SUTGMM PROGRAMME

Server based Unified Thematic Geological Mapping in Makran

GeoNexus

Report on Server-Based Unified Thematic Geological Mapping of Makran

scale 1:100,000 and 1:50,000

November 2024

GeoNexus

SUTGMM PROGRAMME

Server based Unified Thematic Geological Mapping in Makran

Report on Server-Based Unified Thematic Geological Mapping of Makran

scale 1:100,000 and 1:50,000

Geology by: *H. Nazari, S. Arefipour, and M. Fonoudi*

Structural balanced sections by: *H. Nazari and S. Arefipour*

Petrography by: *Gh. Hoseinyar*

Remote sensing and machine learning by: *J. Karami, S. and Arefipour*

Paleontology by: *J. Daneshian and M. R. Partoazar*

Final report and editing by: *A. Fathian*

Executive supervisors: *A. Zarasvandi and M. Moghadam*

Supervisor in chief: *H. Nazari*

GeoNexus

GeoNexus

November 2024

Research Institute for Earth Sciences

UNESCO Chair on Coastal Geo-Hazards Analysis

UNESCO Chair on Coastal Geo-Hazard Analysis

Research Institute for Earth Sciences Geological Survey of Iran

unesco Chair

INTELLIGENT GEO-EXPLORATION IGE

GeoNexus

Datum

Server-Based Unified Thematic Geological Mapping of Makran (SUTGMM) employs the WGS 1984 datum for accurate georeferencing. The map projection used is the Universal Transverse Mercator (UTM), specifically UTM Zone 41N, which ensures precise positioning within the region. The map is provided at a scale of 1:50,000, referenced to Sheet No. 8141-4, ensuring consistency and accuracy in the spatial representation of geological features.

GeoNexus

GeoNexus

Abstract

The Server-Based Unified Thematic Geological Mapping of Makran (SUTGMM) is a comprehensive geospatial study conducted at a scale of 1:50,000, focusing on the Makran region, located in southeastern Iran along the northern margin of the Oman Sea. This region is characterized by diverse geological formations resulting from the collision of the Arabian and Eurasian plates, including volcanic and sedimentary sequences, turbidite basins, and Quaternary deposits. Makran's rich geological heritage, coupled with its historical importance, makes it a prime subject for advanced geoscientific research and mapping.

The SUTGMM project (Sheet No. 8141-4) aims to prepare detailed geological maps for the area covered by four previously published 1:100,000 geological sheets: Chabahar, Pir Sohrab, Konarak, and Kahir. Additionally, the project includes nine 1:50,000 geological sheets: Ab Sard, Chabahar, Gor, Gurdim, Kahir, Konarak, Kuh-e-kand Koruch, Park Bala, and Zirdan. A buffer zone ranging from 13 to 28 km has also been defined around the core area to facilitate better analysis of geological features that extend beyond the sheets. These maps integrate data from multiple remote sensing sources such as Sentinel-1, Sentinel-2, Landsat 8, and ASTER, as well as digital elevation models (DEMs) to capture spectral, geological, and topographical information at various resolutions.

Utilizing a novel approach combining cloud computing, machine learning, and object-based image analysis, the project leverages the power of *Google Earth Engine* for the processing and analysis of large datasets. The random forest algorithm, used for geological classification, has enabled the creation of a unified geological map with an accuracy of 85%, highlighting the effectiveness of this integrated approach.

This project has provided valuable insights into the complex geological context of the Makran region. The geological units mapped in SUTGMM represent a time range from the Oligocene to the Quaternary period. This includes older formations from the Oligocene and Miocene, as well as more recent Pleistocene and Quaternary deposits. The units highlight the region's complex geodynamic evolution, influenced by both tectonic activity and sedimentary processes.

The GeoNexus geodatabase, as the final product of the SUTGMM project, represents a major advancement in geological mapping by using cloud computing, machine learning, field surveys, and multi-source data integration to enhance the accuracy, efficiency, and comprehensiveness of geological outputs. Ultimately, the findings from this study are expected to support sustainable development efforts and foster a deeper understanding of the Makran region's geodynamic processes.

GeoNexus

GeoNexus

Acknowledgment

We would like to express our deepest gratitude to Kor, Rezaie and Afarin from Iranian National Institute for Oceanography and Atmospheric Science, Chabahar Campus for their invaluable support and logistical assistance during the course of this project. Their contributions were instrumental in ensuring the success of our field operations.

We are also grateful to R. Mohtashamipour, R. Lak and M. Majidifar for their support that significantly advanced our project.

This project has been enriched by the cooperation of many individuals and institutions, and we sincerely appreciate their support.

GeoNexus

GeoNexus

Contents

1 INTRODUCTION 1

1.1 Historical and Geographical Context 1
1.2 Scope and Data Collection 1
1.3 Objectives 3
1.4 Data Sources and Accessibility 5
1.4.1 Unlocking Trapped Data 5
1.4.2 Contribution to the Bibliography and Digital Resources 5
1.5 Study Area and Area of Interest (AOI) 6

2 GEOLOGICAL AND TECTONIC SETTING 9

2.1 Tectonic Setting of Makran 9
2.1.1 Subduction Characteristics and Volcanic Arcs 12
2.1.2 Accretionary Wedge 14
2.1.3 Accretionary Wedge Stratigraphy 15
2.1.4 Uplift along the Coast 17
2.2 Structural Features of Makran 18
2.2.1 Folds 18
2.2.1.1 Types and Styles of Folds 18
2.2.1.2 Orientation and Distribution 18
2.2.1.3 Mechanisms and Implications 19
2.2.2 Faults 19
2.2.2.1 Thrust Faults 20
2.2.2.2 Flat and Ramp Systems 21
2.2.2.3 Backthrusts 21
2.2.2.4 Normal Faults 21
2.2.2.5 Strike-Slip Faults 22
2.3 Structural Synthesis 22
2.3.1 Deformation Gradient 22
2.3.2 Temporal Evolution 23
2.3.3 Strain Partitioning 23
2.3.3.1 Main Stress Regimes 23
2.3.4 Low-Temperature Thermochronology of the Makran Accretionary Wedge 24
2.3.4.1 Apatite Fission-Track Results and Interpretations 24
2.3.4.2 Zircon Fission-Track Results and Interpretations 26
2.3.5 Implications for Tectonic Models 26
2.4 Seismicity 29

GeoNexus

3 METHODS AND DATA 33

3.1 Converting Archived Paper Data into Digital Resources 34
3.2 Remote Sensing 34
3.2.1 Sensors 35
3.2.2 Data Acquisition Methods 35
3.2.3 Applications in Geological Mapping 35
3.2.4 Mineral Exploration Techniques 36
3.2.5 Data Processing and Interpretation 36
3.2.6 Integration with Other Data 36
3.2.7 Advantages of Remote Sensing 37
3.2.8 Limitations 37
3.2.9 Emerging Trends 37
3.3 Advanced Remote Sensing Sensors and Their Applications in Geology 39
3.4 Cloud Computing 44
3.4.1 Google Earth Engine 45
3.5 Satellite Imagery and Digital Elevation Model (DEM) 51
3.6 Preparation and Processing of Landsat 8 (OLI) Images 52
3.6.1 Modeling 52
3.6.2 Arithmetic Operations 53
3.6.3 Spectral Indices 53
3.6.4 Principal Component Analysis (PCA) 53
3.6.4.1 Feature-Oriented Principal Component Selection (FPCS) 54
3.7 Preparation and Processing of Sentinel-2 (MSI) Images 55
3.8 Preparation and Processing of Sentinel-1 Dual-Polarization C-band SAR Data 56
3.9 Preparation and Processing of SRTM DEM 58
3.10 Fusion of Optical and Radar Images 58
3.11 Object-Based Process for Geological Mapping of Mineral Potential 59
3.12 Image Segmentation 59
3.12.1 Determining the Appropriate Segmentation Scale in the Multiscale Method 60
3.12.2 Segmentation of the Images within the Study Area 61
3.12.3 Preparing Initial Layers for Segmentation 61
3.12.4 Determining Segmentation Parameters 61
3.12.5 Selecting the Optimal Scale in Segmentation 62
3.12.6 Image Segmentation for Preparing a Preliminary Geological Map 63
3.13 Creation of the Initial Geological Map 65
3.14 Machine Learning 67
3.14.1 How Does a Machine Learn? 68
3.14.2 Features of Machine Learning 69
3.14.3 The Need for Machine Learning 69
3.14.4 Classification Algorithms in Machine Learning 69
3.14.4.1 Supervised learning 70
3.14.4.2 Unsupervised Learning 70
3.14.4.3 Reinforcement Learning 70
3.14.5 Random Forest 71
3.14.5.1 Assumptions in Random Forest 72
3.14.5.2 Advantages of Random Forest 73
3.14.6 Random Forest in Extracting Lithological Units 73
3.14.7 Evaluation of the Random Forest Model 75
3.14.7.1 Evaluation of the Model for Test Samples 75
3.14.7.2 Evaluation of the Model for All Training and Test Samples (30% of the Total Samples) 77

GEONEXUS

3.14.7.3 Evaluation of the Model for the Entire Area (8,959 Polygons) ... 79
3.15 Preparation of Integrated Database of SUTGMM ... 82
3.15.1 JavaScript Programming Language ... 83
3.15.2 Map Canvas - WebGIS Main Display Page ... 84
3.15.3 Layer Control ... 84
3.15.4 Navigation Controls ... 88
3.16 Workflow and Protocol ... 89
3.16.1 Phase 1: Data Acquisition and Extraction ... 90
3.16.2 Phase 2: Data Processing and Feature Extraction ... 91
3.16.3 Phase 3: Machine Learning and Initial Classification ... 91
3.16.4 Phase 4: Field Verification and Geodatabase Integration ... 92
3.16.5 Phase 5: Iterative Refinement and Final Outputs ... 93

4 GEOLOGICAL AND STRATIGRAPHIC ANALYSES ... 95

4.1 $OlM^{SH.S}$ Unit (Late Oligocene Shale and Sandstone) ... 108
4.1.1 Previous Studies ... 108
4.1.2 Lithology ... 108
4.1.3 Stratigraphy and Age ... 109
4.1.4 Structural Features ... 109
4.1.5 Paleontological Evidence ... 109
4.1.6 Depositional Environment ... 109
4.2 $OlM^{S.SH.C}$ Unit (Oligocene Shale, Sandstone, and Conglomerate) ... 110
4.2.1 Lithology ... 110
4.2.2 Stratigraphy and Age ... 111
4.2.3 Petrographic Analysis ... 111
4.2.3.1 Sample 24M-42P ... 111
4.2.3.2 Sample 24M-44P ... 112
4.2.4 Structural Features ... 114
4.2.5 Depositional Environment ... 115
4.2.6 Tectonic Implications ... 115
4.3 $M^{S.SH}$ Unit (Oligocene–Late Miocene Shale and Sandstone) ... 115
4.3.1 Previous Studies ... 116
4.3.2 Lithology and Petrography ... 116
4.3.2.1 Sample 24M-25F ... 116
4.3.2.2 Sample 24M-37P ... 118
4.3.2.3 Sample 24M-37Pb ... 119
4.3.2.4 Sample 24M-38F ... 120
4.3.2.5 Sample 24M-53F ... 122
4.3.3 Structural Features ... 123
4.3.4 Depositional Environment ... 123
4.3.5 Tectonic Implications ... 124
4.4 $M^{SH.S}$ Unit (Middle to Late Miocene Shale and Siltstone) ... 124
4.4.1 Lithology and Stratigraphy ... 124
4.4.2 Petrographic Analysis ... 125
4.4.2.1 Sample 24M-23F ... 125
4.4.2.2 Sample 24M-24F ... 126
4.4.2.3 Sample 24M-41P ... 128
4.4.2.4 Sample 24M-55F ... 129
4.4.3 Micropaleontological Analysis ... 130
4.4.3.1 Sample 24M-04W ... 130
4.4.3.2 Sample 24M-05W ... 132

GeoNexus

4.4.3.3 Sample 24M-19W 134
4.4.3.4 Sample 24M-22W 134
4.4.3.5 Sample 24M-45W 135
4.4.4 Age and Correlation 137
4.4.5 Depositional Environment 137
4.5 $M^{S.SI}$ Unit 137
4.5.1 Petrographic Analysis 137
4.5.1.1 Sample 24M-51P 137
4.5.2 Micropaleontological Analysis 139
4.5.2.1 Sample 24M-46W 139
4.5.2.2 Sample 24M-48W 141
4.5.2.3 Sample 24M-49W 142
4.5.2.4 Sample 24M-50W 142
4.5.3 Age and Correlation 143
4.5.4 Depositional Environment 143
4.6 $MPL^{M.S}$ Unit 143
4.6.1 Petrographic Analysis 144
4.6.1.1 Sample 24M-21F 144
4.6.1.2 Sample 24M-26Pa 145
4.6.1.3 Sample 24M-26Pb 147
4.6.1.4 Sample 24M-28F 148
4.6.1.5 Sample 24M-31F 149
4.6.1.6 Sample 24M-32F 150
4.6.1.7 Sample 24M-54P 151
4.6.2 Micropaleontological Analysis 153
4.6.2.1 Sample 24M-20W 153
4.6.2.2 Sample 24M-27W 153
4.6.2.3 Sample 24M-29W 154
4.6.2.4 Sample 24M-34W 155
4.6.3 Age and Correlation 156
4.6.4 Depositional Environment 156
4.7 $MPL^{M.S.C}$ Unit (Late Miocene–Early Pliocene Sandstone and Microconglomerate) 157
4.7.1 Lithology and Petrography 158
4.7.1.1 Sample 24M-7P 158
4.7.1.2 Sample 24M-8P 159
4.7.1.3 Sample 24M-9P 160
4.7.1.4 Sample 24M-13F 161
4.7.1.5 Sample 24M-16F 163
4.7.1.6 Sample 24M-17F 164
4.7.1.7 Sample 24M-40F 165
4.7.2 Micropaleontological Analysis 167
4.7.2.1 Sample 24M-10W 167
4.7.2.2 Sample 24M-11W 168
4.7.2.3 Sample 24M-15W 168
4.7.2.4 Sample 24M-39W 170
4.7.3 Age and Correlation 171
4.7.4 Depositional Environment 171
4.8 PL^{SI} Unit (Pliocene to Pleistocene Siltstones and Argillic Deposits) 172
4.8.1 Lithology and Petrography 172
4.8.1.1 Sample 24M-1F 172
4.8.1.2 Sample 24M-2F 174
4.8.1.3 Sample 24M-35F 175
4.8.1.4 Sample 24M-36F 177

GeoNexus

4.8.2 Micropaleontological Analysis ... *179*
4.8.2.1 Sample 24M-3W ... 179
4.8.3 Age and Correlation ... *180*
4.8.4 Depositional Environment ... *181*
4.9 $Pl^{Sl.C}$ Unit (Pliocene White to Buff Argillic Deposits and Sandy Siltstones) ... 181
4.9.1 Lithology ... *181*
4.9.2 Structural Features ... *182*
4.9.3 Micropaleontological Analysis ... *182*
4.9.4 Age and Correlation ... *182*
4.9.5 Depositional Environment ... *183*
4.10 $Pl^{L.Sl.S}$ Unit (Pliocene Shale and Volcanosedimentary Sandy Tuff) ... 183
4.10.1 Lithology ... *183*
4.10.2 Micropaleontological Analysis ... *184*
4.10.3 Age and Correlation ... *184*
4.10.4 Depositional Environment ... *184*
4.11 $PlPe^{C.S.Sl}$ Unit (Pliocene to Pleistocene Sediments) ... 185
4.11.1 Lithology ... *185*
4.11.2 Micropaleontological Analysis ... *186*
4.11.2.1 Sample 24M-18W ... 186
4.11.3 Age and Correlation ... *187*
4.11.4 Depositional Environment ... *187*
4.12 Q^{A} Unit (Late Pleistocene to Holocene Mud Flat Deposits) ... 188
4.12.1 Lithology ... *188*
4.12.2 Age and Correlation ... *189*
4.12.3 Depositional Environment ... *189*
4.13 Q^{B} Unit (Late Holocene Beach Deposits) ... 190
4.13.1 Lithology ... *190*
4.13.2 Age and Correlation ... *191*
4.13.3 Depositional Environment ... *191*
4.14 Q^{FP} Unit (Quaternary Alluvial Fan Deposits) ... 192
4.14.1 Lithology ... *192*
4.14.2 Age and Correlation ... *193*
4.14.3 Depositional Environment ... *193*
4.15 Q^{SD} Unit (Holocene Sand Dunes) ... 194
4.15.1 Lithology ... *194*
4.15.2 Age and Correlation ... *195*
4.15.3 Depositional Environment ... *195*
4.16 Q^{AL} Unit (Holocene Alluvial Deposits) ... 195
4.16.1 Lithology ... *196*
4.16.2 Age and Correlation ... *196*
4.16.3 Depositional Environment ... *196*

5 STRUCTURAL ANALYSES ... 199

5.1 Folds ... 199
5.1.1 Anticlines ... *199*
5.1.1.1 A001: Plunging Anticline ... 200
5.1.1.2 A002: Overturned Anticline ... 200
5.1.1.3 A003: Anticline ... 200
5.1.1.4 A004: Overturned Anticline ... 200
5.1.1.5 A005: Anticline ... 200
5.1.1.6 A006: Plunging Anticline ... 201

GEONEXUS

5.1.1.7 A007: Symmetrical Anticline 201
5.1.1.8 A008: Symmetrical Anticline 201
5.1.1.9 A009: Symmetrical Anticline 201
5.1.1.10 A010: Symmetrical Anticline 201
5.1.2 Synclines 202
5.1.2.1 S001: Plunging Syncline 203
5.1.2.2 S002: Syncline Axis 203
5.1.2.3 S003: Symmetrical Syncline 203
5.1.2.4 S004: Syncline Axis 203
5.1.2.5 S005: Syncline Axis 203
5.1.2.6 S006: Syncline Axis 203
5.1.2.7 S007: Syncline Axis 204
5.1.2.8 S008: Overturned Syncline 204
5.1.2.9 S009: Overturned Syncline 204
5.1.2.10 S010: Symmetrical Syncline 204
5.1.2.11 S011: Symmetrical Syncline 204
5.1.2.12 S012: Symmetrical Syncline 205
5.2 FAULTS 205
5.2.1 Fault Mechanism Classification and Trends 205
5.2.2 Geographic Distribution and Concentration of Faults 206
5.2.2.1 Central Zone 206
5.2.2.2 Northwestern Zone 206
5.2.2.3 Northeastern Zone 206
5.2.2.4 Southwestern Zone 208
5.2.2.5 Southeastern Zone 208
5.2.3 Fault Concentration Zones 208
5.3 STRUCTURAL BALANCED SECTIONS 209
5.3.1 Data Preparation and Input 210
5.3.1.1 GeoNexus Map and Mapped Units 210
5.3.1.2 Faults and Fold Geometries 210
5.3.1.3 Bedding Data: 211
5.3.2 Data Integration and Input 211
5.3.2.1 Rock Type and Lithological Composition 212
5.3.2.2 Compaction and Porosity 212
5.3.2.3 Mechanical Properties 212
5.3.2.4 Time/Depth Conversion 212
5.3.3 Setting Up Section Lines 213
5.3.3.1 Profile AA' (Chabahar to Park Bala) 213
5.3.3.2 Profile BB' (Chabahar to Zirdan) 213
5.3.3.3 Profile CC' (Konarak to Zirdan) 213
5.3.3.4 Profile DD' (Gurdim to Kuh-e-kand Koruch) 213
5.3.3.5 Profile EE' (Kahir to Gor) 214
5.3.4 Building the Cross-Section 214
5.3.4.1 Surface Line Tracing 214
5.3.4.2 Fault and Horizon Construction 214
5.3.4.3 Folding Models 214
5.3.5 Geometric and Kinematic Balancing 214
5.3.6 Refining and Validating the Balanced Sections 215
5.3.7 Final Visualization and Output 218
5.4 MUD VOLCANOES 218
5.4.1 Inactive Mud Volcano 218
5.4.2 Active Mud Volcano 219
6 SUMMARY AND CONCLUSIONS 221

GeoNexus

6.1 SUMMARY 221
6.1.1 *Integration of Technologies* 221
6.1.2 *Methodological Innovation* 221
6.1.3 *Computational Efficiency* 221
6.1.4 *Accuracy and Reliability* 222
6.1.5 *Scalability and Broader Applications* 222
6.1.6 *Interdisciplinary Collaboration* 222
6.1.7 *Geological Significance* 222
6.1.8 *Optimized GeoNexus Workflow and Protocol* 223
6.2 RECOMMENDATIONS 223
6.3 OUTLOOK 224
6.4 CONCLUSIONS 224

GeoNexus

List of Figures

FIGURE 1-1. THE AREA OF INTEREST (AOI) FOR THE SERVER-BASED UNIFIED THEMATIC GEOLOGICAL MAPPING OF THE MAKRAN (SUTGMM) HIGHLIGHTED WITH A GREEN POLYGON. DARK SHADED RECTANGLES INDICATE THE FOUR 1:100,000 GEOLOGICAL SHEETS OF KAHIR, PIR SOHRAB, KONARAK AND CHABAHAR. 7
FIGURE 1-2. STUDY AREA ENCOMPASSING THE AREA OF INTEREST (AOI) AND THE ADDITIONAL BUFFER ZONE 7
FIGURE 2-1. TECTONIC SETTING OF THE MAKRAN REGION, SHOWING TECTONOSTRATIGRAPHIC ZONES AND MAJOR STRUCTURES, INCLUDING THE ACCRETIONARY WEDGES AND PULL-APART BASINS (HAGHIPOUR AND BURG, 2014; BURG, 2018). 10
FIGURE 2-2. SEISMOTECTONIC CONFIGURATION OF MAKRAN AND SURROUNDING AREAS. THE SUBDUCTION FRONT IN THE OMAN SEA MARKS THE CONVERGENCE BETWEEN THE ARABIAN AND EURASIAN PLATES. FAULT TRACES ARE COMPILED AND MODIFIED AFTER FATHIAN (2022). RED SHADED POLYGON MARK THE AOI. GREY, RED, AND BLUE BEACHBALLS REPRESENT FAULT PLANE SOLUTIONS FROM THE THE GLOBAL CENTROID MOMENT TENSOR (GCMT; HTTPS://WWW.GLOBALCMT.ORG), BODY WAVEFORM, AND THE FIRST MOTIONS CATALOGS (SEE FATHIAN, 2022 AND THE REFERENCES THEREIN). RED ARROWS REPRESENT GPS VELOCITY VECTORS RELATIVE TO A STABLE EURASIAN PLATE (KHORRAMI ET AL., 2019). BACKGROUND IS THE SHADED RELIEF FROM SRTM 90M (FARR ET AL., 2007) AND GEBCO GLOBAL BATHYMETRY 15 ARC-SEC (GEBCO COMPILATION GROUP, 2023) VISUALIZING SURFACE TOPOGRAPHY AND BATHYMETRY. 11
FIGURE 2-3. A) REGIONAL OVERVIEW OF THE MAKRAN ACCRETIONARY WEDGE AND SURROUNDING TECTONIC FEATURES (BURG, 2018). ITALIC B, T, AND S REPRESENT THE BAZMAN, TAFTAN, AND KOH-I-SULTAN VOLCANOES, RESPECTIVELY. WHITE LINES REPRESENT THE LOCATIONS OF CROSS-SECTIONS SHOWN IN PANELS B AND C. B, C) LITHOSPHERIC-SCALE CROSS-SECTIONS ACROSS THE WESTERN (B) AND EASTERN (C) MAKRAN. THESE CROSS SECTIONS ILLUSTRATE THE PRIMARY GEOLOGICAL STRUCTURES AND SEISMICITY, WITH SOLID BLACK CIRCLES REPRESENTING FOCAL MECHANISMS FOR SEISMIC EVENTS, MODIFIED AFTER BYRNE ET AL. (1992) AND UPDATED WITH MAGNITUDE M4 EVENTS UP TO THE PRESENT (BURG, 2018). 13
FIGURE 2-4. A) N–S SECTION ACROSS WESTERN MAKRAN (60°E) SHOWING THE SUBDUCTION OF THE ARABIAN PLATE BENEATH THE EURASIAN PLATE, WITH SEISMIC EVENTS PROJECTED ALONG THE PROFILE, HIGHLIGHTING THE STEEPENING SUBDUCTION SLOPE BENEATH THE JAZ MURIAN DEPRESSION (JACOB ET AL., 1979). B) SEISMIC TOMOGRAPHY (HAFKENSCHEID ET AL., 2006) AND EARTHQUAKES WITH THE SUBDUCTING SLAB BENEATH THE MAKRAN REGION (DOLATI, 2010). 13
FIGURE 2-5. THE STRUCTURE OF THE MAKRAN ACCRETIONARY WEDGE, ILLUSTRATING UNDERPLATED SEDIMENTS BENEATH A GENTLY DIPPING DÉCOLLEMENT (KOPP ET AL., 2000). 14
FIGURE 2-6. SEISMIC PROFILE (A) AND THE INTERPRETATION (B) ACROSS THE WESTERN OFFSHORE MAKRAN ACCRETIONARY PRISM, SHOWING THE SHELF, SLOPE BASINS, AND ACCRETIONARY PRISM. THE M UNCONFORMITY SEPARATES HIMALAYAN TURBIDITES FROM MAKRAN SANDS. THE INTERPRETATION HIGHLIGHTS GROWTH STRATA, SHALE DIAPIRS, THE IMBRICATE ZONE, AND THE DEFORMATION FRONT, WITH POTENTIAL UNDERPLATING AND A DETACHMENT LEVEL IDENTIFIED (GRANDO AND MCCLAY, 2007). 15
FIGURE 2-7. TECTONOSTRATIGRAPHIC ZONES OF THE MAKRAN ACCRETIONARY WEDGE (KAVEH-FIROUZ ET AL., 2023). BT: BASHAKERD THRUST FAULT, SST: SISTAN-SIAHAN THRUST, BPT: BAMPOSHT THRUST FAULT, CHT: CHANF THRUST FAULT, LT: LASHAR THRUST FAULT, PT: PISHAMAK THRUST FAULT, GGT: QASR-E-QAND THRUST FAULT, GT: GATIVAN THRUST FAULT, AND CKT: CHAH KHAN THRUST FAULT. 15
FIGURE 2-8. MORPHOLOGICAL SETTING OF THE COASTAL MAKRAN, SHOWING PALEOSHORELINES ALONG THE CHABAHAR, POZM, TANG AND DARANGO BAYS (GHARIBREZA, 2016). 17
FIGURE 2-9. GEOLOGICAL MAP OF THE MAKRAN ACCRETIONARY WEDGE IN IRAN, SHOWING FISSION-TRACK SAMPLE LOCATIONS (DOLATI, 2010). APATITE SAMPLE LOCATIONS ARE MARKED BY GREEN HEXAGONS, AND ZIRCON SAMPLES BY RED CROSSES. 27
FIGURE 2-10. CROSS SECTIONS, ILLUSTRATING FISSION-TRACK SAMPLE LOCATIONS (DOLATI, 2010). APATITE AND ZIRCON CENTRAL AGES (±2Σ) ARE SHOWN IN GREEN AND RED BOXES, RESPECTIVELY. SEE LOCATIONS OF PROFILES IN FIGURE 2-9. . 28
FIGURE 2-11. MAJOR FOCAL MECHANISMS OVER THE MAKRAN ACCRETIONARY WEDGE AND ADJACENT AREAS, ILLUSTRATING THE SEGMENTATION AND SEISMICITY PATTERNS (DOLATI, 2010). 31

FIGURE 3-1. COMPARISON OF LANDSAT 7 ETM+ AND LANDSAT 8 OLI/TIRS SPECTRAL BANDS, ILLUSTRATING BANDPASS WAVELENGTHS AND ATMOSPHERIC TRANSMISSION PERCENTAGES ACROSS THE ELECTROMAGNETIC SPECTRUM (GRAPHIC BY L. ROCCHIO AND J. BARSI; SOURCE: HTTPS://LANDSAT.GSFC.NASA.GOV/SATELLITES/LANDSAT-8/)..... 38
FIGURE 3-2. COMPARISON OF SPECTRAL RESOLUTION BETWEEN ETM AND ASTER IMAGES. 40
FIGURE 3-3. COMPARISON OF SENTINEL-2 WITH LANDSAT 7 (ETM+) AND LANDSAT 8 BANDS (SOURCE: HTTPS://LANDSAT.GSFC.NASA.GOV/WP-CONTENT/UPLOADS/2015/06/LANDSAT.V.SENTINEL-2.PNG)..... 41
FIGURE 3-4. FOUR ACQUISITION MODES FOR SENTINEL-1 (TORRES ET AL., 2012) 43
FIGURE 3-5. ILLUSTRATION OF THE MAIN COMPONENTS OF A CLOUD COMPUTING SYSTEM. 44
FIGURE 3-6. THE THREE KEY COMPONENTS OF THE *GOOGLE EARTH ENGINE* SYSTEM AS A CLOUD COMPUTING PLATFORM. 45
FIGURE 3-7. COPERNICUS GLOBAL LAND COVER LAYERS: CGLS-LC100 COLLECTION 2. 45
FIGURE 3-8. LEFT) SLGA: SOIL AND LANDSCAPE GRID OF AUSTRALIA (SOIL ATTRIBUTES). RIGHT) SENTINEL-1 SAR GRD: C-BAND SYNTHETIC APERTURE RADAR GROUND RANGE DETECTED..... 46
FIGURE 3-9. VIEW OF THE *GOOGLE EARTH ENGINE* PROGRAMMING ENVIRONMENT FOR SATELLITE IMAGE PROCESSING..... 48
FIGURE 3-10. VIEW OF THE *GOOGLE EARTH ENGINE* PROGRAMMING ENVIRONMENT FOR TOPOGRAPHIC DATA PROCESSING.. 48
FIGURE 3-11. EXECUTION OF *GOOGLE EARTH ENGINE* PROGRAMMING FOR IMPLEMENTING RANDOM FOREST MACHINE LEARNING. 49
FIGURE 3-12. A LANDSAT 8 SCENE COVERING THE STUDY AREA. 52
FIGURE 3-13. LEFT) DISPLAY OF PRINCIPAL COMPONENTS 1, 2, AND 3 FROM PCA OF LANDSAT 8 IMAGE COVERING THE STUDY AREA. RIGHT) UNIFIED OLI SENSOR IMAGE FROM LANDSAT 8 COVERING THE STUDY AREA (BAND COMBINATION 2-4-6). 55
FIGURE 3-14. LEFT) DISPLAY OF PRINCIPAL COMPONENTS 1, 3, AND 4 FROM PCA OF SENTINEL-2 IMAGERY COVERING THE STUDY AREA. RIGHT) UNIFIED MSI SENSOR IMAGERY FROM SENTINEL-2 COVERING THE STUDY AREA (BAND COMBINATION 2-4-9). 56
FIGURE 3-15. LEFT) SENTINEL-1 VH BAND IMAGE WITHIN THE STUDY AREA. RIGHT) UNIFIED MSI SENSOR IMAGE FROM SENTINEL-2 WITHIN THE STUDY AREA (BAND COMBINATION 2-4-9)..... 57
FIGURE 3-16. CLOSE-UP VIEW OF THE RADAR IMAGES OF THE EASTERN PART OF THE AREA. THE UPPER IMAGE CORRESPONDS TO THE VV ACQUISITION, AND THE LOWER IMAGE CORRESPONDS TO THE VH ACQUISITION..... 57
FIGURE 3-17. LEFT) HILLSHADE OF THE STUDY AREA. RIGHT) SRTM DEM OF THE STUDY AREA. 58
FIGURE 3-18. FUSION OF OPTICAL SATELLITE IMAGERY (SENTINEL-2) AND RADAR IMAGES (SENTINEL-1) TO ENHANCE AND EXPOSE TECTONIC STRUCTURES..... 58
FIGURE 3-19. PARAMETER ADJUSTMENT WINDOW FOR SEGMENTATION IN *ECOGNITION* SOFTWARE. 63
FIGURE 3-20. CHANGES IN LOCAL VARIANCE AND RATE OF CHANGE AT DIFFERENT SCALES..... 63
FIGURE 3-21. A PART OF THE STUDY AREA FOR COMPARISON. THE UPPER IMAGE SHOWS THE SENTINEL-2 BAND COMBINATION, AND THE LOWER IMAGE SHOWS THE SEGMENTATION OVERLAID ON IT..... 64
FIGURE 3-22. ANOTHER PART OF THE STUDY AREA FOR COMPARISON. THE UPPER IMAGE SHOWS THE SENTINEL-2 BAND COMBINATION, AND THE LOWER IMAGE SHOWS THE SEGMENTATION OVERLAID ON IT. 64
FIGURE 3-23. A PART OF THE STUDY AREA FOR COMPARISON WITH THE EXISTING GEOLOGICAL MAP. THE UPPER IMAGE SHOWS THE SENTINEL-2 BAND COMBINATION, AND THE LOWER IMAGE SHOWS THE BOUNDARIES OF THE PREPARED GEOLOGICAL UNITS OVERLAID ON IT. 65
FIGURE 3-24. THE SIMILARITY BETWEEN HUMANS AND COMPUTERS IN LEARNING. 68
FIGURE 3-25. BLOCK DIAGRAM EXPLAINING THE WORKING OF A MACHINE LEARNING ALGORITHM..... 68
FIGURE 3-26. TYPES OF LEARNING METHODS IN MACHINE LEARNING ALGORITHMS. 70
FIGURE 3-27. SCHEMATIC DIAGRAM OF RANDOM FOREST STRUCTURE. 71
FIGURE 3-28. A MORE COMPLETE SCHEMATIC DIAGRAM OF RANDOM FOREST STRUCTURE..... 71
FIGURE 3-29. EXAMPLES OF SELECTED POINTS (LIGHT BLUE CIRCLES) FOR THE M-PL^{M,S} LITHOLOGICAL UNIT. 74
FIGURE 3-30. CONFUSION MATRIX FOR TEST SAMPLES (30% OF TRAINING SAMPLES) FOR EVALUATING THE ACCURACY AND EFFICIENCY OF THE RANDOM FOREST MODEL. 77
FIGURE 3-31. CONFUSION MATRIX FOR ALL TRAINING SAMPLES (30% OF TOTAL SAMPLES) FOR EVALUATING THE ACCURACY AND EFFICIENCY OF THE RANDOM FOREST MODEL. 78
FIGURE 3-32. CONFUSION MATRIX FOR THE STUDY AREA (TOTAL OF 8,959 POLYGONS) FOR EVALUATING THE ACCURACY AND EFFICIENCY OF THE RANDOM FOREST MODEL. 79

GeoNexus

FIGURE 3-33. INTEGRATED GEOLOGICAL MAP OF THE MAKRAN STUDY AREA. 81
FIGURE 3-34. VIEW OF THE VISUAL STUDIO CODE PROGRAMMING ENVIRONMENT AND THE JAVASCRIPT CODES FOR THE SUTGMM GEODATABASE. 83
FIGURE 3-35. MAIN PAGE OF THE MAKRAN GEOLOGICAL WEBGIS SYSTEM, SHOWING MULTIPLE GEOREFERENCED POINTS OVERLAID ON A SATELLITE IMAGERY BASEMAP, ALLOWING FOR SPATIAL EXPLORATION AND DATA INTERACTION. 84
FIGURE 3-36. VIEW OF THE LAYER CONTROL TOOL IN THE WEBGIS ENVIRONMENT....85
FIGURE 3-37. A VIEW GEOPORTAIL FRANCE SATELLITE IMAGERY LAYER....85
FIGURE 3-38. A VIEW OF THE STAMEN WATERCOLOR MAP LAYER. 85
FIGURE 3-39. A VIEW OF THE GOOGLE STREET MAP LAYER....86
FIGURE 3-40. GENERATED GEOLOGICAL LAYER WITH THE ABILITY TO QUERY FEATURES OF EACH UNIT. 86
FIGURE 3-41. DISPLAY OF THE PROJECT FIELD SURVEY POINTS....86
FIGURE 3-42. ONLINE SEARCH AND DISPLAY OF VISUAL INFORMATION FOR POINT 1084 ON THE MAP. 87
FIGURE 3-43. ONLINE SEARCH AND DISPLAY OF AUDIO AND VIDEO INFORMATION FOR POINT 1168 ON THE MAP. 87
FIGURE 3-44. ONLINE SEARCH AND DISPLAY OF THE REPORT RELATED TO EACH FIELD INVESTIGATION POINT. 88
FIGURE 3-45. THE INTERACTIVE AND CONTROL CAPABILITIES. 88
FIGURE 3-46. COORDINATE DISPLAY ON THE MAP. 89
FIGURE 3-47. WORKFLOW AND PROTOCOL FOR SERVER-BASED UNIFIED THEMATIC GEOLOGICAL MAPPING OF MAKRAN (SUTGMM) USING MULTI-SOURCE REMOTE SENSING DATA AND MACHINE LEARNING. THE PROCESS INCLUDES FEATURE EXTRACTION FROM SENTINEL-1, SENTINEL-2, LANDSAT 8, ASTER, AND SRTM DEM DATA, SUPERVISED CLASSIFICATION, FIELD-CHECKING, AND ITERATIVE REFINEMENT. THE FINAL OUTPUTS INCLUDE A UNIFIED GEOLOGICAL MAP, STRUCTURAL SECTION, AND INTEGRATED GEODATABASE....92
FIGURE 4-1. SERVER-BASED UNIFIED THEMATIC GEOLOGICAL UNITS OF THE AOI. SOLID GREEN LINES HIGHLIGHT THE TRAJECTORY OF THE STRUCTURAL CROSS-SECTIONS IN CHAPTER 5. 96
FIGURE 4-2. MAPPING FRAMEWORK FOR THE GEONEXUS PROJECT (SUTGMM) IN THE MAKRAN REGION.THE GREEN POLYGON MARKS THE AREA OF INTEREST (AOI) FOR THE SERVER-BASED UNIFIED THEMATIC GEOLOGICAL MAPPING OF MAKRAN (SUTGMM) PROJECT. THE SOLID GREY RECTANGLES WITH RED OUTLINES REPRESENT THE EXTENT OF THE PREVIOUSLY PUBLISHED 1:100,000 GEOLOGICAL MAPS THAT COVER THE STUDY AREA. THE RECTANGLES WITH BLUE OUTLINES CORRESPOND TO THE NINE 1:50,000 GEOLOGICAL SHEETS PUBLISHED AS PART OF THE GEONEXUS GEODATABASE (SUTGMM), WHICH INCLUDE AB SARD, CHABAHAR, GOR, GURDIM, KAHIR, KONARAK, KUH-E-KAND KORUCH, PARK BALA, AND ZIRDAN. 97
FIGURE 4-3. FINAL VERSION OF THE GEONEXUS (SUTGMM) MAP (SHEET NO. 8141-4; SCALE 1:100,00). 98
FIGURE 4-4. FINAL VERSION OF THE AB SARD MAP (SHEET NO. 8041-2; SCALE 1:50,00)....99
FIGURE 4-5. FINAL VERSION OF THE CABAHAR MAP (SHEET NO. 8140-4; SCALE 1:50,00)....100
FIGURE 4-6. FINAL VERSION OF THE GOR MAP (SHEET NO. 8041-4; SCALE 1:50,00). 101
FIGURE 4-7. FINAL VERSION OF THE GURDIM MAP (SHEET NO. 8040-4; SCALE 1:50,00). 102
FIGURE 4-8. FINAL VERSION OF THE KAHIR MAP (SHEET NO. 8041-3; SCALE 1:50,00). 103
FIGURE 4-9. FINAL VERSION OF THE KONARAK MAP (SHEET NO. 8040-1; SCALE 1:50,00). 104
FIGURE 4-10. FINAL VERSION OF THE KUH-E-KAND KORUCH MAP (SHEET NO. 8041-1; SCALE 1:50,00)....105
FIGURE 4-11. FINAL VERSION OF THE PARK BALA MAP (SHEET NO. 8141-3; SCALE 1:50,00). 106
FIGURE 4-12. FINAL VERSION OF THE ZIRDAN MAP (SHEET NO. 8141-4; SCALE 1:50,00). 107
FIGURE 4-13. PHOTOMICROGRAPHS OF SAMPLE 24M-42P IN CROSS-POLARIZED LIGHT (XPL) AND PLANE-POLARIZED LIGHT (PPL) AT VARYING MAGNIFICATIONS. PANELS A, C, AND E ARE IN XPL, AND PANELS B, D, AND F ARE IN PPL....112
FIGURE 4-14. PHOTOMICROGRAPHS OF SAMPLE 24M-44P IN XPL (PANELS A, C, AND E) AND PPL (PANELS B, D, AND F) AT 10X MAGNIFICATIONS....114
FIGURE 4-15. PHOTOMICROGRAPHS OF SAMPLE 24M-25F IN XPL (PANELS A, C, AND E) AND PPL (PANELS B, D, AND F) AT VARYING MAGNIFICATIONS. 117
FIGURE 4-16. PHOTOMICROGRAPHS OF SAMPLE 24M-37P IN XPL (PANELS A, C, AND E) AND PPL (PANELS B, D, AND F) AT VARYING MAGNIFICATIONS. 119
FIGURE 4-17. PHOTOMICROGRAPHS OF SAMPLE 24M-37PB IN XPL (PANELS A, C, AND E) AND PPL (PANELS B, D, AND F) AT VARYING MAGNIFICATIONS. 120

GeoNexus

FIGURE 4-18. PHOTOMICROGRAPHS OF SAMPLE 24M-38P IN XPL (PANELS A, C, AND E) AND PPL (PANELS B, D, AND F) AT VARYING MAGNIFICATIONS. 121
FIGURE 4-19. PHOTOMICROGRAPHS OF SAMPLE 24M-53F IN XPL (PANELS A, C, AND E) AND PPL (PANELS B, D, AND F) AT VARYING MAGNIFICATIONS. 123
FIGURE 4-20. PHOTOMICROGRAPHS OF SAMPLE 24M-23F IN XPL (PANELS A, C, AND E) AND PPL (PANELS B, D, AND F) AT VARYING MAGNIFICATIONS. 126
FIGURE 4-21. PHOTOMICROGRAPHS OF SAMPLE 24M-24F IN XPL (PANELS A, C, D, AND E) AND PPL (PANELS B AND F) AT VARYING MAGNIFICATIONS. 127
FIGURE 4-22. PHOTOMICROGRAPHS OF SAMPLE 24M-41P IN XPL (PANELS A, C, AND E) AND PPL (PANELS B, D, AND F) AT VARYING MAGNIFICATIONS. 129
FIGURE 4-23. SCANNING ELECTRON MICROSCOPE (SEM) IMAGES OF MICROPALEONTOLOGICAL SPECIES OF SAMPLE 24M-04W (PLATE 2), SHOWCASING THEIR MORPHOLOGICAL DETAILS. 1) *LENTICULINA INORNATE;* 2) *AMMONIA SP. CF. A. ASANOI*; 3) *AMMONIA BECCARII DENTATA*; 4) *CIBICIDES SP.*; 5) *AMMONIA TOCHIGIENSIS*; 6) *GLOBOROTALIA ARCHEOMENARDII*; 7) *NONION COSTIFERUM*; 8) *NONION COSTIFERUM*; 9) *AMMONIA BECCARII DENTATA*; 10) *GLOBIGERNELLA OBESA*; 11) *GLOBIGERINOIDES SUBQUADRATUS*; 12) *GLOBOQUADRINA SP. CF. G. VENEZUELANA*. 131
FIGURE 4-24. SEM IMAGES OF MICROPALEONTOLOGICAL SPECIES OF SAMPLE 24M-04W (PLATE 2), SHOWCASING THEIR MORPHOLOGICAL DETAILS. 13) *PARAGLOBOROTALIA MAYERI*; 14) *GLOBIGERINOIDES*; 15) *GLOBIGERINOIDES SUBQUADRATUS*; 16) *GLOBIGERINOIDES SUBQUADRATUS*; 17) *GLOBIGERINOIDES SUBQUADRATUS*; 18) *GLOBIGERINOIDES IMMATURUS*; 19) *GLOBIGERINOIDES SUBQUADRATUS*; 20) *GLOBIGERINOIDES SUBQUADRATUS*. 132
FIGURE 4-25. SEM IMAGES OF MICROPALEONTOLOGICAL SPECIES OF SAMPLE 24M-05W (PLATE 3), SHOWCASING THEIR MORPHOLOGICAL DETAILS. 1) *AMMONIA BECCARII DENTATA*; 2) *AMMONIA BECCARII DENTATA*; 3) *AMMONIA INFLATA*; 4) *NONION SP.*; 5) *GLOBIGERINOIDES ALTIAPERTURUS*; 6) *GLOBIGERINOIDES ALTIAPERTURUS*; 7) *GLOBIGERINOIDES SUBQUADRATUS*; 8) *GLOBIGERINOIDES SUBQUADRATUS*; 9) *GLOBIGERINOIDES IMMATURUS*; 10) *PARAGLOBOROTALIA MAYERI*; 11) *GLOBOROTALIA CLEMENCIAE*. 133
FIGURE 4-26. SEM IMAGES OF MICROPALEONTOLOGICAL SPECIES OF SAMPLE 24M-19W (PLATE 8), SHOWCASING THEIR MORPHOLOGICAL DETAILS. 1) GLOBIGERINOIDES IMMATURUS; 2) GLOBIGERINOIDES IMMATURUS; 3) UVIGERINA AUBERIANA; 4) GLOBOQUADRINA VENEZUELANA; 5) GLOBOROTALIA SP.; 6) GLOBIGERINOIDES IMMATURUS. 134
FIGURE 4-27. SEM IMAGES OF MICROPALEONTOLOGICAL SPECIES OF SAMPLE 24M-22W (PLATE 10), SHOWCASING THEIR MORPHOLOGICAL DETAILS. 1) *QUINQUELOCULINA TRIANGULARIS*; 2) *CYCLOFORINA CONTORTA*; 3) *PLANULINA SP.*; 4) *TEXTULARIA SP.*; 5) *PRAEORBULINA GLOMEROSA*. 135
FIGURE 4-28. SEM IMAGES OF MICROPALEONTOLOGICAL SPECIES OF SAMPLE 24M-45W (PLATE 15), SHOWCASING THEIR MORPHOLOGICAL DETAILS. 1) *GLOBOQUADRINA SP. CF. G. DEHISCENS*; 2) *CATAPSYDRAX SP.*; 3) *UVIGERINA MULTICOSTATA*; 4) *UVIGERINA MULTICOSTATA*; 5) *VALVULINA SP.*; 6) *BULIMINA PYRULA*. 136
FIGURE 4-29. PHOTOMICROGRAPHS OF SAMPLE 24M-51P IN XPL (PANELS A, C, AND E) AND PPL (PANELS B, D, AND F) AT VARYING MAGNIFICATIONS. 139
FIGURE 4-30. SEM IMAGES OF MICROPALEONTOLOGICAL SPECIES OF SAMPLE 24M-46W (PLATE 16), SHOWCASING THEIR MORPHOLOGICAL DETAILS. 1) *UVIGERINA AUBERIANA*; 2) *TEXTULARIA SP. CF. T. MARIAE*; 3) *GLOBIGERINOIDES SP.*; 4) *BULIMINA COSTATA*; 5) *MARATTIONTELLA COMMUNIS*; 6) *NODOSARIA SP. CF. N. RUDIS*; 7) *GLOBIGERINOIDES TRILOBA*; 8) *GLOBIGERINOIDES SP. CF. G.IMMATURUS*; 9, 10) *BULIMINA SPP.*; 11) *BULIMINA PYRULA*. 140
FIGURE 4-31. SEM IMAGES OF MICROPALEONTOLOGICAL SPECIES OF SAMPLE 24M-48W (PLATE 17), SHOWCASING THEIR MORPHOLOGICAL DETAILS. 1) *GLOBIGERINOIDES IMMATURUS*; 2) *GLOBIGERINOIDES TRILOBA*; 3) *CIBICIDES SP.*; 4) *BULIMINA PYRULA*; 5) *GLOBIGERINOIDES IMMATURUS*. 141
FIGURE 4-32. SEM IMAGES OF MICROPALEONTOLOGICAL SPECIES OF SAMPLE 24M-49W (PLATE 18), SHOWCASING THEIR MORPHOLOGICAL DETAILS. 1) *GLOBIGERINOIDES IMMATURUS*; 2) *DENTALINA ELEGANS*. 142
FIGURE 4-33. SEM IMAGES OF MICROPALEONTOLOGICAL SPECIES OF SAMPLE 24M-50W (PLATE 19), SHOWCASING THEIR MORPHOLOGICAL DETAILS. 1) *DENTALINA SCRIPTA*; 2) *GLOBIGERINOIDES IMMATURUS*; 3) *LENTICULINA MEXICANUS*. 143
FIGURE 4-34. PHOTOMICROGRAPHS OF SAMPLE 24M-21F IN XPL (PANELS A, C, E) AND PPL (PANELS B, D, F) AT MAGNIFICATIONS OF 4X (A, B, E, F) AND 10X (C, D). 145
FIGURE 4-35. PHOTOMICROGRAPHS OF SAMPLE 24M-26PA IN XPL (PANELS A, C, E) AND PPL (PANELS B, D, F) AT MAGNIFICATIONS OF 4X (A, B) AND 10X (C, D, E, F). 146

GeoNeXus

FIGURE 4-36. PHOTOMICROGRAPHS OF SAMPLE 24M-26PB IN XPL (PANELS A, C, E) AND PPL (PANELS B, D, F) AT MAGNIFICATIONS OF 4X (A, B) AND 10X (C, D, E, F).....148
FIGURE 4-37. PHOTOMICROGRAPHS OF SAMPLE 24M-28F IN XPL (PANELS A, D, E) AND PPL (PANELS B, C, F) AT MAGNIFICATIONS OF 4X (A, B, D) AND 10X (C, E, F).....149
FIGURE 4-38. PHOTOMICROGRAPHS OF SAMPLE 24M-32F IN XPL (PANELS A, C, F) AND PPL (PANELS B, D, E) AT MAGNIFICATIONS OF 4X (A, B, C) AND 10X (D, E, F).....151
FIGURE 4-39. PHOTOMICROGRAPHS OF SAMPLE 24M-54P IN XPL (PANELS A, B, C, D, E) AND PPL (PANEL F) AT MAGNIFICATIONS OF 4X (A, B, C) AND 10X (D, E, F).....152
FIGURE 4-40. SEM IMAGES OF *NONION SP.* (SAMPLE 24M-20W; PLATE 9), SHOWCASING ITS MORPHOLOGICAL DETAILS.....153
FIGURE 4-41. SEM IMAGES OF MICROPALEONTOLOGICAL SPECIES OF SAMPLE 24M-27W (PLATE 11), SHOWCASING THEIR MORPHOLOGICAL DETAILS. 1) *AMMONIA GAIMARDI*; 2) *HETEROLEPA DUTEMPLEI*; 3) *HETEROLEPA DUTEMPLEI*. 154
FIGURE 4-42. SEM IMAGES OF MICROPALEONTOLOGICAL SPECIES OF SAMPLE 24M-29W (PLATE 12), SHOWCASING THEIR MORPHOLOGICAL DETAILS. 1) *ORBULINA UNIVERSA*; 2) *ORBULINA UNIVERSA*; 3) *ORBULINA SUTURALIS*; 4) *ORBULINA SUTURALIS*; 5) *ORBULINA UNIVESA*; 6) *TEXTULARIA SP.*; 7) *GLOBIGERINOIDES IMMATURUS*; 8) *GLOBOQUADRINA VENEZUELANA*; 9) *ORBULINA SUTURALIS*; 10) *GLOBOQUADRINA VENEZUELANA*; 11) *BULIMINA ELONGATE*; 12) *UVIGERINA AUBERIANA*. 155
FIGURE 4-43. SEM IMAGES OF MICROPALEONTOLOGICAL SPECIES OF SAMPLE 24M-34W (PLATE 13), SHOWCASING THEIR MORPHOLOGICAL DETAILS. 1) *AMMONIA UMBONATE*; 2) *NONION SCAPHA*; 3) *NONION SP.* 156
FIGURE 4-44. A) OUTCROP AT LOCATION P002 SHOWING THINLY BEDDED ARGILLACEOUS ROCK LAYERS OF THE $MPl^{M.S.C}$ UNIT'S. B) LOCATION P031 DISPLAYING LARGE OLISTOLITH BLOCKS EMBEDDED WITHIN THE SEDIMENTARY SEQUENCE. C, D) PROMINENT HOODOO MORPHOLOGY AT LOCATION P032 (C) AND P033 (D), SHOWCASING THE DIFFERENTIAL WEATHERING AND TEXTURAL CONTRASTS BETWEEN WEATHERED AND FRESH SURFACES IN THE MPLM.S.C UNIT'S SANDSTONE BEDS....157
FIGURE 4-45. PHOTOMICROGRAPHS OF SAMPLE 24M-7P IN XPL (PANELS A, C, AND E) AND PPL (PANELS B, D, AND F) AT VARYING MAGNIFICATIONS. 158
FIGURE 4-46. PHOTOMICROGRAPHS OF SAMPLE 24M-8P IN XPL (PANELS A AND E) AND PPL (PANELS B, C, D, AND F) AT VARYING MAGNIFICATIONS. 160
FIGURE 4-47. PHOTOMICROGRAPHS OF SAMPLE 24M-8P IN XPL (PANELS A, C, E, AND F) AND PPL (PANELS B AND D) AT MAGNIFICATIONS OF 4X (A AND B), 10X (C, D, AND E), AND 40X (F).....161
FIGURE 4-48. PHOTOMICROGRAPHS OF SAMPLE 24M-13F IN XPL (PANELS A, C, AND E) AND PPL (PANELS B, D, AND F) AT VARYING MAGNIFICATIONS. 162
FIGURE 4-49. PHOTOMICROGRAPHS OF SAMPLE 24M-16F IN XPL (PANELS A, C, AND E) AND PPL (PANELS B, D, AND F) AT VARYING MAGNIFICATIONS. 163
FIGURE 4-50. PHOTOMICROGRAPHS OF SAMPLE 24M-17F IN XPL (PANELS A, C, AND E) AND PPL (PANELS B, D, AND F) AT VARYING MAGNIFICATIONS. 165
FIGURE 4-51. PHOTOMICROGRAPHS OF SAMPLE 24M-40F IN XPL AT MAGNIFICATION OF 4X. 166
FIGURE 4-52. SEM IMAGES OF MICROPALEONTOLOGICAL SPECIES OF SAMPLE 24M-10W (PLATE 4), SHOWCASING THEIR MORPHOLOGICAL DETAILS. 1) *AMMONIA TOCHIGIENSIS*; 2) *AMMONIA STACHI*; 3) *AMMONIA GAIMARDI*; 4) *AMMONIA MARHAUSAI*; 5) *NONION SP.*; 6) *AMMONIA ANNECTENS*.....167
FIGURE 4-53. SEM IMAGES OF *ORBULINA SP.* (?) (SAMPLE 24M-11W; PLATE 5), SHOWCASING ITS MORPHOLOGICAL DETAILS. 168
FIGURE 4-54. SEM IMAGES OF MICROPALEONTOLOGICAL SPECIES OF SAMPLE 24M-15W (PLATE 6), SHOWCASING THEIR MORPHOLOGICAL DETAILS. 1) *AMMONIA TOCHIGIENSIS*; 2) *AMMONIA GAIMARDI*; 3) *NONION SP.*; 4) *AMMONIA SUMATRANA*; 5) *GLOBIGERINOIDES IMMATURUS*; 6) *GLOBIGERINOIDES IMMATURUS*; 7) *GLOBIGERINOIDES TRILOBA*; 8) *ORBULINA UNIVERSA*; 9) *ORBULINA SUTURALIS*; 10) *GLOBIGERINOIDES IMMATURUS*; 11) *QUINQUELOCULINA SP.* 169
FIGURE 4-55. SEM IMAGES OF MICROPALEONTOLOGICAL SPECIES OF SAMPLE 24M-39W (PLATE 14), SHOWCASING THEIR MORPHOLOGICAL DETAILS. 1) *ELPHIDIUM SP.*; 2) *AMMONIA PUNCTATO GRANOSA*; 3) *AMMONIA SCHROETERIANA*; 4) *NONION COSTIFERUM*; 5) *QUINQUELOCULINA PEREGRINA*; 6) *AMMONIA BECCARII ANNECTENS*.....170
FIGURE 4-56. TIDAL CROSS-BEDDING OBSERVED IN THE Pl^{Si} UNIT AT LOCATION P014. 172
FIGURE 4-57. PHOTOMICROGRAPHS OF SAMPLE 24M-1F IN XPL (PANELS A, C, B, D, AND F) AND PPL (E) AT A MAGNIFICATION OF 4X.....173

GeoNexus

FIGURE 4-58. PHOTOMICROGRAPHS OF SAMPLE 24M-2F IN XPL AT A MAGNIFICATION OF 4X. 175
FIGURE 4-59. PHOTOMICROGRAPHS OF SAMPLE 24M-35F IN XPL (PANELS A, C, AND E) AND PPL (PANELS B, D, AND F) AT VARYING MAGNIFICATIONS. 177
FIGURE 4-60. PHOTOMICROGRAPHS OF SAMPLE 24M-36F IN XPL (PANELS A, C, D, E, AND F) AND PPL (PANELS B) AT A MAGNIFICATION OF 4X. 178
FIGURE 4-61. SEM IMAGES OF MICROPALEONTOLOGICAL SPECIES OF SAMPLE 24M-3W (PLATE 1), SHOWCASING THEIR MORPHOLOGICAL DETAILS. 1) *NONION COSTIFERUM*; 2) *NONION COSTIFERUM*; 3) *AMMONIA SCHROETERIANA*; 4) *AMMONIA SP. CF. A. ASANOI*; 5) *CIBICIDES SP. CF. C. REFULGENS*; 6) *AMMONIA BECCARII BAGNENSIS*; 7) *AMMONIA BECCARII DENTATA*; 8) *AMMONIA BECCARII DENTATA*; 9) *AMMONIA BECCARII DENTATA*; 10) *NONION SCAPHA*; 11) *GLOBIGERINOIDES IMMATURUS*; 12) *UVIGERINA MULTICOSTATA*. 180
FIGURE 4-62. SEM IMAGES OF MICROPALEONTOLOGICAL SPECIES OF SAMPLE 24M-18W (PLATE 7), SHOWCASING THEIR MORPHOLOGICAL DETAILS. 1) *CIBICIDES SP.*, *GLOBIGERINOIDES IMMATURUS*; 2) *CIBICIDES SP.*; 3) *QUINQUELOCULINA SP.*; 4) *PARAGLOBOROTALIA OBESA*; 5) *GLOBOROTALIA SIAKENSIS*; 6) *GLOBIGERINOIDES IMMATURUS*; 7) *CATAPSYDRAX DISSIMILIS*; 8) *GLOBIGERINOIDES IMMATURUS*; 9) *GLOBIGERINOIDES IMMATURUS*; 10) *CATAPSYDRAX DISSIMILIS*; 11) *CATAPSYDRAX DISSIMILIS*; 12) *GLOBIGERINOIDES IMMATURUS*. 186
FIGURE 4-63. A) MUD FLAT IN THE Q^{A} UNIT AT LOCATION P020, ILLUSTRATING TYPICAL CRACKED, FINE-GRAINED SEDIMENT SURFACES CHARACTERISTIC OF LOW-ENERGY DEPOSITIONAL ENVIRONMENTS. B) OUTCROP AT LOCATION P023, DISPLAYING PALEORELIEF WITH YOUNGER TERRACE DEPOSITS AT THE TOP. THE IMAGE ALSO HIGHLIGHTS SYN-SEDIMENTARY FAULTS BOUNDED TO THE EROSIONAL SURFACE. 188
FIGURE 4-64. BEACH DEPOSITS OF THE Q^{B} UNIT AT LOCATION P005. 190
FIGURE 4-65. HOLOCENE SAND DUNES (Q^{SD}) AT LOCATION P013. 194
FIGURE 5-1. FOLD MAP DEPICTING ANTICLINES AND SYNCLINES WITHIN THE SUTGMM AOI. THE GREEN LINES (AA' TO EE') REPRESENT TRANSECT LINES USED FOR CROSS-SECTION CONSTRUCTION. 202
FIGURE 5-2. NORMAL FAULTING IN THE $PL^{L,SI,S}$ UNIT AT LOCATION P061 ALONG FAULT F122. 206
FIGURE 5-3. FAULT MAP OF THE SUTGMM AOI. THE GREEN LINES (AA' TO EE') REPRESENT TRANSECT LINES USED FOR CROSS-SECTION CONSTRUCTION. 207
FIGURE 5-4. MAP SHOWING BEDDING ORIENTATIONS DERIVED FROM FIELD SURVEYS WITHIN THE SUTGMM AOI. BEDDING DIP ANGLES (IN DEGREES) ARE MARKED, AND THE STRIKE SYMBOLS INDICATE THE DIRECTION OF BEDDING PLANES. THE GREEN LINES (AA' TO EE') REPRESENT TRANSECT LINES USED FOR BALANCED SECTIONS CONSTRUCTION. 211
FIGURE 5-5. AA' TO EE' STRUCTURAL BALANCED SECTIONS OF THE SUTGMM PROJECT 217
FIGURE 5-6. INACTIVE MUD VOLCANO AT LOCATION P009. THE PASSIVE VENT OF THE VOLCANO HAS DEFORMED AND DISPLACED THE UPPER STRATIGRAPHIC HORIZONS. 219
FIGURE 5-7. ACTIVE MUD VOLCANO AT LOCATION P1084. A) THE ELEVATED STRUCTURE WITH FRESH MUD CHANNELS INDICATES ONGOING FLUID AND GAS EMISSIONS, SUGGESTING ACTIVE SUBSURFACE OVERPRESSURE. B) CLOSE-UP OF BUBBLING MUD POOLS ON THE SURFACE OF THE ACTIVE MUD VOLCANO, DEMONSTRATING CURRENT ACTIVITY AND FLUID MIGRATION FROM DEPTH. 219

GeoNexus

List of Tables

TABLE 1-1. LIST OF THE MAPS USED IN THE PROJECT. 6
TABLE 2-1. EARTHQUAKE FAULT PLANE SOLUTIONS WITHIN THE STUDY AREA (SEE FIGURE 2-11). M, S, D, AND R REPRESENT MAGNITUDE, STRIKE, DIP, AND RAKE, RESPECTIVELY. DEPTHS ARE IN KM. 30
TABLE 3-1. SPECIFICATIONS OF LANDSAT 7 ETM+ AND LANDSAT 8 OLI/TIRS SENSORS, INCLUDING SPECTRAL BANDS, WAVELENGTHS, GEOMETRIC RESOLUTION, AND RADIOMETRIC RESOLUTION. 39
TABLE 3-2. SPECIFICATIONS OF ASTER SENSOR IMAGES (E.G., ABRAMS ET AL., 2002) 40
TABLE 3-3. SPECTRAL AND SPATIAL CHARACTERISTICS OF SENTINEL-2 IMAGES 41
TABLE 3-4. SPECIFICATIONS OF THE SENTINEL-1 MISSION. 44
TABLE 3-5. LIST OF SATELLITE IMAGERY AND DEM USED IN THE SUTGMM PROJECT 51
TABLE 3-6. SAMPLE CORRELATION MATRIX FOR BANDS 1, 2, 3, 4, 5, AND 7. 54
TABLE 3-7. SAMPLE EIGENVECTORS FROM PCA TRANSFORMATION BETWEEN BANDS 1, 4, 5, AND 7. 55
TABLE 3-8. TECHNICAL SPECIFICATIONS OF SENTINEL-2 SENSOR IMAGES. 56
TABLE 3-9. LIST OF VARIABLES USED IN THE PROCESSING. 65
TABLE 3-10. FREQUENCY OF CLASS SEGMENTS AND NUMBER OF TRAINING SAMPLES. 73
TABLE 3-11. ACCURACY ASSESSMENT METRICS FOR TEST DATA. 76
TABLE 3-12. ACCURACY ASSESSMENT METRICS FOR ALL TRAINING AND TEST DATA. 77
TABLE 3-13. ACCURACY ASSESSMENT METRICS FOR THE ENTIRE DATASET 79
TABLE 4-1. GEO-UNITS' TIME TABLE BASED ON ABSOLUTE AGE DETERMINATION AND PALEONTOLOGICAL STUDIES 97
TABLE 5-1. GEOMETRICAL PARAMETERS OF SOME OF THE FAULTS MEASURED IN THE FIELD SURVEYS. 209
TABLE 5-2. GEOUNITS INPUTPARAMETERS FOR *MOVE 2D* FOR STRUCTURAL BALANCED SECTIONS OF THE SUTGMM PROJECT. 215
TABLE 5-3. MECHANICAL AND LITHOLOGICAL INPUT PARAMETERS USED IN *MOVE 2D* FOR STRUCTURAL BALANCED SECTIONS OF THE SUTGMM PROJECT. 216

GeoNexus

GeoNexus

GeoNexus

1 Introduction

1.1 Historical and Geographical Context

Makran, a region with profound historical and geographical significance, spans the southeast of Iran and southwest of Pakistan. This area, defined by its characteristic east-west mountains and bordered by the Strait of Hormuz and the port of Karachi, is known both for its rugged terrain and strategic maritime significance. Historically, Makran derives its name from an ancient state, documented to have existed over 3000 years ago. This state extended from Kerman to the Mehran River along the Oman Sea, encompassing an area once under the rule of the Achaemenid Empire as its fourteenth state during the 6th century BC (Kent, 1953; Mayrhofer, 1978; Schmitt, 1991).

The stone inscriptions found in Bisotun and Persepolis refer to this ancient state, historically named Mecca, highlighting its significance during the era of Achaemenid rule. Notably, Makran played a pivotal role during Alexander the Great's return from India in 324–325 BC. Historical accounts suggest that as Alexander led his forces through the Makran desert towards Pura (present-day Iran), he encountered severe challenges including extreme conditions that led to significant losses among his troops due to fatigue, thirst, and malnutrition.

The growing wedge of Makran is characterized by its sparse population and predominantly nomadic lifestyle, juxtaposed against a backdrop of increasing urban development along the Oman Sea coast. This unique blend of historical richness and modern evolution presents a compelling area of study for geological and environmental research.

1.2 Scope and Data Collection

The focus of this report is the Server-based Unified Thematic Geological Mapping of the Makran (SUTGMM), conducted at a detailed scale of 1:50,000. The project aims to delineate and understand the complex geological framework and environmental dynamics of the region through comprehensive data collection and analysis.

The methodology employed in this project involves an extensive compilation of various data sources. These include high-resolution satellite images, existing topographical and geological maps, peer-reviewed articles, theses, and other scholarly publications, all of which have been accessed

GEONAS

through open sources. The collected data were meticulously classified, ranked, and integrated into various informational layers crucial for the mapping project.

A specialized location database was developed to house all georeferenced data extracted from the compiled sources. This database includes detailed records of sample points, dating data, field measurement locales, and earthquake event data. It is important to note that while the primary data collection focused on the mapped area, relevant information from adjacent regions was also gathered to ensure a holistic understanding of the broader geological features.

Prior to the commencement of field investigations, extensive digital mapping of faults and geological structures was conducted to prepare for the detailed field assessments. The preparatory geodatabase comprises over 520 distinct points and linear features, all carefully georeferenced to enhance the accuracy and utility of the geological maps being produced.

The mapping of Makran not only serves to enrich our understanding of its complex geological context but also aids in assessing the region's natural resources, potential geohazards, and environmental challenges. The insights gained through this project are expected to inform future developmental planning and conservation efforts, ensuring that the region's growth is sustainable and cognizant of its rich historical and geological heritage.

This initiative underscores the importance of integrating historical data with contemporary scientific research to foster a holistic understanding of geologically significant regions like Makran. Through the meticulous gathering and analysis of geospatial and geological data, this project contributes significantly to our knowledge of the earth's dynamic processes in one of the world's most historically rich regions.

In the dynamic landscape of Earth sciences development, a pioneering project was defined from the perspective of knowledge and technology in the Makran region. This innovative endeavor, which sits at the intersection of cloud computing, machine learning, artificial intelligence, and remote sensing, marks a significant leap in the ability to understand and map a geologically complex area. The Makran region, part of the Sistan and Baluchestan province, presents a geological collection with diverse trends and geological periods. This area, shaped by the ongoing collision of the Arabian and Eurasian plates, includes a diverse array of geological formations, ranging from ophiolite sequences and turbidite basins to Quaternary sediments. While this complexity offers a treasure trove for geological study, it has long posed significant challenges to traditional mapping methods.

With the advent of cloud computing, big data analysis, and the rapid development of cloud infrastructures, a new era of distributed data processing has begun. The rise and development of cloud computing in spatial science fields, such as the *Google Earth Engine* processing system, have revolutionized the accessibility, processing, and analysis of remote sensing data. This case study represented an ambitious project aimed at demonstrating the power of *Google Earth Engine* in object-based image processing and machine learning techniques. The goal of this project was to create a unified, high-precision geological map of the Makran region, capturing the intricate details of the region's geological landscape.

GeoNexus

1.3 Objectives

The objective of this project is to prepare an integrated geological map using cloud computing and machine learning for an area covered by the four 1:100,000 geological sheets of Chabahar, Pir Soharab, Konarak, and Kahir (Figure 1-1). This will be achieved by utilizing various and diverse remote sensing images—including Sentinel-1, Sentinel-2, Landsat 8 (OLI), ASTER emissivity images—and digital elevation data (DEM, Aspect, Slope, and Hillshade) within a cloud environment and cloud computing platforms.

In this plan, a completely different approach will be adopted: instead of using one or two images, an attempt will be made to utilize a diverse archive of existing images as mentioned above. Additionally, thanks to the processing capabilities of supercomputers available on *Google Earth Engine* servers, all processing will be carried out in this cloud environment. Among other significant differences of this project compared to other mapping studies will be the use of various advanced image processing and data mining algorithms, such as mathematical transformations and machine learning on data and images, which largely eliminates errors resulting from traditional mapping methods.

To achieve these objectives, the project execution for preparing the geological map will be organized based on the following process:

1. Data gathering and literature review
    - Review of sources and previous studies: Collecting existing literature and previous research related to the project topic to build a solid foundational understanding.
    - Designing the process structure: Planning the execution framework of the project, including the identification of required data and images such as optical and radar satellite images, elevation data, and geomorphological information.
    - Preparation of geological maps: Collecting and preparing existing geological maps relevant to the study area.
    - Digitization and georeferencing: Digitizing and georeferencing structural maps and dating samples from previous sources and studies to ensure they are compatible with the project's data framework.
2. Preprocessing of data and images
    - Determining suitable image acquisition Times: Selecting images captured during optimal time intervals to ensure data quality and relevance.
    - Noise removal: Applying noise reduction techniques to optical and radar images as well as elevation data to enhance data clarity.
    - Image fusion methods: Using image fusion techniques to create composite images suitable for extracting geological structures and conducting an initial examination of geological units.
3. Data processing and extraction of desired indices

GeoNexus

- Spectral processing of Sentinel-2 data: Performing spectral analyses using methods like Principal Component Analysis (PCA), band ratios, and modeling to extract various geological indices.
- Processing of ASTER imagery: Analyzing VNIR, SWIR, and thermal images from the ASTER sensor to extract geological indices, emissivity data, and other relevant indicators.
- Processing of Sentinel-1 Radar Images: Processed VV and VH polarization radar images to generate Sum, Divide, and Product outputs, enhancing geomorphological and tectonic feature detection.
- Digital Elevation Data (DEM) analysis: Processing DEM data to extract geomorphological indices such as slope, sinusoidal features, aspect, and hillshade representations.

4. Image segmentation
    - Segmentation of high-resolution images: Conducting segmentation on high-resolution Sentinel-2 images to create initial homogeneous land units at the desired mapping scale.
5. Machine Learning Classification
    - Implementation of random forest algorithm: Executing the random forest machine learning algorithm on the segmented images using the extracted indices.
    - Utilization of geological unit information: Incorporating initial information about the geological units in the area to inform and refine the classification process.
6. Field investigations and sampling
    - Designing field routes: Planning field visits and sampling routes targeting specific points identified during the image analysis phase.
    - Collaboration with image processing experts: Working alongside experts to adjust maps and make necessary changes to the number and types of initial classes or indices used, based on field observations.
7. Reviewing sample analysis results and revising initial maps
    - Comprehensive map revision: Using the results from sample analyses and expert insights to thoroughly revise the initial geological maps.
    - Reclassification and extraction: Performing supervised reclassification to accurately determine and extract the number and types of rock units from the satellite images.

By following this structured approach, the project aims to revolutionize the way geological maps are prepared, leveraging advanced technologies and methodologies to enhance accuracy and efficiency.

GeoNexus

1.4 Data Sources and Accessibility

The thematic geological mapping of Makran has been conducted exclusively with unclassified, publicly available data. This approach ensures transparency and broad accessibility, making it a valuable resource for academic researchers, policymakers, and the general public interested in the geological characteristics of Makran. The reliance on freely available data also highlights the project's commitment to utilizing open-source information to foster a collaborative and inclusive research environment. This approach aligns with global scientific standards for data sharing and accessibility, ensuring that the findings and insights from this project contribute to the collective understanding of regional geology without the constraints of classified or proprietary data barriers.

In alignment with the project's objectives, previous geological maps used within this study undergo a meticulous process of georeferencing to ensure accuracy and reliability across various information layers. These maps, once processed, will be publicly accessible, contributing to the body of open-access resources available to the scientific and public community. This deliberate approach not only supports the study's comprehensive bibliographic compilation but also leverages digitized data and previously published reports. By doing so, the project enhances the robustness of its research framework and facilitates a deeper understanding of the geological intricacies of the Makran region.

The compilation of geological data for this project is grounded in the systematic use of both previous and current maps and reports. These data, essential for the thorough analysis and scope of our study, encompass various information layers, each tailored to specific aspects of the geological features under investigation. By integrating these layers, we achieve a multidimensional understanding of the geological and structural complexities of the area.

1.4.1 Unlocking Trapped Data

Geological maps provide invaluable insights into the surface conditions and composition of different regions. For this project, maps published by the Geological Survey of Iran serve as the primary sources. These maps have been meticulously georeferenced, ensuring precise alignment of the data, which enhances their utility in digital GIS platforms. The georeferencing process not only facilitates the overlay and integration with other spatial data but also improves the accuracy of our geological interpretations.

Each map is categorized by its distinct type—primarily Geological Quadrangle Maps—which detail the geological boundaries, fault lines, and lithographic characteristics of the study area. These maps are published at scales conducive to detailed analysis, typically at 1:250,000 for broad regional assessments and 1:100,000 for more focused, local studies. This scale diversity is critical, allowing us to tailor our investigations to the appropriate geographic extents and resolutions necessary for detailed field studies versus broader regional planning and analysis.

1.4.2 Contribution to the Bibliography and Digital Resources

The digitized data from these maps significantly contribute to our project's bibliography, providing a foundation upon which further studies and reports are built. The conversion of these analog maps

GeoNexus

into digital formats makes them accessible for modern geospatial analyses, and remote sensing integration. Table 1-1 lists the maps used in this project, illustrating the range and depth of the resources employed.

Table 1-1. List of the maps used in the project.

Publisher	Date	Map Type	No.	Title	Scale	Unlocking Data
Geological Survey of Iran	1983	Geological Quadrangle Map of Iran	M14	Pishin	1:250,000	Map
Geological Survey of Iran	1983	Geological Quadrangle Map of Iran	M13	Saravan	1:250,000	Map
Geological Survey of Iran	1983	Geological Quadrangle Map of Iran	K14	Fannuj	1:250,000	Map
Geological Survey of Iran	1989	Geological Quadrangle Map of Iran	L14	Nikshahr	1:250,000	Map
Geological Survey of Iran	1994	Geological Quadrangle Map of Iran	8041	Kahir	1:100,000	Fold, Fault, Legend, etc.
Geological Survey of Iran	1995	Geological Quadrangle Map of Iran	8042	Nik Shahr	1:100,000	Map
Geological Survey of Iran	1996	Geological Quadrangle Map of Iran	8140	Chabahar	1:100,000	Fold, Fault, Legend, etc.
Geological Survey of Iran	2004	Geological Quadrangle Map of Iran	8142	Qasr-e-Qand	1:100,000	Map
Geological Survey of Iran	2004	Geological Quadrangle Map of Iran	8141	Pirsohrab	1:100,000	Fold, Fault, Legend, etc.

Each map entry includes crucial details such as the type of map, publication date, scale, and specific features highlighted (e.g., folds, faults), underscoring the rich geological diversity and complexity of the regions studied. This detailed cataloging ensures that all data sources are accurately attributed and readily available for review and further research, adhering to scientific rigor and integrity in the documentation.

By leveraging these comprehensive and meticulously prepared sources, our project stands on a robust platform of verified data, enhancing both the credibility and reliability of our geological assessments.

1.5 Study Area and Area of Interest (AOI)

The goal of this project was to prepare a geological map for an area covered by the four 1:100,000 geological sheets of Chabahar, Pir Soharab, Konarak, and Kahir (Figure 1-1). An additional buffer zone of approximately 13 to 28 km was defined around the AOI (Figure 1-2). This buffer was included for two reasons:

1. Better analysis and interpretation: to analyze and interpret geological trends that sometimes extend beyond the boundaries of the sheets.
2. Integrated mapping: to prepare unified maps of the rock units within these sheets and their surrounding areas.

GeoNexus

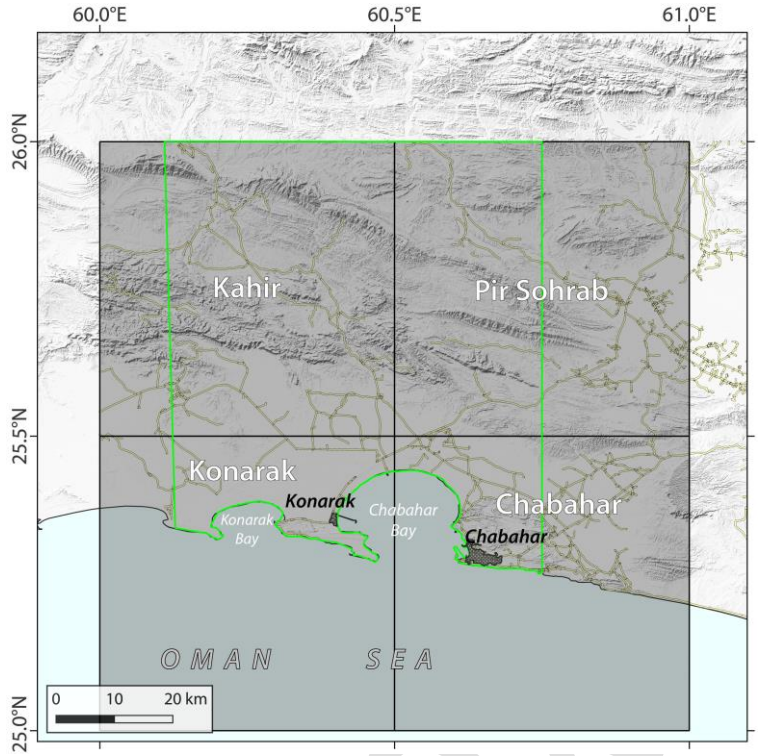


Figure 1-1. The Area of Interest (AOI) for the Server-based Unified Thematic Geological Mapping of the Makran (SUTGMM) highlighted with a green polygon. Dark shaded rectangles indicate the four 1:100,000 geological sheets of Kahir, Pir Sohrab, Konarak and Chabahar.

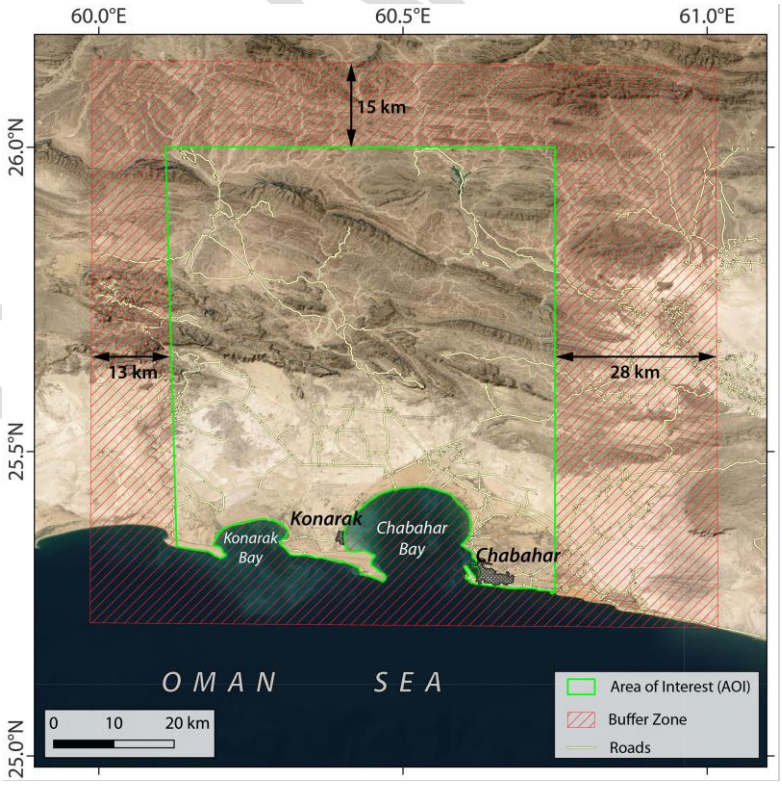


Figure 1-2. Study area encompassing the area of interest (AOI) and the additional buffer zone.

GeoNexus

2 Geological and Tectonic Setting

The tectonic setting of the Makran region has significant implications for understanding the broader geodynamic evolution of the Middle East and the closure of the Neo-Tethys Ocean. The northward subduction of the Arabian Plate beneath Eurasia contrasts with the continental collision in the Zagros Mountains to the west, highlighting the complex tectonic interactions along the plate boundary (Burg, 2018). The presence of Cretaceous and Quaternary volcanic arcs indicates a long history of subduction-related magmatism. The eroded or subducted remnants of older arcs provide insights into the tectonic evolution and fragmentation of the upper plate (Arthurton et al., 1982; Burg, 2018).

The recognition of Jurassic rift-related magmatism and Cretaceous arc magmatism suggests that the Central Iran block underwent significant fragmentation prior to the main collisional events, affecting reconstructions of the orogenic belt (Burg, 2018). The tectonic history of the Makran region can be correlated with that of the Oman Mountains on the subducting Arabian Plate, providing a more comprehensive understanding of regional tectonics (Burg, 2018).

The Makran region exemplifies a complex and evolving tectonic setting (Figure 2-1) shaped by the interplay of subduction, accretion, seismicity, uplift, and sedimentation. The shallow subduction of the Arabian Plate beneath Eurasia has led to the development of one of the world's largest accretionary wedges, characterized by significant sediment accumulation, complex structural deformation, and varied seismic behavior. Understanding the tectonic setting of Makran is crucial for assessing seismic hazards, reconstructing regional geodynamic evolution, and exploring the interactions between tectonics and surface processes. Ongoing research and integration of geological, geophysical, and geomorphological data continue to enhance our knowledge of this dynamic region.

2.1 Tectonic Setting of Makran

The Makran region, located in southeastern Iran and southwestern Pakistan along the northern margin of the Gulf of Oman, is a geologically complex area characterized by an extensive accretionary wedge formed due to the northward subduction of the Arabian Plate beneath the Eurasian Plate (Figure 2-1 and Figure 2-2). This accretionary wedge, known as the Makran accretionary wedge, extends approximately 1,000 km along strike and is bounded by significant

fault systems to the east and west (Arthurton et al., 1982; McCall, 1985; Dolati, 2010; Haghipour and Burg, 2014; Gharibreza, 2016; Burg, 2018).

Geodetic measurements and tectonic reconstructions reveal that the Arabian Plate is actively converging with the Eurasian Plate at rates varying along the strike of the Makran subduction zone (Figure 2-2). Measurements between Muscat in Oman and Chabahar on the Iranian coast indicate a convergence rate of approximately 19 mm/yr (Vernant et al., 2004; Khorrami et al., 2019). This convergence is part of the larger-scale motion of the Arabian Plate as it moves northward, subducting beneath the Eurasian Plate along the Makran Trench (Figure 2-2).

Further geodetic data show that the present-day convergence rate between the Makran coast (e.g., Chabahar GPS station) and stable Eurasia is about 8 mm/yr (Vernant et al., 2004). However, other studies suggest that the convergence rates increase eastward, reaching up to 35.5–42 mm/yr in eastern Makran due to the anticlockwise rotation of the Arabian Plate relative to Eurasia (DeMets et al., 2010; Hatzfeld and Molnar, 2010; Burg, 2018).

The variation in convergence rates along the subduction zone has significant implications for the tectonic evolution and seismicity of the region. The increasing convergence rates from west to east are consistent with the anticlockwise rotation of the Arabian Plate and are corroborated by seafloor spreading rates and fault azimuths for the major plates involved (DeMets et al., 2010).

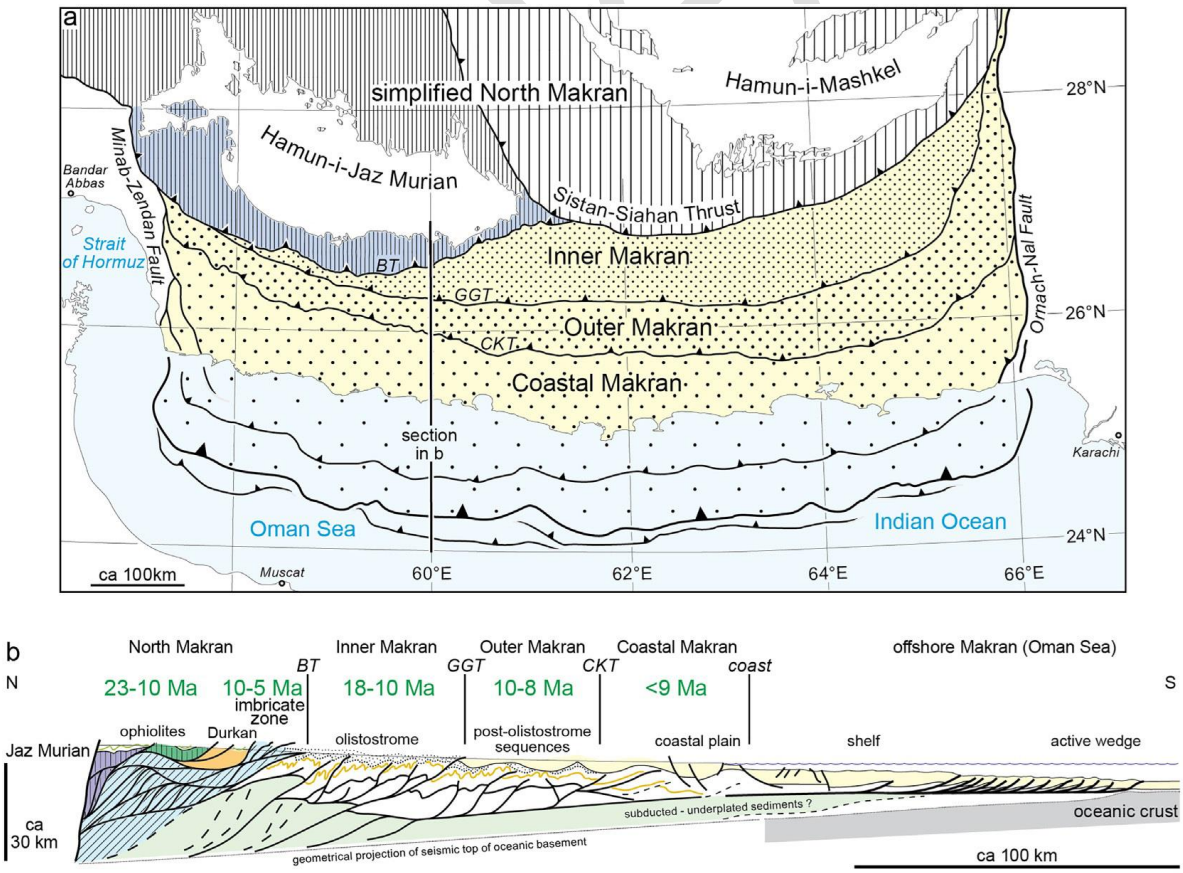


Figure 2-1. Tectonic setting of the Makran region, showing tectonostratigraphic zones and major structures, including the accretionary wedges and pull-apart basins (Haghipour and Burg, 2014; Burg, 2018).

The Makran accretionary wedge is bounded by two major fault systems that play crucial roles in its tectonic configuration (Figure 2-1 and Figure 2-2). To the west lies the dextral (right-lateral) Minab–Zendan Fault System. Specifically, the Minab Fault separates the Makran subduction zone from the Zagros continent–continent collision zone (Stöcklin, 1968; Bird et al., 1975; Dolati, 2010; Haghipour and Burg, 2014). This fault system accommodates the differential motion between the converging plates and acts as a structural boundary between distinct tectonic regimes.

To the east, the sinistral (left-lateral) Chaman–Ornach–Nal Fault System and its offshore continuation, the Owen Fracture Zone, separate Makran and the Arabian Plate from the Indian subcontinent (Figure 2-2). The Indian Plate moves northward at a rate of 40–50 mm/yr relative to Eurasia, significantly faster than the convergence rate along the Makran subduction zone (Paul et al., 2001; Molnar and Stock, 2009; Dolati, 2010; Haghipour and Burg, 2014; Burg, 2018).

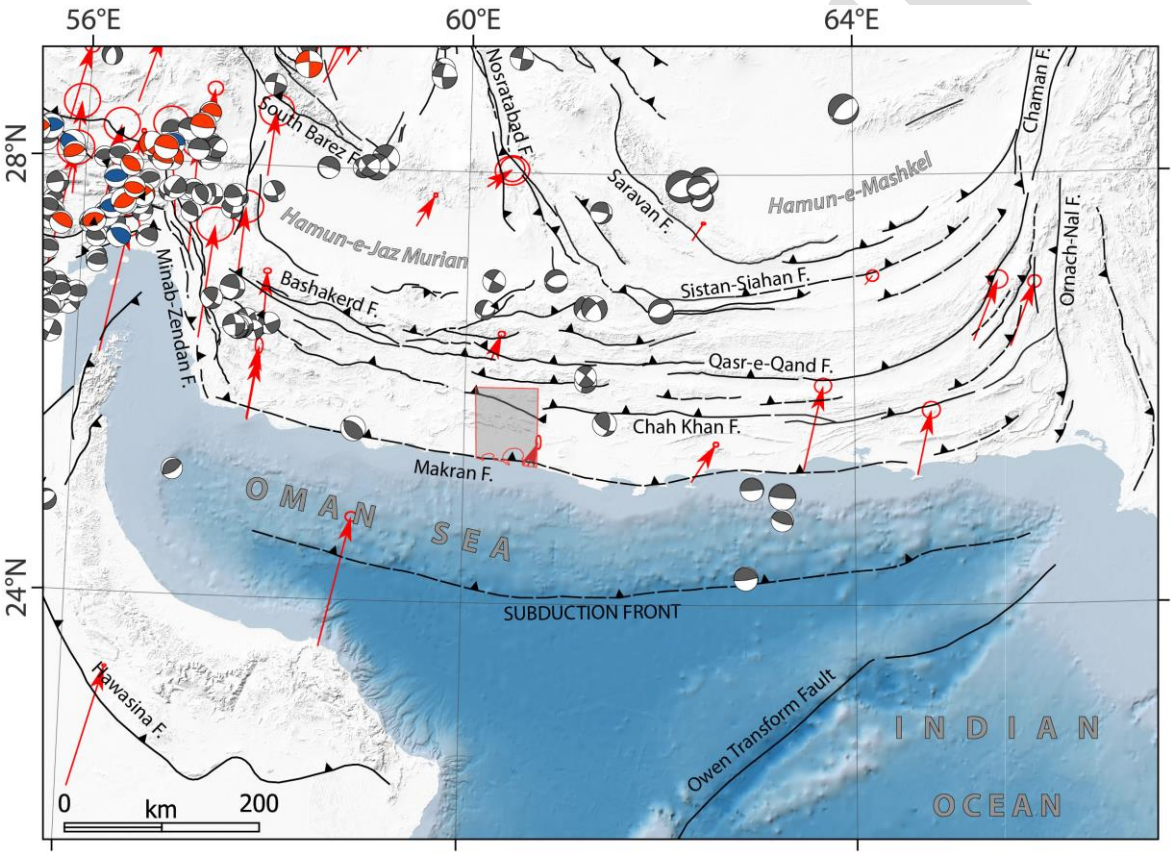


Figure 2-2. Seismotectonic configuration of Makran and surrounding areas. The subduction front in the Oman Sea marks the convergence between the Arabian and Eurasian plates. Fault traces are compiled and modified after Fathian (2022). Red shaded polygon mark the AOI. Grey, red, and blue beachballs represent fault plane solutions from the the Global Centroid Moment Tensor (GCMT; https://www.globalcmt.org), body waveform, and the first motions catalogs (see Fathian, 2022 and the references therein). Red arrows represent GPS velocity vectors relative to a stable Eurasian plate (Khorrami et al., 2019). Background is the shaded relief from SRTM 90m (Farr et al., 2007) and GEBCO Global Bathymetry 15 arc-sec (GEBCO Compilation Group, 2023) visualizing surface topography and bathymetry.

Within the Makran region, the structural configuration is further complicated by several parallel accretionary wedges and pull-apart basins (e.g., Haghipour and Burg, 2014; Gharibreza, 2016). The

Coastal Makran forms the onshore part of the accretionary wedge, comprising deformed Cenozoic terrigenous and mud sediments (Figure 2-1). Seaward of the Coastal Makran lies the Outer Makran, characterized by active sediment accretion and deformation. Further inland, the Inner Makran and North Makran represent more distal parts of the accretionary wedge, with complex sedimentary and structural histories (Figure 2-1b). Inner Makran consists of a thick sequence of upper Eocene to lower Miocene turbidites showing a general thickening- and coarsening-upward trend (e.g., Dolati, 2010; Haghipour and Burg, 2014). North Makran comprises tectonically imbricated upper Cretaceous to Eocene igneous rocks, ophiolites, and associated deep marine sediments (McCall, 1983; Haghipour and Burg, 2014). Additionally, Hamun-e-Jaz Murian and Hamun-e-Mashkel (Figure 2-2) are significant depressions (pull-apart basins) interpreted as forearc basins (Farhoudi and Karig, 1977; Dolati, 2010; Haghipour and Burg, 2014).

The northern boundary of the Makran is delimited by the Quaternary cover of the Jaz Murian depression in Iran and the equivalent Mashkel depression in Pakistan (Burg, 2018). These structural features contribute to the complex tectonic setting and influence sedimentation patterns, seismicity, and surface deformation.

2.1.1 Subduction Characteristics and Volcanic Arcs

The subduction of the oceanic lithosphere of the Arabian Plate beneath the Iranian Lut Block and the Afghan/Helmand Block (Figure 2-3) has been ongoing since the late Cretaceous (Stoneley, 1974; Jacob et al., 1979; McCall and Kidd, 1982; Arthurton et al., 1982; Berberian et al., 1982; Dercourt et al., 1986; Burg, 2018). The initiation of subduction is evidenced by the age of the Makran volcanic arcs, such as Bazman in Iran and the Chagai Hills in Pakistan (Figure 2-3), which date back to the late Cretaceous (Arthurton et al., 1982; Berberian et al., 1982).

The Quaternary Baluchistan volcanic arc, extending from north of the Chagai Hills at the Pakistan–Afghanistan border into southeastern Iran, is associated with the ongoing subduction along the Makran zone (Jacob et al., 1979; Berberian et al., 1982; Dolati, 2010). This volcanic arc comprises three major volcanic centers: Bazman, Taftan, and Koh-i-Sultan. Bazman and Taftan are significant volcanic centers located in southeastern Iran, contributing to the volcanic activity along the arc. Koh-i-Sultan, situated near the Pakistan–Afghanistan border, completes the approximately 300-km-long belt of volcanic centers (Jacob et al., 1979; Berberian et al., 1982). The presence of these volcanic centers indicates active magmatism associated with the subduction process.

A notable feature of the Makran subduction zone is the relatively large gap of 400–600 km between the trench and the volcanic arc. This unusually wide accretionary wedge suggests that the subducting plate dips at a very shallow angle of about 1–2 degrees to the north (e.g., Dolati, 2010). This shallow subduction angle is supported by several lines of evidence. Seismic reflection and refraction studies indicate a gently dipping subducting slab beneath the Makran region (e.g., White and Klitgord, 1976; White and Louden, 1982). Analyses of earthquake hypocenters and focal mechanisms show that seismicity is concentrated at shallow depths, consistent with a shallow subduction angle (Figure 2-3b, c) (Jacob et al., 1979; Byrne et al., 1992; Engdahl et al., 2006; Alinaghi et al., 2007). Additionally, tomographic imaging reveals a shallow slab beneath the Eurasian continent (Figure 2-4), further confirming the low-angle subduction (Bijwaard et al., 1998; Hafkenscheid et al., 2006). The shallow subduction geometry has significant implications for the tectonic evolution, sediment accretion, and seismic behavior of the Makran region.

GeoNexus

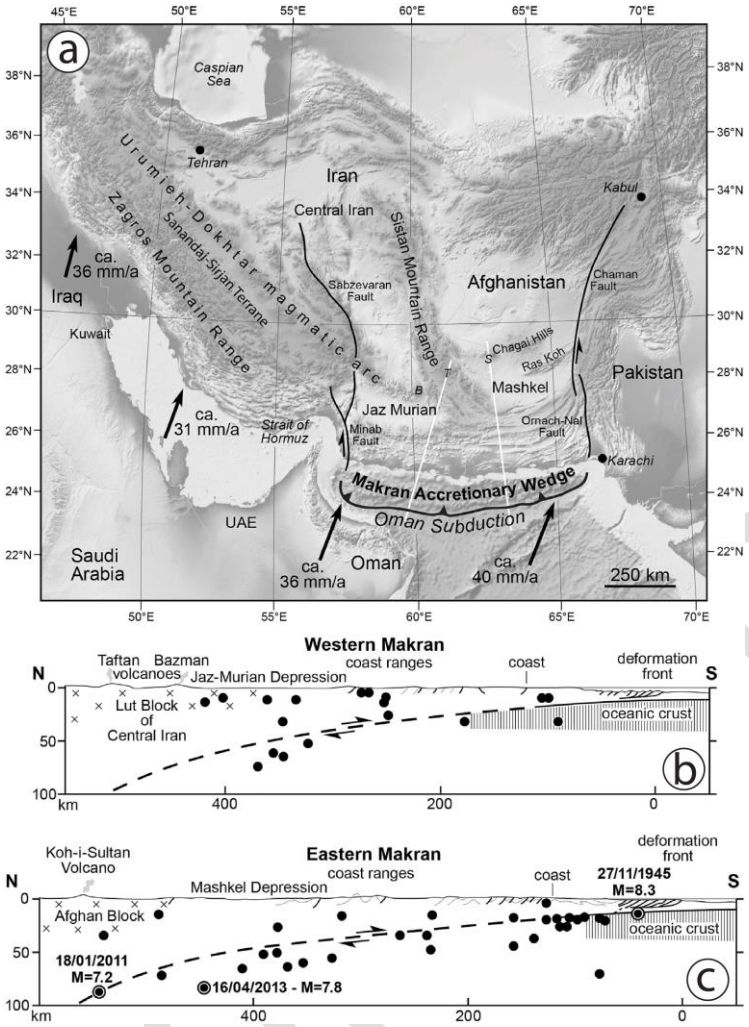


Figure 2-3. a) Regional overview of the Makran accretionary wedge and surrounding tectonic features (Burg, 2018). Italic B, T, and S represent the Bazman, Taftan, and Koh-i-Sultan volcanoes, respectively. White lines represent the locations of cross-sections shown in panels b and c. b, c) Lithospheric-scale cross-sections across the Western (b) and Eastern (c) Makran. These cross sections illustrate the primary geological structures and seismicity, with solid black circles representing focal mechanisms for seismic events, modified after Byrne et al. (1992) and updated with magnitude M4 events up to the present (Burg, 2018).

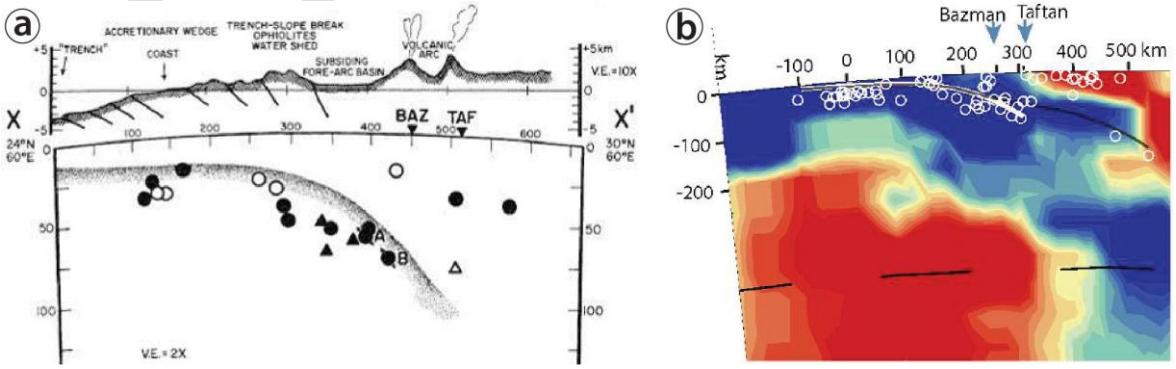


Figure 2-4. a) N–S section across Western Makran (60°E) showing the subduction of the Arabian plate beneath the Eurasian plate, with seismic events projected along the profile, highlighting the steepening subduction slope beneath the Jaz Murian depression (Jacob et al., 1979). b) Seismic tomography (Hafkenscheid et al., 2006) and earthquakes with the subducting slab beneath the Makran region (Dolati, 2010).

2.1.2 Accretionary Wedge

The Makran accretionary wedge is one of the largest in the world, characterized by significant sediment supply from the Indus and other river systems, as well as the shallow subduction angle. It is approximately 300–350 km wide from the submarine deformation front to the Hamun-e-Jaz Murian and Hamun-e-Mashkel depressions (Haghipour and Burg, 2014). The wedge is divided into two main parts. The active submarine wedge, a 100–150-km-wide zone located offshore, is where active sediment accretion and deformation occur as sediments are scraped off the subducting plate and added to the wedge (Burg, 2018). The onshore wedge, a 150–200-km-wide zone on land, comprises deformed sediments that have been uplifted and exposed due to ongoing tectonic processes. These two parts are separated by a narrow coastal belt, only a few km wide, characterized by prominent normal faults and mud volcanoes both onshore and offshore (Von Rad et al., 2000; Back and Morley, 2016; Burg, 2018). This coastal belt represents the transition zone between the active submarine accretion and the uplifted onshore wedge.

Wide-angle seismic lines indicate that the oceanic crust south of the trench has a thickness of approximately 9 km and is overlain by more than 7,000 m of undeformed sediments at the front of the wedge (Figure 2-5) (White and Louden, 1982; Harms et al., 1984; Kopp et al., 2000; Dolati, 2010). The combined thickness of deformed and undeformed sediments reaches over 10 km near the coastline, reflecting significant sediment accumulation due to high sedimentation rates and tectonic convergence (White and Louden, 1982; Harms et al., 1984; Kopp et al., 2000). Interpretations of seismic data place a décollement (detachment) at a depth of approximately 3–4 km (Figure 2-5) near the deformation front (Kopp et al., 2000). Above the décollement, sediments are intensely folded and thrust, contributing to the growth and deformation of the accretionary wedge (Figure 2-6) (White and Klitgord, 1976; Harms et al., 1984; Grando and McClay, 2007; Ellouz-Zimmermann et al., 2007). Sediments below the décollement continue to subduct with the oceanic crust, a process known as underplating (e.g., Platt et al., 1985), which contributes to crustal thickening and may play a role in uplift and exhumation processes (Figure 2-6).

The main accretion phase of the emerged wedge produced growth structures dating from the late Miocene to early Pliocene (Dolati, 2010). Since the late Pliocene, the coastal Makran and mid-slope areas have experienced surface uplift, normal faulting, shale extrusion, and shortening (Harms et al., 1984; Grando and McClay, 2007; Dolati, 2010). These processes contribute to the complex structural architecture of the Makran accretionary wedge and influence seismicity, sedimentation, and surface processes.

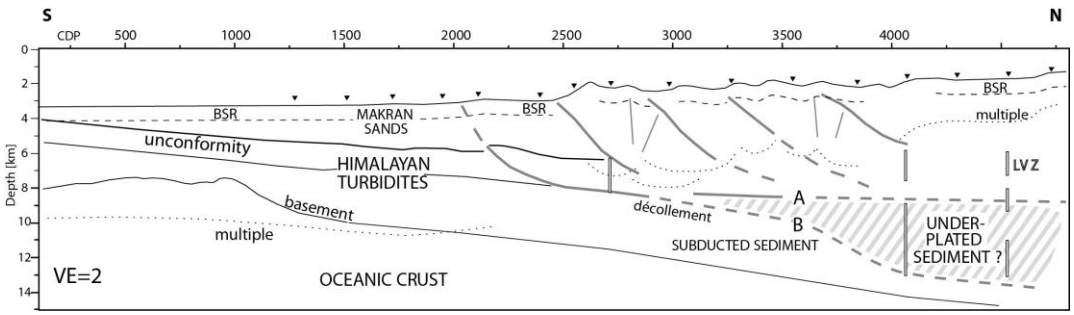


Figure 2-5. The structure of the Makran accretionary wedge, illustrating underplated sediments beneath a gently dipping décollement (Kopp et al., 2000).

GeoNexus

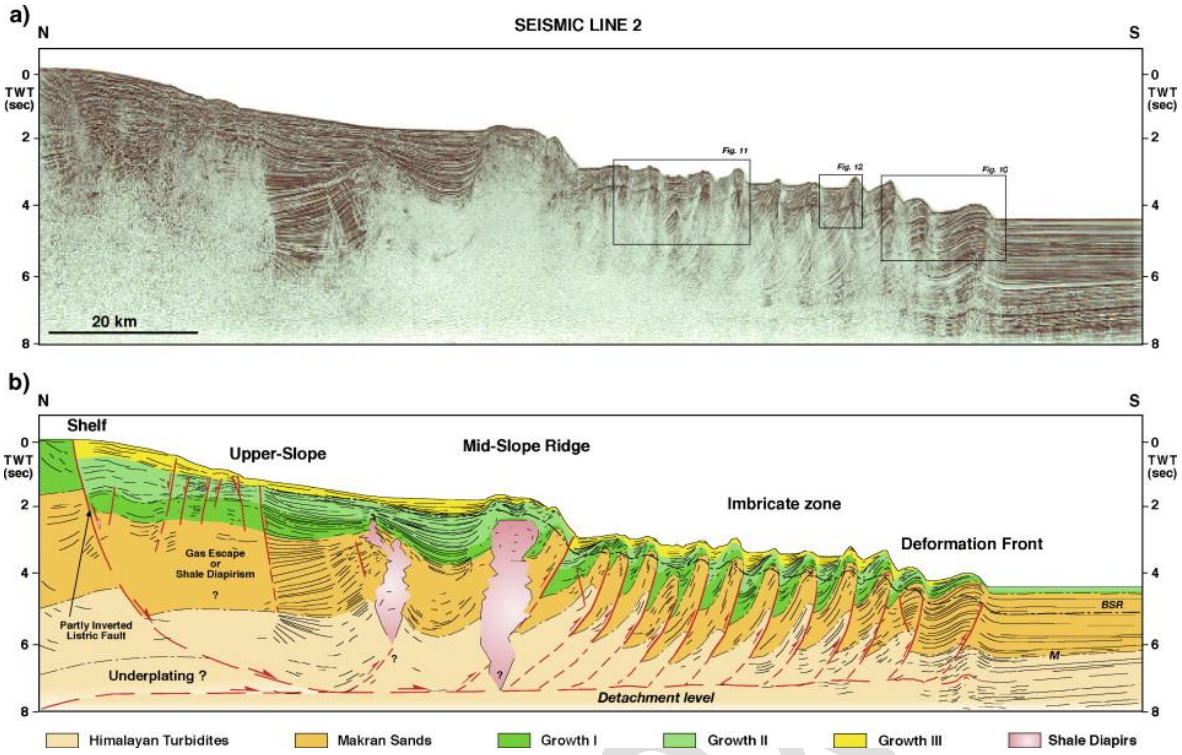


Figure 2-6. Seismic profile (a) and the interpretation (b) across the western offshore Makran accretionary prism, showing the shelf, slope basins, and accretionary prism. The M unconformity separates Himalayan turbidites from Makran Sands. The interpretation highlights growth strata, shale diapirs, the imbricate zone, and the deformation front, with potential underplating and a detachment level identified (Grando and McClay, 2007).

2.1.3 Accretionary Wedge Stratigraphy

The sedimentary architecture of the Makran region is intricately structured within the accretionary wedge and is categorized into four distinct zones (Figure 2-1) from south to north: Coastal Makran, Outer Makran, Inner Makran, and North Makran (e.g., Dolati, 2010; Haghipour and Burg, 2014; Burg, 2018). Each zone exhibits unique sedimentary and igneous characteristics that reflect the evolutionary stages of the accretionary processes in the region (Figure 2-7).

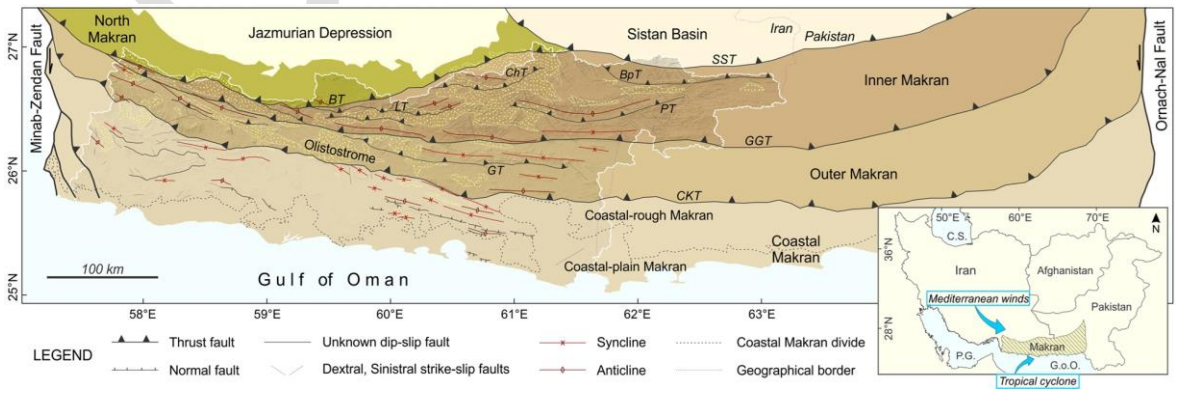


Figure 2-7. Tectonostratigraphic zones of the Makran accretionary wedge (Kaveh-Firouz et al., 2023). BT: Bashakerd thrust fault, SST: Sistan-Siahan Thrust, BpT: Bamposht thrust fault, ChT: Chanf thrust fault, LT: Lashar thrust fault, PT: Pishamak thrust fault, GGT: Qasr-e-Qand thrust fault, GT: Gativan thrust fault, and CKT: Chah Khan thrust fault.

1. Coastal Makran:

To the south of the Outer Makran lies the Coastal Makran zone (Figure 2-7), which represents a wedge-top basin setting. This area showcases a shallowing-upward sequence transitioning from late Miocene slope marls to Pleistocene coastal and continental deposits. The Coastal Makran records the transition from marine to terrestrial environments, influenced by both tectonic uplift and sea-level fluctuations. This province captures the final stages of sedimentary deposition within the accretionary wedge, highlighting the interplay between sediment supply and tectonic forces (Dolati, 2010; Haghipour and Burg, 2014).

2. Outer Makran:

Located between the Qasr-e-Qand and Chah Khan thrust faults (Figure 2-7), the Outer Makran zone comprises lower to middle Miocene siltstones and marls, which include calcareous sandstones that grade up-section into shallower facies indicative of a shelf environment. These sediments include Burdigalian-age deposits and shallow-water carbonate facies that transition upward, indicating a progression towards shallower marine environments. The Outer Makran records a significant phase of sedimentation that reflects changes in sea level and tectonic uplift, contributing to the complex stratigraphic layering observed in this province (Dolati, 2010; Haghipour and Burg, 2014).

3. Inner Makran:

Situated north of the Qasr-e-Qand fault (Figure 2-7), the Inner Makran zone exposes a thick sequence of upper Eocene to lower Miocene terrigenous sandstone and shale sequences, characteristic of "flysch"-type deposits. These sediments are interpreted as part of a proto-Indus fan system, which records the ongoing Himalayan orogeny and the associated sedimentary influx (Kopp et al., 2000; Ellouz-Zimmermann et al., 2007). Syn-sedimentary deformation is evident in this region, marked by growth structures and an upward shallowing trend in sedimentary facies (Dolati, 2010), which reflect active tectonic loading and sedimentation dynamics during deposition.

4. North Makran:

Located to the north of Bashakerd thrust fault (Figure 2-7), the North Makran zone is predominantly characterized by mafic to intermediate igneous rocks. This area features tectonic mélanges, which are complex mixtures of igneous rocks and deep-water sediments, indicative of intense tectonic activity. The sedimentary record here includes Cretaceous deep-water sediments, providing insights into the region's ancient marine environments. Additionally, there are localized occurrences of upper Cretaceous shallow-water limestones. Along the Jaz Murian depression, Paleogene limestones are found unconformably overlying deformed Cretaceous sediments and igneous rocks, illustrating periods of uplift and erosion. Near Espakeh, Eocene sandstone formations are present, adding to the sedimentary diversity of this province (Dolati, 2010; Haghipour and Burg, 2014; Burg, 2018).

An extensive Tortonian olistostrome, dated between 7 and 11 million years ago, plays a significant role in the sedimentary history of the Makran region. This olistostrome comprises giant blocks of both igneous and sedimentary rocks sourced from the North Makran and Inner Makran provinces. Emplaced predominantly over much of the North and Inner Makran areas, the olistostrome was later subjected to partial erosion, shaping the current geological landscape (Burg et al., 2008;

GeoNexus

Haghipour and Burg, 2014). The presence of this large-scale mass transport deposit underscores the dynamic tectonic environment and the processes of sedimentary deformation that have been active in the Makran accretionary wedge.

2.1.4 Uplift along the Coast

The Coastal Makran (Figure 2-8) is an active morphodynamic zone influenced by a combination of tectonic uplift, eustatic sea-level changes, sediment supply, and coastal processes (Gharibreza, 2016). The coastline features multiple marine terraces and raised beaches, indicating phases of uplift and relative sea-level change (Vita-Finzi, 1979, 1987; Gharibreza, 2016). Studies have identified up to 19 marine terraces between the present sea level and elevations of 246 m near Chabahar (Vita-Finzi, 1979). The mean uplift rate along the Iranian coastline is estimated at 1.1–2.6 mm/yr since the mid-Holocene (approximately 6 ka), when sea levels were 2–3 m higher than present (Falcon, 1974; Lambeck, 1996; Gharibreza, 2016).

Radiocarbon dating (^{14}C) of shells and corals from marine terraces provides chronological constraints on uplift and sea-level changes (Vita-Finzi, 1979, 1987; Snead, 1993). For example, shells at 4 m above sea level near Chabahar were dated to 3,670 ± 50 years before present (BP), while higher elevations yielded ages between 28 and 30 kaBP (Vita-Finzi, 1979). The morphology of the coastline (Figure 2-8), including omega-shaped bays and curved bays, reflects the interplay between tectonic uplift, sediment dynamics, and sea-level fluctuations (Gharibreza, 2016). Paleoshorelines serve as indicators of past sea levels and sedimentary environments.

The coastal plain exhibits evidence of progradation due to high sediment supply from rivers and coastal erosion of uplifted terraces. This results in the formation of beach ridges, cheniers, and other coastal landforms. The sorting of sediments along the littoral drift leads to the accumulation of sand and shell-rich ridges, influencing the development of paleoshorelines and the coastal sedimentary record (e.g., Gharibreza, 2016). Eustatic sea-level fluctuations during the late Quaternary, combined with tectonic uplift, have shaped the coastal geomorphology and sedimentation patterns (Lambeck, 1996; Gharibreza, 2016).

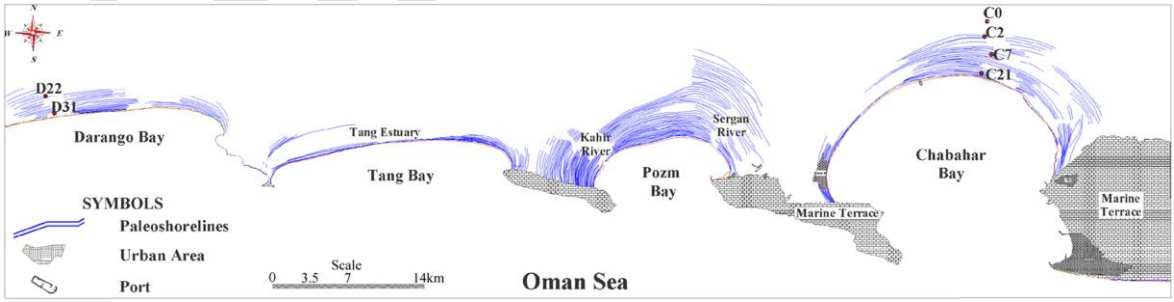


Figure 2-8. Morphological setting of the Coastal Makran, showing paleoshorelines along the Chabahar, Pozm, Tang and Darango bays (Gharibreza, 2016).

2.2 Structural Features of Makran

The Makran accretionary wedge exhibits a complex structural framework resulting from the ongoing northward subduction of the Arabian Plate beneath the Eurasian Plate (e.g., Dolati, 2010). The deformation within the Makran accretionary wedge is manifested through various structural features, predominantly folds and faults, which reflect the intricate interplay of tectonic processes. This section provides an in-depth analysis of these structural features, focusing on their types, distributions, orientations, and the tectonic processes shaping the region.

2.2.1 Folds

Folding is a significant deformation feature within the Makran accretionary wedge, arising from compressional forces associated with subduction and accretion processes (Jacob et al., 1979; McCall and Kidd, 1982; Berberian et al., 1982). The folds exhibit considerable variation in style, scale, and intensity across different structural units, reflecting the heterogeneity of lithologies, and the differences in structural levels, and the evolution of the tectonic regime (Dolati, 2010).

2.2.1.1 Types and Styles of Folds

In the northern parts of the Makran accretionary wedge, particularly within the Inner Makran, folding is intense, characterized by tight to isoclinal folds prevalent in the upper Oligocene turbidites of the Pishamak and Kajeh Thrust Sheets (Dolati, 2010). These folds exhibit steeply dipping to overturned limbs and have wavelengths ranging from centimeters to kilometers. The hinge zones often display well-developed axial plane cleavage, indicative of high strain (Alvarez et al., 1978; Powell, 1979). For instance, in the sandstone-dominated Pirdan Unit of the Pishamak Thrust Sheet, chevron folds are common due to the alternation of competent sandstone layers and weaker shales (Dolati, 2010).

Conversely, in the Coastal Makran and Outer Makran zones, folds are generally open to gentle, with large wavelengths often exceeding 1,000 m and low amplitudes (Harms et al., 1984). These folds are typically symmetric, with rounded to blunt hinge zones, and lack significant axial plane cleavage, suggesting weaker deformation. In the Gativan Thrust Sheet, large box folds with wavelengths greater than 4 km are observed, particularly in lower Miocene sequences (Dolati, 2010).

The Imbricate Zone, located between the Bashakerd Thrust Sheet and the Inner Makran, also exhibits folding but to a lesser degree. Here, open and rounded folds with wavelengths over 100 meters are present, reflecting moderate deformation. These folds have a general east-west trend, consistent with regional tectonic forces, and the axial planes are often weakly developed (Dolati, 2010).

2.2.1.2 Orientation and Distribution

Fold axes within the Makran accretionary wedge generally trend east-west, aligning with the regional tectonic stress field resulting from north-south compression due to subduction (Harms et al., 1984; Dolati, 2010). Measurements indicate that fold axes plunge shallowly to steeply in either direction and can be traced over several km, demonstrating significant structural continuity. In

GeoNexus

some areas, such as within the Lashar, Chanf, and Bamposht Thrust Sheets, fold axes trend northwest-southeast due to local stress variations (Dolati, 2010).

The intensity of axial plane cleavage varies with deformation. In regions with tight folding, such as the Inner Makran, the cleavage is well-developed and indicates significant compressional strain. For example, in the upper Oligocene turbidites, the cleavage is disjunctive and spaced, with domain spacing between 4 to 10 mm, reflecting strong deformation (e.g., Alvarez et al., 1978). In contrast, areas with open folds, like the Coastal Makran, exhibit weak or absent axial plane cleavage due to lower strain levels (Dolati, 2010).

2.2.1.3 Mechanisms and Implications

Flexural slip folding is a dominant mechanism in the Makran accretionary wedge, particularly evident in the competent layers of sandstone where bedding-parallel slip surfaces are common (Ramsay and Huber, 1987). This is supported by the presence of opposed senses of movement on successive fold limbs, indicative of layer-parallel shearing during folding. In the Pishamak Thrust Sheet, the occurrence of boudinaged layers and calcite fibers aligning nearly orthogonal to fold axes further substantiates the flexural slip mechanism (Dolati, 2010).

Fault-propagation folding is also significant, especially in the vicinity of major thrust faults. Asymmetric folds with steep to overturned forelimbs truncated by thrust faults suggest that folding occurred ahead of advancing thrust sheets (e.g., Ramsay and Huber, 1987). For instance, near the Lashar thrust, fault-propagation folds are observed in the hanging wall, where south-vergent folds with steep forelimbs are cut off by ramp faults (Dolati, 2010).

Detachment folding plays a role in the development of large-scale open folds in the Outer Makran and Coastal Makran. The presence of thick shale sequences, such as the upper Oligocene and middle Miocene shales, provides potential detachment horizons that facilitate the formation of broad, gentle folds with large wavelengths (Jamison, 1987; Sepehr et al., 2006; Dolati, 2010). In the Gativan Thrust Sheet, box folds are associated with deeper décollements within these shale units, suggesting a detachment folding mechanism (Dolati, 2010).

The variation in folding styles across the Makran accretionary wedge reflects a deformation gradient, with higher strain and tighter folds in the north, transitioning to lower strain and more open folds towards the south. This gradient corresponds to the position within the accretionary wedge, with the Inner Makran experiencing greater compressional forces due to its proximity to the main subduction zone (Platt et al., 1985; Dolati, 2010).

2.2.2 Faults

Faulting is a critical component of the structural framework of the Makran accretionary wedge, accommodating deformation through thrusting, normal faulting, and strike-slip movements. The intricate fault networks contribute to the complex tectonic evolution of the region.

GeoNexus

2.2.2.1 Thrust Faults

Thrust faulting is the primary mechanism for accommodating convergence within the Makran accretionary wedge, resulting in the stacking of thrust sheets and the development of the accretionary wedge (Jacob et al., 1979; McCall and Kidd, 1982; Harms et al., 1984; Dolati, 2010).

2.2.2.1.1 Bashakerd Thrust and Thrust Sheet

The Bashakerd Thrust marks the northern boundary of the Makran accretionary wedge, placing Cretaceous rocks onto Eocene turbidites of the Lashar Thrust Sheet (Dolati, 2010). The thrust zone exhibits a significant thickness (500–700 m) with intense shearing and the incorporation of marble blocks, indicating high strain levels (Dolati, 2010). The sheared matrix includes dark grey volcaniclastic sandstones and red shales, with blocks of white marble likely derived from the overlying Dur Kan Unit (Dolati, 2010).

Fault planes within the Bashakerd Thrust Zone form an anastomosing network, with both north-dipping and south-dipping reverse faults enveloping tectonic slices and blocks (Dolati, 2010). Measurements indicate that the main fault planes are north- to northeast-dipping reverse faults associated with shallow south-dipping faults, collectively indicating top-to-south movement consistent with regional thrusting directions (Dolati, 2010).

2.2.2.1.2 Lashar, Chanf, and Bamposht Thrusts and Thrust Sheets

These thrusts emplace Eocene to Oligocene turbidites over younger sequences. The Lashar Thrust is particularly well-exposed south of Tang Sarheh, where lower Eocene volcanic rocks are thrust over Oligocene turbidites and the Tortonian olistostrome (Dolati, 2010). The presence of flat and ramp fault systems, fault-propagation folds, and reverse faults with top-to-south movement directions indicate active thrusting and significant deformation (Dolati, 2010).

Measurements of fault planes and slicken lines in the Lashar Thrust Zone reveal northeast-dipping reverse faults, consistent with southeastward to southwestward thrusting (Dolati, 2010). South-vergent asymmetric folds with steep to overturned forelimbs are cut off by ramp faults, suggesting fault-propagation folding.

2.2.2.1.3 Pishamak and Kajeh Thrusts and Thrust Sheets

These thrusts involve the upper Oligocene turbidites thrust over lower Miocene sequences. In the Pishamak Thrust Sheet, S-vergent, close to tight folds are prevalent, and the thrust fault displays north-dipping reverse faults indicating southward movement (Dolati, 2010). The Kajeh Thrust in the western area brings upper Oligocene turbidites onto the Tortonian olistostrome, with evidence of post-olistostrome reactivation (Dolati, 2010).

Fault data in the hanging wall of the Pishamak Thrust indicate north-dipping reverse faults and subvertical sinistral strike-slip faults, consistent with bulk north-south shortening (Dolati, 2010). In the footwall of the Kajeh Thrust, northwest-dipping reverse faults are predominant, with measurements suggesting top-to-south thrusting (Dolati, 2010).

GeoNexus

2.2.2.1.4 Qasr-e-Qand Thrust and Thrust Sheet

This major fault separates Inner and Outer Makran, characterized by thrusting of upper Oligocene turbidites onto lower Miocene marls (Dolati, 2010). Evidence of recent activity includes the thrusting of older rocks onto Holocene conglomerates and the presence of faulted and tilted river terraces (Dolati, 2010). Measurements of fault planes and slicken lines indicate north- to northeast-dipping reverse faults with movement of the hanging wall toward the south-southwest (Dolati, 2010).

2.2.2.1.5 Kahorkan Thrust and Thrust Sheet

In the western Inner Makran, the Kahorkan Thrust emplaces upper Oligocene turbidites over lower-middle Miocene sediments (Dolati, 2010). The thrust is associated with fault-propagation folding, where vertical to overturned forelimbs in the hanging wall are truncated by the thrust fault (Dolati, 2010). Fault data reveal north- to northeast-dipping and south-dipping reverse faults, with a general top-to-south movement (Dolati, 2010).

2.2.2.2 Flat and Ramp Systems

Thrust faults in the Makran accretionary wedge commonly display flat and ramp geometries, where thrust planes follow bedding planes (flats) and cut across layers (ramps) (McClay, 1992; Dolati, 2010). This geometry is evident in the Lashar Thrust Zone, where strata-parallel faults and ramp faults are observed, leading to the development of fault-propagation folds in the hanging wall (Dolati, 2010). These structures are indicative of thin-skinned tectonics prevalent in turbidite sequences.

2.2.2.3 Backthrusts

Backthrusts, or south-dipping reverse faults, are present in the northern parts of the Makran accretionary wedge, particularly in the Imbricate Zone. For example, to the north of Fannuj, the Bashakerd Thrust Sheet is thrust northwestward onto the Imbricate Zone along backthrusts (Dolati, 2010). These structures reflect complex stress regimes within the accretionary wedge and contribute to the intricate structural architecture (Dolati, 2010).

2.2.2.4 Normal Faults

Normal faulting in the Makran accretionary wedge is less extensive but plays a significant role in accommodating extensional stresses, particularly in the Coastal Makran. In the Coastal Makran, normal faults are widespread, cutting through sediments younger than upper Miocene (Dolati, 2010). These faults are typically planar and non-rotational, with displacements ranging from a few meters to several meters (Dolati, 2010). They are associated with extensional tectonics, possibly related to gravitational collapse or regional stress relaxation (Harms et al., 1984; Grando and McClay, 2007).

GeoNexus

Conjugate sets of normal faults are observed, indicating a complex extensional stress field. For instance, conjugate north-northeast- and south-southeast-dipping planes suggest sub-radial extension, while sediment-filled fissures and bookshelf faulting patterns indicate localized extensional regimes (Dolati, 2010).

The presence of normal faults in the Coastal Makran has implications for seismic hazards. Extensional structures can influence stress distribution and may contribute to seismic events (Khan et al., 1991; Dolati, 2010). The normal faulting observed in Pliocene–Pleistocene sediments suggests that extensional tectonics are relatively recent and possibly ongoing.

2.2.2.5 Strike-Slip Faults

Strike-slip faulting is a significant deformation mechanism within the Makran accretionary wedge, accommodating lateral movements and contributing to the complex tectonic fabric.

Two main sets of conjugate strike-slip faults are dominant (Dolati, 2010):

- Northeast–Southwest sinistral (left-lateral) faults: These faults are widespread across the Makran accretionary wedge and often offset major thrusts and folds, indicating a younger deformation phase. Displacements range from a few meters to over 2,000 m, and they significantly influence the topography and river patterns (Dolati, 2010).
- Northwest–Southeast dextral (right-lateral) faults: These faults are conjugate to the sinistral faults, and together they form a pattern consistent with bulk north-northeast–south-southwest compression (Dolati, 2010).

Strike-slip faults cut through Pliocene–Pleistocene sediments and are evident in satellite imagery due to their offsetting of resistant lithologies like sandstone (Dolati, 2010). The youngest strike-slip faults affect the topography and are considered active structures contributing to the ongoing deformation of the Makran accretionary wedge. Similar strike-slip faults have been recognized offshore Pakistan across the active front of the Makran (e.g., Kukowski et al., 2002).

The presence of active strike-slip faulting both onshore and offshore suggests that lateral movements are a significant component of deformation in the Makran accretionary wedge (Kukowski et al., 2002; Dolati, 2010). This has implications for seismic hazard assessments and tectonic models, as these faults can influence the stress distribution and potential for seismic events.

2.3 Structural Synthesis

The structural features of the Makran accretionary wedge result from the interplay of compressional, extensional, and translational tectonic processes associated with subduction and accretion (Byrne et al., 1992; Dolati, 2010).

2.3.1 Deformation Gradient

There is a discernible deformation gradient from north to south within the Makran accretionary wedge. The Inner Makran exhibits intense deformation with tight folding and significant thrusting,

GeoNexus

reflecting strong compressional forces near the subduction zone (Harms et al., 1984; Platt et al., 1985; Dolati, 2010). Towards the south, deformation decreases, with the Outer Makran and Coastal Makran displaying open folds and normal faulting indicative of weaker deformation and extensional regimes.

2.3.2 Temporal Evolution

The structural features suggest multiple phases of deformation:

- Initial compression: The primary phase involved north-south compression due to subduction, leading to thrust faulting and tight folding in the Inner Makran (McCall and Kidd, 1982; Dolati, 2010).
- Strike-slip faulting: A subsequent phase introduced conjugate strike-slip faults, offsetting earlier structures and accommodating lateral movements due to oblique convergence or changes in plate motions (Kukowski et al., 2002; Dolati, 2010).
- Extension: In the Coastal Makran, extensional tectonics became prominent, possibly due to gravitational collapse of the over-thickened wedge or changes in the regional stress field (Harms et al., 1984; Grando and McClay, 2007; Dolati, 2010).

2.3.3 Strain Partitioning

The coexistence of compressional, extensional, and strike-slip structures indicates strain partitioning within the accretionary wedge. This partitioning may be influenced by factors such as variations in sediment thickness, mechanical stratigraphy, rheological contrasts between lithologies, and spatial changes in convergence rates along the subduction zone (Farhoudi and Karig, 1977; Byrne et al., 1992; Dolati, 2010).

2.3.3.1 Main Stress Regimes

Analysis of brittle fault zones within the Makran accretionary wedge reveals critical insights into the paleostress regimes that have shaped the region's structural evolution (Dolati, 2010). Two dominant tectonic regimes have been identified based on fault-slip data and the orientations of principal stress axes:

1. Compression and Transpression
    - Orientation: The maximum principal stress axes (σ_1) generally plunge shallowly towards the NNE or SSW, indicating a regional NNE–SSW compressional stress field.
    - Spatial distribution: This regime is widespread across the Makran accretionary wedge, including the Inner Makran, the Imbricate Zone, and areas adjacent to major thrusts such as the Qasr-e-Qand, Pishamak, and Lashar thrust faults.
    - Kinematic features: Characterized by east-west striking thrusts and conjugate strike-slip faults with NE–SW sinistral and NW–SE dextral movements.

GeoNexus

- Significance: The compressional stress regime aligns with the orientation of folds and major thrust faults, suggesting that these structures formed under the same stress field (Jacob et al., 1979; Harms et al., 1984; Dolati, 2010). This regime reflects the ongoing convergence between the Arabian and Eurasian plates.

2. Extension

   - Orientation: Characterized by steeply plunging maximum principal stress axes (σ_1), indicating a vertical σ_1 and horizontal minimum principal stress axes (σ_3).
   - Spatial distribution: Prominent in the Coastal Makran and, to a lesser extent, along the boundary of the Jaz Murian Depression and north of Fannuj.
   - Kinematic features: Dominated by nearly east-west striking normal faults near the coast, with extension directions varying from N–S inland to E–W near the coast.
   - Significance: Reflects localized tectonic processes such as gravitational collapse or uplift due to underplating, leading to normal faulting and crustal thinning in the Coastal Makran (Harms et al., 1984; Grando and McClay, 2007; Dolati, 2010).

The NNE–SSW compressional stress field is consistent with the present-day convergence direction between the Arabian and Eurasian plates (e.g., Nilforoushan et al., 2003; Reilinger et al., 2006). This stable stress orientation has significantly influenced the development of structural features like folds and thrusts from the Cretaceous to the upper Miocene (Dolati, 2010).

Earthquake focal mechanism data support the compressional regime, indicating nearly N–S compression in the northern Makran accretionary wedge (Byrne et al., 1992; Dolati, 2010). The alignment between paleostress analysis and seismic data enhances confidence in interpreting the regional stress field and understanding seismic hazards.

The extensional regime in the Coastal Makran suggests a complex tectonic history with superimposed extension over regional compression. Factors contributing to this extension include gravitational collapse of the over-thickened wedge and uplift due to sediment underplating (Kopp et al., 2000; Grando and McClay, 2007; Dolati, 2010).

2.3.4 Low-Temperature Thermochronology of the Makran Accretionary Wedge

Low-temperature thermochronology, specifically apatite and zircon fission-track (FT) analysis, provides crucial insights into the burial and exhumation history of the Makran accretionary wedge in southern Iran. These methods allow for the reconstruction of thermal histories associated with sedimentary and tectonic processes, offering temporal constraints on thrust activity and exhumation events (Dolati, 2010).

2.3.4.1 Apatite Fission-Track Results and Interpretations

2.3.4.1.1 Partial Annealing and Thermal Histories

- Partial annealing of apatites: Apatite FT analysis of samples ranging from the late Cretaceous to the Miocene (75–10 Ma) revealed that all have undergone at least partial

annealing since deposition (Dolati, 2010). This indicates that these rocks were subjected to temperatures within the apatite partial annealing zone (APAZ) of 60–110°C (Green et al., 1989).

- Temperature estimates and burial depths: The degree of annealing increases with stratigraphic age, suggesting deeper burial for older units. Samples as young as 10 Ma show slight resetting, implying they reached temperatures above 60°C. Older horizons (>40 Ma) approached temperatures near 110°C, corresponding to burial depths of approximately 5–6 km, assuming a geothermal gradient of 20°C/km (Dolati, 2010).

2.3.4.1.2 Timing of Thrust Activity and Exhumation

- Southward propagation of thrusting: The apatite FT ages indicate a general southward progression of thrust activity over time within the Makran accretionary wedge. Older thrust sheets in the north show earlier exhumation compared to younger, southern sheets (Dolati, 2010).
- Northern Thrust Sheets:
    - Bashakerd Thrust Sheet: Apatite FT ages suggest exhumation occurred between 22.2 ± 7.0 Ma and before 9.6 Ma, as this unit is overlain by the Tortonian olistostrome (11.6–9.6 Ma) (Dolati, 2010).
    - Imbricate Zone: Rapid exhumation is recorded between 15 and 5 Ma, indicating thrust activity during this period (Dolati, 2010).
- Central Thrust Sheets:
    - Chanf and Lashar Thrust Sheets: Exhumation and cooling occurred after 27 Ma, with thrusting activity constrained by overlying sediments and apatite FT ages (Dolati, 2010).
    - Pishamak Thrust Sheet: Cooling ages around 10 Ma suggest thrusting and exhumation occurred before the deposition of the overlying Tortonian sediments (Dolati, 2010).
- Southern Thrust Sheets:
    - Ghasr Ghand and Kahorkan Thrust Sheets: Thrusting activities are constrained between 18 and 7.9 Ma based on apatite FT ages and stratigraphic relationships (Dolati, 2010).

2.3.4.1.3 Exhumation Patterns

The data reveal a disrupted progression of tectonic activity from north to south, consistent with accretionary wedge development models (Dahlen et al., 1984). Exhumation events correspond with periods of thrusting and erosion, contributing to the complex structural architecture of the Makran accretionary wedge.

GeoNexus

2.3.4.2 Zircon Fission-Track Results and Interpretations

2.3.4.2.1 Detrital Zircon Age Populations

- Preservation of detrital ages: Zircon grains did not reach temperatures sufficient for annealing (>240 ± 30°C), preserving their original detrital ages and providing information on sediment sources (Tagami et al., 1998; Dolati, 2010).
- Multiple age populations: Zircon FT analysis identified multiple age populations within the sediments, reflecting diverse provenance and tectonic events (Dolati, 2010).

2.3.4.2.2 Sediment Provenance and Source Regions

- Cretaceous to Oligocene Sediments:
    - Sanandaj-Sirjan zone: Age populations around 144 ± 10 Ma and 77 ± 6 Ma suggest sources from the Sanandaj-Sirjan Belt, which includes Triassic to Cretaceous plutonic and volcanic rocks (Berberian and King, 1981; Alavi, 1994).
    - Active volcanism: Younger zircon ages with minimal lag times (e.g., 54.5 ± 4.8 Ma) indicate synchronous volcanic activity during the late Cretaceous to Eocene, contributing volcanic detritus to the basin (Dolati, 2010).
- Miocene Sediments:
    - Recycling of Accretionary Wedge Material: The presence of similar age populations in Miocene sediments suggests reworking of older accretionary wedge materials, implying uplift and erosion of the wedge during this period (Dolati, 2010).

2.3.5 Implications for Tectonic Models

Understanding the structural features of the Makran accretionary wedge is crucial for refining tectonic models of the region. The complex interplay of folding and faulting reflects the dynamic processes of accretionary wedge development, subduction mechanics, and plate interactions (Byrne et al., 1992; Grando and McClay, 2007; Dolati, 2010). These insights contribute to assessments of seismic hazards, resource exploration, and the broader geodynamic evolution of convergent plate boundaries.

The consistent presence of young zircon populations across stratigraphic units indicates sustained volcanic activity influencing sedimentation from the late Cretaceous through the Oligocene (Dolati, 2010). The recurrence of zircon age populations and evidence of reworked fossils support the notion of sediment recycling within the Makran accretionary wedge during the Miocene (Ellouz-Zimmermann et al., 2007; Dolati, 2010).

GeoNexus

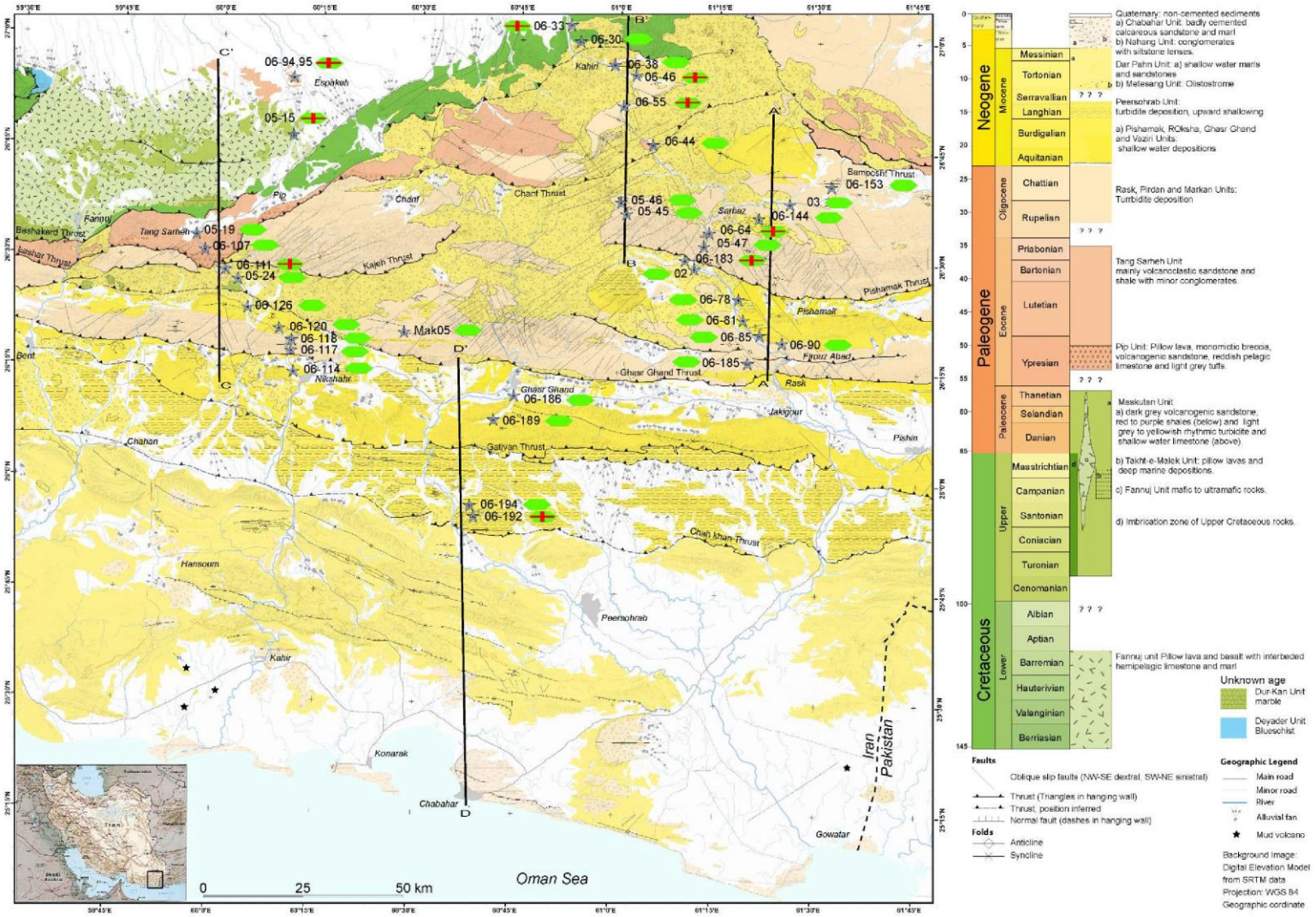


Figure 2-9. Geological map of the Makran accretionary wedge in Iran, showing fission-track sample locations (Dolati, 2010). Apatite sample locations are marked by green hexagons, and zircon samples by red crosses.

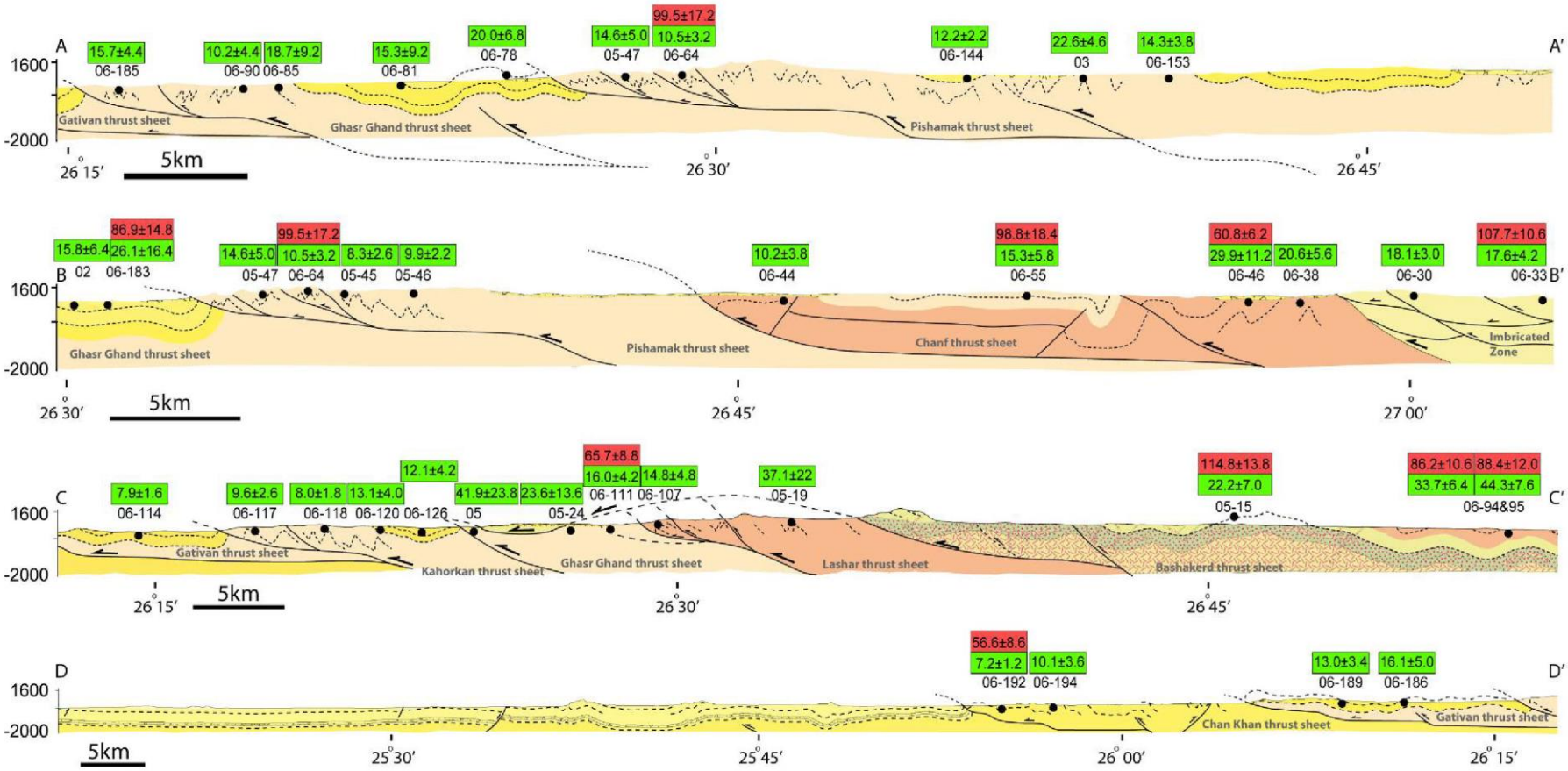


Figure 2-10. Cross sections, illustrating fission-track sample locations (Dolati, 2010). Apatite and zircon central ages (±2σ) are shown in green and red boxes, respectively. See locations of profiles in Figure 2-9.

The integration of apatite FT ages with stratigraphic data constrains the timing of thrust sheet movements, revealing a general trend of younger thrusting towards the south and providing a timeline for the accretionary wedge's development (Dolati, 2010). The varying degrees of annealing and exhumation ages across thrust sheets underscore the role of both sedimentary overburden and tectonic thickening in shaping the thermal and structural evolution of the Makran accretionary wedge (Dolati, 2010). These are aligned with models of accretionary wedge dynamics, where progressive thrusting and frontal accretion lead to the sequential uplift and exhumation of thrust sheets (Dahlen et al., 1984; Platt et al., 1985).

The Makran accretionary wedge exhibits a general southward progression of thrust activity from before 23 Ma in the north to around 7.9 Ma in the south, consistent with accretionary wedge growth patterns (Dolati, 2010). Apatite FT data indicate maximum burial depths of approximately 5–6 km, with subsequent exhumation driven by thrusting and erosion (Dolati, 2010). Detrital zircon ages reveal contributions from the Sanandaj-Sirjan belt and ongoing volcanic activity, with evidence of sediment recycling within the Makran accretionary wedge during the Miocene (Berberian and King, 1981; Dolati, 2010). The combined apatite and zircon FT analyses provide a comprehensive picture of the Makran accretionary wedge's thermo-tectonic evolution, highlighting the interplay between tectonics, sedimentation, and erosion in shaping the region's geological history.

2.4 Seismicity

The recorded seismicity in the Makran region is notably low compared to adjacent areas and most other subduction zones, a phenomenon that has intrigued geoscientists (Dolati, 2010). The seismic behavior of the Makran subduction zone is characterized by distinct segments. The western part of the Makran subduction zone is considered relatively aseismic. Historical records do not indicate any large seismic events, and modern instrumentation has not detected significant shallow seismicity over the past few decades (e.g., Byrne et al., 1992). Most earthquakes in this segment occur at depths of about 70 km within the subducting plate.

In contrast, the eastern segment exhibits higher seismic activity. The most significant event was the M_w 8.1 earthquake of November 1945, which occurred at a depth of 30 km and generated a tsunami that affected the coastlines of Pakistan, Iran, Oman, and India (Page et al., 1979; Byrne et al., 1992; Heidarzadeh et al., 2008). This earthquake ruptured approximately 200 km of the subduction zone. Segmentation of the subduction zone is further evidenced by two seismic events in central Makran that displayed dextral strike-slip motion, suggesting complex stress regimes and potential transform faulting within the subduction zone (Byrne et al., 1992; Dolati, 2010).

The low seismicity in the western segment has raised concerns about the potential for future large earthquakes due to the long seismic gap and accumulated strain (Byrne et al., 1992). The occurrence of the 1945 earthquake in the eastern segment highlights the possibility of megathrust earthquakes and associated tsunamis in the region (Heidarzadeh et al., 2008).

Factors contributing to the seismic behavior include sediment thickness, subduction angle, and thermal regime. The thick sediments in the subduction zone may influence the mechanical properties of the plate interface, potentially affecting seismic coupling and the occurrence of slow slip events or aseismic creep (Kopp et al., 2000; Smith et al., 2012). The shallow subduction angle may lead to a wider seismogenic zone but also complicate stress accumulation and release patterns.

GeoNexus

The low geothermal gradients measured in wells in the onshore Pakistani Makran (about 20°C per km) suggest a cooler subduction zone, which may affect the frictional properties of the plate interface (Harms et al., 1984; Khan et al., 1991).

Table 2-1. Earthquake fault plane solutions within the study area (see Figure 2-11). M, s, d, and r represent magnitude, strike, dip, and rake, respectively. Depths are in km.

No.	Date	Long	Lat	Depth	M	s1	d1	r1	s2	d2	r2	References
1	27.11.1945	63.48	26.15	27.00	7.9	246	7	89	67	83	90	Byrne et al. (1992)
2	05.08.1947	63.49	25.04	20.00	6.8	236	7	68	78	84	93	Byrne et al. (1992)
3	10.01.1979	60.95	26.55	3.00	5.8	256	61	13	160	77	150	Byrne et al. (1992)
4	10.01.1979	61.02	26.48	2.00	5.9	230	82	-4	321	86	-17	Byrne et al. (1992)
5	08.08.1972	61.22	25.14	18.00	5.0	334	15	148	95	82	77	Byrne et al. (1992)
6	03.08.1968	62.87	25.19	26.00	4.7	290	49	-50	58	55	-126	Byrne et al. (1992)
7	13.02.1969	62.75	24.99	18.00	5.1	279	9	84	105	81	91	Byrne et al. (1992)
8	06.08.1972	61.22	25.04	20.00	5.4	321	17	134	96	78	78	Byrne et al. (1992)
9	08.08.1972	61.22	25.14	18.00	5.4	334	15	148	95	82	77	Byrne et al. (1992)
10	18.08.1972	63.14	24.83	20.00	4.6	277	9	84	103	81	91	Byrne et al. (1992)
11	02.09.1973	63.21	24.88	18.00	5.2	281	23	70	123	68	98	Byrne et al. (1992)
12	29.07.1975	63.09	25.22	18.00	5.0	278	27	88	100	63	91	Byrne et al. (1992)
13	10.02.1978	62.40	25.33	18.00	5.1	214	16	19	106	85	105	Byrne et al. (1992)
14	29.05.1963	59.40	27.00	52.00	5.2	46	18	-90	226	72	-90	Chandra (1984)
15	12.08.1963	63.14	25.32	5.00	5.4	190	30	0	100	90	120	Quittmeyer et al. (1984)
16	06.08.1972	61.22	25.04	33.00	5.5	292	22	114	86	70	81	Chandra (1984)
17	08.08.1972	61.22	25.14	30.00	5.5	280	5	90	100	85	90	Chandra (1984)
18	02.09.1973	63.21	24.88	30.00	5.3	270	30	90	90	60	90	Quittmeyer et al. (1984)
19	10.01.1979	60.95	26.55	33.00	5.9	300	40	90	120	50	90	Jackson and McKenzie (1984)
20	10.01.1979	61.02	26.48	33.00	5.9	300	34	90	120	56	90	Jackson and McKenzie (1984)
21	01.01.1980	60.27	26.99	64.10	5.4	208	80	-178	118	88	-10	GCMT
22	07.12.1991	62.94	25.08	15.00	5.6	309	8	133	85	84	85	GCMT
23	30.01.1992	62.88	24.25	15.00	5.8	298	10	126	82	82	84	GCMT
24	17.12.1992	61.43	25.68	37.00	5.7	8	54	142	123	60	43	GCMT
25	24.06.2003	60.91	27.00	72.40	5.5	97	45	-65	244	50	-112	GCMT
26	13.03.2005	62.00	26.73	58.00	6.0	253	37	-89	72	53	-90	GCMT
27	18.07.2006	61.23	26.07	30.80	5.3	107	67	-12	201	79	-157	GCMT
28	30.09.2013	60.18	26.72	16.20	4.7	87	44	-28	198	71	-131	GCMT
29	04.05.2015	61.23	26.12	36.30	5.1	308	83	4	218	86	173	GCMT
30	07.02.2017	63.25	25.01	14.00	6.4	249	6	64	95	84	93	GCMT
31	08.02.2017	63.25	24.79	23.40	5.3	300	19	101	108	71	86	GCMT
32	31.07.2022	63.55	25.05	26.30	5.6	162	39	104	324	52	79	GCMT
33	31.07.2022	63.53	25.01	29.10	5.0	3	46	102	166	46	78	GCMT
34	05.03.2024	59.34	26.89	88.50	5.2	35	71	164	131	75	19	GCMT

GeoNexus

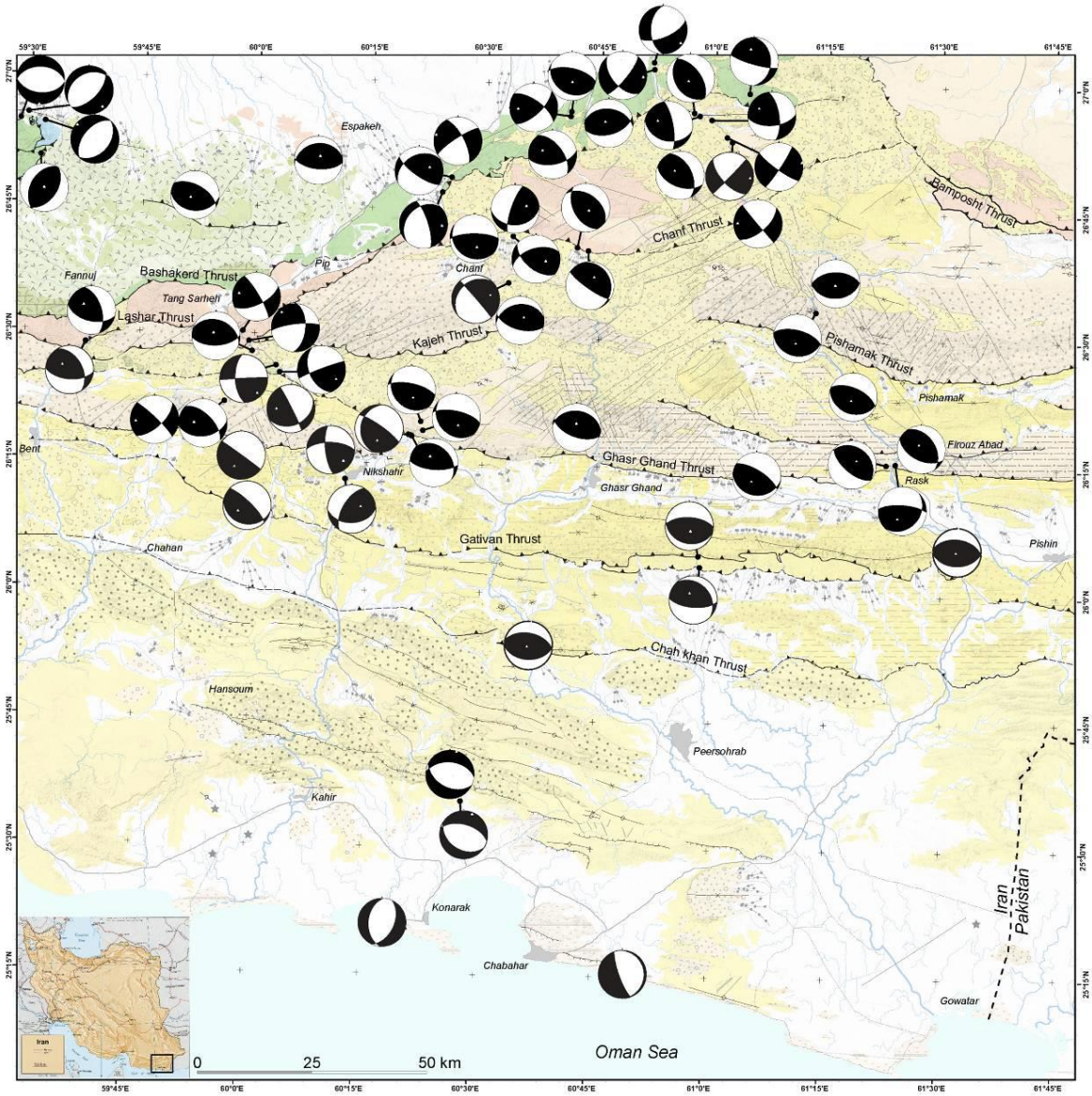


Figure 2-11. Major focal mechanisms over the Makran accretionary wedge and adjacent areas, illustrating the segmentation and seismicity patterns (Dolati, 2010).

GeoNexus

3 Methods and data

The conceptual model of the project represents a harmonious combination of advanced technologies:

1. **Data Integration:** This study included a diverse mix of data sources such as ASTER, Sentinel-1, and Sentinel-2 satellite imagery, topographic data, and geological spectral indices. This multi-source approach allows for a comprehensive view of the landscape of usable data.
2. **Object-Based Approach:** Moving beyond traditional pixel-based analysis, the project employed an object-based method. Sentinel-2 images were initially segmented using *eCognition* software, transforming raster data into meaningful geological entities derived from homogeneous regions. This approach reflects how geologists interpret spatial information from the Earth's surface.
3. **Cloud Processing:** The *Google Earth Engine* provided the core computations of the project. This efficient processing platform enabled the handling of large datasets and complex algorithms, eliminating limitations on access to image resources and intensive computations.
4. **Machine Learning Classification:** At the heart of the project was the random forest algorithm, a powerful machine learning method. This algorithm classified 16 geological classes along with vegetation and water, totaling 18 classes. Spectral features, topography, and shape-based characteristics were used as inputs in this classification.

   The results from the random forest algorithm indicated the effectiveness of this integrated approach; the final geological map achieved an accuracy of 85% with a Kappa coefficient of 0.84. These outcomes highlight the potential of the object-based approach, machine learning, and cloud computing in geological mapping.

This project represented a paradigm shift in how we approach geological mapping. By leveraging cloud computing, we can now process and analyze vast amounts of satellite data in ways previously unimaginable. The integration of machine learning algorithms allowed us to extract meaningful patterns and relationships from these data and images, automating complex classifications that once required extensive manual interpretation.

GeoNexus

Furthermore, the object-based approach, combined with a rich set of data sources, enabled more precise interpretation. This method not only characterized the spectral features of different geological units but also elucidated their spatial relationships and morphological features—a comprehensive approach that aligns more closely with how geologists interpret spatial information.

This project serves as a beacon, charting a course toward a future of rapid, accurate, and large-scale geological mapping, even for the most complex and remote areas. Ultimately, the project demonstrated that with the right combination of data, technology, and expertise, we can achieve new levels of understanding in geological studies.

3.1 Converting Archived Paper Data into Digital Resources

In this study, two key activities were undertaken: (1) Documentary and Data Collection, and (2) Unlocking Data Trapped in Paper. The primary objective of these activities was to enhance the added value of the research and optimize the operational efficiency of the project.

The first activity focused on the systematic collection of data relevant to the project's scope. This was accomplished through extensive searches across various internal and external sources. The data gathered included base maps, project reports, academic theses, and scholarly articles. Each piece of information was carefully reviewed, analyzed, and selected based on its relevance and usefulness for the project's objectives.

The second activity aimed at addressing the limitations posed by the format of the collected data. Many of the sources were originally in non-digital forms—such as paper documents, text manuscripts, and images—which were not directly usable in their original state for advanced digital research. To overcome this challenge, the data was meticulously categorized and positioned based on its inherent value and credibility. Subsequently, a usable geodatabase was generated. This geodatabase includes a variety of digital assets, such as elevation data, images, coordinate data, sampling points, structural sections, stratigraphic columns, as well as texts and tables associated with the selected data.

It is important to note that this report focuses specifically on the outcomes of the second activity. The geodatabase contains all digitized data, and every effort has been made to ensure the comprehensive presentation of this information in the report. By transforming analog data into a structured digital format, the project has significantly enhanced the accessibility and utility of these resources for further analysis and application.

3.2 Remote Sensing

In the study of terrestrial resources, two general methods exist for collecting information: (a) field-based methods and (b) Remote Sensing (RS). One of the modern and effective tools now available in environmental studies, earth sciences, and mineral exploration is the use of remote sensing

GeoNexus

technology and the utilization of satellite data along with high-performance computer systems (Jensen, 2016; Sabins and Ellis, 2020).

The remote sensing began with aerial photographs and entered a new phase with the launch of satellites and the use of multispectral scanners (Drury, 2001). Remote sensing plays a crucial role in modern geological mapping and mineral exploration by providing efficient and cost-effective methods for surveying large areas and identifying potential mineral deposits (Goetz et al., 1983). This technology involves collecting and analyzing images of the Earth's surface using satellite sensors or airborne platforms (Richards, 2013).

Key aspects of remote sensing in geology:

3.2.1 Sensors

Remote sensing in geology utilizes a variety of sensors, each operating in different parts of the electromagnetic spectrum to gather specific types of data. Optical sensors function in the visible and near-infrared range (NIR), capturing images similar to human vision but with additional information from the near-infrared spectrum. Multispectral sensors collect data across multispectral bands, allowing for more detailed analysis by providing information from several discrete wavelengths. Hyperspectral sensors extend this capability by offering detailed spectral information across hundreds of narrow bands, which is essential for identifying specific mineral compositions based on their unique spectral signatures (van der Meer, 2004). Thermal sensors detect and map heat emissions from the Earth's surface, revealing thermal anomalies that may indicate geological activity or the presence of certain materials. Radar systems, operating with microwave frequencies, have the ability to penetrate cloud cover and vegetation, enabling data collection in conditions where optical sensors are limited.

3.2.2 Data Acquisition Methods

The methods of data acquisition in remote sensing include satellite-based platforms, airborne systems, and unmanned aerial vehicles (UAVs). Satellite-based remote sensing provides global coverage with regular revisit times, making it ideal for large-scale geological studies and for monitoring changes over time. Airborne methods involve data collection from aircraft, which offer higher spatial resolution and greater flexibility in both temporal and spatial data acquisition. This allows for targeted surveys and the ability to collect data under specific conditions. UAVs, or drones, deliver very high-resolution data for local areas, enabling detailed mapping and analysis of specific sites of interest, especially where accessibility is challenging or where fine-scale detail is required (e.g., Li et al., 2020).

3.2.3 Applications in Geological Mapping

Remote sensing is extensively used in geological mapping due to its ability to cover large areas efficiently. In lithological mapping, remote sensing helps in the identification and differentiation of rock types and geological units by analyzing their spectral properties and spatial relationships. Structural mapping utilizes remote sensing data to detect faults, folds, and other geological structures, which are crucial for understanding tectonic activities and for exploring mineral

deposits. Geomorphological analysis involves studying landforms and surface processes, providing insights into erosion patterns, sediment deposition, geomorphic features, and landscape evolution. Remote sensing also aids in geobotanical analysis by identifying plant species that indicate specific geological conditions, as certain vegetation types may thrive in soils rich in particular minerals, thus serving as bio-indicators for mineral exploration (e.g., Ghosh and Joshi, 2014).

3.2.4 Mineral Exploration Techniques

In mineral exploration, remote sensing techniques are employed to detect and analyze features indicative of mineralization. Spectral analysis is used to identify specific mineral absorption features within the data, which can point to the presence of certain minerals based on their unique spectral signatures. Alteration mapping involves detecting hydrothermal zones associated with mineral potential by identifying changes in the mineral composition of rocks due to fluid interactions, which often result in characteristic spectral patterns. Lineament and fault analysis is conducted to identify geological structures such as fractures and faults that can control the localization of mineral deposits, providing targets for further exploration.

3.2.5 Data Processing and Interpretation

Processing and interpreting remote sensing data involves several sophisticated techniques to enhance the quality of information extracted. Image enhancement methods improve the visual interpretation of images by adjusting contrast, brightness, and applying filters to highlight specific features. Band ratios and indices are calculated by combining spectral bands in particular ways to emphasize certain materials or conditions, such as vegetation health or mineral content. Principal Component Analysis (PCA) is used to reduce data dimensionality and to emphasize differences between spectral features, aiding in the identification of unique geological signatures. The advent of machine learning and artificial intelligence has revolutionized data processing by enabling automated feature extraction and classification, allowing for more efficient and accurate analysis of large datasets (e.g., Tso and Mather, 2009).

3.2.6 Integration with Other Data

Remote sensing data are often integrated with other datasets to enhance geological interpretations and to provide a more comprehensive understanding of the subsurface. Geographic Information Systems (GIS) combine remote sensing data with other spatial data layers, such as geological maps, soil types, and hydrological data, facilitating multifaceted analysis and visualization. Integration with geophysical data—including magnetic, gravity, and electromagnetic surveys—complements remote sensing by providing information on subsurface properties, which, when combined, offer a fuller picture of geological structures and compositions. Correlating spectral features from remote sensing with known elemental compositions from geochemical data helps in identifying mineral deposits and understanding geological processes, thereby improving the accuracy of exploration models (e.g., Dong et al., 2018).

GeoNexus

3.2.7 Advantages of Remote Sensing

The use of remote sensing in geological studies presents several significant advantages. It offers a cost-effective means of covering large and often inaccessible areas, enabling the surveying of vast regions without the need for extensive ground-based surveys. This is particularly beneficial for accessing remote or hazardous areas where fieldwork is difficult or dangerous, such as mountainous terrains, deserts, or politically unstable regions. Remote sensing also allows for temporal analysis, providing the ability to monitor changes over time, such as erosion, landform development, vegetation growth, or the progression of natural disasters, which is essential for understanding dynamic geological processes and for resource management.

3.2.8 Limitations

Despite its numerous benefits, remote sensing has certain limitations that must be considered. Resolution constraints, especially with satellite-based sensors, can affect the ability to detect small-scale features and subtle variations, potentially overlooking critical geological details. Atmospheric conditions, such as cloud cover, haze, and aerosols, can degrade data quality or obscure the Earth's surface, limiting the effectiveness of optical sensors and sometimes necessitating the use of alternative sensing methods like radar. Additionally, interpretations made from remote sensing data require validation through ground truthing, which involves field verification to confirm the accuracy of remotely sensed information. This process can be resource-intensive and may mitigate some of the cost and accessibility advantages of remote sensing.

3.2.9 Emerging Trends

Emerging trends in remote sensing are enhancing its capabilities and applications in geology. The increased use of hyperspectral sensors allows for detailed mapping of mineral potential by providing precise identification of minerals based on their spectral properties. The development and deployment of UAV-based sensors facilitate high-precision surveys of specific areas, offering unprecedented spatial resolution and flexibility in data acquisition, which is particularly useful for detailed site investigations and for areas that are difficult to access by conventional means. Advancements in machine learning are improving automated image processing and interpretation, enabling more efficient handling of large datasets and enhancing the accuracy of feature extraction and classification. The integration of remote sensing with concurrent field data collection combines real-time measurements with remote observations, improving the reliability and comprehensiveness of geological studies and enabling more responsive decision-making in exploration and resource management (e.g., Breiman, 2001; Pedregosa et al., 2011).

One of the earliest applications of remote sensing in geology was the use of photogeological techniques, which involved interpreting aerial photographs and images from the Multispectral Scanner (MSS) on the Landsat-1 satellite to extract morphological features and identify iron oxide anomalies in the visible wavelength range (NASA, 2016). Following this, products from the French SPOT satellite were utilized by geologists due to their unparalleled spatial resolution and stereoscopic capabilities enabled by spatially overlapping images (Bouvet et al., 2018).

The application of remote sensing in geology accelerated with the advent of the Thematic Mapper (TM) sensor on the Landsat satellites (Goward et al., 2001). For many years, images from this sensor were used in lithological mapping and lineament analysis, especially in mapping alteration minerals associated with hydrothermal processes (Sabins and Ellis, 2020). In 1999, the launch of Landsat 7 with the Enhanced Thematic Mapper Plus (ETM+) sensor provided higher-quality images compared to previous series (NASA, 2016). Unfortunately, in 2003, this sensor experienced a technical failure and lost its full functionality.

Due to the high importance of these images for specialists in various sciences, especially natural sciences, Landsat 8 was launched in 2013 with the Operational Land Imager (OLI) and Thermal Infrared Sensor (TIRS) (Roy et al., 2014). The OLI sensor is similar to the ETM+ but offers differences in spectral resolution. It has nine bands in the reflective wavelength region, seven of which are similar to the previous TM and ETM+ series (NASA, 2016). Two additional bands—the coastal/aerosol band (433–453 nm) and the cirrus band (1360–1390 nm)—have been added. These additions allow scientists to more accurately identify clouds and measure atmospheric water content and cloud thickness, enhancing atmospheric correction and improving the quality of surface observations (Irons et al., 2012).

Furthermore, the OLI/TIRS sensor collects data in a push-broom fashion, using a linear array of detectors to capture imagery as the satellite moves along its orbit, whereas the ETM+ sensor used a whisk-broom method, scanning across the satellite's track with a rotating mirror. The push-broom design results in higher radiometric sensitivity and fewer moving parts, improving data quality and sensor reliability (Storey et al., 2014). Additionally, since the sensors on Landsat 8 have a radiometric resolution of up to 16 bits, they can record and store subtle differences in energy received by the sensor, which is crucial for distinguishing features in areas with low reflectance, such as dense forests or dark geological formations (Roy et al., 2014). The specifications of Landsat 7 and 8 are compared in Table 3-1, and Figure 3-1 illustrates the differences between these two sensors in bandwidth and the position of each band relative to atmospheric windows. Considering these points and the information in Table 2-1, it is easy to understand the higher capability of the Landsat 8 sensor compared to Landsat 7. Therefore, we prioritized using it in this study.

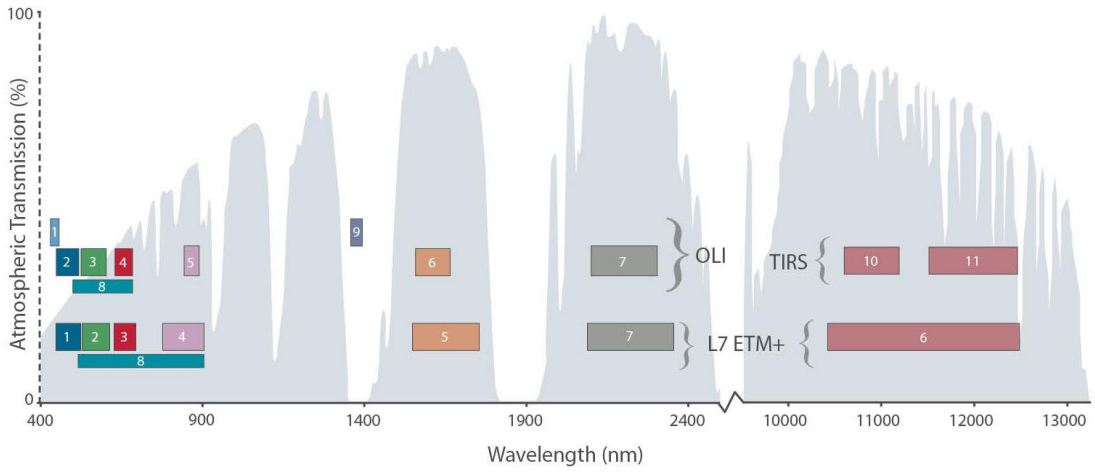


Figure 3-1. Comparison of Landsat 7 ETM+ and Landsat 8 OLI/TIRS spectral bands, illustrating bandpass wavelengths and atmospheric transmission percentages across the electromagnetic spectrum (graphic by L. Rocchio and J. Barsi; source: https://landsat.gsfc.nasa.gov/satellites/landsat-8/).

Table 3-1. Specifications of Landsat 7 ETM+ and Landsat 8 OLI/TIRS Sensors, Including Spectral Bands, Wavelengths, Geometric Resolution, and Radiometric Resolution.

Satellite	Sensor	Spectral Band	Wavelength	Geometric Resolution	Radiometric Resolution
Landsat 8	OLI	Band 1 - Coastal / Aerosol	0.433 - 0.453 µm	30 m	16-bit
		Band 2 - Blue	0.450 - 0.515 µm	30 m	
		Band 3 - Green	0.525 - 0.600 µm	30 m	
		Band 4 - Red	0.630 - 0.680 µm	30 m	
		Band 5 - Near Infrared	0.845 - 0.885 µm	30 m	
		Band 6 - Short Wavelength Infrared	1.560 - 1.660 µm	30 m	
		Band 7 - Short Wavelength Infrared	2.100 - 2.300 µm	30 m	
		Band 8 - Panchromatic	0.500 - 0.680 µm	15 m	
		Band 9 - Cirrus	1.360 - 1.390 µm	30 m	
	TIRS	Band 10 - Long Wavelength Infrared	10.30 - 11.30 µm	100 m	
		Band 11 - Long Wavelength Infrared	11.50 - 12.50 µm	100 m	
Landsat 7	ETM+	Band -1	0.45 to 0.515 µm	30 m	Best 8 of 9 bits
		Band -2	0.525 to 0.605 µm	30 m	
		Band -3	0.63 to 0.690 µm	30 m	
		Band -4	0.75 to 0.90 µm	30 m	
		Band -5	1.55 to 1.75 µm	30 m	
		Band -6	10.40 to 12.5 µm	60 m	
		Band -7	2.09 to 2.35 µm	30 m	
		Panchromatic	0.52 to 0.90 µm	15 m	

3.3 Advanced Remote Sensing Sensors and Their Applications in Geology

Among the widely used sensors in geology and mineral resource exploration is the ASTER (Advanced Spaceborne Thermal Emission and Reflection Radiometer) sensor, which is installed on the Terra satellite. With its relatively suitable spatial and spectral resolution, ASTER has had a significant impact on geological and exploratory studies (Yamaguchi et al., 1998). The sensor's relatively high spectral resolution in the shortwave infrared range, where most minerals have specific spectral absorption features, allows for the differentiation of various alterations (Farrand et al., 2008). Additionally, ASTER is the only sensor considered multi-thermal due to its five spectral bands in the thermal infrared range, making it possible to distinguish rock units through thermal emissivity characteristics (Gillespie et al., 1986).

Characteristics of ASTER Images (Table 3-2):

- Visible and Near-Infrared (VNIR): Provides images with a spatial resolution of 15 m across three bands.

GEONEXUS

- Shortwave Infrared (SWIR): Offers images with a spatial resolution of 30 m across six bands.
- Thermal Infrared (TIR): Delivers images with a spatial resolution of 90 m across five bands (Abrams et al., 2002).

Table 3-2. Specifications of ASTER sensor images (e.g., Abrams et al., 2002)

Characteristic	VNIR	SWIR	TIR
Spectral Range	Band 1: 0.52 - 0.60 µm (Nadir looking)	Band 4: 1.600 - 1.700 µm	Band 10: 8.125 - 8.475 µm
	Band 2: 0.63 - 0.69 µm (Nadir looking)	Band 5: 2.145 - 2.185 µm	Band 11: 8.475 - 8.825 µm
	Band 3: 0.76 - 0.86 µm (Nadir looking)	Band 6: 2.185 - 2.225 µm	Band 12: 8.925 - 9.275 µm
	Band 3: 0.76 - 0.86 µm (Backward looking)	Band 7: 2.235 - 2.285 µm	Band 13: 10.25 - 10.95 µm
		Band 8: 2.295 - 2.365 µm	Band 14: 10.95 - 11.65 µm
		Band 9: 2.360 - 2.430 µm	
Ground Resolution	15 m	30 m	90 m
Data Rate (Mbits/sec)	62	23	4.2
Cross-track Pointing (deg.)	±24	±8.55	±8.55
Cross-track Pointing (km)	±318	±116	±116
Swath Width (km)	60	60	60
Detector Type	Si	PtSi-Si	HgCdTe
Quantization (bits)	8	8	12
System Response Function	VNIR Chart VNIR Dat	SWIR Chart SWIR Data	

One of the advantages of ASTER images over ETM (Enhanced Thematic Mapper) images is their higher spectral resolution, especially in the near-infrared wavelength ranges, which plays a significant role in differentiating alterations. To compare the spectral resolution of these two sensors, the diagram in Figure 3-2 is presented. The most differences are observed in the infrared range, where ASTER has increased the number of spectral bands and reduced their bandwidths, aiding in more precise alteration discrimination.

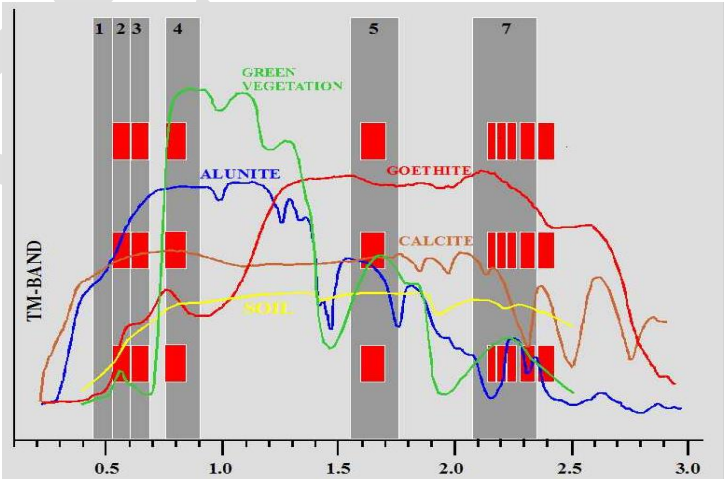


Figure 3-2. Comparison of Spectral Resolution Between ETM and ASTER Images.

GeoNexus

The European Space Agency (ESA) has organized the Copernicus Programme as part of its Earth observation missions (Aschbacher and Milagro-Pérez, 2012). The primary goal of this program is continuous Earth monitoring using high-precision data and images (Drusch et al., 2012). Launched in 2014, the ESA has planned seven missions for the Sentinel program (Sentinel-1 through Sentinel-6). The Sentinel missions include radar and optical imaging of oceans, atmosphere, and land (Torres et al., 2012). Each Sentinel mission consists of two satellites to shorten the Earth's revisit time.

Sentinel-2 Satellites capture high-resolution optical images. Sentinel-2A was launched in June 2015, and Sentinel-2B followed in March 2017 (Gascon et al., 2017). The technical specifications of Sentinel-2 satellites are provided in Table 3-3.

Table 3-3. Spectral and Spatial Characteristics of Sentinel-2 Images

Sentinel-2 Bands	Central Wavelength (µm)	Resolution (m)
Band 1 - Coastal aerosol	0.443	60
Band 2 - Blue	0.49	10
Band 3 - Green	0.56	10
Band 4 - Red	0.665	10
Band 5 - Vegetation Red Edge	0.705	20
Band 6 - Vegetation Red Edge	0.74	20
Band 7 - Vegetation Red Edge	0.783	20
Band 8 - NIR	0.842	10
Band 8A - Vegetation Red Edge	0.865	20
Band 9 - Water vapour	0.945	60
Band 10 - SWIR - Cirrus	1.375	60
Band 11 - SWIR	1.61	20
Band 12 - SWIR	2.19	20

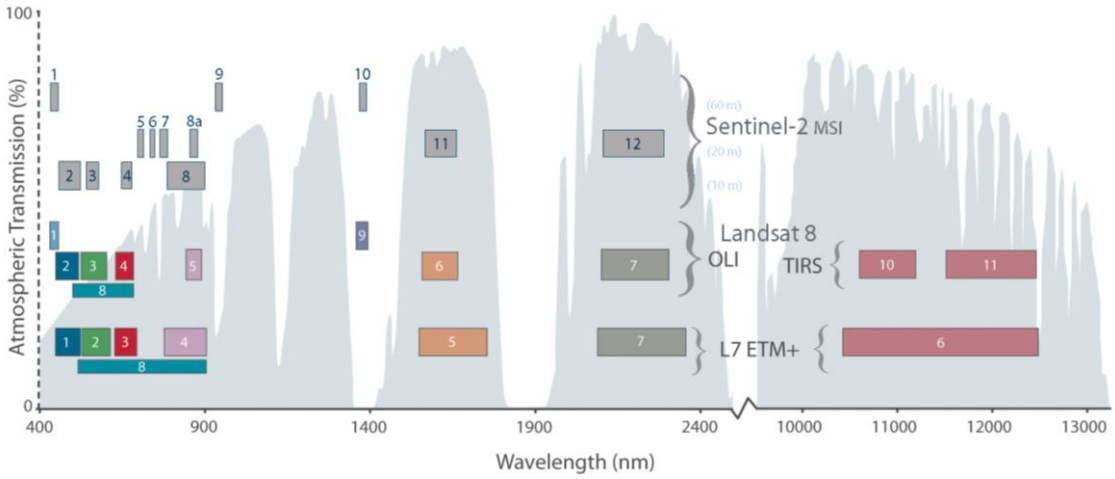


Figure 3-3. Comparison of Sentinel-2 with Landsat 7 (ETM+) and Landsat 8 bands (source: https://landsat.gsfc.nasa.gov/wp-content/uploads/2015/06/Landsat.v.Sentinel-2.png).

Sentinel-1 Satellite is a satellite mission and part of the European Union's Copernicus Programme. Comprising two satellites, Sentinel-1A and Sentinel-1B, it provides continuous all-weather, day-and-night radar imaging of the Earth's surface (Torres et al., 2012). Due to its unique capabilities, this mission has proven to be a valuable tool for geological mapping (Wegnüller et al., 2016), monitoring surface deformation, and geohazards (e.g., Bürgmann et al., 2000; Ferretti et al., 2007).

Key aspects of sentinel-1 in geological mapping:

1. Sensor features:
   - C-band Synthetic Aperture Radar (SAR) operates at a central frequency of 5.4 GHz.
   - All-weather and day-night operation: can penetrate clouds and function in darkness.
   - High-resolution imagery: provides images with resolutions up to 5 m.
2. Imaging modes:
   - Interferometric Wide Swath (IW): primarily used for land monitoring.
   - Wave Mode (WV): for global ocean observation.
   - Strip Map (SM): focused monitoring of small islands.
   - Extra Wide Swath (EW): used for maritime surveillance, sea ice, and polar regions.
3. Applications in Geological Mapping:
   - Geological structures: identification of faults, folds, and lineaments.
   - Geomorphology: mapping landforms and studying surface processes.
   - Lithological mapping: differentiation of rock types based on surface roughness.
   - Monitoring geological hazards: landslides, subsidence, floods, and earthquakes.
   - Mineral exploration: Identifying potential mineral-rich areas.
4. Advantages for geological studies:
   - Effective in cloudy or rainy areas: unaffected by weather conditions.
   - Regular revisit time: frequent coverage allows for up-to-date monitoring.
   - Extensive coverage: each satellite can map the entire Earth every 12 days.
   - Free data access: available to researchers worldwide.
5. Interferometric Capabilities:
   - Surface deformation detection: generates interferograms to detect ground movements.
   - Applications: useful for monitoring volcanic activity, tectonic movements, and land subsidence.
6. Integration with Other Data:
   - Combined analysis: often used alongside optical data (e.g., Sentinel-2) for comprehensive studies.
   - 3D geological mapping: can be integrated with elevation models.
7. Data Processing Techniques:
   - Polarimetric analysis: exploits different polarizations to extract geological information.
   - Synthetic Aperture Radar Interferometry (InSAR): measures surface deformation.
   - Texture analysis: differentiates geological units based on surface roughness.
8. Limitations:

- Radar shadow effects: occur in areas with high relief.

GeoNexus

- Interpretation complexity: requires specialized knowledge for data analysis.
- Lower resolution compared to some commercial SAR satellites

9. Current Research and Future Directions:
    - Algorithm development: creating automatic geological feature extraction algorithms.
    - Machine learning integration: enhancing classification accuracy.
    - Advanced geological mapping: combining Sentinel-1 data with other remote sensing datasets.

Sentinel-1 has significantly contributed to geological mapping by providing extensive and consistent coverage with all-weather imaging capabilities. Its ability to detect subtle ground movements and surface features makes it a valuable tool for understanding geological processes and structures, especially in areas where optical images may be limited by cloud cover or darkness (Ferretti et al., 2007; Wegnüller et al., 2016).

Sentinel-1 satellites are designed to capture radar images (Figure 3-4) both day and night. The first satellite, Sentinel-1A, was launched in April 2014, followed by Sentinel-1B in April 2016 (Table 3-4). These satellites operate in the C-band frequency range, enabling them to collect high-quality radar imagery (e.g., Torres et al., 2012).

By integrating advanced sensors like ASTER, Sentinel-2, and Sentinel-1, modern geological studies have greatly enhanced their capability to map and analyze the Earth's surface. These tools allow geologists to overcome traditional limitations, offering detailed insights into lithology, structural geology, geomorphology, and mineral exploration with unprecedented accuracy and efficiency.

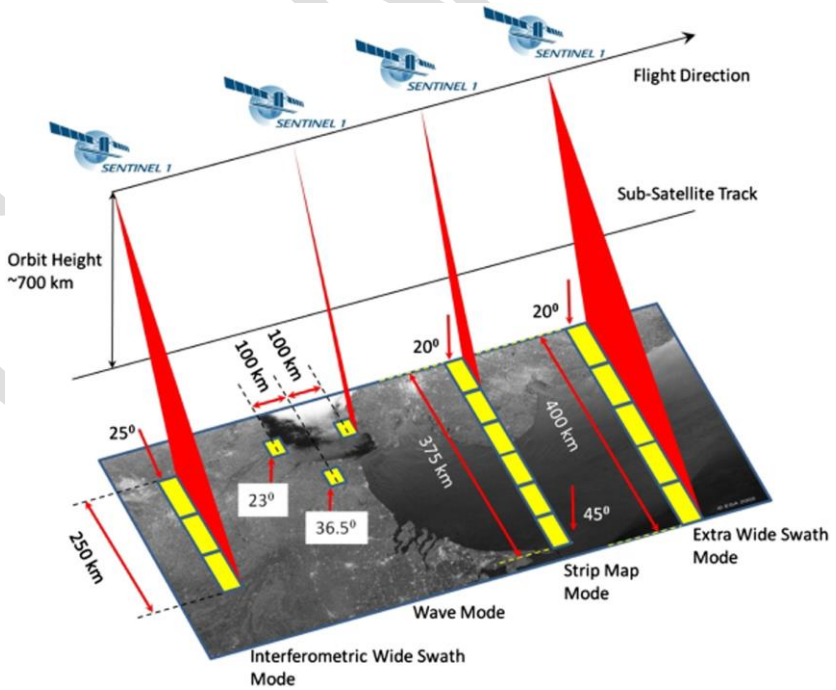


Figure 3-4. Four acquisition modes for Sentinel-1 (Torres et al., 2012)

Table 3-4. Specifications of the Sentinel-1 mission.

Specifications	Sentinel-1 dataset
Satellite	Sentinel-1A; Sentinel-1B (ended)
Launched date	03 April 2014; 25 April 2016 (ended)
Satellite orbit	Descending; Ascending
Incidence angle	~ 43.1°
Repeat cycle	12 days
Imaging frequency	C-band at 5.4 GHz
Imaging mode	IW
Data product	SLC Level-1
Resolution	3.5 m x 22 m (range x azimuth)
Polarization	VV + VH

3.4 Cloud Computing

Cloud computing can be defined as an on-demand system based on computational capabilities, especially in storing massive amounts of data and processing power, which is not directly managed by users. Large cloud infrastructures usually have distributed functions in various locations other than the central core. These cloud systems can be limited to a single organization, in which case they are referred to as private clouds. Alternatively, they can be shared among multiple organizations, known as public clouds. The main philosophy behind such systems is to share information resources to achieve economies of scale and integration. In other words, these systems enable companies to minimize the staggering costs of IT infrastructure.

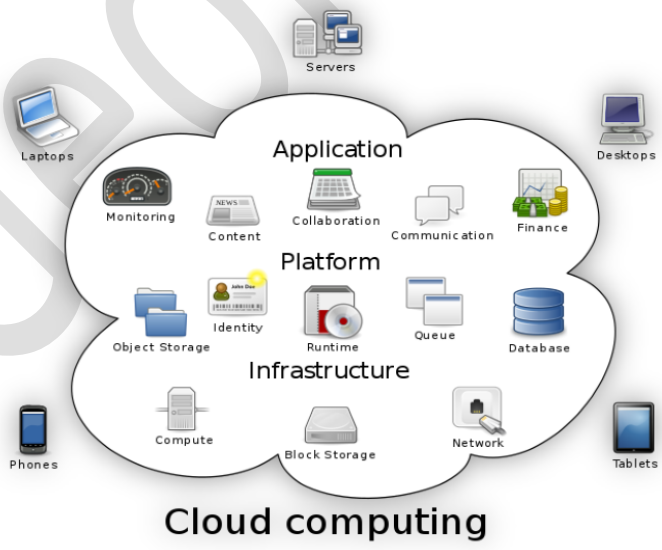


Figure 3-5. illustration of the main components of a cloud computing system.

As shown in Figure 3-5, the three main and fundamental components of such systems are Infrastructure, Platforms, and Applications. In the infrastructure section, two key elements—Storage Blocks and Cloud Processors—play a critical role in cloud systems.

3.4.1 Google Earth Engine

The *Google Earth Engine* system, as a cloud computing platform, enabled—for the first time in history—the rapid processing of vast amounts of satellite imagery (Gorelick et al., 2017). For example, without this system, monitoring changes in vegetation cover, water resources, and land on a global scale would not have been possible (Kumar and Mutanga, 2018). This platform has created a multi-petabyte (10^{15} or 2^{50} bytes) database of satellite images and other geospatial information, along with processing functions and operators on a planetary scale. These two unique capabilities have provided scientists, researchers, and computer programmers with tools to examine environmental changes and trends (Amani et al., 2020). The three components that make up this powerful system are Satellite Imagery, Processing Algorithms, and Environmental Applications (Figure 3-6).

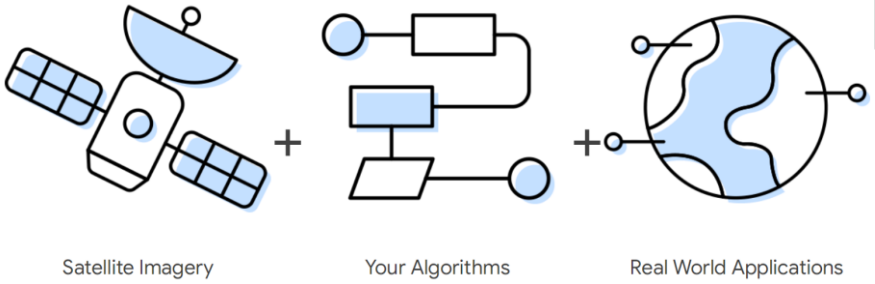


Figure 3-6. The three key components of the *Google Earth Engine* system as a Cloud Computing Platform.

In the *Google Earth Engine* database, there is a comprehensive archive of all satellite images, geophysical data, elevation data, ground information, and indices such as NDVI (Normalized Difference Vegetation Index), LST (Land Surface Temperature), Emissivity, and radar data for various years and time periods. Examples of these information are presented below (Figure 3-7 and Figure 3-8):

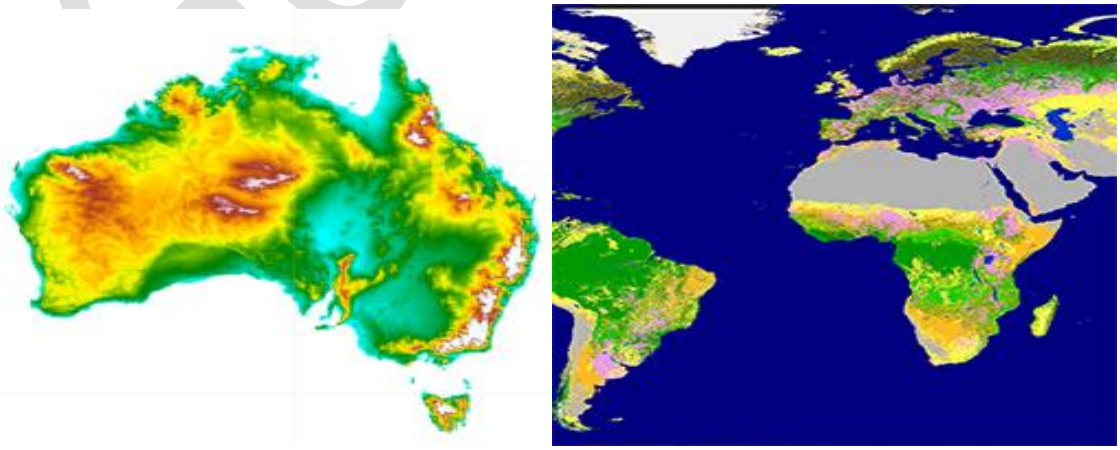


Figure 3-7. Copernicus Global Land Cover Layers: CGLS-LC100 collection 2.

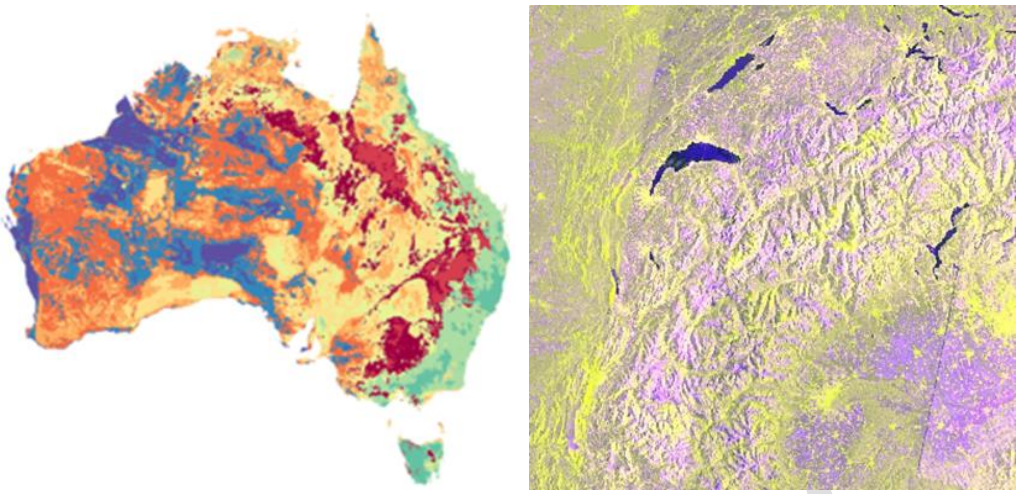


Figure 3-8. Left) SLGA: Soil and Landscape Grid of Australia (Soil Attributes). Right) Sentinel-1 SAR GRD: C-band Synthetic Aperture Radar Ground Range Detected.

In this project, the *Google Earth Engine* cloud processing system was used for data preparation, data processing (Figure 3-9 and Figure 3-10), and machine learning (Figure 3-11). An overview of the workflow within this system is provided below:

1. Data Definition and Preparation
    - Defining the Database: Including Sentinel-1 (SAR data), Sentinel-2 (multispectral), Landsat 8 (multispectral), ASTER datasets (multispectral and thermal), and topographic data (DEM, Slope, Aspect, Sinus) in *Google Earth Engine*.
    - Defining the Area of Interest (AOI): Specifying the study area for the Makran region.
    - Setting Temporal and Quality Filters: Determining time filters and quality thresholds (e.g., cloud cover) for the images.
2. Preprocessing
    - Image Selection: Limiting the image collections based on spatial extent, date range, and cloud cover (for optical images).
    - Radiometric Calibration and Atmospheric Correction: Applying these corrections to optical images (Sentinel-2, Landsat 8, ASTER).
3. Feature Extraction
    - Calculating Spectral Indices: Computing indices (e.g., geological indices) from optical images.
    - Texture Features from SAR Data: Extracting texture information from Sentinel-1 data.
    - Generating Topographic Features: Producing features such as slope, aspect, and sinusoidal representations from elevation data.
    - Creating Band Ratios and Other Features: Developing band ratios and other relevant features for geological mapping.
4. Image Segmentation (Object-Based Approach)

GeoNexus

- Implementing Segmentation Algorithms in *eCognition* Software: Performing image segmentation using specialized software.
- Adjusting Segmentation Parameters: Setting parameters to create homogeneous geological regions based on spectral and shape features.

5. Object Feature Calculation
   - Statistical Measurements: Calculating statistical measures (mean, standard deviation) of spectral bands and indices for each segment.
   - Shape Features: Computing shape characteristics (area, perimeter, and other shape indices).
   - Texture and Topographic Features at Object Level: Integrating texture and topography information at the segment level.
6. Training Data Collection
   - Creating a Training Dataset: Developing a training dataset for initial geological classes using existing geological maps, expert knowledge, or field data based on previous studies.
7. Random Forest Classification
   - Selecting Training Data: Approximately 30% of the data were selected for training the algorithm.
   - Training the random forest classifier: Using object features and training data to train the classifier.
   - Tuning Hyperparameters: Adjusting hyperparameters (number of trees, maximum depth) for optimal performance.
   - Classifying the Entire Area: Applying the trained model to classify the entire study area.
8. Post-Classification Processing
   - Smoothing Classes: Applying relevant filters or other techniques to smooth class boundaries.
   - Merging Small Polygons: Combining small polygons based on similarity to neighboring areas.
   - Refining Class Boundaries: Adjusting and refining class boundaries based on geological knowledge and field visits.
9. Accuracy Assessment
   - Validation: Using a validation dataset to compute the confusion matrix and accuracy metrics (overall accuracy, user's accuracy, producer's accuracy, Kappa coefficient).
10. Final Map Production
    - Generating the Final Classified Map: Creating the final map of geological units.
    - Designing Appropriate Color Schemes: Assigning suitable colors for different geological classes.

GeoNexus

- Adding Map Elements: Including map elements for the final output (e.g., legend, scale bar, north arrow).

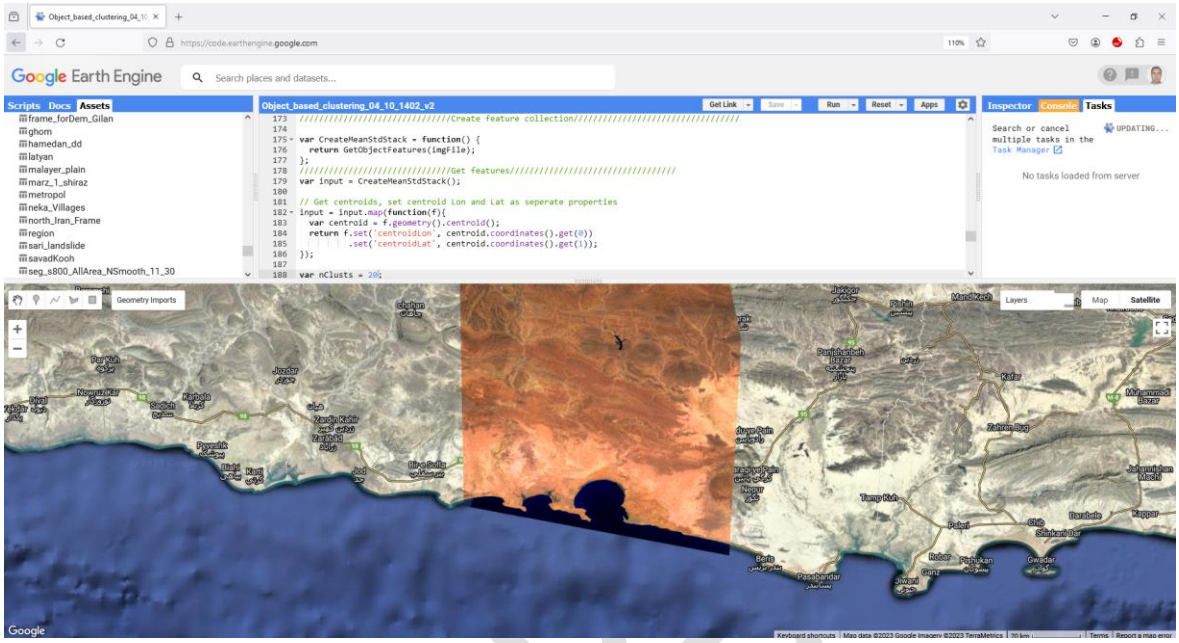


Figure 3-9. View of the *Google Earth Engine* Programming Environment for Satellite Image Processing.

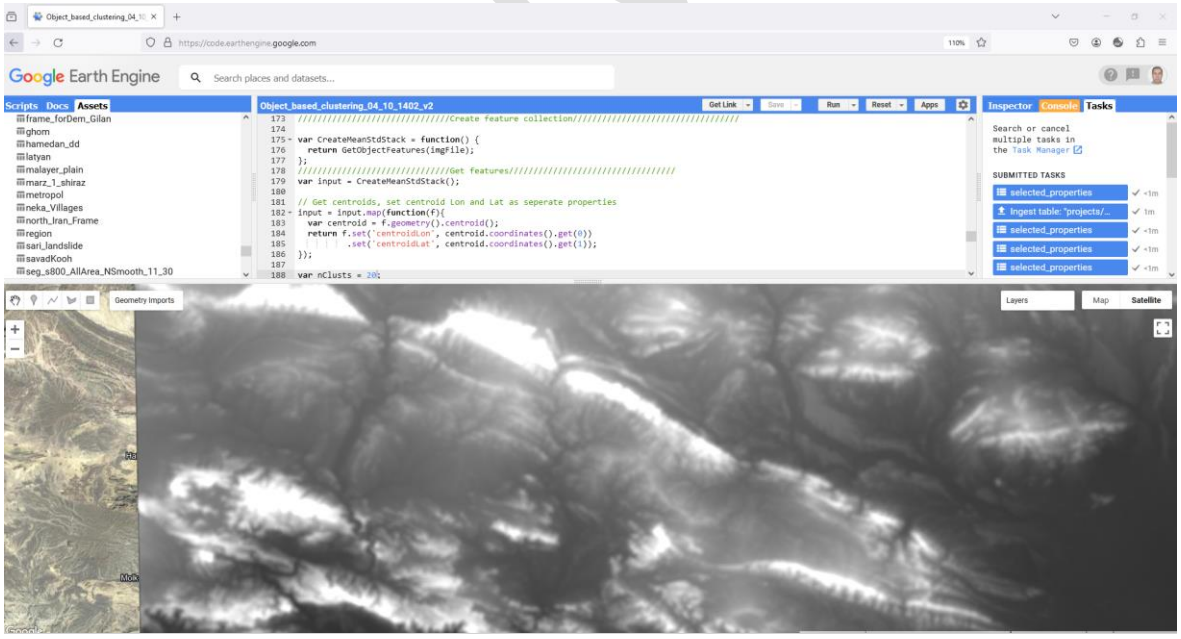


Figure 3-10. View of the *Google Earth Engine* Programming Environment for Topographic Data Processing.

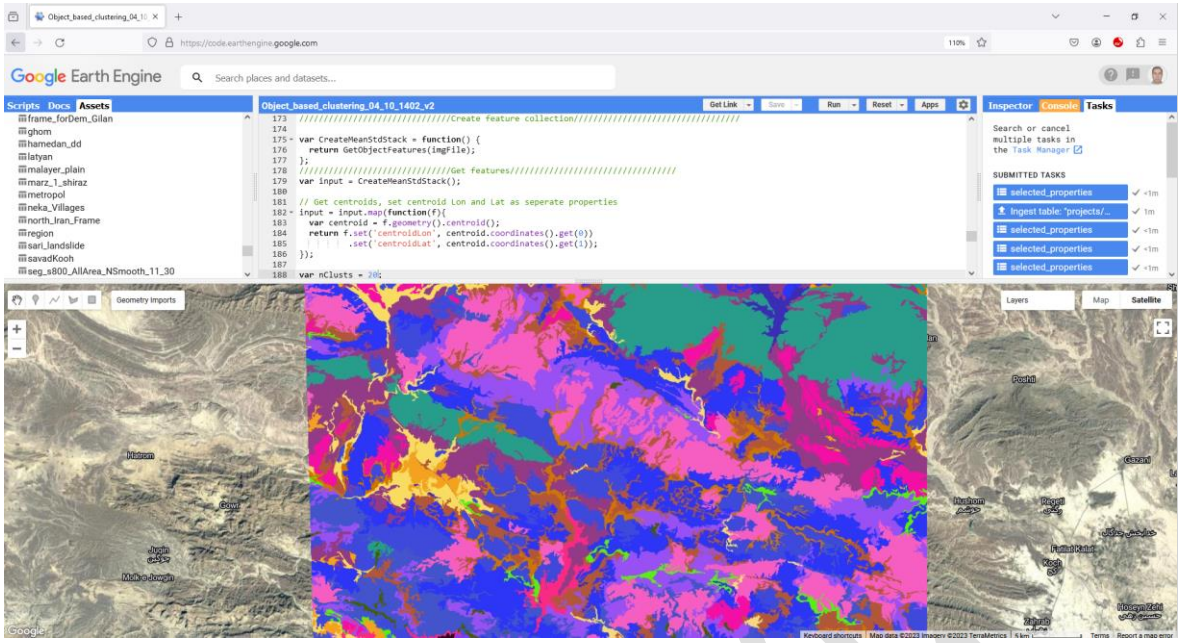


Figure 3-11. Execution of *Google Earth Engine* Programming for Implementing random forest Machine Learning.

Below are some examples of the software environment and related code:

```
// Define the area of interest (Makran region)
var aoi = ee.Geometry.Polygon([/* coordinates of Makran region */]);

// Set the time range
var startDate = '2020-01-01';
var endDate = '2020-12-31';

// Function to mask clouds in Sentinel-2 imagery
function maskS2clouds(image) {
  var qa = image.select('QA60');
  var cloudBitMask = 1 << 10;
  var cirrusBitMask = 1 << 11;
  var mask = qa.bitwiseAnd(cloudBitMask).eq(0).and(
             qa.bitwiseAnd(cirrusBitMask).eq(0));
  return image.updateMask(mask).divide(10000);
}

// Load and preprocess Sentinel-2 data
var s2 = ee.ImageCollection('COPERNICUS/S2_SR')
  .filterBounds(aoi)
  .filterDate(startDate, endDate)
  .filter(ee.Filter.lt('CLOUDY_PIXEL_PERCENTAGE', 20))
  .map(maskS2clouds);

// Load and preprocess Sentinel-1 data
var s1 = ee.ImageCollection('COPERNICUS/S1_GRD')
  .filterBounds(aoi)
  .filterDate(startDate, endDate)
  .filter(ee.Filter.listContains('transmitterReceiverPolarisation', 'VV'))
  .filter(ee.Filter.eq('instrumentMode', 'IW'));

// Load Landsat 8 data
var l8 = ee.ImageCollection('LANDSAT/LC08/C02/T1_L2')
  .filterBounds(aoi)
  .filterDate(startDate, endDate)
  .filter(ee.Filter.lt('CLOUD_COVER', 20));

// Load ASTER data
var aster = ee.ImageCollection('ASTER/AST_L1T_003')
```

```
  .filterBounds(aoi)
  .filterDate(startDate, endDate);

// Load topographic data (SRTM)
var elevation = ee.Image('USGS/SRTMGL1_003').clip(aoi);
var slope = ee.Terrain.slope(elevation);
var aspect = ee.Terrain.aspect(elevation);
// Note: 'sinus' function may not exist in GEE; this line is illustrative
var sinus = ee.Terrain.sinus(elevation);

// Create composites
var s2Composite = s2.median();
var s1Composite = s1.mean();
var l8Composite = l8.median();
var asterComposite = aster.median();

// Calculate indices
var NDCI = s2Composite.normalizedDifference(['B5', 'B4']).rename('NDCI');
var NDFeI = s2Composite.normalizedDifference(['B3', 'B1']).rename('NDFeI');

// Merge all bands
var allBands = s2Composite.addBands(s1Composite)
  .addBands(l8Composite)
  .addBands(asterComposite)
  .addBands(elevation)
  .addBands(slope)
  .addBands(aspect)
  .addBands(NDCI)
  .addBands(NDFeI);

// Perform segmentation
var seeds = ee.Algorithms.Image.Segmentation.seedGrid(20);
var snic = ee.Algorithms.Image.Segmentation.SNIC({
  image: allBands,
  size: 10,
  compactness: 1,
  connectivity: 8,
  neighborhoodSize: 256,
  seeds: seeds
});

var clusters = snic.select('clusters');

// Compute object-level statistics
var objectStats = allBands.addBands(clusters).reduceConnectedComponents({
  reducer: ee.Reducer.mean().combine({
    reducer2: ee.Reducer.stdDev(),
    sharedInputs: true
  }),
  labelBand: 'clusters'
});

// Collect training data
var trainingData = objectStats.sampleRegions({
  collection: trainingSites,
  properties: ['class'],
  scale: 30
});

// Train a Random Forest classifier
var classifier = ee.Classifier.smileRandomForest(50)
  .train({
    features: trainingData,
    classProperty: 'class',
    inputProperties: objectStats.bandNames()
  });

// Classify the image
var classified = objectStats.classify(classifier);

// Post-processing (example: majority filter)
```

```
var filtered = classified.focal_mode({
  radius: 1.5,
  kernelType: 'circle',
  units: 'pixels'
});

// Visualization
var visParams = {
  min: 0,
  max: 5,
  palette: ['red', 'blue', 'green', 'yellow', 'purple', 'orange']
};

Map.centerObject(aoi, 8);
Map.addLayer(filtered, visParams, 'Classified Geological Map');

// Export the result
Export.image.toDrive({
  image: filtered,
  description: 'Makran_Geological_Map',
  scale: 30,
  region: aoi,
  maxPixels: 1e13
});
```

3.5 Satellite Imagery and Digital Elevation Model (DEM)

As previously mentioned, this project utilized a wide range of information and images available in the *Google Earth Engine* database archive (Table 3-5). For satellite imagery, efforts were made to ensure that all images were from the same time period. However, for other data and information such as the emissivity from the ASTER sensor and Digital Elevation Model (DEM) data from the Shuttle Radar Topography Mission (SRTM), the existing archives were used. All of this information and data were processed using their respective algorithms, which are explained in detail in the following sections related to each dataset.

Table 3-5. List of satellite imagery and DEM used in the SUTGMM project.

No.	Data	Type	Acquisition Date	Level of Corrections	Spatial Resolution
1	Sentinel-2	MultiSpectral Instrument (MSI)	July 2019	Geometric correction, atmospheric correction, cloud cover <5%	10 and 20 m
2	Sentinel-1	Dual-polarization C-band Synthetic Aperture Radar (SAR)	July 2019	Calibrated, ortho-corrected product	10, 25, and 40 m
3	Landsat 8	Operational Land Imager (OLI)	July 2019	Atmospherically corrected surface reflectance	30 m
4	ASTER	ASTER (VNIR, SWIR, TIR)	2002	-	15, 30, and 100 m
5	NASA JPL	Shuttle Radar Topography Mission (SRTM)	2002	-	30 m

3.6 Preparation and Processing of Landsat 8 (OLI) Images

For the study area, a single scene from the Operational Land Imager (OLI) sensor of Landsat 8, dated July 2021 (Figure 3-12), was selected. Since the necessary geometric and radiometric corrections had already been applied to these scenes within the *Google Earth Engine* system, a unified image of the study area was prepared for further processing.



Figure 3-12. A Landsat 8 scene covering the study area.

In remote sensing images, processing is conducted to extract two types of information: discrete and continuous data. Generally, the main processing operations on images fall into two categories: Classification and Modeling (e.g., Richards, 2013).

3.6.1 Modeling

The goal of modeling is to extract continuous information. The process involves performing correlation analysis between a specific phenomenon (e.g., geological alterations or mineral contaminations) and the images, ultimately deriving an equation (Lu and Weng, 2007). For example, the relationship between alteration and a satellite band can be expressed as:

$$Y = a \times (DN_i) + b$$

Where Y represents the alteration, DN_i is the digital number of band i, and a and b are coefficients.

In most cases, instead of using the original bands, initial processing such as arithmetic operations (division, subtraction, addition, multiplication) or Principal Component Analysis (PCA) is performed on the images, and then the results are correlated with the phenomena under study (Jensen, 2016).

3.6.2 Arithmetic Operations

Arithmetic operations are common methods in satellite image processing. Among the four basic operations, subtraction and division are used more frequently. For instance, to model geological alterations, different ratios are used depending on the type of alteration. These methods often extract two types of alterations: iron oxide alterations and clay alterations (e.g., Sabins and Ellis, 2020).

Iron oxide alterations exhibit absorption behavior in band 1 of TM images and high reflectance in band 3. Therefore, the ratio of band 3 to band 1 (Ratio (3/1)) is used to enhance iron alterations (Cracknell and Hayes, 2007). Clay alterations have high reflectance in band 5 and low reflectance in band 7 of TM images. Thus, the ratio of band 5 to band 7 (Ratio (5/7)) can highlight areas with clay alteration (van der Meer, 2004).

3.6.3 Spectral Indices

Spectral indices are dimensionless radiometric calculations that usually involve a ratio or linear combination of bands. These calculations do not require additional information; the digital number (DN) values or surface reflectance are sufficient. This method is particularly useful for multispectral data. Band ratioing reduces the effects of topography and shadows and involves the simple division of one band by another.

This method:

- Eliminates topographic effects and shadows.
- Modifies certain noise factors—some are increased, others decreased.
- Reveals differences in brightness levels and clarifies boundaries.

The reflective properties of different phenomena can be examined using their spectral signatures. Based on the spectral properties of the phenomena under consideration, we can decide whether to use this method.

3.6.4 Principal Component Analysis (PCA)

PCA is a well-known method in remote sensing image analysis. Multiple objectives are pursued by employing this technique, such as:

- Dimensionality Reduction: Reducing the data dimensions.
- Change Detection: Identifying changes in multi-temporal images.
- Feature Enhancement: Highlighting specific phenomena.

In this method, the data or image bands are transformed into a new space, and new components replace the original bands (Jolliffe, 2004). In this new space, the correlation between bands is eliminated, and independent bands are created (Richards, 2013).

GeoNexus

3.6.4.1 Feature-Oriented Principal Component Selection (FPCS)

This empirical method, introduced by Crósta in 1989, is often referred to as the Crosta Technique. Instead of using all bands, specific bands are selected, and PCA is performed on them. The phenomenon of interest becomes more prominent in a particular principal component (Crósta and Moore, 1989).

For example, to enhance iron oxide alterations:

- Select bands 1, 3, 4, and 5.
- Perform PCA on these bands.
- The fourth principal component often shows high correlation with iron oxide alterations.

Similarly, for clay alterations:

- Select bands 1, 4, 5, and 7.
- Perform PCA.
- The fourth principal component often shows high correlation with clay alterations.

PCA is used to reduce data dimensions to a smaller number of principal components. In PCA, most information is concentrated in the first few components, while later components contain more noise (Jensen, 2016). This method aggregates information from multiple images into a single image, maximizing the differences in brightness levels (Drury, 2001).

When selecting bands for PCA, it is important to choose bands with less correlation (Lillesand et al., 2015). The less correlated the bands, the more information the combination will contain. Statistical information obtained from PCA can significantly aid in selecting the appropriate identification method. The presence of correlation between bands indicates the existence of shared data or, in other words, data repetition (Eastman, 2006). Therefore, when data fusion aims to obtain maximum possible information, a thorough examination of the correlation matrix (Table 3-6) is necessary (Richards, 2013).

Other important indices include the Eigenvalues and Eigenvectors of the correlation matrix. The Eigenvalue represents the length of each component axis and indicates the amount of information in each component (Table 3-7).

Table 3-6. Sample Correlation Matrix for Bands 1, 2, 3, 4, 5, and 7.

	Band 1	**Band 2**	**Band 3**	**Band 4**	**Band 5**	**Band 7**
Band 1	1					
Band 2	0.97	1				
Band 3	0.93	0.96	1			
Band 4	0.87	0.92	0.97	1		
Band 5	0.77	0.84	0.85	0.85	1	
Band 7	0.75	0.82	0.84	0.84	0.97	1

GeoNeXus

Table 3-7. Sample Eigenvectors from PCA Transformation Between Bands 1, 4, 5, and 7.

Eigenvector	Band 1	Band 4	Band 5	Band 7
PC 1	0.1995	0.3246	0.6323	0.6745
PC 2	0.5757	0.7195	-0.189	-0.339
PC 3	-0.192	0.2523	-0.723	0.6134
PC 4	0.7694	-0.56	-0.203	0.2317

Since there was high correlation among the bands of the OLI images, PCA was performed on these bands to reduce data dimensions and eliminate band correlations. For the study area, bands 1 to 7 of the OLI sensor were transformed into principal components in the *Google Earth Engine* environment. Given that 95% of the information was contained within the first five components, these five components were selected for the next stage. In Figure 3-13, for comparison, the original OLI and the PCA images are presented.

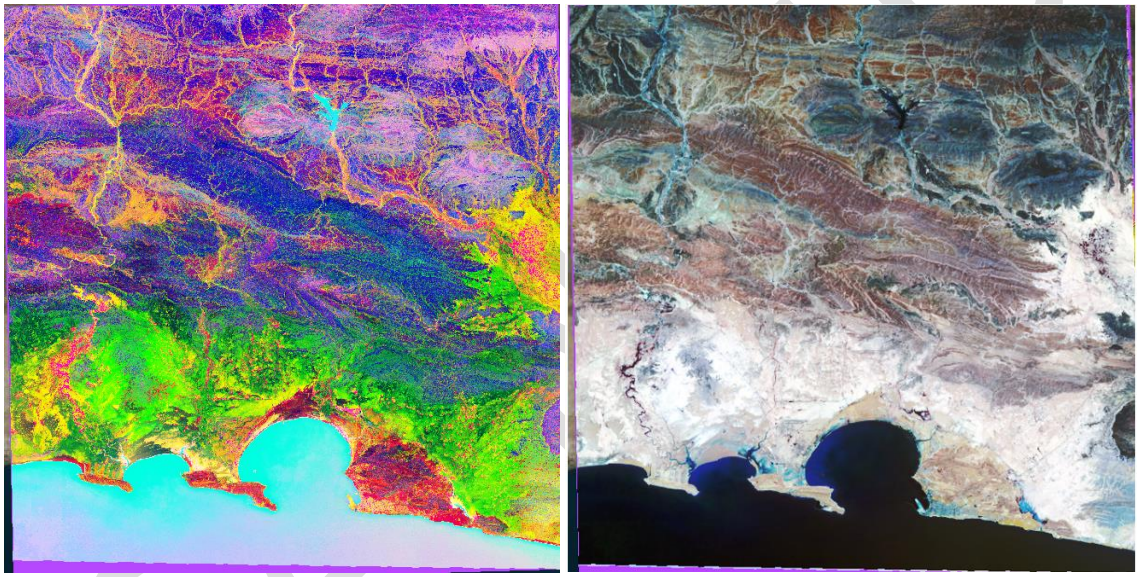


Figure 3-13. Left) Display of principal components 1, 2, and 3 from PCA of Landsat 8 image covering the study area. Right) Unified OLI sensor image from Landsat 8 covering the study area (band combination 2-4-6).

3.7 Preparation and Processing of Sentinel-2 (MSI) Images

The Sentinel-2 satellite captures images with spatial resolutions of 10, 20, and 60 m (Table 3-8). In this project, ten bands from the MSI sensor at 10 and 20 m resolution were used. As explained in the section on processing OLI images, PCA was also applied to these ten bands. Based on the eigenvalues of the components, five components were selected. This processing not only reduced the data dimensions but also increased the contrast and differentiation of geological units (Figure 3-14). These five components were later used in the clustering algorithm to extract geological units.

By applying PCA to both Landsat 8 and Sentinel-2 images, we effectively reduced data redundancy due to high band correlation and enhanced the differentiation of geological units. The principal components obtained were instrumental in subsequent clustering and classification processes to extract detailed geological information from the satellite imagery.

Table 3-8. Technical Specifications of Sentinel-2 Sensor Images.

	Spectral Band	Centre Wavelength (nm)	Band Width (nm)	Spatial Resolution (nm)
B1	Coastal aerosol	443	20	60
B2	Blue (B)	490	65	10
B3	Green (G)	560	35	10
B4	Red (R)	665	30	10
B5	Red-edge 1 (Re1)	705	15	20
B6	Red-edge 2 (Re2)	740	15	20
B7	Red-edge 3 (Re3)	783	20	20
B8	Near infrared (NIR)	842	115	10
B8a	Near infrared narrow (NIRn)	865	20	20
B9	Water vapor	945	20	60
B10	Shortwave infrared/Cirrus	1380	30	60
B11	Shortwave infrared 1 (SWIR1)	1910	90	20
B12	Shortwave infrared 2 (SWIR2)	2190	180	20

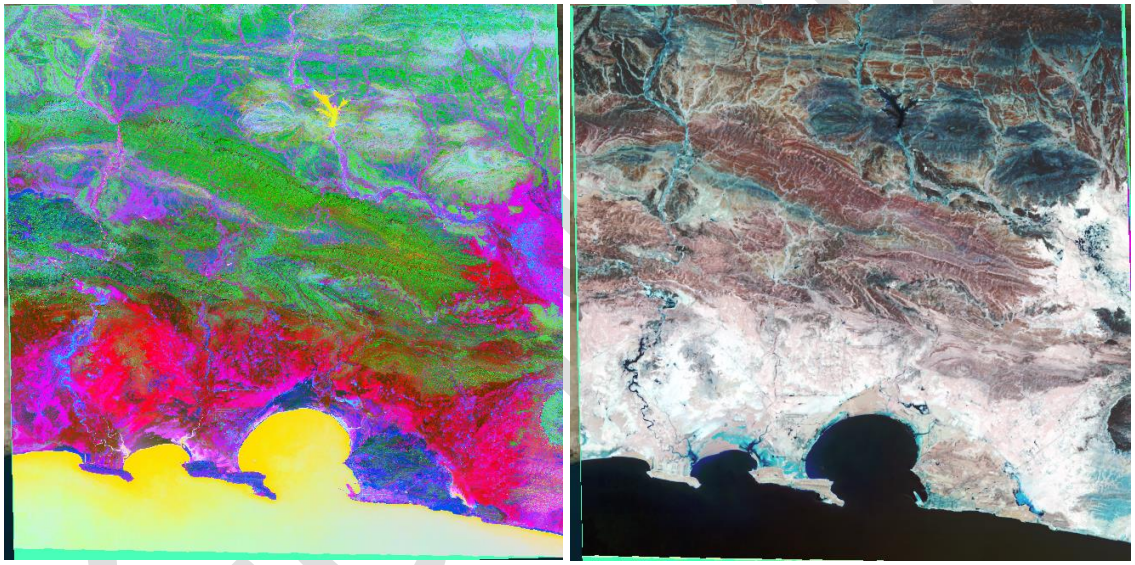


Figure 3-14. Left) Display of principal components 1, 3, and 4 from PCA of Sentinel-2 imagery covering the study area. Right) Unified MSI sensor imagery from Sentinel-2 covering the study area (band combination 2-4-9).

3.8 Preparation and Processing of Sentinel-1 Dual-Polarization C-band SAR Data

Radar images encompass a wide range of geological studies, including topics in engineering geology (such as subsidence and earthquakes), mapping geological structures, and economic geology. Sentinel-1 radar images, due to their dual-mode VV and VH acquisitions (Vertical transmit-Vertical receive and Vertical transmit-Horizontal receive) in the C-band range (wavelengths of 3 to 6 cm), have a very high capability in mapping geological units and faults. Below, a comparison between a radar (VH) image and a Sentinel-2 image clearly demonstrates the ability of this radar imagery to display geological structures. Additionally, in Figure 3-15, the trend of geological structures is seen in a closer view.

In the *Google Earth Engine* environment, by applying mathematical operations on the two images VV and VH (Figure 3-16), the contrast of geological units and structures was enhanced. These processed images were then used as inputs for the learning algorithm in the next stage, significantly impacting the separation of units.

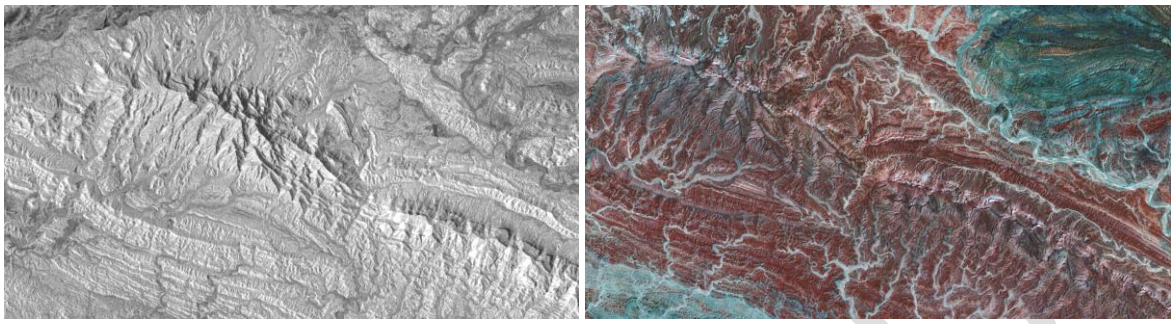


Figure 3-15. Left) Sentinel-1 VH band image within the study area. Right) Unified MSI sensor image from Sentinel-2 within the study area (band combination 2-4-9).

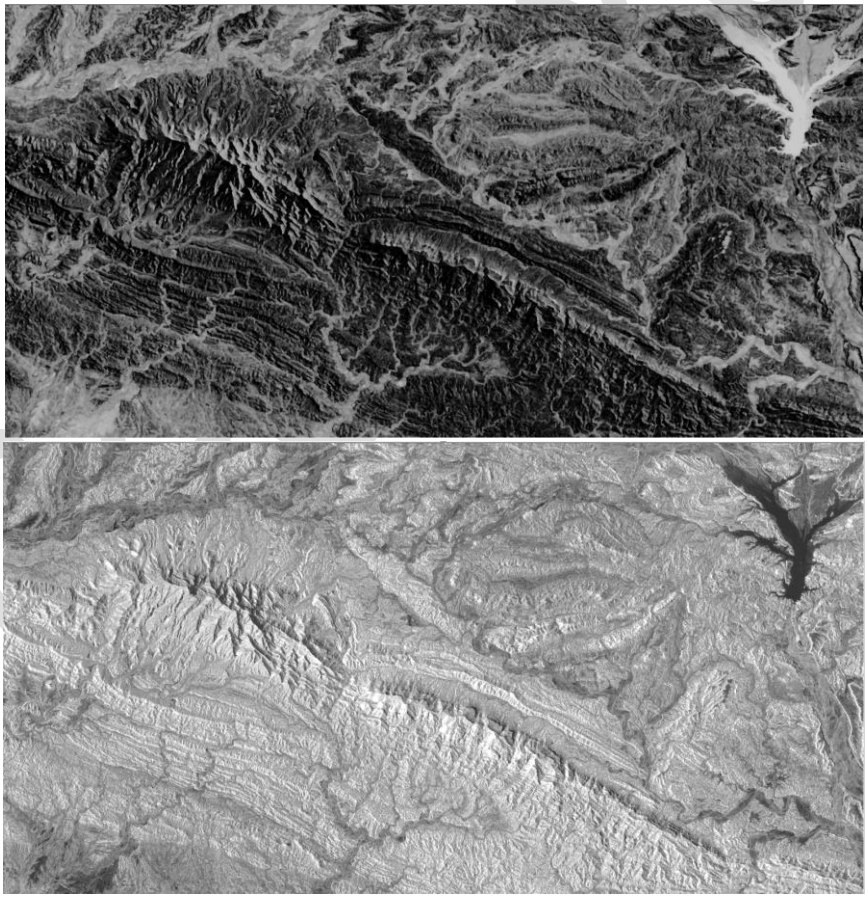


Figure 3-16. Close-up view of the radar images of the eastern part of the area. The upper image corresponds to the VV acquisition, and the lower image corresponds to the VH acquisition.

3.9 Preparation and Processing of SRTM DEM

Among the data that play an important role in identifying and distinguishing geological units—especially when other spectral information is insufficient due to spectral similarity between units—are datasets like the DEM. In this study, elevation data were not used directly; instead, they were processed to derive slope and hillshade information (Figure 3-17).

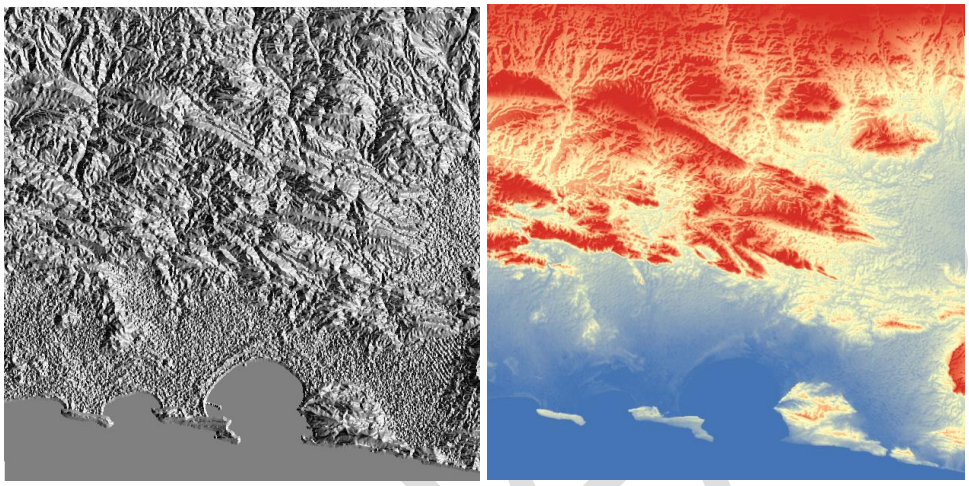


Figure 3-17. Left) Hillshade of the study area. Right) SRTM DEM of the study area.

3.10 Fusion of Optical and Radar Images

As the final step in this section, the process of image fusion between optical images (Sentinel-2) and products derived from radar images (Sentinel-1) was performed to enhance the tectonic structures of the area and extract faults and other structural information. The greatest advantage of this fusion process is creating an image that contains both background information and prominently enhanced structural details (Figure 3-18). This fused image served as the basis for extracting geological structures.

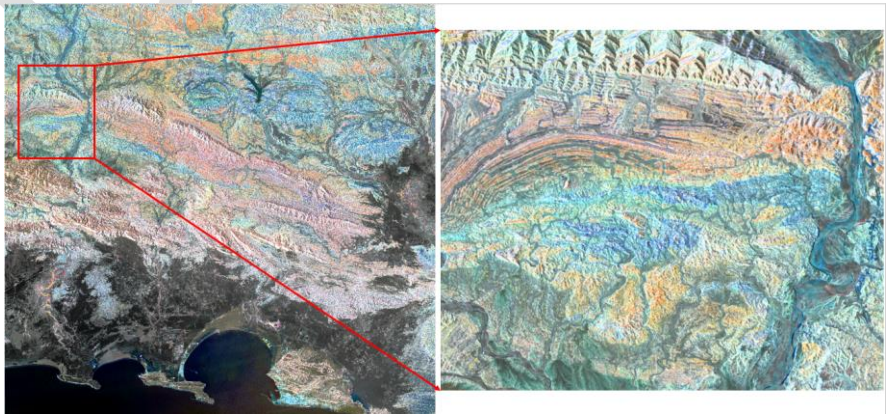


Figure 3-18. Fusion of optical satellite imagery (Sentinel-2) and radar images (Sentinel-1) to enhance and expose tectonic structures.

3.11 Object-Based Process for Geological Mapping of Mineral Potential

In extracting geological information—whether identifying lithological units or promising areas—two general approaches can be employed: pixel-based and object-based methods. In the pixel-based approach, the processing unit is the pixel, and the spectral information of the pixels is utilized. Advantages of this classification include low computational cost and the feasibility of applying it to large areas (Jensen, 2016). However, limitations and disadvantages of this method include its incompatibility with real-world entities and their behavior; in other words, on the ground, there is no entity called a pixel—we deal with land units (Blaschke, 2010). The second limitation pertains to the type and number of features used. In pixel-based methods, features must be homogeneous and from a single source (for example, all inputs are spectral bands), which restricts the use of pixel-based methods (Lu and Weng, 2007).

To mitigate this problem, the object-based classification technique is employed. In object-based classification, instead of using pixels as the smallest classification unit, image objects are used. An object in the image is a homogeneous region where pixels have similar characteristics and corresponds to a geographical entity in the real world (Blaschke et al., 2014). In object-based classification, features are calculated for each segment, and classification is performed at the object level.

In the object-based process of extracting geological maps (lithological units), the first step is to perform segmentation on the images. Typically, in the segmentation phase, the image with the highest spatial accuracy is used. Therefore, in this project, higher spatial resolution images are utilized (Drăguţ et al., 2014).

One of the critical and fundamental aspects of image segmentation is determining the influence of scale and shape in this process. The scale parameter is determined based on the variance within segments; when a lower scale number is set, it means that units with higher homogeneity are grouped together, resulting in smaller segments (Baatz and Schäpe, 2000).

3.12 Image Segmentation

An object can be defined as an image entity consisting of a group of pixels that have similarity in grayscale values within a specific range and are connected in shape, geographical location, and size to real-world objects (Blaschke et al., 2014). Spectrally, objects are homogeneous regions in the image with defined boundaries. Segmentation is used to identify these homogeneous regions. It is one of the most important parts of object-based classification, and the results greatly depend on how the image is segmented (Hay and Castilla, 2008). The two main strategies in segmentation are:

- Top-down segmentation
- Bottom-up segmentation

The bottom-up strategy builds larger image segments by merging smaller ones. Multiscale segmentation utilizes this strategy and is the more common method. It starts merging from individual pixels and iteratively combines existing objects. The scale parameter controls adjacent pixels and thus the growth of segments or image objects. Shape and tone criteria are additional parameters in multiscale segmentation that, together, form the homogeneity criterion. In geology,

both spectral and spatial criteria are important. The scale parameter controls the maximum standard deviation of homogeneity for each object. Lower scales enforce higher homogeneity, resulting in smaller objects, while higher scales allow less homogeneity, producing larger objects (Baatz and Schäpe, 2000).

For example, a segment consists of several pixels where these pixels have high similarity in terms of spectra, color, geometry, shape, and other features. This method is considered the most suitable for separating homogeneous areas and selecting them as objects (Drăguţ et al., 2014). By choosing different scales, compactness, and shapes, varied results can be achieved. A disadvantage of this method is slower processing speed. Nonetheless, the multiscale model is widely regarded as the most popular.

In multiscale segmentation algorithm (Baatz and Schäpe, 2000), scale plays a crucial role in determining segments and influences characteristics like spectral texture and shape. Using region-merging techniques, for a certain number of image segments, average heterogeneity is minimized, and their homogeneity is maximized. As a result, the segmentation algorithm is controlled by a scale factor and a heterogeneity criterion. The scale factor indirectly relates to the average size of segments to be identified. The heterogeneity criterion controls the merging process and is calculated using spectral layers (e.g., multispectral images). It includes two distinct and unique features: color and shape. Color refers to spectral convergence, while shape considers the semantic features of objects and is divided into two unique features: smoothness and compactness. Optimal segmentation parameters depend on the scale and nature of the features to be identified. Once an appropriate scale is identified, the color and shape criteria are adjusted to refine the shape of image segments (Blaschke et al., 2014). Advantages of this method include its applicability to various data types and suitable performance with large image datasets (Blaschke, 2010).

3.12.1 Determining the Appropriate Segmentation Scale in the Multiscale Method

Given that the local variance of spectral heterogeneity of segments in an image is a suitable criterion for adjusting segment sizes in proportion to scale changes, this criterion is used for this purpose. The mechanism of this method is as follows: if the spatial power of the image is smaller than the desired segments, most measured values in the image have high correlation with their neighbors, resulting in decreased local variance. Additionally, if the size of the segments is approximately equal to the spatial resolution of the pixels, the likelihood of similarity between neighboring pixels decreases, leading to an increase in local variance. Local variance essentially extracts spatial autocorrelation, which is one of the fundamental characteristics of an image.

When the size of the segments matches the segments in the real world, the standard deviation increases continuously until this match occurs. At this point, the standard deviation remains constant, and as a result, the local variance increases. When plotting the graph of local variance against the scale parameter, we will have an ascending graph with breakpoints that indicate optimal scales where meaningful segmentation is performed.

In this method, to demonstrate how local variance behaves during the transition from one scale to another, the Rate of Change (ROC) criterion is used. The equation below shows how to calculate the Rate of Change:

GeoNexus

$$ROC = \left[\frac{L_{lv} - (L_{lv} - 1)}{L_{lv} - 1}\right] \times 100$$

Where L_{lv} represents the local variance at the desired levels, and $(L_{lv} - 1)$ represents the local variance at lower scales. In this method, it is assumed that peaks in the ROC graph indicate scales where the image can be segmented most appropriately relative to the data characteristics.

3.12.2 Segmentation of the Images within the Study Area

Segmentation divides the image into separate regions. In other words, segmentation means grouping image elements based on a specific homogeneity criterion. The first step in object-based classification is image segmentation and producing meaningful segments. In this research, due to the widespread use of the multiscale segmentation method, this algorithm was used in the segmentation process (Baatz and Schäpe, 2000).

As mentioned earlier, when using this algorithm, considering optimal segmentation parameters appropriate for the data is crucial. These parameters include selecting the number of input bands, scale number, weights of spectral and shape heterogeneities, and weights of smoothness and compactness parameters (Blaschke, 2010). Due to the absence of ideal parameters for extracting various features, adjustments must be made based on the data used and the desired features to set the best values for these parameters so that the boundaries of the segments produced from image segmentation match the segments in the real world (Drăguţ et al., 2014). For this purpose, images must be segmented in such a way that they can cover different segments in all shapes and sizes (Blaschke et al., 2014).

3.12.3 Preparing Initial Layers for Segmentation

In the object-based process of geological mapping, the first step is to create segmentation on the images. Typically, in the segmentation phase, the image with the highest spatial resolution is used. Therefore, in this project, Sentinel-2 images with ground resolutions of 10 and 20 m were introduced to the *eCognition* software for segmentation. At this stage, the multiscale method was used for segmentation.

3.12.4 Determining Segmentation Parameters

The first step in multiscale segmentation is selecting weights for the scale parameter, spectral and shape heterogeneities, and smoothness and compactness parameters. In choosing these parameters, the most important factor is the amount of internal spectral heterogeneity of the objects. In geology, different classes generally have high internal spectral heterogeneity (Blaschke, 2010). The choice of weight for the compactness parameter depends on the type of dominant feature in the image in terms of its shape and size. The shape parameter expresses the regularity of the geometry of image features, while the compactness parameter expresses the irregularity of features (Baatz and Schäpe, 2000).

GeoNexus

In this research, changes in the local variance of spectral heterogeneity of segments were used to select the scale parameter. To adjust other parameters, the shape parameter was set to 0.4 and the compactness parameter to 0.4 through trial and error (Drăguţ et al., 2014).

The scale parameter controls the merging of adjacent pixels and thus the growth of segments or image objects. In this algorithm, image pixels are considered initial objects, and the growth of these objects continues until the smallest heterogeneity exceeds the defined scale. In object-based classification, identifying the best scale is of great importance. The best scale for extracting each object is the largest scale that, with the minimum number of segments, has the highest conformity with the real world. Also, the larger the segments, the faster the processing speed. Another advantage of the largest possible scale is the reduction of noise in the classification results (Baatz et al., 2004).

As mentioned earlier, the local variance of spectral heterogeneity of closely related segments in the image is a suitable criterion for adjusting the size of segments in proportion to scale changes; therefore, it was used in designing the optimal scale. For this purpose, image segmentation was performed iteratively from the smallest scale to higher scales in the *eCognition* software, and the local variance for each scale was calculated. As segments grow, the variance increases continuously until they match the real world. Thresholds in the rate of change of local variance in the created graph indicate the scale at which the image can be segmented in its most appropriate state (Lillesand et al., 2015).

3.12.5 Selecting the Optimal Scale in Segmentation

Nine bands of Sentinel-2 images were used in the segmentation. The results show the changes in the local variance of spectral heterogeneity of segments against scale. By interpreting this graph, it can be observed that at lower scales, with the increase in segment size, the local variance also increases suddenly, and the rate of change follows an inverse trend. This pattern refers to the transition from the pixel state to the smallest meaningful segment present in the image. The criterion for determining the first scale is the first breakpoint in the change graph after a sharp and continuous decline.

With increasing scale, the rate of change graph displays sudden fluctuations between peaks and troughs, while the local variance graph becomes slightly smoother and flatter. Theoretically, peaks in the rate of change curve indicate levels where the local variance increases due to the matching of segments to their corresponding features in the real world. However, it should be noted that changes occurring due to background segmentation also cause peaks in the rate of change graph.

Considering this, in the current graph, the most prominent peaks compared to their neighbors occur at scales 150, 300, 500, and 800. At scales greater than 800, larger segments are created, which is not desirable for us. Based on experience, scale 300 is suitable for participating in the process of creating image segments.

The next step after selecting the scale parameter is to choose the weights of the color and compactness parameters. Considering the selected scale and performing trial and error, the best weights were found to be 0.4 for the compactness parameter and 0.4 for the shape parameter. The output of this stage is the segmentation map of lithological units. Information from all multi-source

GeoNexus

and multi-scale resources is extracted based on the segments of lithological units. Below are the changes in local variance and the specific parameter adjustment window.

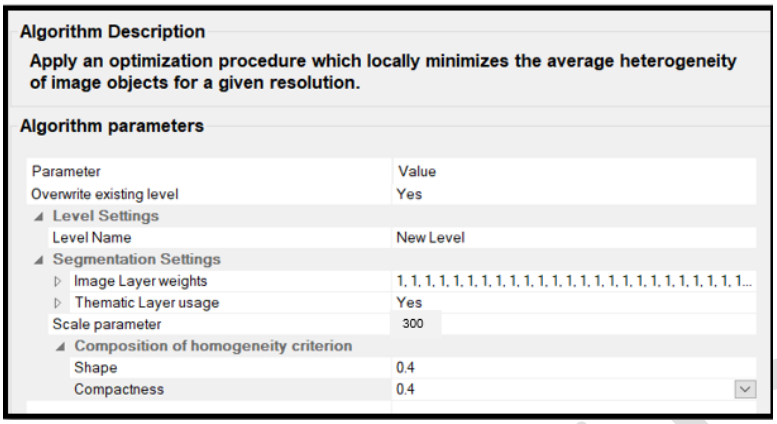


Figure 3-19. Parameter adjustment window for segmentation in *eCognition* Software.

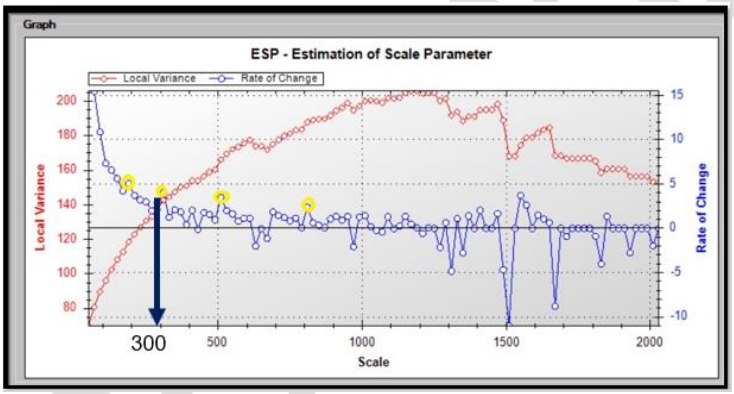


Figure 3-20. Changes in local variance and rate of change at different scales.

3.12.6 Image Segmentation for Preparing a Preliminary Geological Map

At this stage, based on the previous explanations, adjustments of scale parameters and local variance, and expert opinions, a scale of 300 was determined. In Figure 3-21 and Figure 3-22, parts of the study area along with the segmentation overlaid on it are shown. It is clearly visible that the separation has been done effectively.

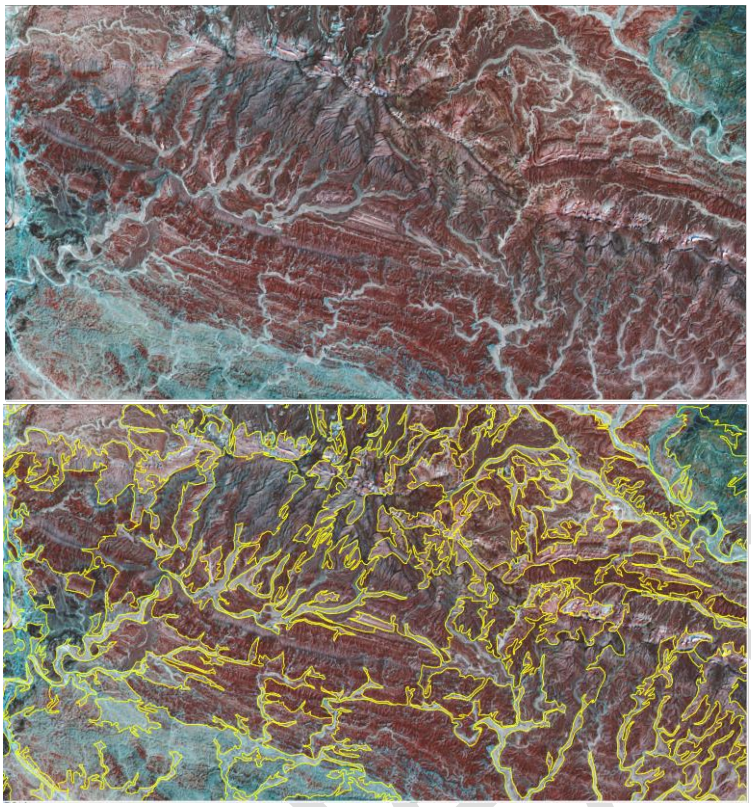


Figure 3-21. A part of the study area for comparison. The upper image shows the Sentinel-2 band combination, and the lower image shows the segmentation overlaid on it.

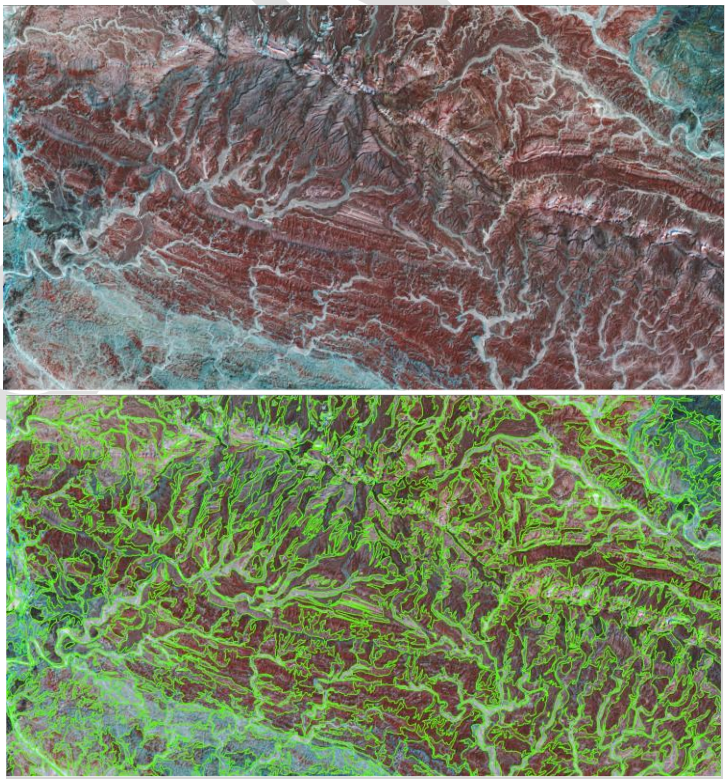


Figure 3-22. Another part of the study area for comparison. The upper image shows the Sentinel-2 band combination, and the lower image shows the segmentation overlaid on it.

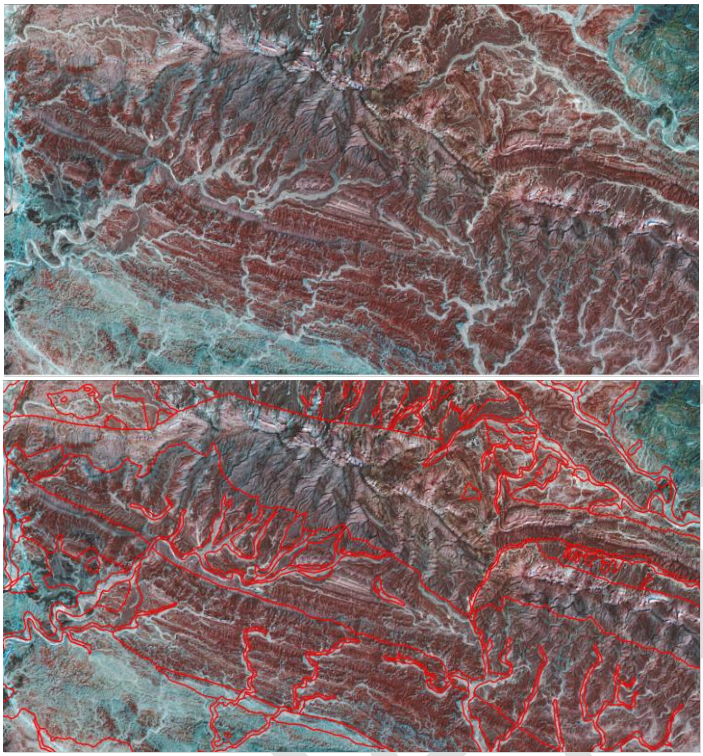


Figure 3-23. A part of the study area for comparison with the existing geological map. The upper image shows the Sentinel-2 band combination, and the lower image shows the boundaries of the prepared geological units overlaid on it.

3.13 Creation of the Initial Geological Map

After preparing the segmentation of the study area, the next step is to create a preliminary geological map based on the features of the segments. The definition of the initial number of classes is based on reviewing existing geological maps, previous projects and studies, and expert knowledge. At this stage, spectral and non-spectral features related to each segment, which contribute to their differentiation and the production of the initial map, are defined.

As previously mentioned, one of the advantages of object-based processing is the ability to use features from various spectral and non-spectral sources. For this reason, in this project, a diverse range of spectral and non-spectral features were used as listed in the table below:

Table 3-9. List of variables used in the processing.

Index	Main Layer/Image	Extracted Features	Description
1	ASTER images (14 bands including VNIR, SWIR, TIR)	Mean of Band 1	VNIR
2		Mean of Band 2	VNIR
3		Mean of Band 3N	VNIR
4		Mean of Band 4	SWIR
5		Mean of Band 5	SWIR
6		Mean of Band 6	SWIR
7		Mean of Band 7	SWIR
8		Mean of Band 8	SWIR

9		Mean of Band 9	SWIR
10		Standard Deviation of Band 1	VNIR
11		Standard Deviation of Band 2	VNIR
12		Standard Deviation of Band 3N	VNIR
13		Standard Deviation of Band 4	SWIR
14		Standard Deviation of Band 5	SWIR
15		Standard Deviation of Band 6	SWIR
16		Standard Deviation of Band 7	SWIR
17		Standard Deviation of Band 8	SWIR
18		Standard Deviation of Band 9	SWIR
19		Mean Emissivity of Band 10	TIR
20		Mean Emissivity of Band 11	TIR
21		Mean Emissivity of Band 12	TIR
22		Mean Emissivity of Band 13	TIR
23		Mean Emissivity of Band 14	TIR
24	Sentinel-2 VNIR & SWIR images	Mean of Band 2	VNIR
25		Mean of Band 3	VNIR
26		Mean of Band 4	VNIR
27		Mean of Band 5	SWIR
28		Mean of Band 6	SWIR
29		Mean of Band 7	SWIR
30		Mean of Band 8	SWIR
31		Mean of Band 11	SWIR
32		Mean of Band 12	SWIR
33		Standard Deviation of Band 2	VNIR
34		Standard Deviation of Band 3	VNIR
35		Standard Deviation of Band 4	VNIR
36		Standard Deviation of Band 5	SWIR
37		Standard Deviation of Band 6	SWIR
38		Standard Deviation of Band 7	SWIR
39		Standard Deviation of Band 8	SWIR
40		Standard Deviation of Band 11	SWIR
41		Standard Deviation of Band 12	SWIR
42	Digital Elevation Model (DEM)	Mean Elevation	
43		Mean Slope	
44		Mean Aspect	
45	Sentinel-1 Radar Satellite (VV and VH bands)	Mean VV Band	
46		Mean VH Band	
47		Standard Deviation of VV Band	
48		Standard Deviation of VH Band	
49		Mean of SUM Product	This layer is the result of processing VV and VH bands
50		Standard Deviation of SUM Product	This layer is the result of processing VV and VH bands
51		Mean of Divide Product	This layer is the result of processing VV and VH bands
52		Standard Deviation of Divide Product	This layer is the result of processing VV and VH bands
53		Mean of Subtract Product	This layer is the result of processing VV and VH bands
54		Standard Deviation of Subtract Product	This layer is the result of processing VV and VH bands
55	Object-based segment information	Mean Asymmetry	These features can only be used in the object-based model
56		Mean Compactness	These features can only be used in the object-based model
57		Mean Border Index	These features can only be used in the object-based model

GeoNexus

58		Mean Curvature	These features can only be used in the object-based model
59		Mean Main Direction	These features can only be used in the object-based model
60		Mean Shape Index	These features can only be used in the object-based model
61		Geological Indices	Used Sentinel-2 images; 20 geological indices were defined for the initial units and extracted from Sentinel-2 images. In the next phase, using feature reduction methods like PCA, seven components were used
62			
63			
64			
65			
66			
67			
68	Landsat 8 VNIR & SWIR images	Mean of Band 2	
69		Mean of Band 3	
70		Mean of Band 4	
71		Mean of Band 5	
72		Mean of Band 6	
73		Mean of Band 7	

After these 73 features were defined for each segment (Table 3-9), in the next stage, using random forest machine learning methods and with the help of 823 samples, the process of separating geological units was carried out. The machine learning method used will be explained in the following sections.

3.14 Machine Learning

Machine learning is a growing technology that enables processing systems to automatically learn from historical data. It uses various algorithms to build mathematical models and make predictions based on existing data or observational information (Alpaydin, 2020). Currently, these algorithms are used for various tasks such as medicine, earth sciences, finance and business topics, face recognition, speech recognition, and many other areas (Jordan and Mitchell, 2015).

In the real world, humans can learn everything from their past experiences due to their ability to learn. Today, computational systems or machines work according to our instructions. But can a machine also learn from past experiences or historical data like a human? This is where the role of machine learning comes into play (Figure 3-24) (Russell and Norvig, 2021).

Machine learning enables systems to continuously update and improve from new data, enhancing the accuracy and efficiency of predictions and decision-making (Kelleher and Tierney, 2018). These capabilities are of particular importance in today's world, especially in scientific and industrial fields, helping researchers and engineers tackle more complex problems.

GeoNexus

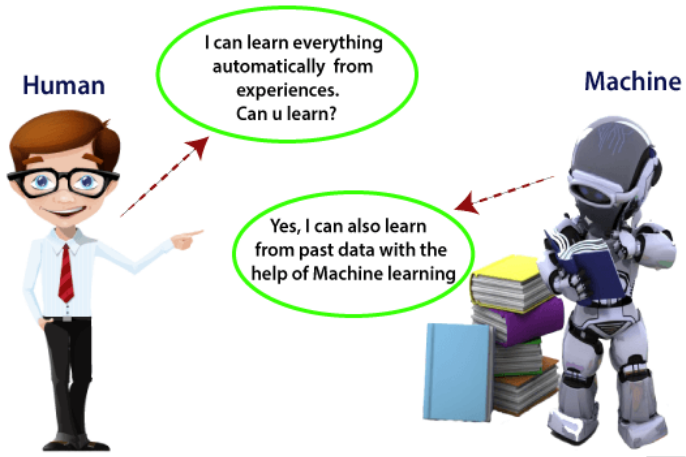


Figure 3-24. The similarity between humans and computers in learning.

Machine learning is introduced as a subset of artificial intelligence and primarily deals with the development of algorithms that allow computers to learn from data and past experiences on their own. The term "machine learning" was first introduced by Arthur Samuel in 1959:

"*Machine learning enables machines to learn automatically from data, improve performance based on experiences, and predict implicit outcomes.*"

Machine learning algorithms build a mathematical model with the help of historical data known as training data, which helps in prediction or decision-making. Machine learning brings together computer science and statistics to create predictive models. It builds algorithms that learn from or utilize historical data. The more information we provide, the better it will perform. A machine has the ability to learn by acquiring more data and can improve its performance.

3.14.1 How Does a Machine Learn?

A machine learning system learns from historical data, builds predictive models, and whenever it receives new data, it predicts the output (Figure 3-25). The accuracy of the predicted output depends on the amount of data because a huge volume of data helps to build a better model that can predict the output more accurately. Suppose we have a complex problem where we need to make predictions. Instead of writing code for it, we just need to feed data to general algorithms, and with the help of these algorithms, the machine builds logic according to the data and predicts the output. Machine learning has changed our way of thinking about problems.

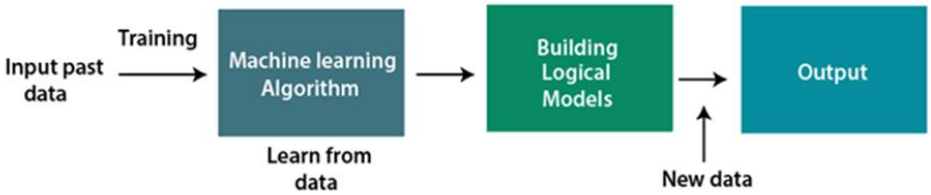


Figure 3-25. Block diagram explaining the working of a machine learning algorithm.

3.14.2 Features of Machine Learning

1. Pattern recognition: Machine learning uses data to identify different patterns in a dataset.
2. Self-improvement: It can learn from past data and improve automatically.
3. Data-driven technology: It is a technology that relies heavily on data.
4. Similarity to data mining: Machine learning is very similar to data mining as it also deals with huge volumes of data.

3.14.3 The Need for Machine Learning

The need for machine learning is increasing day by day. The reason we need machine learning is that it is capable of performing tasks that are very complex for a human to execute directly. Humans have limitations because we cannot manually access huge volumes of data, so for this, we need some computer systems, and this is where machine learning comes in to make things easier for us.

We can train machine learning algorithms by providing them with a large amount of data and allowing them to explore the data, build models, and automatically predict the required output. The performance of a machine learning algorithm depends on the amount of data and can be determined by the cost function. With the help of machine learning, we can save time and money.

The importance of machine learning can be easily understood by its use cases. Currently, machine learning is used in self-driving cars, recognition and separation of land patterns (geological units and mineral potential areas), cyber fraud detection, and face recognition. Various top companies like Netflix and Amazon build machine learning models that use vast amounts of data to analyze user interests and recommend products accordingly.

Below are some key points that show the importance of machine learning:

- Rapid increase in data production: Such as satellite images and other ground data.
- Solving complex problems: That are difficult for humans.
- Decision-making in Earth computations: Making informed decisions in various sectors of earth sciences.
- Discovering hidden patterns: Finding hidden patterns and extracting useful information from ground data.

3.14.4 Classification Algorithms in Machine Learning

At a broad level, machine learning can be classified into three types (Figure 3-26):

1. Supervised learning
2. Unsupervised learning
3. Reinforcement learning

GeoNexus

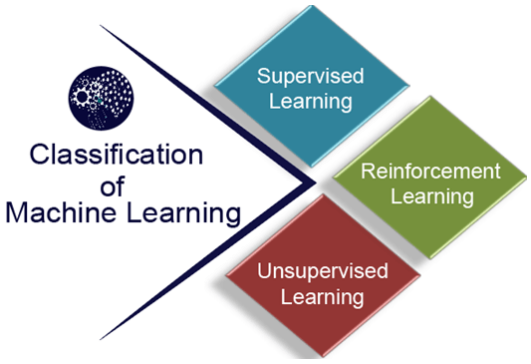


Figure 3-26. Types of learning methods in machine learning algorithms.

3.14.4.1 Supervised learning

Supervised learning is a type of machine learning method in which we provide the machine learning system with labeled sample data to train it, and accordingly, it predicts the output. The system uses labeled data to build a model to understand the dataset and learn about each data point. After completing training and processing, we test the model by providing another set of samples to check whether it predicts the output accurately or not. The goal of supervised learning is to establish a relationship between input data and output data. Supervised learning is based on supervision and is like when a student learns under the guidance of a teacher.

Supervised learning can further be classified into two categories of algorithms:

- Classification
- Regression

3.14.4.2 Unsupervised Learning

Unsupervised learning is a learning method where the machine learns without labeled training data. Training is provided to the machine with datasets that are neither labeled nor classified or categorized, and the algorithm has to act on that data without any supervision. The goal of unsupervised learning is to categorize the input data into groups of objects with similar patterns. In unsupervised learning, we do not have predetermined outcomes. The algorithm tries to find useful patterns from a huge volume of data.

3.14.4.3 Reinforcement Learning

Reinforcement learning is a feedback-based learning method where a learning agent receives a reward for each correct action and a penalty for each incorrect action. The agent automatically learns from this feedback and improves its performance. In reinforcement learning, the agent interacts with the environment and explores it. The algorithm aims to improve its performance through rewards.

GeoNexus

3.14.5 Random Forest

Random forest is a widely used machine learning algorithm that belongs to supervised learning techniques. It can be used for classification and regression problems in Machine Learning (ML) (Breiman, 2001). This method is based on the concept of ensemble learning, which is a process of combining multiple classifiers to solve a complex problem and improve the model's performance (Zhou, 2012).

Random forest is considered a supervised learning algorithm. As its name suggests, this algorithm builds a forest randomly. The constructed "forest" is actually a group of decision trees (Figure 3-27). The work of building a forest using trees is often done by the bagging method. The main idea of the bagging method is that a combination of learning models increases the overall results of the model (Breiman, 1996). Simply put, random forest builds multiple decision trees and merges them together to obtain more accurate and stable predictions (Figure 3-28). One of the advantages of random forest is its applicability to both classification and regression problems, which constitute the majority of current machine learning systems (Liaw and Wiener, 2002).

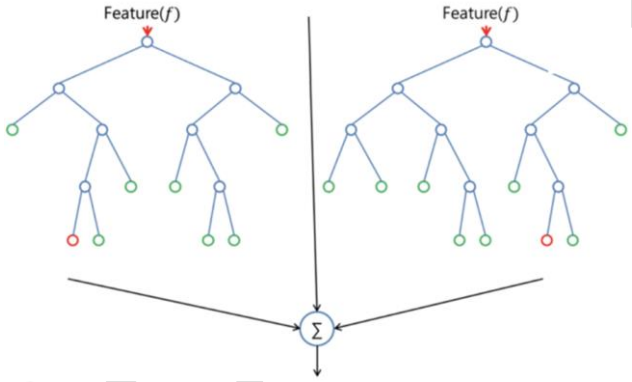


Figure 3-27. Schematic diagram of random forest structure.

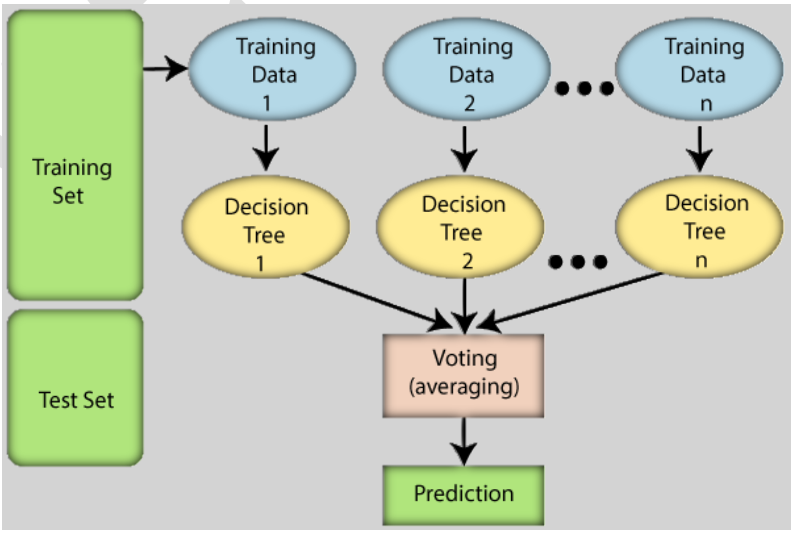


Figure 3-28. A more complete schematic diagram of random forest structure.

3.14.5.1 Assumptions in Random Forest

Since random forest combines multiple trees to predict the class of the dataset, some decision trees may predict the correct output, while others may not. But together, all the trees predict the correct output. Therefore, there are two assumptions for better classification with random forest:

1. Presence of actual values: There should be some actual values in the feature variables of the dataset so that the classifier can predict accurate results rather than a guessed result.
2. Low correlation between trees: The predictions of each tree should have very low correlations.

Below are some points that explain why we should use the random forest algorithm:

- Less Training Time: It requires less training time compared to other algorithms.
- High Accuracy: It predicts output with high accuracy even for large datasets that it runs effectively on.
- Handles Missing Data: It can maintain accuracy even when a large proportion of the data is missing.

Random forest works in two phases: first, it creates the random forest by combining N decision trees, and second, it makes predictions for each tree created in the first phase. The working process can be explained in the following steps and diagram:

Step 1: Randomly select K data points from the training set.

Step 2: Build decision trees associated with the selected data points (subsets).

Step 3: Repeat Steps 1 and 2.

Step 4: For new data points, find the predictions of each decision tree and assign the new data points to the category that wins the majority vote.

Hyperparameters in random forest are used to increase the model's predictive power or to make it faster.

1. Increasing Predictive Power
   - n_estimators: This hyperparameter is the number of trees that the algorithm builds before taking the maximum voting or averages of predictions. Generally, more trees increase performance and make predictions more stable but slow down computations.
   - min_samples_leaf: As the name suggests, this hyperparameter specifies the minimum number of leaves required to split an external node.
2. Increasing Model Speed
   - n_jobs: This hyperparameter tells the engine how many processors it is allowed to use. If its value is 1, it can only use one processor. The value -1 means there is no limit.
   - random_state: Makes the model's output reproducible. When the model has a fixed value for random_state, and if given the same hyperparameters and training data, it will always produce the same results.
   - oob_score: Also known as out-of-bag sampling, this is a method for cross-validation in Random Forest. In this sampling, about one-third of the data is not used for training

GeoNexus

the model and is used to evaluate its performance. These samples are called bag samples. This approach is very similar to the leave-one-out validation method but has almost no computational burden.

3.14.5.2 Advantages of Random Forest

- Versatility: Random forest can perform both classification and regression tasks.
- Handles High Dimensionality: It can manage large datasets with high dimensionality.
- Prevents Overfitting: It increases the accuracy of the model and prevents the overfitting problem.

3.14.6 Random Forest in Extracting Lithological Units

In this project, since the object-based approach was used in image processing and classification, the training samples were selected from among image segments. It should be noted that in the process of converting the Sentinel-2 image, the entire area was first segmented into about 9,000 homogeneous segments based on segmentation parameters. Then, based on Table 3-5 (the images used) and Table 3-9 (the variables extracted from them), 73 spectral, topographic, and shape variables were determined as input features for each segment.

Table 3-10. Frequency of class segments and number of training samples.

No.	Geological Units and Two Classes of Water Bodies and Vegetation Cover	Frequency of Each Class	30% of Each Class Frequency for Training
1	$M\text{-}Pl^{m, s}$	863	259
2	$M\text{-}Pl^{m, s, cong}$	593	178
3	$M^{s, silt}$	848	254
4	$M^{sh, s}$	1,228	368
5	$Olig\text{-}M^{s, sh, cong}$	51	15
6	$Olig\text{-}M^{sh}$	220	66
7	$Olig\text{-}M^{sh, s}$	471	141
8	$Pl\text{-}Pe^{cong.s. silt}$	786	236
9	$Pl^{l.silt. s}$	330	99
10	Pl^{silt}	288	86
11	$Pl^{silt.cong}$	409	123
12	Q^{a}	958	287
13	Q^{al}	825	248
14	Q^{b}	158	47
15	Q^{f}	637	191
16	Q^{sd}	66	20
17	Vegetation	177	53
18	Water	51	15
	Total	**8,959**	**2,688**

GeoNexus

In the classification process with the help of Random Forest, the goal was to extract 18 classes, including 16 lithological units and two classes of water and vegetation cover. Based on statistical criteria, usually 30% of the samples are used to train the algorithm, and then the algorithm classifies the remaining segments based on the training samples (Figure 3-28). Accordingly, and as shown in Table 3-10, out of 8,959 samples, 2,688 samples were randomly selected based on the frequency of each class (Figure 3-29).

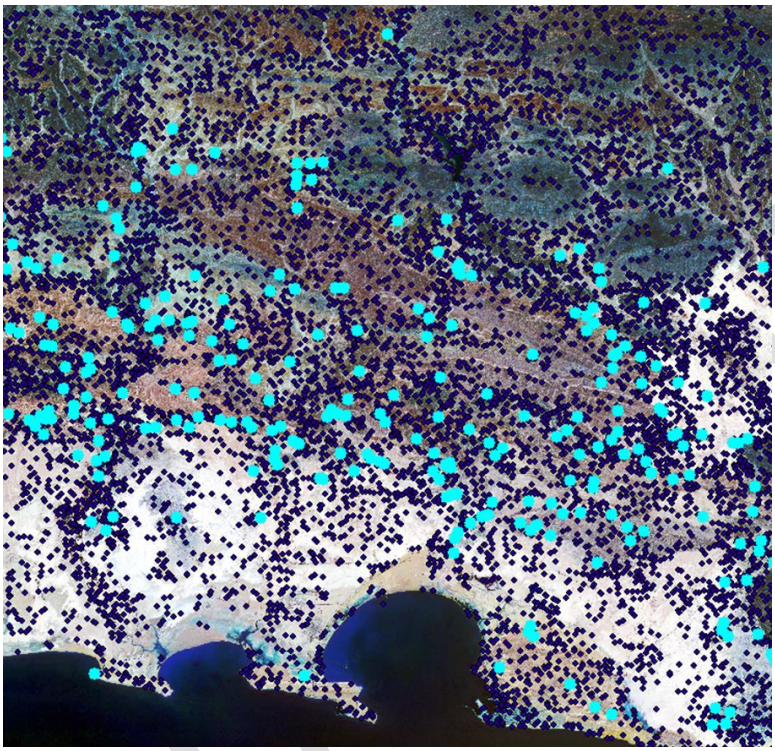


Figure 3-29. Examples of selected points (light blue circles) for the M-Pl^{m,s} lithological unit.

Then, in the process of training the random forest algorithm, 70% of these 30% samples were used for training and 30% for testing the method. For example, for the lithological unit M-Pl^{m,s}, out of 259 samples, 181 samples were used for training and 78 samples were used for evaluating the model. This process was carried out similarly for the remaining units. Below is the sample code executed for random forest machine learning:

```
% Load and prepare your data
% Assuming X is your feature matrix and Y is your target vector with 18 classes
% X should be a matrix where each row is a sample and each column is a feature
% Y should be a vector of class labels (1 to 18)

% Split data into training and testing sets
cv = cvpartition(size(X,1),'HoldOut',0.3);
X_train = X(cv.training,:);
Y_train = Y(cv.training);
X_test = X(cv.test,:);
Y_test = Y(cv.test);

% Train Random Forest model
nTrees = 100; % Number of trees in the forest
```

```
rf_model = TreeBagger(nTrees, X_train, Y_train, 'Method', 'classification');

% Make predictions on the test set
[Y_pred, scores] = predict(rf_model, X_test);

% Convert predictions from cell array to numeric array
Y_pred = str2double(Y_pred);

% Calculate accuracy
accuracy = sum(Y_pred == Y_test) / length(Y_test);

% Calculate confusion matrix
conf_matrix = confusionmat(Y_test, Y_pred);

% Calculate precision, recall, and F1-score for each class
num_classes = 18;
precision = zeros(num_classes, 1);
recall = zeros(num_classes, 1);
f1_score = zeros(num_classes, 1);

for i = 1:num_classes
    true_positives = conf_matrix(i,i);
    false_positives = sum(conf_matrix(:,i)) - true_positives;
    false_negatives = sum(conf_matrix(i,:)) - true_positives;

    precision(i) = true_positives / (true_positives + false_positives);
    recall(i) = true_positives / (true_positives + false_negatives);
    f1_score(i) = 2 * (precision(i) * recall(i)) / (precision(i) + recall(i));
end

% Prepare results for Excel
results = table(Y_test, Y_pred, 'VariableNames', {'True_Class', 'Predicted_Class'});

% Add additional sheets for metrics
accuracy_table = table(accuracy, 'VariableNames', {'Accuracy'});
conf_matrix_table = array2table(conf_matrix, 'VariableNames', cellstr(string(1:18)), 'RowNames',
cellstr(string(1:18)));
metrics_table = table((1:18)', precision, recall, f1_score, 'VariableNames', {'Class', 'Precision',
'Recall', 'F1_Score'});

% Write results to Excel file
filename = 'random_forest_results.xlsx';
writetable(results, filename, 'Sheet', 'Predictions');
writetable(accuracy_table, filename, 'Sheet', 'Accuracy', 'WriteRowNames', true);
writetable(conf_matrix_table, filename, 'Sheet', 'Confusion_Matrix', 'WriteRowNames', true);
writetable(metrics_table, filename, 'Sheet', 'Class_Metrics');

disp('Results have been written to random_forest_results.xlsx');
```

3.14.7 Evaluation of the Random Forest Model

After running the model, its performance evaluation was conducted in the form of a confusion matrix (Figure 3-30).

3.14.7.1 Evaluation of the Model for Test Samples

Table 3-11 presents the overall efficiency of the random forest algorithm for the test data. Note that the test samples constitute 30% of the total samples used in the training and evaluation process of the algorithm.

Table 3-11. Accuracy assessment metrics for test data.

Row	Metric	Value
1	Kappa Index (Kappa)	0.79
2	Variance of Kappa	0.00025
3	Overall Accuracy	0.81
4	Confidence Level	0.95

A Kappa value of 0.79 indicates a significant agreement between the predicted classifications and the actual ones. This means the model performs 79% better than what would be expected by random chance, which is generally considered a good score, indicating strong predictive power across multiple classes. The very low variance (0.00025) suggests that the Kappa statistic is quite stable and reliable. This means that if the classification process were repeated with different samples from the same population, similar Kappa values would likely be obtained.

An overall accuracy of 81% means that 81% of all predictions across all classes were correct. This aligns well with the confusion matrix, where most classes exhibit good accuracy. A confidence level of 0.95 indicates that we can be 95% confident that the true Kappa value for the population falls within a specific range around our calculated Kappa of 0.79.

Based on these metrics, the model generally performs well, with strong agreement between predictions and actual classes. The high Kappa value and low variance suggest that the model's performance is both good and consistent. The 81% overall accuracy confirms the Kappa score, indicating reliable classification across multiple classes. There is still room for improvement, especially in classes with lower individual accuracy, as seen in the confusion matrix.

The confusion matrix (Figure 3-30) represents the performance of the random forest algorithm on the test data for 16 geological classes plus two classes for water bodies and vegetation cover. The model's performance on the test set is moderately good, although it is lower in some classes. In other words, most classes show good accuracy, but there is room for improvement in some classes.

Class performance:

- Best-performing classes: Water: 100% accuracy, Q^{a}: 95.1% accuracy, and $Pl^{silt.cong}$: 89.7% accuracy
- Lowest-performing classes: Q^{sd}: 40% accuracy, Q^{b}: 55.6% accuracy, and Q^{f}: 70.2% accuracy

In conclusion, while the model is promising for several geological classifications, further optimization is needed to improve performance across all classes, especially those with lower accuracy.

GeoNexus

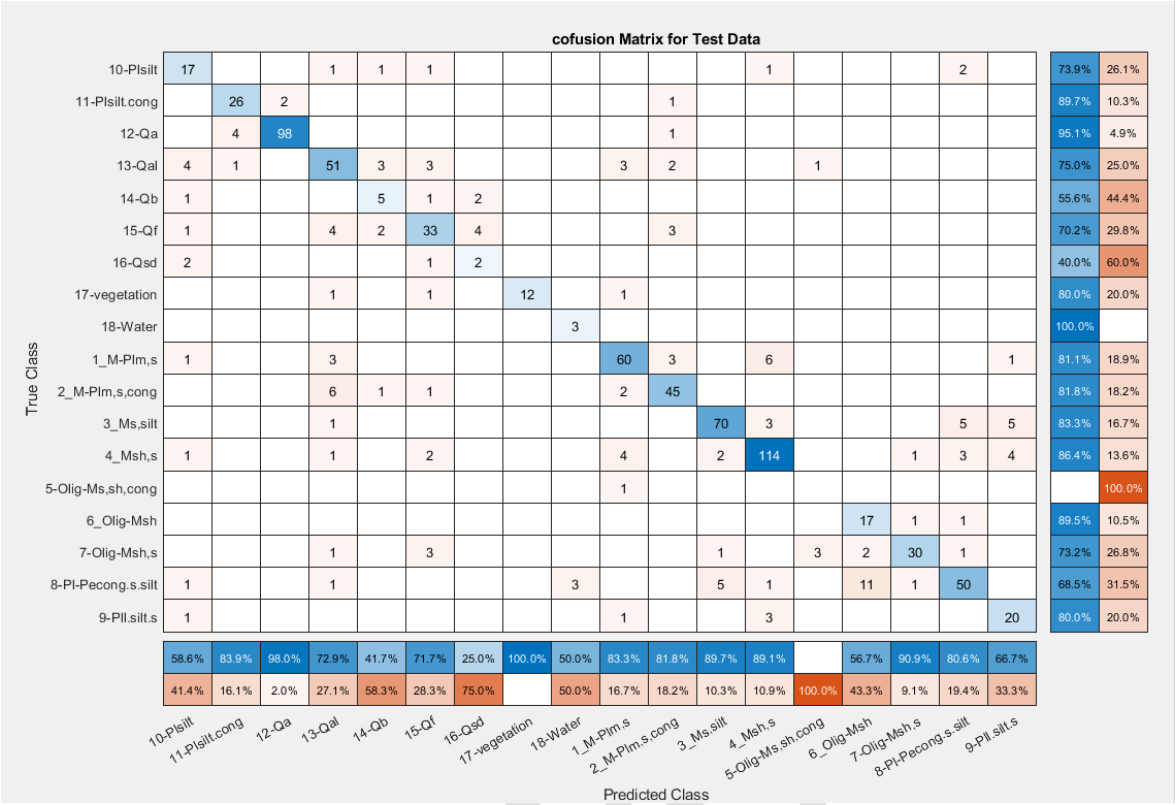


Figure 3-30. Confusion matrix for test samples (30% of training samples) for evaluating the accuracy and efficiency of the random forest model.

3.14.7.2 Evaluation of the Model for All Training and Test Samples (30% of the Total Samples)

A Kappa value of 0.93 indicates an almost perfect agreement between the predicted classifications and the actual ones (Table 3-12). This means the model performs 93% better than what would be expected by random chance, which is an excellent score, indicating very strong predictive power across multiple classes.

Table 3-12. Accuracy assessment metrics for all training and test data.

Row	Metric	Value
1	Kappa Index (Kappa)	0.937
2	Variance of Kappa	0.00005
3	Overall Accuracy (%)	94.3
4	Confidence Level	0.95

An overall accuracy of 94.3% means that 94.3% of all predictions across all classes were correct. This is a very high accuracy, especially for a multi-class geological classification with 16 classes. The very low variance of Kappa (0.00005) indicates that the Kappa statistic is very stable and reliable. This means that if we repeat the classification process with different samples from the same population, we would likely obtain very similar Kappa values.

This model (Figure 3-31) shows exceptional performance for the training and test samples. The high Kappa score and overall accuracy indicate that the model has learned to distinguish between different geological classes with a high degree of accuracy. The low variance in Kappa suggests that this performance is consistent and reliable.

These metrics demonstrate a strong training model that has effectively captured the underlying patterns in the geological data. The model shows very good performance overall, with high accuracy in most classes. The diagonal elements (blue cells) represent correct classifications, which are predominantly high.

Class-specific performance:

- Water: 100% accuracy (though the sample size is small—12 samples).
- Q^{a}: Excellent performance with 98.3% accuracy (285 correct out of 290 samples).
- Q^{sd}: Lowest accuracy at 82.4%, often misclassified as Q^{f}.

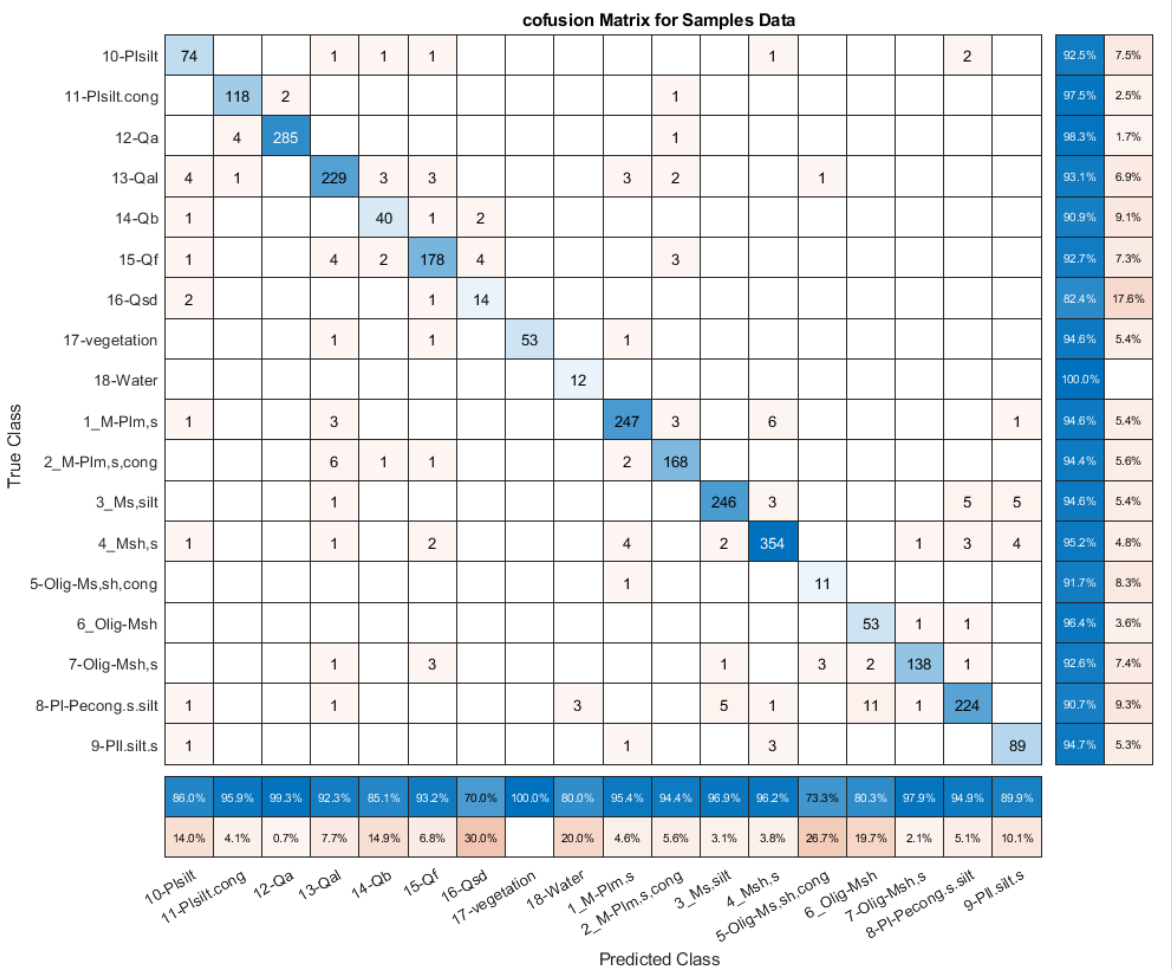


Figure 3-31. Confusion matrix for all training samples (30% of total samples) for evaluating the accuracy and efficiency of the random forest model.

In summary, the model demonstrates high accuracy in classifying geological formations, with only minor confusions between similar classes. The performance is consistent across different sample sizes, indicating a strong and well-trained classifier.

3.14.7.3 Evaluation of the Model for the Entire Area (8,959 Polygons)

A Kappa value of 0.84 indicates a very strong agreement between the predicted classifications and the actual ones (Table 3-13). This means the model performs 84% better than what would be expected by random chance, which is excellent performance, especially for geological classes with inherent complexities. An overall accuracy of 85.6% means that 85.6% of all predictions across the entire area were correct. For a geological classification task with multiple classes, this is a very good accuracy rate.

Table 3-13. Accuracy assessment metrics for the entire dataset.

Row	Metric	Value
1	Kappa Index (Kappa)	0.84
2	Variance of Kappa	0.00005
3	Overall Accuracy (%)	85.6
4	Confidence Level	0.95

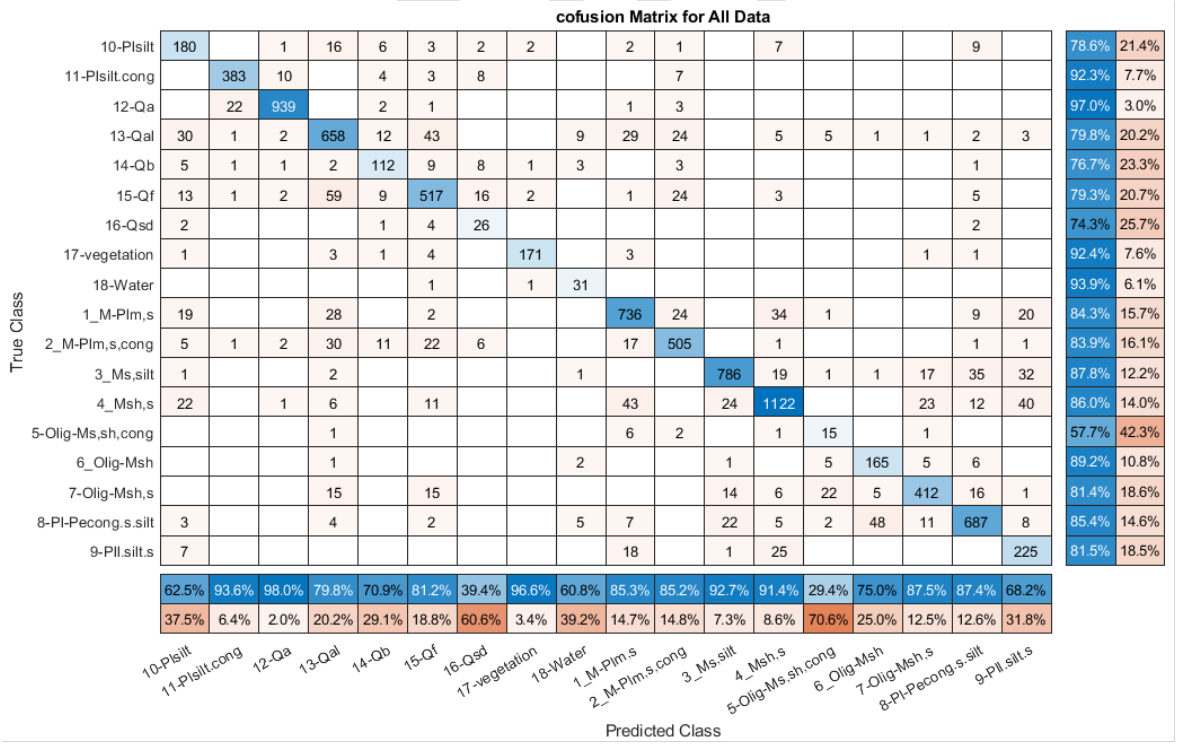


Figure 3-32. Confusion matrix for the study area (total of 8,959 polygons) for evaluating the accuracy and efficiency of the random forest model.

This model (Figure 3-32) demonstrates excellent performance in classifying geological features over a large and diverse area (8,959 polygons and 18 classes). With a Kappa of 0.84 and an overall accuracy of 85.6%, the model shows strong predictive power and reliability in distinguishing between different geological classes. The strong performance on such a large number of samples indicates good generalization capabilities.

It appears that the model has effectively managed the diversity and complexity of geological features across the entire area. The high accuracy and reliability of the model make it suitable for practical applications in geological mapping and classification.

The model shows generally good performance across most classes with varying degrees of accuracy. The diagonal elements (blue cells) represent correct classifications, which are generally high for most classes.

- Class-by-class analysis:
  1. Pl^{silt}: 78.6% (180 correct out of 229) accuracy; significant confusion with Q^{al} and Q^{a}.
  2. Pl^{silt}.Cong: 92.3% (383/415) accuracy; high accuracy.
  3. Q^{a}: 97.0% (939/968) accuracy; excellent performance on a large sample.
  4. Q^{al}: 79.8% (658/825) accuracy; significant confusion with Q^{f} and Q^{b}.
  5. Q^{b}: 76.7% (112/146) accuracy; confusion with Q^{al} and Q^{f}.
  6. Q^{f}: 79.3% (517/652) accuracy; significant confusion with Q^{al}.
  7. Q^{sd}: 74.3% (26/35) accuracy; lowest accuracy, often misclassified as Q^{f}.
  8. Vegetation: 92.4% (171/185) accuracy; high performance.
  9. Water: 93.9% (31/33) accuracy; very high accuracy.
  10. M-$Pl^{m.s}$: 84.3% (736/873) accuracy; some confusion with M-$Pl^{m.s.cong}$ and $M^{s.silt}$.
  11. M-$Pl^{m.s.cong}$: 83.9% (505/602) accuracy; confusion with M-$Pl^{m.s}$ and Q^{al}.
  12. $M^{s.silt}$: 87.8% (786/895) accuracy; some confusion with $M^{sh.s}$ and Pl-$Pe^{cong.s.silt}$.
  13. $M^{sh.s}$: 86.0% (1,122/1,304) accuracy; largest sample size, good performance.
  14. Olig-$M^{s.sh.cong}$: 57.7% (15/26) accuracy; lowest accuracy, significant confusion with $M^{sh.s}$.
  15. OligM^{sh}: 89.2% (165/185) accuracy; high accuracy.
  16. Olig-$M^{sh.s}$: 81.4% (412/506) accuracy; some confusion with Olig-M^{sh} and Pl-$Pe^{cong.s.silt}$.
  17. Pl-$Pe^{cong.s.silt}$: 85.4% (687/804) accuracy; confusion with several classes.
  18. $Pl^{l.silt.s}$: 81.5% (225/276) accuracy; good performance with some confusion.
- Error analysis:
  - Highest Error Rates: Olig-$M^{s.sh.cong}$: 42.3%, Q^{sd}: 25.7%, and Q^{b}: 23.3%.
  - Lowest Error Rates: Q^{a}: 3.0%, Water: 6.1%, and $Pl^{silt.Cong}$: 7.7%

Errors often occur between similar or adjacent geological classes.

- Geological efficiency:
  - The model performs well in identifying major geological formations.
  - Confusions occur between classes that may have similar features or are spatially adjacent.
- Model strengths:
  - Good overall accuracy across a diverse set of geological classes.
  - Strong performance in classes with larger sample sizes (e.g., Q^{a}, $M^{sh.s}$).
- Areas for improvement:
  - Focus on improving classification for Olig-$M^{s.sh.cong}$ and Q^{sd}.

GONEXUS

  - Address confusions between Q^{al} and Q^{f}, which affect a large number of samples.

- Practical implications:
  - The model is generally reliable for geological mapping and classification.
  - It can significantly assist in automating the process of geological data analysis, potentially saving time and resources.

The model's ability to maintain high performance over a large number of polygons suggests it could scale to even larger or more diverse geological datasets. In summary, this confusion matrix demonstrates a good geological classification model with varying performance across different classes. It performed well for most major geological formations. The model's strengths in distinguishing between many classes make it a useful tool for geological analysis, although there is room for refinement in some areas. The varying accuracies across classes indicate that while the model is generally reliable, results should be interpreted considering the specific status of some classes.

By utilizing the Random Forest model and thoroughly evaluating its performance across test samples, training samples, and the entire area, we have developed a robust geological classification. The integrated geological map reflects the model's effectiveness in capturing the geological diversity of the Makran study area (Figure 3-33).

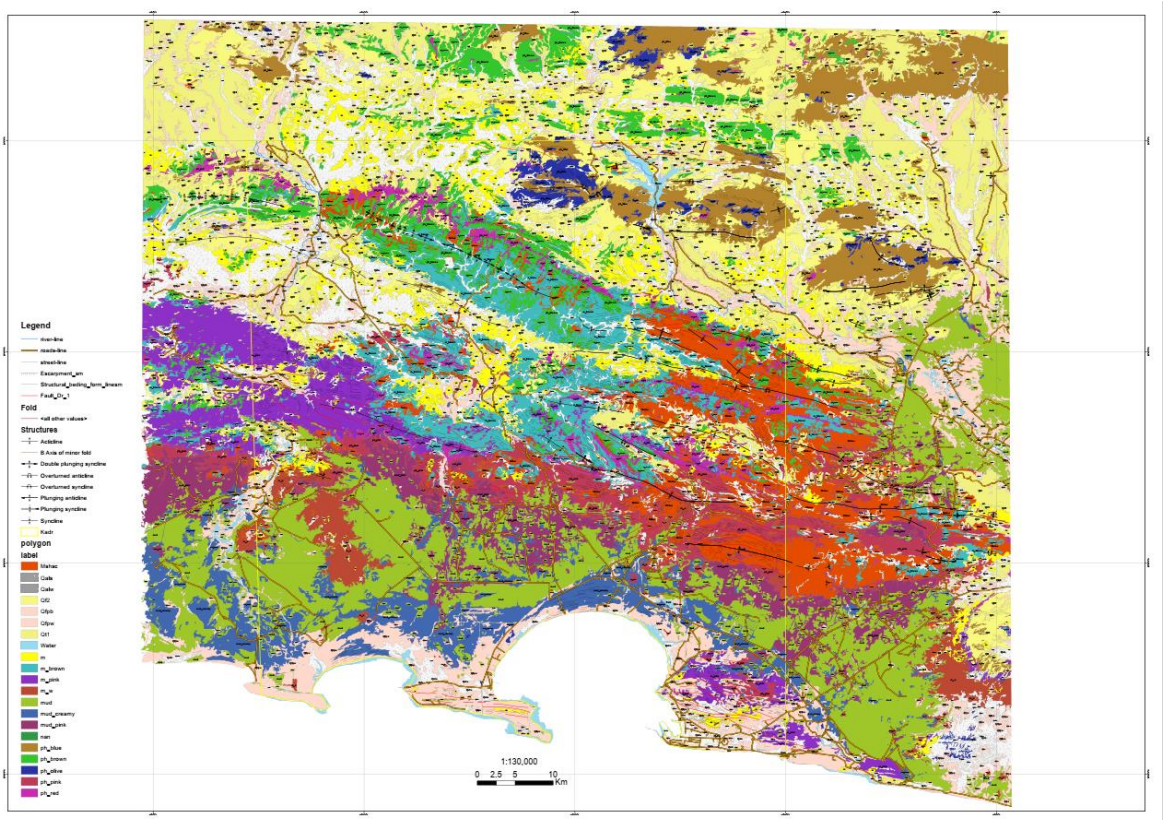


Figure 3-33. Integrated geological map of the Makran study area.

3.15 Preparation of Integrated Database of SUTGMM

The developed Web-GIS system for the Server-based Unified Thematic Geological Mapping of Makran (SUTGMM) represents a significant advancement in the integration and visualization of diverse geological data. Built upon Leaflet, an open-source JavaScript library, this system provides a powerful yet user-friendly interface for displaying and analyzing the varied geological information collected and produced for the Makran region.

At its core, the WebGIS database acts as a centralized repository for a diverse array of spatial, satellite, multimedia (video and audio-visual), and documentary data, collected through advanced remote sensing techniques and extensive field surveys. The primary goal of this system is to provide geologists, researchers, and decision-makers with a comprehensive tool for visualization, analysis, and interpretation of geological results and patterns across the Makran region.

The spatial data component of the database houses satellite images from Sentinel-1, Sentinel-2, and ASTER. These imagery sources offer a wealth of information across various spectral bands, allowing for detailed analysis of surface features and composition. Complementing these satellite data are geological spectral indices that highlight specific mineral compositions and geological formations of interest.

Topographic information constitutes another important layer of the spatial database. Digital Elevation Models (DEMs), along with derived products such as slope, aspect, and hillshade, provide comprehensive data for understanding geological structures and landforms. Integrating these topographic layers with spectral data enables more precise interpretation of geological processes and formations.

A key strength of the database lies in the field data. Multimedia information meticulously collected using the specialized *Epicollect* platform includes a variety of information such as photos, audio files, videos, and other documents. These geotagged real-world data are invaluable for validating remote sensing interpretations. Field notes and observations add a layer of expert interpretation to the raw data.

The segmentation results from the *eCognition* software and subsequent classification outputs from the Random Forest algorithm represent the analytical heart of the database. These layers provide a data-driven approach to geological mapping, marking a significant leap over traditional methods.

The database structure is carefully designed to facilitate the seamless integration of various data types. It allows for efficient querying and analysis across different data layers. The user interface, built using Leaflet in conjunction with custom JavaScript, CSS, and HTML, provides an intuitive and responsive platform for exploring the data. Users can easily switch between different data layers, perform spatial queries, and examine the relationships of various geological units with ease. The browser-based nature of the system ensures broad accessibility without the need for specialized software installation.

In summary, this WebGIS database is a powerful tool for geological research and decision-making in the Makran region. By integrating diverse data sources, utilizing advanced analytical techniques, and providing an accessible user interface, it sets a new standard for geological mapping and analysis.

GeoNexus

3.15.1 JavaScript Programming Language

JavaScript is a high-level, versatile programming language that has become an integral part of web development and, increasingly, spatial data processing and analysis. Originally created to add interactivity to web pages, JavaScript has evolved into a powerful language capable of performing complex tasks, including spatial data processing and visualization. In the context of spatial applications, JavaScript offers several key advantages:

- Client-side processing: JavaScript runs in the user's browser, allowing for quick responses to user interactions and reducing server load for many spatial operations.

- Asynchronous operations: Through features like Promises and async/await, JavaScript can effectively handle the loading and processing of large spatial datasets without crashing the user interface.

- Support for JSON and GeoJSON: JavaScript natively supports JSON (JavaScript Object Notation), making it ideal for working with GeoJSON, a standard format for representing spatial data.

- Extensive Libraries: There are numerous JavaScript libraries specifically designed for spatial operations and mapping.

With JavaScript's key spatial capabilities and data parsing and management, it can handle various spatial data formats, especially GeoJSON. It can programmatically manage spatial information and non-spatial attributes. When combined with HTML5 and CSS3, JavaScript forms a powerful combination for creating complex and responsive applications in WebGIS. Figure 3-34 shows an example of a program written for loading, displaying, and analyzing database information.

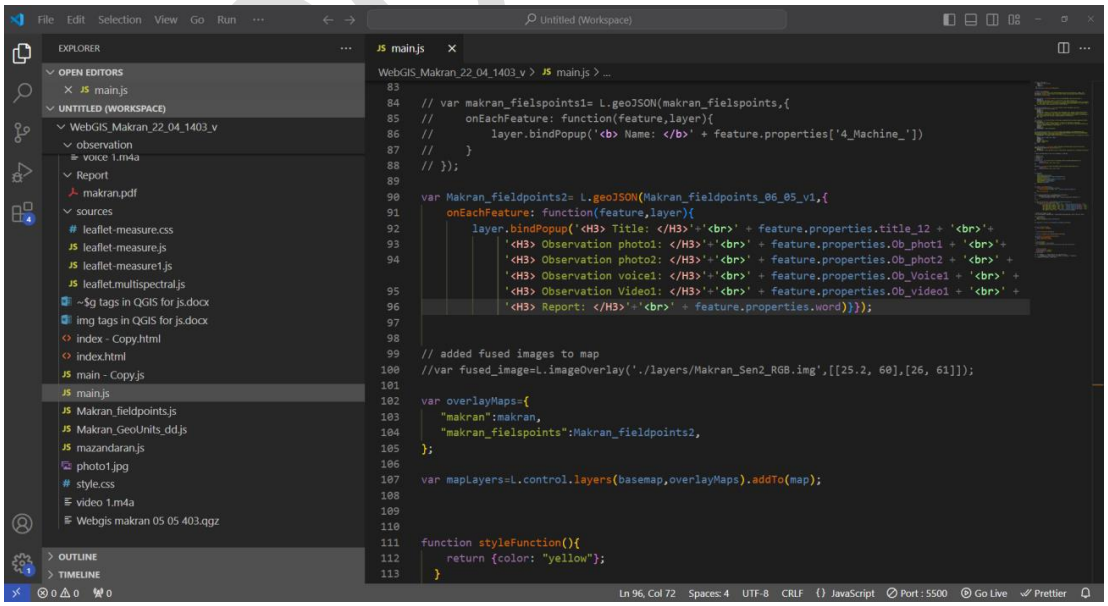


Figure 3-34. View of the Visual Studio Code programming environment and the JavaScript codes for the SUTGMM geodatabase.

3.15.2 Map Canvas - WebGIS Main Display Page

The primary and most prominent element of the WebGIS interface is the map canvas. This is where spatial data are rendered and displayed.

- Typically occupies most of the page space.
- Supports zooming and clicking on features.
- Ability to display multiple data layers simultaneously.
- Supports various base maps (e.g., topographic, satellite imagery, terrain maps).

In Figure 3-35, a view of the main page of the Makran Geological WebGIS is presented, which almost all the necessary tools for displaying and searching for desired information and data are included in this system.

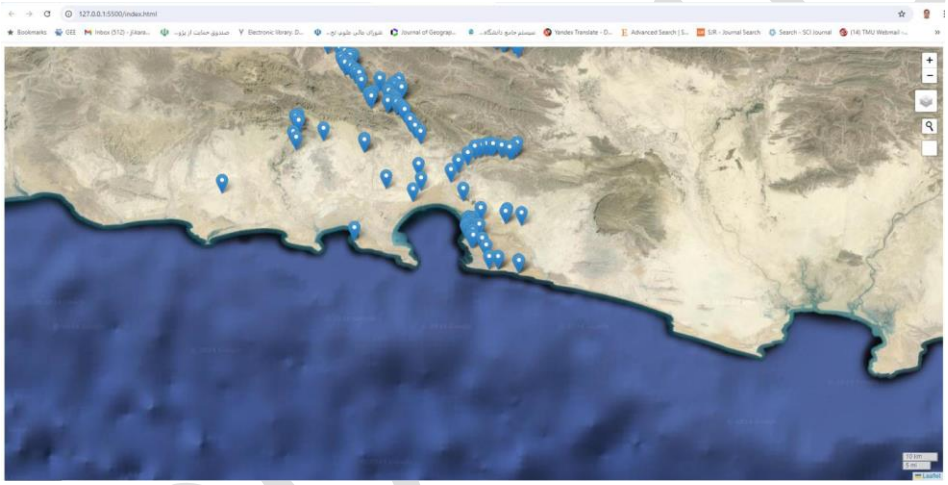


Figure 3-35. Main page of the Makran Geological WebGIS system, showing multiple georeferenced points overlaid on a satellite imagery basemap, allowing for spatial exploration and data interaction.

3.15.3 Layer Control

This interface element allows users to manage the visibility of different data layers (Figure 3-36).

- Usually presented as a list or tree structure.
- Checkboxes to toggle layer visibility.
- May include grouping of layers for different purposes.

For example, different base layers can be changed (Figure 3-37 to Figure 3-39). In this project, in addition to base maps, the generated maps have also been loaded in GeoJSON format (Figure 3-40).

One of the prominent features of this database is the connection of various information to field surveys. This information includes photos, audio, videos, reports, and other non-spatial information that practically get spatial tagging with this system (Figure 3-41 to Figure 3-44). The following capabilities are briefly presented.

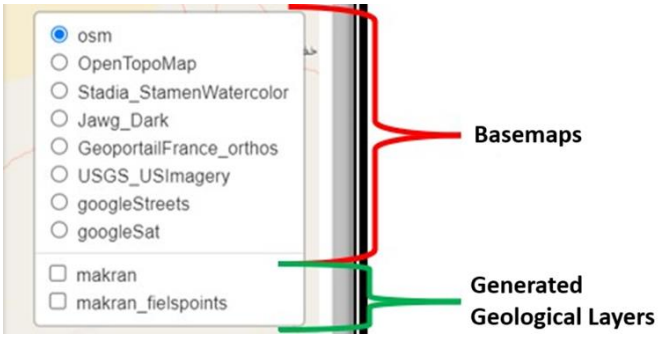


Figure 3-36. View of the layer control tool in the WebGIS environment.



Figure 3-37. A view Geoportail France Satellite Imagery layer.



Figure 3-38. A view of the Stamen Watercolor Map layer.

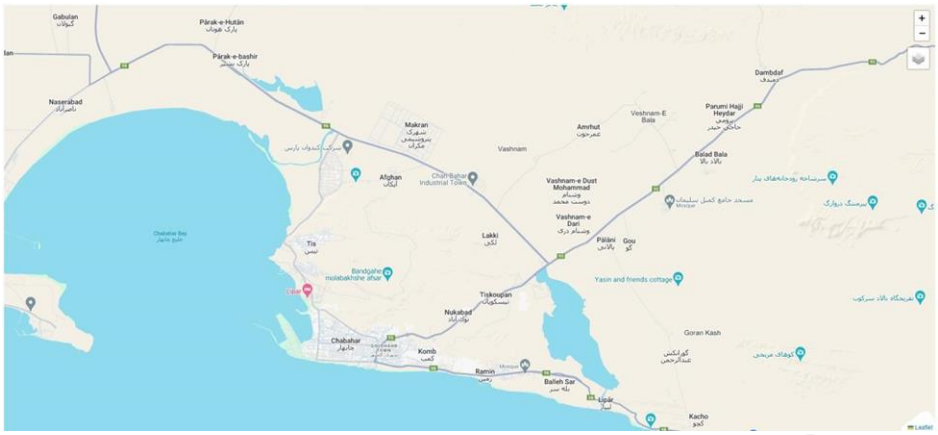


Figure 3-39. A view of the Google Street Map layer.

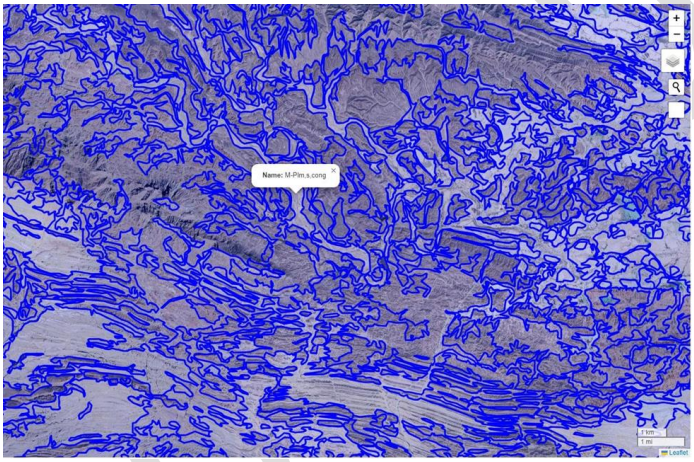


Figure 3-40. Generated geological layer with the ability to query features of each unit.

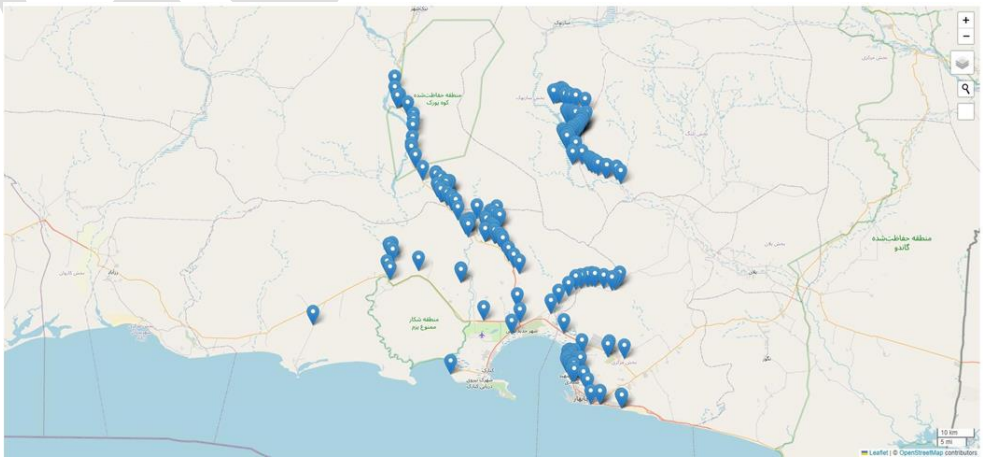


Figure 3-41. Display of the project field survey points.

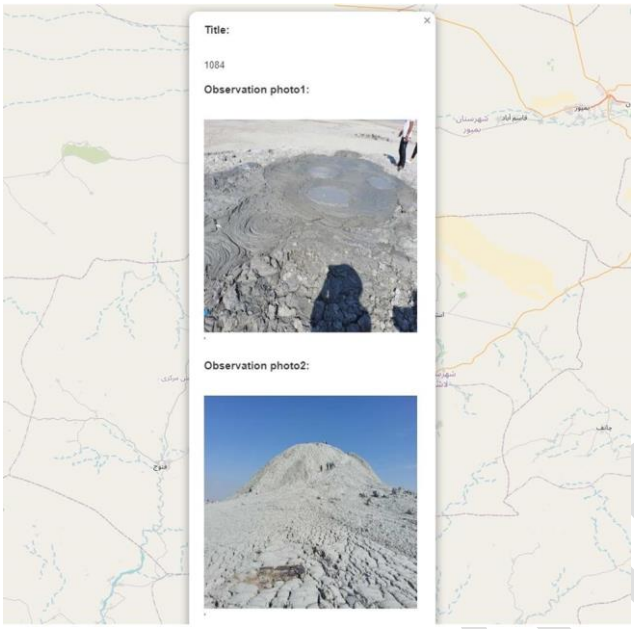


Figure 3-42. Online search and display of visual information for point 1084 on the map.

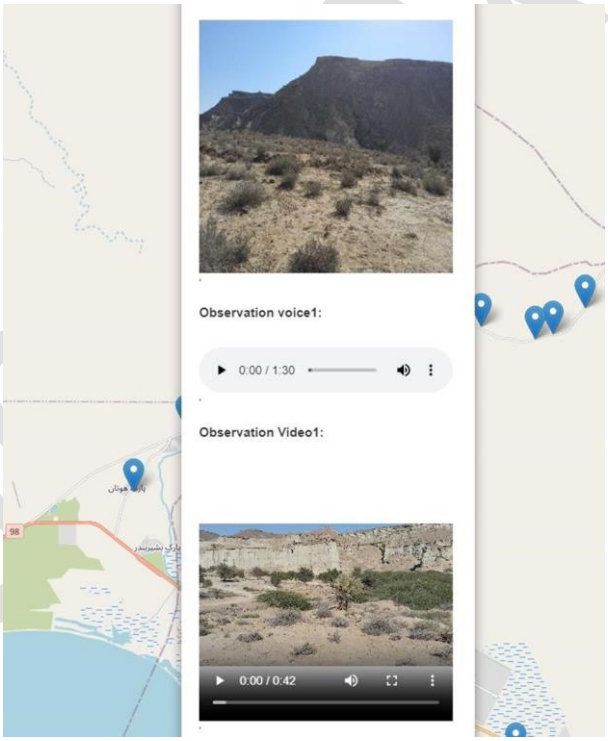


Figure 3-43. Online search and display of audio and video information for point 1168 on the map.

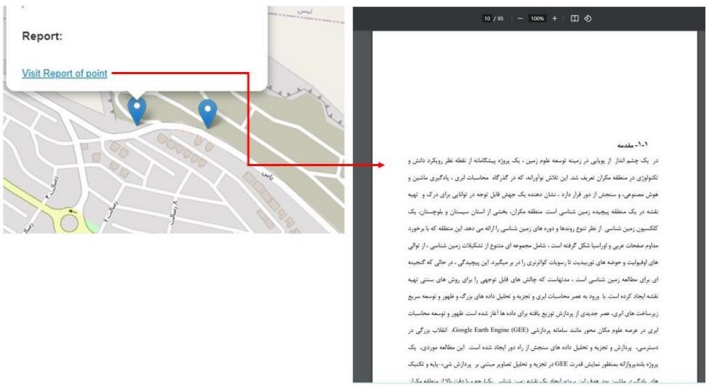


Figure 3-44. Online search and display of the report related to each field investigation point.

3.15.4 Navigation Controls

This plugin allows users to navigate around the map and change the view.

- Zoom in/out buttons: For changing the map scale.
- Pan controls: Often implemented as dragging the map canvas.
- Home button: To return to the initial map extent.
- Geolocation button: To center the map on the user's current location.

On the right side of the display, interactive and control capabilities are provided (Figure 3-45). At the top right, there is the ability to zoom in on the map. Below that, eight base maps are provided, allowing the user to turn on the desired base map according to their needs. This includes various satellite images and terrain maps (e.g., OpenStreetMap). Below that, a search capability is provided, enabling searching for different locations. Below the search tool, line and polygon measurement tools are provided for measuring length, perimeter, and area. Finally, the map scale tool is provided.

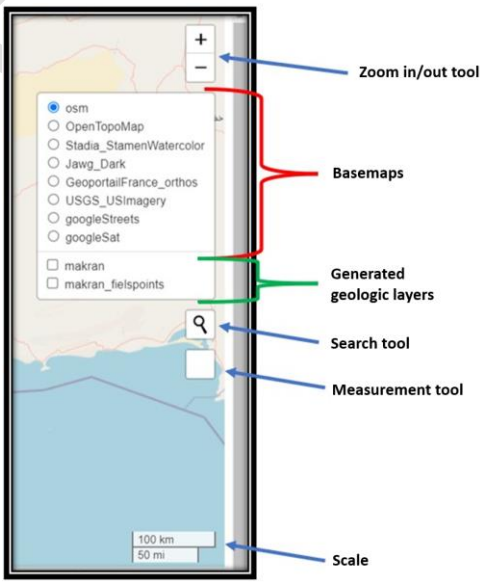


Figure 3-45. The interactive and control capabilities.

- Legend
  - Provides a key to interpret the symbology used on the map.
  - Explains the meaning of colors, shapes, and sizes used for features.
  - May be static or dynamically generated based on visible layers.
  - Often collapsible to save screen space.
- Scale Bar
  - Shows the map scale and helps users understand distances.
  - May be dynamic and update with zoom level changes.
  - Can provide multiple units (e.g., metric and imperial).
- Search Bar
  - Allows users to search for specific locations or features.
- Coordinate Display
  - Shows the coordinates of the current mouse position on the map (Figure 3-46).
  - May support multiple coordinate systems.

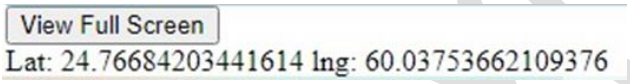


Figure 3-46. Coordinate display on the map.

By integrating these features, the WebGIS system provides a comprehensive platform for users to interact with the geological data of the Makran region effectively. The combination of various data layers, interactive tools, and user-friendly design enhances the ability to analyze and interpret complex geological information.

3.16 Workflow and Protocol

The SUTGMM project represents a significant advancement in modern geological mapping, combining remote sensing, machine learning, and cloud computing to develop a unified, high-resolution geological map of the Makran region. This approach not only accelerates the mapping process but also reduces the number of personnel required to manage large-scale geological surveys. The protocol (Figure 3-47) leverages innovative technologies such as Object-Based Image Analysis (OBIA), machine learning algorithms like Random Forest (RF), and server-based cloud computing to extract and process geological data efficiently. These advances align the project with global trends in geospatial science, where modern workflows emphasize the rapid processing of complex data to produce accurate, data-driven geological maps.

This project aims to create a unified, high-resolution geological map of Makran through a multi-phase approach that integrates diverse datasets and advanced geospatial analysis techniques. The goal is to extract, process, and classify geological and geomorphological features to generate accurate and comprehensive geological outputs.

GeoNexus

3.16.1 Phase 1: Data Acquisition and Extraction

The foundation of the project rests on the integration of multiple datasets, each contributing unique insights into the geological structure of the region. *Google Earth Engine* provides a robust platform for accessing and processing large volumes of satellite data. The project starts with the extraction of data from *Google Earth Engine*'s archive datasets, incorporating various satellite imagery, including Sentinel-1 (VV and VH polarization, 2 band images), Landsat-8 (30 m resolution, 6 band images), Sentinel-2 (10-20 m resolution, 9 band images), ASTER (VNIR, SWIR, and TIR, 14 bands), and SRTM DEM (30-m resolution). These datasets provide essential spectral, geological, and topographical information at various spatial resolutions, forming the foundation of the geological mapping.

Selected datasets for this project include:

- Sentinel-1 (VV and VH polarizations): This dataset plays a crucial role in detecting surface roughness, soil moisture content, and geomorphological variations through the use of synthetic aperture radar (SAR). The polarization data allow for the extraction of statistical features such as mean, minimum, and maximum values, which are essential for segmenting landforms and detecting subtle variations in terrain morphology.
- Sentinel-2 (10- and 20-m resolution, 9-band images): The multi-spectral capabilities of Sentinel-2 are vital for detecting vegetation indices, soil, and water bodies. Its fine spatial resolution enhances the detail of the multi-resolution, multi-scale segmentation, enabling accurate detection of surface features. The spectral bands from Sentinel-2 provide crucial information that supports the classification of geological units based on their unique spectral signatures.
- Landsat-8 (30-m resolution, 6 band images): Landsat-8 offers additional spectral diversity for geological analysis at a coarser resolution compared to Sentinel-2. The combination of mid-infrared and thermal bands contributes to identifying specific rock types and detecting thermal anomalies that may be linked to geothermal activity or subsurface processes. Despite its lower spatial resolution, Landsat-8 data remains integral for broad regional analyses.
- ASTER (VNIR, SWIR, TIR bands): With its fourteen spectral bands, ASTER data significantly enhances the identification of geological units, such as siltstone, travertine, basalt, and ignimbrite. The VNIR, SWIR, and TIR bands provide a multi-dimensional perspective on mineral composition, enabling the extraction of indices that differentiate between lithological units based on their thermal and spectral properties.
- SRTM DEM (30-m resolution): The SRTM DEM data serves as the backbone for topographical analysis, offering crucial information on landform characteristics. From slope to profile convexity and sinuosity, the DEM data provides the essential geometrical parameters required for geomorphological and structural interpretation. This dataset helps in understanding tectonic activity, erosion patterns, and the landform analysis of the region.

GeoNexus

3.16.2 Phase 2: Data Processing and Feature Extraction

After acquiring the datasets, the next phase involves feature extraction, where critical geological and geomorphological characteristics are derived from the various satellite imagery sources. In this step, statistical values (e.g., min, max, and mean) are extracted from Sentinel-1's polarization products to support landform segmentation. This phase also employs OBIA techniques, which are pivotal for segmenting the imagery into meaningful objects based on specific parameters such as texture, shape, and spectral properties. OBIA goes beyond pixel-based classification by considering the spatial context of features, allowing for more accurate segmentation of geological formations.

- Segmentation of Sentinel-2 Images: A multi-resolution and multi-scale segmentation process is applied to the Sentinel-2 data. This segmentation generates objects that are later classified into geological units based on spectral and textural properties. The resolution of Sentinel-2 images (10-20 m) provides the necessary detail for accurately delineating boundaries between rock units, vegetated areas, and geomorphological features.
- Shape Parameters: Shape parameters, such as asymmetry, border index, compactness, ellipticity, density, and roundness, are computed to further characterize geological segments. These parameters provide a quantifiable way to describe the geometry of geological units and are crucial for distinguishing between different rock formations, especially in regions where traditional spectral signatures might overlap (Nazari et al., 2023b; Nazari, 2024; Nazari et al., 2024a).

In this phase, a key innovation is the integration of cloud-based computing to handle vast volumes of data. This allows for faster processing times compared to desktop-based methods and enables the simultaneous extraction of multiple features from various datasets. The flexibility and scalability of cloud computing reduce the need for extensive on-site computational resources, making the process both efficient and cost-effective (Nazari et al., 2022, 2024a).

3.16.3 Phase 3: Machine Learning and Initial Classification

The extracted features from all datasets are aggregated into a comprehensive database, forming the basis for the first phase of supervised classification. In this phase, machine learning algorithms—specifically the Random Forest (RF) classifier—are employed to generate the Preliminary Geomap. The Random Forest algorithm is particularly suited for this task due to its ability to handle high-dimensional datasets and its robustness in processing heterogeneous data from multiple sources.

- Supervised Classification: The first phase of classification involves using a supervised learning model that trains the RF algorithm on labeled datasets, including previously geotagged geological formations and features. The machine learning model learns to recognize patterns in the data, which it then applies to classify segments into geological units.
- Clustering Techniques (Nazari et al., 2024a, 2024b): In parallel with the supervised classification, Fuzzy C-Means (FCM) clustering is applied to group the segmented objects into homogenous clusters based on their spectral and shape properties. This unsupervised method allows for the grouping of data points with partial membership in multiple clusters, which is useful for distinguishing between subtle variations in rock units. FCM is especially

effective in geological applications where the spectral properties of adjacent rock types may overlap, making clear distinctions challenging.

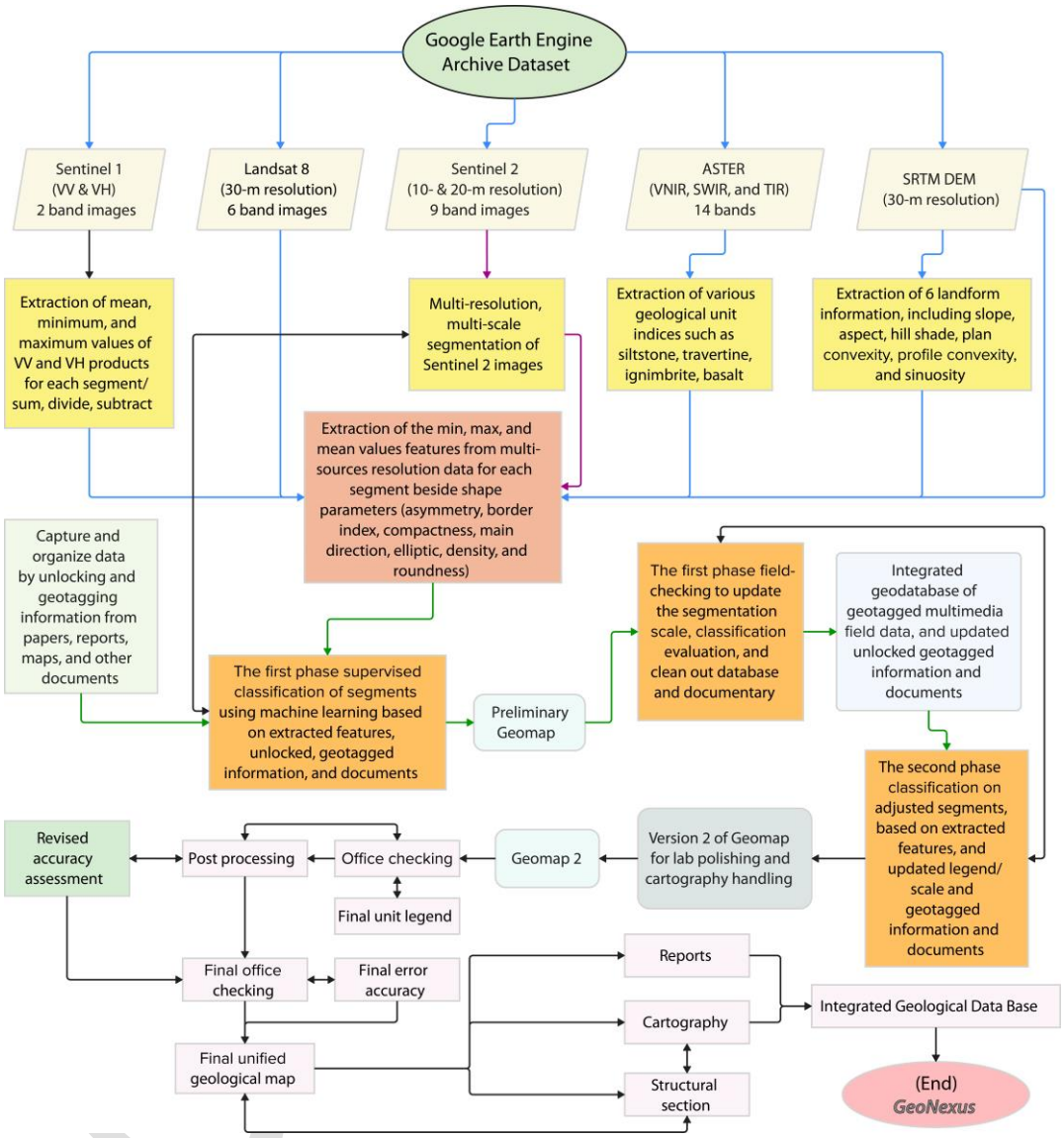


Figure 3-47. Workflow and protocol for Server-based Unified Thematic Geological Mapping of Makran (SUTGMM) using multi-source remote sensing data and machine learning. The process includes feature extraction from Sentinel-1, Sentinel-2, Landsat 8, ASTER, and SRTM DEM data, supervised classification, field-checking, and iterative refinement. The final outputs include a unified geological map, structural section, and integrated geodatabase.

3.16.4 Phase 4: Field Verification and Geodatabase Integration

Once the Preliminary Geomap is generated, the project enters the field-checking phase. This critical step involves ground-truthing the satellite-derived classifications by comparing them to actual geological formations observed in the field. Field teams collect data on rock types, mineral compositions, and structural features, which are then used to refine the classification outputs.

- Field Verification: The first phase of field verification ensures that the segmentation and classification results align with real-world geological features. Any discrepancies are addressed by updating the segmentation scale, evaluating the classification accuracy, and cleaning out obsolete data from the geodatabase.
- Geodatabase Integration: The results from field verification are integrated into a unified geodatabase, which consolidates georeferenced field data, the unlocked trapped data (i.e., historical data from reports, maps, and documents), and satellite-derived features. This geodatabase becomes the core data repository for the project, providing a robust framework for further data refinement and future analyses (Nazari et al., 2023a, 2024a).

3.16.5 Phase 5: Iterative Refinement and Final Outputs

The second phase of classification refines the Preliminary Geomap by adjusting the segments and incorporating updated geotagged data from the field. This results in Geomap 2, which undergoes cartographic processing for lab-based polishing and cartographic handling. At this stage, the focus shifts to ensuring the highest degree of precision and consistency, particularly in how geological units are represented on the final map.

The final step—Post-Processing and Accuracy Assessment—involves a thorough accuracy assessment, where the classified segments are compared against known geological data. Post-processing includes office checks, error analysis, and revisions of the geological legend. These processes ensure that the final unified geological map is of the highest possible accuracy, suitable for research, land-use planning, and resource management applications.

The final outputs include detailed geological reports, a high-resolution geological map, and structural sections, all of which are integrated into a comprehensive GeoNexus geodatabase. This database supports the long-term monitoring and management of the region's geological resources and serves as a foundation for further research.

GeoNexus

GeoNexus

4 Geological and Stratigraphic Analyses

This section delves into the sedimentological characteristics and stratigraphic sequences observed within the mapped area. Each geological unit identified on the map is analyzed for its composition, depositional environment, and temporal succession. The aim is to provide a comprehensive understanding of the stratigraphic framework of the region and to relate these units to the broader tectonic and sedimentary history of the Makran region. The stratigraphy of this area records the long-term evolution of the subduction-related processes and the transition from deep marine to more terrestrial environments during different geological periods.

Detailed field mapping, combined with petrographic and micropaleontological analyses, allows for the characterization of each mapped unit in terms of its lithology, depositional environment, and diagenetic history. Moreover, absolute age dating, supplemented by paleontological data, has helped to establish a chronological framework for the sedimentary sequences. This temporal succession offers insights into the tectonic and paleoenvironmental changes that have shaped the region.

The fieldwork and sampling activities have been carefully designed and performed following the preliminary Geomap (see Chapter 3 for details), leading to a more accurate representation of the Server-Based Unified Thematic Geological Mapping of Makran (SUTGMM). The server-based approach allowed for a significant refinement in mapping workflows, enabling multi-resolution segmentation and classification of Sentinel-2, Landsat-8, ASTER, and SRTM data. These datasets formed the foundation for identifying key sedimentological features, which were further validated and enhanced through micropaleontological, petrographic, and field-based studies.

Key geological units were revised and reclassified based on their spectral, textural, and morphological features. The combination of satellite imagery, field observations, and laboratory analyses has allowed for the identification of depositional sequences spanning from the Oligocene to the present (Table 4-1 and Figure 4-1). Additionally, paleontological dating and petrographic examinations of rock samples have refined the temporal succession of these units, allowing for more accurate age determinations and stratigraphic correlations across the mapped area. The output of this comprehensive analysis forms the basis for version 2 of the GeoMap, with final refinements captured in the GeoNexus database.

GeoNexus

The output of this comprehensive analysis forms the basis for version 2 of the GeoMap (Figure 4-3), with final refinements captured in the GeoNexus database. Additionally, the SUTGMM project has published nine detailed 1:50,000 geological sheets (Figure 4-2), including Ab Sard, Chabahar, Gor, Gurdim, Kahir, Konarak, Kuh-e-kand Koruch, Park Bala, and Zirdan (Figure 4-4 to Figure 4-12). These maps offer an unparalleled level of detail, capturing essential geological features across the Area of Interest (AOI). Each sheet is designed to facilitate in-depth geological analysis at a scale of 1:50,000, ensuring the precise representation of stratigraphic units, structural elements, and surface processes. The high resolution and accuracy of these maps, derived from multi-source remote sensing data and rigorous field validation, provide a valuable resource for both academic research and practical applications in geology, tectonics, and environmental studies. These sheets are integral to understanding the geological evolution of the region, with each map sheet divided into nine distinct 1:150,000 segments for ease of interpretation and use in both research and industry.

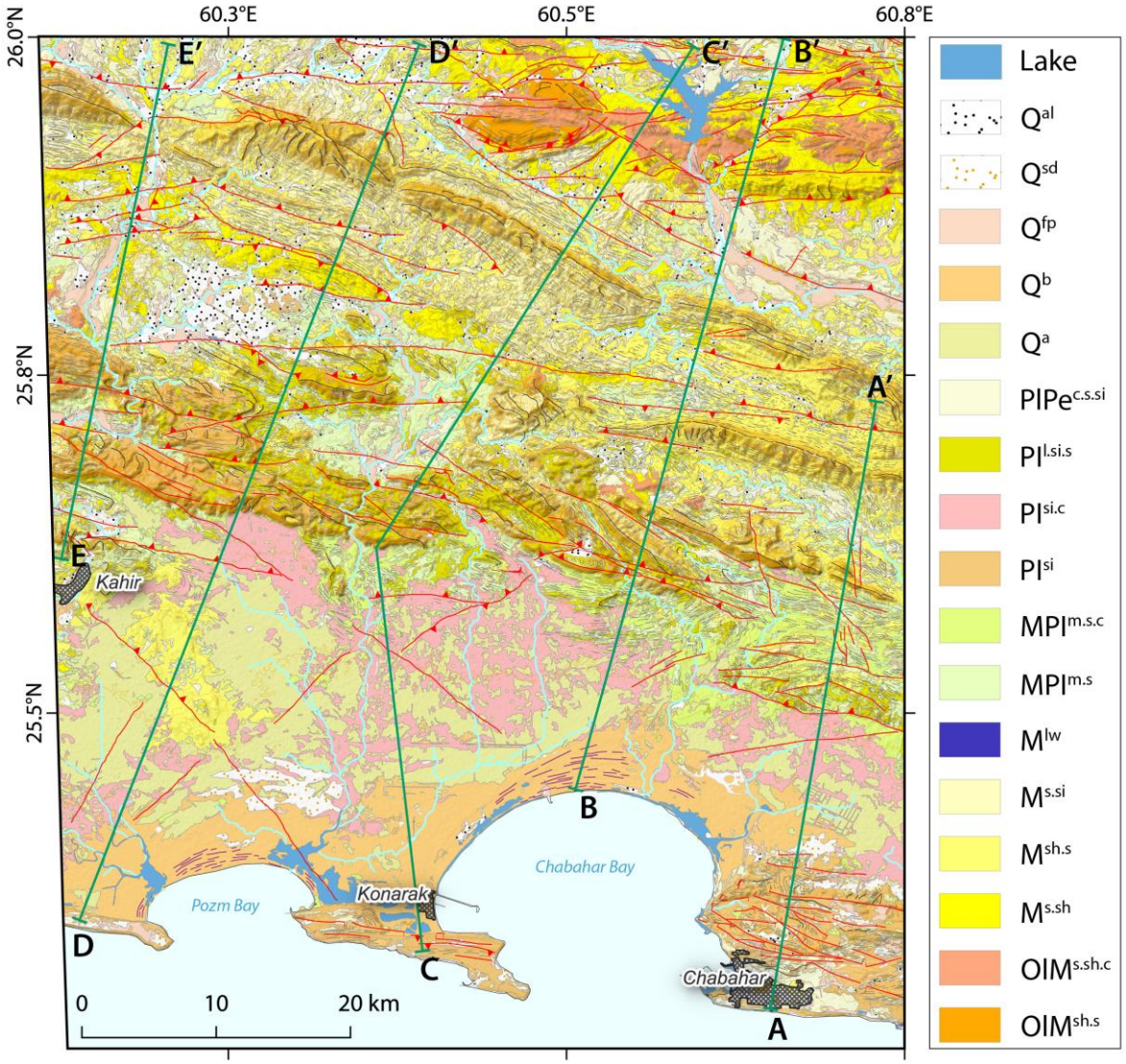


Figure 4-1. Server-based unified thematic geological units of the AOI. Solid green lines highlight the trajectory of the structural cross-sections in Chapter 5.

Table 4-1. Geo-units' time table based on absolute age determination and paleontological studies.

Geo-unit	Absolute Age	Paleontological studies	Reference
Q^{a}	≤ 21.3 kyr		Dolati (2010); Gharibreza (2016)
Q^{b}	≤ 7.3 kyr		Shah-Hosseini et al. (2018); Normand (2019)
$PlPe^{c.s.si}$		Pliocene–Pleistocene	Dolati (2010)
Pl^{si}		Pliocene–Pleistocene	Dolati (2010)
$Pl^{l.si.s}$		Pliocene	Dolati (2010)
$MPl^{m.s.c}$		Middle Miocene (Serravallian) to Early Pliocene	This study
		Late Miocene–Early Pliocene	Dolati (2010)
$MPl^{m.s}$		Early Miocene (Burdigalian)–Early Pliocene	This study
		Late Miocene–Early Pliocene	Dolati (2010)
$M^{s.si}$		Early Miocene (Burdigalian)–Late Miocene (Tortonian)	This study
$M^{sh.s}$		Middle Miocene (Serravallian)–Late Miocene (Tortonian)	This study
		Middle–Late Miocene	Dolati (2010)
$M^{s.sh}$	13.7–6.0 Myr		This study
		Late Oligocene–Middle Miocene	Dolati (2010)
		Oligocene–Late Miocene	Dolati (2010)
$OIM^{s.sh.c}$		Oligocene	Dolati (2010)
$OIM^{sh.s}$		Late Oligocene	Dolati (2010)
		Early Miocene (Late Burdigalian)–Middle Miocene (Early Langhian)	This study

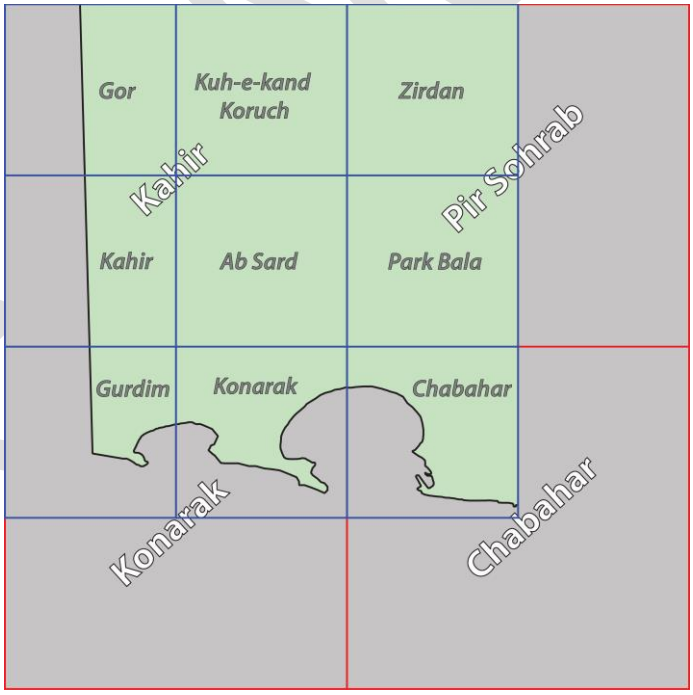


Figure 4-2. Mapping framework for the GeoNexus project (SUTGMM) in the Makran region.The green polygon marks the Area of Interest (AOI) for the Server-Based Unified Thematic Geological Mapping of Makran (SUTGMM) project. The solid grey rectangles with red outlines represent the extent of the previously published 1:100,000 geological maps that cover the study area. The rectangles with blue outlines correspond to the nine 1:50,000 geological sheets published as part of the GeoNexus geodatabase (SUTGMM), which include Ab Sard, Chabahar, Gor, Gurdim, Kahir, Konarak, Kuh-e-kand Koruch, Park Bala, and Zirdan.

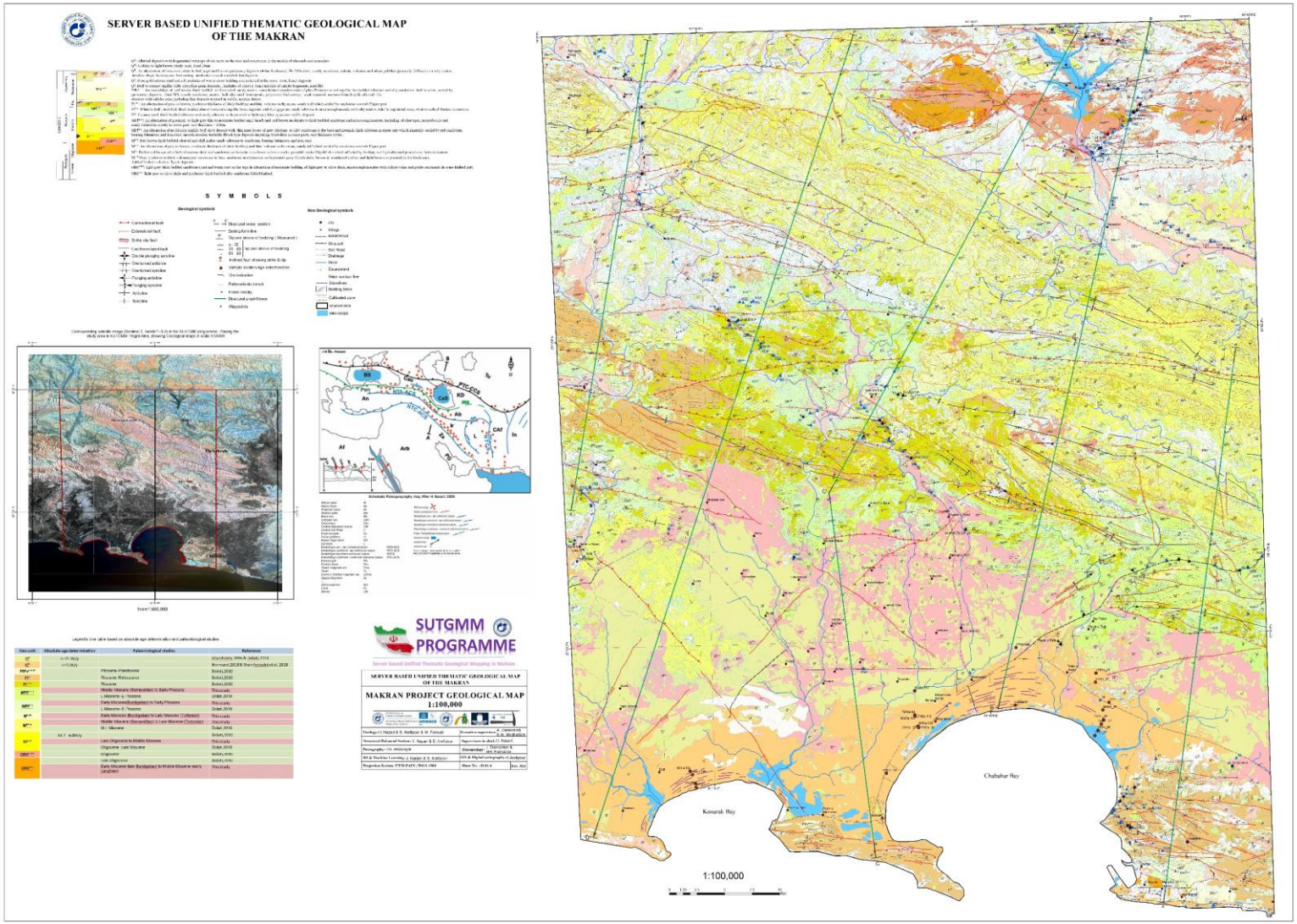


Figure 4-3. Final version of the GeoNexus (SUTGMM) map (Sheet No. 8141-4; scale 1:100,00).

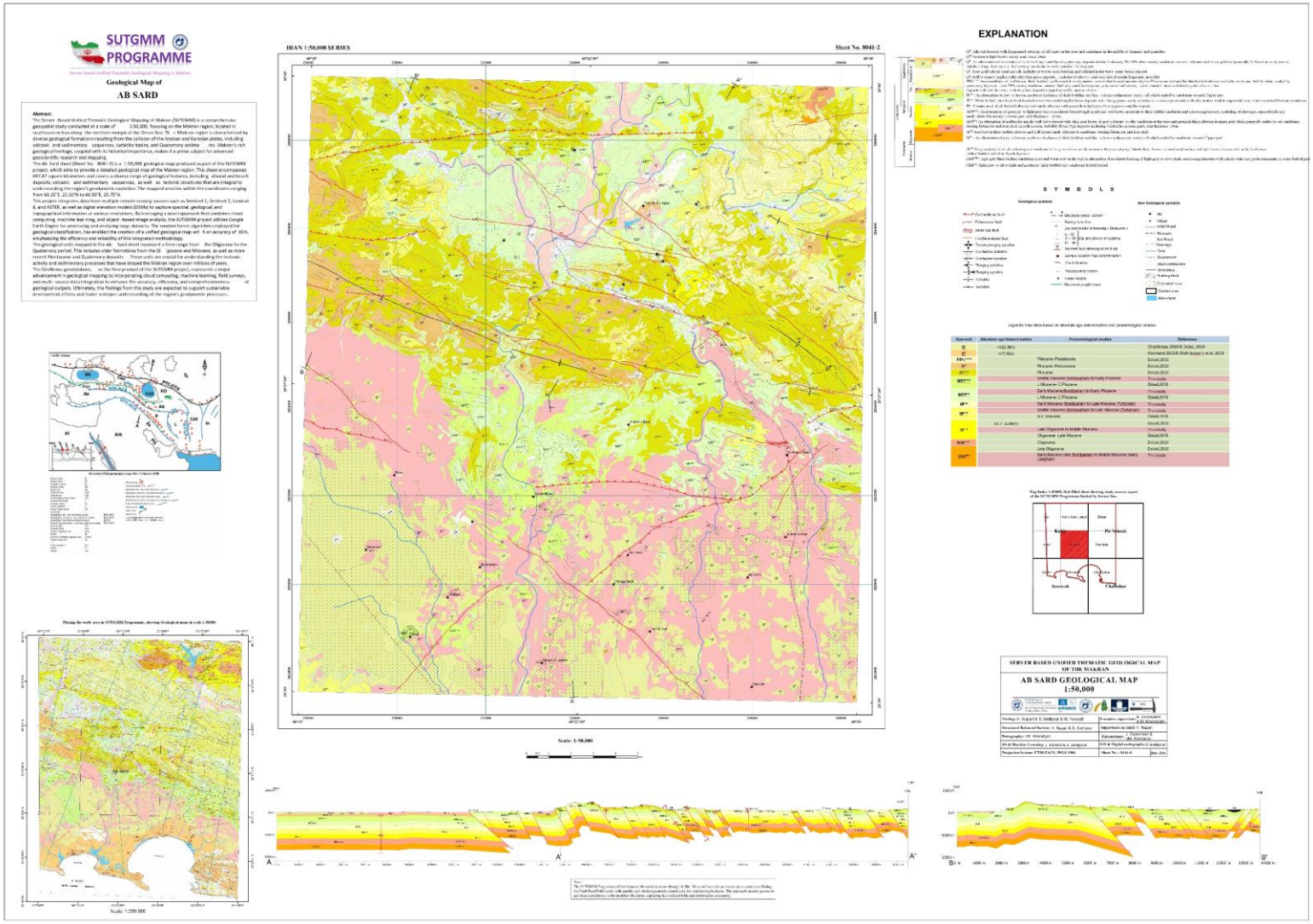


Figure 4-4. Final version of the Ab Sard map (Sheet No. 8041-2; scale 1:50,00).

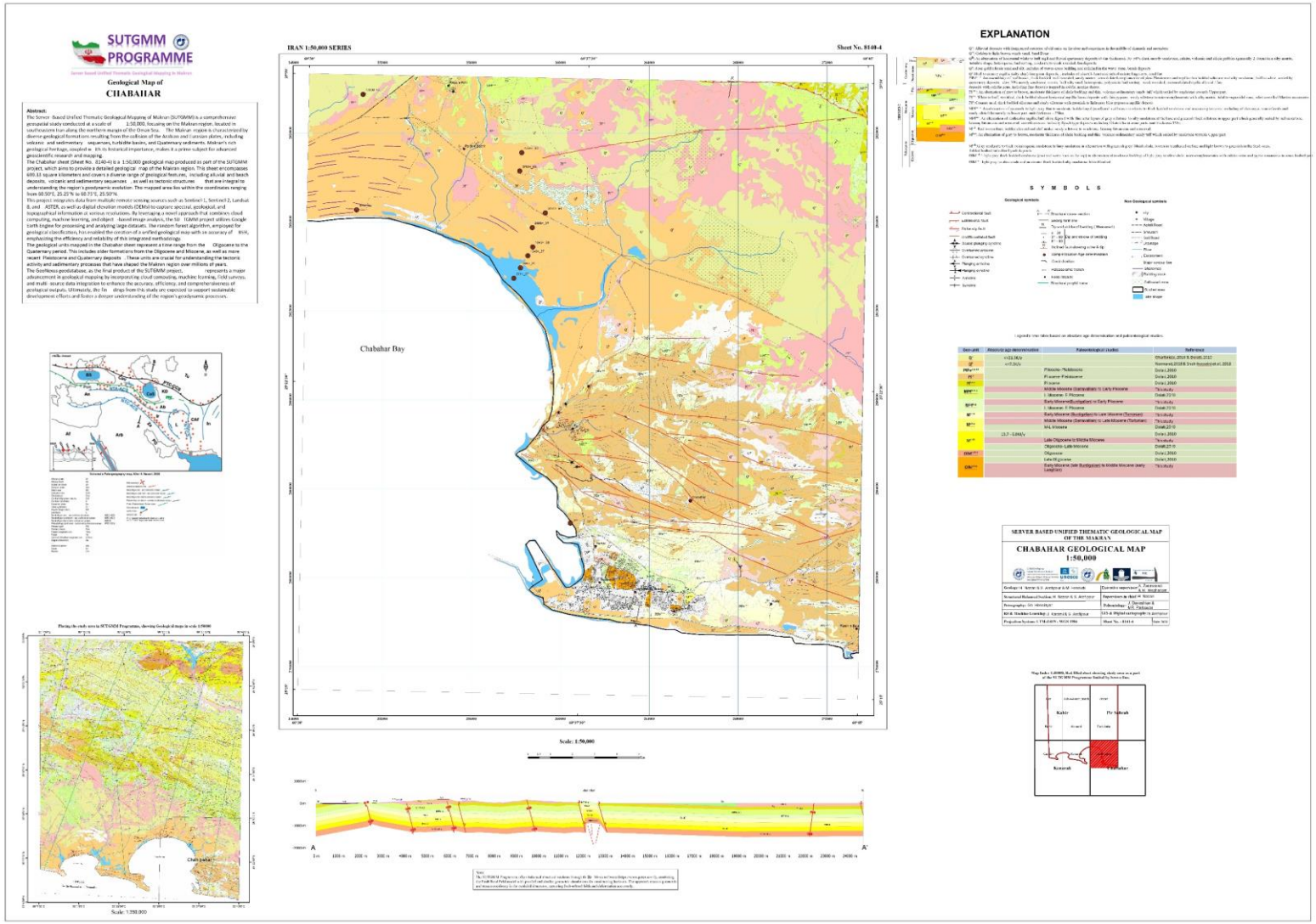


Figure 4-5. Final version of the Cabahar map (Sheet No. 8140-4; scale 1:50,00).

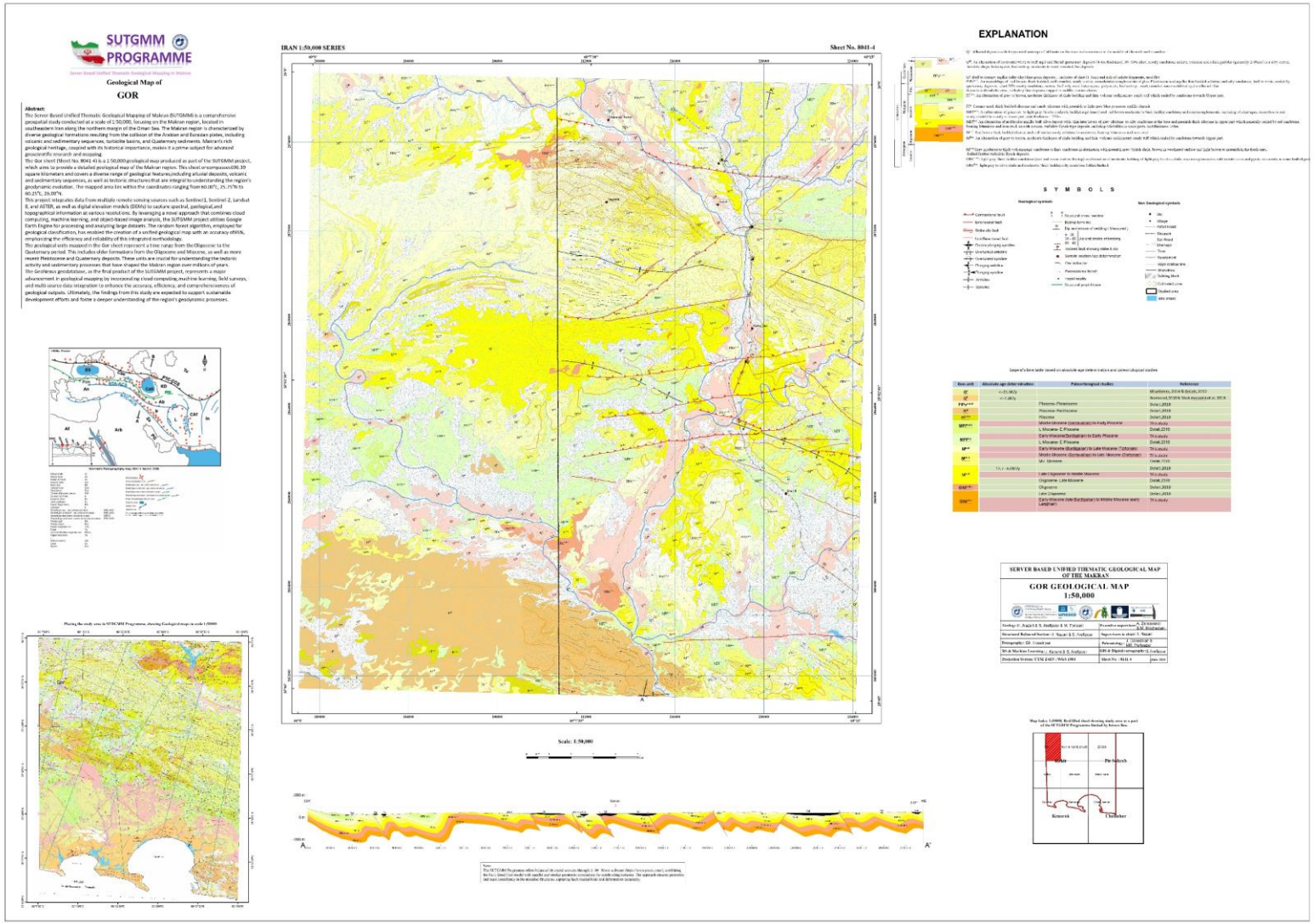


Figure 4-6. Final version of the Gor map (Sheet No. 8041-4; scale 1:50,00).

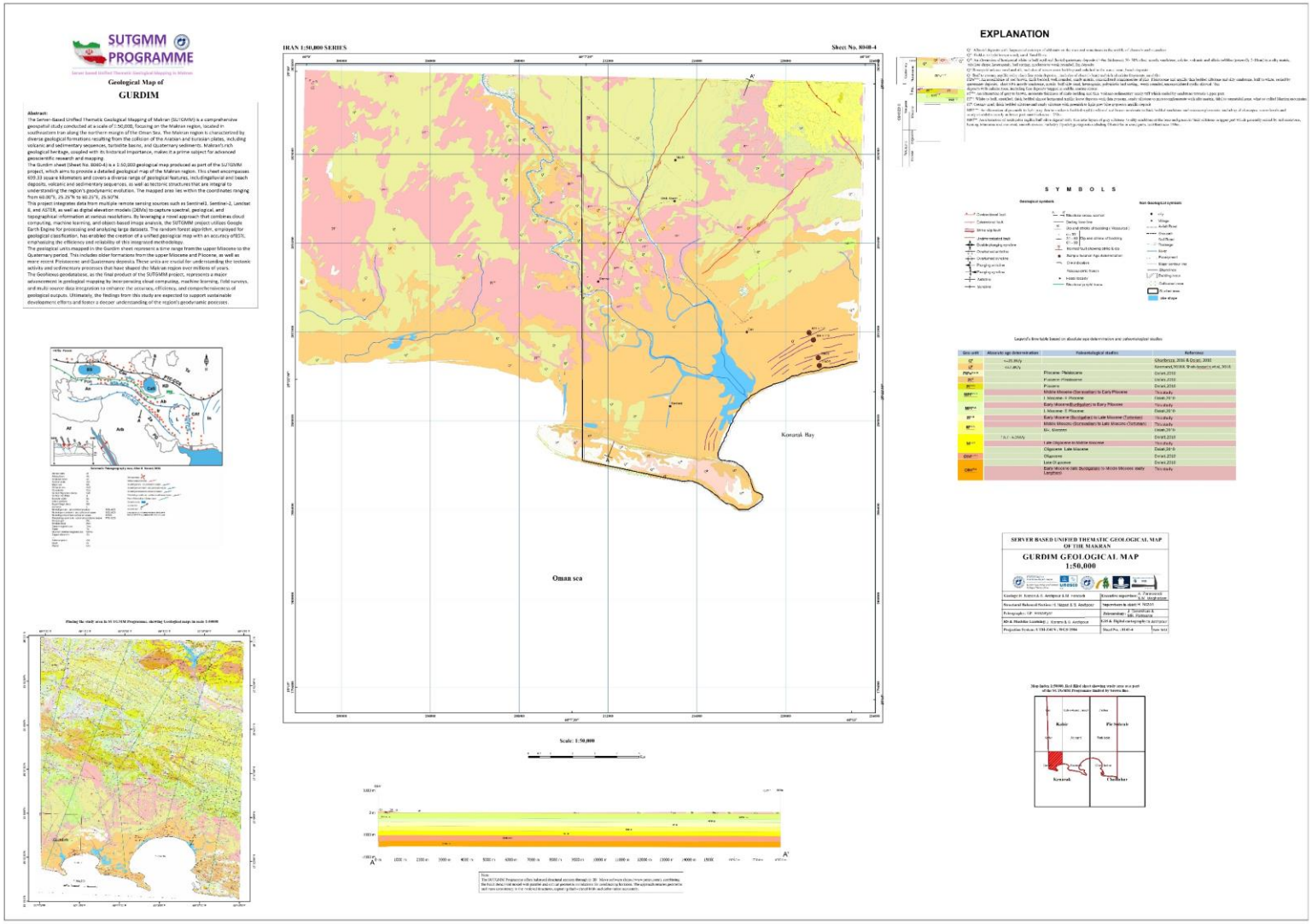


Figure 4-7. Final version of the Gurdim map (Sheet No. 8040-4; scale 1:50,00).

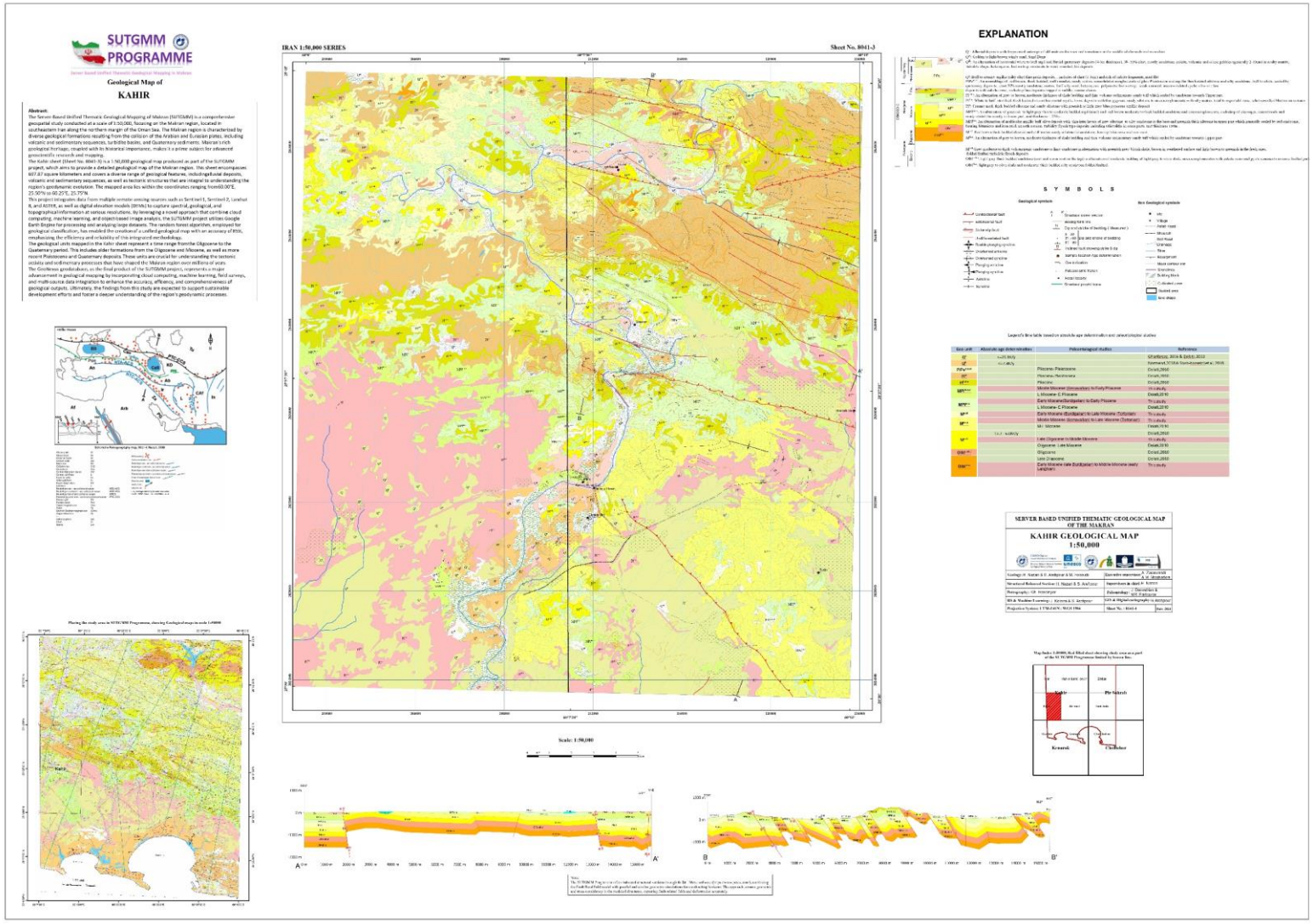


Figure 4-8. Final version of the Kahir map (Sheet No. 8041-3; scale 1:50,00).

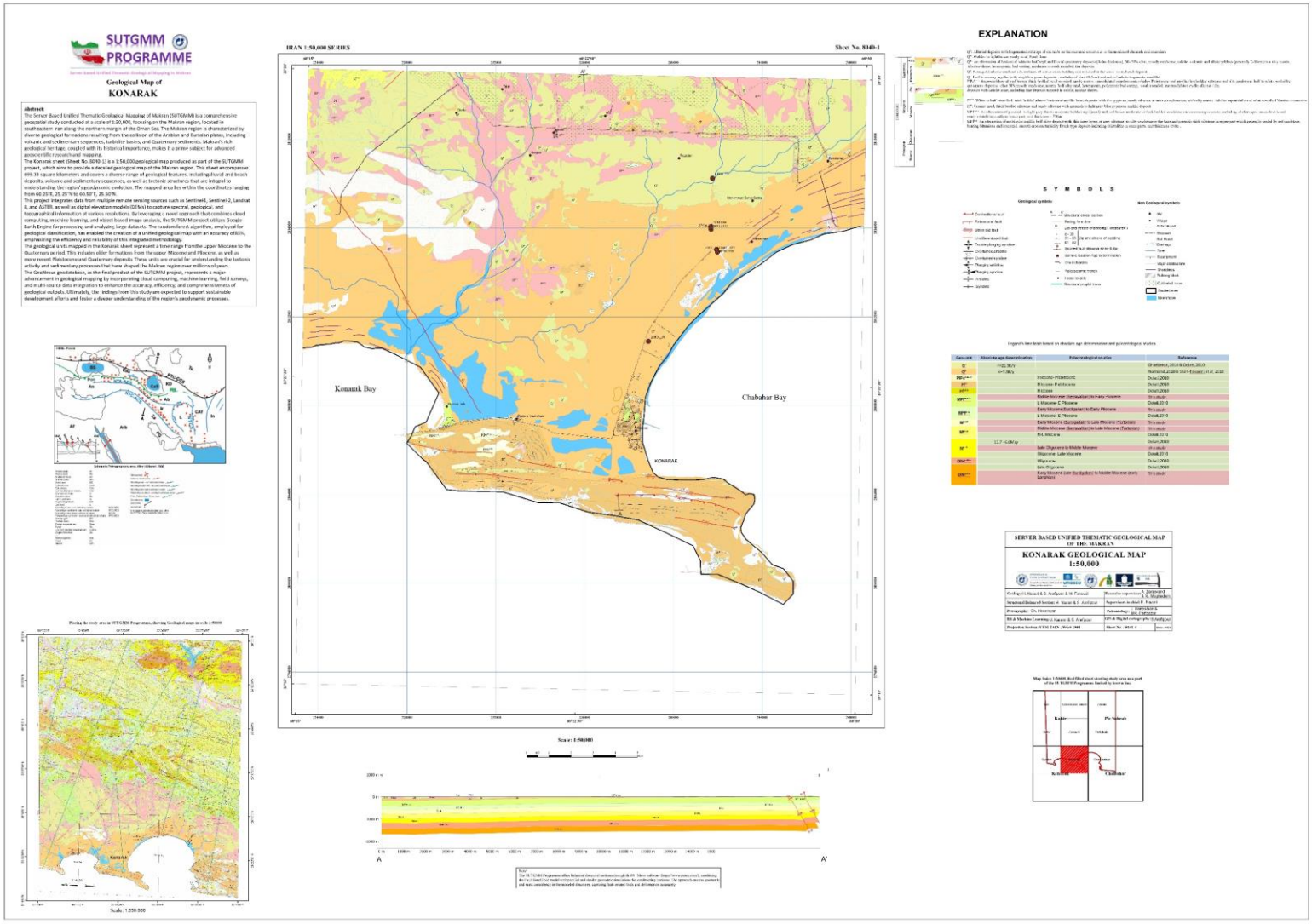


Figure 4-9. Final version of the Konarak map (Sheet No. 8040-1; scale 1:50,00).

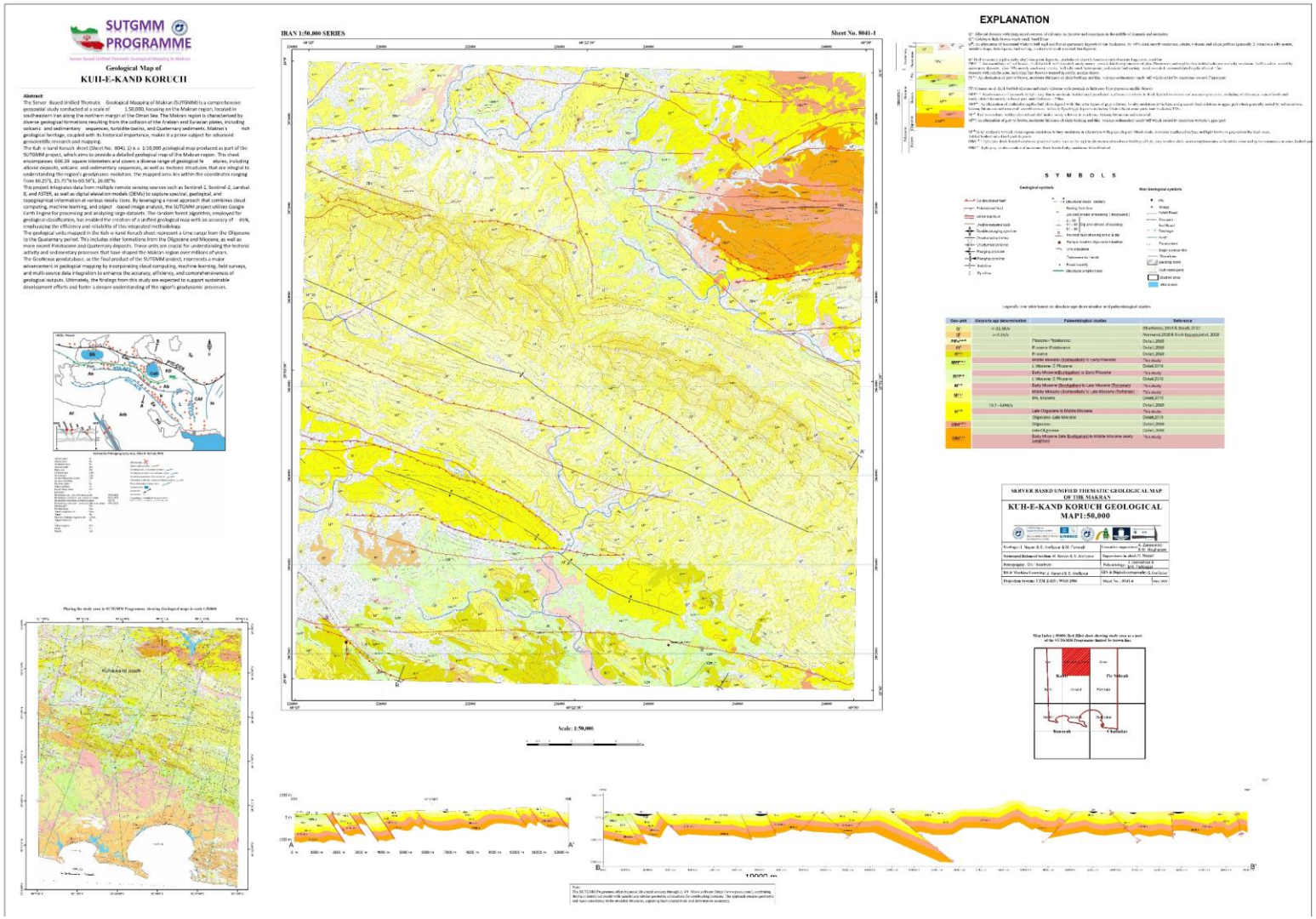


Figure 4-10. Final version of the Kuh-e-kand Koruch map (Sheet No. 8041-1; scale 1:50,00).

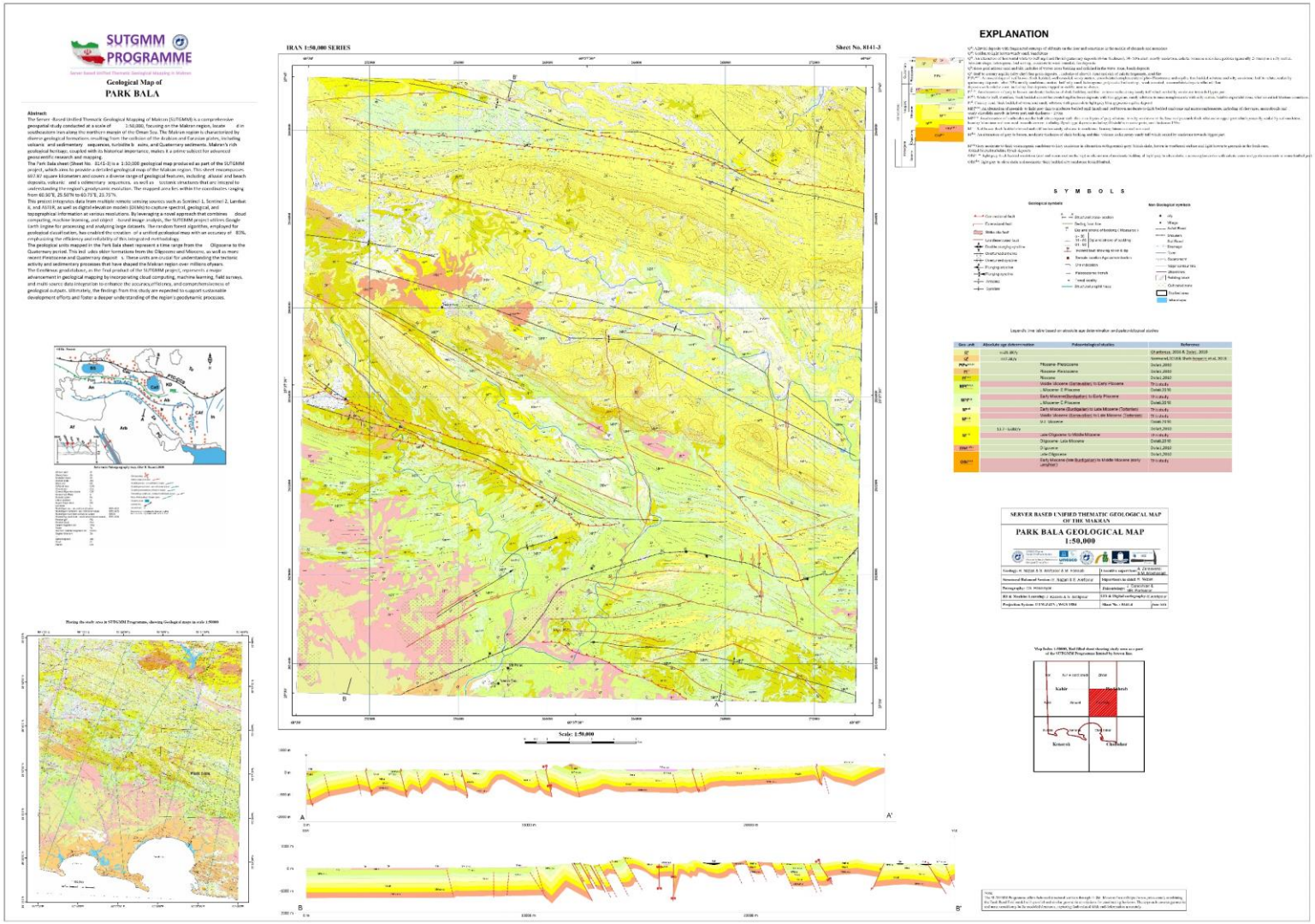


Figure 4-11. Final version of the Park Bala map (Sheet No. 8141-3; scale 1:50,00).

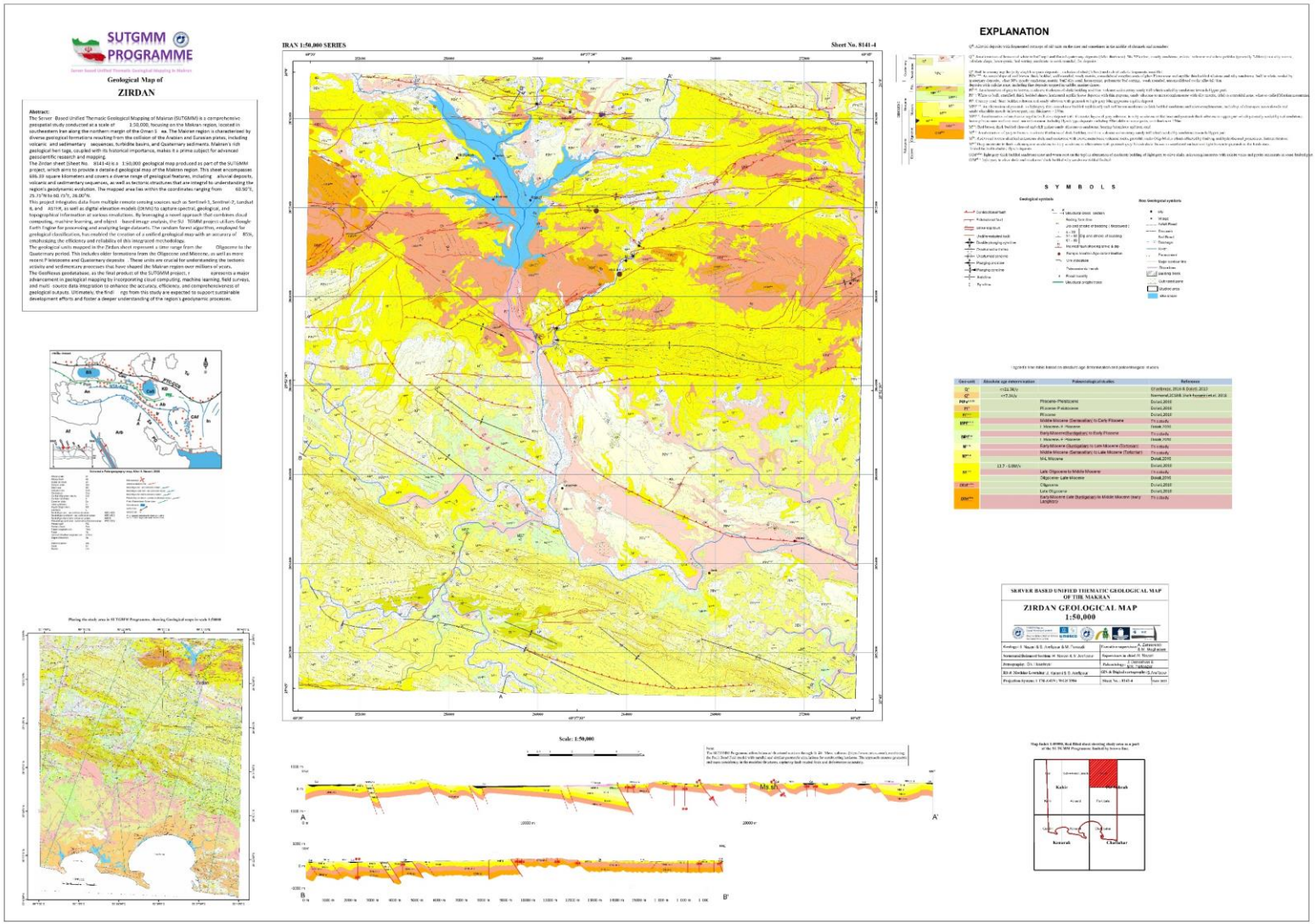


Figure 4-12. Final version of the Zirdan map (Sheet No. 8141-4; scale 1:50,00).

4.1 $OlM^{sh.s}$ Unit (Late Oligocene Shale and Sandstone)

The $OlM^{sh.s}$ Unit represents the oldest geological formation within the study area, dating to the late Oligocene. The unit is represented by 54 mapped polygons within the study area. These outcrops vary in size, reflecting the complex nature of the terrain and the impact of tectonic processes. The individual areas of these outcrops range from approximately 0.0136 sq km to 14.64 sq km (OBJECTID_1: 6108). The cumulative area covered by the $OlM^{sh.s}$ Unit is ~ 38 sq km.

This 350-m thick unit is characterized by light grey to olive shales interbedded with moderate to thick-bedded silty sandstones. These rocks have undergone significant folding and faulting, reflecting the tectonic activities that have shaped the region.

4.1.1 Previous Studies

Previous geological mappings have described formations equivalent to the $OlM^{sh.s}$ Unit under various names. On the 1:250,000 scale geological maps of Nikshahr, Fannuj, and Pishin, similar units have been identified:

- Ruk Unit (McCall, 1985): Described on the Pishin map as rhythmically bedded sandstones and shales of late Eocene to late Oligocene age, with an estimated thickness of 10,000–14,000 m.
- Angohran Unit (Eftekhar-Nejad and McCall, 1993; McCall, 1985): Identified on the Fannuj and Nikshahr maps as massively bedded sandstones with shales and minor siltstones, dated to the Oligocene–early Miocene, with a suggested thickness of 5,000–7,000 m.
- Guredak Unit (Eftekhar-Nejad and McCall, 1993): Found on the Nikshahr map, described as a lower to middle Eocene sandstone-dominated sequence.
- Pirdan Unit (Dolati, 2010): These differing lithological descriptions and nomenclatures, along with more precise stratigraphic ages obtained from recent studies, have led to the redefinition of this unit as the Pirdan Unit (Dolati, 2010). The Pirdan Unit corresponds to the $OlM^{sh.s}$ Unit in this study.

4.1.2 Lithology

The $OlM^{sh.s}$ unit consists predominantly of:

- Shale: Light grey to olive in color, these shales are fine-grained and display fissility. They suggest deposition in a relatively low-energy marine environment.
- Silty Sandstone: These are moderate to thick-bedded, ranging from 10 to 120 cm (Dolati, 2010) in thickness. The sandstones are coarse to fine-grained, green to dark grey, and often display tabular bedding planes. They are commonly volcaniclastic and lack calcareous clasts or cement.

Sedimentary structures such as graded bedding, ripple marks, load casts, groove casts, and flute casts are prevalent (Dolati, 2010), indicating deposition by turbidity currents. The presence of

GeoNexus

channelized sandstones suggests periods of stronger currents capable of transporting coarser material.

Petrographic analyses reveal that the sandstones are composed mainly of quartz grains, with subordinate amounts of feldspar and lithic fragments. The presence of muscovite is notable, increasing from about 5% to 20% towards the west of the study area (Dolati, 2010). The sandstones exhibit textures indicative of rapid deposition from high-density turbidity currents. Grain sizes range from coarse to fine, with good sorting in some layers and poorer sorting in others. The unit has undergone compaction and minor cementation. The lack of calcareous cement suggests limited diagenetic alteration and supports the volcaniclastic nature of the sediments (Dolati, 2010).

4.1.3 Stratigraphy and Age

The unit is assigned to the late Oligocene based on biostratigraphic data, including nannofossils and foraminifera. Samples have yielded ages corresponding to the Chattian stage (approximately 27–23 Ma BP), with some samples indicating ages up to the Rupelian–Chattian boundary (30–27.5 Ma BP) (Dolati, 2010).

The lower boundary of the $OlM^{sh.s}$ Unit is typically obscured by thrust faults, making it difficult to observe directly. The upper boundary transitions into overlying shale-dominated turbidite successions, indicating a shift from inner fan to more distal depositional environments.

4.1.4 Structural Features

The $OlM^{sh.s}$ unit exhibits significant deformation due to tectonic activities associated with the collision between the Arabian and Eurasian plates. The rocks have been subjected to compressional forces, resulting in folding and faulting.

4.1.5 Paleontological Evidence

- Microfossils: The shales contain abundant microfossils, including nannofossils and foraminifera, which have been crucial in dating the unit. The identification of Chattian nannofossil zones (e.g., Zone NP25) supports the late Oligocene age assignment (Dolati, 2010).
- Biostratigraphic correlation: The concordance between nannofossil and foraminifera ages allows for precise stratigraphic correlations within the unit and with other regional formations (Dolati, 2010).

4.1.6 Depositional Environment

The $OlM^{sh.s}$ Unit was deposited in a deep marine setting, specifically within an inner to middle submarine fan environment (Dolati, 2010):

- Inner Fan Deposits: The presence of thick, channelized sandstones suggests deposition by high-energy turbidity currents in proximal settings.

- Sedimentary Structures: Features such as flute casts and groove casts indicate strong and erosive bottom currents, with flow directions predominantly towards the east.
- Upward Thickening Cycles: Observations of 100–300 m thick upward-thickening cycles reflect periodic increases in sediment supply or changes in depositional energy, consistent with submarine fan lobe development.

4.2 $OlM^{s.sh.c}$ Unit (Oligocene Shale, Sandstone, and Conglomerate)

The $OlM^{s.sh.c}$ Unit represents a geological formation within the study area, dating to the Oligocene with a thickness of ~ 250 m. This unit is characterized by light grey thick-bedded sandstones with distinctive sedimentary features, interbedded with light grey to olive shales, and microconglomerates containing calcite veins and pyrite remnants in faulted zones. The unit exhibits significant tectonic deformation, reflecting the complex geological history of the region.

The $OlM^{s.sh.c}$ Unit is an Oligocene-aged geological formation within the study area, characterized by a sequence of interbedded sandstones, shales, and conglomerates. This unit is also equivalent to Pirdan Unit (e.g., Dolati, 2010); however, the unit exhibits distinct lithological features and structural complexities that have been refined and distinguished in our mapping through server-based unified thematic geological mapping. While previous studies have grouped similar formations under broader units, our detailed mapping efforts have identified the $OlM^{s.sh.c}$ Unit as a separate entity.

The unit is represented by 260 mapped polygons within the study area. The individual areas of these outcrops vary greatly, from as small as 0.0008 sq km to as large as 76.36 sq km. Notable large outcrops include OBJECTID_1: 6359 (76.36 sq km), 6305 (28.31 sq km), and 6328 (29.48 sq km). The cumulative area covered by the $OlM^{s.sh.c}$ Unit is ~ 350 sq km.

4.2.1 Lithology

The $OlM^{s.sh.c}$ Unit comprises:

- Sandstone: Light grey, thick-bedded sandstones with notable sedimentary structures such as casts and worm burrows on bed tops. The sandstones are volcaniclastic, lacking calcareous clasts or cement, and exhibit features like graded bedding and ripple marks, indicative of deposition by turbidity currents.
- Shale: Moderate-bedded, light grey to olive shales interbedded with the sandstones, suggesting fluctuations in depositional energy and sediment supply.
- Microconglomerate: Occurs within the unit, containing clasts cemented by calcite veins. In faulted zones, pyrite remnants are observed, pointing to post-depositional mineralization processes.
- Calcite veins and pyrite remnants: The presence of calcite veins and pyrite in faulted parts indicates fluid flow and hydrothermal activity associated with tectonic movements.

GeoNeXus

4.2.2 Stratigraphy and Age

The $OlM^{s.sh.c}$ Unit is assigned an Oligocene age based on stratigraphic position and correlation with similar units identified in previous studies. This unit overlies the older $OlM^{sh.s}$ Unit and is succeeded by younger formations. The transition from thick-bedded sandstones to interbedded shales and conglomerates reflects changes in depositional environments and sediment supply during the Oligocene.

4.2.3 Petrographic Analysis

Two samples from the $OlM^{s.sh.c}$ Unit provide insights into its mineralogical and textural characteristics:

4.2.3.1 Sample 24M-42P

- Location: 25.9281° N latitude, 60.1989° E longitude.
- Rock type: Identified as listvenite, a highly altered or metamorphosed rock resulting from hydrothermal alteration of ultramafic rocks.
- Description:

  The rock exhibits a crystalline texture, with the primary texture completely obliterated due to intense alteration. It is predominantly composed of calcite crystals of varying sizes. The calcite displays rhombohedral crystal forms, and in some areas, the edges of these crystals are coated with brownish clay minerals (?), likely formed from fluid-rock interactions during alteration. These clay minerals could result from the decomposition of silicate minerals under hydrothermal conditions.

  Large grey quartz crystals are present in clusters throughout the rock. These quartz grains have numerous inclusions, suggesting complex growth histories and multiple phases of mineralization. The quartz may have crystallized from silica-rich hydrothermal fluids that permeated the rock during alteration.

  Chromian spinel (chromite) is identified within the sample, indicating an ultramafic protolith. Chromian spinel is a common accessory mineral in peridotites and serpentinites, and its presence supports the interpretation of the rock originating from mantle-derived ultramafic rocks.

  Mineralization is evident, with minerals filling the intercrystalline spaces between calcite crystals. The edges of calcite crystals show signs of oxidation (?), possibly due to exposure to oxidizing fluids or weathering processes post-alteration. Under magnifications of 10x and 40x, small red minerals are observed, which are likely hematite or finely dispersed iron oxides. The red coloration suggests the presence of iron, possibly formed through the oxidation of iron-bearing minerals (Figure 4-13).

- Interpretation:

  The sample represents a listvenite, formed through metasomatic alteration of ultramafic rocks by CO_2-rich hydrothermal fluids. This process involves the carbonation and

GeoNexus

silicification of ultramafic rocks, leading to the replacement of original minerals with calcite and quartz. The presence of chromian spinel confirms the ultramafic nature of the original rock.

The oxidation of calcite edges and the presence of clay minerals suggest secondary alteration processes, possibly related to continued fluid interactions or weathering after the initial metasomatism. The mineralization and filling of intercrystalline spaces indicate episodes of fluid movement, which could be associated with tectonic activity and fracturing that allowed hydrothermal fluids to permeate the rock.

The occurrence of listvenite is significant, as it often forms in zones of major faulting and shearing, where fluids can interact extensively with the host rocks. This sample provides evidence of hydrothermal alteration linked to tectonic processes within the region.

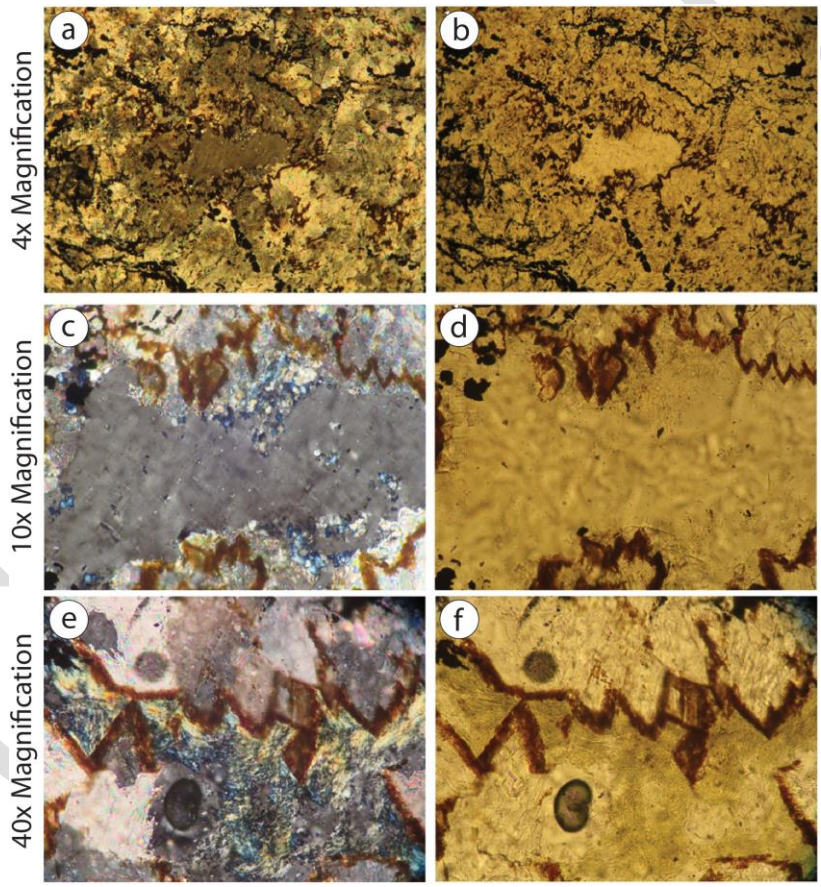


Figure 4-13. Photomicrographs of Sample 24M-42P in cross-polarized light (XPL) and plane-polarized light (PPL) at varying magnifications. Panels a, c, and e are in XPL, and panels b, d, and f are in PPL.

4.2.3.2 Sample 24M-44P

- Location: 25.9281° N latitude, 60.1989° E longitude (same as Sample 24M-42P).

- Rock type: Classified as a mylonitic metabasite, indicating a metamorphosed mafic rock that has undergone intense ductile deformation.
- Description:

  The rock displays a mylonitic texture, characterized by a well-developed foliation resulting from the alignment of minerals under directed stress. This texture indicates significant deformation within a shear zone, where the rock has been subjected to intense shearing forces.

  The sample is extensively chloritized, with chlorite being one of the dominant minerals. Chlorite forms during low-grade metamorphism, typically under greenschist facies conditions. The presence of epidote and amphibole minerals further supports metamorphism under these conditions. Epidote commonly develops in metamorphosed mafic rocks, while amphibole minerals can indicate variations in pressure and temperature during metamorphism.

  Mineralization has occurred along fractures within the rock, leading to the formation of opaque minerals, likely oxides such as magnetite or sulfides like pyrite. These opaque minerals suggest fluid movement and possible hydrothermal activity during or after deformation. The concentration of mineralization along fractures implies that these features served as pathways for fluid flow.

- Interpretation:

  The sample (Figure 4-14) represents a metabasite that has been significantly deformed to form a mylonite. The mylonitic texture indicates that the rock experienced intense ductile deformation, likely within a major shear zone associated with regional tectonic movements.

  The mineral assemblage of chlorite, epidote, and amphibole is characteristic of metamorphism under greenschist facies conditions, corresponding to temperatures of approximately 300–450°C and pressures of 2–10 kbar. This suggests that the rock was metamorphosed at relatively shallow crustal levels during tectonic activity.

  The formation of opaque minerals along fractures points to episodes of fluid infiltration, which may have introduced or redistributed minerals during or after deformation. These fluids could be related to metamorphic devolatilization reactions or external hydrothermal systems.

  Given the complex history indicated by the mylonitic texture and mineralogy, it is recommended that this sample be further examined by a specialist in metamorphic petrology to gain deeper insights into its metamorphic evolution and tectonic significance.

GeoNexus

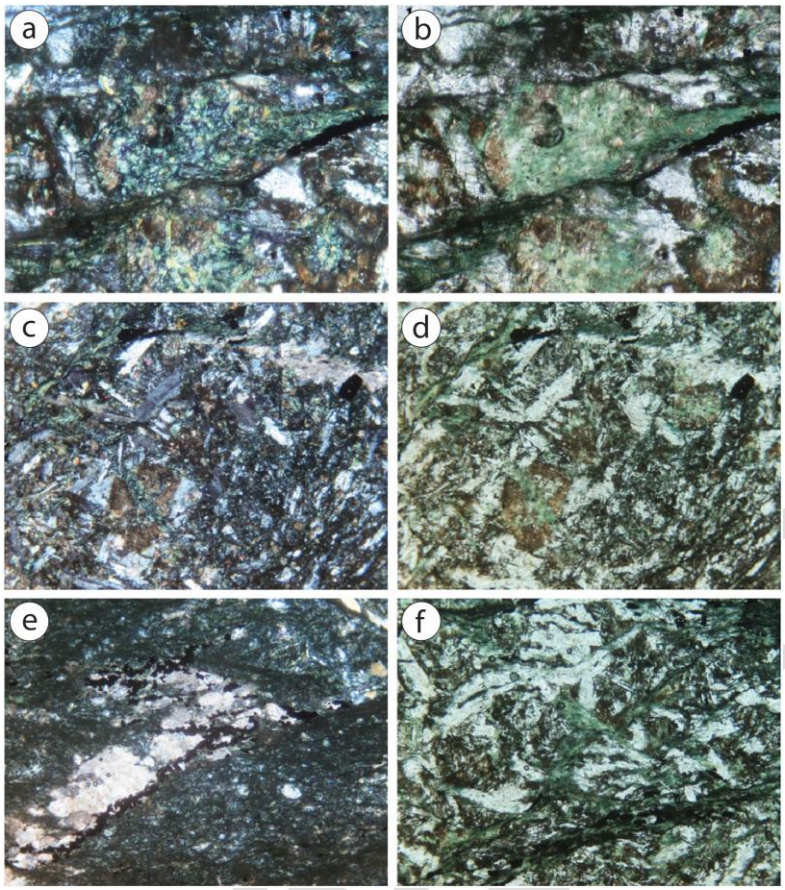


Figure 4-14. Photomicrographs of Sample 24M-44P in XPL (panels a, c, and e) and PPL (panels b, d, and f) at 10x magnifications.

4.2.4 Structural Features

Similar to $OlM^{sh.s}$ Unit, the $OlM^{s.sh.c}$ Unit exhibits significant tectonic deformation, including folding and faulting due to regional compressional forces. Faulted areas contain calcite veins and pyrite, suggesting that these zones acted as pathways for mineralizing fluids. Some rocks within the unit show evidence of metamorphism and hydrothermal alteration, indicating dynamic geological processes at play during and after deposition.

Shear Zones are indicated by the presence of mylonitic textures in rocks such as Sample 24M-44P. These zones represent areas where rocks have undergone intense ductile deformation due to differential stress during tectonic movements. The development of shear zones suggests significant crustal shortening and displacement within the accretionary wedge.

Hydrothermal Alteration is evident in faulted zones, where calcite veins and pyrite remnants are present. These features indicate that faults and fractures acted as conduits for hydrothermal fluids, leading to mineralization and alteration of the surrounding rocks. The interaction between fluids and rocks has contributed to the complexity of the unit's lithology and mineralogy.

4.2.5 Depositional Environment

The sedimentary characteristics of the $OlM^{s.sh.c}$ Unit provide insights into its depositional environment during the Oligocene.

- Submarine Fan Systems: The thick-bedded, channelized sandstones suggest deposition by high-density turbidity currents within submarine fan systems. These environments are associated with continental margins where sediment is transported downslope by gravity flows, depositing sands and conglomerates in deep marine settings.
- Fluctuating Energy Conditions: The alternation of sandstones with shales and microconglomerates reflects variations in depositional energy and sediment supply. High-energy events deposited coarse-grained materials, while quieter periods allowed for the accumulation of fine-grained shales. Such fluctuations could be driven by changes in sea level, tectonic uplift, or variations in sediment source areas.
- Bioturbation and Sedimentary Structures: The presence of worm burrows and other trace fossils indicates that the depositional environment supported benthic organisms. Sedimentary structures like graded bedding and ripple marks provide evidence of current directions and flow regimes during deposition.

4.2.6 Tectonic Implications

The features observed in the $OlM^{s.sh.c}$ Unit have significant implications for the tectonic history of the region.

- Accretionary Processes: The deformation and metamorphism evident in the unit suggest involvement in accretionary processes at a convergent plate margin. The Makran accretionary wedge, formed by the subduction of the Arabian plate beneath the Eurasian plate, provides a tectonic setting where sediments are scraped off the downgoing slab and accreted to the overriding plate, undergoing deformation and metamorphism.
- Ophiolitic Affiliation: The identification of listvenite containing chromian spinel points to the incorporation of ultramafic rocks, possibly derived from ophiolitic sequences, into the sedimentary succession. This incorporation could occur through tectonic emplacement or obduction of oceanic crust onto the continental margin.
- Fluid Flow and Mineralization: The hydrothermal alteration and mineralization within the unit indicate significant fluid flow associated with tectonic activity. Fluids released during metamorphism or introduced from external sources can alter rocks and deposit minerals along fractures and faults. These processes contribute to the complexity of the unit's lithology and provide evidence of the dynamic conditions within the accretionary wedge.

4.3 $M^{s.sh}$ Unit (Oligocene–Late Miocene Shale and Sandstone)

The $M^{s.sh}$ Unit represents an Oligocene to late Miocene geological formation within the study area, characterized by a complex assemblage of sedimentary rocks with volcanic influences. This unit, with a thickness of ~ 200 m, comprises grey, moderate to thick-bedded volcanogenic sandstone

transitioning to limy sandstone, alternating with greenish-grey to bluish shale. On weathered surfaces, the rocks exhibit a brown coloration, while fresh surfaces range from light brown to greenish hues. The $M^{s.sh}$ Unit is notable for its folded and faulted turbiditic flysch deposits, reflecting a dynamic tectonic setting during its formation.

The unit is represented by 516 mapped polygons within the study area. The individual areas of these outcrops vary greatly, from as small as 0.00017 sq km to as large as 123.49 sq km. Notable large outcrops include OBJECTID_1: 4488 (123.49 sq km), 4486 (79.41 sq km), and 4736 (72.74 sq km). The cumulative area covered by the unit is ~ 822 sq km.

4.3.1 Previous Studies

Previous geological investigations have attributed the sediments of the $M^{s.sh}$ Unit to various formations under different nomenclatures.

- Jarut Unit: On the Pishin and Nikshahr geological maps (Geological Survey of Iran, 1989, 1993), the rhythmic sandstone and shale sequences of early to middle Miocene age were designated as the Jarut Unit. This unit was estimated to have a substantial thickness exceeding 5,000 m and was divided into three members.
- Hichan Unit: In the Nikshahr and Fannuj areas, similar rhythmic sandstone and shale deposits of lower Miocene age were referred to as the Hichan Unit. This unit was reported to have a cumulative thickness of approximately 3,000 m.
- Guredak Unit: On the Fannuj quadrangle, McCall (1985) identified these sediments as the Guredak Unit, described as Eocene turbidites.
- OM Formation: Eftekhar-Nejad and McCall (1993) labeled the sediments as "OM" on the Nikshahr map, assigning them a late Oligocene to early Miocene age, although specific lithological descriptions were not provided.
- Pishamak Unit: Notably, the the $M^{s.sh}$ Unit has been associated with the Pishamak Unit (Dolati, 2010), named after a village in the Inner Makran region.

4.3.2 Lithology and Petrography

The $M^{s.sh}$ Unit displays a diverse lithological composition, indicative of varying depositional environments and sediment sources influenced by volcanic activity. Detailed petrographic analyses of several samples have been performed within this unit.

4.3.2.1 Sample 24M-25F

- Location: 25.8866° N latitude, 60.1975° E longitude.
- Rock type: Hybrid Sedimentary–Volcanic Rock.
- Rock name: Volcanic Siltstone to Mudstone.
- Microfacies: Sandy-silty limestone, detrital, ferruginous.

GeoNexus

- Description:

  Sample 24M-25F (Figure 4-15) is characterized by a matrix composed of volcanic ash that has decomposed into calcite. The grains within the rock include quartz, volcanic rock fragments, and feldspar. Due to their small size, distinguishing individual grains under the microscope is challenging. Scattered green grains, possibly epidote, are observed in low abundance. The rock exhibits lamination and minor bioturbation, suggesting deposition in a relatively quiet sedimentary environment with some biological activity. Veins of opaque minerals, likely iron oxides, are present in certain facies, indicating post-depositional mineralization processes. The grains show slight orientation due to compaction, reflecting diagenetic alterations after deposition.

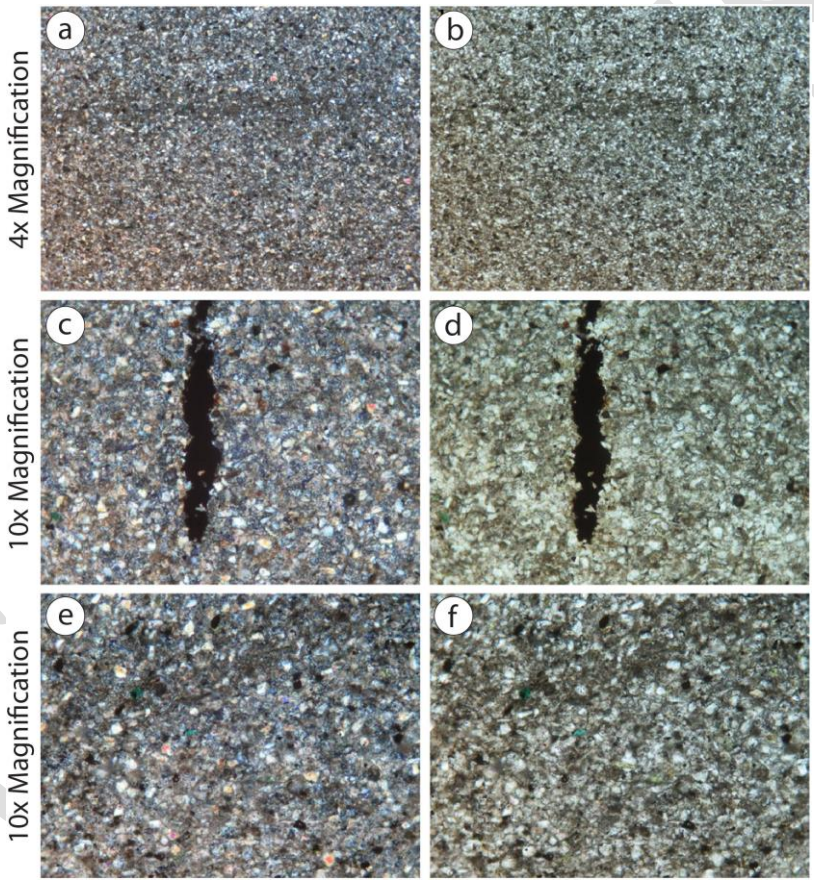


Figure 4-15. Photomicrographs of Sample 24M-25F in XPL (panels a, c, and e) and PPL (panels b, d, and f) at varying magnifications.

- Interpretation:

  This volcanic siltstone to mudstone represents a depositional environment influenced by volcanic activity, where volcanic ash settled and subsequently altered to calcite. The presence of quartz, feldspar, and volcanic rock fragments suggests a mixed provenance, combining both volcanic and sedimentary sources. Minor bioturbation and lamination indicate periods of low-energy conditions allowing for organism activity and fine sediment

deposition. Compaction and orientation of grains reflect diagenetic processes affecting the rock post-deposition. The ferruginous nature indicates iron oxide enrichment, possibly from groundwater percolation or diagenetic alteration.

4.3.2.2 Sample 24M-37P

- Location: 25.949° N latitude, 60.6213° E longitude.
- Rock type: Hybrid Sedimentary–Volcanic Rock.
- Rock name: Fine-Grained Volcanic Sandstone or Epiclastic Volcanic Sandstone.
- Description:

  This sample (Figure 4-16) comprises grains of quartz and feldspar along with volcanic rock fragments. The matrix is partially filled with calcite cement, and in epiclastic regions, it is filled with recrystallized volcanic ash. Mica minerals and glauconite are observed, indicating a marine depositional environment where glauconite typically forms. Some parts of the matrix have undergone recrystallization. Severe decomposition and sericitization are evident on the surfaces of plagioclase and feldspar grains, indicating chemical alteration during diagenesis. Quartz grains mostly exhibit straight extinction under cross-polarized light. The rock displays parallel lamination and possibly cross-lamination, suggesting deposition by currents or waves. The grains are poorly sorted, and the rock is texturally and compositionally immature. No significant mineralization is observed in this facies. Modal composition includes quartz (15–25%), volcanic lithic fragments (40–45%), and feldspar (15–20%).

- Interpretation:

  The fine-grained volcanic sandstone reflects a depositional environment with substantial volcanic input, likely in proximity to volcanic activity. The presence of glauconite and mica suggests marine conditions. Poor sorting and immaturity indicate rapid deposition with minimal transport, preserving the volcanic material's characteristics. Sericitization of feldspars points to chemical weathering and alteration processes during diagenesis.

GeoNexus

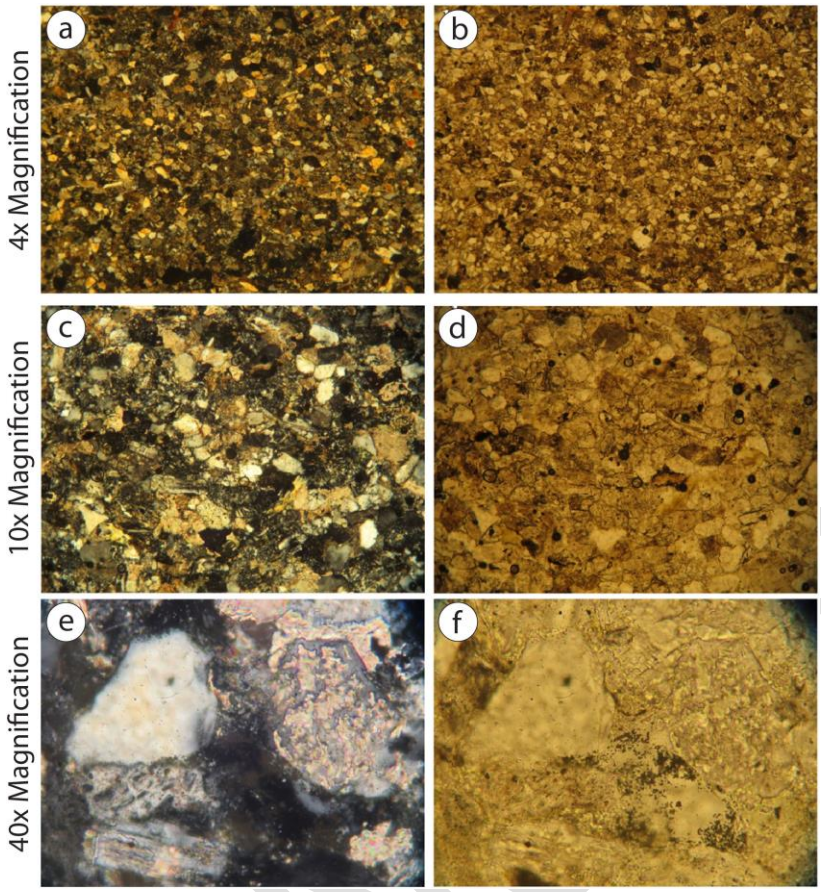


Figure 4-16. Photomicrographs of Sample 24M-37P in XPL (panels a, c, and e) and PPL (panels b, d, and f) at varying magnifications.

4.3.2.3 Sample 24M-37Pb

- Location: 25.949° N latitude, 60.6213° E longitude (same as Sample 24M-37P).
- Rock type: Clastic Sedimentary Rock.
- Rock name: Medium-Grained Sandstone.
- Description:

  Sample 24M-37Pb (Figure 4-17) is a litharenite with calcite cement and volcanic arenite characterized by the presence of quartz, volcanic rock fragments, and feldspar (mainly microcline and orthoclase). A very small amount of skeletal fragments is also present. Quartz grains are angular with straight extinction, indicating limited transport from the source. Volcanic rock fragment grains are semi-rounded, suggesting some degree of transport and abrasion. Sorting is moderate, and the rock remains compositionally immature. Sericitization is less pronounced compared to other samples. The cement is relatively coarse-grained calcite that filled intergranular spaces before burial and compaction, indicating early diagenetic cementation. Overgrowths of silica cement around some quartz grains are observed, pointing to multiple cementation events. Sparse opaque

minerals are present within the facies. Modal composition includes quartz (25–30%), volcanic lithic fragments (40–45%), and feldspar (15–20%).

- Interpretation:

  The medium-grained sandstone reflects a depositional environment where both volcanic and sedimentary materials were mixed. The angular quartz grains and semi-rounded volcanic fragments suggest varying transport histories. Early calcite cementation prevented significant compaction, preserving intergranular porosity. The presence of microcline and orthoclase indicates a felsic source, possibly from continental crustal rocks.

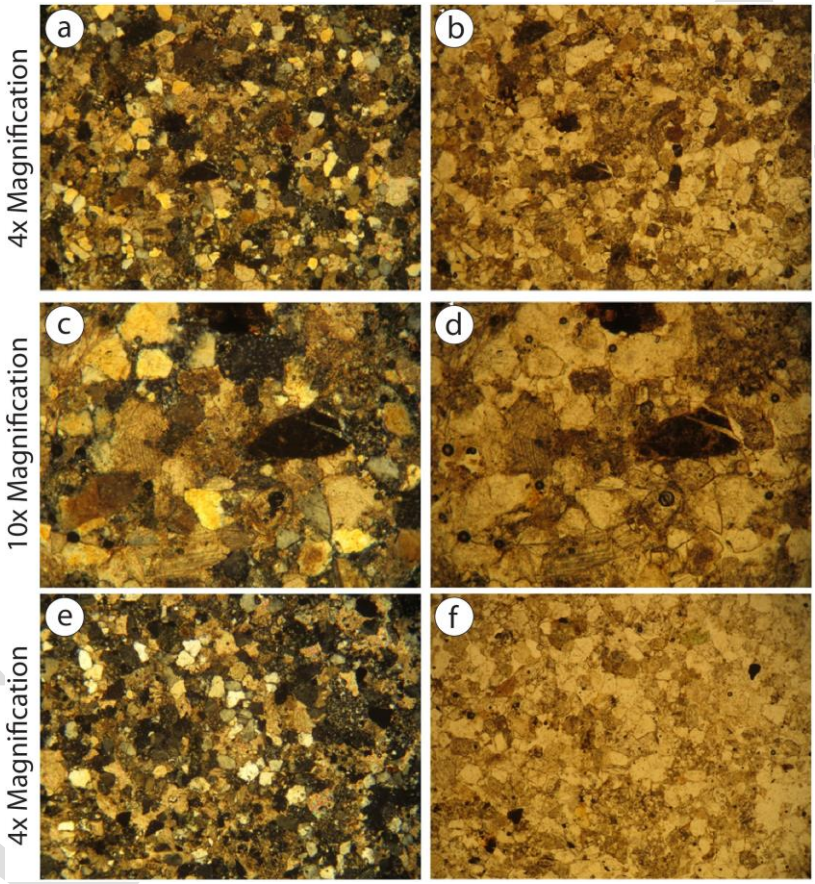


Figure 4-17. Photomicrographs of Sample 24M-37Pb in XPL (panels a, c, and e) and PPL (panels b, d, and f) at varying magnifications.

4.3.2.4 Sample 24M-38F

- Location: 25.949° N latitude, 60.6213° E longitude (same as Sample 24M-37P and Sample 24M-37Pb).
- Rock type: Hybrid Sedimentary–Volcanic Rock (Volcaniclastic).
- Rock name: Tuffaceous Calcareous Sandstone.

- Microfacies: Sandy limestone, ferruginous, calcite veined, bituminous.
- Description:

  This sample (Figure 4-18) contains grains of quartz, limestone rock fragments, volcanic rock fragments, and feldspar, along with foraminifera skeletons, muscovite, and chlorite. The facies exhibits changes, with the matrix in some parts composed of calcareous mud and in others of volcanic ash. The abundance of limestone rock fragments varies and increases in certain horizons, indicating fluctuations in sediment supply. Fractures filled with calcite cement, likely parallel to bedding, suggest syn-depositional or early post-depositional fracturing and cementation. In some areas, the rock lacks matrix and intergranular cement, leading to more severe compaction and the development of serrated and convex–concave grain contacts. Decomposition of volcanic ash and feldspars into calcite is relatively high and severe, indicating significant diagenetic alteration. The rock's modal composition includes quartz (15–20%), volcanic lithic fragments (25–30%), limestone fragments (5–30%), and feldspar (30–40%). The sample includes *Rotalia* sp., *Miliolidae*, and bryozoa with shell fragments.

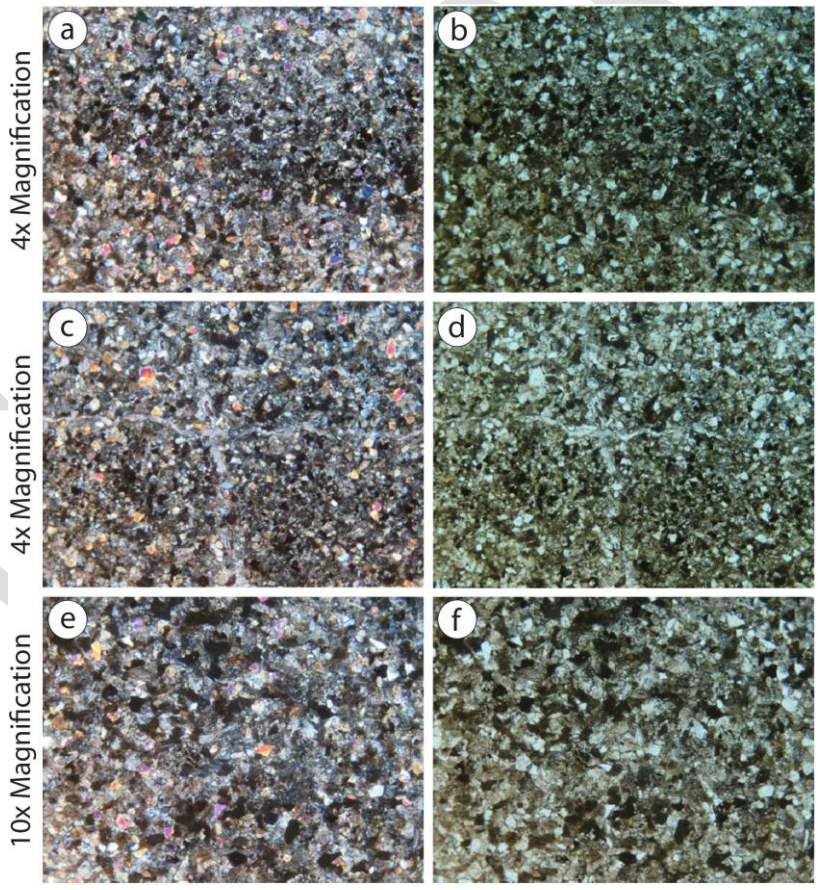


Figure 4-18. Photomicrographs of Sample 24M-38P in XPL (panels a, c, and e) and PPL (panels b, d, and f) at varying magnifications.

- Age Determination:

  Late Eocene to early Miocene.

- Interpretation:

  The tuffaceous calcareous sandstone represents a complex depositional environment with inputs from volcanic activity and carbonate sedimentation. The presence of foraminifera and calcareous mud indicates marine conditions. Variation in limestone fragment abundance suggests changes in proximity to carbonate sources or fluctuations in sea level. Severe alteration of volcanic ash and feldspars to calcite reflects diagenetic processes in a carbonate-rich environment. The ferruginous and bituminous characteristics suggest iron enrichment and the presence of organic matter, possibly indicating reducing conditions during diagenesis. The age determination places the sample in the Late Eocene to Early Miocene, suggesting the inclusion of older sediments.

4.3.2.5 Sample 24M-53F

- Location: 25.8981° N latitude, 60.6131° E longitude.
- Rock type: Hybrid Clastic–Carbonate Sedimentary Rock.
- Rock name: Very Fine-Grained Calcareous Sandstone.
- Microfacies: Sandy limestone, ferruginous.
- Description:

  Grains in this sample (Figure 4-19) are very fine sand-sized, including quartz, feldspar, and volcanic rock fragments, with a lesser abundance of calcareous mud fragments. The matrix is predominantly composed of calcareous mud, although volcanic ash is present in some parts. Intense compaction has resulted in the orientation of grains and volcanic ash, indicating significant diagenetic pressure. Scattered muscovite is observed, aligned in the direction of compaction, suggesting deformation during or after deposition. The calcareous mud has undergone considerable neomorphic recrystallization, pointing to diagenetic changes possibly associated with slight metamorphism. There is a possibility that the rock has experienced very weak metamorphic conditions.

- Interpretation:

  The very fine-grained calcareous sandstone indicates deposition in a low-energy marine environment with significant carbonate mud input. The presence of volcanic ash suggests episodic volcanic activity influencing sedimentation. Intense compaction and grain orientation imply substantial burial depths or tectonic compression. Neomorphic recrystallization of calcareous mud and potential weak metamorphism suggest diagenetic processes at elevated temperatures and pressures, possibly due to tectonic burial.

GeoNexus

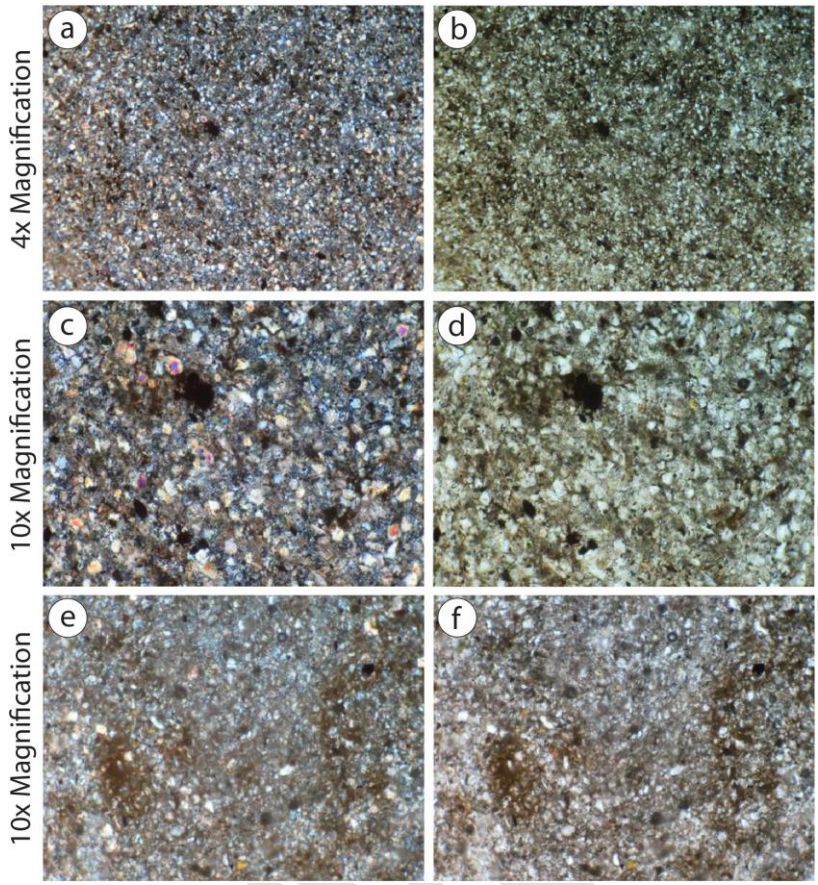


Figure 4-19. Photomicrographs of Sample 24M-53F in XPL (panels a, c, and e) and PPL (panels b, d, and f) at varying magnifications.

4.3.3 Structural Features

The $M^{s.sh}$ Unit exhibits structural complexities indicative of tectonic influences during and after deposition. The rocks are characterized by folded and faulted turbiditic flysch deposits, reflecting compressional tectonic regimes. Deformation has resulted in tight folds and thrust faults, common in accretionary prism settings.

Intense compaction observed in samples like 24M-53F indicates significant overburden pressure or tectonic stress, leading to grain alignment and deformation. Fractures filled with calcite cement, as seen in Sample 24M-38F, suggest syn-depositional or early diagenetic fracturing, potentially due to seismic activity or differential compaction.

4.3.4 Depositional Environment

The $M^{s.sh}$ Unit represents a complex depositional setting influenced by both sedimentary and volcanic processes.

- Volcaniclastic Inputs: The presence of volcanic ash, volcanic rock fragments, and tuffaceous materials indicates active volcanic activity during deposition, suggesting proximity to volcanic centers or influence of airborne volcanic material settling in the basin.

- Marine Conditions: Occurrence of glauconite, foraminifera skeletons, and calcareous mud points to deposition in a marine environment, likely on the continental shelf or slope.
- Turbiditic Deposits: Folded and faulted turbiditic flysch deposits signify sediment gravity flows, such as turbidity currents, transporting material from the continental shelf to deeper basin settings.
- Variations in Energy Conditions: Alternation between sandstones and shales reflects fluctuations in depositional energy, with coarser materials deposited during higher-energy events and finer sediments settling during quieter periods.

4.3.5 Tectonic Implications

Features of the $M^{s.sh}$ Unit provide insights into the tectonic evolution of the region.

- Accretionary Prism Setting: Deformation structures and sedimentary characteristics are consistent with deposition and deformation within an accretionary prism, such as the Makran accretionary wedge, formed by subduction of the Arabian Plate beneath the Eurasian Plate.
- Volcanic Arc Influence: Volcanic components suggest influence from a nearby volcanic arc, providing volcanic ash and pyroclastic material to the sedimentary basin.
- Syn-Depositional Tectonics: Presence of fractures parallel to bedding and early cementation indicates active tectonism during deposition, potentially leading to rapid changes in sedimentation rates and facies.

4.4 $M^{sh.s}$ Unit (Middle to Late Miocene Shale and Siltstone)

The $M^{sh.s}$ Unit represents a sedimentary sequence deposited during the middle to late Miocene. Like $M^{s.sh}$ Unit, this unit lies in Peersohrab Unit (Dolati, 2010), but exhibits different characteristics to distinct it from $M^{s.sh}$ Unit. This unit is characterized by interbedded shales, siltstones, sandstones, and volcaniclastics, reflecting a dynamic depositional environment influenced by both sedimentary and volcanic processes. This report provides a comprehensive analysis of the $M^{sh.s}$ Unit, integrating petrographic and micropaleontological data from various samples to elucidate its lithological characteristics, fossil content, depositional environments, and chronological framework.

The unit is represented by 1305 mapped polygons within the study area. The individual areas of these outcrops vary greatly, from as small as 0.00047 sq km to as large as 256.96 sq km. Notable large outcrops include OBJECTID_1: 5164 (256.96 sq km), 1467 (56.81 sq km), and 5102 (36.22 sq km). The cumulative area covered by the $M^{sh.s}$ Unit is ~ 1263 sq km.

4.4.1 Lithology and Stratigraphy

The $M^{sh.s}$ Unit, with a thickness of ~ 200 m, comprises predominantly clastic sedimentary rocks with significant volcanic input. The lithology includes calcareous siltstones, argillaceous limestones, tuffaceous sandstones, volcanic sandstones, and graywackes. The stratigraphy indicates alternating

GeoNexus

layers of marine sediments and volcanic materials, suggesting episodic volcanic activity during sedimentation.

4.4.2 Petrographic Analysis

4.4.2.1 Sample 24M-23F

- Location: 25.9281° N latitude, 60.1989° E longitude.
- Rock Type: Clastic Sedimentary Rock.
- Rock Name: Calcareous Siltstone to Argillaceous Limestone.
- Microfacies: Sandy-silty limestone, calcite veined, ferruginous.
- Description:

  Sample 24M-23F (Figure 4-20) consists of clastic grains embedded within a matrix of lime mud. The grains range from silt to very fine sand sizes and include feldspar, quartz, volcanic rock fragments, and plagioclase. The grains are angular to sub-angular, suggesting minimal transport from their source, and exhibit moderate sorting.

  The lime mud matrix has undergone neomorphism, resulting in the recrystallization of calcite and the development of interlocking crystal textures. This neomorphic calcite contributes to the rigidity and reduced porosity of the rock.

  Fractures are prevalent throughout the sample, displaying two sets approximately perpendicular to each other. These fractures are filled with blocky calcite cement composed of coarse mosaic crystals rich in inclusions. The calcite cementation occurred during deep burial diagenesis. Prior to cementation, dissolution features along some fractures indicate chemical processes were active before infilling by calcite.

  Iron oxide minerals, possibly hematite or limonite, have weakly developed around the fractures, imparting a slight reddish-brown coloration. Partial bioturbation is observed in some parts of the sample, indicating biological activity during or shortly after deposition.

- Interpretation:

  The calcareous siltstone to argillaceous limestone represents deposition in a marine environment where fine-grained sediments accumulated. The angular nature of the grains and moderate sorting suggest proximity to the source area and limited transport. The presence of volcanic rock fragments indicates volcanic activity in the vicinity during deposition.

  The neomorphism of the lime mud matrix reflects diagenetic alteration under burial conditions, leading to recrystallization of calcite. The fractures filled with blocky calcite cement indicate tectonic activity followed by mineralization during diagenesis. The weak development of iron oxide minerals around fractures suggests minor oxidation processes.

  Bioturbation implies that the depositional environment supported biological activity, possibly in a relatively shallow marine setting with adequate oxygenation.

GeoNexus

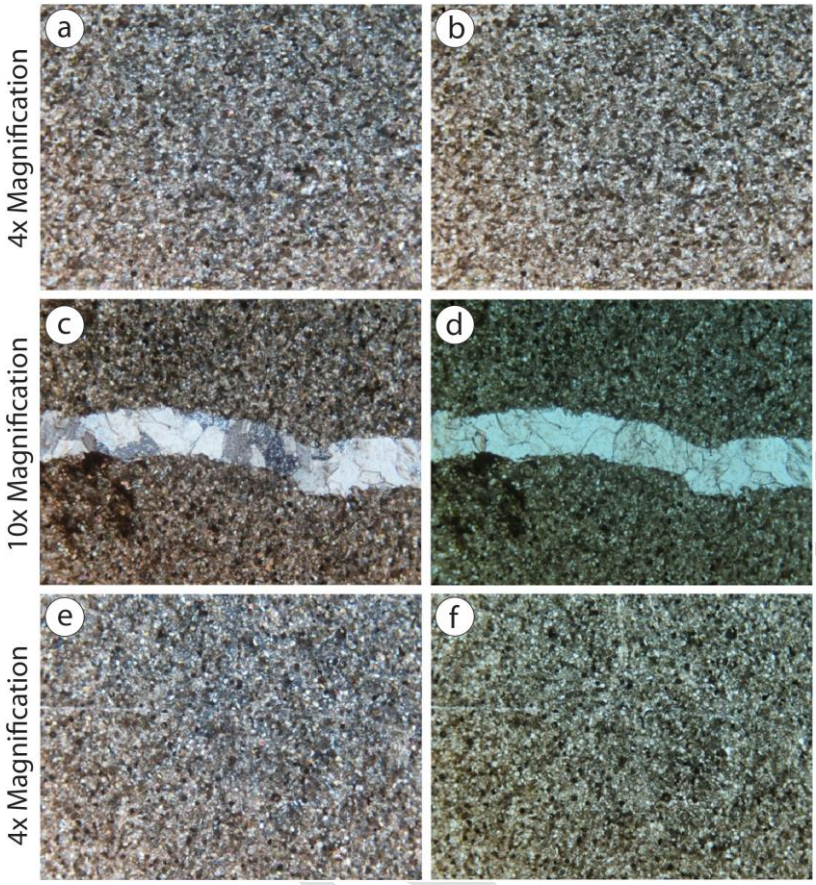


Figure 4-20. Photomicrographs of Sample 24M-23F in XPL (panels a, c, and e) and PPL (panels b, d, and f) at varying magnifications.

4.4.2.2 Sample 24M-24F

- Location: 25.9281° N latitude, 60.1989° E longitude (same as Sample 24M-23F).
- Rock Type: Hybrid Sedimentary–Volcanic Rock.
- Rock Name: Tuffaceous Volcanic Sandstone.
- Microfacies: Sandy-silty limestone.
- Description:

  Sample 24M-24F (Figure 4-21) comprises clastic grains within a matrix of volcanic ash and lime mud. The grains include quartz (30–35%), volcanic rock fragments (20%), feldspar (15–20%), and plagioclase (5–10%). Scattered fragments of lime mudstone are also present.

  The rock exhibits lamination, indicative of sedimentary layering due to fluctuations in depositional energy or sediment supply. Quartz grains are predominantly angular, suggesting minimal transport, while volcanic rock fragments are sub-angular. The volcanic glass within the rock has altered to calcite through devitrification and diagenetic processes.

Fossil fragments, including skeletal remains, are present, indicating a biologically active marine depositional environment. Green minerals, likely chlorite, are observed due to the alteration of mafic minerals or volcanic glass. Opaque minerals, possibly pyrite, are sparsely distributed, suggesting reducing conditions during deposition. This sample includes foraminifera such as *Lenticulina (Robulus) sp.*, *Elphidium? sp.*, and *Miliolidae*.

- Age Determination:

  Paleogene (probably late Eocene to late Oligocene).

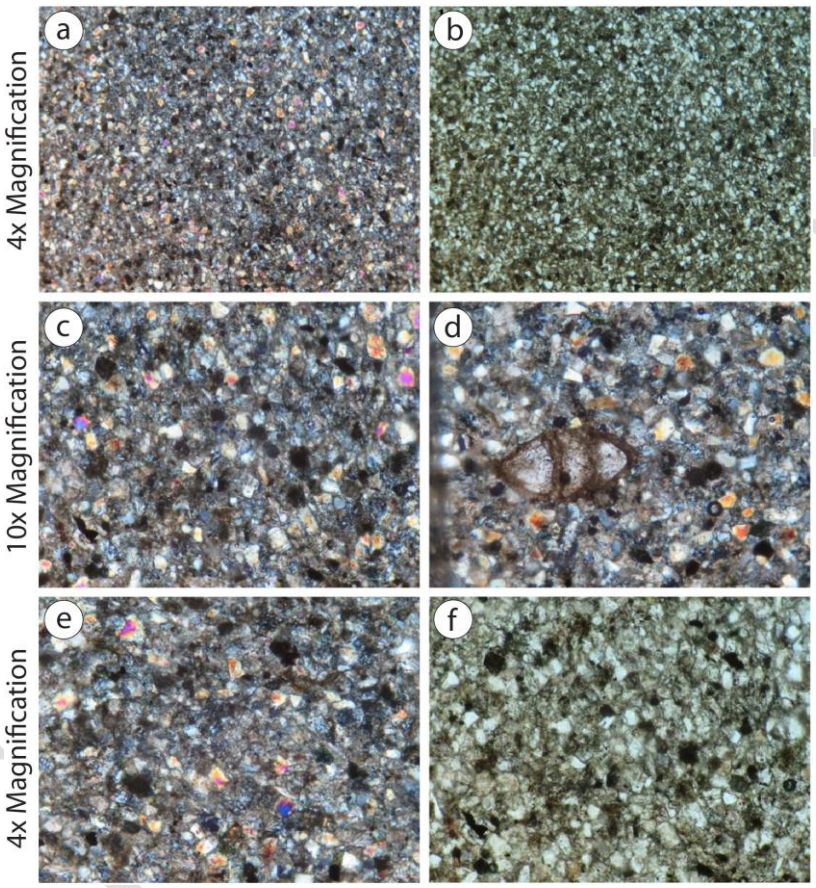


Figure 4-21. Photomicrographs of Sample 24M-24F in XPL (panels a, c, d, and e) and PPL (panels b and f) at varying magnifications.

- Interpretation:

  This tuffaceous volcanic sandstone reflects a depositional environment heavily influenced by volcanic activity, where volcanic ash and clastic sediments were deposited together. The presence of angular quartz and volcanic fragments indicates proximity to the source and rapid deposition. The alteration of volcanic glass to calcite and the presence of chlorite suggest diagenetic processes under low-grade metamorphic conditions.

  The fossil assemblage, including *Lenticulina (Robulus) sp.*, *Elphidium? sp.*, and *Miliolidae*, suggests a Paleogene age, indicating that this sample may represent older strata within the unit. Fossil fragments point to a marine setting with biological activity. The lamination

indicates periodic changes in sedimentation rates or energy conditions. Overall, the rock represents a mixed sedimentary and volcanic environment, possibly near a volcanic island arc or active volcanic center influencing marine sedimentation.

4.4.2.3 Sample 24M-41P

- Location: 25.9959° N latitude, 60.5717° E longitude.
- Rock Type: Hybrid Sedimentary–Volcanic Rock.
- Rock Name: Fine-Grained Volcanic Sandstone.
- Description:

  Sample 24M-41P (Figure 4-22) predominantly consists of quartz (20–25%), volcanic rock fragments (25–30%), and feldspar (15–20%). The matrix is composed of volcanic ash that has undergone alteration and sericitization, transforming into fine-grained sericite minerals.

  A slight orientation of grains is observed, suggesting sedimentary structures such as bedding or alignment due to current activity. The volcanic ash and rock fragments have deformed among the quartz grains, exhibiting flow textures. This deformation likely results from incomplete cooling of volcanic materials before deposition or compaction during diagenesis. Veins of mineralization and occurrences of opaque minerals are present, possibly indicating late-stage hydrothermal activity or diagenetic mineralization processes.

- Interpretation:

  The fine-grained volcanic sandstone represents deposition in an environment with significant volcanic influence, possibly near active volcanic vents. The flow textures and deformation of volcanic materials suggest rapid deposition of hot volcanic materials that were still plastic during emplacement.

  The sericitization of volcanic ash indicates alteration under low-grade metamorphic or diagenetic conditions. The slight grain orientation reflects sedimentary processes such as currents or turbidity flows.

  Mineralization veins and opaque minerals point to hydrothermal fluids circulating through the rock post-deposition, contributing to the alteration and mineralization observed.

GeoNexus

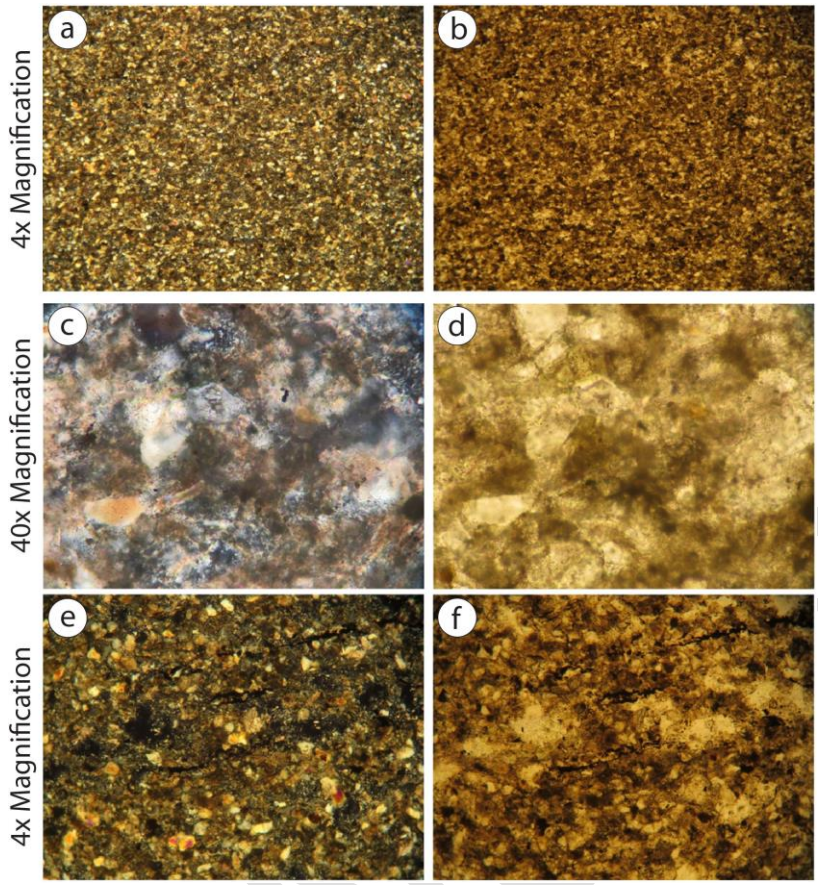


Figure 4-22. Photomicrographs of Sample 24M-41P in XPL (panels a, c, and e) and PPL (panels b, d, and f) at varying magnifications.

4.4.2.4 Sample 24M-55F

- Location: 25.765066° N latitude, 60.272421° E longitude.
- Rock Type: Hybrid Sedimentary–Volcanic Rock.
- Rock Name: Graywacke to Volcanic Siltstone.
- Microfacies: Sandy to silty limestone, detrital.
- Description:

  Sample 24M-55F contains quartz (20–25%), volcanic rock fragments (40–45%), feldspar (10–15%), and fossil fragments (5%), predominantly from bivalves. The matrix consists of volcanic ash, crystallized in some areas, suggesting diagenetic alteration or low-grade metamorphism. The sample includes shell and algal fragments.

  The grains include angular quartz and volcanic rock fragments, indicating limited transport and rapid deposition. The presence of fossils signifies a marine depositional environment. The rock exhibits poor sorting and an immature texture.

- Interpretation:

This graywacke to volcanic siltstone represents a marine environment heavily influenced by volcanic activity, where volcanic ash and clastic sediments were deposited simultaneously. The high content of volcanic fragments and ash indicates proximity to volcanic sources.

The presence of shell and algal fragments suggests a biogenic component to the sedimentation, supporting a marine depositional environment. The age determination of Oligocene–Miocene, based on the stratigraphic position, indicates that this sample may be older than the middle to late Miocene age assigned to the $M^{sh.s}$ Unit.

The presence of marine fossils suggests deposition in a marine setting, possibly on a continental shelf or in a forearc basin adjacent to volcanic activity. The immature texture reflects rapid sedimentation without significant reworking or sorting.

4.4.3 Micropaleontological Analysis

4.4.3.1 Sample 24M-04W

- Location: 25.3642° N latitude, 60.6142° E longitude.
- Description:

  Sample 24M-04W (Figure 4-23 and Figure 4-24) contains a diverse assemblage of both benthic and planktic foraminiferal species.

  Benthic forms identified include *Ammonia sp. cf. A. asanoi*, *Ammonia beccarii dentata*, *Ammonia indica*, *Ammonia punctato granosa*, *Ammonia tochigiensis*, *Cibicides sp.*, *Lenticulina inornata*, *Nodosaria raphanus*, and *Nonion costiferum*.

  Planktic foraminifera present are *Globoquadrina sp. cf. G. venezuelana*, *Globigerinoides immaturus*, *Globigerinoides subquadratus*, *Globigerinella obesa*, *Globoquadrina dehiscens*, *Globorotalia archeomenardii*, and *Paragloborotalia mayeri*.

  The benthic species suggest a marine environment conducive to diverse bottom-dwelling organisms, while the planktic species indicate open marine conditions with sufficient depth and connectivity to global oceans.
- Age Determination:

  The presence of index species *Globorotalia archeomenardii* and *Paragloborotalia mayeri* allows for an accurate age determination, suggesting a middle Miocene (Langhian) age for the sample.
- Interpretation:

  The foraminiferal assemblage indicates deposition during the Middle Miocene in a marine setting. The diversity and abundance of both benthic and planktic forms suggest favorable ecological conditions, including optimal temperature, salinity, and nutrient availability.

  This age determination aligns with the Middle Miocene age defined for the Msh.s unit in the final map legend, supporting the unit's stratigraphic framework.

GeoNexus

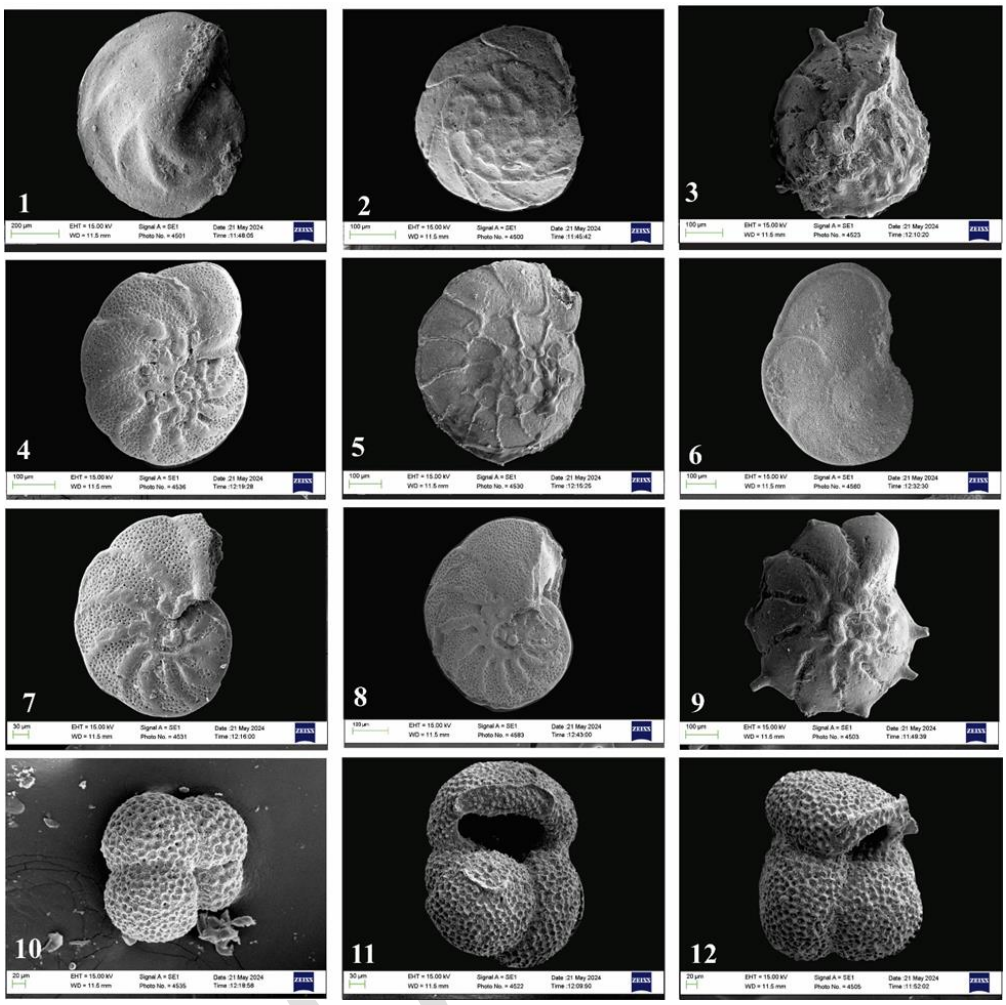


Figure 4-23. Scanning Electron Microscope (SEM) images of micropaleontological species of Sample 24M-04W (Plate 2), showcasing their morphological details. 1) *Lenticulina inornate;* 2) *Ammonia sp. cf. A. asanoi*; 3) *Ammonia beccarii dentata*; 4) *Cibicides sp.*; 5) *Ammonia tochigiensis*; 6) *Globorotalia archeomenardii*; 7) *Nonion costiferum*; 8) *Nonion costiferum*; 9) *Ammonia beccarii dentata*; 10) *Globigernella obesa*; 11) *Globigerinoides subquadratus*; 12) *Globoquadrina sp. cf. G. venezuelana*.

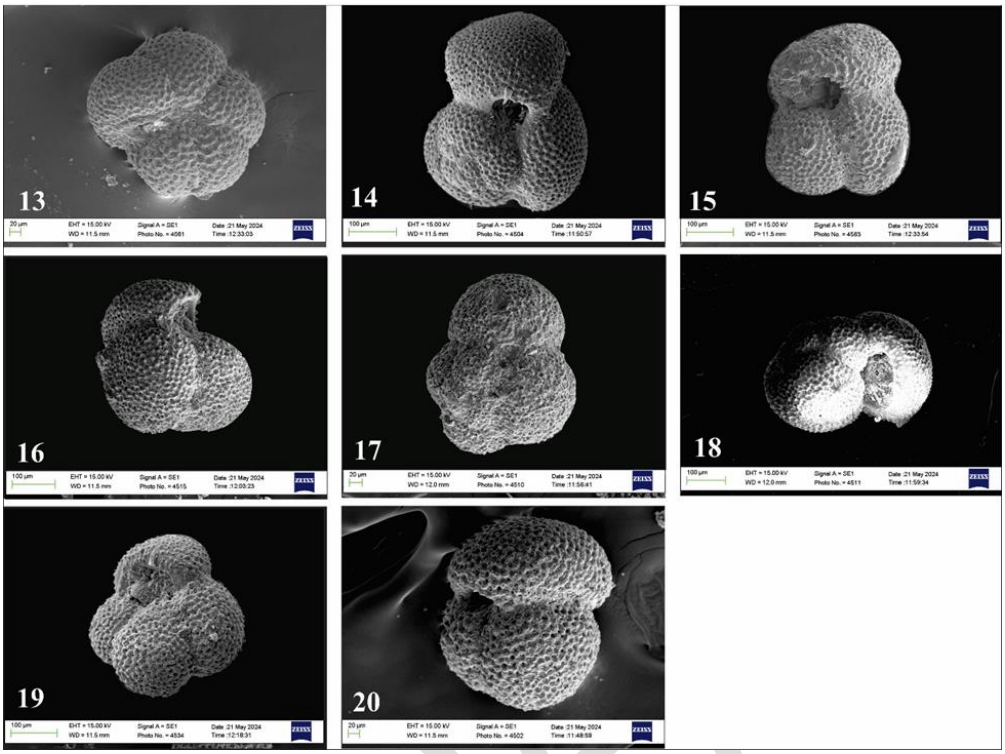


Figure 4-24. SEM images of micropaleontological species of Sample 24M-04W (Plate 2), showcasing their morphological details. 13) *Paragloborotalia mayeri*; 14) *Globigerinoides*; 15) *Globigerinoides subquadratus*; 16) *Globigerinoides subquadratus*; 17) *Globigerinoides subquadratus*; 18) *Globigerinoides immaturus*; 19) *Globigerinoides subquadratus*; 20) *Globigerinoides subquadratus*.

4.4.3.2 Sample 24M-05W

- Location: 25.3753° N latitude, 60.6278° E longitude.
- Description:

  Sample 24M-05W (Figure 4-25) contains benthic foraminifera such as *Ammonia beccarii dentata*, *Ammonia inflata*, *Nodosaria raphanus*, *Nonion sp.*, and *Nonionella sp*. Planktic species include *Globigerinoides altiaperturus*, *Globigerinoides immaturus*, *Globigerinoides subquadratus*, *Globigerinella obesa*, *Globoquadrina dehiscens*, *Globorotalia clemenciae*, and *Paragloborotalia mayeri*.

  The assemblage reflects a marine environment with a mix of shallow-water benthic species and deeper-water planktic species, indicating a range of depositional settings or fluctuating sea levels.

- Age Determination:

  The occurrence of index species *Globigerinoides altiaperturus* and *Globoquadrina dehiscens* permits an accurate age determination, indicating an early Miocene (Burdigalian) age for the sample.

- Interpretation:

The foraminiferal assemblage reflects deposition during the early Miocene in a marine setting. The presence of these index species is crucial for biostratigraphic dating.

- Age Inconsistency:

  The early Miocene age determined for this sample is not consistent with the middle to late Miocene age defined for the $M^{sh.s}$ Unit in the final map legend. This inconsistency suggests that the sample may have been collected from an older stratum within the unit, or that the $M^{sh.s}$ Unit encompasses older sediments than previously recognized.

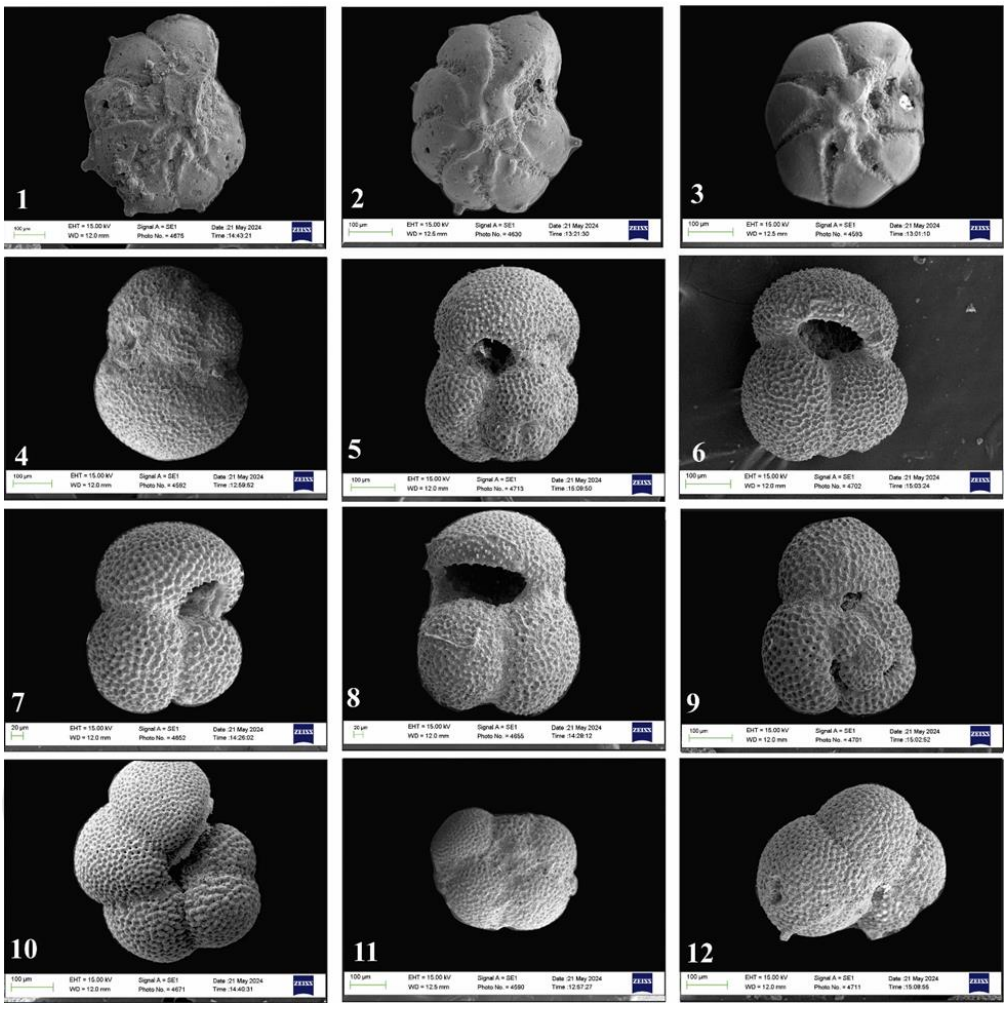


Figure 4-25. SEM images of micropaleontological species of Sample 24M-05W (Plate 3), showcasing their morphological details. 1) *Ammonia beccarii dentata*; 2) *Ammonia beccarii dentata*; 3) *Ammonia inflata*; 4) *Nonion sp.*; 5) *Globigerinoides altiaperturus*; 6) *Globigerinoides altiaperturus*; 7) *Globigerinoides subquadratus*; 8) *Globigerinoides subquadratus*; 9) *Globigerinoides immaturus*; 10) *Paragloborotalia mayeri*; 11) *Globorotalia clemenciae*.

4.4.3.3 Sample 24M-19W

- Location: 25.968171° N latitude, 60.184779° E longitude.
- Description:

  Sample 24M-19W (Figure 4-26) features benthic foraminifera including *Bulimina elongata*, *Heterolepa dutemplei*, *Uvigerina auberiana*, and *Valvulina sp*. Planktic species present are *Dentoglobigerina altispira*, *Globigerina praebulloides*, *Globigerinoides immaturus*, *Globigerinoides subquadratus*, *Globigerinoides triloba*, *Globorotalia sp.*, and *Paragloborotalia mayeri*.

  The benthic species suggest deposition in a marine environment with relatively deeper waters or higher nutrient levels, as indicated by species like *Bulimina elongata* and *Uvigerina auberiana*.

- Age Determination:

  The assemblage permits an age determination ranging from middle Miocene (Serravallian) to late Miocene (Tortonian), based on the presence of index planktic species such as *Paragloborotalia mayeri* and *Dentoglobigerina altispira*.

- Interpretation:

  The foraminiferal assemblage indicates deposition during the middle to late Miocene in a marine setting. This age range is consistent with the middle to late Miocene age defined for the $M^{sh.s}$ Unit, supporting its stratigraphic placement.

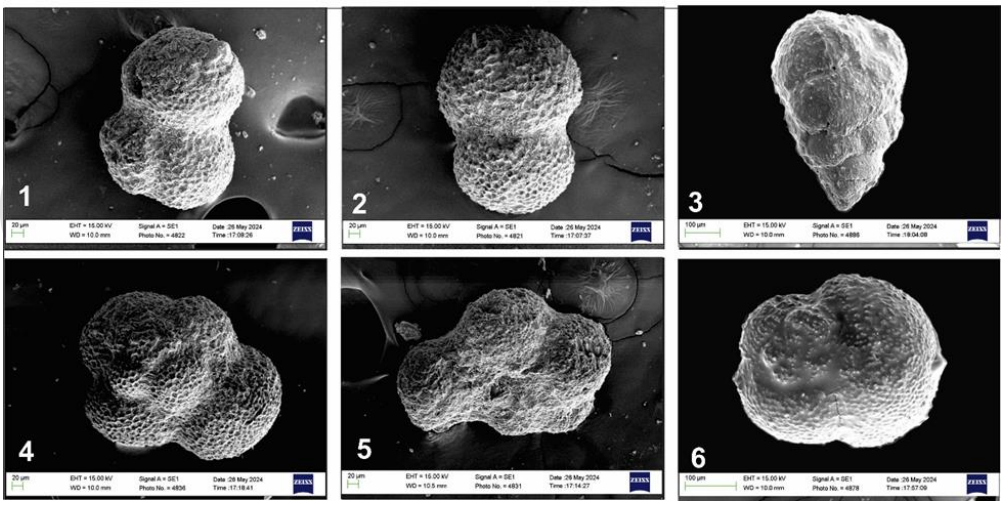


Figure 4-26. SEM images of micropaleontological species of Sample 24M-19W (Plate 8), showcasing their morphological details. 1) Globigerinoides immaturus; 2) Globigerinoides immaturus; 3) Uvigerina auberiana; 4) Globoquadrina venezuelana; 5) Globorotalia sp.; 6) Globigerinoides immaturus.

4.4.3.4 Sample 24M-22W

- Location: 25.9281° N latitude, 60.1989° E longitude.

- Description:

  Sample 24M-22W (Figure 4-27) contains benthic foraminifera such as *Bolivina sp.*, *Cycloforina contorta*, *Planulina sp.*, *Quinqueloculina triangularis*, *Quinqueloculina vulgaris*, *Spiroloculina sp.*, and *Textularia sp*. Planktic forms include *Globigerinoides immaturus* and *Praeorbulina glomerosa*.

  The benthic assemblage includes species characteristic of shallow marine environments, possibly lagoonal or inner shelf settings. The presence of *Praeorbulina glomerosa* is significant for age determination.

- Age Determination:

  The presence of the index planktic species *Praeorbulina glomerosa* and the benthic form *Cycloforina contorta* allows for an age determination of early Miocene (late Burdigalian) to middle Miocene (early Langhian).

- Interpretation:

  The assemblage suggests deposition during the transition from the Early to Middle Miocene in a shallow marine environment. The species present indicate warm, normal marine salinity conditions with good water circulation.

- Age Consideration:

  While the early Langhian age aligns with the middle Miocene age defined for the $M^{sh.s}$ Unit, the late Burdigalian suggests the inclusion of slightly older sediments within the unit.

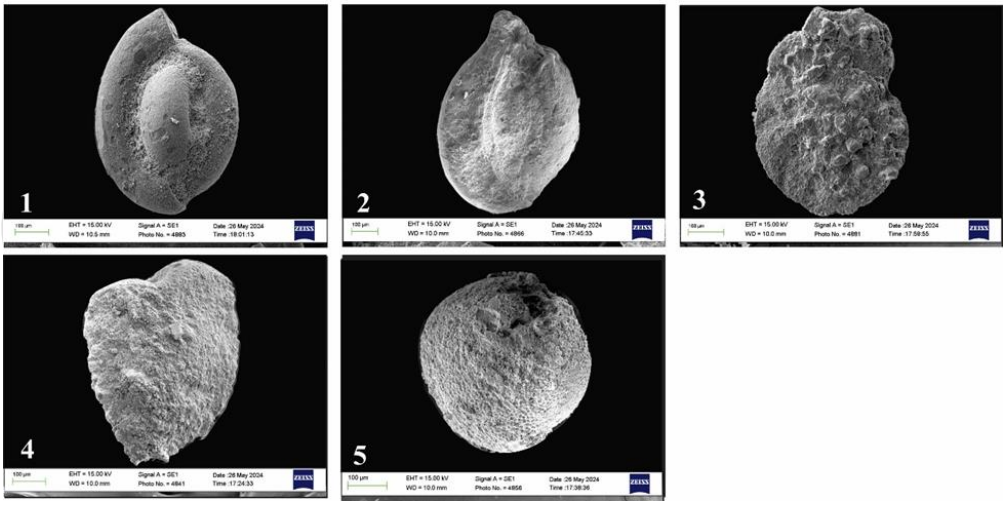


Figure 4-27. SEM images of micropaleontological species of Sample 24M-22W (Plate 10), showcasing their morphological details. 1) *Quinqueloculina triangularis*; 2) *Cycloforina contorta*; 3) *Planulina sp.*; 4) *Textularia sp.*; 5) *Praeorbulina glomerosa*.

4.4.3.5 Sample 24M-45W

- Location: 25.989° N latitude, 60.6025° E longitude.

- Description:

  Sample 24M-45W (Figure 4-28) includes benthic foraminifera such as *Bulimina pyrula*, *Cibicides sp.*, *Gyroidina soldani*, *Heterolepa dutemplei*, Lenticulina sp. cf. L. americanus, *Melonis pompilioides*, *Uvigerina multicostata*, and *Valvulina sp*. Planktic species present are *Catapsydrax sp.*, *Globoquadrina sp. cf. G. dehiscens*, and *Globigerinoides immaturus*.

  The benthic assemblage suggests a relatively deep marine environment with good oxygenation, as indicated by species like *Cibicides sp.* and *Gyroidina soldani*. The presence of *Catapsydrax sp.* is significant for dating.

- Age Determination:

  The occurrence of *Catapsydrax sp.* indicates an early Miocene (Burdigalian) age for the sample.

- Interpretation:

  The foraminiferal assemblage reflects deposition in a marine environment during the early Miocene. The mix of benthic and planktic species suggests normal marine conditions with sufficient depth for planktic forms.

- Age Inconsistency:

  The early Miocene age is not consistent with the middle to late Miocene age defined for the $M^{sh.s}$ Unit in the final map legend. This discrepancy implies that the sample may have originated from an older layer within the unit or that the unit's age range extends into the early Miocene.

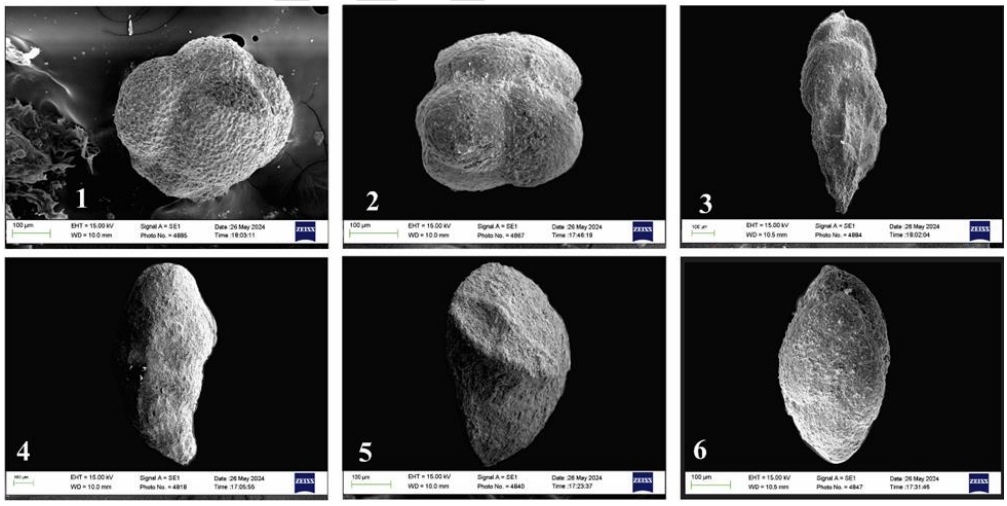


Figure 4-28. SEM images of micropaleontological species of Sample 24M-45W (Plate 15), showcasing their morphological details. 1) *Globoquadrina sp. cf. G. dehiscens*; 2) *Catapsydrax sp.*; 3) *Uvigerina multicostata*; 4) *Uvigerina multicostata*; 5) *Valvulina sp.*; 6) *Bulimina pyrula*.

4.4.4 Age and Correlation

The micropaleontological analyses indicate that the $M^{sh.s}$ Unit includes sediments ranging from the early Miocene (Burdigalian) to the late Miocene (Tortonian). While the unit is defined as middle to late Miocene, the presence of early Miocene fossils suggests that it may encompass older strata or that there is a need to reassess the unit's age boundaries.

4.4.5 Depositional Environment

The $M^{sh.s}$ Unit represents a marine depositional environment with significant volcanic influence. The combination of marine fossils and volcanic materials indicates deposition in a setting affected by volcanic activity, such as a volcanic arc or a forearc basin.

The petrographic analyses reveal rapid deposition of sediments with minimal transport, suggesting proximity to both sediment and volcanic sources. Bioturbation and diverse foraminiferal assemblages point to biologically active environments with varying conditions, from shallow to deeper marine settings.

The presence of older fossils in some samples indicates that the depositional history of the $M^{sh.s}$ Unit is more complex than previously thought, with possible inclusion of older sedimentary materials or reworking of older fossils into younger sediments. This complexity underscores the need for detailed stratigraphic and paleontological studies to refine the understanding of the unit's age and depositional history.

4.5 $M^{s.si}$ Unit

The $M^{s.si}$ is a ~200-m-thick unit, characterized by red-brown, thick-bedded, cleaved, and cliff-forming sandy siltstone to sandstone, bearing bituminous and iron oxide materials. This unit forms prominent cliffs in the study area due to its lithological properties and mechanical strength. The presence of iron oxide contributes to the reddish-brown coloration, while bituminous materials indicate organic content within the sedimentary rocks.

The unit is represented by 947 mapped polygons within the study area. The individual areas of these outcrops vary greatly, from as small as 0.0042 sq km (OBJECTID_1: 6486) to as large as 34.77 sq km (OBJECTID_1: 6885). The cumulative area covered by the $M^{s.si}$ Unit is ~ 710 sq km.

4.5.1 Petrographic Analysis

4.5.1.1 Sample 24M-51P

- Location: 25.9266° N latitude, 60.6435° E longitude.
- Rock Type: Hybrid Sedimentary–Volcanic Rock.
- Rock Name: Fine-Grained Volcanic Sandstone (Tucker, 2001) or Epiclastic Volcanic Sandstone (Fisher, 1961).

- Description:

  Sample 24M-51P (Figure 4-29) is a hybrid rock exhibiting both sedimentary and volcanic characteristics. Based on grain size, it is classified as a fine-grained volcanic sandstone or an epiclastic volcanic sandstone.

  The grains within the rock are composed of:

  - Quartz: Predominantly monocrystalline quartz grains displaying both undulatory and straight extinction. These grains are subangular to angular, suggesting limited transport and proximity to the source area. Polycrystalline quartz grains are present but less common.
  - Feldspar: Feldspar grains are present in lesser amounts compared to quartz. Most feldspar grains show significant alteration, primarily sericitization, indicating chemical weathering and diagenetic processes after deposition.
  - Lithic Fragments: Composed of acidic to intermediate volcanic origin, the lithic fragments are abundant and highlight a substantial volcanic influence during sedimentation.

  The matrix of the rock mainly consists of volcanic ash, which in some areas has altered and shows slight recrystallization. In certain sections, fine-crystalline calcite cement is observed, likely derived from the dissolution of calcium-rich components such as lithic fragments and feldspars.

  Texturally, the rock exhibits very weak lamination, indicating deposition in low-energy conditions. The grains are moderately- to well-sorted, and the overall texture is immature both texturally and compositionally, suggesting rapid deposition with minimal reworking.

- Interpretation:

  Sample 24M-51P (Figure 4-29) represents a depositional environment with significant volcanic influence, likely in proximity to active volcanic regions. The presence of volcanic ash and lithic fragments indicates direct input from volcanic activity during sedimentation.

  The immature texture and angular nature of the grains imply that the sediments were deposited rapidly near their source, without extensive transport. Weak lamination suggests deposition in a low-energy marine environment, possibly below wave base, where fine sediments could settle.

  Diagenetic processes are evident in the alteration of feldspars and the presence of calcite cement. Sericitization of feldspars indicates chemical alteration during or after deposition, while calcite cementation reflects post-depositional processes where dissolved calcium carbonate precipitated within the pore spaces.

  Overall, the petrographic characteristics of this sample highlight the interplay between volcanic activity and sedimentary processes, resulting in a rock that captures both volcanic and sedimentary features.

GeoNexus

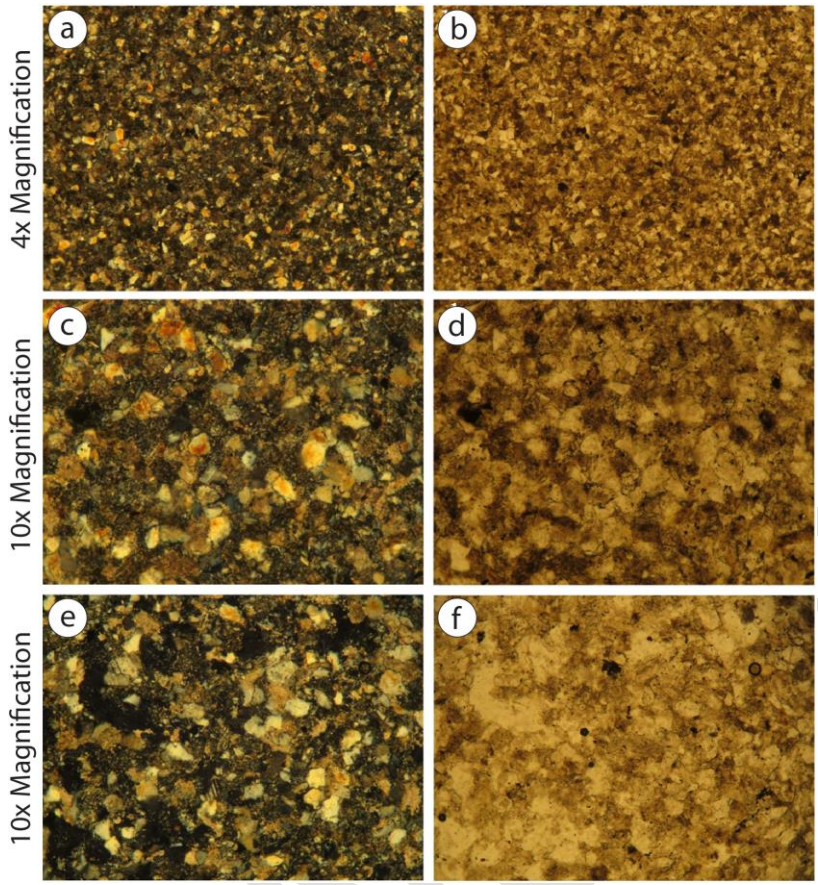


Figure 4-29. Photomicrographs of Sample 24M-51P in XPL (panels a, c, and e) and PPL (panels b, d, and f) at varying magnifications.

4.5.2 Micropaleontological Analysis

4.5.2.1 Sample 24M-46W

- Location: 25.9861° N latitude, 60.6171° E longitude.
- Description:

  Sample 24M-46W (Figure 4-30) contains a diverse assemblage of foraminiferal species, including both benthic and planktic forms. The preservation of planktic foraminifera is weak, and their occurrence is low, which makes age determination challenging based solely on planktic species.

  The benthic foraminiferal assemblage includes species such as *Bolivina beyrichi* group, *Bolivina catanensis*, *Bulimina costata*, *Bulimina pyrula*, *Bulimina spp.*, *Cibicides sp.*, *Gyroidina soldani*, *Heterolepa dutemplei*, *Lenticulina sp.*, *Marattiontella communis*, *Marginulina nodosaria*, *Melonis pompilioides*, *Nodosaria sp. cf. N. rudis*, *Textularia sp. cf. T. mariae*, *Uvigerina auberiana*, and *Uvigerina multicostata*.

Planktic species identified include *Globigerina sp.*, *Globigerinoides immaturus*, *Globigerinoides sp. cf. G. immaturus*, *Globigerinoides triloba*, *Globigerinoides sp.*, *Globoquadrina spp.*, and *Paragloborotalia sp*.

- Age Determination:

  Due to the poor preservation and low abundance of planktic forms, the age determination relies primarily on the benthic assemblage. The presence of species such as *Nodosaria sp. cf. N. rudis*, *Textularia sp. cf. T. mariae*, *Uvigerina auberiana*, and *Uvigerina multicostata* suggests an age ranging from the early Miocene (Burdigalian) to the late Miocene (Tortonian).

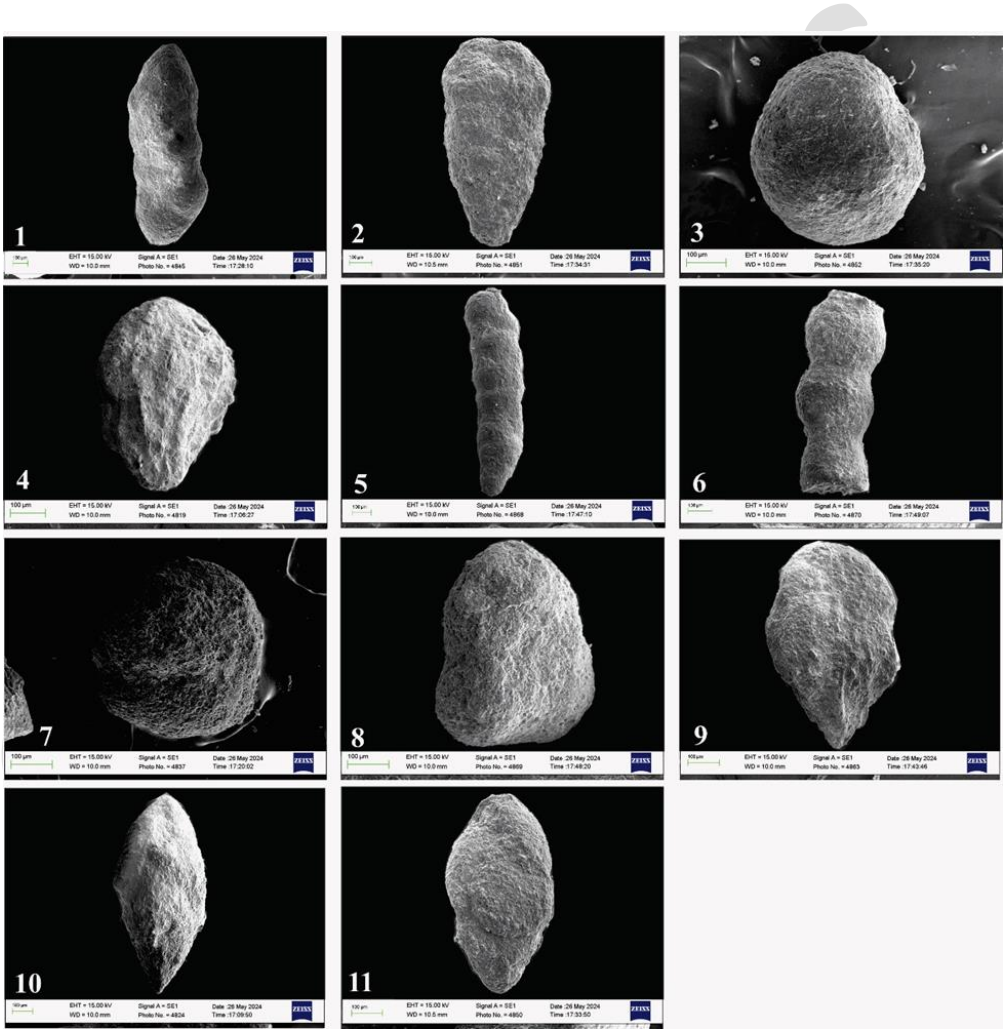


Figure 4-30. SEM images of micropaleontological species of Sample 24M-46W (Plate 16), showcasing their morphological details. 1) *Uvigerina auberiana*; 2) *Textularia sp. cf. T. mariae*; 3) *Globigerinoides sp.*; 4) *Bulimina costata*; 5) *Marattiontella communis*; 6) *Nodosaria sp. cf. N. rudis*; 7) *Globigerinoides triloba*; 8) *Globigerinoides sp. cf. G.immaturus*; 9, 10) *Bulimina spp.*; 11) *Bulimina pyrula*.

- Interpretation:

  The diverse benthic foraminiferal assemblage indicates deposition in a marine environment with varying depths and ecological conditions. The presence of species that span a broad

stratigraphic range suggests either a condensed section or possible reworking of sediments from different ages.

The inconsistency in the age suggested by this sample compared to the age defined for the $M^{s.si}$ Unit in the final map legend (early to middle Miocene) may reflect stratigraphic complexities or local depositional variations within the unit.

4.5.2.2 Sample 24M-48W

- Location: 25.9323° N latitude, 60.6492° E longitude.
- Description:

  Sample 24M-48W (Figure 4-31) contains both benthic and planktic foraminifera. Benthic species identified include *Bulimina pyrula* and *Cibicides sp*. Planktic species include *Globigerina praebulloides*, *Globigerinoides immaturus*, *Globigerinoides triloba*, and *Praeorbulina sp. aff. P. glomerosa*.

- Age Determination:

  The occurrence of the index planktic species *Praeorbulina sp. cf. P. glomerosa* is significant for age determination. This species allows for an age assignment of early Miocene (late Burdigalian) to middle Miocene (early Langhian).

- Interpretation:

  The presence of *Praeorbulina sp. cf. P. glomerosa* provides a reliable biostratigraphic marker, aligning with the age defined for the $M^{s.si}$ Unit in the map legend. The assemblage suggests deposition in an open marine environment with normal salinity and good water circulation.

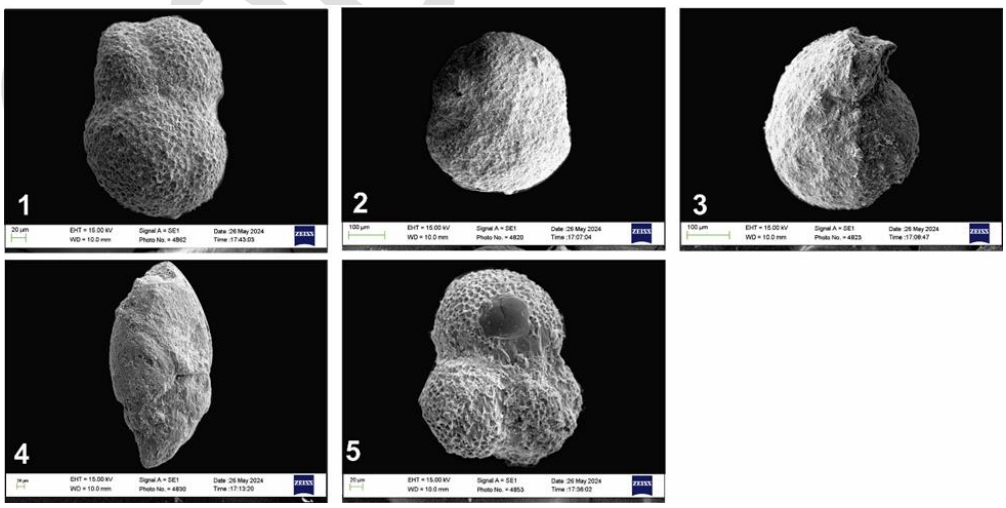


Figure 4-31. SEM images of micropaleontological species of Sample 24M-48W (Plate 17), showcasing their morphological details. 1) *Globigerinoides immaturus*; 2) *Globigerinoides triloba*; 3) *Cibicides sp.*; 4) *Bulimina pyrula*; 5) *Globigerinoides immaturus*.

4.5.2.3 Sample 24M-49W

- Location: 25.9281° N latitude, 60.6466° E longitude.
- Description:

  The sample contains benthic foraminifera such as *Dentalina elegans* and *Melonis pompilioides*, along with planktic species including *Globigerinoides immaturus*, *Globigerinoides sp.*, and *Praeorbulina sp. cf. P. glomerosa*.

- Age Determination:

  Similar to sample 24M-48W (Figure 4-32), the presence of *Praeorbulina sp. cf. P. glomerosa* indicates an age of early Miocene (late Burdigalian) to middle Miocene (early Langhian).

- Interpretation:

  This sample supports the age assignment, consistent with the $M^{s.si}$ Unit. The benthic and planktic assemblage reflects deposition in a marine environment transitioning from shallow to deeper settings.

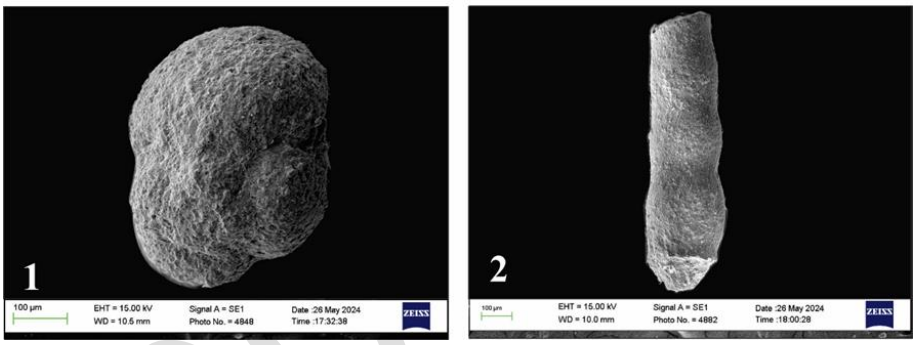


Figure 4-32. SEM images of micropaleontological species of Sample 24M-49W (Plate 18), showcasing their morphological details. 1) *Globigerinoides immaturus*; 2) *Dentalina elegans*.

4.5.2.4 Sample 24M-50W

- Location: 25.9261° N latitude, 60.6435° E longitude.
- Description:

  Sample 24M-50W (Figure 4-33) includes benthic foraminifera such as *Dentalina scripta* and *Lenticulina mexicanus*, along with the planktic species *Globigerinoides immaturus*.

- Age Determination:

  The lack of definitive index species makes precise age determination difficult for this sample. Based on the identified species, the suggested age ranges from the early Miocene (Burdigalian) to Quaternary. The presence of *Dentalina scripta* may indicate a middle Miocene age, but this is considered with low probability.

- Interpretation:

The uncertain age of this sample highlights a potential inconsistency with the age defined for the $M^{s.si}$ Unit in the map legend. Further investigation and additional data are required to clarify the age of this sample.

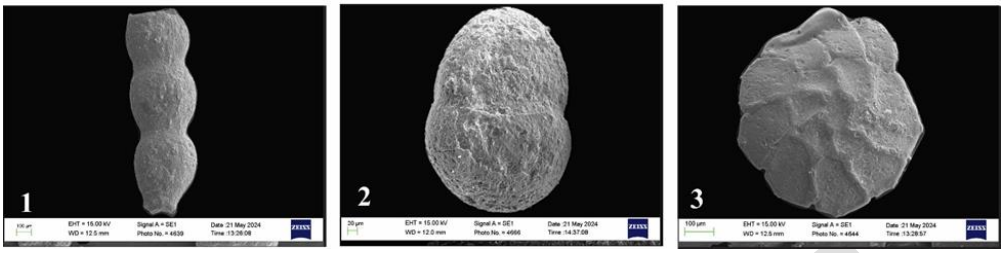


Figure 4-33. SEM images of micropaleontological species of Sample 24M-50W (Plate 19), showcasing their morphological details. 1) *Dentalina scripta*; 2) *Globigerinoides immaturus*; 3) *Lenticulina mexicanus*.

4.5.3 Age and Correlation

The micropaleontological analyses suggest that the $M^{s.si}$ Unit encompasses sediments from the early Miocene (late Burdigalian) to middle Miocene (early Langhian), consistent with the age defined in the final map legend. However, sample 24M-46W indicates a broader age range extending to the late Miocene (Tortonian), which is not entirely consistent with the unit's defined age. Similarly, the uncertain age of sample 24M-50W suggests possible stratigraphic complexities within the unit.

4.5.4 Depositional Environment

The $M^{s.si}$ Unit represents a marine depositional environment influenced by significant volcanic activity. Petrographic evidence, including the presence of volcanic ash and volcanic lithic fragments, indicates proximity to active volcanic sources during sedimentation.

The foraminiferal assemblages reflect normal marine salinity with good water circulation, supporting diverse benthic communities. The immature texture and angular grains in the petrographic sample suggest rapid deposition near the sediment source, while weak lamination indicates low-energy conditions.

4.6 $MPl^{m.s}$ Unit

The ~150-m-thick $MPl^{m.s}$ Unit comprises sedimentary rocks predominantly of late Miocene to early Pliocene, characterized by sandstones, siltstones, mudstones, and occasional hybrid rocks exhibiting both sedimentary and volcanic characteristics. These rocks are significant in the geological framework of the study area due to their diverse lithological properties and depositional histories, reflecting a complex interplay between clastic and volcanic inputs.

The unit is represented by 912 mapped polygons within the study area. The individual areas of these outcrops vary greatly, from as small as 0.0006 sq km (OBJECTID_1: 10455) to as large as 24.34 sq

km (OBJECTID_1: 992). The cumulative area covered by the MPlm.s Unit is approximately 640 sq km.

4.6.1 Petrographic Analysis

4.6.1.1 Sample 24M-21F

- Location: 25.9412° N latitude, 60.1990° E longitude.
- Rock Type: Hybrid Sedimentary–Volcanic Rock.
- Rock Name: Volcanic Sandstone to Tuffaceous Sandstone.
- Microfacies: Poorly Washed Bio-sparite (Silty Argillaceous Limestone), Bearing Iron Oxide, Bituminous, Diagenetic.
- Description:

  Sample 24M-21F (Figure 4-34) is a hybrid rock exhibiting both sedimentary and volcanic characteristics. The grains within the rock are composed of:

  - Feldspar (35–40%): Including both orthoclase and plagioclase feldspars, with plagioclase constituting 10–15% of the total grains.
  - Quartz (15–20%): Grains are angular to subangular, indicating limited transport from the source area.
  - Volcanic Rock Fragments (10–15%): Derived from volcanic materials, reflecting volcanic activity during sedimentation.

  The grains are angular with poor to moderate sorting, set in a matrix of volcanic ash with minor calcareous mud. Texturally, the rock is immature, displaying slight orientation due to compaction and shows lamination. Iron oxide veins and bituminous material are present, suggesting post-depositional mineralization along structural planes. Sparse fossil fragments are observed, though their identification is challenging due to poor preservation. Glauconite occurs sporadically within the sample.

- Interpretation:

  The petrographic characteristics of Sample 24M-21F indicate a depositional environment influenced by significant volcanic activity, likely in proximity to active volcanic regions. The presence of volcanic ash and volcanic rock fragments suggests direct input from volcanic eruptions during sedimentation. The immature texture and angular grains imply rapid deposition near the source area, with minimal transport and reworking. The lamination and slight orientation reflect compaction and low-energy depositional conditions, possibly in a marine setting below wave base. The presence of iron oxide and bituminous material indicates diagenetic processes involving mineralization and organic matter preservation. The presence of glauconite suggests marine conditions with slow sedimentation rates, allowing for authigenic mineral formation.

GeoNexus

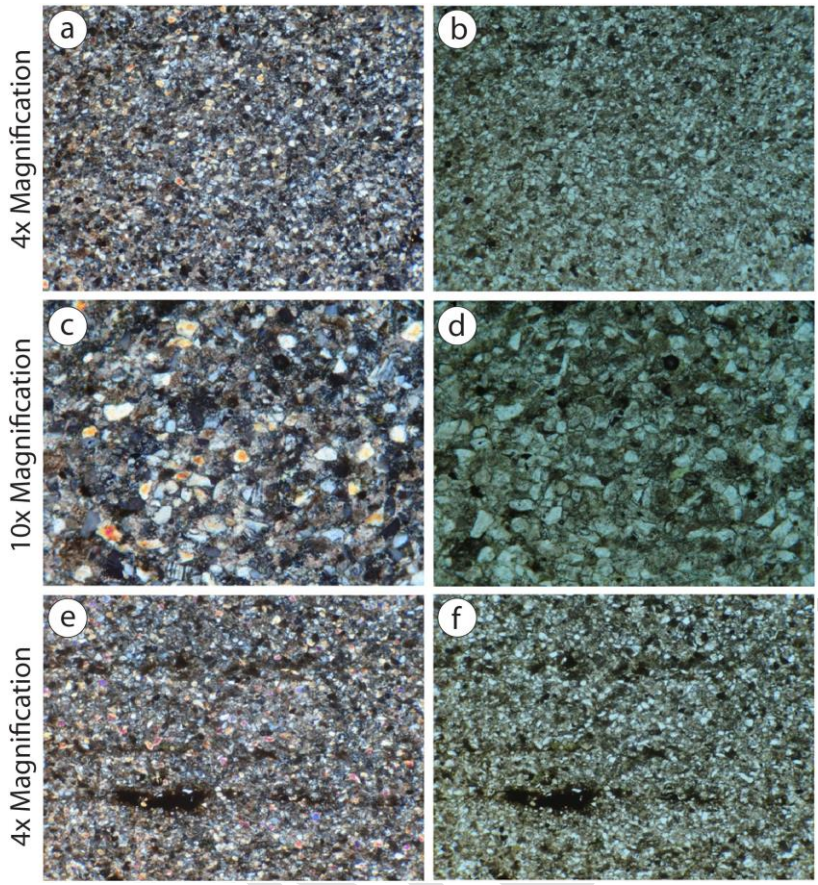


Figure 4-34. Photomicrographs of Sample 24M-21F in XPL (panels a, c, e) and PPL (panels b, d, f) at magnifications of 4x (a, b, e, f) and 10x (c, d).

4.6.1.2 Sample 24M-26Pa

- Location: 25.6490° N latitude, 60.4343° E longitude.
- Rock Type: Clastic Sedimentary Rock.
- Rock Name: Medium- to Fine-Grained Sandstone (Litharenite Arenite with Calcite Cement or Volcanic Arenite with Calcite Cement).
- Microfacies: Sandy Bio-dol-sparite (Sandy Limestone), Detrital, Ferruginous.
- Description:

Sample 24M-26Pa (Figure 4-35) is a medium- to fine-grained sandstone classified as a litharenite arenite with calcite cement. The grains are composed of:

- Quartz: Angular to subangular grains, suggesting limited transport.
- Volcanic Rock Fragments: Reflecting volcanic contributions to the sediment.
- Feldspars: Including orthoclase and calcium-rich feldspars, with plagioclase heavily sericitized, imparting a calcitic appearance.
- Fossil Content: Contains foraminifera such as *Rotalia sp.*, *Textularia sp.*, and *Miliolidae*.

Rare Fossil Fragments: Present in very low abundance and scattered throughout the sample.

In some areas, the matrix consists of volcanic ash, indicating volcanic influence. Grain edges show oxidation. Sorting is moderate to good, and the cement is calcitic with fine to coarse crystals exhibiting clear cleavage. The grains are relatively compacted, with sutured and concave-convex contacts among some grains, indicating pressure solution and diagenetic alteration. Volcanic rock fragments exhibit moderate rounding, suggesting some degree of transport and abrasion. Opaque mineralization occurs in clusters but is not widespread.

- Age Determination:

  Oligocene–Miocene.

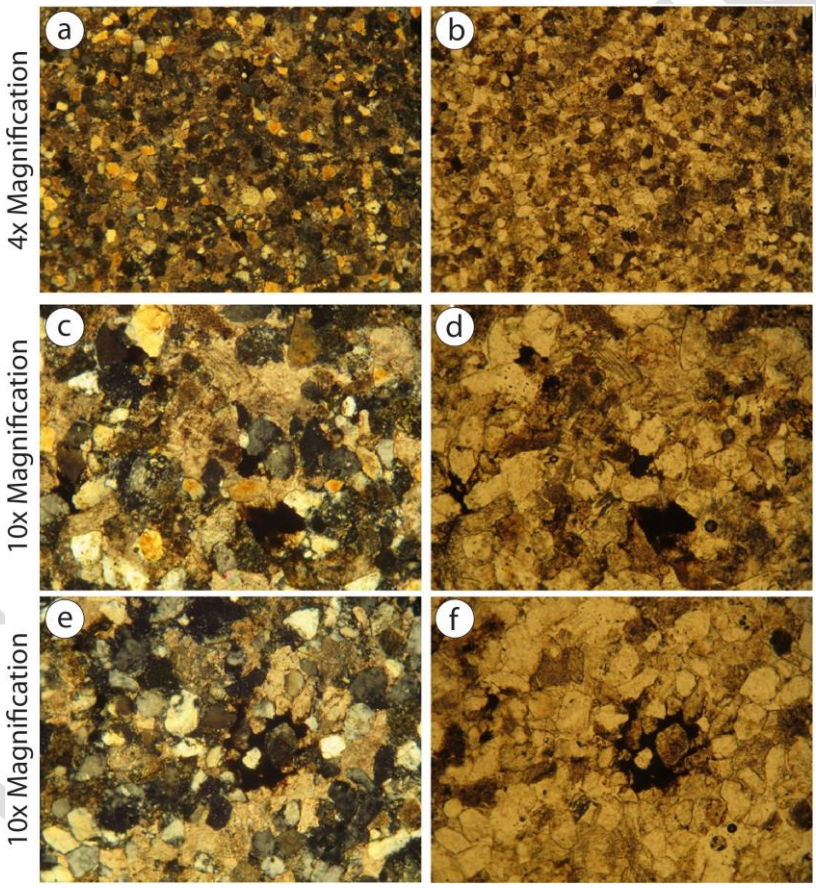


Figure 4-35. Photomicrographs of Sample 24M-26Pa in XPL (panels a, c, e) and PPL (panels b, d, f) at magnifications of 4x (a, b) and 10x (c, d, e, f).

- Interpretation:

  The petrographic features of Sample 24M-26Pa suggest a depositional environment with both clastic and volcanic influences, likely adjacent to volcanic activity. The presence of volcanic ash in the matrix and volcanic rock fragments among the grains indicates direct volcanic input during sedimentation. The moderate to good sorting and angular to subangular grains imply a moderate transport distance from the source area. The calcite

cement indicates diagenetic processes during burial, leading to precipitation within pore spaces. Sericitization of plagioclase grains points to chemical alteration after deposition. The presence of foraminifera (*Rotalia sp.*, *Textularia sp.*, and *Miliolidae*) adds a biogenic component, suggesting a marine influence. The grain contacts and compaction features reflect significant post-depositional modification, including pressure solution and recrystallization.

4.6.1.3 Sample 24M-26Pb

- Location: 25.6490° N latitude, 60.4343° E longitude (same as Sample 24M-26Pa).
- Rock Type: Clastic Sedimentary Rock.
- Rock Name: Medium-Grained Sandstone (Litharenite with Calcite Cement).
- Description:

  Sample 24M-26Pb (Figure 4-36) is a medium-grained sandstone with the following composition:

  - Quartz (~20%): Subangular to subrounded grains.
  - Feldspars (10–15%): Including plagioclase and other feldspars, mostly altered.
  - Rock Fragments (45–55%): Predominantly volcanic in origin, though identification is challenging due to degradation and thin section quality.

  Due to the thick and low-quality thin section, precise grain identification is difficult. Large portions appear as empty spaces, likely from preparation artifacts. Dark grains are mainly rock fragments that are not well-polished. Sorting is moderate, and the cement is calcitic. Some silica cement shows syntaxial overgrowths, indicating diagenetic quartz precipitation. Sutured and concave-convex contacts among grains suggest compaction and pressure solution.

- Interpretation:

  The sample reflects a sandstone with high volcanic rock fragment content, indicating significant volcanic influence during sedimentation. Moderate sorting and grain shapes suggest moderate transport and some reworking. Calcite cement and quartz overgrowths indicate diagenetic processes. Compaction features reflect post-depositional modification under overburden pressure.

GeoNexus

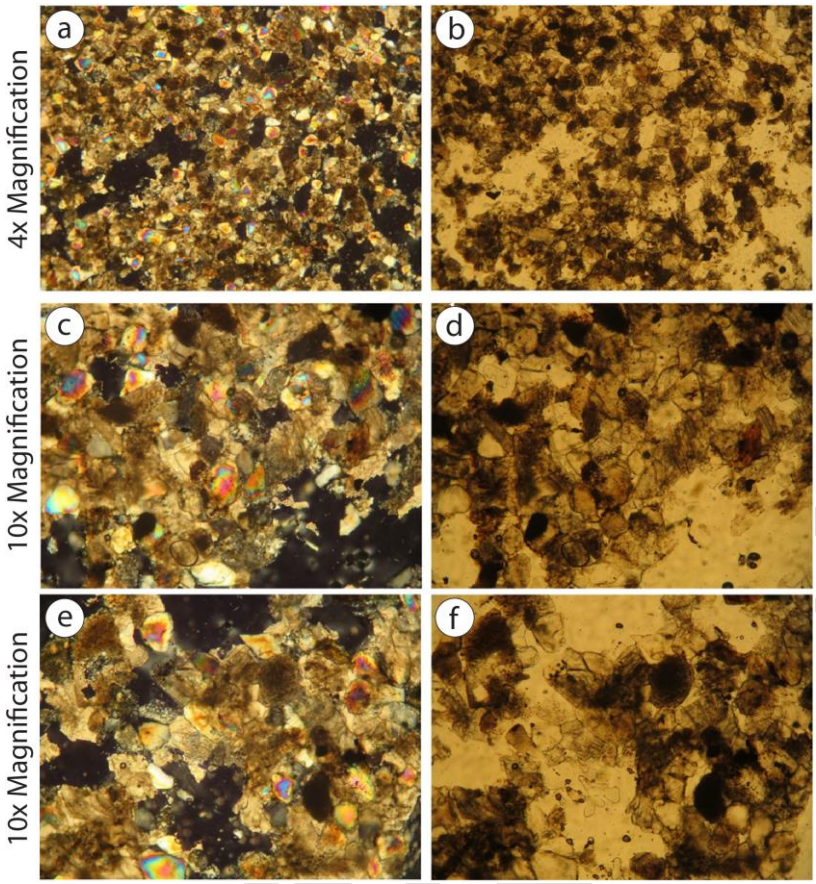


Figure 4-36. Photomicrographs of Sample 24M-26Pb in XPL (panels a, c, e) and PPL (panels b, d, f) at magnifications of 4x (a, b) and 10x (c, d, e, f).

4.6.1.4 Sample 24M-28F

- Location: 25.6848° N latitude, 60.3378° E longitude.
- Rock Type: Hybrid Sedimentary–Volcanic Rock.
- Rock Name: Graywacke to Volcanic Siltstone.
- Microfacies: Silty Argillaceous Limestone (Poorly Washed Silty Bio-sparite), Bearing Iron Oxide, Bituminous, Diagenetic.
- Description:

  Sample 24M-28F (Figure 4-37) exhibits lamination and contains fossil fragments. The rock shows facies changes and contains thin fractures and veins filled with opaque minerals, likely iron oxides. In some areas, minor calcareous mud is present in the matrix. Fossil content includes *Miliolidae*, *Eouvigerina? sp.*, and shell and algal debris. The variation in grain size and composition indicates changes in depositional conditions.

- Interpretation:

  The lamination and fossil fragments suggest deposition in a marine environment with varying energy conditions. The graywacke nature, with a matrix-supported texture,

indicates rapid deposition of mixed sediment sizes, possibly from turbidity currents. Volcanic material reflects volcanic activity during sedimentation. Fractures and mineral-filled veins indicate post-depositional processes such as mineralization along structural features. The presence of iron oxide, bituminous material, and specific fossils like *Miliolidae* and *Eouvigerina? sp.* suggests diagenetic alteration and a marine depositional setting.

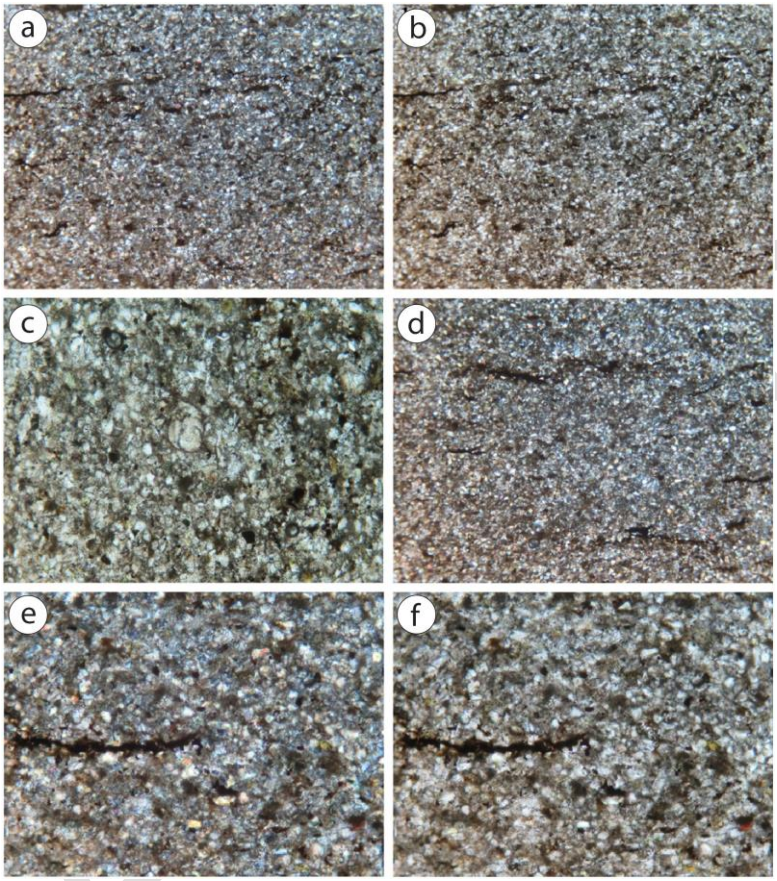


Figure 4-37. Photomicrographs of Sample 24M-28F in XPL (panels a, d, e) and PPL (panels b, c, f) at magnifications of 4x (a, b, d) and 10x (c, e, f).

4.6.1.5 Sample 24M-31F

- Location: 25.6777° N latitude, 60.4094° E longitude.
- Rock Type: Hybrid Sedimentary–Volcanic Rock.
- Rock Name: Calcareous Siltstone to Graywacke.
- Microfacies: Sandy-Silty Limestone, Recrystallized, Detrital, Ferruginous.
- Description:

  Sample 24M-31F contains grains of quartz, feldspars, and volcanic rock fragments. A facies boundary is observed, indicating a change in depositional conditions. Iron oxide formation is noted within this facies. The rock exhibits fine-grained texture with components

indicative of both clastic and volcanic inputs. The rock is recrystallized and ferruginous, suggesting diagenetic processes. Fossils are absent or not identifiable.

- Interpretation:

  The calcareous siltstone suggests deposition in a marine environment with carbonate input. Volcanic material indicates continued volcanic influence. The facies boundary reflects changes in depositional energy or sediment supply. Iron oxide formation suggests diagenetic alteration during burial. The detrital nature and ferruginous characteristics indicate clastic input and post-depositional iron enrichment. The absence of fossils limits precise age determination.

4.6.1.6 Sample 24M-32F

- Location: 25.6806° N latitude, 60.4067° E longitude.
- Rock Type: Hybrid Sedimentary–Volcanic Rock.
- Rock Name: Mudstone to Tuff.
- Microfacies: Sandy Micrite, Calcareous, Detrital.
- Description:

  Sample 24M-32F (Figure 4-38) shows open intersecting fractures with iron oxide impregnation along these features. Dark brown areas, likely containing iron oxide, are observed around fractures and veins. Components are not identifiable due to fine-grained nature. The rock appears homogeneous but reveals structural features under magnification. The rock is calcareous and detrital, but fossils are barren.

- Interpretation:

  The fine-grained texture suggests deposition of volcanic ash or mud in a low-energy environment. Fractures indicate post-depositional tectonic activity. Iron oxide impregnation along fractures suggests fluid movement and mineralization during diagenesis. The calcareous and detrital nature points to a mix of carbonate and clastic sediments. The absence of fossils prevents precise age dating.

GeoNexus

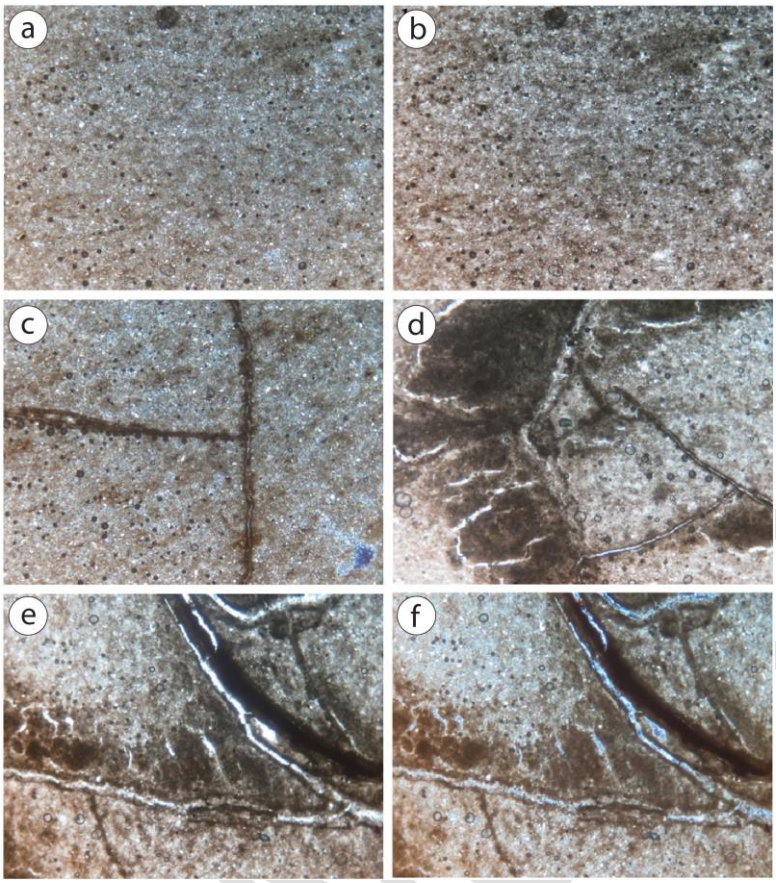


Figure 4-38. Photomicrographs of Sample 24M-32F in XPL (panels a, c, f) and PPL (panels b, d, e) at magnifications of 4x (a, b, c) and 10x (d, e, f).

4.6.1.7 Sample 24M-54P

- Location: 25.7650° N latitude, 60.2813° E longitude.
- Rock Type: Hybrid Clastic-Carbonate Sedimentary Rock.
- Rock Name: Sandy Allochem Limestone to Allochemic Sandstone.
- Microfacies: Sandy Bio-sparite, Strongly Recrystallized, Ferruginous, Bituminous, Tectonized.
- Description:

  Sample 24M-54P (Figure 4-39) transitions between sandy allochem limestone and allochemic sandstone. Clastic grains include quartz, feldspars, and volcanic rock fragments. The matrix consists of micritic limestone that has recrystallized, with calcite cement filling intergranular spaces. Allochems include skeletal fragments of bivalves, echinoderms, corals, green algae, and intraclasts. Fossil content includes *Ammonia beccarii*, *Pseudolituonella reicheli*, *Ammonia sp.*, *Rotalia sp.*, *Textularia sp.*, *Miliolidae*, bivalves, gastropods, shell fragments (*Ostrea latimarginata*), and algal fragments (red algae, *Solenomeris? sp.*). Sorting is poor, and quartz grains exhibit straight extinction. Cement is calcitic, showing at least two generations:

- First Generation: During shallow burial.
- Second Generation: Filling fractures and skeletal molds during deeper burial.

The rock is strongly recrystallized, ferruginous, bituminous, and shows signs of tectonic deformation.

- Age Determination:

  Early Miocene (Aquitanian–Burdigalian).

- Interpretation:

  The sample represents a shallow marine carbonate setting with clastic input. Biogenic allochems and micritic matrix indicate deposition in a carbonate platform. Poor sorting and mixed components suggest fluctuating energy conditions. Calcite cementation and recrystallization indicate diagenetic processes during burial. Opaque minerals suggest post-depositional mineralization. The diverse fossil assemblage, including foraminifera, bivalves, gastropods, and algal fragments, confirms an early Miocene age. The ferruginous and bituminous characteristics indicate iron enrichment and organic matter content. Tectonization reflects structural deformation affecting the rock post-deposition.

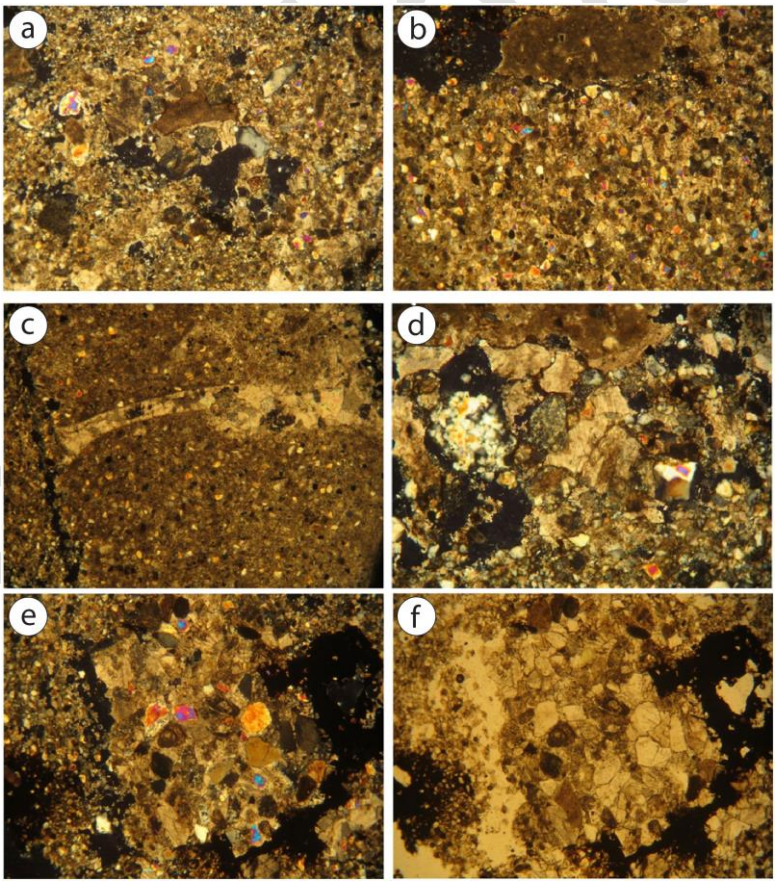


Figure 4-39. Photomicrographs of Sample 24M-54P in XPL (panels a, b, c, d, e) and PPL (panel f) at magnifications of 4x (a, b, c) and 10x (d, e, f).

4.6.2 Micropaleontological Analysis

4.6.2.1 Sample 24M-20W

- Location: 25.9412° N latitude, 60.1990° E longitude.
- Description:

  Benthic species include *Ammonia indica*, *Ammonia tochigiensis*, *Ammonia sp.*, *Bolivina scalprata miocenica*, *Nonion sp.* (Figure 4-40), *Operculina sp.*, and *Quinqueloculina sp. cf. Q. vulgaris*. Planktonic forms are absent.

- Age Determination:

  The absence of index planktonic forms inhibits precise age determination. However, the benthic assemblage suggests an age not older than Miocene. The presence of *Bolivina scalprata miocenica* and *Quinqueloculina sp. cf. Q. vulgaris* allows for an early Miocene (Burdigalian) to early Pliocene age.

- Interpretation:

  The assemblage indicates a marine environment with normal salinity and moderate depth. The age aligns with the $MPl^{m.s}$ Unit. Lack of planktonic forms may reflect shallow water deposition or preservation issues.

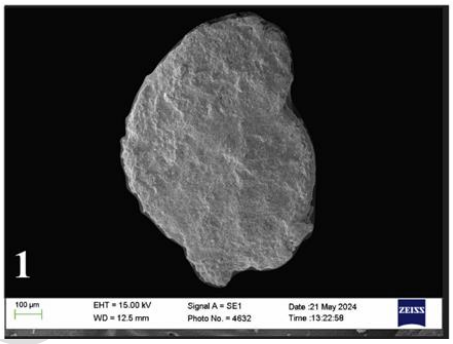


Figure 4-40. SEM images of *Nonion sp.* (Sample 24M-20W; Plate 9), showcasing its morphological details.

4.6.2.2 Sample 24M-27W

- Location: 25.6679° N latitude, 60.3919° E longitude.
- Description:

  Benthic species include *Ammonia beccarii*, *Ammonia gaimardi*, *Ammonia punctato granosa*, *Ammonia schroeteriana*, *Ammonia tochigiensis*, *Ammonia umbonata*, *Heterolepa dutemplei*, and *Nonion sp*. Planktonic species are *Globigerina praebulloides*, *Globigerinoides immaturus*, *Globigerinoides subquadratus*, and *Globigerinoides triloba* (Figure 4-41).

- Age Determination:

The presence of planktonic forms and *Ammonia* species allows for accurate dating. A late Miocene (Tortonian) to early Pliocene age is suggested.

- Interpretation:

  The assemblage reflects open marine conditions with good water circulation. The age aligns with the $MPl^{m.s}$ Unit.

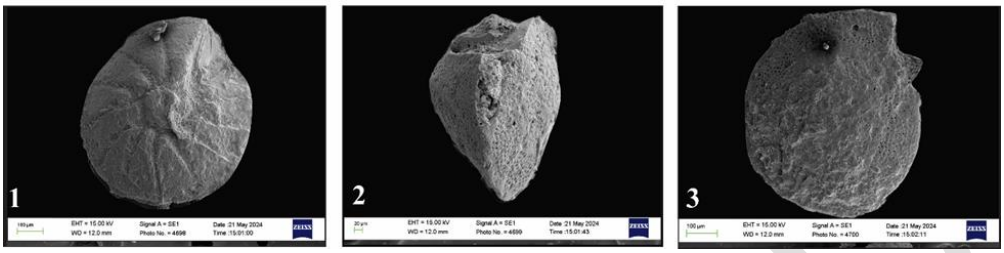


Figure 4-41. SEM images of micropaleontological species of Sample 24M-27W (Plate 11), showcasing their morphological details. 1) *Ammonia gaimardi*; 2) *Heterolepa dutemplei*; 3) *Heterolepa dutemplei*.

4.6.2.3 Sample 24M-29W

- Location: 25.6848° N latitude, 60.3378° E longitude.
- Description:

  Benthic species include *Amphicorina scalaris*, *Anomalina sp.*, *Bolivina sp.*, *Bulimina elongata*, *Lenticulina sp. cf. L. inornata*, *Textularia spp.*, and *Uvigerina auberiana*. Planktonic species are *Dentoglobigerina altispira*, *Globigerina bulloides*, *Globigerinella obesa*, Globoquadrina dehiscens, Globigerinoides immaturus, Orbulina suturalis, *Orbulina universa*, *Paragloborotalia mayeri*, and *Praeorbulina glomerosa* (Figure 4-42).

- Age Determination:

  The presence of index species such as *Orbulina suturalis*, *Orbulina universa*, and *Praeorbulina glomerosa* indicates a middle Miocene (early Langhian) age.

- Interpretation:

  This age is older than the defined unit age of late Miocene to early Pliocene, indicating a potential inconsistency. Portions of the $MPl^{m.s}$ Unit may include older strata or reworked sediments from the middle Miocene. This requires careful stratigraphic analysis.

GeoNexus

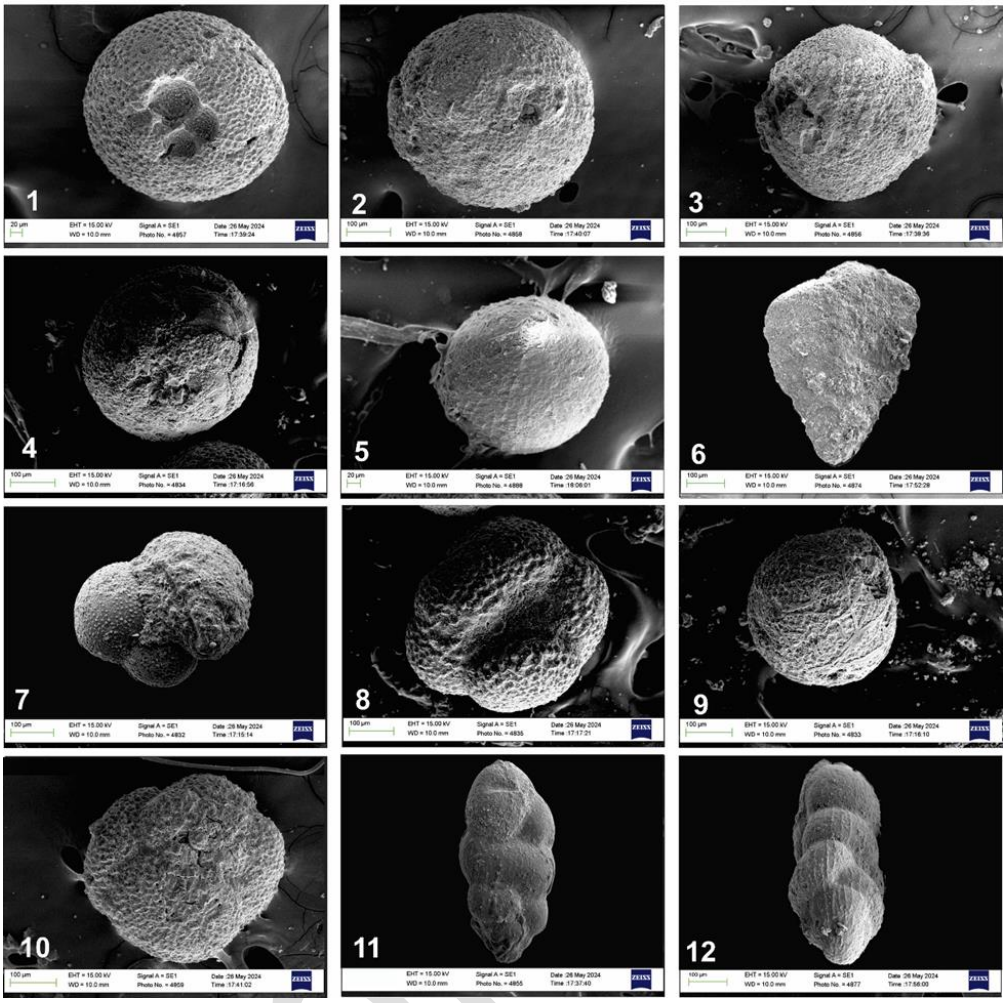


Figure 4-42. SEM images of micropaleontological species of Sample 24M-29W (Plate 12), showcasing their morphological details. 1) *Orbulina universa*; 2) *Orbulina universa*; 3) *Orbulina suturalis*; 4) *Orbulina suturalis*; 5) *Orbulina univesa*; 6) *Textularia sp.*; 7) *Globigerinoides immaturus*; 8) *Globoquadrina venezuelana*; 9) *Orbulina suturalis*; 10) *Globoquadrina venezuelana*; 11) *Bulimina elongate*; 12) *Uvigerina auberiana*.

4.6.2.4 Sample 24M-34W

- Location: 25.7011° N latitude, 60.4239° E longitude.
- Description:

  Benthic species include *Ammonia inflata*, *Ammonia schroeteriana*, *Ammonia tochigiensis*, *Ammonia umbonata*, *Ammonia sp.*, *Nonion costiferum*, *Nonion scapha*, *Nonion sp.*, and *Textularia sp*. (Figure 4-43). Planktonic forms are absent.

- Age Determination:

  The presence of Ammonia species suggests a late Miocene to early Pliocene age.

- Interpretation:

  The assemblage supports the $MPl^{m.s}$ Unit's age. Absence of planktonic forms may indicate shallow marine deposition.

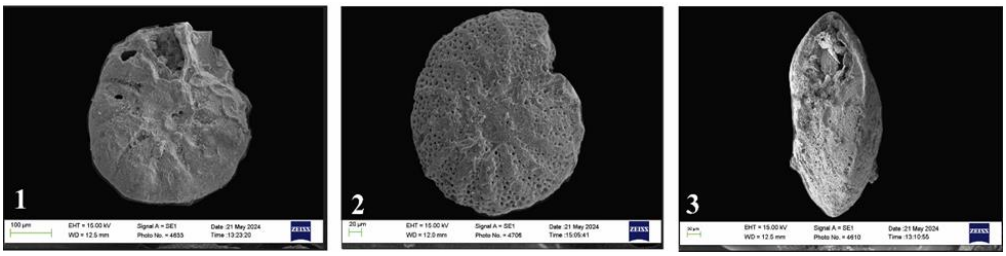


Figure 4-43. SEM images of micropaleontological species of Sample 24M-34W (Plate 13), showcasing their morphological details. 1) *Ammonia umbonate*; 2) *Nonion scapha*; 3) *Nonion sp*.

4.6.3 Age and Correlation

The micropaleontological analyses generally support the late Miocene to early Pliocene of the $MPl^{m.s}$ Unit. However, some samples, such as Sample 24M-21F and Sample 24M-28F, suggest an age of probably Oligocene–Miocene based on lithology and fossil content, which is older than the unit's defined age. Similarly, Sample 24M-54P indicates an early Miocene (Aquitanian–Burdigalian) age. Sample 24M-29W indicates a middle Miocene (early Langhian) age, which is inconsistent with the unit's defined age, as well. These discrepancies suggest that parts of the unit may include older strata or reworked sediments, highlighting the complexity of the geological history and the need for careful stratigraphic analysis.

4.6.4 Depositional Environment

The $MPl^{m.s}$ Unit represents a depositional environment influenced by both clastic and volcanic inputs, within shallow to moderate marine settings. Petrographic analyses indicate deposition near active volcanic regions, as evidenced by volcanic ash matrices and volcanic rock fragments. Immature textures, poor to moderate sorting, and angular grains reflect short transport distances and rapid deposition.

The presence of ferruginous and bituminous characteristics in several samples (e.g., Samples 24M-21F, 24M-28F, and 24M-54P) indicates post-depositional iron enrichment and the presence of organic matter, suggesting reducing conditions during diagenesis. Tectonization observed in Sample 24M-54P reflects structural deformation affecting the rocks after deposition.

Micropaleontological data support marine conditions with normal salinity and good water circulation. Variations in planktonic forms suggest changes in water depth and energy conditions during deposition. The presence of fossils such as foraminifera, shell fragments, and algal debris indicates a productive marine environment with biogenic contributions.

These data largely support the assigned unit age of late Miocene to early Pliocene. However, the older ages suggested by some samples indicate that the $MPl^{m.s}$ Unit may encompass a broader temporal range than previously defined, or that there are complexities in the stratigraphic relationships, such as unconformities, faulting, or folding that have juxtaposed older rocks against younger units. Reworking of older sediments into younger deposits may have occurred, and further detailed stratigraphic and paleontological studies are necessary to refine the age framework of this unit.

GeoNexus

4.7 $MPl^{m.s.c}$ Unit (Late Miocene–Early Pliocene Sandstone and Microconglomerate)

The $MPl^{m.s.c}$ Unit, with ~ 250 m thickness, represents a late Miocene to early Pliocene geological formation within the study area, characterized by alternating sequences of greenish to light grey, thin to moderately bedded marls (argillaceous rocks), and red-brown, moderately to thick-bedded sandstones and microconglomerates (Figure 4-44). The unit features cleavages and macrofossils, with sandy olistoliths particularly concentrated in the lower part. This sedimentary package reflects a diverse depositional environment influenced by both sedimentary and tectonic processes, with unit thickness reaching ~ 250 m. The rocks exhibit variations in color and texture between weathered and fresh surfaces, reflecting their compositional diversity and diagenetic history.

The unit is represented by 654 mapped polygons within the study area. The individual areas of these outcrops vary greatly, from as small as 0.0082 sq km (OBJECTID_1: 1310) to as large as 69.45 sq km (OBJECTID_1: 1483). The cumulative area covered by the $MPl^{m.s.c}$ Unit is ~ 410 sq km.

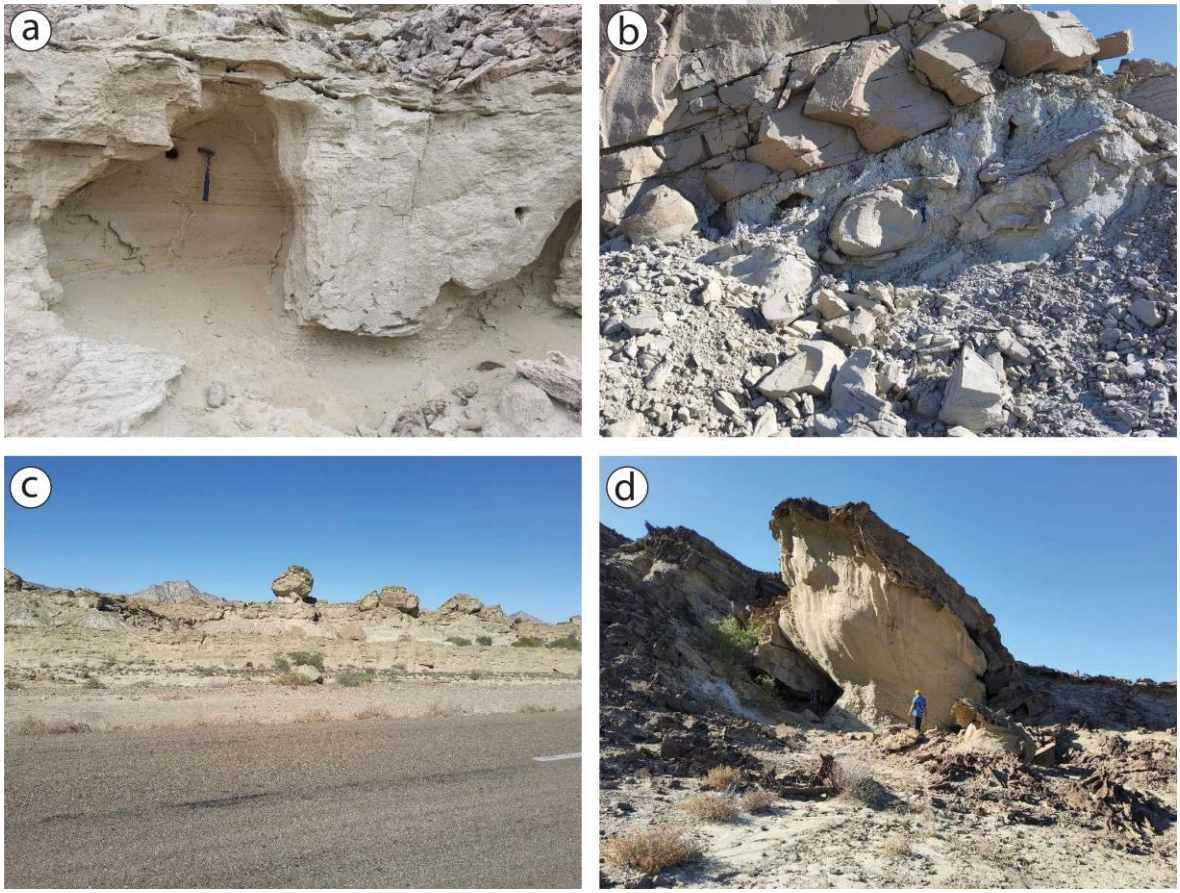


Figure 4-44. a) Outcrop at location P002 showing thinly bedded argillaceous rock layers of the $MPl^{m.s.c}$ Unit's. b) Location P031 displaying large olistolith blocks embedded within the sedimentary sequence. c, d) Prominent hoodoo morphology at location P032 (c) and P033 (d), showcasing the differential weathering and textural contrasts between weathered and fresh surfaces in the MPlm.s.c Unit's sandstone beds.

4.7.1 Lithology and Petrography

4.7.1.1 Sample 24M-7P

- Location: 25.5893° N latitude, 60.4815° E longitude.
- Rock Type: Hybrid Sedimentary–Volcanic Rock.
- Rock Name: Volcanic Siltstone.
- Description:

  Sample 24M-7P (Figure 4-45) is a hybrid rock exhibiting characteristics of both sedimentary and volcanic origins. Classified as a volcanic siltstone, the rock comprises angular grains of quartz and feldspar, along with lithic fragments predominantly of volcanic origin. Muscovite is also present within the sample. The quartz and feldspar grains are angular, suggesting limited transport and rapid deposition. A slight alignment of grains is observed, which may be attributed to compaction rather than metamorphic processes. The matrix filling the intergranular spaces consists of neomorphosed calcareous mud (micrite), indicating diagenetic alteration of the original micritic material. High compaction and the abundance of lithic fragments may have caused the deformation of the grains.

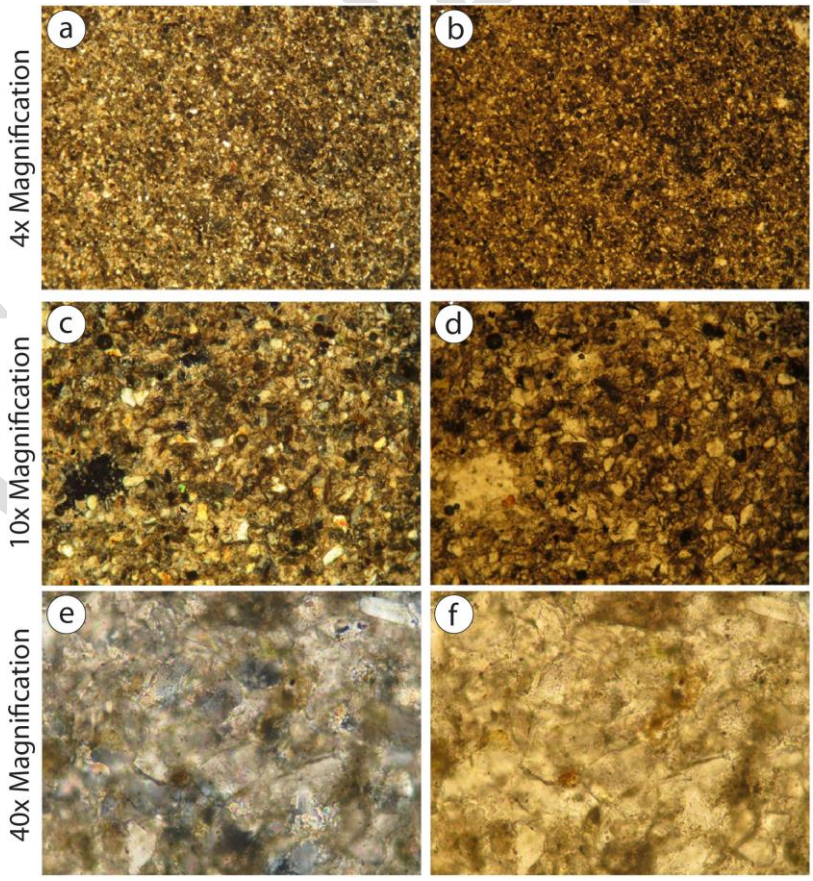


Figure 4-45. Photomicrographs of Sample 24M-7P in XPL (panels a, c, and e) and PPL (panels b, d, and f) at varying magnifications.

- Interpretation:

  The presence of volcanic lithic fragments and angular quartz and feldspar grains suggests proximity to volcanic sources and limited transport distance. The slight grain alignment indicates compaction during burial. The neomorphism of the calcareous mud matrix reflects diagenetic processes that have altered the original sediment. Overall, the rock represents deposition in a volcaniclastic sedimentary environment, possibly in proximity to active volcanic regions.

4.7.1.2 Sample 24M-8P

- Location: 25.5893° N latitude, 60.4815° E longitude.
- Rock Type: Hybrid Clastic–Carbonate Sedimentary Rock.
- Rock Name: Very Fine-Grained Calcareous Sandstone.
- Microfacies : Sandy-bio-sparite (Sandy limestone), calcite veined, argillaceous, ferruginous.
- Description:

  Sample 24M-8P (Figure 4-46) is a hybrid rock combining clastic and carbonate features, classified as a very fine-grained calcareous sandstone. The grains are mainly composed of quartz and volcanic lithic fragments. Quartz grains constitute approximately 20–25% of the grains, while volcanic lithic fragments make up about 30–35%. Plagioclase and other feldspars are present in lesser amounts and are mostly altered, with fine-grained calcite cement forming around or on them. Approximately 7% of the rock consists of fragments and skeletons of foraminifera and bivalves, indicating biogenic input. The grains are embedded in a matrix of neomorphosed calcareous mud. In some areas, grains are enveloped by cement. Short-range stylolites resulting from physicochemical compaction are observed. The clastic grains are angular to sub-angular, suggesting a possible aeolian origin. The sorting of the clastic grains ranges from moderate to poor, reflecting rapid deposition or limited transport. The rock exhibits mineralization, with opaque minerals, likely iron oxides, filling the molds of foraminifera. The rock contains a diverse assemblage of fossils, including foraminifera such as *Ammonia sp.*, *Rotalia sp.*, Rotalidae, Ostracoda, Shell and algal debris (Red algae).

- Age Determination: Early Miocene.
- Interpretation:

  The combination of clastic grains and biogenic components suggests a mixed depositional environment where both terrigenous and marine influences were present. The angularity and poor sorting of the clastic grains imply limited transport and rapid deposition, possibly from wind-blown sources. The presence of stylolites indicates pressure solution during diagenesis. Iron oxide mineralization filling foraminiferal molds suggests post-depositional alteration under oxidizing conditions. Overall, the rock represents deposition in an environment where clastic input from nearby volcanic sources was mixed with marine carbonate sedimentation.

GeoNexus

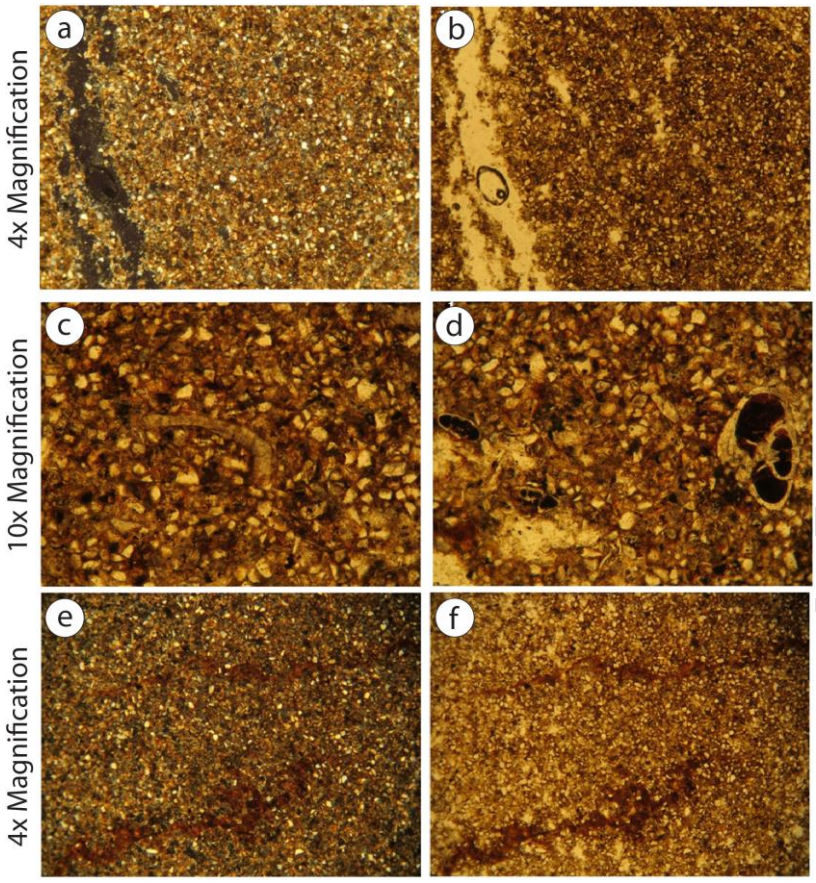


Figure 4-46. Photomicrographs of Sample 24M-8P in XPL (panels a and e) and PPL (panels b, c, d, and f) at varying magnifications.

4.7.1.3 Sample 24M-9P

- Location: 25.3904° N latitude, 60.7160° E longitude.
- Rock Type: Clastic Sedimentary Rock.
- Rock Name: Fine-Grained Sandstone (Litharenite with Calcite Cement).
- Description:

  Sample 24M-9P (Figure 4-47) is a fine-grained sandstone, classified as litharenite with calcite cement. The rock comprises grains of quartz (15–20%), lithic fragments (40–45%), and feldspar (25–30%). The lithic fragments are predominantly volcanic and metamorphic in origin. The lithic grains are sub-rounded, whereas the quartz grains are angular, indicating different transport histories or sources. Fine-grained calcite cement fills the intergranular spaces. Some grains have undergone dissolution, possibly representing leached carbonate allochems, leaving behind molds. Around these voids, dolomite crystals are forming, indicating dolomitization processes where dolomite replaces calcite cement. Opaque minerals are present as cement and vein fillings in void spaces. Pyritization is observed on the rock surface, suggesting the presence of sulfide minerals; polished sections are needed for detailed examination. Compaction appears to be low. In some areas, the

intergranular space is filled with micritic limestone, possibly resulting from neomorphism of calcareous mud. The rock exhibits poor sorting, and the clastic grains are angular.

- Interpretation:

  The high content of lithic fragments and feldspar suggests a proximal source area with rapid deposition, likely near volcanic or metamorphic terrains. The angular quartz grains and poor sorting indicate limited transport and rapid sedimentation. Dissolution features and subsequent dolomitization indicate diagenetic alterations, possibly influenced by fluid migration during burial. The presence of pyrite and other opaque minerals suggests reducing conditions during diagenesis. The mixture of clastic and carbonate components reflects complex depositional and diagenetic histories, indicating interactions between terrigenous input and carbonate sedimentation.

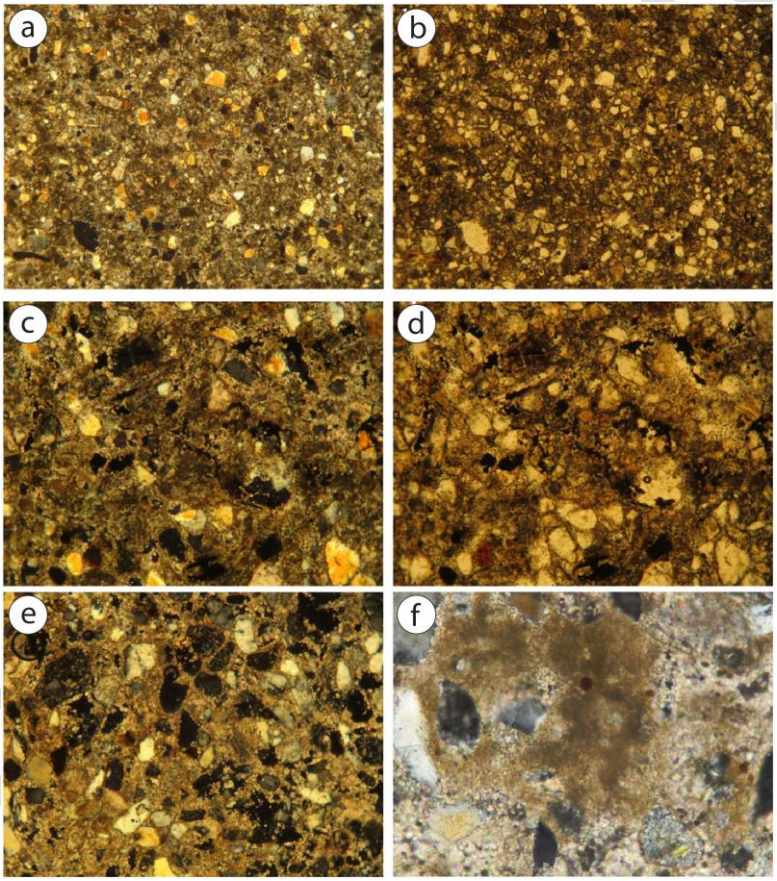


Figure 4-47. Photomicrographs of Sample 24M-8P in XPL (panels a, c, e, and f) and PPL (panels b and d) at magnifications of 4x (a and b), 10x (c, d, and e), and 40x (f).

4.7.1.4 Sample 24M-13F

- Location: 25.5602° N latitude, 60.6730° E longitude.
- Rock Type: Sedimentary–Volcanic Rock.
- Rock Name: Siltstone to Volcanic Siltstone.

- Description:

  Sample 24M-13F (Figure 4-48) is a rock exhibiting both sedimentary and volcanic characteristics, classified as a siltstone to volcanic siltstone. The grains are predominantly angular quartz, along with plagioclase and feldspar. Volcanic lithic fragments are present in small amounts. In parts of the facies, the matrix consists of volcanic ash altered to calcite, indicating diagenetic processes. A slight alignment of grains is observed, suggesting compaction. The composition includes quartz (20–25%), lithic fragments (10%), feldspar (10–15%), and plagioclase (20%).

- Interpretation:

  The dominance of angular quartz grains and the presence of plagioclase, feldspar, and volcanic lithic fragments suggest deposition in an environment influenced by volcanic activity. The volcanic ash matrix altered to calcite reflects diagenetic alteration, possibly due to circulating fluids during burial. The slight grain alignment points to compaction effects during sediment burial. The rock represents deposition where volcanic materials were mixed with clastic sediments, possibly in a marine setting influenced by volcanic eruptions.

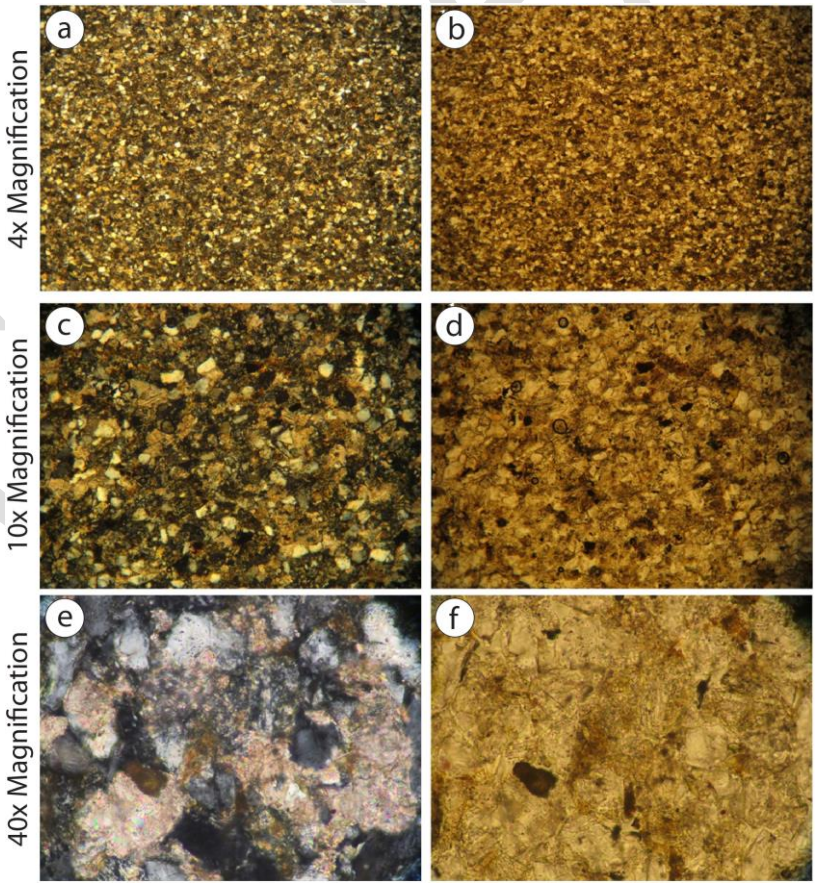


Figure 4-48. Photomicrographs of Sample 24M-13F in XPL (panels a, c, and e) and PPL (panels b, d, and f) at varying magnifications.

4.7.1.5 Sample 24M-16F

- Location: 25.5499° N latitude, 60.7275° E longitude.
- Rock Type: Hybrid Sedimentary–Volcanic Rock.
- Rock Name: Greywacke to Volcanic Siltstone.
- Description:

  Sample 24M-16F (Figure 4-49) is a hybrid rock classified as greywacke to volcanic siltstone. The rock features a volcanic matrix altered to calcite. In some parts, the matrix appears to be a combination of volcanic ash and micritic limestone, making it challenging to distinguish from alteration-derived calcite. Scattered skeletal components are present but are not precisely identifiable due to the quality of the thin section and their small size.

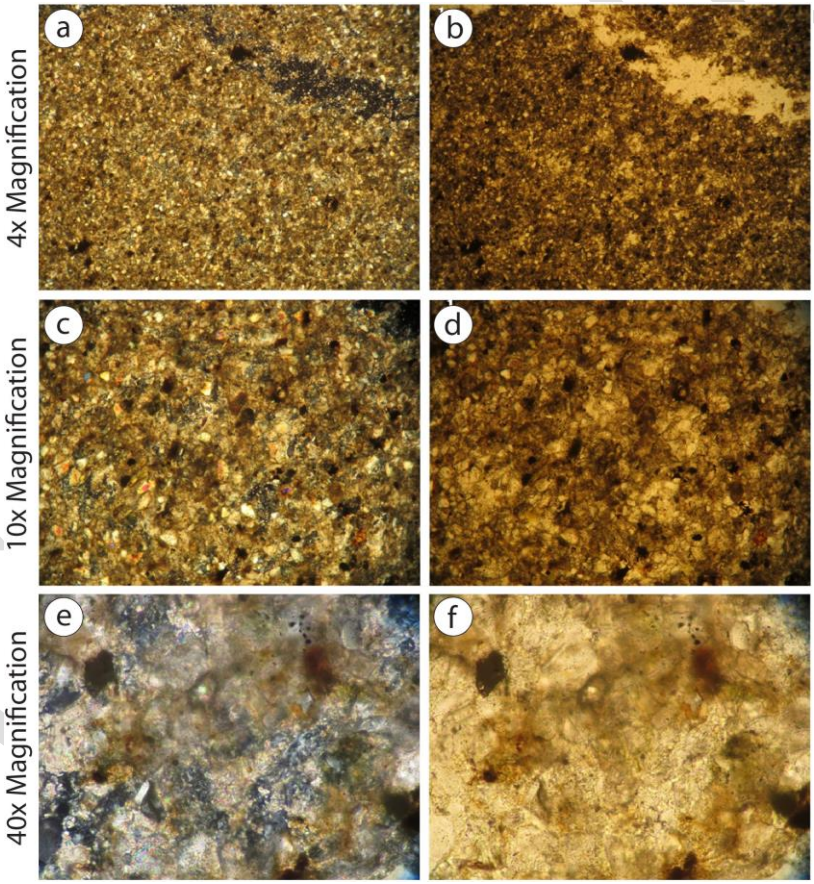


Figure 4-49. Photomicrographs of Sample 24M-16F in XPL (panels a, c, and e) and PPL (panels b, d, and f) at varying magnifications.

- Interpretation:

  The combination of volcanic and sedimentary features indicates deposition in an environment influenced by volcanic activity, possibly a volcaniclastic marine setting. The

alteration of the volcanic matrix to calcite reflects diagenetic processes involving fluid migration and chemical reactions during burial. The presence of skeletal components suggests biogenic activity within the depositional environment. The rock represents a complex interplay between volcanic input, clastic sedimentation, and carbonate deposition.

4.7.1.6 Sample 24M-17F

- Location: 25.5499° N latitude, 60.7275° E longitude.
- Rock Type: Hybrid Clastic–Calcareous Sedimentary Rock.
- Rock Name: Calcareous Siltstone.
- Description:

  Sample 24M-17F (Figure 4-50) is a calcareous siltstone, identified as a muddy micrite to micritic mudrock facies. The rock contains silt-sized clastic grains, occasionally reaching very fine sand size. Grains include quartz, feldspar, plagioclase, and predominantly volcanic lithic fragments. The matrix is neomorphosed, with crystallized micritic limestone evident in many areas, indicating diagenetic recrystallization. Parallel fractures have facilitated fluid infiltration—possibly iron-bearing—leading to the formation of iron oxide cement near these fractures. No fossils are present in this sample.

- Interpretation:

  The fine-grained nature and clastic composition suggest deposition in a low-energy environment with limited transport, possibly a marine setting with volcanic influence. Neomorphism of the micritic matrix indicates diagenetic alteration resulting in recrystallization of the original calcareous mud. Iron oxide cementation along fractures suggests post-depositional alteration under oxidizing conditions. The absence of fossils may be due to unfavorable conditions for biogenic activity or poor preservation. The rock reflects deposition where fine clastic sediments were deposited alongside calcareous mud, with volcanic input and subsequent diagenetic alteration.

GeoNexus

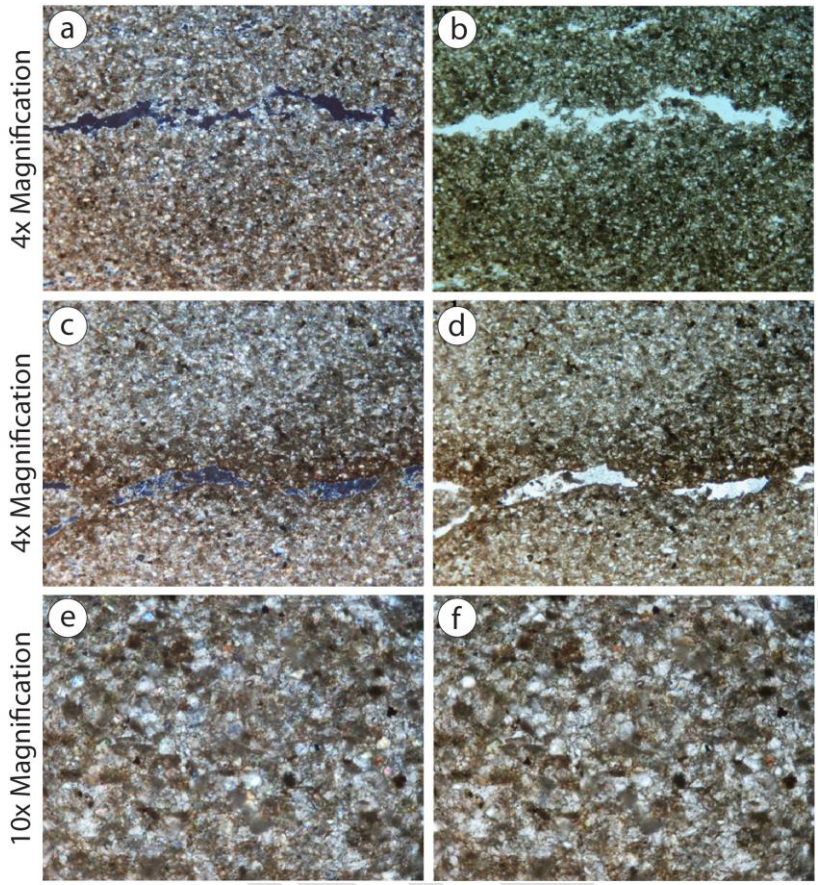


Figure 4-50. Photomicrographs of Sample 24M-17F in XPL (panels a, c, and e) and PPL (panels b, d, and f) at varying magnifications.

4.7.1.7 Sample 24M-40F

- Location: 25.5703° N latitude, 60.3263° E longitude.
- Rock Type: Limestone.
- Rock Name: Peloid-Bioclastic Rudstone.
- Microfacies: Biomicrite, Bioturbation, Bituminous.
- Description:

  Sample 24M-40F (Figure 4-51) is a limestone classified as a peloid-bioclastic rudstone. The rock contains various allochems, including bioclasts of gastropods and benthic foraminifera, along with peloids. The rock contains a diverse assemblage of fossils, including foraminifera such as *Rotalia viennoti*, *Ammonia beccarii*, *Pseudolituonella reicheli*, *Ammonia sp.*, *Rotalia sp.*, *Quinqueloculina sp.*, *Pyrgo sp.*, and *Triloculina? sp*. Other bioclasts include members of the *Rotalidae* and *Miliolidae* families, bivalves, gastropods, worm tubes, and algal fragments (red algae). The rock exhibits evidence of bioturbation, indicating biological reworking of sediments. Bituminous material suggests the presence of organic matter. Large bioclasts of unidentified organisms are also present. Skeletal fragments of echinoderms and bivalves are sporadically distributed throughout the rock. Intraclasts,

though scarce, are among the non-skeletal allochems present. The intergranular spaces are filled with fine-grained sparry calcite cement. Micritization has affected the entire facies, resulting in alteration of original textures. Coarse crystalline calcite cement fills the molds of bioclasts, indicating diagenetic infilling of voids left by dissolved skeletal material. Geopetal fabrics are prominent, particularly within gastropod molds, useful for reconstructing paleohorizontal orientation. Two generations of cement are observed: fine sparry calcite filling intergranular spaces and blocky calcite filling allochem molds.

- Age Determination: Early Miocene (Aquitanian–Burdigalian).
- Interpretation:

  The diversity and abundance of allochems suggest deposition in a shallow, high-energy carbonate environment within the intertidal to subtidal zones. The presence of geopetal structures indicates sedimentation in cavities with a preferred orientation, providing insights into depositional environments. Micritization and multiple cement generations reflect complex diagenetic histories, including alteration of original textures and infilling of void spaces. The rock represents a carbonate platform environment with active biogenic production and sedimentation influenced by high-energy conditions.

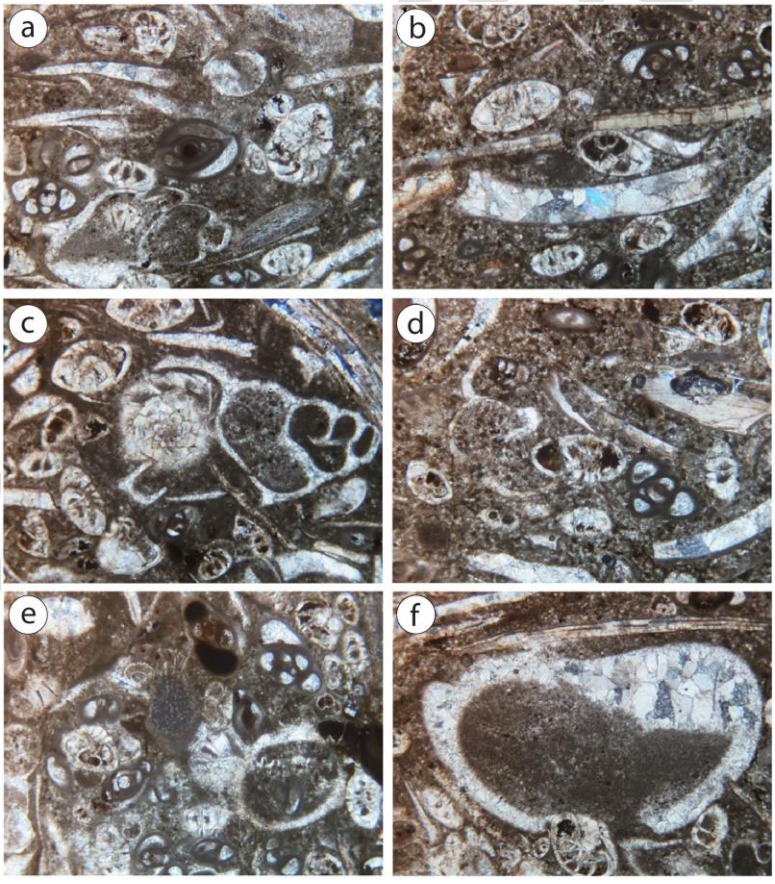


Figure 4-51. Photomicrographs of Sample 24M-40F in XPL at magnification of 4x.

4.7.2 Micropaleontological Analysis

4.7.2.1 Sample 24M-10W

- Location: 25.4937° N latitude, 60.5645° E longitude.
- Description:

  The foraminiferal assemblage in Sample 24M-10W consists of benthic forms, including *Ammonia annectens*, Ammonia gaimardi, Ammonia indica, Ammonia marhausai, *Ammonia schroeteriana*, *Ammonia stachi*, *Ammonia spp.*, and *Nonion spp*. (Figure 4-52). Planktic forms are not available.

- Age Determination:

  The absence of index planktic foraminifera inhibits precise age determination. However, the presence of *Ammonia* species such as *A. gaimardi* and *A. tochigiensis* suggests the age is not older than middle Miocene. The suggested age range is middle Miocene to Pliocene, which is consistent with the unit's defined age of lower Miocene to early Pliocene.

- Interpretation:

  The benthic assemblage indicates deposition in a marine environment, likely within shallow to moderately deep waters. The species present are indicative of normal marine salinity conditions. The lack of planktic forms may suggest deposition in inner shelf environments where planktic foraminifera are less abundant.

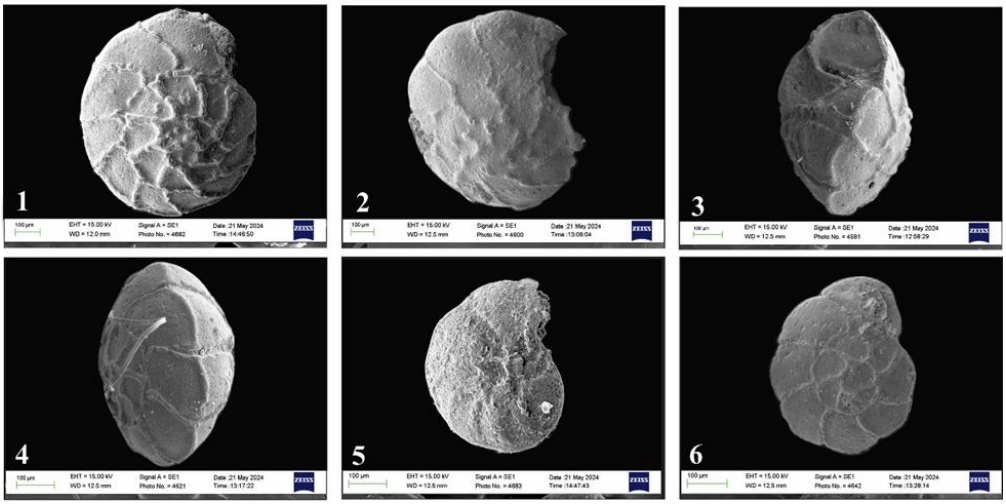


Figure 4-52. SEM images of micropaleontological species of Sample 24M-10W (Plate 4), showcasing their morphological details. 1) *Ammonia tochigiensis*; 2) *Ammonia stachi*; 3) *Ammonia gaimardi*; 4) *Ammonia marhausai*; 5) *Nonion sp.*; 6) *Ammonia annectens*.

4.7.2.2 Sample 24M-11W

- Location: 25.5174° N latitude, 60.5860° E longitude.
- Description:

  In Sample 24M-11W (Figure 4-53), the foraminiferal assemblage includes planktic forms: *Globoquadrina sp.*, *Paragloborotalia mayer*i, and a tentatively identified *? Orbulina sp*. Benthic forms are not available.

- Age Determination:

  The absence of definitive index forms limits precise age determination. Based on the identified species, the suggested age is late Oligocene to middle Miocene. The tentative identification of *? Orbulina sp*. is significant, as the first appearance of *Orbulina* is in the middle Miocene. If this identification is correct, the age would be middle Miocene. However, this potential age may be slightly older than the unit's defined age of lower Miocene to early Pliocene.

- Interpretation:

  The presence of planktic foraminifera suggests deposition in an open marine environment, possibly in outer shelf to upper slope settings. The possible occurrence of Orbulina sp. indicates Middle Miocene age, but due to the tentative identification, further confirmation is needed. The inconsistency between the suggested age and the unit's defined age should be highlighted, as it may indicate inclusion of older sediments or reworking.

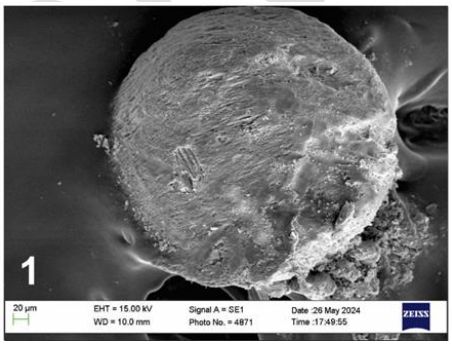


Figure 4-53. SEM images of *Orbulina sp.* (?) (Sample 24M-11W; Plate 5), showcasing its morphological details.

4.7.2.3 Sample 24M-15W

- Location: 25.5499° N latitude, 60.7275° E longitude.
- Description:

  The foraminiferal assemblage in Sample 24M-15W (Figure 4-54) includes both benthic and planktic forms. Benthic forms are *Ammonia gaimardi*, *Ammonia marhausai*, *Ammonia sumatrana*, *Ammonia tochigiensis*, *Ammonia sp.*, *Nonion costiferum*, *Nonion sp.*, *Nonionella sp.*, *Quinqueloculina vulgaris*, and *Quinqueloculina sp*. Planktic forms include

Globigerinoides immaturus, *Globigerinoides subquadratus*, *Globigerinoides triloba*, *Orbulina suturalis*, and *Orbulina universa*.

- Age Determination:

  The presence of index species *Orbulina suturalis* and *Orbulina universa*, alongside benthic forms like *Ammonia gaimardi* and *Ammonia tochigiensis*, allows for an age determination of middle Miocene (Serravallian) to early Pliocene. This age is consistent with the unit's defined timeframe.

- Interpretation:

  The assemblage indicates deposition in a marine environment with both benthic and planktic organisms, suggesting open marine conditions with normal salinity. The presence of *Orbulina* species confirms a middle Miocene to early Pliocene age. The diversity of foraminifera reflects favorable conditions for marine life during deposition.

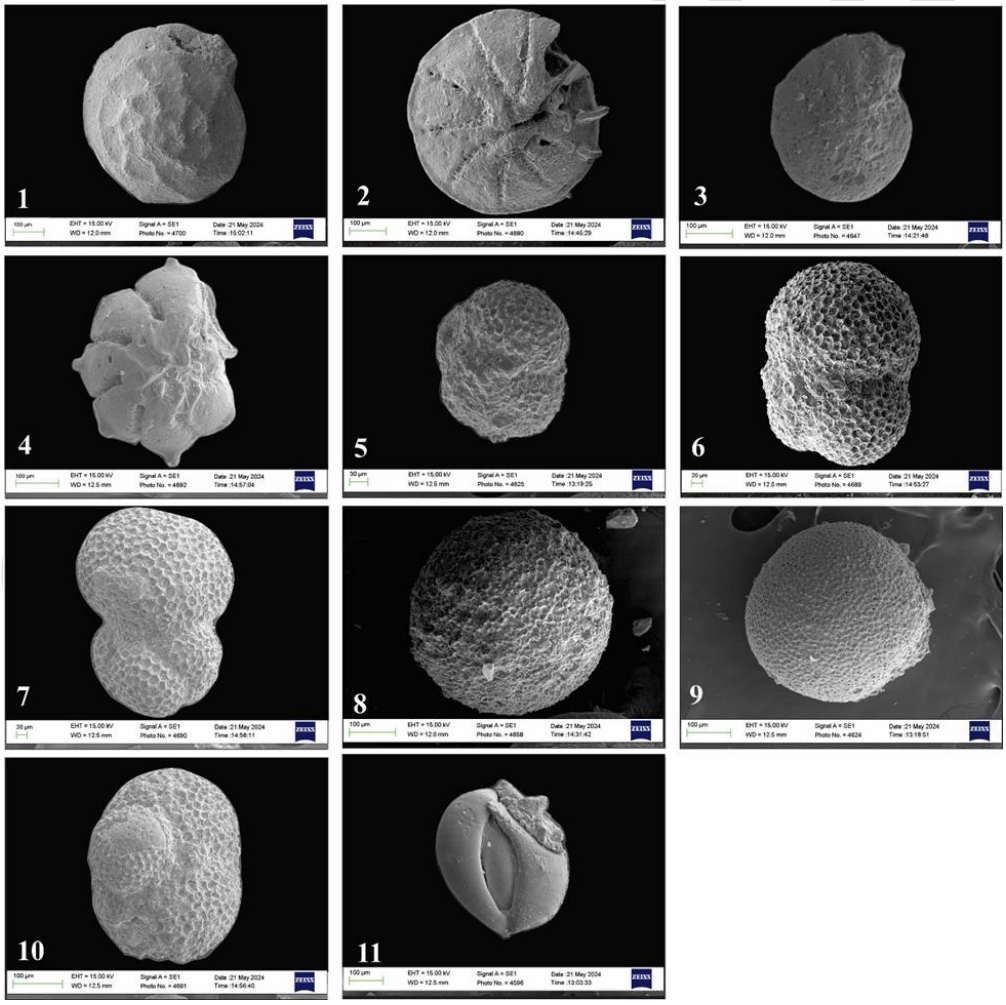


Figure 4-54. SEM images of micropaleontological species of Sample 24M-15W (Plate 6), showcasing their morphological details. 1) *Ammonia tochigiensis*; 2) *Ammonia gaimardi*; 3) *Nonion sp.*; 4) *Ammonia sumatrana*; 5) *Globigerinoides immaturus*; 6) *Globigerinoides immaturus*; 7) *Globigerinoides triloba*; 8) *Orbulina universa*; 9) *Orbulina suturalis*; 10) *Globigerinoides immaturus*; 11) *Quinqueloculina sp*.

4.7.2.4 Sample 24M-39W

- Location: 25.5703° N latitude, 60.3263° E longitude.
- Description:

  The foraminiferal assemblage in Sample 24M-39W (Figure 4-55) consists of benthic forms: *Ammonia beccarii annectens*, *Ammonia beccarii baganensis*, *Ammonia indica*, *Ammonia punctato granosa*, *Ammonia schroeteriana*, *Elphidium sp.*, *Nonion boueanum*, *Nonion costiferum*, *Nonion scapha*, and *Quinqueloculina peregrina*. Planktic forms are not available.

- Age Determination:

  The absence of index planktic foraminifera inhibits precise age determination. However, the presence of *Ammonia* species such as *A. schroeteriana*, *A. inflata*, and *A. tochigiensis* suggests an age not older than late Miocene. The suggested age range is late Miocene to Quaternary, which extends beyond the unit's defined age of lower Miocene to early Pliocene.

- Interpretation:

  The benthic assemblage reflects deposition in a marine environment, possibly shallow marine conditions. The suggested age extending into the Quaternary indicates that this sample may represent younger sediments than the unit's defined age. This discrepancy should be highlighted, as it may result from reworking of sediments, local unconformities, or inaccuracies in the initial age assignment of the unit.

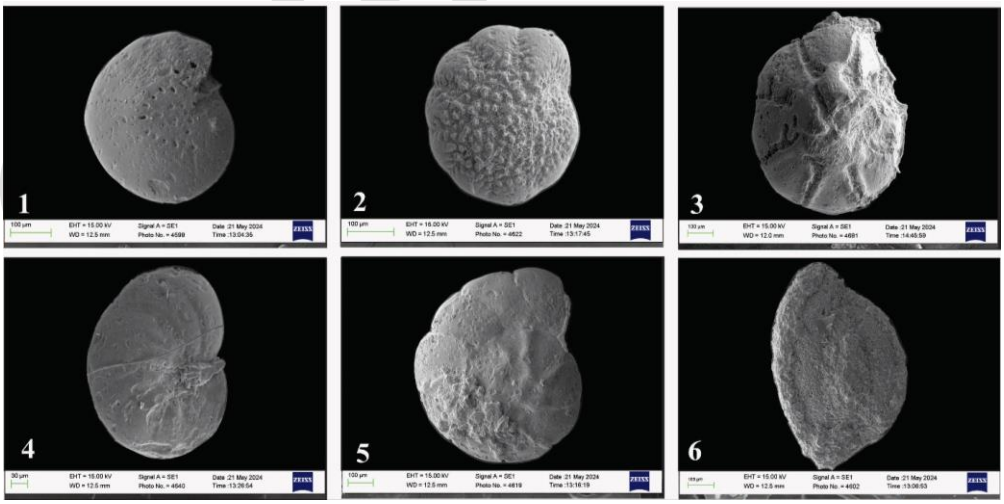


Figure 4-55. SEM images of micropaleontological species of Sample 24M-39W (Plate 14), showcasing their morphological details. 1) *Elphidium sp.*; 2) *Ammonia punctato granosa*; 3) *Ammonia schroeteriana*; 4) *Nonion costiferum*; 5) *Quinqueloculina peregrina*; 6) *Ammonia beccarii annectens*.

4.7.3 Age and Correlation

The $MPl^{m.s.c}$ Unit is defined as spanning from the lower Miocene to early Pliocene. The integrated micropaleontological analyses generally support this age assignment, with the majority of samples falling within this range. Samples 24M-10W and 24M-15W contain foraminiferal assemblages consistent with middle Miocene to early Pliocene age, including key index species such as *Orbulina suturalis* and *Orbulina universa*. However, discrepancies arise with Samples 24M-11W and 24M-39W.

4.7.4 Depositional Environment

The lithological and micropaleontological data suggest that the $MPl^{m.s.c}$ Unit was deposited in a variety of environments influenced by terrestrial, marine, and volcanic processes.

- Volcaniclastic Influence: Samples 24M-7P, 24M-8P, 24M-9P, 24M-13F, 24M-16F, and 24M-17F exhibit characteristics indicative of volcaniclastic input, such as volcanic lithic fragments, altered volcanic ash matrices, and angular clastic grains. This suggests proximity to volcanic sources and deposition influenced by volcanic eruptions, ash falls, and reworking of volcanic materials.
- Mixed Clastic–Carbonate Environments: The combination of clastic sediments with carbonate components, including biogenic material like foraminifera and bivalves, indicates deposition in environments where terrestrial and marine influences intersected. Coastal settings, deltaic environments, and shallow marine shelves where siliciclastic input from land mixed with carbonate production are likely.
- Shallow Marine Carbonate Platforms: Sample 24M-40F represents a limestone deposited in a high-energy shallow marine environment, likely a carbonate platform. The abundance of bioclasts and the presence of peloids and intraclasts indicate active biogenic production and reworking by waves and currents.
- Marine Conditions: Micropaleontological assemblages, particularly in Samples 24M-10W and 24M-15W, suggest deposition in normal marine salinity conditions. The presence of both benthic and planktic foraminifera indicates open marine environments ranging from inner to outer shelf settings.
- Environmental Variability: Variability in sediment types and fossil assemblages within the unit reflects changes in depositional environments over time, possibly due to sea-level fluctuations, volcanic activity, and climatic changes during the Miocene to Pliocene period.

In summary, the $MPl^{m.s.c}$ Unit records a complex depositional history involving the interplay of volcanic activity, clastic sedimentation, carbonate production, and marine processes. Environments range from volcaniclastic settings influenced by active volcanism to shallow marine carbonate platforms and mixed clastic-carbonate coastal zones. Diagenetic alterations observed in the rocks, including neomorphism, micritization, and cementation, further reflect post-depositional processes that have modified the original sediments.

GeoNexus

4.8 Pl^{si} Unit (Pliocene to Pleistocene Siltstones and Argillic Deposits)

This unit comprises creamy mud, thick-bedded siltstone, and sandy siltstone with greenish to light grey-blue gypseous argillic deposits (Figure 4-56). It represents sedimentary sequences deposited during the Pliocene to Pleistocene period. Detailed petrographic and micropaleontological analyses have been conducted to understand the lithology, depositional environments, and age determinations within this unit. The unit has thickness of ~ 100 m.

The Pl^{si} Unit is represented by 310 mapped polygons within the study area. These polygons range in size from as small as 0.0054 sq km to as large as 94.08 sq km. Notable large outcrops include OBJECTID_1: 244 (94.08 sq km), 2409 (65.40 sq km), and 2366 (53.23 sq km). The cumulative area covered by the Pl^{si} Unit is ~ 399 sq km.



Figure 4-56. Tidal cross-bedding observed in the Pl^{si} Unit at location P014.

4.8.1 Lithology and Petrography

4.8.1.1 Sample 24M-1F

- Location: 25.3424° N latitude, 60.6227° E longitude.
- Rock Type: Carbonate Sedimentary Rock
- Rock Name: Limestone
- Microfacies: Intrabioclastic Grainstone to Rudstone with Minor Quartz Grains
- Description:

  Sample 24M-1F (Figure 4-57) is a limestone characterized by an intrabioclastic grainstone to rudstone microfacies, containing minor quartz grains. The grains include various bioclasts of benthic foraminifera such as *Nummulites*, green algae, large bivalves (possibly

rudists), gastropods, bryozoans, red algae (?), coral fragments, and echinoderms. The intergranular space is filled with calcite cement.

Two generations of calcite cement are observed:

- First Generation: Marine cement forming blade-like crystals around grains, enhancing resistance to compaction.
- Second Generation: Fine sparry calcite filling intergranular spaces, possibly formed during meteoric diagenesis and shallow burial, accompanied by dissolution that created moldic porosity.

Porosity types include intergranular, vuggy, and moldic porosity. The rock exhibits significant diagenetic features, including cementation and dissolution.

- Age Determination:

The fossil assemblage, including *Ammonia beccarii*, *Ammonia sp.*, *Rotalia sp.*, *Elphidium sp.*, *Lenticulina (Robulus) sp.*, *Textularia sp.*, *Rotalidae*, *Nodosariidae*, *Miliolidae*, gastropods, echinoid spines, bryozoans with shell fragments, *Ostrea latimarginata*, red algae, and *Lithophyllum sp.*, indicates an early Miocene (Aquitanian) age.

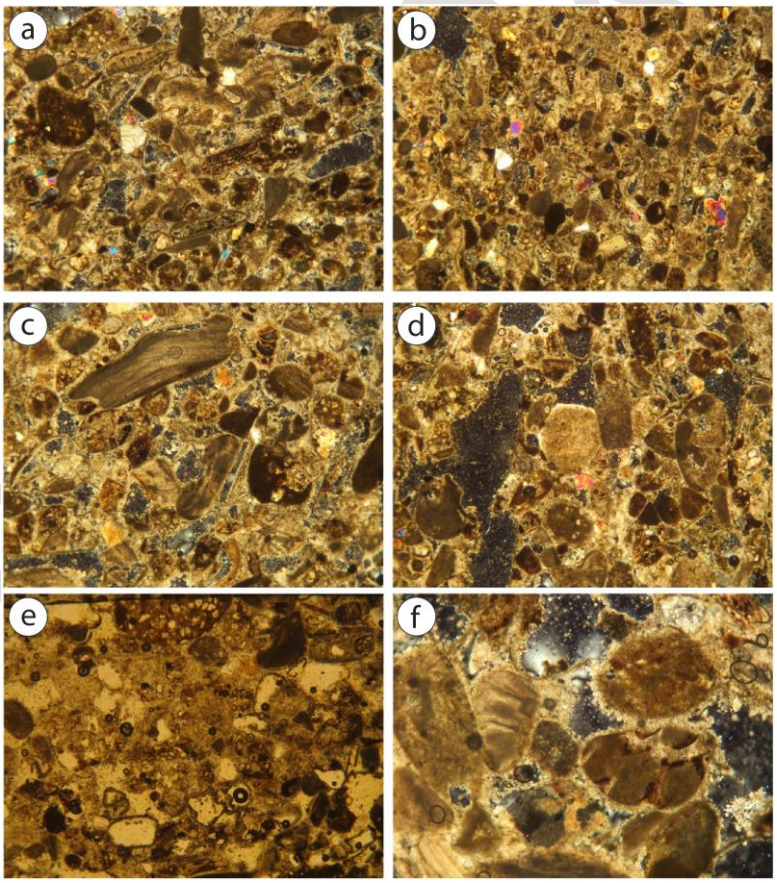


Figure 4-57. Photomicrographs of Sample 24M-1F in XPL (panels a, c, b, d, and f) and PPL (e) at a magnification of 4x.

- Interpretation:

The rock represents deposition in a high-energy shallow marine environment, likely within submarine channels or within the wave and storm influence zone. The abundance of benthic fauna and absence of planktonic fossils suggest a relatively shallow environment. The presence of intrabioclastic grains indicates active reworking and high-energy conditions. Diagenetic features, such as multiple generations of cement and dissolution, reflect complex post-depositional processes.

4.8.1.2 Sample 24M-2F

- Location: 25.3424° N latitude, 60.6227° E longitude.
- Rock type: Carbonate Sedimentary Rock
- Rock name: Limestone
- Microfacies: Poorly Washed Bio-sparite
- Description:

  Sample 24M-2F (Figure 4-58) is a limestone characterized by a poorly washed bio-sparite microfacies. The rock contains abundant allochems, including skeletal fragments of benthic organisms and various intraclasts and extraclasts. The skeletal components are diverse, consisting of:

  - Foraminifera: *Rotalia viennotti*, *Elphidium sp.*, Ammonia sp., Rotalia sp., *Lenticulina sp.*, *Textulariidae*, *Nodosariidae*, *Rotalidae*, *Miliolidae*.
  - Gastropods.
  - Worm tubes: *Kuphus arenarius*.
  - Bryozoans: *Onychocella sp*.
  - Shell fragments: *Ostrea latimarginata* and other bivalves (possibly rudists).
  - Algal fragments: Including red algae (*Lithophyllum sp.*, *Lithothamnium? sp.*).

  Many skeletal grains have undergone dissolution, leaving molds—particularly of bivalves. Intraclasts present in the rock are composed of hybrid sandy limestone to calcareous sandstone facies with a micritic matrix, suggesting erosion from the margins of carbonate basins, transport, and redeposition. The presence of broken skeletal fragments indicates a high-energy depositional environment, likely tidal channels.

  Quartz grains are sporadically distributed throughout the rock, increasing in concentration in some areas. The angular nature of the quartz grains and their random distribution suggest an aeolian origin. The abundance of quartz and clastic grains within the intraclasts varies.

  Extraclasts include clastic rock fragments, especially quartz arenite sandstone fragments. These quartz grains are subrounded to rounded, indicating significant transport and reworking before deposition.

  An erosional boundary is observed at the microscopic scale in the upper part of the sample. Above this boundary, a facies of sandy limestone to bioclastic packstone has been deposited, transitioning upward into a grainstone facies.

GeoNexus

- Age Determination:

  The fossil assemblage, including *Rotalia viennotti*, *Ammonia species*, *Kuphus arenarius*, and red algae, indicates an early Miocene (Aquitanian-Burdigalian) age.

- Interpretation:

  The rock represents deposition in a high-energy shallow marine environment, likely within tidal channels or shoals where strong currents reworked skeletal fragments and intraclasts. The diversity of benthic fauna and the presence of intraclasts suggest active biogenic production and erosion from nearby carbonate platforms. The angular quartz grains imply aeolian input from adjacent land areas. The occurrence of extraclasts with rounded quartz grains indicates prior reworking and long-distance transport, possibly from fluvial sources.

  Diagenetic processes include significant dissolution, particularly of bivalve shells, resulting in moldic porosity. Cementation occurred in two stages: early isopachous fibrous calcite cement around grains and later blocky sparry calcite filling voids left by dissolution.

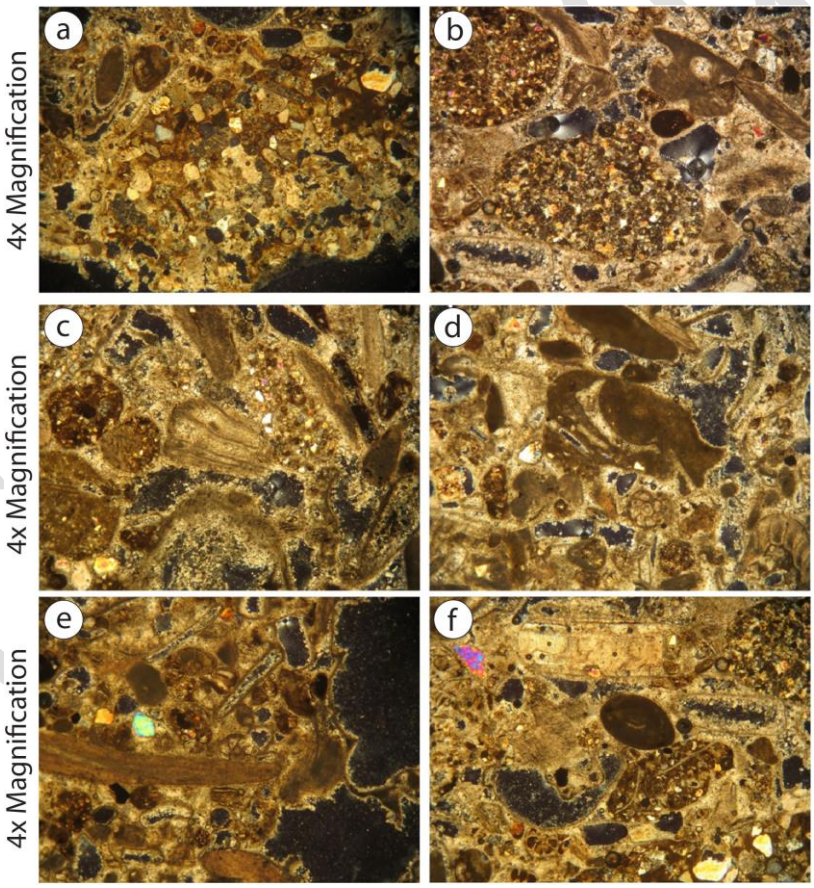


Figure 4-58. Photomicrographs of Sample 24M-2F in XPL at a magnification of 4x.

4.8.1.3 Sample 24M-35F

- Location: 25.3678° N latitude, 60.6173° E longitude.

- Rock type: Clastic Sedimentary Rock
- Rock name: Sandstone
- Microfacies: Sandy Bio-sparite, Ferruginous
- Description:

  Sample 24M-35F (Figure 4-59) is a sandstone classified as litharenite or phyllarenite, exhibiting a sandy bio-sparite microfacies with ferruginous characteristics. The rock is poorly sorted with angular grains, indicating proximity to the source area and rapid deposition. The grain composition includes quartz (15–20%), volcanic lithic fragments, and metamorphic lithic fragments (23–35%). The lithic fragments predominantly consist of gneiss and marble. Sedimentary lithic fragments, such as chert and limestone, are also present. Volcanic lithic fragments are of acidic composition.

  Feldspar is present in very low abundance. Fossils are observed in the sample; however, based on their characteristics, they are likely allochthonous (not originally from the deposition site). Fossils observed in the sample include foraminifera (*Ammonia cf. beccarii*, *Ammonia sp.*, *Rotalia sp*., *Textularia sp*., *Rotalidae*), echinoid fragments, bryozoans with shell and algal debris, and Dasycladacean algae.

  Cementation includes overgrowth of silica around quartz grains and, in some cases, silica filling intergranular spaces. Grain contacts are mainly tangential, with some concavo-convex and occasionally sutured contacts, indicating moderate compaction.

- Age Determination:

  The fossil assemblage, including *Ammonia cf. beccarii* and *Rotalia* species, indicates an early Miocene (Aquitanian-Burdigalian) age.

- Interpretation:

  The angularity and poor sorting of the grains suggest rapid deposition near the source area, likely in a high-relief environment with active erosion. The high content of metamorphic lithic fragments points to erosion from uplifted metamorphic terrains. The presence of acidic volcanic fragments suggests volcanic activity in the source region. Allochthonous fossils imply reworking of older sediments into the depositional environment.

  The ferruginous nature indicates post-depositional iron oxide enrichment, possibly from groundwater percolation. Silica cementation reflects diagenetic processes, possibly from silica-rich fluids during burial.

GeoNexus

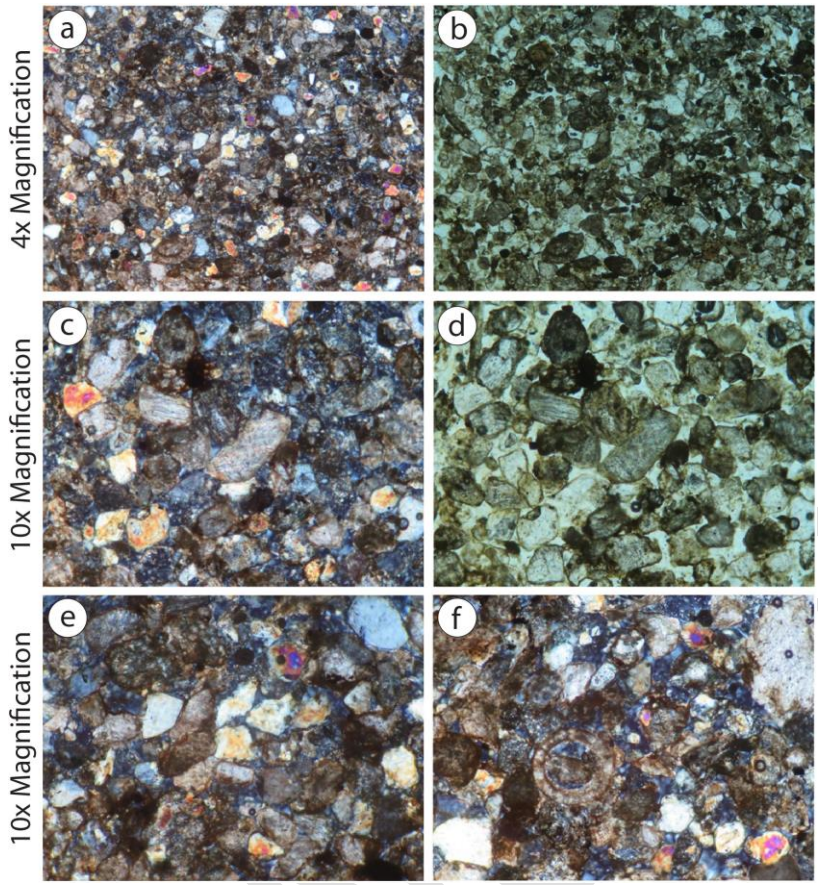


Figure 4-59. Photomicrographs of Sample 24M-35F in XPL (panels a, c, and e) and PPL (panels b, d, and f) at varying magnifications.

4.8.1.4 Sample 24M-36F

- Location: 25.3678° N latitude, 60.6173° E longitude (same as Sample 24M-35F).
- Rock type: Hybrid Clastic–Carbonate Sedimentary Rock
- Rock name: Calcareous Sandstone to Sandy Limestone
- Microfacies: Sandy Bio-sparite (Sandy Limestone)
- Description:

  Sample 24M-36F (Figure 4-60) is a hybrid rock transitioning between calcareous sandstone and sandy limestone, displaying a sandy bio-sparite microfacies. Clastic grains include medium-grained, angular quartz, feldspar, and lithic fragments of igneous and metamorphic origin (possibly marble). Clastic grains include medium-grained, angular quartz, feldspar, and lithic fragments of igneous and metamorphic origin (possibly marble). Grain composition is approximately: quartz (10%), volcanic lithic fragments (25–35%), metamorphic lithic fragments (20–25%), and feldspar (5–10%).

  The skeletal components are diverse, comprising fragments of various bivalves, bryozoans, and benthic foraminifera. The skeletal components include foraminifera (*Rotalia viennotti*, *Dendritina rangi*, *Elphidium sp.*, *Ammonia sp.*, *Rotalia sp.*, *Lenticulina (Robulus) sp.*,

Discorbis sp., *Chapmanina? sp.*, *Nodosariidae*, *Rotalidae*, and *Miliolidae*), bivalves, gastropods, ostracods, Echinoid fragments, bryozoans (*Onychocella sp.*, *Tubucellaria? Sp.*), shell debris (*Ostrea latimarginata*, *Ostrea sp.*), and algal fragments (Red algae). Most skeletal fragments are broken and fragmented, indicating some transport but not extensive. The presence of diverse skeletal components and clastic grains suggests a mixed depositional environment.

- Age Determination:

  The fossil assemblage, including *Rotalia viennotti*, *Dendritina rangi*, and other benthic foraminifera, indicates an early Miocene (Aquitanian-Burdigalian) age.

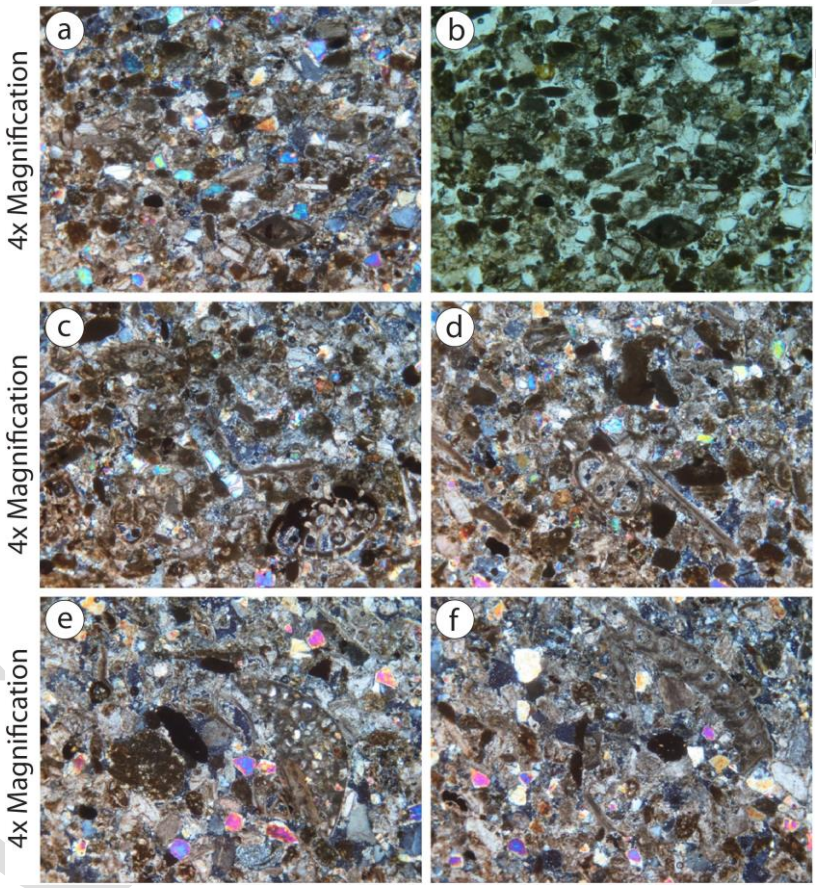


Figure 4-60. Photomicrographs of Sample 24M-36F in XPL (panels a, c, d, e, and f) and PPL (panels b) at a magnification of 4x.

- Interpretation:

  The rock represents deposition in a marine environment where clastic input from nearby terrestrial sources mixed with carbonate sedimentation. The angular quartz grains and feldspar suggest limited transport from the source area. The diverse skeletal components indicate a marine setting with active biogenic production. The broken nature of skeletal fragments implies moderate energy conditions.

The mix of clastic and carbonate materials suggests a nearshore environment influenced by fluvial input or shoreline processes. Diagenetic processes include cementation and minor compaction. The sandy bio-sparite microfacies reflects a sandy limestone with significant biological components, typical of shallow marine environments.

4.8.2 Micropaleontological Analysis

4.8.2.1 Sample 24M-3W

- Location: 25.344074° N latitude, 60.620464° E longitude.
- Description:

  The foraminiferal assemblage in Sample 24M-3W (Figure 4-61) includes both benthic and planktic forms. Benthic forms are *Ammonia beccarii*, *Ammonia beccarii dentata*, *Ammonia beccarii bagnensis*, *Ammonia cf. asanoi*, *Ammonia gaimardi*, *Ammonia indica*, *Ammonia inflata*, *Ammonia schroeteriana*, *Ammonia tochigiensis*, *Ammonia umbonata*, *Cibicides cf. refulgens*, *Elphidium sp.*, *Nonion boueanum*, *Nonion costiferum*, *Nonion scapha*, *Nonionella sp.*, and *Uvigerina multicostata.* Planktic form includes *Globigerinoides immaturus*.

- Age Determination:

  The absence of definitive index planktic foraminifera limits precise age determination. However, the assemblage, particularly the presence of *Ammonia schroeteriana*, *Ammonia tochigiensis*, and *Cibicides cf. refulgens*, suggests that the age is not older than late Miocene. The suggested age range is late Miocene to Pliocene.

- Interpretation:

  The assemblage indicates deposition in a shallow marine environment with normal salinity. Benthic foraminifera suggest inner shelf settings, while the presence of *Globigerinoides immaturus* indicates some open marine influence. The diversity of *Ammonia* species points to warm, temperate waters. The suggested age of late Miocene to Pliocene is slightly older than the unit's defined age of Pliocene to Pleistocene, indicating a potential discrepancy. This inconsistency suggests that the unit may include sediments older than previously recognized or that reworking of older sediments has occurred.

GeoNexus

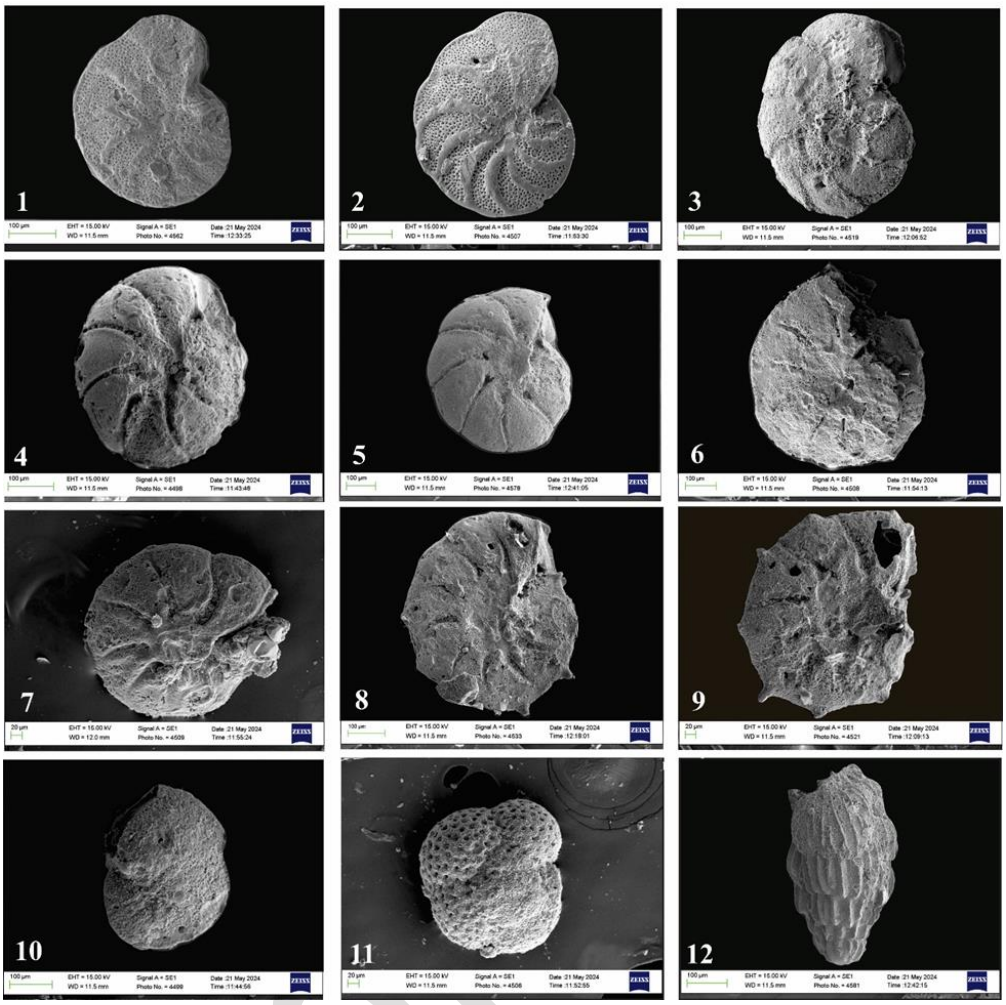


Figure 4-61. SEM images of micropaleontological species of Sample 24M-3W (Plate 1), showcasing their morphological details. 1) *Nonion costiferum*; 2) *Nonion costiferum*; 3) *Ammonia schroeteriana*; 4) *Ammonia sp. cf. A. asanoi*; 5) *Cibicides sp. cf. C. refulgens*; 6) *Ammonia beccarii bagnensis*; 7) *Ammonia beccarii dentata*; 8) *Ammonia beccarii dentata*; 9) *Ammonia beccarii dentata*; 10) *Nonion scapha*; 11) *Globigerinoides immaturus*; 12) *Uvigerina multicostata*.

4.8.3 Age and Correlation

The Pl^{si} Unit is defined as spanning from the Pliocene to Pleistocene. However, the analyses of the samples present discrepancies. Samples 24M-1F, 24M-2F, 24M-35F, and 24M-36F have fossil assemblages indicating an early Miocene (Aquitanian-Burdigalian) age, which is significantly older than the unit's assigned Pliocene to Pleistocene age. Sample 24M-3W suggests an age range of late Miocene to Pliocene, slightly older than the unit's defined age. These discrepancies suggest that the samples may have been collected from older strata within the mapped extent of the Pl^{si} Unit, or there may be complexities in the stratigraphic relationships, such as unconformities, faulting, or folding that have juxtaposed older rocks against younger units, or reworking of older sediments into younger deposits may have occurred. It can also suggest that there may be inaccuracies in field mapping or unit assignments.

4.8.4 Depositional Environment

The lithological and micropaleontological data suggest that the Pl^{si} Unit was deposited in various shallow marine environments influenced by both terrigenous clastic input and marine carbonate production.

- High-Energy Shallow Marine Environments: Samples 24M-1F and 24M-2F represents deposition in tidal channels or shoals, with strong currents reworking skeletal fragments and intraclasts. The abundance of benthic fauna and intraclasts indicates active biogenic production and erosion from nearby carbonate platforms.
- Clastic-Dominated Environments: Samples 24M-35F and 24M-36F show significant clastic input from nearby terrestrial sources, including angular quartz grains, feldspar, and lithic fragments of igneous and metamorphic origin. This suggests deposition near active uplifted terrains undergoing erosion, possibly adjacent to mountainous regions.
- Mixed Clastic–Carbonate Environments: The hybrid nature of some rocks indicates environments where clastic sediments from land mixed with marine carbonates, likely nearshore settings influenced by both marine and fluvial processes.
- Biostratigraphic Indicators: The fossil assemblages support deposition in warm, shallow marine conditions, with influences from both inner shelf and open marine environments. The presence of diverse foraminifera, algae, bryozoans, and other marine organisms reflects a productive ecosystem

Overall, the Pl^{si} Unit records a complex depositional history involving interactions between terrestrial clastic input and marine carbonate sedimentation in shallow marine settings during the Early Miocene to Pleistocene period. The discrepancies in age determinations suggest that the unit may encompass a broader temporal range than previously defined, or that there are stratigraphic complexities that need to be addressed.

4.9 $Pl^{si.c}$ Unit (Pliocene White to Buff Argillic Deposits and Sandy Siltstones)

The $Pl^{si.c}$ Unit is characterized by white to buff, stratified, thick-bedded, almost horizontal argillic loose deposits interbedded with thin gypsum layers. It includes sandy siltstone to microconglomerate with a silty matrix, indicative of deposition in tidal to supratidal zones. This unit forms distinctive landforms locally referred to as the "Martian Mountains." The measured thickness of this unit is ~ 100 m.

The unit is represented by 444 mapped polygons within the study area. The individual areas of these outcrops vary widely, ranging from as small as 0.0041 sq km to as large as 199.87 sq km. Notable large outcrops include OBJECTID_1: 4180 (199.87 sq km), 4002 (128.70 sq km), and 4168 (118.85 sq km). The cumulative area covered by the $Pl^{si.c}$ Unit is ~ 703 sq km.

4.9.1 Lithology

The $Pl^{si.c}$ Unit predominantly consists of:

- Argillic Deposits: White to buff, loosely consolidated clay-rich sediments with stratified, thick bedding and minimal diagenetic alteration.
- Gypsum Layers: Thin interbeds of gypsum (calcium sulfate dihydrate), suggesting periodic evaporitic conditions.
- Sandy Siltstones: Fine-grained clastic rocks composed of silt-sized to fine sand-sized particles.
- Microconglomerates: Coarse-grained clastic rocks containing granule to pebble-sized clasts within a silty matrix.

The argillic deposits exhibit almost horizontal bedding planes, indicating deposition in a relatively stable environment with minimal tectonic disturbance. The thin gypsum layers within the argillic deposits point to episodes of high evaporation rates leading to the precipitation of evaporite minerals.

The sandy siltstones and microconglomerates display varying grain sizes, from fine silt to pebbles, suggesting fluctuations in energy conditions during deposition. The silty matrix within the microconglomerates indicates rapid deposition with poor sorting.

The lithological characteristics suggest that the $Pl^{si.c}$ Unit was deposited in a tidal to supratidal environment during the Pliocene. The presence of argillic deposits and gypsum layers indicates periods of subaerial exposure and evaporation, typical of tidal flats or sabkhas. The sandy siltstones and microconglomerates point to episodic higher energy conditions, possibly due to storm events or seasonal flooding, introducing coarser clastic material into the depositional system.

4.9.2 Structural Features

The $Pl^{si.c}$ Unit exhibits thick, stratified bedding with minimal deformation, indicating deposition in a tectonically stable setting. The almost horizontal bedding planes suggest that the unit has not undergone significant tilting or folding since deposition. No major folds have been documented within this unit, and major fault are also less frequent.

4.9.3 Micropaleontological Analysis

No specific micropaleontological sample data are available for the $Pl^{si.c}$ Unit. Therefore, detailed micropaleontological analysis cannot be conducted at this time.

4.9.4 Age and Correlation

The $Pl^{si.c}$ Unit is assigned a Pliocene age based on its stratigraphic position and regional correlation with similar deposits. The lack of precise micropaleontological data limits the ability to refine the age within the Pliocene.

GeoNexus

4.9.5 Depositional Environment

The sedimentological features of the $Pl^{si.c}$ Unit indicate deposition in tidal to supratidal environments during the Pliocene.

- Tidal Flats and Sabkhas: The argillic deposits with interbedded gypsum layers suggest deposition in tidal flats or coastal sabkha environments, where periodic flooding and evaporation occur.
- Evaporitic Conditions: The presence of gypsum indicates high evaporation rates leading to the precipitation of evaporite minerals, common in arid to semi-arid climates.
- Low to Variable Energy Conditions: The fine-grained argillic deposits reflect low-energy conditions, whereas the sandy siltstones and microconglomerates indicate episodes of increased energy capable of transporting coarser sediments.
- Fluctuating Sea Levels: The alternation between fine-grained sediments and coarser clastic materials may be attributed to changes in sea level or climatic conditions affecting sediment supply and energy levels.

4.10 $Pl^{l.si.s}$ Unit (Pliocene Shale and Volcanosedimentary Sandy Tuff)

The $Pl^{l.si.s}$ Unit is characterized by an alternation of grey to brown shales of moderate bedding thickness and thin beds of volcanosedimentary sandy tuff. Towards the upper part of the sequence, the unit is sealed by sandstone layers. This lithological assemblage reflects a complex interplay between sedimentary and volcanic processes during the Pliocene. The measured thickness of the unit is ~ 100 m.

The unit is represented by 321 mapped polygons within the study area. The individual areas of these outcrops vary significantly, from as small as 0.0657 sq km to as large as 25.50 sq km. Notable large outcrops include OBJECTID_1: 2024 (25.50 sq km), 1747 (25.27 sq km), and 1991 (17.57 sq km). The cumulative area covered by the $Pl^{l.si.s}$ Unit is ~ 254 sq km.

4.10.1 Lithology

The $Pl^{l.si.s}$ Unit predominantly consists of grey to brown shales interbedded with thin layers of sandy tuffs of volcanic origin. The shales exhibit moderate bedding thickness, suggesting relatively consistent depositional conditions over time. These fine-grained sedimentary rocks are indicative of low-energy environments where clay and silt-sized particles settle out of suspension.

The sandy tuff layers represent episodes of volcanic activity, during which pyroclastic materials were deposited within the sedimentary basin. These layers are thin, suggesting that volcanic events were relatively brief or that the influx of volcanic material was limited.

Towards the upper part of the unit, the sequence is sealed by sandstone layers. The sandstones are likely medium to coarse-grained, indicating a shift to higher energy depositional conditions capable

GeoNexus

of transporting and depositing larger sediment particles. This upward transition reflects a significant change in the depositional environment.

The alternation of shales and sandy tuffs suggests a depositional setting influenced by periodic volcanic activity within a predominantly sedimentary basin. The shales indicate quiet, low-energy conditions, possibly in a deep marine or lacustrine environment, while the sandy tuffs reflect volcanic eruptions depositing ash and pyroclastic material.

The presence of sandstone sealing the unit implies a shift to higher energy conditions, such as a regression leading to shallower water depths or an increase in sediment supply from terrestrial sources. This could be due to tectonic uplift, climatic changes, or sea-level fluctuations affecting sedimentation patterns.

4.10.2 Micropaleontological Analysis

No micropaleontological sample data are available for the $Pl^{l.si.s}$ Unit. Therefore, a detailed analysis of microfossil content and precise age determination based on biostratigraphy cannot be conducted at this time.

4.10.3 Age and Correlation

The $Pl^{l.si.s}$ Unit is assigned a Pliocene age based on its stratigraphic position and correlation with regional geological studies, particularly referencing Dolati (2010). The absence of micropaleontological samples limits the ability to refine the age further within the Pliocene. The unit's characteristics are consistent with other Pliocene deposits in the region, supporting this age assignment.

4.10.4 Depositional Environment

The lithological characteristics of the $Pl^{l.si.s}$ Unit indicate a depositional environment that experienced alternating periods of sedimentation and volcanic activity during the Pliocene.

- Low-Energy Aquatic Environment: The grey to brown shales suggest deposition in a calm, low-energy setting such as a deep marine shelf, a quiet deltaic environment, or a lacustrine basin. Fine-grained sediments settled out of suspension over extended periods, forming the shale layers.
- Volcanic Influence: The thin sandy tuff layers represent intermittent volcanic events depositing ash and pyroclastic materials into the basin. This indicates proximity to volcanic sources and suggests that volcanic activity periodically disrupted the sedimentary regime.
- Shift to Higher Energy Conditions: The sandstone layers sealing the unit indicate a transition to higher energy depositional conditions. This could be due to a relative sea-level fall, leading to increased erosion and sediment transport from nearby uplands, or due to tectonic uplift raising the basin floor.

GeoNexus

- Environmental Changes: The vertical succession from shales and tuffs to sandstones reflects environmental changes over time, possibly driven by tectonic movements, climatic shifts, or sea-level fluctuations during the Pliocene.

4.11 $PlPe^{c.s.si}$ Unit (Pliocene to Pleistocene Sediments)

The $PlPe^{c.s.si}$ Unit encompasses a significant assemblage of sedimentary rocks deposited during the Pliocene to Pleistocene. This unit is characterized by a diverse lithology, including red-brown, thick-bedded conglomerates and buff to white, thin-bedded siltstones and silty sandstones. The measured thickness of the unit is approximately 150 m. These sediments reflect dynamic depositional environments influenced by climatic fluctuations, tectonic activities, and sea-level changes during the Pliocene to Pleistocene.

The unit is represented by 861 mapped polygons within the study area. The individual areas of these outcrops vary greatly, from as small as 0.1747 sq km to as large as 97.56 sq km. Notable large outcrops include OBJECTID_1: 10001 (97.56 sq km), 9981 (85.81 sq km), and 9582 (65.12 sq km). The cumulative area covered by the PlPec.s.si unit is ~ 950 sq km.

4.11.1 Lithology

The lithological composition of the $PlPe^{c.s.si}$ Unit is complex, featuring both coarse-grained and fine-grained clastic sediments. The conglomerates are notable for their red-brown color and thick bedding. They consist of approximately 50% clasts, predominantly sandstone, which are well-rounded to weakly rounded. The clasts vary in size and are poorly sorted (bad sorting), indicating rapid deposition likely associated with high-energy environments such as proximal alluvial fans. The matrix of these conglomerates is composed of buff silty sand, contributing to the heterogeneous and polymictic nature of the rock, which suggests multiple source areas and transport paths. These conglomerates are consolidated, reflecting significant lithification processes.

Interbedded with the conglomerates are thin-bedded siltstones and silty sandstones that are buff to white in color. These fine-grained sediments have an argillic texture, indicating a significant clay component, and are generally unconsolidated, suggesting minimal diagenesis. They were likely deposited in lower-energy settings such as floodplains, overbank areas, or distal alluvial environments, where finer sediments could settle.

The unit also includes unconsolidated cyclic alluvial fan deposits with caliche zones. These deposits contain weakly rounded clasts, reflecting limited transport from their source areas. The cyclic nature of these deposits suggests episodic sedimentation events, possibly linked to climatic fluctuations or tectonic uplift, which periodically increased sediment supply. The presence of caliche zones indicates periods of landscape stability and soil formation under arid to semi-arid conditions, pointing to significant climatic influence on sedimentation processes.

Additionally, fine-grained deposits are found trapped in saddle areas near marine shores. These sediments indicate deposition in low-energy environments, potentially influenced by marine processes or protected settings, and may reflect occasional marine incursions due to sea-level changes during the Pliocene to Pleistocene.

GeoNexus

4.11.2 Micropaleontological Analysis

4.11.2.1 Sample 24M-18W

- Location: 26.0291° N latitude, 60.1507° E longitude.
- Description

  The micropaleontological analysis of Sample 24M-18W (Figure 4-62) reveals a diverse assemblage of foraminiferal species. The identified benthic forms include *Cibicides sp.*, *Nonionella sp.*, *Uvigerina sp. cf. U. longa*, *Uvigerina multicostata*, and *Quinqueloculina sp*. The planktic forms identified are *Catapsydrax dissimilis*, *Globigerinoides immaturus*, *Globigerinoides subquadratus*, *Globigerinoides triloba*, *Globorotalia siakensis*, *Paragloborotalia obesa*, and *Praeorbulina sicana*.

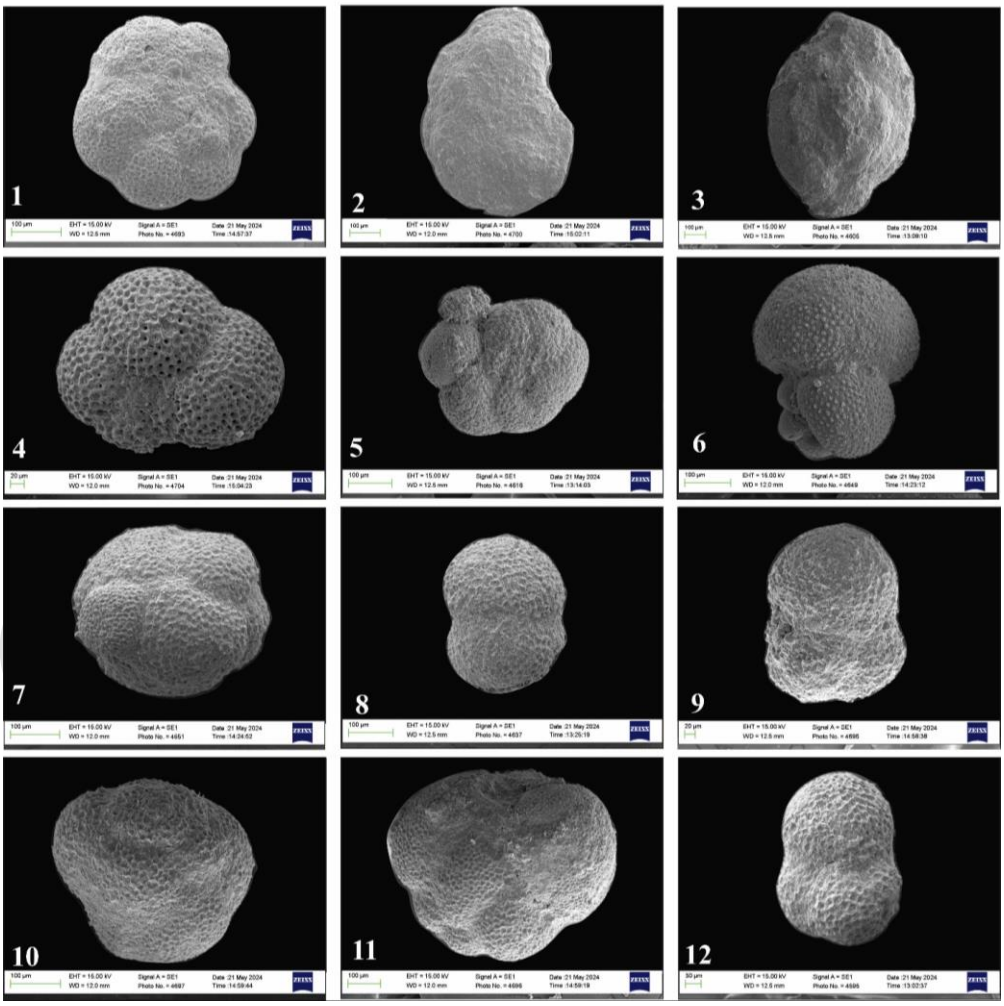


Figure 4-62. SEM images of micropaleontological species of Sample 24M-18W (Plate 7), showcasing their morphological details. 1) *Cibicides sp.*, *Globigerinoides immaturus*; 2) *Cibicides sp.*; 3) *Quinqueloculina sp.*; 4) *Paragloborotalia obesa*; 5) *Globorotalia siakensis*; 6) *Globigerinoides immaturus*; 7) *Catapsydrax dissimilis*; 8) *Globigerinoides immaturus*; 9) *Globigerinoides immaturus*; 10) *Catapsydrax dissimilis*; 11) *Catapsydrax dissimilis*; 12) *Globigerinoides immaturus*.

- Age Determination

  The occurrence of index species such as *Catapsydrax dissimilis* and *Praeorbulina sicana* permits an accurate age determination for the examined sample. Based on the foraminiferal assemblage, the suggested age is early Miocene (late Burdigalian).

- Interpretation

  The early Miocene age determined from the foraminiferal assemblage is not consistent with the Pliocene to Pleistocene age assigned to the PlPec.s.si Unit. This discrepancy suggests that the sample may have been collected from an older formation or that there is reworking of early Miocene sediments within the unit.

4.11.3 Age and Correlation

The $PlPe^{c.s.si}$ Unit is assigned an age ranging from the Pliocene to the Pleistocene based on its stratigraphic position and lithological characteristics. However, the micropaleontological analysis of Sample 24M-18W indicates an early Miocene (late Burdigalian), which is significantly older than the unit's defined age. This inconsistency may be due to:

- Reworking of Older Sediments: Older Miocene sediments could have been eroded and redeposited within the Pliocene to Pleistocene sequences, introducing older microfossils into younger deposits.
- Misidentification of the Unit: The sample may have been collected from a different stratigraphic unit not accurately represented in the map legend.
- Tectonic Activity: Faulting or folding could have juxtaposed older rocks against younger sediments, leading to the inclusion of older material within the unit.

4.11.4 Depositional Environment

The $PlPe^{c.s.si}$ Unit records a complex interplay of depositional processes in environments ranging from high-energy alluvial fans to lower-energy fluvial and coastal settings. The thick-bedded conglomerates with poorly sorted, polymictic clasts suggest deposition by debris flows or high-gradient streams typical of proximal alluvial fans. Cyclic sedimentation patterns indicate repeated episodes of sediment influx, possibly driven by climatic changes or tectonic uplift.

The thin-bedded siltstones and silty sandstones represent deposition in overbank settings or distal alluvial fans where finer sediments could settle. The argillic texture suggests periods of reduced sediment supply or increased weathering, possibly during more humid climatic phases.

Caliche zones within the unit point to periods of landscape stability and soil formation under arid to semi-arid conditions. Fine deposits trapped in saddle areas near marine shores suggest occasional marine influence, indicating fluctuating sea levels during the Pliocene to Pleistocene.

The inconsistency in age determination from the micropaleontological analysis suggests that the unit may include reworked sediments from older formations. This incorporation of older material could be due to erosion of uplifted Miocene strata and redeposition within Pliocene to Pleistocene environments.

GeoNexus

In summary, the $PlPe^{c.s.si}$ Unit reflects dynamic depositional environments influenced by climatic variability, tectonic activity, and sea-level changes during the Pliocene to Pleistocene epochs. The presence of an early Miocene microfaunal assemblage within the unit highlights the complexity of geological processes and the importance of integrating micropaleontological data with lithostratigraphic analysis for accurate geological interpretation.

4.12 Q^a Unit (Late Pleistocene to Holocene Mud Flat Deposits)

The Q^a Unit represents fine-grained sedimentary deposits formed during the late Pleistocene to Holocene, with an absolute age of ≤ 21.3 ka BP (e.g., Gharibreza, 2016). This unit is characterized by buff to creamy argillic silty clay deposits that include clasts ranging from 1 to 3 cm in size and are rich in calcite fragments. These sediments are interpreted as mud flat deposits (Figure 4-63a), indicative of low-energy depositional environments associated with fluctuating water levels and climatic conditions (Figure 4-63b). The measured thickness of this unit is ~ 50 m.

The unit is represented by 1,336 mapped polygons within the study area. The individual areas of these outcrops vary greatly, from as small as 0.0329 sq km to as large as 228.37 sq km. Notable large outcrops include OBJECTID_1: 3326 (228.37 sq km), 2691 (182.88 sq km), and 3567 (84.70 sq km). The cumulative area covered by the Q^a Unit is ~ 1061 sq km.

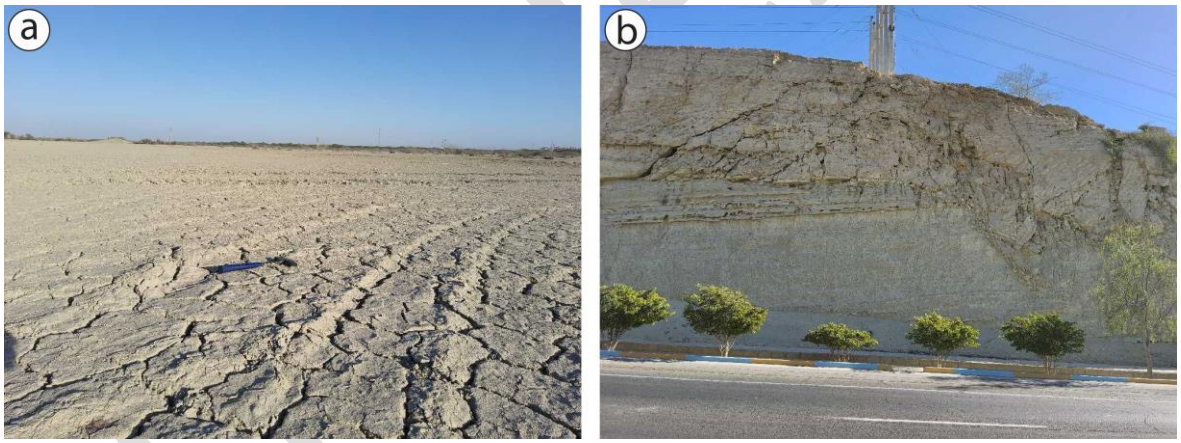


Figure 4-63. a) Mud flat in the Q^a Unit at location P020, illustrating typical cracked, fine-grained sediment surfaces characteristic of low-energy depositional environments. b) Outcrop at location P023, displaying paleorelief with younger terrace deposits at the top. The image also highlights syn-sedimentary faults bounded to the erosional surface.

4.12.1 Lithology

The Q^a Unit exhibits distinctive lithological characteristics dominated by fine-grained sediments. The primary lithology consists of buff to creamy argillic silty clay, indicating a high content of clay minerals and fine silt-sized particles. The argillic nature suggests significant weathering and soil-forming processes. Embedded within the fine-grained matrix are clasts measuring between 1 and 3 cm. These clasts are composed of various lithologies but are notably rich in calcite fragments.

Their presence indicates intermittent higher-energy events capable of transporting coarser material into the predominantly fine-grained environment.

The abundance of calcite fragments points to a source area rich in carbonate rocks or biogenic contributions from organisms that precipitate calcium carbonate. These fragments could also result from the reworking of older carbonate units exposed in the surrounding terrain. The sediments exhibit poor sorting due to the mixture of fine-grained matrix and coarser clasts. The overall texture is indicative of rapid deposition with minimal reworking, characteristic of mud flat environments where energy conditions can vary. The unit has a measured thickness of ~ 50 meters, reflecting substantial sediment accumulation during the late Pleistocene to Holocene.

4.12.2 Age and Correlation

The absolute age of the Q^a Unit is determined to be ≤ 21.3 ka BP (e.g., Gharibreza, 2016), placing it within the late Pleistocene to Holocene transition. This age determination is based on regional correlations and absolute dating methods, such as radiocarbon dating of organic material within the sediments.

The unit correlates with other late Pleistocene to Holocene fine-grained deposits in the region, commonly associated with mud flat environments formed during periods of climatic fluctuation and changing hydrological conditions. The timing corresponds with the last glacial maximum and subsequent deglaciation phases, which influenced sediment supply and depositional patterns.

4.12.3 Depositional Environment

The Q^a Unit is interpreted as representing mud flat depositional environments characterized by low-energy conditions and fine-grained sedimentation. Mud flats typically develop in coastal or lacustrine settings where water movement is minimal, allowing fine particles to settle out of suspension.

Key aspects of the depositional environment include:

- Low-Energy Sedimentation: The dominance of argillic silty clay indicates deposition in a calm environment with limited hydrodynamic energy, allowing fine sediments to accumulate. Such conditions are common in mud flats adjacent to standing bodies of water like lakes or sheltered coastal areas.
- Episodic High-Energy Events: The inclusion of small clasts (1–3 cm) within the fine-grained matrix suggests occasional higher-energy events, such as floods, storms, or seasonal variations, introducing coarser material into the mud flat environment. These events could be linked to climatic fluctuations during the Late Pleistocene to Holocene, including increased precipitation or melting of glacial ice affecting runoff patterns.
- Calcite-Rich Sediments: The richness in calcite fragments implies proximity to carbonate-rich source areas or biogenic activity within the depositional environment. Calcite could precipitate directly from supersaturated waters or be derived from the skeletal remains of organisms inhabiting the mud flats.

GeoNexus

- Pedogenic Processes: The argillic nature of the sediments indicates soil-forming processes, suggesting periods of subaerial exposure. This could result from fluctuations in water levels, with phases of drying allowing for weathering and soil development.
- Climatic Influence: The Late Pleistocene to Holocene was a time of significant climatic change, transitioning from glacial to interglacial conditions. These changes would have influenced sea levels, precipitation patterns, and sediment supply, directly affecting the depositional environment of the Q^a Unit.

4.13 Q^b Unit (Late Holocene Beach Deposits)

The Q^b Unit represents beach deposits formed during the Late Holocene, with an absolute age of ≤ 7.3 ka BP (e.g., Gharibreza, 2016; Normand, 2019). This unit is characterized by rose-gold arkosic sand and silt, featuring wave cross-bedding and caliche formation within the wave zone (Figure 4-64). The calculated thickness of the unit is ~ 50 m, indicating substantial sediment accumulation during this period. These sediments reflect dynamic coastal processes influenced by sea-level fluctuations and climatic conditions in the Holocene.

The unit is represented by 192 mapped polygons within the study area. The individual areas of these outcrops vary greatly, from as small as 0.0691 sq km to as large as 194.02 sq km. Notable large outcrops include OBJECTID_1: 40 (194.02 sq km), 127 (62.56 sq km), and 97 (49.60 sq km). The cumulative area covered by the Q^b Unit is ~ 404 sq km.



Figure 4-64. Beach deposits of the Q^b Unit at location P005.

4.13.1 Lithology

The lithological composition of the Q^b Unit is distinctive, dominated by rose-gold colored arkosic sands and silts. The arkosic nature indicates a high feldspar content, suggesting rapid erosion and minimal chemical weathering of granitic source rocks.

The sediments exhibit several key features. The rose-gold hue is due to the presence of feldspar and iron oxide minerals. The arkosic sands and silts are rich in angular to sub-angular feldspar grains, along with quartz and mica, indicative of a proximal source area and rapid deposition. Wave cross-bedding is prominently observed within the unit. These structures are formed by the migration of ripples and dunes under the influence of oscillatory wave action in a shallow marine environment. The cross-bedding indicates variable current directions and high-energy conditions typical of beach settings.

Caliche layers are developed within the wave zone. Caliche, a hardened deposit of calcium carbonate, forms in arid to semi-arid climates where evaporation rates are high. Its presence suggests periods of subaerial exposure and pedogenic processes occurring within the coastal environment, possibly during low sea-level stands or tidal fluctuations. The sands are medium to coarse-grained, and the silts are fine-grained. The poor sorting and angularity of the grains reflect rapid deposition and limited transport distance from the source rocks. The unit attains a thickness of about 50 m.

4.13.2 Age and Correlation

The absolute age of the Q^b Unit is determined to be less than or equal to 7.3 ka BP (e.g., Gharibreza, 2016; Normand, 2019), placing it within the late Holocene. This age corresponds with a period of significant post-glacial sea-level rise following the last glacial maximum, leading to coastal transgression and the formation of new beach environments.

The unit correlates with other Holocene beach deposits in the region, which are characterized by similar lithologies and sedimentary structures. The arkosic composition and caliche formation are consistent with sediments deposited during periods of rapid sea-level change and climatic fluctuations in arid to semi-arid settings.

4.13.3 Depositional Environment

The Q^b Unit represents deposition in a high-energy coastal environment influenced by wave action, sea-level fluctuations, and climatic conditions during the Late Holocene. The key aspects of the depositional environment include:

- High-Energy Beach Setting: The presence of wave cross-bedding indicates strong wave and current activity typical of beach environments. These conditions facilitate the transportation and deposition of sand and silt-sized particles along the shoreline.
- Proximity to Granitic Source: The arkosic nature of the sediments suggests that the source rocks are granitic and located nearby. The high feldspar content and minimal grain rounding indicate short transport distances and rapid deposition, common in areas where mountains or uplifted terrains are adjacent to the coast.
- Caliche Formation in Wave Zone: The development of caliche within the wave zone implies periods of subaerial exposure, allowing for pedogenic processes. This could be due to fluctuations in sea level, tidal variations, or climatic conditions favoring evaporation over precipitation. The caliche layers reflect episodes of reduced marine influence and increased terrestrial processes within the coastal zone.

GeoNexus

- Climatic Influence: The Late Holocene was a time of climatic variability, with shifts between wetter and drier periods. The arid to semi-arid conditions necessary for caliche formation suggest that evaporation rates were high, impacting sedimentation patterns and diagenetic processes in the beach environment.
- Sea-Level Changes: The age of the unit aligns with known periods of sea-level rise during the Holocene, resulting in the transgression of shorelines. These sea-level changes influenced sediment supply, accommodation space, and the position of depositional environments along the coast.
- Dynamic Coastal Processes: The combination of wave action, sediment supply from proximal sources, and climatic conditions created a dynamic environment where sediments were rapidly deposited, reworked, and occasionally exposed to subaerial conditions, leading to the observed lithological features.

4.14 Q^{fp} Unit (Quaternary Alluvial Fan Deposits)

The Q^{fp} Unit represents Quaternary alluvial fan deposits characterized by an alternation of horizontal white to buff argil and fluvial sediments. With a measured thickness of ~ 50 m, this unit reflects dynamic depositional processes associated with fan environments during the Quaternary period.

The unit is represented by 681 mapped polygons within the study area. The individual areas of these outcrops vary greatly, from as small as 0.0041 sq km to as large as 64.20 sq km. Notable large outcrops include OBJECTID_1: 4426 (64.20 sq km), 8491 (25.97 sq km), and 8503 (19.45 sq km). The cumulative area covered by the Q^{fp} Unit is ~ 385 sq km.

4.14.1 Lithology

The Q^{fp} Unit exhibits a complex lithology composed of both coarse clastic materials and fine-grained sediments. The unit is characterized by an alternation of horizontal layers of white to buff argil (clay-rich material) and fluvial deposits. Individual layers range from 4 to 6 m in thickness, contributing to the overall substantial thickness of the unit.

Clasts constitute 30–50% of the unit and are predominantly composed of sandstone, calcite, volcanic, and silicic pebbles, generally ranging from 2 to 10 cm in size. These clasts are moderately to weakly rounded and exhibit poor sorting, indicating rapid deposition from high-energy processes typical of alluvial fan environments. The heterogeneity and size variation of the clasts suggest a diverse source area, including sedimentary, igneous, and metamorphic rocks.

The clasts are embedded within a silty matrix composed of white to buff argil, reflecting periods of lower energy deposition where finer sediments could settle. The alternation between clastic-rich layers and argil layers indicates fluctuating depositional conditions, possibly due to changes in climate, sediment supply, or tectonic activity influencing the energy levels within the depositional environment.

The tabulate (flat-lying) bedding observed in the unit suggests deposition on a relatively stable surface with minimal post-depositional deformation. The overall poor sorting and moderate to

GeoNexus

weak rounding of the clasts indicate limited transport distance from the source area and rapid deposition, which are characteristic features of proximal alluvial fan deposits.

4.14.2 Age and Correlation

The Q^{fp} Unit is assigned to the Quaternary period based on its stratigraphic position and lithological characteristics. Although specific absolute age determinations are not available for this unit, its features are consistent with Quaternary alluvial fan deposits found in similar geological settings.

The presence of volcanic and silicic pebbles among the clasts suggests a connection to Quaternary volcanic activity in the region. The poor sorting, heterogeneity, and rapid deposition are indicative of depositional processes active during the Quaternary, a period marked by significant climatic fluctuations and tectonic activity that influenced erosion and sedimentation patterns.

Correlation with other Quaternary alluvial fan deposits in adjacent areas supports the assignment of this unit to the Quaternary period. The lack of micropaleontological data limits the precision of age determination, but the geological context provides a reasonable basis for this correlation.

4.14.3 Depositional Environment

The Q^{fp} Unit records sedimentation in an alluvial fan environment characterized by dynamic and high-energy depositional processes. Key aspects of the depositional environment include:

- High-Energy Flows: The moderate to weak rounding of clasts and poor sorting indicate deposition by high-energy flows such as debris flows or flash floods. These processes are capable of transporting a wide range of clast sizes with minimal sorting, typical of alluvial fans at the base of mountainous regions.
- Fluctuating Energy Conditions: The alternation of coarse clastic layers with fine-grained argil layers suggests fluctuations in energy conditions within the depositional environment. During periods of increased water flow or sediment supply, coarser materials were deposited, while quieter periods allowed for the settling of fine-grained argil sediments.
- Source Area Diversity: The clast composition, including sandstone, calcite, volcanic, and silicic pebbles, reflects erosion from a variety of source rocks. This diversity indicates that the alluvial fan was fed by multiple drainages eroding different lithologies, possibly influenced by tectonic uplift and climatic factors enhancing erosion rates.
- Proximity to Source: The limited rounding and poor sorting of the clasts suggest a proximal source area. Sediments were likely transported over short distances from the upland regions to the depositional site, characteristic of alluvial fan systems where steep gradients facilitate rapid sediment delivery.
- Climatic Influence: The Quaternary period experienced significant climatic variability, including glacial and interglacial cycles. These climatic changes would have affected precipitation patterns, vegetation cover, and erosion rates, influencing sediment supply and the frequency of high-energy depositional events in the alluvial fan environment.

GeoNexus

- Tectonic Activity: Regional tectonics may have contributed to the creation of accommodation space for sediment accumulation and influenced the topography driving alluvial fan development. Uplift of source areas would enhance erosion, while subsidence in the depositional area would allow for thicker sediment accumulation.

4.15 Q^{sd} Unit (Holocene Sand Dunes)

The Q^{sd} Unit represents aeolian sand dune deposits (Figure 4-65) formed during the Holocene. These deposits are characterized by golden to light brown wind-blown sands, reflecting dynamic desert environments influenced by climatic conditions prevalent in the Holocene. The unit has a calculated thickness of ~ 50 m, indicating substantial sediment accumulation due to persistent wind activity and sediment supply.

The unit is represented by 72 mapped polygons within the study area. The individual areas of these outcrops vary greatly, from as small as 0.0529 sq km to as large as 19.33 sq km. Notable large outcrops include OBJECTID_1: 10404 (19.33 sq km), 10005 (7.77 sq km), and 10037 (7.45 sq km). The cumulative area covered by the Q^{sd} Unit is ~ 65 sq km.



Figure 4-65. Holocene sand dunes (Q^{sd}) at location P013.

4.15.1 Lithology

The lithology of the Q^{sd} Unit is dominated by unconsolidated, fine to medium-grained sands with a golden to light brown coloration. The sands are primarily composed of quartz grains, with minor contributions from feldspar and heavy minerals. This composition reflects the mineralogy of the source rocks and the effects of mechanical weathering and sorting by wind action.

4.15.2 Age and Correlation

The Q^{sd} Unit is assigned to the Holocene based on its stratigraphic position, depositional characteristics, and correlation with regional aeolian deposits. Sand dune formation is typically associated with arid to semi-arid climatic conditions that prevailed during certain periods of the Holocene.

Although specific absolute age determinations are not available for this unit, its features are consistent with Holocene aeolian deposits found in similar environmental settings. The unit overlies older Quaternary deposits, supporting its assignment to the Holocene. Correlation with nearby well-dated dune fields further substantiates this temporal placement.

4.15.3 Depositional Environment

The Q^{sd} Unit represents an aeolian depositional environment where wind is the primary agent of sediment transport and deposition. Key aspects of the depositional environment include:

- Arid to Semi-Arid Climate: The formation and preservation of sand dunes require dry conditions with limited vegetation cover. During the Holocene, climatic fluctuations led to periods of increased aridity, facilitating the mobilization and accumulation of sand.
- Wind Dynamics: Prevailing wind patterns dictated the transport direction, sorting, and deposition of sand grains. The well-sorted nature of the sands and the development of cross-bedding structures result from consistent wind regimes capable of moving large volumes of sand.
- Dune Morphology: The unit likely comprises various dune types, such as transverse dunes formed by unidirectional winds or barchan dunes shaped under conditions of limited sand supply and a dominant wind direction. The large-scale cross-bedding within the unit reflects the internal structure of these dunes and their migration over time.
- Sediment Source: The sands are derived from the weathering and erosion of nearby rock formations, older alluvial deposits, or exposed lakebeds. The proximity to these sources allows for a continuous supply of sand-sized particles for dune formation.
- Environmental Changes: The initiation and stabilization of dunes are influenced by changes in climate and vegetation. Periods of increased aridity promote dune activity, while wetter conditions lead to vegetation growth that can stabilize dune surfaces and prevent further movement.
- Human Influence: In some regions, human activities such as deforestation or overgrazing can exacerbate dune formation by reducing vegetation cover, though there is no specific evidence of such influences within the Q^{sd} Unit.

4.16 Q^{al} Unit (Holocene Alluvial Deposits)

The Q^{al} Unit represents recent alluvial deposits formed during the Holocene. These unconsolidated sediments have accumulated in river channels, floodplains, and meander belts, reflecting active

fluvial processes that continue to shape the landscape. The unit is characterized by alluvial materials interspersed with fragmented outcrops of older geological units found on terrace risers and occasionally within channels and meanders. The calculated thickness of the unit is ~ 50 m.

The unit is represented by 1031 mapped polygons within the study area. The individual areas of these outcrops vary greatly, from as small as 0.07 sq km to as large as 139.63 sq km. Notable large outcrops include OBJECTID_1: 7766 (139.63 sq km), 7695 (42.84 sq km), and 7730 (28.51 sq km). The cumulative area covered by the Q^{al} Unit is ~ 692.39 sq km.

4.16.1 Lithology

The lithological composition of the Q^{al} Unit is diverse, comprising a mixture of clastic sediments derived from the erosion of upstream rock formations and transported by river systems. The alluvial deposits consist of a heterogeneous mix of clay, silt, sand, gravel, and occasional cobbles. This range of grain sizes reflects the variable energy conditions within the fluvial environment and the diverse geology of the drainage basin.

Embedded within the alluvial sediments are fragments of older geological units. These outcrops appear on the risers of terraces and sometimes within the middle of channels and meanders. They represent remnants of pre-existing formations that have been partially eroded and incorporated into the younger alluvial deposits. The sediments exhibit variable sorting and rounding. Coarser materials like gravel and cobbles are typically sub-angular to sub-rounded, indicating limited transport distance. Fine-grained sediments like silt and clay are well-sorted, having been transported in suspension during lower energy conditions. The sediments display a range of colors from light brown to gray, influenced by the mineral composition and the presence of organic material.

4.16.2 Age and Correlation

The Q^{al} Unit is assigned to the Holocene epoch based on its stratigraphic position, active depositional nature, and lack of consolidation. Alluvial deposits of this kind are characteristic of modern river systems and are continually being reworked and redeposited. The presence of unconsolidated sediments and ongoing fluvial processes supports the assignment of a recent age.

Correlation with other Holocene alluvial deposits in the region confirms the unit's age and depositional environment. The fragmented outcrops of older units within the alluvium indicate active erosion and reworking of pre-existing geological formations, a process consistent with Holocene fluvial dynamics.

4.16.3 Depositional Environment

The Q^{al} Unit represents sedimentation in active fluvial environments, including river channels, floodplains, and meander belts. The depositional environment is characterized by:

- Dynamic Fluvial Processes: The sediments are deposited by rivers and streams through processes such as channel migration, point bar accretion, overbank flooding, and meander formation. These processes lead to the continual reshaping of the river landscape.

GeoNexus

- Variable Energy Conditions: The mixture of grain sizes reflects fluctuating energy levels within the river system. High-energy events like floods can transport and deposit coarser materials, while low-energy conditions favor the deposition of finer sediments.
- Erosion and Deposition Balance: The inclusion of fragmented outcrops of older units signifies active erosion of adjacent or upstream formations. These materials are incorporated into the alluvial deposits, highlighting the balance between erosional and depositional processes in shaping the fluvial environment.
- Floodplain Development: Fine-grained sediments settle on floodplains during periods of overbank flooding. These floodplains are important for soil development and can support diverse ecosystems due to the nutrient-rich sediments.
- Terrace Formation: The presence of terraces with risers indicates changes in river base level, which can result from climatic variations affecting discharge or tectonic activity altering the gradient. These terraces record the historical positions of the river channel.
- Holocene Climatic Influence: During the Holocene, climatic fluctuations influenced precipitation patterns and river discharge, affecting sediment supply and deposition rates. These changes are recorded in the alluvial stratigraphy of the Q^{al} Unit.

GeoNexus

GeoNexus

5 Structural Analyses

This section provides an in-depth analysis of the structural features observed within the mapped area, focusing on the dominant faults and folds that shape the region's geology. The structural framework of the study area reflects the complex tectonic history associated with the Makran accretionary prism and its interactions with the surrounding plates. This chapter discusses the main structural features, including faults and folds, with particular emphasis on their orientation, geometry, and tectonic significance.

In addition to the analysis of faults and folds, structural balanced sections are employed to visualize and interpret the subsurface geometry of these features. These balanced sections, constructed using surface geological data, offer insights into the tectonic evolution of the region and provide a framework for understanding the complex interactions between faults, folds, and stratigraphic units. The balanced sections are a critical tool for reconstructing the deformation history and will be further explored in subsequent sections.

5.1 Folds

The SUTGMM AOI reveals a complex system of folds, including a mix of anticlines and synclines. These folds, developed under compressional tectonic regimes, show varying structural characteristics, such as plunging, overturned, and continuous fold axes. This analysis integrates both the fold map and table, providing a detailed discussion of their distribution, geometry, and tectonic implications.

5.1.1 Anticlines

In the AOI, several prominent anticlines have been identified (Figure 5-1), ranging from simple plunging structures to more complex overturned forms. The varying lengths and orientations of these anticlines reflect a dynamic deformation environment, where different stress regimes and tectonic processes shaped the region.

GeoNexus

5.1.1.1 A001: Plunging Anticline

The A001 fold is a plunging anticline with a total length of ~ 13 km. The fold axis plunges, indicating vertical displacement in addition to horizontal compression. With a bearing of 101°, the fold is fairly linear, as reflected by its sinuosity of 1.0055. The plunging nature suggests the fold may have developed under deeper tectonic forces, such as subsurface warping or crustal bending. The consistent orientation and minimal curvature imply that the A001 fold likely formed under stable compressional conditions, resulting in a well-preserved fold axis.

5.1.1.2 A002: Overturned Anticline

The A002 fold is an overturned anticline, measuring ~ 8.5 km in length. Its fold axis is overturned, meaning one limb has been rotated beyond vertical due to intense tectonic forces. The bearing of the fold is 118°, and its sinuosity of 1.0015 suggests a mostly straight axis with minimal deviation. Overturned anticlines typically form in regions of high tectonic stress, likely near major thrust faults, where compressional forces are strong enough to cause this level of deformation. A002 likely formed in response to significant crustal shortening in the region.

5.1.1.3 A003: Anticline

The A003 fold is a large anticline, spanning ~ 25 km. Its bearing of 290° places it almost perpendicular to other nearby folds, which could indicate different phases of deformation. The fold has a slightly higher sinuosity of 1.0089, suggesting some curvature along its axis. A003 likely formed under regional compressional forces, contributing to its large size and significance as a major structural feature in the area. The minor deviations along the axis may be the result of local faulting or lithological variations.

5.1.1.4 A004: Overturned Anticline

The A004 fold is an overturned anticline with a length of ~ 16.5 km. It trends at 106° and displays a sinuosity of 1.0059, suggesting a mostly linear axis with minor curvature. Like A002, A004 is the result of intense compressional forces that caused one limb of the fold to be overturned. This structure likely formed in a high-strain tectonic environment, possibly near a thrust fault, where the stress regime was strong enough to rotate one side of the fold beyond vertical.

5.1.1.5 A005: Anticline

The A005 fold is an anticline with a total length of ~ 14.5 km. The fold trends at 99° and exhibits a sinuosity of 1.0078, indicating a slightly curved axis. Despite its segmentation, A005 maintains a consistent orientation, suggesting that the folding process was largely uninterrupted by local tectonic complexities. The fold's length and near-linear structure indicate that it formed under steady compressional forces, which allowed for the preservation of its overall geometry.

GeoNexus

5.1.1.6 A006: Plunging Anticline

The A006 fold is a plunging anticline with a total length of ~ 10.5 km. The fold axis plunges, indicating vertical movement as well as horizontal compression. With a bearing of 275°, the fold trends in a westward direction. The sinuosity of 1.0073 suggests a relatively straight fold axis with minor deviations. The plunging nature of A006 points to deeper tectonic influences, potentially linked to subsurface faulting or bending. This fold likely developed as a result of compressional forces acting consistently across a large area, with subsurface warping playing a role in its formation.

5.1.1.7 A007: Symmetrical Anticline

The A007 fold is a symmetrical anticline, extending for ~ 15 km with a bearing of 115°. Symmetrical anticlines have limbs that dip at nearly equal angles, reflecting balanced compressional forces during formation. The fold has a sinuosity of 1.0085, indicating a fairly straight axis with slight curvature. A007 likely formed in a region where compressional forces were evenly distributed, allowing for the creation of this symmetric structure. Its length and straightness suggest a well-preserved fold axis, typical of stable tectonic environments.

5.1.1.8 A008: Symmetrical Anticline

The A008 fold is a small symmetrical anticline with a length of ~ 1.5 km. Its bearing of 85° suggests it trends in an eastward direction. The fold is perfectly straight, with a sinuosity of 1.0000, reflecting no deviation in the fold axis. This symmetry indicates that A008 was formed under balanced tectonic conditions with minimal disturbance. Its small size and perfect symmetry suggest that it formed as part of a localized compressional event, where forces acted uniformly across a short distance.

5.1.1.9 A009: Symmetrical Anticline

The A009 fold is a symmetrical anticline that extends for ~ 7 km. It has a bearing of 114° and a sinuosity of 1.0080, indicating a slightly curved but mostly straight fold axis. The symmetry of the fold implies that it developed under balanced compressional forces, with both limbs dipping at similar angles. A009 is likely part of a broader regional folding event, where consistent tectonic forces created this well-defined anticline.

5.1.1.10 A010: Symmetrical Anticline

The A010 fold is a small symmetrical anticline with a length of ~ 2.3 km. It trends at 173° and has a sinuosity of 1.0000, indicating a perfectly straight axis. Like other symmetrical anticlines, A010 formed in a region where compressional forces were evenly distributed. The fold's short length and straightness suggest it developed as a localized structure, likely in response to uniform tectonic stress.

GeoNexus

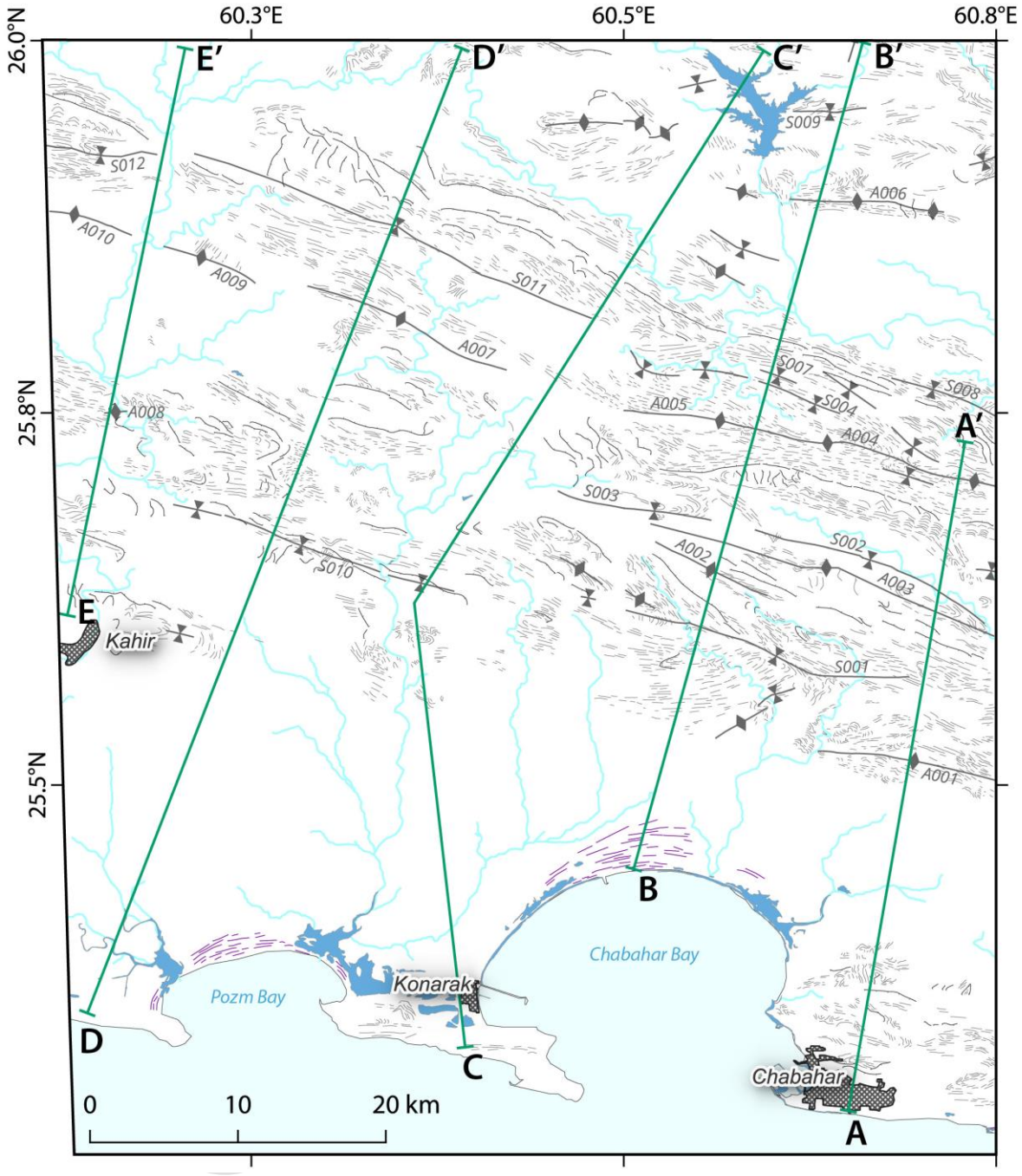


Figure 5-1. Fold map depicting anticlines and synclines within the SUTGMM AOI. The green lines (AA' to EE') represent transect lines used for cross-section construction.

5.1.2 Synclines

Similar to the anticlines, several prominent anticlines have been identified in the AOI, ranging from simple plunging structures to more complex overturned forms. The varying lengths and orientations of these synclines reflect a dynamic deformation environment, where different stress regimes and tectonic processes shaped the region.

5.1.2.1 S001: Plunging Syncline

The S001 fold is a plunging syncline, extending over 20 km with a bearing of 284°. The plunging axis suggests that the fold experienced both vertical displacement and horizontal compression. The fold has a sinuosity of 1.0198, indicating some curvature along its axis. The plunging nature points to deeper tectonic influences, possibly related to subsurface warping or bending. S001 likely formed as part of a regional compressional event, where deeper tectonic forces played a significant role in shaping the fold.

5.1.2.2 S002: Syncline Axis

The S002 syncline stretches for ~ 17.2 km, trending at 114°. Its sinuosity of 1.0160 indicates slight curvature along the fold axis. As a typical syncline, S002 reflects downward flexure in the rock layers, formed due to compressional forces. The curvature of the fold suggests that local tectonic variations, such as nearby faults, may have influenced its development. Despite this, the fold axis remains relatively straight, indicating consistent tectonic forces during formation.

5.1.2.3 S003: Symmetrical Syncline

The S003 fold is a symmetrical syncline with a length of ~ 10.6 km and a bearing of 102°. It exhibits a sinuosity of 1.0062, indicating a mostly straight fold axis with minimal curvature. Symmetrical synclines, like this one, form under balanced compressional forces, where both limbs of the fold dip at equal angles. The straightness and length of S003 suggest it developed as part of a stable tectonic environment with uniform stress distribution.

5.1.2.4 S004: Syncline Axis

The S004 syncline measures ~ 6 km in length, with a bearing of 114°. Its axis is nearly straight, as indicated by a sinuosity of 1.0014. This fold likely formed under consistent compressional forces, with little disruption from local tectonic features. S004 represents a typical syncline, where rock layers are flexed downward as a result of regional tectonic compression.

5.1.2.5 S005: Syncline Axis

The S005 syncline is ~ 3.7 km long and trends at 279°. The fold has a sinuosity of 1.0051, indicating a mostly straight axis with slight curvature. Like other synclines, S005 developed due to compressional forces that caused downward flexure in the rock layers. Its short length and minimal curvature suggest it formed as part of a localized compressional event, where tectonic forces acted uniformly.

5.1.2.6 S006: Syncline Axis

The S006 syncline spans ~ 4.1 km with a bearing of 300°. The fold axis has a sinuosity of 1.1056, indicating some curvature along its length, suggesting that the fold axis is not perfectly straight. This syncline likely formed under localized compressional forces, and the higher sinuosity might be

GeoNexus

the result of minor tectonic disturbances or variations in rock properties during the folding process. Despite the curvature, the overall structure of S006 reflects typical synclinal folding due to compressional forces.

5.1.2.7 S007: Syncline Axis

The S007 syncline is a smaller fold, with a length of ~ 2.6 km. It trends at 292° and has a sinuosity of 1.0004, indicating an almost perfectly straight axis. This straightness suggests that the fold developed under uniform tectonic stress, with minimal disruption or deformation during the folding process. The short length and lack of curvature indicate that S007 likely formed as a local structure in a stable tectonic environment.

5.1.2.8 S008: Overturned Syncline

The S008 fold is an overturned syncline with a total length of more than 16 km. It trends at 111°, and its sinuosity of 1.0085 suggests that the fold axis is relatively straight but exhibits minor curvature. Overturned synclines form when intense compressional forces cause one limb of the fold to rotate beyond vertical. The large size of S008, combined with its overturned structure, suggests that it formed under significant tectonic compression, likely near a major fault system.

5.1.2.9 S009: Overturned Syncline

The S009 fold is another overturned syncline, with a length of ~ 5 km. The fold trends at 87°, and its sinuosity of 1.0079 indicates a relatively straight axis with slight curvature. The overturned nature of this syncline suggests that it formed under intense tectonic forces, where one limb of the fold was rotated beyond vertical. S009 likely developed in a high-strain tectonic environment, where compressional forces were strong enough to cause significant deformation of the rock layers.

5.1.2.10 S010: Symmetrical Syncline

The S010 fold is a symmetrical syncline with a total length of 20 km. The fold trends at 108° 47’ 35.91", indicating a primarily eastward orientation. The fold axis has a sinuosity of 1.0042, reflecting a mostly straight axis with minimal curvature. As a symmetrical syncline, both limbs of the fold dip at similar angles, indicating balanced compressional forces during its formation. The straightness and length of S010 suggest it developed under stable tectonic conditions, making it a well-preserved example of a regional syncline structure.

5.1.2.11 S011: Symmetrical Syncline

The S011 fold is a symmetrical syncline extending for ~ 29.5 km, making it one of the larger folds in the region. It trends at 114°, and its sinuosity of 1.0049 suggests a nearly straight axis with only slight curvature. This symmetry indicates that the fold developed under consistent compressional forces, with both limbs dipping at similar angles. The large size and mostly straight axis of S011

GeoNeXus

imply that it formed as part of a significant regional tectonic event, where widespread compressional forces acted uniformly to create this long, continuous structure.

5.1.2.12 S012: Symmetrical Syncline

The S012 fold is a smaller symmetrical syncline, measuring ~ 7.7 km in length. The fold trends at 275°, indicating a westward orientation. The fold axis has a sinuosity of 1.0190, suggesting a slightly more curved structure compared to other symmetrical synclines in the region. Despite the curvature, the fold maintains its symmetry, with both limbs dipping at equal angles, reflecting balanced tectonic forces. The relatively short length and minor curvature suggest that S012 formed in response to localized compressional stresses, making it a smaller but well-defined syncline.

5.2 Faults

The faults identified and mapped within the SUTGMM AOI (Figure 5-3) illustrate a complex tectonic regime dominated by active deformation. The study area is located in a tectonically active region, which features a complex network of faults including strike-slip, normal, and reverse faults. These faults were mapped and classified as follows: Strike-slip right-lateral, strike-slip left-lateral, reverse faults, and normal faults (Figure 5-3 and Table 5-1). The distribution of faults is spatially varied, with several zones exhibiting higher concentrations of tectonic activity.

5.2.1 Fault Mechanism Classification and Trends

The faults in the AOI are predominantly of strike-slip type, with left-lateral strike-slip being the most prevalent. Normal and reverse faults are also observed but are less frequent. Fault mechanisms are summarized as follows:

- Strike-slip faults (left-lateral and right-lateral) dominate the region, with trends primarily oriented NE-SW and NW-SE. These faults are typically associated with horizontal movement along fault planes.
- Reverse faults exhibit a more N-S or NE-SW orientation and are generally associated with compressional tectonics. These faults are less frequent but are significant in localized areas of the AOI.
- Normal faults are concentrated near the coastal areas, showing a N-S trend. These faults indicate extensional tectonics, which is likely related to the regional crustal thinning or gravitational collapse.

The faults exhibit varying lengths and sinuosity, reflecting the tectonic complexity of the region. Strike-slip faults tend to have longer extents, while reverse and normal faults are generally shorter but more localized.

GeoNexus

5.2.2 Geographic Distribution and Concentration of Faults

The spatial distribution of faults is not uniform across the AOI. Several zones can be defined based on the concentration and orientation of faults, with key faulting trends and mechanisms in each zone:

5.2.2.1 Central Zone

The Central Zone, is characterized by a diverse distribution of normal (Figure 5-2), strike-slip and reverse faults. The most prominent fault in this zone is F001, with a length of ~44 km, representing the longest fault in the AOI. Additional significant faults include F002 (~ 23 km), F021 (~ 22 km), F004 (~ 17 km), and F018 (~ 16 km). The faults in this zone generally trend NW-SE.



Figure 5-2. Normal faulting in the $Pl^{l.si.s}$ Unit at location P061 along Fault F122.

5.2.2.2 Northwestern Zone

The Northwestern Zone features a high concentration of strike-slip faults, particularly left-lateral faults. The dominant fault in this zone is F165 (~ 27 km), followed by F160 (~ 19 km) and F162 (~ 10 km). The main faults in the southwestern parts of this zone predominantly trend NE-SW, consistent with a left-lateral strike-slip mechanism. The northwestern parts are mainly consistent with partially E-W trend of faults accommodating left-lateral component. This zone is tectonically active, with a dense network of strike-slip faults indicating significant horizontal displacement in response to regional shear forces.

5.2.2.3 Northeastern Zone

The Northeastern Zone is characterized by a more complex interplay of faults, with significant contributions from both strike-slip and reverse faulting. The longest faults in this zone include F013, F008, F009, F010, and F014, each of which follows a general NE-SW or N-S trend with an average

length of ~ 10-15 km. This region appears to be influenced by both compressional forces (responsible for reverse faulting) and horizontal shear (strike-slip). The reverse faults in this zone suggest localized compression, which may be related to tectonic collision zones in the broader regional context.

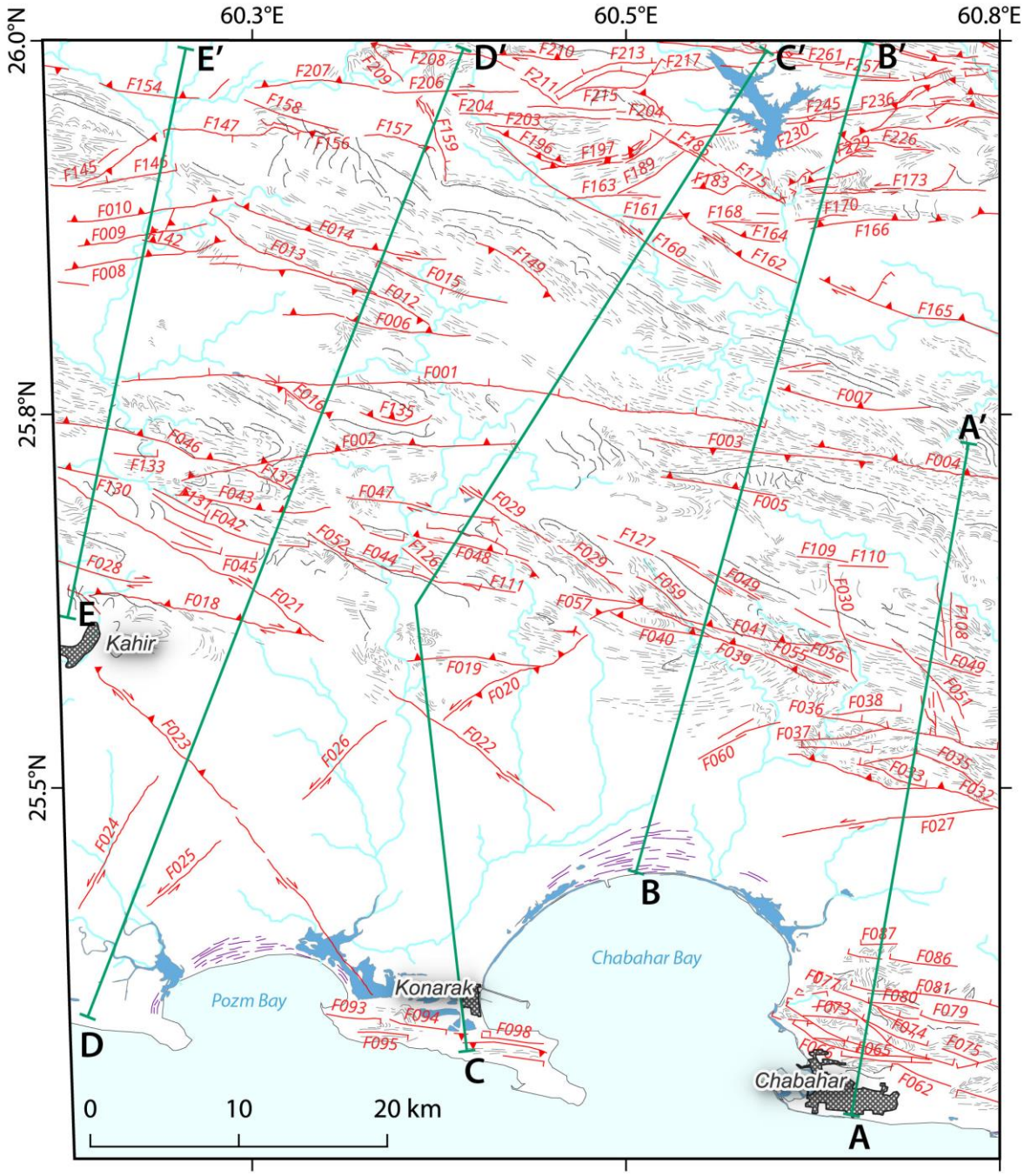


Figure 5-3. Fault map of the SUTGMM AOI. The green lines (AA' to EE') represent transect lines used for cross-section construction.

5.2.2.4 Southwestern Zone

The Southwestern Zone has fewer main faults, but it is still an area of tectonic significance. The largest faults in this region include F023 (~ 30 km), which has two different segments. The NW segment has a reverse mechanism with a right-lateral component, while the SE segment is mainly moving right-laterally. Unlike F0223, the other faults in this zone have a NE-SW trend. F024 (~ 11 km), F025 (~ 7 km), and F026 (~ 8 km) are strike-slip left-lateral faults in this zone. The faults in this zone are primarily strike-slip, with both left-lateral and right-lateral motion observed. This region is influenced by the convergence between tectonic plates, which generates the shear necessary for strike-slip faulting.

5.2.2.5 Southeastern Zone

The Southeastern Zone, which includes areas around Konarak and Chabahar Bay, is characterized by normal and faults with strike-slip component. The faults in this zone generally trend WNW-ESE to E-W, with normal faults dominating the coastal areas. This suggests both extensional and strike-slip tectonic forces, possibly linked to the regional tectonic setting and active margin processes near the coast.

5.2.3 Fault Concentration Zones

Several zones exhibit high concentrations of faults, with particularly intense faulting activity in the Northwestern, Northeastern, and Central zones:

- The Northwestern Zone is densely faulted with a predominance of strike-slip faults, indicating significant lateral tectonic movement.
- The Central Zone has a mix of fault types but shows a clear concentration of normal faults along the coastline, suggesting regional extensional forces.
- The Northeastern Zone is a tectonic transition zone where reverse and strike-slip faults intersect, indicating both compressional and shear forces acting on the region.

The distribution and orientation of faults in the AOI reflect the complex tectonic processes governing the region. The predominance of strike-slip faulting, suggests that the region is experiencing significant horizontal shearing forces, likely related to the larger-scale tectonic interactions between the adjacent plates. The presence of normal faults near the coast suggests local extensional processes, which may be linked to crustal thinning or the gravitational collapse of uplifted regions.

GeoNexus

Table 5-1. Geometrical parameters of some of the faults measured in the field surveys.

Fault Name	Latitude (° N)	Longitude (° E)	Strike (°)	Dip (°)	Rake Strike (°)	Rake Direction (°)	Mechanism
F107	25.765	60.272	260	85	-	-	RRL
F139	25.774	60.263	32	65	-	-	RLN
F016	25.753	60.289	205	74	40	15	RRL
F070	25.342	60.625	5	50	3	114	LL
F172	25.836	60.670	292	60	20	208	NLL
F180	25.894	60.606	250	60	-	-	N
F181	25.895	60.604	178	90	30	30	NLL
F177	25.899	60.600	115	85	10	285	LL
F178	25.898	60.611	320	55	20	228	LL
F179	25.898	60.613	298	70	-	-	N
F222	25.909	60.620	340	35	-	-	LLN
F224	25.911	60.624	310	65	75	320	N
F231	25.928	60.647	152	75	25	258	LLN
F232	25.932	60.649	30	50	37	232	RRL
F265	25.990	60.610	140	60	30	218	NLL
F264	25.989	60.603	140	70	60	85	N
F266	25.999	60.584	160	75	20	70	LLN
F263	25.998	60.579	45	50	45	315	N
F235	25.946	60.626	10	40	45	20	N
F246	25.949	60.621	255	65	-	-	N
F047	25.681	60.407	5	60	27	257	LL
F123	25.678	60.409	340	50	40	42	NRL
F124	25.674	60.414	70	55	45	28	NRL
F122	25.663	60.415	210	50	-	-	NLL
F048	25.655	60.427	20	40	-	-	NLL
F020	25.605	60.466	130	85	-	-	LLR
F142	25.863	60.195	30	40	-	-	R
F143	25.887	60.198	290	73	-	-	RLL
F146	25.914	60.199	185	55	-	-	N
F091	25.375	60.628	120	60	-	-	NLL
F089	25.364	60.614	120	50	-	-	NLL
F088	25.357	60.608	100	75	10	10	LLN
F134	25.629	60.136	40	65	-	-	NRL

GeoNexus

5.3 Structural Balanced Sections

The construction of structural balanced sections in this study was carried out using *Move 2D* software, an advanced structural geology modeling tool, to integrate surface geological data from mapped units, faults, folds, and bedding orientations derived from field surveys and a prepared geological map. This comprehensive approach allowed for the generation of accurate, balanced sections that reflect the complex geological structures of the area. The process included data preparation, setting up the cross-section lines, building the geological model, performing geometric

balancing, and final visualization. Additionally, detailed lithological and mechanical properties were incorporated to refine the model, ensuring that the sections accurately represented both surface and subsurface geology. By employing balanced sections, we ensure that the interpretations are geometrically valid and consistent with physical balancing principles, which is essential for understanding the true nature of the structural framework.

The balanced sections can also serve as a predictive tool for subsurface conditions, providing valuable information for regional tectonic studies, and seismic hazard assessment. By restoring the geological units to their pre-deformation state, we gain insights into the original depositional environments and the subsequent tectonic processes that shaped the region. This restoration not only helps in estimating the amount of crustal shortening but also aids in identifying potential zones of structural weakness, which are crucial for assessing seismic risk in this tectonically active region.

The structural balanced sections on the GeoNexus map cover five key transects (AA', BB', CC', DD', and EE') across the SUTGMM AOI, from the southern coastal areas to the northern limit of the AOI. Each transect captures important structural features such as faults and folds that characterize the Makran accretionary prism. This variability helps us understand the distribution of tectonic stress and the mechanical properties of the sedimentary units.

5.3.1 Data Preparation and Input

5.3.1.1 GeoNexus Map and Mapped Units

The GeoNexus map (SUTGMM) was constructed from extensive field mapping, where lithological boundaries, stratigraphic units, and structural features were identified. Each unit's spatial extent, lithological composition, and surface fault traces were digitized into GIS software and imported into *Move 2D* for structural balanced section construction. The map provided a base layer that helped ensure the geological features in the balanced sections were consistent with field observations.

For each lithological unit (Table 5-2), the geological contacts and unit thicknesses were carefully traced based on the field survey, with additional validation using satellite imagery where available. This base information ensured that each stratigraphic layer in the sections were accurately placed in terms of its spatial extent and thickness.

5.3.1.2 Faults and Fold Geometries

Detailed structural data, including surface fault traces and fold axes, were mapped in the field and digitized for integration into *Move 2D*. This data formed the framework for interpreting subsurface fault geometries and fold structures. Each fault was mapped along its surface expression, and its geometry (e.g., strike, dip and rake) was constrained using field measurements of fault planes, such as fault slickensides or fault breccias, where available. These surface expressions were then projected to depth using fault-bend fold models and *Move 2D*'s structural simulation capabilities. For folds, axial traces and hinge lines were digitized and extrapolated using geometric models to replicate their subsurface geometry.

GeoNexus

5.3.1.3 Bedding Data:

Bedding orientation data (strike and dip) were collected from multiple field stations (Figure 5-4) to guide the placement and orientation of stratigraphic units within the balanced sections. These measurements were essential for determining the true dip of the layers and for simulating folding in areas where deformation had significantly affected the original bedding geometry. Strike and dip data from multiple locations were averaged or interpolated, depending on the complexity of the region, to ensure that bedding planes in the model followed realistic geological patterns.

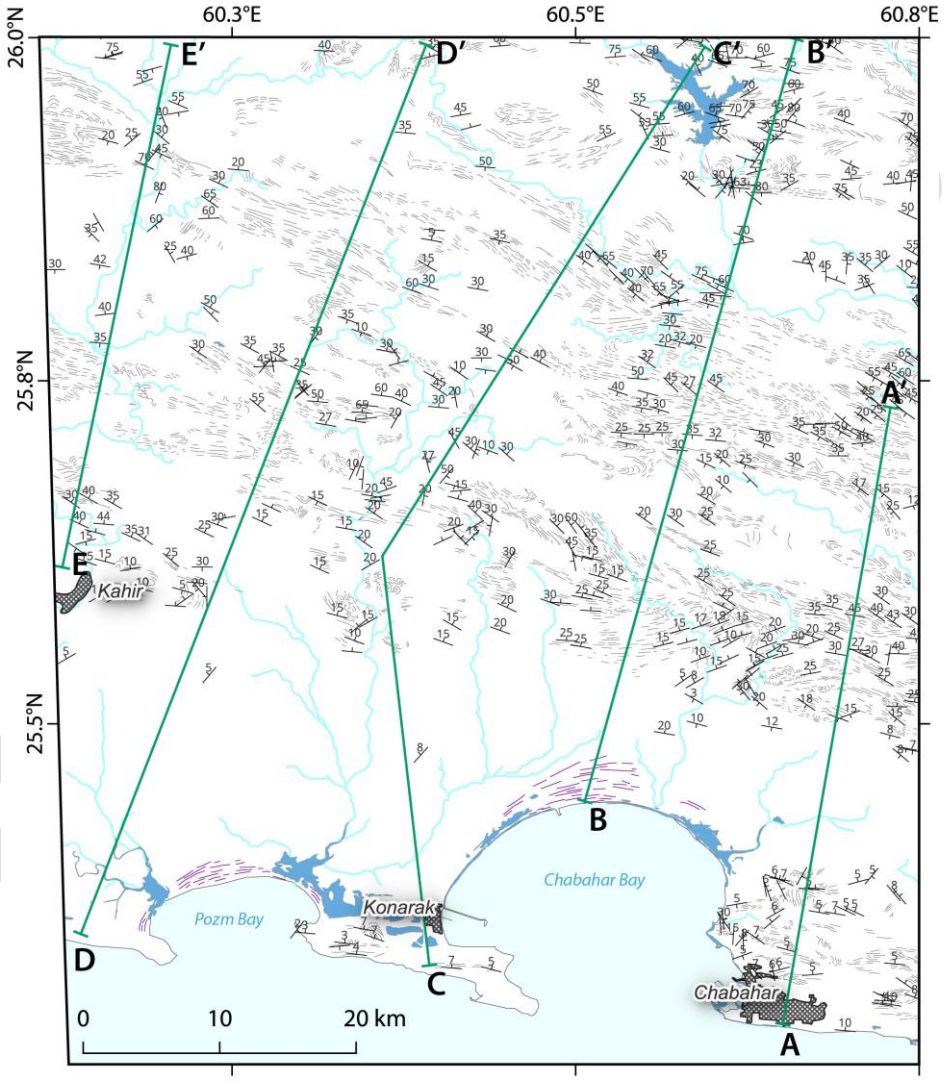


Figure 5-4. Map showing bedding orientations derived from field surveys within the SUTGMM AOI. Bedding dip angles (in degrees) are marked, and the strike symbols indicate the direction of bedding planes. The green lines (AA' to EE') represent transect lines used for balanced sections construction.

5.3.2 Data Integration and Input

To enhance the model's realism, a detailed dataset containing mechanical and lithological properties of the rock units was imported into *Move 2D* (Table 5-3). This dataset provided critical

information on lithology, compaction, porosity, and mechanical behavior, which were used to refine the subsurface model and ensure that the modeled units behaved realistically under tectonic stresses. The following key parameters from the dataset were integrated into the model:

5.3.2.1 Rock Type and Lithological Composition

Each stratigraphic layer was assigned a specific lithological composition, defined in Table 5-3 by percentages of sandstone, shale, and limestone. These percentages were used to represent the relative abundance of each rock type within the model. For example, units with a higher sandstone content were assumed to be more rigid, while those with higher shale content were modeled as more ductile. This lithological variability was critical for simulating fault and fold behavior accurately. The proportions of lithologies influenced the mechanical behavior of each unit under compression and extension, which was essential for constructing realistic deformation features in the sections.

5.3.2.2 Compaction and Porosity

Table 5-3 provides values for Porosity and Depth Coefficient. These parameters were crucial for modeling sedimentary layers, as compaction significantly affects their thickness and mechanical properties with increasing burial depth. In *Move 2D*, these values were used to apply a compaction model that simulated how porosity decreases with depth, causing layers to thin. The porosity data were particularly important for reconstructing sedimentary basins, where variations in compaction control the thickness of stratigraphic units and influence the overall geometry of the cross-section.

5.3.2.3 Mechanical Properties

The Grain Size, Density, Young's Modulus, and Poisson's Ratio columns were input into *Move 2D* to define the mechanical behavior of each lithological unit. Young's Modulus, which measures the stiffness of a material, was especially critical for modeling the elastic response of rocks during deformation. Higher values of Young's Modulus indicated more resistant units, which influenced the way faults propagated through the subsurface. Similarly, Poisson's Ratio, which describes the degree of lateral expansion when a material is compressed, provided insights into how different units would respond to tectonic stresses. These mechanical properties ensured that the simulated geological structures (e.g., faults and folds) reflected the true physical behavior of the units under stress. Units with higher Poisson's Ratios, for instance, were more prone to ductile deformation, influencing fold geometry and fault behavior.

5.3.2.4 Time/Depth Conversion

Table 5-3 included parameters for Time/Depth Conversion, particularly the velocity parameter (V_0), used to convert seismic time data into depth measurements. This conversion was necessary for translating seismic horizons from time-domain interpretations into depth-domain geological cross-sections, providing accurate subsurface depth estimates. The time-depth conversion allowed for the integration of seismic data into the model, aligning the interpreted seismic stratigraphy with the geological cross-section.

GEONEXUS

5.3.3 Setting Up Section Lines

Cross-section lines were carefully placed across the AOI, perpendicular to major geological structures (e.g., faults, folds) to ensure an accurate representation of the subsurface. The cross-section lines were selected based on key outcrop locations and structural features identified during fieldwork. The perpendicular orientation to the regional structural trend was critical for capturing the true geometry of faults and folds, ensuring that any interpreted deformation was consistent with observed surface structures. The cross-section lines also took into account changes in lithology and thickness, ensuring that representative sections of the study area were captured.

5.3.3.1 Profile AA' (Chabahar to Park Bala)

Transect AA' originates in the southern part of the Chabahar sheet, near the southeastern coastal area of Chabahar. The profile extends northward, cutting across the entire Chabahar sheet. As the transect progresses, it crosses into the adjacent Park Bala sheet, extending further into its northeastern corner. The profile's orientation covers a critical range of structural elements from the coastal region of Chabahar up to the more inland and structurally complex terrain of Park Bala, offering key insights into the subsurface tectonic framework (Figure 5-5).

5.3.3.2 Profile BB' (Chabahar to Zirdan)

Transect BB' begins in the northwestern part of the Chabahar sheet, relatively close to the boundary with Konarak. The profile proceeds northward, entering the Park Bala sheet, crossing through its central portion. the profile continues into the Zirdan sheet, where it terminates in the northern region of Zirdan. This transect is strategically designed to capture the structural variations from the southern coastal region up to the northern highlands, covering an extended region of interest that includes important fault systems and tectonic transitions between Chabahar, Park Bala, and Zirdan (Figure 5-5).

5.3.3.3 Profile CC' (Konarak to Zirdan)

Transect CC' originates in the southern part of the Konarak sheet, moving away from the southern coastline. As it extends northward, the profile crosses into the Ab Sard sheet, covering a significant portion of this map sheet. It continues its course into the Zirdan sheet, where it terminates in the northern part of the Zirdan sheet. It captures important structural trends, including fault lines and fold systems that play a crucial role in the subsurface architecture (Figure 5-5).

5.3.3.4 Profile DD' (Gurdim to Kuh-e-kand Koruch)

Transect DD' begins in the southwestern corner of the Gurdim sheet, making its way northward across the region. The profile traverses the Kahir sheet, cutting through its southeastern portion. From Kahir, it proceeds into the northwestern portion of Ab Sard and cuts through central part of the Kuh-e-kand Koruch sheet, and terminates in the northern limit of this sheet. This transect plays a key role in delineating the structural continuity from the southern Gurdim region up to the more rugged terrains of Kuh-e-kand Koruch (Figure 5-5).

GeoNexus

5.3.3.5 Profile EE' (Kahir to Gor)

Transect EE' starts in the wstern part of the Kahir sheet. The profile extends northward, crossing into the northeastern part of the Gor sheet, where it terminates. This transect provides a valuable structural section from the northwester part of Kahir up to the central region of Gor. It covers a broad range of geological features, capturing variations in the stratigraphy and tectonic regimes across this zone (Figure 5-5).

5.3.4 Building the Cross-Section

5.3.4.1 Surface Line Tracing

The surface topography was defined using SRTM 30m (Farr et al., 2007) Digital Elevation Model (DEM), which was imported into *Move 2D*. Alternatively, field observations were used to manually trace the topographic profiles along the cross-section lines. The surface profiles provided the upper boundary for the sections and ensured that geological units matched the topographic constraints of the region.

5.3.4.2 Fault and Horizon Construction

Fault traces and horizon markers (based on lithological unit boundaries) were projected into the sections. Fault planes were extended to depth using structural modeling tools within *Move 2D*, guided by field measurements of fault dip and strike. The integration of mechanical properties from Table 5-3 (e.g., Young's Modulus, density) helped refine the fault geometries, ensuring that more competent units (e.g., sandstone-rich layers) exhibited steeper fault angles, while less competent units (e.g., shale-rich layers) had lower-angle faults. Horizon markers were also constructed based on the mapped stratigraphy, with adjustments made for compaction and porosity changes due to burial depth.

5.3.4.3 Folding Models

Folded strata were modeled using parallel and similar fold geometries, which were extrapolated from field observations. The use of the lithological and mechanical properties (e.g., Poisson's Ratio, grain size; Table 5-3) helped constrain fold geometry by controlling the behavior of different units during folding. For example, thicker or more rigid layers (higher Young's Modulus) resisted deformation and formed broader folds, while more ductile layers (lower Poisson's Ratio) produced tighter folds.

5.3.5 Geometric and Kinematic Balancing

Once the cross-section was constructed, geometric balancing was performed to ensure that the modeled structures (e.g., folds and faults) were geometrically and kinematically consistent. This involved retro-deforming the cross-section to a pre-deformation state using fault-bend fold models. The balancing process verified that the geological structures could have realistically formed from

GeoNexus

an initial, undeformed configuration. The mechanical properties input from Table 5-3, particularly Young's Modulus and Poisson's Ratio, were critical during this step, as they dictated how each unit responded to tectonic forces. Additionally, kinematic restoration was applied to validate the modeled deformation, ensuring that the observed geological structures could evolve from realistic deformation processes.

Table 5-2. Geounits inputparameters for *Move 2D* for structural balanced sections of the SUTGMM project.

Horizon	**Colour**	**Rock Type**	**Age** (Ma)	**Thickness** (m)
Text	Color	Text	Real	Real
#0000FF	#0000CD	#00009B	#000069	#FFFF00
n/a	n/a	n/a	n/a	Metres
dimensionless	dimensionless	dimensionless	dimensionless	dimension
$MPl^{m.s}$	#e9ffbe	Default	5.5	150
$MPl^{m.s.c}$	#e3ff80	Default	5	250
Ml^{w}	#3f36ba	Default	11	10
$M^{s.sh}$	#ffff00	Default	12	200
$M^{s.si}$	#ffffbe	Default	10	200
$M^{sh.s}$	#ffff73	Default	11	200
$OlM^{s.sh.c}$	#ffa77f	Default	13	250
$OlM^{sh.s}$	#ffaa00	Default	15	350
$PlPe^{c.s.si}$	#00ffe4	Default	3	150
$Pl^{l.si.s}$	#e6e600	Default	4	100
Pl^{si}	#f5ca7a	Default	4	100
$Pl^{si.c}$	#ffbebe	Default	4	100
Q^{a}	#eef1a0	Default	1	50
Q^{al}	#ffffff	Default	1	50
Q^{b}	#ffd37f	Default	1	50
Q^{fp}	#ffd9cc	Default	1	50
Q^{sd}	#ffffff	Default	1	50
Water	#66ccff	Default	0	10
vegetation	#ff00ff	Default	0	10

5.3.6 Refining and Validating the Balanced Sections

The balanced sections were iteratively refined by comparing them to both field data and geological interpretations. Adjustments were made to fault angles, fold geometries, and layer thicknesses as necessary. The porosity and compaction data were particularly useful for refining the thickness of sedimentary layers, as burial and compaction can significantly reduce layer thickness over time. The final balanced sections were validated by ensuring that the modeled structures were consistent with surface observations and the regional tectonic framework.

GeoNexus

Table 5-3. Mechanical and lithological input parameters used in *Move 2D* for structural balanced sections of the SUTGMM project.

Name	Name	Elements	Elements	Elements	Compaction	Compaction	Compaction	Time/Depth Conversion	Time/Depth Conversion	Other	Other	Other	Other
Text	Integer	Real	Real	Real	Real	Real	Text	Real	Real	Real	Real	Real	Real
Rock Type	RockPropertyID	Sandstone(%)	Shale(%)	Limestone(%)	Porosity	DepthCoefficient	Compaction Curve	v_0	k	Grain Size	Density	Young Modulus	Poisson Ratio
#00CD00	#009B00	#9B0000	#690000	#00FF00	#FFFF00	#FFCD00	#FF9B00	#FF00FF	#FF00CD	#FF0069	#FFFFFF	#CDFFFF	#9BFFFF
n/a	n/a	Percent	Percent	Percent	Fraction	1/Kilometre	n/a	Metre/Second	n/a	Millimetre	Gram/Cubic Centimetre	Megapascal	n/a
dimensionless	dimensionless	percent	percent	percent	fraction	depth coefficient	dimensionless	velocity	dimensionless	physical size	density	pressure	dimensionless
Sandstone	0	100	0	0	0.49	0.27	Default	3500	0.5	0.375	2500	15000	0.295
Shale	1	0	100	0	0.63	0.52	Default	2500	0.5	0.047	2720	32500	0.3
Limestone	2	0	0	100	0.41	0.4	Default	2600	0.5	0.005	2710	45000	0.215
Default	3				0.56	0.39	Default	2200	0.5	0.211	2680	23750	0.3
ShalySand	4				0.56	0.39	Default	2200	0.5	0.211	2680	23750	0.3
Salt	5				0	0	None	4481	0.5	0	2200	5810	0.4
Chalk	6				0.7	0.71	Default	4481	0.5	0	2200	5810	0.4

GeoNexus

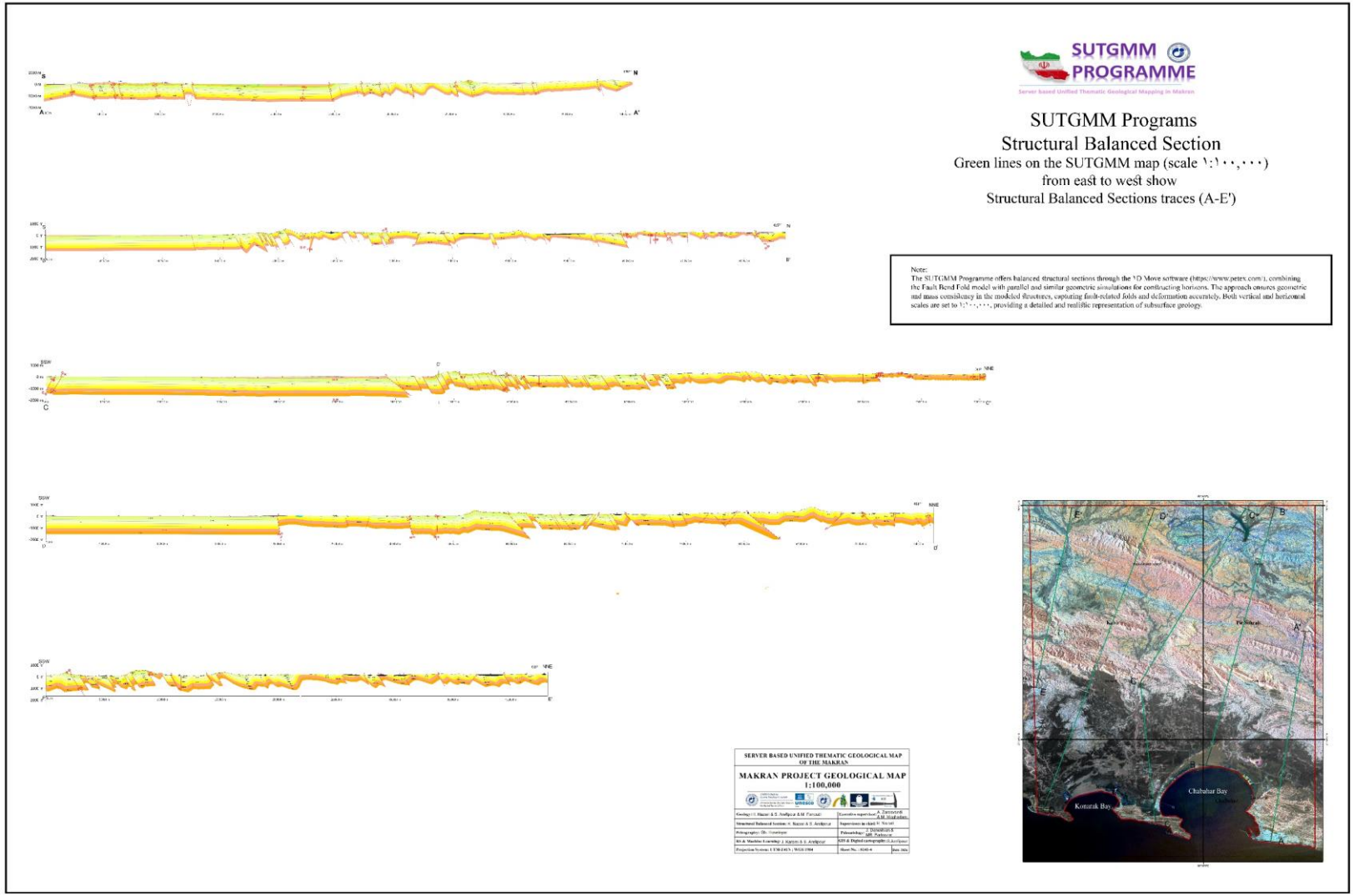


Figure 5-5. AA' to EE' structural balanced sections of the SUTGMM project .

5.3.7 Final Visualization and Output

Once finalized, the balanced sections were exported from *Move 2D* (Figure 5-5) in various formats, including high-resolution images and vector files for further analysis and inclusion in the final GeoNexus maps and the report. The final balanced sections incorporated not only the surface geology but also the detailed mechanical and lithological properties from the data table, ensuring a comprehensive representation of the subsurface geology. These balanced sections provided key insights into the structural complexities of the region, including the relationships between fault geometries, fold structures, and lithological boundaries.

5.4 Mud Volcanoes

Mud volcanoes are formed through the expulsion of mud, water, and gases from depth, often facilitated by tectonic pressures and fluid overpressure within subsurface layers. The mud volcano activity can cause deformation of surrounding and overlying strata, resulting in uplifted zones, fractures, and occasionally large-scale displacement of surface layers. These features can be indicators of subsurface hydrocarbon migration and fluid overpressure zones, as well as evidence of deeper tectonic stresses (Dimitrov, 2002; Kopf, 2002).

Mud volcanoes represent a significant structural feature within the study area, where both active and inactive mud volcanoes were identified and documented, each showing unique structural characteristics that contribute to the broader understanding of deformation patterns and fluid migration pathways.

5.4.1 Inactive Mud Volcano

At location P009, an old, inactive mud volcano was mapped and observed (Figure 5-6). This feature, while no longer actively extruding material, displays significant structural displacement. The old, passive vent of the mud volcano is clearly visible, disrupting the upper horizons and causing noticeable offsets in the stratigraphic layers. This displacement suggests a history of overpressured fluid expulsion, which has since subsided, leaving a preserved structure that now serves as a record of past activity.

The stratigraphic displacement in this inactive mud volcano allows for an assessment of historical tectonic and fluid movement processes within the area. The observed offset within the upper horizons provides clues to the pressures and geological forces that contributed to the mud volcano's formation and eventual inactivity. The structural analysis of this feature aids in understanding the migration pathways of fluids and potential hydrocarbon indicators (e.g., Kopf, 2002) within the study area.

GeoNexus



Figure 5-6. Inactive mud volcano at location P009. The passive vent of the volcano has deformed and displaced the upper stratigraphic horizons.

5.4.2 Active Mud Volcano

An active mud volcano was documented at location P1084 (Figure 5-7). Unlike the inactive volcano (Figure 5-6), this feature shows ongoing activity with fresh mud and gas emissions. Active mud volcanoes are indicative of current subsurface overpressure conditions, where fluids and gases are still being forced upwards. Such activity can reflect ongoing tectonic stress and may highlight zones of weakness within the underlying stratigraphy.

The contrast between the active and inactive mud volcanoes mapped in the SUTGMM project highlights the temporal evolution of these features. By analyzing these mud volcanoes, we gain a better understanding of the tectonic and fluid dynamics at play in this region, as well as the implications for hydrocarbon migration and pressure regimes within subsurface layers.

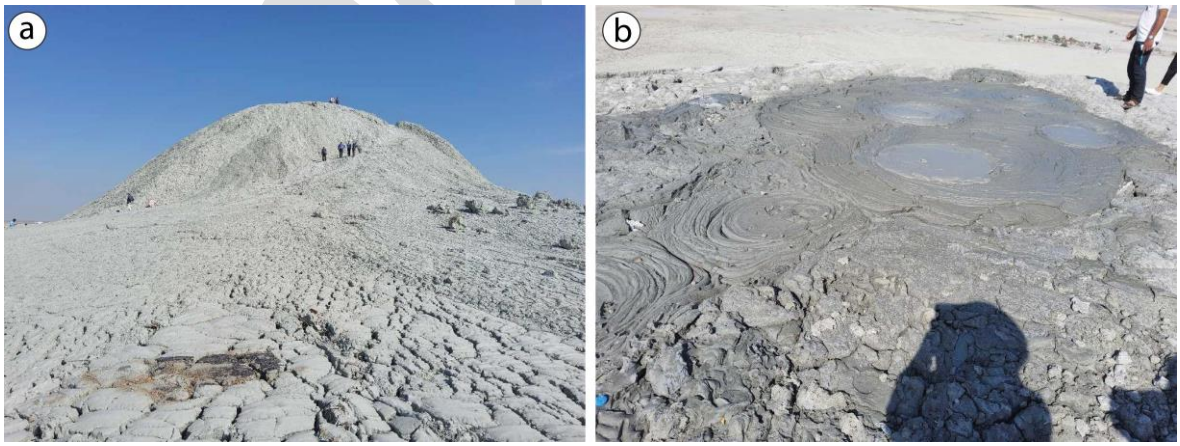


Figure 5-7. Active mud volcano at location P1084. a) The elevated structure with fresh mud channels indicates ongoing fluid and gas emissions, suggesting active subsurface overpressure. b) Close-up of bubbling mud pools on the surface of the active mud volcano, demonstrating current activity and fluid migration from depth.

GeoNexus

6 Summary and Conclusions

6.1 Summary

6.1.1 Integration of Technologies

This project marks a significant leap forward in the field of geological mapping, offering a new standard for accuracy and efficiency through the seamless integration of modern technologies. The combination of cloud computing, machine learning, remote sensing, and object-based image analysis (OBIA) enabled the SUTGMM project to produce high-resolution, reliable geological maps for the Makran region. This technology-driven approach not only enhances the level of detail in the mapping process but also sets the foundation for new methodologies that can be applied to other geologically complex areas globally. The integration of diverse data sources, including Sentinel-1, Sentinel-2, ASTER, Landsat-8, and SRTM DEM, provided a multifaceted view of the region's geological features, allowing for more nuanced and accurate classification.

6.1.2 Methodological Innovation

A major methodological advancement in this project is the shift from traditional pixel-based analysis to the more sophisticated object-based image analysis (OBIA). This transition allowed for better segmentation of the landscape based on the contextual and spatial properties of geological formations, aligning the classification process more closely with the way geologists interpret terrestrial features. The use of multiple datasets spanning various resolutions and spectral ranges provided an in-depth look at the region's geology, leading to a more precise and comprehensive understanding of geological structures and stratigraphy. This innovative workflow significantly reduces both the time and the number of personnel required for large-scale mapping projects.

6.1.3 Computational Efficiency

The project's reliance on *Google Earth Engine* enabled the management and processing of vast volumes of data, overcoming traditional limitations in computational power and accessibility. Cloud computing allowed for the concurrent processing of multi-source remote sensing data, which significantly improved the scalability of the project. This enhanced computational efficiency,

GeoNexus

combined with the use of machine learning algorithms, such as Random Forest (RF), allowed the project to handle complex datasets and execute sophisticated workflows at various spatial scales with ease. This breakthrough demonstrates how cloud-based platforms can streamline and expedite geological mapping projects that traditionally required extensive manual labor and on-site computation.

6.1.4 Accuracy and Reliability

The application of the Random Forest algorithm yielded an accuracy rate of 85%, with a Kappa coefficient of 0.84, demonstrating the robustness of machine learning models in geological classification. These high accuracy levels validate the effectiveness of machine learning approaches in geosciences, especially when combined with field verification techniques. The achieved accuracy further underscores the potential of integrating artificial intelligence (AI) in future geological research, offering a reliable and scalable method for complex geological areas such as the Makran region. This approach can serve as a template for future studies that seek to enhance both the accuracy and efficiency of geological classification processes.

6.1.5 Scalability and Broader Applications

This project acted as a pilot for a new generation of geological mapping methods, providing a blueprint for applying server-based geological mapping to other geologically complex regions across Iran and beyond. The scalability of the SUTGMM workflow demonstrates its potential to revolutionize geological mapping, particularly in regions where traditional methods struggle to capture the intricacies of the terrain. The success in the Makran region showcases the method's adaptability and scalability, offering promising prospects for broader implementation in regional and global geological surveys.

6.1.6 Interdisciplinary Collaboration

The success of this project highlights the importance of interdisciplinary collaboration. Experts from various fields—including geology, remote sensing, computer science, and data engineering—worked together to develop a comprehensive and innovative geological mapping solution. The combination of geological expertise with modern computational techniques demonstrates the transformative power of interdisciplinary efforts. Moving forward, continued collaboration between these disciplines will be critical in refining and expanding the applicability of these methods in geological research and environmental monitoring.

6.1.7 Geological Significance

The detailed geological analysis produced through the SUTGMM project offers a comprehensive understanding of the sedimentary dynamics, stratigraphic sequences, and tectonic features of the Makran region. By documenting and analyzing geological units in great detail, this report contributes to the broader scientific knowledge base of the region. It enhances our understanding of how regional geodynamics have shaped the landscape over millions of years. Furthermore, the

GeoNexus

integration of additional petrological and fossil data will provide a more nuanced interpretation of these processes, supporting future research efforts and resource management decisions.

6.1.8 Optimized GeoNexus Workflow and Protocol

The GeoNexus workflow and protocol (Figure 3-47) developed through the SUTGMM project represent a monumental step forward in cost-effective, large-scale geological mapping. The workflow and protocol demonstrate the transformative potential of combining advanced, modern geospatial technologies, machine learning, and cloud-based computing to streamline the geological mapping process.

One of the most striking achievements of the GeoNexus Protocol is its ability to deliver high-quality geological maps at a fraction of the cost traditionally required for such projects, which results in a cost reduction of nearly 80% and highlights the potential of this approach to transform geological mapping in regions where financial resources are limited.

Furthermore, the time and personnel required for large-scale mapping have been significantly optimized. Traditionally, mapping an area of 30k sq km (scale 1:50,000) would require 15 teams working for 3 years, or alternatively, 1 team working for 15 years. With the GeoNexus workflow, the same task can be completed by 1 team in just 1 year. This dramatic reduction in both time and manpower demonstrates the immense scalability and efficiency of the GeoNexus protocol, making it a viable solution for geological mapping projects of any scale.

6.2 Recommendations

1. Algorithm Development: The methodology developed in this project should be tested in other geologically complex regions to assess its adaptability and robustness. Implementing this standardized workflow in various terrains could lead to a unified approach for geological mapping across diverse geological contexts.
2. Algorithm Refinement: Although the Random Forest algorithm achieved high accuracy, future research should explore other machine learning and deep learning algorithms (e.g., convolutional neural networks) to further enhance accuracy and reliability. Continual refinement of these algorithms is necessary to stay at the forefront of technological advancements in geological mapping.
3. Enhancing Data Resources: Integrating additional types of data—such as hyperspectral images, advanced radar processing, and ground-based spectroscopy—will provide further opportunities for refining geological classifications. These data sources can help improve model performance and enable more detailed interpretations of subsurface structures.
4. User-Friendly Software Development: Developing user-friendly interfaces for this workflow can democratize access to advanced technologies for geologists without extensive programming experience. Such tools will accelerate the adoption of these methods by the broader geological community, especially for non-specialist users.
5. Field Validation: Expanding field implementations to further verify and refine the results will enhance the overall reliability of the generated maps. Ground-truthing remains an

essential step for ensuring that the outputs match real-world geological features, thus improving confidence in the classification system.

6. Collaboration with Geological Institutions: Collaborating with national and international geological organizations will enable the scaling of this methodology to update existing geological maps and implement it on a larger scale. These collaborations will facilitate the exchange of knowledge and resources, fostering advancements in geological research.
7. Environmental Applications: This methodology has the potential for applications beyond geology, including environmental monitoring. The integration of remote sensing data with geospatial analysis can be employed for land-use change detection, vegetation cover analysis, and studying the impacts of climate change on geological formations.
8. 3D Geological Modeling: Future research should investigate the integration of the SUTGMM workflow with 3D geological modeling techniques to produce three-dimensional representations of subsurface geology. This could offer a more comprehensive understanding of geological structures, aiding in exploration and resource management.

6.3 Outlook

In the current phase of the project, sheets Gor, Kahir, and Gurdim are only partially mapped, covering the eastern portions of their frames (Figure 4-2). The SUTGMM project aims to complete these sheets by mapping the missing western areas, thus providing a comprehensive geological framework across the entire study area and achieving a fully integrated set of detailed geological sheets for the region.

6.4 Conclusions

The SUTGMM project represents a significant advancement in geological mapping and analysis, opening new avenues for exploring and understanding complex geological regions. By harnessing the power of modern technologies—such as OBIA, machine learning, and cloud computing—this project not only delivered high-resolution geological maps but also set a precedent for how future geological studies can be conducted with greater accuracy and efficiency. The success of this approach in the GeoNexus/SUTGMM project demonstrates its potential for widespread application, paving the way for more effective geological analyses in regions that were previously difficult to map.

As the methodology continues to evolve through algorithm refinement and field validation, it holds the promise of becoming a cornerstone in the next generation of geological mapping, both in Iran and globally. With these technological advances, geoscientists are better equipped to meet the challenges of modern geological research, enhancing our ability to manage natural resources and mitigate geological hazards.

GeoNexus

GeoNexus

GeoNexus

References

Abrams, M., Hook, S., Ramachandran, B., 2002. ASTER user handbook, version 2. Jet propulsion laboratory 4800, 135.

Alavi, M., 1994. Tectonics of the Zagros orogenic belt of Iran: new data and interpretations. Tectonophysics 229, 211–238.

Alinaghi, A., Koulakov, I., Thybo, H., 2007. Seismic tomographic imaging of P - and S -waves velocity perturbations in the upper mantle beneath Iran. Geophysical Journal International 169, 1089–1102. https://doi.org/10.1111/j.1365-246X.2007.03317.x

Alpaydin, E., 2020. Introduction to machine learning, 4th ed, Adaptive computation and machine learning series. The MIT Press, Cambridge, Massachusetts.

Alvarez, W., Engelder, T., Geiser, P.A., 1978. Classification of solution cleavage in pelagic limestones. Geology 6, 263. https://doi.org/10.1130/0091-7613(1978)6<263:COSCIP>2.0.CO;2

Amani, M., Ghorbanian, A., Ahmadi, S.A., Kakooei, M., Moghimi, A., Mirmazloumi, S.M., Moghaddam, S.H.A., Mahdavi, S., Ghahremanloo, M., Parsian, S., Wu, Q., Brisco, B., 2020. Google Earth Engine Cloud Computing Platform for Remote Sensing Big Data Applications: A Comprehensive Review. IEEE Journal of Selected Topics in Applied Earth Observations and Remote Sensing 13, 5326–5350. https://doi.org/10.1109/JSTARS.2020.3021052

Arthurton, R.S., Farah, A., Ahmed, W., 1982. The Late Cretaceous-Cenozoic history of western Baluchistan Pakistan—the northern margin of the Makran subduction complex. Geological Society, London, Special Publications 10, 373–385. https://doi.org/10.1144/GSL.SP.1982.010.01.25

Aschbacher, J., Milagro-Pérez, M.P., 2012. The European Earth monitoring (GMES) programme: Status and perspectives. Remote Sensing of Environment 120, 3–8. https://doi.org/10.1016/j.rse.2011.08.028

Baatz, M., Schäpe, A., 2000. Multiresolution segmentation: An optimization approach for high quality multi-scale image segmentation. Presented at the Angewandte Geographische Informationsverarbeitung XII, pp. 12–23.

Back, S., Morley, C.K., 2016. Growth faults above shale – Seismic-scale outcrop analogues from the Makran foreland, SW Pakistan. Marine and Petroleum Geology 70, 144–162. https://doi.org/10.1016/j.marpetgeo.2015.11.008

Berberian, F., Muir, I.D., Pankhurst, R.J., Berberian, M., 1982. Late Cretaceous and early Miocene Andean-type plutonic activity in northern Makran and Central Iran. Journal of the Geological Society 139, 605–614. https://doi.org/10.1144/gsjgs.139.5.0605

Berberian, M., King, G.C.P., 1981. Towards a paleogeography and tectonic evolution of Iran. Can. J. Earth Sci. 18, 210–265. https://doi.org/10.1139/e81-019

Bijwaard, H., Spakman, W., Engdahl, E.R., 1998. Closing the gap between regional and global travel time tomography. Journal of Geophysical Research: Solid Earth 103, 30055–30078. https://doi.org/10.1029/98JB02467

Bird, P., Toksöz, M.N., Sleep, N.H., 1975. Thermal and mechanical models of continent-continent convergence zones. J. Geophys. Res. 80, 4405–4416. https://doi.org/10.1029/JB080i032p04405

Blaschke, T., 2010. Object based image analysis for remote sensing. ISPRS Journal of Photogrammetry and Remote Sensing 65, 2–16. https://doi.org/10.1016/j.isprsjprs.2009.06.004

Blaschke, T., Hay, G.J., Kelly, M., Lang, S., Hofmann, P., Addink, E., Queiroz Feitosa, R., Van Der Meer, F., Van Der Werff, H., Van Coillie, F., Tiede, D., 2014. Geographic Object-Based Image Analysis – Towards a new paradigm. ISPRS Journal of Photogrammetry and Remote Sensing 87, 180–191. https://doi.org/10.1016/j.isprsjprs.2013.09.014

Breiman, L., 2001. Random Forests. Machine Learning 45, 5–32. https://doi.org/10.1023/A:1010933404324

Breiman, L., 1996. Bagging predictors. Machine Learning 24, 123–140. https://doi.org/10.1007/BF00058655

Burg, J., Bernoulli, D., Smit, J., Dolati, A., Bahroudi, A., 2008. A giant catastrophic mud-and-debris flow in the Miocene Makran. Terra Nova 20, 188–193. https://doi.org/10.1111/j.1365-3121.2008.00804.x

Burg, J.-P., 2018. Geology of the onshore Makran accretionary wedge: Synthesis and tectonic interpretation. Earth-Science Reviews 185, 1210–1231. https://doi.org/10.1016/j.earscirev.2018.09.011

Bürgmann, R., Rosen, P.A., Fielding, E.J., 2000. Synthetic Aperture Radar Interferometry to Measure Earth's Surface Topography and Its Deformation. Annu. Rev. Earth Planet. Sci. 28, 169–209. https://doi.org/10.1146/annurev.earth.28.1.169

Byrne, D.E., Sykes, L.R., Davis, D.M., 1992. Great thrust earthquakes and aseismic slip along the plate boundary of the Makran Subduction Zone. Journal of Geophysical Research: Solid Earth 97, 449–478. https://doi.org/10.1029/91JB02165

Chandra, U., 1984. Focal mechanism solutions for earthquakes in Iran. Physics of the Earth and Planetary Interiors 34, 9–16. https://doi.org/10.1016/0031-9201(84)90080-3

Cracknell, A.P., Hayes, L., 2007. Introduction to remote sensing, 2nd ed. CRC Press, Boca Raton, Fla.

Crósta, A.P., Moore, J.McM., 1989. Geological mapping using Landsat Thematic Mapper imagery in Almeria Province, south-east Spain. International Journal of Remote Sensing 10, 505–514. https://doi.org/10.1080/01431168908903888

Dahlen, F.A., Suppe, J., Davis, D., 1984. Mechanics of fold-and-thrust belts and accretionary wedges: Cohesive Coulomb Theory. Journal of Geophysical Research: Solid Earth 89, 10087–10101. https://doi.org/10.1029/JB089iB12p10087

DeMets, C., Gordon, R.G., Argus, D.F., 2010. Geologically current plate motions. Geophysical Journal International 181, 1–80. https://doi.org/10.1111/j.1365-246X.2009.04491.x

Dercourt, J., Zonenshain, L.P., Ricou, L.-E., Kazmin, V.G., Le Pichon, X., Knipper, A.L., Grandjacquet, C., Sbortshikov, I.M., Geyssant, J., Lepvrier, C., Pechersky, D.H., Boulin, J., Sibuet, J.-C., Savostin, L.A., Sorokhtin, O., Westphal, M., Bazhenov, M.L., Lauer, J.P., Biju-Duval, B., 1986. Geological evolution of the tethys belt from the atlantic to the pamirs since the LIAS. Tectonophysics 123, 241–315. https://doi.org/10.1016/0040-1951(86)90199-X

Dimitrov, L.I., 2002. Mud volcanoes—the most important pathway for degassing deeply buried sediments. Earth-Science Reviews 59, 49–76. https://doi.org/10.1016/S0012-8252(02)00069-7

Dolati, A., 2010. Stratigraphy, structural geology and low-temperature thermochronology across the Makran accretionary wedge in Iran. ETH Zürich, Switzerland.

GEONEXUS

Dong, J., Liao, M., Xu, Q., Zhang, L., Tang, M., Gong, J., 2018. Detection and displacement characterization of landslides using multi-temporal satellite SAR interferometry: A case study of Danba County in the Dadu River Basin. Engineering Geology 240, 95–109. https://doi.org/10.1016/j.enggeo.2018.04.015

Drăguţ, L., Csillik, O., Eisank, C., Tiede, D., 2014. Automated parameterisation for multi-scale image segmentation on multiple layers. ISPRS Journal of Photogrammetry and Remote Sensing 88, 119–127. https://doi.org/10.1016/j.isprsjprs.2013.11.018

Drury, S.A., 2001. Image interpretation in geology, 3rd ed. Blackwell Science, Malden, MA.

Drusch, M., Del Bello, U., Carlier, S., Colin, O., Fernandez, V., Gascon, F., Hoersch, B., Isola, C., Laberinti, P., Martimort, P., Meygret, A., Spoto, F., Sy, O., Marchese, F., Bargellini, P., 2012. Sentinel-2: ESA's Optical High-Resolution Mission for GMES Operational Services. Remote Sensing of Environment 120, 25–36. https://doi.org/10.1016/j.rse.2011.11.026

Eastman, J.R., 2006. IDRISI Andes: Guide to GIS and Image Processing. Clark Labs, Clark University.

Eftekhar-Nejad, J., McCall, G.J.H., 1993. Explanatory text of the Nikshahr quadrangle Map 1:250000 (No. L 14). Geological survey of Iran.

Ellouz-Zimmermann, N., Deville, E., Müller, C., Lallemant, S., Subhani, A.B., Tabreez, A.R., 2007. Impact of Sedimentation on Convergent Margin Tectonics: Example of the Makran Accretionary Prism (Pakistan), in: Lacombe, O., Roure, F., Lavé, J., Vergés, J. (Eds.), Thrust Belts and Foreland Basins, Frontiers in Earth Sciences. Springer Berlin Heidelberg, Berlin, Heidelberg, pp. 327–350. https://doi.org/10.1007/978-3-540-69426-7_17

Engdahl, E.R., Jackson, J.A., Myers, S.C., Bergman, E.A., Priestley, K., 2006. Relocation and assessment of seismicity in the Iran region. Geophysical Journal International 167, 761–778. https://doi.org/10.1111/j.1365-246X.2006.03127.x

Falcon, N.L., 1974. Southern Iran: Zagros Mountains. Geological Society, London, Special Publications 4, 199–211. https://doi.org/10.1144/GSL.SP.2005.004.01.11

Farhoudi, G., Karig, D.E., 1977. Makran of Iran and Pakistan as an active arc system. Geology 5, 664. https://doi.org/10.1130/0091-7613(1977)5<664:MOIAPA>2.0.CO;2

Farr, T.G., Rosen, P.A., Caro, E., Crippen, R., Duren, R., Hensley, S., Kobrick, M., Paller, M., Rodriguez, E., Roth, L., Seal, D., Shaffer, S., Shimada, J., Umland, J., Werner, M., Oskin, M., Burbank, D., Alsdorf, D., 2007. The Shuttle Radar Topography Mission. Rev. Geophys. 45, RG2004. https://doi.org/10.1029/2005RG000183

Fathian, A., 2022. Active tectonics of the Zagros front (PhD thesis). RWTH Aachen University, Aachen, Germany.

Ferretti, A., Monti-Guarnieri, A., Prati, C., Rocca, F., Massonet, D., 2007. InSAR Principles - Guidelines for SAR Interferometry Processing and Interpretation. ESA Training Manual 19.

Fisher, R.V., 1961. PROPOSED CLASSIFICATION OF VOLCANICLASTIC SEDIMENTS AND ROCKS. Geological Society of America Bulletin 72, 1409. https://doi.org/10.1130/0016-7606(1961)72[1409:PCOVSA]2.0.CO;2

GEBCO Compilation Group, 2023. GEBCO 2023 Global Bathymetry and Topography. https://doi.org/10.5069/G9D21VTT

Geological Survey of Iran, 1993. Geological quadrangle map of Iran, No. M14, Pishin. Scale: 1:250,000.

Geological Survey of Iran, 1989. Geological quadrangle map of Iran, No. L14, Nikshahr. Scale 1:250,000.

Gharibreza, M., 2016. Evolutionary trend of paleoshorelines in the Coastal Makran zone (southeast Iran) since the mid-Holocene. Quaternary International 392, 203–212. https://doi.org/10.1016/j.quaint.2015.06.030

Gillespie, A.R., Kahle, A.B., Walker, R.E., 1986. Color enhancement of highly correlated images. I. Decorrelation and HSI contrast stretches. Remote Sensing of Environment 20, 209–235. https://doi.org/10.1016/0034-4257(86)90044-1

Goetz, A.F.H., Rock, B.N., Rowan, L.C., 1983. Remote sensing for exploration; an overview. Economic Geology 78, 573–590. https://doi.org/10.2113/gsecongeo.78.4.573

Gorelick, N., Hancher, M., Dixon, M., Ilyushchenko, S., Thau, D., Moore, R., 2017. Google Earth Engine: Planetary-scale geospatial analysis for everyone. Remote Sensing of Environment 202, 18–27. https://doi.org/10.1016/j.rse.2017.06.031

Goward, S.N., Masek, J.G., Williams, D.L., Irons, J.R., Thompson, R.J., 2001. The Landsat 7 mission. Remote Sensing of Environment 78, 3–12. https://doi.org/10.1016/S0034-4257(01)00262-0

Grando, G., McClay, K., 2007. Morphotectonics domains and structural styles in the Makran accretionary prism, offshore Iran. Sedimentary Geology 196, 157–179. https://doi.org/10.1016/j.sedgeo.2006.05.030

Green, P.F., Duddy, I.R., Gleadow, A.J.W., Lovering, J.F., 1989. Apatite Fission-Track Analysis as a Paleotemperature Indicator for Hydrocarbon Exploration, in: Naeser, N.D., McCulloh, T.H. (Eds.), Thermal History of Sedimentary Basins. Springer New York, New York, NY, pp. 181–195. https://doi.org/10.1007/978-1-4612-3492-0_11

Hafkenscheid, E., Wortel, M.J.R., Spakman, W., 2006. Subduction history of the Tethyan region derived from seismic tomography and tectonic reconstructions. Journal of Geophysical Research: Solid Earth 111. https://doi.org/10.1029/2005JB003791

Haghipour, N., Burg, J.-P., 2014. Geomorphological analysis of the drainage system on the growing Makran accretionary wedge. Geomorphology 209, 111–132. https://doi.org/10.1016/j.geomorph.2013.11.030

Harms, J.C., Cappel, H.N., Francis, D.C., 1984. The Makran coast of Pakistan: its stratigraphy and hydrocarbon potential. Marine geology and oceanography of Arabian Sea and coastal Pakistan 3.

Hatzfeld, D., Molnar, P., 2010. Comparisons of the kinematics and deep structures of the Zagros and Himalaya and of the Iranian and Tibetan plateaus and geodynamic implications. Reviews of Geophysics 48, RG2005. https://doi.org/10.1029/2009RG000304

Heidarzadeh, M., Pirooz, M.D., Zaker, N.H., Yalciner, A.C., Mokhtari, M., Esmaeily, A., 2008. Historical tsunami in the Makran subduction zone off the southern coasts of Iran and Pakistan and results of numerical modeling. Ocean Engineering 35, 774–786. https://doi.org/10.1016/j.oceaneng.2008.01.017

Irons, J.R., Dwyer, J.L., Barsi, J.A., 2012. The next Landsat satellite: The Landsat Data Continuity Mission. Remote Sensing of Environment 122, 11–21. https://doi.org/10.1016/j.rse.2011.08.026

Jackson, J., McKenzie, D., 1984. Active tectonics of the Alpine-Himalayan Belt between western Turkey and Pakistan. Geophysical Journal International 77, 185–264. https://doi.org/10.1111/j.1365-246X.1984.tb01931.x

Jacob, K.H., Quitmeyer, R., Farah, A., DeJong, K.A., 1979. The Makran region of Pakistan and Iran: trench-arc system with active plate subduction. Quittmeyer, Richard Charles 73.

Jamison, W.R., 1987. Geometric analysis of fold development in overthrust terranes. Journal of Structural Geology 9, 207–219. https://doi.org/10.1016/0191-8141(87)90026-5

Jensen, J.R., 2016. Introductory digital image processing: a remote sensing perspective, 4th ed, Pearson series in geographic information science. Pearson Education, Glenview, Ill.

Jolliffe, I.T., 2004. Principal component analysis, 2nd ed, Springer series in statistics. Springer, New York Berlin Heidelberg.

Jordan, M.I., Mitchell, T.M., 2015. Machine learning: Trends, perspectives, and prospects. Science 349, 255–260. https://doi.org/10.1126/science.aaa8415

Kaveh-Firouz, A., Mohammadi, A., Görüm, T., Sarıkaya, M.A., Alizadeh, H., Akbaş, A., Mirarabi, A., 2023. Main drivers of drainage pattern development in onshore Makran Accretionary

GEONEXUS

Wedge, SE Iran. International Journal of Earth Sciences 112, 539–559. https://doi.org/10.1007/s00531-022-02270-6

Kelleher, J.D., Tierney, B., 2018. Data science, The MIT Press essential knowledge series. The MIT Press, Cambridge, Massachusetts.

Kent, R.G., 1953. Old Persian: Grammar, Texts, Lexicon. American Oriental Society, New Haven.

Khan, M.A., Raza, H.A., Alam, S., 1991. Petroleum geology of the Makran region: implications for hydrocarbon occurrence in cool basins. Journal of Petroleum Geology 14, 5–18. https://doi.org/10.1111/j.1747-5457.1991.tb00295.x

Khorrami, F., Vernant, P., Masson, F., Nilfouroushan, F., Mousavi, Z., Nankali, H., Saadat, S.A., Walpersdorf, A., Hosseini, S., Tavakoli, P., Aghamohammadi, A., Alijanzade, M., 2019. An up-to-date crustal deformation map of Iran using integrated campaign-mode and permanent GPS velocities. Geophysical Journal International 217, 832–843. https://doi.org/10.1093/gji/ggz045

Kopf, A.J., 2002. SIGNIFICANCE OF MUD VOLCANISM. Reviews of Geophysics 40. https://doi.org/10.1029/2000RG000093

Kopp, C., Fruehn, J., Flueh, E.R., Reichert, C., Kukowski, N., Bialas, J., Klaeschen, D., 2000. Structure of the Makran subduction zone from wide-angle and reflection seismic data. Tectonophysics 329, 171–191. https://doi.org/10.1016/S0040-1951(00)00195-5

Kukowski, N., Lallemand, S.E., Malavieille, J., Gutscher, M.-A., Reston, T.J., 2002. Mechanical decoupling and basal duplex formation observed in sandbox experiments with application to the Western Mediterranean Ridge accretionary complex. Marine Geology 186, 29–42. https://doi.org/10.1016/S0025-3227(02)00171-8

Lambeck, K., 1996. Shoreline reconstructions for the Persian Gulf since the last glacial maximum. Earth and Planetary Science Letters 142, 43–57. https://doi.org/10.1016/0012-821X(96)00069-6

Liaw, A., Wiener, M., 2002. Classification and regression by randomForest. R news 2/3.

Lillesand, T.M., Kiefer, R.W., Chipman, J.W., 2015. Remote sensing and image interpretation, 7th ed. John Wiley & Sons, Inc, Hoboken, N.J.

Lu, D., Weng, Q., 2007. A survey of image classification methods and techniques for improving classification performance. International Journal of Remote Sensing 28, 823–870. https://doi.org/10.1080/01431160600746456

Mayrhofer, M., 1978. Handbuch des Altpersischen. Wiesbaden: Harrassowitz.

McCall, G.J.H., 1985. Area report, East Iran Project-Area No: 1 (North Makran & South Baluchestan) (No. Report No.57). Geological Survey of Iran, Tehran.

McCall, G.J.H., 1983. Mélanges of the Makran, southeastern Iran. Hutchinson Ross Publishing Company, Ophiolitic and related mélanges 66, 292–299.

McCall, G.J.H., Kidd, R.G.W., 1982. The Makran, Southeastern Iran: the anatomy of a convergent plate margin active from Cretaceous to Present. Geological Society, London, Special Publications 10, 387–397. https://doi.org/10.1144/GSL.SP.1982.010.01.26

McClay, K.R., 1992. Thrust tectonics. Champan & Hall, London New York Tokyo [etc.].

Molnar, P., Stock, J.M., 2009. Slowing of India's convergence with Eurasia since 20 Ma and its implications for Tibetan mantle dynamics. Tectonics 28, 2008TC002271. https://doi.org/10.1029/2008TC002271

NASA, 2016. Landsat 7 Science Data Users Handbook. NASA's Goddard Space Flight Center.

Nazari, H., 2024. The Server based unified thematic Geological mapping,. Presented at the GEOKURDISTAN VI, 5-7 November 2024, Sulaimani, Kurdistan Region, Iraq.

Nazari, H., Karami, J., Arefipour, S., 2024a. SUTGM PROGRAMME: A New Protocol for Server-Based Unified Thematic Geological Mapping (GeoNexus), UCCGHA 027. UNESCO Chair on Coastal Geo-Hazards Analysis.

Nazari, H., Karami, J., Arefipour, S., 2024b. Geological Mapping in the Era of AI: Leveraging Innovation for Precision and Speed. Presented at the Mediterranean Geoscience Union (MedGU), 25-28 Nov. 2024, Barcelona, Spain.

Nazari, H., Karami, J., Arefipour, S., 2023a. The Server based unified thematic Geological mapping in cloud computing, approach: Deep Machin Learning. Presented at the Regional symposium on Geospatial Information Exchange and Research (GIER), 07-08 March, Muscat, Oman.

Nazari, H., Karami, J., Arefipour, S., 2022. The Server based unified thematic Geological mapping in cloud computing,. Presented at the AAPG Europe Regional Conference: Revitalizing Old Fields and Energy Transition in Mature Basins.

Nazari, H., Karami, J., Arefipour, S., Aghaali, E., 2023b. Using artificial intelligence and Machine learning in the mapping of quaternary units. Quaternary of Iran 8, 379–403.

Nilforoushan, F., Masson, F., Vernant, P., Vigny, C., Martinod, J., Abbassi, M., Nankali, H., Hatzfeld, D., Bayer, R., Tavakoli, F., Ashtiani, A., Doerflinger, E., Daignières, M., Collard, P., Chéry, J., 2003. GPS network monitors the Arabia-Eurasia collision deformation in Iran. Journal of Geodesy 77, 411–422. https://doi.org/10.1007/s00190-003-0326-5

Normand, R., 2019. Geomorphological, sedimentological and structural signals of deformation in a silent subduction zone: an investigation of the Makran (Iran). Université de Genève. https://doi.org/10.13097/ARCHIVE-OUVERTE/UNIGE:117482

Page, W.D., Alt, J.N., Cluff, L.S., Plafker, G., 1979. Evidence for the recurrence of large-magnitude earthquakes along the Makran coast of Iran and Pakistan. Tectonophysics 52, 533–547. https://doi.org/10.1016/0040-1951(79)90269-5

Paul, J., Bürgmann, R., Gaur, V.K., Bilham, R., Larson, K.M., Ananda, M.B., Jade, S., Mukal, M., Anupama, T.S., Satyal, G., Kumar, D., 2001. The motion and active deformation of India. Geophysical Research Letters 28, 647–650. https://doi.org/10.1029/2000GL011832

Pedregosa, F., Varoquaux, G., Gramfort, A., Michel, V., Thirion, B., Grisel, O., Blondel, M., Prettenhofer, P., Weiss, R., Dubourg, V., Vanderplas, J., Passos, A., Cournapeau, D., Brucher, M., Perrot, M., Duchesnay, É., 2011. Scikit-learn: Machine Learning in Python. The Journal of Machine Learning Research 12, 2825–2830.

Platt, J.P., Leggett, J.K., Young, J., Raza, H., Alam, S., 1985. Large-scale sediment underplating in the Makran accretionary prism, southwest Pakistan. Geol 13, 507. https://doi.org/10.1130/0091-7613(1985)13<507:LSUITM>2.0.CO;2

Powell, C.McA., 1979. A morphological classification of rock cleavage. Tectonophysics 58, 21–34. https://doi.org/10.1016/0040-1951(79)90320-2

Quittmeyer, R.C., Kafka, A.L., Armbruster, J.G., 1984. Focal mechanisms and depths of earthquakes in central Pakistan: A tectonic interpretation. Journal of Geophysical Research: Solid Earth 89, 2459–2470. https://doi.org/10.1029/JB089iB04p02459

Ramsay, J.G., Huber, M.I., 1987. The techniques of modern structural geology: Folds and fractures. Academic Press, London.

Reilinger, R., McClusky, S., Vernant, P., Lawrence, S., Ergintav, S., Cakmak, R., Ozener, H., Kadirov, F., Guliev, I., Stepanyan, R., Nadariya, M., Hahubia, G., Mahmoud, S., Sakr, K., ArRajehi, A., Paradissis, D., Al-Aydrus, A., Prilepin, M., Guseva, T., Evren, E., Dmitrotsa, A., Filikov, S.V., Gomez, F., Al-Ghazzi, R., Karam, G., 2006. GPS constraints on continental deformation in the Africa-Arabia-Eurasia continental collision zone and implications for the dynamics of plate interactions. J. Geophys. Res. 111, n/a-n/a. https://doi.org/10.1029/2005JB004051

Richards, J.A., 2013. Remote Sensing Digital Image Analysis: An Introduction, 5th ed. Springer, Berlin.

Roy, D.P., Wulder, M.A., Loveland, T.R., C.E., W., Allen, R.G., Anderson, M.C., Helder, D., Irons, J.R., Johnson, D.M., Kennedy, R., Scambos, T.A., Schaaf, C.B., Schott, J.R., Sheng, Y., Vermote, E.F., Belward, A.S., Bindschadler, R., Cohen, W.B., Gao, F., Hipple, J.D., Hostert, P.,

Huntington, J., Justice, C.O., Kilic, A., Kovalskyy, V., Lee, Z.P., Lymburner, L., Masek, J.G., McCorkel, J., Shuai, Y., Trezza, R., Vogelmann, J., Wynne, R.H., Zhu, Z., 2014. Landsat-8: Science and product vision for terrestrial global change research. Remote Sensing of Environment 145, 154–172. https://doi.org/10.1016/j.rse.2014.02.001

Sabins, F.F.J., Ellis, J.M., 2020. Remote sensing: Principles, Interpretation, and Applications, 4th ed. Waveland Press, Inc, Long Grove (Illinois).

Schmitt, R., 1991. The Bisitun Inscriptions of Darius the Great: Old Persian Text, Corpus Inscriptionum Iranicarum I, 1, Texts I. London.

Sepehr, M., Cosgrove, J., Moieni, M., 2006. The impact of cover rock rheology on the style of folding in the Zagros fold-thrust belt. Tectonophysics 427, 265–281. https://doi.org/10.1016/j.tecto.2006.05.021

Shah-Hosseini, M., Ghanavati, E., Morhange, C., Naderi Beni, A., Lahijani, H.A., Hamzeh, M.A., 2018. The evolution of Chabahar beach ridge system in SE Iran in response to Holocene relative sea level changes. Geomorphology 318, 139–147. https://doi.org/10.1016/j.geomorph.2018.06.009

Smith, G., McNeill, L., Henstock, T.J., Bull, J., 2012. The structure and fault activity of the Makran accretionary prism. Journal of Geophysical Research: Solid Earth 117. https://doi.org/10.1029/2012JB009312

Snead, R.J., 1993. Uplifted marine terraces along the Makran coast of Pakistan and Iran, in: Himalaya to the Sea. Routledge, London, pp. 327–362.

Stöcklin, J., 1968. Structural history and tectonics of Iran: a review. American Association of Petroleum Geologists Bulletin 52, 1229–1258.

Stoneley, R., 1974. Evolution of the Continental Margins Bounding a Former Southern Tethys. The Geology of Continental Margins.

Storey, J., Choate, M., Lee, K., 2014. Landsat 8 Operational Land Imager On-Orbit Geometric Calibration and Performance. Remote Sensing 6, 11127–11152. https://doi.org/10.3390/rs61111127

Tagami, T., Galbraith, R.F., Yamada, R., Laslett, G.M., 1998. Revised Annealing Kinetics of Fission Tracks in Zircon and Geological Implications, in: Van Den Haute, P., De Corte, F. (Eds.), Advances in Fission-Track Geochronology. Springer Netherlands, Dordrecht, pp. 99–112. https://doi.org/10.1007/978-94-015-9133-1_8

Torres, R., Snoeij, P., Geudtner, D., Bibby, D., Davidson, M., Attema, E., Potin, P., Rommen, B., Floury, N., Brown, M., Traver, I.N., Deghaye, P., Duesmann, B., Rosich, B., Miranda, N., Bruno, C., L'Abbate, M., Croci, R., Pietropaolo, A., Huchler, M., Rostan, F., 2012. GMES Sentinel-1 mission. Remote Sensing of Environment 120, 9–24. https://doi.org/10.1016/j.rse.2011.05.028

Tso, B., Mather, P.M., 2009. Classification methods for remotely sensed data, 2nd ed, Environmental engineering. CRC Press, Taylor & FrancisGroup, Boca Raton, Fla. London New York.

Tucker, M.E., 2001. Sedimentary petrology, 3rd ed. Blackwell Science, Oxford.

van der Meer, F., 2004. Analysis of spectral absorption features in hyperspectral imagery. International Journal of Applied Earth Observation and Geoinformation 5, 55–68. https://doi.org/10.1016/j.jag.2003.09.001

Vernant, Ph., Nilforoushan, F., Hatzfeld, D., Abbassi, M.R., Vigny, C., Masson, F., Nankali, H., Martinod, J., Ashtiani, A., Bayer, R., Tavakoli, F., Chéry, J., 2004. Present-day crustal deformation and plate kinematics in the Middle East constrained by GPS measurements in Iran and northern Oman. Geophysical Journal International 157, 381–398. https://doi.org/10.1111/j.1365-246X.2004.02222.x

Vita-Finzi, C., 1987. ^{14}C deformation chronologies in coastal Iran, Greece and Jordan. JGS 144, 553–560. https://doi.org/10.1144/gsjgs.144.4.0553

Vita-Finzi, C., 1979. Contributions to the Quaternary geology of southern Iran. Geological and Mineral Survey of Iran 47, 30–47.

Von Rad, U., Berner, U., Delisle, G., Doose-Rolinski, H., Fechner, N., Linke, P., Lückge, A., Roeser, H.A., Schmaljohann, R., Wiedicke, M., Parties, S. 122/130 S., Block, M., Damm, V., Erbacher, J., Fritsch, J., Harazim, B., Poggenburg, J., Scheeder, G., Schreckenberger, B., Von Mirbach, N., Drews, M., Walter, S., Ali Khan, A., Inam, A., Tahir, M., Tabrez, A.R., Cheema, A.H., Pervaz, M., Ashraf, M., 2000. Gas and fluid venting at the Makran accretionary wedge off Pakistan. Geo-Marine Letters 20, 10–19. https://doi.org/10.1007/s003670000033

Wegnüller, U., Werner, C., Strozzi, T., Wiesmann, A., Frey, O., Santoro, M., 2016. Sentinel-1 Support in the GAMMA Software. Procedia Computer Science 100, 1305–1312. https://doi.org/10.1016/j.procs.2016.09.246

White, R.S., Klitgord, K., 1976. Sediment deformation and plate tectonics in the Gulf of Oman. Earth and Planetary Science Letters 32, 199–209. https://doi.org/10.1016/0012-821X(76)90059-5

White, R.S., Louden, K.E., 1982. The Makran continental margin: structure of a thickly sedimented convergent plate boundary: convergent margins: field investigations of margin structure and stratigraphy. AAPG, Studies in Continental Margin Geology 499–518.

Zhou, Z.-H., 2012. Ensemble methods: foundations and algorithms, Online-Ausg. ed, Chapman & Hall. Taylor & Francis, Boca Raton, FL.

GeoNexus

Appendix

GeoNexus

GeoNexus

Table S1. Summary of mapped polygons for the $OlM^{sh.s}$ Unit.

OBJECTID_1	Join_Count	TARGET_FID	Label	Shape_Area (sqkm)	ORIG_FID	Absolute_Age	Age_paleontology	Unit	Reference
6071	0	6072	ph_olive	0.1068	10		Late Oligocene	OlMsh.s	Dolati (2010)
6072	0	6073	ph_olive	0.1380	10		Late Oligocene	OlMsh.s	Dolati (2010)
6073	0	6074	ph_olive	0.1307	10		Late Oligocene	OlMsh.s	Dolati (2010)
6074	0	6075	ph_olive	0.6026	10		Late Oligocene	OlMsh.s	Dolati (2010)
6075	0	6076	ph_olive	0.1920	10		Late Oligocene	OlMsh.s	Dolati (2010)
6076	0	6077	ph_olive	0.3161	10		Late Oligocene	OlMsh.s	Dolati (2010)
6077	0	6078	ph_olive	0.0194	10		Late Oligocene	OlMsh.s	Dolati (2010)
6078	0	6079	ph_olive	0.0324	10		Late Oligocene	OlMsh.s	Dolati (2010)
6079	0	6080	ph_olive	0.2458	10		Late Oligocene	OlMsh.s	Dolati (2010)
6080	0	6081	ph_olive	0.1932	10		Late Oligocene	OlMsh.s	Dolati (2010)
6081	0	6082	ph_olive	0.3866	10		Late Oligocene	OlMsh.s	Dolati (2010)
6082	0	6083	ph_olive	0.2467	10		Late Oligocene	OlMsh.s	Dolati (2010)
6083	0	6084	ph_olive	0.3452	10		Late Oligocene	OlMsh.s	Dolati (2010)
6084	0	6085	ph_olive	0.1282	10		Late Oligocene	OlMsh.s	Dolati (2010)
6085	0	6086	ph_olive	0.0934	10		Late Oligocene	OlMsh.s	Dolati (2010)
6086	0	6087	ph_olive	1.0558	10		Late Oligocene	OlMsh.s	Dolati (2010)
6087	0	6088	ph_olive	1.0417	10		Late Oligocene	OlMsh.s	Dolati (2010)
6088	0	6089	ph_olive	0.2709	10		Late Oligocene	OlMsh.s	Dolati (2010)
6089	0	6090	ph_olive	0.0394	10		Late Oligocene	OlMsh.s	Dolati (2010)
6090	0	6091	ph_olive	0.2828	10		Late Oligocene	OlMsh.s	Dolati (2010)
6091	0	6092	ph_olive	0.1978	10		Late Oligocene	OlMsh.s	Dolati (2010)
6092	0	6093	ph_olive	0.0338	10		Late Oligocene	OlMsh.s	Dolati (2010)
6093	0	6094	ph_olive	0.0136	10		Late Oligocene	OlMsh.s	Dolati (2010)
6094	0	6095	ph_olive	0.6082	10		Late Oligocene	OlMsh.s	Dolati (2010)
6095	0	6096	ph_olive	0.0523	10		Late Oligocene	OlMsh.s	Dolati (2010)
6096	0	6097	ph_olive	0.4017	10		Late Oligocene	OlMsh.s	Dolati (2010)
6097	0	6098	ph_olive	0.4466	10		Late Oligocene	OlMsh.s	Dolati (2010)
6098	0	6099	ph_olive	1.0477	10		Late Oligocene	OlMsh.s	Dolati (2010)
6099	0	6100	ph_olive	0.5542	10		Late Oligocene	OlMsh.s	Dolati (2010)
6100	0	6101	ph_olive	0.2964	10		Late Oligocene	OlMsh.s	Dolati (2010)
6101	0	6102	ph_olive	0.0239	10		Late Oligocene	OlMsh.s	Dolati (2010)
6102	0	6103	ph_olive	0.0619	10		Late Oligocene	OlMsh.s	Dolati (2010)
6103	0	6104	ph_olive	0.1034	10		Late Oligocene	OlMsh.s	Dolati (2010)
6104	0	6105	ph_olive	0.1360	10		Late Oligocene	OlMsh.s	Dolati (2010)
6105	0	6106	ph_olive	0.0515	10		Late Oligocene	OlMsh.s	Dolati (2010)
6106	0	6107	ph_olive	0.1338	10		Late Oligocene	OlMsh.s	Dolati (2010)
6107	0	6108	ph_olive	0.0638	10		Late Oligocene	OlMsh.s	Dolati (2010)

Geonas

OBJECTID_1	Join_Count	TARGET_FID	Label	Shape_Area (sqkm)	ORIG_FID	Absolute_Age	Age_paleontology	Unit	Reference
6108	0	6109	ph_olive	14.6429	10		Late Oligocene	OlMsh.s	Dolati (2010)
6109	0	6110	ph_olive	0.0487	10		Late Oligocene	OlMsh.s	Dolati (2010)
6110	0	6111	ph_olive	0.2549	10		Late Oligocene	OlMsh.s	Dolati (2010)
6111	0	6112	ph_olive	0.5745	10		Late Oligocene	OlMsh.s	Dolati (2010)
6112	0	6113	ph_olive	1.1481	10		Late Oligocene	OlMsh.s	Dolati (2010)
6113	0	6114	ph_olive	0.0435	10		Late Oligocene	OlMsh.s	Dolati (2010)
6114	0	6115	ph_olive	0.0162	10		Late Oligocene	OlMsh.s	Dolati (2010)
6115	0	6116	ph_olive	0.0349	10		Late Oligocene	OlMsh.s	Dolati (2010)
6116	0	6117	ph_olive	0.0296	10		Late Oligocene	OlMsh.s	Dolati (2010)
6117	0	6118	ph_olive	0.1989	10		Late Oligocene	OlMsh.s	Dolati (2010)
6118	0	6119	ph_olive	0.2426	10		Late Oligocene	OlMsh.s	Dolati (2010)
6119	0	6120	ph_olive	0.2665	10		Late Oligocene	OlMsh.s	Dolati (2010)
6120	0	6121	ph_olive	10.0785	10		Late Oligocene	OlMsh.s	Dolati (2010)
6121	0	6122	ph_olive	0.1646	10		Late Oligocene	OlMsh.s	Dolati (2010)
6122	0	6123	ph_olive	0.0754	10		Late Oligocene	OlMsh.s	Dolati (2010)
6123	0	6124	ph_olive	0.4617	10		Late Oligocene	OlMsh.s	Dolati (2010)
6124	0	6125	ph_olive	0.0574	10		Late Oligocene	OlMsh.s	Dolati (2010)

GeoNews

Table S2. Summary of mapped polygons for the $OlM^{s.sh.c}$ Unit.

OBJECTID_1	Join_Count	TARGET_FID	Label	Shape_Area (sqkm)	ORIG_FID	Absolute_Age	Age_paleontology	Unit	Reference
6125	0	6126	ph_olive_1	0.015	11		Oligocene	OlMs.sh.c	Dolati (2010)
6126	0	6127	ph_olive_1	0.010	11		Oligocene	OlMs.sh.c	Dolati (2010)
6127	0	6128	ph_olive_1	0.013	11		Oligocene	OlMs.sh.c	Dolati (2010)
6128	0	6129	ph_olive_1	0.022	11		Oligocene	OlMs.sh.c	Dolati (2010)
6129	0	6130	ph_olive_1	0.127	11		Oligocene	OlMs.sh.c	Dolati (2010)
6130	0	6131	ph_olive_1	0.815	11		Oligocene	OlMs.sh.c	Dolati (2010)
6131	0	6132	ph_olive_1	0.008	11		Oligocene	OlMs.sh.c	Dolati (2010)
6132	0	6133	ph_olive_1	0.037	11		Oligocene	OlMs.sh.c	Dolati (2010)
6133	0	6134	ph_olive_1	0.008	11		Oligocene	OlMs.sh.c	Dolati (2010)
6134	0	6135	ph_olive_1	0.206	11		Oligocene	OlMs.sh.c	Dolati (2010)
6135	0	6136	ph_olive_1	3.538	11		Oligocene	OlMs.sh.c	Dolati (2010)
6136	0	6137	ph_olive_1	0.095	11		Oligocene	OlMs.sh.c	Dolati (2010)
6137	0	6138	ph_olive_1	0.050	11		Oligocene	OlMs.sh.c	Dolati (2010)
6138	0	6139	ph_olive_1	0.011	11		Oligocene	OlMs.sh.c	Dolati (2010)
6139	0	6140	ph_olive_1	1.276	11		Oligocene	OlMs.sh.c	Dolati (2010)
6140	0	6141	ph_olive_1	0.065	11		Oligocene	OlMs.sh.c	Dolati (2010)
6141	0	6142	ph_olive_1	0.029	11		Oligocene	OlMs.sh.c	Dolati (2010)
6142	0	6143	ph_olive_1	0.084	11		Oligocene	OlMs.sh.c	Dolati (2010)
6143	0	6144	ph_olive_1	0.600	11		Oligocene	OlMs.sh.c	Dolati (2010)
6144	0	6145	ph_olive_1	0.934	11		Oligocene	OlMs.sh.c	Dolati (2010)
6145	0	6146	ph_olive_1	0.216	11		Oligocene	OlMs.sh.c	Dolati (2010)
6146	0	6147	ph_olive_1	0.016	11		Oligocene	OlMs.sh.c	Dolati (2010)
6147	0	6148	ph_olive_1	0.052	11		Oligocene	OlMs.sh.c	Dolati (2010)
6148	0	6149	ph_olive_1	0.012	11		Oligocene	OlMs.sh.c	Dolati (2010)
6149	0	6150	ph_olive_1	0.043	11		Oligocene	OlMs.sh.c	Dolati (2010)
6150	0	6151	ph_olive_1	1.054	11		Oligocene	OlMs.sh.c	Dolati (2010)
6151	0	6152	ph_olive_1	0.012	11		Oligocene	OlMs.sh.c	Dolati (2010)
6152	0	6153	ph_olive_1	1.996	11		Oligocene	OlMs.sh.c	Dolati (2010)
6153	0	6154	ph_olive_1	0.052	11		Oligocene	OlMs.sh.c	Dolati (2010)
6154	0	6155	ph_olive_1	0.030	11		Oligocene	OlMs.sh.c	Dolati (2010)
6155	0	6156	ph_olive_1	2.890	11		Oligocene	OlMs.sh.c	Dolati (2010)
6156	0	6157	ph_olive_1	0.008	11		Oligocene	OlMs.sh.c	Dolati (2010)
6157	0	6158	ph_olive_1	0.158	11		Oligocene	OlMs.sh.c	Dolati (2010)
6158	0	6159	ph_olive_1	0.028	11		Oligocene	OlMs.sh.c	Dolati (2010)
6159	0	6160	ph_olive_1	0.015	11		Oligocene	OlMs.sh.c	Dolati (2010)
6160	0	6161	ph_olive_1	0.138	11		Oligocene	OlMs.sh.c	Dolati (2010)
6161	0	6162	ph_olive_1	0.035	11		Oligocene	OlMs.sh.c	Dolati (2010)
6162	0	6163	ph_olive_1	0.263	11		Oligocene	OlMs.sh.c	Dolati (2010)

GSI NEXUS

OBJECTID_1	Join_Count	TARGET_FID	Label	Shape_Area (sqkm)	ORIG_FID	Absolute_Age	Age_paleontology	Unit	Reference
6163	0	6164	ph_olive_1	0.108	11		Oligocene	OlMs.sh.c	Dolati (2010)
6164	0	6165	ph_olive_1	0.035	11		Oligocene	OlMs.sh.c	Dolati (2010)
6165	0	6166	ph_olive_1	0.242	11		Oligocene	OlMs.sh.c	Dolati (2010)
6166	0	6167	ph_olive_1	0.026	11		Oligocene	OlMs.sh.c	Dolati (2010)
6167	0	6168	ph_olive_1	0.027	11		Oligocene	OlMs.sh.c	Dolati (2010)
6168	0	6169	ph_olive_1	0.016	11		Oligocene	OlMs.sh.c	Dolati (2010)
6169	0	6170	ph_olive_1	0.069	11		Oligocene	OlMs.sh.c	Dolati (2010)
6170	0	6171	ph_olive_1	0.136	11		Oligocene	OlMs.sh.c	Dolati (2010)
6171	0	6172	ph_olive_1	0.276	11		Oligocene	OlMs.sh.c	Dolati (2010)
6172	0	6173	ph_olive_1	0.253	11		Oligocene	OlMs.sh.c	Dolati (2010)
6173	0	6174	ph_olive_1	0.218	11		Oligocene	OlMs.sh.c	Dolati (2010)
6174	0	6175	ph_olive_1	1.168	11		Oligocene	OlMs.sh.c	Dolati (2010)
6175	0	6176	ph_olive_1	0.039	11		Oligocene	OlMs.sh.c	Dolati (2010)
6176	0	6177	ph_olive_1	0.054	11		Oligocene	OlMs.sh.c	Dolati (2010)
6177	0	6178	ph_olive_1	0.263	11		Oligocene	OlMs.sh.c	Dolati (2010)
6178	0	6179	ph_olive_1	0.018	11		Oligocene	OlMs.sh.c	Dolati (2010)
6179	0	6180	ph_olive_1	0.096	11		Oligocene	OlMs.sh.c	Dolati (2010)
6180	0	6181	ph_olive_1	0.560	11		Oligocene	OlMs.sh.c	Dolati (2010)
6181	0	6182	ph_olive_1	1.718	11		Oligocene	OlMs.sh.c	Dolati (2010)
6182	0	6183	ph_olive_1	0.136	11		Oligocene	OlMs.sh.c	Dolati (2010)
6183	0	6184	ph_olive_1	0.340	11		Oligocene	OlMs.sh.c	Dolati (2010)
6185	0	6186	ph_olive_1	1.452	11		Oligocene	OlMs.sh.c	Dolati (2010)
6186	0	6187	ph_olive_1	0.417	11		Oligocene	OlMs.sh.c	Dolati (2010)
6187	0	6188	ph_olive_1	0.944	11		Oligocene	OlMs.sh.c	Dolati (2010)
6188	0	6189	ph_olive_1	2.434	11		Oligocene	OlMs.sh.c	Dolati (2010)
6189	0	6190	ph_olive_1	0.197	11		Oligocene	OlMs.sh.c	Dolati (2010)
6190	0	6191	ph_olive_1	0.114	11		Oligocene	OlMs.sh.c	Dolati (2010)
6191	0	6192	ph_olive_1	0.466	11		Oligocene	OlMs.sh.c	Dolati (2010)
6192	0	6193	ph_olive_1	0.963	11		Oligocene	OlMs.sh.c	Dolati (2010)
6193	0	6194	ph_olive_1	0.028	11		Oligocene	OlMs.sh.c	Dolati (2010)
6194	0	6195	ph_olive_1	0.321	11		Oligocene	OlMs.sh.c	Dolati (2010)
6195	0	6196	ph_olive_1	0.095	11		Oligocene	OlMs.sh.c	Dolati (2010)
6196	0	6197	ph_olive_1	0.094	11		Oligocene	OlMs.sh.c	Dolati (2010)
6197	0	6198	ph_olive_1	3.006	11		Oligocene	OlMs.sh.c	Dolati (2010)
6198	0	6199	ph_olive_1	0.044	11		Oligocene	OlMs.sh.c	Dolati (2010)
6199	0	6200	ph_olive_1	0.092	11		Oligocene	OlMs.sh.c	Dolati (2010)
6200	0	6201	ph_olive_1	0.240	11		Oligocene	OlMs.sh.c	Dolati (2010)
6201	0	6202	ph_olive_1	0.101	11		Oligocene	OlMs.sh.c	Dolati (2010)
6202	0	6203	ph_olive_1	7.936	11		Oligocene	OlMs.sh.c	Dolati (2010)

GSI

OBJECTID_1	Join_Count	TARGET_FID	Label	Shape_Area (sqkm)	ORIG_FID	Absolute_Age	Age_paleontology	Unit	Reference
6203	0	6204	ph_olive_1	0.158	11		Oligocene	OlMs.sh.c	Dolati (2010)
6204	0	6205	ph_olive_1	0.131	11		Oligocene	OlMs.sh.c	Dolati (2010)
6205	0	6206	ph_olive_1	28.313	11		Oligocene	OlMs.sh.c	Dolati (2010)
6206	0	6207	ph_olive_1	0.022	11		Oligocene	OlMs.sh.c	Dolati (2010)
6207	0	6208	ph_olive_1	0.155	11		Oligocene	OlMs.sh.c	Dolati (2010)
6208	0	6209	ph_olive_1	0.332	11		Oligocene	OlMs.sh.c	Dolati (2010)
6209	0	6210	ph_olive_1	0.796	11		Oligocene	OlMs.sh.c	Dolati (2010)
6210	0	6211	ph_olive_1	0.155	11		Oligocene	OlMs.sh.c	Dolati (2010)
6211	0	6212	ph_olive_1	1.429	11		Oligocene	OlMs.sh.c	Dolati (2010)
6212	0	6213	ph_olive_1	0.168	11		Oligocene	OlMs.sh.c	Dolati (2010)
6213	0	6214	ph_olive_1	0.050	11		Oligocene	OlMs.sh.c	Dolati (2010)
6214	0	6215	ph_olive_1	0.099	11		Oligocene	OlMs.sh.c	Dolati (2010)
6215	0	6216	ph_olive_1	0.031	11		Oligocene	OlMs.sh.c	Dolati (2010)
6216	0	6217	ph_olive_1	1.471	11		Oligocene	OlMs.sh.c	Dolati (2010)
6217	0	6218	ph_olive_1	0.551	11		Oligocene	OlMs.sh.c	Dolati (2010)
6218	0	6219	ph_olive_1	0.053	11		Oligocene	OlMs.sh.c	Dolati (2010)
6219	0	6220	ph_olive_1	0.248	11		Oligocene	OlMs.sh.c	Dolati (2010)
6220	0	6221	ph_olive_1	0.555	11		Oligocene	OlMs.sh.c	Dolati (2010)
6221	0	6222	ph_olive_1	0.019	11		Oligocene	OlMs.sh.c	Dolati (2010)
6222	0	6223	ph_olive_1	0.049	11		Oligocene	OlMs.sh.c	Dolati (2010)
6223	0	6224	ph_olive_1	0.129	11		Oligocene	OlMs.sh.c	Dolati (2010)
6224	0	6225	ph_olive_1	0.124	11		Oligocene	OlMs.sh.c	Dolati (2010)
6225	0	6226	ph_olive_1	0.350	11		Oligocene	OlMs.sh.c	Dolati (2010)
6226	0	6227	ph_olive_1	0.375	11		Oligocene	OlMs.sh.c	Dolati (2010)
6227	0	6228	ph_olive_1	7.507	11		Oligocene	OlMs.sh.c	Dolati (2010)
6228	0	6229	ph_olive_1	0.125	11		Oligocene	OlMs.sh.c	Dolati (2010)
6229	0	6230	ph_olive_1	0.089	11		Oligocene	OlMs.sh.c	Dolati (2010)
6230	0	6231	ph_olive_1	0.054	11		Oligocene	OlMs.sh.c	Dolati (2010)
6231	0	6232	ph_olive_1	0.584	11		Oligocene	OlMs.sh.c	Dolati (2010)
6232	0	6233	ph_olive_1	0.235	11		Oligocene	OlMs.sh.c	Dolati (2010)
6233	0	6234	ph_olive_1	0.091	11		Oligocene	OlMs.sh.c	Dolati (2010)
6234	0	6235	ph_olive_1	0.664	11		Oligocene	OlMs.sh.c	Dolati (2010)
6235	0	6236	ph_olive_1	0.895	11		Oligocene	OlMs.sh.c	Dolati (2010)
6236	0	6237	ph_olive_1	0.036	11		Oligocene	OlMs.sh.c	Dolati (2010)
6237	0	6238	ph_olive_1	6.365	11		Oligocene	OlMs.sh.c	Dolati (2010)
6238	0	6239	ph_olive_1	0.811	11		Oligocene	OlMs.sh.c	Dolati (2010)
6239	0	6240	ph_olive_1	0.602	11		Oligocene	OlMs.sh.c	Dolati (2010)
6240	1	6241	ph_olive_1	21.987	11		Oligocene	OlMs.sh.c	Dolati (2010)
6241	0	6242	ph_olive_1	0.138	11		Oligocene	OlMs.sh.c	Dolati (2010)

Geonexus

OBJECTID_1	Join_Count	TARGET_FID	Label	Shape_Area (sqkm)	ORIG_FID	Absolute_Age	Age_paleontology	Unit	Reference
6242	0	6243	ph_olive_1	0.901	11		Oligocene	OlMs.sh.c	Dolati (2010)
6243	0	6244	ph_olive_1	0.771	11		Oligocene	OlMs.sh.c	Dolati (2010)
6244	0	6245	ph_olive_1	0.277	11		Oligocene	OlMs.sh.c	Dolati (2010)
6245	0	6246	ph_olive_1	0.037	11		Oligocene	OlMs.sh.c	Dolati (2010)
6246	0	6247	ph_olive_1	0.124	11		Oligocene	OlMs.sh.c	Dolati (2010)
6247	0	6248	ph_olive_1	0.053	11		Oligocene	OlMs.sh.c	Dolati (2010)
6248	0	6249	ph_olive_1	0.095	11		Oligocene	OlMs.sh.c	Dolati (2010)
6249	0	6250	ph_olive_1	0.455	11		Oligocene	OlMs.sh.c	Dolati (2010)
6250	0	6251	ph_olive_1	0.331	11		Oligocene	OlMs.sh.c	Dolati (2010)
6251	0	6252	ph_olive_1	0.257	11		Oligocene	OlMs.sh.c	Dolati (2010)
6252	0	6253	ph_olive_1	0.604	11		Oligocene	OlMs.sh.c	Dolati (2010)
6253	0	6254	ph_olive_1	28.461	11		Oligocene	OlMs.sh.c	Dolati (2010)
6254	0	6255	ph_olive_1	0.043	11		Oligocene	OlMs.sh.c	Dolati (2010)
6255	0	6256	ph_olive_1	0.563	11		Oligocene	OlMs.sh.c	Dolati (2010)
6256	0	6257	ph_olive_1	0.023	11		Oligocene	OlMs.sh.c	Dolati (2010)
6257	0	6258	ph_olive_1	0.013	11		Oligocene	OlMs.sh.c	Dolati (2010)
6258	0	6259	ph_olive_1	0.320	11		Oligocene	OlMs.sh.c	Dolati (2010)
6259	0	6260	ph_olive_1	0.086	11		Oligocene	OlMs.sh.c	Dolati (2010)
6260	0	6261	ph_olive_1	0.048	11		Oligocene	OlMs.sh.c	Dolati (2010)
6261	0	6262	ph_olive_1	0.112	11		Oligocene	OlMs.sh.c	Dolati (2010)
6262	0	6263	ph_olive_1	0.558	11		Oligocene	OlMs.sh.c	Dolati (2010)
6263	0	6264	ph_olive_1	0.014	11		Oligocene	OlMs.sh.c	Dolati (2010)
6264	0	6265	ph_olive_1	2.468	11		Oligocene	OlMs.sh.c	Dolati (2010)
6265	0	6266	ph_olive_1	0.037	11		Oligocene	OlMs.sh.c	Dolati (2010)
6266	0	6267	ph_olive_1	1.238	11		Oligocene	OlMs.sh.c	Dolati (2010)
6267	0	6268	ph_olive_1	0.195	11		Oligocene	OlMs.sh.c	Dolati (2010)
6268	0	6269	ph_olive_1	0.250	11		Oligocene	OlMs.sh.c	Dolati (2010)
6269	0	6270	ph_olive_1	0.163	11		Oligocene	OlMs.sh.c	Dolati (2010)
6270	0	6271	ph_olive_1	2.137	11		Oligocene	OlMs.sh.c	Dolati (2010)
6271	0	6272	ph_olive_1	0.682	11		Oligocene	OlMs.sh.c	Dolati (2010)
6272	0	6273	ph_olive_1	0.222	11		Oligocene	OlMs.sh.c	Dolati (2010)
6273	0	6274	ph_olive_1	0.271	11		Oligocene	OlMs.sh.c	Dolati (2010)
6274	0	6275	ph_olive_1	0.234	11		Oligocene	OlMs.sh.c	Dolati (2010)
6275	0	6276	ph_olive_1	1.114	11		Oligocene	OlMs.sh.c	Dolati (2010)
6276	0	6277	ph_olive_1	0.022	11		Oligocene	OlMs.sh.c	Dolati (2010)
6277	0	6278	ph_olive_1	0.013	11		Oligocene	OlMs.sh.c	Dolati (2010)
6278	0	6279	ph_olive_1	0.038	11		Oligocene	OlMs.sh.c	Dolati (2010)
6279	0	6280	ph_olive_1	3.120	11		Oligocene	OlMs.sh.c	Dolati (2010)
6280	0	6281	ph_olive_1	0.034	11		Oligocene	OlMs.sh.c	Dolati (2010)

Geonavis

OBJECTID_1	Join_Count	TARGET_FID	Label	Shape_Area (sqkm)	ORIG_FID	Absolute_Age	Age_paleontology	Unit	Reference
6281	0	6282	ph_olive_1	0.072	11		Oligocene	OlMs.sh.c	Dolati (2010)
6282	0	6283	ph_olive_1	0.111	11		Oligocene	OlMs.sh.c	Dolati (2010)
6283	0	6284	ph_olive_1	0.057	11		Oligocene	OlMs.sh.c	Dolati (2010)
6284	0	6285	ph_olive_1	0.205	11		Oligocene	OlMs.sh.c	Dolati (2010)
6285	0	6286	ph_olive_1	0.010	11		Oligocene	OlMs.sh.c	Dolati (2010)
6286	0	6287	ph_olive_1	0.420	11		Oligocene	OlMs.sh.c	Dolati (2010)
6287	0	6288	ph_olive_1	0.118	11		Oligocene	OlMs.sh.c	Dolati (2010)
6288	0	6289	ph_olive_1	0.006	11		Oligocene	OlMs.sh.c	Dolati (2010)
6289	0	6290	ph_olive_1	0.588	11		Oligocene	OlMs.sh.c	Dolati (2010)
6290	0	6291	ph_olive_1	0.036	11		Oligocene	OlMs.sh.c	Dolati (2010)
6291	0	6292	ph_olive_1	0.333	11		Oligocene	OlMs.sh.c	Dolati (2010)
6292	0	6293	ph_olive_1	0.398	11		Oligocene	OlMs.sh.c	Dolati (2010)
6293	0	6294	ph_olive_1	0.237	11		Oligocene	OlMs.sh.c	Dolati (2010)
6294	0	6295	ph_olive_1	0.715	11		Oligocene	OlMs.sh.c	Dolati (2010)
6295	0	6296	ph_olive_1	1.730	11		Oligocene	OlMs.sh.c	Dolati (2010)
6296	0	6297	ph_olive_1	0.367	11		Oligocene	OlMs.sh.c	Dolati (2010)
6297	0	6298	ph_olive_1	0.023	11		Oligocene	OlMs.sh.c	Dolati (2010)
6298	0	6299	ph_olive_1	0.205	11		Oligocene	OlMs.sh.c	Dolati (2010)
6299	0	6300	ph_olive_1	1.379	11		Oligocene	OlMs.sh.c	Dolati (2010)
6300	0	6301	ph_olive_1	0.046	11		Oligocene	OlMs.sh.c	Dolati (2010)
6301	0	6302	ph_olive_1	0.357	11		Oligocene	OlMs.sh.c	Dolati (2010)
6302	0	6303	ph_olive_1	0.238	11		Oligocene	OlMs.sh.c	Dolati (2010)
6303	0	6304	ph_olive_1	0.081	11		Oligocene	OlMs.sh.c	Dolati (2010)
6304	0	6305	ph_olive_1	0.226	11		Oligocene	OlMs.sh.c	Dolati (2010)
6305	0	6306	ph_olive_1	0.232	11		Oligocene	OlMs.sh.c	Dolati (2010)
6306	0	6307	ph_olive_1	0.941	11		Oligocene	OlMs.sh.c	Dolati (2010)
6307	0	6308	ph_olive_1	0.094	11		Oligocene	OlMs.sh.c	Dolati (2010)
6308	0	6309	ph_olive_1	0.434	11		Oligocene	OlMs.sh.c	Dolati (2010)
6309	0	6310	ph_olive_1	0.204	11		Oligocene	OlMs.sh.c	Dolati (2010)
6310	0	6311	ph_olive_1	0.109	11		Oligocene	OlMs.sh.c	Dolati (2010)
6311	0	6312	ph_olive_1	0.196	11		Oligocene	OlMs.sh.c	Dolati (2010)
6312	0	6313	ph_olive_1	0.081	11		Oligocene	OlMs.sh.c	Dolati (2010)
6313	0	6314	ph_olive_1	0.267	11		Oligocene	OlMs.sh.c	Dolati (2010)
6314	0	6315	ph_olive_1	0.155	11		Oligocene	OlMs.sh.c	Dolati (2010)
6315	0	6316	ph_olive_1	0.060	11		Oligocene	OlMs.sh.c	Dolati (2010)
6316	0	6317	ph_olive_1	0.178	11		Oligocene	OlMs.sh.c	Dolati (2010)
6317	0	6318	ph_olive_1	0.342	11		Oligocene	OlMs.sh.c	Dolati (2010)
6318	0	6319	ph_olive_1	0.469	11		Oligocene	OlMs.sh.c	Dolati (2010)
6319	0	6320	ph_olive_1	0.066	11		Oligocene	OlMs.sh.c	Dolati (2010)

Geonexus

OBJECTID_1	Join_Count	TARGET_FID	Label	Shape_Area (sqkm)	ORIG_FID	Absolute_Age	Age_paleontology	Unit	Reference
6320	0	6321	ph_olive_1	0.464	11		Oligocene	OlMs.sh.c	Dolati (2010)
6321	0	6322	ph_olive_1	0.808	11		Oligocene	OlMs.sh.c	Dolati (2010)
6322	0	6323	ph_olive_1	3.247	11		Oligocene	OlMs.sh.c	Dolati (2010)
6323	0	6324	ph_olive_1	0.357	11		Oligocene	OlMs.sh.c	Dolati (2010)
6324	0	6325	ph_olive_1	0.084	11		Oligocene	OlMs.sh.c	Dolati (2010)
6325	0	6326	ph_olive_1	0.171	11		Oligocene	OlMs.sh.c	Dolati (2010)
6326	0	6327	ph_olive_1	0.073	11		Oligocene	OlMs.sh.c	Dolati (2010)
6327	0	6328	ph_olive_1	0.084	11		Oligocene	OlMs.sh.c	Dolati (2010)
6328	0	6329	ph_olive_1	29.480	11		Oligocene	OlMs.sh.c	Dolati (2010)
6329	0	6330	ph_olive_1	0.405	11		Oligocene	OlMs.sh.c	Dolati (2010)
6330	0	6331	ph_olive_1	0.210	11		Oligocene	OlMs.sh.c	Dolati (2010)
6331	0	6332	ph_olive_1	7.786	11		Oligocene	OlMs.sh.c	Dolati (2010)
6332	0	6333	ph_olive_1	0.105	11		Oligocene	OlMs.sh.c	Dolati (2010)
6333	0	6334	ph_olive_1	1.150	11		Oligocene	OlMs.sh.c	Dolati (2010)
6334	0	6335	ph_olive_1	0.078	11		Oligocene	OlMs.sh.c	Dolati (2010)
6335	0	6336	ph_olive_1	8.850	11		Oligocene	OlMs.sh.c	Dolati (2010)
6336	0	6337	ph_olive_1	0.253	11		Oligocene	OlMs.sh.c	Dolati (2010)
6337	0	6338	ph_olive_1	0.104	11		Oligocene	OlMs.sh.c	Dolati (2010)
6338	0	6339	ph_olive_1	0.430	11		Oligocene	OlMs.sh.c	Dolati (2010)
6339	0	6340	ph_olive_1	0.126	11		Oligocene	OlMs.sh.c	Dolati (2010)
6340	0	6341	ph_olive_1	0.570	11		Oligocene	OlMs.sh.c	Dolati (2010)
6341	0	6342	ph_olive_1	0.064	11		Oligocene	OlMs.sh.c	Dolati (2010)
6342	0	6343	ph_olive_1	0.118	11		Oligocene	OlMs.sh.c	Dolati (2010)
6343	0	6344	ph_olive_1	0.669	11		Oligocene	OlMs.sh.c	Dolati (2010)
6344	0	6345	ph_olive_1	0.433	11		Oligocene	OlMs.sh.c	Dolati (2010)
6345	0	6346	ph_olive_1	0.464	11		Oligocene	OlMs.sh.c	Dolati (2010)
6346	0	6347	ph_olive_1	1.795	11		Oligocene	OlMs.sh.c	Dolati (2010)
6347	0	6348	ph_olive_1	0.313	11		Oligocene	OlMs.sh.c	Dolati (2010)
6348	0	6349	ph_olive_1	2.383	11		Oligocene	OlMs.sh.c	Dolati (2010)
6349	0	6350	ph_olive_1	0.782	11		Oligocene	OlMs.sh.c	Dolati (2010)
6350	0	6351	ph_olive_1	0.109	11		Oligocene	OlMs.sh.c	Dolati (2010)
6351	0	6352	ph_olive_1	1.428	11		Oligocene	OlMs.sh.c	Dolati (2010)
6352	0	6353	ph_olive_1	0.100	11		Oligocene	OlMs.sh.c	Dolati (2010)
6353	0	6354	ph_olive_1	0.023	11		Oligocene	OlMs.sh.c	Dolati (2010)
6354	0	6355	ph_olive_1	1.278	11		Oligocene	OlMs.sh.c	Dolati (2010)
6355	0	6356	ph_olive_1	4.945	11		Oligocene	OlMs.sh.c	Dolati (2010)
6356	0	6357	ph_olive_1	0.164	11		Oligocene	OlMs.sh.c	Dolati (2010)
6357	0	6358	ph_olive_1	2.232	11		Oligocene	OlMs.sh.c	Dolati (2010)
6358	0	6359	ph_olive_1	0.019	11		Oligocene	OlMs.sh.c	Dolati (2010)

Geonavis

OBJECTID_1	Join_Count	TARGET_FID	Label	Shape_Area (sqkm)	ORIG_FID	Absolute_Age	Age_paleontology	Unit	Reference
6359	0	6360	ph_olive_1	76.361	11		Oligocene	OlMs.sh.c	Dolati (2010)
6360	0	6361	ph_olive_1	0.766	11		Oligocene	OlMs.sh.c	Dolati (2010)
6361	0	6362	ph_olive_1	14.048	11		Oligocene	OlMs.sh.c	Dolati (2010)
6362	0	6363	ph_olive_1	0.324	11		Oligocene	OlMs.sh.c	Dolati (2010)
6363	0	6364	ph_olive_1	0.317	11		Oligocene	OlMs.sh.c	Dolati (2010)
6364	0	6365	ph_olive_1	3.077	11		Oligocene	OlMs.sh.c	Dolati (2010)
6365	0	6366	ph_olive_1	0.155	11		Oligocene	OlMs.sh.c	Dolati (2010)
6366	0	6367	ph_olive_1	1.230	11		Oligocene	OlMs.sh.c	Dolati (2010)
6367	0	6368	ph_olive_1	3.491	11		Oligocene	OlMs.sh.c	Dolati (2010)
6368	0	6369	ph_olive_1	1.998	11		Oligocene	OlMs.sh.c	Dolati (2010)
6369	0	6370	ph_olive_1	0.212	11		Oligocene	OlMs.sh.c	Dolati (2010)
6370	0	6371	ph_olive_1	0.222	11		Oligocene	OlMs.sh.c	Dolati (2010)
10437	1	10461	ph_olive_1	0.336	0		Oligocene	OlMs.sh.c	Dolati (2010)
10438	1	10462	ph_olive_1	0.274	0		Oligocene	OlMs.sh.c	Dolati (2010)
10439	1	10463	ph_olive_1	0.762	0		Oligocene	OlMs.sh.c	Dolati (2010)
10440	1	10464	ph_olive_1	0.429	0		Oligocene	OlMs.sh.c	Dolati (2010)
10508	0	6274	ph_olive_1	0.001	11		Oligocene	OlMs.sh.c	Dolati (2010)
10509	0	6274	ph_olive_1	0.001	11		Oligocene	OlMs.sh.c	Dolati (2010)
10510	0	6274	ph_olive_1	0.001	11		Oligocene	OlMs.sh.c	Dolati (2010)
10511	0	6274	ph_olive_1	0.003	11		Oligocene	OlMs.sh.c	Dolati (2010)
10512	0	6274	ph_olive_1	0.004	11		Oligocene	OlMs.sh.c	Dolati (2010)
10513	0	6274	ph_olive_1	0.005	11		Oligocene	OlMs.sh.c	Dolati (2010)
10514	0	6274	ph_olive_1	0.006	11		Oligocene	OlMs.sh.c	Dolati (2010)
10515	0	6274	ph_olive_1	0.009	11		Oligocene	OlMs.sh.c	Dolati (2010)
10516	0	6274	ph_olive_1	0.010	11		Oligocene	OlMs.sh.c	Dolati (2010)
10517	0	6274	ph_olive_1	0.024	11		Oligocene	OlMs.sh.c	Dolati (2010)
10523	0	6238	ph_olive_1	0.001	11		Oligocene	OlMs.sh.c	Dolati (2010)

GSI NEXUS

Table S3. Summary of mapped polygons for the $M^{s.sh}$ Unit.

OBJECTID_1	Join_Count	TARGET_FID	Label	Shape_Area (sqkm)	ORIG_FID	Absolute_Age	Age_paleontology	Unit	Reference
4250	0	4250	ph_blue	0.013	8	13.7 - 6.0M	Oligocene- Late Maiocene	Ms.sh	Dolati (2010)
4251	0	4251	ph_blue	0.035	8	13.7 - 6.0M	Oligocene- Late Maiocene	Ms.sh	Dolati (2010)
4252	0	4252	ph_blue	0.028	8	13.7 - 6.0M	Oligocene- Late Maiocene	Ms.sh	Dolati (2010)
4253	0	4253	ph_blue	0.891	8	13.7 - 6.0M	Oligocene- Late Maiocene	Ms.sh	Dolati (2010)
4254	0	4254	ph_blue	0.010	8	13.7 - 6.0M	Oligocene- Late Maiocene	Ms.sh	Dolati (2010)
4255	0	4255	ph_blue	0.015	8	13.7 - 6.0M	Oligocene- Late Maiocene	Ms.sh	Dolati (2010)
4256	0	4256	ph_blue	0.073	8	13.7 - 6.0M	Oligocene- Late Maiocene	Ms.sh	Dolati (2010)
4257	0	4257	ph_blue	0.111	8	13.7 - 6.0M	Oligocene- Late Maiocene	Ms.sh	Dolati (2010)
4258	0	4258	ph_blue	0.451	8	13.7 - 6.0M	Oligocene- Late Maiocene	Ms.sh	Dolati (2010)
4259	0	4259	ph_blue	0.036	8	13.7 - 6.0M	Oligocene- Late Maiocene	Ms.sh	Dolati (2010)
4260	0	4260	ph_blue	0.527	8	13.7 - 6.0M	Oligocene- Late Maiocene	Ms.sh	Dolati (2010)
4261	0	4261	ph_blue	0.282	8	13.7 - 6.0M	Oligocene- Late Maiocene	Ms.sh	Dolati (2010)
4262	0	4262	ph_blue	0.051	8	13.7 - 6.0M	Oligocene- Late Maiocene	Ms.sh	Dolati (2010)
4263	0	4263	ph_blue	0.353	8	13.7 - 6.0M	Oligocene- Late Maiocene	Ms.sh	Dolati (2010)
4264	0	4264	ph_blue	0.540	8	13.7 - 6.0M	Oligocene- Late Maiocene	Ms.sh	Dolati (2010)
4265	0	4265	ph_blue	0.017	8	13.7 - 6.0M	Oligocene- Late Maiocene	Ms.sh	Dolati (2010)
4266	0	4266	ph_blue	0.096	8	13.7 - 6.0M	Oligocene- Late Maiocene	Ms.sh	Dolati (2010)
4267	0	4267	ph_blue	0.012	8	13.7 - 6.0M	Oligocene- Late Maiocene	Ms.sh	Dolati (2010)
4268	0	4268	ph_blue	0.051	8	13.7 - 6.0M	Oligocene- Late Maiocene	Ms.sh	Dolati (2010)
4269	0	4269	ph_blue	0.058	8	13.7 - 6.0M	Oligocene- Late Maiocene	Ms.sh	Dolati (2010)
4270	0	4270	ph_blue	0.024	8	13.7 - 6.0M	Oligocene- Late Maiocene	Ms.sh	Dolati (2010)
4271	0	4271	ph_blue	0.088	8	13.7 - 6.0M	Oligocene- Late Maiocene	Ms.sh	Dolati (2010)
4272	0	4272	ph_blue	0.256	8	13.7 - 6.0M	Oligocene- Late Maiocene	Ms.sh	Dolati (2010)
4273	0	4273	ph_blue	0.047	8	13.7 - 6.0M	Oligocene- Late Maiocene	Ms.sh	Dolati (2010)
4274	0	4274	ph_blue	7.590	8	13.7 - 6.0M	Oligocene- Late Maiocene	Ms.sh	Dolati (2010)
4275	0	4275	ph_blue	0.111	8	13.7 - 6.0M	Oligocene- Late Maiocene	Ms.sh	Dolati (2010)
4276	0	4276	ph_blue	0.028	8	13.7 - 6.0M	Oligocene- Late Maiocene	Ms.sh	Dolati (2010)
4277	0	4277	ph_blue	0.120	8	13.7 - 6.0M	Oligocene- Late Maiocene	Ms.sh	Dolati (2010)
4278	0	4278	ph_blue	0.134	8	13.7 - 6.0M	Oligocene- Late Maiocene	Ms.sh	Dolati (2010)
4279	0	4279	ph_blue	0.071	8	13.7 - 6.0M	Oligocene- Late Maiocene	Ms.sh	Dolati (2010)
4280	0	4280	ph_blue	0.029	8	13.7 - 6.0M	Oligocene- Late Maiocene	Ms.sh	Dolati (2010)
4281	0	4281	ph_blue	0.081	8	13.7 - 6.0M	Oligocene- Late Maiocene	Ms.sh	Dolati (2010)
4282	0	4282	ph_blue	0.064	8	13.7 - 6.0M	Oligocene- Late Maiocene	Ms.sh	Dolati (2010)
4283	0	4283	ph_blue	0.203	8	13.7 - 6.0M	Oligocene- Late Maiocene	Ms.sh	Dolati (2010)
4284	0	4284	ph_blue	0.092	8	13.7 - 6.0M	Oligocene- Late Maiocene	Ms.sh	Dolati (2010)
4285	0	4285	ph_blue	0.152	8	13.7 - 6.0M	Oligocene- Late Maiocene	Ms.sh	Dolati (2010)
4286	0	4286	ph_blue	1.332	8	13.7 - 6.0M	Oligocene- Late Maiocene	Ms.sh	Dolati (2010)

Geoinxus

OBJECTID_1	Join_Count	TARGET_FID	Label	Shape_Area (sqkm)	ORIG_FID	Absolute_Age	Age_paleontology	Unit	Reference
4287	0	4287	ph_blue	0.036	8	13.7 - 6.0M	Oligocene- Late Maiocene	Ms.sh	Dolati (2010)
4288	0	4288	ph_blue	0.049	8	13.7 - 6.0M	Oligocene- Late Maiocene	Ms.sh	Dolati (2010)
4289	0	4289	ph_blue	0.131	8	13.7 - 6.0M	Oligocene- Late Maiocene	Ms.sh	Dolati (2010)
4290	0	4290	ph_blue	0.022	8	13.7 - 6.0M	Oligocene- Late Maiocene	Ms.sh	Dolati (2010)
4291	0	4291	ph_blue	0.586	8	13.7 - 6.0M	Oligocene- Late Maiocene	Ms.sh	Dolati (2010)
4292	0	4292	ph_blue	1.085	8	13.7 - 6.0M	Oligocene- Late Maiocene	Ms.sh	Dolati (2010)
4293	0	4293	ph_blue	1.207	8	13.7 - 6.0M	Oligocene- Late Maiocene	Ms.sh	Dolati (2010)
4294	0	4294	ph_blue	0.025	8	13.7 - 6.0M	Oligocene- Late Maiocene	Ms.sh	Dolati (2010)
4295	0	4295	ph_blue	0.229	8	13.7 - 6.0M	Oligocene- Late Maiocene	Ms.sh	Dolati (2010)
4296	0	4296	ph_blue	0.030	8	13.7 - 6.0M	Oligocene- Late Maiocene	Ms.sh	Dolati (2010)
4297	0	4297	ph_blue	0.532	8	13.7 - 6.0M	Oligocene- Late Maiocene	Ms.sh	Dolati (2010)
4298	0	4298	ph_blue	0.791	8	13.7 - 6.0M	Oligocene- Late Maiocene	Ms.sh	Dolati (2010)
4299	0	4299	ph_blue	0.027	8	13.7 - 6.0M	Oligocene- Late Maiocene	Ms.sh	Dolati (2010)
4300	0	4300	ph_blue	0.025	8	13.7 - 6.0M	Oligocene- Late Maiocene	Ms.sh	Dolati (2010)
4301	0	4301	ph_blue	0.050	8	13.7 - 6.0M	Oligocene- Late Maiocene	Ms.sh	Dolati (2010)
4302	0	4302	ph_blue	0.024	8	13.7 - 6.0M	Oligocene- Late Maiocene	Ms.sh	Dolati (2010)
4303	0	4303	ph_blue	0.595	8	13.7 - 6.0M	Oligocene- Late Maiocene	Ms.sh	Dolati (2010)
4304	0	4304	ph_blue	0.166	8	13.7 - 6.0M	Oligocene- Late Maiocene	Ms.sh	Dolati (2010)
4305	0	4305	ph_blue	0.972	8	13.7 - 6.0M	Oligocene- Late Maiocene	Ms.sh	Dolati (2010)
4306	0	4306	ph_blue	0.041	8	13.7 - 6.0M	Oligocene- Late Maiocene	Ms.sh	Dolati (2010)
4307	0	4307	ph_blue	0.273	8	13.7 - 6.0M	Oligocene- Late Maiocene	Ms.sh	Dolati (2010)
4308	0	4308	ph_blue	0.283	8	13.7 - 6.0M	Oligocene- Late Maiocene	Ms.sh	Dolati (2010)
4309	0	4309	ph_blue	0.100	8	13.7 - 6.0M	Oligocene- Late Maiocene	Ms.sh	Dolati (2010)
4310	0	4310	ph_blue	0.019	8	13.7 - 6.0M	Oligocene- Late Maiocene	Ms.sh	Dolati (2010)
4311	0	4311	ph_blue	0.019	8	13.7 - 6.0M	Oligocene- Late Maiocene	Ms.sh	Dolati (2010)
4312	0	4312	ph_blue	0.885	8	13.7 - 6.0M	Oligocene- Late Maiocene	Ms.sh	Dolati (2010)
4313	0	4313	ph_blue	0.725	8	13.7 - 6.0M	Oligocene- Late Maiocene	Ms.sh	Dolati (2010)
4314	0	4314	ph_blue	0.028	8	13.7 - 6.0M	Oligocene- Late Maiocene	Ms.sh	Dolati (2010)
4315	0	4315	ph_blue	0.231	8	13.7 - 6.0M	Oligocene- Late Maiocene	Ms.sh	Dolati (2010)
4316	0	4316	ph_blue	1.189	8	13.7 - 6.0M	Oligocene- Late Maiocene	Ms.sh	Dolati (2010)
4317	0	4317	ph_blue	0.198	8	13.7 - 6.0M	Oligocene- Late Maiocene	Ms.sh	Dolati (2010)
4318	0	4318	ph_blue	0.012	8	13.7 - 6.0M	Oligocene- Late Maiocene	Ms.sh	Dolati (2010)
4319	0	4319	ph_blue	0.022	8	13.7 - 6.0M	Oligocene- Late Maiocene	Ms.sh	Dolati (2010)
4320	0	4320	ph_blue	0.073	8	13.7 - 6.0M	Oligocene- Late Maiocene	Ms.sh	Dolati (2010)
4321	0	4321	ph_blue	0.844	8	13.7 - 6.0M	Oligocene- Late Maiocene	Ms.sh	Dolati (2010)
4322	0	4322	ph_blue	0.242	8	13.7 - 6.0M	Oligocene- Late Maiocene	Ms.sh	Dolati (2010)
4323	0	4323	ph_blue	0.137	8	13.7 - 6.0M	Oligocene- Late Maiocene	Ms.sh	Dolati (2010)
4324	0	4324	ph_blue	0.059	8	13.7 - 6.0M	Oligocene- Late Maiocene	Ms.sh	Dolati (2010)
4325	0	4325	ph_blue	0.007	8	13.7 - 6.0M	Oligocene- Late Maiocene	Ms.sh	Dolati (2010)

GeoNews

OBJECTID_1	Join_Count	TARGET_FID	Label	Shape_Area (sqkm)	ORIG_FID	Absolute_Age	Age_paleontology	Unit	Reference
4326	0	4326	ph_blue	0.106	8	13.7 - 6.0M	Oligocene- Late Maiocene	Ms.sh	Dolati (2010)
4327	0	4327	ph_blue	0.070	8	13.7 - 6.0M	Oligocene- Late Maiocene	Ms.sh	Dolati (2010)
4328	0	4328	ph_blue	0.092	8	13.7 - 6.0M	Oligocene- Late Maiocene	Ms.sh	Dolati (2010)
4329	0	4329	ph_blue	0.021	8	13.7 - 6.0M	Oligocene- Late Maiocene	Ms.sh	Dolati (2010)
4330	0	4330	ph_blue	0.016	8	13.7 - 6.0M	Oligocene- Late Maiocene	Ms.sh	Dolati (2010)
4331	0	4331	ph_blue	0.058	8	13.7 - 6.0M	Oligocene- Late Maiocene	Ms.sh	Dolati (2010)
4332	0	4332	ph_blue	0.334	8	13.7 - 6.0M	Oligocene- Late Maiocene	Ms.sh	Dolati (2010)
4333	0	4333	ph_blue	0.014	8	13.7 - 6.0M	Oligocene- Late Maiocene	Ms.sh	Dolati (2010)
4334	0	4334	ph_blue	0.034	8	13.7 - 6.0M	Oligocene- Late Maiocene	Ms.sh	Dolati (2010)
4335	0	4335	ph_blue	0.146	8	13.7 - 6.0M	Oligocene- Late Maiocene	Ms.sh	Dolati (2010)
4336	0	4336	ph_blue	0.875	8	13.7 - 6.0M	Oligocene- Late Maiocene	Ms.sh	Dolati (2010)
4337	0	4337	ph_blue	0.423	8	13.7 - 6.0M	Oligocene- Late Maiocene	Ms.sh	Dolati (2010)
4338	0	4338	ph_blue	0.040	8	13.7 - 6.0M	Oligocene- Late Maiocene	Ms.sh	Dolati (2010)
4339	0	4339	ph_blue	0.082	8	13.7 - 6.0M	Oligocene- Late Maiocene	Ms.sh	Dolati (2010)
4340	0	4340	ph_blue	0.023	8	13.7 - 6.0M	Oligocene- Late Maiocene	Ms.sh	Dolati (2010)
4341	0	4341	ph_blue	0.274	8	13.7 - 6.0M	Oligocene- Late Maiocene	Ms.sh	Dolati (2010)
4342	0	4342	ph_blue	0.072	8	13.7 - 6.0M	Oligocene- Late Maiocene	Ms.sh	Dolati (2010)
4343	0	4343	ph_blue	0.045	8	13.7 - 6.0M	Oligocene- Late Maiocene	Ms.sh	Dolati (2010)
4344	0	4344	ph_blue	0.389	8	13.7 - 6.0M	Oligocene- Late Maiocene	Ms.sh	Dolati (2010)
4345	0	4345	ph_blue	0.040	8	13.7 - 6.0M	Oligocene- Late Maiocene	Ms.sh	Dolati (2010)
4346	0	4346	ph_blue	0.031	8	13.7 - 6.0M	Oligocene- Late Maiocene	Ms.sh	Dolati (2010)
4347	0	4347	ph_blue	0.202	8	13.7 - 6.0M	Oligocene- Late Maiocene	Ms.sh	Dolati (2010)
4348	0	4348	ph_blue	0.019	8	13.7 - 6.0M	Oligocene- Late Maiocene	Ms.sh	Dolati (2010)
4349	0	4349	ph_blue	0.040	8	13.7 - 6.0M	Oligocene- Late Maiocene	Ms.sh	Dolati (2010)
4350	0	4350	ph_blue	0.980	8	13.7 - 6.0M	Oligocene- Late Maiocene	Ms.sh	Dolati (2010)
4351	0	4351	ph_blue	1.838	8	13.7 - 6.0M	Oligocene- Late Maiocene	Ms.sh	Dolati (2010)
4352	0	4352	ph_blue	0.013	8	13.7 - 6.0M	Oligocene- Late Maiocene	Ms.sh	Dolati (2010)
4353	0	4353	ph_blue	0.052	8	13.7 - 6.0M	Oligocene- Late Maiocene	Ms.sh	Dolati (2010)
4354	0	4354	ph_blue	0.657	8	13.7 - 6.0M	Oligocene- Late Maiocene	Ms.sh	Dolati (2010)
4355	0	4355	ph_blue	0.484	8	13.7 - 6.0M	Oligocene- Late Maiocene	Ms.sh	Dolati (2010)
4356	0	4356	ph_blue	0.338	8	13.7 - 6.0M	Oligocene- Late Maiocene	Ms.sh	Dolati (2010)
4357	0	4357	ph_blue	0.056	8	13.7 - 6.0M	Oligocene- Late Maiocene	Ms.sh	Dolati (2010)
4358	0	4358	ph_blue	0.015	8	13.7 - 6.0M	Oligocene- Late Maiocene	Ms.sh	Dolati (2010)
4359	0	4359	ph_blue	0.147	8	13.7 - 6.0M	Oligocene- Late Maiocene	Ms.sh	Dolati (2010)
4360	0	4360	ph_blue	0.091	8	13.7 - 6.0M	Oligocene- Late Maiocene	Ms.sh	Dolati (2010)
4361	0	4361	ph_blue	0.589	8	13.7 - 6.0M	Oligocene- Late Maiocene	Ms.sh	Dolati (2010)
4362	0	4362	ph_blue	0.076	8	13.7 - 6.0M	Oligocene- Late Maiocene	Ms.sh	Dolati (2010)
4363	0	4363	ph_blue	0.074	8	13.7 - 6.0M	Oligocene- Late Maiocene	Ms.sh	Dolati (2010)
4364	0	4364	ph_blue	0.390	8	13.7 - 6.0M	Oligocene- Late Maiocene	Ms.sh	Dolati (2010)

Geonics

OBJECTID_1	Join_Count	TARGET_FID	Label	Shape_Area (sqkm)	ORIG_FID	Absolute_Age	Age_paleontology	Unit	Reference
4365	0	4365	ph_blue	0.787	8	13.7 - 6.0M	Oligocene- Late Maiocene	Ms.sh	Dolati (2010)
4366	0	4366	ph_blue	0.152	8	13.7 - 6.0M	Oligocene- Late Maiocene	Ms.sh	Dolati (2010)
4367	0	4367	ph_blue	0.031	8	13.7 - 6.0M	Oligocene- Late Maiocene	Ms.sh	Dolati (2010)
4368	0	4368	ph_blue	0.254	8	13.7 - 6.0M	Oligocene- Late Maiocene	Ms.sh	Dolati (2010)
4369	0	4369	ph_blue	0.537	8	13.7 - 6.0M	Oligocene- Late Maiocene	Ms.sh	Dolati (2010)
4370	0	4370	ph_blue	0.401	8	13.7 - 6.0M	Oligocene- Late Maiocene	Ms.sh	Dolati (2010)
4371	0	4371	ph_blue	0.024	8	13.7 - 6.0M	Oligocene- Late Maiocene	Ms.sh	Dolati (2010)
4372	0	4372	ph_blue	0.534	8	13.7 - 6.0M	Oligocene- Late Maiocene	Ms.sh	Dolati (2010)
4373	0	4373	ph_blue	0.059	8	13.7 - 6.0M	Oligocene- Late Maiocene	Ms.sh	Dolati (2010)
4374	0	4374	ph_blue	1.165	8	13.7 - 6.0M	Oligocene- Late Maiocene	Ms.sh	Dolati (2010)
4375	0	4375	ph_blue	0.025	8	13.7 - 6.0M	Oligocene- Late Maiocene	Ms.sh	Dolati (2010)
4376	0	4376	ph_blue	0.360	8	13.7 - 6.0M	Oligocene- Late Maiocene	Ms.sh	Dolati (2010)
4377	0	4377	ph_blue	0.342	8	13.7 - 6.0M	Oligocene- Late Maiocene	Ms.sh	Dolati (2010)
4378	0	4378	ph_blue	0.545	8	13.7 - 6.0M	Oligocene- Late Maiocene	Ms.sh	Dolati (2010)
4379	0	4379	ph_blue	1.123	8	13.7 - 6.0M	Oligocene- Late Maiocene	Ms.sh	Dolati (2010)
4380	0	4380	ph_blue	0.446	8	13.7 - 6.0M	Oligocene- Late Maiocene	Ms.sh	Dolati (2010)
4381	0	4381	ph_blue	0.572	8	13.7 - 6.0M	Oligocene- Late Maiocene	Ms.sh	Dolati (2010)
4382	0	4382	ph_blue	0.282	8	13.7 - 6.0M	Oligocene- Late Maiocene	Ms.sh	Dolati (2010)
4383	0	4383	ph_blue	0.196	8	13.7 - 6.0M	Oligocene- Late Maiocene	Ms.sh	Dolati (2010)
4384	0	4384	ph_blue	0.023	8	13.7 - 6.0M	Oligocene- Late Maiocene	Ms.sh	Dolati (2010)
4385	0	4385	ph_blue	0.011	8	13.7 - 6.0M	Oligocene- Late Maiocene	Ms.sh	Dolati (2010)
4386	0	4386	ph_blue	0.042	8	13.7 - 6.0M	Oligocene- Late Maiocene	Ms.sh	Dolati (2010)
4387	0	4387	ph_blue	0.378	8	13.7 - 6.0M	Oligocene- Late Maiocene	Ms.sh	Dolati (2010)
4388	0	4388	ph_blue	0.157	8	13.7 - 6.0M	Oligocene- Late Maiocene	Ms.sh	Dolati (2010)
4389	0	4389	ph_blue	1.826	8	13.7 - 6.0M	Oligocene- Late Maiocene	Ms.sh	Dolati (2010)
4390	0	4390	ph_blue	4.670	8	13.7 - 6.0M	Oligocene- Late Maiocene	Ms.sh	Dolati (2010)
4391	0	4391	ph_blue	0.107	8	13.7 - 6.0M	Oligocene- Late Maiocene	Ms.sh	Dolati (2010)
4392	0	4392	ph_blue	0.934	8	13.7 - 6.0M	Oligocene- Late Maiocene	Ms.sh	Dolati (2010)
4393	0	4393	ph_blue	0.379	8	13.7 - 6.0M	Oligocene- Late Maiocene	Ms.sh	Dolati (2010)
4394	0	4394	ph_blue	0.310	8	13.7 - 6.0M	Oligocene- Late Maiocene	Ms.sh	Dolati (2010)
4395	0	4395	ph_blue	1.174	8	13.7 - 6.0M	Oligocene- Late Maiocene	Ms.sh	Dolati (2010)
4396	0	4396	ph_blue	0.094	8	13.7 - 6.0M	Oligocene- Late Maiocene	Ms.sh	Dolati (2010)
4397	0	4397	ph_blue	0.041	8	13.7 - 6.0M	Oligocene- Late Maiocene	Ms.sh	Dolati (2010)
4398	0	4398	ph_blue	0.050	8	13.7 - 6.0M	Oligocene- Late Maiocene	Ms.sh	Dolati (2010)
4399	0	4399	ph_blue	1.394	8	13.7 - 6.0M	Oligocene- Late Maiocene	Ms.sh	Dolati (2010)
4400	0	4400	ph_blue	0.128	8	13.7 - 6.0M	Oligocene- Late Maiocene	Ms.sh	Dolati (2010)
4401	0	4401	ph_blue	0.168	8	13.7 - 6.0M	Oligocene- Late Maiocene	Ms.sh	Dolati (2010)
4402	0	4402	ph_blue	2.051	8	13.7 - 6.0M	Oligocene- Late Maiocene	Ms.sh	Dolati (2010)
4403	0	4403	ph_blue	0.052	8	13.7 - 6.0M	Oligocene- Late Maiocene	Ms.sh	Dolati (2010)

Geonews

OBJECTID_1	Join_Count	TARGET_FID	Label	Shape_Area (sqkm)	ORIG_FID	Absolute_Age	Age_paleontology	Unit	Reference
4404	0	4404	ph_blue	0.313	8	13.7 - 6.0M	Oligocene- Late Maiocene	Ms.sh	Dolati (2010)
4405	0	4405	ph_blue	0.307	8	13.7 - 6.0M	Oligocene- Late Maiocene	Ms.sh	Dolati (2010)
4406	0	4406	ph_blue	0.731	8	13.7 - 6.0M	Oligocene- Late Maiocene	Ms.sh	Dolati (2010)
4407	0	4407	ph_blue	0.201	8	13.7 - 6.0M	Oligocene- Late Maiocene	Ms.sh	Dolati (2010)
4408	0	4408	ph_blue	0.599	8	13.7 - 6.0M	Oligocene- Late Maiocene	Ms.sh	Dolati (2010)
4409	0	4409	ph_blue	0.121	8	13.7 - 6.0M	Oligocene- Late Maiocene	Ms.sh	Dolati (2010)
4410	0	4410	ph_blue	0.241	8	13.7 - 6.0M	Oligocene- Late Maiocene	Ms.sh	Dolati (2010)
4411	0	4411	ph_blue	0.016	8	13.7 - 6.0M	Oligocene- Late Maiocene	Ms.sh	Dolati (2010)
4412	0	4412	ph_blue	0.958	8	13.7 - 6.0M	Oligocene- Late Maiocene	Ms.sh	Dolati (2010)
4413	0	4413	ph_blue	1.132	8	13.7 - 6.0M	Oligocene- Late Maiocene	Ms.sh	Dolati (2010)
4414	0	4414	ph_blue	0.219	8	13.7 - 6.0M	Oligocene- Late Maiocene	Ms.sh	Dolati (2010)
4415	0	4415	ph_blue	8.392	8	13.7 - 6.0M	Oligocene- Late Maiocene	Ms.sh	Dolati (2010)
4416	0	4416	ph_blue	0.345	8	13.7 - 6.0M	Oligocene- Late Maiocene	Ms.sh	Dolati (2010)
4417	0	4417	ph_blue	0.224	8	13.7 - 6.0M	Oligocene- Late Maiocene	Ms.sh	Dolati (2010)
4418	0	4418	ph_blue	1.014	8	13.7 - 6.0M	Oligocene- Late Maiocene	Ms.sh	Dolati (2010)
4419	0	4419	ph_blue	0.264	8	13.7 - 6.0M	Oligocene- Late Maiocene	Ms.sh	Dolati (2010)
4420	0	4420	ph_blue	0.386	8	13.7 - 6.0M	Oligocene- Late Maiocene	Ms.sh	Dolati (2010)
4421	0	4421	ph_blue	0.590	8	13.7 - 6.0M	Oligocene- Late Maiocene	Ms.sh	Dolati (2010)
4422	0	4422	ph_blue	0.281	8	13.7 - 6.0M	Oligocene- Late Maiocene	Ms.sh	Dolati (2010)
4423	0	4423	ph_blue	0.025	8	13.7 - 6.0M	Oligocene- Late Maiocene	Ms.sh	Dolati (2010)
4424	0	4424	ph_blue	0.620	8	13.7 - 6.0M	Oligocene- Late Maiocene	Ms.sh	Dolati (2010)
4425	0	4425	ph_blue	0.135	8	13.7 - 6.0M	Oligocene- Late Maiocene	Ms.sh	Dolati (2010)
4427	0	4427	ph_blue	0.373	8	13.7 - 6.0M	Oligocene- Late Maiocene	Ms.sh	Dolati (2010)
4428	0	4428	ph_blue	0.259	8	13.7 - 6.0M	Oligocene- Late Maiocene	Ms.sh	Dolati (2010)
4429	0	4429	ph_blue	0.134	8	13.7 - 6.0M	Oligocene- Late Maiocene	Ms.sh	Dolati (2010)
4430	0	4430	ph_blue	0.321	8	13.7 - 6.0M	Oligocene- Late Maiocene	Ms.sh	Dolati (2010)
4431	0	4431	ph_blue	1.974	8	13.7 - 6.0M	Oligocene- Late Maiocene	Ms.sh	Dolati (2010)
4432	0	4432	ph_blue	0.091	8	13.7 - 6.0M	Oligocene- Late Maiocene	Ms.sh	Dolati (2010)
4433	0	4433	ph_blue	0.416	8	13.7 - 6.0M	Oligocene- Late Maiocene	Ms.sh	Dolati (2010)
4434	0	4434	ph_blue	1.480	8	13.7 - 6.0M	Oligocene- Late Maiocene	Ms.sh	Dolati (2010)
4435	0	4435	ph_blue	1.192	8	13.7 - 6.0M	Oligocene- Late Maiocene	Ms.sh	Dolati (2010)
4436	0	4436	ph_blue	1.238	8	13.7 - 6.0M	Oligocene- Late Maiocene	Ms.sh	Dolati (2010)
4437	0	4437	ph_blue	0.509	8	13.7 - 6.0M	Oligocene- Late Maiocene	Ms.sh	Dolati (2010)
4438	0	4438	ph_blue	0.329	8	13.7 - 6.0M	Oligocene- Late Maiocene	Ms.sh	Dolati (2010)
4439	0	4439	ph_blue	0.261	8	13.7 - 6.0M	Oligocene- Late Maiocene	Ms.sh	Dolati (2010)
4440	0	4440	ph_blue	16.783	8	13.7 - 6.0M	Oligocene- Late Maiocene	Ms.sh	Dolati (2010)
4441	0	4441	ph_blue	1.824	8	13.7 - 6.0M	Oligocene- Late Maiocene	Ms.sh	Dolati (2010)
4442	0	4442	ph_blue	0.320	8	13.7 - 6.0M	Oligocene- Late Maiocene	Ms.sh	Dolati (2010)
4443	0	4443	ph_blue	0.367	8	13.7 - 6.0M	Oligocene- Late Maiocene	Ms.sh	Dolati (2010)

Geonets

OBJECTID_1	Join_Count	TARGET_FID	Label	Shape_Area (sqkm)	ORIG_FID	Absolute_Age	Age_paleontology	Unit	Reference
4444	0	4444	ph_blue	1.820	8	13.7 - 6.0M	Oligocene- Late Maiocene	Ms.sh	Dolati (2010)
4445	0	4445	ph_blue	0.174	8	13.7 - 6.0M	Oligocene- Late Maiocene	Ms.sh	Dolati (2010)
4446	0	4446	ph_blue	0.480	8	13.7 - 6.0M	Oligocene- Late Maiocene	Ms.sh	Dolati (2010)
4447	0	4447	ph_blue	0.264	8	13.7 - 6.0M	Oligocene- Late Maiocene	Ms.sh	Dolati (2010)
4448	0	4448	ph_blue	0.540	8	13.7 - 6.0M	Oligocene- Late Maiocene	Ms.sh	Dolati (2010)
4449	0	4449	ph_blue	0.020	8	13.7 - 6.0M	Oligocene- Late Maiocene	Ms.sh	Dolati (2010)
4450	0	4450	ph_blue	0.357	8	13.7 - 6.0M	Oligocene- Late Maiocene	Ms.sh	Dolati (2010)
4451	0	4451	ph_blue	0.056	8	13.7 - 6.0M	Oligocene- Late Maiocene	Ms.sh	Dolati (2010)
4452	0	4452	ph_blue	0.184	8	13.7 - 6.0M	Oligocene- Late Maiocene	Ms.sh	Dolati (2010)
4453	0	4453	ph_blue	8.442	8	13.7 - 6.0M	Oligocene- Late Maiocene	Ms.sh	Dolati (2010)
4454	0	4454	ph_blue	0.071	8	13.7 - 6.0M	Oligocene- Late Maiocene	Ms.sh	Dolati (2010)
4455	0	4455	ph_blue	0.093	8	13.7 - 6.0M	Oligocene- Late Maiocene	Ms.sh	Dolati (2010)
4456	0	4456	ph_blue	0.071	8	13.7 - 6.0M	Oligocene- Late Maiocene	Ms.sh	Dolati (2010)
4457	0	4457	ph_blue	0.626	8	13.7 - 6.0M	Oligocene- Late Maiocene	Ms.sh	Dolati (2010)
4458	0	4458	ph_blue	0.155	8	13.7 - 6.0M	Oligocene- Late Maiocene	Ms.sh	Dolati (2010)
4459	0	4459	ph_blue	0.310	8	13.7 - 6.0M	Oligocene- Late Maiocene	Ms.sh	Dolati (2010)
4460	0	4460	ph_blue	0.277	8	13.7 - 6.0M	Oligocene- Late Maiocene	Ms.sh	Dolati (2010)
4461	0	4461	ph_blue	1.484	8	13.7 - 6.0M	Oligocene- Late Maiocene	Ms.sh	Dolati (2010)
4462	0	4462	ph_blue	1.309	8	13.7 - 6.0M	Oligocene- Late Maiocene	Ms.sh	Dolati (2010)
4463	0	4463	ph_blue	2.099	8	13.7 - 6.0M	Oligocene- Late Maiocene	Ms.sh	Dolati (2010)
4464	0	4464	ph_blue	0.441	8	13.7 - 6.0M	Oligocene- Late Maiocene	Ms.sh	Dolati (2010)
4465	0	4465	ph_blue	0.053	8	13.7 - 6.0M	Oligocene- Late Maiocene	Ms.sh	Dolati (2010)
4466	0	4466	ph_blue	0.494	8	13.7 - 6.0M	Oligocene- Late Maiocene	Ms.sh	Dolati (2010)
4467	0	4467	ph_blue	0.472	8	13.7 - 6.0M	Oligocene- Late Maiocene	Ms.sh	Dolati (2010)
4468	0	4468	ph_blue	0.077	8	13.7 - 6.0M	Oligocene- Late Maiocene	Ms.sh	Dolati (2010)
4469	0	4469	ph_blue	0.196	8	13.7 - 6.0M	Oligocene- Late Maiocene	Ms.sh	Dolati (2010)
4470	0	4470	ph_blue	0.438	8	13.7 - 6.0M	Oligocene- Late Maiocene	Ms.sh	Dolati (2010)
4471	0	4471	ph_blue	0.100	8	13.7 - 6.0M	Oligocene- Late Maiocene	Ms.sh	Dolati (2010)
4472	0	4472	ph_blue	0.713	8	13.7 - 6.0M	Oligocene- Late Maiocene	Ms.sh	Dolati (2010)
4473	0	4473	ph_blue	0.094	8	13.7 - 6.0M	Oligocene- Late Maiocene	Ms.sh	Dolati (2010)
4474	0	4474	ph_blue	0.254	8	13.7 - 6.0M	Oligocene- Late Maiocene	Ms.sh	Dolati (2010)
4475	0	4475	ph_blue	0.144	8	13.7 - 6.0M	Oligocene- Late Maiocene	Ms.sh	Dolati (2010)
4476	0	4476	ph_blue	0.362	8	13.7 - 6.0M	Oligocene- Late Maiocene	Ms.sh	Dolati (2010)
4477	0	4477	ph_blue	1.068	8	13.7 - 6.0M	Oligocene- Late Maiocene	Ms.sh	Dolati (2010)
4478	0	4478	ph_blue	0.184	8	13.7 - 6.0M	Oligocene- Late Maiocene	Ms.sh	Dolati (2010)
4479	0	4479	ph_blue	0.065	8	13.7 - 6.0M	Oligocene- Late Maiocene	Ms.sh	Dolati (2010)
4480	0	4480	ph_blue	0.035	8	13.7 - 6.0M	Oligocene- Late Maiocene	Ms.sh	Dolati (2010)
4481	0	4481	ph_blue	2.084	8	13.7 - 6.0M	Oligocene- Late Maiocene	Ms.sh	Dolati (2010)
4482	0	4482	ph_blue	0.518	8	13.7 - 6.0M	Oligocene- Late Maiocene	Ms.sh	Dolati (2010)

GeoNews

OBJECTID_1	Join_Count	TARGET_FID	Label	Shape_Area (sqkm)	ORIG_FID	Absolute_Age	Age_paleontology	Unit	Reference
4484	0	4484	ph_blue	0.767	8	13.7 - 6.0M	Oligocene- Late Maiocene	Ms.sh	Dolati (2010)
4485	0	4485	ph_blue	0.167	8	13.7 - 6.0M	Oligocene- Late Maiocene	Ms.sh	Dolati (2010)
4486	0	4486	ph_blue	79.413	8	13.7 - 6.0M	Oligocene- Late Maiocene	Ms.sh	Dolati (2010)
4487	0	4487	ph_blue	0.806	8	13.7 - 6.0M	Oligocene- Late Maiocene	Ms.sh	Dolati (2010)
4488	0	4488	ph_blue	123.488	8	13.7 - 6.0M	Oligocene- Late Maiocene	Ms.sh	Dolati (2010)
4489	0	4489	ph_blue	0.254	8	13.7 - 6.0M	Oligocene- Late Maiocene	Ms.sh	Dolati (2010)
4490	0	4490	ph_blue	0.030	8	13.7 - 6.0M	Oligocene- Late Maiocene	Ms.sh	Dolati (2010)
4492	0	4492	ph_blue	2.911	8	13.7 - 6.0M	Oligocene- Late Maiocene	Ms.sh	Dolati (2010)
4493	0	4493	ph_blue	0.848	8	13.7 - 6.0M	Oligocene- Late Maiocene	Ms.sh	Dolati (2010)
4494	0	4494	ph_blue	0.581	8	13.7 - 6.0M	Oligocene- Late Maiocene	Ms.sh	Dolati (2010)
4495	0	4495	ph_blue	6.116	8	13.7 - 6.0M	Oligocene- Late Maiocene	Ms.sh	Dolati (2010)
4496	0	4496	ph_blue	0.205	8	13.7 - 6.0M	Oligocene- Late Maiocene	Ms.sh	Dolati (2010)
4498	0	4498	ph_blue	26.369	8	13.7 - 6.0M	Oligocene- Late Maiocene	Ms.sh	Dolati (2010)
4499	0	4499	ph_blue	2.030	8	13.7 - 6.0M	Oligocene- Late Maiocene	Ms.sh	Dolati (2010)
4501	0	4501	ph_blue	0.040	8	13.7 - 6.0M	Oligocene- Late Maiocene	Ms.sh	Dolati (2010)
4502	0	4502	ph_blue	2.739	8	13.7 - 6.0M	Oligocene- Late Maiocene	Ms.sh	Dolati (2010)
4503	0	4503	ph_blue	0.547	8	13.7 - 6.0M	Oligocene- Late Maiocene	Ms.sh	Dolati (2010)
4504	0	4504	ph_blue	0.126	8	13.7 - 6.0M	Oligocene- Late Maiocene	Ms.sh	Dolati (2010)
4505	0	4505	ph_blue	0.114	8	13.7 - 6.0M	Oligocene- Late Maiocene	Ms.sh	Dolati (2010)
4506	0	4506	ph_blue	0.017	8	13.7 - 6.0M	Oligocene- Late Maiocene	Ms.sh	Dolati (2010)
4508	0	4508	ph_blue	0.019	8	13.7 - 6.0M	Oligocene- Late Maiocene	Ms.sh	Dolati (2010)
4509	0	4509	ph_blue	0.021	8	13.7 - 6.0M	Oligocene- Late Maiocene	Ms.sh	Dolati (2010)
4510	0	4510	ph_blue	2.738	8	13.7 - 6.0M	Oligocene- Late Maiocene	Ms.sh	Dolati (2010)
4511	0	4512	ph_blue	0.380	8	13.7 - 6.0M	Oligocene- Late Maiocene	Ms.sh	Dolati (2010)
4512	0	4513	ph_blue	16.248	8	13.7 - 6.0M	Oligocene- Late Maiocene	Ms.sh	Dolati (2010)
4513	0	4514	ph_blue	0.240	8	13.7 - 6.0M	Oligocene- Late Maiocene	Ms.sh	Dolati (2010)
4514	0	4515	ph_blue	2.875	8	13.7 - 6.0M	Oligocene- Late Maiocene	Ms.sh	Dolati (2010)
4515	0	4516	ph_blue	0.184	8	13.7 - 6.0M	Oligocene- Late Maiocene	Ms.sh	Dolati (2010)
4516	0	4517	ph_blue	0.563	8	13.7 - 6.0M	Oligocene- Late Maiocene	Ms.sh	Dolati (2010)
4517	0	4518	ph_blue	22.310	8	13.7 - 6.0M	Oligocene- Late Maiocene	Ms.sh	Dolati (2010)
4518	0	4519	ph_blue	0.698	8	13.7 - 6.0M	Oligocene- Late Maiocene	Ms.sh	Dolati (2010)
4519	0	4520	ph_blue	0.109	8	13.7 - 6.0M	Oligocene- Late Maiocene	Ms.sh	Dolati (2010)
4520	0	4521	ph_blue	0.691	8	13.7 - 6.0M	Oligocene- Late Maiocene	Ms.sh	Dolati (2010)
4521	0	4522	ph_blue	0.514	8	13.7 - 6.0M	Oligocene- Late Maiocene	Ms.sh	Dolati (2010)
4522	0	4523	ph_blue	2.418	8	13.7 - 6.0M	Oligocene- Late Maiocene	Ms.sh	Dolati (2010)
4523	0	4524	ph_blue	0.110	8	13.7 - 6.0M	Oligocene- Late Maiocene	Ms.sh	Dolati (2010)
4524	0	4525	ph_blue	0.256	8	13.7 - 6.0M	Oligocene- Late Maiocene	Ms.sh	Dolati (2010)
4525	0	4526	ph_blue	0.063	8	13.7 - 6.0M	Oligocene- Late Maiocene	Ms.sh	Dolati (2010)
4526	0	4527	ph_blue	2.330	8	13.7 - 6.0M	Oligocene- Late Maiocene	Ms.sh	Dolati (2010)

Preview

OBJECTID_1	Join_Count	TARGET_FID	Label	Shape_Area (sqkm)	ORIG_FID	Absolute_Age	Age_paleontology	Unit	Reference
4527	0	4528	ph_blue	0.107	8	13.7 - 6.0M	Oligocene- Late Maiocene	Ms.sh	Dolati (2010)
4528	0	4529	ph_blue	0.366	8	13.7 - 6.0M	Oligocene- Late Maiocene	Ms.sh	Dolati (2010)
4529	0	4530	ph_blue	0.888	8	13.7 - 6.0M	Oligocene- Late Maiocene	Ms.sh	Dolati (2010)
4530	0	4531	ph_blue	8.628	8	13.7 - 6.0M	Oligocene- Late Maiocene	Ms.sh	Dolati (2010)
4531	0	4532	ph_blue	0.339	8	13.7 - 6.0M	Oligocene- Late Maiocene	Ms.sh	Dolati (2010)
4532	0	4533	ph_blue	1.147	8	13.7 - 6.0M	Oligocene- Late Maiocene	Ms.sh	Dolati (2010)
4533	0	4534	ph_blue	0.126	8	13.7 - 6.0M	Oligocene- Late Maiocene	Ms.sh	Dolati (2010)
4534	0	4535	ph_blue	2.170	8	13.7 - 6.0M	Oligocene- Late Maiocene	Ms.sh	Dolati (2010)
4535	0	4536	ph_blue	1.418	8	13.7 - 6.0M	Oligocene- Late Maiocene	Ms.sh	Dolati (2010)
4536	0	4537	ph_blue	0.842	8	13.7 - 6.0M	Oligocene- Late Maiocene	Ms.sh	Dolati (2010)
4537	0	4538	ph_blue	0.110	8	13.7 - 6.0M	Oligocene- Late Maiocene	Ms.sh	Dolati (2010)
4538	0	4539	ph_blue	0.252	8	13.7 - 6.0M	Oligocene- Late Maiocene	Ms.sh	Dolati (2010)
4539	0	4540	ph_blue	0.860	8	13.7 - 6.0M	Oligocene- Late Maiocene	Ms.sh	Dolati (2010)
4540	0	4541	ph_blue	0.112	8	13.7 - 6.0M	Oligocene- Late Maiocene	Ms.sh	Dolati (2010)
4541	0	4542	ph_blue	0.290	8	13.7 - 6.0M	Oligocene- Late Maiocene	Ms.sh	Dolati (2010)
4542	0	4543	ph_blue	0.143	8	13.7 - 6.0M	Oligocene- Late Maiocene	Ms.sh	Dolati (2010)
4543	0	4544	ph_blue	0.335	8	13.7 - 6.0M	Oligocene- Late Maiocene	Ms.sh	Dolati (2010)
4544	0	4545	ph_blue	0.530	8	13.7 - 6.0M	Oligocene- Late Maiocene	Ms.sh	Dolati (2010)
4545	0	4546	ph_blue	0.201	8	13.7 - 6.0M	Oligocene- Late Maiocene	Ms.sh	Dolati (2010)
4546	0	4547	ph_blue	2.480	8	13.7 - 6.0M	Oligocene- Late Maiocene	Ms.sh	Dolati (2010)
4547	0	4548	ph_blue	1.220	8	13.7 - 6.0M	Oligocene- Late Maiocene	Ms.sh	Dolati (2010)
4548	0	4549	ph_blue	0.276	8	13.7 - 6.0M	Oligocene- Late Maiocene	Ms.sh	Dolati (2010)
4549	0	4550	ph_blue	5.362	8	13.7 - 6.0M	Oligocene- Late Maiocene	Ms.sh	Dolati (2010)
4550	0	4551	ph_blue	0.224	8	13.7 - 6.0M	Oligocene- Late Maiocene	Ms.sh	Dolati (2010)
4551	0	4552	ph_blue	0.093	8	13.7 - 6.0M	Oligocene- Late Maiocene	Ms.sh	Dolati (2010)
4552	0	4553	ph_blue	0.564	8	13.7 - 6.0M	Oligocene- Late Maiocene	Ms.sh	Dolati (2010)
4553	0	4554	ph_blue	1.771	8	13.7 - 6.0M	Oligocene- Late Maiocene	Ms.sh	Dolati (2010)
4554	0	4555	ph_blue	1.002	8	13.7 - 6.0M	Oligocene- Late Maiocene	Ms.sh	Dolati (2010)
4555	0	4556	ph_blue	0.370	8	13.7 - 6.0M	Oligocene- Late Maiocene	Ms.sh	Dolati (2010)
4556	0	4557	ph_blue	5.246	8	13.7 - 6.0M	Oligocene- Late Maiocene	Ms.sh	Dolati (2010)
4557	0	4558	ph_blue	1.605	8	13.7 - 6.0M	Oligocene- Late Maiocene	Ms.sh	Dolati (2010)
4558	0	4559	ph_blue	5.221	8	13.7 - 6.0M	Oligocene- Late Maiocene	Ms.sh	Dolati (2010)
4559	0	4560	ph_blue	0.100	8	13.7 - 6.0M	Oligocene- Late Maiocene	Ms.sh	Dolati (2010)
4560	0	4561	ph_blue	1.163	8	13.7 - 6.0M	Oligocene- Late Maiocene	Ms.sh	Dolati (2010)
4561	0	4562	ph_blue	0.245	8	13.7 - 6.0M	Oligocene- Late Maiocene	Ms.sh	Dolati (2010)
4562	0	4563	ph_blue	0.823	8	13.7 - 6.0M	Oligocene- Late Maiocene	Ms.sh	Dolati (2010)
4563	0	4564	ph_blue	0.247	8	13.7 - 6.0M	Oligocene- Late Maiocene	Ms.sh	Dolati (2010)
4564	0	4565	ph_blue	0.716	8	13.7 - 6.0M	Oligocene- Late Maiocene	Ms.sh	Dolati (2010)
4565	0	4566	ph_blue	0.221	8	13.7 - 6.0M	Oligocene- Late Maiocene	Ms.sh	Dolati (2010)

Geonews

OBJECTID_1	Join_Count	TARGET_FID	Label	Shape_Area (sqkm)	ORIG_FID	Absolute_Age	Age_paleontology	Unit	Reference
4566	0	4567	ph_blue	0.439	8	13.7 - 6.0M	Oligocene- Late Maiocene	Ms.sh	Dolati (2010)
4567	0	4568	ph_blue	0.418	8	13.7 - 6.0M	Oligocene- Late Maiocene	Ms.sh	Dolati (2010)
4568	0	4569	ph_blue	0.172	8	13.7 - 6.0M	Oligocene- Late Maiocene	Ms.sh	Dolati (2010)
4569	0	4570	ph_blue	0.036	8	13.7 - 6.0M	Oligocene- Late Maiocene	Ms.sh	Dolati (2010)
4570	0	4571	ph_blue	0.136	8	13.7 - 6.0M	Oligocene- Late Maiocene	Ms.sh	Dolati (2010)
4571	0	4572	ph_blue	2.219	8	13.7 - 6.0M	Oligocene- Late Maiocene	Ms.sh	Dolati (2010)
4573	0	4574	ph_blue	1.036	8	13.7 - 6.0M	Oligocene- Late Maiocene	Ms.sh	Dolati (2010)
4574	0	4575	ph_blue	0.044	8	13.7 - 6.0M	Oligocene- Late Maiocene	Ms.sh	Dolati (2010)
4575	0	4576	ph_blue	3.826	8	13.7 - 6.0M	Oligocene- Late Maiocene	Ms.sh	Dolati (2010)
4576	0	4577	ph_blue	0.375	8	13.7 - 6.0M	Oligocene- Late Maiocene	Ms.sh	Dolati (2010)
4577	0	4578	ph_blue	0.467	8	13.7 - 6.0M	Oligocene- Late Maiocene	Ms.sh	Dolati (2010)
4578	1	4579	ph_blue	0.647	8	13.7 - 6.0M	Oligocene- Late Maiocene	Ms.sh	Dolati (2010)
4579	0	4580	ph_blue	0.536	8	13.7 - 6.0M	Oligocene- Late Maiocene	Ms.sh	Dolati (2010)
4580	0	4581	ph_blue	1.719	8	13.7 - 6.0M	Oligocene- Late Maiocene	Ms.sh	Dolati (2010)
4581	0	4582	ph_blue	32.150	8	13.7 - 6.0M	Oligocene- Late Maiocene	Ms.sh	Dolati (2010)
4582	0	4583	ph_blue	0.284	8	13.7 - 6.0M	Oligocene- Late Maiocene	Ms.sh	Dolati (2010)
4583	0	4584	ph_blue	0.260	8	13.7 - 6.0M	Oligocene- Late Maiocene	Ms.sh	Dolati (2010)
4584	0	4585	ph_blue	0.504	8	13.7 - 6.0M	Oligocene- Late Maiocene	Ms.sh	Dolati (2010)
4585	0	4586	ph_blue	0.192	8	13.7 - 6.0M	Oligocene- Late Maiocene	Ms.sh	Dolati (2010)
4586	0	4587	ph_blue	0.463	8	13.7 - 6.0M	Oligocene- Late Maiocene	Ms.sh	Dolati (2010)
4587	0	4588	ph_blue	3.370	8	13.7 - 6.0M	Oligocene- Late Maiocene	Ms.sh	Dolati (2010)
4588	0	4589	ph_blue	0.129	8	13.7 - 6.0M	Oligocene- Late Maiocene	Ms.sh	Dolati (2010)
4589	0	4590	ph_blue	0.188	8	13.7 - 6.0M	Oligocene- Late Maiocene	Ms.sh	Dolati (2010)
4590	0	4591	ph_blue	0.873	8	13.7 - 6.0M	Oligocene- Late Maiocene	Ms.sh	Dolati (2010)
4591	0	4592	ph_blue	0.832	8	13.7 - 6.0M	Oligocene- Late Maiocene	Ms.sh	Dolati (2010)
4592	0	4593	ph_blue	0.056	8	13.7 - 6.0M	Oligocene- Late Maiocene	Ms.sh	Dolati (2010)
4593	0	4594	ph_blue	1.204	8	13.7 - 6.0M	Oligocene- Late Maiocene	Ms.sh	Dolati (2010)
4594	0	4595	ph_blue	0.966	8	13.7 - 6.0M	Oligocene- Late Maiocene	Ms.sh	Dolati (2010)
4595	0	4596	ph_blue	0.347	8	13.7 - 6.0M	Oligocene- Late Maiocene	Ms.sh	Dolati (2010)
4596	0	4597	ph_blue	0.598	8	13.7 - 6.0M	Oligocene- Late Maiocene	Ms.sh	Dolati (2010)
4597	0	4598	ph_blue	1.034	8	13.7 - 6.0M	Oligocene- Late Maiocene	Ms.sh	Dolati (2010)
4598	0	4599	ph_blue	0.061	8	13.7 - 6.0M	Oligocene- Late Maiocene	Ms.sh	Dolati (2010)
4599	0	4600	ph_blue	0.072	8	13.7 - 6.0M	Oligocene- Late Maiocene	Ms.sh	Dolati (2010)
4600	0	4601	ph_blue	0.607	8	13.7 - 6.0M	Oligocene- Late Maiocene	Ms.sh	Dolati (2010)
4601	0	4602	ph_blue	0.124	8	13.7 - 6.0M	Oligocene- Late Maiocene	Ms.sh	Dolati (2010)
4602	0	4603	ph_blue	0.921	8	13.7 - 6.0M	Oligocene- Late Maiocene	Ms.sh	Dolati (2010)
4603	0	4604	ph_blue	0.090	8	13.7 - 6.0M	Oligocene- Late Maiocene	Ms.sh	Dolati (2010)
4604	0	4605	ph_blue	0.066	8	13.7 - 6.0M	Oligocene- Late Maiocene	Ms.sh	Dolati (2010)
4605	0	4606	ph_blue	1.354	8	13.7 - 6.0M	Oligocene- Late Maiocene	Ms.sh	Dolati (2010)

Preview

OBJECTID_1	Join_Count	TARGET_FID	Label	Shape_Area (sqkm)	ORIG_FID	Absolute_Age	Age_paleontology	Unit	Reference
4606	0	4607	ph_blue	0.621	8	13.7 - 6.0M	Oligocene- Late Maiocene	Ms.sh	Dolati (2010)
4607	0	4608	ph_blue	0.183	8	13.7 - 6.0M	Oligocene- Late Maiocene	Ms.sh	Dolati (2010)
4608	0	4609	ph_blue	0.409	8	13.7 - 6.0M	Oligocene- Late Maiocene	Ms.sh	Dolati (2010)
4609	0	4610	ph_blue	1.429	8	13.7 - 6.0M	Oligocene- Late Maiocene	Ms.sh	Dolati (2010)
4610	0	4611	ph_blue	2.132	8	13.7 - 6.0M	Oligocene- Late Maiocene	Ms.sh	Dolati (2010)
4611	0	4612	ph_blue	0.203	8	13.7 - 6.0M	Oligocene- Late Maiocene	Ms.sh	Dolati (2010)
4612	0	4613	ph_blue	3.211	8	13.7 - 6.0M	Oligocene- Late Maiocene	Ms.sh	Dolati (2010)
4613	0	4614	ph_blue	2.857	8	13.7 - 6.0M	Oligocene- Late Maiocene	Ms.sh	Dolati (2010)
4614	0	4615	ph_blue	0.942	8	13.7 - 6.0M	Oligocene- Late Maiocene	Ms.sh	Dolati (2010)
4615	0	4616	ph_blue	0.358	8	13.7 - 6.0M	Oligocene- Late Maiocene	Ms.sh	Dolati (2010)
4616	0	4617	ph_blue	0.229	8	13.7 - 6.0M	Oligocene- Late Maiocene	Ms.sh	Dolati (2010)
4617	0	4618	ph_blue	0.568	8	13.7 - 6.0M	Oligocene- Late Maiocene	Ms.sh	Dolati (2010)
4618	0	4619	ph_blue	0.488	8	13.7 - 6.0M	Oligocene- Late Maiocene	Ms.sh	Dolati (2010)
4619	0	4620	ph_blue	0.084	8	13.7 - 6.0M	Oligocene- Late Maiocene	Ms.sh	Dolati (2010)
4620	0	4621	ph_blue	0.528	8	13.7 - 6.0M	Oligocene- Late Maiocene	Ms.sh	Dolati (2010)
4621	0	4622	ph_blue	0.369	8	13.7 - 6.0M	Oligocene- Late Maiocene	Ms.sh	Dolati (2010)
4622	0	4623	ph_blue	0.210	8	13.7 - 6.0M	Oligocene- Late Maiocene	Ms.sh	Dolati (2010)
4623	0	4624	ph_blue	0.564	8	13.7 - 6.0M	Oligocene- Late Maiocene	Ms.sh	Dolati (2010)
4624	0	4625	ph_blue	0.259	8	13.7 - 6.0M	Oligocene- Late Maiocene	Ms.sh	Dolati (2010)
4625	0	4626	ph_blue	0.657	8	13.7 - 6.0M	Oligocene- Late Maiocene	Ms.sh	Dolati (2010)
4626	0	4627	ph_blue	0.059	8	13.7 - 6.0M	Oligocene- Late Maiocene	Ms.sh	Dolati (2010)
4627	0	4628	ph_blue	0.165	8	13.7 - 6.0M	Oligocene- Late Maiocene	Ms.sh	Dolati (2010)
4628	0	4629	ph_blue	0.624	8	13.7 - 6.0M	Oligocene- Late Maiocene	Ms.sh	Dolati (2010)
4629	0	4630	ph_blue	4.366	8	13.7 - 6.0M	Oligocene- Late Maiocene	Ms.sh	Dolati (2010)
4630	0	4631	ph_blue	0.329	8	13.7 - 6.0M	Oligocene- Late Maiocene	Ms.sh	Dolati (2010)
4631	0	4632	ph_blue	0.060	8	13.7 - 6.0M	Oligocene- Late Maiocene	Ms.sh	Dolati (2010)
4632	0	4633	ph_blue	0.035	8	13.7 - 6.0M	Oligocene- Late Maiocene	Ms.sh	Dolati (2010)
4633	0	4634	ph_blue	0.529	8	13.7 - 6.0M	Oligocene- Late Maiocene	Ms.sh	Dolati (2010)
4634	0	4635	ph_blue	0.210	8	13.7 - 6.0M	Oligocene- Late Maiocene	Ms.sh	Dolati (2010)
4635	0	4636	ph_blue	0.123	8	13.7 - 6.0M	Oligocene- Late Maiocene	Ms.sh	Dolati (2010)
4636	0	4637	ph_blue	0.108	8	13.7 - 6.0M	Oligocene- Late Maiocene	Ms.sh	Dolati (2010)
4637	0	4638	ph_blue	0.174	8	13.7 - 6.0M	Oligocene- Late Maiocene	Ms.sh	Dolati (2010)
4638	0	4639	ph_blue	0.757	8	13.7 - 6.0M	Oligocene- Late Maiocene	Ms.sh	Dolati (2010)
4639	0	4640	ph_blue	1.145	8	13.7 - 6.0M	Oligocene- Late Maiocene	Ms.sh	Dolati (2010)
4640	0	4641	ph_blue	0.666	8	13.7 - 6.0M	Oligocene- Late Maiocene	Ms.sh	Dolati (2010)
4641	0	4642	ph_blue	0.333	8	13.7 - 6.0M	Oligocene- Late Maiocene	Ms.sh	Dolati (2010)
4642	0	4643	ph_blue	10.300	8	13.7 - 6.0M	Oligocene- Late Maiocene	Ms.sh	Dolati (2010)
4643	0	4644	ph_blue	0.234	8	13.7 - 6.0M	Oligocene- Late Maiocene	Ms.sh	Dolati (2010)
4644	0	4645	ph_blue	0.906	8	13.7 - 6.0M	Oligocene- Late Maiocene	Ms.sh	Dolati (2010)

GeoNeus

OBJECTID_1	Join_Count	TARGET_FID	Label	Shape_Area (sqkm)	ORIG_FID	Absolute_Age	Age_paleontology	Unit	Reference
4645	0	4646	ph_blue	0.682	8	13.7 - 6.0M	Oligocene- Late Maiocene	Ms.sh	Dolati (2010)
4646	0	4647	ph_blue	0.197	8	13.7 - 6.0M	Oligocene- Late Maiocene	Ms.sh	Dolati (2010)
4647	0	4648	ph_blue	0.099	8	13.7 - 6.0M	Oligocene- Late Maiocene	Ms.sh	Dolati (2010)
4648	0	4649	ph_blue	0.159	8	13.7 - 6.0M	Oligocene- Late Maiocene	Ms.sh	Dolati (2010)
4649	0	4650	ph_blue	0.288	8	13.7 - 6.0M	Oligocene- Late Maiocene	Ms.sh	Dolati (2010)
4650	0	4651	ph_blue	0.495	8	13.7 - 6.0M	Oligocene- Late Maiocene	Ms.sh	Dolati (2010)
4651	0	4652	ph_blue	0.812	8	13.7 - 6.0M	Oligocene- Late Maiocene	Ms.sh	Dolati (2010)
4652	0	4653	ph_blue	0.246	8	13.7 - 6.0M	Oligocene- Late Maiocene	Ms.sh	Dolati (2010)
4653	0	4654	ph_blue	0.169	8	13.7 - 6.0M	Oligocene- Late Maiocene	Ms.sh	Dolati (2010)
4654	0	4655	ph_blue	0.163	8	13.7 - 6.0M	Oligocene- Late Maiocene	Ms.sh	Dolati (2010)
4655	0	4656	ph_blue	0.314	8	13.7 - 6.0M	Oligocene- Late Maiocene	Ms.sh	Dolati (2010)
4656	0	4657	ph_blue	0.044	8	13.7 - 6.0M	Oligocene- Late Maiocene	Ms.sh	Dolati (2010)
4657	0	4658	ph_blue	1.044	8	13.7 - 6.0M	Oligocene- Late Maiocene	Ms.sh	Dolati (2010)
4658	0	4659	ph_blue	0.131	8	13.7 - 6.0M	Oligocene- Late Maiocene	Ms.sh	Dolati (2010)
4659	0	4660	ph_blue	1.031	8	13.7 - 6.0M	Oligocene- Late Maiocene	Ms.sh	Dolati (2010)
4660	0	4661	ph_blue	0.080	8	13.7 - 6.0M	Oligocene- Late Maiocene	Ms.sh	Dolati (2010)
4661	0	4662	ph_blue	0.096	8	13.7 - 6.0M	Oligocene- Late Maiocene	Ms.sh	Dolati (2010)
4662	0	4663	ph_blue	0.217	8	13.7 - 6.0M	Oligocene- Late Maiocene	Ms.sh	Dolati (2010)
4663	0	4664	ph_blue	0.166	8	13.7 - 6.0M	Oligocene- Late Maiocene	Ms.sh	Dolati (2010)
4664	0	4665	ph_blue	0.470	8	13.7 - 6.0M	Oligocene- Late Maiocene	Ms.sh	Dolati (2010)
4665	0	4666	ph_blue	6.478	8	13.7 - 6.0M	Oligocene- Late Maiocene	Ms.sh	Dolati (2010)
4666	0	4667	ph_blue	0.014	8	13.7 - 6.0M	Oligocene- Late Maiocene	Ms.sh	Dolati (2010)
4667	0	4668	ph_blue	0.058	8	13.7 - 6.0M	Oligocene- Late Maiocene	Ms.sh	Dolati (2010)
4668	0	4669	ph_blue	1.273	8	13.7 - 6.0M	Oligocene- Late Maiocene	Ms.sh	Dolati (2010)
4669	0	4670	ph_blue	0.163	8	13.7 - 6.0M	Oligocene- Late Maiocene	Ms.sh	Dolati (2010)
4670	0	4671	ph_blue	1.859	8	13.7 - 6.0M	Oligocene- Late Maiocene	Ms.sh	Dolati (2010)
4671	0	4672	ph_blue	0.029	8	13.7 - 6.0M	Oligocene- Late Maiocene	Ms.sh	Dolati (2010)
4672	0	4673	ph_blue	0.043	8	13.7 - 6.0M	Oligocene- Late Maiocene	Ms.sh	Dolati (2010)
4673	0	4674	ph_blue	0.237	8	13.7 - 6.0M	Oligocene- Late Maiocene	Ms.sh	Dolati (2010)
4674	0	4675	ph_blue	0.045	8	13.7 - 6.0M	Oligocene- Late Maiocene	Ms.sh	Dolati (2010)
4675	0	4676	ph_blue	0.124	8	13.7 - 6.0M	Oligocene- Late Maiocene	Ms.sh	Dolati (2010)
4676	0	4677	ph_blue	0.521	8	13.7 - 6.0M	Oligocene- Late Maiocene	Ms.sh	Dolati (2010)
4677	0	4678	ph_blue	0.127	8	13.7 - 6.0M	Oligocene- Late Maiocene	Ms.sh	Dolati (2010)
4678	0	4679	ph_blue	0.243	8	13.7 - 6.0M	Oligocene- Late Maiocene	Ms.sh	Dolati (2010)
4679	0	4680	ph_blue	2.206	8	13.7 - 6.0M	Oligocene- Late Maiocene	Ms.sh	Dolati (2010)
4680	0	4681	ph_blue	0.317	8	13.7 - 6.0M	Oligocene- Late Maiocene	Ms.sh	Dolati (2010)
4681	0	4682	ph_blue	0.067	8	13.7 - 6.0M	Oligocene- Late Maiocene	Ms.sh	Dolati (2010)
4682	0	4683	ph_blue	3.952	8	13.7 - 6.0M	Oligocene- Late Maiocene	Ms.sh	Dolati (2010)
4683	0	4684	ph_blue	4.348	8	13.7 - 6.0M	Oligocene- Late Maiocene	Ms.sh	Dolati (2010)

Geonets

OBJECTID_1	Join_Count	TARGET_FID	Label	Shape_Area (sqkm)	ORIG_FID	Absolute_Age	Age_paleontology	Unit	Reference
4684	0	4685	ph_blue	0.063	8	13.7 - 6.0M	Oligocene- Late Maiocene	Ms.sh	Dolati (2010)
4685	0	4686	ph_blue	0.161	8	13.7 - 6.0M	Oligocene- Late Maiocene	Ms.sh	Dolati (2010)
4686	0	4687	ph_blue	0.159	8	13.7 - 6.0M	Oligocene- Late Maiocene	Ms.sh	Dolati (2010)
4687	0	4688	ph_blue	0.114	8	13.7 - 6.0M	Oligocene- Late Maiocene	Ms.sh	Dolati (2010)
4688	0	4689	ph_blue	1.776	8	13.7 - 6.0M	Oligocene- Late Maiocene	Ms.sh	Dolati (2010)
4689	0	4690	ph_blue	0.557	8	13.7 - 6.0M	Oligocene- Late Maiocene	Ms.sh	Dolati (2010)
4690	0	4691	ph_blue	0.210	8	13.7 - 6.0M	Oligocene- Late Maiocene	Ms.sh	Dolati (2010)
4691	0	4692	ph_blue	0.042	8	13.7 - 6.0M	Oligocene- Late Maiocene	Ms.sh	Dolati (2010)
4692	0	4693	ph_blue	0.030	8	13.7 - 6.0M	Oligocene- Late Maiocene	Ms.sh	Dolati (2010)
4693	0	4694	ph_blue	0.070	8	13.7 - 6.0M	Oligocene- Late Maiocene	Ms.sh	Dolati (2010)
4694	0	4695	ph_blue	0.818	8	13.7 - 6.0M	Oligocene- Late Maiocene	Ms.sh	Dolati (2010)
4695	0	4696	ph_blue	0.177	8	13.7 - 6.0M	Oligocene- Late Maiocene	Ms.sh	Dolati (2010)
4696	0	4697	ph_blue	0.976	8	13.7 - 6.0M	Oligocene- Late Maiocene	Ms.sh	Dolati (2010)
4697	0	4698	ph_blue	59.070	8	13.7 - 6.0M	Oligocene- Late Maiocene	Ms.sh	Dolati (2010)
4698	0	4699	ph_blue	0.073	8	13.7 - 6.0M	Oligocene- Late Maiocene	Ms.sh	Dolati (2010)
4699	0	4700	ph_blue	0.152	8	13.7 - 6.0M	Oligocene- Late Maiocene	Ms.sh	Dolati (2010)
4700	0	4701	ph_blue	0.073	8	13.7 - 6.0M	Oligocene- Late Maiocene	Ms.sh	Dolati (2010)
4701	0	4702	ph_blue	0.443	8	13.7 - 6.0M	Oligocene- Late Maiocene	Ms.sh	Dolati (2010)
4702	0	4703	ph_blue	0.775	8	13.7 - 6.0M	Oligocene- Late Maiocene	Ms.sh	Dolati (2010)
4703	0	4704	ph_blue	0.161	8	13.7 - 6.0M	Oligocene- Late Maiocene	Ms.sh	Dolati (2010)
4704	0	4705	ph_blue	0.085	8	13.7 - 6.0M	Oligocene- Late Maiocene	Ms.sh	Dolati (2010)
4705	0	4706	ph_blue	0.614	8	13.7 - 6.0M	Oligocene- Late Maiocene	Ms.sh	Dolati (2010)
4706	0	4707	ph_blue	0.297	8	13.7 - 6.0M	Oligocene- Late Maiocene	Ms.sh	Dolati (2010)
4707	0	4708	ph_blue	0.142	8	13.7 - 6.0M	Oligocene- Late Maiocene	Ms.sh	Dolati (2010)
4708	0	4709	ph_blue	0.616	8	13.7 - 6.0M	Oligocene- Late Maiocene	Ms.sh	Dolati (2010)
4709	0	4710	ph_blue	1.598	8	13.7 - 6.0M	Oligocene- Late Maiocene	Ms.sh	Dolati (2010)
4710	0	4711	ph_blue	0.047	8	13.7 - 6.0M	Oligocene- Late Maiocene	Ms.sh	Dolati (2010)
4711	0	4712	ph_blue	0.349	8	13.7 - 6.0M	Oligocene- Late Maiocene	Ms.sh	Dolati (2010)
4712	0	4713	ph_blue	0.192	8	13.7 - 6.0M	Oligocene- Late Maiocene	Ms.sh	Dolati (2010)
4713	0	4714	ph_blue	0.667	8	13.7 - 6.0M	Oligocene- Late Maiocene	Ms.sh	Dolati (2010)
4714	0	4715	ph_blue	0.195	8	13.7 - 6.0M	Oligocene- Late Maiocene	Ms.sh	Dolati (2010)
4715	0	4716	ph_blue	0.094	8	13.7 - 6.0M	Oligocene- Late Maiocene	Ms.sh	Dolati (2010)
4716	0	4717	ph_blue	0.231	8	13.7 - 6.0M	Oligocene- Late Maiocene	Ms.sh	Dolati (2010)
4717	0	4718	ph_blue	0.171	8	13.7 - 6.0M	Oligocene- Late Maiocene	Ms.sh	Dolati (2010)
4718	0	4719	ph_blue	0.933	8	13.7 - 6.0M	Oligocene- Late Maiocene	Ms.sh	Dolati (2010)
4719	0	4720	ph_blue	28.426	8	13.7 - 6.0M	Oligocene- Late Maiocene	Ms.sh	Dolati (2010)
4720	0	4721	ph_blue	0.565	8	13.7 - 6.0M	Oligocene- Late Maiocene	Ms.sh	Dolati (2010)
4721	0	4722	ph_blue	1.347	8	13.7 - 6.0M	Oligocene- Late Maiocene	Ms.sh	Dolati (2010)
4722	0	4723	ph_blue	0.278	8	13.7 - 6.0M	Oligocene- Late Maiocene	Ms.sh	Dolati (2010)

GeoNeus

OBJECTID_1	Join_Count	TARGET_FID	Label	Shape_Area (sqkm)	ORIG_FID	Absolute_Age	Age_paleontology	Unit	Reference
4723	0	4724	ph_blue	2.326	8	13.7 - 6.0M	Oligocene- Late Maiocene	Ms.sh	Dolati (2010)
4724	0	4725	ph_blue	0.896	8	13.7 - 6.0M	Oligocene- Late Maiocene	Ms.sh	Dolati (2010)
4725	0	4726	ph_blue	0.286	8	13.7 - 6.0M	Oligocene- Late Maiocene	Ms.sh	Dolati (2010)
4726	0	4727	ph_blue	0.755	8	13.7 - 6.0M	Oligocene- Late Maiocene	Ms.sh	Dolati (2010)
4727	0	4728	ph_blue	0.514	8	13.7 - 6.0M	Oligocene- Late Maiocene	Ms.sh	Dolati (2010)
4728	0	4729	ph_blue	0.170	8	13.7 - 6.0M	Oligocene- Late Maiocene	Ms.sh	Dolati (2010)
4729	0	4730	ph_blue	0.035	8	13.7 - 6.0M	Oligocene- Late Maiocene	Ms.sh	Dolati (2010)
4730	0	4731	ph_blue	0.298	8	13.7 - 6.0M	Oligocene- Late Maiocene	Ms.sh	Dolati (2010)
4731	0	4732	ph_blue	0.114	8	13.7 - 6.0M	Oligocene- Late Maiocene	Ms.sh	Dolati (2010)
4732	0	4733	ph_blue	0.458	8	13.7 - 6.0M	Oligocene- Late Maiocene	Ms.sh	Dolati (2010)
4733	0	4734	ph_blue	0.073	8	13.7 - 6.0M	Oligocene- Late Maiocene	Ms.sh	Dolati (2010)
4734	0	4735	ph_blue	0.523	8	13.7 - 6.0M	Oligocene- Late Maiocene	Ms.sh	Dolati (2010)
4735	0	4736	ph_blue	0.828	8	13.7 - 6.0M	Oligocene- Late Maiocene	Ms.sh	Dolati (2010)
4736	0	4737	ph_blue	72.740	8	13.7 - 6.0M	Oligocene- Late Maiocene	Ms.sh	Dolati (2010)
4737	0	4738	ph_blue	0.048	8	13.7 - 6.0M	Oligocene- Late Maiocene	Ms.sh	Dolati (2010)
4738	0	4739	ph_blue	0.252	8	13.7 - 6.0M	Oligocene- Late Maiocene	Ms.sh	Dolati (2010)
4739	0	4740	ph_blue	0.809	8	13.7 - 6.0M	Oligocene- Late Maiocene	Ms.sh	Dolati (2010)
4740	0	4741	ph_blue	0.377	8	13.7 - 6.0M	Oligocene- Late Maiocene	Ms.sh	Dolati (2010)
4741	0	4742	ph_blue	0.690	8	13.7 - 6.0M	Oligocene- Late Maiocene	Ms.sh	Dolati (2010)
4742	0	4743	ph_blue	0.405	8	13.7 - 6.0M	Oligocene- Late Maiocene	Ms.sh	Dolati (2010)
4743	0	4744	ph_blue	0.284	8	13.7 - 6.0M	Oligocene- Late Maiocene	Ms.sh	Dolati (2010)
4744	0	4745	ph_blue	0.232	8	13.7 - 6.0M	Oligocene- Late Maiocene	Ms.sh	Dolati (2010)
4745	0	4746	ph_blue	0.497	8	13.7 - 6.0M	Oligocene- Late Maiocene	Ms.sh	Dolati (2010)
4746	0	4747	ph_blue	0.207	8	13.7 - 6.0M	Oligocene- Late Maiocene	Ms.sh	Dolati (2010)
4747	0	4748	ph_blue	0.277	8	13.7 - 6.0M	Oligocene- Late Maiocene	Ms.sh	Dolati (2010)
4748	0	4749	ph_blue	0.348	8	13.7 - 6.0M	Oligocene- Late Maiocene	Ms.sh	Dolati (2010)
4749	0	4750	ph_blue	0.293	8	13.7 - 6.0M	Oligocene- Late Maiocene	Ms.sh	Dolati (2010)
4750	0	4751	ph_blue	0.233	8	13.7 - 6.0M	Oligocene- Late Maiocene	Ms.sh	Dolati (2010)
4751	0	4752	ph_blue	0.333	8	13.7 - 6.0M	Oligocene- Late Maiocene	Ms.sh	Dolati (2010)
4752	0	4753	ph_blue	1.874	8	13.7 - 6.0M	Oligocene- Late Maiocene	Ms.sh	Dolati (2010)
4753	0	4754	ph_blue	0.247	8	13.7 - 6.0M	Oligocene- Late Maiocene	Ms.sh	Dolati (2010)
4754	0	4755	ph_blue	0.846	8	13.7 - 6.0M	Oligocene- Late Maiocene	Ms.sh	Dolati (2010)
4755	0	4756	ph_blue	0.757	8	13.7 - 6.0M	Oligocene- Late Maiocene	Ms.sh	Dolati (2010)
4756	0	4757	ph_blue	0.201	8	13.7 - 6.0M	Oligocene- Late Maiocene	Ms.sh	Dolati (2010)
4757	0	4758	ph_blue	26.153	8	13.7 - 6.0M	Oligocene- Late Maiocene	Ms.sh	Dolati (2010)
4758	0	4759	ph_blue	1.107	8	13.7 - 6.0M	Oligocene- Late Maiocene	Ms.sh	Dolati (2010)
4759	0	4760	ph_blue	0.120	8	13.7 - 6.0M	Oligocene- Late Maiocene	Ms.sh	Dolati (2010)
4760	0	4761	ph_blue	0.457	8			Ms.sh	
8360	0	8361	ph_blue	0.041	14		Oligocene- Late Maiocene	Ms.sh	Dolati (2010)

Geonets

OBJECTID_1	Join_Count	TARGET_FID	Label	Shape_Area (sqkm)	ORIG_FID	Absolute_Age	Age_paleontology	Unit	Reference
10296	1	10299	ph_blue	0.063	19		Oligocene- Late Maiocene	Ms.sh	Dolati (2010)
10419	1	10433	ph_blue	0.007	0		Oligocene- Late Maiocene	Ms.sh	Dolati (2010)
10447	3	7830	ph_blue	0.002	13		Oligocene- Late Maiocene	Ms.sh	Dolati (2010)
10448	3	7830	ph_blue	0.000	13		Oligocene- Late Maiocene	Ms.sh	Dolati (2010)
10458	3	4426	ph_blue	0.001	8	13.7 - 6.0M	Oligocene- Late Maiocene	Ms.sh	Dolati (2010)
10459	1	8323	ph_blue	0.000	14		Oligocene- Late Maiocene	Ms.sh	Dolati (2010)
10460	1	8323	ph_blue	0.000	14		Oligocene- Late Maiocene	Ms.sh	Dolati (2010)
10461	1	8323	ph_blue	0.003	14		Oligocene- Late Maiocene	Ms.sh	Dolati (2010)
10462	0	7634	ph_blue	0.002	13		Oligocene- Late Maiocene	Ms.sh	Dolati (2010)
10463	1	8323	ph_blue	0.005	14		Oligocene- Late Maiocene	Ms.sh	Dolati (2010)
10527	0	1459	ph_blue	0.127	3		Oligocene- Late Maiocene	Ms.sh	Dolati (2010)

GeoNexus

Table S4. Summary of mapped polygons for the $M^{sh.s}$ Unit.

OBJECTID_1	Join_Count	TARGET_FID	Label	Shape_Area (sqkm)	ORIG_FID	Absolute_Age	Age_paleontology	Unit	Reference
1467	0	1467	ph_brow	56.808	3		M-L Miocene	Msh.s	Dolati (2010)
1558	1	1558	ph_brow	25.114	3		M-L Miocene	Msh.s	Dolati (2010)
4761	0	4762	ph_brown	0.153	9		M-L Miocene	Msh.s	Dolati (2010)
4762	0	4763	ph_brown	1.296	9		M-L Miocene	Msh.s	Dolati (2010)
4763	0	4764	ph_brown	0.044	9		M-L Miocene	Msh.s	Dolati (2010)
4764	0	4765	ph_brown	0.045	9		M-L Miocene	Msh.s	Dolati (2010)
4765	0	4766	ph_brown	0.013	9		M-L Miocene	Msh.s	Dolati (2010)
4766	0	4767	ph_brown	0.127	9		M-L Miocene	Msh.s	Dolati (2010)
4767	0	4768	ph_brown	0.139	9		M-L Miocene	Msh.s	Dolati (2010)
4768	0	4769	ph_brown	0.003	9		M-L Miocene	Msh.s	Dolati (2010)
4769	0	4770	ph_brown	0.018	9		M-L Miocene	Msh.s	Dolati (2010)
4770	0	4771	ph_brown	0.000	9		M-L Miocene	Msh.s	Dolati (2010)
4771	0	4772	ph_brown	0.020	9		M-L Miocene	Msh.s	Dolati (2010)
4772	0	4773	ph_brown	0.022	9		M-L Miocene	Msh.s	Dolati (2010)
4773	0	4774	ph_brown	0.463	9		M-L Miocene	Msh.s	Dolati (2010)
4774	0	4775	ph_brown	0.294	9		M-L Miocene	Msh.s	Dolati (2010)
4775	0	4776	ph_brown	0.519	9		M-L Miocene	Msh.s	Dolati (2010)
4776	0	4777	ph_brown	0.045	9		M-L Miocene	Msh.s	Dolati (2010)
4777	0	4778	ph_brown	0.016	9		M-L Miocene	Msh.s	Dolati (2010)
4778	0	4779	ph_brown	0.488	9		M-L Miocene	Msh.s	Dolati (2010)
4779	0	4780	ph_brown	0.203	9		M-L Miocene	Msh.s	Dolati (2010)
4780	0	4781	ph_brown	0.287	9		M-L Miocene	Msh.s	Dolati (2010)
4781	0	4782	ph_brown	0.097	9		M-L Miocene	Msh.s	Dolati (2010)
4782	0	4783	ph_brown	0.430	9		M-L Miocene	Msh.s	Dolati (2010)
4783	0	4784	ph_brown	0.132	9		M-L Miocene	Msh.s	Dolati (2010)
4784	0	4785	ph_brown	0.076	9		M-L Miocene	Msh.s	Dolati (2010)
4785	0	4786	ph_brown	0.090	9		M-L Miocene	Msh.s	Dolati (2010)
4786	0	4787	ph_brown	0.013	9		M-L Miocene	Msh.s	Dolati (2010)
4787	0	4788	ph_brown	0.013	9		M-L Miocene	Msh.s	Dolati (2010)
4788	0	4789	ph_brown	0.027	9		M-L Miocene	Msh.s	Dolati (2010)
4789	0	4790	ph_brown	0.441	9		M-L Miocene	Msh.s	Dolati (2010)
4790	0	4791	ph_brown	0.079	9		M-L Miocene	Msh.s	Dolati (2010)
4791	0	4792	ph_brown	0.086	9		M-L Miocene	Msh.s	Dolati (2010)
4792	0	4793	ph_brown	0.394	9		M-L Miocene	Msh.s	Dolati (2010)
4793	0	4794	ph_brown	0.400	9		M-L Miocene	Msh.s	Dolati (2010)
4794	0	4795	ph_brown	0.119	9		M-L Miocene	Msh.s	Dolati (2010)
4795	0	4796	ph_brown	0.041	9		M-L Miocene	Msh.s	Dolati (2010)

Geonews

OBJECTID_1	Join_Count	TARGET_FID	Label	Shape_Area (sqkm)	ORIG_FID	Absolute_Age	Age_paleontology	Unit	Reference
4796	0	4797	ph_brown	0.046	9		M-L Miocene	Msh.s	Dolati (2010)
4797	0	4798	ph_brown	0.430	9		M-L Miocene	Msh.s	Dolati (2010)
4798	0	4799	ph_brown	0.034	9		M-L Miocene	Msh.s	Dolati (2010)
4799	0	4800	ph_brown	0.030	9		M-L Miocene	Msh.s	Dolati (2010)
4800	0	4801	ph_brown	0.069	9		M-L Miocene	Msh.s	Dolati (2010)
4801	0	4802	ph_brown	0.457	9		M-L Miocene	Msh.s	Dolati (2010)
4802	0	4803	ph_brown	0.082	9		M-L Miocene	Msh.s	Dolati (2010)
4803	0	4804	ph_brown	0.071	9		M-L Miocene	Msh.s	Dolati (2010)
4804	0	4805	ph_brown	0.213	9		M-L Miocene	Msh.s	Dolati (2010)
4805	0	4806	ph_brown	0.139	9		M-L Miocene	Msh.s	Dolati (2010)
4806	0	4807	ph_brown	0.045	9		M-L Miocene	Msh.s	Dolati (2010)
4807	0	4808	ph_brown	0.271	9		M-L Miocene	Msh.s	Dolati (2010)
4808	0	4809	ph_brown	0.034	9		M-L Miocene	Msh.s	Dolati (2010)
4809	0	4810	ph_brown	5.472	9		M-L Miocene	Msh.s	Dolati (2010)
4810	0	4811	ph_brown	0.804	9		M-L Miocene	Msh.s	Dolati (2010)
4811	0	4812	ph_brown	0.980	9		M-L Miocene	Msh.s	Dolati (2010)
4812	0	4813	ph_brown	0.035	9		M-L Miocene	Msh.s	Dolati (2010)
4813	0	4814	ph_brown	0.226	9		M-L Miocene	Msh.s	Dolati (2010)
4814	0	4815	ph_brown	0.143	9		M-L Miocene	Msh.s	Dolati (2010)
4815	0	4816	ph_brown	1.202	9		M-L Miocene	Msh.s	Dolati (2010)
4816	0	4817	ph_brown	11.071	9		M-L Miocene	Msh.s	Dolati (2010)
4817	0	4818	ph_brown	0.900	9		M-L Miocene	Msh.s	Dolati (2010)
4818	0	4819	ph_brown	0.177	9		M-L Miocene	Msh.s	Dolati (2010)
4819	0	4820	ph_brown	0.526	9		M-L Miocene	Msh.s	Dolati (2010)
4820	0	4821	ph_brown	0.055	9		M-L Miocene	Msh.s	Dolati (2010)
4821	0	4822	ph_brown	0.053	9		M-L Miocene	Msh.s	Dolati (2010)
4822	0	4823	ph_brown	0.310	9		M-L Miocene	Msh.s	Dolati (2010)
4823	0	4824	ph_brown	1.255	9		M-L Miocene	Msh.s	Dolati (2010)
4824	0	4825	ph_brown	1.054	9		M-L Miocene	Msh.s	Dolati (2010)
4825	0	4826	ph_brown	0.283	9		M-L Miocene	Msh.s	Dolati (2010)
4826	0	4827	ph_brown	0.332	9		M-L Miocene	Msh.s	Dolati (2010)
4827	0	4828	ph_brown	1.721	9		M-L Miocene	Msh.s	Dolati (2010)
4828	0	4829	ph_brown	0.338	9		M-L Miocene	Msh.s	Dolati (2010)
4829	0	4830	ph_brown	0.167	9		M-L Miocene	Msh.s	Dolati (2010)
4830	0	4831	ph_brown	0.234	9		M-L Miocene	Msh.s	Dolati (2010)
4831	0	4832	ph_brown	0.169	9		M-L Miocene	Msh.s	Dolati (2010)
4832	0	4833	ph_brown	0.675	9		M-L Miocene	Msh.s	Dolati (2010)
4833	0	4834	ph_brown	0.374	9		M-L Miocene	Msh.s	Dolati (2010)
4834	0	4835	ph_brown	0.173	9		M-L Miocene	Msh.s	Dolati (2010)

Geonevis

OBJECTID_1	Join_Count	TARGET_FID	Label	Shape_Area (sqkm)	ORIG_FID	Absolute_Age	Age_paleontology	Unit	Reference
4835	0	4836	ph_brown	0.021	9		M-L Miocene	Msh.s	Dolati (2010)
4836	0	4837	ph_brown	0.024	9		M-L Miocene	Msh.s	Dolati (2010)
4837	0	4838	ph_brown	0.091	9		M-L Miocene	Msh.s	Dolati (2010)
4838	0	4839	ph_brown	0.679	9		M-L Miocene	Msh.s	Dolati (2010)
4839	0	4840	ph_brown	0.192	9		M-L Miocene	Msh.s	Dolati (2010)
4840	0	4841	ph_brown	0.083	9		M-L Miocene	Msh.s	Dolati (2010)
4841	0	4842	ph_brown	0.049	9		M-L Miocene	Msh.s	Dolati (2010)
4842	0	4843	ph_brown	0.304	9		M-L Miocene	Msh.s	Dolati (2010)
4843	0	4844	ph_brown	8.180	9		M-L Miocene	Msh.s	Dolati (2010)
4844	0	4845	ph_brown	0.132	9		M-L Miocene	Msh.s	Dolati (2010)
4845	0	4846	ph_brown	0.043	9		M-L Miocene	Msh.s	Dolati (2010)
4846	0	4847	ph_brown	3.418	9		M-L Miocene	Msh.s	Dolati (2010)
4847	0	4848	ph_brown	0.285	9		M-L Miocene	Msh.s	Dolati (2010)
4848	0	4849	ph_brown	0.211	9		M-L Miocene	Msh.s	Dolati (2010)
4849	0	4850	ph_brown	0.029	9		M-L Miocene	Msh.s	Dolati (2010)
4850	0	4851	ph_brown	1.448	9		M-L Miocene	Msh.s	Dolati (2010)
4851	0	4852	ph_brown	0.325	9		M-L Miocene	Msh.s	Dolati (2010)
4852	0	4853	ph_brown	0.474	9		M-L Miocene	Msh.s	Dolati (2010)
4853	0	4854	ph_brown	1.715	9		M-L Miocene	Msh.s	Dolati (2010)
4854	0	4855	ph_brown	1.191	9		M-L Miocene	Msh.s	Dolati (2010)
4855	0	4856	ph_brown	0.062	9		M-L Miocene	Msh.s	Dolati (2010)
4856	0	4857	ph_brown	0.362	9		M-L Miocene	Msh.s	Dolati (2010)
4857	0	4858	ph_brown	0.402	9		M-L Miocene	Msh.s	Dolati (2010)
4858	0	4859	ph_brown	2.382	9		M-L Miocene	Msh.s	Dolati (2010)
4859	0	4860	ph_brown	2.647	9		M-L Miocene	Msh.s	Dolati (2010)
4860	0	4861	ph_brown	0.449	9		M-L Miocene	Msh.s	Dolati (2010)
4861	0	4862	ph_brown	0.292	9		M-L Miocene	Msh.s	Dolati (2010)
4862	0	4863	ph_brown	1.357	9		M-L Miocene	Msh.s	Dolati (2010)
4863	0	4864	ph_brown	1.870	9		M-L Miocene	Msh.s	Dolati (2010)
4864	0	4865	ph_brown	0.088	9		M-L Miocene	Msh.s	Dolati (2010)
4865	0	4866	ph_brown	0.143	9		M-L Miocene	Msh.s	Dolati (2010)
4866	0	4867	ph_brown	0.697	9		M-L Miocene	Msh.s	Dolati (2010)
4867	0	4868	ph_brown	0.060	9		M-L Miocene	Msh.s	Dolati (2010)
4868	0	4869	ph_brown	0.441	9		M-L Miocene	Msh.s	Dolati (2010)
4869	0	4870	ph_brown	0.092	9		M-L Miocene	Msh.s	Dolati (2010)
4870	0	4871	ph_brown	0.421	9		M-L Miocene	Msh.s	Dolati (2010)
4871	0	4872	ph_brown	0.124	9		M-L Miocene	Msh.s	Dolati (2010)
4872	0	4873	ph_brown	0.436	9		M-L Miocene	Msh.s	Dolati (2010)
4873	0	4874	ph_brown	0.203	9		M-L Miocene	Msh.s	Dolati (2010)

Geonevis

OBJECTID_1	Join_Count	TARGET_FID	Label	Shape_Area (sqkm)	ORIG_FID	Absolute_Age	Age_paleontology	Unit	Reference
4874	0	4875	ph_brown	0.216	9		M-L Miocene	Msh.s	Dolati (2010)
4875	0	4876	ph_brown	0.024	9		M-L Miocene	Msh.s	Dolati (2010)
4876	0	4877	ph_brown	0.038	9		M-L Miocene	Msh.s	Dolati (2010)
4877	0	4878	ph_brown	0.339	9		M-L Miocene	Msh.s	Dolati (2010)
4878	0	4879	ph_brown	0.170	9		M-L Miocene	Msh.s	Dolati (2010)
4879	0	4880	ph_brown	1.367	9		M-L Miocene	Msh.s	Dolati (2010)
4880	0	4881	ph_brown	0.043	9		M-L Miocene	Msh.s	Dolati (2010)
4881	0	4882	ph_brown	0.195	9		M-L Miocene	Msh.s	Dolati (2010)
4882	0	4883	ph_brown	0.327	9		M-L Miocene	Msh.s	Dolati (2010)
4883	0	4884	ph_brown	0.070	9		M-L Miocene	Msh.s	Dolati (2010)
4884	0	4885	ph_brown	0.064	9		M-L Miocene	Msh.s	Dolati (2010)
4885	0	4886	ph_brown	0.134	9		M-L Miocene	Msh.s	Dolati (2010)
4886	0	4887	ph_brown	0.571	9		M-L Miocene	Msh.s	Dolati (2010)
4887	0	4888	ph_brown	0.166	9		M-L Miocene	Msh.s	Dolati (2010)
4888	0	4889	ph_brown	0.889	9		M-L Miocene	Msh.s	Dolati (2010)
4889	0	4890	ph_brown	0.469	9		M-L Miocene	Msh.s	Dolati (2010)
4890	0	4891	ph_brown	0.596	9		M-L Miocene	Msh.s	Dolati (2010)
4891	0	4892	ph_brown	0.059	9		M-L Miocene	Msh.s	Dolati (2010)
4892	0	4893	ph_brown	0.580	9		M-L Miocene	Msh.s	Dolati (2010)
4893	0	4894	ph_brown	0.852	9		M-L Miocene	Msh.s	Dolati (2010)
4894	0	4895	ph_brown	0.238	9		M-L Miocene	Msh.s	Dolati (2010)
4895	0	4896	ph_brown	0.081	9		M-L Miocene	Msh.s	Dolati (2010)
4896	0	4897	ph_brown	0.655	9		M-L Miocene	Msh.s	Dolati (2010)
4897	0	4898	ph_brown	0.314	9		M-L Miocene	Msh.s	Dolati (2010)
4898	0	4899	ph_brown	0.264	9		M-L Miocene	Msh.s	Dolati (2010)
4899	0	4900	ph_brown	0.035	9		M-L Miocene	Msh.s	Dolati (2010)
4900	0	4901	ph_brown	2.180	9		M-L Miocene	Msh.s	Dolati (2010)
4901	0	4902	ph_brown	0.506	9		M-L Miocene	Msh.s	Dolati (2010)
4902	0	4903	ph_brown	0.027	9		M-L Miocene	Msh.s	Dolati (2010)
4903	0	4904	ph_brown	0.383	9		M-L Miocene	Msh.s	Dolati (2010)
4904	0	4905	ph_brown	1.293	9		M-L Miocene	Msh.s	Dolati (2010)
4905	0	4906	ph_brown	0.433	9		M-L Miocene	Msh.s	Dolati (2010)
4906	0	4907	ph_brown	0.505	9		M-L Miocene	Msh.s	Dolati (2010)
4907	0	4908	ph_brown	0.737	9		M-L Miocene	Msh.s	Dolati (2010)
4908	0	4909	ph_brown	0.049	9		M-L Miocene	Msh.s	Dolati (2010)
4909	0	4910	ph_brown	0.040	9		M-L Miocene	Msh.s	Dolati (2010)
4910	0	4911	ph_brown	0.266	9		M-L Miocene	Msh.s	Dolati (2010)
4911	0	4912	ph_brown	0.737	9		M-L Miocene	Msh.s	Dolati (2010)
4912	0	4913	ph_brown	0.062	9		M-L Miocene	Msh.s	Dolati (2010)

Geonevis

OBJECTID_1	Join_Count	TARGET_FID	Label	Shape_Area (sqkm)	ORIG_FID	Absolute_Age	Age_paleontology	Unit	Reference
4913	0	4914	ph_brown	0.092	9		M-L Miocene	Msh.s	Dolati (2010)
4914	0	4915	ph_brown	0.549	9		M-L Miocene	Msh.s	Dolati (2010)
4915	0	4916	ph_brown	0.939	9		M-L Miocene	Msh.s	Dolati (2010)
4916	0	4917	ph_brown	1.177	9		M-L Miocene	Msh.s	Dolati (2010)
4917	0	4918	ph_brown	0.144	9		M-L Miocene	Msh.s	Dolati (2010)
4918	0	4919	ph_brown	1.721	9		M-L Miocene	Msh.s	Dolati (2010)
4919	0	4920	ph_brown	5.717	9		M-L Miocene	Msh.s	Dolati (2010)
4920	0	4921	ph_brown	0.172	9		M-L Miocene	Msh.s	Dolati (2010)
4921	0	4922	ph_brown	0.015	9		M-L Miocene	Msh.s	Dolati (2010)
4922	0	4923	ph_brown	0.050	9		M-L Miocene	Msh.s	Dolati (2010)
4923	0	4924	ph_brown	1.115	9		M-L Miocene	Msh.s	Dolati (2010)
4924	0	4925	ph_brown	1.437	9		M-L Miocene	Msh.s	Dolati (2010)
4925	0	4926	ph_brown	0.233	9		M-L Miocene	Msh.s	Dolati (2010)
4926	0	4927	ph_brown	0.116	9		M-L Miocene	Msh.s	Dolati (2010)
4927	0	4928	ph_brown	0.066	9		M-L Miocene	Msh.s	Dolati (2010)
4928	0	4929	ph_brown	0.153	9		M-L Miocene	Msh.s	Dolati (2010)
4929	0	4930	ph_brown	1.073	9		M-L Miocene	Msh.s	Dolati (2010)
4930	0	4931	ph_brown	2.277	9		M-L Miocene	Msh.s	Dolati (2010)
4931	0	4932	ph_brown	0.423	9		M-L Miocene	Msh.s	Dolati (2010)
4932	0	4933	ph_brown	0.046	9		M-L Miocene	Msh.s	Dolati (2010)
4933	0	4934	ph_brown	0.108	9		M-L Miocene	Msh.s	Dolati (2010)
4934	0	4935	ph_brown	0.417	9		M-L Miocene	Msh.s	Dolati (2010)
4935	0	4936	ph_brown	0.415	9		M-L Miocene	Msh.s	Dolati (2010)
4936	0	4937	ph_brown	0.801	9		M-L Miocene	Msh.s	Dolati (2010)
4937	0	4938	ph_brown	0.115	9		M-L Miocene	Msh.s	Dolati (2010)
4938	0	4939	ph_brown	2.206	9		M-L Miocene	Msh.s	Dolati (2010)
4939	0	4940	ph_brown	0.157	9		M-L Miocene	Msh.s	Dolati (2010)
4940	0	4941	ph_brown	0.049	9		M-L Miocene	Msh.s	Dolati (2010)
4941	0	4942	ph_brown	0.066	9		M-L Miocene	Msh.s	Dolati (2010)
4942	0	4943	ph_brown	0.310	9		M-L Miocene	Msh.s	Dolati (2010)
4943	0	4944	ph_brown	0.091	9		M-L Miocene	Msh.s	Dolati (2010)
4944	0	4945	ph_brown	0.142	9		M-L Miocene	Msh.s	Dolati (2010)
4945	0	4946	ph_brown	0.036	9		M-L Miocene	Msh.s	Dolati (2010)
4946	0	4947	ph_brown	0.112	9		M-L Miocene	Msh.s	Dolati (2010)
4947	0	4948	ph_brown	1.025	9		M-L Miocene	Msh.s	Dolati (2010)
4948	0	4949	ph_brown	0.298	9		M-L Miocene	Msh.s	Dolati (2010)
4949	0	4950	ph_brown	0.053	9		M-L Miocene	Msh.s	Dolati (2010)
4950	0	4951	ph_brown	0.357	9		M-L Miocene	Msh.s	Dolati (2010)
4951	0	4952	ph_brown	0.110	9		M-L Miocene	Msh.s	Dolati (2010)

Geonevis

OBJECTID_1	Join_Count	TARGET_FID	Label	Shape_Area (sqkm)	ORIG_FID	Absolute_Age	Age_paleontology	Unit	Reference
4952	0	4953	ph_brown	0.082	9		M-L Miocene	Msh.s	Dolati (2010)
4953	0	4954	ph_brown	0.346	9		M-L Miocene	Msh.s	Dolati (2010)
4954	0	4955	ph_brown	2.655	9		M-L Miocene	Msh.s	Dolati (2010)
4955	0	4956	ph_brown	0.173	9		M-L Miocene	Msh.s	Dolati (2010)
4956	0	4957	ph_brown	0.073	9		M-L Miocene	Msh.s	Dolati (2010)
4957	0	4958	ph_brown	0.839	9		M-L Miocene	Msh.s	Dolati (2010)
4958	0	4959	ph_brown	0.049	9		M-L Miocene	Msh.s	Dolati (2010)
4959	0	4960	ph_brown	0.077	9		M-L Miocene	Msh.s	Dolati (2010)
4960	0	4961	ph_brown	0.239	9		M-L Miocene	Msh.s	Dolati (2010)
4961	0	4962	ph_brown	0.585	9		M-L Miocene	Msh.s	Dolati (2010)
4962	0	4963	ph_brown	0.044	9		M-L Miocene	Msh.s	Dolati (2010)
4963	0	4964	ph_brown	0.202	9		M-L Miocene	Msh.s	Dolati (2010)
4964	0	4965	ph_brown	0.497	9		M-L Miocene	Msh.s	Dolati (2010)
4965	0	4966	ph_brown	0.254	9		M-L Miocene	Msh.s	Dolati (2010)
4966	0	4967	ph_brown	0.094	9		M-L Miocene	Msh.s	Dolati (2010)
4967	0	4968	ph_brown	1.480	9		M-L Miocene	Msh.s	Dolati (2010)
4968	0	4969	ph_brown	0.041	9		M-L Miocene	Msh.s	Dolati (2010)
4969	0	4970	ph_brown	0.582	9		M-L Miocene	Msh.s	Dolati (2010)
4970	0	4971	ph_brown	0.542	9		M-L Miocene	Msh.s	Dolati (2010)
4971	0	4972	ph_brown	0.079	9		M-L Miocene	Msh.s	Dolati (2010)
4972	0	4973	ph_brown	0.131	9		M-L Miocene	Msh.s	Dolati (2010)
4973	0	4974	ph_brown	0.132	9		M-L Miocene	Msh.s	Dolati (2010)
4974	0	4975	ph_brown	0.158	9		M-L Miocene	Msh.s	Dolati (2010)
4975	0	4976	ph_brown	0.534	9		M-L Miocene	Msh.s	Dolati (2010)
4976	0	4977	ph_brown	0.126	9		M-L Miocene	Msh.s	Dolati (2010)
4977	0	4978	ph_brown	0.738	9		M-L Miocene	Msh.s	Dolati (2010)
4978	0	4979	ph_brown	0.120	9		M-L Miocene	Msh.s	Dolati (2010)
4979	0	4980	ph_brown	0.154	9		M-L Miocene	Msh.s	Dolati (2010)
4980	0	4981	ph_brown	1.231	9		M-L Miocene	Msh.s	Dolati (2010)
4981	0	4982	ph_brown	0.224	9		M-L Miocene	Msh.s	Dolati (2010)
4982	0	4983	ph_brown	0.137	9		M-L Miocene	Msh.s	Dolati (2010)
4983	0	4984	ph_brown	0.056	9		M-L Miocene	Msh.s	Dolati (2010)
4984	0	4985	ph_brown	0.105	9		M-L Miocene	Msh.s	Dolati (2010)
4985	0	4986	ph_brown	0.078	9		M-L Miocene	Msh.s	Dolati (2010)
4986	0	4987	ph_brown	1.693	9		M-L Miocene	Msh.s	Dolati (2010)
4987	0	4988	ph_brown	0.034	9		M-L Miocene	Msh.s	Dolati (2010)
4988	0	4989	ph_brown	1.288	9		M-L Miocene	Msh.s	Dolati (2010)
4989	0	4990	ph_brown	0.551	9		M-L Miocene	Msh.s	Dolati (2010)
4990	0	4991	ph_brown	0.173	9		M-L Miocene	Msh.s	Dolati (2010)

Geonevis

OBJECTID_1	Join_Count	TARGET_FID	Label	Shape_Area (sqkm)	ORIG_FID	Absolute_Age	Age_paleontology	Unit	Reference
4991	0	4992	ph_brown	0.482	9		M-L Miocene	Msh.s	Dolati (2010)
4992	0	4993	ph_brown	0.106	9		M-L Miocene	Msh.s	Dolati (2010)
4993	0	4994	ph_brown	0.829	9		M-L Miocene	Msh.s	Dolati (2010)
4994	0	4995	ph_brown	0.861	9		M-L Miocene	Msh.s	Dolati (2010)
4995	0	4996	ph_brown	0.118	9		M-L Miocene	Msh.s	Dolati (2010)
4996	0	4997	ph_brown	0.431	9		M-L Miocene	Msh.s	Dolati (2010)
4997	0	4998	ph_brown	0.102	9		M-L Miocene	Msh.s	Dolati (2010)
4998	0	4999	ph_brown	0.194	9		M-L Miocene	Msh.s	Dolati (2010)
4999	0	5000	ph_brown	0.181	9		M-L Miocene	Msh.s	Dolati (2010)
5000	0	5001	ph_brown	0.115	9		M-L Miocene	Msh.s	Dolati (2010)
5001	0	5002	ph_brown	3.215	9		M-L Miocene	Msh.s	Dolati (2010)
5002	0	5003	ph_brown	0.388	9		M-L Miocene	Msh.s	Dolati (2010)
5003	0	5004	ph_brown	0.413	9		M-L Miocene	Msh.s	Dolati (2010)
5004	0	5005	ph_brown	0.082	9		M-L Miocene	Msh.s	Dolati (2010)
5005	0	5006	ph_brown	0.051	9		M-L Miocene	Msh.s	Dolati (2010)
5006	0	5007	ph_brown	0.042	9		M-L Miocene	Msh.s	Dolati (2010)
5007	0	5008	ph_brown	0.014	9		M-L Miocene	Msh.s	Dolati (2010)
5008	0	5009	ph_brown	0.190	9		M-L Miocene	Msh.s	Dolati (2010)
5009	0	5010	ph_brown	0.621	9		M-L Miocene	Msh.s	Dolati (2010)
5010	0	5011	ph_brown	0.016	9		M-L Miocene	Msh.s	Dolati (2010)
5011	0	5012	ph_brown	0.048	9		M-L Miocene	Msh.s	Dolati (2010)
5012	0	5013	ph_brown	0.018	9		M-L Miocene	Msh.s	Dolati (2010)
5013	0	5014	ph_brown	0.097	9		M-L Miocene	Msh.s	Dolati (2010)
5014	0	5015	ph_brown	0.312	9		M-L Miocene	Msh.s	Dolati (2010)
5015	0	5016	ph_brown	0.029	9		M-L Miocene	Msh.s	Dolati (2010)
5016	0	5017	ph_brown	0.101	9		M-L Miocene	Msh.s	Dolati (2010)
5017	0	5018	ph_brown	0.019	9		M-L Miocene	Msh.s	Dolati (2010)
5018	0	5019	ph_brown	0.071	9		M-L Miocene	Msh.s	Dolati (2010)
5019	0	5020	ph_brown	0.189	9		M-L Miocene	Msh.s	Dolati (2010)
5020	0	5021	ph_brown	0.041	9		M-L Miocene	Msh.s	Dolati (2010)
5021	0	5022	ph_brown	1.664	9		M-L Miocene	Msh.s	Dolati (2010)
5022	0	5023	ph_brown	0.114	9		M-L Miocene	Msh.s	Dolati (2010)
5023	0	5024	ph_brown	0.195	9		M-L Miocene	Msh.s	Dolati (2010)
5024	0	5025	ph_brown	0.067	9		M-L Miocene	Msh.s	Dolati (2010)
5025	0	5026	ph_brown	0.518	9		M-L Miocene	Msh.s	Dolati (2010)
5026	0	5027	ph_brown	0.419	9		M-L Miocene	Msh.s	Dolati (2010)
5027	0	5028	ph_brown	0.010	9		M-L Miocene	Msh.s	Dolati (2010)
5028	0	5029	ph_brown	8.696	9		M-L Miocene	Msh.s	Dolati (2010)
5029	0	5030	ph_brown	0.446	9		M-L Miocene	Msh.s	Dolati (2010)

Geonevis

OBJECTID_1	Join_Count	TARGET_FID	Label	Shape_Area (sqkm)	ORIG_FID	Absolute_Age	Age_paleontology	Unit	Reference
5030	0	5031	ph_brown	0.054	9		M-L Miocene	Msh.s	Dolati (2010)
5031	0	5032	ph_brown	0.722	9		M-L Miocene	Msh.s	Dolati (2010)
5032	0	5033	ph_brown	0.198	9		M-L Miocene	Msh.s	Dolati (2010)
5033	0	5034	ph_brown	0.018	9		M-L Miocene	Msh.s	Dolati (2010)
5034	0	5035	ph_brown	0.279	9		M-L Miocene	Msh.s	Dolati (2010)
5035	0	5036	ph_brown	0.053	9		M-L Miocene	Msh.s	Dolati (2010)
5036	0	5037	ph_brown	0.157	9		M-L Miocene	Msh.s	Dolati (2010)
5037	0	5038	ph_brown	0.023	9		M-L Miocene	Msh.s	Dolati (2010)
5038	0	5039	ph_brown	0.100	9		M-L Miocene	Msh.s	Dolati (2010)
5039	0	5040	ph_brown	0.008	9		M-L Miocene	Msh.s	Dolati (2010)
5040	0	5041	ph_brown	0.352	9		M-L Miocene	Msh.s	Dolati (2010)
5041	0	5042	ph_brown	0.460	9		M-L Miocene	Msh.s	Dolati (2010)
5042	0	5043	ph_brown	0.045	9		M-L Miocene	Msh.s	Dolati (2010)
5043	0	5044	ph_brown	0.063	9		M-L Miocene	Msh.s	Dolati (2010)
5044	0	5045	ph_brown	0.271	9		M-L Miocene	Msh.s	Dolati (2010)
5045	0	5046	ph_brown	0.075	9		M-L Miocene	Msh.s	Dolati (2010)
5046	0	5047	ph_brown	0.092	9		M-L Miocene	Msh.s	Dolati (2010)
5047	0	5048	ph_brown	0.204	9		M-L Miocene	Msh.s	Dolati (2010)
5048	0	5049	ph_brown	0.032	9		M-L Miocene	Msh.s	Dolati (2010)
5049	0	5050	ph_brown	1.434	9		M-L Miocene	Msh.s	Dolati (2010)
5050	0	5051	ph_brown	0.014	9		M-L Miocene	Msh.s	Dolati (2010)
5051	0	5052	ph_brown	0.031	9		M-L Miocene	Msh.s	Dolati (2010)
5052	0	5053	ph_brown	3.440	9		M-L Miocene	Msh.s	Dolati (2010)
5053	0	5054	ph_brown	0.698	9		M-L Miocene	Msh.s	Dolati (2010)
5054	0	5055	ph_brown	0.060	9		M-L Miocene	Msh.s	Dolati (2010)
5055	0	5056	ph_brown	0.182	9		M-L Miocene	Msh.s	Dolati (2010)
5056	0	5057	ph_brown	0.172	9		M-L Miocene	Msh.s	Dolati (2010)
5057	0	5058	ph_brown	0.013	9		M-L Miocene	Msh.s	Dolati (2010)
5058	0	5059	ph_brown	0.071	9		M-L Miocene	Msh.s	Dolati (2010)
5059	0	5060	ph_brown	0.126	9		M-L Miocene	Msh.s	Dolati (2010)
5060	0	5061	ph_brown	0.213	9		M-L Miocene	Msh.s	Dolati (2010)
5061	0	5062	ph_brown	0.034	9		M-L Miocene	Msh.s	Dolati (2010)
5062	0	5063	ph_brown	1.462	9		M-L Miocene	Msh.s	Dolati (2010)
5063	0	5064	ph_brown	0.329	9		M-L Miocene	Msh.s	Dolati (2010)
5064	0	5065	ph_brown	0.132	9		M-L Miocene	Msh.s	Dolati (2010)
5065	0	5066	ph_brown	3.730	9		M-L Miocene	Msh.s	Dolati (2010)
5066	0	5067	ph_brown	0.037	9		M-L Miocene	Msh.s	Dolati (2010)
5067	0	5068	ph_brown	0.149	9		M-L Miocene	Msh.s	Dolati (2010)
5068	0	5069	ph_brown	0.486	9		M-L Miocene	Msh.s	Dolati (2010)

Geonevis

OBJECTID_1	Join_Count	TARGET_FID	Label	Shape_Area (sqkm)	ORIG_FID	Absolute_Age	Age_paleontology	Unit	Reference
5069	0	5070	ph_brown	0.532	9		M-L Miocene	Msh.s	Dolati (2010)
5070	0	5071	ph_brown	0.010	9		M-L Miocene	Msh.s	Dolati (2010)
5071	0	5072	ph_brown	0.022	9		M-L Miocene	Msh.s	Dolati (2010)
5072	0	5073	ph_brown	0.039	9		M-L Miocene	Msh.s	Dolati (2010)
5073	0	5074	ph_brown	0.056	9		M-L Miocene	Msh.s	Dolati (2010)
5074	0	5075	ph_brown	1.064	9		M-L Miocene	Msh.s	Dolati (2010)
5075	0	5076	ph_brown	0.019	9		M-L Miocene	Msh.s	Dolati (2010)
5076	0	5077	ph_brown	0.027	9		M-L Miocene	Msh.s	Dolati (2010)
5077	0	5078	ph_brown	0.418	9		M-L Miocene	Msh.s	Dolati (2010)
5078	0	5079	ph_brown	0.017	9		M-L Miocene	Msh.s	Dolati (2010)
5079	0	5080	ph_brown	0.009	9		M-L Miocene	Msh.s	Dolati (2010)
5080	0	5081	ph_brown	0.403	9		M-L Miocene	Msh.s	Dolati (2010)
5081	0	5082	ph_brown	1.451	9		M-L Miocene	Msh.s	Dolati (2010)
5082	0	5083	ph_brown	1.292	9		M-L Miocene	Msh.s	Dolati (2010)
5083	0	5084	ph_brown	2.350	9		M-L Miocene	Msh.s	Dolati (2010)
5084	0	5085	ph_brown	0.575	9		M-L Miocene	Msh.s	Dolati (2010)
5085	0	5086	ph_brown	0.146	9		M-L Miocene	Msh.s	Dolati (2010)
5086	0	5087	ph_brown	0.213	9		M-L Miocene	Msh.s	Dolati (2010)
5087	0	5088	ph_brown	0.074	9		M-L Miocene	Msh.s	Dolati (2010)
5088	0	5089	ph_brown	0.054	9		M-L Miocene	Msh.s	Dolati (2010)
5089	0	5090	ph_brown	0.379	9		M-L Miocene	Msh.s	Dolati (2010)
5090	0	5091	ph_brown	0.286	9		M-L Miocene	Msh.s	Dolati (2010)
5091	0	5092	ph_brown	0.026	9		M-L Miocene	Msh.s	Dolati (2010)
5092	0	5093	ph_brown	1.941	9		M-L Miocene	Msh.s	Dolati (2010)
5093	0	5094	ph_brown	0.396	9		M-L Miocene	Msh.s	Dolati (2010)
5094	0	5095	ph_brown	0.340	9		M-L Miocene	Msh.s	Dolati (2010)
5095	0	5096	ph_brown	0.096	9		M-L Miocene	Msh.s	Dolati (2010)
5096	0	5097	ph_brown	0.098	9		M-L Miocene	Msh.s	Dolati (2010)
5097	0	5098	ph_brown	0.068	9		M-L Miocene	Msh.s	Dolati (2010)
5098	0	5099	ph_brown	0.447	9		M-L Miocene	Msh.s	Dolati (2010)
5099	0	5100	ph_brown	0.784	9		M-L Miocene	Msh.s	Dolati (2010)
5100	0	5101	ph_brown	0.099	9		M-L Miocene	Msh.s	Dolati (2010)
5101	0	5102	ph_brown	0.036	9		M-L Miocene	Msh.s	Dolati (2010)
5102	0	5103	ph_brown	36.218	9		M-L Miocene	Msh.s	Dolati (2010)
5103	0	5104	ph_brown	0.052	9		M-L Miocene	Msh.s	Dolati (2010)
5104	0	5105	ph_brown	0.097	9		M-L Miocene	Msh.s	Dolati (2010)
5105	0	5106	ph_brown	1.278	9		M-L Miocene	Msh.s	Dolati (2010)
5106	0	5107	ph_brown	0.332	9		M-L Miocene	Msh.s	Dolati (2010)
5107	0	5108	ph_brown	0.064	9		M-L Miocene	Msh.s	Dolati (2010)

Geonevis

OBJECTID_1	Join_Count	TARGET_FID	Label	Shape_Area (sqkm)	ORIG_FID	Absolute_Age	Age_paleontology	Unit	Reference
5108	0	5109	ph_brown	0.047	9		M-L Miocene	Msh.s	Dolati (2010)
5109	0	5110	ph_brown	0.096	9		M-L Miocene	Msh.s	Dolati (2010)
5110	0	5111	ph_brown	0.075	9		M-L Miocene	Msh.s	Dolati (2010)
5111	0	5112	ph_brown	0.037	9		M-L Miocene	Msh.s	Dolati (2010)
5112	0	5113	ph_brown	0.236	9		M-L Miocene	Msh.s	Dolati (2010)
5113	0	5114	ph_brown	0.177	9		M-L Miocene	Msh.s	Dolati (2010)
5114	0	5115	ph_brown	0.178	9		M-L Miocene	Msh.s	Dolati (2010)
5115	0	5116	ph_brown	0.037	9		M-L Miocene	Msh.s	Dolati (2010)
5116	0	5117	ph_brown	0.604	9		M-L Miocene	Msh.s	Dolati (2010)
5117	0	5118	ph_brown	0.247	9		M-L Miocene	Msh.s	Dolati (2010)
5118	0	5119	ph_brown	0.628	9		M-L Miocene	Msh.s	Dolati (2010)
5119	0	5120	ph_brown	0.183	9		M-L Miocene	Msh.s	Dolati (2010)
5120	0	5121	ph_brown	0.090	9		M-L Miocene	Msh.s	Dolati (2010)
5121	0	5122	ph_brown	0.070	9		M-L Miocene	Msh.s	Dolati (2010)
5122	0	5123	ph_brown	1.334	9		M-L Miocene	Msh.s	Dolati (2010)
5123	0	5124	ph_brown	0.039	9		M-L Miocene	Msh.s	Dolati (2010)
5125	0	5126	ph_brown	0.033	9		M-L Miocene	Msh.s	Dolati (2010)
5126	0	5127	ph_brown	0.454	9		M-L Miocene	Msh.s	Dolati (2010)
5127	0	5128	ph_brown	0.162	9		M-L Miocene	Msh.s	Dolati (2010)
5128	0	5129	ph_brown	1.189	9		M-L Miocene	Msh.s	Dolati (2010)
5129	0	5130	ph_brown	0.060	9		M-L Miocene	Msh.s	Dolati (2010)
5130	0	5131	ph_brown	0.108	9		M-L Miocene	Msh.s	Dolati (2010)
5131	0	5132	ph_brown	0.108	9		M-L Miocene	Msh.s	Dolati (2010)
5132	0	5133	ph_brown	0.780	9		M-L Miocene	Msh.s	Dolati (2010)
5133	0	5134	ph_brown	0.053	9		M-L Miocene	Msh.s	Dolati (2010)
5134	0	5135	ph_brown	0.087	9		M-L Miocene	Msh.s	Dolati (2010)
5135	0	5136	ph_brown	0.350	9		M-L Miocene	Msh.s	Dolati (2010)
5136	0	5137	ph_brown	0.283	9		M-L Miocene	Msh.s	Dolati (2010)
5137	0	5138	ph_brown	0.108	9		M-L Miocene	Msh.s	Dolati (2010)
5138	0	5139	ph_brown	0.465	9		M-L Miocene	Msh.s	Dolati (2010)
5139	0	5140	ph_brown	0.077	9		M-L Miocene	Msh.s	Dolati (2010)
5140	0	5141	ph_brown	0.197	9		M-L Miocene	Msh.s	Dolati (2010)
5141	0	5142	ph_brown	0.300	9		M-L Miocene	Msh.s	Dolati (2010)
5142	0	5143	ph_brown	0.119	9		M-L Miocene	Msh.s	Dolati (2010)
5143	0	5144	ph_brown	0.084	9		M-L Miocene	Msh.s	Dolati (2010)
5144	0	5145	ph_brown	0.444	9		M-L Miocene	Msh.s	Dolati (2010)
5145	0	5146	ph_brown	0.487	9		M-L Miocene	Msh.s	Dolati (2010)
5146	0	5147	ph_brown	0.044	9		M-L Miocene	Msh.s	Dolati (2010)
5147	0	5148	ph_brown	1.549	9		M-L Miocene	Msh.s	Dolati (2010)

Geonevis

OBJECTID_1	Join_Count	TARGET_FID	Label	Shape_Area (sqkm)	ORIG_FID	Absolute_Age	Age_paleontology	Unit	Reference
5148	0	5149	ph_brown	0.031	9		M-L Miocene	Msh.s	Dolati (2010)
5149	0	5150	ph_brown	0.347	9		M-L Miocene	Msh.s	Dolati (2010)
5150	0	5151	ph_brown	0.040	9		M-L Miocene	Msh.s	Dolati (2010)
5151	0	5152	ph_brown	2.061	9		M-L Miocene	Msh.s	Dolati (2010)
5152	0	5153	ph_brown	0.026	9		M-L Miocene	Msh.s	Dolati (2010)
5153	0	5154	ph_brown	0.139	9		M-L Miocene	Msh.s	Dolati (2010)
5154	0	5155	ph_brown	0.749	9		M-L Miocene	Msh.s	Dolati (2010)
5155	0	5156	ph_brown	0.257	9		M-L Miocene	Msh.s	Dolati (2010)
5156	0	5157	ph_brown	0.052	9		M-L Miocene	Msh.s	Dolati (2010)
5157	0	5158	ph_brown	0.388	9		M-L Miocene	Msh.s	Dolati (2010)
5158	0	5159	ph_brown	0.596	9		M-L Miocene	Msh.s	Dolati (2010)
5159	0	5160	ph_brown	0.158	9		M-L Miocene	Msh.s	Dolati (2010)
5160	0	5161	ph_brown	0.030	9		M-L Miocene	Msh.s	Dolati (2010)
5161	0	5162	ph_brown	0.709	9		M-L Miocene	Msh.s	Dolati (2010)
5162	0	5163	ph_brown	0.141	9		M-L Miocene	Msh.s	Dolati (2010)
5163	0	5164	ph_brown	0.497	9		M-L Miocene	Msh.s	Dolati (2010)
5164	0	5165	ph_brown	256.962	9		M-L Miocene	Msh.s	Dolati (2010)
5165	0	5166	ph_brown	0.784	9		M-L Miocene	Msh.s	Dolati (2010)
5166	0	5167	ph_brown	0.525	9		M-L Miocene	Msh.s	Dolati (2010)
5167	0	5168	ph_brown	0.356	9		M-L Miocene	Msh.s	Dolati (2010)
5169	0	5170	ph_brown	1.222	9		M-L Miocene	Msh.s	Dolati (2010)
5170	0	5171	ph_brown	0.072	9		M-L Miocene	Msh.s	Dolati (2010)
5171	0	5172	ph_brown	0.090	9		M-L Miocene	Msh.s	Dolati (2010)
5172	0	5173	ph_brown	0.408	9		M-L Miocene	Msh.s	Dolati (2010)
5173	0	5174	ph_brown	0.314	9		M-L Miocene	Msh.s	Dolati (2010)
5174	0	5175	ph_brown	0.021	9		M-L Miocene	Msh.s	Dolati (2010)
5175	0	5176	ph_brown	0.604	9		M-L Miocene	Msh.s	Dolati (2010)
5176	0	5177	ph_brown	0.126	9		M-L Miocene	Msh.s	Dolati (2010)
5177	0	5178	ph_brown	7.206	9		M-L Miocene	Msh.s	Dolati (2010)
5178	0	5179	ph_brown	0.684	9		M-L Miocene	Msh.s	Dolati (2010)
5179	0	5180	ph_brown	0.729	9		M-L Miocene	Msh.s	Dolati (2010)
5180	0	5181	ph_brown	2.201	9		M-L Miocene	Msh.s	Dolati (2010)
5181	0	5182	ph_brown	0.068	9		M-L Miocene	Msh.s	Dolati (2010)
5182	0	5183	ph_brown	1.073	9		M-L Miocene	Msh.s	Dolati (2010)
5183	0	5184	ph_brown	3.451	9		M-L Miocene	Msh.s	Dolati (2010)
5184	0	5185	ph_brown	0.218	9		M-L Miocene	Msh.s	Dolati (2010)
5185	0	5186	ph_brown	0.039	9		M-L Miocene	Msh.s	Dolati (2010)
5186	0	5187	ph_brown	0.032	9		M-L Miocene	Msh.s	Dolati (2010)
5187	0	5188	ph_brown	0.134	9		M-L Miocene	Msh.s	Dolati (2010)

Geonevis

OBJECTID_1	Join_Count	TARGET_FID	Label	Shape_Area (sqkm)	ORIG_FID	Absolute_Age	Age_paleontology	Unit	Reference
5188	0	5189	ph_brown	0.611	9		M-L Miocene	Msh.s	Dolati (2010)
5189	0	5190	ph_brown	1.312	9		M-L Miocene	Msh.s	Dolati (2010)
5191	0	5192	ph_brown	0.048	9		M-L Miocene	Msh.s	Dolati (2010)
5192	0	5193	ph_brown	0.224	9		M-L Miocene	Msh.s	Dolati (2010)
5193	0	5194	ph_brown	0.012	9		M-L Miocene	Msh.s	Dolati (2010)
5194	0	5195	ph_brown	0.646	9		M-L Miocene	Msh.s	Dolati (2010)
5195	0	5196	ph_brown	0.045	9		M-L Miocene	Msh.s	Dolati (2010)
5196	0	5197	ph_brown	0.261	9		M-L Miocene	Msh.s	Dolati (2010)
5197	0	5198	ph_brown	0.095	9		M-L Miocene	Msh.s	Dolati (2010)
5198	0	5199	ph_brown	1.539	9		M-L Miocene	Msh.s	Dolati (2010)
5199	0	5200	ph_brown	0.045	9		M-L Miocene	Msh.s	Dolati (2010)
5200	0	5201	ph_brown	1.287	9		M-L Miocene	Msh.s	Dolati (2010)
5201	0	5202	ph_brown	0.161	9		M-L Miocene	Msh.s	Dolati (2010)
5202	0	5203	ph_brown	0.040	9		M-L Miocene	Msh.s	Dolati (2010)
5203	0	5204	ph_brown	0.031	9		M-L Miocene	Msh.s	Dolati (2010)
5204	0	5205	ph_brown	0.172	9		M-L Miocene	Msh.s	Dolati (2010)
5205	0	5206	ph_brown	0.153	9		M-L Miocene	Msh.s	Dolati (2010)
5206	0	5207	ph_brown	0.078	9		M-L Miocene	Msh.s	Dolati (2010)
5207	0	5208	ph_brown	0.967	9		M-L Miocene	Msh.s	Dolati (2010)
5209	0	5210	ph_brown	0.063	9		M-L Miocene	Msh.s	Dolati (2010)
5210	0	5211	ph_brown	0.897	9		M-L Miocene	Msh.s	Dolati (2010)
5211	0	5212	ph_brown	0.069	9		M-L Miocene	Msh.s	Dolati (2010)
5212	0	5213	ph_brown	0.344	9		M-L Miocene	Msh.s	Dolati (2010)
5213	0	5214	ph_brown	0.058	9		M-L Miocene	Msh.s	Dolati (2010)
5214	0	5215	ph_brown	0.089	9		M-L Miocene	Msh.s	Dolati (2010)
5215	0	5216	ph_brown	0.149	9		M-L Miocene	Msh.s	Dolati (2010)
5216	0	5217	ph_brown	0.132	9		M-L Miocene	Msh.s	Dolati (2010)
5217	0	5218	ph_brown	1.923	9		M-L Miocene	Msh.s	Dolati (2010)
5218	0	5219	ph_brown	0.382	9		M-L Miocene	Msh.s	Dolati (2010)
5219	0	5220	ph_brown	0.640	9		M-L Miocene	Msh.s	Dolati (2010)
5220	0	5221	ph_brown	0.052	9		M-L Miocene	Msh.s	Dolati (2010)
5221	0	5222	ph_brown	0.164	9		M-L Miocene	Msh.s	Dolati (2010)
5222	0	5223	ph_brown	0.143	9		M-L Miocene	Msh.s	Dolati (2010)
5224	0	5225	ph_brown	0.131	9		M-L Miocene	Msh.s	Dolati (2010)
5225	0	5226	ph_brown	0.085	9		M-L Miocene	Msh.s	Dolati (2010)
5226	0	5227	ph_brown	0.251	9		M-L Miocene	Msh.s	Dolati (2010)
5227	0	5228	ph_brown	0.233	9		M-L Miocene	Msh.s	Dolati (2010)
5228	0	5229	ph_brown	0.025	9		M-L Miocene	Msh.s	Dolati (2010)
5229	0	5230	ph_brown	0.246	9		M-L Miocene	Msh.s	Dolati (2010)

Geonevis

OBJECTID_1	Join_Count	TARGET_FID	Label	Shape_Area (sqkm)	ORIG_FID	Absolute_Age	Age_paleontology	Unit	Reference
5230	0	5231	ph_brown	0.078	9		M-L Miocene	Msh.s	Dolati (2010)
5231	0	5232	ph_brown	0.289	9		M-L Miocene	Msh.s	Dolati (2010)
5233	0	5234	ph_brown	0.196	9		M-L Miocene	Msh.s	Dolati (2010)
5234	0	5235	ph_brown	0.239	9		M-L Miocene	Msh.s	Dolati (2010)
5235	0	5236	ph_brown	0.133	9		M-L Miocene	Msh.s	Dolati (2010)
5236	0	5237	ph_brown	0.052	9		M-L Miocene	Msh.s	Dolati (2010)
5237	0	5238	ph_brown	0.537	9		M-L Miocene	Msh.s	Dolati (2010)
5239	0	5240	ph_brown	0.041	9		M-L Miocene	Msh.s	Dolati (2010)
5240	0	5241	ph_brown	0.163	9		M-L Miocene	Msh.s	Dolati (2010)
5241	0	5242	ph_brown	0.041	9		M-L Miocene	Msh.s	Dolati (2010)
5242	0	5243	ph_brown	0.296	9		M-L Miocene	Msh.s	Dolati (2010)
5243	0	5244	ph_brown	0.064	9		M-L Miocene	Msh.s	Dolati (2010)
5245	0	5246	ph_brown	0.039	9		M-L Miocene	Msh.s	Dolati (2010)
5246	0	5247	ph_brown	0.035	9		M-L Miocene	Msh.s	Dolati (2010)
5247	0	5248	ph_brown	1.945	9		M-L Miocene	Msh.s	Dolati (2010)
5248	0	5249	ph_brown	0.216	9		M-L Miocene	Msh.s	Dolati (2010)
5249	0	5250	ph_brown	0.112	9		M-L Miocene	Msh.s	Dolati (2010)
5250	0	5251	ph_brown	0.327	9		M-L Miocene	Msh.s	Dolati (2010)
5251	0	5252	ph_brown	0.140	9		M-L Miocene	Msh.s	Dolati (2010)
5252	0	5253	ph_brown	0.029	9		M-L Miocene	Msh.s	Dolati (2010)
5253	0	5254	ph_brown	0.010	9		M-L Miocene	Msh.s	Dolati (2010)
5254	0	5255	ph_brown	0.083	9		M-L Miocene	Msh.s	Dolati (2010)
5255	0	5256	ph_brown	0.877	9		M-L Miocene	Msh.s	Dolati (2010)
5256	0	5257	ph_brown	0.072	9		M-L Miocene	Msh.s	Dolati (2010)
5257	0	5258	ph_brown	0.066	9		M-L Miocene	Msh.s	Dolati (2010)
5258	0	5259	ph_brown	0.194	9		M-L Miocene	Msh.s	Dolati (2010)
5259	0	5260	ph_brown	1.149	9		M-L Miocene	Msh.s	Dolati (2010)
5260	0	5261	ph_brown	0.053	9		M-L Miocene	Msh.s	Dolati (2010)
5261	0	5262	ph_brown	0.165	9		M-L Miocene	Msh.s	Dolati (2010)
5262	0	5263	ph_brown	1.615	9		M-L Miocene	Msh.s	Dolati (2010)
5264	0	5265	ph_brown	0.421	9		M-L Miocene	Msh.s	Dolati (2010)
5265	0	5266	ph_brown	0.025	9		M-L Miocene	Msh.s	Dolati (2010)
5266	0	5267	ph_brown	1.392	9		M-L Miocene	Msh.s	Dolati (2010)
5267	0	5268	ph_brown	0.061	9		M-L Miocene	Msh.s	Dolati (2010)
5268	0	5269	ph_brown	0.183	9		M-L Miocene	Msh.s	Dolati (2010)
5269	0	5270	ph_brown	0.048	9		M-L Miocene	Msh.s	Dolati (2010)
5270	0	5271	ph_brown	1.012	9		M-L Miocene	Msh.s	Dolati (2010)
5271	0	5272	ph_brown	2.155	9		M-L Miocene	Msh.s	Dolati (2010)
5272	0	5273	ph_brown	0.570	9		M-L Miocene	Msh.s	Dolati (2010)

Geonevis

OBJECTID_1	Join_Count	TARGET_FID	Label	Shape_Area (sqkm)	ORIG_FID	Absolute_Age	Age_paleontology	Unit	Reference
5273	0	5274	ph_brown	0.405	9		M-L Miocene	Msh.s	Dolati (2010)
5274	0	5275	ph_brown	0.113	9		M-L Miocene	Msh.s	Dolati (2010)
5275	0	5276	ph_brown	0.149	9		M-L Miocene	Msh.s	Dolati (2010)
5276	0	5277	ph_brown	0.447	9		M-L Miocene	Msh.s	Dolati (2010)
5278	0	5279	ph_brown	0.018	9		M-L Miocene	Msh.s	Dolati (2010)
5279	0	5280	ph_brown	0.553	9		M-L Miocene	Msh.s	Dolati (2010)
5280	0	5281	ph_brown	0.044	9		M-L Miocene	Msh.s	Dolati (2010)
5281	0	5282	ph_brown	0.307	9		M-L Miocene	Msh.s	Dolati (2010)
5282	0	5283	ph_brown	0.133	9		M-L Miocene	Msh.s	Dolati (2010)
5283	0	5284	ph_brown	0.074	9		M-L Miocene	Msh.s	Dolati (2010)
5284	0	5285	ph_brown	0.306	9		M-L Miocene	Msh.s	Dolati (2010)
5285	0	5286	ph_brown	0.237	9		M-L Miocene	Msh.s	Dolati (2010)
5286	0	5287	ph_brown	0.843	9		M-L Miocene	Msh.s	Dolati (2010)
5287	0	5288	ph_brown	0.041	9		M-L Miocene	Msh.s	Dolati (2010)
5288	0	5289	ph_brown	1.454	9		M-L Miocene	Msh.s	Dolati (2010)
5289	0	5290	ph_brown	0.178	9		M-L Miocene	Msh.s	Dolati (2010)
5290	0	5291	ph_brown	0.057	9		M-L Miocene	Msh.s	Dolati (2010)
5291	0	5292	ph_brown	0.160	9		M-L Miocene	Msh.s	Dolati (2010)
5292	0	5293	ph_brown	0.201	9		M-L Miocene	Msh.s	Dolati (2010)
5293	0	5294	ph_brown	0.379	9		M-L Miocene	Msh.s	Dolati (2010)
5294	0	5295	ph_brown	0.099	9		M-L Miocene	Msh.s	Dolati (2010)
5296	0	5297	ph_brown	0.060	9		M-L Miocene	Msh.s	Dolati (2010)
5297	0	5298	ph_brown	0.430	9		M-L Miocene	Msh.s	Dolati (2010)
5298	0	5299	ph_brown	0.398	9		M-L Miocene	Msh.s	Dolati (2010)
5299	0	5300	ph_brown	0.367	9		M-L Miocene	Msh.s	Dolati (2010)
5300	0	5301	ph_brown	0.293	9		M-L Miocene	Msh.s	Dolati (2010)
5301	0	5302	ph_brown	0.592	9		M-L Miocene	Msh.s	Dolati (2010)
5302	0	5303	ph_brown	3.562	9		M-L Miocene	Msh.s	Dolati (2010)
5303	0	5304	ph_brown	0.155	9		M-L Miocene	Msh.s	Dolati (2010)
5304	0	5305	ph_brown	0.476	9		M-L Miocene	Msh.s	Dolati (2010)
5305	0	5306	ph_brown	1.763	9		M-L Miocene	Msh.s	Dolati (2010)
5306	0	5307	ph_brown	0.117	9		M-L Miocene	Msh.s	Dolati (2010)
5308	0	5309	ph_brown	0.619	9		M-L Miocene	Msh.s	Dolati (2010)
5309	0	5310	ph_brown	0.161	9		M-L Miocene	Msh.s	Dolati (2010)
5310	0	5311	ph_brown	0.394	9		M-L Miocene	Msh.s	Dolati (2010)
5311	0	5312	ph_brown	0.968	9		M-L Miocene	Msh.s	Dolati (2010)
5312	0	5313	ph_brown	0.499	9		M-L Miocene	Msh.s	Dolati (2010)
5313	0	5314	ph_brown	0.023	9		M-L Miocene	Msh.s	Dolati (2010)
5314	0	5315	ph_brown	0.231	9		M-L Miocene	Msh.s	Dolati (2010)

Geonevis

OBJECTID_1	Join_Count	TARGET_FID	Label	Shape_Area (sqkm)	ORIG_FID	Absolute_Age	Age_paleontology	Unit	Reference
5315	0	5316	ph_brown	0.204	9		M-L Miocene	Msh.s	Dolati (2010)
5316	0	5317	ph_brown	0.105	9		M-L Miocene	Msh.s	Dolati (2010)
5317	0	5318	ph_brown	0.031	9		M-L Miocene	Msh.s	Dolati (2010)
5318	0	5319	ph_brown	0.068	9		M-L Miocene	Msh.s	Dolati (2010)
5321	0	5322	ph_brown	0.037	9		M-L Miocene	Msh.s	Dolati (2010)
5322	0	5323	ph_brown	0.605	9		M-L Miocene	Msh.s	Dolati (2010)
5323	0	5324	ph_brown	0.069	9		M-L Miocene	Msh.s	Dolati (2010)
5324	0	5325	ph_brown	0.705	9		M-L Miocene	Msh.s	Dolati (2010)
5325	0	5326	ph_brown	0.520	9		M-L Miocene	Msh.s	Dolati (2010)
5327	0	5328	ph_brown	0.041	9		M-L Miocene	Msh.s	Dolati (2010)
5328	0	5329	ph_brown	0.071	9		M-L Miocene	Msh.s	Dolati (2010)
5329	0	5330	ph_brown	2.916	9		M-L Miocene	Msh.s	Dolati (2010)
5331	0	5332	ph_brown	0.106	9		M-L Miocene	Msh.s	Dolati (2010)
5333	0	5334	ph_brown	6.569	9		M-L Miocene	Msh.s	Dolati (2010)
5334	0	5335	ph_brown	0.110	9		M-L Miocene	Msh.s	Dolati (2010)
5335	0	5336	ph_brown	1.582	9		M-L Miocene	Msh.s	Dolati (2010)
5336	0	5337	ph_brown	0.310	9		M-L Miocene	Msh.s	Dolati (2010)
5338	0	5339	ph_brown	0.331	9		M-L Miocene	Msh.s	Dolati (2010)
5339	0	5340	ph_brown	0.151	9		M-L Miocene	Msh.s	Dolati (2010)
5340	0	5341	ph_brown	0.111	9		M-L Miocene	Msh.s	Dolati (2010)
5341	0	5342	ph_brown	1.959	9		M-L Miocene	Msh.s	Dolati (2010)
5342	0	5343	ph_brown	0.079	9		M-L Miocene	Msh.s	Dolati (2010)
5343	0	5344	ph_brown	0.084	9		M-L Miocene	Msh.s	Dolati (2010)
5344	0	5345	ph_brown	0.096	9		M-L Miocene	Msh.s	Dolati (2010)
5345	0	5346	ph_brown	0.247	9		M-L Miocene	Msh.s	Dolati (2010)
5346	0	5347	ph_brown	0.239	9		M-L Miocene	Msh.s	Dolati (2010)
5347	0	5348	ph_brown	0.045	9		M-L Miocene	Msh.s	Dolati (2010)
5348	0	5349	ph_brown	0.219	9		M-L Miocene	Msh.s	Dolati (2010)
5350	0	5351	ph_brown	0.232	9		M-L Miocene	Msh.s	Dolati (2010)
5351	0	5352	ph_brown	0.131	9		M-L Miocene	Msh.s	Dolati (2010)
5352	0	5353	ph_brown	4.190	9		M-L Miocene	Msh.s	Dolati (2010)
5353	0	5354	ph_brown	0.207	9		M-L Miocene	Msh.s	Dolati (2010)
5354	0	5355	ph_brown	0.062	9		M-L Miocene	Msh.s	Dolati (2010)
5355	0	5356	ph_brown	5.587	9		M-L Miocene	Msh.s	Dolati (2010)
5356	0	5357	ph_brown	0.082	9		M-L Miocene	Msh.s	Dolati (2010)
5357	0	5358	ph_brown	0.802	9		M-L Miocene	Msh.s	Dolati (2010)
5358	0	5359	ph_brown	0.892	9		M-L Miocene	Msh.s	Dolati (2010)
5359	0	5360	ph_brown	0.145	9		M-L Miocene	Msh.s	Dolati (2010)
5360	0	5361	ph_brown	5.271	9		M-L Miocene	Msh.s	Dolati (2010)

Geonevis

OBJECTID_1	Join_Count	TARGET_FID	Label	Shape_Area (sqkm)	ORIG_FID	Absolute_Age	Age_paleontology	Unit	Reference
5361	0	5362	ph_brown	0.176	9		M-L Miocene	Msh.s	Dolati (2010)
5362	0	5363	ph_brown	0.026	9		M-L Miocene	Msh.s	Dolati (2010)
5363	0	5364	ph_brown	0.730	9		M-L Miocene	Msh.s	Dolati (2010)
5364	0	5365	ph_brown	1.108	9		M-L Miocene	Msh.s	Dolati (2010)
5365	0	5366	ph_brown	0.628	9		M-L Miocene	Msh.s	Dolati (2010)
5366	0	5367	ph_brown	1.130	9		M-L Miocene	Msh.s	Dolati (2010)
5367	0	5368	ph_brown	0.991	9		M-L Miocene	Msh.s	Dolati (2010)
5368	0	5369	ph_brown	0.047	9		M-L Miocene	Msh.s	Dolati (2010)
5369	0	5370	ph_brown	0.080	9		M-L Miocene	Msh.s	Dolati (2010)
5370	0	5371	ph_brown	0.253	9		M-L Miocene	Msh.s	Dolati (2010)
5371	0	5372	ph_brown	0.637	9		M-L Miocene	Msh.s	Dolati (2010)
5372	0	5373	ph_brown	0.177	9		M-L Miocene	Msh.s	Dolati (2010)
5373	0	5374	ph_brown	0.309	9		M-L Miocene	Msh.s	Dolati (2010)
5374	0	5375	ph_brown	1.058	9		M-L Miocene	Msh.s	Dolati (2010)
5375	0	5376	ph_brown	5.137	9		M-L Miocene	Msh.s	Dolati (2010)
5376	0	5377	ph_brown	1.062	9		M-L Miocene	Msh.s	Dolati (2010)
5377	0	5378	ph_brown	0.277	9		M-L Miocene	Msh.s	Dolati (2010)
5378	0	5379	ph_brown	0.442	9		M-L Miocene	Msh.s	Dolati (2010)
5379	0	5380	ph_brown	0.073	9		M-L Miocene	Msh.s	Dolati (2010)
5380	0	5381	ph_brown	0.019	9		M-L Miocene	Msh.s	Dolati (2010)
5381	0	5382	ph_brown	0.149	9		M-L Miocene	Msh.s	Dolati (2010)
5382	0	5383	ph_brown	0.552	9		M-L Miocene	Msh.s	Dolati (2010)
5383	0	5384	ph_brown	0.714	9		M-L Miocene	Msh.s	Dolati (2010)
5384	0	5385	ph_brown	0.035	9		M-L Miocene	Msh.s	Dolati (2010)
5385	0	5386	ph_brown	0.144	9		M-L Miocene	Msh.s	Dolati (2010)
5386	0	5387	ph_brown	0.222	9		M-L Miocene	Msh.s	Dolati (2010)
5387	0	5388	ph_brown	0.051	9		M-L Miocene	Msh.s	Dolati (2010)
5388	0	5389	ph_brown	1.160	9		M-L Miocene	Msh.s	Dolati (2010)
5389	0	5390	ph_brown	0.110	9		M-L Miocene	Msh.s	Dolati (2010)
5390	0	5391	ph_brown	6.847	9		M-L Miocene	Msh.s	Dolati (2010)
5391	0	5392	ph_brown	0.128	9		M-L Miocene	Msh.s	Dolati (2010)
5392	0	5393	ph_brown	0.232	9		M-L Miocene	Msh.s	Dolati (2010)
5393	0	5394	ph_brown	0.554	9		M-L Miocene	Msh.s	Dolati (2010)
5394	0	5395	ph_brown	0.038	9		M-L Miocene	Msh.s	Dolati (2010)
5395	0	5396	ph_brown	0.104	9		M-L Miocene	Msh.s	Dolati (2010)
5396	0	5397	ph_brown	0.476	9		M-L Miocene	Msh.s	Dolati (2010)
5397	0	5398	ph_brown	0.914	9		M-L Miocene	Msh.s	Dolati (2010)
5398	0	5399	ph_brown	0.152	9		M-L Miocene	Msh.s	Dolati (2010)
5399	0	5400	ph_brown	0.466	9		M-L Miocene	Msh.s	Dolati (2010)

Geonevis

OBJECTID_1	Join_Count	TARGET_FID	Label	Shape_Area (sqkm)	ORIG_FID	Absolute_Age	Age_paleontology	Unit	Reference
5400	0	5401	ph_brown	0.186	9		M-L Miocene	Msh.s	Dolati (2010)
5401	0	5402	ph_brown	0.383	9		M-L Miocene	Msh.s	Dolati (2010)
5402	0	5403	ph_brown	0.102	9		M-L Miocene	Msh.s	Dolati (2010)
5403	0	5404	ph_brown	0.288	9		M-L Miocene	Msh.s	Dolati (2010)
5404	0	5405	ph_brown	0.489	9		M-L Miocene	Msh.s	Dolati (2010)
5405	0	5406	ph_brown	0.451	9		M-L Miocene	Msh.s	Dolati (2010)
5406	0	5407	ph_brown	0.041	9		M-L Miocene	Msh.s	Dolati (2010)
5407	0	5408	ph_brown	0.098	9		M-L Miocene	Msh.s	Dolati (2010)
5408	0	5409	ph_brown	0.864	9		M-L Miocene	Msh.s	Dolati (2010)
5409	0	5410	ph_brown	0.808	9		M-L Miocene	Msh.s	Dolati (2010)
5410	0	5411	ph_brown	0.122	9		M-L Miocene	Msh.s	Dolati (2010)
5411	0	5412	ph_brown	1.260	9		M-L Miocene	Msh.s	Dolati (2010)
5412	0	5413	ph_brown	0.780	9		M-L Miocene	Msh.s	Dolati (2010)
5414	0	5415	ph_brown	0.410	9		M-L Miocene	Msh.s	Dolati (2010)
5415	0	5416	ph_brown	0.105	9		M-L Miocene	Msh.s	Dolati (2010)
5416	0	5417	ph_brown	0.517	9		M-L Miocene	Msh.s	Dolati (2010)
5417	0	5418	ph_brown	1.076	9		M-L Miocene	Msh.s	Dolati (2010)
5418	0	5419	ph_brown	0.155	9		M-L Miocene	Msh.s	Dolati (2010)
5419	0	5420	ph_brown	0.071	9		M-L Miocene	Msh.s	Dolati (2010)
5420	0	5421	ph_brown	0.212	9		M-L Miocene	Msh.s	Dolati (2010)
5421	0	5422	ph_brown	0.153	9		M-L Miocene	Msh.s	Dolati (2010)
5422	0	5423	ph_brown	0.180	9		M-L Miocene	Msh.s	Dolati (2010)
5423	0	5424	ph_brown	0.141	9		M-L Miocene	Msh.s	Dolati (2010)
5424	0	5425	ph_brown	3.184	9		M-L Miocene	Msh.s	Dolati (2010)
5425	0	5426	ph_brown	0.041	9		M-L Miocene	Msh.s	Dolati (2010)
5426	0	5427	ph_brown	0.007	9		M-L Miocene	Msh.s	Dolati (2010)
5427	0	5428	ph_brown	0.540	9		M-L Miocene	Msh.s	Dolati (2010)
5428	0	5429	ph_brown	0.625	9		M-L Miocene	Msh.s	Dolati (2010)
5429	0	5430	ph_brown	0.082	9		M-L Miocene	Msh.s	Dolati (2010)
5430	0	5431	ph_brown	0.491	9		M-L Miocene	Msh.s	Dolati (2010)
5431	0	5432	ph_brown	0.107	9		M-L Miocene	Msh.s	Dolati (2010)
5432	0	5433	ph_brown	1.076	9		M-L Miocene	Msh.s	Dolati (2010)
5433	0	5434	ph_brown	0.273	9		M-L Miocene	Msh.s	Dolati (2010)
5434	0	5435	ph_brown	0.572	9		M-L Miocene	Msh.s	Dolati (2010)
5435	0	5436	ph_brown	5.512	9		M-L Miocene	Msh.s	Dolati (2010)
5436	0	5437	ph_brown	0.129	9		M-L Miocene	Msh.s	Dolati (2010)
5437	0	5438	ph_brown	0.583	9		M-L Miocene	Msh.s	Dolati (2010)
5438	0	5439	ph_brown	0.242	9		M-L Miocene	Msh.s	Dolati (2010)
5439	0	5440	ph_brown	1.377	9		M-L Miocene	Msh.s	Dolati (2010)

Geonevis

OBJECTID_1	Join_Count	TARGET_FID	Label	Shape_Area (sqkm)	ORIG_FID	Absolute_Age	Age_paleontology	Unit	Reference
5440	0	5441	ph_brown	0.100	9		M-L Miocene	Msh.s	Dolati (2010)
5441	0	5442	ph_brown	0.723	9		M-L Miocene	Msh.s	Dolati (2010)
5442	0	5443	ph_brown	0.429	9		M-L Miocene	Msh.s	Dolati (2010)
5443	0	5444	ph_brown	2.280	9		M-L Miocene	Msh.s	Dolati (2010)
5444	0	5445	ph_brown	0.867	9		M-L Miocene	Msh.s	Dolati (2010)
5445	0	5446	ph_brown	0.104	9		M-L Miocene	Msh.s	Dolati (2010)
5446	0	5447	ph_brown	0.454	9		M-L Miocene	Msh.s	Dolati (2010)
5447	0	5448	ph_brown	0.200	9		M-L Miocene	Msh.s	Dolati (2010)
5448	0	5449	ph_brown	0.098	9		M-L Miocene	Msh.s	Dolati (2010)
5449	0	5450	ph_brown	0.628	9		M-L Miocene	Msh.s	Dolati (2010)
5450	0	5451	ph_brown	0.150	9		M-L Miocene	Msh.s	Dolati (2010)
5451	0	5452	ph_brown	0.392	9		M-L Miocene	Msh.s	Dolati (2010)
5452	0	5453	ph_brown	0.717	9		M-L Miocene	Msh.s	Dolati (2010)
5453	0	5454	ph_brown	0.103	9		M-L Miocene	Msh.s	Dolati (2010)
5454	0	5455	ph_brown	0.413	9		M-L Miocene	Msh.s	Dolati (2010)
5455	0	5456	ph_brown	0.723	9		M-L Miocene	Msh.s	Dolati (2010)
5456	0	5457	ph_brown	1.474	9		M-L Miocene	Msh.s	Dolati (2010)
5457	0	5458	ph_brown	0.478	9		M-L Miocene	Msh.s	Dolati (2010)
5458	0	5459	ph_brown	2.167	9		M-L Miocene	Msh.s	Dolati (2010)
5459	0	5460	ph_brown	0.135	9		M-L Miocene	Msh.s	Dolati (2010)
5460	0	5461	ph_brown	3.075	9		M-L Miocene	Msh.s	Dolati (2010)
5461	0	5462	ph_brown	0.584	9		M-L Miocene	Msh.s	Dolati (2010)
5462	0	5463	ph_brown	0.025	9		M-L Miocene	Msh.s	Dolati (2010)
5463	0	5464	ph_brown	0.541	9		M-L Miocene	Msh.s	Dolati (2010)
5464	0	5465	ph_brown	0.737	9		M-L Miocene	Msh.s	Dolati (2010)
5465	0	5466	ph_brown	0.432	9		M-L Miocene	Msh.s	Dolati (2010)
5466	0	5467	ph_brown	1.834	9		M-L Miocene	Msh.s	Dolati (2010)
5467	0	5468	ph_brown	0.088	9		M-L Miocene	Msh.s	Dolati (2010)
5468	0	5469	ph_brown	2.219	9		M-L Miocene	Msh.s	Dolati (2010)
5469	0	5470	ph_brown	0.361	9		M-L Miocene	Msh.s	Dolati (2010)
5470	0	5471	ph_brown	0.511	9		M-L Miocene	Msh.s	Dolati (2010)
5471	0	5472	ph_brown	1.664	9		M-L Miocene	Msh.s	Dolati (2010)
5472	0	5473	ph_brown	0.455	9		M-L Miocene	Msh.s	Dolati (2010)
5473	0	5474	ph_brown	0.293	9		M-L Miocene	Msh.s	Dolati (2010)
5474	0	5475	ph_brown	0.008	9		M-L Miocene	Msh.s	Dolati (2010)
5475	0	5476	ph_brown	2.553	9		M-L Miocene	Msh.s	Dolati (2010)
5476	0	5477	ph_brown	0.734	9		M-L Miocene	Msh.s	Dolati (2010)
5477	0	5478	ph_brown	1.726	9		M-L Miocene	Msh.s	Dolati (2010)
5478	0	5479	ph_brown	1.124	9		M-L Miocene	Msh.s	Dolati (2010)

Geonevis

OBJECTID_1	Join_Count	TARGET_FID	Label	Shape_Area (sqkm)	ORIG_FID	Absolute_Age	Age_paleontology	Unit	Reference
5479	0	5480	ph_brown	0.369	9		M-L Miocene	Msh.s	Dolati (2010)
5480	0	5481	ph_brown	0.441	9		M-L Miocene	Msh.s	Dolati (2010)
5481	0	5482	ph_brown	0.123	9		M-L Miocene	Msh.s	Dolati (2010)
5482	0	5483	ph_brown	0.383	9		M-L Miocene	Msh.s	Dolati (2010)
5483	0	5484	ph_brown	1.113	9		M-L Miocene	Msh.s	Dolati (2010)
5484	0	5485	ph_brown	0.477	9		M-L Miocene	Msh.s	Dolati (2010)
5485	0	5486	ph_brown	0.302	9		M-L Miocene	Msh.s	Dolati (2010)
5486	0	5487	ph_brown	0.227	9		M-L Miocene	Msh.s	Dolati (2010)
5487	0	5488	ph_brown	1.785	9		M-L Miocene	Msh.s	Dolati (2010)
5488	0	5489	ph_brown	0.115	9		M-L Miocene	Msh.s	Dolati (2010)
5489	0	5490	ph_brown	1.372	9		M-L Miocene	Msh.s	Dolati (2010)
5490	0	5491	ph_brown	0.813	9		M-L Miocene	Msh.s	Dolati (2010)
5491	0	5492	ph_brown	0.144	9		M-L Miocene	Msh.s	Dolati (2010)
5492	0	5493	ph_brown	0.248	9		M-L Miocene	Msh.s	Dolati (2010)
5493	0	5494	ph_brown	0.191	9		M-L Miocene	Msh.s	Dolati (2010)
5494	0	5495	ph_brown	0.515	9		M-L Miocene	Msh.s	Dolati (2010)
5495	0	5496	ph_brown	0.414	9		M-L Miocene	Msh.s	Dolati (2010)
5496	0	5497	ph_brown	0.722	9		M-L Miocene	Msh.s	Dolati (2010)
5497	0	5498	ph_brown	1.632	9		M-L Miocene	Msh.s	Dolati (2010)
5498	1	5499	ph_brown	11.283	9		M-L Miocene	Msh.s	Dolati (2010)
5499	0	5500	ph_brown	0.347	9		M-L Miocene	Msh.s	Dolati (2010)
5500	0	5501	ph_brown	0.522	9		M-L Miocene	Msh.s	Dolati (2010)
5501	0	5502	ph_brown	0.240	9		M-L Miocene	Msh.s	Dolati (2010)
5502	0	5503	ph_brown	0.078	9		M-L Miocene	Msh.s	Dolati (2010)
5503	0	5504	ph_brown	0.023	9		M-L Miocene	Msh.s	Dolati (2010)
5504	0	5505	ph_brown	0.169	9		M-L Miocene	Msh.s	Dolati (2010)
5505	0	5506	ph_brown	0.111	9		M-L Miocene	Msh.s	Dolati (2010)
5506	0	5507	ph_brown	0.057	9		M-L Miocene	Msh.s	Dolati (2010)
5507	0	5508	ph_brown	1.602	9		M-L Miocene	Msh.s	Dolati (2010)
5508	0	5509	ph_brown	0.351	9		M-L Miocene	Msh.s	Dolati (2010)
5509	0	5510	ph_brown	0.046	9		M-L Miocene	Msh.s	Dolati (2010)
5510	0	5511	ph_brown	1.212	9		M-L Miocene	Msh.s	Dolati (2010)
5511	0	5512	ph_brown	0.682	9		M-L Miocene	Msh.s	Dolati (2010)
5512	0	5513	ph_brown	0.084	9		M-L Miocene	Msh.s	Dolati (2010)
5513	0	5514	ph_brown	0.935	9		M-L Miocene	Msh.s	Dolati (2010)
5514	0	5515	ph_brown	0.813	9		M-L Miocene	Msh.s	Dolati (2010)
5515	0	5516	ph_brown	0.059	9		M-L Miocene	Msh.s	Dolati (2010)
5516	0	5517	ph_brown	0.047	9		M-L Miocene	Msh.s	Dolati (2010)
5517	0	5518	ph_brown	0.145	9		M-L Miocene	Msh.s	Dolati (2010)

Geonevis

OBJECTID_1	Join_Count	TARGET_FID	Label	Shape_Area (sqkm)	ORIG_FID	Absolute_Age	Age_paleontology	Unit	Reference
5518	0	5519	ph_brown	0.538	9		M-L Miocene	Msh.s	Dolati (2010)
5519	0	5520	ph_brown	0.036	9		M-L Miocene	Msh.s	Dolati (2010)
5520	0	5521	ph_brown	0.843	9		M-L Miocene	Msh.s	Dolati (2010)
5521	0	5522	ph_brown	0.090	9		M-L Miocene	Msh.s	Dolati (2010)
5522	0	5523	ph_brown	1.192	9		M-L Miocene	Msh.s	Dolati (2010)
5523	0	5524	ph_brown	0.265	9		M-L Miocene	Msh.s	Dolati (2010)
5524	0	5525	ph_brown	0.788	9		M-L Miocene	Msh.s	Dolati (2010)
5525	0	5526	ph_brown	0.349	9		M-L Miocene	Msh.s	Dolati (2010)
5526	0	5527	ph_brown	2.222	9		M-L Miocene	Msh.s	Dolati (2010)
5527	0	5528	ph_brown	3.346	9		M-L Miocene	Msh.s	Dolati (2010)
5528	0	5529	ph_brown	4.068	9		M-L Miocene	Msh.s	Dolati (2010)
5529	0	5530	ph_brown	0.302	9		M-L Miocene	Msh.s	Dolati (2010)
5530	0	5531	ph_brown	0.283	9		M-L Miocene	Msh.s	Dolati (2010)
5531	0	5532	ph_brown	0.589	9		M-L Miocene	Msh.s	Dolati (2010)
5532	0	5533	ph_brown	1.294	9		M-L Miocene	Msh.s	Dolati (2010)
5533	0	5534	ph_brown	3.098	9		M-L Miocene	Msh.s	Dolati (2010)
5534	0	5535	ph_brown	0.136	9		M-L Miocene	Msh.s	Dolati (2010)
5535	0	5536	ph_brown	0.601	9		M-L Miocene	Msh.s	Dolati (2010)
5536	0	5537	ph_brown	0.184	9		M-L Miocene	Msh.s	Dolati (2010)
5537	0	5538	ph_brown	0.229	9		M-L Miocene	Msh.s	Dolati (2010)
5538	0	5539	ph_brown	1.847	9		M-L Miocene	Msh.s	Dolati (2010)
5539	0	5540	ph_brown	0.836	9		M-L Miocene	Msh.s	Dolati (2010)
5540	0	5541	ph_brown	4.189	9		M-L Miocene	Msh.s	Dolati (2010)
5541	0	5542	ph_brown	0.068	9		M-L Miocene	Msh.s	Dolati (2010)
5542	0	5543	ph_brown	0.389	9		M-L Miocene	Msh.s	Dolati (2010)
5543	0	5544	ph_brown	0.096	9		M-L Miocene	Msh.s	Dolati (2010)
5544	0	5545	ph_brown	0.662	9		M-L Miocene	Msh.s	Dolati (2010)
5545	0	5546	ph_brown	0.192	9		M-L Miocene	Msh.s	Dolati (2010)
5546	0	5547	ph_brown	0.083	9		M-L Miocene	Msh.s	Dolati (2010)
5547	0	5548	ph_brown	0.225	9		M-L Miocene	Msh.s	Dolati (2010)
5548	0	5549	ph_brown	0.117	9		M-L Miocene	Msh.s	Dolati (2010)
5549	0	5550	ph_brown	0.453	9		M-L Miocene	Msh.s	Dolati (2010)
5550	0	5551	ph_brown	0.308	9		M-L Miocene	Msh.s	Dolati (2010)
5551	0	5552	ph_brown	0.099	9		M-L Miocene	Msh.s	Dolati (2010)
5552	0	5553	ph_brown	0.347	9		M-L Miocene	Msh.s	Dolati (2010)
5553	0	5554	ph_brown	0.145	9		M-L Miocene	Msh.s	Dolati (2010)
5554	0	5555	ph_brown	0.088	9		M-L Miocene	Msh.s	Dolati (2010)
5555	0	5556	ph_brown	1.358	9		M-L Miocene	Msh.s	Dolati (2010)
5556	0	5557	ph_brown	1.240	9		M-L Miocene	Msh.s	Dolati (2010)

Geonex

OBJECTID_1	Join_Count	TARGET_FID	Label	Shape_Area (sqkm)	ORIG_FID	Absolute_Age	Age_paleontology	Unit	Reference
5557	0	5558	ph_brown	0.107	9		M-L Miocene	Msh.s	Dolati (2010)
5558	0	5559	ph_brown	0.435	9		M-L Miocene	Msh.s	Dolati (2010)
5559	0	5560	ph_brown	0.125	9		M-L Miocene	Msh.s	Dolati (2010)
5560	0	5561	ph_brown	0.135	9		M-L Miocene	Msh.s	Dolati (2010)
5561	0	5562	ph_brown	0.188	9		M-L Miocene	Msh.s	Dolati (2010)
5562	0	5563	ph_brown	2.931	9		M-L Miocene	Msh.s	Dolati (2010)
5563	0	5564	ph_brown	0.103	9		M-L Miocene	Msh.s	Dolati (2010)
5564	0	5565	ph_brown	0.135	9		M-L Miocene	Msh.s	Dolati (2010)
5565	0	5566	ph_brown	0.214	9		M-L Miocene	Msh.s	Dolati (2010)
5566	0	5567	ph_brown	0.192	9		M-L Miocene	Msh.s	Dolati (2010)
5567	0	5568	ph_brown	0.126	9		M-L Miocene	Msh.s	Dolati (2010)
5568	0	5569	ph_brown	0.006	9		M-L Miocene	Msh.s	Dolati (2010)
5569	0	5570	ph_brown	0.218	9		M-L Miocene	Msh.s	Dolati (2010)
5570	0	5571	ph_brown	1.429	9		M-L Miocene	Msh.s	Dolati (2010)
5571	0	5572	ph_brown	2.344	9		M-L Miocene	Msh.s	Dolati (2010)
5572	0	5573	ph_brown	1.219	9		M-L Miocene	Msh.s	Dolati (2010)
5573	0	5574	ph_brown	2.448	9		M-L Miocene	Msh.s	Dolati (2010)
5574	0	5575	ph_brown	0.161	9		M-L Miocene	Msh.s	Dolati (2010)
5575	0	5576	ph_brown	0.134	9		M-L Miocene	Msh.s	Dolati (2010)
5576	0	5577	ph_brown	4.519	9		M-L Miocene	Msh.s	Dolati (2010)
5577	0	5578	ph_brown	0.094	9		M-L Miocene	Msh.s	Dolati (2010)
5578	0	5579	ph_brown	0.202	9		M-L Miocene	Msh.s	Dolati (2010)
5579	0	5580	ph_brown	0.136	9		M-L Miocene	Msh.s	Dolati (2010)
5580	0	5581	ph_brown	1.233	9		M-L Miocene	Msh.s	Dolati (2010)
5581	0	5582	ph_brown	0.138	9		M-L Miocene	Msh.s	Dolati (2010)
5582	0	5583	ph_brown	0.042	9		M-L Miocene	Msh.s	Dolati (2010)
5583	0	5584	ph_brown	0.130	9		M-L Miocene	Msh.s	Dolati (2010)
5584	0	5585	ph_brown	2.741	9		M-L Miocene	Msh.s	Dolati (2010)
5585	0	5586	ph_brown	0.600	9		M-L Miocene	Msh.s	Dolati (2010)
5586	0	5587	ph_brown	0.423	9		M-L Miocene	Msh.s	Dolati (2010)
5587	0	5588	ph_brown	0.079	9		M-L Miocene	Msh.s	Dolati (2010)
5588	0	5589	ph_brown	0.066	9		M-L Miocene	Msh.s	Dolati (2010)
5589	0	5590	ph_brown	2.307	9		M-L Miocene	Msh.s	Dolati (2010)
5590	0	5591	ph_brown	2.548	9		M-L Miocene	Msh.s	Dolati (2010)
5591	0	5592	ph_brown	0.995	9		M-L Miocene	Msh.s	Dolati (2010)
5592	0	5593	ph_brown	0.026	9		M-L Miocene	Msh.s	Dolati (2010)
5593	0	5594	ph_brown	0.849	9		M-L Miocene	Msh.s	Dolati (2010)
5594	0	5595	ph_brown	0.056	9		M-L Miocene	Msh.s	Dolati (2010)
5595	0	5596	ph_brown	0.187	9		M-L Miocene	Msh.s	Dolati (2010)

Geonevis

OBJECTID_1	Join_Count	TARGET_FID	Label	Shape_Area (sqkm)	ORIG_FID	Absolute_Age	Age_paleontology	Unit	Reference
5596	0	5597	ph_brown	17.523	9		M-L Miocene	Msh.s	Dolati (2010)
5597	0	5598	ph_brown	0.170	9		M-L Miocene	Msh.s	Dolati (2010)
5598	0	5599	ph_brown	0.206	9		M-L Miocene	Msh.s	Dolati (2010)
5599	0	5600	ph_brown	0.114	9		M-L Miocene	Msh.s	Dolati (2010)
5600	0	5601	ph_brown	5.918	9		M-L Miocene	Msh.s	Dolati (2010)
5601	0	5602	ph_brown	0.188	9		M-L Miocene	Msh.s	Dolati (2010)
5602	0	5603	ph_brown	1.008	9		M-L Miocene	Msh.s	Dolati (2010)
5603	0	5604	ph_brown	0.053	9		M-L Miocene	Msh.s	Dolati (2010)
5604	0	5605	ph_brown	0.038	9		M-L Miocene	Msh.s	Dolati (2010)
5605	0	5606	ph_brown	0.240	9		M-L Miocene	Msh.s	Dolati (2010)
5606	0	5607	ph_brown	0.197	9		M-L Miocene	Msh.s	Dolati (2010)
5607	0	5608	ph_brown	0.259	9		M-L Miocene	Msh.s	Dolati (2010)
5608	0	5609	ph_brown	0.781	9		M-L Miocene	Msh.s	Dolati (2010)
5609	0	5610	ph_brown	0.056	9		M-L Miocene	Msh.s	Dolati (2010)
5610	0	5611	ph_brown	0.751	9		M-L Miocene	Msh.s	Dolati (2010)
5611	0	5612	ph_brown	0.798	9		M-L Miocene	Msh.s	Dolati (2010)
5612	0	5613	ph_brown	0.091	9		M-L Miocene	Msh.s	Dolati (2010)
5613	0	5614	ph_brown	0.118	9		M-L Miocene	Msh.s	Dolati (2010)
5614	0	5615	ph_brown	1.435	9		M-L Miocene	Msh.s	Dolati (2010)
5615	0	5616	ph_brown	0.106	9		M-L Miocene	Msh.s	Dolati (2010)
5616	0	5617	ph_brown	0.292	9		M-L Miocene	Msh.s	Dolati (2010)
5617	0	5618	ph_brown	0.114	9		M-L Miocene	Msh.s	Dolati (2010)
5618	0	5619	ph_brown	0.357	9		M-L Miocene	Msh.s	Dolati (2010)
5619	0	5620	ph_brown	0.232	9		M-L Miocene	Msh.s	Dolati (2010)
5620	0	5621	ph_brown	0.111	9		M-L Miocene	Msh.s	Dolati (2010)
5621	0	5622	ph_brown	0.159	9		M-L Miocene	Msh.s	Dolati (2010)
5622	0	5623	ph_brown	0.062	9		M-L Miocene	Msh.s	Dolati (2010)
5623	0	5624	ph_brown	1.276	9		M-L Miocene	Msh.s	Dolati (2010)
5624	0	5625	ph_brown	0.233	9		M-L Miocene	Msh.s	Dolati (2010)
5625	0	5626	ph_brown	1.096	9		M-L Miocene	Msh.s	Dolati (2010)
5626	0	5627	ph_brown	0.440	9		M-L Miocene	Msh.s	Dolati (2010)
5627	0	5628	ph_brown	0.747	9		M-L Miocene	Msh.s	Dolati (2010)
5628	0	5629	ph_brown	0.081	9		M-L Miocene	Msh.s	Dolati (2010)
5629	0	5630	ph_brown	0.071	9		M-L Miocene	Msh.s	Dolati (2010)
5630	0	5631	ph_brown	0.184	9		M-L Miocene	Msh.s	Dolati (2010)
5631	0	5632	ph_brown	0.028	9		M-L Miocene	Msh.s	Dolati (2010)
5632	0	5633	ph_brown	0.854	9		M-L Miocene	Msh.s	Dolati (2010)
5633	0	5634	ph_brown	0.266	9		M-L Miocene	Msh.s	Dolati (2010)
5634	0	5635	ph_brown	0.752	9		M-L Miocene	Msh.s	Dolati (2010)

Geonevis

OBJECTID_1	Join_Count	TARGET_FID	Label	Shape_Area (sqkm)	ORIG_FID	Absolute_Age	Age_paleontology	Unit	Reference
5635	0	5636	ph_brown	0.022	9		M-L Miocene	Msh.s	Dolati (2010)
5636	0	5637	ph_brown	0.191	9		M-L Miocene	Msh.s	Dolati (2010)
5637	0	5638	ph_brown	0.448	9		M-L Miocene	Msh.s	Dolati (2010)
5638	0	5639	ph_brown	0.283	9		M-L Miocene	Msh.s	Dolati (2010)
5639	0	5640	ph_brown	0.198	9		M-L Miocene	Msh.s	Dolati (2010)
5640	0	5641	ph_brown	0.031	9		M-L Miocene	Msh.s	Dolati (2010)
5641	0	5642	ph_brown	0.418	9		M-L Miocene	Msh.s	Dolati (2010)
5642	0	5643	ph_brown	0.042	9		M-L Miocene	Msh.s	Dolati (2010)
5643	0	5644	ph_brown	0.363	9		M-L Miocene	Msh.s	Dolati (2010)
5644	0	5645	ph_brown	0.424	9		M-L Miocene	Msh.s	Dolati (2010)
5645	0	5646	ph_brown	0.163	9		M-L Miocene	Msh.s	Dolati (2010)
5646	0	5647	ph_brown	1.672	9		M-L Miocene	Msh.s	Dolati (2010)
5647	0	5648	ph_brown	0.253	9		M-L Miocene	Msh.s	Dolati (2010)
5648	0	5649	ph_brown	0.159	9		M-L Miocene	Msh.s	Dolati (2010)
5649	0	5650	ph_brown	0.183	9		M-L Miocene	Msh.s	Dolati (2010)
5650	0	5651	ph_brown	0.067	9		M-L Miocene	Msh.s	Dolati (2010)
5651	0	5652	ph_brown	0.144	9		M-L Miocene	Msh.s	Dolati (2010)
5652	0	5653	ph_brown	0.039	9		M-L Miocene	Msh.s	Dolati (2010)
5653	0	5654	ph_brown	0.510	9		M-L Miocene	Msh.s	Dolati (2010)
5654	0	5655	ph_brown	0.608	9		M-L Miocene	Msh.s	Dolati (2010)
5655	0	5656	ph_brown	0.413	9		M-L Miocene	Msh.s	Dolati (2010)
5656	0	5657	ph_brown	0.124	9		M-L Miocene	Msh.s	Dolati (2010)
5657	0	5658	ph_brown	0.418	9		M-L Miocene	Msh.s	Dolati (2010)
5658	0	5659	ph_brown	0.229	9		M-L Miocene	Msh.s	Dolati (2010)
5659	0	5660	ph_brown	0.749	9		M-L Miocene	Msh.s	Dolati (2010)
5660	0	5661	ph_brown	0.078	9		M-L Miocene	Msh.s	Dolati (2010)
5661	0	5662	ph_brown	17.260	9		M-L Miocene	Msh.s	Dolati (2010)
5662	0	5663	ph_brown	0.149	9		M-L Miocene	Msh.s	Dolati (2010)
5663	0	5664	ph_brown	0.259	9		M-L Miocene	Msh.s	Dolati (2010)
5664	0	5665	ph_brown	1.687	9		M-L Miocene	Msh.s	Dolati (2010)
5665	0	5666	ph_brown	0.253	9		M-L Miocene	Msh.s	Dolati (2010)
5666	0	5667	ph_brown	0.191	9		M-L Miocene	Msh.s	Dolati (2010)
5667	0	5668	ph_brown	0.153	9		M-L Miocene	Msh.s	Dolati (2010)
5668	0	5669	ph_brown	0.063	9		M-L Miocene	Msh.s	Dolati (2010)
5669	0	5670	ph_brown	0.141	9		M-L Miocene	Msh.s	Dolati (2010)
5670	0	5671	ph_brown	0.400	9		M-L Miocene	Msh.s	Dolati (2010)
5671	0	5672	ph_brown	1.967	9		M-L Miocene	Msh.s	Dolati (2010)
5672	0	5673	ph_brown	0.169	9		M-L Miocene	Msh.s	Dolati (2010)
5673	0	5674	ph_brown	0.166	9		M-L Miocene	Msh.s	Dolati (2010)

Geonevis

OBJECTID_1	Join_Count	TARGET_FID	Label	Shape_Area (sqkm)	ORIG_FID	Absolute_Age	Age_paleontology	Unit	Reference
5674	0	5675	ph_brown	0.574	9		M-L Miocene	Msh.s	Dolati (2010)
5675	0	5676	ph_brown	1.986	9		M-L Miocene	Msh.s	Dolati (2010)
5676	0	5677	ph_brown	0.443	9		M-L Miocene	Msh.s	Dolati (2010)
5677	0	5678	ph_brown	0.568	9		M-L Miocene	Msh.s	Dolati (2010)
5678	0	5679	ph_brown	1.023	9		M-L Miocene	Msh.s	Dolati (2010)
5679	0	5680	ph_brown	1.453	9		M-L Miocene	Msh.s	Dolati (2010)
5680	0	5681	ph_brown	0.581	9		M-L Miocene	Msh.s	Dolati (2010)
5681	0	5682	ph_brown	0.164	9		M-L Miocene	Msh.s	Dolati (2010)
5682	0	5683	ph_brown	0.134	9		M-L Miocene	Msh.s	Dolati (2010)
5683	0	5684	ph_brown	0.929	9		M-L Miocene	Msh.s	Dolati (2010)
5684	0	5685	ph_brown	2.351	9		M-L Miocene	Msh.s	Dolati (2010)
5685	0	5686	ph_brown	0.054	9		M-L Miocene	Msh.s	Dolati (2010)
5686	0	5687	ph_brown	0.448	9		M-L Miocene	Msh.s	Dolati (2010)
5687	0	5688	ph_brown	0.520	9		M-L Miocene	Msh.s	Dolati (2010)
5688	0	5689	ph_brown	0.256	9		M-L Miocene	Msh.s	Dolati (2010)
5689	0	5690	ph_brown	0.815	9		M-L Miocene	Msh.s	Dolati (2010)
5690	0	5691	ph_brown	1.039	9		M-L Miocene	Msh.s	Dolati (2010)
5691	0	5692	ph_brown	0.876	9		M-L Miocene	Msh.s	Dolati (2010)
5692	0	5693	ph_brown	0.479	9		M-L Miocene	Msh.s	Dolati (2010)
5693	0	5694	ph_brown	0.008	9		M-L Miocene	Msh.s	Dolati (2010)
5694	0	5695	ph_brown	0.058	9		M-L Miocene	Msh.s	Dolati (2010)
5695	0	5696	ph_brown	0.497	9		M-L Miocene	Msh.s	Dolati (2010)
5696	0	5697	ph_brown	1.263	9		M-L Miocene	Msh.s	Dolati (2010)
5697	0	5698	ph_brown	0.050	9		M-L Miocene	Msh.s	Dolati (2010)
5698	0	5699	ph_brown	0.010	9		M-L Miocene	Msh.s	Dolati (2010)
5699	0	5700	ph_brown	0.121	9		M-L Miocene	Msh.s	Dolati (2010)
5700	0	5701	ph_brown	0.127	9		M-L Miocene	Msh.s	Dolati (2010)
5701	0	5702	ph_brown	0.159	9		M-L Miocene	Msh.s	Dolati (2010)
5702	0	5703	ph_brown	4.151	9		M-L Miocene	Msh.s	Dolati (2010)
5703	0	5704	ph_brown	0.070	9		M-L Miocene	Msh.s	Dolati (2010)
5704	0	5705	ph_brown	2.241	9		M-L Miocene	Msh.s	Dolati (2010)
5705	0	5706	ph_brown	0.064	9		M-L Miocene	Msh.s	Dolati (2010)
5706	0	5707	ph_brown	0.415	9		M-L Miocene	Msh.s	Dolati (2010)
5707	0	5708	ph_brown	0.367	9		M-L Miocene	Msh.s	Dolati (2010)
5708	0	5709	ph_brown	0.015	9		M-L Miocene	Msh.s	Dolati (2010)
5709	0	5710	ph_brown	0.011	9		M-L Miocene	Msh.s	Dolati (2010)
5710	0	5711	ph_brown	0.041	9		M-L Miocene	Msh.s	Dolati (2010)
5711	0	5712	ph_brown	0.012	9		M-L Miocene	Msh.s	Dolati (2010)
5712	0	5713	ph_brown	0.626	9		M-L Miocene	Msh.s	Dolati (2010)

Geonevis

OBJECTID_1	Join_Count	TARGET_FID	Label	Shape_Area (sqkm)	ORIG_FID	Absolute_Age	Age_paleontology	Unit	Reference
5713	0	5714	ph_brown	1.808	9		M-L Miocene	Msh.s	Dolati (2010)
5714	0	5715	ph_brown	0.023	9		M-L Miocene	Msh.s	Dolati (2010)
5715	0	5716	ph_brown	0.060	9		M-L Miocene	Msh.s	Dolati (2010)
5716	0	5717	ph_brown	0.064	9		M-L Miocene	Msh.s	Dolati (2010)
5717	0	5718	ph_brown	0.049	9		M-L Miocene	Msh.s	Dolati (2010)
5718	0	5719	ph_brown	0.095	9		M-L Miocene	Msh.s	Dolati (2010)
5719	0	5720	ph_brown	0.025	9		M-L Miocene	Msh.s	Dolati (2010)
5720	0	5721	ph_brown	0.106	9		M-L Miocene	Msh.s	Dolati (2010)
5721	0	5722	ph_brown	0.013	9		M-L Miocene	Msh.s	Dolati (2010)
5722	0	5723	ph_brown	0.055	9		M-L Miocene	Msh.s	Dolati (2010)
5723	0	5724	ph_brown	0.021	9		M-L Miocene	Msh.s	Dolati (2010)
5724	0	5725	ph_brown	0.013	9		M-L Miocene	Msh.s	Dolati (2010)
5725	0	5726	ph_brown	0.091	9		M-L Miocene	Msh.s	Dolati (2010)
5726	0	5727	ph_brown	0.018	9		M-L Miocene	Msh.s	Dolati (2010)
5727	0	5728	ph_brown	0.097	9		M-L Miocene	Msh.s	Dolati (2010)
5728	0	5729	ph_brown	1.297	9		M-L Miocene	Msh.s	Dolati (2010)
5729	0	5730	ph_brown	0.043	9		M-L Miocene	Msh.s	Dolati (2010)
5730	0	5731	ph_brown	0.156	9		M-L Miocene	Msh.s	Dolati (2010)
5731	0	5732	ph_brown	0.086	9		M-L Miocene	Msh.s	Dolati (2010)
5732	0	5733	ph_brown	0.359	9		M-L Miocene	Msh.s	Dolati (2010)
5733	0	5734	ph_brown	0.136	9		M-L Miocene	Msh.s	Dolati (2010)
5734	0	5735	ph_brown	0.311	9		M-L Miocene	Msh.s	Dolati (2010)
5735	0	5736	ph_brown	0.027	9		M-L Miocene	Msh.s	Dolati (2010)
5736	0	5737	ph_brown	2.944	9		M-L Miocene	Msh.s	Dolati (2010)
5737	0	5738	ph_brown	0.030	9		M-L Miocene	Msh.s	Dolati (2010)
5738	0	5739	ph_brown	1.505	9		M-L Miocene	Msh.s	Dolati (2010)
5739	0	5740	ph_brown	0.143	9		M-L Miocene	Msh.s	Dolati (2010)
5740	0	5741	ph_brown	0.061	9		M-L Miocene	Msh.s	Dolati (2010)
5741	0	5742	ph_brown	0.054	9		M-L Miocene	Msh.s	Dolati (2010)
5742	0	5743	ph_brown	0.044	9		M-L Miocene	Msh.s	Dolati (2010)
5743	0	5744	ph_brown	0.388	9		M-L Miocene	Msh.s	Dolati (2010)
5744	0	5745	ph_brown	0.032	9		M-L Miocene	Msh.s	Dolati (2010)
5745	0	5746	ph_brown	2.642	9		M-L Miocene	Msh.s	Dolati (2010)
5746	0	5747	ph_brown	0.434	9		M-L Miocene	Msh.s	Dolati (2010)
5747	0	5748	ph_brown	0.817	9		M-L Miocene	Msh.s	Dolati (2010)
5748	0	5749	ph_brown	0.298	9		M-L Miocene	Msh.s	Dolati (2010)
5749	0	5750	ph_brown	0.058	9		M-L Miocene	Msh.s	Dolati (2010)
5750	0	5751	ph_brown	8.403	9		M-L Miocene	Msh.s	Dolati (2010)
5751	0	5752	ph_brown	0.124	9		M-L Miocene	Msh.s	Dolati (2010)

Geonevis

OBJECTID_1	Join_Count	TARGET_FID	Label	Shape_Area (sqkm)	ORIG_FID	Absolute_Age	Age_paleontology	Unit	Reference
5752	0	5753	ph_brown	0.337	9		M-L Miocene	Msh.s	Dolati (2010)
5753	0	5754	ph_brown	0.298	9		M-L Miocene	Msh.s	Dolati (2010)
5754	0	5755	ph_brown	0.048	9		M-L Miocene	Msh.s	Dolati (2010)
5755	0	5756	ph_brown	0.012	9		M-L Miocene	Msh.s	Dolati (2010)
5756	0	5757	ph_brown	1.757	9		M-L Miocene	Msh.s	Dolati (2010)
5757	0	5758	ph_brown	0.511	9		M-L Miocene	Msh.s	Dolati (2010)
5758	0	5759	ph_brown	0.124	9		M-L Miocene	Msh.s	Dolati (2010)
5759	0	5760	ph_brown	0.041	9		M-L Miocene	Msh.s	Dolati (2010)
5760	0	5761	ph_brown	0.227	9		M-L Miocene	Msh.s	Dolati (2010)
5761	0	5762	ph_brown	1.228	9		M-L Miocene	Msh.s	Dolati (2010)
5762	0	5763	ph_brown	0.052	9		M-L Miocene	Msh.s	Dolati (2010)
5763	0	5764	ph_brown	26.399	9		M-L Miocene	Msh.s	Dolati (2010)
5764	0	5765	ph_brown	2.070	9		M-L Miocene	Msh.s	Dolati (2010)
5765	0	5766	ph_brown	0.013	9		M-L Miocene	Msh.s	Dolati (2010)
5766	0	5767	ph_brown	0.343	9		M-L Miocene	Msh.s	Dolati (2010)
5767	0	5768	ph_brown	0.073	9		M-L Miocene	Msh.s	Dolati (2010)
5768	0	5769	ph_brown	1.411	9		M-L Miocene	Msh.s	Dolati (2010)
5769	0	5770	ph_brown	0.050	9		M-L Miocene	Msh.s	Dolati (2010)
5770	0	5771	ph_brown	0.663	9		M-L Miocene	Msh.s	Dolati (2010)
5771	0	5772	ph_brown	0.012	9		M-L Miocene	Msh.s	Dolati (2010)
5772	0	5773	ph_brown	0.162	9		M-L Miocene	Msh.s	Dolati (2010)
5773	0	5774	ph_brown	0.467	9		M-L Miocene	Msh.s	Dolati (2010)
5774	0	5775	ph_brown	0.197	9		M-L Miocene	Msh.s	Dolati (2010)
5775	0	5776	ph_brown	0.162	9		M-L Miocene	Msh.s	Dolati (2010)
5776	0	5777	ph_brown	0.518	9		M-L Miocene	Msh.s	Dolati (2010)
5777	0	5778	ph_brown	0.418	9		M-L Miocene	Msh.s	Dolati (2010)
5778	0	5779	ph_brown	0.142	9		M-L Miocene	Msh.s	Dolati (2010)
5779	0	5780	ph_brown	2.486	9		M-L Miocene	Msh.s	Dolati (2010)
5780	0	5781	ph_brown	0.494	9		M-L Miocene	Msh.s	Dolati (2010)
5781	0	5782	ph_brown	0.472	9		M-L Miocene	Msh.s	Dolati (2010)
5782	0	5783	ph_brown	1.227	9		M-L Miocene	Msh.s	Dolati (2010)
5783	0	5784	ph_brown	0.039	9		M-L Miocene	Msh.s	Dolati (2010)
5784	0	5785	ph_brown	0.026	9		M-L Miocene	Msh.s	Dolati (2010)
5785	0	5786	ph_brown	0.352	9		M-L Miocene	Msh.s	Dolati (2010)
5786	0	5787	ph_brown	0.227	9		M-L Miocene	Msh.s	Dolati (2010)
5787	0	5788	ph_brown	0.262	9		M-L Miocene	Msh.s	Dolati (2010)
5788	0	5789	ph_brown	0.091	9		M-L Miocene	Msh.s	Dolati (2010)
5789	0	5790	ph_brown	0.027	9		M-L Miocene	Msh.s	Dolati (2010)
5790	0	5791	ph_brown	0.654	9		M-L Miocene	Msh.s	Dolati (2010)

Geonevis

OBJECTID_1	Join_Count	TARGET_FID	Label	Shape_Area (sqkm)	ORIG_FID	Absolute_Age	Age_paleontology	Unit	Reference
5791	0	5792	ph_brown	0.023	9		M-L Miocene	Msh.s	Dolati (2010)
5792	0	5793	ph_brown	0.818	9		M-L Miocene	Msh.s	Dolati (2010)
5793	0	5794	ph_brown	0.696	9		M-L Miocene	Msh.s	Dolati (2010)
5794	0	5795	ph_brown	0.186	9		M-L Miocene	Msh.s	Dolati (2010)
5795	0	5796	ph_brown	0.180	9		M-L Miocene	Msh.s	Dolati (2010)
5796	0	5797	ph_brown	0.643	9		M-L Miocene	Msh.s	Dolati (2010)
5797	0	5798	ph_brown	0.066	9		M-L Miocene	Msh.s	Dolati (2010)
5798	0	5799	ph_brown	2.376	9		M-L Miocene	Msh.s	Dolati (2010)
5799	0	5800	ph_brown	0.632	9		M-L Miocene	Msh.s	Dolati (2010)
5800	0	5801	ph_brown	4.660	9		M-L Miocene	Msh.s	Dolati (2010)
5801	0	5802	ph_brown	3.486	9		M-L Miocene	Msh.s	Dolati (2010)
5802	0	5803	ph_brown	0.459	9		M-L Miocene	Msh.s	Dolati (2010)
5803	0	5804	ph_brown	0.222	9		M-L Miocene	Msh.s	Dolati (2010)
5804	0	5805	ph_brown	1.120	9		M-L Miocene	Msh.s	Dolati (2010)
5805	0	5806	ph_brown	1.188	9		M-L Miocene	Msh.s	Dolati (2010)
5806	0	5807	ph_brown	0.084	9		M-L Miocene	Msh.s	Dolati (2010)
5807	0	5808	ph_brown	1.190	9		M-L Miocene	Msh.s	Dolati (2010)
5808	0	5809	ph_brown	0.159	9		M-L Miocene	Msh.s	Dolati (2010)
5809	0	5810	ph_brown	0.080	9		M-L Miocene	Msh.s	Dolati (2010)
5810	0	5811	ph_brown	0.228	9		M-L Miocene	Msh.s	Dolati (2010)
5811	0	5812	ph_brown	2.021	9		M-L Miocene	Msh.s	Dolati (2010)
5812	0	5813	ph_brown	1.396	9		M-L Miocene	Msh.s	Dolati (2010)
5813	0	5814	ph_brown	0.093	9		M-L Miocene	Msh.s	Dolati (2010)
5814	0	5815	ph_brown	0.570	9		M-L Miocene	Msh.s	Dolati (2010)
5815	0	5816	ph_brown	0.166	9		M-L Miocene	Msh.s	Dolati (2010)
5816	0	5817	ph_brown	0.484	9		M-L Miocene	Msh.s	Dolati (2010)
5817	0	5818	ph_brown	0.226	9		M-L Miocene	Msh.s	Dolati (2010)
5818	0	5819	ph_brown	0.706	9		M-L Miocene	Msh.s	Dolati (2010)
5819	0	5820	ph_brown	0.155	9		M-L Miocene	Msh.s	Dolati (2010)
5820	0	5821	ph_brown	1.525	9		M-L Miocene	Msh.s	Dolati (2010)
5821	0	5822	ph_brown	0.100	9		M-L Miocene	Msh.s	Dolati (2010)
5822	0	5823	ph_brown	0.312	9		M-L Miocene	Msh.s	Dolati (2010)
5823	0	5824	ph_brown	0.255	9		M-L Miocene	Msh.s	Dolati (2010)
5824	0	5825	ph_brown	0.292	9		M-L Miocene	Msh.s	Dolati (2010)
5825	0	5826	ph_brown	0.271	9		M-L Miocene	Msh.s	Dolati (2010)
5826	0	5827	ph_brown	0.075	9		M-L Miocene	Msh.s	Dolati (2010)
5827	0	5828	ph_brown	0.130	9		M-L Miocene	Msh.s	Dolati (2010)
5828	0	5829	ph_brown	0.211	9		M-L Miocene	Msh.s	Dolati (2010)
5829	0	5830	ph_brown	1.597	9		M-L Miocene	Msh.s	Dolati (2010)

Geonevis

OBJECTID_1	Join_Count	TARGET_FID	Label	Shape_Area (sqkm)	ORIG_FID	Absolute_Age	Age_paleontology	Unit	Reference
5830	0	5831	ph_brown	0.226	9		M-L Miocene	Msh.s	Dolati (2010)
5831	0	5832	ph_brown	0.041	9		M-L Miocene	Msh.s	Dolati (2010)
5832	0	5833	ph_brown	5.296	9		M-L Miocene	Msh.s	Dolati (2010)
5833	0	5834	ph_brown	0.125	9		M-L Miocene	Msh.s	Dolati (2010)
5834	0	5835	ph_brown	0.119	9		M-L Miocene	Msh.s	Dolati (2010)
5835	0	5836	ph_brown	0.241	9		M-L Miocene	Msh.s	Dolati (2010)
5836	0	5837	ph_brown	0.080	9		M-L Miocene	Msh.s	Dolati (2010)
5837	0	5838	ph_brown	0.081	9		M-L Miocene	Msh.s	Dolati (2010)
5838	0	5839	ph_brown	0.295	9		M-L Miocene	Msh.s	Dolati (2010)
5839	0	5840	ph_brown	0.453	9		M-L Miocene	Msh.s	Dolati (2010)
5840	0	5841	ph_brown	0.163	9		M-L Miocene	Msh.s	Dolati (2010)
5841	0	5842	ph_brown	0.114	9		M-L Miocene	Msh.s	Dolati (2010)
5842	0	5843	ph_brown	0.124	9		M-L Miocene	Msh.s	Dolati (2010)
5843	0	5844	ph_brown	0.473	9		M-L Miocene	Msh.s	Dolati (2010)
5844	0	5845	ph_brown	0.178	9		M-L Miocene	Msh.s	Dolati (2010)
5845	0	5846	ph_brown	2.204	9		M-L Miocene	Msh.s	Dolati (2010)
5846	0	5847	ph_brown	0.209	9		M-L Miocene	Msh.s	Dolati (2010)
5847	0	5848	ph_brown	3.523	9		M-L Miocene	Msh.s	Dolati (2010)
5848	0	5849	ph_brown	0.294	9		M-L Miocene	Msh.s	Dolati (2010)
5849	0	5850	ph_brown	1.151	9		M-L Miocene	Msh.s	Dolati (2010)
5850	0	5851	ph_brown	0.664	9		M-L Miocene	Msh.s	Dolati (2010)
5851	0	5852	ph_brown	0.075	9		M-L Miocene	Msh.s	Dolati (2010)
5852	0	5853	ph_brown	0.609	9		M-L Miocene	Msh.s	Dolati (2010)
5853	0	5854	ph_brown	0.461	9		M-L Miocene	Msh.s	Dolati (2010)
5854	0	5855	ph_brown	0.235	9		M-L Miocene	Msh.s	Dolati (2010)
5855	0	5856	ph_brown	3.582	9		M-L Miocene	Msh.s	Dolati (2010)
5856	0	5857	ph_brown	2.091	9		M-L Miocene	Msh.s	Dolati (2010)
5857	0	5858	ph_brown	0.132	9		M-L Miocene	Msh.s	Dolati (2010)
5858	0	5859	ph_brown	0.579	9		M-L Miocene	Msh.s	Dolati (2010)
5859	0	5860	ph_brown	0.991	9		M-L Miocene	Msh.s	Dolati (2010)
5860	0	5861	ph_brown	0.238	9		M-L Miocene	Msh.s	Dolati (2010)
5861	0	5862	ph_brown	0.028	9		M-L Miocene	Msh.s	Dolati (2010)
5862	0	5863	ph_brown	0.437	9		M-L Miocene	Msh.s	Dolati (2010)
5863	0	5864	ph_brown	0.103	9		M-L Miocene	Msh.s	Dolati (2010)
5864	0	5865	ph_brown	0.092	9		M-L Miocene	Msh.s	Dolati (2010)
5865	0	5866	ph_brown	0.225	9		M-L Miocene	Msh.s	Dolati (2010)
5866	0	5867	ph_brown	0.699	9		M-L Miocene	Msh.s	Dolati (2010)
5867	0	5868	ph_brown	0.193	9		M-L Miocene	Msh.s	Dolati (2010)
5868	0	5869	ph_brown	0.078	9		M-L Miocene	Msh.s	Dolati (2010)

Geonevis

OBJECTID_1	Join_Count	TARGET_FID	Label	Shape_Area (sqkm)	ORIG_FID	Absolute_Age	Age_paleontology	Unit	Reference
5869	0	5870	ph_brown	0.283	9		M-L Miocene	Msh.s	Dolati (2010)
5870	0	5871	ph_brown	0.195	9		M-L Miocene	Msh.s	Dolati (2010)
5871	0	5872	ph_brown	0.190	9		M-L Miocene	Msh.s	Dolati (2010)
5872	0	5873	ph_brown	0.062	9		M-L Miocene	Msh.s	Dolati (2010)
5873	0	5874	ph_brown	0.549	9		M-L Miocene	Msh.s	Dolati (2010)
5874	0	5875	ph_brown	0.649	9		M-L Miocene	Msh.s	Dolati (2010)
5875	0	5876	ph_brown	0.333	9		M-L Miocene	Msh.s	Dolati (2010)
5876	0	5877	ph_brown	0.381	9		M-L Miocene	Msh.s	Dolati (2010)
5877	0	5878	ph_brown	0.053	9		M-L Miocene	Msh.s	Dolati (2010)
5878	0	5879	ph_brown	1.028	9		M-L Miocene	Msh.s	Dolati (2010)
5879	0	5880	ph_brown	0.080	9		M-L Miocene	Msh.s	Dolati (2010)
5880	0	5881	ph_brown	0.114	9		M-L Miocene	Msh.s	Dolati (2010)
5881	0	5882	ph_brown	0.147	9		M-L Miocene	Msh.s	Dolati (2010)
5882	0	5883	ph_brown	0.430	9		M-L Miocene	Msh.s	Dolati (2010)
5883	0	5884	ph_brown	0.444	9		M-L Miocene	Msh.s	Dolati (2010)
5884	0	5885	ph_brown	0.653	9		M-L Miocene	Msh.s	Dolati (2010)
5885	0	5886	ph_brown	2.474	9		M-L Miocene	Msh.s	Dolati (2010)
5886	0	5887	ph_brown	0.698	9		M-L Miocene	Msh.s	Dolati (2010)
5887	0	5888	ph_brown	3.022	9		M-L Miocene	Msh.s	Dolati (2010)
5888	0	5889	ph_brown	0.008	9		M-L Miocene	Msh.s	Dolati (2010)
5889	0	5890	ph_brown	0.262	9		M-L Miocene	Msh.s	Dolati (2010)
5890	0	5891	ph_brown	0.329	9		M-L Miocene	Msh.s	Dolati (2010)
5891	0	5892	ph_brown	1.680	9		M-L Miocene	Msh.s	Dolati (2010)
5892	0	5893	ph_brown	1.337	9		M-L Miocene	Msh.s	Dolati (2010)
5893	0	5894	ph_brown	0.430	9		M-L Miocene	Msh.s	Dolati (2010)
5894	0	5895	ph_brown	0.017	9		M-L Miocene	Msh.s	Dolati (2010)
5895	0	5896	ph_brown	0.594	9		M-L Miocene	Msh.s	Dolati (2010)
5896	0	5897	ph_brown	0.409	9		M-L Miocene	Msh.s	Dolati (2010)
5897	0	5898	ph_brown	0.335	9		M-L Miocene	Msh.s	Dolati (2010)
5898	0	5899	ph_brown	0.119	9		M-L Miocene	Msh.s	Dolati (2010)
5899	0	5900	ph_brown	1.432	9		M-L Miocene	Msh.s	Dolati (2010)
5900	0	5901	ph_brown	0.428	9		M-L Miocene	Msh.s	Dolati (2010)
5901	0	5902	ph_brown	0.891	9		M-L Miocene	Msh.s	Dolati (2010)
5902	0	5903	ph_brown	0.293	9		M-L Miocene	Msh.s	Dolati (2010)
5903	0	5904	ph_brown	0.219	9		M-L Miocene	Msh.s	Dolati (2010)
5904	0	5905	ph_brown	0.630	9		M-L Miocene	Msh.s	Dolati (2010)
5905	0	5906	ph_brown	0.239	9		M-L Miocene	Msh.s	Dolati (2010)
5906	0	5907	ph_brown	0.400	9		M-L Miocene	Msh.s	Dolati (2010)
5907	0	5908	ph_brown	0.571	9		M-L Miocene	Msh.s	Dolati (2010)

Geonevis

OBJECTID_1	Join_Count	TARGET_FID	Label	Shape_Area (sqkm)	ORIG_FID	Absolute_Age	Age_paleontology	Unit	Reference
5908	0	5909	ph_brown	0.080	9		M-L Miocene	Msh.s	Dolati (2010)
5909	0	5910	ph_brown	0.261	9		M-L Miocene	Msh.s	Dolati (2010)
5910	0	5911	ph_brown	0.205	9		M-L Miocene	Msh.s	Dolati (2010)
5911	0	5912	ph_brown	0.211	9		M-L Miocene	Msh.s	Dolati (2010)
5912	0	5913	ph_brown	0.230	9		M-L Miocene	Msh.s	Dolati (2010)
5913	0	5914	ph_brown	0.086	9		M-L Miocene	Msh.s	Dolati (2010)
5914	0	5915	ph_brown	2.668	9		M-L Miocene	Msh.s	Dolati (2010)
5915	0	5916	ph_brown	0.096	9		M-L Miocene	Msh.s	Dolati (2010)
5916	0	5917	ph_brown	5.995	9		M-L Miocene	Msh.s	Dolati (2010)
5917	0	5918	ph_brown	0.395	9		M-L Miocene	Msh.s	Dolati (2010)
5918	0	5919	ph_brown	2.491	9		M-L Miocene	Msh.s	Dolati (2010)
5919	0	5920	ph_brown	4.539	9		M-L Miocene	Msh.s	Dolati (2010)
5920	0	5921	ph_brown	0.178	9		M-L Miocene	Msh.s	Dolati (2010)
5921	0	5922	ph_brown	0.028	9		M-L Miocene	Msh.s	Dolati (2010)
5922	0	5923	ph_brown	0.547	9		M-L Miocene	Msh.s	Dolati (2010)
5923	0	5924	ph_brown	1.384	9		M-L Miocene	Msh.s	Dolati (2010)
5924	0	5925	ph_brown	0.254	9		M-L Miocene	Msh.s	Dolati (2010)
5925	0	5926	ph_brown	0.539	9		M-L Miocene	Msh.s	Dolati (2010)
5926	0	5927	ph_brown	0.490	9		M-L Miocene	Msh.s	Dolati (2010)
5927	0	5928	ph_brown	17.201	9		M-L Miocene	Msh.s	Dolati (2010)
5928	0	5929	ph_brown	1.062	9		M-L Miocene	Msh.s	Dolati (2010)
5929	0	5930	ph_brown	2.049	9		M-L Miocene	Msh.s	Dolati (2010)
5930	0	5931	ph_brown	0.008	9		M-L Miocene	Msh.s	Dolati (2010)
5931	0	5932	ph_brown	3.906	9		M-L Miocene	Msh.s	Dolati (2010)
5932	0	5933	ph_brown	0.256	9		M-L Miocene	Msh.s	Dolati (2010)
5933	0	5934	ph_brown	0.340	9		M-L Miocene	Msh.s	Dolati (2010)
5934	0	5935	ph_brown	0.463	9		M-L Miocene	Msh.s	Dolati (2010)
5935	0	5936	ph_brown	0.650	9		M-L Miocene	Msh.s	Dolati (2010)
5936	0	5937	ph_brown	0.014	9		M-L Miocene	Msh.s	Dolati (2010)
5937	0	5938	ph_brown	0.264	9		M-L Miocene	Msh.s	Dolati (2010)
5938	0	5939	ph_brown	3.128	9		M-L Miocene	Msh.s	Dolati (2010)
5939	0	5940	ph_brown	0.316	9		M-L Miocene	Msh.s	Dolati (2010)
5940	0	5941	ph_brown	0.585	9		M-L Miocene	Msh.s	Dolati (2010)
5941	0	5942	ph_brown	0.625	9		M-L Miocene	Msh.s	Dolati (2010)
5942	0	5943	ph_brown	0.916	9		M-L Miocene	Msh.s	Dolati (2010)
5943	0	5944	ph_brown	0.122	9		M-L Miocene	Msh.s	Dolati (2010)
5944	0	5945	ph_brown	0.010	9		M-L Miocene	Msh.s	Dolati (2010)
5945	0	5946	ph_brown	2.767	9		M-L Miocene	Msh.s	Dolati (2010)
5946	0	5947	ph_brown	0.025	9		M-L Miocene	Msh.s	Dolati (2010)

Geonevis

OBJECTID_1	Join_Count	TARGET_FID	Label	Shape_Area (sqkm)	ORIG_FID	Absolute_Age	Age_paleontology	Unit	Reference
5947	0	5948	ph_brown	0.167	9		M-L Miocene	Msh.s	Dolati (2010)
5948	0	5949	ph_brown	2.566	9		M-L Miocene	Msh.s	Dolati (2010)
5949	0	5950	ph_brown	0.924	9		M-L Miocene	Msh.s	Dolati (2010)
5950	0	5951	ph_brown	0.344	9		M-L Miocene	Msh.s	Dolati (2010)
5951	0	5952	ph_brown	0.918	9		M-L Miocene	Msh.s	Dolati (2010)
5952	0	5953	ph_brown	0.156	9		M-L Miocene	Msh.s	Dolati (2010)
5953	0	5954	ph_brown	0.474	9		M-L Miocene	Msh.s	Dolati (2010)
5954	0	5955	ph_brown	0.273	9		M-L Miocene	Msh.s	Dolati (2010)
5955	0	5956	ph_brown	0.409	9		M-L Miocene	Msh.s	Dolati (2010)
5956	0	5957	ph_brown	0.019	9		M-L Miocene	Msh.s	Dolati (2010)
5957	0	5958	ph_brown	1.870	9		M-L Miocene	Msh.s	Dolati (2010)
5958	0	5959	ph_brown	0.365	9		M-L Miocene	Msh.s	Dolati (2010)
5959	0	5960	ph_brown	0.076	9		M-L Miocene	Msh.s	Dolati (2010)
5960	0	5961	ph_brown	2.367	9		M-L Miocene	Msh.s	Dolati (2010)
5961	0	5962	ph_brown	0.040	9		M-L Miocene	Msh.s	Dolati (2010)
5962	0	5963	ph_brown	5.711	9		M-L Miocene	Msh.s	Dolati (2010)
5963	0	5964	ph_brown	2.531	9		M-L Miocene	Msh.s	Dolati (2010)
5964	0	5965	ph_brown	0.540	9		M-L Miocene	Msh.s	Dolati (2010)
5965	0	5966	ph_brown	0.869	9		M-L Miocene	Msh.s	Dolati (2010)
5966	0	5967	ph_brown	0.995	9		M-L Miocene	Msh.s	Dolati (2010)
5967	0	5968	ph_brown	1.517	9		M-L Miocene	Msh.s	Dolati (2010)
5968	0	5969	ph_brown	0.459	9		M-L Miocene	Msh.s	Dolati (2010)
5969	0	5970	ph_brown	1.189	9		M-L Miocene	Msh.s	Dolati (2010)
5970	0	5971	ph_brown	0.825	9		M-L Miocene	Msh.s	Dolati (2010)
5971	0	5972	ph_brown	0.403	9		M-L Miocene	Msh.s	Dolati (2010)
5972	0	5973	ph_brown	26.787	9		M-L Miocene	Msh.s	Dolati (2010)
5973	0	5974	ph_brown	1.994	9		M-L Miocene	Msh.s	Dolati (2010)
5974	0	5975	ph_brown	0.485	9		M-L Miocene	Msh.s	Dolati (2010)
5975	0	5976	ph_brown	2.227	9		M-L Miocene	Msh.s	Dolati (2010)
5976	0	5977	ph_brown	3.885	9		M-L Miocene	Msh.s	Dolati (2010)
5977	0	5978	ph_brown	0.233	9		M-L Miocene	Msh.s	Dolati (2010)
5978	0	5979	ph_brown	0.311	9		M-L Miocene	Msh.s	Dolati (2010)
5979	0	5980	ph_brown	0.324	9		M-L Miocene	Msh.s	Dolati (2010)
5980	0	5981	ph_brown	0.330	9		M-L Miocene	Msh.s	Dolati (2010)
5981	0	5982	ph_brown	2.981	9		M-L Miocene	Msh.s	Dolati (2010)
5982	0	5983	ph_brown	2.805	9		M-L Miocene	Msh.s	Dolati (2010)
5983	0	5984	ph_brown	0.111	9		M-L Miocene	Msh.s	Dolati (2010)
5984	0	5985	ph_brown	0.376	9		M-L Miocene	Msh.s	Dolati (2010)
5985	0	5986	ph_brown	0.210	9		M-L Miocene	Msh.s	Dolati (2010)

Geonevis

OBJECTID_1	Join_Count	TARGET_FID	Label	Shape_Area (sqkm)	ORIG_FID	Absolute_Age	Age_paleontology	Unit	Reference
5986	0	5987	ph_brown	0.143	9		M-L Miocene	Msh.s	Dolati (2010)
5987	0	5988	ph_brown	0.047	9		M-L Miocene	Msh.s	Dolati (2010)
5988	0	5989	ph_brown	2.070	9		M-L Miocene	Msh.s	Dolati (2010)
5989	0	5990	ph_brown	0.166	9		M-L Miocene	Msh.s	Dolati (2010)
5990	0	5991	ph_brown	0.748	9		M-L Miocene	Msh.s	Dolati (2010)
5991	0	5992	ph_brown	0.873	9		M-L Miocene	Msh.s	Dolati (2010)
5992	0	5993	ph_brown	0.168	9		M-L Miocene	Msh.s	Dolati (2010)
5993	0	5994	ph_brown	0.303	9		M-L Miocene	Msh.s	Dolati (2010)
5994	0	5995	ph_brown	0.322	9		M-L Miocene	Msh.s	Dolati (2010)
5995	0	5996	ph_brown	0.025	9		M-L Miocene	Msh.s	Dolati (2010)
5996	0	5997	ph_brown	0.593	9		M-L Miocene	Msh.s	Dolati (2010)
5997	0	5998	ph_brown	0.101	9		M-L Miocene	Msh.s	Dolati (2010)
5998	0	5999	ph_brown	0.036	9		M-L Miocene	Msh.s	Dolati (2010)
5999	0	6000	ph_brown	0.057	9		M-L Miocene	Msh.s	Dolati (2010)
6000	0	6001	ph_brown	0.364	9		M-L Miocene	Msh.s	Dolati (2010)
6001	0	6002	ph_brown	0.010	9		M-L Miocene	Msh.s	Dolati (2010)
6002	0	6003	ph_brown	0.185	9		M-L Miocene	Msh.s	Dolati (2010)
6003	0	6004	ph_brown	0.079	9		M-L Miocene	Msh.s	Dolati (2010)
6004	0	6005	ph_brown	0.061	9		M-L Miocene	Msh.s	Dolati (2010)
6005	0	6006	ph_brown	0.882	9		M-L Miocene	Msh.s	Dolati (2010)
6006	0	6007	ph_brown	3.888	9		M-L Miocene	Msh.s	Dolati (2010)
6007	0	6008	ph_brown	0.181	9		M-L Miocene	Msh.s	Dolati (2010)
6008	0	6009	ph_brown	0.333	9		M-L Miocene	Msh.s	Dolati (2010)
6009	0	6010	ph_brown	1.798	9		M-L Miocene	Msh.s	Dolati (2010)
6010	0	6011	ph_brown	0.073	9		M-L Miocene	Msh.s	Dolati (2010)
6011	0	6012	ph_brown	0.282	9		M-L Miocene	Msh.s	Dolati (2010)
6012	0	6013	ph_brown	0.079	9		M-L Miocene	Msh.s	Dolati (2010)
6013	0	6014	ph_brown	0.009	9		M-L Miocene	Msh.s	Dolati (2010)
6014	0	6015	ph_brown	0.930	9		M-L Miocene	Msh.s	Dolati (2010)
6015	0	6016	ph_brown	0.661	9		M-L Miocene	Msh.s	Dolati (2010)
6016	0	6017	ph_brown	0.275	9		M-L Miocene	Msh.s	Dolati (2010)
6017	0	6018	ph_brown	0.962	9		M-L Miocene	Msh.s	Dolati (2010)
6018	0	6019	ph_brown	2.093	9		M-L Miocene	Msh.s	Dolati (2010)
6019	0	6020	ph_brown	0.196	9		M-L Miocene	Msh.s	Dolati (2010)
6020	0	6021	ph_brown	0.279	9		M-L Miocene	Msh.s	Dolati (2010)
6021	0	6022	ph_brown	0.140	9		M-L Miocene	Msh.s	Dolati (2010)
6022	0	6023	ph_brown	0.189	9		M-L Miocene	Msh.s	Dolati (2010)
6023	0	6024	ph_brown	0.875	9		M-L Miocene	Msh.s	Dolati (2010)
6024	0	6025	ph_brown	0.020	9		M-L Miocene	Msh.s	Dolati (2010)

Geonevis

OBJECTID_1	Join_Count	TARGET_FID	Label	Shape_Area (sqkm)	ORIG_FID	Absolute_Age	Age_paleontology	Unit	Reference
6025	0	6026	ph_brown	0.725	9		M-L Miocene	Msh.s	Dolati (2010)
6026	0	6027	ph_brown	0.580	9		M-L Miocene	Msh.s	Dolati (2010)
6027	0	6028	ph_brown	0.264	9		M-L Miocene	Msh.s	Dolati (2010)
6028	0	6029	ph_brown	0.348	9		M-L Miocene	Msh.s	Dolati (2010)
6029	0	6030	ph_brown	0.120	9		M-L Miocene	Msh.s	Dolati (2010)
6030	0	6031	ph_brown	0.269	9		M-L Miocene	Msh.s	Dolati (2010)
6031	0	6032	ph_brown	0.501	9		M-L Miocene	Msh.s	Dolati (2010)
6032	0	6033	ph_brown	0.456	9		M-L Miocene	Msh.s	Dolati (2010)
6033	0	6034	ph_brown	0.583	9		M-L Miocene	Msh.s	Dolati (2010)
6034	0	6035	ph_brown	0.039	9		M-L Miocene	Msh.s	Dolati (2010)
6035	0	6036	ph_brown	1.179	9		M-L Miocene	Msh.s	Dolati (2010)
6036	0	6037	ph_brown	0.245	9		M-L Miocene	Msh.s	Dolati (2010)
6037	0	6038	ph_brown	0.119	9		M-L Miocene	Msh.s	Dolati (2010)
6038	0	6039	ph_brown	0.456	9		M-L Miocene	Msh.s	Dolati (2010)
6039	0	6040	ph_brown	0.365	9		M-L Miocene	Msh.s	Dolati (2010)
6040	0	6041	ph_brown	0.674	9		M-L Miocene	Msh.s	Dolati (2010)
6041	0	6042	ph_brown	1.061	9		M-L Miocene	Msh.s	Dolati (2010)
6042	0	6043	ph_brown	0.060	9		M-L Miocene	Msh.s	Dolati (2010)
6043	0	6044	ph_brown	0.612	9		M-L Miocene	Msh.s	Dolati (2010)
6044	0	6045	ph_brown	0.605	9		M-L Miocene	Msh.s	Dolati (2010)
6045	0	6046	ph_brown	0.338	9		M-L Miocene	Msh.s	Dolati (2010)
6046	0	6047	ph_brown	1.889	9		M-L Miocene	Msh.s	Dolati (2010)
6047	0	6048	ph_brown	0.060	9		M-L Miocene	Msh.s	Dolati (2010)
6048	0	6049	ph_brown	0.074	9		M-L Miocene	Msh.s	Dolati (2010)
6049	0	6050	ph_brown	1.988	9		M-L Miocene	Msh.s	Dolati (2010)
6050	0	6051	ph_brown	0.242	9		M-L Miocene	Msh.s	Dolati (2010)
6051	0	6052	ph_brown	1.895	9		M-L Miocene	Msh.s	Dolati (2010)
6052	0	6053	ph_brown	0.672	9		M-L Miocene	Msh.s	Dolati (2010)
6053	0	6054	ph_brown	0.248	9		M-L Miocene	Msh.s	Dolati (2010)
6054	0	6055	ph_brown	0.706	9		M-L Miocene	Msh.s	Dolati (2010)
6055	0	6056	ph_brown	0.019	9		M-L Miocene	Msh.s	Dolati (2010)
6056	0	6057	ph_brown	0.405	9		M-L Miocene	Msh.s	Dolati (2010)
6057	0	6058	ph_brown	0.789	9		M-L Miocene	Msh.s	Dolati (2010)
6058	0	6059	ph_brown	0.050	9		M-L Miocene	Msh.s	Dolati (2010)
6059	0	6060	ph_brown	0.317	9		M-L Miocene	Msh.s	Dolati (2010)
6060	0	6061	ph_brown	0.456	9		M-L Miocene	Msh.s	Dolati (2010)
6061	0	6062	ph_brown	0.062	9		M-L Miocene	Msh.s	Dolati (2010)
6062	0	6063	ph_brown	3.993	9		M-L Miocene	Msh.s	Dolati (2010)
6063	0	6064	ph_brown	0.062	9		M-L Miocene	Msh.s	Dolati (2010)

Geonevis

OBJECTID_1	Join_Count	TARGET_FID	Label	Shape_Area (sqkm)	ORIG_FID	Absolute_Age	Age_paleontology	Unit	Reference
6064	0	6065	ph_brown	1.015	9		M-L Miocene	Msh.s	Dolati (2010)
6065	0	6066	ph_brown	0.407	9		M-L Miocene	Msh.s	Dolati (2010)
6066	0	6067	ph_brown	0.057	9		M-L Miocene	Msh.s	Dolati (2010)
6067	0	6068	ph_brown	0.031	9		M-L Miocene	Msh.s	Dolati (2010)
6068	0	6069	ph_brown	0.422	9		M-L Miocene	Msh.s	Dolati (2010)
6069	0	6070	ph_brown	0.486	9		M-L Miocene	Msh.s	Dolati (2010)
6070	0	6071	ph_brown	0.052	9		M-L Miocene	Msh.s	Dolati (2010)
7121	1	7122	ph_brown	0.453	12		M-L Miocene	Msh.s	Dolati (2010)
7937	1	7938	ph_brown	0.359	13		M-L Miocene	Msh.s	Dolati (2010)
10430	1	10453	m	0.013	0		M-L Miocene	Msh.s	Dolati (2010)
10432	1	10456	m	0.039	0		M-L Miocene	Msh.s	Dolati (2010)
10433	1	10457	m	0.080	0		M-L Miocene	Msh.s	Dolati (2010)
10435	1	10459	m	0.087	0		M-L Miocene	Msh.s	Dolati (2010)
10442	2	8211	mud_pink	0.005	14		M-L Miocene	Msh.s	
10443	3	2173	mud_pink	0.005	5		M-L Miocene	Msh.s	Dolati (2010)
10444	3	2173	mud_pink	0.001	5		M-L Miocene	Msh.s	Dolati (2010)
10445	3	2173	mud_pink	0.009	5		M-L Miocene	Msh.s	Dolati (2010)
10498	2	244	ph_brow	0.109	2		M-L Miocene	Msh.s	Dolati (2010)
10537	0	5764	ph_brown	2.090	9		M-L Miocene	Msh.s	Dolati (2010)
10541	1	10428	m.w	0.089	0		M-L Miocene	Msh.s	Dolati (2010)

GeoNeuro

Table S5. Summary of mapped polygons for the $M^{s.si}$ Unit.

OBJECTID_1	Join_Count	TARGET_FID	label	Shape_Area (sqkm)	ORIG_FID	Absolute_Age	Age_paleontology	Unit	Reference
6371	0	6372	ph_red	0.022	12			Ms.si	
6372	0	6373	ph_red	0.013	12			Ms.si	
6373	0	6374	ph_red	0.776	12			Ms.si	
6374	0	6375	ph_red	0.038	12			Ms.si	
6375	0	6376	ph_red	0.561	12			Ms.si	
6376	0	6377	ph_red	0.048	12			Ms.si	
6377	0	6378	ph_red	0.020	12			Ms.si	
6378	0	6379	ph_red	0.028	12			Ms.si	
6379	0	6380	ph_red	0.204	12			Ms.si	
6380	0	6381	ph_red	0.405	12			Ms.si	
6381	0	6382	ph_red	0.332	12			Ms.si	
6382	0	6383	ph_red	0.100	12			Ms.si	
6383	0	6384	ph_red	3.110	12			Ms.si	
6384	0	6385	ph_red	0.246	12			Ms.si	
6385	0	6386	ph_red	1.041	12			Ms.si	
6386	0	6387	ph_red	0.149	12			Ms.si	
6387	0	6388	ph_red	0.145	12			Ms.si	
6388	0	6389	ph_red	0.223	12			Ms.si	
6389	0	6390	ph_red	0.169	12			Ms.si	
6390	0	6391	ph_red	0.720	12			Ms.si	
6391	0	6392	ph_red	1.463	12			Ms.si	
6392	0	6393	ph_red	0.044	12			Ms.si	
6393	0	6394	ph_red	0.050	12			Ms.si	
6394	0	6395	ph_red	0.041	12			Ms.si	
6395	0	6396	ph_red	0.006	12			Ms.si	
6396	0	6397	ph_red	0.032	12			Ms.si	
6397	0	6398	ph_red	0.045	12			Ms.si	
6398	0	6399	ph_red	0.104	12			Ms.si	
6399	0	6400	ph_red	0.050	12			Ms.si	
6400	0	6401	ph_red	0.087	12			Ms.si	
6401	0	6402	ph_red	0.059	12			Ms.si	
6402	0	6403	ph_red	0.100	12			Ms.si	
6403	0	6404	ph_red	0.012	12			Ms.si	
6404	0	6405	ph_red	0.035	12			Ms.si	
6405	0	6406	ph_red	0.123	12			Ms.si	
6406	0	6407	ph_red	0.041	12			Ms.si	
6407	0	6408	ph_red	1.024	12			Ms.si	
6408	0	6409	ph_red	0.169	12			Ms.si	

GeoNexus

OBJECTID_1	Join_Count	TARGET_FID	label	Shape_Area (sqkm)	ORIG_FID	Absolute_Age	Age_paleontology	Unit	Reference
6409	0	6410	ph_red	0.132	12			Ms.si	
6410	0	6411	ph_red	0.100	12			Ms.si	
6411	0	6412	ph_red	0.068	12			Ms.si	
6412	0	6413	ph_red	0.079	12			Ms.si	
6413	0	6414	ph_red	0.033	12			Ms.si	
6414	0	6415	ph_red	0.131	12			Ms.si	
6415	0	6416	ph_red	0.132	12			Ms.si	
6416	0	6417	ph_red	0.022	12			Ms.si	
6417	0	6418	ph_red	0.119	12			Ms.si	
6418	0	6419	ph_red	0.301	12			Ms.si	
6419	0	6420	ph_red	0.371	12			Ms.si	
6420	0	6421	ph_red	0.012	12			Ms.si	
6421	0	6422	ph_red	0.020	12			Ms.si	
6422	0	6423	ph_red	0.140	12			Ms.si	
6423	0	6424	ph_red	0.336	12			Ms.si	
6424	0	6425	ph_red	0.341	12			Ms.si	
6425	0	6426	ph_red	0.073	12			Ms.si	
6426	0	6427	ph_red	0.154	12			Ms.si	
6427	0	6428	ph_red	0.051	12			Ms.si	
6428	0	6429	ph_red	0.055	12			Ms.si	
6429	0	6430	ph_red	0.339	12			Ms.si	
6430	0	6431	ph_red	0.213	12			Ms.si	
6431	0	6432	ph_red	0.133	12			Ms.si	
6432	0	6433	ph_red	0.317	12			Ms.si	
6433	0	6434	ph_red	0.624	12			Ms.si	
6434	0	6435	ph_red	0.006	12			Ms.si	
6435	0	6436	ph_red	0.409	12			Ms.si	
6436	0	6437	ph_red	0.530	12			Ms.si	
6437	0	6438	ph_red	0.028	12			Ms.si	
6438	0	6439	ph_red	0.031	12			Ms.si	
6439	0	6440	ph_red	0.006	12			Ms.si	
6440	0	6441	ph_red	0.028	12			Ms.si	
6441	0	6442	ph_red	0.036	12			Ms.si	
6442	0	6443	ph_red	0.155	12			Ms.si	
6443	0	6444	ph_red	0.904	12			Ms.si	
6444	0	6445	ph_red	0.021	12			Ms.si	
6445	0	6446	ph_red	0.101	12			Ms.si	
6446	0	6447	ph_red	0.197	12			Ms.si	
6447	0	6448	ph_red	0.215	12			Ms.si	

GeoNexus

OBJECTID_1	Join_Count	TARGET_FID	label	Shape_Area (sqkm)	ORIG_FID	Absolute_Age	Age_paleontology	Unit	Reference
6448	0	6449	ph_red	1.161	12			Ms.si	
6449	0	6450	ph_red	0.056	12			Ms.si	
6450	0	6451	ph_red	0.016	12			Ms.si	
6451	0	6452	ph_red	0.008	12			Ms.si	
6452	0	6453	ph_red	0.012	12			Ms.si	
6453	0	6454	ph_red	0.053	12			Ms.si	
6454	0	6455	ph_red	0.013	12			Ms.si	
6455	0	6456	ph_red	0.013	12			Ms.si	
6456	0	6457	ph_red	0.260	12			Ms.si	
6457	0	6458	ph_red	0.207	12			Ms.si	
6458	0	6459	ph_red	1.063	12			Ms.si	
6459	0	6460	ph_red	0.008	12			Ms.si	
6460	0	6461	ph_red	0.349	12			Ms.si	
6461	0	6462	ph_red	0.017	12			Ms.si	
6462	0	6463	ph_red	0.462	12			Ms.si	
6463	0	6464	ph_red	0.094	12			Ms.si	
6464	0	6465	ph_red	1.125	12			Ms.si	
6465	0	6466	ph_red	0.007	12			Ms.si	
6466	0	6467	ph_red	0.041	12			Ms.si	
6467	0	6468	ph_red	0.013	12			Ms.si	
6468	0	6469	ph_red	0.129	12			Ms.si	
6469	0	6470	ph_red	0.070	12			Ms.si	
6470	0	6471	ph_red	0.016	12			Ms.si	
6471	0	6472	ph_red	0.007	12			Ms.si	
6472	0	6473	ph_red	0.228	12			Ms.si	
6473	0	6474	ph_red	0.006	12			Ms.si	
6474	0	6475	ph_red	0.113	12			Ms.si	
6475	1	6476	ph_red	0.981	12			Ms.si	
6476	0	6477	ph_red	0.133	12			Ms.si	
6477	0	6478	ph_red	0.024	12			Ms.si	
6478	0	6479	ph_red	0.060	12			Ms.si	
6479	0	6480	ph_red	0.117	12			Ms.si	
6480	0	6481	ph_red	0.035	12			Ms.si	
6481	0	6482	ph_red	0.020	12			Ms.si	
6482	0	6483	ph_red	1.933	12			Ms.si	
6483	0	6484	ph_red	0.116	12			Ms.si	
6484	0	6485	ph_red	0.251	12			Ms.si	
6485	0	6486	ph_red	0.017	12			Ms.si	
6486	0	6487	ph_red	0.004	12			Ms.si	

GeoNexus

OBJECTID_1	Join_Count	TARGET_FID	label	Shape_Area (sqkm)	ORIG_FID	Absolute_Age	Age_paleontology	Unit	Reference
6487	0	6488	ph_red	0.330	12			Ms.si	
6488	0	6489	ph_red	0.051	12			Ms.si	
6489	0	6490	ph_red	0.261	12			Ms.si	
6490	0	6491	ph_red	0.126	12			Ms.si	
6491	0	6492	ph_red	0.337	12			Ms.si	
6492	0	6493	ph_red	0.049	12			Ms.si	
6493	0	6494	ph_red	1.037	12			Ms.si	
6494	0	6495	ph_red	0.069	12			Ms.si	
6495	0	6496	ph_red	0.554	12			Ms.si	
6496	0	6497	ph_red	0.393	12			Ms.si	
6497	0	6498	ph_red	0.061	12			Ms.si	
6498	0	6499	ph_red	0.706	12			Ms.si	
6499	0	6500	ph_red	0.129	12			Ms.si	
6500	0	6501	ph_red	0.019	12			Ms.si	
6501	0	6502	ph_red	0.013	12			Ms.si	
6502	0	6503	ph_red	0.399	12			Ms.si	
6503	0	6504	ph_red	0.373	12			Ms.si	
6504	0	6505	ph_red	0.090	12			Ms.si	
6505	0	6506	ph_red	0.024	12			Ms.si	
6506	0	6507	ph_red	0.031	12			Ms.si	
6507	0	6508	ph_red	0.441	12			Ms.si	
6508	0	6509	ph_red	0.038	12			Ms.si	
6509	0	6510	ph_red	0.382	12			Ms.si	
6510	0	6511	ph_red	0.009	12			Ms.si	
6511	0	6512	ph_red	0.107	12			Ms.si	
6512	0	6513	ph_red	0.693	12			Ms.si	
6513	0	6514	ph_red	3.364	12			Ms.si	
6514	0	6515	ph_red	0.131	12			Ms.si	
6515	0	6516	ph_red	0.042	12			Ms.si	
6516	0	6517	ph_red	0.016	12			Ms.si	
6517	0	6518	ph_red	3.650	12			Ms.si	
6518	0	6519	ph_red	1.099	12			Ms.si	
6519	0	6520	ph_red	0.632	12			Ms.si	
6520	0	6521	ph_red	0.106	12			Ms.si	
6521	0	6522	ph_red	0.126	12			Ms.si	
6522	0	6523	ph_red	1.230	12			Ms.si	
6523	0	6524	ph_red	0.453	12			Ms.si	
6524	0	6525	ph_red	0.026	12			Ms.si	
6525	0	6526	ph_red	0.026	12			Ms.si	

GeoNexus

OBJECTID_1	Join_Count	TARGET_FID	label	Shape_Area (sqkm)	ORIG_FID	Absolute_Age	Age_paleontology	Unit	Reference
6526	0	6527	ph_red	0.196	12			Ms.si	
6527	0	6528	ph_red	0.315	12			Ms.si	
6528	0	6529	ph_red	1.449	12			Ms.si	
6529	0	6530	ph_red	0.219	12			Ms.si	
6530	0	6531	ph_red	0.172	12			Ms.si	
6531	0	6532	ph_red	1.310	12			Ms.si	
6532	0	6533	ph_red	0.227	12			Ms.si	
6533	0	6534	ph_red	0.047	12			Ms.si	
6535	0	6536	ph_red	0.032	12			Ms.si	
6536	0	6537	ph_red	0.010	12			Ms.si	
6537	0	6538	ph_red	0.176	12			Ms.si	
6538	0	6539	ph_red	0.013	12			Ms.si	
6539	0	6540	ph_red	0.098	12			Ms.si	
6540	0	6541	ph_red	0.119	12			Ms.si	
6541	0	6542	ph_red	0.007	12			Ms.si	
6542	0	6543	ph_red	2.309	12			Ms.si	
6543	0	6544	ph_red	0.053	12			Ms.si	
6544	0	6545	ph_red	0.013	12			Ms.si	
6545	0	6546	ph_red	0.038	12			Ms.si	
6546	0	6547	ph_red	0.110	12			Ms.si	
6547	0	6548	ph_red	0.044	12			Ms.si	
6548	0	6549	ph_red	0.008	12			Ms.si	
6549	0	6550	ph_red	0.769	12			Ms.si	
6550	0	6551	ph_red	0.022	12			Ms.si	
6551	0	6552	ph_red	0.020	12			Ms.si	
6552	0	6553	ph_red	0.029	12			Ms.si	
6553	0	6554	ph_red	0.034	12			Ms.si	
6554	0	6555	ph_red	0.107	12			Ms.si	
6555	0	6556	ph_red	0.589	12			Ms.si	
6556	0	6557	ph_red	0.075	12			Ms.si	
6557	0	6558	ph_red	1.856	12			Ms.si	
6558	0	6559	ph_red	0.105	12			Ms.si	
6559	0	6560	ph_red	0.153	12			Ms.si	
6560	0	6561	ph_red	0.449	12			Ms.si	
6561	0	6562	ph_red	0.078	12			Ms.si	
6562	0	6563	ph_red	3.386	12			Ms.si	
6563	0	6564	ph_red	0.075	12			Ms.si	
6564	0	6565	ph_red	0.442	12			Ms.si	
6565	0	6566	ph_red	0.014	12			Ms.si	

GeoNexus

OBJECTID_1	Join_Count	TARGET_FID	label	Shape_Area (sqkm)	ORIG_FID	Absolute_Age	Age_paleontology	Unit	Reference
6566	0	6567	ph_red	0.159	12			Ms.si	
6567	0	6568	ph_red	0.035	12			Ms.si	
6568	0	6569	ph_red	0.229	12			Ms.si	
6569	0	6570	ph_red	0.007	12			Ms.si	
6570	0	6571	ph_red	0.316	12			Ms.si	
6571	0	6572	ph_red	0.133	12			Ms.si	
6572	0	6573	ph_red	0.797	12			Ms.si	
6573	0	6574	ph_red	0.260	12			Ms.si	
6574	0	6575	ph_red	0.738	12			Ms.si	
6575	0	6576	ph_red	0.458	12			Ms.si	
6576	0	6577	ph_red	1.512	12			Ms.si	
6577	0	6578	ph_red	0.049	12			Ms.si	
6578	0	6579	ph_red	0.050	12			Ms.si	
6579	0	6580	ph_red	0.124	12			Ms.si	
6580	0	6581	ph_red	0.452	12			Ms.si	
6581	0	6582	ph_red	0.387	12			Ms.si	
6582	0	6583	ph_red	0.020	12			Ms.si	
6583	0	6584	ph_red	0.066	12			Ms.si	
6584	0	6585	ph_red	0.072	12			Ms.si	
6585	0	6586	ph_red	0.165	12			Ms.si	
6586	0	6587	ph_red	1.088	12			Ms.si	
6588	0	6589	ph_red	0.760	12			Ms.si	
6589	0	6590	ph_red	0.055	12			Ms.si	
6590	0	6591	ph_red	0.025	12			Ms.si	
6591	0	6592	ph_red	0.538	12			Ms.si	
6592	0	6593	ph_red	0.082	12			Ms.si	
6593	0	6594	ph_red	0.267	12			Ms.si	
6594	0	6595	ph_red	0.020	12			Ms.si	
6595	0	6596	ph_red	0.058	12			Ms.si	
6596	0	6597	ph_red	0.046	12			Ms.si	
6597	0	6598	ph_red	0.308	12			Ms.si	
6598	0	6599	ph_red	0.022	12			Ms.si	
6599	0	6600	ph_red	0.014	12			Ms.si	
6600	0	6601	ph_red	0.659	12			Ms.si	
6601	0	6602	ph_red	0.019	12			Ms.si	
6602	0	6603	ph_red	0.454	12			Ms.si	
6603	0	6604	ph_red	0.457	12			Ms.si	
6604	0	6605	ph_red	0.175	12			Ms.si	
6605	0	6606	ph_red	0.063	12			Ms.si	

GeoNexus

OBJECTID_1	Join_Count	TARGET_FID	label	Shape_Area (sqkm)	ORIG_FID	Absolute_Age	Age_paleontology	Unit	Reference
6606	0	6607	ph_red	5.978	12			Ms.si	
6607	0	6608	ph_red	0.194	12			Ms.si	
6608	0	6609	ph_red	1.859	12			Ms.si	
6609	0	6610	ph_red	0.861	12			Ms.si	
6610	0	6611	ph_red	0.111	12			Ms.si	
6611	0	6612	ph_red	0.351	12			Ms.si	
6612	0	6613	ph_red	0.074	12			Ms.si	
6613	0	6614	ph_red	0.006	12			Ms.si	
6614	0	6615	ph_red	0.054	12			Ms.si	
6615	0	6616	ph_red	0.025	12			Ms.si	
6616	0	6617	ph_red	0.098	12			Ms.si	
6617	0	6618	ph_red	0.395	12			Ms.si	
6618	0	6619	ph_red	0.089	12			Ms.si	
6619	0	6620	ph_red	0.654	12			Ms.si	
6620	0	6621	ph_red	0.052	12			Ms.si	
6622	0	6623	ph_red	0.083	12			Ms.si	
6623	0	6624	ph_red	0.009	12			Ms.si	
6624	0	6625	ph_red	0.147	12			Ms.si	
6625	0	6626	ph_red	0.564	12			Ms.si	
6626	0	6627	ph_red	1.766	12			Ms.si	
6627	0	6628	ph_red	0.286	12			Ms.si	
6628	0	6629	ph_red	0.910	12			Ms.si	
6629	0	6630	ph_red	0.431	12			Ms.si	
6630	0	6631	ph_red	0.143	12			Ms.si	
6631	0	6632	ph_red	2.834	12			Ms.si	
6632	0	6633	ph_red	0.433	12			Ms.si	
6633	0	6634	ph_red	0.091	12			Ms.si	
6634	0	6635	ph_red	0.054	12			Ms.si	
6635	0	6636	ph_red	0.788	12			Ms.si	
6636	0	6637	ph_red	0.363	12			Ms.si	
6637	0	6638	ph_red	0.173	12			Ms.si	
6639	0	6640	ph_red	1.133	12			Ms.si	
6640	0	6641	ph_red	0.426	12			Ms.si	
6641	0	6642	ph_red	0.612	12			Ms.si	
6642	0	6643	ph_red	0.085	12			Ms.si	
6643	0	6644	ph_red	0.375	12			Ms.si	
6644	0	6645	ph_red	0.074	12			Ms.si	
6645	0	6646	ph_red	0.131	12			Ms.si	
6646	0	6647	ph_red	0.095	12			Ms.si	

GeoNexus

OBJECTID_1	Join_Count	TARGET_FID	label	Shape_Area (sqkm)	ORIG_FID	Absolute_Age	Age_paleontology	Unit	Reference
6647	0	6648	ph_red	0.291	12			Ms.si	
6648	0	6649	ph_red	0.126	12			Ms.si	
6649	0	6650	ph_red	0.092	12			Ms.si	
6650	0	6651	ph_red	0.020	12			Ms.si	
6651	0	6652	ph_red	0.018	12			Ms.si	
6652	0	6653	ph_red	1.538	12			Ms.si	
6653	0	6654	ph_red	0.305	12			Ms.si	
6654	0	6655	ph_red	0.274	12			Ms.si	
6655	0	6656	ph_red	0.233	12			Ms.si	
6656	0	6657	ph_red	0.160	12			Ms.si	
6657	0	6658	ph_red	0.213	12			Ms.si	
6658	0	6659	ph_red	0.108	12			Ms.si	
6659	0	6660	ph_red	0.019	12			Ms.si	
6660	0	6661	ph_red	0.021	12			Ms.si	
6661	0	6662	ph_red	0.978	12			Ms.si	
6662	0	6663	ph_red	0.010	12			Ms.si	
6663	0	6664	ph_red	0.060	12			Ms.si	
6664	0	6665	ph_red	0.108	12			Ms.si	
6665	0	6666	ph_red	0.059	12			Ms.si	
6666	0	6667	ph_red	0.078	12			Ms.si	
6667	0	6668	ph_red	0.022	12			Ms.si	
6668	0	6669	ph_red	0.046	12			Ms.si	
6669	0	6670	ph_red	0.078	12			Ms.si	
6670	0	6671	ph_red	0.768	12			Ms.si	
6671	0	6672	ph_red	0.052	12			Ms.si	
6672	0	6673	ph_red	0.091	12			Ms.si	
6673	0	6674	ph_red	0.037	12			Ms.si	
6674	0	6675	ph_red	0.246	12			Ms.si	
6675	0	6676	ph_red	0.444	12			Ms.si	
6676	0	6677	ph_red	0.563	12			Ms.si	
6677	0	6678	ph_red	1.546	12			Ms.si	
6678	0	6679	ph_red	0.045	12			Ms.si	
6679	0	6680	ph_red	0.024	12			Ms.si	
6680	0	6681	ph_red	0.179	12			Ms.si	
6681	0	6682	ph_red	0.152	12			Ms.si	
6682	0	6683	ph_red	0.911	12			Ms.si	
6683	0	6684	ph_red	0.131	12			Ms.si	
6685	0	6686	ph_red	0.041	12			Ms.si	
6686	0	6687	ph_red	0.300	12			Ms.si	

GeoNexus

OBJECTID_1	Join_Count	TARGET_FID	label	Shape_Area (sqkm)	ORIG_FID	Absolute_Age	Age_paleontology	Unit	Reference
6687	0	6688	ph_red	0.048	12			Ms.si	
6688	0	6689	ph_red	0.803	12			Ms.si	
6689	0	6690	ph_red	1.919	12			Ms.si	
6690	0	6691	ph_red	0.122	12			Ms.si	
6691	0	6692	ph_red	0.124	12			Ms.si	
6692	0	6693	ph_red	0.173	12			Ms.si	
6693	0	6694	ph_red	0.154	12			Ms.si	
6694	0	6695	ph_red	0.847	12			Ms.si	
6695	0	6696	ph_red	0.503	12			Ms.si	
6696	0	6697	ph_red	0.136	12			Ms.si	
6697	0	6698	ph_red	0.042	12			Ms.si	
6698	0	6699	ph_red	0.046	12			Ms.si	
6699	0	6700	ph_red	0.029	12			Ms.si	
6700	0	6701	ph_red	0.259	12			Ms.si	
6701	0	6702	ph_red	0.096	12			Ms.si	
6702	0	6703	ph_red	0.343	12			Ms.si	
6703	0	6704	ph_red	0.212	12			Ms.si	
6704	0	6705	ph_red	0.035	12			Ms.si	
6705	0	6706	ph_red	0.044	12			Ms.si	
6706	1	6707	ph_red	16.906	12			Ms.si	
6707	0	6708	ph_red	0.387	12			Ms.si	
6708	0	6709	ph_red	0.705	12			Ms.si	
6709	0	6710	ph_red	0.035	12			Ms.si	
6710	0	6711	ph_red	0.021	12			Ms.si	
6711	0	6712	ph_red	0.541	12			Ms.si	
6712	0	6713	ph_red	0.197	12			Ms.si	
6713	0	6714	ph_red	0.130	12			Ms.si	
6714	0	6715	ph_red	0.293	12			Ms.si	
6715	0	6716	ph_red	0.307	12			Ms.si	
6716	0	6717	ph_red	0.377	12			Ms.si	
6717	0	6718	ph_red	0.082	12			Ms.si	
6718	0	6719	ph_red	0.088	12			Ms.si	
6719	0	6720	ph_red	0.019	12			Ms.si	
6720	0	6721	ph_red	0.012	12			Ms.si	
6721	0	6722	ph_red	0.215	12			Ms.si	
6722	0	6723	ph_red	0.143	12			Ms.si	
6723	0	6724	ph_red	0.081	12			Ms.si	
6724	0	6725	ph_red	0.229	12			Ms.si	
6725	0	6726	ph_red	0.099	12			Ms.si	

GeoNexus

OBJECTID_1	Join_Count	TARGET_FID	label	Shape_Area (sqkm)	ORIG_FID	Absolute_Age	Age_paleontology	Unit	Reference
6726	0	6727	ph_red	0.432	12			Ms.si	
6727	0	6728	ph_red	1.068	12			Ms.si	
6728	0	6729	ph_red	0.053	12			Ms.si	
6729	0	6730	ph_red	0.299	12			Ms.si	
6730	0	6731	ph_red	0.331	12			Ms.si	
6731	0	6732	ph_red	0.013	12			Ms.si	
6732	0	6733	ph_red	0.046	12			Ms.si	
6733	0	6734	ph_red	0.234	12			Ms.si	
6734	0	6735	ph_red	0.674	12			Ms.si	
6735	0	6736	ph_red	0.312	12			Ms.si	
6736	0	6737	ph_red	0.315	12			Ms.si	
6737	0	6738	ph_red	0.203	12			Ms.si	
6738	0	6739	ph_red	2.523	12			Ms.si	
6739	0	6740	ph_red	0.283	12			Ms.si	
6740	0	6741	ph_red	0.162	12			Ms.si	
6741	0	6742	ph_red	0.071	12			Ms.si	
6742	0	6743	ph_red	7.704	12			Ms.si	
6743	0	6744	ph_red	1.359	12			Ms.si	
6744	0	6745	ph_red	0.033	12			Ms.si	
6745	0	6746	ph_red	0.972	12			Ms.si	
6746	0	6747	ph_red	0.032	12			Ms.si	
6747	0	6748	ph_red	0.233	12			Ms.si	
6748	0	6749	ph_red	0.015	12			Ms.si	
6749	0	6750	ph_red	0.030	12			Ms.si	
6750	0	6751	ph_red	0.271	12			Ms.si	
6751	0	6752	ph_red	0.061	12			Ms.si	
6752	0	6753	ph_red	0.148	12			Ms.si	
6753	0	6754	ph_red	0.012	12			Ms.si	
6754	0	6755	ph_red	0.548	12			Ms.si	
6755	0	6756	ph_red	0.018	12			Ms.si	
6756	0	6757	ph_red	0.039	12			Ms.si	
6757	0	6758	ph_red	0.251	12			Ms.si	
6758	0	6759	ph_red	1.677	12			Ms.si	
6759	0	6760	ph_red	0.102	12			Ms.si	
6760	0	6761	ph_red	0.015	12			Ms.si	
6761	0	6762	ph_red	1.617	12			Ms.si	
6762	0	6763	ph_red	0.104	12			Ms.si	
6763	0	6764	ph_red	0.883	12			Ms.si	
6764	0	6765	ph_red	0.035	12			Ms.si	

GeoNexus

OBJECTID_1	Join_Count	TARGET_FID	label	Shape_Area (sqkm)	ORIG_FID	Absolute_Age	Age_paleontology	Unit	Reference
6765	0	6766	ph_red	0.233	12			Ms.si	
6766	0	6767	ph_red	0.015	12			Ms.si	
6767	0	6768	ph_red	0.007	12			Ms.si	
6768	0	6769	ph_red	1.292	12			Ms.si	
6769	0	6770	ph_red	0.025	12			Ms.si	
6770	0	6771	ph_red	0.011	12			Ms.si	
6771	0	6772	ph_red	0.275	12			Ms.si	
6772	0	6773	ph_red	0.019	12			Ms.si	
6773	0	6774	ph_red	0.022	12			Ms.si	
6774	0	6775	ph_red	0.211	12			Ms.si	
6775	0	6776	ph_red	0.391	12			Ms.si	
6776	0	6777	ph_red	0.833	12			Ms.si	
6777	0	6778	ph_red	0.219	12			Ms.si	
6778	0	6779	ph_red	0.289	12			Ms.si	
6779	0	6780	ph_red	0.298	12			Ms.si	
6780	0	6781	ph_red	0.445	12			Ms.si	
6781	0	6782	ph_red	0.057	12			Ms.si	
6782	0	6783	ph_red	0.019	12			Ms.si	
6783	0	6784	ph_red	0.023	12			Ms.si	
6784	0	6785	ph_red	0.552	12			Ms.si	
6785	0	6786	ph_red	1.166	12			Ms.si	
6786	0	6787	ph_red	0.010	12			Ms.si	
6787	0	6788	ph_red	0.090	12			Ms.si	
6788	0	6789	ph_red	1.342	12			Ms.si	
6789	0	6790	ph_red	0.329	12			Ms.si	
6790	0	6791	ph_red	0.095	12			Ms.si	
6791	0	6792	ph_red	0.077	12			Ms.si	
6792	0	6793	ph_red	0.025	12			Ms.si	
6793	0	6794	ph_red	2.014	12			Ms.si	
6794	0	6795	ph_red	0.258	12			Ms.si	
6795	0	6796	ph_red	0.060	12			Ms.si	
6796	0	6797	ph_red	0.049	12			Ms.si	
6797	0	6798	ph_red	0.169	12			Ms.si	
6798	0	6799	ph_red	1.351	12			Ms.si	
6799	0	6800	ph_red	5.954	12			Ms.si	
6800	0	6801	ph_red	0.155	12			Ms.si	
6801	0	6802	ph_red	0.348	12			Ms.si	
6802	0	6803	ph_red	0.020	12			Ms.si	
6803	0	6804	ph_red	1.222	12			Ms.si	

GeoNexus

OBJECTID_1	Join_Count	TARGET_FID	label	Shape_Area (sqkm)	ORIG_FID	Absolute_Age	Age_paleontology	Unit	Reference
6804	0	6805	ph_red	0.325	12			Ms.si	
6805	0	6806	ph_red	0.642	12			Ms.si	
6806	0	6807	ph_red	0.080	12			Ms.si	
6807	0	6808	ph_red	0.690	12			Ms.si	
6808	0	6809	ph_red	0.027	12			Ms.si	
6809	0	6810	ph_red	0.067	12			Ms.si	
6810	0	6811	ph_red	0.084	12			Ms.si	
6811	0	6812	ph_red	0.023	12			Ms.si	
6812	0	6813	ph_red	2.031	12			Ms.si	
6813	0	6814	ph_red	1.544	12			Ms.si	
6814	0	6815	ph_red	0.064	12			Ms.si	
6815	0	6816	ph_red	0.080	12			Ms.si	
6816	0	6817	ph_red	0.298	12			Ms.si	
6817	0	6818	ph_red	0.358	12			Ms.si	
6818	0	6819	ph_red	0.504	12			Ms.si	
6819	0	6820	ph_red	0.695	12			Ms.si	
6820	0	6821	ph_red	0.103	12			Ms.si	
6821	0	6822	ph_red	0.020	12			Ms.si	
6822	0	6823	ph_red	0.513	12			Ms.si	
6823	0	6824	ph_red	1.499	12			Ms.si	
6824	0	6825	ph_red	0.096	12			Ms.si	
6825	0	6826	ph_red	0.062	12			Ms.si	
6826	0	6827	ph_red	0.128	12			Ms.si	
6827	0	6828	ph_red	0.236	12			Ms.si	
6828	0	6829	ph_red	1.238	12			Ms.si	
6829	0	6830	ph_red	0.071	12			Ms.si	
6830	0	6831	ph_red	0.630	12			Ms.si	
6831	0	6832	ph_red	0.026	12			Ms.si	
6832	0	6833	ph_red	0.339	12			Ms.si	
6833	0	6834	ph_red	0.136	12			Ms.si	
6834	0	6835	ph_red	0.206	12			Ms.si	
6835	0	6836	ph_red	0.107	12			Ms.si	
6836	0	6837	ph_red	0.469	12			Ms.si	
6837	0	6838	ph_red	0.009	12			Ms.si	
6838	0	6839	ph_red	0.054	12			Ms.si	
6839	0	6840	ph_red	0.160	12			Ms.si	
6840	0	6841	ph_red	0.222	12			Ms.si	
6841	0	6842	ph_red	0.025	12			Ms.si	
6842	0	6843	ph_red	0.330	12			Ms.si	

GeoNexus

OBJECTID_1	Join_Count	TARGET_FID	label	Shape_Area (sqkm)	ORIG_FID	Absolute_Age	Age_paleontology	Unit	Reference
6843	0	6844	ph_red	1.095	12			Ms.si	
6844	0	6845	ph_red	0.339	12			Ms.si	
6845	0	6846	ph_red	0.159	12			Ms.si	
6846	0	6847	ph_red	0.099	12			Ms.si	
6847	0	6848	ph_red	0.114	12			Ms.si	
6848	0	6849	ph_red	0.119	12			Ms.si	
6849	0	6850	ph_red	0.562	12			Ms.si	
6850	0	6851	ph_red	0.700	12			Ms.si	
6851	0	6852	ph_red	4.961	12			Ms.si	
6852	0	6853	ph_red	1.197	12			Ms.si	
6853	0	6854	ph_red	0.713	12			Ms.si	
6854	0	6855	ph_red	0.292	12			Ms.si	
6855	0	6856	ph_red	0.878	12			Ms.si	
6856	0	6857	ph_red	0.670	12			Ms.si	
6857	0	6858	ph_red	1.456	12			Ms.si	
6858	0	6859	ph_red	0.267	12			Ms.si	
6859	0	6860	ph_red	0.575	12			Ms.si	
6860	0	6861	ph_red	0.155	12			Ms.si	
6861	0	6862	ph_red	0.759	12			Ms.si	
6862	0	6863	ph_red	0.094	12			Ms.si	
6863	0	6864	ph_red	0.520	12			Ms.si	
6864	0	6865	ph_red	0.140	12			Ms.si	
6865	0	6866	ph_red	0.197	12			Ms.si	
6866	0	6867	ph_red	0.130	12			Ms.si	
6867	0	6868	ph_red	0.097	12			Ms.si	
6868	0	6869	ph_red	0.212	12			Ms.si	
6869	0	6870	ph_red	0.298	12			Ms.si	
6870	0	6871	ph_red	0.442	12			Ms.si	
6871	0	6872	ph_red	0.688	12			Ms.si	
6872	0	6873	ph_red	0.055	12			Ms.si	
6873	0	6874	ph_red	0.855	12			Ms.si	
6874	0	6875	ph_red	0.060	12			Ms.si	
6875	0	6876	ph_red	0.062	12			Ms.si	
6876	0	6877	ph_red	0.936	12			Ms.si	
6877	0	6878	ph_red	0.183	12			Ms.si	
6878	0	6879	ph_red	0.101	12			Ms.si	
6879	0	6880	ph_red	0.109	12			Ms.si	
6880	0	6881	ph_red	0.308	12			Ms.si	
6881	0	6882	ph_red	0.200	12			Ms.si	

GeoNexus

OBJECTID_1	Join_Count	TARGET_FID	label	Shape_Area (sqkm)	ORIG_FID	Absolute_Age	Age_paleontology	Unit	Reference
6882	0	6883	ph_red	0.132	12			Ms.si	
6883	0	6884	ph_red	0.393	12			Ms.si	
6884	0	6885	ph_red	0.409	12			Ms.si	
6885	1	6886	ph_red	34.768	12			Ms.si	
6886	0	6887	ph_red	0.137	12			Ms.si	
6887	0	6888	ph_red	0.093	12			Ms.si	
6888	0	6889	ph_red	0.025	12			Ms.si	
6889	0	6890	ph_red	0.699	12			Ms.si	
6890	0	6891	ph_red	0.600	12			Ms.si	
6891	0	6892	ph_red	0.104	12			Ms.si	
6892	0	6893	ph_red	0.067	12			Ms.si	
6893	0	6894	ph_red	0.084	12			Ms.si	
6894	0	6895	ph_red	0.543	12			Ms.si	
6895	0	6896	ph_red	1.099	12			Ms.si	
6896	0	6897	ph_red	0.587	12			Ms.si	
6897	0	6898	ph_red	0.297	12			Ms.si	
6898	0	6899	ph_red	0.109	12			Ms.si	
6899	0	6900	ph_red	0.110	12			Ms.si	
6900	0	6901	ph_red	0.062	12			Ms.si	
6901	0	6902	ph_red	0.048	12			Ms.si	
6902	0	6903	ph_red	1.001	12			Ms.si	
6903	0	6904	ph_red	0.193	12			Ms.si	
6904	0	6905	ph_red	0.104	12			Ms.si	
6905	0	6906	ph_red	0.075	12			Ms.si	
6906	0	6907	ph_red	0.917	12			Ms.si	
6907	0	6908	ph_red	2.815	12			Ms.si	
6908	0	6909	ph_red	0.130	12			Ms.si	
6909	0	6910	ph_red	0.546	12			Ms.si	
6910	0	6911	ph_red	0.398	12			Ms.si	
6911	0	6912	ph_red	2.109	12			Ms.si	
6912	0	6913	ph_red	0.164	12			Ms.si	
6913	0	6914	ph_red	0.294	12			Ms.si	
6914	0	6915	ph_red	0.202	12			Ms.si	
6915	0	6916	ph_red	0.422	12			Ms.si	
6916	0	6917	ph_red	2.712	12			Ms.si	
6917	0	6918	ph_red	0.254	12			Ms.si	
6918	0	6919	ph_red	0.042	12			Ms.si	
6919	0	6920	ph_red	2.144	12			Ms.si	
6920	0	6921	ph_red	0.529	12			Ms.si	

GeoNexus

OBJECTID_1	Join_Count	TARGET_FID	label	Shape_Area (sqkm)	ORIG_FID	Absolute_Age	Age_paleontology	Unit	Reference
6921	0	6922	ph_red	0.752	12			Ms.si	
6922	0	6923	ph_red	1.682	12			Ms.si	
6923	0	6924	ph_red	1.169	12			Ms.si	
6924	0	6925	ph_red	0.682	12			Ms.si	
6925	0	6926	ph_red	0.377	12			Ms.si	
6926	0	6927	ph_red	0.155	12			Ms.si	
6927	0	6928	ph_red	0.442	12			Ms.si	
6928	0	6929	ph_red	0.112	12			Ms.si	
6929	0	6930	ph_red	0.017	12			Ms.si	
6930	0	6931	ph_red	0.278	12			Ms.si	
6931	0	6932	ph_red	0.156	12			Ms.si	
6932	0	6933	ph_red	0.433	12			Ms.si	
6933	0	6934	ph_red	2.369	12			Ms.si	
6934	0	6935	ph_red	0.115	12			Ms.si	
6935	1	6936	ph_red	19.683	12			Ms.si	
6936	0	6937	ph_red	0.120	12			Ms.si	
6937	0	6938	ph_red	0.200	12			Ms.si	
6938	0	6939	ph_red	0.384	12			Ms.si	
6939	0	6940	ph_red	0.140	12			Ms.si	
6940	0	6941	ph_red	0.029	12			Ms.si	
6941	0	6942	ph_red	0.048	12			Ms.si	
6942	0	6943	ph_red	0.805	12			Ms.si	
6943	0	6944	ph_red	0.074	12			Ms.si	
6944	0	6945	ph_red	0.085	12			Ms.si	
6945	0	6946	ph_red	0.648	12			Ms.si	
6946	0	6947	ph_red	0.075	12			Ms.si	
6947	0	6948	ph_red	0.813	12			Ms.si	
6948	0	6949	ph_red	0.736	12			Ms.si	
6949	0	6950	ph_red	0.121	12			Ms.si	
6950	0	6951	ph_red	0.493	12			Ms.si	
6951	0	6952	ph_red	0.070	12			Ms.si	
6952	0	6953	ph_red	0.836	12			Ms.si	
6953	0	6954	ph_red	0.076	12			Ms.si	
6954	0	6955	ph_red	9.752	12			Ms.si	
6955	0	6956	ph_red	0.046	12			Ms.si	
6956	0	6957	ph_red	0.133	12			Ms.si	
6957	0	6958	ph_red	0.087	12			Ms.si	
6958	0	6959	ph_red	0.131	12			Ms.si	
6959	0	6960	ph_red	0.421	12			Ms.si	

GeoNexus

OBJECTID_1	Join_Count	TARGET_FID	label	Shape_Area (sqkm)	ORIG_FID	Absolute_Age	Age_paleontology	Unit	Reference
6960	0	6961	ph_red	0.215	12			Ms.si	
6961	0	6962	ph_red	0.215	12			Ms.si	
6962	0	6963	ph_red	0.062	12			Ms.si	
6963	0	6964	ph_red	0.140	12			Ms.si	
6964	0	6965	ph_red	0.205	12			Ms.si	
6965	1	6966	ph_red	25.420	12			Ms.si	
6966	0	6967	ph_red	0.519	12			Ms.si	
6967	0	6968	ph_red	0.288	12			Ms.si	
6968	0	6969	ph_red	0.194	12			Ms.si	
6969	0	6970	ph_red	0.429	12			Ms.si	
6970	0	6971	ph_red	0.274	12			Ms.si	
6971	0	6972	ph_red	2.234	12			Ms.si	
6972	0	6973	ph_red	0.503	12			Ms.si	
6973	0	6974	ph_red	0.649	12			Ms.si	
6974	0	6975	ph_red	0.027	12			Ms.si	
6975	0	6976	ph_red	1.391	12			Ms.si	
6976	0	6977	ph_red	0.102	12			Ms.si	
6977	0	6978	ph_red	0.603	12			Ms.si	
6978	0	6979	ph_red	0.062	12			Ms.si	
6979	0	6980	ph_red	0.188	12			Ms.si	
6980	0	6981	ph_red	0.429	12			Ms.si	
6981	0	6982	ph_red	0.188	12			Ms.si	
6982	0	6983	ph_red	0.077	12			Ms.si	
6983	0	6984	ph_red	0.109	12			Ms.si	
6984	0	6985	ph_red	0.925	12			Ms.si	
6985	0	6986	ph_red	0.057	12			Ms.si	
6986	0	6987	ph_red	0.249	12			Ms.si	
6987	0	6988	ph_red	0.931	12			Ms.si	
6988	0	6989	ph_red	1.699	12			Ms.si	
6989	0	6990	ph_red	0.354	12			Ms.si	
6990	0	6991	ph_red	0.501	12			Ms.si	
6991	0	6992	ph_red	0.148	12			Ms.si	
6992	0	6993	ph_red	0.026	12			Ms.si	
6993	0	6994	ph_red	1.043	12			Ms.si	
6994	0	6995	ph_red	4.441	12			Ms.si	
6995	0	6996	ph_red	0.374	12			Ms.si	
6996	0	6997	ph_red	0.109	12			Ms.si	
6997	0	6998	ph_red	0.327	12			Ms.si	
6998	0	6999	ph_red	5.293	12			Ms.si	

GeoNexus

OBJECTID_1	Join_Count	TARGET_FID	label	Shape_Area (sqkm)	ORIG_FID	Absolute_Age	Age_paleontology	Unit	Reference
6999	0	7000	ph_red	0.282	12			Ms.si	
7000	0	7001	ph_red	0.050	12			Ms.si	
7001	0	7002	ph_red	0.332	12			Ms.si	
7002	0	7003	ph_red	0.874	12			Ms.si	
7003	0	7004	ph_red	1.889	12			Ms.si	
7004	0	7005	ph_red	0.159	12			Ms.si	
7005	0	7006	ph_red	1.271	12			Ms.si	
7006	0	7007	ph_red	0.097	12			Ms.si	
7007	0	7008	ph_red	0.114	12			Ms.si	
7008	0	7009	ph_red	0.280	12			Ms.si	
7009	0	7010	ph_red	0.057	12			Ms.si	
7010	0	7011	ph_red	0.101	12			Ms.si	
7011	0	7012	ph_red	0.619	12			Ms.si	
7012	0	7013	ph_red	0.034	12			Ms.si	
7013	0	7014	ph_red	0.032	12			Ms.si	
7014	0	7015	ph_red	1.311	12			Ms.si	
7015	0	7016	ph_red	1.539	12			Ms.si	
7016	0	7017	ph_red	0.574	12			Ms.si	
7017	0	7018	ph_red	0.183	12			Ms.si	
7018	0	7019	ph_red	0.966	12			Ms.si	
7019	0	7020	ph_red	0.052	12			Ms.si	
7020	0	7021	ph_red	1.410	12			Ms.si	
7021	0	7022	ph_red	0.076	12			Ms.si	
7022	0	7023	ph_red	0.219	12			Ms.si	
7023	0	7024	ph_red	0.465	12			Ms.si	
7024	0	7025	ph_red	0.177	12			Ms.si	
7025	0	7026	ph_red	2.959	12			Ms.si	
7026	0	7027	ph_red	0.113	12			Ms.si	
7027	0	7028	ph_red	0.060	12			Ms.si	
7028	0	7029	ph_red	1.512	12			Ms.si	
7029	0	7030	ph_red	0.089	12			Ms.si	
7030	0	7031	ph_red	4.986	12			Ms.si	
7031	0	7032	ph_red	1.961	12			Ms.si	
7032	0	7033	ph_red	0.650	12			Ms.si	
7033	0	7034	ph_red	0.047	12			Ms.si	
7034	0	7035	ph_red	0.215	12			Ms.si	
7035	0	7036	ph_red	0.017	12			Ms.si	
7036	0	7037	ph_red	0.239	12			Ms.si	
7037	0	7038	ph_red	13.024	12			Ms.si	

GeoNexus

OBJECTID_1	Join_Count	TARGET_FID	label	Shape_Area (sqkm)	ORIG_FID	Absolute_Age	Age_paleontology	Unit	Reference
7038	0	7039	ph_red	1.132	12			Ms.si	
7039	0	7040	ph_red	0.509	12			Ms.si	
7040	0	7041	ph_red	0.393	12			Ms.si	
7041	0	7042	ph_red	2.565	12			Ms.si	
7042	0	7043	ph_red	0.075	12			Ms.si	
7043	0	7044	ph_red	0.102	12			Ms.si	
7044	0	7045	ph_red	0.126	12			Ms.si	
7045	0	7046	ph_red	0.167	12			Ms.si	
7046	0	7047	ph_red	30.568	12			Ms.si	
7047	0	7048	ph_red	0.425	12			Ms.si	
7048	0	7049	ph_red	0.032	12			Ms.si	
7049	0	7050	ph_red	0.041	12			Ms.si	
7050	0	7051	ph_red	0.459	12			Ms.si	
7051	0	7052	ph_red	0.109	12			Ms.si	
7052	0	7053	ph_red	0.021	12			Ms.si	
7053	0	7054	ph_red	0.651	12			Ms.si	
7054	0	7055	ph_red	0.956	12			Ms.si	
7055	0	7056	ph_red	1.436	12			Ms.si	
7056	0	7057	ph_red	0.064	12			Ms.si	
7057	0	7058	ph_red	0.458	12			Ms.si	
7058	0	7059	ph_red	0.142	12			Ms.si	
7059	0	7060	ph_red	0.637	12			Ms.si	
7060	0	7061	ph_red	0.140	12			Ms.si	
7061	0	7062	ph_red	0.955	12			Ms.si	
7062	0	7063	ph_red	0.068	12			Ms.si	
7063	0	7064	ph_red	0.055	12			Ms.si	
7064	0	7065	ph_red	0.204	12			Ms.si	
7065	0	7066	ph_red	0.774	12			Ms.si	
7066	0	7067	ph_red	0.083	12			Ms.si	
7067	0	7068	ph_red	0.506	12			Ms.si	
7068	0	7069	ph_red	0.070	12			Ms.si	
7069	0	7070	ph_red	0.528	12			Ms.si	
7070	0	7071	ph_red	0.030	12			Ms.si	
7071	0	7072	ph_red	0.485	12			Ms.si	
7072	0	7073	ph_red	0.455	12			Ms.si	
7073	0	7074	ph_red	0.770	12			Ms.si	
7074	0	7075	ph_red	0.356	12			Ms.si	
7075	0	7076	ph_red	0.516	12			Ms.si	
7076	0	7077	ph_red	0.144	12			Ms.si	

GeoNexus

OBJECTID_1	Join_Count	TARGET_FID	label	Shape_Area (sqkm)	ORIG_FID	Absolute_Age	Age_paleontology	Unit	Reference
7077	0	7078	ph_red	0.137	12			Ms.si	
7078	0	7079	ph_red	0.032	12			Ms.si	
7079	0	7080	ph_red	0.021	12			Ms.si	
7080	0	7081	ph_red	0.072	12			Ms.si	
7081	0	7082	ph_red	0.061	12			Ms.si	
7082	0	7083	ph_red	0.058	12			Ms.si	
7083	0	7084	ph_red	0.143	12			Ms.si	
7084	0	7085	ph_red	0.293	12			Ms.si	
7085	0	7086	ph_red	0.071	12			Ms.si	
7086	0	7087	ph_red	0.212	12			Ms.si	
7087	0	7088	ph_red	0.746	12			Ms.si	
7088	0	7089	ph_red	0.135	12			Ms.si	
7089	0	7090	ph_red	0.041	12			Ms.si	
7090	0	7091	ph_red	0.136	12			Ms.si	
7091	0	7092	ph_red	0.671	12			Ms.si	
7092	0	7093	ph_red	0.929	12			Ms.si	
7093	0	7094	ph_red	0.670	12			Ms.si	
7094	0	7095	ph_red	1.163	12			Ms.si	
7095	0	7096	ph_red	0.174	12			Ms.si	
7096	0	7097	ph_red	0.066	12			Ms.si	
7097	0	7098	ph_red	0.555	12			Ms.si	
7098	0	7099	ph_red	0.179	12			Ms.si	
7099	0	7100	ph_red	0.030	12			Ms.si	
7100	0	7101	ph_red	0.086	12			Ms.si	
7101	0	7102	ph_red	0.962	12			Ms.si	
7102	0	7103	ph_red	0.153	12			Ms.si	
7103	0	7104	ph_red	0.329	12			Ms.si	
7104	0	7105	ph_red	0.458	12			Ms.si	
7105	0	7106	ph_red	0.022	12			Ms.si	
7106	0	7107	ph_red	0.414	12			Ms.si	
7107	0	7108	ph_red	1.340	12			Ms.si	
7108	0	7109	ph_red	0.084	12			Ms.si	
7109	0	7110	ph_red	0.185	12			Ms.si	
7110	0	7111	ph_red	0.181	12			Ms.si	
7111	0	7112	ph_red	0.048	12			Ms.si	
7112	0	7113	ph_red	0.794	12			Ms.si	
7113	0	7114	ph_red	0.037	12			Ms.si	
7114	0	7115	ph_red	1.476	12			Ms.si	
7115	0	7116	ph_red	0.031	12			Ms.si	

GeoNexus

OBJECTID_1	Join_Count	TARGET_FID	label	Shape_Area (sqkm)	ORIG_FID	Absolute_Age	Age_paleontology	Unit	Reference
7116	0	7117	ph_red	1.574	12			Ms.si	
7117	0	7118	ph_red	0.144	12			Ms.si	
7118	0	7119	ph_red	0.107	12			Ms.si	
7119	0	7120	ph_red	1.678	12			Ms.si	
7120	0	7121	ph_red	0.539	12			Ms.si	
7122	0	7123	ph_red	0.766	12			Ms.si	
7123	0	7124	ph_red	0.248	12			Ms.si	
7124	0	7125	ph_red	0.148	12			Ms.si	
7125	0	7126	ph_red	4.473	12			Ms.si	
7126	0	7127	ph_red	0.851	12			Ms.si	
7127	0	7128	ph_red	4.209	12			Ms.si	
7128	0	7129	ph_red	0.072	12			Ms.si	
7129	0	7130	ph_red	0.666	12			Ms.si	
7130	0	7131	ph_red	7.174	12			Ms.si	
7131	0	7132	ph_red	0.198	12			Ms.si	
7132	0	7133	ph_red	0.328	12			Ms.si	
7133	0	7134	ph_red	0.128	12			Ms.si	
7134	0	7135	ph_red	0.255	12			Ms.si	
7135	0	7136	ph_red	0.188	12			Ms.si	
7136	0	7137	ph_red	0.219	12			Ms.si	
7137	0	7138	ph_red	0.168	12			Ms.si	
7138	0	7139	ph_red	0.023	12			Ms.si	
7139	0	7140	ph_red	4.109	12			Ms.si	
7140	0	7141	ph_red	0.405	12			Ms.si	
7141	0	7142	ph_red	0.023	12			Ms.si	
7142	0	7143	ph_red	0.182	12			Ms.si	
7143	0	7144	ph_red	0.170	12			Ms.si	
7144	0	7145	ph_red	0.770	12			Ms.si	
7145	0	7146	ph_red	0.136	12			Ms.si	
7146	0	7147	ph_red	0.267	12			Ms.si	
7147	0	7148	ph_red	8.513	12			Ms.si	
7148	0	7149	ph_red	5.145	12			Ms.si	
7149	0	7150	ph_red	0.262	12			Ms.si	
7150	0	7151	ph_red	0.494	12			Ms.si	
7151	0	7152	ph_red	0.775	12			Ms.si	
7152	0	7153	ph_red	0.649	12			Ms.si	
7153	0	7154	ph_red	0.533	12			Ms.si	
7154	0	7155	ph_red	0.433	12			Ms.si	
7155	0	7156	ph_red	0.074	12			Ms.si	

GeoNexus

OBJECTID_1	Join_Count	TARGET_FID	label	Shape_Area (sqkm)	ORIG_FID	Absolute_Age	Age_paleontology	Unit	Reference
7156	0	7157	ph_red	0.044	12			Ms.si	
7157	0	7158	ph_red	0.462	12			Ms.si	
7158	0	7159	ph_red	0.190	12			Ms.si	
7159	0	7160	ph_red	0.044	12			Ms.si	
7160	0	7161	ph_red	1.774	12			Ms.si	
7161	0	7162	ph_red	6.490	12			Ms.si	
7162	0	7163	ph_red	0.123	12			Ms.si	
7163	0	7164	ph_red	0.128	12			Ms.si	
7164	0	7165	ph_red	0.216	12			Ms.si	
7165	0	7166	ph_red	8.487	12			Ms.si	
7166	0	7167	ph_red	0.066	12			Ms.si	
7167	0	7168	ph_red	0.468	12			Ms.si	
7168	0	7169	ph_red	3.172	12			Ms.si	
7169	0	7170	ph_red	0.479	12			Ms.si	
7170	0	7171	ph_red	2.898	12			Ms.si	
7171	0	7172	ph_red	0.361	12			Ms.si	
7172	0	7173	ph_red	0.093	12			Ms.si	
7173	0	7174	ph_red	0.008	12			Ms.si	
7174	0	7175	ph_red	0.139	12			Ms.si	
7175	0	7176	ph_red	0.434	12			Ms.si	
7176	0	7177	ph_red	8.018	12			Ms.si	
7177	0	7178	ph_red	0.426	12			Ms.si	
7178	0	7179	ph_red	10.305	12			Ms.si	
7179	0	7180	ph_red	0.170	12			Ms.si	
7180	0	7181	ph_red	0.383	12			Ms.si	
7181	0	7182	ph_red	0.882	12			Ms.si	
7182	0	7183	ph_red	0.042	12			Ms.si	
7183	0	7184	ph_red	0.563	12			Ms.si	
7184	0	7185	ph_red	0.053	12			Ms.si	
7185	0	7186	ph_red	0.814	12			Ms.si	
7186	0	7187	ph_red	0.037	12			Ms.si	
7187	0	7188	ph_red	0.661	12			Ms.si	
7188	0	7189	ph_red	0.395	12			Ms.si	
7189	0	7190	ph_red	1.935	12			Ms.si	
7190	0	7191	ph_red	0.243	12			Ms.si	
7191	0	7192	ph_red	0.383	12			Ms.si	
7192	0	7193	ph_red	0.086	12			Ms.si	
7193	0	7194	ph_red	0.689	12			Ms.si	
7194	0	7195	ph_red	0.907	12			Ms.si	

GeoNexus

OBJECTID_1	Join_Count	TARGET_FID	label	Shape_Area (sqkm)	ORIG_FID	Absolute_Age	Age_paleontology	Unit	Reference
7195	0	7196	ph_red	0.502	12			Ms.si	
7196	0	7197	ph_red	0.415	12			Ms.si	
7197	0	7198	ph_red	0.148	12			Ms.si	
7198	0	7199	ph_red	0.046	12			Ms.si	
7199	0	7200	ph_red	2.785	12			Ms.si	
7200	0	7201	ph_red	1.013	12			Ms.si	
7201	0	7202	ph_red	0.362	12			Ms.si	
7202	0	7203	ph_red	2.580	12			Ms.si	
7203	0	7204	ph_red	0.141	12			Ms.si	
7204	0	7205	ph_red	0.802	12			Ms.si	
7205	0	7206	ph_red	0.259	12			Ms.si	
7206	0	7207	ph_red	0.382	12			Ms.si	
7207	0	7208	ph_red	1.079	12			Ms.si	
7208	0	7209	ph_red	0.447	12			Ms.si	
7209	0	7210	ph_red	7.345	12			Ms.si	
7210	0	7211	ph_red	0.378	12			Ms.si	
7211	0	7212	ph_red	6.446	12			Ms.si	
7212	0	7213	ph_red	0.880	12			Ms.si	
7213	0	7214	ph_red	1.029	12			Ms.si	
7214	0	7215	ph_red	0.625	12			Ms.si	
7215	0	7216	ph_red	1.793	12			Ms.si	
7216	0	7217	ph_red	1.282	12			Ms.si	
7217	0	7218	ph_red	0.256	12			Ms.si	
7218	0	7219	ph_red	1.292	12			Ms.si	
7219	0	7220	ph_red	0.086	12			Ms.si	
7220	0	7221	ph_red	0.073	12			Ms.si	
7221	0	7222	ph_red	0.223	12			Ms.si	
7222	0	7223	ph_red	0.175	12			Ms.si	
7223	0	7224	ph_red	0.067	12			Ms.si	
7224	0	7225	ph_red	0.210	12			Ms.si	
7225	0	7226	ph_red	1.042	12			Ms.si	
7226	0	7227	ph_red	0.079	12			Ms.si	
7227	0	7228	ph_red	0.337	12			Ms.si	
7228	0	7229	ph_red	0.108	12			Ms.si	
7229	0	7230	ph_red	0.092	12			Ms.si	
7230	0	7231	ph_red	0.539	12			Ms.si	
7231	0	7232	ph_red	1.433	12			Ms.si	
7232	0	7233	ph_red	0.928	12			Ms.si	
7233	0	7234	ph_red	0.203	12			Ms.si	

GeoNexus

OBJECTID_1	Join_Count	TARGET_FID	label	Shape_Area (sqkm)	ORIG_FID	Absolute_Age	Age_paleontology	Unit	Reference
7234	0	7235	ph_red	0.052	12			Ms.si	
7235	0	7236	ph_red	0.570	12			Ms.si	
7236	0	7237	ph_red	0.408	12			Ms.si	
7237	0	7238	ph_red	1.601	12			Ms.si	
7238	0	7239	ph_red	0.274	12			Ms.si	
7239	0	7240	ph_red	0.117	12			Ms.si	
7240	0	7241	ph_red	1.089	12			Ms.si	
7241	0	7242	ph_red	1.119	12			Ms.si	
7242	0	7243	ph_red	0.078	12			Ms.si	
7243	0	7244	ph_red	0.084	12			Ms.si	
7244	0	7245	ph_red	1.125	12			Ms.si	
7245	0	7246	ph_red	0.212	12			Ms.si	
7246	0	7247	ph_red	0.292	12			Ms.si	
7247	0	7248	ph_red	0.117	12			Ms.si	
7248	0	7249	ph_red	0.057	12			Ms.si	
7249	0	7250	ph_red	0.521	12			Ms.si	
7250	0	7251	ph_red	0.523	12			Ms.si	
7251	0	7252	ph_red	0.091	12			Ms.si	
7252	0	7253	ph_red	0.213	12			Ms.si	
7253	0	7254	ph_red	0.150	12			Ms.si	
7254	0	7255	ph_red	0.466	12			Ms.si	
7255	0	7256	ph_red	0.179	12			Ms.si	
7256	0	7257	ph_red	0.213	12			Ms.si	
7257	0	7258	ph_red	0.043	12			Ms.si	
7258	0	7259	ph_red	0.224	12			Ms.si	
7259	0	7260	ph_red	0.186	12			Ms.si	
7260	0	7261	ph_red	0.169	12			Ms.si	
7261	0	7262	ph_red	19.456	12			Ms.si	
7262	0	7263	ph_red	0.087	12			Ms.si	
7263	0	7264	ph_red	0.451	12			Ms.si	
7264	0	7265	ph_red	1.590	12			Ms.si	
7265	0	7266	ph_red	2.440	12			Ms.si	
7266	0	7267	ph_red	0.052	12			Ms.si	
7267	0	7268	ph_red	0.692	12			Ms.si	
7268	0	7269	ph_red	3.201	12			Ms.si	
7269	0	7270	ph_red	0.177	12			Ms.si	
7270	0	7271	ph_red	0.290	12			Ms.si	
7271	0	7272	ph_red	0.140	12			Ms.si	
7272	0	7273	ph_red	0.993	12			Ms.si	

GeoNexus

OBJECTID_1	Join_Count	TARGET_FID	label	Shape_Area (sqkm)	ORIG_FID	Absolute_Age	Age_paleontology	Unit	Reference
7273	0	7274	ph_red	0.075	12			Ms.si	
7274	0	7275	ph_red	0.083	12			Ms.si	
7275	0	7276	ph_red	0.305	12			Ms.si	
7276	0	7277	ph_red	0.841	12			Ms.si	
7277	0	7278	ph_red	0.217	12			Ms.si	
7278	0	7279	ph_red	4.392	12			Ms.si	
7279	0	7280	ph_red	0.115	12			Ms.si	
7280	0	7281	ph_red	0.160	12			Ms.si	
7281	0	7282	ph_red	0.062	12			Ms.si	
7282	0	7283	ph_red	1.087	12			Ms.si	
7283	0	7284	ph_red	9.151	12			Ms.si	
7284	0	7285	ph_red	0.723	12			Ms.si	
7285	0	7286	ph_red	0.467	12			Ms.si	
7286	0	7287	ph_red	0.060	12			Ms.si	
7287	0	7288	ph_red	0.062	12			Ms.si	
7288	0	7289	ph_red	0.761	12			Ms.si	
7289	0	7290	ph_red	1.425	12			Ms.si	
7290	0	7291	ph_red	0.229	12			Ms.si	
7291	0	7292	ph_red	0.119	12			Ms.si	
7292	0	7293	ph_red	0.155	12			Ms.si	
7293	0	7294	ph_red	0.114	12			Ms.si	
7294	0	7295	ph_red	0.038	12			Ms.si	
7295	0	7296	ph_red	0.050	12			Ms.si	
7296	0	7297	ph_red	1.997	12			Ms.si	
7297	0	7298	ph_red	0.189	12			Ms.si	
7298	0	7299	ph_red	0.183	12			Ms.si	
7299	0	7300	ph_red	1.269	12			Ms.si	
7300	0	7301	ph_red	0.963	12			Ms.si	
7301	0	7302	ph_red	0.087	12			Ms.si	
7302	0	7303	ph_red	15.942	12			Ms.si	
7303	0	7304	ph_red	0.717	12			Ms.si	
7304	0	7305	ph_red	2.138	12			Ms.si	
7305	0	7306	ph_red	3.152	12			Ms.si	
7306	0	7307	ph_red	2.426	12			Ms.si	
7307	0	7308	ph_red	0.037	12			Ms.si	
7308	0	7309	ph_red	0.884	12			Ms.si	
7309	0	7310	ph_red	2.315	12			Ms.si	
7310	0	7311	ph_red	0.145	12			Ms.si	
7311	0	7312	ph_red	0.405	12			Ms.si	

GeoNexus

OBJECTID_1	Join_Count	TARGET_FID	label	Shape_Area (sqkm)	ORIG_FID	Absolute_Age	Age_paleontology	Unit	Reference
7312	0	7313	ph_red	0.128	12			Ms.si	
7313	0	7314	ph_red	14.378	12			Ms.si	
7314	0	7315	ph_red	1.990	12			Ms.si	
7315	0	7316	ph_red	0.094	12			Ms.si	
7316	0	7317	ph_red	0.133	12			Ms.si	
7317	0	7318	ph_red	0.687	12			Ms.si	
10518	0	6274	ph_red	0.252	11			Ms.si	
10528	0	4488	ph_red	0.197	8			Ms.si	
10530	0	4488	ph_red	0.004	8			Ms.si	
10531	0	7757	ph_red	0.018	13			Ms.si	
10532	0	4488	ph_red	0.008	8			Ms.si	
10540	1	2201	ph_red	0.016	5		Pliocene-Pleistocene	Ms.si	Dolati (2010)

GeoNexus

Table S6. Summary of mapped polygons for the MPl$^{m.s}$ Unit.

OBJECTID_1	Join_Count	TARGET_FID	label	Shape_Area (sqkm)	ORIG_FID	Absolute_Age	Age_paleontology	Unit	Reference
198	0	198	m	0.147	2		L Miocene- E Pliocene	MPlm.s	Dolati (2010)
199	0	199	m	0.103	2		L Miocene- E Pliocene	MPlm.s	Dolati (2010)
200	0	200	m	3.718	2		L Miocene- E Pliocene	MPlm.s	Dolati (2010)
201	0	201	m	0.078	2		L Miocene- E Pliocene	MPlm.s	Dolati (2010)
202	0	202	m	0.084	2		L Miocene- E Pliocene	MPlm.s	Dolati (2010)
204	0	204	m	0.037	2		L Miocene- E Pliocene	MPlm.s	Dolati (2010)
205	0	205	m	0.595	2		L Miocene- E Pliocene	MPlm.s	Dolati (2010)
206	0	206	m	1.246	2		L Miocene- E Pliocene	MPlm.s	Dolati (2010)
207	0	207	m	0.027	2		L Miocene- E Pliocene	MPlm.s	Dolati (2010)
208	0	208	m	0.115	2		L Miocene- E Pliocene	MPlm.s	Dolati (2010)
211	0	211	m	0.128	2		L Miocene- E Pliocene	MPlm.s	Dolati (2010)
212	0	212	m	1.084	2		L Miocene- E Pliocene	MPlm.s	Dolati (2010)
213	0	213	m	0.980	2		L Miocene- E Pliocene	MPlm.s	Dolati (2010)
214	0	214	m	0.065	2		L Miocene- E Pliocene	MPlm.s	Dolati (2010)
216	0	216	m	0.696	2		L Miocene- E Pliocene	MPlm.s	Dolati (2010)
217	0	217	m	0.368	2		L Miocene- E Pliocene	MPlm.s	Dolati (2010)
219	0	219	m	0.020	2		L Miocene- E Pliocene	MPlm.s	Dolati (2010)
221	0	221	m	0.539	2		L Miocene- E Pliocene	MPlm.s	Dolati (2010)
222	0	222	m	0.645	2		L Miocene- E Pliocene	MPlm.s	Dolati (2010)
223	0	223	m	2.228	2		L Miocene- E Pliocene	MPlm.s	Dolati (2010)
225	0	225	m	0.296	2		L Miocene- E Pliocene	MPlm.s	Dolati (2010)
226	0	226	m	0.023	2		L Miocene- E Pliocene	MPlm.s	Dolati (2010)
227	0	227	m	0.373	2		L Miocene- E Pliocene	MPlm.s	Dolati (2010)
228	0	228	m	0.286	2		L Miocene- E Pliocene	MPlm.s	Dolati (2010)
229	0	229	m	1.288	2		L Miocene- E Pliocene	MPlm.s	Dolati (2010)
230	0	230	m	0.176	2		L Miocene- E Pliocene	MPlm.s	Dolati (2010)
231	0	231	m	0.273	2		L Miocene- E Pliocene	MPlm.s	Dolati (2010)
232	0	232	m	0.074	2		L Miocene- E Pliocene	MPlm.s	Dolati (2010)
233	0	233	m	0.034	2		L Miocene- E Pliocene	MPlm.s	Dolati (2010)
235	0	235	m	0.220	2		L Miocene- E Pliocene	MPlm.s	Dolati (2010)
236	0	236	m	0.098	2		L Miocene- E Pliocene	MPlm.s	Dolati (2010)
237	0	237	m	0.172	2		L Miocene- E Pliocene	MPlm.s	Dolati (2010)
239	0	239	m	0.399	2		L Miocene- E Pliocene	MPlm.s	Dolati (2010)
241	0	241	m	0.206	2		L Miocene- E Pliocene	MPlm.s	Dolati (2010)
243	0	243	m	0.031	2		L Miocene- E Pliocene	MPlm.s	Dolati (2010)
246	0	246	m	0.052	2		L Miocene- E Pliocene	MPlm.s	Dolati (2010)
249	0	249	m	0.028	2		L Miocene- E Pliocene	MPlm.s	Dolati (2010)
250	0	250	m	0.073	2		L Miocene- E Pliocene	MPlm.s	Dolati (2010)

GeoNet

OBJECTID_1	Join_Count	TARGET_FID	label	Shape_Area (sqkm)	ORIG_FID	Absolute_Age	Age_paleontology	Unit	Reference
251	0	251	m	0.059	2		L Miocene- E Pliocene	MPlm.s	Dolati (2010)
252	0	252	m	0.077	2		L Miocene- E Pliocene	MPlm.s	Dolati (2010)
253	0	253	m	0.145	2		L Miocene- E Pliocene	MPlm.s	Dolati (2010)
254	0	254	m	0.027	2		L Miocene- E Pliocene	MPlm.s	Dolati (2010)
256	0	256	m	0.057	2		L Miocene- E Pliocene	MPlm.s	Dolati (2010)
257	0	257	m	0.025	2		L Miocene- E Pliocene	MPlm.s	Dolati (2010)
258	0	258	m	0.076	2		L Miocene- E Pliocene	MPlm.s	Dolati (2010)
259	0	259	m	0.028	2		L Miocene- E Pliocene	MPlm.s	Dolati (2010)
260	0	260	m	0.039	2		L Miocene- E Pliocene	MPlm.s	Dolati (2010)
262	0	262	m	0.081	2		L Miocene- E Pliocene	MPlm.s	Dolati (2010)
263	0	263	m	0.296	2		L Miocene- E Pliocene	MPlm.s	Dolati (2010)
264	0	264	m	0.018	2		L Miocene- E Pliocene	MPlm.s	Dolati (2010)
265	0	265	m	0.112	2		L Miocene- E Pliocene	MPlm.s	Dolati (2010)
266	0	266	m	0.042	2		L Miocene- E Pliocene	MPlm.s	Dolati (2010)
269	0	269	m	0.451	2		L Miocene- E Pliocene	MPlm.s	Dolati (2010)
270	0	270	m	0.734	2		L Miocene- E Pliocene	MPlm.s	Dolati (2010)
272	0	272	m	0.192	2		L Miocene- E Pliocene	MPlm.s	Dolati (2010)
273	0	273	m	0.023	2		L Miocene- E Pliocene	MPlm.s	Dolati (2010)
274	0	274	m	0.239	2		L Miocene- E Pliocene	MPlm.s	Dolati (2010)
278	0	278	m	0.093	2		L Miocene- E Pliocene	MPlm.s	Dolati (2010)
279	0	279	m	0.292	2		L Miocene- E Pliocene	MPlm.s	Dolati (2010)
280	0	280	m	0.742	2		L Miocene- E Pliocene	MPlm.s	Dolati (2010)
281	0	281	m	0.271	2		L Miocene- E Pliocene	MPlm.s	Dolati (2010)
283	0	283	m	0.018	2		L Miocene- E Pliocene	MPlm.s	Dolati (2010)
284	0	284	m	0.086	2		L Miocene- E Pliocene	MPlm.s	Dolati (2010)
285	0	285	m	0.526	2		L Miocene- E Pliocene	MPlm.s	Dolati (2010)
286	0	286	m	0.117	2		L Miocene- E Pliocene	MPlm.s	Dolati (2010)
287	0	287	m	0.460	2		L Miocene- E Pliocene	MPlm.s	Dolati (2010)
288	0	288	m	0.790	2		L Miocene- E Pliocene	MPlm.s	Dolati (2010)
289	0	289	m	0.097	2		L Miocene- E Pliocene	MPlm.s	Dolati (2010)
290	0	290	m	0.544	2		L Miocene- E Pliocene	MPlm.s	Dolati (2010)
291	0	291	m	0.486	2		L Miocene- E Pliocene	MPlm.s	Dolati (2010)
292	0	292	m	1.593	2		L Miocene- E Pliocene	MPlm.s	Dolati (2010)
293	0	293	m	0.198	2		L Miocene- E Pliocene	MPlm.s	Dolati (2010)
294	0	294	m	0.035	2		L Miocene- E Pliocene	MPlm.s	Dolati (2010)
295	0	295	m	0.015	2		L Miocene- E Pliocene	MPlm.s	Dolati (2010)
296	0	296	m	0.213	2		L Miocene- E Pliocene	MPlm.s	Dolati (2010)
297	0	297	m	0.020	2		L Miocene- E Pliocene	MPlm.s	Dolati (2010)
298	0	298	m	0.545	2		L Miocene- E Pliocene	MPlm.s	Dolati (2010)

Geonavis

OBJECTID_1	Join_Count	TARGET_FID	label	Shape_Area (sqkm)	ORIG_FID	Absolute_Age	Age_paleontology	Unit	Reference
299	0	299	m	0.040	2		L Miocene- E Pliocene	MPlm.s	Dolati (2010)
300	0	300	m	0.043	2		L Miocene- E Pliocene	MPlm.s	Dolati (2010)
301	0	301	m	0.078	2		L Miocene- E Pliocene	MPlm.s	Dolati (2010)
302	0	302	m	0.062	2		L Miocene- E Pliocene	MPlm.s	Dolati (2010)
303	0	303	m	0.117	2		L Miocene- E Pliocene	MPlm.s	Dolati (2010)
304	0	304	m	6.342	2		L Miocene- E Pliocene	MPlm.s	Dolati (2010)
305	0	305	m	0.067	2		L Miocene- E Pliocene	MPlm.s	Dolati (2010)
306	0	306	m	0.038	2		L Miocene- E Pliocene	MPlm.s	Dolati (2010)
307	0	307	m	0.448	2		L Miocene- E Pliocene	MPlm.s	Dolati (2010)
308	0	308	m	0.102	2		L Miocene- E Pliocene	MPlm.s	Dolati (2010)
309	0	309	m	1.524	2		L Miocene- E Pliocene	MPlm.s	Dolati (2010)
310	0	310	m	0.695	2		L Miocene- E Pliocene	MPlm.s	Dolati (2010)
311	0	311	m	0.215	2		L Miocene- E Pliocene	MPlm.s	Dolati (2010)
312	0	312	m	0.339	2		L Miocene- E Pliocene	MPlm.s	Dolati (2010)
313	0	313	m	0.083	2		L Miocene- E Pliocene	MPlm.s	Dolati (2010)
314	0	314	m	0.266	2		L Miocene- E Pliocene	MPlm.s	Dolati (2010)
315	0	315	m	0.047	2		L Miocene- E Pliocene	MPlm.s	Dolati (2010)
316	0	316	m	0.894	2		L Miocene- E Pliocene	MPlm.s	Dolati (2010)
317	0	317	m	4.564	2		L Miocene- E Pliocene	MPlm.s	Dolati (2010)
318	0	318	m	0.298	2		L Miocene- E Pliocene	MPlm.s	Dolati (2010)
319	0	319	m	0.322	2		L Miocene- E Pliocene	MPlm.s	Dolati (2010)
320	0	320	m	0.662	2		L Miocene- E Pliocene	MPlm.s	Dolati (2010)
321	0	321	m	0.122	2		L Miocene- E Pliocene	MPlm.s	Dolati (2010)
322	0	322	m	0.119	2		L Miocene- E Pliocene	MPlm.s	Dolati (2010)
323	0	323	m	0.067	2		L Miocene- E Pliocene	MPlm.s	Dolati (2010)
324	0	324	m	1.885	2		L Miocene- E Pliocene	MPlm.s	Dolati (2010)
325	0	325	m	0.213	2		L Miocene- E Pliocene	MPlm.s	Dolati (2010)
326	0	326	m	0.061	2		L Miocene- E Pliocene	MPlm.s	Dolati (2010)
327	0	327	m	0.206	2		L Miocene- E Pliocene	MPlm.s	Dolati (2010)
328	0	328	m	0.276	2		L Miocene- E Pliocene	MPlm.s	Dolati (2010)
329	0	329	m	0.036	2		L Miocene- E Pliocene	MPlm.s	Dolati (2010)
330	0	330	m	0.124	2		L Miocene- E Pliocene	MPlm.s	Dolati (2010)
331	0	331	m	0.947	2		L Miocene- E Pliocene	MPlm.s	Dolati (2010)
332	0	332	m	0.333	2		L Miocene- E Pliocene	MPlm.s	Dolati (2010)
333	0	333	m	0.093	2		L Miocene- E Pliocene	MPlm.s	Dolati (2010)
334	0	334	m	0.047	2		L Miocene- E Pliocene	MPlm.s	Dolati (2010)
335	0	335	m	0.212	2		L Miocene- E Pliocene	MPlm.s	Dolati (2010)
336	0	336	m	0.224	2		L Miocene- E Pliocene	MPlm.s	Dolati (2010)
337	0	337	m	0.240	2		L Miocene- E Pliocene	MPlm.s	Dolati (2010)

GeoNeXus

OBJECTID_1	Join_Count	TARGET_FID	label	Shape_Area (sqkm)	ORIG_FID	Absolute_Age	Age_paleontology	Unit	Reference
338	0	338	m	0.056	2		L Miocene- E Pliocene	MPlm.s	Dolati (2010)
339	0	339	m	2.161	2		L Miocene- E Pliocene	MPlm.s	Dolati (2010)
340	0	340	m	0.083	2		L Miocene- E Pliocene	MPlm.s	Dolati (2010)
341	0	341	m	0.220	2		L Miocene- E Pliocene	MPlm.s	Dolati (2010)
342	0	342	m	0.129	2		L Miocene- E Pliocene	MPlm.s	Dolati (2010)
343	0	343	m	0.609	2		L Miocene- E Pliocene	MPlm.s	Dolati (2010)
344	0	344	m	0.097	2		L Miocene- E Pliocene	MPlm.s	Dolati (2010)
345	0	345	m	0.147	2		L Miocene- E Pliocene	MPlm.s	Dolati (2010)
346	0	346	m	0.899	2		L Miocene- E Pliocene	MPlm.s	Dolati (2010)
347	0	347	m	0.109	2		L Miocene- E Pliocene	MPlm.s	Dolati (2010)
348	0	348	m	0.047	2		L Miocene- E Pliocene	MPlm.s	Dolati (2010)
349	0	349	m	0.456	2		L Miocene- E Pliocene	MPlm.s	Dolati (2010)
350	0	350	m	0.304	2		L Miocene- E Pliocene	MPlm.s	Dolati (2010)
351	0	351	m	0.208	2		L Miocene- E Pliocene	MPlm.s	Dolati (2010)
352	0	352	m	0.207	2		L Miocene- E Pliocene	MPlm.s	Dolati (2010)
353	0	353	m	0.752	2		L Miocene- E Pliocene	MPlm.s	Dolati (2010)
354	0	354	m	0.392	2		L Miocene- E Pliocene	MPlm.s	Dolati (2010)
355	0	355	m	0.515	2		L Miocene- E Pliocene	MPlm.s	Dolati (2010)
356	0	356	m	0.013	2		L Miocene- E Pliocene	MPlm.s	Dolati (2010)
357	0	357	m	0.079	2		L Miocene- E Pliocene	MPlm.s	Dolati (2010)
358	0	358	m	8.158	2		L Miocene- E Pliocene	MPlm.s	Dolati (2010)
359	0	359	m	0.080	2		L Miocene- E Pliocene	MPlm.s	Dolati (2010)
360	0	360	m	0.082	2		L Miocene- E Pliocene	MPlm.s	Dolati (2010)
361	0	361	m	0.137	2		L Miocene- E Pliocene	MPlm.s	Dolati (2010)
362	0	362	m	1.215	2		L Miocene- E Pliocene	MPlm.s	Dolati (2010)
363	0	363	m	0.218	2		L Miocene- E Pliocene	MPlm.s	Dolati (2010)
364	0	364	m	0.538	2		L Miocene- E Pliocene	MPlm.s	Dolati (2010)
365	0	365	m	0.166	2		L Miocene- E Pliocene	MPlm.s	Dolati (2010)
366	0	366	m	0.047	2		L Miocene- E Pliocene	MPlm.s	Dolati (2010)
367	0	367	m	19.665	2		L Miocene- E Pliocene	MPlm.s	Dolati (2010)
368	0	368	m	2.772	2		L Miocene- E Pliocene	MPlm.s	Dolati (2010)
369	0	369	m	0.264	2		L Miocene- E Pliocene	MPlm.s	Dolati (2010)
370	0	370	m	0.013	2		L Miocene- E Pliocene	MPlm.s	Dolati (2010)
371	0	371	m	7.576	2		L Miocene- E Pliocene	MPlm.s	Dolati (2010)
372	0	372	m	0.103	2		L Miocene- E Pliocene	MPlm.s	Dolati (2010)
373	0	373	m	0.102	2		L Miocene- E Pliocene	MPlm.s	Dolati (2010)
374	0	374	m	0.160	2		L Miocene- E Pliocene	MPlm.s	Dolati (2010)
375	0	375	m	0.145	2		L Miocene- E Pliocene	MPlm.s	Dolati (2010)
376	0	376	m	0.101	2		L Miocene- E Pliocene	MPlm.s	Dolati (2010)

Geonavis

OBJECTID_1	Join_Count	TARGET_FID	label	Shape_Area (sqkm)	ORIG_FID	Absolute_Age	Age_paleontology	Unit	Reference
377	0	377	m	0.090	2		L Miocene- E Pliocene	MPlm.s	Dolati (2010)
378	0	378	m	1.210	2		L Miocene- E Pliocene	MPlm.s	Dolati (2010)
379	0	379	m	7.514	2		L Miocene- E Pliocene	MPlm.s	Dolati (2010)
380	0	380	m	0.042	2		L Miocene- E Pliocene	MPlm.s	Dolati (2010)
381	0	381	m	0.340	2		L Miocene- E Pliocene	MPlm.s	Dolati (2010)
382	0	382	m	0.135	2		L Miocene- E Pliocene	MPlm.s	Dolati (2010)
383	0	383	m	0.052	2		L Miocene- E Pliocene	MPlm.s	Dolati (2010)
384	0	384	m	0.104	2		L Miocene- E Pliocene	MPlm.s	Dolati (2010)
385	0	385	m	0.044	2		L Miocene- E Pliocene	MPlm.s	Dolati (2010)
386	0	386	m	0.347	2		L Miocene- E Pliocene	MPlm.s	Dolati (2010)
387	0	387	m	0.706	2		L Miocene- E Pliocene	MPlm.s	Dolati (2010)
388	0	388	m	0.320	2		L Miocene- E Pliocene	MPlm.s	Dolati (2010)
389	0	389	m	0.042	2		L Miocene- E Pliocene	MPlm.s	Dolati (2010)
390	0	390	m	0.048	2		L Miocene- E Pliocene	MPlm.s	Dolati (2010)
391	0	391	m	0.021	2		L Miocene- E Pliocene	MPlm.s	Dolati (2010)
392	0	392	m	0.494	2		L Miocene- E Pliocene	MPlm.s	Dolati (2010)
393	0	393	m	0.643	2		L Miocene- E Pliocene	MPlm.s	Dolati (2010)
394	0	394	m	0.020	2		L Miocene- E Pliocene	MPlm.s	Dolati (2010)
395	0	395	m	0.786	2		L Miocene- E Pliocene	MPlm.s	Dolati (2010)
396	0	396	m	0.031	2		L Miocene- E Pliocene	MPlm.s	Dolati (2010)
397	0	397	m	0.121	2		L Miocene- E Pliocene	MPlm.s	Dolati (2010)
398	0	398	m	0.390	2		L Miocene- E Pliocene	MPlm.s	Dolati (2010)
399	0	399	m	0.157	2		L Miocene- E Pliocene	MPlm.s	Dolati (2010)
400	0	400	m	0.897	2		L Miocene- E Pliocene	MPlm.s	Dolati (2010)
401	0	401	m	0.030	2		L Miocene- E Pliocene	MPlm.s	Dolati (2010)
402	0	402	m	0.127	2		L Miocene- E Pliocene	MPlm.s	Dolati (2010)
403	0	403	m	0.123	2		L Miocene- E Pliocene	MPlm.s	Dolati (2010)
404	0	404	m	0.935	2		L Miocene- E Pliocene	MPlm.s	Dolati (2010)
405	0	405	m	1.177	2		L Miocene- E Pliocene	MPlm.s	Dolati (2010)
406	0	406	m	1.486	2		L Miocene- E Pliocene	MPlm.s	Dolati (2010)
407	0	407	m	0.409	2		L Miocene- E Pliocene	MPlm.s	Dolati (2010)
408	0	408	m	0.958	2		L Miocene- E Pliocene	MPlm.s	Dolati (2010)
409	0	409	m	0.299	2		L Miocene- E Pliocene	MPlm.s	Dolati (2010)
410	0	410	m	0.235	2		L Miocene- E Pliocene	MPlm.s	Dolati (2010)
411	0	411	m	0.069	2		L Miocene- E Pliocene	MPlm.s	Dolati (2010)
412	0	412	m	0.071	2		L Miocene- E Pliocene	MPlm.s	Dolati (2010)
413	0	413	m	0.069	2		L Miocene- E Pliocene	MPlm.s	Dolati (2010)
414	0	414	m	0.120	2		L Miocene- E Pliocene	MPlm.s	Dolati (2010)
415	0	415	m	0.369	2		L Miocene- E Pliocene	MPlm.s	Dolati (2010)

GeoNeXus

OBJECTID_1	Join_Count	TARGET_FID	label	Shape_Area (sqkm)	ORIG_FID	Absolute_Age	Age_paleontology	Unit	Reference
416	0	416	m	0.187	2		L Miocene- E Pliocene	MPlm.s	Dolati (2010)
417	0	417	m	0.352	2		L Miocene- E Pliocene	MPlm.s	Dolati (2010)
418	0	418	m	0.356	2		L Miocene- E Pliocene	MPlm.s	Dolati (2010)
419	0	419	m	1.151	2		L Miocene- E Pliocene	MPlm.s	Dolati (2010)
420	0	420	m	0.052	2		L Miocene- E Pliocene	MPlm.s	Dolati (2010)
421	0	421	m	0.018	2		L Miocene- E Pliocene	MPlm.s	Dolati (2010)
422	0	422	m	0.197	2		L Miocene- E Pliocene	MPlm.s	Dolati (2010)
423	0	423	m	0.010	2		L Miocene- E Pliocene	MPlm.s	Dolati (2010)
424	0	424	m	0.129	2		L Miocene- E Pliocene	MPlm.s	Dolati (2010)
425	0	425	m	0.246	2		L Miocene- E Pliocene	MPlm.s	Dolati (2010)
426	0	426	m	0.071	2		L Miocene- E Pliocene	MPlm.s	Dolati (2010)
427	0	427	m	5.327	2		L Miocene- E Pliocene	MPlm.s	Dolati (2010)
428	0	428	m	0.058	2		L Miocene- E Pliocene	MPlm.s	Dolati (2010)
429	0	429	m	0.161	2		L Miocene- E Pliocene	MPlm.s	Dolati (2010)
430	0	430	m	0.272	2		L Miocene- E Pliocene	MPlm.s	Dolati (2010)
431	0	431	m	0.060	2		L Miocene- E Pliocene	MPlm.s	Dolati (2010)
432	0	432	m	0.150	2		L Miocene- E Pliocene	MPlm.s	Dolati (2010)
433	0	433	m	0.165	2		L Miocene- E Pliocene	MPlm.s	Dolati (2010)
434	0	434	m	0.726	2		L Miocene- E Pliocene	MPlm.s	Dolati (2010)
435	0	435	m	0.009	2		L Miocene- E Pliocene	MPlm.s	Dolati (2010)
436	0	436	m	1.059	2		L Miocene- E Pliocene	MPlm.s	Dolati (2010)
437	0	437	m	0.220	2		L Miocene- E Pliocene	MPlm.s	Dolati (2010)
438	0	438	m	0.708	2		L Miocene- E Pliocene	MPlm.s	Dolati (2010)
439	0	439	m	0.150	2		L Miocene- E Pliocene	MPlm.s	Dolati (2010)
440	0	440	m	0.089	2		L Miocene- E Pliocene	MPlm.s	Dolati (2010)
441	0	441	m	0.305	2		L Miocene- E Pliocene	MPlm.s	Dolati (2010)
442	0	442	m	0.835	2		L Miocene- E Pliocene	MPlm.s	Dolati (2010)
443	0	443	m	0.121	2		L Miocene- E Pliocene	MPlm.s	Dolati (2010)
444	0	444	m	0.160	2		L Miocene- E Pliocene	MPlm.s	Dolati (2010)
445	0	445	m	0.059	2		L Miocene- E Pliocene	MPlm.s	Dolati (2010)
446	0	446	m	0.168	2		L Miocene- E Pliocene	MPlm.s	Dolati (2010)
447	0	447	m	0.035	2		L Miocene- E Pliocene	MPlm.s	Dolati (2010)
448	0	448	m	0.148	2		L Miocene- E Pliocene	MPlm.s	Dolati (2010)
449	0	449	m	0.035	2		L Miocene- E Pliocene	MPlm.s	Dolati (2010)
450	0	450	m	0.608	2		L Miocene- E Pliocene	MPlm.s	Dolati (2010)
451	0	451	m	3.039	2		L Miocene- E Pliocene	MPlm.s	Dolati (2010)
452	0	452	m	0.243	2		L Miocene- E Pliocene	MPlm.s	Dolati (2010)
453	0	453	m	1.825	2		L Miocene- E Pliocene	MPlm.s	Dolati (2010)
454	0	454	m	0.083	2		L Miocene- E Pliocene	MPlm.s	Dolati (2010)

Geonavis

OBJECTID_1	Join_Count	TARGET_FID	label	Shape_Area (sqkm)	ORIG_FID	Absolute_Age	Age_paleontology	Unit	Reference
455	0	455	m	2.785	2		L Miocene- E Pliocene	MPlm.s	Dolati (2010)
456	0	456	m	0.040	2		L Miocene- E Pliocene	MPlm.s	Dolati (2010)
457	0	457	m	0.023	2		L Miocene- E Pliocene	MPlm.s	Dolati (2010)
458	0	458	m	0.431	2		L Miocene- E Pliocene	MPlm.s	Dolati (2010)
459	0	459	m	0.035	2		L Miocene- E Pliocene	MPlm.s	Dolati (2010)
460	0	460	m	12.134	2		L Miocene- E Pliocene	MPlm.s	Dolati (2010)
461	0	461	m	0.182	2		L Miocene- E Pliocene	MPlm.s	Dolati (2010)
462	0	462	m	0.038	2		L Miocene- E Pliocene	MPlm.s	Dolati (2010)
463	0	463	m	0.054	2		L Miocene- E Pliocene	MPlm.s	Dolati (2010)
464	0	464	m	0.583	2		L Miocene- E Pliocene	MPlm.s	Dolati (2010)
465	0	465	m	0.066	2		L Miocene- E Pliocene	MPlm.s	Dolati (2010)
466	0	466	m	1.493	2		L Miocene- E Pliocene	MPlm.s	Dolati (2010)
467	0	467	m	0.042	2		L Miocene- E Pliocene	MPlm.s	Dolati (2010)
468	0	468	m	0.072	2		L Miocene- E Pliocene	MPlm.s	Dolati (2010)
469	0	469	m	0.183	2		L Miocene- E Pliocene	MPlm.s	Dolati (2010)
470	0	470	m	0.050	2		L Miocene- E Pliocene	MPlm.s	Dolati (2010)
471	0	471	m	0.091	2		L Miocene- E Pliocene	MPlm.s	Dolati (2010)
472	0	472	m	3.963	2		L Miocene- E Pliocene	MPlm.s	Dolati (2010)
473	0	473	m	0.328	2		L Miocene- E Pliocene	MPlm.s	Dolati (2010)
474	0	474	m	0.072	2		L Miocene- E Pliocene	MPlm.s	Dolati (2010)
475	0	475	m	0.352	2		L Miocene- E Pliocene	MPlm.s	Dolati (2010)
476	0	476	m	0.041	2		L Miocene- E Pliocene	MPlm.s	Dolati (2010)
477	0	477	m	0.035	2		L Miocene- E Pliocene	MPlm.s	Dolati (2010)
478	0	478	m	0.170	2		L Miocene- E Pliocene	MPlm.s	Dolati (2010)
479	0	479	m	0.026	2		L Miocene- E Pliocene	MPlm.s	Dolati (2010)
480	0	480	m	1.945	2		L Miocene- E Pliocene	MPlm.s	Dolati (2010)
481	0	481	m	0.683	2		L Miocene- E Pliocene	MPlm.s	Dolati (2010)
482	0	482	m	0.387	2		L Miocene- E Pliocene	MPlm.s	Dolati (2010)
483	0	483	m	0.337	2		L Miocene- E Pliocene	MPlm.s	Dolati (2010)
484	0	484	m	0.115	2		L Miocene- E Pliocene	MPlm.s	Dolati (2010)
485	0	485	m	0.102	2		L Miocene- E Pliocene	MPlm.s	Dolati (2010)
486	0	486	m	0.395	2		L Miocene- E Pliocene	MPlm.s	Dolati (2010)
487	0	487	m	0.354	2		L Miocene- E Pliocene	MPlm.s	Dolati (2010)
488	0	488	m	0.037	2		L Miocene- E Pliocene	MPlm.s	Dolati (2010)
489	0	489	m	0.489	2		L Miocene- E Pliocene	MPlm.s	Dolati (2010)
490	0	490	m	0.079	2		L Miocene- E Pliocene	MPlm.s	Dolati (2010)
491	0	491	m	0.159	2		L Miocene- E Pliocene	MPlm.s	Dolati (2010)
492	0	492	m	0.138	2		L Miocene- E Pliocene	MPlm.s	Dolati (2010)
493	0	493	m	0.499	2		L Miocene- E Pliocene	MPlm.s	Dolati (2010)

GeoNeXus

OBJECTID_1	Join_Count	TARGET_FID	label	Shape_Area (sqkm)	ORIG_FID	Absolute_Age	Age_paleontology	Unit	Reference
494	0	494	m	0.072	2		L Miocene- E Pliocene	MPlm.s	Dolati (2010)
495	0	495	m	0.099	2		L Miocene- E Pliocene	MPlm.s	Dolati (2010)
496	0	496	m	0.015	2		L Miocene- E Pliocene	MPlm.s	Dolati (2010)
497	0	497	m	0.017	2		L Miocene- E Pliocene	MPlm.s	Dolati (2010)
498	0	498	m	0.094	2		L Miocene- E Pliocene	MPlm.s	Dolati (2010)
499	0	499	m	0.047	2		L Miocene- E Pliocene	MPlm.s	Dolati (2010)
500	0	500	m	0.064	2		L Miocene- E Pliocene	MPlm.s	Dolati (2010)
501	0	501	m	0.095	2		L Miocene- E Pliocene	MPlm.s	Dolati (2010)
502	0	502	m	0.024	2		L Miocene- E Pliocene	MPlm.s	Dolati (2010)
503	0	503	m	0.164	2		L Miocene- E Pliocene	MPlm.s	Dolati (2010)
504	0	504	m	0.192	2		L Miocene- E Pliocene	MPlm.s	Dolati (2010)
505	0	505	m	0.010	2		L Miocene- E Pliocene	MPlm.s	Dolati (2010)
506	0	506	m	0.208	2		L Miocene- E Pliocene	MPlm.s	Dolati (2010)
507	0	507	m	0.013	2		L Miocene- E Pliocene	MPlm.s	Dolati (2010)
508	0	508	m	0.036	2		L Miocene- E Pliocene	MPlm.s	Dolati (2010)
509	0	509	m	0.463	2		L Miocene- E Pliocene	MPlm.s	Dolati (2010)
510	0	510	m	0.024	2		L Miocene- E Pliocene	MPlm.s	Dolati (2010)
511	0	511	m	0.688	2		L Miocene- E Pliocene	MPlm.s	Dolati (2010)
512	0	512	m	0.280	2		L Miocene- E Pliocene	MPlm.s	Dolati (2010)
513	0	513	m	0.285	2		L Miocene- E Pliocene	MPlm.s	Dolati (2010)
514	0	514	m	0.873	2		L Miocene- E Pliocene	MPlm.s	Dolati (2010)
515	0	515	m	0.047	2		L Miocene- E Pliocene	MPlm.s	Dolati (2010)
516	0	516	m	0.238	2		L Miocene- E Pliocene	MPlm.s	Dolati (2010)
517	0	517	m	0.791	2		L Miocene- E Pliocene	MPlm.s	Dolati (2010)
518	0	518	m	0.192	2		L Miocene- E Pliocene	MPlm.s	Dolati (2010)
519	0	519	m	0.147	2		L Miocene- E Pliocene	MPlm.s	Dolati (2010)
520	0	520	m	0.172	2		L Miocene- E Pliocene	MPlm.s	Dolati (2010)
521	0	521	m	0.554	2		L Miocene- E Pliocene	MPlm.s	Dolati (2010)
522	0	522	m	0.092	2		L Miocene- E Pliocene	MPlm.s	Dolati (2010)
523	0	523	m	0.701	2		L Miocene- E Pliocene	MPlm.s	Dolati (2010)
524	0	524	m	1.317	2		L Miocene- E Pliocene	MPlm.s	Dolati (2010)
525	0	525	m	0.216	2		L Miocene- E Pliocene	MPlm.s	Dolati (2010)
526	0	526	m	0.209	2		L Miocene- E Pliocene	MPlm.s	Dolati (2010)
527	0	527	m	0.100	2		L Miocene- E Pliocene	MPlm.s	Dolati (2010)
528	0	528	m	0.062	2		L Miocene- E Pliocene	MPlm.s	Dolati (2010)
529	0	529	m	0.295	2		L Miocene- E Pliocene	MPlm.s	Dolati (2010)
530	0	530	m	0.061	2		L Miocene- E Pliocene	MPlm.s	Dolati (2010)
531	0	531	m	0.141	2		L Miocene- E Pliocene	MPlm.s	Dolati (2010)
532	0	532	m	0.066	2		L Miocene- E Pliocene	MPlm.s	Dolati (2010)

GeoAI

OBJECTID_1	Join_Count	TARGET_FID	label	Shape_Area (sqkm)	ORIG_FID	Absolute_Age	Age_paleontology	Unit	Reference
533	0	533	m	0.238	2		L Miocene- E Pliocene	MPlm.s	Dolati (2010)
534	0	534	m	0.044	2		L Miocene- E Pliocene	MPlm.s	Dolati (2010)
535	0	535	m	0.316	2		L Miocene- E Pliocene	MPlm.s	Dolati (2010)
536	0	536	m	0.049	2		L Miocene- E Pliocene	MPlm.s	Dolati (2010)
537	0	537	m	0.039	2		L Miocene- E Pliocene	MPlm.s	Dolati (2010)
538	0	538	m	0.111	2		L Miocene- E Pliocene	MPlm.s	Dolati (2010)
539	0	539	m	0.048	2		L Miocene- E Pliocene	MPlm.s	Dolati (2010)
540	0	540	m	0.397	2		L Miocene- E Pliocene	MPlm.s	Dolati (2010)
541	0	541	m	0.336	2		L Miocene- E Pliocene	MPlm.s	Dolati (2010)
542	0	542	m	0.157	2		L Miocene- E Pliocene	MPlm.s	Dolati (2010)
543	0	543	m	0.140	2		L Miocene- E Pliocene	MPlm.s	Dolati (2010)
544	0	544	m	0.027	2		L Miocene- E Pliocene	MPlm.s	Dolati (2010)
545	0	545	m	0.017	2		L Miocene- E Pliocene	MPlm.s	Dolati (2010)
546	0	546	m	23.629	2		L Miocene- E Pliocene	MPlm.s	Dolati (2010)
547	0	547	m	1.678	2		L Miocene- E Pliocene	MPlm.s	Dolati (2010)
548	0	548	m	0.131	2		L Miocene- E Pliocene	MPlm.s	Dolati (2010)
549	0	549	m	0.049	2		L Miocene- E Pliocene	MPlm.s	Dolati (2010)
550	0	550	m	0.064	2		L Miocene- E Pliocene	MPlm.s	Dolati (2010)
551	0	551	m	0.219	2		L Miocene- E Pliocene	MPlm.s	Dolati (2010)
552	0	552	m	0.117	2		L Miocene- E Pliocene	MPlm.s	Dolati (2010)
553	0	553	m	0.088	2		L Miocene- E Pliocene	MPlm.s	Dolati (2010)
554	0	554	m	0.188	2		L Miocene- E Pliocene	MPlm.s	Dolati (2010)
555	0	555	m	0.097	2		L Miocene- E Pliocene	MPlm.s	Dolati (2010)
556	0	556	m	0.021	2		L Miocene- E Pliocene	MPlm.s	Dolati (2010)
557	0	557	m	0.339	2		L Miocene- E Pliocene	MPlm.s	Dolati (2010)
558	0	558	m	0.153	2		L Miocene- E Pliocene	MPlm.s	Dolati (2010)
559	0	559	m	3.155	2		L Miocene- E Pliocene	MPlm.s	Dolati (2010)
560	0	560	m	0.447	2		L Miocene- E Pliocene	MPlm.s	Dolati (2010)
561	0	561	m	0.085	2		L Miocene- E Pliocene	MPlm.s	Dolati (2010)
562	0	562	m	0.029	2		L Miocene- E Pliocene	MPlm.s	Dolati (2010)
563	0	563	m	0.736	2		L Miocene- E Pliocene	MPlm.s	Dolati (2010)
564	0	564	m	0.394	2		L Miocene- E Pliocene	MPlm.s	Dolati (2010)
565	0	565	m	0.226	2		L Miocene- E Pliocene	MPlm.s	Dolati (2010)
566	0	566	m	0.172	2		L Miocene- E Pliocene	MPlm.s	Dolati (2010)
567	0	567	m	0.305	2		L Miocene- E Pliocene	MPlm.s	Dolati (2010)
568	0	568	m	0.630	2		L Miocene- E Pliocene	MPlm.s	Dolati (2010)
569	0	569	m	0.031	2		L Miocene- E Pliocene	MPlm.s	Dolati (2010)
570	0	570	m	0.883	2		L Miocene- E Pliocene	MPlm.s	Dolati (2010)
571	0	571	m	0.095	2		L Miocene- E Pliocene	MPlm.s	Dolati (2010)

GeoNeXus

OBJECTID_1	Join_Count	TARGET_FID	label	Shape_Area (sqkm)	ORIG_FID	Absolute_Age	Age_paleontology	Unit	Reference
572	0	572	m	0.431	2		L Miocene- E Pliocene	MPlm.s	Dolati (2010)
573	0	573	m	0.045	2		L Miocene- E Pliocene	MPlm.s	Dolati (2010)
574	0	574	m	1.858	2		L Miocene- E Pliocene	MPlm.s	Dolati (2010)
575	0	575	m	1.812	2		L Miocene- E Pliocene	MPlm.s	Dolati (2010)
576	0	576	m	0.401	2		L Miocene- E Pliocene	MPlm.s	Dolati (2010)
577	0	577	m	0.357	2		L Miocene- E Pliocene	MPlm.s	Dolati (2010)
578	0	578	m	0.072	2		L Miocene- E Pliocene	MPlm.s	Dolati (2010)
579	0	579	m	0.087	2		L Miocene- E Pliocene	MPlm.s	Dolati (2010)
580	0	580	m	0.064	2		L Miocene- E Pliocene	MPlm.s	Dolati (2010)
581	0	581	m	0.111	2		L Miocene- E Pliocene	MPlm.s	Dolati (2010)
582	0	582	m	0.264	2		L Miocene- E Pliocene	MPlm.s	Dolati (2010)
583	0	583	m	0.151	2		L Miocene- E Pliocene	MPlm.s	Dolati (2010)
584	0	584	m	0.699	2		L Miocene- E Pliocene	MPlm.s	Dolati (2010)
585	0	585	m	0.072	2		L Miocene- E Pliocene	MPlm.s	Dolati (2010)
586	0	586	m	0.115	2		L Miocene- E Pliocene	MPlm.s	Dolati (2010)
587	0	587	m	0.323	2		L Miocene- E Pliocene	MPlm.s	Dolati (2010)
588	0	588	m	2.356	2		L Miocene- E Pliocene	MPlm.s	Dolati (2010)
589	0	589	m	0.043	2		L Miocene- E Pliocene	MPlm.s	Dolati (2010)
590	0	590	m	0.870	2		L Miocene- E Pliocene	MPlm.s	Dolati (2010)
591	0	591	m	0.089	2		L Miocene- E Pliocene	MPlm.s	Dolati (2010)
592	0	592	m	0.080	2		L Miocene- E Pliocene	MPlm.s	Dolati (2010)
593	0	593	m	0.039	2		L Miocene- E Pliocene	MPlm.s	Dolati (2010)
594	0	594	m	23.283	2		L Miocene- E Pliocene	MPlm.s	Dolati (2010)
595	0	595	m	0.052	2		L Miocene- E Pliocene	MPlm.s	Dolati (2010)
596	0	596	m	0.147	2		L Miocene- E Pliocene	MPlm.s	Dolati (2010)
597	0	597	m	0.181	2		L Miocene- E Pliocene	MPlm.s	Dolati (2010)
598	0	598	m	0.446	2		L Miocene- E Pliocene	MPlm.s	Dolati (2010)
599	0	599	m	0.281	2		L Miocene- E Pliocene	MPlm.s	Dolati (2010)
600	0	600	m	1.272	2		L Miocene- E Pliocene	MPlm.s	Dolati (2010)
601	0	601	m	0.494	2		L Miocene- E Pliocene	MPlm.s	Dolati (2010)
602	0	602	m	0.231	2		L Miocene- E Pliocene	MPlm.s	Dolati (2010)
603	0	603	m	0.034	2		L Miocene- E Pliocene	MPlm.s	Dolati (2010)
604	0	604	m	0.292	2		L Miocene- E Pliocene	MPlm.s	Dolati (2010)
605	0	605	m	1.352	2		L Miocene- E Pliocene	MPlm.s	Dolati (2010)
606	0	606	m	0.108	2		L Miocene- E Pliocene	MPlm.s	Dolati (2010)
607	0	607	m	1.653	2		L Miocene- E Pliocene	MPlm.s	Dolati (2010)
608	0	608	m	0.231	2		L Miocene- E Pliocene	MPlm.s	Dolati (2010)
609	0	609	m	0.209	2		L Miocene- E Pliocene	MPlm.s	Dolati (2010)
610	0	610	m	0.339	2		L Miocene- E Pliocene	MPlm.s	Dolati (2010)

GeoNavis

OBJECTID_1	Join_Count	TARGET_FID	label	Shape_Area (sqkm)	ORIG_FID	Absolute_Age	Age_paleontology	Unit	Reference
611	0	611	m	3.775	2		L Miocene- E Pliocene	MPlm.s	Dolati (2010)
612	0	612	m	0.054	2		L Miocene- E Pliocene	MPlm.s	Dolati (2010)
613	0	613	m	0.113	2		L Miocene- E Pliocene	MPlm.s	Dolati (2010)
614	0	614	m	0.266	2		L Miocene- E Pliocene	MPlm.s	Dolati (2010)
615	0	615	m	0.403	2		L Miocene- E Pliocene	MPlm.s	Dolati (2010)
616	0	616	m	0.287	2		L Miocene- E Pliocene	MPlm.s	Dolati (2010)
617	0	617	m	0.080	2		L Miocene- E Pliocene	MPlm.s	Dolati (2010)
618	0	618	m	0.086	2		L Miocene- E Pliocene	MPlm.s	Dolati (2010)
619	0	619	m	0.259	2		L Miocene- E Pliocene	MPlm.s	Dolati (2010)
620	0	620	m	0.082	2		L Miocene- E Pliocene	MPlm.s	Dolati (2010)
621	0	621	m	0.872	2		L Miocene- E Pliocene	MPlm.s	Dolati (2010)
622	0	622	m	0.021	2		L Miocene- E Pliocene	MPlm.s	Dolati (2010)
623	0	623	m	2.037	2		L Miocene- E Pliocene	MPlm.s	Dolati (2010)
624	0	624	m	0.558	2		L Miocene- E Pliocene	MPlm.s	Dolati (2010)
625	0	625	m	0.093	2		L Miocene- E Pliocene	MPlm.s	Dolati (2010)
626	0	626	m	0.158	2		L Miocene- E Pliocene	MPlm.s	Dolati (2010)
627	0	627	m	0.051	2		L Miocene- E Pliocene	MPlm.s	Dolati (2010)
628	0	628	m	0.122	2		L Miocene- E Pliocene	MPlm.s	Dolati (2010)
629	0	629	m	0.042	2		L Miocene- E Pliocene	MPlm.s	Dolati (2010)
630	0	630	m	0.960	2		L Miocene- E Pliocene	MPlm.s	Dolati (2010)
631	0	631	m	0.077	2		L Miocene- E Pliocene	MPlm.s	Dolati (2010)
632	0	632	m	0.673	2		L Miocene- E Pliocene	MPlm.s	Dolati (2010)
633	0	633	m	1.229	2		L Miocene- E Pliocene	MPlm.s	Dolati (2010)
634	0	634	m	0.631	2		L Miocene- E Pliocene	MPlm.s	Dolati (2010)
635	0	635	m	0.025	2		L Miocene- E Pliocene	MPlm.s	Dolati (2010)
636	0	636	m	0.101	2		L Miocene- E Pliocene	MPlm.s	Dolati (2010)
637	0	637	m	0.201	2		L Miocene- E Pliocene	MPlm.s	Dolati (2010)
638	0	638	m	0.226	2		L Miocene- E Pliocene	MPlm.s	Dolati (2010)
639	0	639	m	2.606	2		L Miocene- E Pliocene	MPlm.s	Dolati (2010)
640	0	640	m	0.261	2		L Miocene- E Pliocene	MPlm.s	Dolati (2010)
641	0	641	m	0.077	2		L Miocene- E Pliocene	MPlm.s	Dolati (2010)
642	0	642	m	0.023	2		L Miocene- E Pliocene	MPlm.s	Dolati (2010)
643	0	643	m	0.031	2		L Miocene- E Pliocene	MPlm.s	Dolati (2010)
644	0	644	m	0.059	2		L Miocene- E Pliocene	MPlm.s	Dolati (2010)
645	0	645	m	0.171	2		L Miocene- E Pliocene	MPlm.s	Dolati (2010)
646	0	646	m	0.049	2		L Miocene- E Pliocene	MPlm.s	Dolati (2010)
647	0	647	m	0.519	2		L Miocene- E Pliocene	MPlm.s	Dolati (2010)
648	0	648	m	1.538	2		L Miocene- E Pliocene	MPlm.s	Dolati (2010)
649	0	649	m	0.078	2		L Miocene- E Pliocene	MPlm.s	Dolati (2010)

GeoNeXus

OBJECTID_1	Join_Count	TARGET_FID	label	Shape_Area (sqkm)	ORIG_FID	Absolute_Age	Age_paleontology	Unit	Reference
650	0	650	m	0.036	2		L Miocene- E Pliocene	MPlm.s	Dolati (2010)
651	0	651	m	0.299	2		L Miocene- E Pliocene	MPlm.s	Dolati (2010)
652	0	652	m	0.038	2		L Miocene- E Pliocene	MPlm.s	Dolati (2010)
653	0	653	m	0.021	2		L Miocene- E Pliocene	MPlm.s	Dolati (2010)
654	0	654	m	0.038	2		L Miocene- E Pliocene	MPlm.s	Dolati (2010)
655	0	655	m	0.200	2		L Miocene- E Pliocene	MPlm.s	Dolati (2010)
656	0	656	m	0.369	2		L Miocene- E Pliocene	MPlm.s	Dolati (2010)
657	0	657	m	13.227	2		L Miocene- E Pliocene	MPlm.s	Dolati (2010)
658	0	658	m	0.956	2		L Miocene- E Pliocene	MPlm.s	Dolati (2010)
659	0	659	m	0.070	2		L Miocene- E Pliocene	MPlm.s	Dolati (2010)
660	0	660	m	0.011	2		L Miocene- E Pliocene	MPlm.s	Dolati (2010)
661	0	661	m	0.481	2		L Miocene- E Pliocene	MPlm.s	Dolati (2010)
662	0	662	m	0.096	2		L Miocene- E Pliocene	MPlm.s	Dolati (2010)
663	0	663	m	0.083	2		L Miocene- E Pliocene	MPlm.s	Dolati (2010)
664	0	664	m	0.269	2		L Miocene- E Pliocene	MPlm.s	Dolati (2010)
665	0	665	m	0.044	2		L Miocene- E Pliocene	MPlm.s	Dolati (2010)
666	0	666	m	0.401	2		L Miocene- E Pliocene	MPlm.s	Dolati (2010)
667	0	667	m	0.021	2		L Miocene- E Pliocene	MPlm.s	Dolati (2010)
668	0	668	m	0.221	2		L Miocene- E Pliocene	MPlm.s	Dolati (2010)
669	0	669	m	0.114	2		L Miocene- E Pliocene	MPlm.s	Dolati (2010)
670	0	670	m	0.034	2		L Miocene- E Pliocene	MPlm.s	Dolati (2010)
671	0	671	m	0.287	2		L Miocene- E Pliocene	MPlm.s	Dolati (2010)
672	1	672	m	3.090	2		L Miocene- E Pliocene	MPlm.s	Dolati (2010)
673	0	673	m	0.407	2		L Miocene- E Pliocene	MPlm.s	Dolati (2010)
674	0	674	m	0.557	2		L Miocene- E Pliocene	MPlm.s	Dolati (2010)
675	0	675	m	0.151	2		L Miocene- E Pliocene	MPlm.s	Dolati (2010)
676	0	676	m	0.406	2		L Miocene- E Pliocene	MPlm.s	Dolati (2010)
677	0	677	m	0.137	2		L Miocene- E Pliocene	MPlm.s	Dolati (2010)
678	0	678	m	4.167	2		L Miocene- E Pliocene	MPlm.s	Dolati (2010)
679	0	679	m	0.043	2		L Miocene- E Pliocene	MPlm.s	Dolati (2010)
680	0	680	m	0.520	2		L Miocene- E Pliocene	MPlm.s	Dolati (2010)
681	0	681	m	0.341	2		L Miocene- E Pliocene	MPlm.s	Dolati (2010)
682	0	682	m	0.216	2		L Miocene- E Pliocene	MPlm.s	Dolati (2010)
683	0	683	m	0.143	2		L Miocene- E Pliocene	MPlm.s	Dolati (2010)
684	0	684	m	0.624	2		L Miocene- E Pliocene	MPlm.s	Dolati (2010)
685	0	685	m	0.147	2		L Miocene- E Pliocene	MPlm.s	Dolati (2010)
686	0	686	m	0.189	2		L Miocene- E Pliocene	MPlm.s	Dolati (2010)
687	0	687	m	0.334	2		L Miocene- E Pliocene	MPlm.s	Dolati (2010)
688	0	688	m	0.209	2		L Miocene- E Pliocene	MPlm.s	Dolati (2010)

Geonavis

OBJECTID_1	Join_Count	TARGET_FID	label	Shape_Area (sqkm)	ORIG_FID	Absolute_Age	Age_paleontology	Unit	Reference
689	0	689	m	0.661	2		L Miocene- E Pliocene	MPlm.s	Dolati (2010)
690	0	690	m	1.392	2		L Miocene- E Pliocene	MPlm.s	Dolati (2010)
691	0	691	m	0.113	2		L Miocene- E Pliocene	MPlm.s	Dolati (2010)
692	0	692	m	0.083	2		L Miocene- E Pliocene	MPlm.s	Dolati (2010)
693	0	693	m	3.506	2		L Miocene- E Pliocene	MPlm.s	Dolati (2010)
694	0	694	m	0.436	2		L Miocene- E Pliocene	MPlm.s	Dolati (2010)
695	0	695	m	0.034	2		L Miocene- E Pliocene	MPlm.s	Dolati (2010)
696	0	696	m	0.071	2		L Miocene- E Pliocene	MPlm.s	Dolati (2010)
697	0	697	m	0.149	2		L Miocene- E Pliocene	MPlm.s	Dolati (2010)
698	0	698	m	0.030	2		L Miocene- E Pliocene	MPlm.s	Dolati (2010)
699	0	699	m	0.041	2		L Miocene- E Pliocene	MPlm.s	Dolati (2010)
700	0	700	m	0.092	2		L Miocene- E Pliocene	MPlm.s	Dolati (2010)
701	1	701	m	0.331	2		L Miocene- E Pliocene	MPlm.s	Dolati (2010)
702	0	702	m	5.581	2		L Miocene- E Pliocene	MPlm.s	Dolati (2010)
703	0	703	m	0.090	2		L Miocene- E Pliocene	MPlm.s	Dolati (2010)
704	0	704	m	0.623	2		L Miocene- E Pliocene	MPlm.s	Dolati (2010)
705	0	705	m	0.110	2		L Miocene- E Pliocene	MPlm.s	Dolati (2010)
706	0	706	m	0.078	2		L Miocene- E Pliocene	MPlm.s	Dolati (2010)
707	0	707	m	0.056	2		L Miocene- E Pliocene	MPlm.s	Dolati (2010)
708	0	708	m	0.195	2		L Miocene- E Pliocene	MPlm.s	Dolati (2010)
709	0	709	m	0.150	2		L Miocene- E Pliocene	MPlm.s	Dolati (2010)
710	0	710	m	0.107	2		L Miocene- E Pliocene	MPlm.s	Dolati (2010)
711	0	711	m	0.537	2		L Miocene- E Pliocene	MPlm.s	Dolati (2010)
712	0	712	m	1.541	2		L Miocene- E Pliocene	MPlm.s	Dolati (2010)
713	0	713	m	0.118	2		L Miocene- E Pliocene	MPlm.s	Dolati (2010)
714	0	714	m	0.164	2		L Miocene- E Pliocene	MPlm.s	Dolati (2010)
715	0	715	m	0.040	2		L Miocene- E Pliocene	MPlm.s	Dolati (2010)
716	0	716	m	0.026	2		L Miocene- E Pliocene	MPlm.s	Dolati (2010)
717	0	717	m	0.280	2		L Miocene- E Pliocene	MPlm.s	Dolati (2010)
718	0	718	m	0.062	2		L Miocene- E Pliocene	MPlm.s	Dolati (2010)
719	0	719	m	0.183	2		L Miocene- E Pliocene	MPlm.s	Dolati (2010)
720	0	720	m	0.034	2		L Miocene- E Pliocene	MPlm.s	Dolati (2010)
721	0	721	m	0.059	2		L Miocene- E Pliocene	MPlm.s	Dolati (2010)
722	0	722	m	0.109	2		L Miocene- E Pliocene	MPlm.s	Dolati (2010)
723	0	723	m	0.160	2		L Miocene- E Pliocene	MPlm.s	Dolati (2010)
724	0	724	m	0.022	2		L Miocene- E Pliocene	MPlm.s	Dolati (2010)
725	0	725	m	0.010	2		L Miocene- E Pliocene	MPlm.s	Dolati (2010)
726	0	726	m	0.064	2		L Miocene- E Pliocene	MPlm.s	Dolati (2010)
727	0	727	m	0.952	2		L Miocene- E Pliocene	MPlm.s	Dolati (2010)

GeoNeXus

OBJECTID_1	Join_Count	TARGET_FID	label	Shape_Area (sqkm)	ORIG_FID	Absolute_Age	Age_paleontology	Unit	Reference
728	0	728	m	0.102	2		L Miocene- E Pliocene	MPlm.s	Dolati (2010)
729	0	729	m	0.104	2		L Miocene- E Pliocene	MPlm.s	Dolati (2010)
730	0	730	m	0.014	2		L Miocene- E Pliocene	MPlm.s	Dolati (2010)
731	0	731	m	3.584	2		L Miocene- E Pliocene	MPlm.s	Dolati (2010)
732	0	732	m	0.118	2		L Miocene- E Pliocene	MPlm.s	Dolati (2010)
733	0	733	m	0.171	2		L Miocene- E Pliocene	MPlm.s	Dolati (2010)
734	0	734	m	0.206	2		L Miocene- E Pliocene	MPlm.s	Dolati (2010)
735	0	735	m	0.060	2		L Miocene- E Pliocene	MPlm.s	Dolati (2010)
736	0	736	m	0.344	2		L Miocene- E Pliocene	MPlm.s	Dolati (2010)
737	0	737	m	0.076	2		L Miocene- E Pliocene	MPlm.s	Dolati (2010)
738	0	738	m	0.587	2		L Miocene- E Pliocene	MPlm.s	Dolati (2010)
740	0	740	m	0.072	2		L Miocene- E Pliocene	MPlm.s	Dolati (2010)
741	0	741	m	0.425	2		L Miocene- E Pliocene	MPlm.s	Dolati (2010)
742	0	742	m	0.109	2		L Miocene- E Pliocene	MPlm.s	Dolati (2010)
743	0	743	m	0.723	2		L Miocene- E Pliocene	MPlm.s	Dolati (2010)
744	0	744	m	0.383	2		L Miocene- E Pliocene	MPlm.s	Dolati (2010)
745	0	745	m	1.295	2		L Miocene- E Pliocene	MPlm.s	Dolati (2010)
746	0	746	m	0.031	2		L Miocene- E Pliocene	MPlm.s	Dolati (2010)
747	0	747	m	0.045	2		L Miocene- E Pliocene	MPlm.s	Dolati (2010)
748	0	748	m	5.030	2		L Miocene- E Pliocene	MPlm.s	Dolati (2010)
749	0	749	m	0.959	2		L Miocene- E Pliocene	MPlm.s	Dolati (2010)
750	0	750	m	0.134	2		L Miocene- E Pliocene	MPlm.s	Dolati (2010)
751	0	751	m	0.252	2		L Miocene- E Pliocene	MPlm.s	Dolati (2010)
752	0	752	m	0.264	2		L Miocene- E Pliocene	MPlm.s	Dolati (2010)
753	0	753	m	0.088	2		L Miocene- E Pliocene	MPlm.s	Dolati (2010)
754	0	754	m	1.255	2		L Miocene- E Pliocene	MPlm.s	Dolati (2010)
755	0	755	m	0.688	2		L Miocene- E Pliocene	MPlm.s	Dolati (2010)
756	0	756	m	0.617	2		L Miocene- E Pliocene	MPlm.s	Dolati (2010)
757	0	757	m	0.591	2		L Miocene- E Pliocene	MPlm.s	Dolati (2010)
758	0	758	m	0.143	2		L Miocene- E Pliocene	MPlm.s	Dolati (2010)
759	0	759	m	0.082	2		L Miocene- E Pliocene	MPlm.s	Dolati (2010)
760	0	760	m	0.159	2		L Miocene- E Pliocene	MPlm.s	Dolati (2010)
761	0	761	m	0.575	2		L Miocene- E Pliocene	MPlm.s	Dolati (2010)
762	0	762	m	0.101	2		L Miocene- E Pliocene	MPlm.s	Dolati (2010)
763	0	763	m	0.136	2		L Miocene- E Pliocene	MPlm.s	Dolati (2010)
764	0	764	m	0.598	2		L Miocene- E Pliocene	MPlm.s	Dolati (2010)
765	0	765	m	0.197	2		L Miocene- E Pliocene	MPlm.s	Dolati (2010)
766	0	766	m	0.038	2		L Miocene- E Pliocene	MPlm.s	Dolati (2010)
767	0	767	m	0.810	2		L Miocene- E Pliocene	MPlm.s	Dolati (2010)

Geonavis

OBJECTID_1	Join_Count	TARGET_FID	label	Shape_Area (sqkm)	ORIG_FID	Absolute_Age	Age_paleontology	Unit	Reference
768	0	768	m	0.076	2		L Miocene- E Pliocene	MPlm.s	Dolati (2010)
769	0	769	m	0.026	2		L Miocene- E Pliocene	MPlm.s	Dolati (2010)
770	0	770	m	0.619	2		L Miocene- E Pliocene	MPlm.s	Dolati (2010)
771	0	771	m	0.064	2		L Miocene- E Pliocene	MPlm.s	Dolati (2010)
772	0	772	m	0.208	2		L Miocene- E Pliocene	MPlm.s	Dolati (2010)
773	0	773	m	0.852	2		L Miocene- E Pliocene	MPlm.s	Dolati (2010)
774	0	774	m	5.275	2		L Miocene- E Pliocene	MPlm.s	Dolati (2010)
775	0	775	m	0.124	2		L Miocene- E Pliocene	MPlm.s	Dolati (2010)
776	0	776	m	0.022	2		L Miocene- E Pliocene	MPlm.s	Dolati (2010)
777	0	777	m	0.926	2		L Miocene- E Pliocene	MPlm.s	Dolati (2010)
778	0	778	m	0.742	2		L Miocene- E Pliocene	MPlm.s	Dolati (2010)
779	0	779	m	0.479	2		L Miocene- E Pliocene	MPlm.s	Dolati (2010)
780	0	780	m	0.007	2		L Miocene- E Pliocene	MPlm.s	Dolati (2010)
781	0	781	m	0.124	2		L Miocene- E Pliocene	MPlm.s	Dolati (2010)
782	0	782	m	0.012	2		L Miocene- E Pliocene	MPlm.s	Dolati (2010)
783	0	783	m	0.102	2		L Miocene- E Pliocene	MPlm.s	Dolati (2010)
784	0	784	m	0.147	2		L Miocene- E Pliocene	MPlm.s	Dolati (2010)
785	0	785	m	0.640	2		L Miocene- E Pliocene	MPlm.s	Dolati (2010)
786	0	786	m	0.307	2		L Miocene- E Pliocene	MPlm.s	Dolati (2010)
787	0	787	m	0.383	2		L Miocene- E Pliocene	MPlm.s	Dolati (2010)
788	0	788	m	0.341	2		L Miocene- E Pliocene	MPlm.s	Dolati (2010)
789	0	789	m	0.240	2		L Miocene- E Pliocene	MPlm.s	Dolati (2010)
790	0	790	m	0.114	2		L Miocene- E Pliocene	MPlm.s	Dolati (2010)
791	0	791	m	0.300	2		L Miocene- E Pliocene	MPlm.s	Dolati (2010)
792	0	792	m	0.124	2		L Miocene- E Pliocene	MPlm.s	Dolati (2010)
793	0	793	m	0.362	2		L Miocene- E Pliocene	MPlm.s	Dolati (2010)
794	0	794	m	0.176	2		L Miocene- E Pliocene	MPlm.s	Dolati (2010)
795	0	795	m	0.209	2		L Miocene- E Pliocene	MPlm.s	Dolati (2010)
796	0	796	m	0.384	2		L Miocene- E Pliocene	MPlm.s	Dolati (2010)
797	0	797	m	0.083	2		L Miocene- E Pliocene	MPlm.s	Dolati (2010)
798	0	798	m	0.384	2		L Miocene- E Pliocene	MPlm.s	Dolati (2010)
799	0	799	m	0.275	2		L Miocene- E Pliocene	MPlm.s	Dolati (2010)
800	0	800	m	0.099	2		L Miocene- E Pliocene	MPlm.s	Dolati (2010)
801	0	801	m	0.145	2		L Miocene- E Pliocene	MPlm.s	Dolati (2010)
802	0	802	m	0.270	2		L Miocene- E Pliocene	MPlm.s	Dolati (2010)
803	0	803	m	0.784	2		L Miocene- E Pliocene	MPlm.s	Dolati (2010)
804	0	804	m	0.022	2		L Miocene- E Pliocene	MPlm.s	Dolati (2010)
805	0	805	m	0.426	2		L Miocene- E Pliocene	MPlm.s	Dolati (2010)
806	0	806	m	0.078	2		L Miocene- E Pliocene	MPlm.s	Dolati (2010)

GeoNeus

OBJECTID_1	Join_Count	TARGET_FID	label	Shape_Area (sqkm)	ORIG_FID	Absolute_Age	Age_paleontology	Unit	Reference
807	0	807	m	0.118	2		L Miocene- E Pliocene	MPlm.s	Dolati (2010)
808	0	808	m	0.037	2		L Miocene- E Pliocene	MPlm.s	Dolati (2010)
809	0	809	m	0.362	2		L Miocene- E Pliocene	MPlm.s	Dolati (2010)
810	0	810	m	0.022	2		L Miocene- E Pliocene	MPlm.s	Dolati (2010)
811	0	811	m	0.091	2		L Miocene- E Pliocene	MPlm.s	Dolati (2010)
812	0	812	m	0.108	2		L Miocene- E Pliocene	MPlm.s	Dolati (2010)
813	0	813	m	0.130	2		L Miocene- E Pliocene	MPlm.s	Dolati (2010)
814	0	814	m	0.477	2		L Miocene- E Pliocene	MPlm.s	Dolati (2010)
815	0	815	m	9.195	2		L Miocene- E Pliocene	MPlm.s	Dolati (2010)
816	0	816	m	0.045	2		L Miocene- E Pliocene	MPlm.s	Dolati (2010)
817	0	817	m	0.471	2		L Miocene- E Pliocene	MPlm.s	Dolati (2010)
818	0	818	m	0.142	2		L Miocene- E Pliocene	MPlm.s	Dolati (2010)
819	0	819	m	0.636	2		L Miocene- E Pliocene	MPlm.s	Dolati (2010)
820	0	820	m	0.083	2		L Miocene- E Pliocene	MPlm.s	Dolati (2010)
821	0	821	m	0.844	2		L Miocene- E Pliocene	MPlm.s	Dolati (2010)
822	0	822	m	0.016	2		L Miocene- E Pliocene	MPlm.s	Dolati (2010)
823	0	823	m	0.298	2		L Miocene- E Pliocene	MPlm.s	Dolati (2010)
824	0	824	m	0.179	2		L Miocene- E Pliocene	MPlm.s	Dolati (2010)
825	0	825	m	0.087	2		L Miocene- E Pliocene	MPlm.s	Dolati (2010)
826	0	826	m	0.037	2		L Miocene- E Pliocene	MPlm.s	Dolati (2010)
827	0	827	m	0.016	2		L Miocene- E Pliocene	MPlm.s	Dolati (2010)
828	0	828	m	0.042	2		L Miocene- E Pliocene	MPlm.s	Dolati (2010)
829	0	829	m	0.586	2		L Miocene- E Pliocene	MPlm.s	Dolati (2010)
830	0	830	m	0.264	2		L Miocene- E Pliocene	MPlm.s	Dolati (2010)
831	0	831	m	3.142	2		L Miocene- E Pliocene	MPlm.s	Dolati (2010)
832	0	832	m	0.059	2		L Miocene- E Pliocene	MPlm.s	Dolati (2010)
833	0	833	m	0.246	2		L Miocene- E Pliocene	MPlm.s	Dolati (2010)
834	0	834	m	0.033	2		L Miocene- E Pliocene	MPlm.s	Dolati (2010)
835	0	835	m	0.066	2		L Miocene- E Pliocene	MPlm.s	Dolati (2010)
836	0	836	m	1.390	2		L Miocene- E Pliocene	MPlm.s	Dolati (2010)
837	0	837	m	0.503	2		L Miocene- E Pliocene	MPlm.s	Dolati (2010)
838	0	838	m	2.011	2		L Miocene- E Pliocene	MPlm.s	Dolati (2010)
839	0	839	m	0.020	2		L Miocene- E Pliocene	MPlm.s	Dolati (2010)
840	0	840	m	0.170	2		L Miocene- E Pliocene	MPlm.s	Dolati (2010)
841	0	841	m	0.280	2		L Miocene- E Pliocene	MPlm.s	Dolati (2010)
842	0	842	m	0.092	2		L Miocene- E Pliocene	MPlm.s	Dolati (2010)
843	0	843	m	0.061	2		L Miocene- E Pliocene	MPlm.s	Dolati (2010)
844	0	844	m	0.067	2		L Miocene- E Pliocene	MPlm.s	Dolati (2010)
846	0	846	m	0.678	2		L Miocene- E Pliocene	MPlm.s	Dolati (2010)

GeoAI

OBJECTID_1	Join_Count	TARGET_FID	label	Shape_Area (sqkm)	ORIG_FID	Absolute_Age	Age_paleontology	Unit	Reference
847	0	847	m	5.150	2		L Miocene- E Pliocene	MPlm.s	Dolati (2010)
848	0	848	m	0.029	2		L Miocene- E Pliocene	MPlm.s	Dolati (2010)
849	0	849	m	0.249	2		L Miocene- E Pliocene	MPlm.s	Dolati (2010)
851	0	851	m	2.203	2		L Miocene- E Pliocene	MPlm.s	Dolati (2010)
852	0	852	m	0.212	2		L Miocene- E Pliocene	MPlm.s	Dolati (2010)
853	0	853	m	0.715	2		L Miocene- E Pliocene	MPlm.s	Dolati (2010)
854	0	854	m	1.667	2		L Miocene- E Pliocene	MPlm.s	Dolati (2010)
855	0	855	m	1.842	2		L Miocene- E Pliocene	MPlm.s	Dolati (2010)
856	0	856	m	0.265	2		L Miocene- E Pliocene	MPlm.s	Dolati (2010)
857	0	857	m	3.342	2		L Miocene- E Pliocene	MPlm.s	Dolati (2010)
858	0	858	m	0.025	2		L Miocene- E Pliocene	MPlm.s	Dolati (2010)
859	0	859	m	0.275	2		L Miocene- E Pliocene	MPlm.s	Dolati (2010)
860	0	860	m	0.078	2		L Miocene- E Pliocene	MPlm.s	Dolati (2010)
861	0	861	m	2.921	2		L Miocene- E Pliocene	MPlm.s	Dolati (2010)
862	0	862	m	0.257	2		L Miocene- E Pliocene	MPlm.s	Dolati (2010)
863	0	863	m	0.479	2		L Miocene- E Pliocene	MPlm.s	Dolati (2010)
864	0	864	m	0.205	2		L Miocene- E Pliocene	MPlm.s	Dolati (2010)
865	0	865	m	0.175	2		L Miocene- E Pliocene	MPlm.s	Dolati (2010)
866	0	866	m	0.093	2		L Miocene- E Pliocene	MPlm.s	Dolati (2010)
867	0	867	m	0.015	2		L Miocene- E Pliocene	MPlm.s	Dolati (2010)
868	0	868	m	0.845	2		L Miocene- E Pliocene	MPlm.s	Dolati (2010)
869	0	869	m	0.459	2		L Miocene- E Pliocene	MPlm.s	Dolati (2010)
870	1	870	m	13.381	2		L Miocene- E Pliocene	MPlm.s	Dolati (2010)
871	0	871	m	1.044	2		L Miocene- E Pliocene	MPlm.s	Dolati (2010)
872	0	872	m	0.089	2		L Miocene- E Pliocene	MPlm.s	Dolati (2010)
873	0	873	m	0.014	2		L Miocene- E Pliocene	MPlm.s	Dolati (2010)
874	0	874	m	0.547	2		L Miocene- E Pliocene	MPlm.s	Dolati (2010)
875	0	875	m	0.166	2		L Miocene- E Pliocene	MPlm.s	Dolati (2010)
876	0	876	m	0.193	2		L Miocene- E Pliocene	MPlm.s	Dolati (2010)
877	0	877	m	2.055	2		L Miocene- E Pliocene	MPlm.s	Dolati (2010)
878	0	878	m	0.416	2		L Miocene- E Pliocene	MPlm.s	Dolati (2010)
879	0	879	m	0.054	2		L Miocene- E Pliocene	MPlm.s	Dolati (2010)
880	0	880	m	0.016	2		L Miocene- E Pliocene	MPlm.s	Dolati (2010)
881	0	881	m	0.462	2		L Miocene- E Pliocene	MPlm.s	Dolati (2010)
882	0	882	m	0.775	2		L Miocene- E Pliocene	MPlm.s	Dolati (2010)
883	0	883	m	0.165	2		L Miocene- E Pliocene	MPlm.s	Dolati (2010)
884	0	884	m	0.062	2		L Miocene- E Pliocene	MPlm.s	Dolati (2010)
885	0	885	m	0.132	2		L Miocene- E Pliocene	MPlm.s	Dolati (2010)
886	0	886	m	0.680	2		L Miocene- E Pliocene	MPlm.s	Dolati (2010)

GeoNeXus

OBJECTID_1	Join_Count	TARGET_FID	label	Shape_Area (sqkm)	ORIG_FID	Absolute_Age	Age_paleontology	Unit	Reference
887	0	887	m	0.098	2		L Miocene- E Pliocene	MPlm.s	Dolati (2010)
888	0	888	m	0.041	2		L Miocene- E Pliocene	MPlm.s	Dolati (2010)
889	0	889	m	2.297	2		L Miocene- E Pliocene	MPlm.s	Dolati (2010)
890	0	890	m	0.026	2		L Miocene- E Pliocene	MPlm.s	Dolati (2010)
891	0	891	m	2.614	2		L Miocene- E Pliocene	MPlm.s	Dolati (2010)
892	0	892	m	0.044	2		L Miocene- E Pliocene	MPlm.s	Dolati (2010)
893	0	893	m	0.398	2		L Miocene- E Pliocene	MPlm.s	Dolati (2010)
894	0	894	m	0.103	2		L Miocene- E Pliocene	MPlm.s	Dolati (2010)
895	0	895	m	0.353	2		L Miocene- E Pliocene	MPlm.s	Dolati (2010)
896	0	896	m	0.290	2		L Miocene- E Pliocene	MPlm.s	Dolati (2010)
897	0	897	m	16.958	2		L Miocene- E Pliocene	MPlm.s	Dolati (2010)
898	0	898	m	0.418	2		L Miocene- E Pliocene	MPlm.s	Dolati (2010)
899	0	899	m	2.804	2		L Miocene- E Pliocene	MPlm.s	Dolati (2010)
900	0	900	m	0.066	2		L Miocene- E Pliocene	MPlm.s	Dolati (2010)
901	0	901	m	0.033	2		L Miocene- E Pliocene	MPlm.s	Dolati (2010)
902	0	902	m	0.122	2		L Miocene- E Pliocene	MPlm.s	Dolati (2010)
903	0	903	m	1.672	2		L Miocene- E Pliocene	MPlm.s	Dolati (2010)
904	0	904	m	0.886	2		L Miocene- E Pliocene	MPlm.s	Dolati (2010)
905	0	905	m	0.123	2		L Miocene- E Pliocene	MPlm.s	Dolati (2010)
906	0	906	m	0.080	2		L Miocene- E Pliocene	MPlm.s	Dolati (2010)
907	0	907	m	0.085	2		L Miocene- E Pliocene	MPlm.s	Dolati (2010)
908	0	908	m	0.138	2		L Miocene- E Pliocene	MPlm.s	Dolati (2010)
909	0	909	m	10.622	2		L Miocene- E Pliocene	MPlm.s	Dolati (2010)
910	0	910	m	0.244	2		L Miocene- E Pliocene	MPlm.s	Dolati (2010)
911	0	911	m	0.377	2		L Miocene- E Pliocene	MPlm.s	Dolati (2010)
912	0	912	m	0.271	2		L Miocene- E Pliocene	MPlm.s	Dolati (2010)
913	0	913	m	0.352	2		L Miocene- E Pliocene	MPlm.s	Dolati (2010)
914	0	914	m	0.097	2		L Miocene- E Pliocene	MPlm.s	Dolati (2010)
915	0	915	m	3.595	2		L Miocene- E Pliocene	MPlm.s	Dolati (2010)
916	0	916	m	0.302	2		L Miocene- E Pliocene	MPlm.s	Dolati (2010)
917	0	917	m	0.759	2		L Miocene- E Pliocene	MPlm.s	Dolati (2010)
918	0	918	m	0.258	2		L Miocene- E Pliocene	MPlm.s	Dolati (2010)
919	0	919	m	0.226	2		L Miocene- E Pliocene	MPlm.s	Dolati (2010)
920	0	920	m	0.060	2		L Miocene- E Pliocene	MPlm.s	Dolati (2010)
921	0	921	m	0.471	2		L Miocene- E Pliocene	MPlm.s	Dolati (2010)
922	0	922	m	0.100	2		L Miocene- E Pliocene	MPlm.s	Dolati (2010)
923	0	923	m	2.659	2		L Miocene- E Pliocene	MPlm.s	Dolati (2010)
924	0	924	m	1.247	2		L Miocene- E Pliocene	MPlm.s	Dolati (2010)
925	0	925	m	0.333	2		L Miocene- E Pliocene	MPlm.s	Dolati (2010)

Geonavis

OBJECTID_1	Join_Count	TARGET_FID	label	Shape_Area (sqkm)	ORIG_FID	Absolute_Age	Age_paleontology	Unit	Reference
926	0	926	m	0.196	2		L Miocene- E Pliocene	MPlm.s	Dolati (2010)
927	0	927	m	0.040	2		L Miocene- E Pliocene	MPlm.s	Dolati (2010)
928	0	928	m	0.138	2		L Miocene- E Pliocene	MPlm.s	Dolati (2010)
930	0	930	m	0.624	2		L Miocene- E Pliocene	MPlm.s	Dolati (2010)
931	0	931	m	0.322	2		L Miocene- E Pliocene	MPlm.s	Dolati (2010)
933	0	933	m	0.984	2		L Miocene- E Pliocene	MPlm.s	Dolati (2010)
934	0	934	m	0.105	2		L Miocene- E Pliocene	MPlm.s	Dolati (2010)
935	0	935	m	1.989	2		L Miocene- E Pliocene	MPlm.s	Dolati (2010)
936	0	936	m	0.041	2		L Miocene- E Pliocene	MPlm.s	Dolati (2010)
937	0	937	m	0.095	2		L Miocene- E Pliocene	MPlm.s	Dolati (2010)
938	0	938	m	0.141	2		L Miocene- E Pliocene	MPlm.s	Dolati (2010)
939	0	939	m	0.439	2		L Miocene- E Pliocene	MPlm.s	Dolati (2010)
940	0	940	m	0.058	2		L Miocene- E Pliocene	MPlm.s	Dolati (2010)
941	0	941	m	0.079	2		L Miocene- E Pliocene	MPlm.s	Dolati (2010)
942	0	942	m	0.099	2		L Miocene- E Pliocene	MPlm.s	Dolati (2010)
943	0	943	m	0.312	2		L Miocene- E Pliocene	MPlm.s	Dolati (2010)
944	0	944	m	0.020	2		L Miocene- E Pliocene	MPlm.s	Dolati (2010)
945	0	945	m	0.042	2		L Miocene- E Pliocene	MPlm.s	Dolati (2010)
946	0	946	m	0.193	2		L Miocene- E Pliocene	MPlm.s	Dolati (2010)
947	0	947	m	0.294	2		L Miocene- E Pliocene	MPlm.s	Dolati (2010)
949	0	949	m	0.068	2		L Miocene- E Pliocene	MPlm.s	Dolati (2010)
950	0	950	m	0.145	2		L Miocene- E Pliocene	MPlm.s	Dolati (2010)
951	0	951	m	0.452	2		L Miocene- E Pliocene	MPlm.s	Dolati (2010)
952	0	952	m	0.587	2		L Miocene- E Pliocene	MPlm.s	Dolati (2010)
953	0	953	m	0.054	2		L Miocene- E Pliocene	MPlm.s	Dolati (2010)
954	0	954	m	0.598	2		L Miocene- E Pliocene	MPlm.s	Dolati (2010)
955	0	955	m	0.259	2		L Miocene- E Pliocene	MPlm.s	Dolati (2010)
956	0	956	m	0.106	2		L Miocene- E Pliocene	MPlm.s	Dolati (2010)
957	0	957	m	1.075	2		L Miocene- E Pliocene	MPlm.s	Dolati (2010)
958	0	958	m	0.816	2		L Miocene- E Pliocene	MPlm.s	Dolati (2010)
959	0	959	m	0.424	2		L Miocene- E Pliocene	MPlm.s	Dolati (2010)
960	0	960	m	1.760	2		L Miocene- E Pliocene	MPlm.s	Dolati (2010)
961	0	961	m	0.563	2		L Miocene- E Pliocene	MPlm.s	Dolati (2010)
962	0	962	m	0.081	2		L Miocene- E Pliocene	MPlm.s	Dolati (2010)
963	0	963	m	0.051	2		L Miocene- E Pliocene	MPlm.s	Dolati (2010)
965	0	965	m	0.031	2		L Miocene- E Pliocene	MPlm.s	Dolati (2010)
966	0	966	m	0.076	2		L Miocene- E Pliocene	MPlm.s	Dolati (2010)
967	0	967	m	0.145	2		L Miocene- E Pliocene	MPlm.s	Dolati (2010)
968	0	968	m	6.129	2		L Miocene- E Pliocene	MPlm.s	Dolati (2010)

GeoNeXus

OBJECTID_1	Join_Count	TARGET_FID	label	Shape_Area (sqkm)	ORIG_FID	Absolute_Age	Age_paleontology	Unit	Reference
969	0	969	m	0.301	2		L Miocene- E Pliocene	MPlm.s	Dolati (2010)
970	0	970	m	0.216	2		L Miocene- E Pliocene	MPlm.s	Dolati (2010)
971	0	971	m	3.323	2		L Miocene- E Pliocene	MPlm.s	Dolati (2010)
972	0	972	m	0.436	2		L Miocene- E Pliocene	MPlm.s	Dolati (2010)
973	0	973	m	0.766	2		L Miocene- E Pliocene	MPlm.s	Dolati (2010)
974	0	974	m	1.604	2		L Miocene- E Pliocene	MPlm.s	Dolati (2010)
975	0	975	m	0.600	2		L Miocene- E Pliocene	MPlm.s	Dolati (2010)
976	0	976	m	0.543	2		L Miocene- E Pliocene	MPlm.s	Dolati (2010)
977	0	977	m	0.350	2		L Miocene- E Pliocene	MPlm.s	Dolati (2010)
978	0	978	m	0.167	2		L Miocene- E Pliocene	MPlm.s	Dolati (2010)
979	0	979	m	0.276	2		L Miocene- E Pliocene	MPlm.s	Dolati (2010)
980	0	980	m	0.177	2		L Miocene- E Pliocene	MPlm.s	Dolati (2010)
981	0	981	m	0.057	2		L Miocene- E Pliocene	MPlm.s	Dolati (2010)
982	0	982	m	0.631	2		L Miocene- E Pliocene	MPlm.s	Dolati (2010)
983	0	983	m	0.055	2		L Miocene- E Pliocene	MPlm.s	Dolati (2010)
984	0	984	m	0.088	2		L Miocene- E Pliocene	MPlm.s	Dolati (2010)
985	0	985	m	0.172	2		L Miocene- E Pliocene	MPlm.s	Dolati (2010)
986	0	986	m	1.417	2		L Miocene- E Pliocene	MPlm.s	Dolati (2010)
987	0	987	m	0.679	2		L Miocene- E Pliocene	MPlm.s	Dolati (2010)
988	0	988	m	1.466	2		L Miocene- E Pliocene	MPlm.s	Dolati (2010)
989	0	989	m	0.022	2		L Miocene- E Pliocene	MPlm.s	Dolati (2010)
990	0	990	m	0.485	2		L Miocene- E Pliocene	MPlm.s	Dolati (2010)
991	0	991	m	0.988	2		L Miocene- E Pliocene	MPlm.s	Dolati (2010)
992	0	992	m	24.342	2		L Miocene- E Pliocene	MPlm.s	Dolati (2010)
993	0	993	m	0.103	2		L Miocene- E Pliocene	MPlm.s	Dolati (2010)
994	0	994	m	1.162	2		L Miocene- E Pliocene	MPlm.s	Dolati (2010)
995	0	995	m	0.118	2		L Miocene- E Pliocene	MPlm.s	Dolati (2010)
996	0	996	m	0.018	2		L Miocene- E Pliocene	MPlm.s	Dolati (2010)
997	0	997	m	1.638	2		L Miocene- E Pliocene	MPlm.s	Dolati (2010)
998	0	998	m	0.091	2		L Miocene- E Pliocene	MPlm.s	Dolati (2010)
999	0	999	m	0.095	2		L Miocene- E Pliocene	MPlm.s	Dolati (2010)
1000	0	1000	m	0.206	2		L Miocene- E Pliocene	MPlm.s	Dolati (2010)
1001	0	1001	m	0.048	2		L Miocene- E Pliocene	MPlm.s	Dolati (2010)
1002	0	1002	m	0.162	2		L Miocene- E Pliocene	MPlm.s	Dolati (2010)
1003	0	1003	m	1.314	2		L Miocene- E Pliocene	MPlm.s	Dolati (2010)
1004	0	1004	m	0.210	2		L Miocene- E Pliocene	MPlm.s	Dolati (2010)
1005	0	1005	m	1.508	2		L Miocene- E Pliocene	MPlm.s	Dolati (2010)
1006	0	1006	m	1.371	2		L Miocene- E Pliocene	MPlm.s	Dolati (2010)
1007	0	1007	m	0.040	2		L Miocene- E Pliocene	MPlm.s	Dolati (2010)

GeoAI

OBJECTID_1	Join_Count	TARGET_FID	label	Shape_Area (sqkm)	ORIG_FID	Absolute_Age	Age_paleontology	Unit	Reference
1008	0	1008	m	0.087	2		L Miocene- E Pliocene	MPlm.s	Dolati (2010)
1009	0	1009	m	1.462	2		L Miocene- E Pliocene	MPlm.s	Dolati (2010)
1010	0	1010	m	0.040	2		L Miocene- E Pliocene	MPlm.s	Dolati (2010)
1011	0	1011	m	0.034	2		L Miocene- E Pliocene	MPlm.s	Dolati (2010)
1012	0	1012	m	0.117	2		L Miocene- E Pliocene	MPlm.s	Dolati (2010)
1013	0	1013	m	0.236	2		L Miocene- E Pliocene	MPlm.s	Dolati (2010)
1014	0	1014	m	0.119	2		L Miocene- E Pliocene	MPlm.s	Dolati (2010)
1015	0	1015	m	8.671	2		L Miocene- E Pliocene	MPlm.s	Dolati (2010)
1016	0	1016	m	0.436	2		L Miocene- E Pliocene	MPlm.s	Dolati (2010)
1017	0	1017	m	1.694	2		L Miocene- E Pliocene	MPlm.s	Dolati (2010)
1018	0	1018	m	0.583	2		L Miocene- E Pliocene	MPlm.s	Dolati (2010)
1019	0	1019	m	0.683	2		L Miocene- E Pliocene	MPlm.s	Dolati (2010)
1020	0	1020	m	0.110	2		L Miocene- E Pliocene	MPlm.s	Dolati (2010)
1021	0	1021	m	0.215	2		L Miocene- E Pliocene	MPlm.s	Dolati (2010)
1022	0	1022	m	0.158	2		L Miocene- E Pliocene	MPlm.s	Dolati (2010)
1023	0	1023	m	0.199	2		L Miocene- E Pliocene	MPlm.s	Dolati (2010)
1024	0	1024	m	0.258	2		L Miocene- E Pliocene	MPlm.s	Dolati (2010)
1025	0	1025	m	0.121	2		L Miocene- E Pliocene	MPlm.s	Dolati (2010)
1026	0	1026	m	1.232	2		L Miocene- E Pliocene	MPlm.s	Dolati (2010)
1027	0	1027	m	0.403	2		L Miocene- E Pliocene	MPlm.s	Dolati (2010)
1028	0	1028	m	0.081	2		L Miocene- E Pliocene	MPlm.s	Dolati (2010)
1029	0	1029	m	0.595	2		L Miocene- E Pliocene	MPlm.s	Dolati (2010)
1030	0	1030	m	0.085	2		L Miocene- E Pliocene	MPlm.s	Dolati (2010)
1031	0	1031	m	0.096	2		L Miocene- E Pliocene	MPlm.s	Dolati (2010)
1032	0	1032	m	0.143	2		L Miocene- E Pliocene	MPlm.s	Dolati (2010)
1033	0	1033	m	0.115	2		L Miocene- E Pliocene	MPlm.s	Dolati (2010)
1034	0	1034	m	0.120	2		L Miocene- E Pliocene	MPlm.s	Dolati (2010)
1035	0	1035	m	0.083	2		L Miocene- E Pliocene	MPlm.s	Dolati (2010)
1036	0	1036	m	0.243	2		L Miocene- E Pliocene	MPlm.s	Dolati (2010)
1037	0	1037	m	0.403	2		L Miocene- E Pliocene	MPlm.s	Dolati (2010)
1038	0	1038	m	0.052	2		L Miocene- E Pliocene	MPlm.s	Dolati (2010)
1039	0	1039	m	0.136	2		L Miocene- E Pliocene	MPlm.s	Dolati (2010)
1040	0	1040	m	0.657	2		L Miocene- E Pliocene	MPlm.s	Dolati (2010)
1041	0	1041	m	0.160	2		L Miocene- E Pliocene	MPlm.s	Dolati (2010)
1042	0	1042	m	0.045	2		L Miocene- E Pliocene	MPlm.s	Dolati (2010)
1043	0	1043	m	0.058	2		L Miocene- E Pliocene	MPlm.s	Dolati (2010)
1044	0	1044	m	0.164	2		L Miocene- E Pliocene	MPlm.s	Dolati (2010)
1045	0	1045	m	0.040	2		L Miocene- E Pliocene	MPlm.s	Dolati (2010)
1046	0	1046	m	1.722	2		L Miocene- E Pliocene	MPlm.s	Dolati (2010)

GeoNeXus

OBJECTID_1	Join_Count	TARGET_FID	label	Shape_Area (sqkm)	ORIG_FID	Absolute_Age	Age_paleontology	Unit	Reference
1047	0	1047	m	0.120	2		L Miocene- E Pliocene	MPlm.s	Dolati (2010)
1048	0	1048	m	0.012	2		L Miocene- E Pliocene	MPlm.s	Dolati (2010)
1049	0	1049	m	0.375	2		L Miocene- E Pliocene	MPlm.s	Dolati (2010)
1050	0	1050	m	0.068	2		L Miocene- E Pliocene	MPlm.s	Dolati (2010)
1051	0	1051	m	1.008	2		L Miocene- E Pliocene	MPlm.s	Dolati (2010)
1052	0	1052	m	0.272	2		L Miocene- E Pliocene	MPlm.s	Dolati (2010)
1053	0	1053	m	5.060	2		L Miocene- E Pliocene	MPlm.s	Dolati (2010)
1054	0	1054	m	2.526	2		L Miocene- E Pliocene	MPlm.s	Dolati (2010)
1055	0	1055	m	0.052	2		L Miocene- E Pliocene	MPlm.s	Dolati (2010)
1056	0	1056	m	0.300	2		L Miocene- E Pliocene	MPlm.s	Dolati (2010)
1057	0	1057	m	0.381	2		L Miocene- E Pliocene	MPlm.s	Dolati (2010)
1058	0	1058	m	0.822	2		L Miocene- E Pliocene	MPlm.s	Dolati (2010)
1059	0	1059	m	0.679	2		L Miocene- E Pliocene	MPlm.s	Dolati (2010)
1060	0	1060	m	6.710	2		L Miocene- E Pliocene	MPlm.s	Dolati (2010)
1061	0	1061	m	1.159	2		L Miocene- E Pliocene	MPlm.s	Dolati (2010)
1062	0	1062	m	2.665	2		L Miocene- E Pliocene	MPlm.s	Dolati (2010)
1063	0	1063	m	0.637	2		L Miocene- E Pliocene	MPlm.s	Dolati (2010)
1064	0	1064	m	0.208	2		L Miocene- E Pliocene	MPlm.s	Dolati (2010)
1065	0	1065	m	10.591	2		L Miocene- E Pliocene	MPlm.s	Dolati (2010)
1066	0	1066	m	1.710	2		L Miocene- E Pliocene	MPlm.s	Dolati (2010)
1067	0	1067	m	1.412	2		L Miocene- E Pliocene	MPlm.s	Dolati (2010)
1068	0	1068	m	0.477	2		L Miocene- E Pliocene	MPlm.s	Dolati (2010)
1069	0	1069	m	6.039	2		L Miocene- E Pliocene	MPlm.s	Dolati (2010)
1070	0	1070	m	0.779	2		L Miocene- E Pliocene	MPlm.s	Dolati (2010)
1071	0	1071	m	0.200	2		L Miocene- E Pliocene	MPlm.s	Dolati (2010)
1072	0	1072	m	0.615	2		L Miocene- E Pliocene	MPlm.s	Dolati (2010)
1073	0	1073	m	0.701	2		L Miocene- E Pliocene	MPlm.s	Dolati (2010)
1074	0	1074	m	0.204	2		L Miocene- E Pliocene	MPlm.s	Dolati (2010)
1075	0	1075	m	0.305	2		L Miocene- E Pliocene	MPlm.s	Dolati (2010)
1076	0	1076	m	4.868	2		L Miocene- E Pliocene	MPlm.s	Dolati (2010)
1077	0	1077	m	0.564	2		L Miocene- E Pliocene	MPlm.s	Dolati (2010)
1078	0	1078	m	0.384	2		L Miocene- E Pliocene	MPlm.s	Dolati (2010)
1079	0	1079	m	0.787	2		L Miocene- E Pliocene	MPlm.s	Dolati (2010)
1080	0	1080	m	0.046	2		L Miocene- E Pliocene	MPlm.s	Dolati (2010)
1081	0	1081	m	0.564	2		L Miocene- E Pliocene	MPlm.s	Dolati (2010)
1082	0	1082	m	0.073	2		L Miocene- E Pliocene	MPlm.s	Dolati (2010)
1083	0	1083	m	0.246	2		L Miocene- E Pliocene	MPlm.s	Dolati (2010)
1084	0	1084	m	0.216	2		L Miocene- E Pliocene	MPlm.s	Dolati (2010)
1085	0	1085	m	0.129	2		L Miocene- E Pliocene	MPlm.s	Dolati (2010)

GeoAI

OBJECTID_1	Join_Count	TARGET_FID	label	Shape_Area (sqkm)	ORIG_FID	Absolute_Age	Age_paleontology	Unit	Reference
1086	0	1086	m	0.357	2		L Miocene- E Pliocene	MPlm.s	Dolati (2010)
1087	0	1087	m	0.545	2		L Miocene- E Pliocene	MPlm.s	Dolati (2010)
1089	0	1089	m	0.562	2		L Miocene- E Pliocene	MPlm.s	Dolati (2010)
1090	0	1090	m	0.262	2		L Miocene- E Pliocene	MPlm.s	Dolati (2010)
1091	0	1091	m	0.082	2		L Miocene- E Pliocene	MPlm.s	Dolati (2010)
1092	0	1092	m	0.089	2		L Miocene- E Pliocene	MPlm.s	Dolati (2010)
1093	0	1093	m	0.180	2		L Miocene- E Pliocene	MPlm.s	Dolati (2010)
1094	0	1094	m	0.055	2		L Miocene- E Pliocene	MPlm.s	Dolati (2010)
1095	0	1095	m	0.386	2		L Miocene- E Pliocene	MPlm.s	Dolati (2010)
1096	0	1096	m	0.289	2		L Miocene- E Pliocene	MPlm.s	Dolati (2010)
1097	0	1097	m	0.060	2		L Miocene- E Pliocene	MPlm.s	Dolati (2010)
1098	0	1098	m	0.322	2		L Miocene- E Pliocene	MPlm.s	Dolati (2010)
1099	0	1099	m	0.337	2		L Miocene- E Pliocene	MPlm.s	Dolati (2010)
1100	0	1100	m	0.377	2		L Miocene- E Pliocene	MPlm.s	Dolati (2010)
1101	0	1101	m	0.344	2		L Miocene- E Pliocene	MPlm.s	Dolati (2010)
1102	0	1102	m	0.120	2		L Miocene- E Pliocene	MPlm.s	Dolati (2010)
1103	0	1103	m	0.101	2		L Miocene- E Pliocene	MPlm.s	Dolati (2010)
1104	0	1104	m	0.267	2		L Miocene- E Pliocene	MPlm.s	Dolati (2010)
1106	0	1106	m	0.232	2		L Miocene- E Pliocene	MPlm.s	Dolati (2010)
1107	0	1107	m	0.124	2		L Miocene- E Pliocene	MPlm.s	Dolati (2010)
1108	0	1108	m	0.433	2		L Miocene- E Pliocene	MPlm.s	Dolati (2010)
1109	0	1109	m	0.960	2		L Miocene- E Pliocene	MPlm.s	Dolati (2010)
1110	0	1110	m	6.519	2		L Miocene- E Pliocene	MPlm.s	Dolati (2010)
1111	0	1111	m	0.036	2		L Miocene- E Pliocene	MPlm.s	Dolati (2010)
1112	0	1112	m	1.295	2		L Miocene- E Pliocene	MPlm.s	Dolati (2010)
1113	0	1113	m	1.372	2		L Miocene- E Pliocene	MPlm.s	Dolati (2010)
1114	0	1114	m	0.244	2		L Miocene- E Pliocene	MPlm.s	Dolati (2010)
1115	0	1115	m	0.012	2		L Miocene- E Pliocene	MPlm.s	Dolati (2010)
1116	0	1116	m	0.212	2		L Miocene- E Pliocene	MPlm.s	Dolati (2010)
1117	0	1117	m	0.553	2		L Miocene- E Pliocene	MPlm.s	Dolati (2010)
1118	0	1118	m	0.865	2		L Miocene- E Pliocene	MPlm.s	Dolati (2010)
1119	0	1119	m	0.013	2		L Miocene- E Pliocene	MPlm.s	Dolati (2010)
1120	0	1120	m	0.251	2		L Miocene- E Pliocene	MPlm.s	Dolati (2010)
1121	0	1121	m	0.371	2		L Miocene- E Pliocene	MPlm.s	Dolati (2010)
1122	0	1122	m	1.144	2		L Miocene- E Pliocene	MPlm.s	Dolati (2010)
1123	0	1123	m	0.078	2		L Miocene- E Pliocene	MPlm.s	Dolati (2010)
1124	0	1124	m	1.212	2		L Miocene- E Pliocene	MPlm.s	Dolati (2010)
1125	0	1125	m	0.428	2		L Miocene- E Pliocene	MPlm.s	Dolati (2010)
1126	0	1126	m	0.950	2		L Miocene- E Pliocene	MPlm.s	Dolati (2010)

GeoNeus

OBJECTID_1	Join_Count	TARGET_FID	label	Shape_Area (sqkm)	ORIG_FID	Absolute_Age	Age_paleontology	Unit	Reference
1127	0	1127	m	0.212	2		L Miocene- E Pliocene	MPlm.s	Dolati (2010)
1128	0	1128	m	0.367	2		L Miocene- E Pliocene	MPlm.s	Dolati (2010)
2055	2	2055	m	0.933	4		L Miocene- E Pliocene	MPlm.s	Dolati (2010)
10411	1	10420	m	0.073	0		L Miocene- E Pliocene	MPlm.s	Dolati (2010)
10416	2	10427	m	0.114	0		L Miocene- E Pliocene	MPlm.s	Dolati (2010)
10420	1	10434	m	0.004	0		L Miocene- E Pliocene	MPlm.s	Dolati (2010)
10421	1	10436	m	0.013	0		L Miocene- E Pliocene	MPlm.s	Dolati (2010)
10422	2	10438	m	0.016	0		L Miocene- E Pliocene	MPlm.s	Dolati (2010)
10423	1	10439	m	0.007	0		L Miocene- E Pliocene	MPlm.s	Dolati (2010)
10424	1	10441	m	0.002	0		L Miocene- E Pliocene	MPlm.s	Dolati (2010)
10425	1	10443	m	0.006	0		L Miocene- E Pliocene	MPlm.s	Dolati (2010)
10434	1	10458	m	0.010	0		L Miocene- E Pliocene	MPlm.s	Dolati (2010)
10454	1	9566	m	0.002	17		L Miocene- E Pliocene	MPlm.s	Dolati (2010)
10455	1	9566	m	0.001	17		L Miocene- E Pliocene	MPlm.s	Dolati (2010)
10456	0	8541	m	0.001	15		L Miocene- E Pliocene	MPlm.s	Dolati (2010)
10457	0	4452	m	0.004	8			MPlm.s	Dolati (2010)

GeoNeAIS

Table S7. Summary of mapped polygons for the MPl$^{m.s.c}$ Unit.

OBJECTID_1	Join_Count	TARGET_FID	label	Shape_Area (sqkm)	ORIG_FID	Absolute_Age	Age_paleontology	Unit	Reference
1129	0	1129	m.w	1.635	3		L Miocene- E Pliocene	MPlm.s.c	Dolati (2010)
1130	0	1130	m.w	0.099	3		L Miocene- E Pliocene	MPlm.s.c	Dolati (2010)
1131	0	1131	m.w	0.095	3		L Miocene- E Pliocene	MPlm.s.c	Dolati (2010)
1132	0	1132	m.w	1.174	3		L Miocene- E Pliocene	MPlm.s.c	Dolati (2010)
1133	0	1133	m.w	0.012	3		L Miocene- E Pliocene	MPlm.s.c	Dolati (2010)
1134	0	1134	m.w	0.025	3		L Miocene- E Pliocene	MPlm.s.c	Dolati (2010)
1135	0	1135	m.w	2.544	3		L Miocene- E Pliocene	MPlm.s.c	Dolati (2010)
1136	0	1136	m.w	0.067	3		L Miocene- E Pliocene	MPlm.s.c	Dolati (2010)
1137	0	1137	m.w	0.127	3		L Miocene- E Pliocene	MPlm.s.c	Dolati (2010)
1138	0	1138	m.w	0.023	3		L Miocene- E Pliocene	MPlm.s.c	Dolati (2010)
1139	0	1139	m.w	0.639	3		L Miocene- E Pliocene	MPlm.s.c	Dolati (2010)
1140	0	1140	m.w	0.069	3		L Miocene- E Pliocene	MPlm.s.c	Dolati (2010)
1141	0	1141	m.w	0.149	3		L Miocene- E Pliocene	MPlm.s.c	Dolati (2010)
1142	0	1142	m.w	0.093	3		L Miocene- E Pliocene	MPlm.s.c	Dolati (2010)
1143	0	1143	m.w	0.029	3		L Miocene- E Pliocene	MPlm.s.c	Dolati (2010)
1144	0	1144	m.w	0.534	3		L Miocene- E Pliocene	MPlm.s.c	Dolati (2010)
1145	0	1145	m.w	0.025	3		L Miocene- E Pliocene	MPlm.s.c	Dolati (2010)
1146	0	1146	m.w	0.052	3		L Miocene- E Pliocene	MPlm.s.c	Dolati (2010)
1147	0	1147	m.w	0.344	3		L Miocene- E Pliocene	MPlm.s.c	Dolati (2010)
1148	0	1148	m.w	1.780	3		L Miocene- E Pliocene	MPlm.s.c	Dolati (2010)
1149	0	1149	m.w	0.055	3		L Miocene- E Pliocene	MPlm.s.c	Dolati (2010)
1150	0	1150	m.w	0.021	3		L Miocene- E Pliocene	MPlm.s.c	Dolati (2010)
1151	0	1151	m.w	0.064	3		L Miocene- E Pliocene	MPlm.s.c	Dolati (2010)
1152	0	1152	m.w	11.878	3		L Miocene- E Pliocene	MPlm.s.c	Dolati (2010)
1153	0	1153	m.w	0.149	3		L Miocene- E Pliocene	MPlm.s.c	Dolati (2010)
1154	0	1154	m.w	0.142	3		L Miocene- E Pliocene	MPlm.s.c	Dolati (2010)
1155	0	1155	m.w	0.081	3		L Miocene- E Pliocene	MPlm.s.c	Dolati (2010)
1156	0	1156	m.w	0.421	3		L Miocene- E Pliocene	MPlm.s.c	Dolati (2010)
1157	0	1157	m.w	0.281	3		L Miocene- E Pliocene	MPlm.s.c	Dolati (2010)
1158	0	1158	m.w	0.183	3		L Miocene- E Pliocene	MPlm.s.c	Dolati (2010)
1159	0	1159	m.w	0.051	3		L Miocene- E Pliocene	MPlm.s.c	Dolati (2010)
1160	0	1160	m.w	0.273	3		L Miocene- E Pliocene	MPlm.s.c	Dolati (2010)
1161	0	1161	m.w	0.306	3		L Miocene- E Pliocene	MPlm.s.c	Dolati (2010)
1162	0	1162	m.w	0.114	3		L Miocene- E Pliocene	MPlm.s.c	Dolati (2010)
1163	0	1163	m.w	0.036	3		L Miocene- E Pliocene	MPlm.s.c	Dolati (2010)
1164	0	1164	m.w	0.073	3		L Miocene- E Pliocene	MPlm.s.c	Dolati (2010)
1165	0	1165	m.w	0.032	3		L Miocene- E Pliocene	MPlm.s.c	Dolati (2010)
1166	0	1166	m.w	0.184	3		L Miocene- E Pliocene	MPlm.s.c	Dolati (2010)

GeoNeAS

OBJECTID_1	Join_Count	TARGET_FID	label	Shape_Area (sqkm)	ORIG_FID	Absolute_Age	Age_paleontology	Unit	Reference
1167	0	1167	m.w	5.222	3		L Miocene- E Pliocene	MPlm.s.c	Dolati (2010)
1168	0	1168	m.w	1.086	3		L Miocene- E Pliocene	MPlm.s.c	Dolati (2010)
1169	0	1169	m.w	0.024	3		L Miocene- E Pliocene	MPlm.s.c	Dolati (2010)
1170	0	1170	m.w	0.071	3		L Miocene- E Pliocene	MPlm.s.c	Dolati (2010)
1171	0	1171	m.w	0.033	3		L Miocene- E Pliocene	MPlm.s.c	Dolati (2010)
1172	0	1172	m.w	0.219	3		L Miocene- E Pliocene	MPlm.s.c	Dolati (2010)
1173	0	1173	m.w	3.019	3		L Miocene- E Pliocene	MPlm.s.c	Dolati (2010)
1174	0	1174	m.w	0.697	3		L Miocene- E Pliocene	MPlm.s.c	Dolati (2010)
1175	0	1175	m.w	0.297	3		L Miocene- E Pliocene	MPlm.s.c	Dolati (2010)
1176	0	1176	m.w	0.074	3		L Miocene- E Pliocene	MPlm.s.c	Dolati (2010)
1177	0	1177	m.w	0.011	3		L Miocene- E Pliocene	MPlm.s.c	Dolati (2010)
1179	0	1179	m.w	0.258	3		L Miocene- E Pliocene	MPlm.s.c	Dolati (2010)
1180	0	1180	m.w	0.820	3		L Miocene- E Pliocene	MPlm.s.c	Dolati (2010)
1181	0	1181	m.w	0.054	3		L Miocene- E Pliocene	MPlm.s.c	Dolati (2010)
1183	0	1183	m.w	0.048	3		L Miocene- E Pliocene	MPlm.s.c	Dolati (2010)
1184	0	1184	m.w	0.147	3		L Miocene- E Pliocene	MPlm.s.c	Dolati (2010)
1185	0	1185	m.w	0.030	3		L Miocene- E Pliocene	MPlm.s.c	Dolati (2010)
1186	0	1186	m.w	0.047	3		L Miocene- E Pliocene	MPlm.s.c	Dolati (2010)
1187	0	1187	m.w	0.314	3		L Miocene- E Pliocene	MPlm.s.c	Dolati (2010)
1188	0	1188	m.w	0.507	3		L Miocene- E Pliocene	MPlm.s.c	Dolati (2010)
1189	0	1189	m.w	0.082	3		L Miocene- E Pliocene	MPlm.s.c	Dolati (2010)
1190	0	1190	m.w	0.378	3		L Miocene- E Pliocene	MPlm.s.c	Dolati (2010)
1191	0	1191	m.w	0.076	3		L Miocene- E Pliocene	MPlm.s.c	Dolati (2010)
1192	0	1192	m.w	0.227	3		L Miocene- E Pliocene	MPlm.s.c	Dolati (2010)
1193	0	1193	m.w	0.145	3		L Miocene- E Pliocene	MPlm.s.c	Dolati (2010)
1194	0	1194	m.w	0.032	3		L Miocene- E Pliocene	MPlm.s.c	Dolati (2010)
1195	0	1195	m.w	0.018	3		L Miocene- E Pliocene	MPlm.s.c	Dolati (2010)
1196	0	1196	m.w	0.009	3		L Miocene- E Pliocene	MPlm.s.c	Dolati (2010)
1197	0	1197	m.w	0.067	3		L Miocene- E Pliocene	MPlm.s.c	Dolati (2010)
1198	0	1198	m.w	0.026	3		L Miocene- E Pliocene	MPlm.s.c	Dolati (2010)
1199	0	1199	m.w	0.231	3		L Miocene- E Pliocene	MPlm.s.c	Dolati (2010)
1200	0	1200	m.w	0.146	3		L Miocene- E Pliocene	MPlm.s.c	Dolati (2010)
1201	0	1201	m.w	0.022	3		L Miocene- E Pliocene	MPlm.s.c	Dolati (2010)
1202	0	1202	m.w	0.056	3		L Miocene- E Pliocene	MPlm.s.c	Dolati (2010)
1203	0	1203	m.w	0.036	3		L Miocene- E Pliocene	MPlm.s.c	Dolati (2010)
1204	0	1204	m.w	0.073	3		L Miocene- E Pliocene	MPlm.s.c	Dolati (2010)
1205	0	1205	m.w	0.010	3		L Miocene- E Pliocene	MPlm.s.c	Dolati (2010)
1206	0	1206	m.w	1.356	3		L Miocene- E Pliocene	MPlm.s.c	Dolati (2010)
1207	0	1207	m.w	0.013	3		L Miocene- E Pliocene	MPlm.s.c	Dolati (2010)

GeoMLS

OBJECTID_1	Join_Count	TARGET_FID	label	Shape_Area (sqkm)	ORIG_FID	Absolute_Age	Age_paleontology	Unit	Reference
1208	0	1208	m.w	0.349	3		L Miocene- E Pliocene	MPlm.s.c	Dolati (2010)
1209	0	1209	m.w	0.024	3		L Miocene- E Pliocene	MPlm.s.c	Dolati (2010)
1210	0	1210	m.w	0.077	3		L Miocene- E Pliocene	MPlm.s.c	Dolati (2010)
1211	0	1211	m.w	0.080	3		L Miocene- E Pliocene	MPlm.s.c	Dolati (2010)
1212	0	1212	m.w	0.015	3		L Miocene- E Pliocene	MPlm.s.c	Dolati (2010)
1213	0	1213	m.w	0.149	3		L Miocene- E Pliocene	MPlm.s.c	Dolati (2010)
1214	0	1214	m.w	0.030	3		L Miocene- E Pliocene	MPlm.s.c	Dolati (2010)
1215	0	1215	m.w	0.336	3		L Miocene- E Pliocene	MPlm.s.c	Dolati (2010)
1216	0	1216	m.w	0.060	3		L Miocene- E Pliocene	MPlm.s.c	Dolati (2010)
1217	0	1217	m.w	0.419	3		L Miocene- E Pliocene	MPlm.s.c	Dolati (2010)
1218	0	1218	m.w	0.074	3		L Miocene- E Pliocene	MPlm.s.c	Dolati (2010)
1219	0	1219	m.w	0.011	3		L Miocene- E Pliocene	MPlm.s.c	Dolati (2010)
1220	0	1220	m.w	0.016	3		L Miocene- E Pliocene	MPlm.s.c	Dolati (2010)
1221	0	1221	m.w	0.359	3		L Miocene- E Pliocene	MPlm.s.c	Dolati (2010)
1222	0	1222	m.w	0.191	3		L Miocene- E Pliocene	MPlm.s.c	Dolati (2010)
1223	0	1223	m.w	0.067	3		L Miocene- E Pliocene	MPlm.s.c	Dolati (2010)
1224	0	1224	m.w	66.189	3		L Miocene- E Pliocene	MPlm.s.c	Dolati (2010)
1225	0	1225	m.w	0.026	3		L Miocene- E Pliocene	MPlm.s.c	Dolati (2010)
1226	0	1226	m.w	0.028	3		L Miocene- E Pliocene	MPlm.s.c	Dolati (2010)
1227	0	1227	m.w	0.626	3		L Miocene- E Pliocene	MPlm.s.c	Dolati (2010)
1228	0	1228	m.w	0.013	3		L Miocene- E Pliocene	MPlm.s.c	Dolati (2010)
1229	0	1229	m.w	0.014	3		L Miocene- E Pliocene	MPlm.s.c	Dolati (2010)
1230	0	1230	m.w	0.045	3		L Miocene- E Pliocene	MPlm.s.c	Dolati (2010)
1231	0	1231	m.w	0.059	3		L Miocene- E Pliocene	MPlm.s.c	Dolati (2010)
1232	0	1232	m.w	0.029	3		L Miocene- E Pliocene	MPlm.s.c	Dolati (2010)
1233	0	1233	m.w	0.017	3		L Miocene- E Pliocene	MPlm.s.c	Dolati (2010)
1234	0	1234	m.w	0.043	3		L Miocene- E Pliocene	MPlm.s.c	Dolati (2010)
1235	0	1235	m.w	0.462	3		L Miocene- E Pliocene	MPlm.s.c	Dolati (2010)
1236	0	1236	m.w	0.399	3		L Miocene- E Pliocene	MPlm.s.c	Dolati (2010)
1237	0	1237	m.w	0.046	3		L Miocene- E Pliocene	MPlm.s.c	Dolati (2010)
1238	0	1238	m.w	0.024	3		L Miocene- E Pliocene	MPlm.s.c	Dolati (2010)
1239	0	1239	m.w	0.049	3		L Miocene- E Pliocene	MPlm.s.c	Dolati (2010)
1240	0	1240	m.w	0.017	3		L Miocene- E Pliocene	MPlm.s.c	Dolati (2010)
1242	0	1242	m.w	0.115	3		L Miocene- E Pliocene	MPlm.s.c	Dolati (2010)
1243	0	1243	m.w	0.338	3		L Miocene- E Pliocene	MPlm.s.c	Dolati (2010)
1244	0	1244	m.w	0.179	3		L Miocene- E Pliocene	MPlm.s.c	Dolati (2010)
1245	0	1245	m.w	0.558	3		L Miocene- E Pliocene	MPlm.s.c	Dolati (2010)
1246	0	1246	m.w	0.057	3		L Miocene- E Pliocene	MPlm.s.c	Dolati (2010)
1247	0	1247	m.w	0.037	3		L Miocene- E Pliocene	MPlm.s.c	Dolati (2010)

GeoNeXus

OBJECTID_1	Join_Count	TARGET_FID	label	Shape_Area (sqkm)	ORIG_FID	Absolute_Age	Age_paleontology	Unit	Reference
1248	0	1248	m.w	0.056	3		L Miocene- E Pliocene	MPlm.s.c	Dolati (2010)
1249	0	1249	m.w	0.042	3		L Miocene- E Pliocene	MPlm.s.c	Dolati (2010)
1250	0	1250	m.w	0.163	3		L Miocene- E Pliocene	MPlm.s.c	Dolati (2010)
1251	0	1251	m.w	6.856	3		L Miocene- E Pliocene	MPlm.s.c	Dolati (2010)
1252	0	1252	m.w	0.258	3		L Miocene- E Pliocene	MPlm.s.c	Dolati (2010)
1253	0	1253	m.w	0.037	3		L Miocene- E Pliocene	MPlm.s.c	Dolati (2010)
1254	0	1254	m.w	0.062	3		L Miocene- E Pliocene	MPlm.s.c	Dolati (2010)
1255	0	1255	m.w	0.063	3		L Miocene- E Pliocene	MPlm.s.c	Dolati (2010)
1256	0	1256	m.w	0.030	3		L Miocene- E Pliocene	MPlm.s.c	Dolati (2010)
1257	0	1257	m.w	0.017	3		L Miocene- E Pliocene	MPlm.s.c	Dolati (2010)
1258	0	1258	m.w	0.043	3		L Miocene- E Pliocene	MPlm.s.c	Dolati (2010)
1259	0	1259	m.w	0.078	3		L Miocene- E Pliocene	MPlm.s.c	Dolati (2010)
1260	0	1260	m.w	0.459	3		L Miocene- E Pliocene	MPlm.s.c	Dolati (2010)
1261	0	1261	m.w	0.120	3		L Miocene- E Pliocene	MPlm.s.c	Dolati (2010)
1263	0	1263	m.w	0.100	3		L Miocene- E Pliocene	MPlm.s.c	Dolati (2010)
1264	0	1264	m.w	0.023	3		L Miocene- E Pliocene	MPlm.s.c	Dolati (2010)
1265	0	1265	m.w	0.049	3		L Miocene- E Pliocene	MPlm.s.c	Dolati (2010)
1266	0	1266	m.w	0.027	3		L Miocene- E Pliocene	MPlm.s.c	Dolati (2010)
1267	0	1267	m.w	0.064	3		L Miocene- E Pliocene	MPlm.s.c	Dolati (2010)
1268	0	1268	m.w	0.052	3		L Miocene- E Pliocene	MPlm.s.c	Dolati (2010)
1269	0	1269	m.w	0.249	3		L Miocene- E Pliocene	MPlm.s.c	Dolati (2010)
1270	0	1270	m.w	0.059	3		L Miocene- E Pliocene	MPlm.s.c	Dolati (2010)
1271	0	1271	m.w	0.770	3		L Miocene- E Pliocene	MPlm.s.c	Dolati (2010)
1272	0	1272	m.w	0.228	3		L Miocene- E Pliocene	MPlm.s.c	Dolati (2010)
1273	0	1273	m.w	0.013	3		L Miocene- E Pliocene	MPlm.s.c	Dolati (2010)
1274	0	1274	m.w	0.059	3		L Miocene- E Pliocene	MPlm.s.c	Dolati (2010)
1275	0	1275	m.w	0.651	3		L Miocene- E Pliocene	MPlm.s.c	Dolati (2010)
1276	0	1276	m.w	0.033	3		L Miocene- E Pliocene	MPlm.s.c	Dolati (2010)
1277	0	1277	m.w	0.017	3		L Miocene- E Pliocene	MPlm.s.c	Dolati (2010)
1278	0	1278	m.w	0.121	3		L Miocene- E Pliocene	MPlm.s.c	Dolati (2010)
1279	0	1279	m.w	0.171	3		L Miocene- E Pliocene	MPlm.s.c	Dolati (2010)
1280	0	1280	m.w	0.019	3		L Miocene- E Pliocene	MPlm.s.c	Dolati (2010)
1281	0	1281	m.w	0.012	3		L Miocene- E Pliocene	MPlm.s.c	Dolati (2010)
1282	0	1282	m.w	0.199	3		L Miocene- E Pliocene	MPlm.s.c	Dolati (2010)
1283	0	1283	m.w	0.105	3		L Miocene- E Pliocene	MPlm.s.c	Dolati (2010)
1284	0	1284	m.w	0.133	3		L Miocene- E Pliocene	MPlm.s.c	Dolati (2010)
1285	0	1285	m.w	0.196	3		L Miocene- E Pliocene	MPlm.s.c	Dolati (2010)
1286	0	1286	m.w	0.132	3		L Miocene- E Pliocene	MPlm.s.c	Dolati (2010)
1287	0	1287	m.w	0.027	3		L Miocene- E Pliocene	MPlm.s.c	Dolati (2010)

GeoMLA

OBJECTID_1	Join_Count	TARGET_FID	label	Shape_Area (sqkm)	ORIG_FID	Absolute_Age	Age_paleontology	Unit	Reference
1288	0	1288	m.w	0.128	3		L Miocene- E Pliocene	MPlm.s.c	Dolati (2010)
1289	0	1289	m.w	0.090	3		L Miocene- E Pliocene	MPlm.s.c	Dolati (2010)
1290	0	1290	m.w	0.040	3		L Miocene- E Pliocene	MPlm.s.c	Dolati (2010)
1291	0	1291	m.w	0.026	3		L Miocene- E Pliocene	MPlm.s.c	Dolati (2010)
1292	0	1292	m.w	1.696	3		L Miocene- E Pliocene	MPlm.s.c	Dolati (2010)
1293	0	1293	m.w	0.036	3		L Miocene- E Pliocene	MPlm.s.c	Dolati (2010)
1294	0	1294	m.w	0.039	3		L Miocene- E Pliocene	MPlm.s.c	Dolati (2010)
1295	0	1295	m.w	0.041	3		L Miocene- E Pliocene	MPlm.s.c	Dolati (2010)
1296	0	1296	m.w	0.077	3		L Miocene- E Pliocene	MPlm.s.c	Dolati (2010)
1297	0	1297	m.w	0.087	3		L Miocene- E Pliocene	MPlm.s.c	Dolati (2010)
1298	0	1298	m.w	1.609	3		L Miocene- E Pliocene	MPlm.s.c	Dolati (2010)
1299	0	1299	m.w	0.181	3		L Miocene- E Pliocene	MPlm.s.c	Dolati (2010)
1300	0	1300	m.w	0.022	3		L Miocene- E Pliocene	MPlm.s.c	Dolati (2010)
1301	0	1301	m.w	0.065	3		L Miocene- E Pliocene	MPlm.s.c	Dolati (2010)
1302	0	1302	m.w	0.397	3		L Miocene- E Pliocene	MPlm.s.c	Dolati (2010)
1303	0	1303	m.w	0.158	3		L Miocene- E Pliocene	MPlm.s.c	Dolati (2010)
1304	0	1304	m.w	0.388	3		L Miocene- E Pliocene	MPlm.s.c	Dolati (2010)
1305	0	1305	m.w	0.012	3		L Miocene- E Pliocene	MPlm.s.c	Dolati (2010)
1306	0	1306	m.w	4.608	3		L Miocene- E Pliocene	MPlm.s.c	Dolati (2010)
1307	0	1307	m.w	0.025	3		L Miocene- E Pliocene	MPlm.s.c	Dolati (2010)
1308	0	1308	m.w	0.014	3		L Miocene- E Pliocene	MPlm.s.c	Dolati (2010)
1309	0	1309	m.w	0.213	3		L Miocene- E Pliocene	MPlm.s.c	Dolati (2010)
1310	0	1310	m.w	0.008	3		L Miocene- E Pliocene	MPlm.s.c	Dolati (2010)
1311	0	1311	m.w	0.057	3		L Miocene- E Pliocene	MPlm.s.c	Dolati (2010)
1312	0	1312	m.w	0.023	3		L Miocene- E Pliocene	MPlm.s.c	Dolati (2010)
1313	0	1313	m.w	0.043	3		L Miocene- E Pliocene	MPlm.s.c	Dolati (2010)
1314	0	1314	m.w	0.092	3		L Miocene- E Pliocene	MPlm.s.c	Dolati (2010)
1315	0	1315	m.w	0.260	3		L Miocene- E Pliocene	MPlm.s.c	Dolati (2010)
1316	0	1316	m.w	0.556	3		L Miocene- E Pliocene	MPlm.s.c	Dolati (2010)
1317	0	1317	m.w	0.079	3		L Miocene- E Pliocene	MPlm.s.c	Dolati (2010)
1318	0	1318	m.w	0.033	3		L Miocene- E Pliocene	MPlm.s.c	Dolati (2010)
1319	0	1319	m.w	0.349	3		L Miocene- E Pliocene	MPlm.s.c	Dolati (2010)
1320	0	1320	m.w	0.036	3		L Miocene- E Pliocene	MPlm.s.c	Dolati (2010)
1321	0	1321	m.w	0.896	3		L Miocene- E Pliocene	MPlm.s.c	Dolati (2010)
1322	0	1322	m.w	0.029	3		L Miocene- E Pliocene	MPlm.s.c	Dolati (2010)
1323	0	1323	m.w	0.021	3		L Miocene- E Pliocene	MPlm.s.c	Dolati (2010)
1324	0	1324	m.w	0.130	3		L Miocene- E Pliocene	MPlm.s.c	Dolati (2010)
1325	0	1325	m.w	0.600	3		L Miocene- E Pliocene	MPlm.s.c	Dolati (2010)
1326	0	1326	m.w	0.343	3		L Miocene- E Pliocene	MPlm.s.c	Dolati (2010)

GeoNeXus

OBJECTID_1	Join_Count	TARGET_FID	label	Shape_Area (sqkm)	ORIG_FID	Absolute_Age	Age_paleontology	Unit	Reference
1327	0	1327	m.w	0.537	3		L Miocene- E Pliocene	MPlm.s.c	Dolati (2010)
1328	0	1328	m.w	0.449	3		L Miocene- E Pliocene	MPlm.s.c	Dolati (2010)
1329	0	1329	m.w	0.026	3		L Miocene- E Pliocene	MPlm.s.c	Dolati (2010)
1330	0	1330	m.w	0.267	3		L Miocene- E Pliocene	MPlm.s.c	Dolati (2010)
1331	0	1331	m.w	0.038	3		L Miocene- E Pliocene	MPlm.s.c	Dolati (2010)
1332	0	1332	m.w	0.101	3		L Miocene- E Pliocene	MPlm.s.c	Dolati (2010)
1333	0	1333	m.w	0.100	3		L Miocene- E Pliocene	MPlm.s.c	Dolati (2010)
1334	0	1334	m.w	0.622	3		L Miocene- E Pliocene	MPlm.s.c	Dolati (2010)
1335	0	1335	m.w	0.597	3		L Miocene- E Pliocene	MPlm.s.c	Dolati (2010)
1336	0	1336	m.w	0.043	3		L Miocene- E Pliocene	MPlm.s.c	Dolati (2010)
1337	0	1337	m.w	0.154	3		L Miocene- E Pliocene	MPlm.s.c	Dolati (2010)
1338	0	1338	m.w	0.059	3		L Miocene- E Pliocene	MPlm.s.c	Dolati (2010)
1339	0	1339	m.w	0.065	3		L Miocene- E Pliocene	MPlm.s.c	Dolati (2010)
1340	0	1340	m.w	0.051	3		L Miocene- E Pliocene	MPlm.s.c	Dolati (2010)
1341	0	1341	m.w	0.224	3		L Miocene- E Pliocene	MPlm.s.c	Dolati (2010)
1342	0	1342	m.w	0.156	3		L Miocene- E Pliocene	MPlm.s.c	Dolati (2010)
1343	0	1343	m.w	0.186	3		L Miocene- E Pliocene	MPlm.s.c	Dolati (2010)
1344	0	1344	m.w	1.417	3		L Miocene- E Pliocene	MPlm.s.c	Dolati (2010)
1345	0	1345	m.w	0.055	3		L Miocene- E Pliocene	MPlm.s.c	Dolati (2010)
1346	0	1346	m.w	0.213	3		L Miocene- E Pliocene	MPlm.s.c	Dolati (2010)
1347	0	1347	m.w	0.143	3		L Miocene- E Pliocene	MPlm.s.c	Dolati (2010)
1348	0	1348	m.w	0.022	3		L Miocene- E Pliocene	MPlm.s.c	Dolati (2010)
1349	0	1349	m.w	0.090	3		L Miocene- E Pliocene	MPlm.s.c	Dolati (2010)
1350	0	1350	m.w	0.040	3		L Miocene- E Pliocene	MPlm.s.c	Dolati (2010)
1351	0	1351	m.w	0.128	3		L Miocene- E Pliocene	MPlm.s.c	Dolati (2010)
1352	0	1352	m.w	0.047	3		L Miocene- E Pliocene	MPlm.s.c	Dolati (2010)
1353	0	1353	m.w	0.044	3		L Miocene- E Pliocene	MPlm.s.c	Dolati (2010)
1354	0	1354	m.w	0.053	3		L Miocene- E Pliocene	MPlm.s.c	Dolati (2010)
1355	0	1355	m.w	0.124	3		L Miocene- E Pliocene	MPlm.s.c	Dolati (2010)
1356	0	1356	m.w	0.077	3		L Miocene- E Pliocene	MPlm.s.c	Dolati (2010)
1357	0	1357	m.w	0.368	3		L Miocene- E Pliocene	MPlm.s.c	Dolati (2010)
1358	0	1358	m.w	0.175	3		L Miocene- E Pliocene	MPlm.s.c	Dolati (2010)
1359	0	1359	m.w	0.049	3		L Miocene- E Pliocene	MPlm.s.c	Dolati (2010)
1360	0	1360	m.w	0.038	3		L Miocene- E Pliocene	MPlm.s.c	Dolati (2010)
1361	0	1361	m.w	0.107	3		L Miocene- E Pliocene	MPlm.s.c	Dolati (2010)
1362	0	1362	m.w	0.079	3		L Miocene- E Pliocene	MPlm.s.c	Dolati (2010)
1363	0	1363	m.w	0.415	3		L Miocene- E Pliocene	MPlm.s.c	Dolati (2010)
1364	0	1364	m.w	0.101	3		L Miocene- E Pliocene	MPlm.s.c	Dolati (2010)
1365	0	1365	m.w	0.132	3		L Miocene- E Pliocene	MPlm.s.c	Dolati (2010)

GeoMap

OBJECTID_1	Join_Count	TARGET_FID	label	Shape_Area (sqkm)	ORIG_FID	Absolute_Age	Age_paleontology	Unit	Reference
1366	0	1366	m.w	2.539	3		L Miocene- E Pliocene	MPlm.s.c	Dolati (2010)
1367	0	1367	m.w	0.042	3		L Miocene- E Pliocene	MPlm.s.c	Dolati (2010)
1368	0	1368	m.w	0.237	3		L Miocene- E Pliocene	MPlm.s.c	Dolati (2010)
1369	0	1369	m.w	0.038	3		L Miocene- E Pliocene	MPlm.s.c	Dolati (2010)
1370	0	1370	m.w	0.119	3		L Miocene- E Pliocene	MPlm.s.c	Dolati (2010)
1371	0	1371	m.w	17.405	3		L Miocene- E Pliocene	MPlm.s.c	Dolati (2010)
1372	0	1372	m.w	0.031	3		L Miocene- E Pliocene	MPlm.s.c	Dolati (2010)
1373	0	1373	m.w	0.018	3		L Miocene- E Pliocene	MPlm.s.c	Dolati (2010)
1374	0	1374	m.w	0.050	3		L Miocene- E Pliocene	MPlm.s.c	Dolati (2010)
1375	0	1375	m.w	0.016	3		L Miocene- E Pliocene	MPlm.s.c	Dolati (2010)
1376	0	1376	m.w	0.059	3		L Miocene- E Pliocene	MPlm.s.c	Dolati (2010)
1377	0	1377	m.w	0.017	3		L Miocene- E Pliocene	MPlm.s.c	Dolati (2010)
1378	0	1378	m.w	0.092	3		L Miocene- E Pliocene	MPlm.s.c	Dolati (2010)
1379	0	1379	m.w	0.049	3		L Miocene- E Pliocene	MPlm.s.c	Dolati (2010)
1380	0	1380	m.w	0.219	3		L Miocene- E Pliocene	MPlm.s.c	Dolati (2010)
1381	0	1381	m.w	0.023	3		L Miocene- E Pliocene	MPlm.s.c	Dolati (2010)
1382	0	1382	m.w	0.177	3		L Miocene- E Pliocene	MPlm.s.c	Dolati (2010)
1383	0	1383	m.w	0.022	3		L Miocene- E Pliocene	MPlm.s.c	Dolati (2010)
1384	0	1384	m.w	1.732	3		L Miocene- E Pliocene	MPlm.s.c	Dolati (2010)
1385	0	1385	m.w	0.230	3		L Miocene- E Pliocene	MPlm.s.c	Dolati (2010)
1386	0	1386	m.w	0.025	3		L Miocene- E Pliocene	MPlm.s.c	Dolati (2010)
1387	0	1387	m.w	0.201	3		L Miocene- E Pliocene	MPlm.s.c	Dolati (2010)
1388	0	1388	m.w	1.311	3		L Miocene- E Pliocene	MPlm.s.c	Dolati (2010)
1389	0	1389	m.w	0.263	3		L Miocene- E Pliocene	MPlm.s.c	Dolati (2010)
1390	0	1390	m.w	0.020	3		L Miocene- E Pliocene	MPlm.s.c	Dolati (2010)
1391	0	1391	m.w	0.047	3		L Miocene- E Pliocene	MPlm.s.c	Dolati (2010)
1392	0	1392	m.w	0.152	3		L Miocene- E Pliocene	MPlm.s.c	Dolati (2010)
1393	0	1393	m.w	0.069	3		L Miocene- E Pliocene	MPlm.s.c	Dolati (2010)
1394	0	1394	m.w	0.083	3		L Miocene- E Pliocene	MPlm.s.c	Dolati (2010)
1395	0	1395	m.w	0.057	3		L Miocene- E Pliocene	MPlm.s.c	Dolati (2010)
1396	0	1396	m.w	0.030	3		L Miocene- E Pliocene	MPlm.s.c	Dolati (2010)
1397	0	1397	m.w	0.046	3		L Miocene- E Pliocene	MPlm.s.c	Dolati (2010)
1398	0	1398	m.w	0.161	3		L Miocene- E Pliocene	MPlm.s.c	Dolati (2010)
1399	0	1399	m.w	0.012	3		L Miocene- E Pliocene	MPlm.s.c	Dolati (2010)
1400	0	1400	m.w	0.172	3		L Miocene- E Pliocene	MPlm.s.c	Dolati (2010)
1401	0	1401	m.w	0.033	3		L Miocene- E Pliocene	MPlm.s.c	Dolati (2010)
1402	0	1402	m.w	0.047	3		L Miocene- E Pliocene	MPlm.s.c	Dolati (2010)
1403	0	1403	m.w	0.083	3		L Miocene- E Pliocene	MPlm.s.c	Dolati (2010)
1404	0	1404	m.w	0.115	3		L Miocene- E Pliocene	MPlm.s.c	Dolati (2010)

GeoNeXus

OBJECTID_1	Join_Count	TARGET_FID	label	Shape_Area (sqkm)	ORIG_FID	Absolute_Age	Age_paleontology	Unit	Reference
1405	0	1405	m.w	0.053	3		L Miocene- E Pliocene	MPlm.s.c	Dolati (2010)
1406	0	1406	m.w	0.323	3		L Miocene- E Pliocene	MPlm.s.c	Dolati (2010)
1407	0	1407	m.w	0.573	3		L Miocene- E Pliocene	MPlm.s.c	Dolati (2010)
1408	0	1408	m.w	0.070	3		L Miocene- E Pliocene	MPlm.s.c	Dolati (2010)
1409	0	1409	m.w	0.138	3		L Miocene- E Pliocene	MPlm.s.c	Dolati (2010)
1410	0	1410	m.w	0.054	3		L Miocene- E Pliocene	MPlm.s.c	Dolati (2010)
1411	0	1411	m.w	0.287	3		L Miocene- E Pliocene	MPlm.s.c	Dolati (2010)
1412	0	1412	m.w	0.074	3		L Miocene- E Pliocene	MPlm.s.c	Dolati (2010)
1413	0	1413	m.w	0.390	3		L Miocene- E Pliocene	MPlm.s.c	Dolati (2010)
1414	0	1414	m.w	0.443	3		L Miocene- E Pliocene	MPlm.s.c	Dolati (2010)
1415	0	1415	m.w	0.060	3		L Miocene- E Pliocene	MPlm.s.c	Dolati (2010)
1416	0	1416	m.w	0.596	3		L Miocene- E Pliocene	MPlm.s.c	Dolati (2010)
1417	0	1417	m.w	0.023	3		L Miocene- E Pliocene	MPlm.s.c	Dolati (2010)
1418	0	1418	m.w	0.029	3		L Miocene- E Pliocene	MPlm.s.c	Dolati (2010)
1419	0	1419	m.w	0.080	3		L Miocene- E Pliocene	MPlm.s.c	Dolati (2010)
1420	0	1420	m.w	0.023	3		L Miocene- E Pliocene	MPlm.s.c	Dolati (2010)
1421	0	1421	m.w	0.022	3		L Miocene- E Pliocene	MPlm.s.c	Dolati (2010)
1422	0	1422	m.w	1.203	3		L Miocene- E Pliocene	MPlm.s.c	Dolati (2010)
1423	0	1423	m.w	0.043	3		L Miocene- E Pliocene	MPlm.s.c	Dolati (2010)
1424	0	1424	m.w	0.053	3		L Miocene- E Pliocene	MPlm.s.c	Dolati (2010)
1425	0	1425	m.w	0.048	3		L Miocene- E Pliocene	MPlm.s.c	Dolati (2010)
1426	0	1426	m.w	0.065	3		L Miocene- E Pliocene	MPlm.s.c	Dolati (2010)
1427	0	1427	m.w	0.026	3		L Miocene- E Pliocene	MPlm.s.c	Dolati (2010)
1428	0	1428	m.w	0.038	3		L Miocene- E Pliocene	MPlm.s.c	Dolati (2010)
1429	0	1429	m.w	0.180	3		L Miocene- E Pliocene	MPlm.s.c	Dolati (2010)
1430	0	1430	m.w	0.120	3		L Miocene- E Pliocene	MPlm.s.c	Dolati (2010)
1431	0	1431	m.w	0.095	3		L Miocene- E Pliocene	MPlm.s.c	Dolati (2010)
1432	0	1432	m.w	0.136	3		L Miocene- E Pliocene	MPlm.s.c	Dolati (2010)
1433	0	1433	m.w	0.198	3		L Miocene- E Pliocene	MPlm.s.c	Dolati (2010)
1434	0	1434	m.w	0.260	3		L Miocene- E Pliocene	MPlm.s.c	Dolati (2010)
1435	0	1435	m.w	0.251	3		L Miocene- E Pliocene	MPlm.s.c	Dolati (2010)
1436	0	1436	m.w	0.098	3		L Miocene- E Pliocene	MPlm.s.c	Dolati (2010)
1437	0	1437	m.w	0.353	3		L Miocene- E Pliocene	MPlm.s.c	Dolati (2010)
1438	0	1438	m.w	0.064	3		L Miocene- E Pliocene	MPlm.s.c	Dolati (2010)
1439	0	1439	m.w	0.269	3		L Miocene- E Pliocene	MPlm.s.c	Dolati (2010)
1440	0	1440	m.w	0.150	3		L Miocene- E Pliocene	MPlm.s.c	Dolati (2010)
1441	0	1441	m.w	0.085	3		L Miocene- E Pliocene	MPlm.s.c	Dolati (2010)
1442	0	1442	m.w	0.034	3		L Miocene- E Pliocene	MPlm.s.c	Dolati (2010)
1443	0	1443	m.w	0.052	3		L Miocene- E Pliocene	MPlm.s.c	Dolati (2010)

GeoNode

OBJECTID_1	Join_Count	TARGET_FID	label	Shape_Area (sqkm)	ORIG_FID	Absolute_Age	Age_paleontology	Unit	Reference
1444	0	1444	m.w	1.009	3		L Miocene- E Pliocene	MPlm.s.c	Dolati (2010)
1445	0	1445	m.w	0.098	3		L Miocene- E Pliocene	MPlm.s.c	Dolati (2010)
1446	0	1446	m.w	0.884	3		L Miocene- E Pliocene	MPlm.s.c	Dolati (2010)
1447	0	1447	m.w	0.228	3		L Miocene- E Pliocene	MPlm.s.c	Dolati (2010)
1448	0	1448	m.w	0.057	3		L Miocene- E Pliocene	MPlm.s.c	Dolati (2010)
1449	0	1449	m.w	0.402	3		L Miocene- E Pliocene	MPlm.s.c	Dolati (2010)
1450	0	1450	m.w	0.044	3		L Miocene- E Pliocene	MPlm.s.c	Dolati (2010)
1451	0	1451	m.w	0.045	3		L Miocene- E Pliocene	MPlm.s.c	Dolati (2010)
1452	0	1452	m.w	0.019	3		L Miocene- E Pliocene	MPlm.s.c	Dolati (2010)
1453	0	1453	m.w	0.060	3		L Miocene- E Pliocene	MPlm.s.c	Dolati (2010)
1454	0	1454	m.w	0.037	3		L Miocene- E Pliocene	MPlm.s.c	Dolati (2010)
1455	0	1455	m.w	0.165	3		L Miocene- E Pliocene	MPlm.s.c	Dolati (2010)
1456	0	1456	m.w	0.158	3		L Miocene- E Pliocene	MPlm.s.c	Dolati (2010)
1457	0	1457	m.w	0.075	3		L Miocene- E Pliocene	MPlm.s.c	Dolati (2010)
1458	0	1458	m.w	0.782	3		L Miocene- E Pliocene	MPlm.s.c	Dolati (2010)
1459	0	1459	m.w	25.473	3		L Miocene- E Pliocene	MPlm.s.c	Dolati (2010)
1460	0	1460	m.w	0.058	3		L Miocene- E Pliocene	MPlm.s.c	Dolati (2010)
1461	0	1461	m.w	0.015	3		L Miocene- E Pliocene	MPlm.s.c	Dolati (2010)
1462	0	1462	m.w	0.075	3		L Miocene- E Pliocene	MPlm.s.c	Dolati (2010)
1463	0	1463	m.w	0.179	3		L Miocene- E Pliocene	MPlm.s.c	Dolati (2010)
1464	0	1464	m.w	0.068	3		L Miocene- E Pliocene	MPlm.s.c	Dolati (2010)
1465	0	1465	m.w	0.173	3		L Miocene- E Pliocene	MPlm.s.c	Dolati (2010)
1466	0	1466	m.w	0.549	3		L Miocene- E Pliocene	MPlm.s.c	Dolati (2010)
1468	0	1468	m.w	0.103	3		L Miocene- E Pliocene	MPlm.s.c	Dolati (2010)
1469	0	1469	m.w	0.721	3		L Miocene- E Pliocene	MPlm.s.c	Dolati (2010)
1470	0	1470	m.w	0.052	3		L Miocene- E Pliocene	MPlm.s.c	Dolati (2010)
1471	0	1471	m.w	0.071	3		L Miocene- E Pliocene	MPlm.s.c	Dolati (2010)
1472	0	1472	m.w	0.059	3		L Miocene- E Pliocene	MPlm.s.c	Dolati (2010)
1473	0	1473	m.w	0.108	3		L Miocene- E Pliocene	MPlm.s.c	Dolati (2010)
1474	0	1474	m.w	0.121	3		L Miocene- E Pliocene	MPlm.s.c	Dolati (2010)
1475	0	1475	m.w	0.031	3		L Miocene- E Pliocene	MPlm.s.c	Dolati (2010)
1476	0	1476	m.w	0.383	3		L Miocene- E Pliocene	MPlm.s.c	Dolati (2010)
1477	0	1477	m.w	0.061	3		L Miocene- E Pliocene	MPlm.s.c	Dolati (2010)
1478	0	1478	m.w	0.029	3		L Miocene- E Pliocene	MPlm.s.c	Dolati (2010)
1479	0	1479	m.w	0.339	3		L Miocene- E Pliocene	MPlm.s.c	Dolati (2010)
1480	0	1480	m.w	0.096	3		L Miocene- E Pliocene	MPlm.s.c	Dolati (2010)
1481	0	1481	m.w	0.084	3		L Miocene- E Pliocene	MPlm.s.c	Dolati (2010)
1482	0	1482	m.w	0.088	3		L Miocene- E Pliocene	MPlm.s.c	Dolati (2010)
1483	3	1483	m.w	69.452	3		L Miocene- E Pliocene	MPlm.s.c	Dolati (2010)

GeoNeXus

OBJECTID_1	Join_Count	TARGET_FID	label	Shape_Area (sqkm)	ORIG_FID	Absolute_Age	Age_paleontology	Unit	Reference
1484	0	1484	m.w	0.047	3		L Miocene- E Pliocene	MPlm.s.c	Dolati (2010)
1485	0	1485	m.w	0.143	3		L Miocene- E Pliocene	MPlm.s.c	Dolati (2010)
1486	0	1486	m.w	0.014	3		L Miocene- E Pliocene	MPlm.s.c	Dolati (2010)
1487	0	1487	m.w	0.088	3		L Miocene- E Pliocene	MPlm.s.c	Dolati (2010)
1488	0	1488	m.w	0.127	3		L Miocene- E Pliocene	MPlm.s.c	Dolati (2010)
1489	0	1489	m.w	0.047	3		L Miocene- E Pliocene	MPlm.s.c	Dolati (2010)
1490	0	1490	m.w	0.100	3		L Miocene- E Pliocene	MPlm.s.c	Dolati (2010)
1491	0	1491	m.w	0.217	3		L Miocene- E Pliocene	MPlm.s.c	Dolati (2010)
1492	0	1492	m.w	0.072	3		L Miocene- E Pliocene	MPlm.s.c	Dolati (2010)
1493	0	1493	m.w	0.044	3		L Miocene- E Pliocene	MPlm.s.c	Dolati (2010)
1494	0	1494	m.w	0.010	3		L Miocene- E Pliocene	MPlm.s.c	Dolati (2010)
1495	0	1495	m.w	0.141	3		L Miocene- E Pliocene	MPlm.s.c	Dolati (2010)
1496	0	1496	m.w	0.065	3		L Miocene- E Pliocene	MPlm.s.c	Dolati (2010)
1497	0	1497	m.w	0.057	3		L Miocene- E Pliocene	MPlm.s.c	Dolati (2010)
1498	0	1498	m.w	0.047	3		L Miocene- E Pliocene	MPlm.s.c	Dolati (2010)
1499	0	1499	m.w	0.160	3		L Miocene- E Pliocene	MPlm.s.c	Dolati (2010)
1500	0	1500	m.w	0.245	3		L Miocene- E Pliocene	MPlm.s.c	Dolati (2010)
1501	0	1501	m.w	0.072	3		L Miocene- E Pliocene	MPlm.s.c	Dolati (2010)
1502	0	1502	m.w	0.223	3		L Miocene- E Pliocene	MPlm.s.c	Dolati (2010)
1503	0	1503	m.w	0.062	3		L Miocene- E Pliocene	MPlm.s.c	Dolati (2010)
1504	0	1504	m.w	0.374	3		L Miocene- E Pliocene	MPlm.s.c	Dolati (2010)
1505	0	1505	m.w	0.146	3		L Miocene- E Pliocene	MPlm.s.c	Dolati (2010)
1506	0	1506	m.w	0.031	3		L Miocene- E Pliocene	MPlm.s.c	Dolati (2010)
1507	0	1507	m.w	0.049	3		L Miocene- E Pliocene	MPlm.s.c	Dolati (2010)
1508	0	1508	m.w	0.046	3		L Miocene- E Pliocene	MPlm.s.c	Dolati (2010)
1509	0	1509	m.w	0.057	3		L Miocene- E Pliocene	MPlm.s.c	Dolati (2010)
1510	0	1510	m.w	0.027	3		L Miocene- E Pliocene	MPlm.s.c	Dolati (2010)
1511	0	1511	m.w	0.103	3		L Miocene- E Pliocene	MPlm.s.c	Dolati (2010)
1512	0	1512	m.w	0.240	3		L Miocene- E Pliocene	MPlm.s.c	Dolati (2010)
1513	0	1513	m.w	0.060	3		L Miocene- E Pliocene	MPlm.s.c	Dolati (2010)
1514	0	1514	m.w	0.035	3		L Miocene- E Pliocene	MPlm.s.c	Dolati (2010)
1515	0	1515	m.w	0.023	3		L Miocene- E Pliocene	MPlm.s.c	Dolati (2010)
1516	0	1516	m.w	0.082	3		L Miocene- E Pliocene	MPlm.s.c	Dolati (2010)
1517	0	1517	m.w	0.052	3		L Miocene- E Pliocene	MPlm.s.c	Dolati (2010)
1518	0	1518	m.w	0.044	3		L Miocene- E Pliocene	MPlm.s.c	Dolati (2010)
1519	0	1519	m.w	0.098	3		L Miocene- E Pliocene	MPlm.s.c	Dolati (2010)
1520	0	1520	m.w	0.109	3		L Miocene- E Pliocene	MPlm.s.c	Dolati (2010)
1521	0	1521	m.w	0.023	3		L Miocene- E Pliocene	MPlm.s.c	Dolati (2010)
1522	0	1522	m.w	0.018	3		L Miocene- E Pliocene	MPlm.s.c	Dolati (2010)

GeoMap

OBJECTID_1	Join_Count	TARGET_FID	label	Shape_Area (sqkm)	ORIG_FID	Absolute_Age	Age_paleontology	Unit	Reference
1523	0	1523	m.w	0.211	3		L Miocene- E Pliocene	MPlm.s.c	Dolati (2010)
1524	0	1524	m.w	0.167	3		L Miocene- E Pliocene	MPlm.s.c	Dolati (2010)
1525	0	1525	m.w	0.100	3		L Miocene- E Pliocene	MPlm.s.c	Dolati (2010)
1526	0	1526	m.w	0.249	3		L Miocene- E Pliocene	MPlm.s.c	Dolati (2010)
1527	0	1527	m.w	0.177	3		L Miocene- E Pliocene	MPlm.s.c	Dolati (2010)
1528	0	1528	m.w	0.141	3		L Miocene- E Pliocene	MPlm.s.c	Dolati (2010)
1529	0	1529	m.w	0.084	3		L Miocene- E Pliocene	MPlm.s.c	Dolati (2010)
1530	0	1530	m.w	1.168	3		L Miocene- E Pliocene	MPlm.s.c	Dolati (2010)
1531	0	1531	m.w	0.034	3		L Miocene- E Pliocene	MPlm.s.c	Dolati (2010)
1532	0	1532	m.w	0.145	3		L Miocene- E Pliocene	MPlm.s.c	Dolati (2010)
1533	0	1533	m.w	0.092	3		L Miocene- E Pliocene	MPlm.s.c	Dolati (2010)
1534	0	1534	m.w	0.069	3		L Miocene- E Pliocene	MPlm.s.c	Dolati (2010)
1535	0	1535	m.w	7.420	3		L Miocene- E Pliocene	MPlm.s.c	Dolati (2010)
1536	0	1536	m.w	0.190	3		L Miocene- E Pliocene	MPlm.s.c	Dolati (2010)
1537	0	1537	m.w	0.049	3		L Miocene- E Pliocene	MPlm.s.c	Dolati (2010)
1538	0	1538	m.w	0.021	3		L Miocene- E Pliocene	MPlm.s.c	Dolati (2010)
1539	0	1539	m.w	0.120	3		L Miocene- E Pliocene	MPlm.s.c	Dolati (2010)
1540	0	1540	m.w	0.118	3		L Miocene- E Pliocene	MPlm.s.c	Dolati (2010)
1541	0	1541	m.w	0.034	3		L Miocene- E Pliocene	MPlm.s.c	Dolati (2010)
1542	0	1542	m.w	0.082	3		L Miocene- E Pliocene	MPlm.s.c	Dolati (2010)
1543	0	1543	m.w	0.017	3		L Miocene- E Pliocene	MPlm.s.c	Dolati (2010)
1544	2	1544	m.w	16.148	3		L Miocene- E Pliocene	MPlm.s.c	Dolati (2010)
1545	0	1545	m.w	2.602	3		L Miocene- E Pliocene	MPlm.s.c	Dolati (2010)
1546	0	1546	m.w	0.163	3		L Miocene- E Pliocene	MPlm.s.c	Dolati (2010)
1547	0	1547	m.w	0.071	3		L Miocene- E Pliocene	MPlm.s.c	Dolati (2010)
1548	0	1548	m.w	0.123	3		L Miocene- E Pliocene	MPlm.s.c	Dolati (2010)
1549	0	1549	m.w	0.069	3		L Miocene- E Pliocene	MPlm.s.c	Dolati (2010)
1550	0	1550	m.w	0.148	3		L Miocene- E Pliocene	MPlm.s.c	Dolati (2010)
1551	0	1551	m.w	0.078	3		L Miocene- E Pliocene	MPlm.s.c	Dolati (2010)
1552	0	1552	m.w	0.048	3		L Miocene- E Pliocene	MPlm.s.c	Dolati (2010)
1553	0	1553	m.w	0.114	3		L Miocene- E Pliocene	MPlm.s.c	Dolati (2010)
1554	0	1554	m.w	0.308	3		L Miocene- E Pliocene	MPlm.s.c	Dolati (2010)
1555	0	1555	m.w	0.054	3		L Miocene- E Pliocene	MPlm.s.c	Dolati (2010)
1556	0	1556	m.w	0.096	3		L Miocene- E Pliocene	MPlm.s.c	Dolati (2010)
1557	0	1557	m.w	0.608	3		L Miocene- E Pliocene	MPlm.s.c	Dolati (2010)
1559	0	1559	m.w	0.070	3		L Miocene- E Pliocene	MPlm.s.c	Dolati (2010)
1560	0	1560	m.w	0.235	3		L Miocene- E Pliocene	MPlm.s.c	Dolati (2010)
1561	0	1561	m.w	0.054	3		L Miocene- E Pliocene	MPlm.s.c	Dolati (2010)
1562	0	1562	m.w	0.031	3		L Miocene- E Pliocene	MPlm.s.c	Dolati (2010)

GeoNeXus

OBJECTID_1	Join_Count	TARGET_FID	label	Shape_Area (sqkm)	ORIG_FID	Absolute_Age	Age_paleontology	Unit	Reference
1563	0	1563	m.w	2.881	3		L Miocene- E Pliocene	MPlm.s.c	Dolati (2010)
1564	0	1564	m.w	0.078	3		L Miocene- E Pliocene	MPlm.s.c	Dolati (2010)
1565	0	1565	m.w	0.081	3		L Miocene- E Pliocene	MPlm.s.c	Dolati (2010)
1566	0	1566	m.w	0.404	3		L Miocene- E Pliocene	MPlm.s.c	Dolati (2010)
1567	0	1567	m.w	0.036	3		L Miocene- E Pliocene	MPlm.s.c	Dolati (2010)
1568	0	1568	m.w	0.031	3		L Miocene- E Pliocene	MPlm.s.c	Dolati (2010)
1569	0	1569	m.w	0.067	3		L Miocene- E Pliocene	MPlm.s.c	Dolati (2010)
1570	0	1570	m.w	0.072	3		L Miocene- E Pliocene	MPlm.s.c	Dolati (2010)
1571	0	1571	m.w	0.066	3		L Miocene- E Pliocene	MPlm.s.c	Dolati (2010)
1572	0	1572	m.w	0.208	3		L Miocene- E Pliocene	MPlm.s.c	Dolati (2010)
1573	0	1573	m.w	0.200	3		L Miocene- E Pliocene	MPlm.s.c	Dolati (2010)
1574	0	1574	m.w	1.768	3		L Miocene- E Pliocene	MPlm.s.c	Dolati (2010)
1575	0	1575	m.w	0.325	3		L Miocene- E Pliocene	MPlm.s.c	Dolati (2010)
1576	0	1576	m.w	0.093	3		L Miocene- E Pliocene	MPlm.s.c	Dolati (2010)
1577	0	1577	m.w	0.176	3		L Miocene- E Pliocene	MPlm.s.c	Dolati (2010)
1578	0	1578	m.w	0.158	3		L Miocene- E Pliocene	MPlm.s.c	Dolati (2010)
1579	0	1579	m.w	8.514	3		L Miocene- E Pliocene	MPlm.s.c	Dolati (2010)
1580	0	1580	m.w	0.068	3		L Miocene- E Pliocene	MPlm.s.c	Dolati (2010)
1581	0	1581	m.w	4.096	3		L Miocene- E Pliocene	MPlm.s.c	Dolati (2010)
1582	0	1582	m.w	0.178	3		L Miocene- E Pliocene	MPlm.s.c	Dolati (2010)
1583	0	1583	m.w	19.234	3		L Miocene- E Pliocene	MPlm.s.c	Dolati (2010)
1584	0	1584	m.w	0.040	3		L Miocene- E Pliocene	MPlm.s.c	Dolati (2010)
1585	0	1585	m.w	0.279	3		L Miocene- E Pliocene	MPlm.s.c	Dolati (2010)
1586	0	1586	m.w	0.066	3		L Miocene- E Pliocene	MPlm.s.c	Dolati (2010)
1587	0	1587	m.w	0.048	3		L Miocene- E Pliocene	MPlm.s.c	Dolati (2010)
1588	0	1588	m.w	0.031	3		L Miocene- E Pliocene	MPlm.s.c	Dolati (2010)
1589	0	1589	m.w	2.498	3		L Miocene- E Pliocene	MPlm.s.c	Dolati (2010)
1590	0	1590	m.w	0.017	3		L Miocene- E Pliocene	MPlm.s.c	Dolati (2010)
1591	0	1591	m.w	0.157	3		L Miocene- E Pliocene	MPlm.s.c	Dolati (2010)
1592	0	1592	m.w	0.043	3		L Miocene- E Pliocene	MPlm.s.c	Dolati (2010)
1593	0	1593	m.w	0.524	3		L Miocene- E Pliocene	MPlm.s.c	Dolati (2010)
1594	0	1594	m.w	1.339	3		L Miocene- E Pliocene	MPlm.s.c	Dolati (2010)
1595	0	1595	m.w	0.104	3		L Miocene- E Pliocene	MPlm.s.c	Dolati (2010)
1596	0	1596	m.w	2.152	3		L Miocene- E Pliocene	MPlm.s.c	Dolati (2010)
1597	0	1597	m.w	2.536	3		L Miocene- E Pliocene	MPlm.s.c	Dolati (2010)
1598	0	1598	m.w	0.693	3		L Miocene- E Pliocene	MPlm.s.c	Dolati (2010)
1599	0	1599	m.w	0.053	3		L Miocene- E Pliocene	MPlm.s.c	Dolati (2010)
1600	0	1600	m.w	0.034	3		L Miocene- E Pliocene	MPlm.s.c	Dolati (2010)
1601	0	1601	m.w	0.042	3		L Miocene- E Pliocene	MPlm.s.c	Dolati (2010)

GeoNode

OBJECTID_1	Join_Count	TARGET_FID	label	Shape_Area (sqkm)	ORIG_FID	Absolute_Age	Age_paleontology	Unit	Reference
1602	0	1602	m.w	0.194	3		L Miocene- E Pliocene	MPlm.s.c	Dolati (2010)
1603	0	1603	m.w	0.071	3		L Miocene- E Pliocene	MPlm.s.c	Dolati (2010)
1604	0	1604	m.w	0.411	3		L Miocene- E Pliocene	MPlm.s.c	Dolati (2010)
1605	0	1605	m.w	0.022	3		L Miocene- E Pliocene	MPlm.s.c	Dolati (2010)
1606	0	1606	m.w	0.043	3		L Miocene- E Pliocene	MPlm.s.c	Dolati (2010)
1607	0	1607	m.w	1.251	3		L Miocene- E Pliocene	MPlm.s.c	Dolati (2010)
1608	0	1608	m.w	0.068	3		L Miocene- E Pliocene	MPlm.s.c	Dolati (2010)
1609	0	1609	m.w	0.187	3		L Miocene- E Pliocene	MPlm.s.c	Dolati (2010)
1610	0	1610	m.w	0.178	3		L Miocene- E Pliocene	MPlm.s.c	Dolati (2010)
1611	0	1611	m.w	0.097	3		L Miocene- E Pliocene	MPlm.s.c	Dolati (2010)
1612	0	1612	m.w	0.054	3		L Miocene- E Pliocene	MPlm.s.c	Dolati (2010)
1613	0	1613	m.w	0.526	3		L Miocene- E Pliocene	MPlm.s.c	Dolati (2010)
1614	0	1614	m.w	0.432	3		L Miocene- E Pliocene	MPlm.s.c	Dolati (2010)
1615	0	1615	m.w	0.076	3		L Miocene- E Pliocene	MPlm.s.c	Dolati (2010)
1616	0	1616	m.w	0.033	3		L Miocene- E Pliocene	MPlm.s.c	Dolati (2010)
1617	0	1617	m.w	0.045	3		L Miocene- E Pliocene	MPlm.s.c	Dolati (2010)
1618	0	1618	m.w	0.413	3		L Miocene- E Pliocene	MPlm.s.c	Dolati (2010)
1619	0	1619	m.w	0.024	3		L Miocene- E Pliocene	MPlm.s.c	Dolati (2010)
1620	0	1620	m.w	0.224	3		L Miocene- E Pliocene	MPlm.s.c	Dolati (2010)
1621	0	1621	m.w	0.259	3		L Miocene- E Pliocene	MPlm.s.c	Dolati (2010)
1622	0	1622	m.w	0.065	3		L Miocene- E Pliocene	MPlm.s.c	Dolati (2010)
1623	0	1623	m.w	2.015	3		L Miocene- E Pliocene	MPlm.s.c	Dolati (2010)
1624	0	1624	m.w	0.107	3		L Miocene- E Pliocene	MPlm.s.c	Dolati (2010)
1625	0	1625	m.w	2.274	3		L Miocene- E Pliocene	MPlm.s.c	Dolati (2010)
1626	0	1626	m.w	0.930	3		L Miocene- E Pliocene	MPlm.s.c	Dolati (2010)
1627	0	1627	m.w	0.054	3		L Miocene- E Pliocene	MPlm.s.c	Dolati (2010)
1628	0	1628	m.w	0.041	3		L Miocene- E Pliocene	MPlm.s.c	Dolati (2010)
1629	0	1629	m.w	0.122	3		L Miocene- E Pliocene	MPlm.s.c	Dolati (2010)
1630	0	1630	m.w	0.029	3		L Miocene- E Pliocene	MPlm.s.c	Dolati (2010)
1631	0	1631	m.w	0.184	3		L Miocene- E Pliocene	MPlm.s.c	Dolati (2010)
1632	0	1632	m.w	1.651	3		L Miocene- E Pliocene	MPlm.s.c	Dolati (2010)
1633	0	1633	m.w	1.552	3		L Miocene- E Pliocene	MPlm.s.c	Dolati (2010)
1634	0	1634	m.w	0.117	3		L Miocene- E Pliocene	MPlm.s.c	Dolati (2010)
1635	0	1635	m.w	0.273	3		L Miocene- E Pliocene	MPlm.s.c	Dolati (2010)
1636	0	1636	m.w	0.106	3		L Miocene- E Pliocene	MPlm.s.c	Dolati (2010)
1637	0	1637	m.w	0.450	3		L Miocene- E Pliocene	MPlm.s.c	Dolati (2010)
1638	0	1638	m.w	0.107	3		L Miocene- E Pliocene	MPlm.s.c	Dolati (2010)
1639	0	1639	m.w	0.017	3		L Miocene- E Pliocene	MPlm.s.c	Dolati (2010)
1640	0	1640	m.w	0.033	3		L Miocene- E Pliocene	MPlm.s.c	Dolati (2010)

GeoNeXus

OBJECTID_1	Join_Count	TARGET_FID	label	Shape_Area (sqkm)	ORIG_FID	Absolute_Age	Age_paleontology	Unit	Reference
1641	0	1641	m.w	0.014	3		L Miocene- E Pliocene	MPlm.s.c	Dolati (2010)
1642	0	1642	m.w	0.452	3		L Miocene- E Pliocene	MPlm.s.c	Dolati (2010)
1643	0	1643	m.w	0.019	3		L Miocene- E Pliocene	MPlm.s.c	Dolati (2010)
1645	0	1645	m.w	0.127	3		L Miocene- E Pliocene	MPlm.s.c	Dolati (2010)
1646	0	1646	m.w	0.357	3		L Miocene- E Pliocene	MPlm.s.c	Dolati (2010)
1648	0	1648	m.w	0.037	3		L Miocene- E Pliocene	MPlm.s.c	Dolati (2010)
1649	0	1649	m.w	0.034	3		L Miocene- E Pliocene	MPlm.s.c	Dolati (2010)
1650	0	1650	m.w	0.068	3		L Miocene- E Pliocene	MPlm.s.c	Dolati (2010)
1651	0	1651	m.w	0.019	3		L Miocene- E Pliocene	MPlm.s.c	Dolati (2010)
1652	0	1652	m.w	0.043	3		L Miocene- E Pliocene	MPlm.s.c	Dolati (2010)
1653	0	1653	m.w	0.076	3		L Miocene- E Pliocene	MPlm.s.c	Dolati (2010)
1654	0	1654	m.w	0.017	3		L Miocene- E Pliocene	MPlm.s.c	Dolati (2010)
1655	0	1655	m.w	0.169	3		L Miocene- E Pliocene	MPlm.s.c	Dolati (2010)
1656	0	1656	m.w	0.317	3		L Miocene- E Pliocene	MPlm.s.c	Dolati (2010)
1657	0	1657	m.w	0.387	3		L Miocene- E Pliocene	MPlm.s.c	Dolati (2010)
1658	0	1658	m.w	0.074	3		L Miocene- E Pliocene	MPlm.s.c	Dolati (2010)
1659	0	1659	m.w	0.009	3		L Miocene- E Pliocene	MPlm.s.c	Dolati (2010)
1660	0	1660	m.w	0.196	3		L Miocene- E Pliocene	MPlm.s.c	Dolati (2010)
1661	0	1661	m.w	0.095	3		L Miocene- E Pliocene	MPlm.s.c	Dolati (2010)
1662	0	1662	m.w	0.120	3		L Miocene- E Pliocene	MPlm.s.c	Dolati (2010)
1663	0	1663	m.w	0.024	3		L Miocene- E Pliocene	MPlm.s.c	Dolati (2010)
1664	0	1664	m.w	0.070	3		L Miocene- E Pliocene	MPlm.s.c	Dolati (2010)
1665	0	1665	m.w	0.070	3		L Miocene- E Pliocene	MPlm.s.c	Dolati (2010)
1666	0	1666	m.w	0.651	3		L Miocene- E Pliocene	MPlm.s.c	Dolati (2010)
1667	0	1667	m.w	0.140	3		L Miocene- E Pliocene	MPlm.s.c	Dolati (2010)
1668	0	1668	m.w	0.975	3		L Miocene- E Pliocene	MPlm.s.c	Dolati (2010)
1669	0	1669	m.w	0.044	3		L Miocene- E Pliocene	MPlm.s.c	Dolati (2010)
1670	0	1670	m.w	0.129	3		L Miocene- E Pliocene	MPlm.s.c	Dolati (2010)
1671	0	1671	m.w	0.063	3		L Miocene- E Pliocene	MPlm.s.c	Dolati (2010)
1672	0	1672	m.w	0.023	3		L Miocene- E Pliocene	MPlm.s.c	Dolati (2010)
1673	0	1673	m.w	0.287	3		L Miocene- E Pliocene	MPlm.s.c	Dolati (2010)
1674	0	1674	m.w	0.033	3		L Miocene- E Pliocene	MPlm.s.c	Dolati (2010)
1675	0	1675	m.w	0.265	3		L Miocene- E Pliocene	MPlm.s.c	Dolati (2010)
1676	0	1676	m.w	0.009	3		L Miocene- E Pliocene	MPlm.s.c	Dolati (2010)
1677	0	1677	m.w	0.263	3		L Miocene- E Pliocene	MPlm.s.c	Dolati (2010)
1678	0	1678	m.w	0.896	3		L Miocene- E Pliocene	MPlm.s.c	Dolati (2010)
1679	0	1679	m.w	0.823	3		L Miocene- E Pliocene	MPlm.s.c	Dolati (2010)
1680	0	1680	m.w	0.292	3		L Miocene- E Pliocene	MPlm.s.c	Dolati (2010)
1681	0	1681	m.w	0.015	3		L Miocene- E Pliocene	MPlm.s.c	Dolati (2010)

GeoMLA

OBJECTID_1	Join_Count	TARGET_FID	label	Shape_Area (sqkm)	ORIG_FID	Absolute_Age	Age_paleontology	Unit	Reference
1682	0	1682	m.w	0.048	3		L Miocene- E Pliocene	MPlm.s.c	Dolati (2010)
1683	0	1683	m.w	0.431	3		L Miocene- E Pliocene	MPlm.s.c	Dolati (2010)
1684	0	1684	m.w	0.246	3		L Miocene- E Pliocene	MPlm.s.c	Dolati (2010)
1685	0	1685	m.w	0.049	3		L Miocene- E Pliocene	MPlm.s.c	Dolati (2010)
1686	0	1686	m.w	0.068	3		L Miocene- E Pliocene	MPlm.s.c	Dolati (2010)
1687	0	1687	m.w	0.917	3		L Miocene- E Pliocene	MPlm.s.c	Dolati (2010)
1688	0	1688	m.w	0.038	3		L Miocene- E Pliocene	MPlm.s.c	Dolati (2010)
1689	0	1689	m.w	0.102	3		L Miocene- E Pliocene	MPlm.s.c	Dolati (2010)
1690	0	1690	m.w	0.023	3		L Miocene- E Pliocene	MPlm.s.c	Dolati (2010)
1691	0	1691	m.w	0.062	3		L Miocene- E Pliocene	MPlm.s.c	Dolati (2010)
1692	0	1692	m.w	0.171	3		L Miocene- E Pliocene	MPlm.s.c	Dolati (2010)
1693	0	1693	m.w	0.527	3		L Miocene- E Pliocene	MPlm.s.c	Dolati (2010)
1694	0	1694	m.w	0.083	3		L Miocene- E Pliocene	MPlm.s.c	Dolati (2010)
1695	0	1695	m.w	0.066	3		L Miocene- E Pliocene	MPlm.s.c	Dolati (2010)
1696	0	1696	m.w	0.021	3		L Miocene- E Pliocene	MPlm.s.c	Dolati (2010)
1697	0	1697	m.w	0.013	3		L Miocene- E Pliocene	MPlm.s.c	Dolati (2010)
1698	0	1698	m.w	0.058	3		L Miocene- E Pliocene	MPlm.s.c	Dolati (2010)
1699	0	1699	m.w	0.206	3		L Miocene- E Pliocene	MPlm.s.c	Dolati (2010)
1700	0	1700	m.w	0.233	3		L Miocene- E Pliocene	MPlm.s.c	Dolati (2010)
1701	0	1701	m.w	0.064	3		L Miocene- E Pliocene	MPlm.s.c	Dolati (2010)
1702	0	1702	m.w	0.060	3		L Miocene- E Pliocene	MPlm.s.c	Dolati (2010)
1703	0	1703	m.w	0.014	3		L Miocene- E Pliocene	MPlm.s.c	Dolati (2010)
1704	0	1704	m.w	0.024	3		L Miocene- E Pliocene	MPlm.s.c	Dolati (2010)
1705	0	1705	m.w	0.170	3		L Miocene- E Pliocene	MPlm.s.c	Dolati (2010)
1706	0	1706	m.w	0.078	3		L Miocene- E Pliocene	MPlm.s.c	Dolati (2010)
1707	0	1707	m.w	0.041	3		L Miocene- E Pliocene	MPlm.s.c	Dolati (2010)
1708	0	1708	m.w	0.199	3		L Miocene- E Pliocene	MPlm.s.c	Dolati (2010)
1709	0	1709	m.w	0.047	3		L Miocene- E Pliocene	MPlm.s.c	Dolati (2010)
1710	0	1710	m.w	0.040	3		L Miocene- E Pliocene	MPlm.s.c	Dolati (2010)
1711	0	1711	m.w	0.447	3		L Miocene- E Pliocene	MPlm.s.c	Dolati (2010)
1712	0	1712	m.w	0.041	3		L Miocene- E Pliocene	MPlm.s.c	Dolati (2010)
1713	0	1713	m.w	0.043	3		L Miocene- E Pliocene	MPlm.s.c	Dolati (2010)
1714	0	1714	m.w	0.034	3		L Miocene- E Pliocene	MPlm.s.c	Dolati (2010)
1715	0	1715	m.w	0.056	3		L Miocene- E Pliocene	MPlm.s.c	Dolati (2010)
1716	0	1716	m.w	0.053	3		L Miocene- E Pliocene	MPlm.s.c	Dolati (2010)
1717	0	1717	m.w	0.389	3		L Miocene- E Pliocene	MPlm.s.c	Dolati (2010)
1718	0	1718	m.w	0.527	3		L Miocene- E Pliocene	MPlm.s.c	Dolati (2010)
1719	0	1719	m.w	0.389	3		L Miocene- E Pliocene	MPlm.s.c	Dolati (2010)
1720	0	1720	m.w	0.108	3		L Miocene- E Pliocene	MPlm.s.c	Dolati (2010)

GeoNeXus

OBJECTID_1	Join_Count	TARGET_FID	label	Shape_Area (sqkm)	ORIG_FID	Absolute_Age	Age_paleontology	Unit	Reference
1721	0	1721	m.w	0.088	3		L Miocene- E Pliocene	MPlm.s.c	Dolati (2010)
1722	0	1722	m.w	0.248	3		L Miocene- E Pliocene	MPlm.s.c	Dolati (2010)
1723	0	1723	m.w	0.076	3		L Miocene- E Pliocene	MPlm.s.c	Dolati (2010)
1724	0	1724	m.w	0.301	3		L Miocene- E Pliocene	MPlm.s.c	Dolati (2010)
1725	0	1725	m.w	0.236	3		L Miocene- E Pliocene	MPlm.s.c	Dolati (2010)
1726	0	1726	m.w	0.607	3		L Miocene- E Pliocene	MPlm.s.c	Dolati (2010)
1727	0	1727	m.w	0.446	3		L Miocene- E Pliocene	MPlm.s.c	Dolati (2010)
1728	0	1728	m.w	0.046	3		L Miocene- E Pliocene	MPlm.s.c	Dolati (2010)
1729	0	1729	m.w	0.430	3		L Miocene- E Pliocene	MPlm.s.c	Dolati (2010)
1730	0	1730	m.w	0.019	3		L Miocene- E Pliocene	MPlm.s.c	Dolati (2010)
1731	0	1731	m.w	0.220	3		L Miocene- E Pliocene	MPlm.s.c	Dolati (2010)
1732	0	1732	m.w	0.436	3		L Miocene- E Pliocene	MPlm.s.c	Dolati (2010)
1733	0	1733	m.w	0.080	3		L Miocene- E Pliocene	MPlm.s.c	Dolati (2010)
1734	0	1734	m.w	0.067	3		L Miocene- E Pliocene	MPlm.s.c	Dolati (2010)
1735	0	1735	m.w	0.046	3		L Miocene- E Pliocene	MPlm.s.c	Dolati (2010)
1736	0	1736	m.w	0.195	3		L Miocene- E Pliocene	MPlm.s.c	Dolati (2010)
1737	0	1737	m.w	0.109	3		L Miocene- E Pliocene	MPlm.s.c	Dolati (2010)
1738	0	1738	m.w	0.071	3		L Miocene- E Pliocene	MPlm.s.c	Dolati (2010)
1739	0	1739	m.w	0.424	3		L Miocene- E Pliocene	MPlm.s.c	Dolati (2010)
1740	0	1740	m.w	0.288	3		L Miocene- E Pliocene	MPlm.s.c	Dolati (2010)
1741	0	1741	m.w	0.236	3		L Miocene- E Pliocene	MPlm.s.c	Dolati (2010)
1742	0	1742	m.w	0.065	3		L Miocene- E Pliocene	MPlm.s.c	Dolati (2010)
1743	0	1743	m.w	0.162	3		L Miocene- E Pliocene	MPlm.s.c	Dolati (2010)
1744	0	1744	m.w	0.224	3		L Miocene- E Pliocene	MPlm.s.c	Dolati (2010)
1745	0	1745	m.w	0.083	3		L Miocene- E Pliocene	MPlm.s.c	Dolati (2010)
1746	0	1746	m.w	2.495	3		L Miocene- E Pliocene	MPlm.s.c	Dolati (2010)
1748	0	1748	m.w	0.724	3		L Miocene- E Pliocene	MPlm.s.c	Dolati (2010)
1749	0	1749	m.w	0.493	3		L Miocene- E Pliocene	MPlm.s.c	Dolati (2010)
1750	0	1750	m.w	0.046	3		L Miocene- E Pliocene	MPlm.s.c	Dolati (2010)
1751	0	1751	m.w	0.039	3		L Miocene- E Pliocene	MPlm.s.c	Dolati (2010)
1752	0	1752	m.w	0.015	3		L Miocene- E Pliocene	MPlm.s.c	Dolati (2010)
1753	0	1753	m.w	0.114	3		L Miocene- E Pliocene	MPlm.s.c	Dolati (2010)
1754	0	1754	m.w	0.032	3		L Miocene- E Pliocene	MPlm.s.c	Dolati (2010)
1755	0	1755	m.w	0.621	3		L Miocene- E Pliocene	MPlm.s.c	Dolati (2010)
1756	0	1756	m.w	0.041	3		L Miocene- E Pliocene	MPlm.s.c	Dolati (2010)
1757	0	1757	m.w	0.030	3		L Miocene- E Pliocene	MPlm.s.c	Dolati (2010)
1758	0	1758	m.w	0.028	3		L Miocene- E Pliocene	MPlm.s.c	Dolati (2010)
1759	0	1759	m.w	0.081	3		L Miocene- E Pliocene	MPlm.s.c	Dolati (2010)
1760	0	1760	m.w	0.024	3		L Miocene- E Pliocene	MPlm.s.c	Dolati (2010)

GeoMap

OBJECTID_1	Join_Count	TARGET_FID	label	Shape_Area (sqkm)	ORIG_FID	Absolute_Age	Age_paleontology	Unit	Reference
1761	0	1761	m.w	0.186	3		L Miocene- E Pliocene	MPlm.s.c	Dolati (2010)
1762	0	1762	m.w	0.136	3		L Miocene- E Pliocene	MPlm.s.c	Dolati (2010)
1763	0	1763	m.w	0.053	3		L Miocene- E Pliocene	MPlm.s.c	Dolati (2010)
1764	0	1764	m.w	0.055	3		L Miocene- E Pliocene	MPlm.s.c	Dolati (2010)
1765	0	1765	m.w	0.784	3		L Miocene- E Pliocene	MPlm.s.c	Dolati (2010)
1766	0	1766	m.w	0.065	3		L Miocene- E Pliocene	MPlm.s.c	Dolati (2010)
1767	0	1767	m.w	0.027	3		L Miocene- E Pliocene	MPlm.s.c	Dolati (2010)
1768	0	1768	m.w	0.273	3		L Miocene- E Pliocene	MPlm.s.c	Dolati (2010)
1769	0	1769	m.w	0.043	3		L Miocene- E Pliocene	MPlm.s.c	Dolati (2010)
1770	0	1770	m.w	0.152	3		L Miocene- E Pliocene	MPlm.s.c	Dolati (2010)
1771	0	1771	m.w	0.019	3		L Miocene- E Pliocene	MPlm.s.c	Dolati (2010)
1772	0	1772	m.w	1.388	3		L Miocene- E Pliocene	MPlm.s.c	Dolati (2010)
1773	0	1773	m.w	0.084	3		L Miocene- E Pliocene	MPlm.s.c	Dolati (2010)
1774	0	1774	m.w	0.041	3		L Miocene- E Pliocene	MPlm.s.c	Dolati (2010)
1775	0	1775	m.w	1.014	3		L Miocene- E Pliocene	MPlm.s.c	Dolati (2010)
1776	0	1776	m.w	0.557	3		L Miocene- E Pliocene	MPlm.s.c	Dolati (2010)
1777	0	1777	m.w	0.035	3		L Miocene- E Pliocene	MPlm.s.c	Dolati (2010)
1778	0	1778	m.w	0.301	3		L Miocene- E Pliocene	MPlm.s.c	Dolati (2010)
1779	0	1779	m.w	0.141	3		L Miocene- E Pliocene	MPlm.s.c	Dolati (2010)
1780	0	1780	m.w	0.029	3		L Miocene- E Pliocene	MPlm.s.c	Dolati (2010)
1781	0	1781	m.w	0.040	3		L Miocene- E Pliocene	MPlm.s.c	Dolati (2010)
1782	0	1782	m.w	0.113	3		L Miocene- E Pliocene	MPlm.s.c	Dolati (2010)
3028	0	3028	m.w	0.037	6		L Miocene- E Pliocene	MPlm.s.c	Dolati (2010)
8460	1	8461	m.w	0.188	15		L Miocene- E Pliocene	MPlm.s.c	Dolati (2010)
10406	1	10414	m.w	0.027	0		L Miocene- E Pliocene	MPlm.s.c	Dolati (2010)
10407	1	10415	m.w	0.028	0		L Miocene- E Pliocene	MPlm.s.c	Dolati (2010)
10408	1	10417	m.w	0.054	0		L Miocene- E Pliocene	MPlm.s.c	Dolati (2010)
10409	1	10418	m.w	0.019	0		L Miocene- E Pliocene	MPlm.s.c	Dolati (2010)
10410	1	10419	m.w	0.067	0		L Miocene- E Pliocene	MPlm.s.c	Dolati (2010)
10417	1	10428	m.w	0.451	0		L Miocene- E Pliocene	MPlm.s.c	Dolati (2010)
10538	2	244	m.w	0.159	2		L Miocene- E Pliocene	MPlm.s.c	Dolati (2010)

GeoMaps

Table S8. Summary of mapped polygons for the Pl^{si} Unit.

OBJECTID_1	Join_Count	TARGET_FID	Label	Shape_Area(sqkm)	ORIG_FID	Absolute_Age	Age_paleontology	Unit	Reference
244	2	244	m_pink	94.080	2		L Miocene- E Pliocene	Plsi	Dolati (2010)
2112	0	2112	m_pink	1.308	5		Pliocene- Pleistocene	Plsi	Dolati (2010)
2113	0	2113	m_pink	0.703	5		Pliocene- Pleistocene	Plsi	Dolati (2010)
2114	0	2114	m_pink	0.025	5		Pliocene- Pleistocene	Plsi	Dolati (2010)
2115	0	2115	m_pink	1.597	5		Pliocene- Pleistocene	Plsi	Dolati (2010)
2116	0	2116	m_pink	0.011	5		Pliocene- Pleistocene	Plsi	Dolati (2010)
2117	0	2117	m_pink	0.066	5		Pliocene- Pleistocene	Plsi	Dolati (2010)
2118	0	2118	m_pink	0.160	5		Pliocene- Pleistocene	Plsi	Dolati (2010)
2119	0	2119	m_pink	0.325	5		Pliocene- Pleistocene	Plsi	Dolati (2010)
2120	0	2120	m_pink	0.030	5		Pliocene- Pleistocene	Plsi	Dolati (2010)
2121	0	2121	m_pink	0.040	5		Pliocene- Pleistocene	Plsi	Dolati (2010)
2122	0	2122	m_pink	0.345	5		Pliocene- Pleistocene	Plsi	Dolati (2010)
2123	0	2123	m_pink	0.066	5		Pliocene- Pleistocene	Plsi	Dolati (2010)
2124	0	2124	m_pink	0.987	5		Pliocene- Pleistocene	Plsi	Dolati (2010)
2125	0	2125	m_pink	0.087	5		Pliocene- Pleistocene	Plsi	Dolati (2010)
2126	0	2126	m_pink	0.041	5		Pliocene- Pleistocene	Plsi	Dolati (2010)
2127	0	2127	m_pink	2.427	5		Pliocene- Pleistocene	Plsi	Dolati (2010)
2128	0	2128	m_pink	0.084	5		Pliocene- Pleistocene	Plsi	Dolati (2010)
2129	0	2129	m_pink	0.678	5		Pliocene- Pleistocene	Plsi	Dolati (2010)
2130	0	2130	m_pink	2.536	5		Pliocene- Pleistocene	Plsi	Dolati (2010)
2131	0	2131	m_pink	0.840	5		Pliocene- Pleistocene	Plsi	Dolati (2010)
2132	0	2132	m_pink	1.301	5		Pliocene- Pleistocene	Plsi	Dolati (2010)
2133	0	2133	m_pink	0.501	5		Pliocene- Pleistocene	Plsi	Dolati (2010)
2134	0	2134	m_pink	0.028	5		Pliocene- Pleistocene	Plsi	Dolati (2010)
2135	0	2135	m_pink	0.042	5		Pliocene- Pleistocene	Plsi	Dolati (2010)
2136	0	2136	m_pink	0.108	5		Pliocene- Pleistocene	Plsi	Dolati (2010)
2137	0	2137	m_pink	0.013	5		Pliocene- Pleistocene	Plsi	Dolati (2010)
2138	0	2138	m_pink	0.115	5		Pliocene- Pleistocene	Plsi	Dolati (2010)
2139	0	2139	m_pink	0.040	5		Pliocene- Pleistocene	Plsi	Dolati (2010)
2140	0	2140	m_pink	0.696	5		Pliocene- Pleistocene	Plsi	Dolati (2010)
2141	0	2141	m_pink	0.684	5		Pliocene- Pleistocene	Plsi	Dolati (2010)
2142	0	2142	m_pink	0.047	5		Pliocene- Pleistocene	Plsi	Dolati (2010)
2143	0	2143	m_pink	0.244	5		Pliocene- Pleistocene	Plsi	Dolati (2010)
2145	0	2145	m_pink	0.094	5		Pliocene- Pleistocene	Plsi	Dolati (2010)
2146	0	2146	m_pink	0.191	5		Pliocene- Pleistocene	Plsi	Dolati (2010)
2147	0	2147	m_pink	0.969	5		Pliocene- Pleistocene	Plsi	Dolati (2010)
2148	0	2148	m_pink	0.119	5		Pliocene- Pleistocene	Plsi	Dolati (2010)

Geonemis

OBJECTID_1	Join_Count	TARGET_FID	Label	Shape_Area(sqkm)	ORIG_FID	Absolute_Age	Age_paleontology	Unit	Reference
2149	0	2149	m_pink	0.176	5		Pliocene- Pleistocene	Plsi	Dolati (2010)
2150	0	2150	m_pink	0.025	5		Pliocene- Pleistocene	Plsi	Dolati (2010)
2151	0	2151	m_pink	0.150	5		Pliocene- Pleistocene	Plsi	Dolati (2010)
2153	0	2153	m_pink	0.094	5		Pliocene- Pleistocene	Plsi	Dolati (2010)
2155	0	2155	m_pink	0.032	5		Pliocene- Pleistocene	Plsi	Dolati (2010)
2156	0	2156	m_pink	0.039	5		Pliocene- Pleistocene	Plsi	Dolati (2010)
2157	0	2157	m_pink	0.734	5		Pliocene- Pleistocene	Plsi	Dolati (2010)
2158	0	2158	m_pink	0.291	5		Pliocene- Pleistocene	Plsi	Dolati (2010)
2159	0	2159	m_pink	0.352	5		Pliocene- Pleistocene	Plsi	Dolati (2010)
2161	0	2161	m_pink	0.016	5		Pliocene- Pleistocene	Plsi	Dolati (2010)
2162	0	2162	m_pink	29.882	5		Pliocene- Pleistocene	Plsi	Dolati (2010)
2163	0	2163	m_pink	1.137	5		Pliocene- Pleistocene	Plsi	Dolati (2010)
2164	0	2164	m_pink	0.205	5		Pliocene- Pleistocene	Plsi	Dolati (2010)
2166	0	2166	m_pink	0.009	5		Pliocene- Pleistocene	Plsi	Dolati (2010)
2167	0	2167	m_pink	10.096	5		Pliocene- Pleistocene	Plsi	Dolati (2010)
2168	0	2168	m_pink	0.394	5		Pliocene- Pleistocene	Plsi	Dolati (2010)
2169	0	2169	m_pink	0.223	5		Pliocene- Pleistocene	Plsi	Dolati (2010)
2170	0	2170	m_pink	0.226	5		Pliocene- Pleistocene	Plsi	Dolati (2010)
2171	0	2171	m_pink	0.018	5		Pliocene- Pleistocene	Plsi	Dolati (2010)
2172	0	2172	m_pink	0.012	5		Pliocene- Pleistocene	Plsi	Dolati (2010)
2174	0	2174	m_pink	0.010	5		Pliocene- Pleistocene	Plsi	Dolati (2010)
2175	0	2175	m_pink	0.035	5		Pliocene- Pleistocene	Plsi	Dolati (2010)
2176	0	2176	m_pink	0.079	5		Pliocene- Pleistocene	Plsi	Dolati (2010)
2177	0	2177	m_pink	0.172	5		Pliocene- Pleistocene	Plsi	Dolati (2010)
2178	0	2178	m_pink	0.071	5		Pliocene- Pleistocene	Plsi	Dolati (2010)
2179	0	2179	m_pink	0.266	5		Pliocene- Pleistocene	Plsi	Dolati (2010)
2180	0	2180	m_pink	0.064	5		Pliocene- Pleistocene	Plsi	Dolati (2010)
2181	0	2181	m_pink	0.053	5		Pliocene- Pleistocene	Plsi	Dolati (2010)
2182	0	2182	m_pink	0.087	5		Pliocene- Pleistocene	Plsi	Dolati (2010)
2183	0	2183	m_pink	0.078	5		Pliocene- Pleistocene	Plsi	Dolati (2010)
2184	0	2184	m_pink	0.427	5		Pliocene- Pleistocene	Plsi	Dolati (2010)
2185	0	2185	m_pink	0.096	5		Pliocene- Pleistocene	Plsi	Dolati (2010)
2186	0	2186	m_pink	0.016	5		Pliocene- Pleistocene	Plsi	Dolati (2010)
2187	0	2187	m_pink	0.021	5		Pliocene- Pleistocene	Plsi	Dolati (2010)
2188	0	2188	m_pink	0.072	5		Pliocene- Pleistocene	Plsi	Dolati (2010)
2189	0	2189	m_pink	0.047	5		Pliocene- Pleistocene	Plsi	Dolati (2010)
2190	0	2190	m_pink	0.009	5		Pliocene- Pleistocene	Plsi	Dolati (2010)
2191	0	2191	m_pink	0.314	5		Pliocene- Pleistocene	Plsi	Dolati (2010)
2192	0	2192	m_pink	0.103	5		Pliocene- Pleistocene	Plsi	Dolati (2010)

GSI Nov 25

OBJECTID_1	Join_Count	TARGET_FID	Label	Shape_Area(sqkm)	ORIG_FID	Absolute_Age	Age_paleontology	Unit	Reference
2193	0	2193	m_pink	0.395	5		Pliocene- Pleistocene	Plsi	Dolati (2010)
2194	0	2194	m_pink	0.055	5		Pliocene- Pleistocene	Plsi	Dolati (2010)
2195	0	2195	m_pink	0.263	5		Pliocene- Pleistocene	Plsi	Dolati (2010)
2196	0	2196	m_pink	0.187	5		Pliocene- Pleistocene	Plsi	Dolati (2010)
2197	0	2197	m_pink	0.053	5		Pliocene- Pleistocene	Plsi	Dolati (2010)
2198	0	2198	m_pink	0.153	5		Pliocene- Pleistocene	Plsi	Dolati (2010)
2199	0	2199	m_pink	0.012	5		Pliocene- Pleistocene	Plsi	Dolati (2010)
2200	0	2200	m_pink	0.064	5		Pliocene- Pleistocene	Plsi	Dolati (2010)
2202	0	2202	m_pink	0.073	5		Pliocene- Pleistocene	Plsi	Dolati (2010)
2203	0	2203	m_pink	0.167	5		Pliocene- Pleistocene	Plsi	Dolati (2010)
2204	0	2204	m_pink	0.133	5		Pliocene- Pleistocene	Plsi	Dolati (2010)
2205	0	2205	m_pink	0.084	5		Pliocene- Pleistocene	Plsi	Dolati (2010)
2206	0	2206	m_pink	0.136	5		Pliocene- Pleistocene	Plsi	Dolati (2010)
2207	0	2207	m_pink	0.301	5		Pliocene- Pleistocene	Plsi	Dolati (2010)
2208	0	2208	m_pink	0.105	5		Pliocene- Pleistocene	Plsi	Dolati (2010)
2209	0	2209	m_pink	0.058	5		Pliocene- Pleistocene	Plsi	Dolati (2010)
2210	0	2210	m_pink	0.538	5		Pliocene- Pleistocene	Plsi	Dolati (2010)
2211	0	2211	m_pink	0.027	5		Pliocene- Pleistocene	Plsi	Dolati (2010)
2212	0	2212	m_pink	0.229	5		Pliocene- Pleistocene	Plsi	Dolati (2010)
2213	0	2213	m_pink	0.543	5		Pliocene- Pleistocene	Plsi	Dolati (2010)
2214	0	2214	m_pink	0.172	5		Pliocene- Pleistocene	Plsi	Dolati (2010)
2215	0	2215	m_pink	0.279	5		Pliocene- Pleistocene	Plsi	Dolati (2010)
2216	0	2216	m_pink	0.139	5		Pliocene- Pleistocene	Plsi	Dolati (2010)
2217	0	2217	m_pink	0.807	5		Pliocene- Pleistocene	Plsi	Dolati (2010)
2218	0	2218	m_pink	0.584	5		Pliocene- Pleistocene	Plsi	Dolati (2010)
2219	0	2219	m_pink	0.027	5		Pliocene- Pleistocene	Plsi	Dolati (2010)
2220	0	2220	m_pink	0.189	5		Pliocene- Pleistocene	Plsi	Dolati (2010)
2221	0	2221	m_pink	0.043	5		Pliocene- Pleistocene	Plsi	Dolati (2010)
2222	0	2222	m_pink	0.143	5		Pliocene- Pleistocene	Plsi	Dolati (2010)
2223	0	2223	m_pink	0.027	5		Pliocene- Pleistocene	Plsi	Dolati (2010)
2224	0	2224	m_pink	0.370	5		Pliocene- Pleistocene	Plsi	Dolati (2010)
2225	0	2225	m_pink	0.037	5		Pliocene- Pleistocene	Plsi	Dolati (2010)
2226	0	2226	m_pink	0.038	5		Pliocene- Pleistocene	Plsi	Dolati (2010)
2227	0	2227	m_pink	0.090	5		Pliocene- Pleistocene	Plsi	Dolati (2010)
2228	0	2228	m_pink	0.042	5		Pliocene- Pleistocene	Plsi	Dolati (2010)
2229	0	2229	m_pink	0.049	5		Pliocene- Pleistocene	Plsi	Dolati (2010)
2230	0	2230	m_pink	0.119	5		Pliocene- Pleistocene	Plsi	Dolati (2010)
2231	0	2231	m_pink	0.063	5		Pliocene- Pleistocene	Plsi	Dolati (2010)
2232	0	2232	m_pink	0.041	5		Pliocene- Pleistocene	Plsi	Dolati (2010)

Geonavis

OBJECTID_1	Join_Count	TARGET_FID	Label	Shape_Area(sqkm)	ORIG_FID	Absolute_Age	Age_paleontology	Unit	Reference
2233	0	2233	m_pink	0.065	5		Pliocene- Pleistocene	Plsi	Dolati (2010)
2234	0	2234	m_pink	0.085	5		Pliocene- Pleistocene	Plsi	Dolati (2010)
2235	0	2235	m_pink	0.110	5		Pliocene- Pleistocene	Plsi	Dolati (2010)
2236	0	2236	m_pink	0.256	5		Pliocene- Pleistocene	Plsi	Dolati (2010)
2237	0	2237	m_pink	0.040	5		Pliocene- Pleistocene	Plsi	Dolati (2010)
2238	0	2238	m_pink	0.770	5		Pliocene- Pleistocene	Plsi	Dolati (2010)
2239	0	2239	m_pink	0.705	5		Pliocene- Pleistocene	Plsi	Dolati (2010)
2240	0	2240	m_pink	2.906	5		Pliocene- Pleistocene	Plsi	Dolati (2010)
2241	0	2241	m_pink	0.038	5		Pliocene- Pleistocene	Plsi	Dolati (2010)
2242	0	2242	m_pink	0.758	5		Pliocene- Pleistocene	Plsi	Dolati (2010)
2243	1	2243	m_pink	0.077	5		Pliocene- Pleistocene	Plsi	Dolati (2010)
2244	0	2244	m_pink	0.044	5		Pliocene- Pleistocene	Plsi	Dolati (2010)
2245	0	2245	m_pink	0.043	5		Pliocene- Pleistocene	Plsi	Dolati (2010)
2246	0	2246	m_pink	0.192	5		Pliocene- Pleistocene	Plsi	Dolati (2010)
2247	0	2247	m_pink	0.117	5		Pliocene- Pleistocene	Plsi	Dolati (2010)
2248	0	2248	m_pink	0.744	5		Pliocene- Pleistocene	Plsi	Dolati (2010)
2249	0	2249	m_pink	0.073	5		Pliocene- Pleistocene	Plsi	Dolati (2010)
2250	0	2250	m_pink	0.014	5		Pliocene- Pleistocene	Plsi	Dolati (2010)
2251	0	2251	m_pink	0.087	5		Pliocene- Pleistocene	Plsi	Dolati (2010)
2252	0	2252	m_pink	0.292	5		Pliocene- Pleistocene	Plsi	Dolati (2010)
2253	0	2253	m_pink	0.109	5		Pliocene- Pleistocene	Plsi	Dolati (2010)
2254	0	2254	m_pink	0.046	5		Pliocene- Pleistocene	Plsi	Dolati (2010)
2255	1	2255	m_pink	0.088	5		Pliocene- Pleistocene	Plsi	Dolati (2010)
2256	0	2256	m_pink	0.047	5		Pliocene- Pleistocene	Plsi	Dolati (2010)
2257	0	2257	m_pink	0.030	5		Pliocene- Pleistocene	Plsi	Dolati (2010)
2258	0	2258	m_pink	0.089	5		Pliocene- Pleistocene	Plsi	Dolati (2010)
2259	0	2259	m_pink	0.908	5		Pliocene- Pleistocene	Plsi	Dolati (2010)
2260	0	2260	m_pink	0.157	5		Pliocene- Pleistocene	Plsi	Dolati (2010)
2261	0	2261	m_pink	1.893	5		Pliocene- Pleistocene	Plsi	Dolati (2010)
2262	1	2262	m_pink	1.261	5		Pliocene- Pleistocene	Plsi	Dolati (2010)
2263	0	2263	m_pink	0.195	5		Pliocene- Pleistocene	Plsi	Dolati (2010)
2264	0	2264	m_pink	0.146	5		Pliocene- Pleistocene	Plsi	Dolati (2010)
2265	0	2265	m_pink	0.344	5		Pliocene- Pleistocene	Plsi	Dolati (2010)
2266	0	2266	m_pink	1.621	5		Pliocene- Pleistocene	Plsi	Dolati (2010)
2267	0	2267	m_pink	0.128	5		Pliocene- Pleistocene	Plsi	Dolati (2010)
2268	0	2268	m_pink	0.104	5		Pliocene- Pleistocene	Plsi	Dolati (2010)
2269	0	2269	m_pink	0.040	5		Pliocene- Pleistocene	Plsi	Dolati (2010)
2270	1	2270	m_pink	1.682	5		Pliocene- Pleistocene	Plsi	Dolati (2010)
2271	0	2271	m_pink	0.134	5		Pliocene- Pleistocene	Plsi	Dolati (2010)

GSI NOVUS

OBJECTID_1	Join_Count	TARGET_FID	Label	Shape_Area(sqkm)	ORIG_FID	Absolute_Age	Age_paleontology	Unit	Reference
2272	0	2272	m_pink	5.445	5		Pliocene- Pleistocene	Plsi	Dolati (2010)
2273	0	2273	m_pink	0.254	5		Pliocene- Pleistocene	Plsi	Dolati (2010)
2274	0	2274	m_pink	0.093	5		Pliocene- Pleistocene	Plsi	Dolati (2010)
2275	0	2275	m_pink	0.191	5		Pliocene- Pleistocene	Plsi	Dolati (2010)
2276	0	2276	m_pink	0.062	5		Pliocene- Pleistocene	Plsi	Dolati (2010)
2277	0	2277	m_pink	0.074	5		Pliocene- Pleistocene	Plsi	Dolati (2010)
2278	0	2278	m_pink	0.143	5		Pliocene- Pleistocene	Plsi	Dolati (2010)
2279	0	2279	m_pink	0.221	5		Pliocene- Pleistocene	Plsi	Dolati (2010)
2280	0	2280	m_pink	0.098	5		Pliocene- Pleistocene	Plsi	Dolati (2010)
2281	0	2281	m_pink	0.570	5		Pliocene- Pleistocene	Plsi	Dolati (2010)
2282	0	2282	m_pink	0.060	5		Pliocene- Pleistocene	Plsi	Dolati (2010)
2283	0	2283	m_pink	0.077	5		Pliocene- Pleistocene	Plsi	Dolati (2010)
2284	0	2284	m_pink	0.480	5		Pliocene- Pleistocene	Plsi	Dolati (2010)
2285	0	2285	m_pink	0.213	5		Pliocene- Pleistocene	Plsi	Dolati (2010)
2286	0	2286	m_pink	0.473	5		Pliocene- Pleistocene	Plsi	Dolati (2010)
2287	0	2287	m_pink	0.727	5		Pliocene- Pleistocene	Plsi	Dolati (2010)
2288	0	2288	m_pink	0.104	5		Pliocene- Pleistocene	Plsi	Dolati (2010)
2289	0	2289	m_pink	0.565	5		Pliocene- Pleistocene	Plsi	Dolati (2010)
2290	0	2290	m_pink	0.011	5		Pliocene- Pleistocene	Plsi	Dolati (2010)
2291	0	2291	m_pink	0.091	5		Pliocene- Pleistocene	Plsi	Dolati (2010)
2292	0	2292	m_pink	0.104	5		Pliocene- Pleistocene	Plsi	Dolati (2010)
2293	0	2293	m_pink	0.019	5		Pliocene- Pleistocene	Plsi	Dolati (2010)
2294	0	2294	m_pink	3.696	5		Pliocene- Pleistocene	Plsi	Dolati (2010)
2295	0	2295	m_pink	7.754	5		Pliocene- Pleistocene	Plsi	Dolati (2010)
2296	0	2296	m_pink	0.123	5		Pliocene- Pleistocene	Plsi	Dolati (2010)
2297	0	2297	m_pink	0.111	5		Pliocene- Pleistocene	Plsi	Dolati (2010)
2298	0	2298	m_pink	0.181	5		Pliocene- Pleistocene	Plsi	Dolati (2010)
2299	0	2299	m_pink	0.013	5		Pliocene- Pleistocene	Plsi	Dolati (2010)
2300	0	2300	m_pink	21.030	5		Pliocene- Pleistocene	Plsi	Dolati (2010)
2301	0	2301	m_pink	0.056	5		Pliocene- Pleistocene	Plsi	Dolati (2010)
2302	0	2302	m_pink	0.019	5		Pliocene- Pleistocene	Plsi	Dolati (2010)
2303	0	2303	m_pink	0.635	5		Pliocene- Pleistocene	Plsi	Dolati (2010)
2304	0	2304	m_pink	0.304	5		Pliocene- Pleistocene	Plsi	Dolati (2010)
2305	0	2305	m_pink	0.058	5		Pliocene- Pleistocene	Plsi	Dolati (2010)
2306	0	2306	m_pink	0.094	5		Pliocene- Pleistocene	Plsi	Dolati (2010)
2307	0	2307	m_pink	0.180	5		Pliocene- Pleistocene	Plsi	Dolati (2010)
2308	0	2308	m_pink	0.198	5		Pliocene- Pleistocene	Plsi	Dolati (2010)
2309	0	2309	m_pink	2.034	5		Pliocene- Pleistocene	Plsi	Dolati (2010)
2310	0	2310	m_pink	0.097	5		Pliocene- Pleistocene	Plsi	Dolati (2010)

Geonavis

OBJECTID_1	Join_Count	TARGET_FID	Label	Shape_Area(sqkm)	ORIG_FID	Absolute_Age	Age_paleontology	Unit	Reference
2311	0	2311	m_pink	0.041	5		Pliocene- Pleistocene	Plsi	Dolati (2010)
2312	0	2312	m_pink	0.330	5		Pliocene- Pleistocene	Plsi	Dolati (2010)
2313	0	2313	m_pink	2.911	5		Pliocene- Pleistocene	Plsi	Dolati (2010)
2314	0	2314	m_pink	0.803	5		Pliocene- Pleistocene	Plsi	Dolati (2010)
2315	0	2315	m_pink	0.096	5		Pliocene- Pleistocene	Plsi	Dolati (2010)
2316	0	2316	m_pink	0.046	5		Pliocene- Pleistocene	Plsi	Dolati (2010)
2317	0	2317	m_pink	0.048	5		Pliocene- Pleistocene	Plsi	Dolati (2010)
2318	0	2318	m_pink	0.051	5		Pliocene- Pleistocene	Plsi	Dolati (2010)
2319	0	2319	m_pink	1.753	5		Pliocene- Pleistocene	Plsi	Dolati (2010)
2320	0	2320	m_pink	0.098	5		Pliocene- Pleistocene	Plsi	Dolati (2010)
2321	0	2321	m_pink	0.614	5		Pliocene- Pleistocene	Plsi	Dolati (2010)
2322	0	2322	m_pink	0.040	5		Pliocene- Pleistocene	Plsi	Dolati (2010)
2323	0	2323	m_pink	0.405	5		Pliocene- Pleistocene	Plsi	Dolati (2010)
2324	0	2324	m_pink	0.190	5		Pliocene- Pleistocene	Plsi	Dolati (2010)
2325	0	2325	m_pink	0.044	5		Pliocene- Pleistocene	Plsi	Dolati (2010)
2326	0	2326	m_pink	0.598	5		Pliocene- Pleistocene	Plsi	Dolati (2010)
2327	0	2327	m_pink	1.688	5		Pliocene- Pleistocene	Plsi	Dolati (2010)
2328	0	2328	m_pink	0.146	5		Pliocene- Pleistocene	Plsi	Dolati (2010)
2329	0	2329	m_pink	0.162	5		Pliocene- Pleistocene	Plsi	Dolati (2010)
2330	0	2330	m_pink	0.441	5		Pliocene- Pleistocene	Plsi	Dolati (2010)
2331	0	2331	m_pink	0.017	5		Pliocene- Pleistocene	Plsi	Dolati (2010)
2332	0	2332	m_pink	0.034	5		Pliocene- Pleistocene	Plsi	Dolati (2010)
2333	0	2333	m_pink	0.055	5		Pliocene- Pleistocene	Plsi	Dolati (2010)
2334	0	2334	m_pink	0.046	5		Pliocene- Pleistocene	Plsi	Dolati (2010)
2335	0	2335	m_pink	0.150	5		Pliocene- Pleistocene	Plsi	Dolati (2010)
2336	0	2336	m_pink	0.368	5		Pliocene- Pleistocene	Plsi	Dolati (2010)
2337	0	2337	m_pink	0.270	5		Pliocene- Pleistocene	Plsi	Dolati (2010)
2338	0	2338	m_pink	0.039	5		Pliocene- Pleistocene	Plsi	Dolati (2010)
2339	0	2339	m_pink	0.024	5		Pliocene- Pleistocene	Plsi	Dolati (2010)
2340	0	2340	m_pink	0.721	5		Pliocene- Pleistocene	Plsi	Dolati (2010)
2341	0	2341	m_pink	0.134	5		Pliocene- Pleistocene	Plsi	Dolati (2010)
2342	0	2342	m_pink	0.407	5		Pliocene- Pleistocene	Plsi	Dolati (2010)
2343	0	2343	m_pink	0.062	5		Pliocene- Pleistocene	Plsi	Dolati (2010)
2344	0	2344	m_pink	0.076	5		Pliocene- Pleistocene	Plsi	Dolati (2010)
2345	0	2345	m_pink	0.034	5		Pliocene- Pleistocene	Plsi	Dolati (2010)
2346	0	2346	m_pink	3.278	5		Pliocene- Pleistocene	Plsi	Dolati (2010)
2347	0	2347	m_pink	0.007	5		Pliocene- Pleistocene	Plsi	Dolati (2010)
2348	0	2348	m_pink	0.339	5		Pliocene- Pleistocene	Plsi	Dolati (2010)
2349	0	2349	m_pink	0.028	5		Pliocene- Pleistocene	Plsi	Dolati (2010)

GSI Nov 25

OBJECTID_1	Join_Count	TARGET_FID	Label	Shape_Area(sqkm)	ORIG_FID	Absolute_Age	Age_paleontology	Unit	Reference
2350	0	2350	m_pink	0.035	5		Pliocene- Pleistocene	Plsi	Dolati (2010)
2351	0	2351	m_pink	0.060	5		Pliocene- Pleistocene	Plsi	Dolati (2010)
2352	0	2352	m_pink	0.288	5		Pliocene- Pleistocene	Plsi	Dolati (2010)
2353	0	2353	m_pink	0.030	5		Pliocene- Pleistocene	Plsi	Dolati (2010)
2354	0	2354	m_pink	0.059	5		Pliocene- Pleistocene	Plsi	Dolati (2010)
2355	0	2355	m_pink	0.108	5		Pliocene- Pleistocene	Plsi	Dolati (2010)
2356	0	2356	m_pink	0.066	5		Pliocene- Pleistocene	Plsi	Dolati (2010)
2357	0	2357	m_pink	0.224	5		Pliocene- Pleistocene	Plsi	Dolati (2010)
2358	0	2358	m_pink	0.036	5		Pliocene- Pleistocene	Plsi	Dolati (2010)
2359	0	2359	m_pink	0.289	5		Pliocene- Pleistocene	Plsi	Dolati (2010)
2360	0	2360	m_pink	0.054	5		Pliocene- Pleistocene	Plsi	Dolati (2010)
2361	0	2361	m_pink	0.621	5		Pliocene- Pleistocene	Plsi	Dolati (2010)
2362	0	2362	m_pink	0.149	5		Pliocene- Pleistocene	Plsi	Dolati (2010)
2363	0	2363	m_pink	1.979	5		Pliocene- Pleistocene	Plsi	Dolati (2010)
2364	0	2364	m_pink	0.223	5		Pliocene- Pleistocene	Plsi	Dolati (2010)
2365	0	2365	m_pink	0.044	5		Pliocene- Pleistocene	Plsi	Dolati (2010)
2366	0	2366	m_pink	53.231	5		Pliocene- Pleistocene	Plsi	Dolati (2010)
2367	0	2367	m_pink	3.546	5		Pliocene- Pleistocene	Plsi	Dolati (2010)
2368	0	2368	m_pink	0.071	5		Pliocene- Pleistocene	Plsi	Dolati (2010)
2369	0	2369	m_pink	0.035	5		Pliocene- Pleistocene	Plsi	Dolati (2010)
2370	0	2370	m_pink	0.069	5		Pliocene- Pleistocene	Plsi	Dolati (2010)
2371	0	2371	m_pink	0.244	5		Pliocene- Pleistocene	Plsi	Dolati (2010)
2372	0	2372	m_pink	0.650	5		Pliocene- Pleistocene	Plsi	Dolati (2010)
2373	0	2373	m_pink	0.055	5		Pliocene- Pleistocene	Plsi	Dolati (2010)
2374	0	2374	m_pink	0.063	5		Pliocene- Pleistocene	Plsi	Dolati (2010)
2375	0	2375	m_pink	0.360	5		Pliocene- Pleistocene	Plsi	Dolati (2010)
2376	0	2376	m_pink	0.233	5		Pliocene- Pleistocene	Plsi	Dolati (2010)
2377	0	2377	m_pink	0.008	5		Pliocene- Pleistocene	Plsi	Dolati (2010)
2378	0	2378	m_pink	3.113	5		Pliocene- Pleistocene	Plsi	Dolati (2010)
2379	0	2379	m_pink	0.034	5		Pliocene- Pleistocene	Plsi	Dolati (2010)
2380	0	2380	m_pink	0.019	5		Pliocene- Pleistocene	Plsi	Dolati (2010)
2381	0	2381	m_pink	0.146	5		Pliocene- Pleistocene	Plsi	Dolati (2010)
2382	0	2382	m_pink	0.020	5		Pliocene- Pleistocene	Plsi	Dolati (2010)
2383	0	2383	m_pink	0.830	5		Pliocene- Pleistocene	Plsi	Dolati (2010)
2384	0	2384	m_pink	4.110	5		Pliocene- Pleistocene	Plsi	Dolati (2010)
2385	0	2385	m_pink	0.070	5		Pliocene- Pleistocene	Plsi	Dolati (2010)
2386	0	2386	m_pink	0.031	5		Pliocene- Pleistocene	Plsi	Dolati (2010)
2387	0	2387	m_pink	0.024	5		Pliocene- Pleistocene	Plsi	Dolati (2010)
2388	0	2388	m_pink	1.494	5		Pliocene- Pleistocene	Plsi	Dolati (2010)

Geonavis

OBJECTID_1	Join_Count	TARGET_FID	Label	Shape_Area(sqkm)	ORIG_FID	Absolute_Age	Age_paleontology	Unit	Reference
2389	0	2389	m_pink	0.091	5		Pliocene- Pleistocene	Plsi	Dolati (2010)
2390	0	2390	m_pink	0.032	5		Pliocene- Pleistocene	Plsi	Dolati (2010)
2391	0	2391	m_pink	0.051	5		Pliocene- Pleistocene	Plsi	Dolati (2010)
2392	0	2392	m_pink	0.168	5		Pliocene- Pleistocene	Plsi	Dolati (2010)
2393	0	2393	m_pink	0.131	5		Pliocene- Pleistocene	Plsi	Dolati (2010)
2394	0	2394	m_pink	2.641	5		Pliocene- Pleistocene	Plsi	Dolati (2010)
2395	0	2395	m_pink	6.253	5		Pliocene- Pleistocene	Plsi	Dolati (2010)
2396	0	2396	m_pink	0.068	5		Pliocene- Pleistocene	Plsi	Dolati (2010)
2397	0	2397	m_pink	0.021	5		Pliocene- Pleistocene	Plsi	Dolati (2010)
2398	0	2398	m_pink	0.063	5		Pliocene- Pleistocene	Plsi	Dolati (2010)
2399	0	2399	m_pink	0.101	5		Pliocene- Pleistocene	Plsi	Dolati (2010)
2400	0	2400	m_pink	0.011	5		Pliocene- Pleistocene	Plsi	Dolati (2010)
2401	0	2401	m_pink	0.015	5		Pliocene- Pleistocene	Plsi	Dolati (2010)
2402	0	2402	m_pink	0.645	5		Pliocene- Pleistocene	Plsi	Dolati (2010)
2403	0	2403	m_pink	0.023	5		Pliocene- Pleistocene	Plsi	Dolati (2010)
2404	0	2404	m_pink	0.005	5		Pliocene- Pleistocene	Plsi	Dolati (2010)
2405	0	2405	m_pink	1.482	5		Pliocene- Pleistocene	Plsi	Dolati (2010)
2406	0	2406	m_pink	0.176	5		Pliocene- Pleistocene	Plsi	Dolati (2010)
2407	0	2407	m_pink	0.030	5		Pliocene- Pleistocene	Plsi	Dolati (2010)
2408	0	2408	m_pink	0.045	5		Pliocene- Pleistocene	Plsi	Dolati (2010)
2409	0	2409	m_pink	65.403	5		Pliocene- Pleistocene	Plsi	Dolati (2010)
2410	0	2410	m_pink	1.082	5		Pliocene- Pleistocene	Plsi	Dolati (2010)
2411	0	2411	m_pink	0.307	5		Pliocene- Pleistocene	Plsi	Dolati (2010)
2412	0	2412	m_pink	0.776	5		Pliocene- Pleistocene	Plsi	Dolati (2010)
2413	0	2413	m_pink	0.314	5		Pliocene- Pleistocene	Plsi	Dolati (2010)
2414	0	2414	m_pink	0.120	5		Pliocene- Pleistocene	Plsi	Dolati (2010)
2415	0	2415	m_pink	0.078	5		Pliocene- Pleistocene	Plsi	Dolati (2010)
2416	0	2416	m_pink	0.096	5		Pliocene- Pleistocene	Plsi	Dolati (2010)
2417	0	2417	m_pink	0.130	5		Pliocene- Pleistocene	Plsi	Dolati (2010)
2418	0	2418	m_pink	0.083	5		Pliocene- Pleistocene	Plsi	Dolati (2010)
2419	0	2419	m_pink	0.271	5		Pliocene- Pleistocene	Plsi	Dolati (2010)
2420	0	2420	m_pink	0.012	5		Pliocene- Pleistocene	Plsi	Dolati (2010)
2421	0	2421	m_pink	0.033	5		Pliocene- Pleistocene	Plsi	Dolati (2010)
2422	0	2422	m_pink	0.063	5		Pliocene- Pleistocene	Plsi	Dolati (2010)
2423	0	2423	m_pink	0.334	5		Pliocene- Pleistocene	Plsi	Dolati (2010)
2424	0	2424	m_pink	0.083	5		Pliocene- Pleistocene	Plsi	Dolati (2010)
2425	0	2425	m_pink	0.160	5		Pliocene- Pleistocene	Plsi	Dolati (2010)
10024	1	10026	m_pink	0.085	18			Plsi	
10029	1	10031	m_pink	0.536	18			Plsi	

GSI NOVUS

Table S9. Summary of mapped polygons for the $Pl^{si.c}$ Unit.

OBJECTID_1	Join_Count	TARGET_FID	Label	Shape_Area (sqkm)	ORIG_FID	Absolute_Age	Age_paleontology	Unit	Reference
3798	0	3798	mud_pink	0.013	7		Pliocene	Plsi.c	
3799	0	3799	mud_pink	0.089	7		Pliocene	Plsi.c	
3800	0	3800	mud_pink	0.012	7		Pliocene	Plsi.c	
3801	0	3801	mud_pink	0.010	7		Pliocene	Plsi.c	
3802	0	3802	mud_pink	0.004	7		Pliocene	Plsi.c	
3803	0	3803	mud_pink	0.101	7		Pliocene	Plsi.c	
3804	0	3804	mud_pink	0.109	7		Pliocene	Plsi.c	
3805	0	3805	mud_pink	0.008	7		Pliocene	Plsi.c	
3806	0	3806	mud_pink	0.100	7		Pliocene	Plsi.c	
3807	0	3807	mud_pink	0.314	7		Pliocene	Plsi.c	
3808	0	3808	mud_pink	0.117	7		Pliocene	Plsi.c	
3809	0	3809	mud_pink	0.055	7		Pliocene	Plsi.c	
3810	0	3810	mud_pink	0.063	7		Pliocene	Plsi.c	
3811	0	3811	mud_pink	0.578	7		Pliocene	Plsi.c	
3812	0	3812	mud_pink	0.953	7		Pliocene	Plsi.c	
3813	0	3813	mud_pink	0.220	7		Pliocene	Plsi.c	
3814	0	3814	mud_pink	0.041	7		Pliocene	Plsi.c	
3815	0	3815	mud_pink	0.075	7		Pliocene	Plsi.c	
3816	0	3816	mud_pink	0.136	7		Pliocene	Plsi.c	
3817	0	3817	mud_pink	0.021	7		Pliocene	Plsi.c	
3818	0	3818	mud_pink	0.066	7		Pliocene	Plsi.c	
3819	0	3819	mud_pink	0.119	7		Pliocene	Plsi.c	
3820	0	3820	mud_pink	0.476	7		Pliocene	Plsi.c	
3821	0	3821	mud_pink	0.082	7		Pliocene	Plsi.c	
3822	0	3822	mud_pink	0.058	7		Pliocene	Plsi.c	
3823	0	3823	mud_pink	0.088	7		Pliocene	Plsi.c	
3824	0	3824	mud_pink	0.057	7		Pliocene	Plsi.c	
3825	0	3825	mud_pink	0.544	7		Pliocene	Plsi.c	
3826	0	3826	mud_pink	0.052	7		Pliocene	Plsi.c	
3827	0	3827	mud_pink	0.239	7		Pliocene	Plsi.c	
3828	0	3828	mud_pink	0.025	7		Pliocene	Plsi.c	
3829	0	3829	mud_pink	1.125	7		Pliocene	Plsi.c	
3830	0	3830	mud_pink	0.744	7		Pliocene	Plsi.c	

GeoNexus

OBJECTID_1	Join_Count	TARGET_FID	Label	Shape_Area (sqkm)	ORIG_FID	Absolute_Age	Age_paleontology	Unit	Reference
3831	0	3831	mud_pink	0.007	7		Pliocene	Plsi.c	
3832	0	3832	mud_pink	0.531	7		Pliocene	Plsi.c	
3833	0	3833	mud_pink	0.041	7		Pliocene	Plsi.c	
3834	0	3834	mud_pink	0.801	7		Pliocene	Plsi.c	
3835	0	3835	mud_pink	0.061	7		Pliocene	Plsi.c	
3836	0	3836	mud_pink	0.072	7		Pliocene	Plsi.c	
3837	0	3837	mud_pink	0.016	7		Pliocene	Plsi.c	
3838	0	3838	mud_pink	0.197	7		Pliocene	Plsi.c	
3839	0	3839	mud_pink	0.112	7		Pliocene	Plsi.c	
3840	0	3840	mud_pink	0.126	7		Pliocene	Plsi.c	
3841	0	3841	mud_pink	0.157	7		Pliocene	Plsi.c	
3842	0	3842	mud_pink	0.041	7		Pliocene	Plsi.c	
3843	0	3843	mud_pink	0.021	7		Pliocene	Plsi.c	
3844	0	3844	mud_pink	0.072	7		Pliocene	Plsi.c	
3845	0	3845	mud_pink	0.007	7		Pliocene	Plsi.c	
3846	0	3846	mud_pink	0.079	7		Pliocene	Plsi.c	
3847	0	3847	mud_pink	0.064	7		Pliocene	Plsi.c	
3848	0	3848	mud_pink	0.074	7		Pliocene	Plsi.c	
3849	0	3849	mud_pink	0.879	7		Pliocene	Plsi.c	
3850	0	3850	mud_pink	5.305	7		Pliocene	Plsi.c	
3851	0	3851	mud_pink	0.353	7		Pliocene	Plsi.c	
3852	0	3852	mud_pink	0.042	7		Pliocene	Plsi.c	
3853	0	3853	mud_pink	0.129	7		Pliocene	Plsi.c	
3854	0	3854	mud_pink	0.179	7		Pliocene	Plsi.c	
3855	0	3855	mud_pink	0.035	7		Pliocene	Plsi.c	
3856	0	3856	mud_pink	0.410	7		Pliocene	Plsi.c	
3857	0	3857	mud_pink	0.135	7		Pliocene	Plsi.c	
3858	0	3858	mud_pink	0.302	7		Pliocene	Plsi.c	
3859	0	3859	mud_pink	1.011	7		Pliocene	Plsi.c	
3860	0	3860	mud_pink	4.496	7		Pliocene	Plsi.c	
3861	0	3861	mud_pink	0.682	7		Pliocene	Plsi.c	
3862	0	3862	mud_pink	0.055	7		Pliocene	Plsi.c	
3863	0	3863	mud_pink	0.200	7		Pliocene	Plsi.c	
3864	0	3864	mud_pink	0.496	7		Pliocene	Plsi.c	

GeoNexus

OBJECTID_1	Join_Count	TARGET_FID	Label	Shape_Area (sqkm)	ORIG_FID	Absolute_Age	Age_paleontology	Unit	Reference
3865	0	3865	mud_pink	0.223	7		Pliocene	Plsi.c	
3867	0	3867	mud_pink	0.007	7		Pliocene	Plsi.c	
3868	0	3868	mud_pink	0.213	7		Pliocene	Plsi.c	
3869	0	3869	mud_pink	0.004	7		Pliocene	Plsi.c	
3870	0	3870	mud_pink	0.190	7		Pliocene	Plsi.c	
3871	0	3871	mud_pink	0.280	7		Pliocene	Plsi.c	
3872	0	3872	mud_pink	0.083	7		Pliocene	Plsi.c	
3873	0	3873	mud_pink	0.088	7		Pliocene	Plsi.c	
3874	0	3874	mud_pink	0.193	7		Pliocene	Plsi.c	
3875	0	3875	mud_pink	0.012	7		Pliocene	Plsi.c	
3877	0	3877	mud_pink	0.195	7		Pliocene	Plsi.c	
3878	0	3878	mud_pink	0.281	7		Pliocene	Plsi.c	
3879	0	3879	mud_pink	0.073	7		Pliocene	Plsi.c	
3881	0	3881	mud_pink	0.037	7		Pliocene	Plsi.c	
3882	0	3882	mud_pink	0.102	7		Pliocene	Plsi.c	
3883	0	3883	mud_pink	0.103	7		Pliocene	Plsi.c	
3884	0	3884	mud_pink	0.090	7		Pliocene	Plsi.c	
3885	0	3885	mud_pink	0.102	7		Pliocene	Plsi.c	
3886	0	3886	mud_pink	0.095	7		Pliocene	Plsi.c	
3887	0	3887	mud_pink	0.092	7		Pliocene	Plsi.c	
3888	0	3888	mud_pink	0.016	7		Pliocene	Plsi.c	
3889	0	3889	mud_pink	1.153	7		Pliocene	Plsi.c	
3891	0	3891	mud_pink	0.127	7		Pliocene	Plsi.c	
3892	0	3892	mud_pink	0.272	7		Pliocene	Plsi.c	
3893	0	3893	mud_pink	1.163	7		Pliocene	Plsi.c	
3894	0	3894	mud_pink	0.025	7		Pliocene	Plsi.c	
3895	0	3895	mud_pink	0.582	7		Pliocene	Plsi.c	
3896	0	3896	mud_pink	0.057	7		Pliocene	Plsi.c	
3897	0	3897	mud_pink	0.018	7		Pliocene	Plsi.c	
3898	0	3898	mud_pink	0.046	7		Pliocene	Plsi.c	
3899	0	3899	mud_pink	0.178	7		Pliocene	Plsi.c	
3900	0	3900	mud_pink	0.052	7		Pliocene	Plsi.c	
3901	0	3901	mud_pink	0.086	7		Pliocene	Plsi.c	
3902	0	3902	mud_pink	0.065	7		Pliocene	Plsi.c	

GeoNexus

OBJECTID_1	Join_Count	TARGET_FID	Label	Shape_Area (sqkm)	ORIG_FID	Absolute_Age	Age_paleontology	Unit	Reference
3903	0	3903	mud_pink	0.031	7		Pliocene	Plsi.c	
3904	0	3904	mud_pink	0.042	7		Pliocene	Plsi.c	
3905	0	3905	mud_pink	4.488	7		Pliocene	Plsi.c	
3906	0	3906	mud_pink	0.109	7		Pliocene	Plsi.c	
3907	0	3907	mud_pink	1.816	7		Pliocene	Plsi.c	
3908	0	3908	mud_pink	0.089	7		Pliocene	Plsi.c	
3909	0	3909	mud_pink	0.144	7		Pliocene	Plsi.c	
3910	0	3910	mud_pink	0.038	7		Pliocene	Plsi.c	
3911	0	3911	mud_pink	1.181	7		Pliocene	Plsi.c	
3912	0	3912	mud_pink	0.246	7		Pliocene	Plsi.c	
3913	0	3913	mud_pink	0.758	7		Pliocene	Plsi.c	
3914	0	3914	mud_pink	0.011	7		Pliocene	Plsi.c	
3916	0	3916	mud_pink	0.217	7		Pliocene	Plsi.c	
3917	0	3917	mud_pink	0.016	7		Pliocene	Plsi.c	
3918	0	3918	mud_pink	2.951	7		Pliocene	Plsi.c	
3919	0	3919	mud_pink	0.333	7		Pliocene	Plsi.c	
3920	0	3920	mud_pink	0.031	7		Pliocene	Plsi.c	
3921	0	3921	mud_pink	0.333	7		Pliocene	Plsi.c	
3922	0	3922	mud_pink	1.707	7		Pliocene	Plsi.c	
3923	0	3923	mud_pink	0.742	7		Pliocene	Plsi.c	
3924	0	3924	mud_pink	0.969	7		Pliocene	Plsi.c	
3925	0	3925	mud_pink	0.054	7		Pliocene	Plsi.c	
3927	0	3927	mud_pink	0.540	7		Pliocene	Plsi.c	
3928	0	3928	mud_pink	0.215	7		Pliocene	Plsi.c	
3929	0	3929	mud_pink	0.039	7		Pliocene	Plsi.c	
3930	0	3930	mud_pink	0.032	7		Pliocene	Plsi.c	
3931	0	3931	mud_pink	0.054	7		Pliocene	Plsi.c	
3932	0	3932	mud_pink	0.005	7		Pliocene	Plsi.c	
3933	0	3933	mud_pink	0.218	7		Pliocene	Plsi.c	
3934	0	3934	mud_pink	0.459	7		Pliocene	Plsi.c	
3935	0	3935	mud_pink	1.416	7		Pliocene	Plsi.c	
3936	0	3936	mud_pink	0.059	7		Pliocene	Plsi.c	
3937	0	3937	mud_pink	0.545	7		Pliocene	Plsi.c	
3938	0	3938	mud_pink	0.242	7		Pliocene	Plsi.c	

GeoNexus

OBJECTID_1	Join_Count	TARGET_FID	Label	Shape_Area (sqkm)	ORIG_FID	Absolute_Age	Age_paleontology	Unit	Reference
3939	0	3939	mud_pink	1.160	7		Pliocene	Plsi.c	
3940	0	3940	mud_pink	0.023	7		Pliocene	Plsi.c	
3941	0	3941	mud_pink	0.195	7		Pliocene	Plsi.c	
3942	0	3942	mud_pink	0.726	7		Pliocene	Plsi.c	
3943	0	3943	mud_pink	0.139	7		Pliocene	Plsi.c	
3944	0	3944	mud_pink	0.152	7		Pliocene	Plsi.c	
3945	0	3945	mud_pink	0.136	7		Pliocene	Plsi.c	
3946	0	3946	mud_pink	0.011	7		Pliocene	Plsi.c	
3947	0	3947	mud_pink	0.032	7		Pliocene	Plsi.c	
3948	0	3948	mud_pink	6.625	7		Pliocene	Plsi.c	
3949	0	3949	mud_pink	0.069	7		Pliocene	Plsi.c	
3950	0	3950	mud_pink	0.019	7		Pliocene	Plsi.c	
3952	0	3952	mud_pink	0.021	7		Pliocene	Plsi.c	
3954	0	3954	mud_pink	0.005	7		Pliocene	Plsi.c	
3955	0	3955	mud_pink	0.211	7		Pliocene	Plsi.c	
3956	0	3956	mud_pink	0.061	7		Pliocene	Plsi.c	
3957	0	3957	mud_pink	0.278	7		Pliocene	Plsi.c	
3958	0	3958	mud_pink	0.166	7		Pliocene	Plsi.c	
3960	0	3960	mud_pink	0.218	7		Pliocene	Plsi.c	
3961	0	3961	mud_pink	0.406	7		Pliocene	Plsi.c	
3962	0	3962	mud_pink	6.069	7		Pliocene	Plsi.c	
3963	0	3963	mud_pink	0.073	7		Pliocene	Plsi.c	
3964	0	3964	mud_pink	0.369	7		Pliocene	Plsi.c	
3965	0	3965	mud_pink	0.058	7		Pliocene	Plsi.c	
3966	0	3966	mud_pink	0.044	7		Pliocene	Plsi.c	
3967	0	3967	mud_pink	0.380	7		Pliocene	Plsi.c	
3968	0	3968	mud_pink	0.428	7		Pliocene	Plsi.c	
3969	0	3969	mud_pink	0.017	7		Pliocene	Plsi.c	
3970	0	3970	mud_pink	0.446	7		Pliocene	Plsi.c	
3971	0	3971	mud_pink	0.141	7		Pliocene	Plsi.c	
3972	0	3972	mud_pink	0.393	7		Pliocene	Plsi.c	
3973	0	3973	mud_pink	0.087	7		Pliocene	Plsi.c	
3974	0	3974	mud_pink	0.048	7		Pliocene	Plsi.c	
3975	0	3975	mud_pink	0.015	7		Pliocene	Plsi.c	

GeoNexus

OBJECTID_1	Join_Count	TARGET_FID	Label	Shape_Area (sqkm)	ORIG_FID	Absolute_Age	Age_paleontology	Unit	Reference
3976	0	3976	mud_pink	0.204	7		Pliocene	Plsi.c	
3977	0	3977	mud_pink	0.179	7		Pliocene	Plsi.c	
3978	0	3978	mud_pink	0.233	7		Pliocene	Plsi.c	
3979	0	3979	mud_pink	0.063	7		Pliocene	Plsi.c	
3980	0	3980	mud_pink	0.234	7		Pliocene	Plsi.c	
3981	0	3981	mud_pink	0.200	7		Pliocene	Plsi.c	
3982	0	3982	mud_pink	0.033	7		Pliocene	Plsi.c	
3983	0	3983	mud_pink	0.118	7		Pliocene	Plsi.c	
3984	0	3984	mud_pink	0.029	7		Pliocene	Plsi.c	
3985	0	3985	mud_pink	1.346	7		Pliocene	Plsi.c	
3986	0	3986	mud_pink	0.131	7		Pliocene	Plsi.c	
3987	0	3987	mud_pink	0.035	7		Pliocene	Plsi.c	
3988	0	3988	mud_pink	1.104	7		Pliocene	Plsi.c	
3989	0	3989	mud_pink	0.661	7		Pliocene	Plsi.c	
3990	0	3990	mud_pink	0.033	7		Pliocene	Plsi.c	
3991	0	3991	mud_pink	0.020	7		Pliocene	Plsi.c	
3992	0	3992	mud_pink	0.043	7		Pliocene	Plsi.c	
3993	0	3993	mud_pink	0.566	7		Pliocene	Plsi.c	
3994	0	3994	mud_pink	0.023	7		Pliocene	Plsi.c	
3995	0	3995	mud_pink	0.123	7		Pliocene	Plsi.c	
3996	0	3996	mud_pink	0.037	7		Pliocene	Plsi.c	
3997	0	3997	mud_pink	1.165	7		Pliocene	Plsi.c	
3998	0	3998	mud_pink	0.596	7		Pliocene	Plsi.c	
3999	0	3999	mud_pink	0.030	7		Pliocene	Plsi.c	
4000	0	4000	mud_pink	0.403	7		Pliocene	Plsi.c	
4001	0	4001	mud_pink	0.056	7		Pliocene	Plsi.c	
4002	0	4002	mud_pink	128.703	7		Pliocene	Plsi.c	
4003	0	4003	mud_pink	0.409	7		Pliocene	Plsi.c	
4004	0	4004	mud_pink	0.123	7		Pliocene	Plsi.c	
4005	0	4005	mud_pink	0.066	7		Pliocene	Plsi.c	
4006	0	4006	mud_pink	0.049	7		Pliocene	Plsi.c	
4007	0	4007	mud_pink	0.013	7		Pliocene	Plsi.c	
4008	0	4008	mud_pink	0.008	7		Pliocene	Plsi.c	
4009	0	4009	mud_pink	0.073	7		Pliocene	Plsi.c	

GeoNexus

OBJECTID_1	Join_Count	TARGET_FID	Label	Shape_Area (sqkm)	ORIG_FID	Absolute_Age	Age_paleontology	Unit	Reference
4010	0	4010	mud_pink	0.215	7		Pliocene	Plsi.c	
4011	0	4011	mud_pink	0.064	7		Pliocene	Plsi.c	
4012	0	4012	mud_pink	0.095	7		Pliocene	Plsi.c	
4013	0	4013	mud_pink	1.582	7		Pliocene	Plsi.c	
4014	0	4014	mud_pink	0.733	7		Pliocene	Plsi.c	
4015	0	4015	mud_pink	0.105	7		Pliocene	Plsi.c	
4016	0	4016	mud_pink	0.130	7		Pliocene	Plsi.c	
4017	0	4017	mud_pink	1.207	7		Pliocene	Plsi.c	
4018	0	4018	mud_pink	0.076	7		Pliocene	Plsi.c	
4019	0	4019	mud_pink	0.505	7		Pliocene	Plsi.c	
4020	0	4020	mud_pink	0.095	7		Pliocene	Plsi.c	
4021	0	4021	mud_pink	0.736	7		Pliocene	Plsi.c	
4022	0	4022	mud_pink	0.030	7		Pliocene	Plsi.c	
4023	0	4023	mud_pink	0.296	7		Pliocene	Plsi.c	
4024	0	4024	mud_pink	0.035	7		Pliocene	Plsi.c	
4025	0	4025	mud_pink	0.034	7		Pliocene	Plsi.c	
4026	0	4026	mud_pink	0.101	7		Pliocene	Plsi.c	
4027	0	4027	mud_pink	0.088	7		Pliocene	Plsi.c	
4028	0	4028	mud_pink	0.415	7		Pliocene	Plsi.c	
4029	0	4029	mud_pink	0.213	7		Pliocene	Plsi.c	
4030	0	4030	mud_pink	0.395	7		Pliocene	Plsi.c	
4031	0	4031	mud_pink	0.048	7		Pliocene	Plsi.c	
4032	0	4032	mud_pink	0.195	7		Pliocene	Plsi.c	
4033	0	4033	mud_pink	0.138	7		Pliocene	Plsi.c	
4034	0	4034	mud_pink	0.499	7		Pliocene	Plsi.c	
4035	0	4035	mud_pink	0.081	7		Pliocene	Plsi.c	
4036	0	4036	mud_pink	0.743	7		Pliocene	Plsi.c	
4037	0	4037	mud_pink	0.036	7		Pliocene	Plsi.c	
4038	0	4038	mud_pink	0.390	7		Pliocene	Plsi.c	
4039	0	4039	mud_pink	0.127	7		Pliocene	Plsi.c	
4040	0	4040	mud_pink	0.106	7		Pliocene	Plsi.c	
4041	0	4041	mud_pink	0.134	7		Pliocene	Plsi.c	
4042	0	4042	mud_pink	0.068	7		Pliocene	Plsi.c	
4043	0	4043	mud_pink	0.037	7		Pliocene	Plsi.c	

GeoNexus

OBJECTID_1	Join_Count	TARGET_FID	Label	Shape_Area (sqkm)	ORIG_FID	Absolute_Age	Age_paleontology	Unit	Reference
4044	0	4044	mud_pink	0.832	7		Pliocene	Plsi.c	
4045	0	4045	mud_pink	0.082	7		Pliocene	Plsi.c	
4046	0	4046	mud_pink	0.288	7		Pliocene	Plsi.c	
4047	0	4047	mud_pink	0.101	7		Pliocene	Plsi.c	
4048	0	4048	mud_pink	0.461	7		Pliocene	Plsi.c	
4049	0	4049	mud_pink	0.072	7		Pliocene	Plsi.c	
4050	0	4050	mud_pink	0.170	7		Pliocene	Plsi.c	
4051	0	4051	mud_pink	0.014	7		Pliocene	Plsi.c	
4052	0	4052	mud_pink	0.078	7		Pliocene	Plsi.c	
4053	0	4053	mud_pink	0.115	7		Pliocene	Plsi.c	
4054	0	4054	mud_pink	0.123	7		Pliocene	Plsi.c	
4055	0	4055	mud_pink	0.128	7		Pliocene	Plsi.c	
4056	0	4056	mud_pink	0.229	7		Pliocene	Plsi.c	
4057	0	4057	mud_pink	0.141	7		Pliocene	Plsi.c	
4058	0	4058	mud_pink	12.864	7		Pliocene	Plsi.c	
4059	0	4059	mud_pink	0.204	7		Pliocene	Plsi.c	
4060	0	4060	mud_pink	0.068	7		Pliocene	Plsi.c	
4061	0	4061	mud_pink	0.037	7		Pliocene	Plsi.c	
4062	0	4062	mud_pink	0.730	7		Pliocene	Plsi.c	
4063	0	4063	mud_pink	0.050	7		Pliocene	Plsi.c	
4064	0	4064	mud_pink	0.265	7		Pliocene	Plsi.c	
4065	0	4065	mud_pink	0.026	7		Pliocene	Plsi.c	
4066	0	4066	mud_pink	0.007	7		Pliocene	Plsi.c	
4067	0	4067	mud_pink	0.332	7		Pliocene	Plsi.c	
4068	0	4068	mud_pink	0.427	7		Pliocene	Plsi.c	
4069	0	4069	mud_pink	0.209	7		Pliocene	Plsi.c	
4070	0	4070	mud_pink	0.160	7		Pliocene	Plsi.c	
4071	0	4071	mud_pink	3.151	7		Pliocene	Plsi.c	
4072	0	4072	mud_pink	0.229	7		Pliocene	Plsi.c	
4073	0	4073	mud_pink	0.314	7		Pliocene	Plsi.c	
4074	0	4074	mud_pink	0.013	7		Pliocene	Plsi.c	
4075	0	4075	mud_pink	0.145	7		Pliocene	Plsi.c	
4076	0	4076	mud_pink	0.054	7		Pliocene	Plsi.c	
4077	0	4077	mud_pink	0.050	7		Pliocene	Plsi.c	

GeoNexus

OBJECTID_1	Join_Count	TARGET_FID	Label	Shape_Area (sqkm)	ORIG_FID	Absolute_Age	Age_paleontology	Unit	Reference
4078	0	4078	mud_pink	15.834	7		Pliocene	Plsi.c	
4079	0	4079	mud_pink	0.032	7		Pliocene	Plsi.c	
4080	0	4080	mud_pink	0.017	7		Pliocene	Plsi.c	
4081	0	4081	mud_pink	0.105	7		Pliocene	Plsi.c	
4082	0	4082	mud_pink	0.049	7		Pliocene	Plsi.c	
4083	0	4083	mud_pink	0.189	7		Pliocene	Plsi.c	
4084	0	4084	mud_pink	0.204	7		Pliocene	Plsi.c	
4085	0	4085	mud_pink	0.505	7		Pliocene	Plsi.c	
4086	0	4086	mud_pink	1.848	7		Pliocene	Plsi.c	
4087	0	4087	mud_pink	0.040	7		Pliocene	Plsi.c	
4088	0	4088	mud_pink	0.542	7		Pliocene	Plsi.c	
4089	0	4089	mud_pink	1.292	7		Pliocene	Plsi.c	
4090	0	4090	mud_pink	0.039	7		Pliocene	Plsi.c	
4091	0	4091	mud_pink	0.045	7		Pliocene	Plsi.c	
4093	0	4093	mud_pink	0.111	7		Pliocene	Plsi.c	
4094	0	4094	mud_pink	0.051	7		Pliocene	Plsi.c	
4095	0	4095	mud_pink	0.139	7		Pliocene	Plsi.c	
4096	0	4096	mud_pink	0.007	7		Pliocene	Plsi.c	
4097	0	4097	mud_pink	0.235	7		Pliocene	Plsi.c	
4098	0	4098	mud_pink	0.044	7		Pliocene	Plsi.c	
4099	0	4099	mud_pink	0.257	7		Pliocene	Plsi.c	
4100	0	4100	mud_pink	0.084	7		Pliocene	Plsi.c	
4101	0	4101	mud_pink	0.148	7		Pliocene	Plsi.c	
4102	0	4102	mud_pink	0.063	7		Pliocene	Plsi.c	
4103	0	4103	mud_pink	0.172	7		Pliocene	Plsi.c	
4104	0	4104	mud_pink	0.024	7		Pliocene	Plsi.c	
4105	0	4105	mud_pink	0.015	7		Pliocene	Plsi.c	
4106	0	4106	mud_pink	0.123	7		Pliocene	Plsi.c	
4107	0	4107	mud_pink	0.410	7		Pliocene	Plsi.c	
4108	0	4108	mud_pink	0.277	7		Pliocene	Plsi.c	
4109	0	4109	mud_pink	3.411	7		Pliocene	Plsi.c	
4110	0	4110	mud_pink	0.161	7		Pliocene	Plsi.c	
4111	0	4111	mud_pink	0.080	7		Pliocene	Plsi.c	
4112	0	4112	mud_pink	0.028	7		Pliocene	Plsi.c	

GeoNexus

OBJECTID_1	Join_Count	TARGET_FID	Label	Shape_Area (sqkm)	ORIG_FID	Absolute_Age	Age_paleontology	Unit	Reference
4113	0	4113	mud_pink	0.242	7		Pliocene	Plsi.c	
4114	0	4114	mud_pink	0.039	7		Pliocene	Plsi.c	
4115	0	4115	mud_pink	0.155	7		Pliocene	Plsi.c	
4116	0	4116	mud_pink	0.019	7		Pliocene	Plsi.c	
4117	0	4117	mud_pink	0.405	7		Pliocene	Plsi.c	
4118	0	4118	mud_pink	0.107	7		Pliocene	Plsi.c	
4119	0	4119	mud_pink	0.248	7		Pliocene	Plsi.c	
4120	0	4120	mud_pink	0.497	7		Pliocene	Plsi.c	
4121	0	4121	mud_pink	0.038	7		Pliocene	Plsi.c	
4122	0	4122	mud_pink	0.442	7		Pliocene	Plsi.c	
4123	0	4123	mud_pink	0.088	7		Pliocene	Plsi.c	
4124	0	4124	mud_pink	0.522	7		Pliocene	Plsi.c	
4125	0	4125	mud_pink	0.257	7		Pliocene	Plsi.c	
4126	0	4126	mud_pink	0.379	7		Pliocene	Plsi.c	
4127	0	4127	mud_pink	0.313	7		Pliocene	Plsi.c	
4128	0	4128	mud_pink	0.049	7		Pliocene	Plsi.c	
4129	0	4129	mud_pink	0.010	7		Pliocene	Plsi.c	
4130	0	4130	mud_pink	0.161	7		Pliocene	Plsi.c	
4131	0	4131	mud_pink	0.634	7		Pliocene	Plsi.c	
4132	0	4132	mud_pink	0.167	7		Pliocene	Plsi.c	
4133	0	4133	mud_pink	4.066	7		Pliocene	Plsi.c	
4134	0	4134	mud_pink	0.039	7		Pliocene	Plsi.c	
4135	0	4135	mud_pink	0.067	7		Pliocene	Plsi.c	
4136	0	4136	mud_pink	0.232	7		Pliocene	Plsi.c	
4137	0	4137	mud_pink	0.701	7		Pliocene	Plsi.c	
4138	0	4138	mud_pink	0.924	7		Pliocene	Plsi.c	
4139	0	4139	mud_pink	0.454	7		Pliocene	Plsi.c	
4140	0	4140	mud_pink	0.444	7		Pliocene	Plsi.c	
4141	0	4141	mud_pink	0.327	7		Pliocene	Plsi.c	
4142	0	4142	mud_pink	0.128	7		Pliocene	Plsi.c	
4143	0	4143	mud_pink	0.426	7		Pliocene	Plsi.c	
4144	0	4144	mud_pink	0.037	7		Pliocene	Plsi.c	
4145	0	4145	mud_pink	0.046	7		Pliocene	Plsi.c	
4146	0	4146	mud_pink	0.038	7		Pliocene	Plsi.c	

GeoNexus

OBJECTID_1	Join_Count	TARGET_FID	Label	Shape_Area (sqkm)	ORIG_FID	Absolute_Age	Age_paleontology	Unit	Reference
4147	0	4147	mud_pink	0.556	7		Pliocene	Plsi.c	
4148	0	4148	mud_pink	0.234	7		Pliocene	Plsi.c	
4149	0	4149	mud_pink	0.017	7		Pliocene	Plsi.c	
4150	0	4150	mud_pink	0.014	7		Pliocene	Plsi.c	
4151	0	4151	mud_pink	0.053	7		Pliocene	Plsi.c	
4152	0	4152	mud_pink	3.319	7		Pliocene	Plsi.c	
4153	0	4153	mud_pink	0.047	7		Pliocene	Plsi.c	
4154	0	4154	mud_pink	0.060	7		Pliocene	Plsi.c	
4155	0	4155	mud_pink	0.201	7		Pliocene	Plsi.c	
4156	0	4156	mud_pink	0.970	7		Pliocene	Plsi.c	
4157	0	4157	mud_pink	0.132	7		Pliocene	Plsi.c	
4158	0	4158	mud_pink	0.063	7		Pliocene	Plsi.c	
4159	0	4159	mud_pink	0.473	7		Pliocene	Plsi.c	
4160	0	4160	mud_pink	0.119	7		Pliocene	Plsi.c	
4161	0	4161	mud_pink	0.466	7		Pliocene	Plsi.c	
4162	0	4162	mud_pink	0.071	7		Pliocene	Plsi.c	
4163	0	4163	mud_pink	0.591	7		Pliocene	Plsi.c	
4164	0	4164	mud_pink	0.160	7		Pliocene	Plsi.c	
4165	0	4165	mud_pink	0.231	7		Pliocene	Plsi.c	
4166	0	4166	mud_pink	0.088	7		Pliocene	Plsi.c	
4167	0	4167	mud_pink	2.645	7		Pliocene	Plsi.c	
4168	0	4168	mud_pink	118.853	7		Pliocene	Plsi.c	
4169	0	4169	mud_pink	0.028	7		Pliocene	Plsi.c	
4170	0	4170	mud_pink	0.503	7		Pliocene	Plsi.c	
4171	0	4171	mud_pink	0.075	7		Pliocene	Plsi.c	
4172	0	4172	mud_pink	0.048	7		Pliocene	Plsi.c	
4173	0	4173	mud_pink	0.161	7		Pliocene	Plsi.c	
4174	0	4174	mud_pink	0.872	7		Pliocene	Plsi.c	
4175	0	4175	mud_pink	3.625	7		Pliocene	Plsi.c	
4176	0	4176	mud_pink	2.076	7		Pliocene	Plsi.c	
4177	0	4177	mud_pink	0.030	7		Pliocene	Plsi.c	
4178	0	4178	mud_pink	0.054	7		Pliocene	Plsi.c	
4179	0	4179	mud_pink	4.902	7		Pliocene	Plsi.c	
4180	0	4180	mud_pink	199.871	7		Pliocene	Plsi.c	

GeoNexus

OBJECTID_1	Join_Count	TARGET_FID	Label	Shape_Area (sqkm)	ORIG_FID	Absolute_Age	Age_paleontology	Unit	Reference
4181	0	4181	mud_pink	0.070	7		Pliocene	Plsi.c	
4182	0	4182	mud_pink	0.072	7		Pliocene	Plsi.c	
4183	0	4183	mud_pink	1.078	7		Pliocene	Plsi.c	
4184	0	4184	mud_pink	0.349	7		Pliocene	Plsi.c	
4185	0	4185	mud_pink	0.278	7		Pliocene	Plsi.c	
4186	0	4186	mud_pink	0.052	7		Pliocene	Plsi.c	
4187	0	4187	mud_pink	0.679	7		Pliocene	Plsi.c	
4188	0	4188	mud_pink	0.232	7		Pliocene	Plsi.c	
4189	0	4189	mud_pink	0.020	7		Pliocene	Plsi.c	
4190	0	4190	mud_pink	0.346	7		Pliocene	Plsi.c	
4191	0	4191	mud_pink	0.167	7		Pliocene	Plsi.c	
4192	0	4192	mud_pink	0.014	7		Pliocene	Plsi.c	
4193	0	4193	mud_pink	0.761	7		Pliocene	Plsi.c	
4194	0	4194	mud_pink	0.165	7		Pliocene	Plsi.c	
4195	0	4195	mud_pink	0.238	7		Pliocene	Plsi.c	
4196	0	4196	mud_pink	16.371	7		Pliocene	Plsi.c	
4197	0	4197	mud_pink	0.029	7		Pliocene	Plsi.c	
4198	0	4198	mud_pink	0.055	7		Pliocene	Plsi.c	
4199	0	4199	mud_pink	0.030	7		Pliocene	Plsi.c	
4200	0	4200	mud_pink	0.019	7		Pliocene	Plsi.c	
4201	0	4201	mud_pink	0.491	7		Pliocene	Plsi.c	
4202	0	4202	mud_pink	0.674	7		Pliocene	Plsi.c	
4203	0	4203	mud_pink	0.157	7		Pliocene	Plsi.c	
4204	0	4204	mud_pink	0.045	7		Pliocene	Plsi.c	
4205	0	4205	mud_pink	1.799	7		Pliocene	Plsi.c	
4206	0	4206	mud_pink	0.144	7		Pliocene	Plsi.c	
4207	0	4207	mud_pink	0.019	7		Pliocene	Plsi.c	
4211	0	4211	mud_pink	0.578	7		Pliocene	Plsi.c	
4212	0	4212	mud_pink	0.086	7		Pliocene	Plsi.c	
4213	0	4213	mud_pink	0.334	7		Pliocene	Plsi.c	
4214	0	4214	mud_pink	0.189	7		Pliocene	Plsi.c	
4215	0	4215	mud_pink	0.023	7		Pliocene	Plsi.c	
4216	0	4216	mud_pink	0.027	7		Pliocene	Plsi.c	
4217	0	4217	mud_pink	0.119	7		Pliocene	Plsi.c	

GeoNexus

OBJECTID_1	Join_Count	TARGET_FID	Label	Shape_Area (sqkm)	ORIG_FID	Absolute_Age	Age_paleontology	Unit	Reference
4218	0	4218	mud_pink	0.714	7		Pliocene	Plsi.c	
4219	0	4219	mud_pink	0.229	7		Pliocene	Plsi.c	
4220	0	4220	mud_pink	7.034	7		Pliocene	Plsi.c	
4221	0	4221	mud_pink	0.004	7		Pliocene	Plsi.c	
4222	0	4222	mud_pink	0.034	7		Pliocene	Plsi.c	
4223	0	4223	mud_pink	0.788	7		Pliocene	Plsi.c	
4224	0	4224	mud_pink	1.143	7		Pliocene	Plsi.c	
4225	0	4225	mud_pink	0.558	7		Pliocene	Plsi.c	
4226	0	4226	mud_pink	0.244	7		Pliocene	Plsi.c	
4227	0	4227	mud_pink	0.022	7		Pliocene	Plsi.c	
4228	0	4228	mud_pink	0.030	7		Pliocene	Plsi.c	
4230	0	4230	mud_pink	2.038	7		Pliocene	Plsi.c	
4232	0	4232	mud_pink	0.168	7		Pliocene	Plsi.c	
4233	0	4233	mud_pink	0.185	7		Pliocene	Plsi.c	
4235	0	4235	mud_pink	0.093	7		Pliocene	Plsi.c	
4236	0	4236	mud_pink	0.217	7		Pliocene	Plsi.c	
4237	0	4237	mud_pink	0.008	7		Pliocene	Plsi.c	
4238	0	4238	mud_pink	0.044	7		Pliocene	Plsi.c	
4239	0	4239	mud_pink	0.124	7		Pliocene	Plsi.c	
4241	0	4241	mud_pink	0.114	7		Pliocene	Plsi.c	
4243	0	4243	mud_pink	0.182	7		Pliocene	Plsi.c	
4244	0	4244	mud_pink	0.197	7		Pliocene	Plsi.c	
4245	0	4245	mud_pink	0.047	7		Pliocene	Plsi.c	
4246	0	4246	mud_pink	0.699	7		Pliocene	Plsi.c	
4247	0	4247	mud_pink	2.888	7		Pliocene	Plsi.c	
4248	0	4248	mud_pink	0.406	7		Pliocene	Plsi.c	
4249	0	4249	mud_pink	0.252	7		Pliocene	Plsi.c	
8350	3	8351	mud_pink	2.865	14		Pliocene	Plsi.c	
10398	1	10405	mud_pink	0.065	0		Pliocene	Plsi.c	
10402	1	10409	mud_pink	0.022	0		Pliocene	Plsi.c	
10403	1	10410	mud_pink	0.231	0		Pliocene	Plsi.c	
10465	0	4168	mud_pink	31.672	7		Pliocene	Plsi.c	
10474	0	4180	mud_pink	0.308	7		Pliocene	Plsi.c	
10487	0	4229	mud_pink	0.151	7		Pliocene	Plsi.c	

GeoNexus

OBJECTID_1	Join_Count	TARGET_FID	Label	Shape_Area (sqkm)	ORIG_FID	Absolute_Age	Age_paleontology	Unit	Reference
10492	0	4196	mud_pink	0.039	7		Pliocene	Plsi.c	
10494	0	4196	mud_pink	1.236	7		Pliocene	Plsi.c	
10497	0	4196	mud_pink	3.126	7		Pliocene	Plsi.c	

GeoNexus

Table S10. Summary of mapped polygons for the $Pl^{l.si.s}$ Unit.

OBJECTID_1	Join_Count	TARGET_FID	Label	Shape_Area (sqkm)	ORIG_FID	Absolute_Age	Age_paleontology	Unit	Reference
1747	0	1747	m_brown	25.272	3		Pliocene	Pll.si.s	Dolati (2010)
1783	0	1783	m_brown	0.124	4		Pliocene	Pll.si.s	Dolati (2010)
1784	0	1784	m_brown	0.066	4		Pliocene	Pll.si.s	Dolati (2010)
1785	0	1785	m_brown	0.416	4		Pliocene	Pll.si.s	Dolati (2010)
1786	0	1786	m_brown	0.251	4		Pliocene	Pll.si.s	Dolati (2010)
1787	0	1787	m_brown	0.588	4		Pliocene	Pll.si.s	Dolati (2010)
1788	0	1788	m_brown	0.361	4		Pliocene	Pll.si.s	Dolati (2010)
1789	0	1789	m_brown	0.322	4		Pliocene	Pll.si.s	Dolati (2010)
1790	0	1790	m_brown	0.026	4		Pliocene	Pll.si.s	Dolati (2010)
1791	0	1791	m_brown	0.102	4		Pliocene	Pll.si.s	Dolati (2010)
1792	0	1792	m_brown	0.261	4		Pliocene	Pll.si.s	Dolati (2010)
1793	0	1793	m_brown	1.007	4		Pliocene	Pll.si.s	Dolati (2010)
1794	0	1794	m_brown	0.058	4		Pliocene	Pll.si.s	Dolati (2010)
1795	0	1795	m_brown	0.793	4		Pliocene	Pll.si.s	Dolati (2010)
1796	0	1796	m_brown	0.393	4		Pliocene	Pll.si.s	Dolati (2010)
1797	0	1797	m_brown	0.202	4		Pliocene	Pll.si.s	Dolati (2010)
1798	0	1798	m_brown	0.054	4		Pliocene	Pll.si.s	Dolati (2010)
1799	0	1799	m_brown	0.878	4		Pliocene	Pll.si.s	Dolati (2010)
1800	0	1800	m_brown	0.461	4		Pliocene	Pll.si.s	Dolati (2010)
1801	0	1801	m_brown	0.187	4		Pliocene	Pll.si.s	Dolati (2010)
1802	0	1802	m_brown	0.062	4		Pliocene	Pll.si.s	Dolati (2010)
1803	0	1803	m_brown	0.025	4		Pliocene	Pll.si.s	Dolati (2010)
1804	0	1804	m_brown	0.565	4		Pliocene	Pll.si.s	Dolati (2010)
1805	0	1805	m_brown	0.289	4		Pliocene	Pll.si.s	Dolati (2010)
1806	0	1806	m_brown	1.456	4		Pliocene	Pll.si.s	Dolati (2010)
1807	0	1807	m_brown	0.026	4		Pliocene	Pll.si.s	Dolati (2010)
1808	0	1808	m_brown	5.666	4		Pliocene	Pll.si.s	Dolati (2010)
1809	0	1809	m_brown	0.030	4		Pliocene	Pll.si.s	Dolati (2010)
1810	0	1810	m_brown	0.350	4		Pliocene	Pll.si.s	Dolati (2010)
1811	0	1811	m_brown	1.246	4		Pliocene	Pll.si.s	Dolati (2010)
1812	0	1812	m_brown	0.099	4		Pliocene	Pll.si.s	Dolati (2010)
1813	0	1813	m_brown	0.109	4		Pliocene	Pll.si.s	Dolati (2010)
1814	0	1814	m_brown	1.504	4		Pliocene	Pll.si.s	Dolati (2010)
1815	0	1815	m_brown	0.388	4		Pliocene	Pll.si.s	Dolati (2010)
1816	0	1816	m_brown	0.125	4		Pliocene	Pll.si.s	Dolati (2010)
1817	0	1817	m_brown	0.022	4		Pliocene	Pll.si.s	Dolati (2010)
1818	0	1818	m_brown	0.060	4		Pliocene	Pll.si.s	Dolati (2010)
1819	0	1819	m_brown	0.061	4		Pliocene	Pll.si.s	Dolati (2010)

Geonevis

OBJECTID_1	Join_Count	TARGET_FID	Label	Shape_Area (sqkm)	ORIG_FID	Absolute_Age	Age_paleontology	Unit	Reference
1820	0	1820	m_brown	0.976	4		Pliocene	Pll.si.s	Dolati (2010)
1821	0	1821	m_brown	0.081	4		Pliocene	Pll.si.s	Dolati (2010)
1822	0	1822	m_brown	0.022	4		Pliocene	Pll.si.s	Dolati (2010)
1823	0	1823	m_brown	0.323	4		Pliocene	Pll.si.s	Dolati (2010)
1824	0	1824	m_brown	0.059	4		Pliocene	Pll.si.s	Dolati (2010)
1825	0	1825	m_brown	0.234	4		Pliocene	Pll.si.s	Dolati (2010)
1826	0	1826	m_brown	0.418	4		Pliocene	Pll.si.s	Dolati (2010)
1827	0	1827	m_brown	0.035	4		Pliocene	Pll.si.s	Dolati (2010)
1828	0	1828	m_brown	0.033	4		Pliocene	Pll.si.s	Dolati (2010)
1829	0	1829	m_brown	0.153	4		Pliocene	Pll.si.s	Dolati (2010)
1830	0	1830	m_brown	0.047	4		Pliocene	Pll.si.s	Dolati (2010)
1831	0	1831	m_brown	0.225	4		Pliocene	Pll.si.s	Dolati (2010)
1832	0	1832	m_brown	0.173	4		Pliocene	Pll.si.s	Dolati (2010)
1833	0	1833	m_brown	0.135	4		Pliocene	Pll.si.s	Dolati (2010)
1834	0	1834	m_brown	0.225	4		Pliocene	Pll.si.s	Dolati (2010)
1835	0	1835	m_brown	0.044	4		Pliocene	Pll.si.s	Dolati (2010)
1836	0	1836	m_brown	0.250	4		Pliocene	Pll.si.s	Dolati (2010)
1837	0	1837	m_brown	0.046	4		Pliocene	Pll.si.s	Dolati (2010)
1838	0	1838	m_brown	0.318	4		Pliocene	Pll.si.s	Dolati (2010)
1839	0	1839	m_brown	1.354	4		Pliocene	Pll.si.s	Dolati (2010)
1840	0	1840	m_brown	0.266	4		Pliocene	Pll.si.s	Dolati (2010)
1841	0	1841	m_brown	0.047	4		Pliocene	Pll.si.s	Dolati (2010)
1842	0	1842	m_brown	0.110	4		Pliocene	Pll.si.s	Dolati (2010)
1843	0	1843	m_brown	0.090	4		Pliocene	Pll.si.s	Dolati (2010)
1844	0	1844	m_brown	0.031	4		Pliocene	Pll.si.s	Dolati (2010)
1845	0	1845	m_brown	0.073	4		Pliocene	Pll.si.s	Dolati (2010)
1846	0	1846	m_brown	0.040	4		Pliocene	Pll.si.s	Dolati (2010)
1847	0	1847	m_brown	0.140	4		Pliocene	Pll.si.s	Dolati (2010)
1848	0	1848	m_brown	0.366	4		Pliocene	Pll.si.s	Dolati (2010)
1849	0	1849	m_brown	0.230	4		Pliocene	Pll.si.s	Dolati (2010)
1850	0	1850	m_brown	0.116	4		Pliocene	Pll.si.s	Dolati (2010)
1851	0	1851	m_brown	0.238	4		Pliocene	Pll.si.s	Dolati (2010)
1852	0	1852	m_brown	1.600	4		Pliocene	Pll.si.s	Dolati (2010)
1853	0	1853	m_brown	0.584	4		Pliocene	Pll.si.s	Dolati (2010)
1854	0	1854	m_brown	0.070	4		Pliocene	Pll.si.s	Dolati (2010)
1855	0	1855	m_brown	0.135	4		Pliocene	Pll.si.s	Dolati (2010)
1856	0	1856	m_brown	0.031	4		Pliocene	Pll.si.s	Dolati (2010)
1857	0	1857	m_brown	0.103	4		Pliocene	Pll.si.s	Dolati (2010)
1858	0	1858	m_brown	0.043	4		Pliocene	Pll.si.s	Dolati (2010)

Geonevus

OBJECTID_1	Join_Count	TARGET_FID	Label	Shape_Area (sqkm)	ORIG_FID	Absolute_Age	Age_paleontology	Unit	Reference
1859	0	1859	m_brown	0.079	4		Pliocene	Pll.si.s	Dolati (2010)
1860	0	1860	m_brown	0.857	4		Pliocene	Pll.si.s	Dolati (2010)
1861	0	1861	m_brown	0.130	4		Pliocene	Pll.si.s	Dolati (2010)
1862	0	1862	m_brown	2.392	4		Pliocene	Pll.si.s	Dolati (2010)
1863	0	1863	m_brown	0.273	4		Pliocene	Pll.si.s	Dolati (2010)
1864	0	1864	m_brown	0.042	4		Pliocene	Pll.si.s	Dolati (2010)
1865	0	1865	m_brown	0.162	4		Pliocene	Pll.si.s	Dolati (2010)
1866	0	1866	m_brown	0.181	4		Pliocene	Pll.si.s	Dolati (2010)
1867	0	1867	m_brown	0.154	4		Pliocene	Pll.si.s	Dolati (2010)
1868	0	1868	m_brown	0.035	4		Pliocene	Pll.si.s	Dolati (2010)
1869	0	1869	m_brown	1.175	4		Pliocene	Pll.si.s	Dolati (2010)
1870	0	1870	m_brown	0.388	4		Pliocene	Pll.si.s	Dolati (2010)
1871	0	1871	m_brown	0.040	4		Pliocene	Pll.si.s	Dolati (2010)
1872	0	1872	m_brown	0.068	4		Pliocene	Pll.si.s	Dolati (2010)
1873	0	1873	m_brown	0.172	4		Pliocene	Pll.si.s	Dolati (2010)
1874	0	1874	m_brown	0.184	4		Pliocene	Pll.si.s	Dolati (2010)
1875	0	1875	m_brown	0.121	4		Pliocene	Pll.si.s	Dolati (2010)
1876	0	1876	m_brown	0.157	4		Pliocene	Pll.si.s	Dolati (2010)
1877	0	1877	m_brown	0.717	4		Pliocene	Pll.si.s	Dolati (2010)
1878	0	1878	m_brown	0.063	4		Pliocene	Pll.si.s	Dolati (2010)
1879	0	1879	m_brown	0.259	4		Pliocene	Pll.si.s	Dolati (2010)
1880	0	1880	m_brown	0.036	4		Pliocene	Pll.si.s	Dolati (2010)
1881	0	1881	m_brown	0.276	4		Pliocene	Pll.si.s	Dolati (2010)
1882	0	1882	m_brown	2.157	4		Pliocene	Pll.si.s	Dolati (2010)
1883	0	1883	m_brown	0.037	4		Pliocene	Pll.si.s	Dolati (2010)
1884	0	1884	m_brown	0.049	4		Pliocene	Pll.si.s	Dolati (2010)
1885	0	1885	m_brown	0.662	4		Pliocene	Pll.si.s	Dolati (2010)
1886	0	1886	m_brown	0.060	4		Pliocene	Pll.si.s	Dolati (2010)
1887	0	1887	m_brown	0.452	4		Pliocene	Pll.si.s	Dolati (2010)
1888	0	1888	m_brown	3.121	4		Pliocene	Pll.si.s	Dolati (2010)
1889	0	1889	m_brown	0.095	4		Pliocene	Pll.si.s	Dolati (2010)
1890	0	1890	m_brown	1.410	4		Pliocene	Pll.si.s	Dolati (2010)
1891	0	1891	m_brown	0.116	4		Pliocene	Pll.si.s	Dolati (2010)
1892	0	1892	m_brown	0.029	4		Pliocene	Pll.si.s	Dolati (2010)
1893	0	1893	m_brown	0.080	4		Pliocene	Pll.si.s	Dolati (2010)
1894	0	1894	m_brown	0.099	4		Pliocene	Pll.si.s	Dolati (2010)
1895	0	1895	m_brown	0.069	4		Pliocene	Pll.si.s	Dolati (2010)
1896	0	1896	m_brown	0.084	4		Pliocene	Pll.si.s	Dolati (2010)
1897	0	1897	m_brown	1.116	4		Pliocene	Pll.si.s	Dolati (2010)

Geoverse

OBJECTID_1	Join_Count	TARGET_FID	Label	Shape_Area (sqkm)	ORIG_FID	Absolute_Age	Age_paleontology	Unit	Reference
1898	0	1898	m_brown	0.018	4		Pliocene	Pll.si.s	Dolati (2010)
1899	0	1899	m_brown	0.078	4		Pliocene	Pll.si.s	Dolati (2010)
1900	0	1900	m_brown	0.342	4		Pliocene	Pll.si.s	Dolati (2010)
1901	0	1901	m_brown	0.053	4		Pliocene	Pll.si.s	Dolati (2010)
1902	0	1902	m_brown	0.170	4		Pliocene	Pll.si.s	Dolati (2010)
1903	0	1903	m_brown	0.047	4		Pliocene	Pll.si.s	Dolati (2010)
1904	0	1904	m_brown	0.008	4		Pliocene	Pll.si.s	Dolati (2010)
1905	0	1905	m_brown	0.353	4		Pliocene	Pll.si.s	Dolati (2010)
1906	0	1906	m_brown	0.335	4		Pliocene	Pll.si.s	Dolati (2010)
1907	0	1907	m_brown	0.540	4		Pliocene	Pll.si.s	Dolati (2010)
1908	0	1908	m_brown	0.015	4		Pliocene	Pll.si.s	Dolati (2010)
1909	0	1909	m_brown	0.029	4		Pliocene	Pll.si.s	Dolati (2010)
1910	0	1910	m_brown	0.075	4		Pliocene	Pll.si.s	Dolati (2010)
1911	0	1911	m_brown	0.034	4		Pliocene	Pll.si.s	Dolati (2010)
1912	0	1912	m_brown	0.101	4		Pliocene	Pll.si.s	Dolati (2010)
1913	0	1913	m_brown	0.014	4		Pliocene	Pll.si.s	Dolati (2010)
1914	0	1914	m_brown	0.165	4		Pliocene	Pll.si.s	Dolati (2010)
1915	0	1915	m_brown	7.336	4		Pliocene	Pll.si.s	Dolati (2010)
1916	0	1916	m_brown	0.029	4		Pliocene	Pll.si.s	Dolati (2010)
1917	0	1917	m_brown	0.010	4		Pliocene	Pll.si.s	Dolati (2010)
1918	0	1918	m_brown	0.515	4		Pliocene	Pll.si.s	Dolati (2010)
1919	0	1919	m_brown	0.088	4		Pliocene	Pll.si.s	Dolati (2010)
1920	0	1920	m_brown	2.259	4		Pliocene	Pll.si.s	Dolati (2010)
1921	0	1921	m_brown	0.027	4		Pliocene	Pll.si.s	Dolati (2010)
1922	0	1922	m_brown	0.104	4		Pliocene	Pll.si.s	Dolati (2010)
1923	0	1923	m_brown	0.795	4		Pliocene	Pll.si.s	Dolati (2010)
1924	0	1924	m_brown	0.775	4		Pliocene	Pll.si.s	Dolati (2010)
1925	0	1925	m_brown	0.219	4		Pliocene	Pll.si.s	Dolati (2010)
1926	0	1926	m_brown	0.049	4		Pliocene	Pll.si.s	Dolati (2010)
1927	0	1927	m_brown	0.103	4		Pliocene	Pll.si.s	Dolati (2010)
1928	0	1928	m_brown	0.076	4		Pliocene	Pll.si.s	Dolati (2010)
1929	0	1929	m_brown	0.063	4		Pliocene	Pll.si.s	Dolati (2010)
1930	0	1930	m_brown	0.062	4		Pliocene	Pll.si.s	Dolati (2010)
1931	0	1931	m_brown	0.030	4		Pliocene	Pll.si.s	Dolati (2010)
1932	0	1932	m_brown	0.034	4		Pliocene	Pll.si.s	Dolati (2010)
1933	0	1933	m_brown	0.202	4		Pliocene	Pll.si.s	Dolati (2010)
1934	0	1934	m_brown	0.257	4		Pliocene	Pll.si.s	Dolati (2010)
1935	0	1935	m_brown	0.020	4		Pliocene	Pll.si.s	Dolati (2010)
1936	0	1936	m_brown	0.361	4		Pliocene	Pll.si.s	Dolati (2010)

geonevis

OBJECTID_1	Join_Count	TARGET_FID	Label	Shape_Area (sqkm)	ORIG_FID	Absolute_Age	Age_paleontology	Unit	Reference
1937	0	1937	m_brown	2.655	4		Pliocene	Pll.si.s	Dolati (2010)
1938	0	1938	m_brown	0.452	4		Pliocene	Pll.si.s	Dolati (2010)
1939	0	1939	m_brown	0.103	4		Pliocene	Pll.si.s	Dolati (2010)
1940	0	1940	m_brown	0.024	4		Pliocene	Pll.si.s	Dolati (2010)
1941	0	1941	m_brown	0.047	4		Pliocene	Pll.si.s	Dolati (2010)
1942	0	1942	m_brown	0.012	4		Pliocene	Pll.si.s	Dolati (2010)
1943	0	1943	m_brown	0.076	4		Pliocene	Pll.si.s	Dolati (2010)
1944	0	1944	m_brown	0.065	4		Pliocene	Pll.si.s	Dolati (2010)
1945	0	1945	m_brown	1.186	4		Pliocene	Pll.si.s	Dolati (2010)
1946	0	1946	m_brown	0.168	4		Pliocene	Pll.si.s	Dolati (2010)
1947	0	1947	m_brown	0.048	4		Pliocene	Pll.si.s	Dolati (2010)
1948	0	1948	m_brown	0.527	4		Pliocene	Pll.si.s	Dolati (2010)
1949	0	1949	m_brown	0.032	4		Pliocene	Pll.si.s	Dolati (2010)
1950	0	1950	m_brown	0.051	4		Pliocene	Pll.si.s	Dolati (2010)
1951	0	1951	m_brown	0.089	4		Pliocene	Pll.si.s	Dolati (2010)
1952	0	1952	m_brown	0.476	4		Pliocene	Pll.si.s	Dolati (2010)
1953	0	1953	m_brown	0.533	4		Pliocene	Pll.si.s	Dolati (2010)
1954	0	1954	m_brown	0.620	4		Pliocene	Pll.si.s	Dolati (2010)
1955	0	1955	m_brown	0.066	4		Pliocene	Pll.si.s	Dolati (2010)
1956	0	1956	m_brown	1.286	4		Pliocene	Pll.si.s	Dolati (2010)
1957	0	1957	m_brown	0.125	4		Pliocene	Pll.si.s	Dolati (2010)
1958	0	1958	m_brown	1.209	4		Pliocene	Pll.si.s	Dolati (2010)
1959	0	1959	m_brown	0.268	4		Pliocene	Pll.si.s	Dolati (2010)
1960	0	1960	m_brown	0.134	4		Pliocene	Pll.si.s	Dolati (2010)
1961	0	1961	m_brown	2.456	4		Pliocene	Pll.si.s	Dolati (2010)
1962	0	1962	m_brown	0.106	4		Pliocene	Pll.si.s	Dolati (2010)
1963	0	1963	m_brown	0.049	4		Pliocene	Pll.si.s	Dolati (2010)
1964	0	1964	m_brown	1.229	4		Pliocene	Pll.si.s	Dolati (2010)
1965	0	1965	m_brown	0.174	4		Pliocene	Pll.si.s	Dolati (2010)
1966	0	1966	m_brown	0.078	4		Pliocene	Pll.si.s	Dolati (2010)
1967	0	1967	m_brown	0.110	4		Pliocene	Pll.si.s	Dolati (2010)
1968	0	1968	m_brown	0.262	4		Pliocene	Pll.si.s	Dolati (2010)
1969	0	1969	m_brown	0.023	4		Pliocene	Pll.si.s	Dolati (2010)
1970	0	1970	m_brown	0.139	4		Pliocene	Pll.si.s	Dolati (2010)
1971	0	1971	m_brown	2.117	4		Pliocene	Pll.si.s	Dolati (2010)
1972	0	1972	m_brown	0.082	4		Pliocene	Pll.si.s	Dolati (2010)
1973	0	1973	m_brown	0.123	4		Pliocene	Pll.si.s	Dolati (2010)
1974	0	1974	m_brown	0.578	4		Pliocene	Pll.si.s	Dolati (2010)
1975	0	1975	m_brown	0.371	4		Pliocene	Pll.si.s	Dolati (2010)

Geoverse

OBJECTID_1	Join_Count	TARGET_FID	Label	Shape_Area (sqkm)	ORIG_FID	Absolute_Age	Age_paleontology	Unit	Reference
1976	0	1976	m_brown	0.123	4		Pliocene	Pll.si.s	Dolati (2010)
1977	0	1977	m_brown	0.335	4		Pliocene	Pll.si.s	Dolati (2010)
1978	0	1978	m_brown	1.527	4		Pliocene	Pll.si.s	Dolati (2010)
1979	0	1979	m_brown	0.239	4		Pliocene	Pll.si.s	Dolati (2010)
1981	0	1981	m_brown	0.037	4		Pliocene	Pll.si.s	Dolati (2010)
1982	0	1982	m_brown	0.287	4		Pliocene	Pll.si.s	Dolati (2010)
1983	0	1983	m_brown	0.227	4		Pliocene	Pll.si.s	Dolati (2010)
1984	0	1984	m_brown	0.141	4		Pliocene	Pll.si.s	Dolati (2010)
1985	0	1985	m_brown	0.042	4		Pliocene	Pll.si.s	Dolati (2010)
1986	0	1986	m_brown	0.286	4		Pliocene	Pll.si.s	Dolati (2010)
1987	0	1987	m_brown	14.256	4		Pliocene	Pll.si.s	Dolati (2010)
1988	0	1988	m_brown	0.902	4		Pliocene	Pll.si.s	Dolati (2010)
1989	0	1989	m_brown	0.028	4		Pliocene	Pll.si.s	Dolati (2010)
1990	0	1990	m_brown	0.144	4		Pliocene	Pll.si.s	Dolati (2010)
1991	1	1991	m_brown	17.572	4		Pliocene	Pll.si.s	Dolati (2010)
1992	0	1992	m_brown	0.473	4		Pliocene	Pll.si.s	Dolati (2010)
1993	0	1993	m_brown	0.122	4		Pliocene	Pll.si.s	Dolati (2010)
1994	0	1994	m_brown	0.428	4		Pliocene	Pll.si.s	Dolati (2010)
1995	0	1995	m_brown	0.065	4		Pliocene	Pll.si.s	Dolati (2010)
1996	0	1996	m_brown	0.730	4		Pliocene	Pll.si.s	Dolati (2010)
1997	0	1997	m_brown	0.724	4		Pliocene	Pll.si.s	Dolati (2010)
1998	0	1998	m_brown	1.092	4		Pliocene	Pll.si.s	Dolati (2010)
1999	0	1999	m_brown	0.081	4		Pliocene	Pll.si.s	Dolati (2010)
2000	0	2000	m_brown	0.441	4		Pliocene	Pll.si.s	Dolati (2010)
2001	0	2001	m_brown	2.595	4		Pliocene	Pll.si.s	Dolati (2010)
2002	0	2002	m_brown	1.109	4		Pliocene	Pll.si.s	Dolati (2010)
2003	0	2003	m_brown	0.056	4		Pliocene	Pll.si.s	Dolati (2010)
2004	0	2004	m_brown	4.058	4		Pliocene	Pll.si.s	Dolati (2010)
2005	0	2005	m_brown	0.317	4		Pliocene	Pll.si.s	Dolati (2010)
2006	0	2006	m_brown	0.390	4		Pliocene	Pll.si.s	Dolati (2010)
2007	0	2007	m_brown	0.483	4		Pliocene	Pll.si.s	Dolati (2010)
2008	0	2008	m_brown	0.035	4		Pliocene	Pll.si.s	Dolati (2010)
2009	0	2009	m_brown	1.033	4		Pliocene	Pll.si.s	Dolati (2010)
2010	0	2010	m_brown	0.200	4		Pliocene	Pll.si.s	Dolati (2010)
2011	0	2011	m_brown	0.181	4		Pliocene	Pll.si.s	Dolati (2010)
2012	0	2012	m_brown	1.780	4		Pliocene	Pll.si.s	Dolati (2010)
2013	0	2013	m_brown	0.464	4		Pliocene	Pll.si.s	Dolati (2010)
2014	0	2014	m_brown	0.382	4		Pliocene	Pll.si.s	Dolati (2010)
2015	0	2015	m_brown	0.164	4		Pliocene	Pll.si.s	Dolati (2010)

geonevis

OBJECTID_1	Join_Count	TARGET_FID	Label	Shape_Area (sqkm)	ORIG_FID	Absolute_Age	Age_paleontology	Unit	Reference
2016	0	2016	m_brown	8.152	4		Pliocene	Pll.si.s	Dolati (2010)
2017	0	2017	m_brown	0.350	4		Pliocene	Pll.si.s	Dolati (2010)
2018	0	2018	m_brown	1.683	4		Pliocene	Pll.si.s	Dolati (2010)
2019	0	2019	m_brown	0.043	4		Pliocene	Pll.si.s	Dolati (2010)
2020	0	2020	m_brown	0.972	4		Pliocene	Pll.si.s	Dolati (2010)
2021	0	2021	m_brown	0.034	4		Pliocene	Pll.si.s	Dolati (2010)
2022	0	2022	m_brown	0.147	4		Pliocene	Pll.si.s	Dolati (2010)
2023	0	2023	m_brown	0.165	4		Pliocene	Pll.si.s	Dolati (2010)
2024	0	2024	m_brown	25.495	4		Pliocene	Pll.si.s	Dolati (2010)
2025	0	2025	m_brown	0.108	4		Pliocene	Pll.si.s	Dolati (2010)
2026	0	2026	m_brown	2.555	4		Pliocene	Pll.si.s	Dolati (2010)
2027	0	2027	m_brown	0.075	4		Pliocene	Pll.si.s	Dolati (2010)
2028	0	2028	m_brown	0.366	4		Pliocene	Pll.si.s	Dolati (2010)
2029	0	2029	m_brown	0.240	4		Pliocene	Pll.si.s	Dolati (2010)
2030	0	2030	m_brown	0.644	4		Pliocene	Pll.si.s	Dolati (2010)
2031	0	2031	m_brown	0.574	4		Pliocene	Pll.si.s	Dolati (2010)
2032	0	2032	m_brown	0.182	4		Pliocene	Pll.si.s	Dolati (2010)
2033	0	2033	m_brown	0.651	4		Pliocene	Pll.si.s	Dolati (2010)
2034	0	2034	m_brown	0.092	4		Pliocene	Pll.si.s	Dolati (2010)
2035	0	2035	m_brown	0.108	4		Pliocene	Pll.si.s	Dolati (2010)
2036	0	2036	m_brown	0.051	4		Pliocene	Pll.si.s	Dolati (2010)
2037	0	2037	m_brown	1.566	4		Pliocene	Pll.si.s	Dolati (2010)
2038	0	2038	m_brown	0.157	4		Pliocene	Pll.si.s	Dolati (2010)
2039	0	2039	m_brown	3.176	4		Pliocene	Pll.si.s	Dolati (2010)
2040	0	2040	m_brown	0.072	4		Pliocene	Pll.si.s	Dolati (2010)
2041	0	2041	m_brown	0.240	4		Pliocene	Pll.si.s	Dolati (2010)
2042	0	2042	m_brown	0.018	4		Pliocene	Pll.si.s	Dolati (2010)
2045	0	2045	m_brown	0.329	4		Pliocene	Pll.si.s	Dolati (2010)
2046	0	2046	m_brown	1.201	4		Pliocene	Pll.si.s	Dolati (2010)
2048	0	2048	m_brown	0.417	4		Pliocene	Pll.si.s	Dolati (2010)
2049	0	2049	m_brown	0.115	4		Pliocene	Pll.si.s	Dolati (2010)
2050	0	2050	m_brown	0.036	4		Pliocene	Pll.si.s	Dolati (2010)
2051	0	2051	m_brown	3.820	4		Pliocene	Pll.si.s	Dolati (2010)
2052	0	2052	m_brown	0.108	4		Pliocene	Pll.si.s	Dolati (2010)
2054	0	2054	m_brown	0.580	4		Pliocene	Pll.si.s	Dolati (2010)
2056	0	2056	m_brown	0.573	4		Pliocene	Pll.si.s	Dolati (2010)
2057	0	2057	m_brown	1.195	4		Pliocene	Pll.si.s	Dolati (2010)
2058	0	2058	m_brown	0.388	4		Pliocene	Pll.si.s	Dolati (2010)
2059	0	2059	m_brown	1.671	4		Pliocene	Pll.si.s	Dolati (2010)

GeoNeus

OBJECTID_1	Join_Count	TARGET_FID	Label	Shape_Area (sqkm)	ORIG_FID	Absolute_Age	Age_paleontology	Unit	Reference
2060	0	2060	m_brown	0.456	4		Pliocene	Pll.si.s	Dolati (2010)
2061	0	2061	m_brown	0.171	4		Pliocene	Pll.si.s	Dolati (2010)
2062	0	2062	m_brown	10.675	4		Pliocene	Pll.si.s	Dolati (2010)
2065	0	2065	m_brown	2.208	4		Pliocene	Pll.si.s	Dolati (2010)
2066	0	2066	m_brown	0.324	4		Pliocene	Pll.si.s	Dolati (2010)
2068	0	2068	m_brown	1.463	4		Pliocene	Pll.si.s	Dolati (2010)
2069	0	2069	m_brown	0.378	4		Pliocene	Pll.si.s	Dolati (2010)
2071	0	2071	m_brown	0.259	4		Pliocene	Pll.si.s	Dolati (2010)
2073	0	2073	m_brown	0.310	4		Pliocene	Pll.si.s	Dolati (2010)
2074	0	2074	m_brown	0.171	4		Pliocene	Pll.si.s	Dolati (2010)
2075	0	2075	m_brown	0.878	4		Pliocene	Pll.si.s	Dolati (2010)
2076	0	2076	m_brown	0.223	4		Pliocene	Pll.si.s	Dolati (2010)
2077	0	2077	m_brown	0.432	4		Pliocene	Pll.si.s	Dolati (2010)
2078	0	2078	m_brown	0.197	4		Pliocene	Pll.si.s	Dolati (2010)
2080	0	2080	m_brown	0.134	4		Pliocene	Pll.si.s	Dolati (2010)
2082	0	2082	m_brown	1.207	4		Pliocene	Pll.si.s	Dolati (2010)
2084	0	2084	m_brown	0.193	4		Pliocene	Pll.si.s	Dolati (2010)
2085	0	2085	m_brown	0.805	4		Pliocene	Pll.si.s	Dolati (2010)
2087	0	2087	m_brown	0.230	4		Pliocene	Pll.si.s	Dolati (2010)
2088	0	2088	m_brown	0.106	4		Pliocene	Pll.si.s	Dolati (2010)
2089	0	2089	m_brown	1.115	4		Pliocene	Pll.si.s	Dolati (2010)
2090	0	2090	m_brown	0.069	4		Pliocene	Pll.si.s	Dolati (2010)
2091	0	2091	m_brown	0.265	4		Pliocene	Pll.si.s	Dolati (2010)
2092	0	2092	m_brown	0.057	4		Pliocene	Pll.si.s	Dolati (2010)
2093	0	2093	m_brown	0.451	4		Pliocene	Pll.si.s	Dolati (2010)
2094	0	2094	m_brown	1.066	4		Pliocene	Pll.si.s	Dolati (2010)
2095	0	2095	m_brown	1.050	4		Pliocene	Pll.si.s	Dolati (2010)
2096	0	2096	m_brown	0.784	4		Pliocene	Pll.si.s	Dolati (2010)
2097	0	2097	m_brown	0.673	4		Pliocene	Pll.si.s	Dolati (2010)
2098	0	2098	m_brown	1.297	4		Pliocene	Pll.si.s	Dolati (2010)
2099	0	2099	m_brown	1.316	4		Pliocene	Pll.si.s	Dolati (2010)
2101	0	2101	m_brown	0.083	4		Pliocene	Pll.si.s	Dolati (2010)
2102	0	2102	m_brown	1.601	4		Pliocene	Pll.si.s	Dolati (2010)
2104	0	2104	m_brown	0.089	4		Pliocene	Pll.si.s	Dolati (2010)
2105	0	2105	m_brown	0.030	4		Pliocene	Pll.si.s	Dolati (2010)
2108	0	2108	m_brown	0.184	4		Pliocene	Pll.si.s	Dolati (2010)
2109	0	2109	m_brown	0.652	4		Pliocene	Pll.si.s	Dolati (2010)
2110	0	2110	m_brown	0.173	4		Pliocene	Pll.si.s	Dolati (2010)
2111	0	2111	m_brown	0.536	4		Pliocene	Pll.si.s	Dolati (2010)

geonevis

OBJECTID_1	Join_Count	TARGET_FID	Label	Shape_Area (sqkm)	ORIG_FID	Absolute_Age	Age_paleontology	Unit	Reference
5124	1	5125	m_brown	1.708	9		Pliocene	Pll.si.s	Dolati (2010)
5320	1	5321	m_brown	0.284	9		Pliocene	Pll.si.s	Dolati (2010)
6534	1	6535	m_brown	0.243	12		Pliocene	Pll.si.s	Dolati (2010)
6587	1	6588	m_brown	0.170	12		Pliocene	Pll.si.s	Dolati (2010)
6621	1	6622	m_brown	0.543	12		Pliocene	Pll.si.s	Dolati (2010)
6638	1	6639	m_brown	0.573	12		Pliocene	Pll.si.s	Dolati (2010)
10412	1	10421	m_brown	0.017	0		Pliocene	Pll.si.s	Dolati (2010)
10413	1	10423	m_brown	0.255	0		Pliocene	Pll.si.s	Dolati (2010)
10414	3	10424	m_brown	0.627	0		Pliocene	Pll.si.s	Dolati (2010)
10415	1	10425	m_brown	0.003	0		Pliocene	Pll.si.s	Dolati (2010)

GeoNexus

Table S11. Summary of mapped polygons for the PlPe$^{c.s.si}$ Unit.

OBJECTID_1	Join_Count	TARGET_FID	Label	Shape_Area (sqkm)	ORIG_FID	Absolute_Age	Age_paleontology	Unit	Reference
203	0	203	Plc-Qt	0.175	2		Pliocene- Pleistocene	PlPec.s.si	Dolati (2010)
209	0	209	Plc-Qt	0.657	2		Pliocene- Pleistocene	PlPec.s.si	Dolati (2010)
210	0	210	Plc-Qt	0.604	2		Pliocene- Pleistocene	PlPec.s.si	Dolati (2010)
215	0	215	Plc-Qt	1.380	2		Pliocene- Pleistocene	PlPec.s.si	Dolati (2010)
218	0	218	Plc-Qt	0.249	2		Pliocene- Pleistocene	PlPec.s.si	Dolati (2010)
220	0	220	Plc-Qt	4.941	2		Pliocene- Pleistocene	PlPec.s.si	Dolati (2010)
224	0	224	Plc-Qt	0.676	2		Pliocene- Pleistocene	PlPec.s.si	Dolati (2010)
234	0	234	Plc-Qt	0.894	2		Pliocene- Pleistocene	PlPec.s.si	Dolati (2010)
238	0	238	Plc-Qt	8.712	2		Pliocene- Pleistocene	PlPec.s.si	Dolati (2010)
240	0	240	Plc-Qt	0.042	2		Pliocene- Pleistocene	PlPec.s.si	Dolati (2010)
242	0	242	Plc-Qt	1.346	2		Pliocene- Pleistocene	PlPec.s.si	Dolati (2010)
245	0	245	Plc-Qt	0.039	2		Pliocene- Pleistocene	PlPec.s.si	Dolati (2010)
247	0	247	Plc-Qt	0.564	2		Pliocene- Pleistocene	PlPec.s.si	Dolati (2010)
248	0	248	Plc-Qt	0.317	2		Pliocene- Pleistocene	PlPec.s.si	Dolati (2010)
255	0	255	Plc-Qt	2.194	2		Pliocene- Pleistocene	PlPec.s.si	Dolati (2010)
267	0	267	Plc-Qt	1.020	2		Pliocene- Pleistocene	PlPec.s.si	Dolati (2010)
268	0	268	Plc-Qt	0.330	2		Pliocene- Pleistocene	PlPec.s.si	Dolati (2010)
271	0	271	Plc-Qt	0.061	2		Pliocene- Pleistocene	PlPec.s.si	Dolati (2010)
276	0	276	Plc-Qt	1.278	2		Pliocene- Pleistocene	PlPec.s.si	Dolati (2010)
282	0	282	Plc-Qt	1.168	2		Pliocene- Pleistocene	PlPec.s.si	Dolati (2010)
2144	1	2144	Plc-Qt	3.232	5		Pliocene- Pleistocene	PlPec.s.si	Dolati (2010)
8809	1	8810	Qt	0.473	16		Pliocene- Pleistocene	PlPec.s.si	Dolati (2010)
9189	0	9190	Qt	0.039	17		Pliocene- Pleistocene	PlPec.s.si	Dolati (2010)
9190	0	9191	Qt	0.679	17		Pliocene- Pleistocene	PlPec.s.si	Dolati (2010)
9191	0	9192	Qt	0.109	17		Pliocene- Pleistocene	PlPec.s.si	Dolati (2010)
9192	0	9193	Qt	0.019	17		Pliocene- Pleistocene	PlPec.s.si	Dolati (2010)
9193	0	9194	Qt	0.011	17		Pliocene- Pleistocene	PlPec.s.si	Dolati (2010)
9194	0	9195	Qt	0.014	17		Pliocene- Pleistocene	PlPec.s.si	Dolati (2010)
9195	0	9196	Qt	0.786	17		Pliocene- Pleistocene	PlPec.s.si	Dolati (2010)
9196	0	9197	Qt	0.029	17		Pliocene- Pleistocene	PlPec.s.si	Dolati (2010)
9197	0	9198	Qt	0.041	17		Pliocene- Pleistocene	PlPec.s.si	Dolati (2010)
9198	0	9199	Qt	0.171	17		Pliocene- Pleistocene	PlPec.s.si	Dolati (2010)
9199	0	9200	Qt	0.074	17		Pliocene- Pleistocene	PlPec.s.si	Dolati (2010)
9200	0	9201	Qt	0.243	17		Pliocene- Pleistocene	PlPec.s.si	Dolati (2010)
9201	0	9202	Qt	0.194	17		Pliocene- Pleistocene	PlPec.s.si	Dolati (2010)
9202	0	9203	Qt	0.229	17		Pliocene- Pleistocene	PlPec.s.si	Dolati (2010)
9203	0	9204	Qt	0.074	17		Pliocene- Pleistocene	PlPec.s.si	Dolati (2010)
9204	0	9205	Qt	0.131	17		Pliocene- Pleistocene	PlPec.s.si	Dolati (2010)

GSI Only

OBJECTID_1	Join_Count	TARGET_FID	Label	Shape_Area (sqkm)	ORIG_FID	Absolute_Age	Age_paleontology	Unit	Reference
9205	0	9206	Qt	0.052	17		Pliocene- Pleistocene	PlPec.s.si	Dolati (2010)
9206	0	9207	Qt	0.028	17		Pliocene- Pleistocene	PlPec.s.si	Dolati (2010)
9207	0	9208	Qt	0.074	17		Pliocene- Pleistocene	PlPec.s.si	Dolati (2010)
9208	0	9209	Qt	0.085	17		Pliocene- Pleistocene	PlPec.s.si	Dolati (2010)
9209	0	9210	Qt	0.004	17		Pliocene- Pleistocene	PlPec.s.si	Dolati (2010)
9210	0	9211	Qt	0.211	17		Pliocene- Pleistocene	PlPec.s.si	Dolati (2010)
9211	0	9212	Qt	0.453	17		Pliocene- Pleistocene	PlPec.s.si	Dolati (2010)
9212	0	9213	Qt	0.004	17		Pliocene- Pleistocene	PlPec.s.si	Dolati (2010)
9213	0	9214	Qt	0.439	17		Pliocene- Pleistocene	PlPec.s.si	Dolati (2010)
9214	0	9215	Qt	0.085	17		Pliocene- Pleistocene	PlPec.s.si	Dolati (2010)
9215	0	9216	Qt	0.413	17		Pliocene- Pleistocene	PlPec.s.si	Dolati (2010)
9216	0	9217	Qt	0.189	17		Pliocene- Pleistocene	PlPec.s.si	Dolati (2010)
9217	0	9218	Qt	17.773	17		Pliocene- Pleistocene	PlPec.s.si	Dolati (2010)
9218	0	9219	Qt	0.152	17		Pliocene- Pleistocene	PlPec.s.si	Dolati (2010)
9219	0	9220	Qt	0.012	17		Pliocene- Pleistocene	PlPec.s.si	Dolati (2010)
9220	0	9221	Qt	0.005	17		Pliocene- Pleistocene	PlPec.s.si	Dolati (2010)
9221	0	9222	Qt	0.605	17		Pliocene- Pleistocene	PlPec.s.si	Dolati (2010)
9222	0	9223	Qt	0.002	17		Pliocene- Pleistocene	PlPec.s.si	Dolati (2010)
9223	0	9224	Qt	0.058	17		Pliocene- Pleistocene	PlPec.s.si	Dolati (2010)
9224	0	9225	Qt	0.047	17		Pliocene- Pleistocene	PlPec.s.si	Dolati (2010)
9225	0	9226	Qt	0.146	17		Pliocene- Pleistocene	PlPec.s.si	Dolati (2010)
9226	0	9227	Qt	0.341	17		Pliocene- Pleistocene	PlPec.s.si	Dolati (2010)
9227	0	9228	Qt	0.016	17		Pliocene- Pleistocene	PlPec.s.si	Dolati (2010)
9228	0	9229	Qt	0.343	17		Pliocene- Pleistocene	PlPec.s.si	Dolati (2010)
9229	0	9230	Qt	0.139	17		Pliocene- Pleistocene	PlPec.s.si	Dolati (2010)
9230	0	9231	Qt	0.058	17		Pliocene- Pleistocene	PlPec.s.si	Dolati (2010)
9231	0	9232	Qt	0.041	17		Pliocene- Pleistocene	PlPec.s.si	Dolati (2010)
9232	0	9233	Qt	0.322	17		Pliocene- Pleistocene	PlPec.s.si	Dolati (2010)
9233	0	9234	Qt	0.141	17		Pliocene- Pleistocene	PlPec.s.si	Dolati (2010)
9234	0	9235	Qt	0.011	17		Pliocene- Pleistocene	PlPec.s.si	Dolati (2010)
9235	0	9236	Qt	0.036	17		Pliocene- Pleistocene	PlPec.s.si	Dolati (2010)
9236	0	9237	Qt	0.044	17		Pliocene- Pleistocene	PlPec.s.si	Dolati (2010)
9237	0	9238	Qt	0.503	17		Pliocene- Pleistocene	PlPec.s.si	Dolati (2010)
9238	0	9239	Qt	0.269	17		Pliocene- Pleistocene	PlPec.s.si	Dolati (2010)
9239	0	9240	Qt	0.048	17		Pliocene- Pleistocene	PlPec.s.si	Dolati (2010)
9240	0	9241	Qt	0.049	17		Pliocene- Pleistocene	PlPec.s.si	Dolati (2010)
9241	0	9242	Qt	0.105	17		Pliocene- Pleistocene	PlPec.s.si	Dolati (2010)
9242	0	9243	Qt	0.108	17		Pliocene- Pleistocene	PlPec.s.si	Dolati (2010)
9243	0	9244	Qt	0.397	17		Pliocene- Pleistocene	PlPec.s.si	Dolati (2010)

GeoNVS

OBJECTID_1	Join_Count	TARGET_FID	Label	Shape_Area (sqkm)	ORIG_FID	Absolute_Age	Age_paleontology	Unit	Reference
9244	0	9245	Qt	0.155	17		Pliocene- Pleistocene	PlPec.s.si	Dolati (2010)
9245	0	9246	Qt	2.623	17		Pliocene- Pleistocene	PlPec.s.si	Dolati (2010)
9246	0	9247	Qt	0.023	17		Pliocene- Pleistocene	PlPec.s.si	Dolati (2010)
9247	0	9248	Qt	0.132	17		Pliocene- Pleistocene	PlPec.s.si	Dolati (2010)
9248	0	9249	Qt	0.060	17		Pliocene- Pleistocene	PlPec.s.si	Dolati (2010)
9249	0	9250	Qt	0.066	17		Pliocene- Pleistocene	PlPec.s.si	Dolati (2010)
9250	0	9251	Qt	0.060	17		Pliocene- Pleistocene	PlPec.s.si	Dolati (2010)
9251	0	9252	Qt	0.201	17		Pliocene- Pleistocene	PlPec.s.si	Dolati (2010)
9252	0	9253	Qt	0.029	17		Pliocene- Pleistocene	PlPec.s.si	Dolati (2010)
9253	0	9254	Qt	0.169	17		Pliocene- Pleistocene	PlPec.s.si	Dolati (2010)
9254	0	9255	Qt	0.164	17		Pliocene- Pleistocene	PlPec.s.si	Dolati (2010)
9255	0	9256	Qt	0.334	17		Pliocene- Pleistocene	PlPec.s.si	Dolati (2010)
9256	0	9257	Qt	0.050	17		Pliocene- Pleistocene	PlPec.s.si	Dolati (2010)
9257	0	9258	Qt	0.247	17		Pliocene- Pleistocene	PlPec.s.si	Dolati (2010)
9258	0	9259	Qt	0.107	17		Pliocene- Pleistocene	PlPec.s.si	Dolati (2010)
9259	0	9260	Qt	0.347	17		Pliocene- Pleistocene	PlPec.s.si	Dolati (2010)
9260	0	9261	Qt	0.482	17		Pliocene- Pleistocene	PlPec.s.si	Dolati (2010)
9261	0	9262	Qt	0.065	17		Pliocene- Pleistocene	PlPec.s.si	Dolati (2010)
9262	0	9263	Qt	0.119	17		Pliocene- Pleistocene	PlPec.s.si	Dolati (2010)
9263	0	9264	Qt	0.132	17		Pliocene- Pleistocene	PlPec.s.si	Dolati (2010)
9264	0	9265	Qt	0.122	17		Pliocene- Pleistocene	PlPec.s.si	Dolati (2010)
9265	0	9266	Qt	0.157	17		Pliocene- Pleistocene	PlPec.s.si	Dolati (2010)
9266	0	9267	Qt	0.070	17		Pliocene- Pleistocene	PlPec.s.si	Dolati (2010)
9267	0	9268	Qt	0.023	17		Pliocene- Pleistocene	PlPec.s.si	Dolati (2010)
9268	0	9269	Qt	0.419	17		Pliocene- Pleistocene	PlPec.s.si	Dolati (2010)
9269	0	9270	Qt	0.441	17		Pliocene- Pleistocene	PlPec.s.si	Dolati (2010)
9270	0	9271	Qt	0.805	17		Pliocene- Pleistocene	PlPec.s.si	Dolati (2010)
9271	0	9272	Qt	0.073	17		Pliocene- Pleistocene	PlPec.s.si	Dolati (2010)
9272	0	9273	Qt	0.631	17		Pliocene- Pleistocene	PlPec.s.si	Dolati (2010)
9273	0	9274	Qt	0.236	17		Pliocene- Pleistocene	PlPec.s.si	Dolati (2010)
9274	0	9275	Qt	0.334	17		Pliocene- Pleistocene	PlPec.s.si	Dolati (2010)
9275	0	9276	Qt	0.041	17		Pliocene- Pleistocene	PlPec.s.si	Dolati (2010)
9276	0	9277	Qt	0.237	17		Pliocene- Pleistocene	PlPec.s.si	Dolati (2010)
9277	0	9278	Qt	0.268	17		Pliocene- Pleistocene	PlPec.s.si	Dolati (2010)
9278	0	9279	Qt	0.189	17		Pliocene- Pleistocene	PlPec.s.si	Dolati (2010)
9279	0	9280	Qt	14.465	17		Pliocene- Pleistocene	PlPec.s.si	Dolati (2010)
9280	0	9281	Qt	0.324	17		Pliocene- Pleistocene	PlPec.s.si	Dolati (2010)
9281	0	9282	Qt	0.470	17		Pliocene- Pleistocene	PlPec.s.si	Dolati (2010)
9282	0	9283	Qt	0.268	17		Pliocene- Pleistocene	PlPec.s.si	Dolati (2010)

GeoNLP

OBJECTID_1	Join_Count	TARGET_FID	Label	Shape_Area (sqkm)	ORIG_FID	Absolute_Age	Age_paleontology	Unit	Reference
9283	0	9284	Qt	0.188	17		Pliocene- Pleistocene	PlPec.s.si	Dolati (2010)
9284	0	9285	Qt	0.087	17		Pliocene- Pleistocene	PlPec.s.si	Dolati (2010)
9285	0	9286	Qt	0.006	17		Pliocene- Pleistocene	PlPec.s.si	Dolati (2010)
9286	0	9287	Qt	0.435	17		Pliocene- Pleistocene	PlPec.s.si	Dolati (2010)
9287	0	9288	Qt	3.489	17		Pliocene- Pleistocene	PlPec.s.si	Dolati (2010)
9288	0	9289	Qt	0.460	17		Pliocene- Pleistocene	PlPec.s.si	Dolati (2010)
9289	0	9290	Qt	0.109	17		Pliocene- Pleistocene	PlPec.s.si	Dolati (2010)
9290	0	9291	Qt	0.074	17		Pliocene- Pleistocene	PlPec.s.si	Dolati (2010)
9291	0	9292	Qt	0.532	17		Pliocene- Pleistocene	PlPec.s.si	Dolati (2010)
9292	0	9293	Qt	0.265	17		Pliocene- Pleistocene	PlPec.s.si	Dolati (2010)
9293	0	9294	Qt	0.279	17		Pliocene- Pleistocene	PlPec.s.si	Dolati (2010)
9294	0	9295	Qt	0.267	17		Pliocene- Pleistocene	PlPec.s.si	Dolati (2010)
9295	0	9296	Qt	0.106	17		Pliocene- Pleistocene	PlPec.s.si	Dolati (2010)
9296	0	9297	Qt	0.277	17		Pliocene- Pleistocene	PlPec.s.si	Dolati (2010)
9297	0	9298	Qt	1.638	17		Pliocene- Pleistocene	PlPec.s.si	Dolati (2010)
9298	0	9299	Qt	0.073	17		Pliocene- Pleistocene	PlPec.s.si	Dolati (2010)
9299	0	9300	Qt	0.177	17		Pliocene- Pleistocene	PlPec.s.si	Dolati (2010)
9300	0	9301	Qt	0.531	17		Pliocene- Pleistocene	PlPec.s.si	Dolati (2010)
9301	0	9302	Qt	0.012	17		Pliocene- Pleistocene	PlPec.s.si	Dolati (2010)
9302	0	9303	Qt	0.029	17		Pliocene- Pleistocene	PlPec.s.si	Dolati (2010)
9303	0	9304	Qt	0.109	17		Pliocene- Pleistocene	PlPec.s.si	Dolati (2010)
9304	0	9305	Qt	0.017	17		Pliocene- Pleistocene	PlPec.s.si	Dolati (2010)
9305	0	9306	Qt	0.007	17		Pliocene- Pleistocene	PlPec.s.si	Dolati (2010)
9306	0	9307	Qt	0.336	17		Pliocene- Pleistocene	PlPec.s.si	Dolati (2010)
9307	0	9308	Qt	0.507	17		Pliocene- Pleistocene	PlPec.s.si	Dolati (2010)
9308	0	9309	Qt	0.031	17		Pliocene- Pleistocene	PlPec.s.si	Dolati (2010)
9309	0	9310	Qt	0.614	17		Pliocene- Pleistocene	PlPec.s.si	Dolati (2010)
9310	0	9311	Qt	0.020	17		Pliocene- Pleistocene	PlPec.s.si	Dolati (2010)
9311	0	9312	Qt	0.326	17		Pliocene- Pleistocene	PlPec.s.si	Dolati (2010)
9312	0	9313	Qt	0.053	17		Pliocene- Pleistocene	PlPec.s.si	Dolati (2010)
9313	0	9314	Qt	0.013	17		Pliocene- Pleistocene	PlPec.s.si	Dolati (2010)
9314	0	9315	Qt	0.013	17		Pliocene- Pleistocene	PlPec.s.si	Dolati (2010)
9315	0	9316	Qt	0.455	17		Pliocene- Pleistocene	PlPec.s.si	Dolati (2010)
9316	0	9317	Qt	0.132	17		Pliocene- Pleistocene	PlPec.s.si	Dolati (2010)
9317	0	9318	Qt	0.685	17		Pliocene- Pleistocene	PlPec.s.si	Dolati (2010)
9318	0	9319	Qt	0.356	17		Pliocene- Pleistocene	PlPec.s.si	Dolati (2010)
9319	0	9320	Qt	0.050	17		Pliocene- Pleistocene	PlPec.s.si	Dolati (2010)
9320	0	9321	Qt	0.028	17		Pliocene- Pleistocene	PlPec.s.si	Dolati (2010)
9321	0	9322	Qt	0.037	17		Pliocene- Pleistocene	PlPec.s.si	Dolati (2010)

GeoNeus

OBJECTID_1	Join_Count	TARGET_FID	Label	Shape_Area (sqkm)	ORIG_FID	Absolute_Age	Age_paleontology	Unit	Reference
9322	0	9323	Qt	0.228	17		Pliocene- Pleistocene	PlPec.s.si	Dolati (2010)
9323	0	9324	Qt	0.010	17		Pliocene- Pleistocene	PlPec.s.si	Dolati (2010)
9324	0	9325	Qt	0.018	17		Pliocene- Pleistocene	PlPec.s.si	Dolati (2010)
9325	0	9326	Qt	0.080	17		Pliocene- Pleistocene	PlPec.s.si	Dolati (2010)
9326	0	9327	Qt	0.012	17		Pliocene- Pleistocene	PlPec.s.si	Dolati (2010)
9327	0	9328	Qt	0.019	17		Pliocene- Pleistocene	PlPec.s.si	Dolati (2010)
9328	0	9329	Qt	0.282	17		Pliocene- Pleistocene	PlPec.s.si	Dolati (2010)
9329	0	9330	Qt	0.209	17		Pliocene- Pleistocene	PlPec.s.si	Dolati (2010)
9330	0	9331	Qt	0.020	17		Pliocene- Pleistocene	PlPec.s.si	Dolati (2010)
9331	0	9332	Qt	0.006	17		Pliocene- Pleistocene	PlPec.s.si	Dolati (2010)
9332	0	9333	Qt	0.119	17		Pliocene- Pleistocene	PlPec.s.si	Dolati (2010)
9333	0	9334	Qt	0.554	17		Pliocene- Pleistocene	PlPec.s.si	Dolati (2010)
9334	0	9335	Qt	0.191	17		Pliocene- Pleistocene	PlPec.s.si	Dolati (2010)
9335	0	9336	Qt	0.048	17		Pliocene- Pleistocene	PlPec.s.si	Dolati (2010)
9336	0	9337	Qt	3.687	17		Pliocene- Pleistocene	PlPec.s.si	Dolati (2010)
9337	0	9338	Qt	0.142	17		Pliocene- Pleistocene	PlPec.s.si	Dolati (2010)
9338	0	9339	Qt	0.527	17		Pliocene- Pleistocene	PlPec.s.si	Dolati (2010)
9339	0	9340	Qt	3.042	17		Pliocene- Pleistocene	PlPec.s.si	Dolati (2010)
9340	0	9341	Qt	0.035	17		Pliocene- Pleistocene	PlPec.s.si	Dolati (2010)
9341	0	9342	Qt	0.125	17		Pliocene- Pleistocene	PlPec.s.si	Dolati (2010)
9342	0	9343	Qt	0.070	17		Pliocene- Pleistocene	PlPec.s.si	Dolati (2010)
9343	0	9344	Qt	1.546	17		Pliocene- Pleistocene	PlPec.s.si	Dolati (2010)
9344	0	9345	Qt	0.045	17		Pliocene- Pleistocene	PlPec.s.si	Dolati (2010)
9345	0	9346	Qt	0.355	17		Pliocene- Pleistocene	PlPec.s.si	Dolati (2010)
9346	0	9347	Qt	0.049	17		Pliocene- Pleistocene	PlPec.s.si	Dolati (2010)
9347	0	9348	Qt	0.056	17		Pliocene- Pleistocene	PlPec.s.si	Dolati (2010)
9348	0	9349	Qt	0.020	17		Pliocene- Pleistocene	PlPec.s.si	Dolati (2010)
9349	0	9350	Qt	1.069	17		Pliocene- Pleistocene	PlPec.s.si	Dolati (2010)
9350	0	9351	Qt	0.644	17		Pliocene- Pleistocene	PlPec.s.si	Dolati (2010)
9351	0	9352	Qt	0.252	17		Pliocene- Pleistocene	PlPec.s.si	Dolati (2010)
9352	0	9353	Qt	0.034	17		Pliocene- Pleistocene	PlPec.s.si	Dolati (2010)
9353	0	9354	Qt	0.399	17		Pliocene- Pleistocene	PlPec.s.si	Dolati (2010)
9354	0	9355	Qt	0.096	17		Pliocene- Pleistocene	PlPec.s.si	Dolati (2010)
9355	0	9356	Qt	0.045	17		Pliocene- Pleistocene	PlPec.s.si	Dolati (2010)
9356	0	9357	Qt	0.056	17		Pliocene- Pleistocene	PlPec.s.si	Dolati (2010)
9357	0	9358	Qt	0.446	17		Pliocene- Pleistocene	PlPec.s.si	Dolati (2010)
9358	0	9359	Qt	0.340	17		Pliocene- Pleistocene	PlPec.s.si	Dolati (2010)
9359	0	9360	Qt	0.025	17		Pliocene- Pleistocene	PlPec.s.si	Dolati (2010)
9360	0	9361	Qt	0.292	17		Pliocene- Pleistocene	PlPec.s.si	Dolati (2010)

GeoNLP

OBJECTID_1	Join_Count	TARGET_FID	Label	Shape_Area (sqkm)	ORIG_FID	Absolute_Age	Age_paleontology	Unit	Reference
9361	0	9362	Qt	0.120	17		Pliocene- Pleistocene	PlPec.s.si	Dolati (2010)
9362	0	9363	Qt	0.130	17		Pliocene- Pleistocene	PlPec.s.si	Dolati (2010)
9363	0	9364	Qt	0.078	17		Pliocene- Pleistocene	PlPec.s.si	Dolati (2010)
9364	0	9365	Qt	0.014	17		Pliocene- Pleistocene	PlPec.s.si	Dolati (2010)
9365	0	9366	Qt	0.449	17		Pliocene- Pleistocene	PlPec.s.si	Dolati (2010)
9366	0	9367	Qt	0.208	17		Pliocene- Pleistocene	PlPec.s.si	Dolati (2010)
9367	0	9368	Qt	0.061	17		Pliocene- Pleistocene	PlPec.s.si	Dolati (2010)
9368	0	9369	Qt	0.089	17		Pliocene- Pleistocene	PlPec.s.si	Dolati (2010)
9369	0	9370	Qt	0.343	17		Pliocene- Pleistocene	PlPec.s.si	Dolati (2010)
9370	0	9371	Qt	0.061	17		Pliocene- Pleistocene	PlPec.s.si	Dolati (2010)
9371	0	9372	Qt	0.351	17		Pliocene- Pleistocene	PlPec.s.si	Dolati (2010)
9372	0	9373	Qt	0.061	17		Pliocene- Pleistocene	PlPec.s.si	Dolati (2010)
9373	0	9374	Qt	0.037	17		Pliocene- Pleistocene	PlPec.s.si	Dolati (2010)
9374	0	9375	Qt	0.116	17		Pliocene- Pleistocene	PlPec.s.si	Dolati (2010)
9375	0	9376	Qt	0.013	17		Pliocene- Pleistocene	PlPec.s.si	Dolati (2010)
9376	0	9377	Qt	0.039	17		Pliocene- Pleistocene	PlPec.s.si	Dolati (2010)
9377	0	9378	Qt	0.171	17		Pliocene- Pleistocene	PlPec.s.si	Dolati (2010)
9378	0	9379	Qt	0.053	17		Pliocene- Pleistocene	PlPec.s.si	Dolati (2010)
9379	0	9380	Qt	0.480	17		Pliocene- Pleistocene	PlPec.s.si	Dolati (2010)
9380	0	9381	Qt	0.234	17		Pliocene- Pleistocene	PlPec.s.si	Dolati (2010)
9381	0	9382	Qt	0.021	17		Pliocene- Pleistocene	PlPec.s.si	Dolati (2010)
9382	0	9383	Qt	0.179	17		Pliocene- Pleistocene	PlPec.s.si	Dolati (2010)
9383	0	9384	Qt	0.112	17		Pliocene- Pleistocene	PlPec.s.si	Dolati (2010)
9384	0	9385	Qt	0.063	17		Pliocene- Pleistocene	PlPec.s.si	Dolati (2010)
9385	0	9386	Qt	0.084	17		Pliocene- Pleistocene	PlPec.s.si	Dolati (2010)
9386	0	9387	Qt	0.029	17		Pliocene- Pleistocene	PlPec.s.si	Dolati (2010)
9387	0	9388	Qt	0.058	17		Pliocene- Pleistocene	PlPec.s.si	Dolati (2010)
9388	0	9389	Qt	0.289	17		Pliocene- Pleistocene	PlPec.s.si	Dolati (2010)
9389	1	9390	Plc-Qt	1.808	17		Pliocene- Pleistocene	PlPec.s.si	Dolati (2010)
9390	0	9391	Qt	0.073	17		Pliocene- Pleistocene	PlPec.s.si	Dolati (2010)
9391	0	9392	Qt	0.057	17		Pliocene- Pleistocene	PlPec.s.si	Dolati (2010)
9392	0	9393	Qt	0.083	17		Pliocene- Pleistocene	PlPec.s.si	Dolati (2010)
9393	0	9394	Qt	1.269	17		Pliocene- Pleistocene	PlPec.s.si	Dolati (2010)
9394	0	9395	Qt	0.263	17		Pliocene- Pleistocene	PlPec.s.si	Dolati (2010)
9395	0	9396	Qt	0.421	17		Pliocene- Pleistocene	PlPec.s.si	Dolati (2010)
9396	0	9397	Qt	0.026	17		Pliocene- Pleistocene	PlPec.s.si	Dolati (2010)
9397	0	9398	Qt	0.490	17		Pliocene- Pleistocene	PlPec.s.si	Dolati (2010)
9398	0	9399	Qt	0.053	17		Pliocene- Pleistocene	PlPec.s.si	Dolati (2010)
9399	0	9400	Qt	0.158	17		Pliocene- Pleistocene	PlPec.s.si	Dolati (2010)

GeoNeus

OBJECTID_1	Join_Count	TARGET_FID	Label	Shape_Area (sqkm)	ORIG_FID	Absolute_Age	Age_paleontology	Unit	Reference
9400	0	9401	Qt	0.036	17		Pliocene- Pleistocene	PlPec.s.si	Dolati (2010)
9401	0	9402	Qt	0.011	17		Pliocene- Pleistocene	PlPec.s.si	Dolati (2010)
9402	0	9403	Qt	0.073	17		Pliocene- Pleistocene	PlPec.s.si	Dolati (2010)
9403	0	9404	Qt	0.021	17		Pliocene- Pleistocene	PlPec.s.si	Dolati (2010)
9404	0	9405	Qt	0.185	17		Pliocene- Pleistocene	PlPec.s.si	Dolati (2010)
9405	0	9406	Qt	11.279	17		Pliocene- Pleistocene	PlPec.s.si	Dolati (2010)
9406	0	9407	Qt	0.021	17		Pliocene- Pleistocene	PlPec.s.si	Dolati (2010)
9407	0	9408	Qt	0.114	17		Pliocene- Pleistocene	PlPec.s.si	Dolati (2010)
9408	0	9409	Qt	0.619	17		Pliocene- Pleistocene	PlPec.s.si	Dolati (2010)
9409	0	9410	Qt	0.071	17		Pliocene- Pleistocene	PlPec.s.si	Dolati (2010)
9410	0	9411	Qt	0.494	17		Pliocene- Pleistocene	PlPec.s.si	Dolati (2010)
9411	0	9412	Qt	1.229	17		Pliocene- Pleistocene	PlPec.s.si	Dolati (2010)
9412	0	9413	Qt	0.582	17		Pliocene- Pleistocene	PlPec.s.si	Dolati (2010)
9413	0	9414	Qt	0.103	17		Pliocene- Pleistocene	PlPec.s.si	Dolati (2010)
9414	0	9415	Qt	0.833	17		Pliocene- Pleistocene	PlPec.s.si	Dolati (2010)
9415	0	9416	Qt	0.325	17		Pliocene- Pleistocene	PlPec.s.si	Dolati (2010)
9416	0	9417	Qt	0.065	17		Pliocene- Pleistocene	PlPec.s.si	Dolati (2010)
9417	0	9418	Qt	0.044	17		Pliocene- Pleistocene	PlPec.s.si	Dolati (2010)
9418	0	9419	Qt	0.111	17		Pliocene- Pleistocene	PlPec.s.si	Dolati (2010)
9419	0	9420	Qt	0.035	17		Pliocene- Pleistocene	PlPec.s.si	Dolati (2010)
9420	0	9421	Qt	0.164	17		Pliocene- Pleistocene	PlPec.s.si	Dolati (2010)
9421	0	9422	Qt	3.129	17		Pliocene- Pleistocene	PlPec.s.si	Dolati (2010)
9422	0	9423	Qt	0.021	17		Pliocene- Pleistocene	PlPec.s.si	Dolati (2010)
9423	0	9424	Qt	0.055	17		Pliocene- Pleistocene	PlPec.s.si	Dolati (2010)
9424	0	9425	Qt	0.054	17		Pliocene- Pleistocene	PlPec.s.si	Dolati (2010)
9425	0	9426	Qt	0.233	17		Pliocene- Pleistocene	PlPec.s.si	Dolati (2010)
9426	0	9427	Qt	2.933	17		Pliocene- Pleistocene	PlPec.s.si	Dolati (2010)
9427	0	9428	Qt	0.050	17		Pliocene- Pleistocene	PlPec.s.si	Dolati (2010)
9428	0	9429	Qt	0.272	17		Pliocene- Pleistocene	PlPec.s.si	Dolati (2010)
9429	0	9430	Qt	0.034	17		Pliocene- Pleistocene	PlPec.s.si	Dolati (2010)
9430	0	9431	Qt	0.072	17		Pliocene- Pleistocene	PlPec.s.si	Dolati (2010)
9431	0	9432	Qt	0.535	17		Pliocene- Pleistocene	PlPec.s.si	Dolati (2010)
9432	0	9433	Qt	0.063	17		Pliocene- Pleistocene	PlPec.s.si	Dolati (2010)
9433	0	9434	Qt	0.009	17		Pliocene- Pleistocene	PlPec.s.si	Dolati (2010)
9434	0	9435	Qt	0.068	17		Pliocene- Pleistocene	PlPec.s.si	Dolati (2010)
9435	0	9436	Qt	0.201	17		Pliocene- Pleistocene	PlPec.s.si	Dolati (2010)
9436	0	9437	Qt	0.173	17		Pliocene- Pleistocene	PlPec.s.si	Dolati (2010)
9437	0	9438	Qt	0.111	17		Pliocene- Pleistocene	PlPec.s.si	Dolati (2010)
9438	0	9439	Qt	0.504	17		Pliocene- Pleistocene	PlPec.s.si	Dolati (2010)

GeoNLP

OBJECTID_1	Join_Count	TARGET_FID	Label	Shape_Area (sqkm)	ORIG_FID	Absolute_Age	Age_paleontology	Unit	Reference
9439	0	9440	Qt	0.044	17		Pliocene- Pleistocene	PlPec.s.si	Dolati (2010)
9440	0	9441	Qt	0.232	17		Pliocene- Pleistocene	PlPec.s.si	Dolati (2010)
9441	0	9442	Qt	0.059	17		Pliocene- Pleistocene	PlPec.s.si	Dolati (2010)
9442	0	9443	Qt	1.074	17		Pliocene- Pleistocene	PlPec.s.si	Dolati (2010)
9443	0	9444	Qt	5.571	17		Pliocene- Pleistocene	PlPec.s.si	Dolati (2010)
9444	0	9445	Qt	0.035	17		Pliocene- Pleistocene	PlPec.s.si	Dolati (2010)
9445	0	9446	Qt	0.125	17		Pliocene- Pleistocene	PlPec.s.si	Dolati (2010)
9446	0	9447	Qt	0.085	17		Pliocene- Pleistocene	PlPec.s.si	Dolati (2010)
9447	0	9448	Qt	0.952	17		Pliocene- Pleistocene	PlPec.s.si	Dolati (2010)
9448	0	9449	Qt	0.119	17		Pliocene- Pleistocene	PlPec.s.si	Dolati (2010)
9449	0	9450	Qt	1.134	17		Pliocene- Pleistocene	PlPec.s.si	Dolati (2010)
9450	0	9451	Qt	0.110	17		Pliocene- Pleistocene	PlPec.s.si	Dolati (2010)
9451	0	9452	Qt	0.013	17		Pliocene- Pleistocene	PlPec.s.si	Dolati (2010)
9452	0	9453	Qt	0.096	17		Pliocene- Pleistocene	PlPec.s.si	Dolati (2010)
9453	0	9454	Qt	1.261	17		Pliocene- Pleistocene	PlPec.s.si	Dolati (2010)
9454	0	9455	Qt	0.085	17		Pliocene- Pleistocene	PlPec.s.si	Dolati (2010)
9455	0	9456	Qt	0.046	17		Pliocene- Pleistocene	PlPec.s.si	Dolati (2010)
9456	0	9457	Qt	0.418	17		Pliocene- Pleistocene	PlPec.s.si	Dolati (2010)
9457	0	9458	Qt	0.684	17		Pliocene- Pleistocene	PlPec.s.si	Dolati (2010)
9458	0	9459	Qt	2.855	17		Pliocene- Pleistocene	PlPec.s.si	Dolati (2010)
9459	0	9460	Qt	0.054	17		Pliocene- Pleistocene	PlPec.s.si	Dolati (2010)
9460	0	9461	Qt	0.630	17		Pliocene- Pleistocene	PlPec.s.si	Dolati (2010)
9461	0	9462	Qt	0.094	17		Pliocene- Pleistocene	PlPec.s.si	Dolati (2010)
9462	0	9463	Qt	0.762	17		Pliocene- Pleistocene	PlPec.s.si	Dolati (2010)
9463	0	9464	Qt	0.125	17		Pliocene- Pleistocene	PlPec.s.si	Dolati (2010)
9464	0	9465	Qt	0.444	17		Pliocene- Pleistocene	PlPec.s.si	Dolati (2010)
9465	0	9466	Qt	0.161	17		Pliocene- Pleistocene	PlPec.s.si	Dolati (2010)
9466	0	9467	Qt	1.189	17		Pliocene- Pleistocene	PlPec.s.si	Dolati (2010)
9467	0	9468	Qt	0.496	17		Pliocene- Pleistocene	PlPec.s.si	Dolati (2010)
9468	0	9469	Qt	4.778	17		Pliocene- Pleistocene	PlPec.s.si	Dolati (2010)
9469	0	9470	Qt	0.082	17		Pliocene- Pleistocene	PlPec.s.si	Dolati (2010)
9470	0	9471	Qt	0.111	17		Pliocene- Pleistocene	PlPec.s.si	Dolati (2010)
9471	0	9472	Qt	0.286	17		Pliocene- Pleistocene	PlPec.s.si	Dolati (2010)
9472	0	9473	Qt	0.070	17		Pliocene- Pleistocene	PlPec.s.si	Dolati (2010)
9473	0	9474	Qt	0.145	17		Pliocene- Pleistocene	PlPec.s.si	Dolati (2010)
9474	0	9475	Qt	0.144	17		Pliocene- Pleistocene	PlPec.s.si	Dolati (2010)
9475	0	9476	Qt	0.048	17		Pliocene- Pleistocene	PlPec.s.si	Dolati (2010)
9476	0	9477	Qt	0.060	17		Pliocene- Pleistocene	PlPec.s.si	Dolati (2010)
9477	0	9478	Qt	0.009	17		Pliocene- Pleistocene	PlPec.s.si	Dolati (2010)

GeoNeus

OBJECTID_1	Join_Count	TARGET_FID	Label	Shape_Area (sqkm)	ORIG_FID	Absolute_Age	Age_paleontology	Unit	Reference
9478	0	9479	Qt	0.097	17		Pliocene- Pleistocene	PlPec.s.si	Dolati (2010)
9479	0	9480	Qt	0.186	17		Pliocene- Pleistocene	PlPec.s.si	Dolati (2010)
9480	0	9481	Qt	0.309	17		Pliocene- Pleistocene	PlPec.s.si	Dolati (2010)
9481	0	9482	Qt	0.191	17		Pliocene- Pleistocene	PlPec.s.si	Dolati (2010)
9482	0	9483	Qt	0.085	17		Pliocene- Pleistocene	PlPec.s.si	Dolati (2010)
9483	0	9484	Qt	0.571	17		Pliocene- Pleistocene	PlPec.s.si	Dolati (2010)
9484	0	9485	Qt	2.113	17		Pliocene- Pleistocene	PlPec.s.si	Dolati (2010)
9485	0	9486	Qt	0.472	17		Pliocene- Pleistocene	PlPec.s.si	Dolati (2010)
9486	0	9487	Qt	0.133	17		Pliocene- Pleistocene	PlPec.s.si	Dolati (2010)
9487	0	9488	Qt	0.505	17		Pliocene- Pleistocene	PlPec.s.si	Dolati (2010)
9488	0	9489	Qt	0.465	17		Pliocene- Pleistocene	PlPec.s.si	Dolati (2010)
9489	0	9490	Qt	0.093	17		Pliocene- Pleistocene	PlPec.s.si	Dolati (2010)
9490	0	9491	Qt	0.035	17		Pliocene- Pleistocene	PlPec.s.si	Dolati (2010)
9491	0	9492	Qt	0.781	17		Pliocene- Pleistocene	PlPec.s.si	Dolati (2010)
9492	0	9493	Qt	0.133	17		Pliocene- Pleistocene	PlPec.s.si	Dolati (2010)
9493	0	9494	Qt	0.149	17		Pliocene- Pleistocene	PlPec.s.si	Dolati (2010)
9494	0	9495	Qt	0.044	17		Pliocene- Pleistocene	PlPec.s.si	Dolati (2010)
9495	0	9496	Qt	0.452	17		Pliocene- Pleistocene	PlPec.s.si	Dolati (2010)
9496	0	9497	Qt	4.311	17		Pliocene- Pleistocene	PlPec.s.si	Dolati (2010)
9497	0	9498	Qt	0.281	17		Pliocene- Pleistocene	PlPec.s.si	Dolati (2010)
9498	0	9499	Qt	2.873	17		Pliocene- Pleistocene	PlPec.s.si	Dolati (2010)
9499	0	9500	Qt	0.929	17		Pliocene- Pleistocene	PlPec.s.si	Dolati (2010)
9500	0	9501	Qt	2.059	17		Pliocene- Pleistocene	PlPec.s.si	Dolati (2010)
9501	0	9502	Qt	0.250	17		Pliocene- Pleistocene	PlPec.s.si	Dolati (2010)
9502	0	9503	Qt	0.245	17		Pliocene- Pleistocene	PlPec.s.si	Dolati (2010)
9503	1	9504	Plc-Qt	5.872	17		Pliocene- Pleistocene	PlPec.s.si	Dolati (2010)
9504	0	9505	Qt	0.188	17		Pliocene- Pleistocene	PlPec.s.si	Dolati (2010)
9505	0	9506	Qt	0.032	17		Pliocene- Pleistocene	PlPec.s.si	Dolati (2010)
9506	0	9507	Qt	0.021	17		Pliocene- Pleistocene	PlPec.s.si	Dolati (2010)
9507	0	9508	Qt	3.054	17		Pliocene- Pleistocene	PlPec.s.si	Dolati (2010)
9508	0	9509	Qt	0.052	17		Pliocene- Pleistocene	PlPec.s.si	Dolati (2010)
9509	0	9510	Qt	0.167	17		Pliocene- Pleistocene	PlPec.s.si	Dolati (2010)
9510	0	9511	Qt	0.324	17		Pliocene- Pleistocene	PlPec.s.si	Dolati (2010)
9511	0	9512	Qt	0.024	17		Pliocene- Pleistocene	PlPec.s.si	Dolati (2010)
9512	0	9513	Qt	0.053	17		Pliocene- Pleistocene	PlPec.s.si	Dolati (2010)
9513	0	9514	Qt	4.076	17		Pliocene- Pleistocene	PlPec.s.si	Dolati (2010)
9514	0	9515	Qt	0.377	17		Pliocene- Pleistocene	PlPec.s.si	Dolati (2010)
9515	0	9516	Qt	1.956	17		Pliocene- Pleistocene	PlPec.s.si	Dolati (2010)
9516	0	9517	Qt	0.099	17		Pliocene- Pleistocene	PlPec.s.si	Dolati (2010)

GeoNeuro

OBJECTID_1	Join_Count	TARGET_FID	Label	Shape_Area (sqkm)	ORIG_FID	Absolute_Age	Age_paleontology	Unit	Reference
9517	0	9518	Qt	0.151	17		Pliocene- Pleistocene	PlPec.s.si	Dolati (2010)
9518	0	9519	Qt	0.194	17		Pliocene- Pleistocene	PlPec.s.si	Dolati (2010)
9519	0	9520	Qt	0.199	17		Pliocene- Pleistocene	PlPec.s.si	Dolati (2010)
9520	0	9521	Qt	0.131	17		Pliocene- Pleistocene	PlPec.s.si	Dolati (2010)
9521	0	9522	Qt	0.041	17		Pliocene- Pleistocene	PlPec.s.si	Dolati (2010)
9522	0	9523	Qt	0.044	17		Pliocene- Pleistocene	PlPec.s.si	Dolati (2010)
9523	0	9524	Qt	0.959	17		Pliocene- Pleistocene	PlPec.s.si	Dolati (2010)
9524	0	9525	Qt	0.030	17		Pliocene- Pleistocene	PlPec.s.si	Dolati (2010)
9525	0	9526	Qt	0.070	17		Pliocene- Pleistocene	PlPec.s.si	Dolati (2010)
9526	0	9527	Qt	0.138	17		Pliocene- Pleistocene	PlPec.s.si	Dolati (2010)
9527	0	9528	Qt	0.272	17		Pliocene- Pleistocene	PlPec.s.si	Dolati (2010)
9528	0	9529	Qt	0.422	17		Pliocene- Pleistocene	PlPec.s.si	Dolati (2010)
9529	0	9530	Qt	0.464	17		Pliocene- Pleistocene	PlPec.s.si	Dolati (2010)
9530	0	9531	Qt	0.059	17		Pliocene- Pleistocene	PlPec.s.si	Dolati (2010)
9531	0	9532	Qt	0.052	17		Pliocene- Pleistocene	PlPec.s.si	Dolati (2010)
9532	0	9533	Qt	0.228	17		Pliocene- Pleistocene	PlPec.s.si	Dolati (2010)
9533	0	9534	Qt	0.120	17		Pliocene- Pleistocene	PlPec.s.si	Dolati (2010)
9534	0	9535	Qt	0.039	17		Pliocene- Pleistocene	PlPec.s.si	Dolati (2010)
9535	0	9536	Qt	0.030	17		Pliocene- Pleistocene	PlPec.s.si	Dolati (2010)
9536	0	9537	Qt	0.188	17		Pliocene- Pleistocene	PlPec.s.si	Dolati (2010)
9537	0	9538	Qt	5.750	17		Pliocene- Pleistocene	PlPec.s.si	Dolati (2010)
9538	0	9539	Qt	0.039	17		Pliocene- Pleistocene	PlPec.s.si	Dolati (2010)
9539	0	9540	Qt	0.270	17		Pliocene- Pleistocene	PlPec.s.si	Dolati (2010)
9540	0	9541	Qt	0.181	17		Pliocene- Pleistocene	PlPec.s.si	Dolati (2010)
9541	0	9542	Qt	0.268	17		Pliocene- Pleistocene	PlPec.s.si	Dolati (2010)
9542	0	9543	Qt	0.144	17		Pliocene- Pleistocene	PlPec.s.si	Dolati (2010)
9543	0	9544	Qt	0.206	17		Pliocene- Pleistocene	PlPec.s.si	Dolati (2010)
9544	0	9545	Qt	0.192	17		Pliocene- Pleistocene	PlPec.s.si	Dolati (2010)
9545	0	9546	Qt	0.019	17		Pliocene- Pleistocene	PlPec.s.si	Dolati (2010)
9546	0	9547	Qt	0.200	17		Pliocene- Pleistocene	PlPec.s.si	Dolati (2010)
9547	0	9548	Qt	1.213	17		Pliocene- Pleistocene	PlPec.s.si	Dolati (2010)
9548	0	9549	Qt	0.330	17		Pliocene- Pleistocene	PlPec.s.si	Dolati (2010)
9549	0	9550	Qt	0.677	17		Pliocene- Pleistocene	PlPec.s.si	Dolati (2010)
9550	0	9551	Qt	0.125	17		Pliocene- Pleistocene	PlPec.s.si	Dolati (2010)
9551	0	9552	Qt	0.045	17		Pliocene- Pleistocene	PlPec.s.si	Dolati (2010)
9552	0	9553	Qt	0.043	17		Pliocene- Pleistocene	PlPec.s.si	Dolati (2010)
9553	0	9554	Qt	0.043	17		Pliocene- Pleistocene	PlPec.s.si	Dolati (2010)
9554	0	9555	Qt	0.040	17		Pliocene- Pleistocene	PlPec.s.si	Dolati (2010)
9555	0	9556	Qt	0.499	17		Pliocene- Pleistocene	PlPec.s.si	Dolati (2010)

GeoNeus

OBJECTID_1	Join_Count	TARGET_FID	Label	Shape_Area (sqkm)	ORIG_FID	Absolute_Age	Age_paleontology	Unit	Reference
9556	0	9557	Qt	0.087	17		Pliocene- Pleistocene	PlPec.s.si	Dolati (2010)
9557	0	9558	Qt	0.113	17		Pliocene- Pleistocene	PlPec.s.si	Dolati (2010)
9558	0	9559	Qt	0.083	17		Pliocene- Pleistocene	PlPec.s.si	Dolati (2010)
9559	0	9560	Qt	0.590	17		Pliocene- Pleistocene	PlPec.s.si	Dolati (2010)
9560	0	9561	Qt	0.054	17		Pliocene- Pleistocene	PlPec.s.si	Dolati (2010)
9561	0	9562	Qt	0.035	17		Pliocene- Pleistocene	PlPec.s.si	Dolati (2010)
9562	0	9563	Qt	0.195	17		Pliocene- Pleistocene	PlPec.s.si	Dolati (2010)
9563	0	9564	Qt	0.054	17		Pliocene- Pleistocene	PlPec.s.si	Dolati (2010)
9564	0	9565	Qt	1.145	17		Pliocene- Pleistocene	PlPec.s.si	Dolati (2010)
9565	1	9566	Plc-Qt	19.592	17		Pliocene- Pleistocene	PlPec.s.si	Dolati (2010)
9566	0	9567	Qt	0.506	17		Pliocene- Pleistocene	PlPec.s.si	Dolati (2010)
9567	0	9568	Qt	0.060	17		Pliocene- Pleistocene	PlPec.s.si	Dolati (2010)
9568	0	9569	Qt	0.161	17		Pliocene- Pleistocene	PlPec.s.si	Dolati (2010)
9569	0	9570	Qt	0.169	17		Pliocene- Pleistocene	PlPec.s.si	Dolati (2010)
9570	0	9571	Qt	0.126	17		Pliocene- Pleistocene	PlPec.s.si	Dolati (2010)
9571	0	9572	Qt	0.015	17		Pliocene- Pleistocene	PlPec.s.si	Dolati (2010)
9572	0	9573	Qt	0.180	17		Pliocene- Pleistocene	PlPec.s.si	Dolati (2010)
9573	0	9574	Qt	0.706	17		Pliocene- Pleistocene	PlPec.s.si	Dolati (2010)
9574	0	9575	Qt	0.105	17		Pliocene- Pleistocene	PlPec.s.si	Dolati (2010)
9575	0	9576	Qt	0.069	17		Pliocene- Pleistocene	PlPec.s.si	Dolati (2010)
9576	0	9577	Qt	0.104	17		Pliocene- Pleistocene	PlPec.s.si	Dolati (2010)
9577	0	9578	Qt	0.183	17		Pliocene- Pleistocene	PlPec.s.si	Dolati (2010)
9578	0	9579	Qt	0.457	17		Pliocene- Pleistocene	PlPec.s.si	Dolati (2010)
9579	0	9580	Qt	0.234	17		Pliocene- Pleistocene	PlPec.s.si	Dolati (2010)
9580	0	9581	Qt	0.349	17		Pliocene- Pleistocene	PlPec.s.si	Dolati (2010)
9581	0	9582	Qt	7.629	17		Pliocene- Pleistocene	PlPec.s.si	Dolati (2010)
9582	0	9583	Qt	65.122	17		Pliocene- Pleistocene	PlPec.s.si	Dolati (2010)
9583	0	9584	Qt	0.180	17		Pliocene- Pleistocene	PlPec.s.si	Dolati (2010)
9584	0	9585	Qt	0.099	17		Pliocene- Pleistocene	PlPec.s.si	Dolati (2010)
9585	0	9586	Qt	0.070	17		Pliocene- Pleistocene	PlPec.s.si	Dolati (2010)
9587	0	9588	Qt	0.575	17		Pliocene- Pleistocene	PlPec.s.si	Dolati (2010)
9588	0	9589	Qt	1.164	17		Pliocene- Pleistocene	PlPec.s.si	Dolati (2010)
9589	0	9590	Qt	0.026	17		Pliocene- Pleistocene	PlPec.s.si	Dolati (2010)
9590	0	9591	Qt	0.626	17		Pliocene- Pleistocene	PlPec.s.si	Dolati (2010)
9591	0	9592	Qt	0.436	17		Pliocene- Pleistocene	PlPec.s.si	Dolati (2010)
9592	0	9593	Qt	0.160	17		Pliocene- Pleistocene	PlPec.s.si	Dolati (2010)
9593	0	9594	Qt	0.068	17		Pliocene- Pleistocene	PlPec.s.si	Dolati (2010)
9594	0	9595	Qt	0.147	17		Pliocene- Pleistocene	PlPec.s.si	Dolati (2010)
9595	0	9596	Qt	0.480	17		Pliocene- Pleistocene	PlPec.s.si	Dolati (2010)

GeoNeW

OBJECTID_1	Join_Count	TARGET_FID	Label	Shape_Area (sqkm)	ORIG_FID	Absolute_Age	Age_paleontology	Unit	Reference
9596	0	9597	Qt	0.147	17		Pliocene- Pleistocene	PlPec.s.si	Dolati (2010)
9597	0	9598	Qt	0.122	17		Pliocene- Pleistocene	PlPec.s.si	Dolati (2010)
9598	0	9599	Qt	0.283	17		Pliocene- Pleistocene	PlPec.s.si	Dolati (2010)
9599	0	9600	Qt	0.535	17		Pliocene- Pleistocene	PlPec.s.si	Dolati (2010)
9600	0	9601	Qt	0.653	17		Pliocene- Pleistocene	PlPec.s.si	Dolati (2010)
9601	0	9602	Qt	0.080	17		Pliocene- Pleistocene	PlPec.s.si	Dolati (2010)
9602	0	9603	Qt	0.781	17		Pliocene- Pleistocene	PlPec.s.si	Dolati (2010)
9603	0	9604	Qt	0.163	17		Pliocene- Pleistocene	PlPec.s.si	Dolati (2010)
9604	0	9605	Qt	0.369	17		Pliocene- Pleistocene	PlPec.s.si	Dolati (2010)
9605	0	9606	Qt	0.814	17		Pliocene- Pleistocene	PlPec.s.si	Dolati (2010)
9606	0	9607	Qt	0.431	17		Pliocene- Pleistocene	PlPec.s.si	Dolati (2010)
9607	0	9608	Qt	0.436	17		Pliocene- Pleistocene	PlPec.s.si	Dolati (2010)
9608	0	9609	Qt	0.170	17		Pliocene- Pleistocene	PlPec.s.si	Dolati (2010)
9609	0	9610	Qt	0.072	17		Pliocene- Pleistocene	PlPec.s.si	Dolati (2010)
9610	0	9611	Qt	0.107	17		Pliocene- Pleistocene	PlPec.s.si	Dolati (2010)
9611	0	9612	Qt	0.227	17		Pliocene- Pleistocene	PlPec.s.si	Dolati (2010)
9612	0	9613	Qt	0.906	17		Pliocene- Pleistocene	PlPec.s.si	Dolati (2010)
9613	0	9614	Qt	0.715	17		Pliocene- Pleistocene	PlPec.s.si	Dolati (2010)
9614	0	9616	Qt	0.189	17		Pliocene- Pleistocene	PlPec.s.si	Dolati (2010)
9616	0	9618	Qt	0.081	17		Pliocene- Pleistocene	PlPec.s.si	Dolati (2010)
9617	0	9619	Qt	0.907	17		Pliocene- Pleistocene	PlPec.s.si	Dolati (2010)
9618	0	9620	Qt	2.941	17		Pliocene- Pleistocene	PlPec.s.si	Dolati (2010)
9619	0	9621	Qt	0.145	17		Pliocene- Pleistocene	PlPec.s.si	Dolati (2010)
9620	0	9622	Qt	0.347	17		Pliocene- Pleistocene	PlPec.s.si	Dolati (2010)
9621	0	9623	Qt	0.273	17		Pliocene- Pleistocene	PlPec.s.si	Dolati (2010)
9622	0	9624	Qt	0.123	17		Pliocene- Pleistocene	PlPec.s.si	Dolati (2010)
9623	0	9625	Qt	0.556	17		Pliocene- Pleistocene	PlPec.s.si	Dolati (2010)
9624	0	9626	Qt	0.488	17		Pliocene- Pleistocene	PlPec.s.si	Dolati (2010)
9625	0	9627	Qt	0.031	17		Pliocene- Pleistocene	PlPec.s.si	Dolati (2010)
9626	0	9628	Qt	1.237	17		Pliocene- Pleistocene	PlPec.s.si	Dolati (2010)
9627	0	9629	Qt	0.153	17		Pliocene- Pleistocene	PlPec.s.si	Dolati (2010)
9628	0	9630	Qt	0.061	17		Pliocene- Pleistocene	PlPec.s.si	Dolati (2010)
9629	0	9631	Qt	1.490	17		Pliocene- Pleistocene	PlPec.s.si	Dolati (2010)
9630	0	9632	Qt	0.355	17		Pliocene- Pleistocene	PlPec.s.si	Dolati (2010)
9631	0	9633	Qt	0.272	17		Pliocene- Pleistocene	PlPec.s.si	Dolati (2010)
9632	0	9634	Qt	0.107	17		Pliocene- Pleistocene	PlPec.s.si	Dolati (2010)
9633	0	9635	Qt	0.034	17		Pliocene- Pleistocene	PlPec.s.si	Dolati (2010)
9634	0	9636	Qt	0.207	17		Pliocene- Pleistocene	PlPec.s.si	Dolati (2010)
9635	0	9637	Qt	0.371	17		Pliocene- Pleistocene	PlPec.s.si	Dolati (2010)

GeoNeus

OBJECTID_1	Join_Count	TARGET_FID	Label	Shape_Area (sqkm)	ORIG_FID	Absolute_Age	Age_paleontology	Unit	Reference
9636	0	9638	Qt	0.128	17		Pliocene- Pleistocene	PlPec.s.si	Dolati (2010)
9637	0	9639	Qt	0.020	17		Pliocene- Pleistocene	PlPec.s.si	Dolati (2010)
9638	0	9640	Qt	0.082	17		Pliocene- Pleistocene	PlPec.s.si	Dolati (2010)
9639	0	9641	Qt	1.328	17		Pliocene- Pleistocene	PlPec.s.si	Dolati (2010)
9640	0	9642	Qt	0.052	17		Pliocene- Pleistocene	PlPec.s.si	Dolati (2010)
9641	0	9643	Qt	0.123	17		Pliocene- Pleistocene	PlPec.s.si	Dolati (2010)
9642	0	9644	Qt	1.134	17		Pliocene- Pleistocene	PlPec.s.si	Dolati (2010)
9643	0	9645	Qt	0.152	17		Pliocene- Pleistocene	PlPec.s.si	Dolati (2010)
9644	0	9646	Qt	0.232	17		Pliocene- Pleistocene	PlPec.s.si	Dolati (2010)
9645	0	9647	Qt	0.080	17		Pliocene- Pleistocene	PlPec.s.si	Dolati (2010)
9646	0	9648	Qt	0.245	17		Pliocene- Pleistocene	PlPec.s.si	Dolati (2010)
9647	0	9649	Qt	0.400	17		Pliocene- Pleistocene	PlPec.s.si	Dolati (2010)
9648	0	9650	Qt	0.354	17		Pliocene- Pleistocene	PlPec.s.si	Dolati (2010)
9649	0	9651	Qt	1.210	17		Pliocene- Pleistocene	PlPec.s.si	Dolati (2010)
9650	0	9652	Qt	0.175	17		Pliocene- Pleistocene	PlPec.s.si	Dolati (2010)
9651	0	9653	Qt	1.664	17		Pliocene- Pleistocene	PlPec.s.si	Dolati (2010)
9652	0	9654	Qt	0.162	17		Pliocene- Pleistocene	PlPec.s.si	Dolati (2010)
9653	0	9655	Qt	0.199	17		Pliocene- Pleistocene	PlPec.s.si	Dolati (2010)
9654	0	9656	Qt	0.057	17		Pliocene- Pleistocene	PlPec.s.si	Dolati (2010)
9655	0	9657	Qt	1.616	17		Pliocene- Pleistocene	PlPec.s.si	Dolati (2010)
9656	0	9658	Qt	0.273	17		Pliocene- Pleistocene	PlPec.s.si	Dolati (2010)
9657	0	9659	Qt	0.368	17		Pliocene- Pleistocene	PlPec.s.si	Dolati (2010)
9658	0	9660	Qt	0.027	17		Pliocene- Pleistocene	PlPec.s.si	Dolati (2010)
9659	0	9661	Qt	0.268	17		Pliocene- Pleistocene	PlPec.s.si	Dolati (2010)
9660	0	9662	Qt	0.070	17		Pliocene- Pleistocene	PlPec.s.si	Dolati (2010)
9661	0	9663	Qt	0.345	17		Pliocene- Pleistocene	PlPec.s.si	Dolati (2010)
9662	0	9664	Qt	0.060	17		Pliocene- Pleistocene	PlPec.s.si	Dolati (2010)
9663	0	9665	Qt	0.344	17		Pliocene- Pleistocene	PlPec.s.si	Dolati (2010)
9664	0	9666	Qt	0.117	17		Pliocene- Pleistocene	PlPec.s.si	Dolati (2010)
9665	0	9667	Qt	0.136	17		Pliocene- Pleistocene	PlPec.s.si	Dolati (2010)
9666	0	9668	Qt	0.528	17		Pliocene- Pleistocene	PlPec.s.si	Dolati (2010)
9667	0	9669	Qt	1.240	17		Pliocene- Pleistocene	PlPec.s.si	Dolati (2010)
9668	0	9670	Qt	0.148	17		Pliocene- Pleistocene	PlPec.s.si	Dolati (2010)
9669	0	9671	Qt	0.217	17		Pliocene- Pleistocene	PlPec.s.si	Dolati (2010)
9670	0	9672	Qt	0.095	17		Pliocene- Pleistocene	PlPec.s.si	Dolati (2010)
9671	0	9673	Qt	2.115	17		Pliocene- Pleistocene	PlPec.s.si	Dolati (2010)
9672	0	9674	Qt	0.129	17		Pliocene- Pleistocene	PlPec.s.si	Dolati (2010)
9673	0	9675	Qt	0.447	17		Pliocene- Pleistocene	PlPec.s.si	Dolati (2010)
9674	0	9676	Qt	6.110	17		Pliocene- Pleistocene	PlPec.s.si	Dolati (2010)

GeoNLP

OBJECTID_1	Join_Count	TARGET_FID	Label	Shape_Area (sqkm)	ORIG_FID	Absolute_Age	Age_paleontology	Unit	Reference
9675	0	9677	Qt	0.278	17		Pliocene- Pleistocene	PlPec.s.si	Dolati (2010)
9676	0	9678	Qt	5.675	17		Pliocene- Pleistocene	PlPec.s.si	Dolati (2010)
9677	0	9679	Qt	0.487	17		Pliocene- Pleistocene	PlPec.s.si	Dolati (2010)
9678	0	9680	Qt	1.197	17		Pliocene- Pleistocene	PlPec.s.si	Dolati (2010)
9679	0	9681	Qt	0.393	17		Pliocene- Pleistocene	PlPec.s.si	Dolati (2010)
9680	0	9682	Qt	0.144	17		Pliocene- Pleistocene	PlPec.s.si	Dolati (2010)
9681	0	9683	Qt	0.253	17		Pliocene- Pleistocene	PlPec.s.si	Dolati (2010)
9682	0	9684	Qt	2.446	17		Pliocene- Pleistocene	PlPec.s.si	Dolati (2010)
9683	0	9685	Qt	0.358	17		Pliocene- Pleistocene	PlPec.s.si	Dolati (2010)
9684	0	9686	Qt	0.157	17		Pliocene- Pleistocene	PlPec.s.si	Dolati (2010)
9685	0	9687	Qt	0.466	17		Pliocene- Pleistocene	PlPec.s.si	Dolati (2010)
9686	0	9688	Qt	0.147	17		Pliocene- Pleistocene	PlPec.s.si	Dolati (2010)
9687	0	9689	Qt	0.548	17		Pliocene- Pleistocene	PlPec.s.si	Dolati (2010)
9688	0	9690	Qt	0.373	17		Pliocene- Pleistocene	PlPec.s.si	Dolati (2010)
9689	0	9691	Qt	0.774	17		Pliocene- Pleistocene	PlPec.s.si	Dolati (2010)
9690	0	9692	Qt	1.843	17		Pliocene- Pleistocene	PlPec.s.si	Dolati (2010)
9691	0	9693	Qt	0.075	17		Pliocene- Pleistocene	PlPec.s.si	Dolati (2010)
9692	0	9694	Qt	0.109	17		Pliocene- Pleistocene	PlPec.s.si	Dolati (2010)
9693	0	9695	Qt	0.211	17		Pliocene- Pleistocene	PlPec.s.si	Dolati (2010)
9694	0	9696	Qt	0.093	17		Pliocene- Pleistocene	PlPec.s.si	Dolati (2010)
9695	0	9697	Qt	0.146	17		Pliocene- Pleistocene	PlPec.s.si	Dolati (2010)
9696	0	9698	Qt	0.195	17		Pliocene- Pleistocene	PlPec.s.si	Dolati (2010)
9697	0	9699	Qt	2.292	17		Pliocene- Pleistocene	PlPec.s.si	Dolati (2010)
9698	0	9700	Qt	0.743	17		Pliocene- Pleistocene	PlPec.s.si	Dolati (2010)
9699	0	9701	Qt	4.870	17		Pliocene- Pleistocene	PlPec.s.si	Dolati (2010)
9700	0	9702	Qt	3.190	17		Pliocene- Pleistocene	PlPec.s.si	Dolati (2010)
9701	0	9703	Qt	0.557	17		Pliocene- Pleistocene	PlPec.s.si	Dolati (2010)
9702	0	9704	Qt	1.525	17		Pliocene- Pleistocene	PlPec.s.si	Dolati (2010)
9703	0	9705	Qt	0.046	17		Pliocene- Pleistocene	PlPec.s.si	Dolati (2010)
9704	0	9706	Qt	3.514	17		Pliocene- Pleistocene	PlPec.s.si	Dolati (2010)
9705	0	9707	Qt	2.090	17		Pliocene- Pleistocene	PlPec.s.si	Dolati (2010)
9706	0	9708	Qt	0.276	17		Pliocene- Pleistocene	PlPec.s.si	Dolati (2010)
9707	0	9709	Qt	0.255	17		Pliocene- Pleistocene	PlPec.s.si	Dolati (2010)
9708	0	9710	Qt	0.096	17		Pliocene- Pleistocene	PlPec.s.si	Dolati (2010)
9709	0	9711	Qt	0.353	17		Pliocene- Pleistocene	PlPec.s.si	Dolati (2010)
9710	0	9712	Qt	0.046	17		Pliocene- Pleistocene	PlPec.s.si	Dolati (2010)
9711	0	9713	Qt	1.013	17		Pliocene- Pleistocene	PlPec.s.si	Dolati (2010)
9712	0	9714	Qt	0.360	17		Pliocene- Pleistocene	PlPec.s.si	Dolati (2010)
9713	0	9715	Qt	0.260	17		Pliocene- Pleistocene	PlPec.s.si	Dolati (2010)

GeoNVS

OBJECTID_1	Join_Count	TARGET_FID	Label	Shape_Area (sqkm)	ORIG_FID	Absolute_Age	Age_paleontology	Unit	Reference
9714	0	9716	Qt	0.053	17		Pliocene- Pleistocene	PlPec.s.si	Dolati (2010)
9715	0	9717	Qt	0.268	17		Pliocene- Pleistocene	PlPec.s.si	Dolati (2010)
9716	0	9718	Qt	0.867	17		Pliocene- Pleistocene	PlPec.s.si	Dolati (2010)
9717	0	9719	Qt	0.950	17		Pliocene- Pleistocene	PlPec.s.si	Dolati (2010)
9718	0	9720	Qt	0.078	17		Pliocene- Pleistocene	PlPec.s.si	Dolati (2010)
9719	0	9721	Qt	0.706	17		Pliocene- Pleistocene	PlPec.s.si	Dolati (2010)
9720	0	9722	Qt	59.799	17		Pliocene- Pleistocene	PlPec.s.si	Dolati (2010)
9721	0	9723	Qt	0.408	17		Pliocene- Pleistocene	PlPec.s.si	Dolati (2010)
9722	0	9724	Qt	17.565	17		Pliocene- Pleistocene	PlPec.s.si	Dolati (2010)
9723	0	9725	Qt	0.027	17		Pliocene- Pleistocene	PlPec.s.si	Dolati (2010)
9724	0	9726	Qt	0.108	17		Pliocene- Pleistocene	PlPec.s.si	Dolati (2010)
9725	0	9727	Qt	0.679	17		Pliocene- Pleistocene	PlPec.s.si	Dolati (2010)
9726	0	9728	Qt	0.332	17		Pliocene- Pleistocene	PlPec.s.si	Dolati (2010)
9727	0	9729	Qt	31.908	17		Pliocene- Pleistocene	PlPec.s.si	Dolati (2010)
9728	0	9730	Qt	1.116	17		Pliocene- Pleistocene	PlPec.s.si	Dolati (2010)
9729	0	9731	Qt	0.117	17		Pliocene- Pleistocene	PlPec.s.si	Dolati (2010)
9730	0	9732	Qt	0.299	17		Pliocene- Pleistocene	PlPec.s.si	Dolati (2010)
9731	0	9733	Qt	0.486	17		Pliocene- Pleistocene	PlPec.s.si	Dolati (2010)
9732	0	9734	Qt	0.096	17		Pliocene- Pleistocene	PlPec.s.si	Dolati (2010)
9733	0	9735	Qt	0.022	17		Pliocene- Pleistocene	PlPec.s.si	Dolati (2010)
9734	0	9736	Qt	0.754	17		Pliocene- Pleistocene	PlPec.s.si	Dolati (2010)
9735	0	9737	Qt	0.046	17		Pliocene- Pleistocene	PlPec.s.si	Dolati (2010)
9736	0	9738	Qt	0.023	17		Pliocene- Pleistocene	PlPec.s.si	Dolati (2010)
9737	0	9739	Qt	0.106	17		Pliocene- Pleistocene	PlPec.s.si	Dolati (2010)
9738	0	9740	Qt	0.130	17		Pliocene- Pleistocene	PlPec.s.si	Dolati (2010)
9739	0	9741	Qt	0.330	17		Pliocene- Pleistocene	PlPec.s.si	Dolati (2010)
9740	0	9742	Qt	0.097	17		Pliocene- Pleistocene	PlPec.s.si	Dolati (2010)
9741	0	9743	Qt	0.079	17		Pliocene- Pleistocene	PlPec.s.si	Dolati (2010)
9742	0	9744	Qt	0.015	17		Pliocene- Pleistocene	PlPec.s.si	Dolati (2010)
9743	0	9745	Qt	0.541	17		Pliocene- Pleistocene	PlPec.s.si	Dolati (2010)
9744	0	9746	Qt	0.037	17		Pliocene- Pleistocene	PlPec.s.si	Dolati (2010)
9745	0	9747	Qt	0.066	17		Pliocene- Pleistocene	PlPec.s.si	Dolati (2010)
9746	0	9748	Qt	0.584	17		Pliocene- Pleistocene	PlPec.s.si	Dolati (2010)
9747	0	9749	Qt	0.911	17		Pliocene- Pleistocene	PlPec.s.si	Dolati (2010)
9748	0	9750	Qt	3.848	17		Pliocene- Pleistocene	PlPec.s.si	Dolati (2010)
9749	0	9751	Qt	0.038	17		Pliocene- Pleistocene	PlPec.s.si	Dolati (2010)
9750	0	9752	Qt	0.170	17		Pliocene- Pleistocene	PlPec.s.si	Dolati (2010)
9751	0	9753	Qt	0.765	17		Pliocene- Pleistocene	PlPec.s.si	Dolati (2010)
9752	0	9754	Qt	0.247	17		Pliocene- Pleistocene	PlPec.s.si	Dolati (2010)

GeoNeuro

OBJECTID_1	Join_Count	TARGET_FID	Label	Shape_Area (sqkm)	ORIG_FID	Absolute_Age	Age_paleontology	Unit	Reference
9753	0	9755	Qt	0.076	17		Pliocene- Pleistocene	PlPec.s.si	Dolati (2010)
9754	0	9756	Qt	0.098	17		Pliocene- Pleistocene	PlPec.s.si	Dolati (2010)
9755	0	9757	Qt	0.972	17		Pliocene- Pleistocene	PlPec.s.si	Dolati (2010)
9756	0	9758	Qt	0.788	17		Pliocene- Pleistocene	PlPec.s.si	Dolati (2010)
9757	0	9759	Qt	3.203	17		Pliocene- Pleistocene	PlPec.s.si	Dolati (2010)
9758	0	9760	Qt	0.347	17		Pliocene- Pleistocene	PlPec.s.si	Dolati (2010)
9759	0	9761	Qt	0.523	17		Pliocene- Pleistocene	PlPec.s.si	Dolati (2010)
9760	0	9762	Qt	0.173	17		Pliocene- Pleistocene	PlPec.s.si	Dolati (2010)
9761	0	9763	Qt	0.046	17		Pliocene- Pleistocene	PlPec.s.si	Dolati (2010)
9762	0	9764	Qt	2.004	17		Pliocene- Pleistocene	PlPec.s.si	Dolati (2010)
9763	0	9765	Qt	1.483	17		Pliocene- Pleistocene	PlPec.s.si	Dolati (2010)
9764	0	9766	Qt	4.491	17		Pliocene- Pleistocene	PlPec.s.si	Dolati (2010)
9765	0	9767	Qt	0.078	17		Pliocene- Pleistocene	PlPec.s.si	Dolati (2010)
9766	0	9768	Qt	0.803	17		Pliocene- Pleistocene	PlPec.s.si	Dolati (2010)
9767	0	9769	Qt	0.021	17		Pliocene- Pleistocene	PlPec.s.si	Dolati (2010)
9768	0	9770	Qt	0.261	17		Pliocene- Pleistocene	PlPec.s.si	Dolati (2010)
9769	0	9771	Qt	2.598	17		Pliocene- Pleistocene	PlPec.s.si	Dolati (2010)
9770	0	9772	Qt	0.128	17		Pliocene- Pleistocene	PlPec.s.si	Dolati (2010)
9771	0	9773	Qt	0.144	17		Pliocene- Pleistocene	PlPec.s.si	Dolati (2010)
9772	0	9774	Qt	0.117	17		Pliocene- Pleistocene	PlPec.s.si	Dolati (2010)
9773	0	9775	Qt	1.238	17		Pliocene- Pleistocene	PlPec.s.si	Dolati (2010)
9774	0	9776	Qt	0.333	17		Pliocene- Pleistocene	PlPec.s.si	Dolati (2010)
9775	0	9777	Qt	3.259	17		Pliocene- Pleistocene	PlPec.s.si	Dolati (2010)
9776	0	9778	Qt	0.139	17		Pliocene- Pleistocene	PlPec.s.si	Dolati (2010)
9777	0	9779	Qt	0.163	17		Pliocene- Pleistocene	PlPec.s.si	Dolati (2010)
9778	0	9780	Qt	0.028	17		Pliocene- Pleistocene	PlPec.s.si	Dolati (2010)
9779	0	9781	Qt	0.181	17		Pliocene- Pleistocene	PlPec.s.si	Dolati (2010)
9780	0	9782	Qt	2.271	17		Pliocene- Pleistocene	PlPec.s.si	Dolati (2010)
9781	0	9783	Qt	0.190	17		Pliocene- Pleistocene	PlPec.s.si	Dolati (2010)
9782	0	9784	Qt	0.118	17		Pliocene- Pleistocene	PlPec.s.si	Dolati (2010)
9783	0	9785	Qt	0.062	17		Pliocene- Pleistocene	PlPec.s.si	Dolati (2010)
9784	0	9786	Qt	0.023	17		Pliocene- Pleistocene	PlPec.s.si	Dolati (2010)
9785	0	9787	Qt	0.221	17		Pliocene- Pleistocene	PlPec.s.si	Dolati (2010)
9786	0	9788	Qt	0.217	17		Pliocene- Pleistocene	PlPec.s.si	Dolati (2010)
9787	0	9789	Qt	0.142	17		Pliocene- Pleistocene	PlPec.s.si	Dolati (2010)
9788	0	9790	Qt	0.064	17		Pliocene- Pleistocene	PlPec.s.si	Dolati (2010)
9789	0	9791	Qt	0.153	17		Pliocene- Pleistocene	PlPec.s.si	Dolati (2010)
9790	0	9792	Qt	0.255	17		Pliocene- Pleistocene	PlPec.s.si	Dolati (2010)
9791	0	9793	Qt	4.729	17		Pliocene- Pleistocene	PlPec.s.si	Dolati (2010)

GeoNeus

OBJECTID_1	Join_Count	TARGET_FID	Label	Shape_Area (sqkm)	ORIG_FID	Absolute_Age	Age_paleontology	Unit	Reference
9792	0	9794	Qt	0.099	17		Pliocene- Pleistocene	PlPec.s.si	Dolati (2010)
9793	0	9795	Qt	0.561	17		Pliocene- Pleistocene	PlPec.s.si	Dolati (2010)
9794	0	9796	Qt	0.336	17		Pliocene- Pleistocene	PlPec.s.si	Dolati (2010)
9795	0	9797	Qt	0.427	17		Pliocene- Pleistocene	PlPec.s.si	Dolati (2010)
9796	0	9798	Qt	0.523	17		Pliocene- Pleistocene	PlPec.s.si	Dolati (2010)
9797	0	9799	Qt	0.185	17		Pliocene- Pleistocene	PlPec.s.si	Dolati (2010)
9798	0	9800	Qt	0.067	17		Pliocene- Pleistocene	PlPec.s.si	Dolati (2010)
9799	0	9801	Qt	0.737	17		Pliocene- Pleistocene	PlPec.s.si	Dolati (2010)
9800	0	9802	Qt	8.010	17		Pliocene- Pleistocene	PlPec.s.si	Dolati (2010)
9801	0	9803	Qt	1.563	17		Pliocene- Pleistocene	PlPec.s.si	Dolati (2010)
9802	0	9804	Qt	0.341	17		Pliocene- Pleistocene	PlPec.s.si	Dolati (2010)
9803	0	9805	Qt	0.374	17		Pliocene- Pleistocene	PlPec.s.si	Dolati (2010)
9804	0	9806	Qt	0.115	17		Pliocene- Pleistocene	PlPec.s.si	Dolati (2010)
9805	0	9807	Qt	0.241	17		Pliocene- Pleistocene	PlPec.s.si	Dolati (2010)
9806	0	9808	Qt	0.657	17		Pliocene- Pleistocene	PlPec.s.si	Dolati (2010)
9807	0	9809	Qt	0.071	17		Pliocene- Pleistocene	PlPec.s.si	Dolati (2010)
9808	0	9810	Qt	0.347	17		Pliocene- Pleistocene	PlPec.s.si	Dolati (2010)
9809	0	9811	Qt	0.127	17		Pliocene- Pleistocene	PlPec.s.si	Dolati (2010)
9810	0	9812	Qt	0.188	17		Pliocene- Pleistocene	PlPec.s.si	Dolati (2010)
9811	0	9813	Qt	0.111	17		Pliocene- Pleistocene	PlPec.s.si	Dolati (2010)
9812	0	9814	Qt	1.030	17		Pliocene- Pleistocene	PlPec.s.si	Dolati (2010)
9813	0	9815	Qt	0.168	17		Pliocene- Pleistocene	PlPec.s.si	Dolati (2010)
9814	0	9816	Qt	0.048	17		Pliocene- Pleistocene	PlPec.s.si	Dolati (2010)
9815	0	9817	Qt	0.280	17		Pliocene- Pleistocene	PlPec.s.si	Dolati (2010)
9816	0	9818	Qt	0.300	17		Pliocene- Pleistocene	PlPec.s.si	Dolati (2010)
9817	0	9819	Qt	0.223	17		Pliocene- Pleistocene	PlPec.s.si	Dolati (2010)
9818	0	9820	Qt	0.497	17		Pliocene- Pleistocene	PlPec.s.si	Dolati (2010)
9819	0	9821	Qt	0.271	17		Pliocene- Pleistocene	PlPec.s.si	Dolati (2010)
9820	0	9822	Qt	0.298	17		Pliocene- Pleistocene	PlPec.s.si	Dolati (2010)
9821	0	9823	Qt	0.094	17		Pliocene- Pleistocene	PlPec.s.si	Dolati (2010)
9822	0	9824	Qt	0.164	17		Pliocene- Pleistocene	PlPec.s.si	Dolati (2010)
9823	0	9825	Qt	0.041	17		Pliocene- Pleistocene	PlPec.s.si	Dolati (2010)
9824	0	9826	Qt	0.121	17		Pliocene- Pleistocene	PlPec.s.si	Dolati (2010)
9825	0	9827	Qt	4.329	17		Pliocene- Pleistocene	PlPec.s.si	Dolati (2010)
9826	0	9828	Qt	3.781	17		Pliocene- Pleistocene	PlPec.s.si	Dolati (2010)
9827	0	9829	Qt	0.096	17		Pliocene- Pleistocene	PlPec.s.si	Dolati (2010)
9828	0	9830	Qt	2.329	17		Pliocene- Pleistocene	PlPec.s.si	Dolati (2010)
9829	0	9831	Qt	0.102	17		Pliocene- Pleistocene	PlPec.s.si	Dolati (2010)
9830	0	9832	Qt	0.147	17		Pliocene- Pleistocene	PlPec.s.si	Dolati (2010)

GeoNLP

OBJECTID_1	Join_Count	TARGET_FID	Label	Shape_Area (sqkm)	ORIG_FID	Absolute_Age	Age_paleontology	Unit	Reference
9831	0	9833	Qt	0.651	17		Pliocene- Pleistocene	PlPec.s.si	Dolati (2010)
9832	0	9834	Qt	0.183	17		Pliocene- Pleistocene	PlPec.s.si	Dolati (2010)
9833	0	9835	Qt	0.273	17		Pliocene- Pleistocene	PlPec.s.si	Dolati (2010)
9834	0	9836	Qt	0.114	17		Pliocene- Pleistocene	PlPec.s.si	Dolati (2010)
9835	0	9837	Qt	0.150	17		Pliocene- Pleistocene	PlPec.s.si	Dolati (2010)
9836	0	9838	Qt	1.270	17		Pliocene- Pleistocene	PlPec.s.si	Dolati (2010)
9837	0	9839	Qt	2.548	17		Pliocene- Pleistocene	PlPec.s.si	Dolati (2010)
9838	0	9840	Qt	1.206	17		Pliocene- Pleistocene	PlPec.s.si	Dolati (2010)
9839	0	9841	Qt	0.063	17		Pliocene- Pleistocene	PlPec.s.si	Dolati (2010)
9840	0	9842	Qt	0.537	17		Pliocene- Pleistocene	PlPec.s.si	Dolati (2010)
9841	0	9843	Qt	0.278	17		Pliocene- Pleistocene	PlPec.s.si	Dolati (2010)
9842	0	9844	Qt	0.494	17		Pliocene- Pleistocene	PlPec.s.si	Dolati (2010)
9843	0	9845	Qt	0.085	17		Pliocene- Pleistocene	PlPec.s.si	Dolati (2010)
9844	0	9846	Qt	0.028	17		Pliocene- Pleistocene	PlPec.s.si	Dolati (2010)
9845	0	9847	Qt	0.847	17		Pliocene- Pleistocene	PlPec.s.si	Dolati (2010)
9846	0	9848	Qt	0.187	17		Pliocene- Pleistocene	PlPec.s.si	Dolati (2010)
9847	0	9849	Qt	0.048	17		Pliocene- Pleistocene	PlPec.s.si	Dolati (2010)
9848	0	9850	Qt	0.962	17		Pliocene- Pleistocene	PlPec.s.si	Dolati (2010)
9849	0	9851	Qt	0.111	17		Pliocene- Pleistocene	PlPec.s.si	Dolati (2010)
9850	0	9852	Qt	16.625	17		Pliocene- Pleistocene	PlPec.s.si	Dolati (2010)
9851	0	9853	Qt	0.107	17		Pliocene- Pleistocene	PlPec.s.si	Dolati (2010)
9852	0	9854	Qt	0.052	17		Pliocene- Pleistocene	PlPec.s.si	Dolati (2010)
9853	0	9855	Qt	0.098	17		Pliocene- Pleistocene	PlPec.s.si	Dolati (2010)
9854	0	9856	Qt	0.235	17		Pliocene- Pleistocene	PlPec.s.si	Dolati (2010)
9855	0	9857	Qt	1.019	17		Pliocene- Pleistocene	PlPec.s.si	Dolati (2010)
9856	0	9858	Qt	0.128	17		Pliocene- Pleistocene	PlPec.s.si	Dolati (2010)
9857	0	9859	Qt	2.671	17		Pliocene- Pleistocene	PlPec.s.si	Dolati (2010)
9858	0	9860	Qt	0.086	17		Pliocene- Pleistocene	PlPec.s.si	Dolati (2010)
9859	0	9861	Qt	0.196	17		Pliocene- Pleistocene	PlPec.s.si	Dolati (2010)
9860	0	9862	Qt	2.921	17		Pliocene- Pleistocene	PlPec.s.si	Dolati (2010)
9861	0	9863	Qt	0.191	17		Pliocene- Pleistocene	PlPec.s.si	Dolati (2010)
9863	0	9865	Qt	0.098	17		Pliocene- Pleistocene	PlPec.s.si	Dolati (2010)
9864	0	9866	Qt	0.385	17		Pliocene- Pleistocene	PlPec.s.si	Dolati (2010)
9865	0	9867	Qt	0.020	17		Pliocene- Pleistocene	PlPec.s.si	Dolati (2010)
9866	0	9868	Qt	2.521	17		Pliocene- Pleistocene	PlPec.s.si	Dolati (2010)
9867	0	9869	Qt	0.121	17		Pliocene- Pleistocene	PlPec.s.si	Dolati (2010)
9868	0	9870	Qt	2.975	17		Pliocene- Pleistocene	PlPec.s.si	Dolati (2010)
9869	0	9871	Qt	0.127	17		Pliocene- Pleistocene	PlPec.s.si	Dolati (2010)
9870	0	9872	Qt	0.317	17		Pliocene- Pleistocene	PlPec.s.si	Dolati (2010)

GeoNeus

OBJECTID_1	Join_Count	TARGET_FID	Label	Shape_Area (sqkm)	ORIG_FID	Absolute_Age	Age_paleontology	Unit	Reference
9871	0	9873	Qt	0.020	17		Pliocene- Pleistocene	PlPec.s.si	Dolati (2010)
9872	0	9874	Qt	0.066	17		Pliocene- Pleistocene	PlPec.s.si	Dolati (2010)
9873	0	9875	Qt	0.040	17		Pliocene- Pleistocene	PlPec.s.si	Dolati (2010)
9874	0	9876	Qt	0.057	17		Pliocene- Pleistocene	PlPec.s.si	Dolati (2010)
9875	0	9877	Qt	0.210	17		Pliocene- Pleistocene	PlPec.s.si	Dolati (2010)
9876	0	9878	Qt	0.363	17		Pliocene- Pleistocene	PlPec.s.si	Dolati (2010)
9877	0	9879	Qt	1.148	17		Pliocene- Pleistocene	PlPec.s.si	Dolati (2010)
9878	0	9880	Qt	0.452	17		Pliocene- Pleistocene	PlPec.s.si	Dolati (2010)
9879	0	9881	Qt	0.952	17		Pliocene- Pleistocene	PlPec.s.si	Dolati (2010)
9880	0	9882	Qt	0.414	17		Pliocene- Pleistocene	PlPec.s.si	Dolati (2010)
9881	0	9883	Qt	0.641	17		Pliocene- Pleistocene	PlPec.s.si	Dolati (2010)
9882	0	9884	Qt	1.089	17		Pliocene- Pleistocene	PlPec.s.si	Dolati (2010)
9883	0	9885	Qt	0.336	17		Pliocene- Pleistocene	PlPec.s.si	Dolati (2010)
9884	0	9886	Qt	3.596	17		Pliocene- Pleistocene	PlPec.s.si	Dolati (2010)
9885	0	9887	Qt	1.187	17		Pliocene- Pleistocene	PlPec.s.si	Dolati (2010)
9886	0	9888	Qt	0.604	17		Pliocene- Pleistocene	PlPec.s.si	Dolati (2010)
9887	0	9889	Qt	0.232	17		Pliocene- Pleistocene	PlPec.s.si	Dolati (2010)
9888	0	9890	Qt	0.098	17		Pliocene- Pleistocene	PlPec.s.si	Dolati (2010)
9889	0	9891	Qt	0.226	17		Pliocene- Pleistocene	PlPec.s.si	Dolati (2010)
9890	0	9892	Qt	0.822	17		Pliocene- Pleistocene	PlPec.s.si	Dolati (2010)
9891	0	9893	Qt	0.274	17		Pliocene- Pleistocene	PlPec.s.si	Dolati (2010)
9892	0	9894	Qt	0.063	17		Pliocene- Pleistocene	PlPec.s.si	Dolati (2010)
9893	0	9895	Qt	0.121	17		Pliocene- Pleistocene	PlPec.s.si	Dolati (2010)
9894	0	9896	Qt	0.184	17		Pliocene- Pleistocene	PlPec.s.si	Dolati (2010)
9895	0	9897	Qt	0.135	17		Pliocene- Pleistocene	PlPec.s.si	Dolati (2010)
9896	0	9898	Qt	0.277	17		Pliocene- Pleistocene	PlPec.s.si	Dolati (2010)
9897	0	9899	Qt	0.259	17		Pliocene- Pleistocene	PlPec.s.si	Dolati (2010)
9898	0	9900	Qt	0.427	17		Pliocene- Pleistocene	PlPec.s.si	Dolati (2010)
9899	0	9901	Qt	0.059	17		Pliocene- Pleistocene	PlPec.s.si	Dolati (2010)
9900	0	9902	Qt	0.684	17		Pliocene- Pleistocene	PlPec.s.si	Dolati (2010)
9901	0	9903	Qt	0.277	17		Pliocene- Pleistocene	PlPec.s.si	Dolati (2010)
9902	0	9904	Qt	0.218	17		Pliocene- Pleistocene	PlPec.s.si	Dolati (2010)
9903	0	9905	Qt	2.595	17		Pliocene- Pleistocene	PlPec.s.si	Dolati (2010)
9904	0	9906	Qt	0.346	17		Pliocene- Pleistocene	PlPec.s.si	Dolati (2010)
9905	0	9907	Qt	0.075	17		Pliocene- Pleistocene	PlPec.s.si	Dolati (2010)
9906	0	9908	Qt	0.075	17		Pliocene- Pleistocene	PlPec.s.si	Dolati (2010)
9907	0	9909	Qt	0.292	17		Pliocene- Pleistocene	PlPec.s.si	Dolati (2010)
9908	0	9910	Qt	0.148	17		Pliocene- Pleistocene	PlPec.s.si	Dolati (2010)
9909	0	9911	Qt	1.343	17		Pliocene- Pleistocene	PlPec.s.si	Dolati (2010)

GeoNLP

OBJECTID_1	Join_Count	TARGET_FID	Label	Shape_Area (sqkm)	ORIG_FID	Absolute_Age	Age_paleontology	Unit	Reference
9910	0	9912	Qt	0.872	17		Pliocene- Pleistocene	PlPec.s.si	Dolati (2010)
9911	0	9913	Qt	0.375	17		Pliocene- Pleistocene	PlPec.s.si	Dolati (2010)
9912	0	9914	Qt	0.662	17		Pliocene- Pleistocene	PlPec.s.si	Dolati (2010)
9913	0	9915	Qt	0.276	17		Pliocene- Pleistocene	PlPec.s.si	Dolati (2010)
9914	0	9916	Qt	0.038	17		Pliocene- Pleistocene	PlPec.s.si	Dolati (2010)
9915	0	9917	Qt	0.880	17		Pliocene- Pleistocene	PlPec.s.si	Dolati (2010)
9916	0	9918	Qt	0.353	17		Pliocene- Pleistocene	PlPec.s.si	Dolati (2010)
9917	0	9919	Qt	0.154	17		Pliocene- Pleistocene	PlPec.s.si	Dolati (2010)
9918	0	9920	Qt	0.026	17		Pliocene- Pleistocene	PlPec.s.si	Dolati (2010)
9919	0	9921	Qt	0.226	17		Pliocene- Pleistocene	PlPec.s.si	Dolati (2010)
9920	0	9922	Qt	0.734	17		Pliocene- Pleistocene	PlPec.s.si	Dolati (2010)
9921	0	9923	Qt	0.053	17		Pliocene- Pleistocene	PlPec.s.si	Dolati (2010)
9922	0	9924	Qt	0.384	17		Pliocene- Pleistocene	PlPec.s.si	Dolati (2010)
9923	0	9925	Qt	0.674	17		Pliocene- Pleistocene	PlPec.s.si	Dolati (2010)
9924	0	9926	Qt	0.127	17		Pliocene- Pleistocene	PlPec.s.si	Dolati (2010)
9925	0	9927	Qt	0.058	17		Pliocene- Pleistocene	PlPec.s.si	Dolati (2010)
9926	0	9928	Qt	18.533	17		Pliocene- Pleistocene	PlPec.s.si	Dolati (2010)
9927	0	9929	Qt	0.360	17		Pliocene- Pleistocene	PlPec.s.si	Dolati (2010)
9928	0	9930	Qt	0.436	17		Pliocene- Pleistocene	PlPec.s.si	Dolati (2010)
9929	0	9931	Qt	0.051	17		Pliocene- Pleistocene	PlPec.s.si	Dolati (2010)
9930	0	9932	Qt	1.312	17		Pliocene- Pleistocene	PlPec.s.si	Dolati (2010)
9931	0	9933	Qt	0.139	17		Pliocene- Pleistocene	PlPec.s.si	Dolati (2010)
9932	0	9934	Qt	1.008	17		Pliocene- Pleistocene	PlPec.s.si	Dolati (2010)
9933	0	9935	Qt	1.175	17		Pliocene- Pleistocene	PlPec.s.si	Dolati (2010)
9934	0	9936	Qt	0.550	17		Pliocene- Pleistocene	PlPec.s.si	Dolati (2010)
9935	0	9937	Qt	0.131	17		Pliocene- Pleistocene	PlPec.s.si	Dolati (2010)
9936	0	9938	Qt	0.250	17		Pliocene- Pleistocene	PlPec.s.si	Dolati (2010)
9937	0	9939	Qt	0.175	17		Pliocene- Pleistocene	PlPec.s.si	Dolati (2010)
9938	0	9940	Qt	1.181	17		Pliocene- Pleistocene	PlPec.s.si	Dolati (2010)
9939	0	9941	Qt	0.515	17		Pliocene- Pleistocene	PlPec.s.si	Dolati (2010)
9940	0	9942	Qt	1.092	17		Pliocene- Pleistocene	PlPec.s.si	Dolati (2010)
9941	0	9943	Qt	0.542	17		Pliocene- Pleistocene	PlPec.s.si	Dolati (2010)
9942	0	9944	Qt	0.351	17		Pliocene- Pleistocene	PlPec.s.si	Dolati (2010)
9943	0	9945	Qt	1.326	17		Pliocene- Pleistocene	PlPec.s.si	Dolati (2010)
9944	0	9946	Qt	1.408	17		Pliocene- Pleistocene	PlPec.s.si	Dolati (2010)
9945	0	9947	Qt	0.815	17		Pliocene- Pleistocene	PlPec.s.si	Dolati (2010)
9946	0	9948	Qt	0.371	17		Pliocene- Pleistocene	PlPec.s.si	Dolati (2010)
9947	0	9949	Qt	2.101	17		Pliocene- Pleistocene	PlPec.s.si	Dolati (2010)
9948	0	9950	Qt	0.183	17		Pliocene- Pleistocene	PlPec.s.si	Dolati (2010)

GeoNeus

OBJECTID_1	Join_Count	TARGET_FID	Label	Shape_Area (sqkm)	ORIG_FID	Absolute_Age	Age_paleontology	Unit	Reference
9949	0	9951	Qt	0.072	17		Pliocene- Pleistocene	PlPec.s.si	Dolati (2010)
9950	0	9952	Qt	0.621	17		Pliocene- Pleistocene	PlPec.s.si	Dolati (2010)
9951	0	9953	Qt	0.828	17		Pliocene- Pleistocene	PlPec.s.si	Dolati (2010)
9952	0	9954	Qt	0.243	17		Pliocene- Pleistocene	PlPec.s.si	Dolati (2010)
9953	0	9955	Qt	0.249	17		Pliocene- Pleistocene	PlPec.s.si	Dolati (2010)
9954	0	9956	Qt	0.619	17		Pliocene- Pleistocene	PlPec.s.si	Dolati (2010)
9955	0	9957	Qt	0.205	17		Pliocene- Pleistocene	PlPec.s.si	Dolati (2010)
9956	0	9958	Qt	0.509	17		Pliocene- Pleistocene	PlPec.s.si	Dolati (2010)
9957	0	9959	Qt	0.956	17		Pliocene- Pleistocene	PlPec.s.si	Dolati (2010)
9958	0	9960	Qt	0.106	17		Pliocene- Pleistocene	PlPec.s.si	Dolati (2010)
9959	0	9961	Qt	0.488	17		Pliocene- Pleistocene	PlPec.s.si	Dolati (2010)
9960	0	9962	Qt	0.088	17		Pliocene- Pleistocene	PlPec.s.si	Dolati (2010)
9961	0	9963	Qt	0.165	17		Pliocene- Pleistocene	PlPec.s.si	Dolati (2010)
9962	0	9964	Qt	2.436	17		Pliocene- Pleistocene	PlPec.s.si	Dolati (2010)
9963	0	9965	Qt	1.109	17		Pliocene- Pleistocene	PlPec.s.si	Dolati (2010)
9964	0	9966	Qt	0.040	17		Pliocene- Pleistocene	PlPec.s.si	Dolati (2010)
9965	0	9967	Qt	0.791	17		Pliocene- Pleistocene	PlPec.s.si	Dolati (2010)
9966	0	9968	Qt	5.518	17		Pliocene- Pleistocene	PlPec.s.si	Dolati (2010)
9967	0	9969	Qt	0.077	17		Pliocene- Pleistocene	PlPec.s.si	Dolati (2010)
9968	0	9970	Qt	0.170	17		Pliocene- Pleistocene	PlPec.s.si	Dolati (2010)
9969	0	9971	Qt	3.563	17		Pliocene- Pleistocene	PlPec.s.si	Dolati (2010)
9970	0	9972	Qt	0.185	17		Pliocene- Pleistocene	PlPec.s.si	Dolati (2010)
9971	0	9973	Qt	0.420	17		Pliocene- Pleistocene	PlPec.s.si	Dolati (2010)
9972	0	9974	Qt	0.337	17		Pliocene- Pleistocene	PlPec.s.si	Dolati (2010)
9973	0	9975	Qt	3.083	17		Pliocene- Pleistocene	PlPec.s.si	Dolati (2010)
9974	0	9976	Qt	0.191	17		Pliocene- Pleistocene	PlPec.s.si	Dolati (2010)
9975	0	9977	Qt	0.106	17		Pliocene- Pleistocene	PlPec.s.si	Dolati (2010)
9976	0	9978	Qt	0.050	17		Pliocene- Pleistocene	PlPec.s.si	Dolati (2010)
9977	0	9979	Qt	5.107	17		Pliocene- Pleistocene	PlPec.s.si	Dolati (2010)
9978	0	9980	Qt	12.251	17		Pliocene- Pleistocene	PlPec.s.si	Dolati (2010)
9979	0	9981	Qt	0.722	17		Pliocene- Pleistocene	PlPec.s.si	Dolati (2010)
9980	0	9982	Qt	0.077	17		Pliocene- Pleistocene	PlPec.s.si	Dolati (2010)
9981	0	9983	Qt	85.807	17		Pliocene- Pleistocene	PlPec.s.si	Dolati (2010)
9982	0	9984	Qt	0.356	17		Pliocene- Pleistocene	PlPec.s.si	Dolati (2010)
9983	0	9985	Qt	0.648	17		Pliocene- Pleistocene	PlPec.s.si	Dolati (2010)
9984	0	9986	Qt	0.157	17		Pliocene- Pleistocene	PlPec.s.si	Dolati (2010)
9985	0	9987	Qt	0.067	17		Pliocene- Pleistocene	PlPec.s.si	Dolati (2010)
9986	0	9988	Qt	0.044	17		Pliocene- Pleistocene	PlPec.s.si	Dolati (2010)
9987	0	9989	Qt	0.761	17		Pliocene- Pleistocene	PlPec.s.si	Dolati (2010)

GeoNLP

OBJECTID_1	Join_Count	TARGET_FID	Label	Shape_Area (sqkm)	ORIG_FID	Absolute_Age	Age_paleontology	Unit	Reference
9988	0	9990	Qt	2.284	17		Pliocene- Pleistocene	PlPec.s.si	Dolati (2010)
9989	0	9991	Qt	0.391	17		Pliocene- Pleistocene	PlPec.s.si	Dolati (2010)
9990	0	9992	Qt	2.161	17		Pliocene- Pleistocene	PlPec.s.si	Dolati (2010)
9991	0	9993	Qt	0.183	17		Pliocene- Pleistocene	PlPec.s.si	Dolati (2010)
9992	0	9994	Qt	2.635	17		Pliocene- Pleistocene	PlPec.s.si	Dolati (2010)
9993	0	9995	Qt	0.126	17		Pliocene- Pleistocene	PlPec.s.si	Dolati (2010)
9994	0	9996	Qt	6.783	17		Pliocene- Pleistocene	PlPec.s.si	Dolati (2010)
9995	0	9997	Qt	0.026	17		Pliocene- Pleistocene	PlPec.s.si	Dolati (2010)
9996	0	9998	Qt	7.481	17		Pliocene- Pleistocene	PlPec.s.si	Dolati (2010)
9997	0	9999	Qt	0.291	17		Pliocene- Pleistocene	PlPec.s.si	Dolati (2010)
9998	0	10000	Qt	0.110	17		Pliocene- Pleistocene	PlPec.s.si	Dolati (2010)
9999	0	10001	Qt	0.537	17		Pliocene- Pleistocene	PlPec.s.si	Dolati (2010)
10000	0	10002	Qt	0.174	17		Pliocene- Pleistocene	PlPec.s.si	Dolati (2010)
10001	0	10003	Qt	97.555	17		Pliocene- Pleistocene	PlPec.s.si	Dolati (2010)
10002	0	10004	Qt	8.001	17		Pliocene- Pleistocene	PlPec.s.si	Dolati (2010)
10003	0	10005	Qt	0.346	17		Pliocene- Pleistocene	PlPec.s.si	Dolati (2010)
10338	1	10341	Plc-Qt	0.461	20		Pliocene- Pleistocene	PlPec.s.si	Dolati (2010)
10379	1	10382	Plc-Qt	0.196	0		Pliocene- Pleistocene	PlPec.s.si	Dolati (2010)
10380	3	10383	Plc-Qt	1.316	0		Pliocene- Pleistocene	PlPec.s.si	Dolati (2010)
10381	1	10384	Plc-Qt	0.244	0		Pliocene- Pleistocene	PlPec.s.si	Dolati (2010)
10382	1	10385	Plc-Qt	0.280	0		Pliocene- Pleistocene	PlPec.s.si	Dolati (2010)
10383	1	10386	Plc-Qt	0.068	0		Pliocene- Pleistocene	PlPec.s.si	Dolati (2010)
10384	1	10387	Plc-Qt	0.324	0		Pliocene- Pleistocene	PlPec.s.si	Dolati (2010)
10385	1	10388	Plc-Qt	0.061	0		Pliocene- Pleistocene	PlPec.s.si	Dolati (2010)
10386	1	10389	Plc-Qt	0.746	0		Pliocene- Pleistocene	PlPec.s.si	Dolati (2010)
10387	1	10390	Plc-Qt	0.389	0		Pliocene- Pleistocene	PlPec.s.si	Dolati (2010)
10388	2	10391	Plc-Qt	0.141	0		Pliocene- Pleistocene	PlPec.s.si	Dolati (2010)
10389	1	10392	Plc-Qt	0.761	0		Pliocene- Pleistocene	PlPec.s.si	Dolati (2010)
10390	2	10397	Plc-Qt	0.126	0		Pliocene- Pleistocene	PlPec.s.si	Dolati (2010)
10391	2	10398	Plc-Qt	0.103	0		Pliocene- Pleistocene	PlPec.s.si	Dolati (2010)
10392	0	10399	Plc-Qt	0.440	0		Pliocene- Pleistocene	PlPec.s.si	Dolati (2010)
10393	0	10400	Plc-Qt	0.077	0		Pliocene- Pleistocene	PlPec.s.si	Dolati (2010)
10394	1	10401	Plc-Qt	0.244	0		Pliocene- Pleistocene	PlPec.s.si	Dolati (2010)
10395	1	10402	Plc-Qt	0.764	0		Pliocene- Pleistocene	PlPec.s.si	Dolati (2010)
10396	1	10403	Plc-Qt	1.026	0		Pliocene- Pleistocene	PlPec.s.si	Dolati (2010)
10426	1	10444	Qt	0.025	0		Pliocene- Pleistocene	PlPec.s.si	Dolati (2010)
10427	1	10447	Qt	0.022	0		Pliocene- Pleistocene	PlPec.s.si	Dolati (2010)
10428	1	10448	Qt	0.118	0		Pliocene- Pleistocene	PlPec.s.si	Dolati (2010)
10429	1	10451	Qt	0.458	0		Pliocene- Pleistocene	PlPec.s.si	Dolati (2010)

GeoNeWS

OBJECTID_1	Join_Count	TARGET_FID	Label	Shape_Area (sqkm)	ORIG_FID	Absolute_Age	Age_paleontology	Unit	Reference
10450	0	4500	Qt	0.036	8			PlPec.s.si	
10451	0	4500	Qt	0.039	8			PlPec.s.si	Dolati (2010)
10452	3	9587	Qt	0.012	17		Pliocene- Pleistocene	PlPec.s.si	Dolati (2010)
10453	3	9587	Qt	0.017	17		Pliocene- Pleistocene	PlPec.s.si	Dolati (2010)

GeoNexus

Table S12. Summary of mapped polygons for the Q^a Unit.

OBJECTID_1	Join_Count	TARGET_FID	Label	Shape_Area (sqkm)	ORIG_FID	Absolute_Age	Age_paleontology	Unit	Reference
2426	0	2426	mud	0.102	6	≤ 21.3K	Pleistocene-mid Holocene	Qa	Gharibreza (2016); Dolati (2010)
2427	0	2427	mud	0.084	6	≤ 21.3K	Pleistocene-mid Holocene	Qa	Gharibreza (2016); Dolati (2010)
2428	0	2428	mud	0.035	6	≤ 21.3K	Pleistocene-mid Holocene	Qa	Gharibreza (2016); Dolati (2010)
2429	0	2429	mud	0.033	6	≤ 21.3K	Pleistocene-mid Holocene	Qa	Gharibreza (2016); Dolati (2010)
2430	0	2430	mud	0.105	6	≤ 21.3K	Pleistocene-mid Holocene	Qa	Gharibreza (2016); Dolati (2010)
2431	0	2431	mud	0.310	6	≤ 21.3K	Pleistocene-mid Holocene	Qa	Gharibreza (2016); Dolati (2010)
2432	0	2432	mud	0.069	6	≤ 21.3K	Pleistocene-mid Holocene	Qa	Gharibreza (2016); Dolati (2010)
2433	0	2433	mud	0.058	6	≤ 21.3K	Pleistocene-mid Holocene	Qa	Gharibreza (2016); Dolati (2010)
2434	0	2434	mud	0.164	6	≤ 21.3K	Pleistocene-mid Holocene	Qa	Gharibreza (2016); Dolati (2010)
2435	0	2435	mud	0.079	6	≤ 21.3K	Pleistocene-mid Holocene	Qa	Gharibreza (2016); Dolati (2010)
2436	0	2436	mud	0.134	6	≤ 21.3K	Pleistocene-mid Holocene	Qa	Gharibreza (2016); Dolati (2010)
2437	0	2437	mud	0.072	6	≤ 21.3K	Pleistocene-mid Holocene	Qa	Gharibreza (2016); Dolati (2010)
2438	0	2438	mud	0.317	6	≤ 21.3K	Pleistocene-mid Holocene	Qa	Gharibreza (2016); Dolati (2010)
2439	0	2439	mud	0.277	6	≤ 21.3K	Pleistocene-mid Holocene	Qa	Gharibreza (2016); Dolati (2010)
2440	0	2440	mud	0.055	6	≤ 21.3K	Pleistocene-mid Holocene	Qa	Gharibreza (2016); Dolati (2010)
2441	0	2441	mud	1.258	6	≤ 21.3K	Pleistocene-mid Holocene	Qa	Gharibreza (2016); Dolati (2010)
2442	0	2442	mud	0.110	6	≤ 21.3K	Pleistocene-mid Holocene	Qa	Gharibreza (2016); Dolati (2010)
2443	0	2443	mud	6.569	6	≤ 21.3K	Pleistocene-mid Holocene	Qa	Gharibreza (2016); Dolati (2010)
2444	0	2444	mud	0.012	6	≤ 21.3K	Pleistocene-mid Holocene	Qa	Gharibreza (2016); Dolati (2010)
2445	0	2445	mud	0.073	6	≤ 21.3K	Pleistocene-mid Holocene	Qa	Gharibreza (2016); Dolati (2010)
2446	0	2446	mud	0.017	6	≤ 21.3K	Pleistocene-mid Holocene	Qa	Gharibreza (2016); Dolati (2010)
2447	0	2447	mud	0.004	6	≤ 21.3K	Pleistocene-mid Holocene	Qa	Gharibreza (2016); Dolati (2010)
2448	0	2448	mud	0.290	6	≤ 21.3K	Pleistocene-mid Holocene	Qa	Gharibreza (2016); Dolati (2010)
2449	0	2449	mud	0.097	6	≤ 21.3K	Pleistocene-mid Holocene	Qa	Gharibreza (2016); Dolati (2010)
2450	0	2450	mud	0.337	6	≤ 21.3K	Pleistocene-mid Holocene	Qa	Gharibreza (2016); Dolati (2010)
2451	0	2451	mud	0.232	6	≤ 21.3K	Pleistocene-mid Holocene	Qa	Gharibreza (2016); Dolati (2010)
2452	0	2452	mud	0.012	6	≤ 21.3K	Pleistocene-mid Holocene	Qa	Gharibreza (2016); Dolati (2010)
2453	0	2453	mud	0.002	6	≤ 21.3K	Pleistocene-mid Holocene	Qa	Gharibreza (2016); Dolati (2010)
2454	0	2454	mud	0.015	6	≤ 21.3K	Pleistocene-mid Holocene	Qa	Gharibreza (2016); Dolati (2010)
2455	0	2455	mud	0.033	6	≤ 21.3K	Pleistocene-mid Holocene	Qa	Gharibreza (2016); Dolati (2010)
2456	0	2456	mud	0.032	6	≤ 21.3K	Pleistocene-mid Holocene	Qa	Gharibreza (2016); Dolati (2010)
2457	0	2457	mud	0.008	6	≤ 21.3K	Pleistocene-mid Holocene	Qa	Gharibreza (2016); Dolati (2010)
2458	0	2458	mud	0.122	6	≤ 21.3K	Pleistocene-mid Holocene	Qa	Gharibreza (2016); Dolati (2010)
2459	0	2459	mud	0.095	6	≤ 21.3K	Pleistocene-mid Holocene	Qa	Gharibreza (2016); Dolati (2010)
2460	0	2460	mud	0.038	6	≤ 21.3K	Pleistocene-mid Holocene	Qa	Gharibreza (2016); Dolati (2010)
2461	0	2461	mud	0.011	6	≤ 21.3K	Pleistocene-mid Holocene	Qa	Gharibreza (2016); Dolati (2010)
2462	0	2462	mud	0.191	6	≤ 21.3K	Pleistocene-mid Holocene	Qa	Gharibreza (2016); Dolati (2010)
2463	0	2463	mud	0.024	6	≤ 21.3K	Pleistocene-mid Holocene	Qa	Gharibreza (2016); Dolati (2010)

Preview

OBJECTID_1	Join_Count	TARGET_FID	Label	Shape_Area (sqkm)	ORIG_FID	Absolute_Age	Age_paleontology	Unit	Reference
2464	0	2464	mud	0.146	6	≤ 21.3K	Pleistocene-mid Holocene	Qa	Gharibreza (2016); Dolati (2010)
2465	0	2465	mud	0.195	6	≤ 21.3K	Pleistocene-mid Holocene	Qa	Gharibreza (2016); Dolati (2010)
2466	0	2466	mud	0.008	6	≤ 21.3K	Pleistocene-mid Holocene	Qa	Gharibreza (2016); Dolati (2010)
2467	0	2467	mud	0.020	6	≤ 21.3K	Pleistocene-mid Holocene	Qa	Gharibreza (2016); Dolati (2010)
2468	0	2468	mud	0.084	6	≤ 21.3K	Pleistocene-mid Holocene	Qa	Gharibreza (2016); Dolati (2010)
2469	0	2469	mud	0.014	6	≤ 21.3K	Pleistocene-mid Holocene	Qa	Gharibreza (2016); Dolati (2010)
2470	0	2470	mud	0.296	6	≤ 21.3K	Pleistocene-mid Holocene	Qa	Gharibreza (2016); Dolati (2010)
2471	0	2471	mud	0.076	6	≤ 21.3K	Pleistocene-mid Holocene	Qa	Gharibreza (2016); Dolati (2010)
2472	0	2472	mud	0.018	6	≤ 21.3K	Pleistocene-mid Holocene	Qa	Gharibreza (2016); Dolati (2010)
2473	0	2473	mud	0.048	6	≤ 21.3K	Pleistocene-mid Holocene	Qa	Gharibreza (2016); Dolati (2010)
2474	0	2474	mud	0.406	6	≤ 21.3K	Pleistocene-mid Holocene	Qa	Gharibreza (2016); Dolati (2010)
2475	0	2475	mud	0.057	6	≤ 21.3K	Pleistocene-mid Holocene	Qa	Gharibreza (2016); Dolati (2010)
2476	0	2476	mud	0.027	6	≤ 21.3K	Pleistocene-mid Holocene	Qa	Gharibreza (2016); Dolati (2010)
2477	0	2477	mud	0.018	6	≤ 21.3K	Pleistocene-mid Holocene	Qa	Gharibreza (2016); Dolati (2010)
2478	0	2478	mud	0.010	6	≤ 21.3K	Pleistocene-mid Holocene	Qa	Gharibreza (2016); Dolati (2010)
2479	0	2479	mud	0.042	6	≤ 21.3K	Pleistocene-mid Holocene	Qa	Gharibreza (2016); Dolati (2010)
2480	0	2480	mud	0.007	6	≤ 21.3K	Pleistocene-mid Holocene	Qa	Gharibreza (2016); Dolati (2010)
2481	0	2481	mud	0.039	6	≤ 21.3K	Pleistocene-mid Holocene	Qa	Gharibreza (2016); Dolati (2010)
2482	0	2482	mud	0.003	6	≤ 21.3K	Pleistocene-mid Holocene	Qa	Gharibreza (2016); Dolati (2010)
2483	0	2483	mud	0.003	6	≤ 21.3K	Pleistocene-mid Holocene	Qa	Gharibreza (2016); Dolati (2010)
2484	0	2484	mud	0.020	6	≤ 21.3K	Pleistocene-mid Holocene	Qa	Gharibreza (2016); Dolati (2010)
2485	0	2485	mud	0.039	6	≤ 21.3K	Pleistocene-mid Holocene	Qa	Gharibreza (2016); Dolati (2010)
2486	0	2486	mud	0.320	6	≤ 21.3K	Pleistocene-mid Holocene	Qa	Gharibreza (2016); Dolati (2010)
2487	0	2487	mud	0.004	6	≤ 21.3K	Pleistocene-mid Holocene	Qa	Gharibreza (2016); Dolati (2010)
2488	0	2488	mud	0.040	6	≤ 21.3K	Pleistocene-mid Holocene	Qa	Gharibreza (2016); Dolati (2010)
2489	0	2489	mud	0.026	6	≤ 21.3K	Pleistocene-mid Holocene	Qa	Gharibreza (2016); Dolati (2010)
2490	0	2490	mud	0.031	6	≤ 21.3K	Pleistocene-mid Holocene	Qa	Gharibreza (2016); Dolati (2010)
2491	0	2491	mud	0.019	6	≤ 21.3K	Pleistocene-mid Holocene	Qa	Gharibreza (2016); Dolati (2010)
2492	0	2492	mud	0.180	6	≤ 21.3K	Pleistocene-mid Holocene	Qa	Gharibreza (2016); Dolati (2010)
2493	0	2493	mud	0.194	6	≤ 21.3K	Pleistocene-mid Holocene	Qa	Gharibreza (2016); Dolati (2010)
2494	0	2494	mud	0.019	6	≤ 21.3K	Pleistocene-mid Holocene	Qa	Gharibreza (2016); Dolati (2010)
2495	0	2495	mud	0.397	6	≤ 21.3K	Pleistocene-mid Holocene	Qa	Gharibreza (2016); Dolati (2010)
2496	0	2496	mud	0.023	6	≤ 21.3K	Pleistocene-mid Holocene	Qa	Gharibreza (2016); Dolati (2010)
2497	0	2497	mud	0.160	6	≤ 21.3K	Pleistocene-mid Holocene	Qa	Gharibreza (2016); Dolati (2010)
2498	0	2498	mud	0.125	6	≤ 21.3K	Pleistocene-mid Holocene	Qa	Gharibreza (2016); Dolati (2010)
2499	0	2499	mud	0.068	6	≤ 21.3K	Pleistocene-mid Holocene	Qa	Gharibreza (2016); Dolati (2010)
2500	0	2500	mud	0.126	6	≤ 21.3K	Pleistocene-mid Holocene	Qa	Gharibreza (2016); Dolati (2010)
2501	0	2501	mud	0.110	6	≤ 21.3K	Pleistocene-mid Holocene	Qa	Gharibreza (2016); Dolati (2010)
2502	0	2502	mud	0.121	6	≤ 21.3K	Pleistocene-mid Holocene	Qa	Gharibreza (2016); Dolati (2010)

Preview

OBJECTID_1	Join_Count	TARGET_FID	Label	Shape_Area (sqkm)	ORIG_FID	Absolute_Age	Age_paleontology	Unit	Reference
2503	0	2503	mud	0.117	6	≤ 21.3K	Pleistocene-mid Holocene	Qa	Gharibreza (2016); Dolati (2010)
2504	0	2504	mud	0.013	6	≤ 21.3K	Pleistocene-mid Holocene	Qa	Gharibreza (2016); Dolati (2010)
2505	0	2505	mud	0.188	6	≤ 21.3K	Pleistocene-mid Holocene	Qa	Gharibreza (2016); Dolati (2010)
2506	0	2506	mud	0.071	6	≤ 21.3K	Pleistocene-mid Holocene	Qa	Gharibreza (2016); Dolati (2010)
2507	0	2507	mud	0.051	6	≤ 21.3K	Pleistocene-mid Holocene	Qa	Gharibreza (2016); Dolati (2010)
2508	0	2508	mud	0.044	6	≤ 21.3K	Pleistocene-mid Holocene	Qa	Gharibreza (2016); Dolati (2010)
2509	0	2509	mud	0.033	6	≤ 21.3K	Pleistocene-mid Holocene	Qa	Gharibreza (2016); Dolati (2010)
2510	0	2510	mud	0.029	6	≤ 21.3K	Pleistocene-mid Holocene	Qa	Gharibreza (2016); Dolati (2010)
2511	0	2511	mud	0.041	6	≤ 21.3K	Pleistocene-mid Holocene	Qa	Gharibreza (2016); Dolati (2010)
2512	0	2512	mud	0.100	6	≤ 21.3K	Pleistocene-mid Holocene	Qa	Gharibreza (2016); Dolati (2010)
2513	0	2513	mud	0.982	6	≤ 21.3K	Pleistocene-mid Holocene	Qa	Gharibreza (2016); Dolati (2010)
2514	0	2514	mud	0.054	6	≤ 21.3K	Pleistocene-mid Holocene	Qa	Gharibreza (2016); Dolati (2010)
2515	0	2515	mud	0.097	6	≤ 21.3K	Pleistocene-mid Holocene	Qa	Gharibreza (2016); Dolati (2010)
2516	0	2516	mud	0.021	6	≤ 21.3K	Pleistocene-mid Holocene	Qa	Gharibreza (2016); Dolati (2010)
2517	0	2517	mud	0.659	6	≤ 21.3K	Pleistocene-mid Holocene	Qa	Gharibreza (2016); Dolati (2010)
2518	0	2518	mud	0.526	6	≤ 21.3K	Pleistocene-mid Holocene	Qa	Gharibreza (2016); Dolati (2010)
2519	0	2519	mud	0.031	6	≤ 21.3K	Pleistocene-mid Holocene	Qa	Gharibreza (2016); Dolati (2010)
2520	0	2520	mud	0.076	6	≤ 21.3K	Pleistocene-mid Holocene	Qa	Gharibreza (2016); Dolati (2010)
2521	0	2521	mud	0.064	6	≤ 21.3K	Pleistocene-mid Holocene	Qa	Gharibreza (2016); Dolati (2010)
2522	0	2522	mud	0.135	6	≤ 21.3K	Pleistocene-mid Holocene	Qa	Gharibreza (2016); Dolati (2010)
2523	0	2523	mud	0.039	6	≤ 21.3K	Pleistocene-mid Holocene	Qa	Gharibreza (2016); Dolati (2010)
2524	0	2524	mud	0.036	6	≤ 21.3K	Pleistocene-mid Holocene	Qa	Gharibreza (2016); Dolati (2010)
2525	0	2525	mud	0.170	6	≤ 21.3K	Pleistocene-mid Holocene	Qa	Gharibreza (2016); Dolati (2010)
2526	0	2526	mud	0.012	6	≤ 21.3K	Pleistocene-mid Holocene	Qa	Gharibreza (2016); Dolati (2010)
2527	0	2527	mud	0.304	6	≤ 21.3K	Pleistocene-mid Holocene	Qa	Gharibreza (2016); Dolati (2010)
2528	0	2528	mud	0.092	6	≤ 21.3K	Pleistocene-mid Holocene	Qa	Gharibreza (2016); Dolati (2010)
2529	0	2529	mud	0.016	6	≤ 21.3K	Pleistocene-mid Holocene	Qa	Gharibreza (2016); Dolati (2010)
2530	0	2530	mud	0.024	6	≤ 21.3K	Pleistocene-mid Holocene	Qa	Gharibreza (2016); Dolati (2010)
2531	0	2531	mud	0.096	6	≤ 21.3K	Pleistocene-mid Holocene	Qa	Gharibreza (2016); Dolati (2010)
2532	0	2532	mud	0.487	6	≤ 21.3K	Pleistocene-mid Holocene	Qa	Gharibreza (2016); Dolati (2010)
2533	0	2533	mud	2.497	6	≤ 21.3K	Pleistocene-mid Holocene	Qa	Gharibreza (2016); Dolati (2010)
2534	0	2534	mud	0.190	6	≤ 21.3K	Pleistocene-mid Holocene	Qa	Gharibreza (2016); Dolati (2010)
2535	0	2535	mud	0.500	6	≤ 21.3K	Pleistocene-mid Holocene	Qa	Gharibreza (2016); Dolati (2010)
2536	0	2536	mud	0.029	6	≤ 21.3K	Pleistocene-mid Holocene	Qa	Gharibreza (2016); Dolati (2010)
2537	0	2537	mud	0.016	6	≤ 21.3K	Pleistocene-mid Holocene	Qa	Gharibreza (2016); Dolati (2010)
2538	0	2538	mud	0.015	6	≤ 21.3K	Pleistocene-mid Holocene	Qa	Gharibreza (2016); Dolati (2010)
2539	0	2539	mud	0.021	6	≤ 21.3K	Pleistocene-mid Holocene	Qa	Gharibreza (2016); Dolati (2010)
2540	0	2540	mud	0.040	6	≤ 21.3K	Pleistocene-mid Holocene	Qa	Gharibreza (2016); Dolati (2010)
2541	0	2541	mud	0.060	6	≤ 21.3K	Pleistocene-mid Holocene	Qa	Gharibreza (2016); Dolati (2010)

Preview

OBJECTID_1	Join_Count	TARGET_FID	Label	Shape_Area (sqkm)	ORIG_FID	Absolute_Age	Age_paleontology	Unit	Reference
2542	0	2542	mud	0.096	6	≤ 21.3K	Pleistocene-mid Holocene	Qa	Gharibreza (2016); Dolati (2010)
2543	0	2543	mud	0.094	6	≤ 21.3K	Pleistocene-mid Holocene	Qa	Gharibreza (2016); Dolati (2010)
2544	0	2544	mud	1.010	6	≤ 21.3K	Pleistocene-mid Holocene	Qa	Gharibreza (2016); Dolati (2010)
2545	0	2545	mud	0.042	6	≤ 21.3K	Pleistocene-mid Holocene	Qa	Gharibreza (2016); Dolati (2010)
2546	0	2546	mud	0.088	6	≤ 21.3K	Pleistocene-mid Holocene	Qa	Gharibreza (2016); Dolati (2010)
2547	0	2547	mud	0.053	6	≤ 21.3K	Pleistocene-mid Holocene	Qa	Gharibreza (2016); Dolati (2010)
2548	0	2548	mud	0.634	6	≤ 21.3K	Pleistocene-mid Holocene	Qa	Gharibreza (2016); Dolati (2010)
2549	0	2549	mud	0.064	6	≤ 21.3K	Pleistocene-mid Holocene	Qa	Gharibreza (2016); Dolati (2010)
2550	0	2550	mud	0.055	6	≤ 21.3K	Pleistocene-mid Holocene	Qa	Gharibreza (2016); Dolati (2010)
2551	0	2551	mud	0.013	6	≤ 21.3K	Pleistocene-mid Holocene	Qa	Gharibreza (2016); Dolati (2010)
2552	0	2552	mud	0.144	6	≤ 21.3K	Pleistocene-mid Holocene	Qa	Gharibreza (2016); Dolati (2010)
2553	0	2553	mud	0.103	6	≤ 21.3K	Pleistocene-mid Holocene	Qa	Gharibreza (2016); Dolati (2010)
2554	0	2554	mud	0.060	6	≤ 21.3K	Pleistocene-mid Holocene	Qa	Gharibreza (2016); Dolati (2010)
2555	0	2555	mud	0.089	6	≤ 21.3K	Pleistocene-mid Holocene	Qa	Gharibreza (2016); Dolati (2010)
2556	0	2556	mud	0.048	6	≤ 21.3K	Pleistocene-mid Holocene	Qa	Gharibreza (2016); Dolati (2010)
2557	0	2557	mud	0.124	6	≤ 21.3K	Pleistocene-mid Holocene	Qa	Gharibreza (2016); Dolati (2010)
2558	0	2558	mud	1.010	6	≤ 21.3K	Pleistocene-mid Holocene	Qa	Gharibreza (2016); Dolati (2010)
2559	0	2559	mud	0.088	6	≤ 21.3K	Pleistocene-mid Holocene	Qa	Gharibreza (2016); Dolati (2010)
2560	0	2560	mud	0.019	6	≤ 21.3K	Pleistocene-mid Holocene	Qa	Gharibreza (2016); Dolati (2010)
2561	0	2561	mud	0.013	6	≤ 21.3K	Pleistocene-mid Holocene	Qa	Gharibreza (2016); Dolati (2010)
2562	0	2562	mud	0.027	6	≤ 21.3K	Pleistocene-mid Holocene	Qa	Gharibreza (2016); Dolati (2010)
2563	0	2563	mud	0.030	6	≤ 21.3K	Pleistocene-mid Holocene	Qa	Gharibreza (2016); Dolati (2010)
2564	0	2564	mud	0.015	6	≤ 21.3K	Pleistocene-mid Holocene	Qa	Gharibreza (2016); Dolati (2010)
2565	0	2565	mud	0.009	6	≤ 21.3K	Pleistocene-mid Holocene	Qa	Gharibreza (2016); Dolati (2010)
2566	0	2566	mud	0.691	6	≤ 21.3K	Pleistocene-mid Holocene	Qa	Gharibreza (2016); Dolati (2010)
2567	0	2567	mud	0.023	6	≤ 21.3K	Pleistocene-mid Holocene	Qa	Gharibreza (2016); Dolati (2010)
2568	0	2568	mud	0.231	6	≤ 21.3K	Pleistocene-mid Holocene	Qa	Gharibreza (2016); Dolati (2010)
2569	0	2569	mud	0.119	6	≤ 21.3K	Pleistocene-mid Holocene	Qa	Gharibreza (2016); Dolati (2010)
2570	0	2570	mud	0.165	6	≤ 21.3K	Pleistocene-mid Holocene	Qa	Gharibreza (2016); Dolati (2010)
2571	0	2571	mud	0.109	6	≤ 21.3K	Pleistocene-mid Holocene	Qa	Gharibreza (2016); Dolati (2010)
2572	0	2572	mud	0.011	6	≤ 21.3K	Pleistocene-mid Holocene	Qa	Gharibreza (2016); Dolati (2010)
2573	0	2573	mud	0.224	6	≤ 21.3K	Pleistocene-mid Holocene	Qa	Gharibreza (2016); Dolati (2010)
2574	0	2574	mud	0.071	6	≤ 21.3K	Pleistocene-mid Holocene	Qa	Gharibreza (2016); Dolati (2010)
2575	0	2575	mud	0.022	6	≤ 21.3K	Pleistocene-mid Holocene	Qa	Gharibreza (2016); Dolati (2010)
2576	0	2576	mud	0.263	6	≤ 21.3K	Pleistocene-mid Holocene	Qa	Gharibreza (2016); Dolati (2010)
2577	0	2577	mud	0.176	6	≤ 21.3K	Pleistocene-mid Holocene	Qa	Gharibreza (2016); Dolati (2010)
2578	0	2578	mud	0.015	6	≤ 21.3K	Pleistocene-mid Holocene	Qa	Gharibreza (2016); Dolati (2010)
2579	0	2579	mud	0.002	6	≤ 21.3K	Pleistocene-mid Holocene	Qa	Gharibreza (2016); Dolati (2010)
2580	0	2580	mud	0.082	6	≤ 21.3K	Pleistocene-mid Holocene	Qa	Gharibreza (2016); Dolati (2010)

Preview

OBJECTID_1	Join_Count	TARGET_FID	Label	Shape_Area (sqkm)	ORIG_FID	Absolute_Age	Age_paleontology	Unit	Reference
2581	0	2581	mud	0.291	6	≤ 21.3K	Pleistocene-mid Holocene	Qa	Gharibreza (2016); Dolati (2010)
2582	0	2582	mud	0.280	6	≤ 21.3K	Pleistocene-mid Holocene	Qa	Gharibreza (2016); Dolati (2010)
2583	0	2583	mud	0.372	6	≤ 21.3K	Pleistocene-mid Holocene	Qa	Gharibreza (2016); Dolati (2010)
2584	0	2584	mud	0.106	6	≤ 21.3K	Pleistocene-mid Holocene	Qa	Gharibreza (2016); Dolati (2010)
2585	0	2585	mud	0.036	6	≤ 21.3K	Pleistocene-mid Holocene	Qa	Gharibreza (2016); Dolati (2010)
2586	0	2586	mud	0.122	6	≤ 21.3K	Pleistocene-mid Holocene	Qa	Gharibreza (2016); Dolati (2010)
2587	0	2587	mud	0.001	6	≤ 21.3K	Pleistocene-mid Holocene	Qa	Gharibreza (2016); Dolati (2010)
2588	0	2588	mud	0.090	6	≤ 21.3K	Pleistocene-mid Holocene	Qa	Gharibreza (2016); Dolati (2010)
2589	0	2589	mud	0.013	6	≤ 21.3K	Pleistocene-mid Holocene	Qa	Gharibreza (2016); Dolati (2010)
2590	0	2590	mud	0.054	6	≤ 21.3K	Pleistocene-mid Holocene	Qa	Gharibreza (2016); Dolati (2010)
2591	0	2591	mud	0.195	6	≤ 21.3K	Pleistocene-mid Holocene	Qa	Gharibreza (2016); Dolati (2010)
2592	0	2592	mud	0.022	6	≤ 21.3K	Pleistocene-mid Holocene	Qa	Gharibreza (2016); Dolati (2010)
2593	0	2593	mud	0.016	6	≤ 21.3K	Pleistocene-mid Holocene	Qa	Gharibreza (2016); Dolati (2010)
2594	0	2594	mud	1.050	6	≤ 21.3K	Pleistocene-mid Holocene	Qa	Gharibreza (2016); Dolati (2010)
2595	0	2595	mud	0.163	6	≤ 21.3K	Pleistocene-mid Holocene	Qa	Gharibreza (2016); Dolati (2010)
2596	0	2596	mud	0.017	6	≤ 21.3K	Pleistocene-mid Holocene	Qa	Gharibreza (2016); Dolati (2010)
2597	0	2597	mud	0.046	6	≤ 21.3K	Pleistocene-mid Holocene	Qa	Gharibreza (2016); Dolati (2010)
2598	0	2598	mud	0.035	6	≤ 21.3K	Pleistocene-mid Holocene	Qa	Gharibreza (2016); Dolati (2010)
2599	0	2599	mud	0.049	6	≤ 21.3K	Pleistocene-mid Holocene	Qa	Gharibreza (2016); Dolati (2010)
2600	0	2600	mud	0.044	6	≤ 21.3K	Pleistocene-mid Holocene	Qa	Gharibreza (2016); Dolati (2010)
2602	0	2602	mud	0.060	6	≤ 21.3K	Pleistocene-mid Holocene	Qa	Gharibreza (2016); Dolati (2010)
2603	0	2603	mud	0.018	6	≤ 21.3K	Pleistocene-mid Holocene	Qa	Gharibreza (2016); Dolati (2010)
2604	0	2604	mud	0.000	6	≤ 21.3K	Pleistocene-mid Holocene	Qa	Gharibreza (2016); Dolati (2010)
2605	0	2605	mud	0.002	6	≤ 21.3K	Pleistocene-mid Holocene	Qa	Gharibreza (2016); Dolati (2010)
2606	0	2606	mud	0.415	6	≤ 21.3K	Pleistocene-mid Holocene	Qa	Gharibreza (2016); Dolati (2010)
2607	0	2607	mud	2.445	6	≤ 21.3K	Pleistocene-mid Holocene	Qa	Gharibreza (2016); Dolati (2010)
2608	0	2608	mud	0.420	6	≤ 21.3K	Pleistocene-mid Holocene	Qa	Gharibreza (2016); Dolati (2010)
2609	0	2609	mud	0.168	6	≤ 21.3K	Pleistocene-mid Holocene	Qa	Gharibreza (2016); Dolati (2010)
2610	0	2610	mud	0.041	6	≤ 21.3K	Pleistocene-mid Holocene	Qa	Gharibreza (2016); Dolati (2010)
2611	0	2611	mud	0.020	6	≤ 21.3K	Pleistocene-mid Holocene	Qa	Gharibreza (2016); Dolati (2010)
2612	0	2612	mud	0.064	6	≤ 21.3K	Pleistocene-mid Holocene	Qa	Gharibreza (2016); Dolati (2010)
2613	0	2613	mud	0.059	6	≤ 21.3K	Pleistocene-mid Holocene	Qa	Gharibreza (2016); Dolati (2010)
2614	0	2614	mud	0.056	6	≤ 21.3K	Pleistocene-mid Holocene	Qa	Gharibreza (2016); Dolati (2010)
2615	0	2615	mud	0.011	6	≤ 21.3K	Pleistocene-mid Holocene	Qa	Gharibreza (2016); Dolati (2010)
2616	0	2616	mud	0.334	6	≤ 21.3K	Pleistocene-mid Holocene	Qa	Gharibreza (2016); Dolati (2010)
2617	0	2617	mud	1.796	6	≤ 21.3K	Pleistocene-mid Holocene	Qa	Gharibreza (2016); Dolati (2010)
2618	0	2618	mud	0.013	6	≤ 21.3K	Pleistocene-mid Holocene	Qa	Gharibreza (2016); Dolati (2010)
2619	0	2619	mud	23.532	6	≤ 21.3K	Pleistocene-mid Holocene	Qa	Gharibreza (2016); Dolati (2010)
2620	0	2620	mud	0.280	6	≤ 21.3K	Pleistocene-mid Holocene	Qa	Gharibreza (2016); Dolati (2010)

Preview

OBJECTID_1	Join_Count	TARGET_FID	Label	Shape_Area (sqkm)	ORIG_FID	Absolute_Age	Age_paleontology	Unit	Reference
2621	0	2621	mud	0.154	6	≤ 21.3K	Pleistocene-mid Holocene	Qa	Gharibreza (2016); Dolati (2010)
2622	0	2622	mud	0.043	6	≤ 21.3K	Pleistocene-mid Holocene	Qa	Gharibreza (2016); Dolati (2010)
2623	0	2623	mud	0.048	6	≤ 21.3K	Pleistocene-mid Holocene	Qa	Gharibreza (2016); Dolati (2010)
2624	0	2624	mud	0.088	6	≤ 21.3K	Pleistocene-mid Holocene	Qa	Gharibreza (2016); Dolati (2010)
2625	0	2625	mud	0.332	6	≤ 21.3K	Pleistocene-mid Holocene	Qa	Gharibreza (2016); Dolati (2010)
2626	0	2626	mud	0.060	6	≤ 21.3K	Pleistocene-mid Holocene	Qa	Gharibreza (2016); Dolati (2010)
2627	0	2627	mud	0.046	6	≤ 21.3K	Pleistocene-mid Holocene	Qa	Gharibreza (2016); Dolati (2010)
2628	0	2628	mud	0.023	6	≤ 21.3K	Pleistocene-mid Holocene	Qa	Gharibreza (2016); Dolati (2010)
2629	0	2629	mud	0.087	6	≤ 21.3K	Pleistocene-mid Holocene	Qa	Gharibreza (2016); Dolati (2010)
2630	0	2630	mud	0.022	6	≤ 21.3K	Pleistocene-mid Holocene	Qa	Gharibreza (2016); Dolati (2010)
2631	0	2631	mud	0.022	6	≤ 21.3K	Pleistocene-mid Holocene	Qa	Gharibreza (2016); Dolati (2010)
2632	0	2632	mud	0.040	6	≤ 21.3K	Pleistocene-mid Holocene	Qa	Gharibreza (2016); Dolati (2010)
2633	0	2633	mud	0.011	6	≤ 21.3K	Pleistocene-mid Holocene	Qa	Gharibreza (2016); Dolati (2010)
2634	0	2634	mud	0.030	6	≤ 21.3K	Pleistocene-mid Holocene	Qa	Gharibreza (2016); Dolati (2010)
2635	0	2635	mud	0.013	6	≤ 21.3K	Pleistocene-mid Holocene	Qa	Gharibreza (2016); Dolati (2010)
2636	0	2636	mud	0.120	6	≤ 21.3K	Pleistocene-mid Holocene	Qa	Gharibreza (2016); Dolati (2010)
2637	0	2637	mud	0.238	6	≤ 21.3K	Pleistocene-mid Holocene	Qa	Gharibreza (2016); Dolati (2010)
2638	0	2638	mud	0.104	6	≤ 21.3K	Pleistocene-mid Holocene	Qa	Gharibreza (2016); Dolati (2010)
2639	0	2639	mud	0.280	6	≤ 21.3K	Pleistocene-mid Holocene	Qa	Gharibreza (2016); Dolati (2010)
2640	0	2640	mud	0.052	6	≤ 21.3K	Pleistocene-mid Holocene	Qa	Gharibreza (2016); Dolati (2010)
2641	0	2641	mud	0.020	6	≤ 21.3K	Pleistocene-mid Holocene	Qa	Gharibreza (2016); Dolati (2010)
2642	0	2642	mud	0.023	6	≤ 21.3K	Pleistocene-mid Holocene	Qa	Gharibreza (2016); Dolati (2010)
2643	0	2643	mud	0.017	6	≤ 21.3K	Pleistocene-mid Holocene	Qa	Gharibreza (2016); Dolati (2010)
2644	0	2644	mud	0.129	6	≤ 21.3K	Pleistocene-mid Holocene	Qa	Gharibreza (2016); Dolati (2010)
2645	0	2645	mud	1.375	6	≤ 21.3K	Pleistocene-mid Holocene	Qa	Gharibreza (2016); Dolati (2010)
2646	0	2646	mud	0.178	6	≤ 21.3K	Pleistocene-mid Holocene	Qa	Gharibreza (2016); Dolati (2010)
2647	0	2647	mud	0.249	6	≤ 21.3K	Pleistocene-mid Holocene	Qa	Gharibreza (2016); Dolati (2010)
2648	0	2648	mud	0.085	6	≤ 21.3K	Pleistocene-mid Holocene	Qa	Gharibreza (2016); Dolati (2010)
2649	0	2649	mud	0.068	6	≤ 21.3K	Pleistocene-mid Holocene	Qa	Gharibreza (2016); Dolati (2010)
2650	0	2650	mud	0.147	6	≤ 21.3K	Pleistocene-mid Holocene	Qa	Gharibreza (2016); Dolati (2010)
2651	0	2651	mud	0.158	6	≤ 21.3K	Pleistocene-mid Holocene	Qa	Gharibreza (2016); Dolati (2010)
2652	0	2652	mud	0.051	6	≤ 21.3K	Pleistocene-mid Holocene	Qa	Gharibreza (2016); Dolati (2010)
2653	0	2653	mud	0.242	6	≤ 21.3K	Pleistocene-mid Holocene	Qa	Gharibreza (2016); Dolati (2010)
2654	0	2654	mud	0.033	6	≤ 21.3K	Pleistocene-mid Holocene	Qa	Gharibreza (2016); Dolati (2010)
2655	0	2655	mud	0.097	6	≤ 21.3K	Pleistocene-mid Holocene	Qa	Gharibreza (2016); Dolati (2010)
2656	0	2656	mud	0.146	6	≤ 21.3K	Pleistocene-mid Holocene	Qa	Gharibreza (2016); Dolati (2010)
2657	0	2657	mud	0.030	6	≤ 21.3K	Pleistocene-mid Holocene	Qa	Gharibreza (2016); Dolati (2010)
2658	0	2658	mud	0.150	6	≤ 21.3K	Pleistocene-mid Holocene	Qa	Gharibreza (2016); Dolati (2010)
2659	0	2659	mud	0.081	6	≤ 21.3K	Pleistocene-mid Holocene	Qa	Gharibreza (2016); Dolati (2010)

Preview

OBJECTID_1	Join_Count	TARGET_FID	Label	Shape_Area (sqkm)	ORIG_FID	Absolute_Age	Age_paleontology	Unit	Reference
2660	0	2660	mud	0.050	6	≤ 21.3K	Pleistocene-mid Holocene	Qa	Gharibreza (2016); Dolati (2010)
2661	0	2661	mud	0.102	6	≤ 21.3K	Pleistocene-mid Holocene	Qa	Gharibreza (2016); Dolati (2010)
2662	0	2662	mud	0.502	6	≤ 21.3K	Pleistocene-mid Holocene	Qa	Gharibreza (2016); Dolati (2010)
2663	0	2663	mud	0.027	6	≤ 21.3K	Pleistocene-mid Holocene	Qa	Gharibreza (2016); Dolati (2010)
2664	0	2664	mud	0.629	6	≤ 21.3K	Pleistocene-mid Holocene	Qa	Gharibreza (2016); Dolati (2010)
2665	0	2665	mud	0.033	6	≤ 21.3K	Pleistocene-mid Holocene	Qa	Gharibreza (2016); Dolati (2010)
2666	0	2666	mud	0.131	6	≤ 21.3K	Pleistocene-mid Holocene	Qa	Gharibreza (2016); Dolati (2010)
2667	0	2667	mud	0.086	6	≤ 21.3K	Pleistocene-mid Holocene	Qa	Gharibreza (2016); Dolati (2010)
2668	0	2668	mud	0.038	6	≤ 21.3K	Pleistocene-mid Holocene	Qa	Gharibreza (2016); Dolati (2010)
2669	0	2669	mud	0.033	6	≤ 21.3K	Pleistocene-mid Holocene	Qa	Gharibreza (2016); Dolati (2010)
2670	0	2670	mud	0.048	6	≤ 21.3K	Pleistocene-mid Holocene	Qa	Gharibreza (2016); Dolati (2010)
2671	0	2671	mud	0.177	6	≤ 21.3K	Pleistocene-mid Holocene	Qa	Gharibreza (2016); Dolati (2010)
2672	0	2672	mud	0.049	6	≤ 21.3K	Pleistocene-mid Holocene	Qa	Gharibreza (2016); Dolati (2010)
2673	0	2673	mud	0.019	6	≤ 21.3K	Pleistocene-mid Holocene	Qa	Gharibreza (2016); Dolati (2010)
2674	0	2674	mud	0.060	6	≤ 21.3K	Pleistocene-mid Holocene	Qa	Gharibreza (2016); Dolati (2010)
2675	0	2675	mud	0.019	6	≤ 21.3K	Pleistocene-mid Holocene	Qa	Gharibreza (2016); Dolati (2010)
2676	0	2676	mud	0.164	6	≤ 21.3K	Pleistocene-mid Holocene	Qa	Gharibreza (2016); Dolati (2010)
2677	0	2677	mud	0.117	6	≤ 21.3K	Pleistocene-mid Holocene	Qa	Gharibreza (2016); Dolati (2010)
2678	0	2678	mud	0.012	6	≤ 21.3K	Pleistocene-mid Holocene	Qa	Gharibreza (2016); Dolati (2010)
2679	0	2679	mud	0.058	6	≤ 21.3K	Pleistocene-mid Holocene	Qa	Gharibreza (2016); Dolati (2010)
2680	0	2680	mud	0.035	6	≤ 21.3K	Pleistocene-mid Holocene	Qa	Gharibreza (2016); Dolati (2010)
2681	0	2681	mud	0.039	6	≤ 21.3K	Pleistocene-mid Holocene	Qa	Gharibreza (2016); Dolati (2010)
2682	0	2682	mud	0.118	6	≤ 21.3K	Pleistocene-mid Holocene	Qa	Gharibreza (2016); Dolati (2010)
2683	0	2683	mud	0.038	6	≤ 21.3K	Pleistocene-mid Holocene	Qa	Gharibreza (2016); Dolati (2010)
2684	0	2684	mud	0.031	6	≤ 21.3K	Pleistocene-mid Holocene	Qa	Gharibreza (2016); Dolati (2010)
2685	0	2685	mud	0.858	6	≤ 21.3K	Pleistocene-mid Holocene	Qa	Gharibreza (2016); Dolati (2010)
2686	0	2686	mud	0.130	6	≤ 21.3K	Pleistocene-mid Holocene	Qa	Gharibreza (2016); Dolati (2010)
2687	0	2687	mud	0.010	6	≤ 21.3K	Pleistocene-mid Holocene	Qa	Gharibreza (2016); Dolati (2010)
2688	0	2688	mud	0.067	6	≤ 21.3K	Pleistocene-mid Holocene	Qa	Gharibreza (2016); Dolati (2010)
2689	0	2689	mud	0.036	6	≤ 21.3K	Pleistocene-mid Holocene	Qa	Gharibreza (2016); Dolati (2010)
2690	0	2690	mud	0.073	6	≤ 21.3K	Pleistocene-mid Holocene	Qa	Gharibreza (2016); Dolati (2010)
2691	0	2691	mud	182.879	6	≤ 21.3K	Pleistocene-mid Holocene	Qa	Gharibreza (2016); Dolati (2010)
2692	0	2692	mud	0.069	6	≤ 21.3K	Pleistocene-mid Holocene	Qa	Gharibreza (2016); Dolati (2010)
2693	0	2693	mud	0.027	6	≤ 21.3K	Pleistocene-mid Holocene	Qa	Gharibreza (2016); Dolati (2010)
2694	0	2694	mud	0.350	6	≤ 21.3K	Pleistocene-mid Holocene	Qa	Gharibreza (2016); Dolati (2010)
2695	0	2695	mud	0.024	6	≤ 21.3K	Pleistocene-mid Holocene	Qa	Gharibreza (2016); Dolati (2010)
2696	0	2696	mud	0.055	6	≤ 21.3K	Pleistocene-mid Holocene	Qa	Gharibreza (2016); Dolati (2010)
2697	0	2697	mud	6.776	6	≤ 21.3K	Pleistocene-mid Holocene	Qa	Gharibreza (2016); Dolati (2010)
2698	0	2698	mud	0.004	6	≤ 21.3K	Pleistocene-mid Holocene	Qa	Gharibreza (2016); Dolati (2010)

Preview

OBJECTID_1	Join_Count	TARGET_FID	Label	Shape_Area (sqkm)	ORIG_FID	Absolute_Age	Age_paleontology	Unit	Reference
2700	0	2700	mud	0.227	6	≤ 21.3K	Pleistocene-mid Holocene	Qa	Gharibreza (2016); Dolati (2010)
2701	0	2701	mud	0.108	6	≤ 21.3K	Pleistocene-mid Holocene	Qa	Gharibreza (2016); Dolati (2010)
2702	0	2702	mud	0.077	6	≤ 21.3K	Pleistocene-mid Holocene	Qa	Gharibreza (2016); Dolati (2010)
2703	0	2703	mud	1.041	6	≤ 21.3K	Pleistocene-mid Holocene	Qa	Gharibreza (2016); Dolati (2010)
2704	0	2704	mud	0.261	6	≤ 21.3K	Pleistocene-mid Holocene	Qa	Gharibreza (2016); Dolati (2010)
2705	0	2705	mud	0.032	6	≤ 21.3K	Pleistocene-mid Holocene	Qa	Gharibreza (2016); Dolati (2010)
2706	0	2706	mud	0.581	6	≤ 21.3K	Pleistocene-mid Holocene	Qa	Gharibreza (2016); Dolati (2010)
2707	0	2707	mud	0.043	6	≤ 21.3K	Pleistocene-mid Holocene	Qa	Gharibreza (2016); Dolati (2010)
2708	0	2708	mud	0.051	6	≤ 21.3K	Pleistocene-mid Holocene	Qa	Gharibreza (2016); Dolati (2010)
2709	0	2709	mud	0.591	6	≤ 21.3K	Pleistocene-mid Holocene	Qa	Gharibreza (2016); Dolati (2010)
2710	0	2710	mud	0.070	6	≤ 21.3K	Pleistocene-mid Holocene	Qa	Gharibreza (2016); Dolati (2010)
2711	0	2711	mud	0.169	6	≤ 21.3K	Pleistocene-mid Holocene	Qa	Gharibreza (2016); Dolati (2010)
2712	0	2712	mud	0.032	6	≤ 21.3K	Pleistocene-mid Holocene	Qa	Gharibreza (2016); Dolati (2010)
2713	0	2713	mud	0.113	6	≤ 21.3K	Pleistocene-mid Holocene	Qa	Gharibreza (2016); Dolati (2010)
2714	0	2714	mud	0.414	6	≤ 21.3K	Pleistocene-mid Holocene	Qa	Gharibreza (2016); Dolati (2010)
2715	0	2715	mud	0.152	6	≤ 21.3K	Pleistocene-mid Holocene	Qa	Gharibreza (2016); Dolati (2010)
2716	0	2716	mud	0.190	6	≤ 21.3K	Pleistocene-mid Holocene	Qa	Gharibreza (2016); Dolati (2010)
2717	0	2717	mud	0.292	6	≤ 21.3K	Pleistocene-mid Holocene	Qa	Gharibreza (2016); Dolati (2010)
2718	0	2718	mud	2.570	6	≤ 21.3K	Pleistocene-mid Holocene	Qa	Gharibreza (2016); Dolati (2010)
2719	0	2719	mud	0.024	6	≤ 21.3K	Pleistocene-mid Holocene	Qa	Gharibreza (2016); Dolati (2010)
2720	0	2720	mud	0.080	6	≤ 21.3K	Pleistocene-mid Holocene	Qa	Gharibreza (2016); Dolati (2010)
2721	0	2721	mud	0.355	6	≤ 21.3K	Pleistocene-mid Holocene	Qa	Gharibreza (2016); Dolati (2010)
2722	0	2722	mud	0.060	6	≤ 21.3K	Pleistocene-mid Holocene	Qa	Gharibreza (2016); Dolati (2010)
2723	0	2723	mud	0.010	6	≤ 21.3K	Pleistocene-mid Holocene	Qa	Gharibreza (2016); Dolati (2010)
2724	0	2724	mud	0.278	6	≤ 21.3K	Pleistocene-mid Holocene	Qa	Gharibreza (2016); Dolati (2010)
2725	0	2725	mud	0.039	6	≤ 21.3K	Pleistocene-mid Holocene	Qa	Gharibreza (2016); Dolati (2010)
2726	0	2726	mud	0.068	6	≤ 21.3K	Pleistocene-mid Holocene	Qa	Gharibreza (2016); Dolati (2010)
2727	0	2727	mud	0.297	6	≤ 21.3K	Pleistocene-mid Holocene	Qa	Gharibreza (2016); Dolati (2010)
2728	0	2728	mud	0.115	6	≤ 21.3K	Pleistocene-mid Holocene	Qa	Gharibreza (2016); Dolati (2010)
2729	0	2729	mud	0.085	6	≤ 21.3K	Pleistocene-mid Holocene	Qa	Gharibreza (2016); Dolati (2010)
2730	0	2730	mud	0.080	6	≤ 21.3K	Pleistocene-mid Holocene	Qa	Gharibreza (2016); Dolati (2010)
2731	0	2731	mud	0.313	6	≤ 21.3K	Pleistocene-mid Holocene	Qa	Gharibreza (2016); Dolati (2010)
2732	0	2732	mud	0.054	6	≤ 21.3K	Pleistocene-mid Holocene	Qa	Gharibreza (2016); Dolati (2010)
2733	0	2733	mud	1.335	6	≤ 21.3K	Pleistocene-mid Holocene	Qa	Gharibreza (2016); Dolati (2010)
2734	0	2734	mud	1.202	6	≤ 21.3K	Pleistocene-mid Holocene	Qa	Gharibreza (2016); Dolati (2010)
2735	0	2735	mud	0.373	6	≤ 21.3K	Pleistocene-mid Holocene	Qa	Gharibreza (2016); Dolati (2010)
2736	0	2736	mud	0.347	6	≤ 21.3K	Pleistocene-mid Holocene	Qa	Gharibreza (2016); Dolati (2010)
2737	0	2737	mud	0.084	6	≤ 21.3K	Pleistocene-mid Holocene	Qa	Gharibreza (2016); Dolati (2010)
2738	0	2738	mud	0.037	6	≤ 21.3K	Pleistocene-mid Holocene	Qa	Gharibreza (2016); Dolati (2010)

Preview

OBJECTID_1	Join_Count	TARGET_FID	Label	Shape_Area (sqkm)	ORIG_FID	Absolute_Age	Age_paleontology	Unit	Reference
2739	0	2739	mud	0.005	6	≤ 21.3K	Pleistocene-mid Holocene	Qa	Gharibreza (2016); Dolati (2010)
2740	0	2740	mud	0.041	6	≤ 21.3K	Pleistocene-mid Holocene	Qa	Gharibreza (2016); Dolati (2010)
2741	0	2741	mud	0.022	6	≤ 21.3K	Pleistocene-mid Holocene	Qa	Gharibreza (2016); Dolati (2010)
2742	0	2742	mud	0.257	6	≤ 21.3K	Pleistocene-mid Holocene	Qa	Gharibreza (2016); Dolati (2010)
2743	0	2743	mud	0.121	6	≤ 21.3K	Pleistocene-mid Holocene	Qa	Gharibreza (2016); Dolati (2010)
2744	0	2744	mud	6.692	6	≤ 21.3K	Pleistocene-mid Holocene	Qa	Gharibreza (2016); Dolati (2010)
2745	0	2745	mud	0.027	6	≤ 21.3K	Pleistocene-mid Holocene	Qa	Gharibreza (2016); Dolati (2010)
2748	0	2748	mud	0.176	6	≤ 21.3K	Pleistocene-mid Holocene	Qa	Gharibreza (2016); Dolati (2010)
2749	0	2749	mud	0.003	6	≤ 21.3K	Pleistocene-mid Holocene	Qa	Gharibreza (2016); Dolati (2010)
2750	0	2750	mud	0.018	6	≤ 21.3K	Pleistocene-mid Holocene	Qa	Gharibreza (2016); Dolati (2010)
2751	0	2751	mud	0.062	6	≤ 21.3K	Pleistocene-mid Holocene	Qa	Gharibreza (2016); Dolati (2010)
2752	0	2752	mud	0.283	6	≤ 21.3K	Pleistocene-mid Holocene	Qa	Gharibreza (2016); Dolati (2010)
2753	0	2753	mud	0.237	6	≤ 21.3K	Pleistocene-mid Holocene	Qa	Gharibreza (2016); Dolati (2010)
2754	0	2754	mud	0.020	6	≤ 21.3K	Pleistocene-mid Holocene	Qa	Gharibreza (2016); Dolati (2010)
2755	0	2755	mud	0.014	6	≤ 21.3K	Pleistocene-mid Holocene	Qa	Gharibreza (2016); Dolati (2010)
2756	0	2756	mud	0.031	6	≤ 21.3K	Pleistocene-mid Holocene	Qa	Gharibreza (2016); Dolati (2010)
2757	0	2757	mud	1.802	6	≤ 21.3K	Pleistocene-mid Holocene	Qa	Gharibreza (2016); Dolati (2010)
2758	0	2758	mud	0.031	6	≤ 21.3K	Pleistocene-mid Holocene	Qa	Gharibreza (2016); Dolati (2010)
2759	0	2759	mud	0.014	6	≤ 21.3K	Pleistocene-mid Holocene	Qa	Gharibreza (2016); Dolati (2010)
2760	0	2760	mud	0.025	6	≤ 21.3K	Pleistocene-mid Holocene	Qa	Gharibreza (2016); Dolati (2010)
2761	0	2761	mud	0.049	6	≤ 21.3K	Pleistocene-mid Holocene	Qa	Gharibreza (2016); Dolati (2010)
2762	0	2762	mud	0.027	6	≤ 21.3K	Pleistocene-mid Holocene	Qa	Gharibreza (2016); Dolati (2010)
2763	0	2763	mud	0.425	6	≤ 21.3K	Pleistocene-mid Holocene	Qa	Gharibreza (2016); Dolati (2010)
2764	0	2764	mud	0.079	6	≤ 21.3K	Pleistocene-mid Holocene	Qa	Gharibreza (2016); Dolati (2010)
2765	0	2765	mud	0.041	6	≤ 21.3K	Pleistocene-mid Holocene	Qa	Gharibreza (2016); Dolati (2010)
2766	0	2766	mud	0.105	6	≤ 21.3K	Pleistocene-mid Holocene	Qa	Gharibreza (2016); Dolati (2010)
2767	0	2767	mud	0.116	6	≤ 21.3K	Pleistocene-mid Holocene	Qa	Gharibreza (2016); Dolati (2010)
2768	0	2768	mud	0.063	6	≤ 21.3K	Pleistocene-mid Holocene	Qa	Gharibreza (2016); Dolati (2010)
2769	0	2769	mud	0.182	6	≤ 21.3K	Pleistocene-mid Holocene	Qa	Gharibreza (2016); Dolati (2010)
2770	0	2770	mud	0.016	6	≤ 21.3K	Pleistocene-mid Holocene	Qa	Gharibreza (2016); Dolati (2010)
2771	0	2771	mud	0.789	6	≤ 21.3K	Pleistocene-mid Holocene	Qa	Gharibreza (2016); Dolati (2010)
2772	0	2772	mud	0.116	6	≤ 21.3K	Pleistocene-mid Holocene	Qa	Gharibreza (2016); Dolati (2010)
2773	0	2773	mud	0.163	6	≤ 21.3K	Pleistocene-mid Holocene	Qa	Gharibreza (2016); Dolati (2010)
2774	0	2774	mud	0.142	6	≤ 21.3K	Pleistocene-mid Holocene	Qa	Gharibreza (2016); Dolati (2010)
2775	0	2775	mud	0.211	6	≤ 21.3K	Pleistocene-mid Holocene	Qa	Gharibreza (2016); Dolati (2010)
2776	0	2776	mud	0.015	6	≤ 21.3K	Pleistocene-mid Holocene	Qa	Gharibreza (2016); Dolati (2010)
2777	0	2777	mud	0.017	6	≤ 21.3K	Pleistocene-mid Holocene	Qa	Gharibreza (2016); Dolati (2010)
2778	0	2778	mud	0.061	6	≤ 21.3K	Pleistocene-mid Holocene	Qa	Gharibreza (2016); Dolati (2010)
2779	0	2779	mud	0.036	6	≤ 21.3K	Pleistocene-mid Holocene	Qa	Gharibreza (2016); Dolati (2010)

Preview

OBJECTID_1	Join_Count	TARGET_FID	Label	Shape_Area (sqkm)	ORIG_FID	Absolute_Age	Age_paleontology	Unit	Reference
2780	0	2780	mud	1.888	6	≤ 21.3K	Pleistocene-mid Holocene	Qa	Gharibreza (2016); Dolati (2010)
2781	0	2781	mud	0.030	6	≤ 21.3K	Pleistocene-mid Holocene	Qa	Gharibreza (2016); Dolati (2010)
2782	0	2782	mud	0.051	6	≤ 21.3K	Pleistocene-mid Holocene	Qa	Gharibreza (2016); Dolati (2010)
2783	0	2783	mud	0.089	6	≤ 21.3K	Pleistocene-mid Holocene	Qa	Gharibreza (2016); Dolati (2010)
2784	0	2784	mud	0.065	6	≤ 21.3K	Pleistocene-mid Holocene	Qa	Gharibreza (2016); Dolati (2010)
2785	0	2785	mud	0.142	6	≤ 21.3K	Pleistocene-mid Holocene	Qa	Gharibreza (2016); Dolati (2010)
2786	0	2786	mud	0.043	6	≤ 21.3K	Pleistocene-mid Holocene	Qa	Gharibreza (2016); Dolati (2010)
2787	0	2787	mud	0.689	6	≤ 21.3K	Pleistocene-mid Holocene	Qa	Gharibreza (2016); Dolati (2010)
2788	0	2788	mud	0.007	6	≤ 21.3K	Pleistocene-mid Holocene	Qa	Gharibreza (2016); Dolati (2010)
2789	0	2789	mud	0.305	6	≤ 21.3K	Pleistocene-mid Holocene	Qa	Gharibreza (2016); Dolati (2010)
2790	0	2790	mud	1.282	6	≤ 21.3K	Pleistocene-mid Holocene	Qa	Gharibreza (2016); Dolati (2010)
2791	0	2791	mud	0.206	6	≤ 21.3K	Pleistocene-mid Holocene	Qa	Gharibreza (2016); Dolati (2010)
2792	0	2792	mud	0.006	6	≤ 21.3K	Pleistocene-mid Holocene	Qa	Gharibreza (2016); Dolati (2010)
2793	0	2793	mud	0.033	6	≤ 21.3K	Pleistocene-mid Holocene	Qa	Gharibreza (2016); Dolati (2010)
2795	0	2795	mud	0.062	6	≤ 21.3K	Pleistocene-mid Holocene	Qa	Gharibreza (2016); Dolati (2010)
2796	0	2796	mud	0.008	6	≤ 21.3K	Pleistocene-mid Holocene	Qa	Gharibreza (2016); Dolati (2010)
2797	0	2797	mud	0.020	6	≤ 21.3K	Pleistocene-mid Holocene	Qa	Gharibreza (2016); Dolati (2010)
2798	0	2798	mud	3.809	6	≤ 21.3K	Pleistocene-mid Holocene	Qa	Gharibreza (2016); Dolati (2010)
2799	0	2799	mud	0.142	6	≤ 21.3K	Pleistocene-mid Holocene	Qa	Gharibreza (2016); Dolati (2010)
2800	0	2800	mud	0.249	6	≤ 21.3K	Pleistocene-mid Holocene	Qa	Gharibreza (2016); Dolati (2010)
2801	0	2801	mud	0.093	6	≤ 21.3K	Pleistocene-mid Holocene	Qa	Gharibreza (2016); Dolati (2010)
2802	0	2802	mud	0.180	6	≤ 21.3K	Pleistocene-mid Holocene	Qa	Gharibreza (2016); Dolati (2010)
2803	0	2803	mud	0.023	6	≤ 21.3K	Pleistocene-mid Holocene	Qa	Gharibreza (2016); Dolati (2010)
2804	0	2804	mud	0.224	6	≤ 21.3K	Pleistocene-mid Holocene	Qa	Gharibreza (2016); Dolati (2010)
2805	0	2805	mud	0.059	6	≤ 21.3K	Pleistocene-mid Holocene	Qa	Gharibreza (2016); Dolati (2010)
2806	0	2806	mud	0.153	6	≤ 21.3K	Pleistocene-mid Holocene	Qa	Gharibreza (2016); Dolati (2010)
2807	0	2807	mud	0.149	6	≤ 21.3K	Pleistocene-mid Holocene	Qa	Gharibreza (2016); Dolati (2010)
2808	0	2808	mud	0.129	6	≤ 21.3K	Pleistocene-mid Holocene	Qa	Gharibreza (2016); Dolati (2010)
2809	0	2809	mud	0.806	6	≤ 21.3K	Pleistocene-mid Holocene	Qa	Gharibreza (2016); Dolati (2010)
2810	0	2810	mud	0.085	6	≤ 21.3K	Pleistocene-mid Holocene	Qa	Gharibreza (2016); Dolati (2010)
2811	0	2811	mud	0.199	6	≤ 21.3K	Pleistocene-mid Holocene	Qa	Gharibreza (2016); Dolati (2010)
2812	0	2812	mud	0.154	6	≤ 21.3K	Pleistocene-mid Holocene	Qa	Gharibreza (2016); Dolati (2010)
2813	0	2813	mud	4.265	6	≤ 21.3K	Pleistocene-mid Holocene	Qa	Gharibreza (2016); Dolati (2010)
2814	0	2814	mud	0.062	6	≤ 21.3K	Pleistocene-mid Holocene	Qa	Gharibreza (2016); Dolati (2010)
2815	0	2815	mud	0.113	6	≤ 21.3K	Pleistocene-mid Holocene	Qa	Gharibreza (2016); Dolati (2010)
2816	0	2816	mud	0.293	6	≤ 21.3K	Pleistocene-mid Holocene	Qa	Gharibreza (2016); Dolati (2010)
2817	0	2817	mud	0.023	6	≤ 21.3K	Pleistocene-mid Holocene	Qa	Gharibreza (2016); Dolati (2010)
2819	0	2819	mud	0.028	6	≤ 21.3K	Pleistocene-mid Holocene	Qa	Gharibreza (2016); Dolati (2010)
2820	0	2820	mud	0.826	6	≤ 21.3K	Pleistocene-mid Holocene	Qa	Gharibreza (2016); Dolati (2010)

Geonews

OBJECTID_1	Join_Count	TARGET_FID	Label	Shape_Area (sqkm)	ORIG_FID	Absolute_Age	Age_paleontology	Unit	Reference
2821	0	2821	mud	0.055	6	≤ 21.3K	Pleistocene-mid Holocene	Qa	Gharibreza (2016); Dolati (2010)
2822	0	2822	mud	0.089	6	≤ 21.3K	Pleistocene-mid Holocene	Qa	Gharibreza (2016); Dolati (2010)
2823	0	2823	mud	0.201	6	≤ 21.3K	Pleistocene-mid Holocene	Qa	Gharibreza (2016); Dolati (2010)
2824	0	2824	mud	0.052	6	≤ 21.3K	Pleistocene-mid Holocene	Qa	Gharibreza (2016); Dolati (2010)
2825	0	2825	mud	1.470	6	≤ 21.3K	Pleistocene-mid Holocene	Qa	Gharibreza (2016); Dolati (2010)
2826	0	2826	mud	0.021	6	≤ 21.3K	Pleistocene-mid Holocene	Qa	Gharibreza (2016); Dolati (2010)
2827	0	2827	mud	0.024	6	≤ 21.3K	Pleistocene-mid Holocene	Qa	Gharibreza (2016); Dolati (2010)
2828	0	2828	mud	0.133	6	≤ 21.3K	Pleistocene-mid Holocene	Qa	Gharibreza (2016); Dolati (2010)
2829	0	2829	mud	1.857	6	≤ 21.3K	Pleistocene-mid Holocene	Qa	Gharibreza (2016); Dolati (2010)
2830	0	2830	mud	0.424	6	≤ 21.3K	Pleistocene-mid Holocene	Qa	Gharibreza (2016); Dolati (2010)
2831	0	2831	mud	0.723	6	≤ 21.3K	Pleistocene-mid Holocene	Qa	Gharibreza (2016); Dolati (2010)
2832	0	2832	mud	0.860	6	≤ 21.3K	Pleistocene-mid Holocene	Qa	Gharibreza (2016); Dolati (2010)
2833	0	2833	mud	0.023	6	≤ 21.3K	Pleistocene-mid Holocene	Qa	Gharibreza (2016); Dolati (2010)
2834	0	2834	mud	0.150	6	≤ 21.3K	Pleistocene-mid Holocene	Qa	Gharibreza (2016); Dolati (2010)
2835	0	2835	mud	0.214	6	≤ 21.3K	Pleistocene-mid Holocene	Qa	Gharibreza (2016); Dolati (2010)
2836	0	2836	mud	0.213	6	≤ 21.3K	Pleistocene-mid Holocene	Qa	Gharibreza (2016); Dolati (2010)
2837	0	2837	mud	0.135	6	≤ 21.3K	Pleistocene-mid Holocene	Qa	Gharibreza (2016); Dolati (2010)
2838	0	2838	mud	0.006	6	≤ 21.3K	Pleistocene-mid Holocene	Qa	Gharibreza (2016); Dolati (2010)
2839	0	2839	mud	0.535	6	≤ 21.3K	Pleistocene-mid Holocene	Qa	Gharibreza (2016); Dolati (2010)
2840	0	2840	mud	0.036	6	≤ 21.3K	Pleistocene-mid Holocene	Qa	Gharibreza (2016); Dolati (2010)
2841	0	2841	mud	0.204	6	≤ 21.3K	Pleistocene-mid Holocene	Qa	Gharibreza (2016); Dolati (2010)
2842	0	2842	mud	0.033	6	≤ 21.3K	Pleistocene-mid Holocene	Qa	Gharibreza (2016); Dolati (2010)
2843	0	2843	mud	0.026	6	≤ 21.3K	Pleistocene-mid Holocene	Qa	Gharibreza (2016); Dolati (2010)
2844	0	2844	mud	0.120	6	≤ 21.3K	Pleistocene-mid Holocene	Qa	Gharibreza (2016); Dolati (2010)
2845	0	2845	mud	0.046	6	≤ 21.3K	Pleistocene-mid Holocene	Qa	Gharibreza (2016); Dolati (2010)
2846	0	2846	mud	0.058	6	≤ 21.3K	Pleistocene-mid Holocene	Qa	Gharibreza (2016); Dolati (2010)
2847	0	2847	mud	1.236	6	≤ 21.3K	Pleistocene-mid Holocene	Qa	Gharibreza (2016); Dolati (2010)
2848	0	2848	mud	0.088	6	≤ 21.3K	Pleistocene-mid Holocene	Qa	Gharibreza (2016); Dolati (2010)
2849	0	2849	mud	0.008	6	≤ 21.3K	Pleistocene-mid Holocene	Qa	Gharibreza (2016); Dolati (2010)
2850	0	2850	mud	0.026	6	≤ 21.3K	Pleistocene-mid Holocene	Qa	Gharibreza (2016); Dolati (2010)
2851	0	2851	mud	0.043	6	≤ 21.3K	Pleistocene-mid Holocene	Qa	Gharibreza (2016); Dolati (2010)
2852	0	2852	mud	0.125	6	≤ 21.3K	Pleistocene-mid Holocene	Qa	Gharibreza (2016); Dolati (2010)
2853	0	2853	mud	0.051	6	≤ 21.3K	Pleistocene-mid Holocene	Qa	Gharibreza (2016); Dolati (2010)
2854	0	2854	mud	0.090	6	≤ 21.3K	Pleistocene-mid Holocene	Qa	Gharibreza (2016); Dolati (2010)
2855	0	2855	mud	0.056	6	≤ 21.3K	Pleistocene-mid Holocene	Qa	Gharibreza (2016); Dolati (2010)
2856	0	2856	mud	0.096	6	≤ 21.3K	Pleistocene-mid Holocene	Qa	Gharibreza (2016); Dolati (2010)
2857	0	2857	mud	0.156	6	≤ 21.3K	Pleistocene-mid Holocene	Qa	Gharibreza (2016); Dolati (2010)
2858	0	2858	mud	0.444	6	≤ 21.3K	Pleistocene-mid Holocene	Qa	Gharibreza (2016); Dolati (2010)
2859	0	2859	mud	0.028	6	≤ 21.3K	Pleistocene-mid Holocene	Qa	Gharibreza (2016); Dolati (2010)

Preview

OBJECTID_1	Join_Count	TARGET_FID	Label	Shape_Area (sqkm)	ORIG_FID	Absolute_Age	Age_paleontology	Unit	Reference
2860	0	2860	mud	0.060	6	≤ 21.3K	Pleistocene-mid Holocene	Qa	Gharibreza (2016); Dolati (2010)
2861	0	2861	mud	0.062	6	≤ 21.3K	Pleistocene-mid Holocene	Qa	Gharibreza (2016); Dolati (2010)
2862	0	2862	mud	0.106	6	≤ 21.3K	Pleistocene-mid Holocene	Qa	Gharibreza (2016); Dolati (2010)
2863	0	2863	mud	0.058	6	≤ 21.3K	Pleistocene-mid Holocene	Qa	Gharibreza (2016); Dolati (2010)
2864	0	2864	mud	0.115	6	≤ 21.3K	Pleistocene-mid Holocene	Qa	Gharibreza (2016); Dolati (2010)
2865	0	2865	mud	0.959	6	≤ 21.3K	Pleistocene-mid Holocene	Qa	Gharibreza (2016); Dolati (2010)
2866	0	2866	mud	0.085	6	≤ 21.3K	Pleistocene-mid Holocene	Qa	Gharibreza (2016); Dolati (2010)
2867	0	2867	mud	0.050	6	≤ 21.3K	Pleistocene-mid Holocene	Qa	Gharibreza (2016); Dolati (2010)
2868	0	2868	mud	0.175	6	≤ 21.3K	Pleistocene-mid Holocene	Qa	Gharibreza (2016); Dolati (2010)
2869	0	2869	mud	0.157	6	≤ 21.3K	Pleistocene-mid Holocene	Qa	Gharibreza (2016); Dolati (2010)
2870	0	2870	mud	0.027	6	≤ 21.3K	Pleistocene-mid Holocene	Qa	Gharibreza (2016); Dolati (2010)
2871	0	2871	mud	0.077	6	≤ 21.3K	Pleistocene-mid Holocene	Qa	Gharibreza (2016); Dolati (2010)
2872	0	2872	mud	0.024	6	≤ 21.3K	Pleistocene-mid Holocene	Qa	Gharibreza (2016); Dolati (2010)
2873	0	2873	mud	0.010	6	≤ 21.3K	Pleistocene-mid Holocene	Qa	Gharibreza (2016); Dolati (2010)
2874	0	2874	mud	0.367	6	≤ 21.3K	Pleistocene-mid Holocene	Qa	Gharibreza (2016); Dolati (2010)
2875	0	2875	mud	0.090	6	≤ 21.3K	Pleistocene-mid Holocene	Qa	Gharibreza (2016); Dolati (2010)
2876	0	2876	mud	0.102	6	≤ 21.3K	Pleistocene-mid Holocene	Qa	Gharibreza (2016); Dolati (2010)
2877	0	2877	mud	0.066	6	≤ 21.3K	Pleistocene-mid Holocene	Qa	Gharibreza (2016); Dolati (2010)
2878	0	2878	mud	0.064	6	≤ 21.3K	Pleistocene-mid Holocene	Qa	Gharibreza (2016); Dolati (2010)
2879	0	2879	mud	0.029	6	≤ 21.3K	Pleistocene-mid Holocene	Qa	Gharibreza (2016); Dolati (2010)
2880	0	2880	mud	0.055	6	≤ 21.3K	Pleistocene-mid Holocene	Qa	Gharibreza (2016); Dolati (2010)
2881	0	2881	mud	0.322	6	≤ 21.3K	Pleistocene-mid Holocene	Qa	Gharibreza (2016); Dolati (2010)
2882	0	2882	mud	0.027	6	≤ 21.3K	Pleistocene-mid Holocene	Qa	Gharibreza (2016); Dolati (2010)
2883	0	2883	mud	0.009	6	≤ 21.3K	Pleistocene-mid Holocene	Qa	Gharibreza (2016); Dolati (2010)
2884	0	2884	mud	0.058	6	≤ 21.3K	Pleistocene-mid Holocene	Qa	Gharibreza (2016); Dolati (2010)
2885	0	2885	mud	0.179	6	≤ 21.3K	Pleistocene-mid Holocene	Qa	Gharibreza (2016); Dolati (2010)
2886	0	2886	mud	0.024	6	≤ 21.3K	Pleistocene-mid Holocene	Qa	Gharibreza (2016); Dolati (2010)
2887	0	2887	mud	0.033	6	≤ 21.3K	Pleistocene-mid Holocene	Qa	Gharibreza (2016); Dolati (2010)
2888	0	2888	mud	0.669	6	≤ 21.3K	Pleistocene-mid Holocene	Qa	Gharibreza (2016); Dolati (2010)
2890	0	2890	mud	0.326	6	≤ 21.3K	Pleistocene-mid Holocene	Qa	Gharibreza (2016); Dolati (2010)
2891	0	2891	mud	0.231	6	≤ 21.3K	Pleistocene-mid Holocene	Qa	Gharibreza (2016); Dolati (2010)
2892	0	2892	mud	0.061	6	≤ 21.3K	Pleistocene-mid Holocene	Qa	Gharibreza (2016); Dolati (2010)
2893	0	2893	mud	0.020	6	≤ 21.3K	Pleistocene-mid Holocene	Qa	Gharibreza (2016); Dolati (2010)
2894	0	2894	mud	0.027	6	≤ 21.3K	Pleistocene-mid Holocene	Qa	Gharibreza (2016); Dolati (2010)
2895	0	2895	mud	0.093	6	≤ 21.3K	Pleistocene-mid Holocene	Qa	Gharibreza (2016); Dolati (2010)
2896	0	2896	mud	0.049	6	≤ 21.3K	Pleistocene-mid Holocene	Qa	Gharibreza (2016); Dolati (2010)
2897	0	2897	mud	0.080	6	≤ 21.3K	Pleistocene-mid Holocene	Qa	Gharibreza (2016); Dolati (2010)
2898	0	2898	mud	0.050	6	≤ 21.3K	Pleistocene-mid Holocene	Qa	Gharibreza (2016); Dolati (2010)
2899	0	2899	mud	0.170	6	≤ 21.3K	Pleistocene-mid Holocene	Qa	Gharibreza (2016); Dolati (2010)

Preview

OBJECTID_1	Join_Count	TARGET_FID	Label	Shape_Area (sqkm)	ORIG_FID	Absolute_Age	Age_paleontology	Unit	Reference
2900	0	2900	mud	0.031	6	≤ 21.3K	Pleistocene-mid Holocene	Qa	Gharibreza (2016); Dolati (2010)
2901	0	2901	mud	0.191	6	≤ 21.3K	Pleistocene-mid Holocene	Qa	Gharibreza (2016); Dolati (2010)
2902	0	2902	mud	0.752	6	≤ 21.3K	Pleistocene-mid Holocene	Qa	Gharibreza (2016); Dolati (2010)
2903	0	2903	mud	0.144	6	≤ 21.3K	Pleistocene-mid Holocene	Qa	Gharibreza (2016); Dolati (2010)
2904	0	2904	mud	0.039	6	≤ 21.3K	Pleistocene-mid Holocene	Qa	Gharibreza (2016); Dolati (2010)
2905	0	2905	mud	0.024	6	≤ 21.3K	Pleistocene-mid Holocene	Qa	Gharibreza (2016); Dolati (2010)
2906	0	2906	mud	2.628	6	≤ 21.3K	Pleistocene-mid Holocene	Qa	Gharibreza (2016); Dolati (2010)
2907	0	2907	mud	0.032	6	≤ 21.3K	Pleistocene-mid Holocene	Qa	Gharibreza (2016); Dolati (2010)
2908	0	2908	mud	0.227	6	≤ 21.3K	Pleistocene-mid Holocene	Qa	Gharibreza (2016); Dolati (2010)
2909	0	2909	mud	0.207	6	≤ 21.3K	Pleistocene-mid Holocene	Qa	Gharibreza (2016); Dolati (2010)
2910	0	2910	mud	0.060	6	≤ 21.3K	Pleistocene-mid Holocene	Qa	Gharibreza (2016); Dolati (2010)
2911	0	2911	mud	0.035	6	≤ 21.3K	Pleistocene-mid Holocene	Qa	Gharibreza (2016); Dolati (2010)
2912	0	2912	mud	0.324	6	≤ 21.3K	Pleistocene-mid Holocene	Qa	Gharibreza (2016); Dolati (2010)
2913	0	2913	mud	0.106	6	≤ 21.3K	Pleistocene-mid Holocene	Qa	Gharibreza (2016); Dolati (2010)
2914	0	2914	mud	0.031	6	≤ 21.3K	Pleistocene-mid Holocene	Qa	Gharibreza (2016); Dolati (2010)
2915	0	2915	mud	0.149	6	≤ 21.3K	Pleistocene-mid Holocene	Qa	Gharibreza (2016); Dolati (2010)
2916	0	2916	mud	0.407	6	≤ 21.3K	Pleistocene-mid Holocene	Qa	Gharibreza (2016); Dolati (2010)
2917	0	2917	mud	0.125	6	≤ 21.3K	Pleistocene-mid Holocene	Qa	Gharibreza (2016); Dolati (2010)
2919	0	2919	mud	0.068	6	≤ 21.3K	Pleistocene-mid Holocene	Qa	Gharibreza (2016); Dolati (2010)
2920	0	2920	mud	0.065	6	≤ 21.3K	Pleistocene-mid Holocene	Qa	Gharibreza (2016); Dolati (2010)
2921	0	2921	mud	0.131	6	≤ 21.3K	Pleistocene-mid Holocene	Qa	Gharibreza (2016); Dolati (2010)
2922	0	2922	mud	0.106	6	≤ 21.3K	Pleistocene-mid Holocene	Qa	Gharibreza (2016); Dolati (2010)
2923	0	2923	mud	0.405	6	≤ 21.3K	Pleistocene-mid Holocene	Qa	Gharibreza (2016); Dolati (2010)
2924	0	2924	mud	0.206	6	≤ 21.3K	Pleistocene-mid Holocene	Qa	Gharibreza (2016); Dolati (2010)
2925	0	2925	mud	0.021	6	≤ 21.3K	Pleistocene-mid Holocene	Qa	Gharibreza (2016); Dolati (2010)
2926	0	2926	mud	0.019	6	≤ 21.3K	Pleistocene-mid Holocene	Qa	Gharibreza (2016); Dolati (2010)
2927	0	2927	mud	0.063	6	≤ 21.3K	Pleistocene-mid Holocene	Qa	Gharibreza (2016); Dolati (2010)
2928	0	2928	mud	0.202	6	≤ 21.3K	Pleistocene-mid Holocene	Qa	Gharibreza (2016); Dolati (2010)
2929	0	2929	mud	0.088	6	≤ 21.3K	Pleistocene-mid Holocene	Qa	Gharibreza (2016); Dolati (2010)
2930	0	2930	mud	0.096	6	≤ 21.3K	Pleistocene-mid Holocene	Qa	Gharibreza (2016); Dolati (2010)
2931	0	2931	mud	0.012	6	≤ 21.3K	Pleistocene-mid Holocene	Qa	Gharibreza (2016); Dolati (2010)
2932	0	2932	mud	0.089	6	≤ 21.3K	Pleistocene-mid Holocene	Qa	Gharibreza (2016); Dolati (2010)
2933	0	2933	mud	0.623	6	≤ 21.3K	Pleistocene-mid Holocene	Qa	Gharibreza (2016); Dolati (2010)
2934	0	2934	mud	0.126	6	≤ 21.3K	Pleistocene-mid Holocene	Qa	Gharibreza (2016); Dolati (2010)
2935	0	2935	mud	0.035	6	≤ 21.3K	Pleistocene-mid Holocene	Qa	Gharibreza (2016); Dolati (2010)
2936	0	2936	mud	0.014	6	≤ 21.3K	Pleistocene-mid Holocene	Qa	Gharibreza (2016); Dolati (2010)
2937	0	2937	mud	0.085	6	≤ 21.3K	Pleistocene-mid Holocene	Qa	Gharibreza (2016); Dolati (2010)
2938	0	2938	mud	0.035	6	≤ 21.3K	Pleistocene-mid Holocene	Qa	Gharibreza (2016); Dolati (2010)
2939	0	2939	mud	0.035	6	≤ 21.3K	Pleistocene-mid Holocene	Qa	Gharibreza (2016); Dolati (2010)

Preview

OBJECTID_1	Join_Count	TARGET_FID	Label	Shape_Area (sqkm)	ORIG_FID	Absolute_Age	Age_paleontology	Unit	Reference
2940	0	2940	mud	0.130	6	≤ 21.3K	Pleistocene-mid Holocene	Qa	Gharibreza (2016); Dolati (2010)
2941	0	2941	mud	0.041	6	≤ 21.3K	Pleistocene-mid Holocene	Qa	Gharibreza (2016); Dolati (2010)
2942	0	2942	mud	0.081	6	≤ 21.3K	Pleistocene-mid Holocene	Qa	Gharibreza (2016); Dolati (2010)
2943	0	2943	mud	0.027	6	≤ 21.3K	Pleistocene-mid Holocene	Qa	Gharibreza (2016); Dolati (2010)
2944	0	2944	mud	0.048	6	≤ 21.3K	Pleistocene-mid Holocene	Qa	Gharibreza (2016); Dolati (2010)
2945	0	2945	mud	0.039	6	≤ 21.3K	Pleistocene-mid Holocene	Qa	Gharibreza (2016); Dolati (2010)
2946	0	2946	mud	0.048	6	≤ 21.3K	Pleistocene-mid Holocene	Qa	Gharibreza (2016); Dolati (2010)
2947	0	2947	mud	0.168	6	≤ 21.3K	Pleistocene-mid Holocene	Qa	Gharibreza (2016); Dolati (2010)
2948	0	2948	mud	0.103	6	≤ 21.3K	Pleistocene-mid Holocene	Qa	Gharibreza (2016); Dolati (2010)
2949	0	2949	mud	29.632	6	≤ 21.3K	Pleistocene-mid Holocene	Qa	Gharibreza (2016); Dolati (2010)
2950	0	2950	mud	0.116	6	≤ 21.3K	Pleistocene-mid Holocene	Qa	Gharibreza (2016); Dolati (2010)
2951	0	2951	mud	0.227	6	≤ 21.3K	Pleistocene-mid Holocene	Qa	Gharibreza (2016); Dolati (2010)
2952	0	2952	mud	0.196	6	≤ 21.3K	Pleistocene-mid Holocene	Qa	Gharibreza (2016); Dolati (2010)
2953	0	2953	mud	0.043	6	≤ 21.3K	Pleistocene-mid Holocene	Qa	Gharibreza (2016); Dolati (2010)
2954	0	2954	mud	0.143	6	≤ 21.3K	Pleistocene-mid Holocene	Qa	Gharibreza (2016); Dolati (2010)
2955	0	2955	mud	0.487	6	≤ 21.3K	Pleistocene-mid Holocene	Qa	Gharibreza (2016); Dolati (2010)
2956	0	2956	mud	0.041	6	≤ 21.3K	Pleistocene-mid Holocene	Qa	Gharibreza (2016); Dolati (2010)
2957	0	2957	mud	0.056	6	≤ 21.3K	Pleistocene-mid Holocene	Qa	Gharibreza (2016); Dolati (2010)
2958	0	2958	mud	0.104	6	≤ 21.3K	Pleistocene-mid Holocene	Qa	Gharibreza (2016); Dolati (2010)
2959	0	2959	mud	0.033	6	≤ 21.3K	Pleistocene-mid Holocene	Qa	Gharibreza (2016); Dolati (2010)
2960	0	2960	mud	0.095	6	≤ 21.3K	Pleistocene-mid Holocene	Qa	Gharibreza (2016); Dolati (2010)
2961	0	2961	mud	0.376	6	≤ 21.3K	Pleistocene-mid Holocene	Qa	Gharibreza (2016); Dolati (2010)
2962	0	2962	mud	0.081	6	≤ 21.3K	Pleistocene-mid Holocene	Qa	Gharibreza (2016); Dolati (2010)
2963	0	2963	mud	1.098	6	≤ 21.3K	Pleistocene-mid Holocene	Qa	Gharibreza (2016); Dolati (2010)
2964	0	2964	mud	0.049	6	≤ 21.3K	Pleistocene-mid Holocene	Qa	Gharibreza (2016); Dolati (2010)
2965	0	2965	mud	0.081	6	≤ 21.3K	Pleistocene-mid Holocene	Qa	Gharibreza (2016); Dolati (2010)
2966	0	2966	mud	0.010	6	≤ 21.3K	Pleistocene-mid Holocene	Qa	Gharibreza (2016); Dolati (2010)
2967	0	2967	mud	0.136	6	≤ 21.3K	Pleistocene-mid Holocene	Qa	Gharibreza (2016); Dolati (2010)
2968	0	2968	mud	0.053	6	≤ 21.3K	Pleistocene-mid Holocene	Qa	Gharibreza (2016); Dolati (2010)
2969	0	2969	mud	0.053	6	≤ 21.3K	Pleistocene-mid Holocene	Qa	Gharibreza (2016); Dolati (2010)
2970	0	2970	mud	0.145	6	≤ 21.3K	Pleistocene-mid Holocene	Qa	Gharibreza (2016); Dolati (2010)
2971	0	2971	mud	0.058	6	≤ 21.3K	Pleistocene-mid Holocene	Qa	Gharibreza (2016); Dolati (2010)
2972	0	2972	mud	0.031	6	≤ 21.3K	Pleistocene-mid Holocene	Qa	Gharibreza (2016); Dolati (2010)
2973	0	2973	mud	0.953	6	≤ 21.3K	Pleistocene-mid Holocene	Qa	Gharibreza (2016); Dolati (2010)
2974	0	2974	mud	0.036	6	≤ 21.3K	Pleistocene-mid Holocene	Qa	Gharibreza (2016); Dolati (2010)
2975	0	2975	mud	0.130	6	≤ 21.3K	Pleistocene-mid Holocene	Qa	Gharibreza (2016); Dolati (2010)
2976	0	2976	mud	0.036	6	≤ 21.3K	Pleistocene-mid Holocene	Qa	Gharibreza (2016); Dolati (2010)
2977	0	2977	mud	0.055	6	≤ 21.3K	Pleistocene-mid Holocene	Qa	Gharibreza (2016); Dolati (2010)
2978	0	2978	mud	0.029	6	≤ 21.3K	Pleistocene-mid Holocene	Qa	Gharibreza (2016); Dolati (2010)

Preview

OBJECTID_1	Join_Count	TARGET_FID	Label	Shape_Area (sqkm)	ORIG_FID	Absolute_Age	Age_paleontology	Unit	Reference
2979	0	2979	mud	1.810	6	≤ 21.3K	Pleistocene-mid Holocene	Qa	Gharibreza (2016); Dolati (2010)
2980	0	2980	mud	0.331	6	≤ 21.3K	Pleistocene-mid Holocene	Qa	Gharibreza (2016); Dolati (2010)
2981	0	2981	mud	0.034	6	≤ 21.3K	Pleistocene-mid Holocene	Qa	Gharibreza (2016); Dolati (2010)
2982	0	2982	mud	0.475	6	≤ 21.3K	Pleistocene-mid Holocene	Qa	Gharibreza (2016); Dolati (2010)
2983	0	2983	mud	0.015	6	≤ 21.3K	Pleistocene-mid Holocene	Qa	Gharibreza (2016); Dolati (2010)
2984	0	2984	mud	0.206	6	≤ 21.3K	Pleistocene-mid Holocene	Qa	Gharibreza (2016); Dolati (2010)
2985	0	2985	mud	0.075	6	≤ 21.3K	Pleistocene-mid Holocene	Qa	Gharibreza (2016); Dolati (2010)
2986	0	2986	mud	0.129	6	≤ 21.3K	Pleistocene-mid Holocene	Qa	Gharibreza (2016); Dolati (2010)
2987	0	2987	mud	0.027	6	≤ 21.3K	Pleistocene-mid Holocene	Qa	Gharibreza (2016); Dolati (2010)
2988	0	2988	mud	0.028	6	≤ 21.3K	Pleistocene-mid Holocene	Qa	Gharibreza (2016); Dolati (2010)
2989	0	2989	mud	0.140	6	≤ 21.3K	Pleistocene-mid Holocene	Qa	Gharibreza (2016); Dolati (2010)
2990	0	2990	mud	0.179	6	≤ 21.3K	Pleistocene-mid Holocene	Qa	Gharibreza (2016); Dolati (2010)
2991	0	2991	mud	0.074	6	≤ 21.3K	Pleistocene-mid Holocene	Qa	Gharibreza (2016); Dolati (2010)
2992	0	2992	mud	0.064	6	≤ 21.3K	Pleistocene-mid Holocene	Qa	Gharibreza (2016); Dolati (2010)
2993	0	2993	mud	0.188	6	≤ 21.3K	Pleistocene-mid Holocene	Qa	Gharibreza (2016); Dolati (2010)
2994	0	2994	mud	0.401	6	≤ 21.3K	Pleistocene-mid Holocene	Qa	Gharibreza (2016); Dolati (2010)
2995	0	2995	mud	0.047	6	≤ 21.3K	Pleistocene-mid Holocene	Qa	Gharibreza (2016); Dolati (2010)
2996	0	2996	mud	0.965	6	≤ 21.3K	Pleistocene-mid Holocene	Qa	Gharibreza (2016); Dolati (2010)
2997	0	2997	mud	0.072	6	≤ 21.3K	Pleistocene-mid Holocene	Qa	Gharibreza (2016); Dolati (2010)
2998	0	2998	mud	0.048	6	≤ 21.3K	Pleistocene-mid Holocene	Qa	Gharibreza (2016); Dolati (2010)
2999	0	2999	mud	0.169	6	≤ 21.3K	Pleistocene-mid Holocene	Qa	Gharibreza (2016); Dolati (2010)
3000	0	3000	mud	0.559	6	≤ 21.3K	Pleistocene-mid Holocene	Qa	Gharibreza (2016); Dolati (2010)
3001	0	3001	mud	0.057	6	≤ 21.3K	Pleistocene-mid Holocene	Qa	Gharibreza (2016); Dolati (2010)
3002	0	3002	mud	0.483	6	≤ 21.3K	Pleistocene-mid Holocene	Qa	Gharibreza (2016); Dolati (2010)
3003	0	3003	mud	0.036	6	≤ 21.3K	Pleistocene-mid Holocene	Qa	Gharibreza (2016); Dolati (2010)
3004	0	3004	mud	0.049	6	≤ 21.3K	Pleistocene-mid Holocene	Qa	Gharibreza (2016); Dolati (2010)
3005	0	3005	mud	0.056	6	≤ 21.3K	Pleistocene-mid Holocene	Qa	Gharibreza (2016); Dolati (2010)
3006	0	3006	mud	0.187	6	≤ 21.3K	Pleistocene-mid Holocene	Qa	Gharibreza (2016); Dolati (2010)
3007	0	3007	mud	0.424	6	≤ 21.3K	Pleistocene-mid Holocene	Qa	Gharibreza (2016); Dolati (2010)
3008	0	3008	mud	0.035	6	≤ 21.3K	Pleistocene-mid Holocene	Qa	Gharibreza (2016); Dolati (2010)
3009	0	3009	mud	0.129	6	≤ 21.3K	Pleistocene-mid Holocene	Qa	Gharibreza (2016); Dolati (2010)
3010	0	3010	mud	0.063	6	≤ 21.3K	Pleistocene-mid Holocene	Qa	Gharibreza (2016); Dolati (2010)
3011	0	3011	mud	0.064	6	≤ 21.3K	Pleistocene-mid Holocene	Qa	Gharibreza (2016); Dolati (2010)
3012	0	3012	mud	0.074	6	≤ 21.3K	Pleistocene-mid Holocene	Qa	Gharibreza (2016); Dolati (2010)
3013	0	3013	mud	0.122	6	≤ 21.3K	Pleistocene-mid Holocene	Qa	Gharibreza (2016); Dolati (2010)
3014	0	3014	mud	0.089	6	≤ 21.3K	Pleistocene-mid Holocene	Qa	Gharibreza (2016); Dolati (2010)
3015	0	3015	mud	0.937	6	≤ 21.3K	Pleistocene-mid Holocene	Qa	Gharibreza (2016); Dolati (2010)
3016	0	3016	mud	0.013	6	≤ 21.3K	Pleistocene-mid Holocene	Qa	Gharibreza (2016); Dolati (2010)
3017	0	3017	mud	0.096	6	≤ 21.3K	Pleistocene-mid Holocene	Qa	Gharibreza (2016); Dolati (2010)

Preview

OBJECTID_1	Join_Count	TARGET_FID	Label	Shape_Area (sqkm)	ORIG_FID	Absolute_Age	Age_paleontology	Unit	Reference
3018	0	3018	mud	0.050	6	≤ 21.3K	Pleistocene-mid Holocene	Qa	Gharibreza (2016); Dolati (2010)
3019	0	3019	mud	0.029	6	≤ 21.3K	Pleistocene-mid Holocene	Qa	Gharibreza (2016); Dolati (2010)
3020	0	3020	mud	0.016	6	≤ 21.3K	Pleistocene-mid Holocene	Qa	Gharibreza (2016); Dolati (2010)
3021	0	3021	mud	0.078	6	≤ 21.3K	Pleistocene-mid Holocene	Qa	Gharibreza (2016); Dolati (2010)
3022	0	3022	mud	0.037	6	≤ 21.3K	Pleistocene-mid Holocene	Qa	Gharibreza (2016); Dolati (2010)
3023	0	3023	mud	0.073	6	≤ 21.3K	Pleistocene-mid Holocene	Qa	Gharibreza (2016); Dolati (2010)
3024	0	3024	mud	0.140	6	≤ 21.3K	Pleistocene-mid Holocene	Qa	Gharibreza (2016); Dolati (2010)
3025	0	3025	mud	0.020	6	≤ 21.3K	Pleistocene-mid Holocene	Qa	Gharibreza (2016); Dolati (2010)
3026	0	3026	mud	1.968	6	≤ 21.3K	Pleistocene-mid Holocene	Qa	Gharibreza (2016); Dolati (2010)
3027	0	3027	mud	0.102	6	≤ 21.3K	Pleistocene-mid Holocene	Qa	Gharibreza (2016); Dolati (2010)
3029	0	3029	mud	0.061	6	≤ 21.3K	Pleistocene-mid Holocene	Qa	Gharibreza (2016); Dolati (2010)
3030	0	3030	mud	0.018	6	≤ 21.3K	Pleistocene-mid Holocene	Qa	Gharibreza (2016); Dolati (2010)
3031	0	3031	mud	0.083	6	≤ 21.3K	Pleistocene-mid Holocene	Qa	Gharibreza (2016); Dolati (2010)
3032	0	3032	mud	0.131	6	≤ 21.3K	Pleistocene-mid Holocene	Qa	Gharibreza (2016); Dolati (2010)
3033	0	3033	mud	11.999	6	≤ 21.3K	Pleistocene-mid Holocene	Qa	Gharibreza (2016); Dolati (2010)
3034	0	3034	mud	0.050	6	≤ 21.3K	Pleistocene-mid Holocene	Qa	Gharibreza (2016); Dolati (2010)
3035	0	3035	mud	0.055	6	≤ 21.3K	Pleistocene-mid Holocene	Qa	Gharibreza (2016); Dolati (2010)
3036	0	3036	mud	0.012	6	≤ 21.3K	Pleistocene-mid Holocene	Qa	Gharibreza (2016); Dolati (2010)
3037	0	3037	mud	0.031	6	≤ 21.3K	Pleistocene-mid Holocene	Qa	Gharibreza (2016); Dolati (2010)
3038	0	3038	mud	0.326	6	≤ 21.3K	Pleistocene-mid Holocene	Qa	Gharibreza (2016); Dolati (2010)
3039	0	3039	mud	0.765	6	≤ 21.3K	Pleistocene-mid Holocene	Qa	Gharibreza (2016); Dolati (2010)
3040	0	3040	mud	0.059	6	≤ 21.3K	Pleistocene-mid Holocene	Qa	Gharibreza (2016); Dolati (2010)
3041	0	3041	mud	1.588	6	≤ 21.3K	Pleistocene-mid Holocene	Qa	Gharibreza (2016); Dolati (2010)
3042	0	3042	mud	0.078	6	≤ 21.3K	Pleistocene-mid Holocene	Qa	Gharibreza (2016); Dolati (2010)
3043	0	3043	mud	8.100	6	≤ 21.3K	Pleistocene-mid Holocene	Qa	Gharibreza (2016); Dolati (2010)
3044	0	3044	mud	0.111	6	≤ 21.3K	Pleistocene-mid Holocene	Qa	Gharibreza (2016); Dolati (2010)
3045	0	3045	mud	3.230	6	≤ 21.3K	Pleistocene-mid Holocene	Qa	Gharibreza (2016); Dolati (2010)
3046	0	3046	mud	0.172	6	≤ 21.3K	Pleistocene-mid Holocene	Qa	Gharibreza (2016); Dolati (2010)
3047	0	3047	mud	0.080	6	≤ 21.3K	Pleistocene-mid Holocene	Qa	Gharibreza (2016); Dolati (2010)
3048	0	3048	mud	0.613	6	≤ 21.3K	Pleistocene-mid Holocene	Qa	Gharibreza (2016); Dolati (2010)
3049	0	3049	mud	0.108	6	≤ 21.3K	Pleistocene-mid Holocene	Qa	Gharibreza (2016); Dolati (2010)
3050	0	3050	mud	0.612	6	≤ 21.3K	Pleistocene-mid Holocene	Qa	Gharibreza (2016); Dolati (2010)
3051	0	3051	mud	0.166	6	≤ 21.3K	Pleistocene-mid Holocene	Qa	Gharibreza (2016); Dolati (2010)
3052	0	3052	mud	0.054	6	≤ 21.3K	Pleistocene-mid Holocene	Qa	Gharibreza (2016); Dolati (2010)
3053	0	3053	mud	0.140	6	≤ 21.3K	Pleistocene-mid Holocene	Qa	Gharibreza (2016); Dolati (2010)
3054	0	3054	mud	0.021	6	≤ 21.3K	Pleistocene-mid Holocene	Qa	Gharibreza (2016); Dolati (2010)
3055	0	3055	mud	0.017	6	≤ 21.3K	Pleistocene-mid Holocene	Qa	Gharibreza (2016); Dolati (2010)
3056	0	3056	mud	0.047	6	≤ 21.3K	Pleistocene-mid Holocene	Qa	Gharibreza (2016); Dolati (2010)
3057	0	3057	mud	0.161	6	≤ 21.3K	Pleistocene-mid Holocene	Qa	Gharibreza (2016); Dolati (2010)

Preview

OBJECTID_1	Join_Count	TARGET_FID	Label	Shape_Area (sqkm)	ORIG_FID	Absolute_Age	Age_paleontology	Unit	Reference
3058	0	3058	mud	0.329	6	≤ 21.3K	Pleistocene-mid Holocene	Qa	Gharibreza (2016); Dolati (2010)
3059	0	3059	mud	0.068	6	≤ 21.3K	Pleistocene-mid Holocene	Qa	Gharibreza (2016); Dolati (2010)
3060	0	3060	mud	0.042	6	≤ 21.3K	Pleistocene-mid Holocene	Qa	Gharibreza (2016); Dolati (2010)
3061	0	3061	mud	0.024	6	≤ 21.3K	Pleistocene-mid Holocene	Qa	Gharibreza (2016); Dolati (2010)
3062	0	3062	mud	0.805	6	≤ 21.3K	Pleistocene-mid Holocene	Qa	Gharibreza (2016); Dolati (2010)
3063	0	3063	mud	0.472	6	≤ 21.3K	Pleistocene-mid Holocene	Qa	Gharibreza (2016); Dolati (2010)
3064	0	3064	mud	0.050	6	≤ 21.3K	Pleistocene-mid Holocene	Qa	Gharibreza (2016); Dolati (2010)
3065	0	3065	mud	0.249	6	≤ 21.3K	Pleistocene-mid Holocene	Qa	Gharibreza (2016); Dolati (2010)
3066	0	3066	mud	0.506	6	≤ 21.3K	Pleistocene-mid Holocene	Qa	Gharibreza (2016); Dolati (2010)
3067	0	3067	mud	0.023	6	≤ 21.3K	Pleistocene-mid Holocene	Qa	Gharibreza (2016); Dolati (2010)
3068	0	3068	mud	0.040	6	≤ 21.3K	Pleistocene-mid Holocene	Qa	Gharibreza (2016); Dolati (2010)
3069	0	3069	mud	0.061	6	≤ 21.3K	Pleistocene-mid Holocene	Qa	Gharibreza (2016); Dolati (2010)
3070	0	3070	mud	0.054	6	≤ 21.3K	Pleistocene-mid Holocene	Qa	Gharibreza (2016); Dolati (2010)
3071	0	3071	mud	0.024	6	≤ 21.3K	Pleistocene-mid Holocene	Qa	Gharibreza (2016); Dolati (2010)
3072	0	3072	mud	0.391	6	≤ 21.3K	Pleistocene-mid Holocene	Qa	Gharibreza (2016); Dolati (2010)
3073	0	3073	mud	0.448	6	≤ 21.3K	Pleistocene-mid Holocene	Qa	Gharibreza (2016); Dolati (2010)
3074	0	3074	mud	0.397	6	≤ 21.3K	Pleistocene-mid Holocene	Qa	Gharibreza (2016); Dolati (2010)
3075	0	3075	mud	0.300	6	≤ 21.3K	Pleistocene-mid Holocene	Qa	Gharibreza (2016); Dolati (2010)
3076	0	3076	mud	0.015	6	≤ 21.3K	Pleistocene-mid Holocene	Qa	Gharibreza (2016); Dolati (2010)
3077	0	3077	mud	0.863	6	≤ 21.3K	Pleistocene-mid Holocene	Qa	Gharibreza (2016); Dolati (2010)
3078	0	3078	mud	0.193	6	≤ 21.3K	Pleistocene-mid Holocene	Qa	Gharibreza (2016); Dolati (2010)
3079	0	3079	mud	0.028	6	≤ 21.3K	Pleistocene-mid Holocene	Qa	Gharibreza (2016); Dolati (2010)
3080	0	3080	mud	0.449	6	≤ 21.3K	Pleistocene-mid Holocene	Qa	Gharibreza (2016); Dolati (2010)
3081	0	3081	mud	0.033	6	≤ 21.3K	Pleistocene-mid Holocene	Qa	Gharibreza (2016); Dolati (2010)
3082	0	3082	mud	0.048	6	≤ 21.3K	Pleistocene-mid Holocene	Qa	Gharibreza (2016); Dolati (2010)
3083	0	3083	mud	0.040	6	≤ 21.3K	Pleistocene-mid Holocene	Qa	Gharibreza (2016); Dolati (2010)
3084	0	3084	mud	0.034	6	≤ 21.3K	Pleistocene-mid Holocene	Qa	Gharibreza (2016); Dolati (2010)
3085	0	3085	mud	0.101	6	≤ 21.3K	Pleistocene-mid Holocene	Qa	Gharibreza (2016); Dolati (2010)
3086	0	3086	mud	0.008	6	≤ 21.3K	Pleistocene-mid Holocene	Qa	Gharibreza (2016); Dolati (2010)
3087	0	3087	mud	0.106	6	≤ 21.3K	Pleistocene-mid Holocene	Qa	Gharibreza (2016); Dolati (2010)
3088	0	3088	mud	0.207	6	≤ 21.3K	Pleistocene-mid Holocene	Qa	Gharibreza (2016); Dolati (2010)
3089	0	3089	mud	0.030	6	≤ 21.3K	Pleistocene-mid Holocene	Qa	Gharibreza (2016); Dolati (2010)
3090	0	3090	mud	1.160	6	≤ 21.3K	Pleistocene-mid Holocene	Qa	Gharibreza (2016); Dolati (2010)
3091	0	3091	mud	0.024	6	≤ 21.3K	Pleistocene-mid Holocene	Qa	Gharibreza (2016); Dolati (2010)
3092	0	3092	mud	0.104	6	≤ 21.3K	Pleistocene-mid Holocene	Qa	Gharibreza (2016); Dolati (2010)
3093	0	3093	mud	0.165	6	≤ 21.3K	Pleistocene-mid Holocene	Qa	Gharibreza (2016); Dolati (2010)
3094	0	3094	mud	0.024	6	≤ 21.3K	Pleistocene-mid Holocene	Qa	Gharibreza (2016); Dolati (2010)
3095	0	3095	mud	0.137	6	≤ 21.3K	Pleistocene-mid Holocene	Qa	Gharibreza (2016); Dolati (2010)
3096	0	3096	mud	0.313	6	≤ 21.3K	Pleistocene-mid Holocene	Qa	Gharibreza (2016); Dolati (2010)

Preview

OBJECTID_1	Join_Count	TARGET_FID	Label	Shape_Area (sqkm)	ORIG_FID	Absolute_Age	Age_paleontology	Unit	Reference
3097	0	3097	mud	0.621	6	≤ 21.3K	Pleistocene-mid Holocene	Qa	Gharibreza (2016); Dolati (2010)
3098	0	3098	mud	0.105	6	≤ 21.3K	Pleistocene-mid Holocene	Qa	Gharibreza (2016); Dolati (2010)
3099	0	3099	mud	0.027	6	≤ 21.3K	Pleistocene-mid Holocene	Qa	Gharibreza (2016); Dolati (2010)
3100	0	3100	mud	0.039	6	≤ 21.3K	Pleistocene-mid Holocene	Qa	Gharibreza (2016); Dolati (2010)
3101	0	3101	mud	0.068	6	≤ 21.3K	Pleistocene-mid Holocene	Qa	Gharibreza (2016); Dolati (2010)
3102	0	3102	mud	0.070	6	≤ 21.3K	Pleistocene-mid Holocene	Qa	Gharibreza (2016); Dolati (2010)
3103	0	3103	mud	0.055	6	≤ 21.3K	Pleistocene-mid Holocene	Qa	Gharibreza (2016); Dolati (2010)
3104	0	3104	mud	0.039	6	≤ 21.3K	Pleistocene-mid Holocene	Qa	Gharibreza (2016); Dolati (2010)
3105	0	3105	mud	0.099	6	≤ 21.3K	Pleistocene-mid Holocene	Qa	Gharibreza (2016); Dolati (2010)
3106	0	3106	mud	0.029	6	≤ 21.3K	Pleistocene-mid Holocene	Qa	Gharibreza (2016); Dolati (2010)
3107	0	3107	mud	0.132	6	≤ 21.3K	Pleistocene-mid Holocene	Qa	Gharibreza (2016); Dolati (2010)
3108	0	3108	mud	0.084	6	≤ 21.3K	Pleistocene-mid Holocene	Qa	Gharibreza (2016); Dolati (2010)
3109	0	3109	mud	0.779	6	≤ 21.3K	Pleistocene-mid Holocene	Qa	Gharibreza (2016); Dolati (2010)
3110	0	3110	mud	0.024	6	≤ 21.3K	Pleistocene-mid Holocene	Qa	Gharibreza (2016); Dolati (2010)
3111	0	3111	mud	0.046	6	≤ 21.3K	Pleistocene-mid Holocene	Qa	Gharibreza (2016); Dolati (2010)
3112	0	3112	mud	24.957	6	≤ 21.3K	Pleistocene-mid Holocene	Qa	Gharibreza (2016); Dolati (2010)
3113	0	3113	mud	0.071	6	≤ 21.3K	Pleistocene-mid Holocene	Qa	Gharibreza (2016); Dolati (2010)
3114	0	3114	mud	0.118	6	≤ 21.3K	Pleistocene-mid Holocene	Qa	Gharibreza (2016); Dolati (2010)
3115	0	3115	mud	0.101	6	≤ 21.3K	Pleistocene-mid Holocene	Qa	Gharibreza (2016); Dolati (2010)
3116	0	3116	mud	0.179	6	≤ 21.3K	Pleistocene-mid Holocene	Qa	Gharibreza (2016); Dolati (2010)
3117	0	3117	mud	2.526	6	≤ 21.3K	Pleistocene-mid Holocene	Qa	Gharibreza (2016); Dolati (2010)
3118	0	3118	mud	2.581	6	≤ 21.3K	Pleistocene-mid Holocene	Qa	Gharibreza (2016); Dolati (2010)
3119	0	3119	mud	0.399	6	≤ 21.3K	Pleistocene-mid Holocene	Qa	Gharibreza (2016); Dolati (2010)
3120	0	3120	mud	0.068	6	≤ 21.3K	Pleistocene-mid Holocene	Qa	Gharibreza (2016); Dolati (2010)
3121	0	3121	mud	0.205	6	≤ 21.3K	Pleistocene-mid Holocene	Qa	Gharibreza (2016); Dolati (2010)
3122	0	3122	mud	0.465	6	≤ 21.3K	Pleistocene-mid Holocene	Qa	Gharibreza (2016); Dolati (2010)
3123	0	3123	mud	0.012	6	≤ 21.3K	Pleistocene-mid Holocene	Qa	Gharibreza (2016); Dolati (2010)
3124	0	3124	mud	0.155	6	≤ 21.3K	Pleistocene-mid Holocene	Qa	Gharibreza (2016); Dolati (2010)
3125	0	3125	mud	0.541	6	≤ 21.3K	Pleistocene-mid Holocene	Qa	Gharibreza (2016); Dolati (2010)
3126	0	3126	mud	0.246	6	≤ 21.3K	Pleistocene-mid Holocene	Qa	Gharibreza (2016); Dolati (2010)
3127	0	3127	mud	0.020	6	≤ 21.3K	Pleistocene-mid Holocene	Qa	Gharibreza (2016); Dolati (2010)
3128	0	3128	mud	18.225	6	≤ 21.3K	Pleistocene-mid Holocene	Qa	Gharibreza (2016); Dolati (2010)
3129	0	3129	mud	0.566	6	≤ 21.3K	Pleistocene-mid Holocene	Qa	Gharibreza (2016); Dolati (2010)
3130	0	3130	mud	0.172	6	≤ 21.3K	Pleistocene-mid Holocene	Qa	Gharibreza (2016); Dolati (2010)
3131	0	3131	mud	0.008	6	≤ 21.3K	Pleistocene-mid Holocene	Qa	Gharibreza (2016); Dolati (2010)
3132	0	3132	mud	0.325	6	≤ 21.3K	Pleistocene-mid Holocene	Qa	Gharibreza (2016); Dolati (2010)
3133	0	3133	mud	0.029	6	≤ 21.3K	Pleistocene-mid Holocene	Qa	Gharibreza (2016); Dolati (2010)
3134	0	3134	mud	0.046	6	≤ 21.3K	Pleistocene-mid Holocene	Qa	Gharibreza (2016); Dolati (2010)
3135	0	3135	mud	0.043	6	≤ 21.3K	Pleistocene-mid Holocene	Qa	Gharibreza (2016); Dolati (2010)

Geonews

OBJECTID_1	Join_Count	TARGET_FID	Label	Shape_Area (sqkm)	ORIG_FID	Absolute_Age	Age_paleontology	Unit	Reference
3136	0	3136	mud	0.336	6	≤ 21.3K	Pleistocene-mid Holocene	Qa	Gharibreza (2016); Dolati (2010)
3137	0	3137	mud	0.032	6	≤ 21.3K	Pleistocene-mid Holocene	Qa	Gharibreza (2016); Dolati (2010)
3138	0	3138	mud	0.088	6	≤ 21.3K	Pleistocene-mid Holocene	Qa	Gharibreza (2016); Dolati (2010)
3139	0	3139	mud	0.112	6	≤ 21.3K	Pleistocene-mid Holocene	Qa	Gharibreza (2016); Dolati (2010)
3140	0	3140	mud	0.598	6	≤ 21.3K	Pleistocene-mid Holocene	Qa	Gharibreza (2016); Dolati (2010)
3141	0	3141	mud	0.040	6	≤ 21.3K	Pleistocene-mid Holocene	Qa	Gharibreza (2016); Dolati (2010)
3142	0	3142	mud	0.032	6	≤ 21.3K	Pleistocene-mid Holocene	Qa	Gharibreza (2016); Dolati (2010)
3143	0	3143	mud	0.536	6	≤ 21.3K	Pleistocene-mid Holocene	Qa	Gharibreza (2016); Dolati (2010)
3144	0	3144	mud	0.446	6	≤ 21.3K	Pleistocene-mid Holocene	Qa	Gharibreza (2016); Dolati (2010)
3145	0	3145	mud	1.405	6	≤ 21.3K	Pleistocene-mid Holocene	Qa	Gharibreza (2016); Dolati (2010)
3146	0	3146	mud	0.052	6	≤ 21.3K	Pleistocene-mid Holocene	Qa	Gharibreza (2016); Dolati (2010)
3147	0	3147	mud	0.045	6	≤ 21.3K	Pleistocene-mid Holocene	Qa	Gharibreza (2016); Dolati (2010)
3148	0	3148	mud	0.816	6	≤ 21.3K	Pleistocene-mid Holocene	Qa	Gharibreza (2016); Dolati (2010)
3149	0	3149	mud	0.040	6	≤ 21.3K	Pleistocene-mid Holocene	Qa	Gharibreza (2016); Dolati (2010)
3150	0	3150	mud	0.091	6	≤ 21.3K	Pleistocene-mid Holocene	Qa	Gharibreza (2016); Dolati (2010)
3151	0	3151	mud	0.046	6	≤ 21.3K	Pleistocene-mid Holocene	Qa	Gharibreza (2016); Dolati (2010)
3152	0	3152	mud	5.268	6	≤ 21.3K	Pleistocene-mid Holocene	Qa	Gharibreza (2016); Dolati (2010)
3153	0	3153	mud	0.081	6	≤ 21.3K	Pleistocene-mid Holocene	Qa	Gharibreza (2016); Dolati (2010)
3154	0	3154	mud	0.060	6	≤ 21.3K	Pleistocene-mid Holocene	Qa	Gharibreza (2016); Dolati (2010)
3155	0	3155	mud	0.162	6	≤ 21.3K	Pleistocene-mid Holocene	Qa	Gharibreza (2016); Dolati (2010)
3157	0	3157	mud	0.033	6	≤ 21.3K	Pleistocene-mid Holocene	Qa	Gharibreza (2016); Dolati (2010)
3158	0	3158	mud	0.213	6	≤ 21.3K	Pleistocene-mid Holocene	Qa	Gharibreza (2016); Dolati (2010)
3159	0	3159	mud	0.051	6	≤ 21.3K	Pleistocene-mid Holocene	Qa	Gharibreza (2016); Dolati (2010)
3160	0	3160	mud	0.244	6	≤ 21.3K	Pleistocene-mid Holocene	Qa	Gharibreza (2016); Dolati (2010)
3161	0	3161	mud	0.077	6	≤ 21.3K	Pleistocene-mid Holocene	Qa	Gharibreza (2016); Dolati (2010)
3162	0	3162	mud	0.382	6	≤ 21.3K	Pleistocene-mid Holocene	Qa	Gharibreza (2016); Dolati (2010)
3163	0	3163	mud	0.045	6	≤ 21.3K	Pleistocene-mid Holocene	Qa	Gharibreza (2016); Dolati (2010)
3164	0	3164	mud	0.902	6	≤ 21.3K	Pleistocene-mid Holocene	Qa	Gharibreza (2016); Dolati (2010)
3165	0	3165	mud	0.118	6	≤ 21.3K	Pleistocene-mid Holocene	Qa	Gharibreza (2016); Dolati (2010)
3166	0	3166	mud	0.088	6	≤ 21.3K	Pleistocene-mid Holocene	Qa	Gharibreza (2016); Dolati (2010)
3167	0	3167	mud	68.755	6	≤ 21.3K	Pleistocene-mid Holocene	Qa	Gharibreza (2016); Dolati (2010)
3168	0	3168	mud	0.188	6	≤ 21.3K	Pleistocene-mid Holocene	Qa	Gharibreza (2016); Dolati (2010)
3169	0	3169	mud	0.039	6	≤ 21.3K	Pleistocene-mid Holocene	Qa	Gharibreza (2016); Dolati (2010)
3170	0	3170	mud	0.315	6	≤ 21.3K	Pleistocene-mid Holocene	Qa	Gharibreza (2016); Dolati (2010)
3171	0	3171	mud	0.046	6	≤ 21.3K	Pleistocene-mid Holocene	Qa	Gharibreza (2016); Dolati (2010)
3172	0	3172	mud	0.039	6	≤ 21.3K	Pleistocene-mid Holocene	Qa	Gharibreza (2016); Dolati (2010)
3173	0	3173	mud	4.057	6	≤ 21.3K	Pleistocene-mid Holocene	Qa	Gharibreza (2016); Dolati (2010)
3174	0	3174	mud	0.162	6	≤ 21.3K	Pleistocene-mid Holocene	Qa	Gharibreza (2016); Dolati (2010)
3175	0	3175	mud	0.290	6	≤ 21.3K	Pleistocene-mid Holocene	Qa	Gharibreza (2016); Dolati (2010)

Preview

OBJECTID_1	Join_Count	TARGET_FID	Label	Shape_Area (sqkm)	ORIG_FID	Absolute_Age	Age_paleontology	Unit	Reference
3176	0	3176	mud	0.056	6	≤ 21.3K	Pleistocene-mid Holocene	Qa	Gharibreza (2016); Dolati (2010)
3177	0	3177	mud	0.144	6	≤ 21.3K	Pleistocene-mid Holocene	Qa	Gharibreza (2016); Dolati (2010)
3178	0	3178	mud	2.953	6	≤ 21.3K	Pleistocene-mid Holocene	Qa	Gharibreza (2016); Dolati (2010)
3179	0	3179	mud	0.262	6	≤ 21.3K	Pleistocene-mid Holocene	Qa	Gharibreza (2016); Dolati (2010)
3180	0	3180	mud	0.481	6	≤ 21.3K	Pleistocene-mid Holocene	Qa	Gharibreza (2016); Dolati (2010)
3181	0	3181	mud	0.124	6	≤ 21.3K	Pleistocene-mid Holocene	Qa	Gharibreza (2016); Dolati (2010)
3182	0	3182	mud	0.262	6	≤ 21.3K	Pleistocene-mid Holocene	Qa	Gharibreza (2016); Dolati (2010)
3183	0	3183	mud	0.044	6	≤ 21.3K	Pleistocene-mid Holocene	Qa	Gharibreza (2016); Dolati (2010)
3184	0	3184	mud	0.045	6	≤ 21.3K	Pleistocene-mid Holocene	Qa	Gharibreza (2016); Dolati (2010)
3185	0	3185	mud	0.117	6	≤ 21.3K	Pleistocene-mid Holocene	Qa	Gharibreza (2016); Dolati (2010)
3186	0	3186	mud	0.012	6	≤ 21.3K	Pleistocene-mid Holocene	Qa	Gharibreza (2016); Dolati (2010)
3187	0	3187	mud	0.028	6	≤ 21.3K	Pleistocene-mid Holocene	Qa	Gharibreza (2016); Dolati (2010)
3188	0	3188	mud	0.065	6	≤ 21.3K	Pleistocene-mid Holocene	Qa	Gharibreza (2016); Dolati (2010)
3189	0	3189	mud	0.040	6	≤ 21.3K	Pleistocene-mid Holocene	Qa	Gharibreza (2016); Dolati (2010)
3190	0	3190	mud	0.141	6	≤ 21.3K	Pleistocene-mid Holocene	Qa	Gharibreza (2016); Dolati (2010)
3191	0	3191	mud	0.054	6	≤ 21.3K	Pleistocene-mid Holocene	Qa	Gharibreza (2016); Dolati (2010)
3192	0	3192	mud	0.049	6	≤ 21.3K	Pleistocene-mid Holocene	Qa	Gharibreza (2016); Dolati (2010)
3193	0	3193	mud	0.704	6	≤ 21.3K	Pleistocene-mid Holocene	Qa	Gharibreza (2016); Dolati (2010)
3194	0	3194	mud	0.134	6	≤ 21.3K	Pleistocene-mid Holocene	Qa	Gharibreza (2016); Dolati (2010)
3195	0	3195	mud	0.041	6	≤ 21.3K	Pleistocene-mid Holocene	Qa	Gharibreza (2016); Dolati (2010)
3196	0	3196	mud	0.067	6	≤ 21.3K	Pleistocene-mid Holocene	Qa	Gharibreza (2016); Dolati (2010)
3197	0	3197	mud	0.079	6	≤ 21.3K	Pleistocene-mid Holocene	Qa	Gharibreza (2016); Dolati (2010)
3198	0	3198	mud	0.053	6	≤ 21.3K	Pleistocene-mid Holocene	Qa	Gharibreza (2016); Dolati (2010)
3199	0	3199	mud	0.031	6	≤ 21.3K	Pleistocene-mid Holocene	Qa	Gharibreza (2016); Dolati (2010)
3200	0	3200	mud	0.646	6	≤ 21.3K	Pleistocene-mid Holocene	Qa	Gharibreza (2016); Dolati (2010)
3201	0	3201	mud	1.190	6	≤ 21.3K	Pleistocene-mid Holocene	Qa	Gharibreza (2016); Dolati (2010)
3202	0	3202	mud	0.025	6	≤ 21.3K	Pleistocene-mid Holocene	Qa	Gharibreza (2016); Dolati (2010)
3203	0	3203	mud	0.021	6	≤ 21.3K	Pleistocene-mid Holocene	Qa	Gharibreza (2016); Dolati (2010)
3204	0	3204	mud	0.411	6	≤ 21.3K	Pleistocene-mid Holocene	Qa	Gharibreza (2016); Dolati (2010)
3205	0	3205	mud	0.050	6	≤ 21.3K	Pleistocene-mid Holocene	Qa	Gharibreza (2016); Dolati (2010)
3206	0	3206	mud	0.142	6	≤ 21.3K	Pleistocene-mid Holocene	Qa	Gharibreza (2016); Dolati (2010)
3207	0	3207	mud	0.314	6	≤ 21.3K	Pleistocene-mid Holocene	Qa	Gharibreza (2016); Dolati (2010)
3208	0	3208	mud	0.055	6	≤ 21.3K	Pleistocene-mid Holocene	Qa	Gharibreza (2016); Dolati (2010)
3209	0	3209	mud	0.239	6	≤ 21.3K	Pleistocene-mid Holocene	Qa	Gharibreza (2016); Dolati (2010)
3210	0	3210	mud	0.231	6	≤ 21.3K	Pleistocene-mid Holocene	Qa	Gharibreza (2016); Dolati (2010)
3211	0	3211	mud	0.005	6	≤ 21.3K	Pleistocene-mid Holocene	Qa	Gharibreza (2016); Dolati (2010)
3212	0	3212	mud	0.046	6	≤ 21.3K	Pleistocene-mid Holocene	Qa	Gharibreza (2016); Dolati (2010)
3213	0	3213	mud	0.251	6	≤ 21.3K	Pleistocene-mid Holocene	Qa	Gharibreza (2016); Dolati (2010)
3215	0	3215	mud	0.035	6	≤ 21.3K	Pleistocene-mid Holocene	Qa	Gharibreza (2016); Dolati (2010)

Preview

OBJECTID_1	Join_Count	TARGET_FID	Label	Shape_Area (sqkm)	ORIG_FID	Absolute_Age	Age_paleontology	Unit	Reference
3216	0	3216	mud	0.506	6	≤ 21.3K	Pleistocene-mid Holocene	Qa	Gharibreza (2016); Dolati (2010)
3217	0	3217	mud	0.027	6	≤ 21.3K	Pleistocene-mid Holocene	Qa	Gharibreza (2016); Dolati (2010)
3218	0	3218	mud	0.062	6	≤ 21.3K	Pleistocene-mid Holocene	Qa	Gharibreza (2016); Dolati (2010)
3219	0	3219	mud	0.031	6	≤ 21.3K	Pleistocene-mid Holocene	Qa	Gharibreza (2016); Dolati (2010)
3220	0	3220	mud	0.272	6	≤ 21.3K	Pleistocene-mid Holocene	Qa	Gharibreza (2016); Dolati (2010)
3221	0	3221	mud	0.035	6	≤ 21.3K	Pleistocene-mid Holocene	Qa	Gharibreza (2016); Dolati (2010)
3222	0	3222	mud	1.376	6	≤ 21.3K	Pleistocene-mid Holocene	Qa	Gharibreza (2016); Dolati (2010)
3223	0	3223	mud	0.084	6	≤ 21.3K	Pleistocene-mid Holocene	Qa	Gharibreza (2016); Dolati (2010)
3224	0	3224	mud	0.150	6	≤ 21.3K	Pleistocene-mid Holocene	Qa	Gharibreza (2016); Dolati (2010)
3225	0	3225	mud	0.092	6	≤ 21.3K	Pleistocene-mid Holocene	Qa	Gharibreza (2016); Dolati (2010)
3226	0	3226	mud	1.178	6	≤ 21.3K	Pleistocene-mid Holocene	Qa	Gharibreza (2016); Dolati (2010)
3227	0	3227	mud	0.032	6	≤ 21.3K	Pleistocene-mid Holocene	Qa	Gharibreza (2016); Dolati (2010)
3228	0	3228	mud	0.061	6	≤ 21.3K	Pleistocene-mid Holocene	Qa	Gharibreza (2016); Dolati (2010)
3229	0	3229	mud	0.040	6	≤ 21.3K	Pleistocene-mid Holocene	Qa	Gharibreza (2016); Dolati (2010)
3230	0	3230	mud	0.069	6	≤ 21.3K	Pleistocene-mid Holocene	Qa	Gharibreza (2016); Dolati (2010)
3231	0	3231	mud	0.069	6	≤ 21.3K	Pleistocene-mid Holocene	Qa	Gharibreza (2016); Dolati (2010)
3232	0	3232	mud	5.520	6	≤ 21.3K	Pleistocene-mid Holocene	Qa	Gharibreza (2016); Dolati (2010)
3233	0	3233	mud	0.342	6	≤ 21.3K	Pleistocene-mid Holocene	Qa	Gharibreza (2016); Dolati (2010)
3234	0	3234	mud	0.347	6	≤ 21.3K	Pleistocene-mid Holocene	Qa	Gharibreza (2016); Dolati (2010)
3235	0	3235	mud	0.108	6	≤ 21.3K	Pleistocene-mid Holocene	Qa	Gharibreza (2016); Dolati (2010)
3236	0	3236	mud	0.452	6	≤ 21.3K	Pleistocene-mid Holocene	Qa	Gharibreza (2016); Dolati (2010)
3237	0	3237	mud	0.165	6	≤ 21.3K	Pleistocene-mid Holocene	Qa	Gharibreza (2016); Dolati (2010)
3238	0	3238	mud	0.079	6	≤ 21.3K	Pleistocene-mid Holocene	Qa	Gharibreza (2016); Dolati (2010)
3239	0	3239	mud	0.031	6	≤ 21.3K	Pleistocene-mid Holocene	Qa	Gharibreza (2016); Dolati (2010)
3240	0	3240	mud	0.008	6	≤ 21.3K	Pleistocene-mid Holocene	Qa	Gharibreza (2016); Dolati (2010)
3241	0	3241	mud	0.065	6	≤ 21.3K	Pleistocene-mid Holocene	Qa	Gharibreza (2016); Dolati (2010)
3242	0	3242	mud	0.024	6	≤ 21.3K	Pleistocene-mid Holocene	Qa	Gharibreza (2016); Dolati (2010)
3243	0	3243	mud	0.067	6	≤ 21.3K	Pleistocene-mid Holocene	Qa	Gharibreza (2016); Dolati (2010)
3244	0	3244	mud	0.045	6	≤ 21.3K	Pleistocene-mid Holocene	Qa	Gharibreza (2016); Dolati (2010)
3245	0	3245	mud	0.166	6	≤ 21.3K	Pleistocene-mid Holocene	Qa	Gharibreza (2016); Dolati (2010)
3246	0	3246	mud	0.012	6	≤ 21.3K	Pleistocene-mid Holocene	Qa	Gharibreza (2016); Dolati (2010)
3247	0	3247	mud	0.918	6	≤ 21.3K	Pleistocene-mid Holocene	Qa	Gharibreza (2016); Dolati (2010)
3248	0	3248	mud	0.028	6	≤ 21.3K	Pleistocene-mid Holocene	Qa	Gharibreza (2016); Dolati (2010)
3249	0	3249	mud	0.300	6	≤ 21.3K	Pleistocene-mid Holocene	Qa	Gharibreza (2016); Dolati (2010)
3250	0	3250	mud	0.081	6	≤ 21.3K	Pleistocene-mid Holocene	Qa	Gharibreza (2016); Dolati (2010)
3251	0	3251	mud	0.089	6	≤ 21.3K	Pleistocene-mid Holocene	Qa	Gharibreza (2016); Dolati (2010)
3252	0	3252	mud	0.215	6	≤ 21.3K	Pleistocene-mid Holocene	Qa	Gharibreza (2016); Dolati (2010)
3253	0	3253	mud	0.185	6	≤ 21.3K	Pleistocene-mid Holocene	Qa	Gharibreza (2016); Dolati (2010)
3254	0	3254	mud	0.565	6	≤ 21.3K	Pleistocene-mid Holocene	Qa	Gharibreza (2016); Dolati (2010)

Reviews

OBJECTID_1	Join_Count	TARGET_FID	Label	Shape_Area (sqkm)	ORIG_FID	Absolute_Age	Age_paleontology	Unit	Reference
3255	0	3255	mud	0.044	6	≤ 21.3K	Pleistocene-mid Holocene	Qa	Gharibreza (2016); Dolati (2010)
3256	0	3256	mud	0.025	6	≤ 21.3K	Pleistocene-mid Holocene	Qa	Gharibreza (2016); Dolati (2010)
3257	0	3257	mud	0.091	6	≤ 21.3K	Pleistocene-mid Holocene	Qa	Gharibreza (2016); Dolati (2010)
3258	0	3258	mud	0.193	6	≤ 21.3K	Pleistocene-mid Holocene	Qa	Gharibreza (2016); Dolati (2010)
3259	0	3259	mud	0.259	6	≤ 21.3K	Pleistocene-mid Holocene	Qa	Gharibreza (2016); Dolati (2010)
3260	0	3260	mud	0.078	6	≤ 21.3K	Pleistocene-mid Holocene	Qa	Gharibreza (2016); Dolati (2010)
3261	0	3261	mud	0.152	6	≤ 21.3K	Pleistocene-mid Holocene	Qa	Gharibreza (2016); Dolati (2010)
3262	0	3262	mud	0.092	6	≤ 21.3K	Pleistocene-mid Holocene	Qa	Gharibreza (2016); Dolati (2010)
3263	0	3263	mud	0.116	6	≤ 21.3K	Pleistocene-mid Holocene	Qa	Gharibreza (2016); Dolati (2010)
3264	0	3264	mud	0.016	6	≤ 21.3K	Pleistocene-mid Holocene	Qa	Gharibreza (2016); Dolati (2010)
3265	0	3265	mud	0.039	6	≤ 21.3K	Pleistocene-mid Holocene	Qa	Gharibreza (2016); Dolati (2010)
3266	0	3266	mud	0.201	6	≤ 21.3K	Pleistocene-mid Holocene	Qa	Gharibreza (2016); Dolati (2010)
3267	0	3267	mud	0.219	6	≤ 21.3K	Pleistocene-mid Holocene	Qa	Gharibreza (2016); Dolati (2010)
3268	0	3268	mud	0.024	6	≤ 21.3K	Pleistocene-mid Holocene	Qa	Gharibreza (2016); Dolati (2010)
3269	0	3269	mud	0.605	6	≤ 21.3K	Pleistocene-mid Holocene	Qa	Gharibreza (2016); Dolati (2010)
3270	0	3270	mud	0.054	6	≤ 21.3K	Pleistocene-mid Holocene	Qa	Gharibreza (2016); Dolati (2010)
3271	0	3271	mud	0.076	6	≤ 21.3K	Pleistocene-mid Holocene	Qa	Gharibreza (2016); Dolati (2010)
3272	0	3272	mud	0.048	6	≤ 21.3K	Pleistocene-mid Holocene	Qa	Gharibreza (2016); Dolati (2010)
3273	0	3273	mud	0.182	6	≤ 21.3K	Pleistocene-mid Holocene	Qa	Gharibreza (2016); Dolati (2010)
3274	0	3274	mud	1.342	6	≤ 21.3K	Pleistocene-mid Holocene	Qa	Gharibreza (2016); Dolati (2010)
3275	0	3275	mud	0.060	6	≤ 21.3K	Pleistocene-mid Holocene	Qa	Gharibreza (2016); Dolati (2010)
3276	0	3276	mud	0.126	6	≤ 21.3K	Pleistocene-mid Holocene	Qa	Gharibreza (2016); Dolati (2010)
3277	0	3277	mud	0.060	6	≤ 21.3K	Pleistocene-mid Holocene	Qa	Gharibreza (2016); Dolati (2010)
3278	0	3278	mud	0.184	6	≤ 21.3K	Pleistocene-mid Holocene	Qa	Gharibreza (2016); Dolati (2010)
3279	0	3279	mud	0.942	6	≤ 21.3K	Pleistocene-mid Holocene	Qa	Gharibreza (2016); Dolati (2010)
3280	0	3280	mud	0.052	6	≤ 21.3K	Pleistocene-mid Holocene	Qa	Gharibreza (2016); Dolati (2010)
3281	0	3281	mud	0.072	6	≤ 21.3K	Pleistocene-mid Holocene	Qa	Gharibreza (2016); Dolati (2010)
3282	0	3282	mud	0.129	6	≤ 21.3K	Pleistocene-mid Holocene	Qa	Gharibreza (2016); Dolati (2010)
3283	0	3283	mud	0.279	6	≤ 21.3K	Pleistocene-mid Holocene	Qa	Gharibreza (2016); Dolati (2010)
3284	0	3284	mud	0.232	6	≤ 21.3K	Pleistocene-mid Holocene	Qa	Gharibreza (2016); Dolati (2010)
3285	0	3285	mud	0.106	6	≤ 21.3K	Pleistocene-mid Holocene	Qa	Gharibreza (2016); Dolati (2010)
3286	0	3286	mud	0.079	6	≤ 21.3K	Pleistocene-mid Holocene	Qa	Gharibreza (2016); Dolati (2010)
3287	0	3287	mud	0.123	6	≤ 21.3K	Pleistocene-mid Holocene	Qa	Gharibreza (2016); Dolati (2010)
3288	0	3288	mud	0.279	6	≤ 21.3K	Pleistocene-mid Holocene	Qa	Gharibreza (2016); Dolati (2010)
3289	0	3289	mud	0.025	6	≤ 21.3K	Pleistocene-mid Holocene	Qa	Gharibreza (2016); Dolati (2010)
3290	0	3290	mud	0.076	6	≤ 21.3K	Pleistocene-mid Holocene	Qa	Gharibreza (2016); Dolati (2010)
3291	0	3291	mud	0.150	6	≤ 21.3K	Pleistocene-mid Holocene	Qa	Gharibreza (2016); Dolati (2010)
3292	0	3292	mud	0.580	6	≤ 21.3K	Pleistocene-mid Holocene	Qa	Gharibreza (2016); Dolati (2010)
3293	0	3293	mud	0.075	6	≤ 21.3K	Pleistocene-mid Holocene	Qa	Gharibreza (2016); Dolati (2010)

Preview

OBJECTID_1	Join_Count	TARGET_FID	Label	Shape_Area (sqkm)	ORIG_FID	Absolute_Age	Age_paleontology	Unit	Reference
3294	0	3294	mud	0.208	6	≤ 21.3K	Pleistocene-mid Holocene	Qa	Gharibreza (2016); Dolati (2010)
3295	0	3295	mud	0.024	6	≤ 21.3K	Pleistocene-mid Holocene	Qa	Gharibreza (2016); Dolati (2010)
3296	0	3296	mud	3.919	6	≤ 21.3K	Pleistocene-mid Holocene	Qa	Gharibreza (2016); Dolati (2010)
3297	0	3297	mud	0.463	6	≤ 21.3K	Pleistocene-mid Holocene	Qa	Gharibreza (2016); Dolati (2010)
3298	0	3298	mud	0.045	6	≤ 21.3K	Pleistocene-mid Holocene	Qa	Gharibreza (2016); Dolati (2010)
3299	0	3299	mud	0.057	6	≤ 21.3K	Pleistocene-mid Holocene	Qa	Gharibreza (2016); Dolati (2010)
3300	0	3300	mud	0.125	6	≤ 21.3K	Pleistocene-mid Holocene	Qa	Gharibreza (2016); Dolati (2010)
3301	0	3301	mud	0.775	6	≤ 21.3K	Pleistocene-mid Holocene	Qa	Gharibreza (2016); Dolati (2010)
3302	0	3302	mud	0.077	6	≤ 21.3K	Pleistocene-mid Holocene	Qa	Gharibreza (2016); Dolati (2010)
3303	0	3303	mud	0.141	6	≤ 21.3K	Pleistocene-mid Holocene	Qa	Gharibreza (2016); Dolati (2010)
3304	0	3304	mud	0.147	6	≤ 21.3K	Pleistocene-mid Holocene	Qa	Gharibreza (2016); Dolati (2010)
3305	0	3305	mud	0.473	6	≤ 21.3K	Pleistocene-mid Holocene	Qa	Gharibreza (2016); Dolati (2010)
3306	0	3306	mud	0.049	6	≤ 21.3K	Pleistocene-mid Holocene	Qa	Gharibreza (2016); Dolati (2010)
3307	0	3307	mud	0.023	6	≤ 21.3K	Pleistocene-mid Holocene	Qa	Gharibreza (2016); Dolati (2010)
3308	0	3308	mud	3.819	6	≤ 21.3K	Pleistocene-mid Holocene	Qa	Gharibreza (2016); Dolati (2010)
3309	0	3309	mud	0.404	6	≤ 21.3K	Pleistocene-mid Holocene	Qa	Gharibreza (2016); Dolati (2010)
3310	0	3310	mud	0.078	6	≤ 21.3K	Pleistocene-mid Holocene	Qa	Gharibreza (2016); Dolati (2010)
3311	0	3311	mud	0.057	6	≤ 21.3K	Pleistocene-mid Holocene	Qa	Gharibreza (2016); Dolati (2010)
3312	0	3312	mud	0.280	6	≤ 21.3K	Pleistocene-mid Holocene	Qa	Gharibreza (2016); Dolati (2010)
3313	0	3313	mud	0.175	6	≤ 21.3K	Pleistocene-mid Holocene	Qa	Gharibreza (2016); Dolati (2010)
3314	0	3314	mud	0.030	6	≤ 21.3K	Pleistocene-mid Holocene	Qa	Gharibreza (2016); Dolati (2010)
3315	0	3315	mud	0.015	6	≤ 21.3K	Pleistocene-mid Holocene	Qa	Gharibreza (2016); Dolati (2010)
3316	0	3316	mud	0.058	6	≤ 21.3K	Pleistocene-mid Holocene	Qa	Gharibreza (2016); Dolati (2010)
3317	0	3317	mud	0.050	6	≤ 21.3K	Pleistocene-mid Holocene	Qa	Gharibreza (2016); Dolati (2010)
3318	0	3318	mud	0.045	6	≤ 21.3K	Pleistocene-mid Holocene	Qa	Gharibreza (2016); Dolati (2010)
3319	0	3319	mud	0.038	6	≤ 21.3K	Pleistocene-mid Holocene	Qa	Gharibreza (2016); Dolati (2010)
3320	0	3320	mud	0.027	6	≤ 21.3K	Pleistocene-mid Holocene	Qa	Gharibreza (2016); Dolati (2010)
3321	0	3321	mud	0.072	6	≤ 21.3K	Pleistocene-mid Holocene	Qa	Gharibreza (2016); Dolati (2010)
3322	0	3322	mud	4.688	6	≤ 21.3K	Pleistocene-mid Holocene	Qa	Gharibreza (2016); Dolati (2010)
3323	0	3323	mud	0.144	6	≤ 21.3K	Pleistocene-mid Holocene	Qa	Gharibreza (2016); Dolati (2010)
3324	0	3324	mud	0.311	6	≤ 21.3K	Pleistocene-mid Holocene	Qa	Gharibreza (2016); Dolati (2010)
3325	0	3325	mud	0.682	6	≤ 21.3K	Pleistocene-mid Holocene	Qa	Gharibreza (2016); Dolati (2010)
3326	0	3326	mud	228.372	6	≤ 21.3K	Pleistocene-mid Holocene	Qa	Gharibreza (2016); Dolati (2010)
3327	0	3327	mud	0.034	6	≤ 21.3K	Pleistocene-mid Holocene	Qa	Gharibreza (2016); Dolati (2010)
3328	0	3328	mud	0.317	6	≤ 21.3K	Pleistocene-mid Holocene	Qa	Gharibreza (2016); Dolati (2010)
3329	0	3329	mud	0.239	6	≤ 21.3K	Pleistocene-mid Holocene	Qa	Gharibreza (2016); Dolati (2010)
3330	0	3330	mud	0.067	6	≤ 21.3K	Pleistocene-mid Holocene	Qa	Gharibreza (2016); Dolati (2010)
3331	0	3331	mud	0.105	6	≤ 21.3K	Pleistocene-mid Holocene	Qa	Gharibreza (2016); Dolati (2010)
3332	0	3332	mud	1.521	6	≤ 21.3K	Pleistocene-mid Holocene	Qa	Gharibreza (2016); Dolati (2010)

Geonews

OBJECTID_1	Join_Count	TARGET_FID	Label	Shape_Area (sqkm)	ORIG_FID	Absolute_Age	Age_paleontology	Unit	Reference
3333	0	3333	mud	0.022	6	≤ 21.3K	Pleistocene-mid Holocene	Qa	Gharibreza (2016); Dolati (2010)
3334	0	3334	mud	0.023	6	≤ 21.3K	Pleistocene-mid Holocene	Qa	Gharibreza (2016); Dolati (2010)
3335	0	3335	mud	0.031	6	≤ 21.3K	Pleistocene-mid Holocene	Qa	Gharibreza (2016); Dolati (2010)
3336	0	3336	mud	0.272	6	≤ 21.3K	Pleistocene-mid Holocene	Qa	Gharibreza (2016); Dolati (2010)
3337	0	3337	mud	0.050	6	≤ 21.3K	Pleistocene-mid Holocene	Qa	Gharibreza (2016); Dolati (2010)
3338	0	3338	mud	0.083	6	≤ 21.3K	Pleistocene-mid Holocene	Qa	Gharibreza (2016); Dolati (2010)
3339	0	3339	mud	0.116	6	≤ 21.3K	Pleistocene-mid Holocene	Qa	Gharibreza (2016); Dolati (2010)
3340	0	3340	mud	0.020	6	≤ 21.3K	Pleistocene-mid Holocene	Qa	Gharibreza (2016); Dolati (2010)
3341	0	3341	mud	0.151	6	≤ 21.3K	Pleistocene-mid Holocene	Qa	Gharibreza (2016); Dolati (2010)
3342	0	3342	mud	0.018	6	≤ 21.3K	Pleistocene-mid Holocene	Qa	Gharibreza (2016); Dolati (2010)
3343	0	3343	mud	0.032	6	≤ 21.3K	Pleistocene-mid Holocene	Qa	Gharibreza (2016); Dolati (2010)
3344	0	3344	mud	0.062	6	≤ 21.3K	Pleistocene-mid Holocene	Qa	Gharibreza (2016); Dolati (2010)
3346	0	3346	mud	0.030	6	≤ 21.3K	Pleistocene-mid Holocene	Qa	Gharibreza (2016); Dolati (2010)
3347	0	3347	mud	0.607	6	≤ 21.3K	Pleistocene-mid Holocene	Qa	Gharibreza (2016); Dolati (2010)
3348	0	3348	mud	0.014	6	≤ 21.3K	Pleistocene-mid Holocene	Qa	Gharibreza (2016); Dolati (2010)
3349	0	3349	mud	0.137	6	≤ 21.3K	Pleistocene-mid Holocene	Qa	Gharibreza (2016); Dolati (2010)
3350	0	3350	mud	0.032	6	≤ 21.3K	Pleistocene-mid Holocene	Qa	Gharibreza (2016); Dolati (2010)
3351	0	3351	mud	0.102	6	≤ 21.3K	Pleistocene-mid Holocene	Qa	Gharibreza (2016); Dolati (2010)
3352	0	3352	mud	0.033	6	≤ 21.3K	Pleistocene-mid Holocene	Qa	Gharibreza (2016); Dolati (2010)
3353	0	3353	mud	0.176	6	≤ 21.3K	Pleistocene-mid Holocene	Qa	Gharibreza (2016); Dolati (2010)
3354	0	3354	mud	0.066	6	≤ 21.3K	Pleistocene-mid Holocene	Qa	Gharibreza (2016); Dolati (2010)
3355	0	3355	mud	0.156	6	≤ 21.3K	Pleistocene-mid Holocene	Qa	Gharibreza (2016); Dolati (2010)
3356	0	3356	mud	0.090	6	≤ 21.3K	Pleistocene-mid Holocene	Qa	Gharibreza (2016); Dolati (2010)
3357	0	3357	mud	0.014	6	≤ 21.3K	Pleistocene-mid Holocene	Qa	Gharibreza (2016); Dolati (2010)
3358	0	3358	mud	0.037	6	≤ 21.3K	Pleistocene-mid Holocene	Qa	Gharibreza (2016); Dolati (2010)
3359	0	3359	mud	0.077	6	≤ 21.3K	Pleistocene-mid Holocene	Qa	Gharibreza (2016); Dolati (2010)
3360	0	3360	mud	0.236	6	≤ 21.3K	Pleistocene-mid Holocene	Qa	Gharibreza (2016); Dolati (2010)
3361	0	3361	mud	0.177	6	≤ 21.3K	Pleistocene-mid Holocene	Qa	Gharibreza (2016); Dolati (2010)
3362	0	3362	mud	0.096	6	≤ 21.3K	Pleistocene-mid Holocene	Qa	Gharibreza (2016); Dolati (2010)
3363	0	3363	mud	0.022	6	≤ 21.3K	Pleistocene-mid Holocene	Qa	Gharibreza (2016); Dolati (2010)
3364	0	3364	mud	0.464	6	≤ 21.3K	Pleistocene-mid Holocene	Qa	Gharibreza (2016); Dolati (2010)
3365	0	3365	mud	4.074	6	≤ 21.3K	Pleistocene-mid Holocene	Qa	Gharibreza (2016); Dolati (2010)
3366	0	3366	mud	0.057	6	≤ 21.3K	Pleistocene-mid Holocene	Qa	Gharibreza (2016); Dolati (2010)
3367	0	3367	mud	0.056	6	≤ 21.3K	Pleistocene-mid Holocene	Qa	Gharibreza (2016); Dolati (2010)
3368	0	3368	mud	0.108	6	≤ 21.3K	Pleistocene-mid Holocene	Qa	Gharibreza (2016); Dolati (2010)
3369	0	3369	mud	0.052	6	≤ 21.3K	Pleistocene-mid Holocene	Qa	Gharibreza (2016); Dolati (2010)
3370	0	3370	mud	0.175	6	≤ 21.3K	Pleistocene-mid Holocene	Qa	Gharibreza (2016); Dolati (2010)
3371	0	3371	mud	0.294	6	≤ 21.3K	Pleistocene-mid Holocene	Qa	Gharibreza (2016); Dolati (2010)
3372	0	3372	mud	0.392	6	≤ 21.3K	Pleistocene-mid Holocene	Qa	Gharibreza (2016); Dolati (2010)

Preview

OBJECTID_1	Join_Count	TARGET_FID	Label	Shape_Area (sqkm)	ORIG_FID	Absolute_Age	Age_paleontology	Unit	Reference
3373	0	3373	mud	0.055	6	≤ 21.3K	Pleistocene-mid Holocene	Qa	Gharibreza (2016); Dolati (2010)
3374	0	3374	mud	0.055	6	≤ 21.3K	Pleistocene-mid Holocene	Qa	Gharibreza (2016); Dolati (2010)
3375	0	3375	mud	0.036	6	≤ 21.3K	Pleistocene-mid Holocene	Qa	Gharibreza (2016); Dolati (2010)
3376	0	3376	mud	0.043	6	≤ 21.3K	Pleistocene-mid Holocene	Qa	Gharibreza (2016); Dolati (2010)
3377	0	3377	mud	0.170	6	≤ 21.3K	Pleistocene-mid Holocene	Qa	Gharibreza (2016); Dolati (2010)
3378	0	3378	mud	0.077	6	≤ 21.3K	Pleistocene-mid Holocene	Qa	Gharibreza (2016); Dolati (2010)
3379	0	3379	mud	0.079	6	≤ 21.3K	Pleistocene-mid Holocene	Qa	Gharibreza (2016); Dolati (2010)
3380	0	3380	mud	0.195	6	≤ 21.3K	Pleistocene-mid Holocene	Qa	Gharibreza (2016); Dolati (2010)
3381	0	3381	mud	0.077	6	≤ 21.3K	Pleistocene-mid Holocene	Qa	Gharibreza (2016); Dolati (2010)
3382	0	3382	mud	0.321	6	≤ 21.3K	Pleistocene-mid Holocene	Qa	Gharibreza (2016); Dolati (2010)
3383	0	3383	mud	0.136	6	≤ 21.3K	Pleistocene-mid Holocene	Qa	Gharibreza (2016); Dolati (2010)
3384	0	3384	mud	0.053	6	≤ 21.3K	Pleistocene-mid Holocene	Qa	Gharibreza (2016); Dolati (2010)
3385	0	3385	mud	0.028	6	≤ 21.3K	Pleistocene-mid Holocene	Qa	Gharibreza (2016); Dolati (2010)
3386	0	3386	mud	0.072	6	≤ 21.3K	Pleistocene-mid Holocene	Qa	Gharibreza (2016); Dolati (2010)
3387	0	3387	mud	0.219	6	≤ 21.3K	Pleistocene-mid Holocene	Qa	Gharibreza (2016); Dolati (2010)
3388	0	3388	mud	0.044	6	≤ 21.3K	Pleistocene-mid Holocene	Qa	Gharibreza (2016); Dolati (2010)
3389	0	3389	mud	0.085	6	≤ 21.3K	Pleistocene-mid Holocene	Qa	Gharibreza (2016); Dolati (2010)
3390	0	3390	mud	0.053	6	≤ 21.3K	Pleistocene-mid Holocene	Qa	Gharibreza (2016); Dolati (2010)
3391	0	3391	mud	0.071	6	≤ 21.3K	Pleistocene-mid Holocene	Qa	Gharibreza (2016); Dolati (2010)
3392	0	3392	mud	0.020	6	≤ 21.3K	Pleistocene-mid Holocene	Qa	Gharibreza (2016); Dolati (2010)
3393	0	3393	mud	0.026	6	≤ 21.3K	Pleistocene-mid Holocene	Qa	Gharibreza (2016); Dolati (2010)
3394	0	3394	mud	0.071	6	≤ 21.3K	Pleistocene-mid Holocene	Qa	Gharibreza (2016); Dolati (2010)
3395	0	3395	mud	5.406	6	≤ 21.3K	Pleistocene-mid Holocene	Qa	Gharibreza (2016); Dolati (2010)
3396	0	3396	mud	0.092	6	≤ 21.3K	Pleistocene-mid Holocene	Qa	Gharibreza (2016); Dolati (2010)
3397	0	3397	mud	0.018	6	≤ 21.3K	Pleistocene-mid Holocene	Qa	Gharibreza (2016); Dolati (2010)
3399	0	3399	mud	0.024	6	≤ 21.3K	Pleistocene-mid Holocene	Qa	Gharibreza (2016); Dolati (2010)
3400	0	3400	mud	0.228	6	≤ 21.3K	Pleistocene-mid Holocene	Qa	Gharibreza (2016); Dolati (2010)
3401	0	3401	mud	0.022	6	≤ 21.3K	Pleistocene-mid Holocene	Qa	Gharibreza (2016); Dolati (2010)
3402	0	3402	mud	0.041	6	≤ 21.3K	Pleistocene-mid Holocene	Qa	Gharibreza (2016); Dolati (2010)
3404	0	3404	mud	0.109	6	≤ 21.3K	Pleistocene-mid Holocene	Qa	Gharibreza (2016); Dolati (2010)
3405	0	3405	mud	0.025	6	≤ 21.3K	Pleistocene-mid Holocene	Qa	Gharibreza (2016); Dolati (2010)
3406	0	3406	mud	0.013	6	≤ 21.3K	Pleistocene-mid Holocene	Qa	Gharibreza (2016); Dolati (2010)
3407	0	3407	mud	0.062	6	≤ 21.3K	Pleistocene-mid Holocene	Qa	Gharibreza (2016); Dolati (2010)
3408	0	3408	mud	0.040	6	≤ 21.3K	Pleistocene-mid Holocene	Qa	Gharibreza (2016); Dolati (2010)
3410	0	3410	mud	0.014	6	≤ 21.3K	Pleistocene-mid Holocene	Qa	Gharibreza (2016); Dolati (2010)
3411	0	3411	mud	0.048	6	≤ 21.3K	Pleistocene-mid Holocene	Qa	Gharibreza (2016); Dolati (2010)
3412	0	3412	mud	0.024	6	≤ 21.3K	Pleistocene-mid Holocene	Qa	Gharibreza (2016); Dolati (2010)
3413	0	3413	mud	0.063	6	≤ 21.3K	Pleistocene-mid Holocene	Qa	Gharibreza (2016); Dolati (2010)
3414	0	3414	mud	0.066	6	≤ 21.3K	Pleistocene-mid Holocene	Qa	Gharibreza (2016); Dolati (2010)

Preview

OBJECTID_1	Join_Count	TARGET_FID	Label	Shape_Area (sqkm)	ORIG_FID	Absolute_Age	Age_paleontology	Unit	Reference
3415	0	3415	mud	0.195	6	≤ 21.3K	Pleistocene-mid Holocene	Qa	Gharibreza (2016); Dolati (2010)
3417	0	3417	mud	0.062	6	≤ 21.3K	Pleistocene-mid Holocene	Qa	Gharibreza (2016); Dolati (2010)
3418	0	3418	mud	0.159	6	≤ 21.3K	Pleistocene-mid Holocene	Qa	Gharibreza (2016); Dolati (2010)
3420	0	3420	mud	0.037	6	≤ 21.3K	Pleistocene-mid Holocene	Qa	Gharibreza (2016); Dolati (2010)
3421	0	3421	mud	0.124	6	≤ 21.3K	Pleistocene-mid Holocene	Qa	Gharibreza (2016); Dolati (2010)
3422	0	3422	mud	0.015	6	≤ 21.3K	Pleistocene-mid Holocene	Qa	Gharibreza (2016); Dolati (2010)
3423	0	3423	mud	0.030	6	≤ 21.3K	Pleistocene-mid Holocene	Qa	Gharibreza (2016); Dolati (2010)
3424	0	3424	mud	0.016	6	≤ 21.3K	Pleistocene-mid Holocene	Qa	Gharibreza (2016); Dolati (2010)
3425	0	3425	mud	0.057	6	≤ 21.3K	Pleistocene-mid Holocene	Qa	Gharibreza (2016); Dolati (2010)
3426	0	3426	mud	0.046	6	≤ 21.3K	Pleistocene-mid Holocene	Qa	Gharibreza (2016); Dolati (2010)
3427	0	3427	mud	0.029	6	≤ 21.3K	Pleistocene-mid Holocene	Qa	Gharibreza (2016); Dolati (2010)
3428	0	3428	mud	0.064	6	≤ 21.3K	Pleistocene-mid Holocene	Qa	Gharibreza (2016); Dolati (2010)
3429	0	3429	mud	0.035	6	≤ 21.3K	Pleistocene-mid Holocene	Qa	Gharibreza (2016); Dolati (2010)
3430	0	3430	mud	0.112	6	≤ 21.3K	Pleistocene-mid Holocene	Qa	Gharibreza (2016); Dolati (2010)
3431	0	3431	mud	0.010	6	≤ 21.3K	Pleistocene-mid Holocene	Qa	Gharibreza (2016); Dolati (2010)
3434	0	3434	mud	0.348	6	≤ 21.3K	Pleistocene-mid Holocene	Qa	Gharibreza (2016); Dolati (2010)
3435	0	3435	mud	0.026	6	≤ 21.3K	Pleistocene-mid Holocene	Qa	Gharibreza (2016); Dolati (2010)
3436	0	3436	mud	0.030	6	≤ 21.3K	Pleistocene-mid Holocene	Qa	Gharibreza (2016); Dolati (2010)
3437	0	3437	mud	0.022	6	≤ 21.3K	Pleistocene-mid Holocene	Qa	Gharibreza (2016); Dolati (2010)
3438	0	3438	mud	0.034	6	≤ 21.3K	Pleistocene-mid Holocene	Qa	Gharibreza (2016); Dolati (2010)
3439	0	3439	mud	0.013	6	≤ 21.3K	Pleistocene-mid Holocene	Qa	Gharibreza (2016); Dolati (2010)
3440	0	3440	mud	0.030	6	≤ 21.3K	Pleistocene-mid Holocene	Qa	Gharibreza (2016); Dolati (2010)
3441	0	3441	mud	0.155	6	≤ 21.3K	Pleistocene-mid Holocene	Qa	Gharibreza (2016); Dolati (2010)
3442	0	3442	mud	0.039	6	≤ 21.3K	Pleistocene-mid Holocene	Qa	Gharibreza (2016); Dolati (2010)
3443	0	3443	mud	0.574	6	≤ 21.3K	Pleistocene-mid Holocene	Qa	Gharibreza (2016); Dolati (2010)
3444	0	3444	mud	0.309	6	≤ 21.3K	Pleistocene-mid Holocene	Qa	Gharibreza (2016); Dolati (2010)
3445	0	3445	mud	0.034	6	≤ 21.3K	Pleistocene-mid Holocene	Qa	Gharibreza (2016); Dolati (2010)
3446	0	3446	mud	0.130	6	≤ 21.3K	Pleistocene-mid Holocene	Qa	Gharibreza (2016); Dolati (2010)
3447	0	3447	mud	0.037	6	≤ 21.3K	Pleistocene-mid Holocene	Qa	Gharibreza (2016); Dolati (2010)
3448	0	3448	mud	0.041	6	≤ 21.3K	Pleistocene-mid Holocene	Qa	Gharibreza (2016); Dolati (2010)
3449	0	3449	mud	0.026	6	≤ 21.3K	Pleistocene-mid Holocene	Qa	Gharibreza (2016); Dolati (2010)
3450	0	3450	mud	0.413	6	≤ 21.3K	Pleistocene-mid Holocene	Qa	Gharibreza (2016); Dolati (2010)
3451	0	3451	mud	0.113	6	≤ 21.3K	Pleistocene-mid Holocene	Qa	Gharibreza (2016); Dolati (2010)
3452	0	3452	mud	0.069	6	≤ 21.3K	Pleistocene-mid Holocene	Qa	Gharibreza (2016); Dolati (2010)
3453	0	3453	mud	0.068	6	≤ 21.3K	Pleistocene-mid Holocene	Qa	Gharibreza (2016); Dolati (2010)
3454	0	3454	mud	0.620	6	≤ 21.3K	Pleistocene-mid Holocene	Qa	Gharibreza (2016); Dolati (2010)
3455	0	3455	mud	0.031	6	≤ 21.3K	Pleistocene-mid Holocene	Qa	Gharibreza (2016); Dolati (2010)
3456	0	3456	mud	0.527	6	≤ 21.3K	Pleistocene-mid Holocene	Qa	Gharibreza (2016); Dolati (2010)
3457	0	3457	mud	0.039	6	≤ 21.3K	Pleistocene-mid Holocene	Qa	Gharibreza (2016); Dolati (2010)

Preview

OBJECTID_1	Join_Count	TARGET_FID	Label	Shape_Area (sqkm)	ORIG_FID	Absolute_Age	Age_paleontology	Unit	Reference
3458	0	3458	mud	0.070	6	≤ 21.3K	Pleistocene-mid Holocene	Qa	Gharibreza (2016); Dolati (2010)
3459	0	3459	mud	0.029	6	≤ 21.3K	Pleistocene-mid Holocene	Qa	Gharibreza (2016); Dolati (2010)
3460	0	3460	mud	0.027	6	≤ 21.3K	Pleistocene-mid Holocene	Qa	Gharibreza (2016); Dolati (2010)
3461	0	3461	mud	0.012	6	≤ 21.3K	Pleistocene-mid Holocene	Qa	Gharibreza (2016); Dolati (2010)
3462	0	3462	mud	0.165	6	≤ 21.3K	Pleistocene-mid Holocene	Qa	Gharibreza (2016); Dolati (2010)
3463	0	3463	mud	0.174	6	≤ 21.3K	Pleistocene-mid Holocene	Qa	Gharibreza (2016); Dolati (2010)
3464	0	3464	mud	0.067	6	≤ 21.3K	Pleistocene-mid Holocene	Qa	Gharibreza (2016); Dolati (2010)
3465	0	3465	mud	0.007	6	≤ 21.3K	Pleistocene-mid Holocene	Qa	Gharibreza (2016); Dolati (2010)
3466	0	3466	mud	0.047	6	≤ 21.3K	Pleistocene-mid Holocene	Qa	Gharibreza (2016); Dolati (2010)
3467	0	3467	mud	0.004	6	≤ 21.3K	Pleistocene-mid Holocene	Qa	Gharibreza (2016); Dolati (2010)
3468	0	3468	mud	0.033	6	≤ 21.3K	Pleistocene-mid Holocene	Qa	Gharibreza (2016); Dolati (2010)
3469	0	3469	mud	0.134	6	≤ 21.3K	Pleistocene-mid Holocene	Qa	Gharibreza (2016); Dolati (2010)
3470	0	3470	mud	0.020	6	≤ 21.3K	Pleistocene-mid Holocene	Qa	Gharibreza (2016); Dolati (2010)
3471	0	3471	mud	0.120	6	≤ 21.3K	Pleistocene-mid Holocene	Qa	Gharibreza (2016); Dolati (2010)
3472	0	3472	mud	0.022	6	≤ 21.3K	Pleistocene-mid Holocene	Qa	Gharibreza (2016); Dolati (2010)
3473	0	3473	mud	0.037	6	≤ 21.3K	Pleistocene-mid Holocene	Qa	Gharibreza (2016); Dolati (2010)
3474	0	3474	mud	0.623	6	≤ 21.3K	Pleistocene-mid Holocene	Qa	Gharibreza (2016); Dolati (2010)
3475	0	3475	mud	0.045	6	≤ 21.3K	Pleistocene-mid Holocene	Qa	Gharibreza (2016); Dolati (2010)
3476	0	3476	mud	0.030	6	≤ 21.3K	Pleistocene-mid Holocene	Qa	Gharibreza (2016); Dolati (2010)
3477	0	3477	mud	0.013	6	≤ 21.3K	Pleistocene-mid Holocene	Qa	Gharibreza (2016); Dolati (2010)
3478	0	3478	mud	0.102	6	≤ 21.3K	Pleistocene-mid Holocene	Qa	Gharibreza (2016); Dolati (2010)
3479	0	3479	mud	0.109	6	≤ 21.3K	Pleistocene-mid Holocene	Qa	Gharibreza (2016); Dolati (2010)
3480	0	3480	mud	0.036	6	≤ 21.3K	Pleistocene-mid Holocene	Qa	Gharibreza (2016); Dolati (2010)
3482	0	3482	mud	0.228	6	≤ 21.3K	Pleistocene-mid Holocene	Qa	Gharibreza (2016); Dolati (2010)
3483	0	3483	mud	0.023	6	≤ 21.3K	Pleistocene-mid Holocene	Qa	Gharibreza (2016); Dolati (2010)
3484	0	3484	mud	0.556	6	≤ 21.3K	Pleistocene-mid Holocene	Qa	Gharibreza (2016); Dolati (2010)
3485	0	3485	mud	0.035	6	≤ 21.3K	Pleistocene-mid Holocene	Qa	Gharibreza (2016); Dolati (2010)
3486	0	3486	mud	0.022	6	≤ 21.3K	Pleistocene-mid Holocene	Qa	Gharibreza (2016); Dolati (2010)
3487	0	3487	mud	0.680	6	≤ 21.3K	Pleistocene-mid Holocene	Qa	Gharibreza (2016); Dolati (2010)
3488	0	3488	mud	0.019	6	≤ 21.3K	Pleistocene-mid Holocene	Qa	Gharibreza (2016); Dolati (2010)
3489	0	3489	mud	0.057	6	≤ 21.3K	Pleistocene-mid Holocene	Qa	Gharibreza (2016); Dolati (2010)
3490	0	3490	mud	0.048	6	≤ 21.3K	Pleistocene-mid Holocene	Qa	Gharibreza (2016); Dolati (2010)
3491	0	3491	mud	0.051	6	≤ 21.3K	Pleistocene-mid Holocene	Qa	Gharibreza (2016); Dolati (2010)
3492	0	3492	mud	0.048	6	≤ 21.3K	Pleistocene-mid Holocene	Qa	Gharibreza (2016); Dolati (2010)
3493	0	3493	mud	0.015	6	≤ 21.3K	Pleistocene-mid Holocene	Qa	Gharibreza (2016); Dolati (2010)
3494	0	3494	mud	0.028	6	≤ 21.3K	Pleistocene-mid Holocene	Qa	Gharibreza (2016); Dolati (2010)
3495	0	3495	mud	0.012	6	≤ 21.3K	Pleistocene-mid Holocene	Qa	Gharibreza (2016); Dolati (2010)
3496	0	3496	mud	0.010	6	≤ 21.3K	Pleistocene-mid Holocene	Qa	Gharibreza (2016); Dolati (2010)
3497	0	3497	mud	0.049	6	≤ 21.3K	Pleistocene-mid Holocene	Qa	Gharibreza (2016); Dolati (2010)

Preview

OBJECTID_1	Join_Count	TARGET_FID	Label	Shape_Area (sqkm)	ORIG_FID	Absolute_Age	Age_paleontology	Unit	Reference
3498	0	3498	mud	0.045	6	≤ 21.3K	Pleistocene-mid Holocene	Qa	Gharibreza (2016); Dolati (2010)
3499	0	3499	mud	0.250	6	≤ 21.3K	Pleistocene-mid Holocene	Qa	Gharibreza (2016); Dolati (2010)
3500	0	3500	mud	0.155	6	≤ 21.3K	Pleistocene-mid Holocene	Qa	Gharibreza (2016); Dolati (2010)
3501	0	3501	mud	0.013	6	≤ 21.3K	Pleistocene-mid Holocene	Qa	Gharibreza (2016); Dolati (2010)
3502	0	3502	mud	0.049	6	≤ 21.3K	Pleistocene-mid Holocene	Qa	Gharibreza (2016); Dolati (2010)
3503	0	3503	mud	0.658	6	≤ 21.3K	Pleistocene-mid Holocene	Qa	Gharibreza (2016); Dolati (2010)
3504	0	3504	mud	0.204	6	≤ 21.3K	Pleistocene-mid Holocene	Qa	Gharibreza (2016); Dolati (2010)
3505	0	3505	mud	0.028	6	≤ 21.3K	Pleistocene-mid Holocene	Qa	Gharibreza (2016); Dolati (2010)
3506	0	3506	mud	0.014	6	≤ 21.3K	Pleistocene-mid Holocene	Qa	Gharibreza (2016); Dolati (2010)
3508	0	3508	mud	0.091	6	≤ 21.3K	Pleistocene-mid Holocene	Qa	Gharibreza (2016); Dolati (2010)
3509	0	3509	mud	0.557	6	≤ 21.3K	Pleistocene-mid Holocene	Qa	Gharibreza (2016); Dolati (2010)
3510	0	3510	mud	0.017	6	≤ 21.3K	Pleistocene-mid Holocene	Qa	Gharibreza (2016); Dolati (2010)
3511	0	3511	mud	0.006	6	≤ 21.3K	Pleistocene-mid Holocene	Qa	Gharibreza (2016); Dolati (2010)
3512	0	3512	mud	0.056	6	≤ 21.3K	Pleistocene-mid Holocene	Qa	Gharibreza (2016); Dolati (2010)
3513	0	3513	mud	0.024	6	≤ 21.3K	Pleistocene-mid Holocene	Qa	Gharibreza (2016); Dolati (2010)
3514	0	3514	mud	0.020	6	≤ 21.3K	Pleistocene-mid Holocene	Qa	Gharibreza (2016); Dolati (2010)
3515	0	3515	mud	0.018	6	≤ 21.3K	Pleistocene-mid Holocene	Qa	Gharibreza (2016); Dolati (2010)
3516	0	3516	mud	0.056	6	≤ 21.3K	Pleistocene-mid Holocene	Qa	Gharibreza (2016); Dolati (2010)
3517	0	3517	mud	0.026	6	≤ 21.3K	Pleistocene-mid Holocene	Qa	Gharibreza (2016); Dolati (2010)
3518	0	3518	mud	0.033	6	≤ 21.3K	Pleistocene-mid Holocene	Qa	Gharibreza (2016); Dolati (2010)
3519	0	3519	mud	0.070	6	≤ 21.3K	Pleistocene-mid Holocene	Qa	Gharibreza (2016); Dolati (2010)
3520	0	3520	mud	0.046	6	≤ 21.3K	Pleistocene-mid Holocene	Qa	Gharibreza (2016); Dolati (2010)
3521	0	3521	mud	0.003	6	≤ 21.3K	Pleistocene-mid Holocene	Qa	Gharibreza (2016); Dolati (2010)
3522	0	3522	mud	0.134	6	≤ 21.3K	Pleistocene-mid Holocene	Qa	Gharibreza (2016); Dolati (2010)
3524	0	3524	mud	0.005	6	≤ 21.3K	Pleistocene-mid Holocene	Qa	Gharibreza (2016); Dolati (2010)
3525	0	3525	mud	0.035	6	≤ 21.3K	Pleistocene-mid Holocene	Qa	Gharibreza (2016); Dolati (2010)
3526	0	3526	mud	0.040	6	≤ 21.3K	Pleistocene-mid Holocene	Qa	Gharibreza (2016); Dolati (2010)
3527	0	3527	mud	0.041	6	≤ 21.3K	Pleistocene-mid Holocene	Qa	Gharibreza (2016); Dolati (2010)
3528	0	3528	mud	0.016	6	≤ 21.3K	Pleistocene-mid Holocene	Qa	Gharibreza (2016); Dolati (2010)
3529	0	3529	mud	0.082	6	≤ 21.3K	Pleistocene-mid Holocene	Qa	Gharibreza (2016); Dolati (2010)
3530	0	3530	mud	0.029	6	≤ 21.3K	Pleistocene-mid Holocene	Qa	Gharibreza (2016); Dolati (2010)
3531	0	3531	mud	0.030	6	≤ 21.3K	Pleistocene-mid Holocene	Qa	Gharibreza (2016); Dolati (2010)
3532	0	3532	mud	0.020	6	≤ 21.3K	Pleistocene-mid Holocene	Qa	Gharibreza (2016); Dolati (2010)
3533	0	3533	mud	0.036	6	≤ 21.3K	Pleistocene-mid Holocene	Qa	Gharibreza (2016); Dolati (2010)
3534	0	3534	mud	0.024	6	≤ 21.3K	Pleistocene-mid Holocene	Qa	Gharibreza (2016); Dolati (2010)
3535	0	3535	mud	0.029	6	≤ 21.3K	Pleistocene-mid Holocene	Qa	Gharibreza (2016); Dolati (2010)
3536	0	3536	mud	0.031	6	≤ 21.3K	Pleistocene-mid Holocene	Qa	Gharibreza (2016); Dolati (2010)
3537	0	3537	mud	0.018	6	≤ 21.3K	Pleistocene-mid Holocene	Qa	Gharibreza (2016); Dolati (2010)
3538	0	3538	mud	0.115	6	≤ 21.3K	Pleistocene-mid Holocene	Qa	Gharibreza (2016); Dolati (2010)

Preview

OBJECTID_1	Join_Count	TARGET_FID	Label	Shape_Area (sqkm)	ORIG_FID	Absolute_Age	Age_paleontology	Unit	Reference
3539	0	3539	mud	0.051	6	≤ 21.3K	Pleistocene-mid Holocene	Qa	Gharibreza (2016); Dolati (2010)
3540	0	3540	mud	0.051	6	≤ 21.3K	Pleistocene-mid Holocene	Qa	Gharibreza (2016); Dolati (2010)
3541	0	3541	mud	0.971	6	≤ 21.3K	Pleistocene-mid Holocene	Qa	Gharibreza (2016); Dolati (2010)
3542	0	3542	mud	0.059	6	≤ 21.3K	Pleistocene-mid Holocene	Qa	Gharibreza (2016); Dolati (2010)
3543	0	3543	mud	0.060	6	≤ 21.3K	Pleistocene-mid Holocene	Qa	Gharibreza (2016); Dolati (2010)
3544	0	3544	mud	0.192	6	≤ 21.3K	Pleistocene-mid Holocene	Qa	Gharibreza (2016); Dolati (2010)
3545	0	3545	mud	0.077	6	≤ 21.3K	Pleistocene-mid Holocene	Qa	Gharibreza (2016); Dolati (2010)
3546	0	3546	mud	0.018	6	≤ 21.3K	Pleistocene-mid Holocene	Qa	Gharibreza (2016); Dolati (2010)
3547	0	3547	mud	0.020	6	≤ 21.3K	Pleistocene-mid Holocene	Qa	Gharibreza (2016); Dolati (2010)
3548	0	3548	mud	0.087	6	≤ 21.3K	Pleistocene-mid Holocene	Qa	Gharibreza (2016); Dolati (2010)
3549	0	3549	mud	1.443	6	≤ 21.3K	Pleistocene-mid Holocene	Qa	Gharibreza (2016); Dolati (2010)
3550	0	3550	mud	0.202	6	≤ 21.3K	Pleistocene-mid Holocene	Qa	Gharibreza (2016); Dolati (2010)
3551	0	3551	mud	1.052	6	≤ 21.3K	Pleistocene-mid Holocene	Qa	Gharibreza (2016); Dolati (2010)
3552	0	3552	mud	0.057	6	≤ 21.3K	Pleistocene-mid Holocene	Qa	Gharibreza (2016); Dolati (2010)
3553	0	3553	mud	0.029	6	≤ 21.3K	Pleistocene-mid Holocene	Qa	Gharibreza (2016); Dolati (2010)
3554	0	3554	mud	5.135	6	≤ 21.3K	Pleistocene-mid Holocene	Qa	Gharibreza (2016); Dolati (2010)
3555	0	3555	mud	0.053	6	≤ 21.3K	Pleistocene-mid Holocene	Qa	Gharibreza (2016); Dolati (2010)
3556	0	3556	mud	0.078	6	≤ 21.3K	Pleistocene-mid Holocene	Qa	Gharibreza (2016); Dolati (2010)
3557	0	3557	mud	0.406	6	≤ 21.3K	Pleistocene-mid Holocene	Qa	Gharibreza (2016); Dolati (2010)
3558	0	3558	mud	0.049	6	≤ 21.3K	Pleistocene-mid Holocene	Qa	Gharibreza (2016); Dolati (2010)
3559	0	3559	mud	0.059	6	≤ 21.3K	Pleistocene-mid Holocene	Qa	Gharibreza (2016); Dolati (2010)
3560	0	3560	mud	0.015	6	≤ 21.3K	Pleistocene-mid Holocene	Qa	Gharibreza (2016); Dolati (2010)
3561	0	3561	mud	0.071	6	≤ 21.3K	Pleistocene-mid Holocene	Qa	Gharibreza (2016); Dolati (2010)
3562	0	3562	mud	0.004	6	≤ 21.3K	Pleistocene-mid Holocene	Qa	Gharibreza (2016); Dolati (2010)
3563	0	3563	mud	0.296	6	≤ 21.3K	Pleistocene-mid Holocene	Qa	Gharibreza (2016); Dolati (2010)
3564	0	3564	mud	0.038	6	≤ 21.3K	Pleistocene-mid Holocene	Qa	Gharibreza (2016); Dolati (2010)
3565	0	3565	mud	0.156	6	≤ 21.3K	Pleistocene-mid Holocene	Qa	Gharibreza (2016); Dolati (2010)
3566	0	3566	mud	0.101	6	≤ 21.3K	Pleistocene-mid Holocene	Qa	Gharibreza (2016); Dolati (2010)
3567	0	3567	mud	84.697	6	≤ 21.3K	Pleistocene-mid Holocene	Qa	Gharibreza (2016); Dolati (2010)
3568	0	3568	mud	0.187	6	≤ 21.3K	Pleistocene-mid Holocene	Qa	Gharibreza (2016); Dolati (2010)
3569	0	3569	mud	0.008	6	≤ 21.3K	Pleistocene-mid Holocene	Qa	Gharibreza (2016); Dolati (2010)
3570	0	3570	mud	0.111	6	≤ 21.3K	Pleistocene-mid Holocene	Qa	Gharibreza (2016); Dolati (2010)
3571	0	3571	mud	0.035	6	≤ 21.3K	Pleistocene-mid Holocene	Qa	Gharibreza (2016); Dolati (2010)
3572	0	3572	mud	0.006	6	≤ 21.3K	Pleistocene-mid Holocene	Qa	Gharibreza (2016); Dolati (2010)
3573	0	3573	mud	0.067	6	≤ 21.3K	Pleistocene-mid Holocene	Qa	Gharibreza (2016); Dolati (2010)
3575	0	3575	mud	0.023	6	≤ 21.3K	Pleistocene-mid Holocene	Qa	Gharibreza (2016); Dolati (2010)
3576	0	3576	mud	0.012	6	≤ 21.3K	Pleistocene-mid Holocene	Qa	Gharibreza (2016); Dolati (2010)
3577	0	3577	mud	0.556	6	≤ 21.3K	Pleistocene-mid Holocene	Qa	Gharibreza (2016); Dolati (2010)
3578	0	3578	mud	0.111	6	≤ 21.3K	Pleistocene-mid Holocene	Qa	Gharibreza (2016); Dolati (2010)

Geonews

OBJECTID_1	Join_Count	TARGET_FID	Label	Shape_Area (sqkm)	ORIG_FID	Absolute_Age	Age_paleontology	Unit	Reference
3579	0	3579	mud	0.288	6	≤ 21.3K	Pleistocene-mid Holocene	Qa	Gharibreza (2016); Dolati (2010)
3580	0	3580	mud	0.028	6	≤ 21.3K	Pleistocene-mid Holocene	Qa	Gharibreza (2016); Dolati (2010)
3581	0	3581	mud	0.026	6	≤ 21.3K	Pleistocene-mid Holocene	Qa	Gharibreza (2016); Dolati (2010)
3582	0	3582	mud	0.198	6	≤ 21.3K	Pleistocene-mid Holocene	Qa	Gharibreza (2016); Dolati (2010)
3583	0	3583	mud	0.139	6	≤ 21.3K	Pleistocene-mid Holocene	Qa	Gharibreza (2016); Dolati (2010)
3584	0	3584	mud	0.040	6	≤ 21.3K	Pleistocene-mid Holocene	Qa	Gharibreza (2016); Dolati (2010)
3586	0	3586	mud	0.114	6	≤ 21.3K	Pleistocene-mid Holocene	Qa	Gharibreza (2016); Dolati (2010)
3587	0	3587	mud	0.904	6	≤ 21.3K	Pleistocene-mid Holocene	Qa	Gharibreza (2016); Dolati (2010)
3588	0	3588	mud	0.018	6	≤ 21.3K	Pleistocene-mid Holocene	Qa	Gharibreza (2016); Dolati (2010)
3589	0	3589	mud	0.026	6	≤ 21.3K	Pleistocene-mid Holocene	Qa	Gharibreza (2016); Dolati (2010)
3590	0	3590	mud	0.026	6	≤ 21.3K	Pleistocene-mid Holocene	Qa	Gharibreza (2016); Dolati (2010)
3591	0	3591	mud	0.015	6	≤ 21.3K	Pleistocene-mid Holocene	Qa	Gharibreza (2016); Dolati (2010)
3592	0	3592	mud	0.013	6	≤ 21.3K	Pleistocene-mid Holocene	Qa	Gharibreza (2016); Dolati (2010)
3593	0	3593	mud	0.017	6	≤ 21.3K	Pleistocene-mid Holocene	Qa	Gharibreza (2016); Dolati (2010)
3594	0	3594	mud	0.472	6	≤ 21.3K	Pleistocene-mid Holocene	Qa	Gharibreza (2016); Dolati (2010)
3596	0	3596	mud	0.006	6	≤ 21.3K	Pleistocene-mid Holocene	Qa	Gharibreza (2016); Dolati (2010)
3597	0	3597	mud	0.012	6	≤ 21.3K	Pleistocene-mid Holocene	Qa	Gharibreza (2016); Dolati (2010)
3598	0	3598	mud	0.009	6	≤ 21.3K	Pleistocene-mid Holocene	Qa	Gharibreza (2016); Dolati (2010)
3599	0	3599	mud	0.010	6	≤ 21.3K	Pleistocene-mid Holocene	Qa	Gharibreza (2016); Dolati (2010)
3600	0	3600	mud	0.495	6	≤ 21.3K	Pleistocene-mid Holocene	Qa	Gharibreza (2016); Dolati (2010)
3601	0	3601	mud	0.065	6	≤ 21.3K	Pleistocene-mid Holocene	Qa	Gharibreza (2016); Dolati (2010)
3602	0	3602	mud	0.172	6	≤ 21.3K	Pleistocene-mid Holocene	Qa	Gharibreza (2016); Dolati (2010)
3603	0	3603	mud	0.017	6	≤ 21.3K	Pleistocene-mid Holocene	Qa	Gharibreza (2016); Dolati (2010)
3604	0	3604	mud	0.005	6	≤ 21.3K	Pleistocene-mid Holocene	Qa	Gharibreza (2016); Dolati (2010)
3606	0	3606	mud	0.027	6	≤ 21.3K	Pleistocene-mid Holocene	Qa	Gharibreza (2016); Dolati (2010)
3607	0	3607	mud	0.076	6	≤ 21.3K	Pleistocene-mid Holocene	Qa	Gharibreza (2016); Dolati (2010)
3608	0	3608	mud	8.638	6	≤ 21.3K	Pleistocene-mid Holocene	Qa	Gharibreza (2016); Dolati (2010)
3609	0	3609	mud	1.264	6	≤ 21.3K	Pleistocene-mid Holocene	Qa	Gharibreza (2016); Dolati (2010)
3610	0	3610	mud	0.122	6	≤ 21.3K	Pleistocene-mid Holocene	Qa	Gharibreza (2016); Dolati (2010)
3611	0	3611	mud	0.015	6	≤ 21.3K	Pleistocene-mid Holocene	Qa	Gharibreza (2016); Dolati (2010)
3612	0	3612	mud	0.074	6	≤ 21.3K	Pleistocene-mid Holocene	Qa	Gharibreza (2016); Dolati (2010)
3614	0	3614	mud	0.203	6	≤ 21.3K	Pleistocene-mid Holocene	Qa	Gharibreza (2016); Dolati (2010)
3616	0	3616	mud	0.028	6	≤ 21.3K	Pleistocene-mid Holocene	Qa	Gharibreza (2016); Dolati (2010)
3617	0	3617	mud	0.012	6	≤ 21.3K	Pleistocene-mid Holocene	Qa	Gharibreza (2016); Dolati (2010)
3618	0	3618	mud	0.067	6	≤ 21.3K	Pleistocene-mid Holocene	Qa	Gharibreza (2016); Dolati (2010)
3619	0	3619	mud	0.025	6	≤ 21.3K	Pleistocene-mid Holocene	Qa	Gharibreza (2016); Dolati (2010)
3620	0	3620	mud	0.156	6	≤ 21.3K	Pleistocene-mid Holocene	Qa	Gharibreza (2016); Dolati (2010)
3621	0	3621	mud	0.659	6	≤ 21.3K	Pleistocene-mid Holocene	Qa	Gharibreza (2016); Dolati (2010)
3622	0	3622	mud	0.073	6	≤ 21.3K	Pleistocene-mid Holocene	Qa	Gharibreza (2016); Dolati (2010)

Preview

OBJECTID_1	Join_Count	TARGET_FID	Label	Shape_Area (sqkm)	ORIG_FID	Absolute_Age	Age_paleontology	Unit	Reference
3623	0	3623	mud	0.003	6	≤ 21.3K	Pleistocene-mid Holocene	Qa	Gharibreza (2016); Dolati (2010)
3626	0	3626	mud	0.036	6	≤ 21.3K	Pleistocene-mid Holocene	Qa	Gharibreza (2016); Dolati (2010)
3627	0	3627	mud	0.273	6	≤ 21.3K	Pleistocene-mid Holocene	Qa	Gharibreza (2016); Dolati (2010)
3628	0	3628	mud	0.092	6	≤ 21.3K	Pleistocene-mid Holocene	Qa	Gharibreza (2016); Dolati (2010)
3629	0	3629	mud	0.123	6	≤ 21.3K	Pleistocene-mid Holocene	Qa	Gharibreza (2016); Dolati (2010)
3630	0	3630	mud	0.208	6	≤ 21.3K	Pleistocene-mid Holocene	Qa	Gharibreza (2016); Dolati (2010)
3631	0	3631	mud	0.061	6	≤ 21.3K	Pleistocene-mid Holocene	Qa	Gharibreza (2016); Dolati (2010)
3632	0	3632	mud	0.018	6	≤ 21.3K	Pleistocene-mid Holocene	Qa	Gharibreza (2016); Dolati (2010)
3633	0	3633	mud	0.105	6	≤ 21.3K	Pleistocene-mid Holocene	Qa	Gharibreza (2016); Dolati (2010)
3634	0	3634	mud	0.006	6	≤ 21.3K	Pleistocene-mid Holocene	Qa	Gharibreza (2016); Dolati (2010)
3635	0	3635	mud	0.014	6	≤ 21.3K	Pleistocene-mid Holocene	Qa	Gharibreza (2016); Dolati (2010)
3636	0	3636	mud	0.211	6	≤ 21.3K	Pleistocene-mid Holocene	Qa	Gharibreza (2016); Dolati (2010)
3637	0	3637	mud	0.269	6	≤ 21.3K	Pleistocene-mid Holocene	Qa	Gharibreza (2016); Dolati (2010)
3638	0	3638	mud	0.039	6	≤ 21.3K	Pleistocene-mid Holocene	Qa	Gharibreza (2016); Dolati (2010)
3639	0	3639	mud	0.030	6	≤ 21.3K	Pleistocene-mid Holocene	Qa	Gharibreza (2016); Dolati (2010)
3640	0	3640	mud	0.233	6	≤ 21.3K	Pleistocene-mid Holocene	Qa	Gharibreza (2016); Dolati (2010)
3641	0	3641	mud	0.005	6	≤ 21.3K	Pleistocene-mid Holocene	Qa	Gharibreza (2016); Dolati (2010)
3642	0	3642	mud	0.155	6	≤ 21.3K	Pleistocene-mid Holocene	Qa	Gharibreza (2016); Dolati (2010)
3644	0	3644	mud	0.006	6	≤ 21.3K	Pleistocene-mid Holocene	Qa	Gharibreza (2016); Dolati (2010)
3646	0	3646	mud	0.062	6	≤ 21.3K	Pleistocene-mid Holocene	Qa	Gharibreza (2016); Dolati (2010)
3647	0	3647	mud	0.028	6	≤ 21.3K	Pleistocene-mid Holocene	Qa	Gharibreza (2016); Dolati (2010)
3648	0	3648	mud	0.115	6	≤ 21.3K	Pleistocene-mid Holocene	Qa	Gharibreza (2016); Dolati (2010)
3649	0	3649	mud	0.044	6	≤ 21.3K	Pleistocene-mid Holocene	Qa	Gharibreza (2016); Dolati (2010)
3650	0	3650	mud	0.047	6	≤ 21.3K	Pleistocene-mid Holocene	Qa	Gharibreza (2016); Dolati (2010)
3652	0	3652	mud	0.075	6	≤ 21.3K	Pleistocene-mid Holocene	Qa	Gharibreza (2016); Dolati (2010)
3653	0	3653	mud	0.195	6	≤ 21.3K	Pleistocene-mid Holocene	Qa	Gharibreza (2016); Dolati (2010)
3654	0	3654	mud	0.035	6	≤ 21.3K	Pleistocene-mid Holocene	Qa	Gharibreza (2016); Dolati (2010)
3655	0	3655	mud	0.015	6	≤ 21.3K	Pleistocene-mid Holocene	Qa	Gharibreza (2016); Dolati (2010)
3656	0	3656	mud	0.222	6	≤ 21.3K	Pleistocene-mid Holocene	Qa	Gharibreza (2016); Dolati (2010)
3657	0	3657	mud	0.102	6	≤ 21.3K	Pleistocene-mid Holocene	Qa	Gharibreza (2016); Dolati (2010)
3658	0	3658	mud	0.010	6	≤ 21.3K	Pleistocene-mid Holocene	Qa	Gharibreza (2016); Dolati (2010)
3659	0	3659	mud	0.134	6	≤ 21.3K	Pleistocene-mid Holocene	Qa	Gharibreza (2016); Dolati (2010)
3661	0	3661	mud	0.060	6	≤ 21.3K	Pleistocene-mid Holocene	Qa	Gharibreza (2016); Dolati (2010)
3662	0	3662	mud	0.028	6	≤ 21.3K	Pleistocene-mid Holocene	Qa	Gharibreza (2016); Dolati (2010)
3664	0	3664	mud	0.404	6	≤ 21.3K	Pleistocene-mid Holocene	Qa	Gharibreza (2016); Dolati (2010)
3665	0	3665	mud	0.094	6	≤ 21.3K	Pleistocene-mid Holocene	Qa	Gharibreza (2016); Dolati (2010)
3666	0	3666	mud	0.049	6	≤ 21.3K	Pleistocene-mid Holocene	Qa	Gharibreza (2016); Dolati (2010)
3667	0	3667	mud	0.013	6	≤ 21.3K	Pleistocene-mid Holocene	Qa	Gharibreza (2016); Dolati (2010)
3668	0	3668	mud	0.040	6	≤ 21.3K	Pleistocene-mid Holocene	Qa	Gharibreza (2016); Dolati (2010)

Preview

OBJECTID_1	Join_Count	TARGET_FID	Label	Shape_Area (sqkm)	ORIG_FID	Absolute_Age	Age_paleontology	Unit	Reference
3669	0	3669	mud	0.328	6	≤ 21.3K	Pleistocene-mid Holocene	Qa	Gharibreza (2016); Dolati (2010)
3670	0	3670	mud	0.012	6	≤ 21.3K	Pleistocene-mid Holocene	Qa	Gharibreza (2016); Dolati (2010)
3671	0	3671	mud	0.033	6	≤ 21.3K	Pleistocene-mid Holocene	Qa	Gharibreza (2016); Dolati (2010)
3672	0	3672	mud	0.011	6	≤ 21.3K	Pleistocene-mid Holocene	Qa	Gharibreza (2016); Dolati (2010)
3673	0	3673	mud	0.004	6	≤ 21.3K	Pleistocene-mid Holocene	Qa	Gharibreza (2016); Dolati (2010)
3674	0	3674	mud	0.229	6	≤ 21.3K	Pleistocene-mid Holocene	Qa	Gharibreza (2016); Dolati (2010)
3675	0	3675	mud	0.036	6	≤ 21.3K	Pleistocene-mid Holocene	Qa	Gharibreza (2016); Dolati (2010)
3676	0	3676	mud	0.131	6	≤ 21.3K	Pleistocene-mid Holocene	Qa	Gharibreza (2016); Dolati (2010)
3677	0	3677	mud	0.034	6	≤ 21.3K	Pleistocene-mid Holocene	Qa	Gharibreza (2016); Dolati (2010)
3678	0	3678	mud	0.023	6	≤ 21.3K	Pleistocene-mid Holocene	Qa	Gharibreza (2016); Dolati (2010)
3679	0	3679	mud	0.012	6	≤ 21.3K	Pleistocene-mid Holocene	Qa	Gharibreza (2016); Dolati (2010)
3680	0	3680	mud	0.091	6	≤ 21.3K	Pleistocene-mid Holocene	Qa	Gharibreza (2016); Dolati (2010)
3681	0	3681	mud	0.016	6	≤ 21.3K	Pleistocene-mid Holocene	Qa	Gharibreza (2016); Dolati (2010)
3682	0	3682	mud	0.171	6	≤ 21.3K	Pleistocene-mid Holocene	Qa	Gharibreza (2016); Dolati (2010)
3683	0	3683	mud	0.012	6	≤ 21.3K	Pleistocene-mid Holocene	Qa	Gharibreza (2016); Dolati (2010)
3684	0	3684	mud	0.034	6	≤ 21.3K	Pleistocene-mid Holocene	Qa	Gharibreza (2016); Dolati (2010)
3686	0	3686	mud	0.105	6	≤ 21.3K	Pleistocene-mid Holocene	Qa	Gharibreza (2016); Dolati (2010)
3687	0	3687	mud	0.111	6	≤ 21.3K	Pleistocene-mid Holocene	Qa	Gharibreza (2016); Dolati (2010)
3688	0	3688	mud	0.178	6	≤ 21.3K	Pleistocene-mid Holocene	Qa	Gharibreza (2016); Dolati (2010)
3689	0	3689	mud	0.017	6	≤ 21.3K	Pleistocene-mid Holocene	Qa	Gharibreza (2016); Dolati (2010)
3690	0	3690	mud	0.051	6	≤ 21.3K	Pleistocene-mid Holocene	Qa	Gharibreza (2016); Dolati (2010)
3691	0	3691	mud	0.156	6	≤ 21.3K	Pleistocene-mid Holocene	Qa	Gharibreza (2016); Dolati (2010)
3692	0	3692	mud	0.012	6	≤ 21.3K	Pleistocene-mid Holocene	Qa	Gharibreza (2016); Dolati (2010)
3693	0	3693	mud	0.080	6	≤ 21.3K	Pleistocene-mid Holocene	Qa	Gharibreza (2016); Dolati (2010)
3694	0	3694	mud	0.043	6	≤ 21.3K	Pleistocene-mid Holocene	Qa	Gharibreza (2016); Dolati (2010)
3695	0	3695	mud	0.015	6	≤ 21.3K	Pleistocene-mid Holocene	Qa	Gharibreza (2016); Dolati (2010)
3696	0	3696	mud	0.023	6	≤ 21.3K	Pleistocene-mid Holocene	Qa	Gharibreza (2016); Dolati (2010)
3697	0	3697	mud	0.011	6	≤ 21.3K	Pleistocene-mid Holocene	Qa	Gharibreza (2016); Dolati (2010)
3698	0	3698	mud	0.021	6	≤ 21.3K	Pleistocene-mid Holocene	Qa	Gharibreza (2016); Dolati (2010)
3699	0	3699	mud	0.021	6	≤ 21.3K	Pleistocene-mid Holocene	Qa	Gharibreza (2016); Dolati (2010)
3700	0	3700	mud	0.029	6	≤ 21.3K	Pleistocene-mid Holocene	Qa	Gharibreza (2016); Dolati (2010)
3701	0	3701	mud	0.020	6	≤ 21.3K	Pleistocene-mid Holocene	Qa	Gharibreza (2016); Dolati (2010)
3702	0	3702	mud	0.013	6	≤ 21.3K	Pleistocene-mid Holocene	Qa	Gharibreza (2016); Dolati (2010)
3703	0	3703	mud	0.144	6	≤ 21.3K	Pleistocene-mid Holocene	Qa	Gharibreza (2016); Dolati (2010)
3704	0	3704	mud	0.028	6	≤ 21.3K	Pleistocene-mid Holocene	Qa	Gharibreza (2016); Dolati (2010)
3705	0	3705	mud	0.017	6	≤ 21.3K	Pleistocene-mid Holocene	Qa	Gharibreza (2016); Dolati (2010)
3706	0	3706	mud	0.020	6	≤ 21.3K	Pleistocene-mid Holocene	Qa	Gharibreza (2016); Dolati (2010)
3707	0	3707	mud	0.047	6	≤ 21.3K	Pleistocene-mid Holocene	Qa	Gharibreza (2016); Dolati (2010)
3708	0	3708	mud	0.708	6	≤ 21.3K	Pleistocene-mid Holocene	Qa	Gharibreza (2016); Dolati (2010)

Geonews

OBJECTID_1	Join_Count	TARGET_FID	Label	Shape_Area (sqkm)	ORIG_FID	Absolute_Age	Age_paleontology	Unit	Reference
3709	0	3709	mud	0.038	6	≤ 21.3K	Pleistocene-mid Holocene	Qa	Gharibreza (2016); Dolati (2010)
3710	0	3710	mud	0.081	6	≤ 21.3K	Pleistocene-mid Holocene	Qa	Gharibreza (2016); Dolati (2010)
3711	0	3711	mud	0.071	6	≤ 21.3K	Pleistocene-mid Holocene	Qa	Gharibreza (2016); Dolati (2010)
3712	0	3712	mud	0.033	6	≤ 21.3K	Pleistocene-mid Holocene	Qa	Gharibreza (2016); Dolati (2010)
3713	0	3713	mud	0.024	6	≤ 21.3K	Pleistocene-mid Holocene	Qa	Gharibreza (2016); Dolati (2010)
3714	0	3714	mud	0.041	6	≤ 21.3K	Pleistocene-mid Holocene	Qa	Gharibreza (2016); Dolati (2010)
3715	0	3715	mud	0.096	6	≤ 21.3K	Pleistocene-mid Holocene	Qa	Gharibreza (2016); Dolati (2010)
3716	0	3716	mud	0.010	6	≤ 21.3K	Pleistocene-mid Holocene	Qa	Gharibreza (2016); Dolati (2010)
3717	0	3717	mud	0.611	6	≤ 21.3K	Pleistocene-mid Holocene	Qa	Gharibreza (2016); Dolati (2010)
3718	0	3718	mud	0.244	6	≤ 21.3K	Pleistocene-mid Holocene	Qa	Gharibreza (2016); Dolati (2010)
3719	0	3719	mud	0.016	6	≤ 21.3K	Pleistocene-mid Holocene	Qa	Gharibreza (2016); Dolati (2010)
3720	0	3720	mud	0.305	6	≤ 21.3K	Pleistocene-mid Holocene	Qa	Gharibreza (2016); Dolati (2010)
3721	0	3721	mud	0.459	6	≤ 21.3K	Pleistocene-mid Holocene	Qa	Gharibreza (2016); Dolati (2010)
3722	0	3722	mud	0.017	6	≤ 21.3K	Pleistocene-mid Holocene	Qa	Gharibreza (2016); Dolati (2010)
3724	0	3724	mud	0.187	6	≤ 21.3K	Pleistocene-mid Holocene	Qa	Gharibreza (2016); Dolati (2010)
3725	0	3725	mud	0.013	6	≤ 21.3K	Pleistocene-mid Holocene	Qa	Gharibreza (2016); Dolati (2010)
3726	0	3726	mud	0.070	6	≤ 21.3K	Pleistocene-mid Holocene	Qa	Gharibreza (2016); Dolati (2010)
3727	0	3727	mud	0.157	6	≤ 21.3K	Pleistocene-mid Holocene	Qa	Gharibreza (2016); Dolati (2010)
3728	0	3728	mud	0.032	6	≤ 21.3K	Pleistocene-mid Holocene	Qa	Gharibreza (2016); Dolati (2010)
3729	0	3729	mud	0.097	6	≤ 21.3K	Pleistocene-mid Holocene	Qa	Gharibreza (2016); Dolati (2010)
3730	0	3730	mud	0.058	6	≤ 21.3K	Pleistocene-mid Holocene	Qa	Gharibreza (2016); Dolati (2010)
3731	0	3731	mud	0.646	6	≤ 21.3K	Pleistocene-mid Holocene	Qa	Gharibreza (2016); Dolati (2010)
3732	0	3732	mud	0.017	6	≤ 21.3K	Pleistocene-mid Holocene	Qa	Gharibreza (2016); Dolati (2010)
3733	0	3733	mud	0.996	6	≤ 21.3K	Pleistocene-mid Holocene	Qa	Gharibreza (2016); Dolati (2010)
3734	0	3734	mud	0.302	6	≤ 21.3K	Pleistocene-mid Holocene	Qa	Gharibreza (2016); Dolati (2010)
3735	0	3735	mud	0.133	6	≤ 21.3K	Pleistocene-mid Holocene	Qa	Gharibreza (2016); Dolati (2010)
3736	0	3736	mud	0.173	6	≤ 21.3K	Pleistocene-mid Holocene	Qa	Gharibreza (2016); Dolati (2010)
3737	0	3737	mud	4.215	6	≤ 21.3K	Pleistocene-mid Holocene	Qa	Gharibreza (2016); Dolati (2010)
3738	0	3738	mud	0.330	6	≤ 21.3K	Pleistocene-mid Holocene	Qa	Gharibreza (2016); Dolati (2010)
3739	0	3739	mud	0.089	6	≤ 21.3K	Pleistocene-mid Holocene	Qa	Gharibreza (2016); Dolati (2010)
3740	0	3740	mud	0.189	6	≤ 21.3K	Pleistocene-mid Holocene	Qa	Gharibreza (2016); Dolati (2010)
3741	0	3741	mud	0.242	6	≤ 21.3K	Pleistocene-mid Holocene	Qa	Gharibreza (2016); Dolati (2010)
3742	0	3742	mud	0.053	6	≤ 21.3K	Pleistocene-mid Holocene	Qa	Gharibreza (2016); Dolati (2010)
3743	0	3743	mud	0.019	6	≤ 21.3K	Pleistocene-mid Holocene	Qa	Gharibreza (2016); Dolati (2010)
3744	0	3744	mud	0.023	6	≤ 21.3K	Pleistocene-mid Holocene	Qa	Gharibreza (2016); Dolati (2010)
3745	0	3745	mud	0.027	6	≤ 21.3K	Pleistocene-mid Holocene	Qa	Gharibreza (2016); Dolati (2010)
3746	0	3746	mud	0.202	6	≤ 21.3K	Pleistocene-mid Holocene	Qa	Gharibreza (2016); Dolati (2010)
3747	0	3747	mud	0.186	6	≤ 21.3K	Pleistocene-mid Holocene	Qa	Gharibreza (2016); Dolati (2010)
3748	0	3748	mud	0.050	6	≤ 21.3K	Pleistocene-mid Holocene	Qa	Gharibreza (2016); Dolati (2010)

Reviews

OBJECTID_1	Join_Count	TARGET_FID	Label	Shape_Area (sqkm)	ORIG_FID	Absolute_Age	Age_paleontology	Unit	Reference
3749	0	3749	mud	0.330	6	≤ 21.3K	Pleistocene-mid Holocene	Qa	Gharibreza (2016); Dolati (2010)
3750	0	3750	mud	0.085	6	≤ 21.3K	Pleistocene-mid Holocene	Qa	Gharibreza (2016); Dolati (2010)
3751	0	3751	mud	0.069	6	≤ 21.3K	Pleistocene-mid Holocene	Qa	Gharibreza (2016); Dolati (2010)
3752	0	3752	mud	0.036	6	≤ 21.3K	Pleistocene-mid Holocene	Qa	Gharibreza (2016); Dolati (2010)
3753	0	3753	mud	0.135	6	≤ 21.3K	Pleistocene-mid Holocene	Qa	Gharibreza (2016); Dolati (2010)
3754	0	3754	mud	0.028	6	≤ 21.3K	Pleistocene-mid Holocene	Qa	Gharibreza (2016); Dolati (2010)
3755	0	3755	mud	0.014	6	≤ 21.3K	Pleistocene-mid Holocene	Qa	Gharibreza (2016); Dolati (2010)
3756	0	3756	mud	0.016	6	≤ 21.3K	Pleistocene-mid Holocene	Qa	Gharibreza (2016); Dolati (2010)
3757	0	3757	mud	0.038	6	≤ 21.3K	Pleistocene-mid Holocene	Qa	Gharibreza (2016); Dolati (2010)
3758	0	3758	mud	0.031	6	≤ 21.3K	Pleistocene-mid Holocene	Qa	Gharibreza (2016); Dolati (2010)
3759	0	3759	mud	0.019	6	≤ 21.3K	Pleistocene-mid Holocene	Qa	Gharibreza (2016); Dolati (2010)
3760	0	3760	mud	1.727	6	≤ 21.3K	Pleistocene-mid Holocene	Qa	Gharibreza (2016); Dolati (2010)
3761	0	3761	mud	69.141	6	≤ 21.3K	Pleistocene-mid Holocene	Qa	Gharibreza (2016); Dolati (2010)
3762	0	3762	mud	0.547	6	≤ 21.3K	Pleistocene-mid Holocene	Qa	Gharibreza (2016); Dolati (2010)
3763	0	3763	mud	0.015	6	≤ 21.3K	Pleistocene-mid Holocene	Qa	Gharibreza (2016); Dolati (2010)
3764	0	3764	mud	0.019	6	≤ 21.3K	Pleistocene-mid Holocene	Qa	Gharibreza (2016); Dolati (2010)
3765	0	3765	mud	0.398	6	≤ 21.3K	Pleistocene-mid Holocene	Qa	Gharibreza (2016); Dolati (2010)
3766	0	3766	mud	0.174	6	≤ 21.3K	Pleistocene-mid Holocene	Qa	Gharibreza (2016); Dolati (2010)
3767	0	3767	mud	0.157	6	≤ 21.3K	Pleistocene-mid Holocene	Qa	Gharibreza (2016); Dolati (2010)
3768	0	3768	mud	0.016	6	≤ 21.3K	Pleistocene-mid Holocene	Qa	Gharibreza (2016); Dolati (2010)
3769	0	3769	mud	0.026	6	≤ 21.3K	Pleistocene-mid Holocene	Qa	Gharibreza (2016); Dolati (2010)
3770	0	3770	mud	0.069	6	≤ 21.3K	Pleistocene-mid Holocene	Qa	Gharibreza (2016); Dolati (2010)
3771	0	3771	mud	0.024	6	≤ 21.3K	Pleistocene-mid Holocene	Qa	Gharibreza (2016); Dolati (2010)
3772	0	3772	mud	0.027	6	≤ 21.3K	Pleistocene-mid Holocene	Qa	Gharibreza (2016); Dolati (2010)
3773	0	3773	mud	0.029	6	≤ 21.3K	Pleistocene-mid Holocene	Qa	Gharibreza (2016); Dolati (2010)
3774	0	3774	mud	0.010	6	≤ 21.3K	Pleistocene-mid Holocene	Qa	Gharibreza (2016); Dolati (2010)
3775	0	3775	mud	0.006	6	≤ 21.3K	Pleistocene-mid Holocene	Qa	Gharibreza (2016); Dolati (2010)
3776	0	3776	mud	0.013	6	≤ 21.3K	Pleistocene-mid Holocene	Qa	Gharibreza (2016); Dolati (2010)
3777	0	3777	mud	0.015	6	≤ 21.3K	Pleistocene-mid Holocene	Qa	Gharibreza (2016); Dolati (2010)
3778	0	3778	mud	0.003	6	≤ 21.3K	Pleistocene-mid Holocene	Qa	Gharibreza (2016); Dolati (2010)
3779	0	3779	mud	0.005	6	≤ 21.3K	Pleistocene-mid Holocene	Qa	Gharibreza (2016); Dolati (2010)
3780	0	3780	mud	0.027	6	≤ 21.3K	Pleistocene-mid Holocene	Qa	Gharibreza (2016); Dolati (2010)
3781	0	3781	mud	0.037	6	≤ 21.3K	Pleistocene-mid Holocene	Qa	Gharibreza (2016); Dolati (2010)
3783	0	3783	mud	0.066	6	≤ 21.3K	Pleistocene-mid Holocene	Qa	Gharibreza (2016); Dolati (2010)
3784	0	3784	mud	0.031	6	≤ 21.3K	Pleistocene-mid Holocene	Qa	Gharibreza (2016); Dolati (2010)
3785	0	3785	mud	0.020	6	≤ 21.3K	Pleistocene-mid Holocene	Qa	Gharibreza (2016); Dolati (2010)
3786	0	3786	mud	0.012	6	≤ 21.3K	Pleistocene-mid Holocene	Qa	Gharibreza (2016); Dolati (2010)
3787	0	3787	mud	0.049	6	≤ 21.3K	Pleistocene-mid Holocene	Qa	Gharibreza (2016); Dolati (2010)
3788	0	3788	mud	0.080	6	≤ 21.3K	Pleistocene-mid Holocene	Qa	Gharibreza (2016); Dolati (2010)

Preview

OBJECTID_1	Join_Count	TARGET_FID	Label	Shape_Area (sqkm)	ORIG_FID	Absolute_Age	Age_paleontology	Unit	Reference
3789	0	3789	mud	0.012	6	≤ 21.3K	Pleistocene-mid Holocene	Qa	Gharibreza (2016); Dolati (2010)
3790	0	3790	mud	0.013	6	≤ 21.3K	Pleistocene-mid Holocene	Qa	Gharibreza (2016); Dolati (2010)
3791	0	3791	mud	0.009	6	≤ 21.3K	Pleistocene-mid Holocene	Qa	Gharibreza (2016); Dolati (2010)
3792	0	3792	mud	0.077	6	≤ 21.3K	Pleistocene-mid Holocene	Qa	Gharibreza (2016); Dolati (2010)
3793	0	3793	mud	0.077	6	≤ 21.3K	Pleistocene-mid Holocene	Qa	Gharibreza (2016); Dolati (2010)
3794	0	3794	mud	0.007	6	≤ 21.3K	Pleistocene-mid Holocene	Qa	Gharibreza (2016); Dolati (2010)
3795	0	3795	mud	0.033	6	≤ 21.3K	Pleistocene-mid Holocene	Qa	Gharibreza (2016); Dolati (2010)
3796	0	3796	mud	0.023	6	≤ 21.3K	Pleistocene-mid Holocene	Qa	Gharibreza (2016); Dolati (2010)
3797	0	3797	mud	0.010	6	≤ 21.3K	Pleistocene-mid Holocene	Qa	Gharibreza (2016); Dolati (2010)
10400	1	10407	mud	0.040	0			Qa	Gharibreza (2016); Dolati (2010)
10401	0	10408	mud	0.015	0			Qa	Gharibreza (2016); Dolati (2010)

GeoNexus

Table S13. Summary of mapped polygons for the Q^b Unit.

OBJECTID_1	Join_Count	TARGET_FID	Label	Shape_Area (sqkm)	ORIG_FID	Absolute_Age	Age_paleontology	Unit	Reference
1	0	1	beach	0.130	1	≤ 7.3K		Qb	Normand (2018)
2	0	2	beach	1.239	1	≤ 7.3K		Qb	Normand (2018); Shah-hosseini et al. (2018)
3	0	3	beach	5.285	1	≤ 7.3K		Qb	Normand (2018); Shah-hosseini et al. (2018)
4	0	4	beach	0.389	1	≤ 7.3K		Qb	Normand (2018); Shah-hosseini et al. (2018)
5	0	5	beach	0.069	1	≤ 7.3K		Qb	Normand (2018); Shah-hosseini et al. (2018)
6	0	6	beach	0.033	1	≤ 7.3K		Qb	Normand (2018); Shah-hosseini et al. (2018)
7	0	7	beach	0.711	1	≤ 7.3K		Qb	Normand (2018); Shah-hosseini et al. (2018)
8	0	8	beach	0.041	1	≤ 7.3K		Qb	Normand (2018); Shah-hosseini et al. (2018)
9	0	9	beach	1.155	1	≤ 7.3K		Qb	Normand (2018); Shah-hosseini et al. (2018)
10	0	10	beach	0.084	1	≤ 7.3K		Qb	Normand (2018); Shah-hosseini et al. (2018)
11	0	11	beach	0.059	1	≤ 7.3K		Qb	Normand (2018); Shah-hosseini et al. (2018)
12	0	12	beach	1.846	1	≤ 7.3K		Qb	Normand (2018); Shah-hosseini et al. (2018)
13	0	13	beach	0.026	1	≤ 7.3K		Qb	Normand (2018); Shah-hosseini et al. (2018)
14	0	14	beach	0.018	1	≤ 7.3K		Qb	Normand (2018); Shah-hosseini et al. (2018)
15	0	15	beach	0.175	1	≤ 7.3K		Qb	Normand (2018); Shah-hosseini et al. (2018)
16	2	16	beach	0.069	1	≤ 7.3K		Qb	Normand (2018); Shah-hosseini et al. (2018)
17	0	17	beach	0.044	1	≤ 7.3K		Qb	Normand (2018); Shah-hosseini et al. (2018)
18	0	18	beach	0.048	1	≤ 7.3K		Qb	Normand (2018); Shah-hosseini et al. (2018)
19	0	19	beach	0.177	1	≤ 7.3K		Qb	Normand (2018); Shah-hosseini et al. (2018)
20	0	20	beach	0.039	1	≤ 7.3K		Qb	Normand (2018); Shah-hosseini et al. (2018)
21	0	21	beach	1.001	1	≤ 7.3K		Qb	Normand (2018); Shah-hosseini et al. (2018)
22	0	22	beach	0.109	1	≤ 7.3K		Qb	Normand (2018); Shah-hosseini et al. (2018)
23	0	23	beach	0.193	1	≤ 7.3K		Qb	Normand (2018); Shah-hosseini et al. (2018)
24	0	24	beach	0.718	1	≤ 7.3K		Qb	Normand (2018); Shah-hosseini et al. (2018)
25	0	25	beach	0.078	1	≤ 7.3K		Qb	Normand (2018); Shah-hosseini et al. (2018)
26	0	26	beach	0.495	1	≤ 7.3K		Qb	Normand (2018); Shah-hosseini et al. (2018)
27	0	27	beach	0.086	1	≤ 7.3K		Qb	Normand (2018); Shah-hosseini et al. (2018)
28	0	28	beach	0.100	1	≤ 7.3K		Qb	Normand (2018); Shah-hosseini et al. (2018)
29	0	29	beach	0.022	1	≤ 7.3K		Qb	Normand (2018); Shah-hosseini et al. (2018)
30	0	30	beach	0.057	1	≤ 7.3K		Qb	Normand (2018); Shah-hosseini et al. (2018)
31	0	31	beach	0.020	1	≤ 7.3K		Qb	Normand (2018); Shah-hosseini et al. (2018)
32	0	32	beach	0.023	1	≤ 7.3K		Qb	Normand (2018); Shah-hosseini et al. (2018)
33	0	33	beach	0.027	1	≤ 7.3K		Qb	Normand (2018); Shah-hosseini et al. (2018)
34	0	34	beach	1.199	1	≤ 7.3K		Qb	Normand (2018); Shah-hosseini et al. (2018)
35	0	35	beach	0.067	1	≤ 7.3K		Qb	Normand (2018); Shah-hosseini et al. (2018)
36	0	36	beach	0.027	1	≤ 7.3K		Qb	Normand (2018); Shah-hosseini et al. (2018)
38	0	38	beach	0.295	1	≤ 7.3K		Qb	Normand (2018); Shah-hosseini et al. (2018)
39	0	39	beach	0.015	1	≤ 7.3K		Qb	Normand (2018); Shah-hosseini et al. (2018)

GSI Review

OBJECTID_1	Join_Count	TARGET_FID	Label	Shape_Area (sqkm)	ORIG_FID	Absolute_Age	Age_paleontology	Unit	Reference
40	0	40	beach	194.020	1	≤ 7.3K		Qb	Normand (2018); Shah-hosseini et al. (2018)
42	0	42	beach	0.297	1	≤ 7.3K		Qb	Normand (2018); Shah-hosseini et al. (2018)
43	0	43	beach	0.101	1	≤ 7.3K		Qb	Normand (2018); Shah-hosseini et al. (2018)
44	0	44	beach	0.842	1	≤ 7.3K		Qb	Normand (2018); Shah-hosseini et al. (2018)
45	0	45	beach	0.281	1	≤ 7.3K		Qb	Normand (2018); Shah-hosseini et al. (2018)
46	0	46	beach	0.029	1	≤ 7.3K		Qb	Normand (2018); Shah-hosseini et al. (2018)
47	0	47	beach	0.643	1	≤ 7.3K		Qb	Normand (2018); Shah-hosseini et al. (2018)
48	0	48	beach	0.383	1	≤ 7.3K		Qb	Normand (2018); Shah-hosseini et al. (2018)
49	0	49	beach	0.130	1	≤ 7.3K		Qb	Normand (2018); Shah-hosseini et al. (2018)
50	0	50	beach	0.414	1	≤ 7.3K		Qb	Normand (2018); Shah-hosseini et al. (2018)
51	0	51	beach	0.023	1	≤ 7.3K		Qb	Normand (2018); Shah-hosseini et al. (2018)
52	0	52	beach	1.304	1	≤ 7.3K		Qb	Normand (2018); Shah-hosseini et al. (2018)
53	0	53	beach	3.229	1	≤ 7.3K		Qb	Normand (2018); Shah-hosseini et al. (2018)
54	0	54	beach	0.050	1	≤ 7.3K		Qb	Normand (2018); Shah-hosseini et al. (2018)
55	0	55	beach	0.453	1	≤ 7.3K		Qb	Normand (2018); Shah-hosseini et al. (2018)
56	0	56	beach	0.024	1	≤ 7.3K		Qb	Normand (2018); Shah-hosseini et al. (2018)
57	0	57	beach	0.155	1	≤ 7.3K		Qb	Normand (2018); Shah-hosseini et al. (2018)
58	0	58	beach	0.152	1	≤ 7.3K		Qb	Normand (2018); Shah-hosseini et al. (2018)
59	0	59	beach	0.054	1	≤ 7.3K		Qb	Normand (2018); Shah-hosseini et al. (2018)
60	0	60	beach	0.077	1	≤ 7.3K		Qb	Normand (2018); Shah-hosseini et al. (2018)
61	0	61	beach	0.029	1	≤ 7.3K		Qb	Normand (2018); Shah-hosseini et al. (2018)
62	0	62	beach	0.051	1	≤ 7.3K		Qb	Normand (2018); Shah-hosseini et al. (2018)
63	0	63	beach	0.043	1	≤ 7.3K		Qb	Normand (2018); Shah-hosseini et al. (2018)
64	0	64	beach	0.069	1	≤ 7.3K		Qb	Normand (2018); Shah-hosseini et al. (2018)
65	0	65	beach	0.252	1	≤ 7.3K		Qb	Normand (2018); Shah-hosseini et al. (2018)
66	0	66	beach	16.165	1	≤ 7.3K		Qb	Normand (2018); Shah-hosseini et al. (2018)
67	0	67	beach	0.214	1	≤ 7.3K		Qb	Normand (2018); Shah-hosseini et al. (2018)
68	0	68	beach	0.040	1	≤ 7.3K		Qb	Normand (2018); Shah-hosseini et al. (2018)
69	0	69	beach	0.108	1	≤ 7.3K		Qb	Normand (2018); Shah-hosseini et al. (2018)
70	0	70	beach	1.330	1	≤ 7.3K		Qb	Normand (2018); Shah-hosseini et al. (2018)
71	0	71	beach	0.043	1	≤ 7.3K		Qb	Normand (2018); Shah-hosseini et al. (2018)
72	0	72	beach	0.049	1	≤ 7.3K		Qb	Normand (2018); Shah-hosseini et al. (2018)
73	0	73	beach	0.054	1	≤ 7.3K		Qb	Normand (2018); Shah-hosseini et al. (2018)
74	0	74	beach	0.393	1	≤ 7.3K		Qb	Normand (2018); Shah-hosseini et al. (2018)
76	0	76	beach	0.252	1	≤ 7.3K		Qb	Normand (2018); Shah-hosseini et al. (2018)
77	0	77	beach	0.023	1	≤ 7.3K		Qb	Normand (2018); Shah-hosseini et al. (2018)
78	0	78	beach	0.615	1	≤ 7.3K		Qb	Normand (2018); Shah-hosseini et al. (2018)
79	0	79	beach	0.129	1	≤ 7.3K		Qb	Normand (2018); Shah-hosseini et al. (2018)
80	0	80	beach	0.055	1	≤ 7.3K		Qb	Normand (2018); Shah-hosseini et al. (2018)

preview

OBJECTID_1	Join_Count	TARGET_FID	Label	Shape_Area (sqkm)	ORIG_FID	Absolute_Age	Age_paleontology	Unit	Reference
82	1	82	beach	6.123	1	≤ 7.3K		Qb	Normand (2018); Shah-hosseini et al. (2018)
83	0	83	beach	0.264	1	≤ 7.3K		Qb	Normand (2018); Shah-hosseini et al. (2018)
84	0	84	beach	0.029	1	≤ 7.3K		Qb	Normand (2018); Shah-hosseini et al. (2018)
85	0	85	beach	0.158	1	≤ 7.3K		Qb	Normand (2018); Shah-hosseini et al. (2018)
86	0	86	beach	0.056	1	≤ 7.3K		Qb	Normand (2018); Shah-hosseini et al. (2018)
87	0	87	beach	0.100	1	≤ 7.3K		Qb	Normand (2018); Shah-hosseini et al. (2018)
88	0	88	beach	0.127	1	≤ 7.3K		Qb	Normand (2018); Shah-hosseini et al. (2018)
89	0	89	beach	0.236	1	≤ 7.3K		Qb	Normand (2018); Shah-hosseini et al. (2018)
90	0	90	beach	0.125	1	≤ 7.3K		Qb	Normand (2018); Shah-hosseini et al. (2018)
91	0	91	beach	0.304	1	≤ 7.3K		Qb	Normand (2018); Shah-hosseini et al. (2018)
92	0	92	beach	0.009	1	≤ 7.3K		Qb	Normand (2018); Shah-hosseini et al. (2018)
93	0	93	beach	0.113	1	≤ 7.3K		Qb	Normand (2018); Shah-hosseini et al. (2018)
94	0	94	beach	0.016	1	≤ 7.3K		Qb	Normand (2018); Shah-hosseini et al. (2018)
95	0	95	beach	0.023	1	≤ 7.3K		Qb	Normand (2018); Shah-hosseini et al. (2018)
96	0	96	beach	2.419	1	≤ 7.3K		Qb	Normand (2018); Shah-hosseini et al. (2018)
97	0	97	beach	49.602	1	≤ 7.3K		Qb	Normand (2018); Shah-hosseini et al. (2018)
98	0	98	beach	0.054	1	≤ 7.3K		Qb	Normand (2018); Shah-hosseini et al. (2018)
99	0	99	beach	0.033	1	≤ 7.3K		Qb	Normand (2018); Shah-hosseini et al. (2018)
100	0	100	beach	0.069	1	≤ 7.3K		Qb	Normand (2018); Shah-hosseini et al. (2018)
101	0	101	beach	0.406	1	≤ 7.3K		Qb	Normand (2018); Shah-hosseini et al. (2018)
102	0	102	beach	0.085	1	≤ 7.3K		Qb	Normand (2018); Shah-hosseini et al. (2018)
103	0	103	beach	0.095	1	≤ 7.3K		Qb	Normand (2018); Shah-hosseini et al. (2018)
104	0	104	beach	0.019	1	≤ 7.3K		Qb	Normand (2018); Shah-hosseini et al. (2018)
105	0	105	beach	0.067	1	≤ 7.3K		Qb	Normand (2018); Shah-hosseini et al. (2018)
106	0	106	beach	0.133	1	≤ 7.3K		Qb	Normand (2018); Shah-hosseini et al. (2018)
107	0	107	beach	12.077	1	≤ 7.3K		Qb	Normand (2018); Shah-hosseini et al. (2018)
108	0	108	beach	0.064	1	≤ 7.3K		Qb	Normand (2018); Shah-hosseini et al. (2018)
109	0	109	beach	0.031	1	≤ 7.3K		Qb	Normand (2018); Shah-hosseini et al. (2018)
110	0	110	beach	1.587	1	≤ 7.3K		Qb	Normand (2018); Shah-hosseini et al. (2018)
111	0	111	beach	0.645	1	≤ 7.3K		Qb	Normand (2018); Shah-hosseini et al. (2018)
112	0	112	beach	0.093	1	≤ 7.3K		Qb	Normand (2018); Shah-hosseini et al. (2018)
113	0	113	beach	0.253	1	≤ 7.3K		Qb	Normand (2018); Shah-hosseini et al. (2018)
114	0	114	beach	0.027	1	≤ 7.3K		Qb	Normand (2018); Shah-hosseini et al. (2018)
115	0	115	beach	0.075	1	≤ 7.3K		Qb	Normand (2018); Shah-hosseini et al. (2018)
116	0	116	beach	0.172	1	≤ 7.3K		Qb	Normand (2018); Shah-hosseini et al. (2018)
117	0	117	beach	0.165	1	≤ 7.3K		Qb	Normand (2018); Shah-hosseini et al. (2018)
118	0	118	beach	0.655	1	≤ 7.3K		Qb	Normand (2018); Shah-hosseini et al. (2018)
119	0	119	beach	0.026	1	≤ 7.3K		Qb	Normand (2018); Shah-hosseini et al. (2018)
120	0	120	beach	0.042	1	≤ 7.3K		Qb	Normand (2018); Shah-hosseini et al. (2018)

Geonews

OBJECTID_1	Join_Count	TARGET_FID	Label	Shape_Area (sqkm)	ORIG_FID	Absolute_Age	Age_paleontology	Unit	Reference
121	0	121	beach	0.165	1	≤ 7.3K		Qb	Normand (2018); Shah-hosseini et al. (2018)
122	0	122	beach	0.064	1	≤ 7.3K		Qb	Normand (2018); Shah-hosseini et al. (2018)
123	0	123	beach	0.780	1	≤ 7.3K		Qb	Normand (2018); Shah-hosseini et al. (2018)
124	0	124	beach	0.078	1	≤ 7.3K		Qb	Normand (2018); Shah-hosseini et al. (2018)
125	0	125	beach	0.062	1	≤ 7.3K		Qb	Normand (2018); Shah-hosseini et al. (2018)
126	0	126	beach	0.393	1	≤ 7.3K		Qb	Normand (2018); Shah-hosseini et al. (2018)
127	0	127	beach	62.563	1	≤ 7.3K		Qb	Normand (2018); Shah-hosseini et al. (2018)
128	0	128	beach	0.134	1	≤ 7.3K		Qb	Normand (2018); Shah-hosseini et al. (2018)
129	0	129	beach	0.070	1	≤ 7.3K		Qb	Normand (2018); Shah-hosseini et al. (2018)
130	0	130	beach	0.880	1	≤ 7.3K		Qb	Normand (2018); Shah-hosseini et al. (2018)
131	0	131	beach	0.129	1	≤ 7.3K		Qb	Normand (2018); Shah-hosseini et al. (2018)
132	0	132	beach	0.010	1	≤ 7.3K		Qb	Normand (2018); Shah-hosseini et al. (2018)
133	0	133	beach	0.067	1	≤ 7.3K		Qb	Normand (2018); Shah-hosseini et al. (2018)
134	0	134	beach	0.322	1	≤ 7.3K		Qb	Normand (2018); Shah-hosseini et al. (2018)
135	0	135	beach	0.348	1	≤ 7.3K		Qb	Normand (2018); Shah-hosseini et al. (2018)
136	0	136	beach	0.107	1	≤ 7.3K		Qb	Normand (2018); Shah-hosseini et al. (2018)
137	0	137	beach	0.050	1	≤ 7.3K		Qb	Normand (2018); Shah-hosseini et al. (2018)
138	0	138	beach	0.069	1	≤ 7.3K		Qb	Normand (2018); Shah-hosseini et al. (2018)
139	0	139	beach	0.031	1	≤ 7.3K		Qb	Normand (2018); Shah-hosseini et al. (2018)
140	0	140	beach	0.100	1	≤ 7.3K		Qb	Normand (2018); Shah-hosseini et al. (2018)
141	0	141	beach	0.037	1	≤ 7.3K		Qb	Normand (2018); Shah-hosseini et al. (2018)
142	0	142	beach	0.233	1	≤ 7.3K		Qb	Normand (2018); Shah-hosseini et al. (2018)
143	0	143	beach	0.013	1	≤ 7.3K		Qb	Normand (2018); Shah-hosseini et al. (2018)
144	0	144	beach	0.614	1	≤ 7.3K		Qb	Normand (2018); Shah-hosseini et al. (2018)
145	0	145	beach	0.023	1	≤ 7.3K		Qb	Normand (2018); Shah-hosseini et al. (2018)
146	0	146	beach	0.013	1	≤ 7.3K		Qb	Normand (2018); Shah-hosseini et al. (2018)
147	0	147	beach	0.075	1	≤ 7.3K		Qb	Normand (2018); Shah-hosseini et al. (2018)
148	0	148	beach	0.199	1	≤ 7.3K		Qb	Normand (2018); Shah-hosseini et al. (2018)
149	0	149	beach	0.325	1	≤ 7.3K		Qb	Normand (2018); Shah-hosseini et al. (2018)
150	0	150	beach	0.289	1	≤ 7.3K		Qb	Normand (2018); Shah-hosseini et al. (2018)
151	0	151	beach	0.006	1	≤ 7.3K		Qb	Normand (2018); Shah-hosseini et al. (2018)
152	0	152	beach	1.043	1	≤ 7.3K		Qb	Normand (2018); Shah-hosseini et al. (2018)
153	0	153	beach	0.073	1	≤ 7.3K		Qb	Normand (2018); Shah-hosseini et al. (2018)
154	0	154	beach	0.448	1	≤ 7.3K		Qb	Normand (2018); Shah-hosseini et al. (2018)
155	0	155	beach	0.044	1	≤ 7.3K		Qb	Normand (2018); Shah-hosseini et al. (2018)
156	0	156	beach	0.011	1	≤ 7.3K		Qb	Normand (2018); Shah-hosseini et al. (2018)
157	0	157	beach	0.068	1	≤ 7.3K		Qb	Normand (2018); Shah-hosseini et al. (2018)
158	0	158	beach	4.870	1	≤ 7.3K		Qb	Normand (2018); Shah-hosseini et al. (2018)
159	0	159	beach	0.517	1	≤ 7.3K		Qb	Normand (2018); Shah-hosseini et al. (2018)

geoNeus

OBJECTID_1	Join_Count	TARGET_FID	Label	Shape_Area (sqkm)	ORIG_FID	Absolute_Age	Age_paleontology	Unit	Reference
160	0	160	beach	0.030	1	≤ 7.3K		Qb	Normand (2018); Shah-hosseini et al. (2018)
161	0	161	beach	0.522	1	≤ 7.3K		Qb	Normand (2018); Shah-hosseini et al. (2018)
162	0	162	beach	0.024	1	≤ 7.3K		Qb	Normand (2018); Shah-hosseini et al. (2018)
163	0	163	beach	0.119	1	≤ 7.3K		Qb	Normand (2018); Shah-hosseini et al. (2018)
164	0	164	beach	0.044	1	≤ 7.3K		Qb	Normand (2018); Shah-hosseini et al. (2018)
166	0	166	beach	0.038	1	≤ 7.3K		Qb	Normand (2018); Shah-hosseini et al. (2018)
167	0	167	beach	0.083	1	≤ 7.3K		Qb	Normand (2018); Shah-hosseini et al. (2018)
168	0	168	beach	0.535	1	≤ 7.3K		Qb	Normand (2018); Shah-hosseini et al. (2018)
169	0	169	beach	0.122	1	≤ 7.3K		Qb	Normand (2018); Shah-hosseini et al. (2018)
170	0	170	beach	0.033	1	≤ 7.3K		Qb	Normand (2018); Shah-hosseini et al. (2018)
171	0	171	beach	0.737	1	≤ 7.3K		Qb	Normand (2018); Shah-hosseini et al. (2018)
172	0	172	beach	0.082	1	≤ 7.3K		Qb	Normand (2018); Shah-hosseini et al. (2018)
173	0	173	beach	0.176	1	≤ 7.3K		Qb	Normand (2018); Shah-hosseini et al. (2018)
174	0	174	beach	0.608	1	≤ 7.3K		Qb	Normand (2018); Shah-hosseini et al. (2018)
175	0	175	beach	0.665	1	≤ 7.3K		Qb	Normand (2018); Shah-hosseini et al. (2018)
176	0	176	beach	0.890	1	≤ 7.3K		Qb	Normand (2018); Shah-hosseini et al. (2018)
177	0	177	beach	0.985	1	≤ 7.3K		Qb	Normand (2018); Shah-hosseini et al. (2018)
178	0	178	beach	2.050	1	≤ 7.3K		Qb	Normand (2018); Shah-hosseini et al. (2018)
179	0	179	beach	0.058	1	≤ 7.3K		Qb	Normand (2018); Shah-hosseini et al. (2018)
180	0	180	beach	0.400	1	≤ 7.3K		Qb	Normand (2018); Shah-hosseini et al. (2018)
181	0	181	beach	0.337	1	≤ 7.3K		Qb	Normand (2018); Shah-hosseini et al. (2018)
182	0	182	beach	1.190	1	≤ 7.3K		Qb	Normand (2018); Shah-hosseini et al. (2018)
183	0	183	beach	0.338	1	≤ 7.3K		Qb	Normand (2018); Shah-hosseini et al. (2018)
184	0	184	beach	0.121	1	≤ 7.3K		Qb	Normand (2018); Shah-hosseini et al. (2018)
185	0	185	beach	0.255	1	≤ 7.3K		Qb	Normand (2018); Shah-hosseini et al. (2018)
186	0	186	beach	0.024	1	≤ 7.3K		Qb	Normand (2018); Shah-hosseini et al. (2018)
187	0	187	beach	0.007	1	≤ 7.3K		Qb	Normand (2018); Shah-hosseini et al. (2018)
188	0	188	beach	0.168	1	≤ 7.3K		Qb	Normand (2018); Shah-hosseini et al. (2018)
189	0	189	beach	0.035	1	≤ 7.3K		Qb	Normand (2018); Shah-hosseini et al. (2018)
190	0	190	beach	0.121	1	≤ 7.3K		Qb	Normand (2018); Shah-hosseini et al. (2018)
191	0	191	beach	1.441	1	≤ 7.3K		Qb	Normand (2018); Shah-hosseini et al. (2018)
192	0	192	beach	0.230	1	≤ 7.3K		Qb	Normand (2018); Shah-hosseini et al. (2018)
193	0	193	beach	0.136	1	≤ 7.3K		Qb	Normand (2018); Shah-hosseini et al. (2018)
194	0	194	beach	0.035	1	≤ 7.3K		Qb	Normand (2018); Shah-hosseini et al. (2018)
195	0	195	beach	0.040	1	≤ 7.3K		Qb	Normand (2018); Shah-hosseini et al. (2018)
196	0	196	beach	0.066	1	≤ 7.3K		Qb	Normand (2018); Shah-hosseini et al. (2018)
197	0	197	beach	0.525	1	≤ 7.3K		Qb	Normand (2018); Shah-hosseini et al. (2018)

Geonerds

Table S14. Summary of mapped polygons for the Q^{fp} Unit.

OBJECTID_1	Join_Count	TARGET_FID	Label	Shape_Area (sqkm)	ORIG_FID	Absolute_Age	Age_paleontology	Unit	Reference
4426	3	4426	Qfpb	64.201	8	13.7 - 6.0M	Oligocene- Late Maiocene	Qfp	Dolati (2010)
7746	1	7747	Qfpb	0.665	13			Qfp	
8432	0	8433	Qfpb	0.842	15			Qfp	
8433	0	8434	Qfpb	0.004	15			Qfp	
8434	0	8435	Qfpb	0.097	15			Qfp	
8435	0	8436	Qfpb	0.183	15			Qfp	
8436	0	8437	Qfpb	0.012	15			Qfp	
8437	0	8438	Qfpb	0.326	15			Qfp	
8438	0	8439	Qfpb	0.136	15			Qfp	
8439	0	8440	Qfpb	0.024	15			Qfp	
8440	0	8441	Qfpb	0.016	15			Qfp	
8441	0	8442	Qfpb	0.018	15			Qfp	
8442	0	8443	Qfpb	0.425	15			Qfp	
8443	0	8444	Qfpb	0.501	15			Qfp	
8444	0	8445	Qfpb	0.019	15			Qfp	
8445	0	8446	Qfpb	0.237	15			Qfp	
8446	0	8447	Qfpb	0.014	15			Qfp	
8447	0	8448	Qfpb	0.043	15			Qfp	
8448	0	8449	Qfpb	0.115	15			Qfp	
8449	0	8450	Qfpb	0.085	15			Qfp	
8450	0	8451	Qfpb	0.426	15			Qfp	
8451	0	8452	Qfpb	0.631	15			Qfp	
8452	0	8453	Qfpb	0.372	15			Qfp	
8453	0	8454	Qfpb	0.033	15			Qfp	
8454	0	8455	Qfpb	0.030	15			Qfp	
8455	0	8456	Qfpb	0.015	15			Qfp	
8456	0	8457	Qfpb	0.117	15			Qfp	
8457	0	8458	Qfpb	0.062	15			Qfp	
8458	0	8459	Qfpb	0.056	15			Qfp	
8459	0	8460	Qfpb	0.125	15			Qfp	
8461	0	8462	Qfpb	0.496	15			Qfp	
8462	0	8463	Qfpb	0.024	15			Qfp	
8463	0	8464	Qfpb	0.123	15			Qfp	
8464	0	8465	Qfpb	0.110	15			Qfp	
8465	0	8466	Qfpb	0.138	15			Qfp	
8466	0	8467	Qfpb	0.023	15			Qfp	
8467	0	8468	Qfpb	0.009	15			Qfp	
8468	0	8469	Qfpb	0.172	15			Qfp	

GeoNexus

OBJECTID_1	Join_Count	TARGET_FID	Label	Shape_Area (sqkm)	ORIG_FID	Absolute_Age	Age_paleontology	Unit	Reference
8469	0	8470	Qfpb	0.045	15			Qfp	
8470	0	8471	Qfpb	0.065	15			Qfp	
8471	0	8472	Qfpb	0.022	15			Qfp	
8472	0	8473	Qfpb	0.011	15			Qfp	
8473	0	8474	Qfpb	0.031	15			Qfp	
8474	0	8475	Qfpb	0.126	15			Qfp	
8475	0	8476	Qfpb	0.037	15			Qfp	
8476	0	8477	Qfpb	0.065	15			Qfp	
8477	0	8478	Qfpb	0.482	15			Qfp	
8478	0	8479	Qfpb	0.050	15			Qfp	
8479	0	8480	Qfpb	0.118	15			Qfp	
8480	0	8481	Qfpb	0.275	15			Qfp	
8481	0	8482	Qfpb	0.060	15			Qfp	
8482	0	8483	Qfpb	0.071	15			Qfp	
8486	0	8487	Qfpb	0.018	15			Qfp	
8487	0	8488	Qfpb	2.409	15			Qfp	
8489	0	8490	Qfpb	0.012	15			Qfp	
8491	0	8492	Qfpb	25.971	15			Qfp	
8494	0	8495	Qfpb	0.168	15			Qfp	
8495	0	8496	Qfpb	0.112	15			Qfp	
8497	0	8498	Qfpb	0.027	15			Qfp	
8498	0	8499	Qfpb	0.094	15			Qfp	
8499	0	8500	Qfpb	0.035	15			Qfp	
8500	0	8501	Qfpb	12.559	15			Qfp	
8501	0	8502	Qfpb	0.083	15			Qfp	
8502	0	8503	Qfpb	0.182	15			Qfp	
8503	0	8504	Qfpb	19.454	15			Qfp	
8505	0	8506	Qfpb	1.670	15			Qfp	
8506	0	8507	Qfpb	0.656	15			Qfp	
8508	0	8509	Qfpb	0.014	15			Qfp	
8509	0	8510	Qfpb	0.052	15			Qfp	
8510	0	8511	Qfpb	0.942	15			Qfp	
8511	0	8512	Qfpb	0.067	15			Qfp	
8512	0	8513	Qfpb	0.175	15			Qfp	
8513	0	8514	Qfpb	0.285	15			Qfp	
8514	0	8515	Qfpb	0.182	15			Qfp	
8515	0	8516	Qfpb	0.168	15			Qfp	
8516	0	8517	Qfpb	0.193	15			Qfp	
8517	0	8518	Qfpb	0.281	15			Qfp	

Geonexus

OBJECTID_1	Join_Count	TARGET_FID	Label	Shape_Area (sqkm)	ORIG_FID	Absolute_Age	Age_paleontology	Unit	Reference
8518	0	8519	Qfpb	0.320	15			Qfp	
8519	0	8520	Qfpb	0.646	15			Qfp	
8521	0	8522	Qfpb	0.505	15			Qfp	
8523	0	8524	Qfpb	0.885	15			Qfp	
8528	0	8529	Qfpb	0.033	15			Qfp	
8529	0	8530	Qfpb	0.509	15			Qfp	
8534	0	8535	Qfpb	0.123	15			Qfp	
8536	0	8537	Qfpb	0.136	15			Qfp	
8537	0	8538	Qfpb	0.114	15			Qfp	
8538	0	8539	Qfpb	0.017	15			Qfp	
8542	0	8543	Qfpb	0.076	15			Qfp	
8543	0	8544	Qfpb	0.122	15			Qfp	
8544	0	8545	Qfpb	0.312	15			Qfp	
8545	0	8546	Qfpb	0.535	15			Qfp	
8546	0	8547	Qfpb	0.243	15			Qfp	
8548	0	8549	Qfpb	1.150	15			Qfp	
8549	0	8550	Qfpb	0.506	15			Qfp	
8550	0	8551	Qfpb	0.439	15			Qfp	
8551	0	8552	Qfpb	0.135	15			Qfp	
8552	0	8553	Qfpb	0.440	15			Qfp	
8553	0	8554	Qfpb	0.610	15			Qfp	
8554	0	8555	Qfpb	0.469	15			Qfp	
8556	0	8557	Qfpb	0.296	15			Qfp	
8557	0	8558	Qfpb	0.051	15			Qfp	
8559	0	8560	Qfpb	1.251	15			Qfp	
8560	0	8561	Qfpb	0.172	15			Qfp	
8562	0	8563	Qfpb	0.769	15			Qfp	
8563	0	8564	Qfpb	0.580	15			Qfp	
8564	0	8565	Qfpb	0.050	15			Qfp	
8565	0	8566	Qfpb	1.240	15			Qfp	
8566	0	8567	Qfpb	0.561	15			Qfp	
8568	0	8569	Qfpb	0.609	15			Qfp	
8569	0	8570	Qfpb	0.023	15			Qfp	
8570	0	8571	Qfpb	0.101	15			Qfp	
8571	0	8572	Qfpb	0.322	15			Qfp	
8573	0	8574	Qfpb	0.446	15			Qfp	
8574	0	8575	Qfpb	0.448	15			Qfp	
8575	0	8576	Qfpb	0.614	15			Qfp	
8576	0	8577	Qfpb	0.553	15			Qfp	

GeoNexus

OBJECTID_1	Join_Count	TARGET_FID	Label	Shape_Area (sqkm)	ORIG_FID	Absolute_Age	Age_paleontology	Unit	Reference
8577	0	8578	Qfpb	0.478	15			Qfp	
8578	0	8579	Qfpb	1.124	15			Qfp	
8579	0	8580	Qfpb	0.025	15			Qfp	
8580	0	8581	Qfpb	0.173	15			Qfp	
8581	0	8582	Qfpb	0.817	15			Qfp	
8582	0	8583	Qfpb	0.052	15			Qfp	
8583	0	8584	Qfpb	0.281	15			Qfp	
8584	0	8585	Qfpb	0.229	15			Qfp	
8585	0	8586	Qfpb	0.326	15			Qfp	
8586	0	8587	Qfpb	0.096	15			Qfp	
8587	0	8588	Qfpb	0.151	15			Qfp	
8588	0	8589	Qfpb	0.030	15			Qfp	
8589	0	8590	Qfpb	0.222	15			Qfp	
8590	0	8591	Qfpb	0.158	15			Qfp	
8591	0	8592	Qfpb	0.536	15			Qfp	
8592	0	8593	Qfpb	0.060	15			Qfp	
8593	0	8594	Qfpb	0.029	15			Qfp	
8594	0	8595	Qfpb	0.198	15			Qfp	
8595	0	8596	Qfpb	0.122	15			Qfp	
8596	0	8597	Qfpb	0.098	15			Qfp	
8597	0	8598	Qfpb	0.152	15			Qfp	
8598	0	8599	Qfpb	1.181	15			Qfp	
8599	0	8600	Qfpb	0.479	15			Qfp	
8601	0	8602	Qfpb	1.471	15			Qfp	
8602	0	8603	Qfpb	0.796	15			Qfp	
8603	0	8604	Qfpb	0.153	15			Qfp	
8604	0	8605	Qfpb	0.162	15			Qfp	
8605	0	8606	Qfpb	0.822	15			Qfp	
8606	0	8607	Qfpb	0.344	15			Qfp	
8607	0	8608	Qfpb	0.158	15			Qfp	
8608	0	8609	Qfpb	0.146	15			Qfp	
8609	0	8610	Qfpb	0.099	15			Qfp	
8610	0	8611	Qfpb	0.434	15			Qfp	
8611	0	8612	Qfpb	0.083	15			Qfp	
8612	0	8613	Qfpb	1.223	15			Qfp	
8613	0	8614	Qfpb	0.324	15			Qfp	
8614	0	8615	Qfpb	0.288	15			Qfp	
8615	0	8616	Qfpb	0.093	15			Qfp	
8616	0	8617	Qfpb	0.314	15			Qfp	

GeoNexus

OBJECTID_1	Join_Count	TARGET_FID	Label	Shape_Area (sqkm)	ORIG_FID	Absolute_Age	Age_paleontology	Unit	Reference
8617	0	8618	Qfpb	0.494	15			Qfp	
8618	0	8619	Qfpb	0.960	15			Qfp	
8619	0	8620	Qfpb	0.732	15			Qfp	
8620	0	8621	Qfpb	0.445	15			Qfp	
8621	0	8622	Qfpb	0.261	15			Qfp	
8622	0	8623	Qfpb	0.775	15			Qfp	
8623	0	8624	Qfpb	0.417	15			Qfp	
8624	0	8625	Qfpb	0.303	15			Qfp	
8625	0	8626	Qfpb	0.217	15			Qfp	
8626	0	8627	Qfpb	0.595	15			Qfp	
8627	0	8628	Qfpb	0.078	15			Qfp	
8628	0	8629	Qfpb	0.480	15			Qfp	
8629	0	8630	Qfpb	1.010	15			Qfp	
8630	0	8631	Qfpb	0.258	15			Qfp	
8631	0	8632	Qfpb	0.224	15			Qfp	
8632	0	8633	Qfpb	1.753	15			Qfp	
8633	0	8634	Qfpb	0.506	15			Qfp	
8634	0	8635	Qfpb	0.132	15			Qfp	
8636	0	8637	Qfpb	0.313	15			Qfp	
8637	0	8638	Qfpb	0.133	15			Qfp	
8638	0	8639	Qfpb	0.387	15			Qfp	
8639	0	8640	Qfpb	1.974	15			Qfp	
8640	0	8641	Qfpb	0.079	15			Qfp	
8641	0	8642	Qfpb	0.188	15			Qfp	
8642	0	8643	Qfpb	0.130	15			Qfp	
8643	0	8644	Qfpb	0.058	15			Qfp	
8644	0	8645	Qfpb	0.102	15			Qfp	
8645	0	8646	Qfpb	0.505	15			Qfp	
8646	0	8647	Qfpb	0.067	15			Qfp	
8647	0	8648	Qfpb	0.255	15			Qfp	
8648	0	8649	Qfpb	0.099	15			Qfp	
8649	0	8650	Qfpb	0.315	15			Qfp	
8650	0	8651	Qfpb	0.935	15			Qfp	
8651	0	8652	Qfpb	0.149	15			Qfp	
8652	0	8653	Qfpb	3.012	15			Qfp	
8653	0	8654	Qfpb	0.085	15			Qfp	
8654	0	8655	Qfpb	0.160	15			Qfp	
8655	0	8656	Qfpb	0.030	15			Qfp	
8656	0	8657	Qfpb	0.047	15			Qfp	

GeoNexus

OBJECTID_1	Join_Count	TARGET_FID	Label	Shape_Area (sqkm)	ORIG_FID	Absolute_Age	Age_paleontology	Unit	Reference
8657	0	8658	Qfpb	0.673	15			Qfp	
8658	0	8659	Qfpb	1.255	15			Qfp	
8659	0	8660	Qfpb	1.161	15			Qfp	
8660	0	8661	Qfpb	0.684	15			Qfp	
8661	0	8662	Qfpb	0.422	15			Qfp	
8662	0	8663	Qfpb	0.458	15			Qfp	
8663	0	8664	Qfpb	0.203	15			Qfp	
8664	0	8665	Qfpb	0.913	15			Qfp	
8665	0	8666	Qfpb	0.950	15			Qfp	
8666	0	8667	Qfpb	0.079	15			Qfp	
8667	0	8668	Qfpb	0.165	15			Qfp	
8668	0	8669	Qfpb	0.057	15			Qfp	
8669	0	8670	Qfpb	0.054	15			Qfp	
8670	0	8671	Qfpb	0.189	15			Qfp	
8671	0	8672	Qfpb	0.089	15			Qfp	
8672	0	8673	Qfpb	0.014	15			Qfp	
8673	0	8674	Qfpb	0.590	15			Qfp	
8674	0	8675	Qfpb	0.615	15			Qfp	
8675	0	8676	Qfpb	0.405	15			Qfp	
8676	0	8677	Qfpb	0.099	15			Qfp	
8677	0	8678	Qfpb	0.030	15			Qfp	
8678	0	8679	Qfpb	3.058	15			Qfp	
8679	0	8680	Qfpb	0.105	15			Qfp	
8680	0	8681	Qfpb	0.418	15			Qfp	
8681	0	8682	Qfpb	0.063	15			Qfp	
8682	0	8683	Qfpb	1.162	15			Qfp	
8683	0	8684	Qfpb	0.062	15			Qfp	
8684	0	8685	Qfpb	2.016	15			Qfp	
8685	0	8686	Qfpb	0.243	15			Qfp	
8686	0	8687	Qfpb	0.149	15			Qfp	
8687	0	8688	Qfpb	0.114	15			Qfp	
8688	0	8689	Qfpb	0.087	15			Qfp	
8689	0	8690	Qfpb	0.260	15			Qfp	
8690	0	8691	Qfpb	0.107	15			Qfp	
8691	0	8692	Qfpb	0.702	15			Qfp	
8692	0	8693	Qfpb	0.143	15			Qfp	
8693	0	8694	Qfpb	0.313	15			Qfp	
8694	0	8695	Qfpb	0.067	15			Qfp	
8695	0	8696	Qfpb	0.939	15			Qfp	

Geonexus

OBJECTID_1	Join_Count	TARGET_FID	Label	Shape_Area (sqkm)	ORIG_FID	Absolute_Age	Age_paleontology	Unit	Reference
8696	0	8697	Qfpb	0.202	15			Qfp	
8697	0	8698	Qfpb	0.057	15			Qfp	
8698	0	8699	Qfpb	0.313	15			Qfp	
8699	0	8700	Qfpb	0.099	15			Qfp	
8700	0	8701	Qfpb	0.308	15			Qfp	
8701	0	8702	Qfpb	1.772	15			Qfp	
8702	0	8703	Qfpb	0.057	15			Qfp	
8703	0	8704	Qfpb	7.561	15			Qfp	
8704	0	8705	Qfpb	0.489	15			Qfp	
8705	0	8706	Qfpb	0.405	15			Qfp	
8706	0	8707	Qfpb	0.552	15			Qfp	
8707	0	8708	Qfpb	0.272	15			Qfp	
8708	0	8709	Qfpb	6.355	15			Qfp	
8709	0	8710	Qfpb	0.257	15			Qfp	
8710	0	8711	Qfpb	5.054	15			Qfp	
8711	0	8712	Qfpb	0.284	15			Qfp	
8712	0	8713	Qfpb	0.369	15			Qfp	
8713	0	8714	Qfpb	0.104	15			Qfp	
8714	0	8715	Qfpb	0.470	15			Qfp	
8715	0	8716	Qfpb	0.504	15			Qfp	
8716	0	8717	Qfpb	0.182	15			Qfp	
8717	0	8718	Qfpb	0.442	15			Qfp	
8718	0	8719	Qfpb	0.213	15			Qfp	
8719	0	8720	Qfpb	0.492	15			Qfp	
8720	0	8721	Qfpb	0.037	15			Qfp	
8721	0	8722	Qfpb	0.163	15			Qfp	
8722	0	8723	Qfpb	0.289	15			Qfp	
8723	0	8724	Qfpb	0.165	15			Qfp	
8724	0	8725	Qfpb	0.490	15			Qfp	
8725	0	8726	Qfpb	0.113	15			Qfp	
8726	0	8727	Qfpb	0.972	15			Qfp	
8727	0	8728	Qfpb	0.054	15			Qfp	
8728	0	8729	Qfpb	1.033	15			Qfp	
8729	0	8730	Qfpb	0.535	15			Qfp	
8730	0	8731	Qfpb	0.315	15			Qfp	
8731	0	8732	Qfpb	0.084	15			Qfp	
8732	0	8733	Qfpb	0.392	15			Qfp	
8733	0	8734	Qfpb	0.316	15			Qfp	
8734	0	8735	Qfpb	0.623	15			Qfp	

GeoNexus

OBJECTID_1	Join_Count	TARGET_FID	Label	Shape_Area (sqkm)	ORIG_FID	Absolute_Age	Age_paleontology	Unit	Reference
8735	0	8736	Qfpb	0.480	15			Qfp	
8736	0	8737	Qfpb	0.298	15			Qfp	
8737	0	8738	Qfpb	0.697	15			Qfp	
8738	0	8739	Qfpb	0.114	15			Qfp	
8739	0	8740	Qfpb	0.486	15			Qfp	
8740	0	8741	Qfpb	0.203	15			Qfp	
8741	0	8742	Qfpb	0.341	15			Qfp	
8742	0	8743	Qfpb	0.041	15			Qfp	
8743	0	8744	Qfpb	0.312	15			Qfp	
8744	0	8745	Qfpb	0.043	15			Qfp	
8745	0	8746	Qfpb	0.050	15			Qfp	
8746	0	8747	Qfpb	0.288	15			Qfp	
8747	0	8748	Qfpb	0.082	15			Qfp	
8748	0	8749	Qfpb	0.143	15			Qfp	
8749	0	8750	Qfpb	0.354	15			Qfp	
8750	0	8751	Qfpb	0.169	15			Qfp	
8751	0	8752	Qfpb	0.115	15			Qfp	
8752	0	8753	Qfpb	0.183	15			Qfp	
8753	0	8754	Qfpb	0.769	15			Qfp	
8754	0	8755	Qfpb	0.618	15			Qfp	
8755	0	8756	Qfpb	0.140	15			Qfp	
8756	0	8757	Qfpb	1.965	15			Qfp	
8757	0	8758	Qfpb	0.994	15			Qfp	
8758	0	8759	Qfpb	0.090	15			Qfp	
8759	0	8760	Qfpb	0.972	15			Qfp	
8760	0	8761	Qfpb	1.194	15			Qfp	
8761	0	8762	Qfpb	0.767	15			Qfp	
8762	0	8763	Qfpb	2.008	15			Qfp	
8763	0	8764	Qfpb	0.359	15			Qfp	
8764	0	8765	Qfpb	0.845	15			Qfp	
8765	0	8766	Qfpw	0.125	16			Qfp	
8766	0	8767	Qfpw	0.021	16			Qfp	
8767	0	8768	Qfpw	1.494	16			Qfp	
8768	0	8769	Qfpw	0.115	16			Qfp	
8769	0	8770	Qfpw	0.078	16			Qfp	
8770	0	8771	Qfpw	0.364	16			Qfp	
8771	0	8772	Qfpw	3.323	16			Qfp	
8772	0	8773	Qfpw	0.448	16			Qfp	
8773	0	8774	Qfpw	0.089	16			Qfp	

Geonexus

OBJECTID_1	Join_Count	TARGET_FID	Label	Shape_Area (sqkm)	ORIG_FID	Absolute_Age	Age_paleontology	Unit	Reference
8774	0	8775	Qfpw	0.034	16			Qfp	
8775	0	8776	Qfpw	0.059	16			Qfp	
8776	0	8777	Qfpw	0.024	16			Qfp	
8777	0	8778	Qfpw	0.365	16			Qfp	
8778	0	8779	Qfpw	0.849	16			Qfp	
8779	0	8780	Qfpw	0.297	16			Qfp	
8780	0	8781	Qfpw	0.709	16			Qfp	
8781	0	8782	Qfpw	0.282	16			Qfp	
8782	0	8783	Qfpw	0.165	16			Qfp	
8783	0	8784	Qfpw	0.283	16			Qfp	
8784	0	8785	Qfpw	0.630	16			Qfp	
8785	0	8786	Qfpw	1.121	16			Qfp	
8786	0	8787	Qfpw	0.666	16			Qfp	
8787	0	8788	Qfpw	1.107	16			Qfp	
8788	0	8789	Qfpw	0.110	16			Qfp	
8789	0	8790	Qfpw	0.113	16			Qfp	
8790	0	8791	Qfpw	0.073	16			Qfp	
8791	0	8792	Qfpw	0.144	16			Qfp	
8792	0	8793	Qfpw	0.145	16			Qfp	
8793	0	8794	Qfpw	0.364	16			Qfp	
8794	0	8795	Qfpw	0.162	16			Qfp	
8795	0	8796	Qfpw	0.153	16			Qfp	
8796	0	8797	Qfpw	0.312	16			Qfp	
8797	0	8798	Qfpw	1.136	16			Qfp	
8798	0	8799	Qfpw	1.704	16			Qfp	
8799	0	8800	Qfpw	0.106	16			Qfp	
8800	0	8801	Qfpw	2.466	16			Qfp	
8802	0	8803	Qfpw	0.085	16			Qfp	
8803	0	8804	Qfpw	0.107	16			Qfp	
8804	0	8805	Qfpw	1.110	16			Qfp	
8805	0	8806	Qfpw	0.117	16			Qfp	
8806	0	8807	Qfpw	0.017	16			Qfp	
8807	0	8808	Qfpw	1.066	16			Qfp	
8808	0	8809	Qfpw	0.548	16			Qfp	
8810	0	8811	Qfpw	0.004	16			Qfp	
8811	0	8812	Qfpw	0.582	16			Qfp	
8812	0	8813	Qfpw	0.010	16			Qfp	
8813	0	8814	Qfpw	0.067	16			Qfp	
8814	0	8815	Qfpw	0.081	16			Qfp	

GeoNexus

OBJECTID_1	Join_Count	TARGET_FID	Label	Shape_Area (sqkm)	ORIG_FID	Absolute_Age	Age_paleontology	Unit	Reference
8815	0	8816	Qfpw	0.014	16			Qfp	
8816	0	8817	Qfpw	0.027	16			Qfp	
8817	0	8818	Qfpw	0.023	16			Qfp	
8818	0	8819	Qfpw	0.788	16			Qfp	
8819	0	8820	Qfpw	0.146	16			Qfp	
8820	0	8821	Qfpw	0.023	16			Qfp	
8821	0	8822	Qfpw	0.108	16			Qfp	
8822	0	8823	Qfpw	0.042	16			Qfp	
8823	0	8824	Qfpw	0.046	16			Qfp	
8824	0	8825	Qfpw	0.104	16			Qfp	
8825	0	8826	Qfpw	0.089	16			Qfp	
8826	0	8827	Qfpw	1.967	16			Qfp	
8827	0	8828	Qfpw	0.061	16			Qfp	
8828	0	8829	Qfpw	0.028	16			Qfp	
8829	0	8830	Qfpw	0.212	16			Qfp	
8830	0	8831	Qfpw	0.236	16			Qfp	
8831	0	8832	Qfpw	0.067	16			Qfp	
8832	0	8833	Qfpw	0.088	16			Qfp	
8833	0	8834	Qfpw	0.107	16			Qfp	
8834	0	8835	Qfpw	0.108	16			Qfp	
8835	0	8836	Qfpw	0.010	16			Qfp	
8836	0	8837	Qfpw	0.301	16			Qfp	
8837	0	8838	Qfpw	0.082	16			Qfp	
8838	0	8839	Qfpw	0.008	16			Qfp	
8839	0	8840	Qfpw	0.064	16			Qfp	
8840	0	8841	Qfpw	0.301	16			Qfp	
8841	0	8842	Qfpw	0.117	16			Qfp	
8842	0	8843	Qfpw	0.061	16			Qfp	
8843	0	8844	Qfpw	0.148	16			Qfp	
8844	0	8845	Qfpw	0.054	16			Qfp	
8845	0	8846	Qfpw	0.038	16			Qfp	
8846	0	8847	Qfpw	0.108	16			Qfp	
8847	0	8848	Qfpw	0.133	16			Qfp	
8848	0	8849	Qfpw	0.073	16			Qfp	
8849	0	8850	Qfpw	0.024	16			Qfp	
8850	0	8851	Qfpw	0.034	16			Qfp	
8851	0	8852	Qfpw	0.147	16			Qfp	
8852	0	8853	Qfpw	0.147	16			Qfp	
8853	0	8854	Qfpw	0.037	16			Qfp	

GeoNexus

OBJECTID_1	Join_Count	TARGET_FID	Label	Shape_Area (sqkm)	ORIG_FID	Absolute_Age	Age_paleontology	Unit	Reference
8854	0	8855	Qfpw	0.173	16			Qfp	
8855	0	8856	Qfpw	0.148	16			Qfp	
8856	0	8857	Qfpw	0.666	16			Qfp	
8857	0	8858	Qfpw	0.195	16			Qfp	
8858	0	8859	Qfpw	0.223	16			Qfp	
8859	0	8860	Qfpw	0.112	16			Qfp	
8860	0	8861	Qfpw	0.121	16			Qfp	
8861	0	8862	Qfpw	0.480	16			Qfp	
8862	0	8863	Qfpw	0.088	16			Qfp	
8863	0	8864	Qfpw	0.073	16			Qfp	
8864	0	8865	Qfpw	0.449	16			Qfp	
8865	0	8866	Qfpw	0.079	16			Qfp	
8866	0	8867	Qfpw	0.117	16			Qfp	
8867	0	8868	Qfpw	0.082	16			Qfp	
8868	0	8869	Qfpw	0.047	16			Qfp	
8869	0	8870	Qfpw	0.103	16			Qfp	
8870	0	8871	Qfpw	0.032	16			Qfp	
8871	0	8872	Qfpw	0.025	16			Qfp	
8872	0	8873	Qfpw	0.030	16			Qfp	
8873	0	8874	Qfpw	3.325	16			Qfp	
8874	0	8875	Qfpw	0.096	16			Qfp	
8875	0	8876	Qfpw	0.019	16			Qfp	
8876	0	8877	Qfpw	1.647	16			Qfp	
8877	0	8878	Qfpw	0.014	16			Qfp	
8878	0	8879	Qfpw	0.332	16			Qfp	
8879	0	8880	Qfpw	0.067	16			Qfp	
8880	0	8881	Qfpw	0.400	16			Qfp	
8881	0	8882	Qfpw	0.315	16			Qfp	
8882	0	8883	Qfpw	0.742	16			Qfp	
8883	0	8884	Qfpw	0.023	16			Qfp	
8884	0	8885	Qfpw	0.020	16			Qfp	
8885	0	8886	Qfpw	0.008	16			Qfp	
8886	0	8887	Qfpw	0.075	16			Qfp	
8887	0	8888	Qfpw	0.638	16			Qfp	
8888	0	8889	Qfpw	0.174	16			Qfp	
8889	0	8890	Qfpw	0.282	16			Qfp	
8890	0	8891	Qfpw	0.069	16			Qfp	
8891	0	8892	Qfpw	0.370	16			Qfp	
8892	0	8893	Qfpw	0.376	16			Qfp	

GeoNexus

OBJECTID_1	Join_Count	TARGET_FID	Label	Shape_Area (sqkm)	ORIG_FID	Absolute_Age	Age_paleontology	Unit	Reference
8893	0	8894	Qfpw	0.158	16			Qfp	
8894	0	8895	Qfpw	0.006	16			Qfp	
8895	0	8896	Qfpw	0.949	16			Qfp	
8896	0	8897	Qfpw	0.017	16			Qfp	
8897	0	8898	Qfpw	0.179	16			Qfp	
8898	0	8899	Qfpw	0.010	16			Qfp	
8899	0	8900	Qfpw	0.063	16			Qfp	
8900	0	8901	Qfpw	0.045	16			Qfp	
8901	0	8902	Qfpw	0.040	16			Qfp	
8902	0	8903	Qfpw	0.006	16			Qfp	
8903	0	8904	Qfpw	0.053	16			Qfp	
8904	0	8905	Qfpw	0.292	16			Qfp	
8905	0	8906	Qfpw	0.229	16			Qfp	
8906	0	8907	Qfpw	0.367	16			Qfp	
8907	0	8908	Qfpw	0.048	16			Qfp	
8908	0	8909	Qfpw	0.234	16			Qfp	
8909	0	8910	Qfpw	0.105	16			Qfp	
8910	0	8911	Qfpw	0.571	16			Qfp	
8911	0	8912	Qfpw	0.122	16			Qfp	
8912	0	8913	Qfpw	0.840	16			Qfp	
8913	0	8914	Qfpw	0.417	16			Qfp	
8914	0	8915	Qfpw	0.308	16			Qfp	
8915	0	8916	Qfpw	0.200	16			Qfp	
8916	0	8917	Qfpw	0.123	16			Qfp	
8917	0	8918	Qfpw	3.732	16			Qfp	
8918	0	8919	Qfpw	0.014	16			Qfp	
8919	0	8920	Qfpw	0.140	16			Qfp	
8920	0	8921	Qfpw	0.030	16			Qfp	
8921	0	8922	Qfpw	0.118	16			Qfp	
8922	0	8923	Qfpw	0.022	16			Qfp	
8923	0	8924	Qfpw	0.047	16			Qfp	
8924	0	8925	Qfpw	0.086	16			Qfp	
8925	0	8926	Qfpw	0.039	16			Qfp	
8926	0	8927	Qfpw	0.087	16			Qfp	
8927	0	8928	Qfpw	2.433	16			Qfp	
8928	0	8929	Qfpw	0.134	16			Qfp	
8929	0	8930	Qfpw	0.431	16			Qfp	
8930	0	8931	Qfpw	0.018	16			Qfp	
8931	0	8932	Qfpw	0.047	16			Qfp	

Geonexus

OBJECTID_1	Join_Count	TARGET_FID	Label	Shape_Area (sqkm)	ORIG_FID	Absolute_Age	Age_paleontology	Unit	Reference
8932	0	8933	Qfpw	0.537	16			Qfp	
8933	0	8934	Qfpw	0.254	16			Qfp	
8934	0	8935	Qfpw	0.069	16			Qfp	
8935	0	8936	Qfpw	0.051	16			Qfp	
8936	0	8937	Qfpw	0.148	16			Qfp	
8937	0	8938	Qfpw	0.406	16			Qfp	
8938	0	8939	Qfpw	0.033	16			Qfp	
8939	0	8940	Qfpw	0.086	16			Qfp	
8940	0	8941	Qfpw	0.494	16			Qfp	
8941	0	8942	Qfpw	0.110	16			Qfp	
8942	0	8943	Qfpw	0.140	16			Qfp	
8943	0	8944	Qfpw	0.056	16			Qfp	
8944	0	8945	Qfpw	0.058	16			Qfp	
8945	0	8946	Qfpw	0.051	16			Qfp	
8946	0	8947	Qfpw	0.046	16			Qfp	
8947	0	8948	Qfpw	0.559	16			Qfp	
8948	0	8949	Qfpw	0.933	16			Qfp	
8949	0	8950	Qfpw	0.020	16			Qfp	
8950	0	8951	Qfpw	0.073	16			Qfp	
8951	0	8952	Qfpw	7.074	16			Qfp	
8952	0	8953	Qfpw	0.079	16			Qfp	
8953	0	8954	Qfpw	0.062	16			Qfp	
8954	0	8955	Qfpw	0.041	16			Qfp	
8955	0	8956	Qfpw	0.150	16			Qfp	
8956	0	8957	Qfpw	0.037	16			Qfp	
8957	0	8958	Qfpw	0.105	16			Qfp	
8958	0	8959	Qfpw	0.077	16			Qfp	
8959	0	8960	Qfpw	0.043	16			Qfp	
8960	0	8961	Qfpw	0.671	16			Qfp	
8961	0	8962	Qfpw	0.038	16			Qfp	
8962	0	8963	Qfpw	0.043	16			Qfp	
8963	0	8964	Qfpw	0.077	16			Qfp	
8964	0	8965	Qfpw	0.206	16			Qfp	
8965	0	8966	Qfpw	4.288	16			Qfp	
8966	0	8967	Qfpw	0.086	16			Qfp	
8967	0	8968	Qfpw	0.095	16			Qfp	
8968	0	8969	Qfpw	0.120	16			Qfp	
8969	0	8970	Qfpw	0.039	16			Qfp	
8970	0	8971	Qfpw	0.260	16			Qfp	

GeoNexus

OBJECTID_1	Join_Count	TARGET_FID	Label	Shape_Area (sqkm)	ORIG_FID	Absolute_Age	Age_paleontology	Unit	Reference
8971	0	8972	Qfpw	0.492	16			Qfp	
8972	0	8973	Qfpw	0.043	16			Qfp	
8973	0	8974	Qfpw	1.109	16			Qfp	
8974	0	8975	Qfpw	0.392	16			Qfp	
8975	0	8976	Qfpw	0.097	16			Qfp	
8976	0	8977	Qfpw	1.574	16			Qfp	
8977	0	8978	Qfpw	1.004	16			Qfp	
8978	0	8979	Qfpw	0.434	16			Qfp	
8979	0	8980	Qfpw	0.059	16			Qfp	
8980	0	8981	Qfpw	0.042	16			Qfp	
8981	0	8982	Qfpw	0.158	16			Qfp	
8982	0	8983	Qfpw	0.062	16			Qfp	
8983	0	8984	Qfpw	0.097	16			Qfp	
8984	0	8985	Qfpw	0.101	16			Qfp	
8985	0	8986	Qfpw	0.368	16			Qfp	
8986	0	8987	Qfpw	0.078	16			Qfp	
8987	0	8988	Qfpw	0.627	16			Qfp	
8988	0	8989	Qfpw	0.209	16			Qfp	
8989	0	8990	Qfpw	0.117	16			Qfp	
8990	0	8991	Qfpw	0.135	16			Qfp	
8991	0	8992	Qfpw	1.633	16			Qfp	
8992	0	8993	Qfpw	0.038	16			Qfp	
8993	0	8994	Qfpw	0.110	16			Qfp	
8994	0	8995	Qfpw	0.061	16			Qfp	
8996	0	8997	Qfpw	0.166	16			Qfp	
8997	0	8998	Qfpw	0.030	16			Qfp	
9000	0	9001	Qfpw	0.072	16			Qfp	
9003	0	9004	Qfpw	0.173	16			Qfp	
9004	0	9005	Qfpw	0.065	16			Qfp	
9005	0	9006	Qfpw	0.431	16			Qfp	
9007	0	9008	Qfpw	0.096	16			Qfp	
9008	0	9009	Qfpw	0.268	16			Qfp	
9009	0	9010	Qfpw	0.015	16			Qfp	
9010	0	9011	Qfpw	0.053	16			Qfp	
9011	0	9012	Qfpw	9.880	16			Qfp	
9014	0	9015	Qfpw	0.185	16			Qfp	
9016	0	9017	Qfpw	0.011	16			Qfp	
9018	0	9019	Qfpw	0.012	16			Qfp	
9019	0	9020	Qfpw	0.170	16			Qfp	

GeoNexus

OBJECTID_1	Join_Count	TARGET_FID	Label	Shape_Area (sqkm)	ORIG_FID	Absolute_Age	Age_paleontology	Unit	Reference
9020	0	9021	Qfpw	0.007	16			Qfp	
9021	0	9022	Qfpw	0.020	16			Qfp	
9022	0	9023	Qfpw	0.117	16			Qfp	
9023	0	9024	Qfpw	0.501	16			Qfp	
9024	0	9025	Qfpw	0.049	16			Qfp	
9025	0	9026	Qfpw	0.020	16			Qfp	
9026	0	9027	Qfpw	0.172	16			Qfp	
9027	0	9028	Qfpw	0.048	16			Qfp	
9028	0	9029	Qfpw	1.163	16			Qfp	
9029	0	9030	Qfpw	0.009	16			Qfp	
9030	0	9031	Qfpw	0.033	16			Qfp	
9031	0	9032	Qfpw	0.182	16			Qfp	
9032	0	9033	Qfpw	0.180	16			Qfp	
9033	0	9034	Qfpw	0.042	16			Qfp	
9034	0	9035	Qfpw	0.302	16			Qfp	
9035	0	9036	Qfpw	0.290	16			Qfp	
9036	0	9037	Qfpw	0.230	16			Qfp	
9037	0	9038	Qfpw	0.174	16			Qfp	
9038	0	9039	Qfpw	0.023	16			Qfp	
9039	0	9040	Qfpw	0.009	16			Qfp	
9040	0	9041	Qfpw	0.050	16			Qfp	
9041	0	9042	Qfpw	0.147	16			Qfp	
9042	0	9043	Qfpw	0.825	16			Qfp	
9043	0	9044	Qfpw	0.279	16			Qfp	
9044	0	9045	Qfpw	0.165	16			Qfp	
9045	0	9046	Qfpw	0.071	16			Qfp	
9046	0	9047	Qfpw	0.394	16			Qfp	
9047	0	9048	Qfpw	0.041	16			Qfp	
9048	0	9049	Qfpw	0.110	16			Qfp	
9049	0	9050	Qfpw	0.105	16			Qfp	
9050	0	9051	Qfpw	0.114	16			Qfp	
9051	0	9052	Qfpw	0.084	16			Qfp	
9052	0	9053	Qfpw	0.109	16			Qfp	
9053	0	9054	Qfpw	0.865	16			Qfp	
9054	0	9055	Qfpw	0.287	16			Qfp	
9055	0	9056	Qfpw	0.438	16			Qfp	
9056	0	9057	Qfpw	0.160	16			Qfp	
9058	0	9059	Qfpw	0.071	16			Qfp	
9059	0	9060	Qfpw	0.697	16			Qfp	

GeoNexus

OBJECTID_1	Join_Count	TARGET_FID	Label	Shape_Area (sqkm)	ORIG_FID	Absolute_Age	Age_paleontology	Unit	Reference
9060	0	9061	Qfpw	0.191	16			Qfp	
9062	0	9063	Qfpw	3.957	16			Qfp	
9064	0	9065	Qfpw	0.027	16			Qfp	
9065	0	9066	Qfpw	1.780	16			Qfp	
9067	0	9068	Qfpw	0.260	16			Qfp	
9068	0	9069	Qfpw	0.008	16			Qfp	
9069	0	9070	Qfpw	0.009	16			Qfp	
9071	0	9072	Qfpw	1.054	16			Qfp	
9072	0	9073	Qfpw	0.008	16			Qfp	
9075	0	9076	Qfpw	0.017	16			Qfp	
9076	0	9077	Qfpw	0.248	16			Qfp	
9078	0	9079	Qfpw	0.820	16			Qfp	
9080	0	9081	Qfpw	0.031	16			Qfp	
9081	0	9082	Qfpw	0.031	16			Qfp	
9084	0	9085	Qfpw	0.155	16			Qfp	
9085	0	9086	Qfpw	0.107	16			Qfp	
9086	0	9087	Qfpw	0.120	16			Qfp	
9087	0	9088	Qfpw	0.065	16			Qfp	
9090	0	9091	Qfpw	0.511	16			Qfp	
9091	0	9092	Qfpw	0.057	16			Qfp	
9093	0	9094	Qfpw	0.011	16			Qfp	
9094	0	9095	Qfpw	0.883	16			Qfp	
9095	0	9096	Qfpw	0.088	16			Qfp	
9096	0	9097	Qfpw	2.055	16			Qfp	
9097	0	9098	Qfpw	0.757	16			Qfp	
9098	0	9099	Qfpw	0.873	16			Qfp	
9099	0	9100	Qfpw	1.332	16			Qfp	
9100	0	9101	Qfpw	0.006	16			Qfp	
9101	0	9102	Qfpw	0.645	16			Qfp	
9102	0	9103	Qfpw	0.385	16			Qfp	
9103	0	9104	Qfpw	0.085	16			Qfp	
9107	0	9108	Qfpw	1.740	16			Qfp	
9108	0	9109	Qfpw	0.087	16			Qfp	
9109	0	9110	Qfpw	0.038	16			Qfp	
9110	0	9111	Qfpw	0.084	16			Qfp	
9111	0	9112	Qfpw	0.052	16			Qfp	
9112	0	9113	Qfpw	0.007	16			Qfp	
9113	0	9114	Qfpw	0.988	16			Qfp	
9114	0	9115	Qfpw	0.639	16			Qfp	

Geonexus

OBJECTID_1	Join_Count	TARGET_FID	Label	Shape_Area (sqkm)	ORIG_FID	Absolute_Age	Age_paleontology	Unit	Reference
9116	0	9117	Qfpw	0.126	16			Qfp	
9117	0	9118	Qfpw	0.057	16			Qfp	
9118	0	9119	Qfpw	0.022	16			Qfp	
9120	0	9121	Qfpw	0.059	16			Qfp	
9121	0	9122	Qfpw	0.064	16			Qfp	
9122	0	9123	Qfpw	0.193	16			Qfp	
9123	0	9124	Qfpw	0.041	16			Qfp	
9124	0	9125	Qfpw	0.077	16			Qfp	
9127	0	9128	Qfpw	0.308	16			Qfp	
9128	0	9129	Qfpw	0.016	16			Qfp	
9129	0	9130	Qfpw	0.202	16			Qfp	
9130	0	9131	Qfpw	0.096	16			Qfp	
9135	0	9136	Qfpw	0.047	16			Qfp	
9136	0	9137	Qfpw	0.063	16			Qfp	
9137	0	9138	Qfpw	0.196	16			Qfp	
9138	0	9139	Qfpw	0.038	16			Qfp	
9139	0	9140	Qfpw	0.213	16			Qfp	
9141	0	9142	Qfpw	0.234	16			Qfp	
9145	0	9146	Qfpw	0.005	16			Qfp	
9146	0	9147	Qfpw	0.095	16			Qfp	
9147	0	9148	Qfpw	0.025	16			Qfp	
9148	0	9149	Qfpw	0.436	16			Qfp	
9149	0	9150	Qfpw	0.322	16			Qfp	
9150	0	9151	Qfpw	0.126	16			Qfp	
9151	0	9152	Qfpw	0.065	16			Qfp	
9153	0	9154	Qfpw	0.029	16			Qfp	
9154	0	9155	Qfpw	0.872	16			Qfp	
9155	0	9156	Qfpw	0.098	16			Qfp	
9156	0	9157	Qfpw	0.013	16			Qfp	
9157	0	9158	Qfpw	0.017	16			Qfp	
9158	0	9159	Qfpw	1.077	16			Qfp	
9159	0	9160	Qfpw	0.082	16			Qfp	
9160	0	9161	Qfpw	0.016	16			Qfp	
9161	0	9162	Qfpw	0.120	16			Qfp	
9162	0	9163	Qfpw	0.023	16			Qfp	
9163	0	9164	Qfpw	0.596	16			Qfp	
9164	0	9165	Qfpw	0.149	16			Qfp	
9165	0	9166	Qfpw	0.563	16			Qfp	
9166	0	9167	Qfpw	0.074	16			Qfp	

GeoNexus

OBJECTID_1	Join_Count	TARGET_FID	Label	Shape_Area (sqkm)	ORIG_FID	Absolute_Age	Age_paleontology	Unit	Reference
9167	0	9168	Qfpw	0.054	16			Qfp	
9168	0	9169	Qfpw	0.289	16			Qfp	
9169	0	9170	Qfpw	0.071	16			Qfp	
9170	0	9171	Qfpw	0.034	16			Qfp	
9171	0	9172	Qfpw	0.012	16			Qfp	
9172	0	9173	Qfpw	0.013	16			Qfp	
9173	0	9174	Qfpw	0.331	16			Qfp	
9174	0	9175	Qfpw	0.142	16			Qfp	
9175	0	9176	Qfpw	0.018	16			Qfp	
9176	0	9177	Qfpw	0.027	16			Qfp	
9177	0	9178	Qfpw	0.339	16			Qfp	
9178	0	9179	Qfpw	0.059	16			Qfp	
9181	0	9182	Qfpw	0.046	16			Qfp	
9182	0	9183	Qfpw	0.098	16			Qfp	
9183	0	9184	Qfpw	0.020	16			Qfp	
9185	0	9186	Qfpw	0.201	16			Qfp	
9187	0	9188	Qfpw	0.017	16			Qfp	
9188	0	9189	Qfpw	0.074	16			Qfp	
10490	0	8492	Qfpb	0.798	15			Qfp	

GeoNexus

Table S15. Summary of mapped polygons for the Q^{sd} Unit.

OBJECTID_1	Join_Count	TARGET_FID	Label	Shape_Area (sqkm)	ORIG_FID	Absolute_Age	Age_paleontology	Unit	Reference
10004	0	10006	sand dune	0.053	18			Qsd	
10005	0	10007	sand dune	7.768	18			Qsd	
10006	0	10008	sand dune	0.252	18			Qsd	
10007	0	10009	sand dune	0.061	18			Qsd	
10008	0	10010	sand dune	0.191	18			Qsd	
10009	0	10011	sand dune	0.036	18			Qsd	
10010	0	10012	sand dune	0.046	18			Qsd	
10011	0	10013	sand dune	0.429	18			Qsd	
10012	0	10014	sand dune	0.225	18			Qsd	
10013	0	10015	sand dune	0.760	18			Qsd	
10014	0	10016	sand dune	0.219	18			Qsd	
10015	0	10017	sand dune	0.037	18			Qsd	
10016	0	10018	sand dune	0.341	18			Qsd	
10017	0	10019	sand dune	0.062	18			Qsd	
10018	0	10020	sand dune	0.802	18			Qsd	
10019	0	10021	sand dune	0.476	18			Qsd	
10020	0	10022	sand dune	0.266	18			Qsd	
10021	0	10023	sand dune	0.173	18			Qsd	
10022	0	10024	sand dune	0.950	18			Qsd	
10023	0	10025	sand dune	0.824	18			Qsd	
10025	0	10027	sand dune	0.157	18			Qsd	
10026	0	10028	sand dune	0.015	18			Qsd	
10027	0	10029	sand dune	0.561	18			Qsd	
10028	0	10030	sand dune	0.245	18			Qsd	
10030	0	10032	sand dune	0.107	18			Qsd	
10031	0	10033	sand dune	1.005	18			Qsd	
10032	0	10034	sand dune	1.318	18			Qsd	
10033	0	10035	sand dune	0.558	18			Qsd	
10034	0	10036	sand dune	1.400	18			Qsd	
10035	0	10037	sand dune	1.413	18			Qsd	
10036	0	10038	sand dune	0.081	18			Qsd	
10037	0	10039	sand dune	7.445	18			Qsd	
10038	0	10040	sand dune	0.264	18			Qsd	
10039	0	10041	sand dune	0.126	18			Qsd	
10040	0	10042	sand dune	0.115	18			Qsd	
10041	0	10043	sand dune	0.121	18			Qsd	
10042	0	10044	sand dune	4.904	18			Qsd	
10043	0	10045	sand dune	0.096	18			Qsd	

GeoNexus

OBJECTID_1	Join_Count	TARGET_FID	Label	Shape_Area (sqkm)	ORIG_FID	Absolute_Age	Age_paleontology	Unit	Reference
10044	0	10046	sand dune	0.095	18			Qsd	
10045	0	10047	sand dune	0.019	18			Qsd	
10046	0	10048	sand dune	0.162	18			Qsd	
10047	0	10049	sand dune	0.065	18			Qsd	
10048	0	10050	sand dune	0.012	18			Qsd	
10049	0	10051	sand dune	0.439	18			Qsd	
10050	0	10052	sand dune	0.301	18			Qsd	
10051	0	10053	sand dune	0.010	18			Qsd	
10052	0	10054	sand dune	0.500	18			Qsd	
10053	0	10055	sand dune	0.258	18			Qsd	
10054	0	10056	sand dune	0.111	18			Qsd	
10055	0	10057	sand dune	0.437	18			Qsd	
10056	0	10058	sand dune	0.155	18			Qsd	
10057	0	10059	sand dune	0.109	18			Qsd	
10058	1	10060	Qtsd	0.385	18			Qsd	
10059	0	10061	sand dune	0.139	18			Qsd	
10060	0	10062	sand dune	0.091	18			Qsd	
10061	0	10063	sand dune	0.075	18			Qsd	
10062	0	10064	sand dune	0.616	18			Qsd	
10063	0	10065	sand dune	0.119	18			Qsd	
10064	0	10066	sand dune	0.172	18			Qsd	
10065	0	10067	sand dune	0.109	18			Qsd	
10066	0	10068	sand dune	0.558	18			Qsd	
10067	0	10069	sand dune	0.196	18			Qsd	
10068	0	10070	sand dune	1.290	18			Qsd	
10069	0	10071	sand dune	0.158	18			Qsd	
10070	0	10072	sand dune	1.166	18			Qsd	
10071	0	10073	sand dune	0.103	18			Qsd	
10072	0	10074	sand dune	1.401	18			Qsd	
10377	1	10380	Qtsd	0.002	0			Qsd	
10378	1	10381	Qtsd	0.096	0			Qsd	
10397	1	10404	Qtsd	1.193	0			Qsd	
10399	1	10406	Qtsd	1.690	0			Qsd	
10404	1	10411	Qtsd	19.333	0			Qsd	

Geonexus

Table S16. Summary of mapped polygons for the Q^{al} Unit.

OBJECTID_1	Join_Count	TARGET_FID	Label	Shape_Area (sqkm)	ORIG_FID	Absolute_Age	Age_paleontology	Unit	Reference
2083	0	2083	Qals	0.438	4			Qal	
2103	0	2103	Qals	0.276	4			Qal	
2107	0	2107	Qals	0.530	4			Qal	-
7318	0	7319	Qals	0.224	13			Qal	
7319	0	7320	Qals	0.070	13			Qal	
7320	0	7321	Qals	0.192	13			Qal	
7321	0	7322	Qals	0.442	13			Qal	
7322	0	7323	Qals	16.767	13			Qal	
7326	0	7327	Qals	0.067	13			Qal	
7329	0	7330	Qals	0.148	13			Qal	
7331	0	7332	Qals	0.044	13			Qal	
7333	0	7334	Qals	0.032	13			Qal	
7334	0	7335	Qals	0.119	13			Qal	
7335	0	7336	Qals	0.356	13			Qal	
7337	0	7338	Qals	0.900	13			Qal	
7338	0	7339	Qals	0.495	13			Qal	
7339	0	7340	Qals	0.215	13			Qal	
7340	0	7341	Qals	0.124	13			Qal	
7341	0	7342	Qals	0.074	13			Qal	
7342	0	7343	Qals	0.045	13			Qal	
7343	0	7344	Qals	0.301	13			Qal	
7344	0	7345	Qals	0.338	13			Qal	
7345	0	7346	Qals	0.129	13			Qal	
7346	0	7347	Qals	6.565	13			Qal	
7347	0	7348	Qals	1.563	13			Qal	
7348	0	7349	Qals	0.386	13			Qal	
7349	0	7350	Qals	0.055	13			Qal	
7350	0	7351	Qals	0.197	13			Qal	
7351	0	7352	Qals	0.136	13			Qal	
7352	0	7353	Qals	0.056	13			Qal	
7353	0	7354	Qals	0.023	13			Qal	
7354	0	7355	Qals	0.030	13			Qal	
7355	0	7356	Qals	0.037	13			Qal	
7356	0	7357	Qals	0.703	13			Qal	
7357	0	7358	Qals	2.501	13			Qal	
7358	0	7359	Qals	0.042	13			Qal	
7359	0	7360	Qals	0.185	13			Qal	
7360	0	7361	Qals	0.221	13			Qal	

GeoNexus

OBJECTID_1	Join_Count	TARGET_FID	Label	Shape_Area (sqkm)	ORIG_FID	Absolute_Age	Age_paleontology	Unit	Reference
7361	0	7362	Qals	0.021	13			Qal	
7362	0	7363	Qals	0.032	13			Qal	
7363	0	7364	Qals	0.074	13			Qal	
7364	0	7365	Qals	1.315	13			Qal	
7365	0	7366	Qals	0.242	13			Qal	
7366	0	7367	Qals	1.275	13			Qal	
7367	0	7368	Qals	0.062	13			Qal	
7368	0	7369	Qals	0.022	13			Qal	
7369	0	7370	Qals	0.053	13			Qal	
7370	0	7371	Qals	0.169	13			Qal	
7371	0	7372	Qals	0.120	13			Qal	
7372	0	7373	Qals	0.164	13			Qal	
7373	0	7374	Qals	0.279	13			Qal	
7374	0	7375	Qals	1.483	13			Qal	
7375	0	7376	Qals	0.296	13			Qal	
7376	0	7377	Qals	0.231	13			Qal	
7377	0	7378	Qals	1.039	13			Qal	
7378	0	7379	Qals	0.044	13			Qal	
7379	0	7380	Qals	0.141	13			Qal	
7380	0	7381	Qals	0.608	13			Qal	
7381	0	7382	Qals	0.119	13			Qal	
7382	0	7383	Qals	0.659	13			Qal	
7383	0	7384	Qals	0.056	13			Qal	
7384	0	7385	Qals	0.037	13			Qal	
7385	0	7386	Qals	0.471	13			Qal	
7386	0	7387	Qals	0.700	13			Qal	
7387	0	7388	Qals	0.078	13			Qal	
7388	0	7389	Qals	0.281	13			Qal	
7389	0	7390	Qals	0.295	13			Qal	
7390	0	7391	Qals	0.137	13			Qal	
7391	0	7392	Qals	0.048	13			Qal	
7392	0	7393	Qals	0.213	13			Qal	
7393	0	7394	Qals	0.015	13			Qal	
7394	0	7395	Qals	0.044	13			Qal	
7395	0	7396	Qals	0.091	13			Qal	
7396	0	7397	Qals	0.456	13			Qal	
7397	0	7398	Qals	0.044	13			Qal	
7398	0	7399	Qals	0.320	13			Qal	
7399	0	7400	Qals	0.040	13			Qal	

GeoNexus

OBJECTID_1	Join_Count	TARGET_FID	Label	Shape_Area (sqkm)	ORIG_FID	Absolute_Age	Age_paleontology	Unit	Reference
7400	0	7401	Qals	0.716	13			Qal	
7401	0	7402	Qals	0.222	13			Qal	
7402	0	7403	Qals	0.142	13			Qal	
7403	0	7404	Qals	1.809	13			Qal	
7404	0	7405	Qals	0.135	13			Qal	
7405	0	7406	Qals	0.164	13			Qal	
7406	0	7407	Qals	0.296	13			Qal	
7407	0	7408	Qals	2.416	13			Qal	
7408	0	7409	Qals	0.363	13			Qal	
7409	0	7410	Qals	0.046	13			Qal	
7410	0	7411	Qals	0.456	13			Qal	
7411	0	7412	Qals	0.055	13			Qal	
7412	0	7413	Qals	0.338	13			Qal	
7413	0	7414	Qals	0.392	13			Qal	
7414	0	7415	Qals	0.391	13			Qal	
7415	0	7416	Qals	0.092	13			Qal	
7416	0	7417	Qals	1.023	13			Qal	
7417	0	7418	Qals	0.241	13			Qal	
7418	0	7419	Qals	0.142	13			Qal	
7419	0	7420	Qals	0.069	13			Qal	
7420	0	7421	Qals	2.010	13			Qal	
7421	0	7422	Qals	0.746	13			Qal	
7422	0	7423	Qals	0.085	13			Qal	
7423	0	7424	Qals	0.897	13			Qal	
7424	0	7425	Qals	0.052	13			Qal	
7425	0	7426	Qals	0.107	13			Qal	
7426	0	7427	Qals	0.221	13			Qal	
7427	0	7428	Qals	0.094	13			Qal	
7428	0	7429	Qals	0.624	13			Qal	
7429	0	7430	Qals	0.611	13			Qal	
7430	0	7431	Qals	0.099	13			Qal	
7431	0	7432	Qals	0.295	13			Qal	
7432	0	7433	Qals	0.201	13			Qal	
7433	0	7434	Qals	0.595	13			Qal	
7434	0	7435	Qals	0.057	13			Qal	
7435	0	7436	Qals	0.463	13			Qal	
7436	0	7437	Qals	1.687	13			Qal	
7437	0	7438	Qals	0.403	13			Qal	
7438	0	7439	Qals	0.124	13			Qal	

GeoNexus

OBJECTID_1	Join_Count	TARGET_FID	Label	Shape_Area (sqkm)	ORIG_FID	Absolute_Age	Age_paleontology	Unit	Reference
7439	0	7440	Qals	0.055	13			Qal	
7440	0	7441	Qals	0.018	13			Qal	
7441	0	7442	Qals	0.028	13			Qal	
7442	0	7443	Qals	0.049	13			Qal	
7443	0	7444	Qals	1.968	13			Qal	
7444	0	7445	Qals	0.156	13			Qal	
7445	0	7446	Qals	0.204	13			Qal	
7446	0	7447	Qals	0.368	13			Qal	
7447	0	7448	Qals	0.376	13			Qal	
7448	0	7449	Qals	0.043	13			Qal	
7449	0	7450	Qals	0.058	13			Qal	
7450	0	7451	Qals	0.308	13			Qal	
7451	0	7452	Qals	0.035	13			Qal	
7452	0	7453	Qals	0.129	13			Qal	
7453	0	7454	Qals	0.014	13			Qal	
7454	0	7455	Qals	0.700	13			Qal	
7455	0	7456	Qals	0.987	13			Qal	
7456	0	7457	Qals	0.181	13			Qal	
7457	0	7458	Qals	0.173	13			Qal	
7458	0	7459	Qals	0.040	13			Qal	
7459	0	7460	Qals	0.254	13			Qal	
7460	0	7461	Qals	0.599	13			Qal	
7461	0	7462	Qals	0.458	13			Qal	
7462	0	7463	Qals	0.123	13			Qal	
7463	0	7464	Qals	0.898	13			Qal	
7464	0	7465	Qals	0.117	13			Qal	
7465	0	7466	Qals	0.421	13			Qal	
7466	0	7467	Qals	0.132	13			Qal	
7467	0	7468	Qals	0.860	13			Qal	
7468	0	7469	Qals	0.501	13			Qal	
7469	0	7470	Qals	0.145	13			Qal	
7470	0	7471	Qals	0.103	13			Qal	
7471	0	7472	Qals	3.143	13			Qal	
7472	0	7473	Qals	0.085	13			Qal	
7473	0	7474	Qals	0.061	13			Qal	
7474	0	7475	Qals	1.000	13			Qal	
7475	0	7476	Qals	0.544	13			Qal	
7476	0	7477	Qals	0.138	13			Qal	
7477	0	7478	Qals	0.046	13			Qal	

GeoNexus

OBJECTID_1	Join_Count	TARGET_FID	Label	Shape_Area (sqkm)	ORIG_FID	Absolute_Age	Age_paleontology	Unit	Reference
7478	0	7479	Qals	0.630	13			Qal	
7479	0	7480	Qals	0.137	13			Qal	
7480	0	7481	Qals	0.200	13			Qal	
7481	0	7482	Qals	1.605	13			Qal	
7482	0	7483	Qals	0.031	13			Qal	
7483	0	7484	Qals	0.717	13			Qal	
7484	0	7485	Qals	0.384	13			Qal	
7485	0	7486	Qals	0.029	13			Qal	
7486	0	7487	Qals	0.458	13			Qal	
7487	0	7488	Qals	0.851	13			Qal	
7488	0	7489	Qals	0.312	13			Qal	
7489	0	7490	Qals	0.715	13			Qal	
7490	0	7491	Qals	0.200	13			Qal	
7491	0	7492	Qals	0.435	13			Qal	
7492	0	7493	Qals	0.371	13			Qal	
7493	0	7494	Qals	0.063	13			Qal	
7494	0	7495	Qals	0.747	13			Qal	
7495	0	7496	Qals	0.107	13			Qal	
7496	0	7497	Qals	0.028	13			Qal	
7497	0	7498	Qals	0.324	13			Qal	
7498	0	7499	Qals	0.005	13			Qal	
7499	0	7500	Qals	0.042	13			Qal	
7500	0	7501	Qals	0.151	13			Qal	
7501	0	7502	Qals	0.392	13			Qal	
7502	0	7503	Qals	0.214	13			Qal	
7503	0	7504	Qals	0.052	13			Qal	
7504	0	7505	Qals	0.210	13			Qal	
7505	0	7506	Qals	0.116	13			Qal	
7506	0	7507	Qals	0.530	13			Qal	
7507	0	7508	Qals	0.188	13			Qal	
7508	0	7509	Qals	0.212	13			Qal	
7509	0	7510	Qals	0.537	13			Qal	
7510	0	7511	Qals	0.075	13			Qal	
7511	0	7512	Qals	0.354	13			Qal	
7512	0	7513	Qals	0.235	13			Qal	
7513	0	7514	Qals	0.094	13			Qal	
7514	0	7515	Qals	0.792	13			Qal	
7515	0	7516	Qals	0.065	13			Qal	
7516	0	7517	Qals	0.096	13			Qal	

GeoNexus

OBJECTID_1	Join_Count	TARGET_FID	Label	Shape_Area (sqkm)	ORIG_FID	Absolute_Age	Age_paleontology	Unit	Reference
7517	0	7518	Qals	3.093	13			Qal	
7518	0	7519	Qals	2.208	13			Qal	
7519	0	7520	Qals	0.378	13			Qal	
7520	0	7521	Qals	0.178	13			Qal	
7521	0	7522	Qals	0.636	13			Qal	
7522	0	7523	Qals	0.145	13			Qal	
7523	0	7524	Qals	0.053	13			Qal	
7524	0	7525	Qals	0.428	13			Qal	
7525	0	7526	Qals	1.047	13			Qal	
7526	0	7527	Qals	2.156	13			Qal	
7527	0	7528	Qals	0.020	13			Qal	
7528	0	7529	Qals	0.012	13			Qal	
7529	0	7530	Qals	0.059	13			Qal	
7530	0	7531	Qals	1.678	13			Qal	
7531	0	7532	Qals	0.261	13			Qal	
7532	0	7533	Qals	0.434	13			Qal	
7533	0	7534	Qals	0.324	13			Qal	
7534	0	7535	Qals	0.024	13			Qal	
7536	0	7537	Qals	0.060	13			Qal	
7537	0	7538	Qals	0.010	13			Qal	
7538	0	7539	Qals	0.054	13			Qal	
7539	0	7540	Qals	0.494	13			Qal	
7540	0	7541	Qals	0.427	13			Qal	
7541	0	7542	Qals	0.078	13			Qal	
7542	0	7543	Qals	0.994	13			Qal	
7543	0	7544	Qals	0.142	13			Qal	
7544	0	7545	Qals	1.100	13			Qal	
7545	0	7546	Qals	0.138	13			Qal	
7546	0	7547	Qals	0.272	13			Qal	
7547	0	7548	Qals	6.851	13			Qal	
7548	0	7549	Qals	0.120	13			Qal	
7550	0	7551	Qals	0.137	13			Qal	
7551	0	7552	Qals	0.251	13			Qal	
7552	0	7553	Qals	0.027	13			Qal	
7553	0	7554	Qals	0.527	13			Qal	
7554	0	7555	Qals	0.095	13			Qal	
7555	0	7556	Qals	0.317	13			Qal	
7556	0	7557	Qals	0.213	13			Qal	
7557	0	7558	Qals	0.212	13			Qal	

GeoNexus

OBJECTID_1	Join_Count	TARGET_FID	Label	Shape_Area (sqkm)	ORIG_FID	Absolute_Age	Age_paleontology	Unit	Reference
7558	0	7559	Qals	0.143	13			Qal	
7559	0	7560	Qals	0.729	13			Qal	
7560	0	7561	Qals	3.264	13			Qal	
7561	0	7562	Qals	0.079	13			Qal	
7562	0	7563	Qals	0.238	13			Qal	
7563	0	7564	Qals	0.112	13			Qal	
7564	0	7565	Qals	0.157	13			Qal	
7565	0	7566	Qals	0.080	13			Qal	
7566	0	7567	Qals	0.056	13			Qal	
7567	0	7568	Qals	0.079	13			Qal	
7568	0	7569	Qals	0.355	13			Qal	
7569	0	7570	Qals	3.854	13			Qal	
7570	0	7571	Qals	0.029	13			Qal	
7571	0	7572	Qals	0.136	13			Qal	
7572	0	7573	Qals	0.611	13			Qal	
7573	0	7574	Qals	0.205	13			Qal	
7574	0	7575	Qals	0.073	13			Qal	
7575	0	7576	Qals	0.176	13			Qal	
7576	0	7577	Qals	0.151	13			Qal	
7577	0	7578	Qals	0.471	13			Qal	
7578	0	7579	Qals	0.029	13			Qal	
7579	0	7580	Qals	0.409	13			Qal	
7580	0	7581	Qals	0.048	13			Qal	
7581	0	7582	Qals	0.135	13			Qal	
7582	0	7583	Qals	0.613	13			Qal	
7583	0	7584	Qals	0.272	13			Qal	
7584	0	7585	Qals	0.097	13			Qal	
7585	0	7586	Qals	0.437	13			Qal	
7586	0	7587	Qals	0.219	13			Qal	
7587	0	7588	Qals	0.339	13			Qal	
7588	0	7589	Qals	0.045	13			Qal	
7589	0	7590	Qals	0.029	13			Qal	
7590	0	7591	Qals	0.681	13			Qal	
7591	0	7592	Qals	8.260	13			Qal	
7592	0	7593	Qals	0.107	13			Qal	
7593	0	7594	Qals	0.273	13			Qal	
7594	0	7595	Qals	0.447	13			Qal	
7595	0	7596	Qals	0.047	13			Qal	
7596	0	7597	Qals	0.457	13			Qal	

GeoNexus

OBJECTID_1	Join_Count	TARGET_FID	Label	Shape_Area (sqkm)	ORIG_FID	Absolute_Age	Age_paleontology	Unit	Reference
7598	0	7599	Qals	5.292	13			Qal	
7600	0	7601	Qals	2.422	13			Qal	
7601	0	7602	Qals	0.098	13			Qal	
7602	0	7603	Qals	0.044	13			Qal	
7603	0	7604	Qals	0.032	13			Qal	
7604	0	7605	Qals	0.394	13			Qal	
7605	0	7606	Qals	0.087	13			Qal	
7608	0	7609	Qals	0.293	13			Qal	
7609	0	7610	Qals	0.044	13			Qal	
7610	0	7611	Qals	0.034	13			Qal	
7611	0	7612	Qals	0.009	13			Qal	
7612	0	7613	Qals	0.079	13			Qal	
7613	0	7614	Qals	0.381	13			Qal	
7614	0	7615	Qals	0.032	13			Qal	
7615	0	7616	Qals	0.163	13			Qal	
7616	0	7617	Qals	0.285	13			Qal	
7617	0	7618	Qals	1.024	13			Qal	
7618	0	7619	Qals	0.582	13			Qal	
7620	0	7621	Qals	0.073	13			Qal	
7622	0	7623	Qals	0.033	13			Qal	
7623	0	7624	Qals	0.238	13			Qal	
7624	0	7625	Qals	0.140	13			Qal	
7625	0	7626	Qals	0.668	13			Qal	
7626	0	7627	Qals	0.555	13			Qal	
7627	0	7628	Qals	0.040	13			Qal	
7628	0	7629	Qals	0.251	13			Qal	
7629	0	7630	Qals	4.944	13			Qal	
7630	0	7631	Qals	0.144	13			Qal	
7631	0	7632	Qals	0.163	13			Qal	
7632	0	7633	Qals	1.508	13			Qal	
7634	0	7635	Qals	0.114	13			Qal	
7635	0	7636	Qals	0.030	13			Qal	
7636	0	7637	Qals	0.056	13			Qal	
7637	0	7638	Qals	0.006	13			Qal	
7638	0	7639	Qals	0.086	13			Qal	
7639	0	7640	Qals	1.659	13			Qal	
7640	0	7641	Qals	0.059	13			Qal	
7641	0	7642	Qals	0.285	13			Qal	
7642	0	7643	Qals	0.399	13			Qal	

GeoNexus

OBJECTID_1	Join_Count	TARGET_FID	Label	Shape_Area (sqkm)	ORIG_FID	Absolute_Age	Age_paleontology	Unit	Reference
7643	0	7644	Qals	0.055	13			Qal	
7644	0	7645	Qals	0.132	13			Qal	
7645	0	7646	Qals	0.032	13			Qal	
7646	0	7647	Qals	3.587	13			Qal	
7647	0	7648	Qals	0.162	13			Qal	
7648	0	7649	Qals	1.105	13			Qal	
7649	0	7650	Qals	0.522	13			Qal	
7650	0	7651	Qals	1.298	13			Qal	
7651	0	7652	Qals	0.065	13			Qal	
7652	0	7653	Qals	0.110	13			Qal	
7653	0	7654	Qals	1.918	13			Qal	
7654	0	7655	Qals	0.166	13			Qal	
7656	0	7657	Qals	0.139	13			Qal	
7657	0	7658	Qals	0.145	13			Qal	
7658	0	7659	Qals	0.022	13			Qal	
7659	0	7660	Qals	0.059	13			Qal	
7660	0	7661	Qals	0.348	13			Qal	
7661	0	7662	Qals	0.341	13			Qal	
7662	0	7663	Qals	0.023	13			Qal	
7664	0	7665	Qals	0.076	13			Qal	
7665	0	7666	Qals	0.005	13			Qal	
7667	0	7668	Qals	0.038	13			Qal	
7668	0	7669	Qals	0.026	13			Qal	
7670	0	7671	Qals	0.114	13			Qal	
7671	0	7672	Qals	0.008	13			Qal	
7672	0	7673	Qals	0.218	13			Qal	
7673	0	7674	Qals	0.018	13			Qal	
7674	0	7675	Qals	0.023	13			Qal	
7676	0	7677	Qals	0.015	13			Qal	
7679	0	7680	Qals	0.041	13			Qal	
7680	0	7681	Qals	1.394	13			Qal	
7681	0	7682	Qals	0.078	13			Qal	
7682	0	7683	Qals	0.318	13			Qal	
7683	0	7684	Qals	0.013	13			Qal	
7684	0	7685	Qals	0.335	13			Qal	
7685	0	7686	Qals	0.187	13			Qal	
7686	0	7687	Qals	0.030	13			Qal	
7687	0	7688	Qals	0.120	13			Qal	
7688	0	7689	Qals	0.028	13			Qal	

GeoNexus

OBJECTID_1	Join_Count	TARGET_FID	Label	Shape_Area (sqkm)	ORIG_FID	Absolute_Age	Age_paleontology	Unit	Reference
7689	0	7690	Qals	0.169	13			Qal	
7690	0	7691	Qals	0.054	13			Qal	
7691	0	7692	Qals	0.117	13			Qal	
7692	0	7693	Qals	0.532	13			Qal	
7693	0	7694	Qals	0.774	13			Qal	
7694	0	7695	Qals	0.095	13			Qal	
7695	0	7696	Qals	42.844	13			Qal	
7696	0	7697	Qals	0.077	13			Qal	
7697	0	7698	Qals	0.070	13			Qal	
7698	0	7699	Qals	0.750	13			Qal	
7699	0	7700	Qals	0.131	13			Qal	
7700	0	7701	Qals	0.280	13			Qal	
7701	0	7702	Qals	0.081	13			Qal	
7702	0	7703	Qals	0.101	13			Qal	
7703	0	7704	Qals	2.988	13			Qal	
7704	0	7705	Qals	0.425	13			Qal	
7705	0	7706	Qals	0.017	13			Qal	
7706	0	7707	Qals	0.270	13			Qal	
7707	0	7708	Qals	0.559	13			Qal	
7708	0	7709	Qals	0.027	13			Qal	
7710	0	7711	Qals	0.056	13			Qal	
7711	0	7712	Qals	0.427	13			Qal	
7712	0	7713	Qals	0.291	13			Qal	
7713	0	7714	Qals	0.245	13			Qal	
7714	0	7715	Qals	0.089	13			Qal	
7715	0	7716	Qals	0.053	13			Qal	
7716	0	7717	Qals	0.177	13			Qal	
7717	0	7718	Qals	0.058	13			Qal	
7718	0	7719	Qals	6.510	13			Qal	
7719	0	7720	Qals	0.233	13			Qal	
7720	0	7721	Qals	0.177	13			Qal	
7721	0	7722	Qals	0.197	13			Qal	
7722	0	7723	Qals	0.041	13			Qal	
7723	0	7724	Qals	0.094	13			Qal	
7724	0	7725	Qals	0.013	13			Qal	
7725	0	7726	Qals	0.051	13			Qal	
7726	0	7727	Qals	0.438	13			Qal	
7727	0	7728	Qals	0.717	13			Qal	
7728	0	7729	Qals	8.384	13			Qal	

GeoNexus

OBJECTID_1	Join_Count	TARGET_FID	Label	Shape_Area (sqkm)	ORIG_FID	Absolute_Age	Age_paleontology	Unit	Reference
7729	0	7730	Qals	0.029	13			Qal	
7730	0	7731	Qals	28.509	13			Qal	
7731	0	7732	Qals	0.088	13			Qal	
7732	0	7733	Qals	0.618	13			Qal	
7733	0	7734	Qals	0.358	13			Qal	
7735	0	7736	Qals	0.327	13			Qal	
7736	0	7737	Qals	0.061	13			Qal	
7737	0	7738	Qals	1.015	13			Qal	
7738	0	7739	Qals	0.118	13			Qal	
7739	0	7740	Qals	0.879	13			Qal	
7740	0	7741	Qals	0.692	13			Qal	
7741	0	7742	Qals	0.130	13			Qal	
7742	0	7743	Qals	0.142	13			Qal	
7743	0	7744	Qals	0.173	13			Qal	
7744	0	7745	Qals	0.028	13			Qal	
7745	0	7746	Qals	0.343	13			Qal	
7747	0	7748	Qals	0.283	13			Qal	
7748	0	7749	Qals	0.135	13			Qal	
7749	0	7750	Qals	0.024	13			Qal	
7750	0	7751	Qals	0.068	13			Qal	
7751	0	7752	Qals	1.602	13			Qal	
7752	0	7753	Qals	0.470	13			Qal	
7753	0	7754	Qals	0.952	13			Qal	
7754	0	7755	Qals	0.191	13			Qal	
7755	0	7756	Qals	0.094	13			Qal	
7756	0	7757	Qals	4.722	13			Qal	
7757	0	7758	Qals	0.156	13			Qal	
7758	0	7759	Qals	0.015	13			Qal	
7759	0	7760	Qals	0.074	13			Qal	
7760	0	7761	Qals	3.283	13			Qal	
7761	0	7762	Qals	0.047	13			Qal	
7762	0	7763	Qals	0.171	13			Qal	
7763	0	7764	Qals	0.241	13			Qal	
7764	0	7765	Qals	2.695	13			Qal	
7765	0	7766	Qals	0.177	13			Qal	
7766	0	7767	Qals	139.630	13			Qal	
7767	0	7768	Qals	0.010	13			Qal	
7768	0	7769	Qals	0.036	13			Qal	
7770	0	7771	Qals	0.019	13			Qal	

GeoNexus

OBJECTID_1	Join_Count	TARGET_FID	Label	Shape_Area (sqkm)	ORIG_FID	Absolute_Age	Age_paleontology	Unit	Reference
7771	0	7772	Qals	0.206	13			Qal	
7773	0	7774	Qals	0.183	13			Qal	
7774	0	7775	Qals	0.121	13			Qal	
7775	0	7776	Qals	0.208	13			Qal	
7776	0	7777	Qals	0.033	13			Qal	
7777	0	7778	Qals	0.022	13			Qal	
7778	0	7779	Qals	1.530	13			Qal	
7779	0	7780	Qals	0.150	13			Qal	
7780	0	7781	Qals	2.478	13			Qal	
7781	0	7782	Qals	0.463	13			Qal	
7782	0	7783	Qals	0.041	13			Qal	
7783	0	7784	Qals	7.657	13			Qal	
7784	0	7785	Qals	0.084	13			Qal	
7785	0	7786	Qals	0.034	13			Qal	
7786	0	7787	Qals	0.051	13			Qal	
7787	0	7788	Qals	0.028	13			Qal	
7788	0	7789	Qals	0.045	13			Qal	
7789	0	7790	Qals	0.137	13			Qal	
7790	0	7791	Qals	0.110	13			Qal	
7791	0	7792	Qals	0.038	13			Qal	
7792	0	7793	Qals	0.029	13			Qal	
7793	0	7794	Qals	0.031	13			Qal	
7794	0	7795	Qals	0.133	13			Qal	
7795	0	7796	Qals	0.026	13			Qal	
7796	0	7797	Qals	0.430	13			Qal	
7797	0	7798	Qals	0.279	13			Qal	
7798	0	7799	Qals	0.022	13			Qal	
7799	0	7800	Qals	0.017	13			Qal	
7800	0	7801	Qals	0.043	13			Qal	
7801	0	7802	Qals	0.543	13			Qal	
7802	0	7803	Qals	0.026	13			Qal	
7803	0	7804	Qals	0.024	13			Qal	
7804	0	7805	Qals	0.024	13			Qal	
7805	0	7806	Qals	0.237	13			Qal	
7806	0	7807	Qals	0.044	13			Qal	
7807	0	7808	Qals	0.031	13			Qal	
7808	0	7809	Qals	0.055	13			Qal	
7809	0	7810	Qals	0.089	13			Qal	
7810	0	7811	Qals	0.032	13			Qal	

GeoNexus

OBJECTID_1	Join_Count	TARGET_FID	Label	Shape_Area (sqkm)	ORIG_FID	Absolute_Age	Age_paleontology	Unit	Reference
7812	0	7813	Qals	0.118	13			Qal	
7813	0	7814	Qals	0.017	13			Qal	
7814	0	7815	Qals	2.594	13			Qal	
7815	0	7816	Qals	1.673	13			Qal	
7816	0	7817	Qals	0.037	13			Qal	
7817	0	7818	Qals	0.022	13			Qal	
7818	0	7819	Qals	0.061	13			Qal	
7819	0	7820	Qals	0.180	13			Qal	
7820	0	7821	Qals	0.028	13			Qal	
7821	0	7822	Qals	0.021	13			Qal	
7822	0	7823	Qals	0.007	13			Qal	
7823	0	7824	Qals	16.290	13			Qal	
7824	0	7825	Qals	0.080	13			Qal	
7825	0	7826	Qals	0.008	13			Qal	
7827	0	7828	Qals	0.266	13			Qal	
7828	0	7829	Qals	0.011	13			Qal	
7829	3	7830	Qalw	0.085	13			Qal	
7830	0	7831	Qals	0.020	13			Qal	
7831	0	7832	Qals	10.987	13			Qal	
7832	0	7833	Qals	0.131	13			Qal	
7833	0	7834	Qals	0.047	13			Qal	
7834	0	7835	Qals	0.004	13			Qal	
7835	0	7836	Qals	0.052	13			Qal	
7836	0	7837	Qals	0.079	13			Qal	
7837	0	7838	Qals	0.237	13			Qal	
7838	0	7839	Qals	0.021	13			Qal	
7839	0	7840	Qals	0.279	13			Qal	
7840	0	7841	Qals	0.032	13			Qal	
7841	0	7842	Qals	0.026	13			Qal	
7842	0	7843	Qals	0.035	13			Qal	
7843	0	7844	Qals	0.144	13			Qal	
7844	0	7845	Qals	0.064	13			Qal	
7845	0	7846	Qals	0.050	13			Qal	
7846	0	7847	Qals	0.059	13			Qal	
7847	0	7848	Qals	0.017	13			Qal	
7848	0	7849	Qals	0.056	13			Qal	
7849	0	7850	Qals	0.209	13			Qal	
7850	0	7851	Qals	0.027	13			Qal	
7852	0	7853	Qals	0.018	13			Qal	

GeoNexus

OBJECTID_1	Join_Count	TARGET_FID	Label	Shape_Area (sqkm)	ORIG_FID	Absolute_Age	Age_paleontology	Unit	Reference
7853	0	7854	Qals	0.767	13			Qal	
7854	0	7855	Qals	0.044	13			Qal	
7855	0	7856	Qals	0.017	13			Qal	
7856	0	7857	Qals	0.042	13			Qal	
7857	0	7858	Qals	0.013	13			Qal	
7858	0	7859	Qals	0.047	13			Qal	
7859	0	7860	Qals	0.027	13			Qal	
7860	0	7861	Qals	0.398	13			Qal	
7861	0	7862	Qals	0.704	13			Qal	
7862	0	7863	Qals	0.081	13			Qal	
7864	0	7865	Qals	0.029	13			Qal	
7865	0	7866	Qals	0.011	13			Qal	
7866	0	7867	Qals	0.117	13			Qal	
7867	0	7868	Qals	0.009	13			Qal	
7868	0	7869	Qals	0.007	13			Qal	
7869	0	7870	Qals	0.294	13			Qal	
7870	0	7871	Qals	0.012	13			Qal	
7871	0	7872	Qals	0.014	13			Qal	
7872	0	7873	Qals	0.036	13			Qal	
7873	0	7874	Qals	0.097	13			Qal	
7874	0	7875	Qals	0.072	13			Qal	
7875	0	7876	Qals	0.012	13			Qal	
7876	0	7877	Qals	0.033	13			Qal	
7877	0	7878	Qals	0.003	13			Qal	
7878	0	7879	Qals	4.658	13			Qal	
7879	0	7880	Qals	0.026	13			Qal	
7880	0	7881	Qals	0.108	13			Qal	
7881	0	7882	Qals	0.180	13			Qal	
7882	0	7883	Qals	0.040	13			Qal	
7883	0	7884	Qals	0.683	13			Qal	
7884	0	7885	Qals	0.105	13			Qal	
7885	0	7886	Qals	0.010	13			Qal	
7886	0	7887	Qals	0.036	13			Qal	
7887	0	7888	Qals	5.849	13			Qal	
7888	0	7889	Qals	0.321	13			Qal	
7889	0	7890	Qals	1.776	13			Qal	
7890	0	7891	Qals	0.037	13			Qal	
7891	0	7892	Qals	0.010	13			Qal	
7892	0	7893	Qals	0.029	13			Qal	

GeoNexus

OBJECTID_1	Join_Count	TARGET_FID	Label	Shape_Area (sqkm)	ORIG_FID	Absolute_Age	Age_paleontology	Unit	Reference
7893	1	7894	Qals	0.218	13			Qal	
7894	0	7895	Qals	0.013	13			Qal	
7895	0	7896	Qals	1.863	13			Qal	
7896	0	7897	Qals	0.010	13			Qal	
7897	0	7898	Qals	0.230	13			Qal	
7898	0	7899	Qals	0.106	13			Qal	
7899	0	7900	Qals	0.022	13			Qal	
7900	0	7901	Qals	1.203	13			Qal	
7902	0	7903	Qals	0.020	13			Qal	
7903	0	7904	Qals	0.024	13			Qal	
7904	0	7905	Qals	0.032	13			Qal	
7906	0	7907	Qals	0.284	13			Qal	
7907	0	7908	Qals	0.085	13			Qal	
7908	0	7909	Qals	0.063	13			Qal	
7909	0	7910	Qals	0.135	13			Qal	
7910	0	7911	Qals	0.024	13			Qal	
7911	0	7912	Qals	0.183	13			Qal	
7912	0	7913	Qals	0.017	13			Qal	
7913	0	7914	Qals	0.061	13			Qal	
7914	0	7915	Qals	0.066	13			Qal	
7915	0	7916	Qals	0.256	13			Qal	
7916	0	7917	Qals	0.192	13			Qal	
7917	0	7918	Qals	0.499	13			Qal	
7918	0	7919	Qals	0.024	13			Qal	
7919	0	7920	Qals	0.014	13			Qal	
7920	0	7921	Qals	0.084	13			Qal	
7921	0	7922	Qals	0.221	13			Qal	
7922	0	7923	Qals	0.012	13			Qal	
7923	0	7924	Qals	0.030	13			Qal	
7924	0	7925	Qals	0.036	13			Qal	
7925	0	7926	Qals	0.041	13			Qal	
7926	0	7927	Qals	0.134	13			Qal	
7927	0	7928	Qals	0.045	13			Qal	
7928	0	7929	Qals	0.373	13			Qal	
7929	0	7930	Qals	0.871	13			Qal	
7930	0	7931	Qals	0.021	13			Qal	
7931	0	7932	Qals	0.082	13			Qal	
7932	0	7933	Qals	0.241	13			Qal	
7933	0	7934	Qals	0.297	13			Qal	

GeoNexus

OBJECTID_1	Join_Count	TARGET_FID	Label	Shape_Area (sqkm)	ORIG_FID	Absolute_Age	Age_paleontology	Unit	Reference
7934	0	7935	Qals	1.022	13			Qal	
7935	0	7936	Qals	0.180	13			Qal	
7936	0	7937	Qals	0.173	13			Qal	
7938	0	7939	Qals	0.077	13			Qal	
7939	0	7940	Qals	0.039	13			Qal	
7940	0	7941	Qals	0.197	13			Qal	
7942	0	7943	Qals	0.189	13			Qal	
7943	0	7944	Qals	0.249	13			Qal	
7944	0	7945	Qals	0.321	13			Qal	
7946	0	7947	Qals	0.185	13			Qal	
7947	0	7948	Qals	0.055	13			Qal	
7948	0	7949	Qals	0.118	13			Qal	
7949	0	7950	Qals	0.749	13			Qal	
7950	0	7951	Qals	0.238	13			Qal	
7951	0	7952	Qals	0.299	13			Qal	
7952	0	7953	Qals	0.014	13			Qal	
7953	0	7954	Qals	0.128	13			Qal	
7954	0	7955	Qals	0.034	13			Qal	
7955	0	7956	Qals	0.066	13			Qal	
7956	0	7957	Qals	0.011	13			Qal	
7957	0	7958	Qals	0.033	13			Qal	
7958	0	7959	Qals	0.017	13			Qal	
7959	0	7960	Qals	0.254	13			Qal	
7960	0	7961	Qals	0.013	13			Qal	
7961	0	7962	Qals	0.363	13			Qal	
7962	0	7963	Qals	0.098	13			Qal	
7963	0	7964	Qals	2.999	13			Qal	
7964	0	7965	Qals	0.024	13			Qal	
7965	0	7966	Qals	0.070	13			Qal	
7966	0	7967	Qals	0.137	13			Qal	
7967	0	7968	Qals	0.038	13			Qal	
7968	0	7969	Qals	0.073	13			Qal	
7969	0	7970	Qals	0.028	13			Qal	
7971	0	7972	Qals	0.087	13			Qal	
7972	0	7973	Qals	0.033	13			Qal	
7973	0	7974	Qals	0.010	13			Qal	
7974	0	7975	Qals	0.028	13			Qal	
7975	0	7976	Qals	0.511	13			Qal	
7976	0	7977	Qals	0.388	13			Qal	

GeoNexus

OBJECTID_1	Join_Count	TARGET_FID	Label	Shape_Area (sqkm)	ORIG_FID	Absolute_Age	Age_paleontology	Unit	Reference
7977	0	7978	Qals	0.142	13			Qal	
7978	0	7979	Qals	0.016	13			Qal	
7979	0	7980	Qals	0.035	13			Qal	
7980	0	7981	Qals	0.231	13			Qal	
7981	0	7982	Qals	0.197	13			Qal	
7982	0	7983	Qals	0.045	13			Qal	
7983	0	7984	Qals	0.038	13			Qal	
7984	0	7985	Qals	0.785	13			Qal	
7985	0	7986	Qals	0.024	13			Qal	
7986	0	7987	Qals	0.208	13			Qal	
7987	0	7988	Qals	0.053	13			Qal	
7988	0	7989	Qals	0.610	13			Qal	
7989	0	7990	Qals	0.052	13			Qal	
7990	0	7991	Qals	0.027	13			Qal	
7991	0	7992	Qals	0.146	13			Qal	
7992	0	7993	Qals	28.304	13			Qal	
7993	0	7994	Qals	0.181	13			Qal	
7994	0	7995	Qals	0.029	13			Qal	
7995	0	7996	Qals	0.184	13			Qal	
7996	0	7997	Qals	0.194	13			Qal	
7997	0	7998	Qals	0.031	13			Qal	
7998	0	7999	Qals	0.078	13			Qal	
7999	0	8000	Qals	0.121	13			Qal	
8000	0	8001	Qals	0.380	13			Qal	
8001	0	8002	Qals	0.055	13			Qal	
8002	0	8003	Qals	0.067	13			Qal	
8003	0	8004	Qals	0.040	13			Qal	
8004	0	8005	Qals	7.785	13			Qal	
8005	0	8006	Qals	0.517	13			Qal	
8006	0	8007	Qals	1.490	13			Qal	
8007	0	8008	Qals	0.043	13			Qal	
8008	0	8009	Qals	0.061	13			Qal	
8009	0	8010	Qals	0.401	13			Qal	
8010	0	8011	Qals	0.189	13			Qal	
8011	0	8012	Qals	0.099	13			Qal	
8012	0	8013	Qals	0.106	13			Qal	
8013	0	8014	Qals	0.093	13			Qal	
8014	0	8015	Qals	0.031	13			Qal	
8015	0	8016	Qals	4.167	13			Qal	

GeoNexus

OBJECTID_1	Join_Count	TARGET_FID	Label	Shape_Area (sqkm)	ORIG_FID	Absolute_Age	Age_paleontology	Unit	Reference
8016	0	8017	Qals	0.187	13			Qal	
8017	0	8018	Qals	0.043	13			Qal	
8019	0	8020	Qals	0.547	13			Qal	
8020	0	8021	Qals	0.107	13			Qal	
8021	0	8022	Qals	0.165	13			Qal	
8022	0	8023	Qals	0.046	13			Qal	
8023	0	8024	Qals	0.438	13			Qal	
8024	0	8025	Qals	0.085	13			Qal	
8025	0	8026	Qals	0.254	13			Qal	
8026	0	8027	Qals	0.057	13			Qal	
8027	0	8028	Qals	0.009	13			Qal	
8028	0	8029	Qals	0.182	13			Qal	
8029	0	8030	Qals	0.137	13			Qal	
8030	0	8031	Qals	0.013	13			Qal	
8031	0	8032	Qals	0.198	13			Qal	
8032	0	8033	Qals	0.031	13			Qal	
8033	0	8034	Qals	0.087	13			Qal	
8034	0	8035	Qals	10.515	13			Qal	
8035	0	8036	Qals	1.157	13			Qal	
8036	0	8037	Qals	0.030	13			Qal	
8037	0	8038	Qals	0.322	13			Qal	
8038	0	8039	Qals	0.014	13			Qal	
8039	0	8040	Qals	0.045	13			Qal	
8040	0	8041	Qals	0.058	13			Qal	
8041	0	8042	Qals	0.017	13			Qal	
8042	0	8043	Qals	8.224	13			Qal	
8043	0	8044	Qals	0.341	13			Qal	
8044	0	8045	Qals	0.075	13			Qal	
8045	0	8046	Qals	0.269	13			Qal	
8046	0	8047	Qals	1.907	13			Qal	
8047	0	8048	Qals	3.574	13			Qal	
8048	0	8049	Qals	0.352	13			Qal	
8049	0	8050	Qals	0.473	13			Qal	
8050	0	8051	Qals	0.146	13			Qal	
8051	0	8052	Qals	0.482	13			Qal	
8052	0	8053	Qals	0.334	13			Qal	
8053	0	8054	Qals	0.011	13			Qal	
8054	0	8055	Qals	0.041	13			Qal	
8055	0	8056	Qals	1.147	13			Qal	

GeoNexus

OBJECTID_1	Join_Count	TARGET_FID	Label	Shape_Area (sqkm)	ORIG_FID	Absolute_Age	Age_paleontology	Unit	Reference
8056	0	8057	Qals	0.291	13			Qal	
8057	0	8058	Qals	0.038	13			Qal	
8058	0	8059	Qals	0.833	13			Qal	
8059	0	8060	Qals	0.166	13			Qal	
8060	0	8061	Qals	0.329	13			Qal	
8061	0	8062	Qals	0.331	13			Qal	
8062	0	8063	Qals	0.084	13			Qal	
8063	0	8064	Qals	0.345	13			Qal	
8064	0	8065	Qals	0.158	13			Qal	
8065	0	8066	Qals	0.043	13			Qal	
8066	0	8067	Qals	0.028	13			Qal	
8067	0	8068	Qals	0.002	13			Qal	
8068	0	8069	Qals	0.009	13			Qal	
8069	0	8070	Qals	0.007	13			Qal	
8070	0	8071	Qals	0.022	13			Qal	
8071	0	8072	Qals	0.057	13			Qal	
8072	0	8073	Qals	0.266	13			Qal	
8074	0	8075	Qals	1.807	13			Qal	
8075	0	8076	Qals	0.081	13			Qal	
8076	0	8077	Qals	0.153	13			Qal	
8077	0	8078	Qals	0.150	13			Qal	
8078	0	8079	Qals	0.071	13			Qal	
8079	0	8080	Qals	0.019	13			Qal	
8080	0	8081	Qals	0.119	13			Qal	
8081	0	8082	Qals	0.044	13			Qal	
8082	0	8083	Qals	0.084	13			Qal	
8083	0	8084	Qals	9.230	13			Qal	
8084	0	8085	Qals	0.103	13			Qal	
8085	0	8086	Qals	0.002	13			Qal	
8086	0	8087	Qals	0.025	13			Qal	
8087	0	8088	Qals	0.303	13			Qal	
8088	0	8089	Qals	0.007	13			Qal	
8089	0	8090	Qals	0.207	13			Qal	
8090	0	8091	Qals	0.702	13			Qal	
8091	0	8092	Qals	0.238	13			Qal	
8092	0	8093	Qals	0.429	13			Qal	
8093	0	8094	Qals	0.095	13			Qal	
8094	0	8095	Qals	0.580	13			Qal	
8095	0	8096	Qals	2.346	13			Qal	

GeoNexus

OBJECTID_1	Join_Count	TARGET_FID	Label	Shape_Area (sqkm)	ORIG_FID	Absolute_Age	Age_paleontology	Unit	Reference
8096	0	8097	Qals	0.009	13			Qal	
8097	0	8098	Qals	0.061	13			Qal	
8098	0	8099	Qals	0.079	13			Qal	
8099	0	8100	Qals	0.016	13			Qal	
8100	0	8101	Qals	0.186	13			Qal	
8101	0	8102	Qals	0.006	13			Qal	
8102	0	8103	Qals	0.929	13			Qal	
8103	0	8104	Qals	0.474	13			Qal	
8104	0	8105	Qals	0.265	13			Qal	
8105	0	8106	Qals	0.093	13			Qal	
8106	0	8107	Qals	0.723	13			Qal	
8107	0	8108	Qals	0.197	13			Qal	
8108	0	8109	Qals	0.171	13			Qal	
8109	0	8110	Qals	0.189	13			Qal	
8110	0	8111	Qals	1.305	13			Qal	
8111	0	8112	Qals	2.812	13			Qal	
8112	0	8113	Qals	0.043	13			Qal	
8113	0	8114	Qals	0.080	13			Qal	
8114	0	8115	Qals	0.218	13			Qal	
8115	0	8116	Qals	0.333	13			Qal	
8116	0	8117	Qalw	0.007	14			Qal	
8117	0	8118	Qalw	0.171	14			Qal	
8118	0	8119	Qalw	0.009	14			Qal	
8119	0	8120	Qalw	0.012	14			Qal	
8120	0	8121	Qalw	0.081	14			Qal	
8122	0	8123	Qalw	0.042	14			Qal	
8124	0	8125	Qalw	0.074	14			Qal	
8129	0	8130	Qalw	0.170	14			Qal	
8131	0	8132	Qalw	0.003	14			Qal	
8132	0	8133	Qalw	0.184	14			Qal	
8133	0	8134	Qalw	0.025	14			Qal	
8134	0	8135	Qalw	0.089	14			Qal	
8137	0	8138	Qalw	0.025	14			Qal	
8138	0	8139	Qalw	0.179	14			Qal	
8139	0	8140	Qalw	0.048	14			Qal	
8140	0	8141	Qalw	0.039	14			Qal	
8141	0	8142	Qalw	0.022	14			Qal	
8142	0	8143	Qalw	0.012	14			Qal	
8147	0	8148	Qalw	0.147	14			Qal	

GeoNexus

OBJECTID_1	Join_Count	TARGET_FID	Label	Shape_Area (sqkm)	ORIG_FID	Absolute_Age	Age_paleontology	Unit	Reference
8149	0	8150	Qalw	0.138	14			Qal	
8150	0	8151	Qalw	0.166	14			Qal	
8151	0	8152	Qalw	0.025	14			Qal	
8152	0	8153	Qalw	0.020	14			Qal	
8153	0	8154	Qalw	0.010	14			Qal	
8154	0	8155	Qalw	0.024	14			Qal	
8156	0	8157	Qalw	0.058	14			Qal	
8157	0	8158	Qalw	0.098	14			Qal	
8159	0	8160	Qalw	0.109	14			Qal	
8160	0	8161	Qalw	0.035	14			Qal	
8161	0	8162	Qalw	0.020	14			Qal	
8162	0	8163	Qalw	0.009	14			Qal	
8164	0	8165	Qalw	0.134	14			Qal	
8165	0	8166	Qalw	0.042	14			Qal	
8166	0	8167	Qalw	0.005	14			Qal	
8167	0	8168	Qalw	0.127	14			Qal	
8168	0	8169	Qalw	0.160	14			Qal	
8170	0	8171	Qalw	0.012	14			Qal	
8171	0	8172	Qalw	0.129	14			Qal	
8172	0	8173	Qalw	0.019	14			Qal	
8173	0	8174	Qalw	0.258	14			Qal	
8174	0	8175	Qalw	3.774	14			Qal	
8175	0	8176	Qalw	0.602	14			Qal	
8176	0	8177	Qalw	0.771	14			Qal	
8177	0	8178	Qalw	3.865	14			Qal	
8178	0	8179	Qalw	0.100	14			Qal	
8181	0	8182	Qalw	4.959	14			Qal	
8183	0	8184	Qalw	0.068	14			Qal	
8187	0	8188	Qalw	0.872	14			Qal	
8188	0	8189	Qalw	0.067	14			Qal	
8189	0	8190	Qalw	0.257	14			Qal	
8190	0	8191	Qalw	0.137	14			Qal	
8191	0	8192	Qalw	0.044	14			Qal	
8192	0	8193	Qalw	0.062	14			Qal	
8193	0	8194	Qalw	0.024	14			Qal	
8194	0	8195	Qalw	0.246	14			Qal	
8195	0	8196	Qalw	0.034	14			Qal	
8198	0	8199	Qalw	0.122	14			Qal	
8200	0	8201	Qalw	0.120	14			Qal	

GeoNexus

OBJECTID_1	Join_Count	TARGET_FID	Label	Shape_Area (sqkm)	ORIG_FID	Absolute_Age	Age_paleontology	Unit	Reference
8201	0	8202	Qalw	0.030	14			Qal	
8202	0	8203	Qalw	0.046	14			Qal	
8203	0	8204	Qalw	0.008	14			Qal	
8204	0	8205	Qalw	0.091	14			Qal	
8205	0	8206	Qalw	0.020	14			Qal	
8206	0	8207	Qalw	0.105	14			Qal	
8207	0	8208	Qalw	0.038	14			Qal	
8208	0	8209	Qalw	0.252	14			Qal	
8209	0	8210	Qalw	0.005	14			Qal	
8211	0	8212	Qalw	0.010	14			Qal	
8212	0	8213	Qalw	0.012	14			Qal	
8213	0	8214	Qalw	0.099	14			Qal	
8214	0	8215	Qalw	0.033	14			Qal	
8215	0	8216	Qalw	0.052	14			Qal	
8216	0	8217	Qalw	0.043	14			Qal	
8217	0	8218	Qalw	0.115	14			Qal	
8218	0	8219	Qalw	0.034	14			Qal	
8219	0	8220	Qalw	0.019	14			Qal	
8220	0	8221	Qalw	0.045	14			Qal	
8221	0	8222	Qalw	0.175	14			Qal	
8222	0	8223	Qalw	0.005	14			Qal	
8223	0	8224	Qalw	0.006	14			Qal	
8224	0	8225	Qalw	0.063	14			Qal	
8225	0	8226	Qalw	0.039	14			Qal	
8226	0	8227	Qalw	0.235	14			Qal	
8228	0	8229	Qalw	0.096	14			Qal	
8229	0	8230	Qalw	0.024	14			Qal	
8230	0	8231	Qalw	0.004	14			Qal	
8231	0	8232	Qalw	0.020	14			Qal	
8232	0	8233	Qalw	0.128	14			Qal	
8233	0	8234	Qalw	0.050	14			Qal	
8234	0	8235	Qalw	0.373	14			Qal	
8235	0	8236	Qalw	0.032	14			Qal	
8236	0	8237	Qalw	0.027	14			Qal	
8237	0	8238	Qalw	1.350	14			Qal	
8238	0	8239	Qalw	0.160	14			Qal	
8239	0	8240	Qalw	0.117	14			Qal	
8240	0	8241	Qalw	0.755	14			Qal	
8241	0	8242	Qalw	0.042	14			Qal	

GeoNexus

OBJECTID_1	Join_Count	TARGET_FID	Label	Shape_Area (sqkm)	ORIG_FID	Absolute_Age	Age_paleontology	Unit	Reference
8242	0	8243	Qalw	0.030	14			Qal	
8243	0	8244	Qalw	0.016	14			Qal	
8244	0	8245	Qalw	0.005	14			Qal	
8245	0	8246	Qalw	0.003	14			Qal	
8246	0	8247	Qalw	0.051	14			Qal	
8247	0	8248	Qalw	0.017	14			Qal	
8248	0	8249	Qalw	0.025	14			Qal	
8249	0	8250	Qalw	0.033	14			Qal	
8250	0	8251	Qalw	0.012	14			Qal	
8251	0	8252	Qalw	0.015	14			Qal	
8252	0	8253	Qalw	0.008	14			Qal	
8253	0	8254	Qalw	0.004	14			Qal	
8254	0	8255	Qalw	0.021	14			Qal	
8255	0	8256	Qalw	0.128	14			Qal	
8256	0	8257	Qalw	0.013	14			Qal	
8257	0	8258	Qalw	0.008	14			Qal	
8258	0	8259	Qalw	0.014	14			Qal	
8259	0	8260	Qalw	0.006	14			Qal	
8260	0	8261	Qalw	0.004	14			Qal	
8261	0	8262	Qalw	0.143	14			Qal	
8262	0	8263	Qalw	0.255	14			Qal	
8263	0	8264	Qalw	0.124	14			Qal	
8264	0	8265	Qalw	0.024	14			Qal	
8265	0	8266	Qalw	0.016	14			Qal	
8266	0	8267	Qalw	0.021	14			Qal	
8267	0	8268	Qalw	0.033	14			Qal	
8268	0	8269	Qalw	0.118	14			Qal	
8269	0	8270	Qalw	0.035	14			Qal	
8270	0	8271	Qalw	0.020	14			Qal	
8271	0	8272	Qalw	0.018	14			Qal	
8272	0	8273	Qalw	0.413	14			Qal	
8273	0	8274	Qalw	0.146	14			Qal	
8274	0	8275	Qalw	0.016	14			Qal	
8275	0	8276	Qalw	0.225	14			Qal	
8276	0	8277	Qalw	0.030	14			Qal	
8277	0	8278	Qalw	0.241	14			Qal	
8278	0	8279	Qalw	0.026	14			Qal	
8279	0	8280	Qalw	0.018	14			Qal	
8280	0	8281	Qalw	0.138	14			Qal	

GeoNexus

OBJECTID_1	Join_Count	TARGET_FID	Label	Shape_Area (sqkm)	ORIG_FID	Absolute_Age	Age_paleontology	Unit	Reference
8281	0	8282	Qalw	0.029	14			Qal	
8282	0	8283	Qalw	0.264	14			Qal	
8283	0	8284	Qalw	0.023	14			Qal	
8284	0	8285	Qalw	0.034	14			Qal	
8285	0	8286	Qalw	0.005	14			Qal	
8286	0	8287	Qalw	0.020	14			Qal	
8287	0	8288	Qalw	0.075	14			Qal	
8288	0	8289	Qalw	0.049	14			Qal	
8289	0	8290	Qalw	0.006	14			Qal	
8290	0	8291	Qalw	0.150	14			Qal	
8291	0	8292	Qalw	0.015	14			Qal	
8292	0	8293	Qalw	0.020	14			Qal	
8293	0	8294	Qalw	0.106	14			Qal	
8294	0	8295	Qalw	0.052	14			Qal	
8295	0	8296	Qalw	0.351	14			Qal	
8296	0	8297	Qalw	0.044	14			Qal	
8297	0	8298	Qalw	0.013	14			Qal	
8299	0	8300	Qalw	0.011	14			Qal	
8301	0	8302	Qalw	0.079	14			Qal	
8302	0	8303	Qalw	0.108	14			Qal	
8303	0	8304	Qalw	0.560	14			Qal	
8304	0	8305	Qalw	0.005	14			Qal	
8305	0	8306	Qalw	0.057	14			Qal	
8306	0	8307	Qalw	0.003	14			Qal	
8307	0	8308	Qalw	0.020	14			Qal	
8309	0	8310	Qalw	0.031	14			Qal	
8310	0	8311	Qalw	0.015	14			Qal	
8312	0	8313	Qalw	0.044	14			Qal	
8313	0	8314	Qalw	0.032	14			Qal	
8315	0	8316	Qalw	0.013	14			Qal	
8316	0	8317	Qalw	0.014	14			Qal	
8317	0	8318	Qalw	0.005	14			Qal	
8318	0	8319	Qalw	0.062	14			Qal	
8319	0	8320	Qalw	0.089	14			Qal	
8323	0	8324	Qalw	0.160	14			Qal	
8324	0	8325	Qalw	0.011	14			Qal	
8325	0	8326	Qalw	0.355	14			Qal	
8326	0	8327	Qalw	0.078	14			Qal	
8327	0	8328	Qalw	0.068	14			Qal	

GeoNexus

OBJECTID_1	Join_Count	TARGET_FID	Label	Shape_Area (sqkm)	ORIG_FID	Absolute_Age	Age_paleontology	Unit	Reference
8328	0	8329	Qalw	0.165	14			Qal	
8329	0	8330	Qalw	0.075	14			Qal	
8330	0	8331	Qalw	0.154	14			Qal	
8331	0	8332	Qalw	0.107	14			Qal	
8332	0	8333	Qalw	0.040	14			Qal	
8333	0	8334	Qalw	0.124	14			Qal	
8334	0	8335	Qalw	0.045	14			Qal	
8335	0	8336	Qalw	1.568	14			Qal	
8336	0	8337	Qalw	0.046	14			Qal	
8337	0	8338	Qalw	1.535	14			Qal	
8338	0	8339	Qalw	0.644	14			Qal	
8340	0	8341	Qalw	0.544	14			Qal	
8341	0	8342	Qalw	3.051	14			Qal	
8342	0	8343	Qalw	0.125	14			Qal	
8344	0	8345	Qalw	1.423	14			Qal	
8345	0	8346	Qalw	1.353	14			Qal	
8347	0	8348	Qalw	0.436	14			Qal	
8348	0	8349	Qalw	0.142	14			Qal	
8349	0	8350	Qalw	0.104	14			Qal	
8351	0	8352	Qalw	0.021	14			Qal	
8352	0	8353	Qalw	0.140	14			Qal	
8354	0	8355	Qalw	0.479	14			Qal	
8355	0	8356	Qalw	0.117	14			Qal	
8356	0	8357	Qalw	0.035	14			Qal	
8357	0	8358	Qalw	0.021	14			Qal	
8358	0	8359	Qalw	0.257	14			Qal	
8359	0	8360	Qalw	0.065	14			Qal	
8361	0	8362	Qalw	0.015	14			Qal	
8363	0	8364	Qalw	0.363	14			Qal	
8364	0	8365	Qalw	0.043	14			Qal	
8365	0	8366	Qalw	0.061	14			Qal	
8366	0	8367	Qalw	0.043	14			Qal	
8367	0	8368	Qalw	0.071	14			Qal	
8368	0	8369	Qalw	0.057	14			Qal	
8369	0	8370	Qalw	0.725	14			Qal	
8370	0	8371	Qalw	0.091	14			Qal	
8371	0	8372	Qalw	0.030	14			Qal	
8372	0	8373	Qalw	0.178	14			Qal	
8373	0	8374	Qalw	0.356	14			Qal	

GeoNexus

OBJECTID_1	Join_Count	TARGET_FID	Label	Shape_Area (sqkm)	ORIG_FID	Absolute_Age	Age_paleontology	Unit	Reference
8374	0	8375	Qalw	0.123	14			Qal	
8375	0	8376	Qalw	0.236	14			Qal	
8376	0	8377	Qalw	0.257	14			Qal	
8377	0	8378	Qalw	0.308	14			Qal	
8378	0	8379	Qalw	0.050	14			Qal	
8379	0	8380	Qalw	0.078	14			Qal	
8380	0	8381	Qalw	0.005	14			Qal	
8381	0	8382	Qalw	2.214	14			Qal	
8382	0	8383	Qalw	0.366	14			Qal	
8383	0	8384	Qalw	1.080	14			Qal	
8384	0	8385	Qalw	0.064	14			Qal	
8385	0	8386	Qalw	0.035	14			Qal	
8386	0	8387	Qalw	0.041	14			Qal	
8387	0	8388	Qalw	0.272	14			Qal	
8389	0	8390	Qalw	0.297	14			Qal	
8390	0	8391	Qalw	0.534	14			Qal	
8391	0	8392	Qalw	0.020	14			Qal	
8393	0	8394	Qalw	0.490	14			Qal	
8394	0	8395	Qalw	0.013	14			Qal	
8395	0	8396	Qalw	0.394	14			Qal	
8396	0	8397	Qalw	0.075	14			Qal	
8398	0	8399	Qalw	0.070	14			Qal	
8399	0	8400	Qalw	0.182	14			Qal	
8400	0	8401	Qalw	0.270	14			Qal	
8401	0	8402	Qalw	1.359	14			Qal	
8402	0	8403	Qalw	0.056	14			Qal	
8403	0	8404	Qalw	0.667	14			Qal	
8404	0	8405	Qalw	0.155	14			Qal	
8405	0	8406	Qalw	0.027	14			Qal	
8406	0	8407	Qalw	0.089	14			Qal	
8407	0	8408	Qalw	0.027	14			Qal	
8408	0	8409	Qalw	0.123	14			Qal	
8409	0	8410	Qalw	0.109	14			Qal	
8410	0	8411	Qalw	0.127	14			Qal	
8411	0	8412	Qalw	3.147	14			Qal	
8412	0	8413	Qalw	0.101	14			Qal	
8413	0	8414	Qalw	0.108	14			Qal	
8414	0	8415	Qalw	0.075	14			Qal	
8415	0	8416	Qalw	0.210	14			Qal	

GeoNexus

OBJECTID_1	Join_Count	TARGET_FID	Label	Shape_Area (sqkm)	ORIG_FID	Absolute_Age	Age_paleontology	Unit	Reference
8416	0	8417	Qalw	0.112	14			Qal	
8417	0	8418	Qalw	0.174	14			Qal	
8418	0	8419	Qalw	0.142	14			Qal	
8419	0	8420	Qalw	0.027	14			Qal	
8420	0	8421	Qalw	0.078	14			Qal	
8421	0	8422	Qalw	0.105	14			Qal	
8422	0	8423	Qalw	0.181	14			Qal	
8423	0	8424	Qalw	0.261	14			Qal	
8424	0	8425	Qalw	0.439	14			Qal	
8425	0	8426	Qalw	2.635	14			Qal	
8426	0	8427	Qalw	0.059	14			Qal	
8428	0	8429	Qalw	0.066	14			Qal	
8429	0	8430	Qalw	0.270	14			Qal	
8430	0	8431	Qalw	0.093	14			Qal	
8431	0	8432	Qalw	0.931	14			Qal	
10449	0	8361	Qalw	0.021	14			Qal	
10483	0	7838	Qals	0.320	13			Qal	
10533	0	7767	Qals	0.000	13			Qal	

GeoNexus

Table S17. Summary of the mapped faults in the SUTGMM project. Mec.:Mechanism; Sin.: Sinuosity.

Fault	Mec.	Length (km)	Strike (°)	START_X (° E)	START_Y (° N)	END_X (° E)	END_Y (° N)	Sin.
F001	N	43.85	274.6	60.593	25.741	60.163	25.772	1.01
F002	R	22.87	83.0	60.203	25.706	60.427	25.730	1.01
F003	R	15.09	276.9	60.665	25.717	60.516	25.734	1.00
F004	R	16.62	100.1	60.624	25.729	60.785	25.703	1.01
F005	LLR	7.84	100.1	60.523	25.708	60.600	25.696	1.00
F006	R	8.57	99.1	60.313	25.815	60.396	25.803	1.02
F006	R	4.13	92.3	60.271	25.817	60.311	25.815	1.01
F007	R	10.46	97.8	60.601	25.768	60.703	25.755	1.01
F008	R	11.08	78.4	60.125	25.846	60.232	25.866	1.01
F009	RLL	8.83	79.1	60.134	25.863	60.219	25.877	1.01
F010	LLR	11.34	81.2	60.126	25.879	60.237	25.895	1.01
F012	R	15.82	287.1	60.368	25.810	60.222	25.851	1.03
F013	NRL	13.16	118.3	60.222	25.885	60.333	25.831	1.04
F014	RRL	15.05	106.6	60.239	25.892	60.380	25.854	1.02
F015	N	9.23	109.7	60.334	25.853	60.420	25.825	1.01
F016	RRL	5.24	295.7	60.304	25.752	60.259	25.771	1.04
F017	RRL	0.98	181.4	60.272	25.766	60.272	25.757	1.01
F018	RLL	15.57	101.4	60.141	25.629	60.289	25.602	1.02
F019	R	9.00	92.5	60.354	25.585	60.443	25.581	1.01
F020	LLR	8.23	239.2	60.446	25.582	60.378	25.545	1.03
F020	LLR	3.71	51.5	60.446	25.582	60.474	25.602	1.03
F021	RL	21.94	124.3	60.121	25.708	60.298	25.598	1.02
F022	RL	14.40	128.7	60.342	25.565	60.452	25.485	1.01
F023	RRL	14.25	137.4	60.146	25.579	60.240	25.486	1.02
F023	RL	12.40	144.8	60.260	25.452	60.330	25.362	1.01
F023	RL	3.26	143.9	60.239	25.480	60.258	25.457	1.01
F024	LL	11.32	28.4	60.134	25.419	60.187	25.508	1.01
F025	LL	7.00	45.6	60.180	25.421	60.229	25.465	1.01
F026	LL	8.17	224.0	60.340	25.545	60.284	25.492	1.01
F027	LL	14.37	81.7	60.605	25.467	60.745	25.486	1.01
F028	LL	6.50	104.2	60.121	25.652	60.183	25.638	1.01
F029	RL	5.63	128.5	60.455	25.662	60.498	25.631	1.02
F029	RL	7.31	125.2	60.391	25.702	60.449	25.665	1.01
F030	RL	9.09	167.5	60.635	25.650	60.654	25.571	1.02
F032	R	15.18	105.8	60.609	25.522	60.750	25.486	1.03
F033	N	4.96	290.0	60.700	25.501	60.655	25.516	1.02
F034	N	4.95	274.5	60.664	25.524	60.616	25.527	1.01
F035	N	8.49	281.6	60.735	25.502	60.659	25.516	1.09
F036	N	12.57	281.5	60.748	25.526	60.628	25.548	1.02
F037	N	6.44	261.9	60.675	25.540	60.613	25.532	1.01
F038	N	4.65	266.9	60.684	25.551	60.638	25.549	1.01
F039	R	13.76	112.9	60.520	25.618	60.642	25.571	1.03
F040	R	6.89	105.5	60.490	25.618	60.555	25.601	1.01
F041	R	15.00	103.1	60.503	25.628	60.645	25.598	1.03
F042	N	8.84	295.8	60.262	25.663	60.184	25.697	1.01
F043	R	6.13	100.9	60.199	25.696	60.258	25.686	1.00
F043	R	3.98	85.8	60.263	25.685	60.302	25.688	1.01
F044	N	9.59	286.4	60.402	25.632	60.312	25.656	1.02
F045	N	2.06	277.4	60.253	25.653	60.232	25.655	1.00
F045	N	3.41	285.9	60.229	25.656	60.196	25.665	1.00
F046	R	12.91	104.2	60.119	25.744	60.242	25.716	1.01
F047	LL	10.51	99.5	60.313	25.695	60.415	25.679	1.01
F048	RLL	5.94	102.7	60.360	25.668	60.417	25.656	1.00
F048	NLL	1.57	108.2	60.420	25.656	60.435	25.652	1.00
F049	RL	4.59	107.4	60.694	25.587	60.737	25.575	1.00
F049	RL	2.70	120.3	60.613	25.620	60.636	25.608	1.00

GeoNexus

Fault	Mec.	Length (km)	Strike (°)	START_X (° E)	START_Y (° N)	END_X (° E)	END_Y (° N)	Sin.
F049	RL	2.82	116.9	60.524	25.659	60.549	25.647	1.00
F049	RL	4.02	121.7	60.555	25.645	60.589	25.626	1.00
F049	RL	3.95	109.7	60.647	25.603	60.684	25.591	1.00
F050	RL	4.88	126.2	60.532	25.655	60.571	25.629	1.00
F051	RL	7.78	140.7	60.678	25.599	60.726	25.546	1.02
F052	RL	4.85	126.7	60.288	25.671	60.326	25.645	1.01
F053	RL	3.60	115.7	60.191	25.680	60.223	25.666	1.00
F054	RL	2.28	119.7	60.202	25.671	60.222	25.661	1.00
F055	RL	4.78	112.5	60.593	25.590	60.637	25.574	1.00
F056	RL	3.74	112.5	60.614	25.591	60.649	25.578	1.00
F057	LL	4.26	99.1	60.464	25.630	60.506	25.623	1.00
F058	LLR	3.76	72.2	60.476	25.613	60.511	25.623	1.03
F059	RL	4.49	130.4	60.507	25.641	60.541	25.615	1.01
F060	LL	3.67	60.1	60.548	25.519	60.580	25.536	1.00
F060	LL	3.15	70.3	60.574	25.534	60.603	25.544	1.01
F061	LL	2.77	58.2	60.562	25.533	60.585	25.546	1.00
F062	N	4.32	112.9	60.678	25.315	60.717	25.300	1.01
F062	N	5.87	109.5	60.722	25.298	60.777	25.280	1.00
F063	NLL	3.25	274.6	60.792	25.274	60.761	25.277	1.01
F064	NLL	1.57	276.7	60.769	25.278	60.754	25.280	1.00
F065	NLL	6.12	95.0	60.644	25.321	60.704	25.316	1.00
F066	NLL	9.83	106.1	60.611	25.342	60.703	25.318	1.03
F067	N	9.61	300.3	60.718	25.314	60.638	25.357	1.02
F068	NLL	7.79	118.2	60.607	25.354	60.675	25.321	1.01
F069	NLL	2.09	276.9	60.646	25.330	60.626	25.332	1.00
F070	LL	0.39	86.2	60.621	25.342	60.625	25.342	1.00
F071	NLL	0.65	111.4	60.598	25.347	60.604	25.345	1.00
F072	NLL	1.31	276.2	60.622	25.344	60.609	25.345	1.00
F073	NLL	3.64	275.6	60.655	25.344	60.619	25.347	1.00
F074	NLL	4.84	114.5	60.658	25.345	60.701	25.327	1.01
F075	NLL	2.62	292.6	60.736	25.316	60.712	25.325	1.00
F076	NLL	2.68	74.7	60.722	25.312	60.747	25.319	1.00
F077	NLL	6.16	110.6	60.639	25.365	60.696	25.345	1.01
F078	NLL	3.15	307.8	60.693	25.335	60.668	25.352	1.02
F079	NLL	4.03	100.4	60.697	25.348	60.736	25.341	1.01
F080	NLL	3.41	98.0	60.662	25.356	60.696	25.352	1.01
F081	NLL	10.17	99.2	60.650	25.368	60.750	25.353	1.00
F082	NLL	1.49	264.7	60.639	25.355	60.625	25.354	1.02
F083	LL	0.48	91.7	60.614	25.361	60.619	25.361	1.00
F084	NLL	0.99	259.9	60.634	25.364	60.625	25.362	1.00
F085	NLL	2.31	100.2	60.648	25.389	60.671	25.385	1.00
F086	NLL	4.58	97.1	60.676	25.386	60.721	25.381	1.00
F087	NLL	2.44	88.6	60.657	25.395	60.681	25.396	1.00
F088	LLN	0.37	190.3	60.608	25.359	60.607	25.356	1.00
F089	NLL	0.44	208.7	60.615	25.366	60.613	25.362	1.00
F090	NLL	0.75	195.7	60.629	25.377	60.627	25.371	1.00
F091	NLL	0.45	207.5	60.628	25.376	60.626	25.373	1.00
F092	NLL	2.77	278.8	60.445	25.317	60.418	25.321	1.00
F093	NLL	3.68	275.6	60.336	25.345	60.300	25.349	1.00
F094	NLL	3.91	281.3	60.380	25.338	60.342	25.345	1.01
F095	NLL	3.40	273.9	60.354	25.334	60.321	25.336	1.00
F096	RLL	5.74	277.5	60.447	25.323	60.391	25.329	1.01
F097	RLL	0.89	274.2	60.394	25.335	60.385	25.336	1.00
F098	NLL	4.17	96.2	60.403	25.333	60.445	25.329	1.00
F099	NLL	0.51	273.7	60.409	25.337	60.404	25.337	1.00
F100	RL	0.71	174.8	60.697	25.561	60.698	25.555	1.00
F101	RL	0.68	176.2	60.703	25.560	60.703	25.554	1.00
F102	RL	1.08	178.8	60.706	25.564	60.706	25.554	1.00

GeoNexus

Fault	**Mec.**	**Length** (km)	**Strike** (°)	**START_X** (° E)	**START_Y** (° N)	**END_X** (° E)	**END_Y** (° N)	**Sin.**
F103	RL	1.57	162.8	60.708	25.565	60.713	25.551	1.00
F104	RL	2.01	164.8	60.718	25.548	60.723	25.531	1.03
F105	RL	1.75	176.1	60.706	25.551	60.707	25.536	1.01
F106	RL	1.44	150.1	60.700	25.553	60.707	25.542	1.04
F107	RL	5.77	174.2	60.709	25.637	60.714	25.586	1.01
F108	RL	4.02	179.5	60.718	25.631	60.718	25.595	1.01
F109	LL	3.43	96.8	60.615	25.655	60.648	25.651	1.00
F110	LL	3.35	92.2	60.642	25.649	60.675	25.648	1.00
F111	LL	3.54	100.5	60.391	25.637	60.426	25.631	1.00
F112	LL	0.26	75.1	60.463	25.604	60.465	25.605	1.02
F113	LL	1.36	93.6	60.452	25.606	60.465	25.605	1.03
F114	LL	0.72	94.2	60.458	25.605	60.465	25.604	1.01
F115	LLN	0.13	112.0	60.466	25.605	60.467	25.605	1.02
F116	LLN	0.06	119.8	60.465	25.605	60.466	25.605	1.01
F117	LLN	0.01	102.3	60.466	25.605	60.466	25.605	1.00
F118	LLN	0.04	282.3	60.466	25.605	60.465	25.605	1.02
F119	LLR	1.68	314.3	60.442	25.641	60.430	25.651	1.02
F120	N	2.32	284.4	60.351	25.665	60.329	25.671	1.00
F121	N	0.13	32.7	60.466	25.605	60.466	25.606	1.02
F122	NLL	5.63	106.3	60.367	25.674	60.420	25.660	1.02
F123	NRL	0.78	267.4	60.411	25.678	60.403	25.678	1.04
F124	NRL	1.48	148.2	60.410	25.680	60.417	25.669	1.03
F125	RL	1.40	134.9	60.315	25.682	60.325	25.673	1.02
F126	RL	3.19	133.1	60.350	25.660	60.374	25.641	1.00
F127	RL	2.81	111.9	60.492	25.665	60.518	25.656	1.00
F128	RL	0.71	115.6	60.481	25.669	60.488	25.666	1.00
F129	RL	1.02	98.5	60.487	25.645	60.497	25.643	1.00
F130	R	4.09	102.4	60.120	25.715	60.160	25.707	1.00
F131	N	4.06	299.9	60.219	25.682	60.184	25.700	1.00
F132	N	1.99	274.2	60.288	25.661	60.268	25.663	1.00
F133	N	2.90	275.1	60.187	25.722	60.158	25.724	1.00
F134	NRL	1.13	114.8	60.127	25.633	60.137	25.629	1.00
F135	R	5.18	92.8	60.322	25.751	60.370	25.749	1.08
F136	R	2.19	89.3	60.337	25.749	60.357	25.749	1.08
F137	RL	3.38	115.5	60.246	25.713	60.276	25.700	1.02
F138	RL	1.66	138.7	60.137	25.628	60.148	25.616	1.00
F139	RLN	0.86	307.8	60.266	25.772	60.259	25.777	1.00
F140	LL	2.70	88.6	60.214	25.855	60.241	25.856	1.00
F141	LL	2.04	97.1	60.120	25.839	60.140	25.836	1.00
F142	R	2.98	106.1	60.177	25.867	60.205	25.859	1.00
F143	RLL	1.62	200.3	60.198	25.887	60.192	25.874	1.00
F144	LL	1.68	51.9	60.147	25.918	60.160	25.928	1.01
F145	LLR	8.54	241.7	60.187	25.938	60.115	25.904	1.06
F146	N	6.75	259.2	60.199	25.913	60.134	25.902	1.01
F147	N	9.64	90.8	60.191	25.940	60.282	25.939	1.05
F149	R	7.09	309.6	60.452	25.826	60.400	25.865	1.04
F150	LL	2.31	89.9	60.609	25.779	60.632	25.779	1.00
F151	LL	2.08	77.5	60.603	25.780	60.623	25.784	1.00
F152	LL	1.90	79.9	60.618	25.781	60.636	25.784	1.01
F153	LL	1.94	42.9	60.221	25.961	60.234	25.974	1.00
F154	R	6.81	99.6	60.148	25.972	60.214	25.962	1.01
F155	R	1.64	279.9	60.127	25.981	60.111	25.983	1.00
F156	R	5.61	279.8	60.306	25.939	60.256	25.947	1.10
F157	R	5.09	283.5	60.372	25.926	60.325	25.937	1.05
F158	RL	6.65	109.5	60.245	25.960	60.307	25.940	1.00
F159	NRL	6.56	163.2	60.361	25.961	60.379	25.906	1.03
F160	RL	18.54	305.3	60.563	25.838	60.413	25.933	1.01
F161	LL	4.01	90.0	60.498	25.883	60.538	25.883	1.01

GeoNexus

Fault	Mec.	Length (km)	Strike (°)	START_X (° E)	START_Y (° N)	END_X (° E)	END_Y (° N)	Sin.
F162	RRL	9.68	124.4	60.536	25.887	60.614	25.838	1.01
F163	LL	6.27	89.1	60.461	25.895	60.523	25.895	1.01
F164	RRL	4.79	106.8	60.558	25.878	60.603	25.866	1.02
F165	RRL	27.02	112.2	60.630	25.841	60.874	25.750	1.02
F166	R	7.23	84.6	60.624	25.874	60.695	25.880	1.01
F166	R	1.12	81.8	60.702	25.879	60.713	25.880	1.01
F167	R	1.86	80.5	60.731	25.882	60.749	25.884	1.03
F168	LL	4.76	90.5	60.554	25.878	60.602	25.878	1.01
F169	LL	1.05	78.4	60.622	25.879	60.632	25.880	1.01
F170	LL	3.55	83.5	60.613	25.880	60.648	25.883	1.02
F171	LL	1.45	91.2	60.588	25.884	60.602	25.884	1.00
F172	NLL	1.66	213.6	60.671	25.839	60.662	25.827	1.02
F172	NLL	0.76	223.5	60.677	25.845	60.672	25.840	1.01
F173	LL	3.60	90.0	60.705	25.900	60.740	25.900	1.01
F173	LL	1.78	94.4	60.686	25.901	60.704	25.900	1.01
F173	LL	2.04	89.0	60.663	25.901	60.684	25.901	1.01
F173	LL	1.76	92.1	60.647	25.901	60.664	25.900	1.01
F173	LL	2.25	98.3	60.622	25.901	60.644	25.898	1.04
F173	LL	2.31	88.8	60.644	25.898	60.666	25.899	1.02
F174	LL	2.17	85.7	60.620	25.901	60.642	25.902	1.01
F175	RL	5.24	124.2	60.563	25.918	60.605	25.891	1.01
F176	RL	2.71	118.3	60.577	25.905	60.601	25.894	1.02
F177	LL	0.41	19.5	60.600	25.899	60.601	25.902	1.00
F178	LL	0.14	226.5	60.612	25.899	60.611	25.898	1.00
F179	N	0.36	203.7	60.614	25.899	60.612	25.896	1.01
F180	N	0.40	156.7	60.605	25.895	60.606	25.891	1.01
F181	NLL	0.38	87.5	60.604	25.895	60.607	25.895	1.00
F182	LL	2.36	72.4	60.544	25.906	60.566	25.913	1.01
F183	R	3.87	88.1	60.545	25.901	60.580	25.902	1.08
F184	RL	2.19	303.6	60.560	25.916	60.542	25.927	1.02
F185	RL	2.78	301.8	60.552	25.919	60.529	25.932	1.02
F186	RL	2.46	300.0	60.537	25.929	60.517	25.940	1.02
F187	LLR	2.19	77.1	60.617	25.904	60.638	25.908	1.02
F188	LL	1.56	75.1	60.641	25.908	60.655	25.912	1.02
F189	LL	5.42	234.8	60.538	25.926	60.495	25.898	1.01
F190	LL	3.16	53.9	60.500	25.918	60.525	25.935	1.02
F190	LL	0.59	42.2	60.526	25.937	60.530	25.941	1.02
F191	R	2.97	44.9	60.498	25.921	60.517	25.938	1.11
F192	R	1.74	80.7	60.481	25.916	60.498	25.919	1.01
F193	R	4.15	82.0	60.443	25.914	60.484	25.919	1.01
F194	R	1.88	52.5	60.498	25.923	60.512	25.933	1.05
F195	R	2.86	111.1	60.434	25.925	60.460	25.916	1.03
F196	R	5.94	117.2	60.407	25.942	60.459	25.918	1.02
F197	R	3.52	258.6	60.495	25.923	60.461	25.917	1.01
F198	LL	1.17	48.3	60.502	25.926	60.511	25.933	1.03
F199	LL	3.54	77.2	60.539	25.931	60.573	25.938	1.02
F200	LL	1.15	75.9	60.577	25.938	60.588	25.941	1.02
F201	LL	1.13	252.7	60.573	25.942	60.562	25.939	1.01
F202	LL	0.76	71.1	60.575	25.942	60.582	25.945	1.03
F203	LL	5.16	94.1	60.400	25.944	60.450	25.941	1.01
F204	LL	3.28	97.0	60.494	25.948	60.526	25.944	1.02
F204	LL	3.56	90.9	60.528	25.944	60.563	25.944	1.01
F204	LL	7.78	272.9	60.489	25.948	60.412	25.951	1.01
F204	LL	2.51	93.6	60.389	25.951	60.414	25.950	1.01
F205	LL	0.60	89.9	60.494	25.952	60.500	25.953	1.01
F205	LL	5.96	91.4	60.434	25.956	60.493	25.954	1.01
F206	LL	9.10	90.3	60.338	25.967	60.428	25.966	1.01
F207	R	8.47	90.5	60.252	25.969	60.335	25.968	1.02

GeoNexus

Fault	**Mec.**	**Length** (km)	**Strike** (°)	**START_X** (° E)	**START_Y** (° N)	**END_X** (° E)	**END_Y** (° N)	**Sin.**
F208	LL	9.87	101.9	60.331	25.998	60.425	25.980	1.03
F209	RRL	3.44	142.1	60.330	25.997	60.351	25.973	1.03
F210	LLR	5.55	93.6	60.413	25.991	60.468	25.987	1.01
F211	RL	3.16	127.5	60.430	25.974	60.454	25.958	1.03
F212	LL	2.30	55.6	60.452	25.965	60.471	25.976	1.01
F213	LLN	5.04	80.2	60.472	25.978	60.520	25.985	1.02
F214	LLN	6.61	73.7	60.455	25.961	60.513	25.976	1.08
F215	LL	4.21	266.4	60.507	25.969	60.466	25.966	1.02
F216	LLN	2.81	218.9	60.524	25.988	60.507	25.969	1.03
F217	LLN	4.21	82.8	60.518	25.978	60.559	25.982	1.02
F218	LL	1.51	94.7	60.563	25.983	60.578	25.982	1.00
F219	LL	1.00	83.5	60.582	25.984	60.592	25.985	1.01
F220	R	3.52	130.5	60.505	25.966	60.530	25.946	1.05
F221	LL	0.98	59.3	60.624	25.911	60.633	25.915	1.01
F222	LLN	0.13	268.5	60.620	25.909	60.619	25.909	1.02
F223	LLR	1.75	53.8	60.609	25.903	60.622	25.912	1.05
F224	N	0.13	211.8	60.624	25.912	60.624	25.911	1.00
F225	N	2.38	223.4	60.720	25.915	60.705	25.901	1.07
F226	LL	4.62	91.5	60.645	25.930	60.690	25.929	1.02
F227	LL	2.03	92.4	60.686	25.927	60.706	25.926	1.02
F228	LL	1.51	92.0	60.650	25.923	60.665	25.923	1.01
F229	LLN	2.91	71.5	60.641	25.918	60.667	25.926	1.04
F230	LL	2.44	241.8	60.628	25.938	60.607	25.928	1.02
F231	LLN	0.93	238.1	60.649	25.930	60.641	25.925	1.00
F232	RRL	1.17	131.8	60.642	25.938	60.651	25.931	1.01
F233	LL	8.79	83.8	60.664	25.940	60.750	25.948	1.02
F234	LLR	4.11	54.3	60.650	25.934	60.682	25.955	1.04
F235	N	3.00	265.6	60.637	25.947	60.607	25.944	1.01
F236	LL	4.98	82.9	60.657	25.951	60.706	25.957	1.01
F236	LL	2.05	75.3	60.637	25.947	60.656	25.951	1.01
F237	LLN	1.70	89.0	60.707	25.957	60.723	25.957	1.03
F238	LLR	2.66	105.6	60.724	25.957	60.749	25.951	1.00
F239	LL	0.52	87.9	60.711	25.959	60.716	25.959	1.01
F240	LL	0.92	91.4	60.715	25.960	60.724	25.960	1.01
F241	LL	0.30	85.9	60.728	25.961	60.731	25.961	1.01
F242	LL	1.62	85.1	60.704	25.961	60.719	25.962	1.01
F243	LLR	2.19	93.0	60.727	25.964	60.749	25.963	1.02
F244	N	1.68	53.8	60.701	25.949	60.714	25.958	1.02
F245	LL	3.67	81.2	60.622	25.949	60.657	25.954	1.01
F245	LL	1.26	84.0	60.608	25.948	60.621	25.949	1.01
F246	N	0.33	331.5	60.623	25.947	60.621	25.949	1.00
F247	RLL	0.76	249.1	60.679	25.958	60.673	25.956	1.02
F248	RLL	2.67	237.5	60.701	25.970	60.680	25.958	1.06
F249	RLL	1.32	225.9	60.691	25.967	60.682	25.959	1.04
F250	RLL	1.34	52.8	60.691	25.961	60.702	25.968	1.02
F251	LLR	1.82	241.9	60.718	25.975	60.703	25.967	1.02
F252	LL	0.55	91.6	60.744	25.980	60.750	25.980	1.00
F253	LLN	1.58	78.8	60.727	25.976	60.742	25.979	1.03
F254	LL	1.33	90.3	60.724	25.981	60.737	25.981	1.01
F255	LLN	2.44	66.6	60.693	25.973	60.715	25.982	1.03
F255	LLN	1.90	71.5	60.700	25.975	60.718	25.980	1.03
F256	LL	3.22	89.7	60.657	25.974	60.689	25.974	1.00
F257	LLN	5.31	98.1	60.630	25.982	60.682	25.975	1.00
F258	LLR	4.39	94.2	60.603	25.989	60.646	25.986	1.02
F259	LL	0.58	78.7	60.640	25.984	60.646	25.985	1.01
F260	LL	1.21	87.7	60.612	25.983	60.624	25.984	1.00
F261	RL	6.21	95.5	60.558	25.996	60.618	25.991	1.02
F262	LLR	5.02	97.4	60.523	25.999	60.572	25.993	1.01

GeoNexus

Fault	**Mec.**	**Length** (km)	**Strike** (°)	**START_X** (° E)	**START_Y** (° N)	**END_X** (° E)	**END_Y** (° N)	**Sin.**
F263	N	1.60	293.0	60.592	25.993	60.578	25.998	1.02
F264	N	0.80	242.0	60.603	25.989	60.596	25.986	1.01
F265	NLL	0.18	46.1	60.609	25.989	60.610	25.990	1.00
F265	NLL	0.13	54.9	60.610	25.990	60.612	25.991	1.00
F266	LLN	0.49	68.8	60.584	25.998	60.588	26.000	1.00
F267	LLR	3.72	102.5	60.684	25.992	60.720	25.984	1.00
F268	LLR	3.90	285.5	60.703	25.989	60.665	25.998	1.00
F269	LL	1.68	95.3	60.726	25.986	60.743	25.984	1.00
F270	R	3.55	96.9	60.701	25.993	60.735	25.989	1.04
F271	RLN	1.05	121.6	60.737	25.999	60.746	25.994	1.02
F272	RLN	1.15	290.0	60.740	25.999	60.729	26.002	1.03
F273	RLN	1.48	294.9	60.750	25.995	60.737	26.000	1.04
F274	R	6.39	97.4	60.793	25.698	60.855	25.691	1.01
F275		9.72	97.3	60.270	25.813	60.365	25.802	1.01
F276		4.33	113.7	60.179	25.853	60.217	25.837	1.02
F277		3.85	113.6	60.224	25.834	60.259	25.820	1.01
F278		10.71	118.8	60.334	25.724	60.424	25.679	1.04
F279		10.33	82.9	60.463	25.733	60.565	25.745	1.01
F280		5.96	110.1	60.654	25.717	60.709	25.698	1.00
F281		2.31	113.3	60.128	25.733	60.149	25.725	1.00
F282		0.94	104.4	60.116	25.735	60.125	25.733	1.00
F283		0.60	108.9	60.175	25.703	60.181	25.701	1.00
F284		1.83	117.3	60.149	25.714	60.165	25.706	1.00
F285		1.50	121.8	60.143	25.719	60.156	25.712	1.00
F286		1.47	99.3	60.120	25.724	60.135	25.721	1.00
F287		0.70	141.9	60.137	25.701	60.141	25.696	1.00
F288		1.65	109.5	60.397	25.593	60.413	25.588	1.00
F289		3.97	37.5	60.462	25.577	60.485	25.604	1.02
F290		0.18	104.3	60.463	25.606	60.465	25.605	1.02
F291		0.07	100.0	60.466	25.605	60.466	25.605	1.02
F292		0.08	287.3	60.467	25.605	60.466	25.605	1.03
F293		0.05	235.9	60.467	25.605	60.466	25.605	1.02
F294		0.08	130.7	60.466	25.605	60.467	25.605	1.04
F295		0.05	96.8	60.468	25.604	60.468	25.604	1.01
F296		1.32	289.4	60.451	25.606	60.439	25.610	1.02
F297		0.03	59.1	60.434	25.649	60.434	25.650	1.02
F298		0.01	214.1	60.434	25.649	60.434	25.649	1.02
F299		0.02	226.0	60.434	25.649	60.434	25.649	1.01
F300		0.01	54.3	60.434	25.649	60.434	25.650	1.01
F301		0.16	288.7	60.435	25.649	60.433	25.650	1.02
F302		0.09	90.1	60.434	25.650	60.435	25.650	1.02
F303		0.06	86.7	60.434	25.650	60.435	25.650	1.01
F304		0.02	302.7	60.433	25.650	60.433	25.650	1.03
F305		0.09	279.4	60.433	25.650	60.432	25.650	1.02
F306		2.78	57.9	60.411	25.635	60.434	25.648	1.03
F307		0.92	237.4	60.408	25.633	60.401	25.629	1.07
F308		0.85	27.0	60.399	25.623	60.403	25.629	1.02
F309		0.61	42.8	60.435	25.649	60.439	25.653	1.02
F310		0.39	122.0	60.413	25.671	60.416	25.669	1.00
F311		0.69	105.2	60.639	25.521	60.645	25.520	1.00
F312		0.72	97.8	60.641	25.524	60.648	25.523	1.00
F313		0.84	103.4	60.651	25.524	60.660	25.522	1.00
F314		3.25	219.0	60.753	25.565	60.732	25.543	1.01
F315		4.63	115.4	60.725	25.546	60.763	25.530	1.11
F316		3.66	72.8	60.714	25.567	60.748	25.576	1.02
F317		1.21	113.4	60.633	25.545	60.644	25.541	1.01
F318		2.12	104.7	60.625	25.544	60.645	25.539	1.02
F319		4.91	193.9	60.653	25.591	60.643	25.551	1.08

GeoNexus

Fault	Mec.	Length (km)	Strike (°)	START_X (° E)	START_Y (° N)	END_X (° E)	END_Y (° N)	Sin.
F320		0.99	145.5	60.744	25.494	60.750	25.486	1.00
F321		2.15	107.0	60.290	25.691	60.310	25.685	1.02
F322		0.11	123.8	60.459	25.446	60.460	25.446	1.01
F323		0.10	314.2	60.458	25.446	60.458	25.447	1.01
F324		0.07	107.5	60.460	25.445	60.461	25.445	1.02
F325		0.12	102.2	60.461	25.445	60.462	25.445	1.02
F326		7.01	39.2	60.533	25.769	60.575	25.815	1.06
F327		0.63	99.6	60.743	25.988	60.749	25.987	1.03
F328		1.47	106.0	60.470	25.988	60.484	25.985	1.01
F329		1.58	116.5	60.452	25.995	60.466	25.988	1.00
F330		0.50	207.2	60.630	25.985	60.628	25.981	1.01
F331		0.75	57.2	60.629	25.982	60.635	25.986	1.01
F332		1.89	89.7	60.631	25.990	60.649	25.991	1.05
F333		2.01	86.2	60.638	25.994	60.657	25.996	1.02
F334		1.40	98.0	60.642	25.998	60.655	25.996	1.02
F335		1.70	97.6	60.586	25.991	60.602	25.989	1.02
F336		1.69	90.7	60.581	25.982	60.598	25.982	1.02
F337		0.28	68.6	60.701	25.971	60.703	25.972	1.01
F338		0.50	278.6	60.707	25.970	60.702	25.971	1.02
F339		0.94	79.0	60.709	25.961	60.718	25.962	1.03
F340		0.82	93.1	60.714	25.961	60.722	25.960	1.01
F341		1.08	82.3	60.717	25.960	60.727	25.961	1.03
F342		0.27	76.7	60.723	25.960	60.725	25.961	1.05
F343		0.54	81.3	60.719	25.976	60.725	25.976	1.07
F344		0.88	73.2	60.720	25.975	60.728	25.977	1.03
F345		0.29	71.0	60.719	25.980	60.722	25.981	1.04
F346		0.63	69.1	60.726	25.976	60.732	25.978	1.02
F347		0.72	58.3	60.719	25.978	60.725	25.981	1.04
F348		1.73	88.5	60.714	25.978	60.731	25.978	1.02
F349		0.51	60.3	60.723	25.979	60.728	25.981	1.04
F350		1.49	83.3	60.726	25.975	60.740	25.976	1.03
F351		0.97	90.7	60.737	25.962	60.747	25.962	1.02
F352		0.44	75.5	60.734	25.961	60.738	25.962	1.03
F353		3.12	57.5	60.730	25.910	60.755	25.925	1.04
F354		1.43	42.4	60.718	25.902	60.728	25.911	1.03
F355		3.93	41.6	60.724	25.909	60.749	25.935	1.04
F356		1.95	36.6	60.732	25.920	60.744	25.934	1.02
F357		1.08	12.9	60.717	25.902	60.720	25.912	1.03
F358		1.35	22.6	60.720	25.907	60.725	25.918	1.01
F359		3.49	239.3	60.756	25.916	60.727	25.900	1.03
F360		1.33	308.9	60.537	25.936	60.527	25.944	1.02
F361		1.47	189.4	60.521	25.923	60.519	25.910	1.02
F362		1.11	107.7	60.508	25.942	60.517	25.939	1.11
F363		1.35	31.9	60.533	25.945	60.540	25.955	1.02
F364		4.42	268.0	60.490	25.947	60.446	25.945	1.01
F365		2.19	107.5	60.489	25.977	60.510	25.971	1.01
F366		2.17	125.5	60.455	25.932	60.473	25.920	1.01
F367		3.96	88.2	60.246	25.844	60.285	25.845	1.02
F368		1.70	77.9	60.228	25.851	60.244	25.854	1.02
F369		4.27	296.8	60.295	25.826	60.258	25.843	1.03
F370		0.68	75.7	60.617	25.909	60.624	25.910	1.02
F371		0.37	55.1	60.619	25.910	60.622	25.912	1.02
F372		0.40	85.8	60.619	25.910	60.623	25.910	1.00
F373		0.12	57.2	60.621	25.912	60.622	25.913	1.02
F374		0.42	62.3	60.622	25.912	60.626	25.914	1.02
F375		0.17	112.1	60.620	25.911	60.622	25.910	1.03
F376		0.58	61.7	60.640	25.921	60.645	25.923	1.02
F377		0.75	62.2	60.600	25.899	60.606	25.902	1.03

GeoNexus

Fault	Mec.	Length (km)	Strike (°)	START_X (° E)	START_Y (° N)	END_X (° E)	END_Y (° N)	Sin.
F378		0.74	42.7	60.617	25.909	60.622	25.914	1.03
F379		3.03	78.5	60.542	25.957	60.571	25.962	1.02
F380		1.80	98.6	60.201	25.854	60.219	25.851	1.02
F381		2.80	81.3	60.245	25.896	60.272	25.899	1.03
F382		3.38	59.5	60.263	25.893	60.292	25.908	1.02
F383		2.50	73.3	60.201	25.881	60.224	25.888	1.01
F384		0.76	34.0	60.623	25.972	60.627	25.978	1.01
F385		0.90	95.1	60.601	25.984	60.610	25.984	1.01
F386		0.34	80.5	60.595	25.983	60.598	25.984	1.02
F387		0.75	77.1	60.587	25.982	60.595	25.983	1.01
F388		3.62	51.7	60.207	25.917	60.235	25.937	1.03
F389		2.90	175.1	60.540	25.923	60.543	25.897	1.02
F390		0.10	78.6	60.618	25.910	60.619	25.910	1.03
F391		0.17	73.3	60.617	25.908	60.619	25.909	1.03
F392		0.19	61.7	60.617	25.908	60.619	25.908	1.03
F393		0.11	52.1	60.617	25.907	60.618	25.908	1.02
F394		0.42	54.0	60.611	25.898	60.615	25.900	1.01
F395		0.44	214.0	60.618	25.904	60.615	25.900	1.03
F396		0.51	252.4	60.619	25.901	60.615	25.899	1.02
F397		0.88	69.1	60.618	25.899	60.626	25.902	1.04
F398		0.05	56.8	60.611	25.897	60.611	25.897	1.02
F399		3.01	93.0	60.553	25.927	60.582	25.926	1.04
F400		0.32	288.1	60.638	25.985	60.635	25.986	1.02
F401		0.07	89.9	60.610	25.949	60.610	25.949	579.03
F402		0.08	297.9	60.611	25.949	60.610	25.950	1.59
F403		0.07	306.6	60.610	25.950	60.610	25.950	2.23
F404		0.24	234.3	60.610	25.897	60.609	25.896	1.02
F405		0.14	218.6	60.608	25.895	60.607	25.894	1.00
F406		2.83	153.1	60.607	25.889	60.620	25.866	1.01
F407		0.41	250.4	60.612	25.901	60.608	25.900	1.03
F408		0.15	141.5	60.622	25.949	60.622	25.948	1.00
F409		0.86	187.0	60.619	25.958	60.618	25.951	1.00
F410		0.22	222.7	60.605	25.992	60.604	25.991	1.00
F411		0.31	115.2	60.612	25.991	60.615	25.990	1.00
F412		0.79	102.9	60.578	25.999	60.585	25.997	1.00
F413		0.41	268.6	60.597	26.001	60.593	26.001	1.00
F414		0.20	248.2	60.591	26.001	60.589	26.000	1.00
F415		0.23	75.3	60.599	26.001	60.602	26.002	1.00
F416		0.44	61.0	60.603	26.002	60.607	26.004	1.00
F417		1.68	64.8	60.575	25.997	60.590	26.004	1.04
F418		0.32	69.8	60.591	26.004	60.594	26.005	1.00
F419		2.72	49.4	60.208	25.948	60.229	25.964	1.01
F420		0.95	283.2	60.123	25.879	60.114	25.881	1.03
F421		8.44	41.3	60.232	25.963	60.287	26.020	1.01

GeoNexus

Table S18- Summary of the measured bedding planes.

OBJECTID	Title	Latitude (° N)	Longitude (° E)	Strike (°)	Dip (°)
1	1145	25.719	60.318	10	27
2	1144	25.735	60.312	5	50
3	1143	25.761	60.273	358	45
4	1142	25.762	60.274	310	25
5	1140	25.774	60.263	28	35
6	1139	25.765	60.281	358	50
7	1138	25.764	60.280	80	35
8	1136	25.746	60.301	52	20
9	1135	25.743	60.301	322	45
10	1134	25.742	60.301	320	35
11	1131	25.555	60.645	330	30
12	1130	25.554	60.706	4	27
13	1129	25.552	60.735	2	40
14	1128	25.561	60.748	182	45
15	1127	25.805	60.750	54	45
16	1125	25.819	60.713	238	30
17	1124	25.819	60.710	340	35
18	1123	25.824	60.689	20	55
19	1122	25.829	60.681	270	45
20	1120	25.836	60.670	250	20
21	1119	25.837	60.665	10	40
22	1117	25.851	60.622	350	5
23	1116	25.855	60.622	200	70
24	1115	25.892	60.613	290	25
25	1114	25.888	60.607	130	30
26	1112	25.894	60.606	350	25
27	1111	25.895	60.604	230	30
28	1108	25.897	60.610	295	30
29	1106	25.898	60.613	260	30
30	1104	25.911	60.624	200	45
31	1103	25.916	60.633	300	50
32	1101	25.927	60.644	358	85
33	1099	25.928	60.647	320	35
34	1098	25.932	60.649	10	50
35	1097	25.944	60.659	130	80
36	1096	25.977	60.656	20	75
37	1095	25.985	60.631	15	75
38	1094	25.986	60.617	0	70
39	1093	25.990	60.610	260	50
40	1092	25.989	60.603	58	70
41	1091	26.000	60.597	2	45
42	1090	26.002	60.592	40	45
43	1089	26.000	60.592	290	45
44	1088	25.999	60.584	10	50
45	1087	25.998	60.579	320	80
46	1085	25.349	60.298	128	2
47	1077	25.946	60.626	130	75
48	1074	25.951	60.606	358	50
49	1073	25.368	60.617	170	5
50	1066	25.691	60.393	75	27
51	1065	25.681	60.407	130	50
52	71	25.701	60.424	40	30
53	70	25.700	60.428	110	20
54	69	25.708	60.412	60	45
55	62	25.665	60.414	15	20
56	60	25.722	60.369	300	20

GeoNexus

OBJECTID	Title	Latitude (° N)	Longitude (° E)	Strike (°)	Dip (°)
57	58	25.688	60.344	110	20
58	57	25.678	60.344	275	35
59	55	25.685	60.338	295	10
60	56	25.666	60.390	100	20
61	53	25.655	60.427	44	40
62	51	25.644	60.438	280	30
63	50	25.621	60.452	300	30
64	47	25.843	60.205	60	25
65	46	25.863	60.195	140	60
66	44	25.887	60.198	110	80
67	43	25.914	60.199	205	45
68	42	25.928	60.199	40	30
69	41	25.941	60.199	250	20
70	40	25.968	60.185	340	55
71	39	25.988	60.163	342	75
72	38	25.987	60.163	345	75
73	37	25.986	60.158	5	45
74	36	26.005	60.150	50	85
75	34	25.550	60.727	280	55
76	32	25.560	60.673	340	30
77	31	25.559	60.662	10	30
78	30	25.553	60.631	28	28
79	28	25.517	60.586	210	3
80	27	25.494	60.565	10	20
81	23	25.330	60.622	160	5
82	22	25.589	60.481	20	30
83	12	25.277	60.696	5	10
84	9	25.346	60.614	274	15
85	4	25.357	60.608	55	25
86	3	25.358	60.608	85	30
87	2	25.344	60.620	310	5
88	1	25.342	60.623	90	8
89	1152	25.632	60.144	165	15
90	1151	25.627	60.137	215	15
91	1150	25.617	60.144	200	15
92	1147	25.597	60.214	196	5
93	1146	25.478	60.387	312	8
94	0	0.000	0.000	45	46
95	0	0.000	0.000	190	42
96	0	0.000	0.000	5	44
97	0	0.000	0.000	35	31
98	0	0.000	0.000	40	25
99	0	0.000	0.000	5	40
100	0	0.000	0.000	3	6
101	0	0.000	0.000	35	13
102	0	0.000	0.000	165	35
103	0	0.000	0.000	23	55
104	0	0.000	0.000	170	60
105	0	0.000	0.000	30	35
106	0	0.000	0.000	345	50
107	0	0.000	0.000	5	35
108	0	0.000	0.000	350	45
109	0	0.000	0.000	345	65
110	0	0.000	0.000	355	60
111	0	0.000	0.000	193	35
112	0	0.000	0.000	185	35
113	0	0.000	0.000	10	5
114	0	0.000	0.000	10	30

GeoNexus

OBJECTID	Title	Latitude (° N)	Longitude (° E)	Strike (°)	Dip (°)
115	0	0.000	0.000	18	30
116	0	0.000	0.000	165	40
117	0	0.000	0.000	320	25
118	0	0.000	0.000	310	25
119	0	0.000	0.000	25	70
120	0	0.000	0.000	195	20
121	0	0.000	0.000	5	20
122	0	0.000	0.000	25	30
123	0	0.000	0.000	30	15
124	0	0.000	0.000	358	60
125	0	0.000	0.000	35	65
126	0	0.000	0.000	240	50
127	0	0.000	0.000	225	35
128	0	0.000	0.000	30	50
129	0	0.000	0.000	35	30
130	0	0.000	0.000	28	35
131	0	0.000	0.000	25	25
132	0	0.000	0.000	125	30
133	0	0.000	0.000	200	35
134	0	0.000	0.000	200	10
135	0	0.000	0.000	10	30
136	0	0.000	0.000	345	40
137	0	0.000	0.000	30	40
138	0	0.000	0.000	260	20
139	0	0.000	0.000	35	45
140	0	0.000	0.000	5	30
141	0	0.000	0.000	35	10
142	0	0.000	0.000	188	20
143	0	0.000	0.000	210	50
144	0	0.000	0.000	28	50
145	0	0.000	0.000	28	40
146	0	0.000	0.000	30	30
147	0	0.000	0.000	180	30
148	0	0.000	0.000	42	30
149	0	0.000	0.000	200	10
150	0	0.000	0.000	25	40
151	0	0.000	0.000	5	60
152	0	0.000	0.000	5	65
153	0	0.000	0.000	10	45
154	0	0.000	0.000	355	60
155	0	0.000	0.000	185	35
156	0	0.000	0.000	180	30
157	0	0.000	0.000	40	55
158	0	0.000	0.000	25	35
159	0	0.000	0.000	25	40
160	0	0.000	0.000	35	30
161	0	0.000	0.000	30	40
162	0	0.000	0.000	15	15
163	0	0.000	0.000	350	10
164	0	0.000	0.000	10	10
165	0	0.000	0.000	15	65
166	0	0.000	0.000	330	10
167	0	0.000	0.000	4	12
168	0	0.000	0.000	325	15
169	0	0.000	0.000	230	20
170	0	0.000	0.000	270	10
171	0	0.000	0.000	330	5
172	0	0.000	0.000	310	5

GeoNexus

OBJECTID	Title	Latitude (° N)	Longitude (° E)	Strike (°)	Dip (°)
173	0	0.000	0.000	20	10
174	0	0.000	0.000	320	10
175	0	0.000	0.000	330	15
176	0	0.000	0.000	15	15
177	0	0.000	0.000	20	15
178	0	0.000	0.000	330	20
179	0	0.000	0.000	3	25
180	0	0.000	0.000	4	25
181	0	0.000	0.000	20	20
182	0	0.000	0.000	25	20
183	0	0.000	0.000	30	15
184	0	0.000	0.000	260	20
185	0	0.000	0.000	60	45
186	0	0.000	0.000	55	50
187	0	0.000	0.000	35	30
188	0	0.000	0.000	335	30
189	0	0.000	0.000	135	15
190	0	0.000	0.000	150	20
191	0	0.000	0.000	175	15
192	0	0.000	0.000	195	40
193	0	0.000	0.000	45	30
194	0	0.000	0.000	35	20
195	0	0.000	0.000	10	15
196	0	0.000	0.000	35	20
197	0	0.000	0.000	185	20
198	0	0.000	0.000	340	45
199	0	0.000	0.000	10	20
200	0	0.000	0.000	205	15
201	0	0.000	0.000	160	20
202	0	0.000	0.000	25	30
203	0	0.000	0.000	25	15
204	0	0.000	0.000	350	30
205	0	0.000	0.000	20	30
206	0	0.000	0.000	2	60
207	0	0.000	0.000	355	75
208	0	0.000	0.000	20	50
209	0	0.000	0.000	15	55
210	0	0.000	0.000	38	41
211	0	0.000	0.000	65	53
212	0	0.000	0.000	335	55
213	0	0.000	0.000	355	50
214	0	0.000	0.000	15	30
215	0	0.000	0.000	355	55
216	0	0.000	0.000	65	40
217	0	0.000	0.000	20	65
218	0	0.000	0.000	20	65
219	0	0.000	0.000	350	60
220	0	0.000	0.000	350	60
221	0	0.000	0.000	20	60
222	0	0.000	0.000	35	55
223	0	0.000	0.000	345	60
224	0	0.000	0.000	355	70
225	0	0.000	0.000	3	47
226	0	0.000	0.000	165	60
227	0	0.000	0.000	315	45
228	0	0.000	0.000	325	45
229	0	0.000	0.000	20	40
230	0	0.000	0.000	25	45

GeoNexus

OBJECTID	Title	Latitude (° N)	Longitude (° E)	Strike (°)	Dip (°)
231	0	0.000	0.000	3	52
232	0	0.000	0.000	330	70
233	0	0.000	0.000	8	70
234	0	0.000	0.000	35	60
235	0	0.000	0.000	35	40
236	0	0.000	0.000	20	40
237	0	0.000	0.000	220	70
238	0	0.000	0.000	220	75
239	0	0.000	0.000	95	45
240	0	0.000	0.000	350	40
241	0	0.000	0.000	25	50
242	0	0.000	0.000	355	40
243	0	0.000	0.000	355	45
244	0	0.000	0.000	25	60
245	0	0.000	0.000	345	23
246	0	0.000	0.000	180	80
247	0	0.000	0.000	215	75
248	0	0.000	0.000	30	40
249	0	0.000	0.000	25	40
250	0	0.000	0.000	38	10
251	0	0.000	0.000	3	20
252	0	0.000	0.000	40	35
253	0	0.000	0.000	95	35
254	0	0.000	0.000	35	75
255	0	0.000	0.000	30	65
256	0	0.000	0.000	215	60
257	0	0.000	0.000	220	50
258	0	0.000	0.000	210	45
259	0	0.000	0.000	210	55
260	0	0.000	0.000	220	45
261	0	0.000	0.000	215	25
262	0	0.000	0.000	225	30
263	0	0.000	0.000	220	45
264	0	0.000	0.000	210	45
265	0	0.000	0.000	220	48
266	0	0.000	0.000	220	25
267	0	0.000	0.000	215	20
268	0	0.000	0.000	40	35
269	0	0.000	0.000	20	35
270	0	0.000	0.000	30	25
271	0	0.000	0.000	30	25
272	0	0.000	0.000	210	50
273	0	0.000	0.000	180	55
274	0	0.000	0.000	180	50
275	0	0.000	0.000	25	35
276	0	0.000	0.000	175	40
277	0	0.000	0.000	210	35
278	0	0.000	0.000	190	35
279	0	0.000	0.000	200	30
280	0	0.000	0.000	165	12
281	0	0.000	0.000	220	15
282	0	0.000	0.000	205	30
283	0	0.000	0.000	230	25
284	0	0.000	0.000	225	10
285	0	0.000	0.000	200	25
286	0	0.000	0.000	0	35
287	0	0.000	0.000	35	30
288	0	0.000	0.000	35	43

GeoNexus

OBJECTID	Title	Latitude (° N)	Longitude (° E)	Strike (°)	Dip (°)
289	0	0.000	0.000	35	40
290	0	0.000	0.000	10	45
291	0	0.000	0.000	15	35
292	0	0.000	0.000	5	35
293	0	0.000	0.000	25	25
294	0	0.000	0.000	350	20
295	0	0.000	0.000	340	20
296	0	0.000	0.000	345	18
297	0	0.000	0.000	340	20
298	0	0.000	0.000	340	22
299	0	0.000	0.000	345	25
300	0	0.000	0.000	350	25
301	0	0.000	0.000	330	15
302	0	0.000	0.000	320	25
303	0	0.000	0.000	30	25
304	0	0.000	0.000	345	15
305	0	0.000	0.000	5	30
306	0	0.000	0.000	8	25
307	0	0.000	0.000	2	35
308	0	0.000	0.000	220	15
309	0	0.000	0.000	200	18
310	0	0.000	0.000	215	18
311	0	0.000	0.000	220	20
312	0	0.000	0.000	230	30
313	0	0.000	0.000	240	25
314	0	0.000	0.000	10	30
315	0	0.000	0.000	320	25
316	0	0.000	0.000	330	15
317	0	0.000	0.000	330	10
318	0	0.000	0.000	340	15
319	0	0.000	0.000	340	10
320	0	0.000	0.000	330	8
321	0	0.000	0.000	325	5
322	0	0.000	0.000	10	25
323	0	0.000	0.000	345	15
324	0	0.000	0.000	345	17
325	0	0.000	0.000	340	17
326	0	0.000	0.000	345	15
327	0	0.000	0.000	340	15
328	0	0.000	0.000	340	15
329	0	0.000	0.000	335	10
330	0	0.000	0.000	20	25
331	0	0.000	0.000	35	25
332	0	0.000	0.000	25	20
333	0	0.000	0.000	325	15
334	0	0.000	0.000	3	25
335	0	0.000	0.000	25	25
336	0	0.000	0.000	15	25
337	0	0.000	0.000	10	25
338	0	0.000	0.000	15	15
339	0	0.000	0.000	20	15
340	0	0.000	0.000	195	8
341	0	0.000	0.000	50	35
342	0	0.000	0.000	50	45
343	0	0.000	0.000	35	25
344	0	0.000	0.000	30	20
345	0	0.000	0.000	220	10
346	0	0.000	0.000	220	20

GeoNexus

OBJECTID	Title	Latitude (° N)	Longitude (° E)	Strike (°)	Dip (°)
347	0	0.000	0.000	205	15
348	0	0.000	0.000	190	12
349	0	0.000	0.000	185	25
350	0	0.000	0.000	180	25
351	0	0.000	0.000	185	35
352	0	0.000	0.000	5	32
353	0	0.000	0.000	35	30
354	0	0.000	0.000	35	20
355	0	0.000	0.000	180	25
356	0	0.000	0.000	40	27
357	0	0.000	0.000	45	45
358	0	0.000	0.000	35	32
359	0	0.000	0.000	5	50
360	0	0.000	0.000	200	40
361	0	0.000	0.000	195	43
362	0	0.000	0.000	185	30
363	0	0.000	0.000	195	20
364	0	0.000	0.000	10	20
365	0	0.000	0.000	198	30
366	0	0.000	0.000	190	35
367	0	0.000	0.000	185	20
368	0	0.000	0.000	180	45
369	0	0.000	0.000	25	60
370	0	0.000	0.000	30	50
371	0	0.000	0.000	200	65
372	0	0.000	0.000	25	75
373	0	0.000	0.000	35	75
374	0	0.000	0.000	140	55
375	0	0.000	0.000	170	45
376	0	0.000	0.000	170	40
377	0	0.000	0.000	200	40
378	0	0.000	0.000	220	65
379	0	0.000	0.000	230	70
380	0	0.000	0.000	225	70
381	0	0.000	0.000	220	40
382	0	0.000	0.000	195	45
383	0	0.000	0.000	220	40
384	0	0.000	0.000	225	45
385	0	0.000	0.000	220	65
386	0	0.000	0.000	220	70
387	0	0.000	0.000	215	40
388	0	0.000	0.000	45	45
389	0	0.000	0.000	3	30
390	0	0.000	0.000	40	42
391	0	0.000	0.000	220	20
392	0	0.000	0.000	185	63
393	0	0.000	0.000	260	10
394	0	0.000	0.000	220	42
395	0	0.000	0.000	220	8
396	0	0.000	0.000	190	7
397	0	0.000	0.000	195	8
398	0	0.000	0.000	190	12
399	0	0.000	0.000	195	10
400	0	0.000	0.000	330	6
401	0	0.000	0.000	320	10
402	0	0.000	0.000	10	7
403	0	0.000	0.000	5	10
404	0	0.000	0.000	5	5

GeoNexus

OBJECTID	Title	Latitude (° N)	Longitude (° E)	Strike (°)	Dip (°)
405	0	0.000	0.000	120	10
406	0	0.000	0.000	10	10
407	0	0.000	0.000	20	6
408	0	0.000	0.000	25	7
409	0	0.000	0.000	70	7
410	0	0.000	0.000	80	6
411	0	0.000	0.000	35	7
412	0	0.000	0.000	50	7
413	0	0.000	0.000	260	6
414	0	0.000	0.000	15	5
415	0	0.000	0.000	5	5
416	0	0.000	0.000	25	5
417	0	0.000	0.000	345	5
418	0	0.000	0.000	130	5
419	0	0.000	0.000	50	8
420	0	0.000	0.000	50	10
421	0	0.000	0.000	25	5
422	0	0.000	0.000	345	6
423	0	0.000	0.000	355	5
424	0	0.000	0.000	10	10
425	0	0.000	0.000	10	9
426	0	0.000	0.000	7	7
427	0	0.000	0.000	25	7
428	0	0.000	0.000	20	8
429	0	0.000	0.000	15	5
430	0	0.000	0.000	7	4
431	0	0.000	0.000	5	3
432	0	0.000	0.000	10	7
433	0	0.000	0.000	20	7
434	0	0.000	0.000	7	3
435	0	0.000	0.000	175	4

GeoNexus

GeoNexus

GeoNexus

GeoNexus

Abstract

This report presents the findings of the Server-Based Unified Thematic Geological Mapping of Makran (SUTGMM) project, a groundbreaking geospatial study conducted at a 1:50,000 scale in southeastern Iran. The Makran region, positioned along the northern margin of the Oman Sea, is a key geological area shaped by the complex collision of the Arabian and Eurasian plates. The project offers a detailed analysis of the region's diverse geological formations, including volcanic sequences, sedimentary basins, and Quaternary deposits, which reveal the area's dynamic geologic history. Utilizing state-of-the-art technologies such as cloud computing, machine learning, and object-based image analysis (OBIA), the SUTGMM project integrates data from Sentinel-1, Sentinel-2, Landsat-8, and ASTER, alongside digital elevation models (DEMs). Processed via *Google Earth Engine*, this innovative approach enabled the production of a unified geological map with 85% accuracy, providing new insights into the region's stratigraphy and tectonic processes. The final output includes geological maps, covering key areas of Makran, supported by the GeoNexus geodatabase. This geodatabase consolidates multi-source data, field surveys, and advanced algorithms to produce highly detailed and accurate geological interpretations. The GeoNexus/SUTGMM project represents a cost reduction of 80% compared to traditional methods and achieves a more than 90% reduction in time and personnel, making it a highly efficient and cost-effective, yet precise and comprehensive solution for large-scale geological mapping. The SUTGMM project represents a significant advancement in cost-effective geological mapping, reducing both time and resources traditionally required for such large-scale studies, while improving precision and comprehensiveness.

GeoNexus